AD-A010 505

SYMPOSIUM ON NAVAL HYDRODYNAMICS (9TH). VOLUME 1. UNCONVENTIONAL SHIPS; OCEAN ENGINEERING. HELD AT PARIS (FRANCE) ON AUGUST 20-25, 1972

R. Brard, et al

Office of Naval Research
Arlington, Virginia

1972

DISTRIBUTED BY:

NTIS

National Technical Information Service
U. S. DEPARTMENT OF COMMERCE

Best
Available
Copy

AD A010505

164073

0

Ninth Symposium

NAVAL HYDRODYNAMICS

VOLUME I

UNCONVENTIONAL SHIPS

SEAKEEPING

DDC
RECEIVED
JUN 12 1975

Reproduced by
NATIONAL TECHNICAL
INFORMATION SERVICE
US Department of Commerce
Springfield, VA. 22151

DISTRIBUTION STATEMENT A
Approved for public release;
Distribution Unlimited

ACR-203
Office of Naval Research
Department of the Navy

Ninth Symposium

NAVAL HYDRODYNAMICS

VOLUME 1

UNCONVENTIONAL SHIPS
OCEAN ENGINEERING

sponsored by the

OFFICE OF NAVAL RESEARCH

the

MINISTERE D'ETAT CHARGE DE LA DEFENSE NATIONALE

and the

ASSOCIATION TECHNIQUE MARITIME ET AERONAUTIQUE

August 20-25, 1972

Paris, France

DDC
RECEIVED
JUN 12 1975
D

R. BRARD
A. CASTERA
Editors

ACR-203

OFFICE OF NAVAL RESEARCH—DEPARTMENT OF THE NAVY

Arlington, Va.

For sale by the Superintendent of Documents, U.S. Government Printing Office
Washington, D.C. 20402 -
Stock Number 0851-00062

DISTRIBUTION STATEMENT A
Approved for public release;
Distribution Unlimited

PREVIOUS BOOKS IN THE NAVAL HYDRODYNAMICS SERIES

"First Symposium on Naval Hydrodynamics," National Academy of Sciences–National Research Council, Publication 515, 1957, Washington, D.C.; PB133732, paper copy $6.00, 335-mm microfilm $1.45.

"Second Symposium on Naval Hydrodynamics: Hydrodynamic Noise and Cavity Flow," Office of Naval Reserach, Department of the Navy, ACR-38, 1958; PB157668, paper copy $10.00, 35-mm microfilm $1.45.

"Third Symposium on Naval Hydrodynamics: High-Performance Ships," Office of Naval Research, Department of the Navy, ACR-65, 1960; AD430729, paper copy $6.00, 35-mm microfilm $1.45.

"Fourth Symposium on Naval Hydrodynamics: Propulsion and Hydroelasticity," Office of Naval Research, Department of the Navy, ACR-92, 1962; AD447732, paper copy $9.00, 35-mm microfilm $1.45.

"The Collected Papers of Sir Thomas Havelock on Hydrodynamics," Office of Naval Research, Department of the Navy, ACR-103, 1963; AD623589, paper copy $6.00, microfiche $1.45.

"Fifth Symposium on Naval Hydrodynamics: Ship Motions and Drag Reduction," Office of Naval Research, Department of the Navy, ACR-112, 1964; AD640539, paper copy $15.00, microfiche $1.45.

"Sixth Symposium on Naval Hydrodynamics: Physics of Fluids, Maneuverability and Ocean Platform Ocean Waves, and Ship-Generated Waves and Wave Resistance," Office of Naval Research, Department of the Navy, ACR-136, 1966; AD676079, paper copy $10.00, microfiche $1.45.

"Seventh Symposium on Naval Hydrodynamics: Unsteady Propeller Forces, Fundamental Hydrodynamics, Unconventional Propulsion," Office of Naval Research, Department of the Navy, DR-148, 1968. AD721180; Available from Superintendent of Documents, U.S. Government Printing Office, Washington, D.C. 20402, Clothbound, 1690 pages, illustrated (Catalog No. D 210.15:DR-148; Stock No. 0851-0049), $13.00; microfiche $1.45.

"Eighth Symposium on Naval Hydrodynamics: Hydrodynamics in the Ocean Environment," Office of Naval Research, Department of the Navy, ACR-179, 1970; AD748721; Available from Superintendent of Documents, U.S. Government Printing Office, Washington, D.C., 20404, Clothbound, 1185 pages, illustrated (Catalog No. D 210.15: ACR-179; Stock No. 0851-0056), $10.00; microfiche $1.45.

NOTE: The above books are available on microfilm and microfiche from the National Technical Information Service, U.S. Department of Commerce, Springfield, Virginia 22151. The first six books are also available from NTIS in paper copies. The catalog numbers and the prices for paper, clothbound, and microform copies are shown for each book.

Statements and opinions contained herein are those of the authors and are not to be construed as official or reflecting the views of the Navy Department or of the naval service at large.

PREFACE

The Ninth Symposium on Naval Hydrodynamics continues in all aspects the precedent, established by previous symposia in this series, of providing an international forum for the presentation and exchange of the most recent research results in selected fields of naval hydrodynamics. The Symposium was held in Paris, France on 20-25 August 1972 under the joint sponsorship of the Office of Naval Research, the Ministère d'Etat chargé de la Défense Nationale and the Association Technique Maritime et Aeroanutique.

The technical program of the Symposium was devoted to three subject areas of current naval and maritime interest. These subject areas are covered in the Proceedings in two volumes:

Volume 1 — The Hydrodynamics of Unconventional Ships
— Hydrodynamic Aspects of Ocean Engineering
Volume 2 — Frontier Problems in Hydrodynamics.

The planning, organization and management of a Symposium such as this is an undertaking of considerable magnitude, and many people have made invaluable contributions to the resolution of the myriad of large and small problems which invariably arise. The Office of Naval Research is acutely aware of the fact that the success of the Ninth Symposium is directly attributable to these people and wishes to take this opportunity to express its heartfelt gratitude to them. We are particularly indebted to Vice Admiral Raymond THIENNOT, Directeur Technique des Constructions Navales, Ministère d'Etat chargé de la Défense Nationale, to Professor Jean DUBOIS, Directeur des Recherches et Moyens d'Essais, Ministère d'Etat chargé de la Défense Nationale, and to Monsieur Jean MARIE, Président de l'Association Technique Maritime et Aeronautique, who provided the formal structure which made this joint undertaking possible. The detailed organization and management of the Ninth Symposium lay in the capable and competent hands of Vice Admiral Roger BRARD, Président de la Academie des Sciences, and Rear Admiral André CASTERA, Directeur du Bassin d'Essais des Carènes, who were most ably assisted in this endeavor by the charming Madame Jean TATON. Throughout the long days of planning and preparation the experienced and practical counsel of Mr. Stanley DOROFF of the Office of Naval Research provided continuous guidance which contributed in an immeasurable way to the success of the Ninth Symposium on Hydrodynamics.

Ralph D. Cooper

RALPH D. COOPER
Fluid Dynamics Program
Office of Naval Research

VOLUME 1

CONTENTS

Page

Preface iii

Introductory Address xv
Roger Brard, Chairman, French Organizing Committee

Opening Address xvii
Jean Blancard, Délégué Ministériel pour l'Armement Paris, France

Address xix
Honorable Robert A. Frosch, Assistant Secretary of the Navy for Research and Development, Washington, U.S.A.

UNCONVENTIONAL SHIPS

WATER-JET PROPULSION FOR HIGH-SPEED SURFACE SHIPS 3
J. Duport, M. Visconti and J. Merle (SOGREAH), France

DISCUSSION 29
William B. Morgan, Naval Ship Research and Development Center, Bethesda, Maryland

REPLY TO DISCUSSION 29
J. Duport, SOGREAH, Grenoble, France

THE FORCES ON AN AIR-CUSHION VEHICLE EXECUTING AN UNSTEADY MOTION 35
Lawrence J. Doctors, University of New South Wales, Sydney, Australia

DISCUSSION 95
Jorgens Strom-Tejsen, Naval Ship Research and Development Center, Bethesda, Maryland

Page

REPLY TC DISCUSSION 96
Lawrence J. Doctors, University of New South Wales, Sydney, Australia

A LINEARIZED POTENTIAL FLOW THEORY FOR THE MOTIONS OF AMPHIBIOUS AND NON AMPHIBIOUS AIR CUSHION VEHICLES IN A SEAWAY 99
Dr. T.K.S. Murthy, Portsmouth Polytechnic, U.K.

DISCUSSION 255
Lawrence J. Doctors, University of New South Wales, Sydney, Australia

REPLY TO DISCUSSION 256
T.K.S. Murthy, Portsmouth Polytechnic, U.K.

DISCUSSION 257
Roger Brard, Bassin d'Essais des Carènes, Paris, France

REPLY TO DISCUSSION 258
T.K.S. Murthy, Portsmouth Polytechnic, U.K.

DISCUSSION 258
Paul Kaplan, Oceanics Inc. Plainview, New York

REPLY TO DISCUSSION 259
T.K.S. Murthy, Portsmouth Polytechnic, U.K.

ON THE DETERMINATION OF AEROHYDRODYNAMIC PERFORMANCE OF AIR CUSHION VEHICLES 261
S.D. Prokhorov, V.N. Treshchevsky and L.D. Volkov Kryloff Ship Research Institute, Leningrad, U.S.S.R.

DISCUSSION 288
Paul Kaplan, Oceanics Inc. Plainview, New York

REPLY TO DISCUSSION 289
Vjacheslav N. Treshchevsky, Kryloff Research Institute, Leningrad, U.S.S.R.

HYDRODYNAMICS AND SIMULATION IN THE CANADIAN HYDROFOIL PROGRAM 293
R.T. Schmitke and E.A. Jones, Defence Research Establishment Atlantic, Dartmouth, N.S., Canada

DISCUSSION 339
Christopher Hook, Hydrofin, Bosham, Sussex, U.K.

Page

REPLY TO DISCUSSION 339
Rodney T. Schmitke, Defence Research Establishment Atlantic, Dartmouth, N.S., Canada

DISCUSSION 340
Reuven Leopold, U.S. Navy Naval Ship Engineering Center, Hyattsville, Maryland

REPLY TO DISCUSSION 340
Rodney T. Schmitke, Defence Research Establishment Atlantic, Dartmouth, N.S., Canada

DISCUSSION 341
Reuven Leopold, U.S. Navy Naval Ship Engineering Center, Hyattsville, Maryland

REPLY TO DISCUSSION 341
Rodney T. Schmitke, Defence Research Establishment Atlantic, Dartmouth, N.S., Canada

BENDING FLUTTER AND TORSIONAL FLUTTER OF FLEXIBLE HYDROFOIL STRUTS 343
Peter K. Besch and Yuan-Ning Liu, Naval Ship Research and Development Center, Bethesda, Maryland

DISCUSSION 395
Reuven Leopold, U.S. Navy Naval Ship Engineering Center, Hyattsville, Maryland

REPLY TO DISCUSSION 395
Peter K. Besch, Naval Ship Research and Development Center, Bethesda, Maryland

DISCUSSION 396
Reuven Leopold, U.S. Navy Naval Ship Engineering Center, Hyattsville, Maryland

REPLY TO DISCUSSION 396
Peter K. Besch, Naval Ship Research and Development Center, Bethesda, Maryland

DISCUSSION 397
John P. Breslin, Stevens Institute of Technology, Hoboken, New Jersey

REPLY TO DISCUSSION 397
Peter K. Besch, Naval Ship Research and Development Center, Bethesda, Maryland

Page

DISCUSSION 398
John P. Breslin, Steve Institute of Technology, Hoboken, New Jersey

REPLY TO DISCUSSION 398
Peter K. Besch, Naval Ship Research and Development Center, Bethesda, Maryland

DISCUSSION 398
John P. Breslin, Stevens Institute of Technology, Hoboken, New Jersey

REPLY TO DISCUSSION 399
Peter K. Besch, Naval Ship Research and Development Center, Bethesda, Maryland

DISCUSSION 399
Reuven Leopold, U.S. Navy Naval Ship Engineering Center, Hyattsville, Maryland

ON THE DESIGN OF THE PROPULSION SYSTEMS WITH "Z" DRIVES FOR HYDROFOIL SHIPS 401
A.A. Rousetsky, Kryloff Ship Research Institute, Leningrad, U.S.S.R.

DISCUSSION 411
Henry M. Cheng, Office of the Chief of Naval Operation, U.S.A.

REPLY TO DISCUSSION 412
Vjacheslav N. Treshchevsky, Kryloff Research Institute, Leningrad, U.S.S.R.

DISCUSSION 412
Reuven Leopold, U.S. Navy Naval Ship Engineering Center, Hyattsville, Maryland.

DISCUSSION 413
Jorgens Strom-Tejsen, Naval Ship Research and Development Center, Bethesda, Maryland

DISCUSSION 415
William B. Morgan, Naval Ship Research and Development Center, Bethesda, Maryland

DISCUSSION 415
Horst Nowacki, University of Michigan, Ann Harbor, Michigan

Page

REPLY TO DISCUSSION 416
Vjacheslav N. Treshchevsky, Kryloff Research Institute, Leningrad, U.S.S.R.

DISCUSSION 417
Reuven Leopold, U.S. Navy Naval Ship Engineering Center, Hyattsville, Maryland

REPLY TO DISCUSSION 417
Vjacheslav N. Treshchevsky, Kryloff Research Institute, Leningrad, U.S.S.R.

HYDRODYNAMIC DEVELOPMENT OF A HIGH SPEED PLANING HULL FOR ROUGH WATER 419
Daniel Savitsky, Stevens Institute of Technology, Hoboken, New Jersey, John K. Roper, Atlantic Hydrofoils, Inc. Hancock, N.H. and Lawrence Benen, Naval Ship Systems Command, U.S. Navy

DISCUSSION 459
Manley Saint-Denis, University of Hawai, Honolulu

DISCUSSION 460
Reuven Leopold, U.S. Navy Naval Ship Engineering Center, Hyattsville, Maryland

REPLY TO DISCUSSION 460
Daniel Savitsky, Stevens Institute of Technology, Hoboken, New Jersey

DISCUSSION 461
Reuven Leopold, U.S. Navy Naval Ship Engineering Center, Hyattsville, Maryland

REPLY TO DISCUSSION 461
Daniel Savitsky, Stevens Institute of Technology, Hoboken, New Jersey

MOTION AND RESISTANCE OF A LOW-WATERPLANE CATAMARAN 463
P.C. Pien and C.M. Lee, Naval Ship Research and Development Center, Bethesda, Maryland

DISCUSSION 541
J.N. Newman, Massachusetts Institute of Technology, Cambridge, Massachusetts

Page

DISCUSSION 542
Robert F. Beck, University of Michigan, Ann Arbor, Michigan

REPLY TO DISCUSSION 543
Choung M. Lee, Naval Ship Research and Development Center, Bethesda, Maryland

DISCUSSION 544
T.K.S. Murthy, Portsmouth Polytechnic, Portsmouth, U.K.

REPLY TO DISCUSSION 545
Choung M. Lee, Naval Ship Research and Development Center, Bethesda, Maryland

HYDRODYNAMIC DESIGN OF AN S^3 SEMI-SUBMERGED SHIP 549
Thomas G. Lang, PhD, Naval Undersea Research and Development Center, San Diego, California

DISCUSSION 573
Gerald E. Bellows, Universität Hamburg, Institut für Schiffbau, Hamburg, Germany

REPLY TO DISCUSSION 573
Thomas G. Lang, Naval Undersea Research and Development Center, San Diego, California

DISCUSSION 574
Nils Salvesen, Naval Ship Research and Development Center, Bethesda, Maryland

REPLY TO DISCUSSION 576
Thomas G. Lang, Naval Undersea Research and Development Center, San Diego, California

DISCUSSION 577
Edmund P. Lover, Admiralty Experiment Works Haslar, Gosport, Hants, U.K.

REPLY TO DISCUSSION 577
Thomas G. Lang, Naval Undersea Research and Development Center, San Diego, California

DISCUSSION 578
Hans Edstrand, Statens Skeppsprovningsanstalt Göteborg, Sweden

Page

REPLY TO DISCUSSION 578
Thomas G. Lang, Naval Undersea Research and Development Center, San Diego, California

DISCUSSION 579
Christopher Hook, Hydrofin, Bosham, Sussex, U.K.

REPLY TO DISCUSSION 580
Thomas G. Lang, Naval Undersea Research and Development Center, San Diego, California

PROPELLER EXCITATION AND RESPONSE OF 230 000 TDW TANKERS 581
C.A. Johnsson, The Swedish State Shipbuilding Experimental Tank, Göteborg, Sweden and
T. Søntvedt, Det norske Veritas, Oslo, Norway

DISCUSSION 655
William B. Morgan, Naval Ship Research and Development Center, Bethesda, Maryland

REPLY TO DISCUSSION 656
Carl-Anders Johnsson, Statens Skeppsprovnings-anstalt, Göteborg, Sweden

DISCUSSION 658
Marinus Oosterveld, Netherlands Ship Model Basin Wageningen, Netherlands

REPLY TO DISCUSSION 659
Carl-Anders Johnsson, Statens Skeppsprovnings-anstalt, Göteborg, Sweden

DISCUSSION 660
Edmund V. Telfer, R.I.N.A., Ewell, Surrey, U.K.

REPLY TO DISCUSSION 660
Carl-Anders Johnsson, Statens Skeppsprovnings-anstalt, Göteborg, Sweden

DISCUSSION 661
Harrison Lackenby, British Ship Research Association, Wallsend, Northumberland, U.K.

REPLY TO DISCUSSION 661
Carl-Anders Johnsson, Statens Skeppsprovnings-anstalt, Göteborg, Sweden

Page

DISCUSSION 662
Finn C. Michelsen, Norges Tekniske Høgskole, Trondheim, Norway

REPLY TO DISCUSSION 663
Carl-Anders Johnsson, Statens Skeppsprovnings-anstalt, Göteborg, Sweden

DISCUSSION 664
John P. Breslin, Stevens Institute of Technology, Hoboken, New Jersey

REPLY TO DISCUSSION 665
Carl-Anders Johnsson, Statens Skeppsprovnings-anstalt, Göteborg, Sweden

DISCUSSION 666
Erling Huse, Ship Research Institute of Norway, Trondheim, Norway

REPLY TO DISCUSSION 668
Carl-Anders Johnsson, Statens Skeppsprovnings-anstalt, Göteborg, Sweden

MOTIONS OF MOORED SHIPS IN SIX DEGREES OF FREEDOM 671
I-Min Yang, Tetra Tech. Inc., Pasadena, California

DISCUSSION 679
Manley Saint-Denis, University of Hawai, Honolulu

REPLY TO DISCUSSION 680
I-Min Yang, Tetra Tech. Inc. Pasadena, California

DISCUSSION 681
Paul Kaplan, Oceanics Inc., New York

REPLY TO DISCUSSION 683
I-Min Yang, Tetra Tech. Inc. Pasadena, California

DISCUSSION 684
Ernest O. Tuck, University of Adelaide, Australia

DISCUSSION 685
Grand Lewison, National Physical Lab., Feltham, Middlesex, U.K.

Page

REPLY TO DISCUSSION 685
I-Min Yang, Tetra Tech, Inc. Pasadena, California

DISCUSSION 685
Grant Lewison, National Physical Lab., Feltham, Middlesex, U.K.

REPLY TO DISCUSSION 686
I-Min Yang, Tetra Tech, Inc., Pasadena, California

ANALYSIS OF SHIP-SIDE WAVE PROFILES, WITH SPECIAL REFERENCE TO HULL'S SHELTERING EFFECT 687
Kazuhiro Mori, Takao Inui and Hisashi Kajitani, University of Tokyo, Japan

DISCUSSION 745
Klaus W. Eggers, Institut für Schiffbau der Universität Hamburg, Germany

REPLY TO DISCUSSION 746
Kazuhiro Mori, University of Tokyo, Japan

DISCUSSION 746
Roger Brard, Bassin d'Essais des Carènes, Paris, France

REPLY TO DISCUSSION 749
Kazuhiro Mori, University of Tokyo, Japan

DISCUSSION 756
Louis Landweber, University of Iowa, Iowa City

REPLY TO DISCUSSION 757
Kazuhiro Mori, University of Tokyo, Japan

OCEAN ENGINEERING

Page

WAVE-INDUCED EDDIES AND "LIFT" FORCES ON CIRCULAR CYLINDERS 761
R. L. Wiegel and R.C. Delmonte, University of California, Berkeley, California

DISCUSSION 792
Choung M. Lee, Naval Ship Research and Development Center, Bethesda, Maryland

REPLY TO DISCUSSION 792
Robert L. Wiegel, University of California, Berkeley, California

ANALYSES OF MULTIPLE-FLOAT-SUPPORTED PLATFORMS IN WAVES 793
C.H. Kim and J.A. Mercier, Stevens Institute of Technology, Hoboken, New Jersey

DISCUSSION 955
Michel K. Ochi, Naval Ship Research and Development Center, Bethesda, Maryland

REPLY TO DISCUSSION 956
John A. Mercier, Stevens Institute of Technology, Hoboken, New Jersey

SOME ASPECTS OF VERY LARGE OFFSHORE STRUCTURES 957
G. Van Oortmerssen, Netherlands Ship Model Basin, Wageningen, Netherlands

DISCUSSION 998
C.M. Lee, Naval Ship Research and Development Center, Bethesda, Maryland

REPLY TO DISCUSSION 998
G. Van Oortmerssen, Netherlands Ship Model Basin, Wageningen, Netherlands

DISCUSSION 999
E.J. Plate, University of Karlsruhe, Germany

REPLY TO DISCUSSION 999
G. Van Oortmerssen, Netherlands Ship Model Basin, Wageningen, Netherlands

Page

DISCUSSION 1000
J.P. Breslin, Stevens Institute of Technology, Hoboken, New Jersey

REPLY TO DISCUSSION 1000
G. Van Oortmerssen, Netherlands Ship Model Basin, Wageningen, Netherlands

UNSTABLE MOTION OF FREE SPAR BUOYS IN WAVES 1003
J-C. Dern, Bassin d'Essais des Carènes, Paris, France

AUTO-OSCILLATIONS OF ANCHORED VESSELS UNDER THE ACTION OF WIND AND CURRENT 1079
A.V. Gerassimov, R.Y. Pershitz, N.N. Rakhmanin, Kryloff Ship Research Institute, Leningrad, U.S.S.R.

DISCUSSION 1106
J-C. Dern, Bassin d'Essais des Carènes, Paris, France

REPLY TO DISCUSSION 1107
N.N. Rakhmanin, Kryloff Ship Research Institute, Leningrad, U.S.S.R.

OPENING CEREMONY

INTRODUCTORY ADDRESS

Roger BRARD
Chairman, French Organizing Committee

Ladies and Gentlemen,

As an introduction to the Opening Ceremony of the Ninth ONR-Symposium on Naval Hydrodynamics I would first like to say how pleased and honored we felt when Dr. Frosch accepted the invitation to attend the said ceremony and to speak on behalf of the United States Navy. The presence of such a high ranking official of the United States Department of Defence is a very unusual privilege.

To welcome the Assistant Secretary of the Navy for Research and Development it was only befitting that the French Government representative be Mr. Jean Blancard, Délégué Ministériel pour l'Armement, who ranks immediately after the Ministre d'Etat chargé de la Défense Nationale.

As Délégué Ministériel pour l'Armement, Mr. Jean Blancard is responsible for all the armament programs of the French Armed Forces, Army, Navy and Air Force. This includes the procurement of all the materials, either from the military establishments or from the industry, and also all the activities in Research and Development.

In particular, the Direction Technique des Constructions Navales, which is in charge of designing and building the naval ships, comes under his supervision. So does the Direction des Recherches et Moyens d'Essais which deals with fundamental research and evaluation of new scientific concepts.

Mr. Jean Blancard's academic achievements comprise ranking first at both Ecole Polytechnique and Ecole Nationale Supé-

rieure des Mines. Before being appointed as Délégué Ministériel pour l'Armement, Mr. Jean Blancard has held very important positions either in Government agencies or Government controlled industries. He has for instance been Directeur des Carburants and, as such, has for several years supervised the French Government controlled oil companies. He has also been deputy of the Minister of Defence for the Air Force. Recently he was president of the SNECMA, the major French jet engines manufacturer.

The great interest taken by Mr. Jean Blancard in the three themes of our Symposium accounts for his accepting readily to preside over the Opening Ceremony.

Thank you for your attention.

OPENING ADDRESS

Jean BLANCARD
Délégué Ministériel pour l'Armement
Paris, France

Ladies and Gentlemen,

I thank Ingénieur Général Brard for having successfully explained in a few words what the "Délégation Ministérielle pour l'Armement" is.

I am very happy to open the Ninth Symposium on Naval Hydrodynamics. I would first like to emphasize two particular reasons why it gives me great pleasure :

- the first one is that this Symposium be held in France, in Paris. It is traditional that the Symposia take place alternately in the United States and in a foreign country. This is the first time that the Symposium on Naval Hydrodynamics takes place in Paris, and I feel particularly glad for it.

- the second reason is the number and quality of the representatives from the twenty two countries who favoured us with a positive answer to our invitation. This shows the utmost importance attached to the problems of Naval Hydrodynamics.

Whatever the positions I have held and that Mr. Brard just recalled, I am not at all a theoretician in Naval Hydrodynamics. From my student time, some forty years ago, I remember that the intricate equations of hydrodynamics were stretching unendingly on the blackboard, and when the professor had finished writing them down, he would add : "The solutions are not known, so one has to resort to experiment".

Looking at your technical program, I can see that a rather important part of it is devoted to what you call frontier problems, a somewhat strange term for the non specialist. This shows that there still exist numerous unsolved problems in naval hydrodynamics, and

that scientists still have a wide field of research ahead of them.

I would like to make two remarks :

- The first one concerns the importance that what you call Ocean Engineering begins to take. For twenty five years I have been an oil prospector, and therefore I have known the beginning of off-shore prospection. The oil prospectors at first behaved like landsmen, that is that they cautiously began by erecting fixed drilling platforms to keep their feet dry. Progressively, through advances in Naval Hydrodynamics, their technique evolved, and did so with a striking rapidity if one recalls that only ten years ago the North Sea had never been crossed by a geophysical ship. In these ten years, through survey of currents and winds and study of seakeeping qualities of platforms, all the difficulties were overcome, and this interior european sea has became one of the main sources of oil for Europe, so much so that the supply from the North Sea would compensate possible difficulties in the Middle East. This could be obtained thanks to Naval Hydrodynamics.

- The second remark I shall make concerns the importance that you give to unconventional ships. It is a difficult problem for the leaders of our Navies, to know at any time what are the techniques to be applied to have better naval ships when needed. New techniques are never sufficiently called upon to adapt the existing material to the wars of to-morrow.

Even if it is true - and I believe that this was said by an American Admiral - that wars are won with outdated weaponry, a certain balance has however to be kept. No doubt that the leaders of our Navies have the final say in deciding what is needed for to-morrow, but it is the aims of a Symposium such as this one, of scientists such as you are, to give them the necessary elements to define their policy.

I would not like to be too long and delay your work any further. I only want to thank Dr. Frosch, Assistant Secretary of the Navy for Research and Development, and Mr. Ralph D. Cooper from Office of Naval Research, whose presence here proves the great interest taken by the American Authorities in your studies.

In conclusion I wish you full success in your work as well as a pleasant stay in Paris.

Thank you, Ladies and Gentlemen, for your attention.

ADDRESS

Honorable Robert A. FROSCH
Assistant Secretary of the Navy
for Research and Development
Washington, U.S.A.

It is a great pleasure to be here, not only because of my pleasure in assisting at this inaugural ceremony for the Ninth Symposium on Naval Hydrodynamics but because it is a particular pleasure for me to be able to share this platform with Mr. Blancard, with whom I have had a number of pleasant and fruitful discussions on various aspects of naval warfare and naval technology. We are very happy to have this Symposium in France not only because of traditional friendships but because of my view of the importance of the French contributions to ocean engineering in general, the French pioneering work with the bathyscaph, the advanced diving experiments of the French Navy, of Comex, of the Cousteau group and some of the unique Government and industry relationships, such as Cnexo, for the exploitation and investigation of the oceans. All of these pioneering works make it appropriate to have such a conference here in France.

It is excellent to see 12 nations contributing to a programme attended by 22, to exchange information on this particular branch of ocean engineering, which I think is significant and important to ocean engineering in general and to the basic purpose for which we all work in ocean engineering - namely, the careful use and exploitation of the oceans for the benefit of all of us.

I speak here as an outsider to naval hydrodynamics and in some sense as a consumer of naval hydrodynamics as a scientific and engineering element in ocean engineering, of naval warfare matters and of contributions to general oceanographic and oceanological matters. Viewing it as an outsider one can frequently see things that are not apparent to an insider or look different to an insider and it seems to me that we have been going through a period of very important change in naval hydrodynamics. Perhaps it looks more gradual to those who have been working on it, but to those of us who have not been working in detail on the subject it appears as though

there is a renaissance or efflorescence of ideas, a great expansion of new things in the subject.

I am thinking, for example, of what I might call the super ship, changing very rapidly from ships whose tonnage was measured in tens of thousands to ships whose tonnage is measured in hundreds of thousands. I am thinking also of the fact that the hydrofoil has come from being a curiosity to being a useful vessel not only in a naval warfare sense but, as importantly, in the sense of transportation. I have been in several European cities in which the hydrofoil is beginning to be part of the bus transportation of the city or the region, and I think we shall see this more and more. As I look at my own country and particularly my own locality of Washington DC I know that we have available, already constructed by nature, a number of highways that we do not use. You have begun to use them in Europe with hydrofoils and I think this will spread all over the world so that the waterways may become the autoroutes for many places where it is possible to do this.

Along with the hydrofoils we have begun to exploit the surface effects vehicles in the same way, first for transportation, but several navies are looking at them as possible advanced warships.

As an entirely different trend of development, but also important in the development of ships for the future and growing, as far as I can tell, from the floating oil platform techniques which Mr. Blancard has mentioned and separately coming together from a very old technique, the catamaran, we have now the various versions of what might be called low water plane catamaran or the semi-submerged ship that are being looked at in several countries and will probably have a place for ship transportation somewhere intermediate between the monohull of the conventional type and the hydrofoil or surface effect ship. But that, of course, remains for the future and perhaps this is the first international symposium in which that kind of ship will be discussed in some detail.

These transportation modes, as I might call them, are all obvious contributions not only to naval matters in the specific sense but to ocean matters in the general transportation sense. This is extremely important because for all the improvements in air transportation still most of the trade and tonnage of the world moves by sea and it appears to me that the laws of nature are such that this will go on perhaps indefinitely, at least so far as aerodynamics do not permit us to produce an aircraft which can go a long distance and carry enough fuel to get back as well as any cargo, so that all

our heavy and bulky materials will certainly continue to move by sea. So the work in naval hydrodynamics as a contribution to improved sea transportation remains as important or more important to trade and international relationships as it has ever been.

Beyond ships and ship transportation, however, we are entering an era of the use and exploitation of the oceans in which other contributions of hydrodynamic understanding will be important. We are beginning the expansion of our examinations of the oceans to a complete sensor and surveying system so that we may know the properties of the oceans and of the weather over the oceans all over the world. We have the beginnings of the means to do this in various types of buoys and instruments but many of the hydrodynamic problems associated with the long-term mooring and movement of buoys in the oceans have only begun to be broached and there will be a good deal of work ahead if we are able to make really permanent stations at sea so that we can understand the influence of the weather on the oceans, the oceans on the weather and both on the entire global environment.

As we become more concerned about the degradation of the environment and the problems of pollution, some of which are upon us and some of which we can see coming rapidly, we are looking to new means for unloading the ships that I have discussed earlier and of moving them about in such a way that we can prevent catastrophes and problems from occurring. This has begun to increase interest in offshore terminals, offshore storage and the means for moving equipment from these offshore platforms to the land. These structures and terminals also pose new problems in ocean engineering and new questions of hydrodynamics, of structures, of wave forces, of the movement of sediments on the bottom. These too will pose problems for this branch of the engineering profession.

In addition to these problems of manmade equipment and structures we have continuing and increasing human interest in the nature of the coastline itself, in the forces that shape the coastline, either to construct it or to destroy it, and we always have the interest in learning how either to control these forces and movements or to predict them and understand in what says we can live with them. These also are traditional problems of naval hydrodynamics in the broadest sense and problems that are very far from being solved. So it is clear to me that in all these areas of transportation, of terminals, of major structures at sea, of sensors to understand what happens at sea and have an understanding of the very workings of the natural forces themselves, this subject of naval hydrodyna-

mics is important and full of problems that are interesting in themselves, but also of great importance for the human interprise of keeping our lives, our civilisation and our planet together in the best possible way.

For these reasons I am delighted to be here to help to open this Ninth International Symposium on Naval Hydrodynamics.

UNCONVENTIONAL SHIPS

Monday, August 21, 1972

Morning Session

Chairman : R. Brard
Bassin d'Essais des Carènes, Paris

	Page
Water-Jet Propulsion for High-Speed Surface Ships J. Duport, M. Visconti, J. Merle (S. O. G. R. E. A. H., France)	3
The Forces on an Air-Cushion Vehicle Executing an Unsteady Motion. L. J. Doctors (University of New South Wales, Australia).	35
A linearized Potential Flow Theory for the Motions of Amphibious and Non Amphibious Air Cushion Vehicles in a Seaway. T. K. S. Murthy (Portsmouth Polytechnic, U. K.)	99
On the Determination of Aerohydrodynamic Performance of Air Cushion Vehicles. S. D. Prokhorov, V. N. Treshchevsky, L. D. Volkov (Kryloff Research Institute, Leningrad, U. S. S. R.).	261

WATER-JET PROPULSION FOR HIGH-SPEED SURFACE SHIPS

Jacques Duport, Michel Visconti, Jean Merle

SOGREAH
Grenoble, France

ABSTRACT

Free-stream subcavitating propellers are not proper for very high-speed surface crafts. The range of speed where subcavitating impellers can be used is largely increased when the propulsion flow is separated from the main external flow, i.e. when water-jet propulsion systems are being used.

A great variety of water-jet propellers can be proposed depending mainly on the jet-velocity ratio (then on the rate of flow), and the arrangement of water circuits (either fully or partially submerged, either straight-flow or elbowed circuits, etc.).

A common method of approach, applying to any of these, is proposed for the determination of the hydrodynamic characteristics of the propeller system. This concerns principally :

. Energy balance of both internal and external flows,
. Mutual interaction of both flows (including eventual hull interaction),
. Cavitation limits,
. Dimensionless hydrodynamic parameters.

The hydrodynamics of internal flow can be to a large extent analysed separately from the external flow analysis. This is a source of considerable simplification for both theoretical and experimental approaches.

Preceding page blank

The authors show that his can be applied (while with some precautions) to short-ducted, nacelle-type propellers. They describe an unconventional test-facility which has been specially developed for the design-study of high specific-speed impellers now applied to a 50 knots water-jet propeller. Comparison of prototype and predicted performances of this propeller is in favour of the applicability of the "partially separated" hydrodynamic approach.

I. WHY IS WATER JET PROPULSION OF INTEREST FOR RAPID SURFACE VESSELS

The use of subcavitating free stream propeller in surface vessels is practically limited beyond speeds of approximately 40 knots. The main cause of this limitation is that the propeller thrust behind the propeller requires that flow speed is at least equal to forward drive speed and, consequently, relative speed at the rotor is considerably higher than forward drive speed.

Thus even if a very low load coefficient is adopted, the inception of cavitation is inevitable.

If the subcavitating impellers are to be used in the high velocity range then the drive flux must be separated from the main flowstream i.e. water jets must be used. These comprise :

- an immersed water intake,
- an internal hydraulic circuit,
- a pump,
- a discharge nozzle.

With this arrangement the practical range of subcavitating impellers may be extended, principally, for the following reasons :

- selected impeller approach and discharge speeds may be adopted independently of forward drive speed (of the ship)
- use may be made, if necessary, of impellers other than the axial flow type which is suitable for free stream propellers(centrifugal pumps, mixed flow pumps, multistage pumps, etc.)

Naturally the question must be raised as to the viability of extending the use of subcavitating impellers.

A discussion of this question would involve a comparative analysis of all systems which have been, or which could be, used for the propulsion of rapid surface ships. This would exceed the scope of the present subject and we present graph fig. 1, extracted from Mr Myers paper at the SNAME Hydrofoil Symposium 1965, to which has been added a curve for the "straight flow jet propeller" which we will discuss later.

The existence of viable field of use for jet propellers (i. e. Z flow or "water-jets" or straight flow) is even more evident if reference is made to available thrust at the propeller at intermediate speeds (and not simply efficiency at cruising speed as shown in figure 1). In fact all rapid ships where the hull is designed to lift at cruising speed suffer from relatively high resistance at intermediate speeds and from this aspect, the performance of jet propellers is of particular interest, as will be demonstrated.

II. TYPES OF WATER JET PROPELLERS FOR RAPID SURFACE VESSELS

To the best of our knowledge, two main types of water jet have been developed, or proposed, for fast surface vessels and they may be differentiated by the general arrangement of the internal drive circuit.

- the type which we propose to call "Z flow jet propeller" (ZFJP) comprising an inlet component (scoop) the forward part of which is open, and a discharge nozzle at the rear the axis of which is offset in height compared to that of the water inlet axis. Between these two components, the circuit proper is rectilinear, or practically so. One of the two elbows of the circuit may be formed by the pump volute. This arrangement (specifically used by Boeing for hydrofoil drive, is essentially based upon the advantage of fitting the pump within the hull of the ship with in-line or parallel shaft drive).

- the type which we propose to refer to as "Straight flow jet propeller (SFJP) the inlet component and the discharge nozzle being aligned, implying that the whole of the propeller is submerged.

Other circuit arrangements are, a priori, feasible, for example those with a lateral water intake to provide a "Γ" shape, or those (Ω shape) in which the discharge nozzle would be lowered to surface level, so as to reduce head generated by the pump.

However neither of these arrangements has been adopted for rapid surface vessels.

As regards the former (Γ), the cavitation limit characteristics of the lateral water intake are considerably less advantageous that those of the frontal intake, so prohibiting its use at high speeds for surface vessels.

The latter arrangement (Ω) is of no practical interest since the additional weight and the head loss in the "return sector" more than offset the reduction of geometric head.

The Z flow propeller practically always includes a relatively long internal hydraulic circuit, part of which is situated above the free stream surface, where as the straight flow propeller generally has a short hydraulic circuit and is often called a pumpjet and in some ways, it is related to ducted propellers (ducted propellers with a decelerating nozzle).

The internal losses in the Z flow propeller circuit can be relatively high so that the head produced by the pump results not only from the kinetic energy added to the jet but also from the internal head loss and the geometric head. For this reason and also due to weight consideration the optimization of this type of propeller generally leads to a relatively high ratio of jet speed versus forward drive speed and lower efficiency than that of a "straight flow" propeller which can accept a relatively low ratio.

III. PERFORMANCE AND QUALITY PARAMETERS CHARACTERISING A PROPELLER

We have indicated in § 2 that efficency is neither the only one nor the most important parameter to take into account when selecting the type or optimising the characteristics of a propeller to be adopted for high-speed surface ship.

Restricting ourselves to hydrodynamic considerations concerning both the propeller and the ship, we propose to define some simple parameters, which might express the main preoccupations of a fast-ship designer.

3.1. Efficiency, the most usual concept, needs some clarification, which cannot be achieved by just transferring to jet propellers the considerations which have been developped for conventional free-stream propellers.

We think that there is no ambiguity about the definition of "input power", which should be in any case the shaft power of the impeller, and which we designate by Ps. This implies, however that the power transmission efficiency should be taken into account through another way in the selection and optimisation procedure.

"Usefull Power" on the contrary, as it is the case for conventional propeller may be more ambiguous, as long as the "thrust" concept has not been clarified.

In case of jet propeller it is easy to define the "gross thrust" Tg of the propulsion unit : this is the trust which results from the jet reaction. In case of a drowned jet with a uniform distribution of velocity, this being parallel to the drive speed, it writes :

$$Tg = \dot{M} (Vj - V)$$

Tg = gross thrust
M = rate of mass-flow
Vj = jet velocity
V = ship speed

This gross-thrust is equal to the longitudinal component of hydrodynamic forces transmitted to the ship by the propelling flux ; these forces are transmitted not only to the surface of the internal circuit but also partially to the ship hull if the intake mouth of the propeller circuit is located close to it, (to this extent, gross thrust of a jet propeller is not to be compared to the thrust of a conventional "open-water" propeller).

It is not enough to consider gross thrust of a jet propeller. This is because :

- the wetted structures of the propulsion unit are the source of a supplementary resistance which is not taken into account in the gross-thrust. This supplementary resistance is due to the external flow surrounding the wetted structures ; it can be for instance : the friction and wave resistance of struts connecting the propulsion unit (or the intake scoop) to the ship, or the external resistance of the nacelle of a "Straight Flow" propulsion unit, etc.

We propose to designate by Rp this "propeller own resistance" (which includes the resistance of associated struts).

- the flow around the hull (or foils in case of hydrofoils) can be modified due to the presence of the propulsion unit (shape modification) or the suction effect of the intake mouth. If it is so, the ship resistance may be modified, compared to the observed figure in the absence of the propulsion unit. This may occur for instance if a nacelle type SFJP or the scoop of a ZFJP is combined with the wing systems of a hydrofoil ship : the drag of the wing system can then be altered. We shall designate by Ri the supplementary resistance induced by the propeller (this introduces a correction factor which to some extent is analogous to the "suction coefficient" of conventional propellers, but does not at all respond to the same approach).

The net thrust is :

$$T_n = T_g - R_p - R_i$$

It must be noticed that separate determination of R_p and R_i is not always possible, since it may happen that they cannot be simply added.

Anyhow the value of $R_p + R_i$ can be reached through the thrust and resistance balance of the ship with and without propeller. This value depends not only upon the propeller design but also the ship design. For that reason it is interesting to consider gross efficiency as well as net efficiency.

. gross efficiency η_g is the one determined from the gross thrust :

$$\eta_g = \frac{T_g \cdot V}{P_s}$$

. net efficiency :

$$\eta_n = \frac{T_n \cdot V}{P_s}$$

3.2. Weight balance of the ship is also an important parameter when rapid surface ships are concerned, since they normally operate with either partially or fully emersed hulls. The contribution of the propulsion unit on this balance results :

. from the own apparent weight W_{AP} of the propulsion unit (circuit, pump, etc.), the power-transmission gear and emersed part of circuit-water.

. from the lift L_P of the propulsion unit due to external flow around the drowned parts of this unit, and/or the eventual inclination of the jet.

We propose to consider the "relative weight balance" of the propulsion unit :

$$RWB = \frac{W_{AP} - L_P}{T_g}$$

This parameter should be normally related to cruise conditions, but it may be interesting also to refer to RWB under take-off conditions.

3.3. We have mentionned earlier that the cruising speed condition is not the only one to be considered when dealing with high speed surface ships. The thrust requirement may be rather severe at intermediate speeds, in relation with some kind of "take-off" procedure. It is not possible to express these "medium speed" requirements in general terms since they depend largely upon the type, the size and more generally the "project programme" of the ship.

On the other side it seems rather easy to summarize approximately the "medium-speed thrust performance" of a given propulsion unit into two simple parameters which we propose to designate respectively by :

. "peak thrust ratio" : $tp = \frac{T_P}{T_C}$

. "peak thrust relative speed : $vp = \frac{V_P}{V_C}$

where : T_P is the maximum thrust as defined below,

T_C is the rated thrust at cruising speed,

V_P is the "peak thrust velocity" as defined below,

V_C is the rated cruising speed.

To define T_P and V_P let us consider the trust versus speed diagram(fig. 2). Two main limiting curves can be drawn on this diagram: the one wich corresponds to a constant shaft power equal to that required at cruising conditions, the one which corresponds to the cavitation limit of the internal circuit and pump. Both lines intersect at a point where the thrust is the highest one obtainable within the limits of the cruise condition shaft power and in view of cavitation limits. The coordinates of this point are T_P and V_P respectively.

Comparing two propeller types which might lead to equivalent performances at cruise conditions, one may be induced to select the one with the highest peak thrust ratio.

There is no precise general indication about the desirable "peak thrust relative speed". However it must be noted that a high peak thrust ratio cannot occur at high relative speed, but more at relative speed between, say, 0.3 to 0.6.

A "low peak thrust relative speed" would mean that the efficiency decreases rapidly with the ship speed and that the available thrust at medium speed may be not sufficiently high.

3.4. Following examples of performances can be proposed, according to the information we have in hands.

Straight-flow jet propeller

The 800 Kw, 50 kn prototype of SFJP which we have developped performs the following characteristics.

$$\eta g = 0,73$$

$$\eta n = 0,655$$

$$t_p = 1,5$$

$$v_p = 0,55$$

$$RWB = -0,3$$

The negative RWB figure is derived from a hydrofoil projected application where, due to optimised lift of the propeller, the lift exceeds the weight of the propulsion unit and its transmission

mechanism.

Z F propeller - 45 knots

η_g = 0,50 approximately

t_p = 1,12 to 1,2 approximately

The limitation seems to be due to the constant power condition more than to cavitation limitation.

RWB = 0,10 to 0,15

Super-cavitating propeller - 55 knots

η_g = 0,63

η_n = 0,57

RWB = 0,15 to 0,20

tp = slighthy higher than one ; the limitation is the "constant power", not the cavitation limit.

IV. EFFECT OF CAVITATION LIMITS UPON CERTAIN JET PROPULSION UNIT CHARACTERISTICS

Certain conditions must be respected to avoid the inception of cavitation within the internal circuit of a jet propulsion unit. These conditions directly affect the efficiency which is to be expected of such units with the limit of efficiency depending, among other things, upon the forward speed of the vessel for which the propulsion unit is designed.

4.1. Z Flow jet propeller (ZFJP)

As already stated, these propulsion units are fitted with a scoop and a forward intake followed by an elbow. Vaned elbows are generally used to reduce external dimensions and head losses to a minimum while avoiding cavitation.

The critical cavitation condition of an elbow is expressed by the Thoma parameter :

$$\sigma = \frac{NPSH}{Ve^2/2g}$$

NPSH being the net positive suction head at the elbow intake,

Ve is the mean velocity in the intake section of the elbow.

To the best of our knowledge, even with an extremely good vane profile, σ must be at least 0,35.

If this condition is to be respected then a diverging section is required at high speed so that the velocity at the elbow intake is lower than forward speed.

This limit has a direct effect upon the central cross-section of the scoop and upon strut thickness.

Scoop drag (friction and wave resistance) depends upon :

- the shape of the cross-section of the scoop and the intake pipe,
- the fairing and dimensions of the scoop and the strut,
- dimensions.

In order to calculate simply the incidence of the non-cavitation condition of the elbow upon propulsion unit performance, we will suppose that the external centre section for optimised shapes of scoop and strut is proportional to the cross-section of the elbow intake.

Scoop and strut drag D may thus be expressed as :

$$D = \frac{1}{2} K C_x \rho Se V^2$$

where

K is the form factor

C_x is the coefficient of drag

ρ is water density

Se is the elbow cross-section

V is forward speed

Moreover the gross thrust of the propulsion unit may be expressed as :

$$T_g = \rho Q V (w-1)$$

where

$$w = \frac{V_J}{V} \text{ and } V_J \text{ is jet velocity.}$$

The critical cavitation condition may be used to calculate Se :

$$Se = Q\sqrt{\frac{\sigma_e}{2g\,(NPSH)}}$$

where σ_e is the "critical" value of σ
From these equations it is possible to calculate the non-dimensional parameter :

$$\frac{T_g}{D} = 2\,(w-1)\frac{1}{KCx}\quad\frac{1}{V}\sqrt{\frac{2g\ NPSH}{\sigma_e}}$$

This equation shows that, for a given forward speed (and thus a given NPSH) T_G/D increases with w , which is evident since an increase in w for a given thrust leads to a decrease in the rate of propulsive flow. This effect though beneficial upon scoop drag, reduces the theoretical drive efficiency which is equal to $\frac{2}{w+1}$. This will not be expanded in this discussion since the optimisation of w also involves head losses in the circuit and the weight balance.

It should also be noted that $\frac{T_g}{D}$ decreases when the forward speed of the ship increases.

Moreover the non-cavitation condition of external flow and the external streamlining of the scoop will increase coefficients K and Cx. Beyond a speed of approximately 50 knot , sub-cavitational flow can not be maintained around the scoop and supercavitational conditions of external flow would lead to an increase in KCx.

4.2. SFJP

The non-cavitation condition for the external circuit may not, in this case, be expressed so simply a· for the scoop elbow of the ZFJP.

The critical conditions for the inception of cavitation in the pump involve the pump characteristics :

$$Cm = \frac{Q}{Sr\sqrt{2gH}}$$

in which :

Q is the rate of propulsive flow

Sr is the cross-section of the impeller

H is the head generated by the pump

$$\psi = \frac{H}{u^2/2g}$$

in which :

u is the peripheral velocity of the impeller.

Finally for the given value of Cm and ψ the pump cavitation limit is expressed by the Thomas parameter :

$$\sigma = \frac{NPSH}{H}$$

A complete examination of this question, which will not be given here, reveals the following principal considerations :

In propulsion units for high forward speeds : a diverging section before reaching the pump inlet is, in every case, necessary : for example at speeds of 50 knots pump intake speed has had to be reduced by approximately 80% of the forward drive speed.

As with the ZFJP scoop, increase in speed to slightly over 50 knots results in a slight increase of coefficient K and, beyond a certain limit speed, super-cavitating external flow is required.

Finally, it may be seen quite readily that available pump σ for a given w decreases as velocity increases, this may be compensated by :

- either reducing w by discarding the optimum values resulting from compromise between theoretical efficiency and nacelle drag,

- or by adopting a 2 stage pump.

V. HYDRODYNAMIC STUDIES OF JET PROPELLERS

5.1. Advantages and limitations of separating the study of internal and external circuits

For long circuit water-jet propulsion units of the Z flow-type, separate examination of the hydraulics of the external and internal circuits, and particularly the pump, is clearly well-founded and advantageous. The internal and external flux have to be examined conjointly only in the study of the immersed scoop.

In the design studies of nacelle type propulsion units of the "straight flow" type we considered that the same separate theoretical and experimental approach was also of great interest for the following reasons :

. theoretical analysis of the internal flow and circuit design is much simplified if it is considered separately from the external circuit. This is particularly significant when applied to the pump design.

. experimental approach also is very much facilitated. For example the test rig allocated for internal circuit study may be used for measuring directly all characteristics of the internal flux (rate of flow, momentum, thrust, cavitation limits, etc.) without any interference of the external flow.
High enough Reynolds number and a proper cavitation simulation can be obtained with a reasonably small test rig as the one described below. If equivalent limits were to be attained in a hydrodynamic tunnel then the vein size would have to be at least 1,2 metres in diameter with a vacuum of 0,5 m absolute, a flow speed of 12m/s and discharge of $14 m^3/s$ so that the facility would be considerably larger than that described below whose discharge is limited to $0,5\ m^3/s$. Moreover, in such a tunnel facility, cavitation around the nacelle would limit investigation of the cavitation limits of the internal circuit. Nevertheless separate study of the two flux gives rise to certain difficulties since the internal flow is influenced by the external flow as is clearly shown, for instance in theories concerning ducted propellers.

However in the case of "straight flow" propulsion units of the type which we have developped for rapid surface ships, this effect of

the external flow upon the internal flow is relatively low and can be approximately taken into account in the "separate flow" approach.

For instance the transversal distribution of approach velocity into the pump may be simulated by properly adjusting the profile of the intake bell-mouth of the model. This adjustment is based upon calculation (perfect fluid and boundary layer) and upon smaller scale tests of the complete propulsion unit in a hydrodynamic tunnel.

As regards the discharge nozzle, the absence of external flow in the test rig described below, slightly modifies the jet contraction compared with the prototype nozzle. Therefore we carried out model tests of the pump with various nozzle diameters and finalised the nozzle diameter adjustment during the prototype tests in the TOULOUSE high-speed towing-tank.

5.2. Methods of approach applied to the design studies of jet propellers

The methods mentionned hereafter are the ones we applied for finalising the hydraulic design of the straight flow 50 knots jet propeller dealt with in § 7. However the same general way could be followed for Z flow jet propeller design, with some adaptation.

a) Intake mouth of the nacelle

Analysis of flow in this part of the machine requires the consideration of both internal and external flow. Two main methods have been used :

- potential flow axisymmetric computation with a special attention towards the cavitation limits of the circular leading edge area.

- experimental study on a hydrodynamic tunnel where the internal flow was separately controlled (see fig. 3).

These approaches could well be adapted to the design studies of intake scoop of a Z flow jet propeller.

b) Driving pump

A special test rig had to be developped for that purpose as will be explained in § 6.

c) Nacelle body and rejection nozzle

- conventionnal friction resistance computations were applied to predict the nacelle external friction drag.

- experimental study of a complete small scale model of the propulsion unit (fig. 4) was carried out, having in view the determination of cavitation limits of the external flow and the lift coefficient of the propeller.

During these tests the internal rate of flow was simulated with help of a small internal pump similar to that of the prototype but no shaft power measurement was made since the impeller Reynolds number and bearing friction torque were not proper for that purpose.

d) Integral test of the entire propulsion unit

Since the effect of mutual interaction of external and internal flows is of the same order of magnitude as the one of scale effects, we decided to run integral accurate tests only on the full-size prototype unit. As already mentionned this implies that the hydraulic design of some parts of the propulsion units (mainly the rejection nozzle) has to be finalised during the prototype test. This is presently carried out as explained in § 7.

VI. TEST RIG FOR HIGH SPECIFIC SPEED PROPELLER-PUMP DRIVE UNITS

6.1. Description of the test-rig

If centrifugal or mixed flow pumps are involved, conventional test rigs may be used to perfect the hydraulic design of pumps used in water-jet drive units. The only significant difference between these and normal pumps is the relatively higher velocity at the volute outlet.

However the test rigs normally used for propeller pumps are not suitable for solving the problems associated with high specific speed propeller pumps, used in the SFJP.

Firstly the head generated by these pumps is often relatively low in comparison with the kinetic head corresponding to approach velocity and to discharge velocity so that accurate measurement of the generated head is difficult. Moreover pump efficiency, as a propeller, depends upon both generated head and also upon the transversal

velocity distribution at the nozzle outlet, i-e the momentum communicated to the jet. For these reasons we have found it necessary to construct a specialized test-rig in which the momentum transmitted to the propulsive flux is measured directly and not solely the increment of energy transmitted to the said flux. The design of this test-rig also allowed for the necessity of simulating head (captation energy) due to the forward drive speed of the ship. Thus a circulatory pump had to be used.

The simulation of cavitation conditions is achieved by the control of absolute pressure on both sides of the model pump.

The figures 5 and 6 show the basic arrangement of the test rig.

Maximum impeller diameter is 300 mm. The model, placed between two tanks, allows visualisation of the impeller, distributor and diffuser.

Water circulation is ensured by a 520 l/s pump with 9 metre head at 835 rpm driven by a DC thyristorised motor at variable speed between 0 and 2 500 rpm. A 1/3 reduction unit is mounted between the pump and the motor. Motor speed stability is controlled to within 1/100.

The 500 mm diameter piping is fitted with two vaned elbows, a manually controlled 500 mm diameter valve, a 350 mm diameter vertical turbine flowmeter with calibrating piping.

The 2.2. metre diameter upstream tank was specially designed to ensure correct feed to the pump : uniform flow distribution, absence of vortex, etc.

The water level is regulated by a capacitance sensor acting upon rotation velocity of the circulation pump. The water level is Zp = 1,8 metres above the plane of the impeller. Absolute air pressure above the water surface may vary between 0,05 and 1,7 atmospheres. The upper tank also supports the two water-floating bearings - diameter 360 mm and 160 mm of the stator casing. Internal stiffeners avoid displacement between these bearings. The tank also supports the thrust-balance and the torque balance.

The lower tank, diameter 2,5 metres, was specially designed to dampen jet energy without sucking unwanted air to the pump while ensuring a stable level. The facility may be operated with the nozzle either drowned or not. Absolute pressure above the water

level may also be varied between 0,05 and 1,4 atmospheres. Water head between the two tanks is measured accurately by a differential manometer (mercury weighing). Air pressure in the upper tank is weighed in the same manner.

Model rotation is ensured by an asynchronous motor, between 300 and 1 750 rpm whose speed is varied through a frequency converter. Resultant stability is to within 1/1000 of rotation speed.

The whole body of the jet propeller (i.e. intake bell-mouth, pump and nozzle) is rigidly connected to a main stator structure which is vertically guided in two self-centering guide-bearings fed with water under pressure. The vertical resultant of weight and hydraulic thrust acting on this structure is measured through a weighing-balance to which it is connected through a oil pressure frictionless thrust bearing. Since the total weight of the balanced body, and pressures on both sides of each guide-bearings are known, it is possible to derive from the balance measurement the net thrust due to the jet effect. Because of the absence of friction in the guide and thrust bearings, it is also possible to measure the stator torque (which corresponds to the jet rotational momentum).

The stator of the driving motor is mounted in the above-mentionned stator body with help of self-centering guide and thrust bearings fed with oil under pressure, thus allowing for accurate driving torque measurement, then accurate shaft-power determination. The friction torque of the shaft guide bearings situated in the propeller body is not directly measured but is taken into account through a precalibration procedure. A pressure sensor in the oil floating shaft thrust bearing is used to measure rotor thrust after calibration.

The 360 mm diameter water floating bearing, mounted between the two tanks serves as a water seal. Its leakage rate is calibrated and is approximately 0,15 l/s. The 160 mm diameter upper floating bearing serves as an air seal. Its leakage is also taken into account.

This rig is equipped with centralised remote control and measurement equipment.

The flow, head and pressure characteristics of the rig are such that it proves very useful for perfecting propeller pumps for SFJP type drive, covering the forward speed range from 0 (fixed point propellers) up to approximately 100 knots.

6.2. The following figures can be directly derived from the measurements made with a propeller of diameter D on the test rig described above :

. the head H applied between the external limits of the propulsion unit model ; this head simulates the effect of kinetic energy due to the forward speed V of the ship.

. the rate of mass-flow $\dot{M}$ passing through the propeller.

. the component of the jet momentum $\mathcal{M}$ in the axial direction.

. the shaft power P_s

. the rotational speed N

. the net positive suction head NPSH.

From these figures, it is possible to determine :

The equivalent ship speed : $V = \sqrt{2gH}$

The gross thrust : $T_g = \mathcal{M} - \dot{M}V$

(i.e. the gross thrust obtainable at speed V from a propulsion unit operating under the same internal hydraulic conditions as the model)

The gross efficiency $\eta_g = \dfrac{V \cdot T_G}{P}$

The thrust coefficient $C_T = \dfrac{T_G}{\frac{1}{2}\rho V^2 S_R}$ with $S_R = \dfrac{\Pi D^2}{4}$

The rpm coefficient $u = \dfrac{ND}{V}$

The cavitation coefficient $h_{NA} = \dfrac{NPSH}{V^2/2g}$

The dimensionless parameters defined above can be plotted in a diagram as the one represented in fig. 7 and then applied through similarity considerations to the determination of a prototype propulsion unit of given dimension and speed.

VII. TESTS ON THE 50 KNOT SOGREAH PROPULSION UNIT SFJP TYPE IN THE CEAT (Centre d'Essais Aéronautique de Toulouse) HIGH-SPEED TOWING TANK

After completion of tests carried out on the internal circuit, using the test rig already described, and on the external circuit in the tunnel, we designed and constructed a 800 kw prototype unit for complete testing in the CEAT high-speed towing tank. Impeller diameter is 0,772 m for the prototype compared with 0,268 for the impeller of the model while the ratio of power consumed under cruising conditions was 800/7 Kw for the two types of test.

The graph 8 shows the comparison of efficiency obtained on the test rig for the scale model and in the tank for the prototype.

Curve 1 represents the net efficiency obtained with the 0,772 diameter prototype. This efficiency takes account of the nacelle drag.

Curve 3 is derived from curve 1 by subtracting the external drag losses of the nacelle and therefore represents the gross efficiency as defined above.

Curve 2 represents gross efficiency obtained with the scale model, diameter 0,268 m. Comparison of curves 2 and 3 shows that the variation of efficiency with the thrust coefficient is properly predicted from the model. The difference in efficiency between model and prototype is of order of magnitude which can be anticipated from scale effect consideration.

Figure 9 shows the net thrust Tn versus V characteristics - the limiting curves are those derived from the model test results.

The points represent the results obtained to date on the 0,772 m prototype with operation near to the diagram limits.

The test program will be continued for even closer approach to the operating limits. It must be noted here that the drag losses are likely to be reduced if the trailing edge profile of the nozzle is modified which will help to improve overall efficiency.

The following characteristic parameters may be noted from both figures :

$\eta_g = 0,73$

$\eta n = 0,655$

$t_P = 1,50$

$v_P = 0,55$

VIII. CONCLUSION

A general method of approach has been briefly described, this applying to the hydraulic design studies of jet propellers for high speed surface ships. The validity of this method where internal and external flows are to a large extent separately considered had to be proven, at least for application to short ducted straight flow jet propellers.

The tests of a 50 knot , 800 Kw prototype propulsion unit in the high speed towing tank of CEAT in Toulouse has shown a good accordance between the prototype performances and the predicted characteristics which had been derived from the proposed approach method. The descrepancies are within the limits of the expected scale effect which is normally observed when dealing with reduced model approachs.

We have also proposed some simple dimensionless parameters for the sake of comparison of various types of propellers applicable to rapid surface-ships. The prototype test proved the high performances of the Straight-Flow-Jet Propeller unit, and its potential interest in this field of application.

* * *

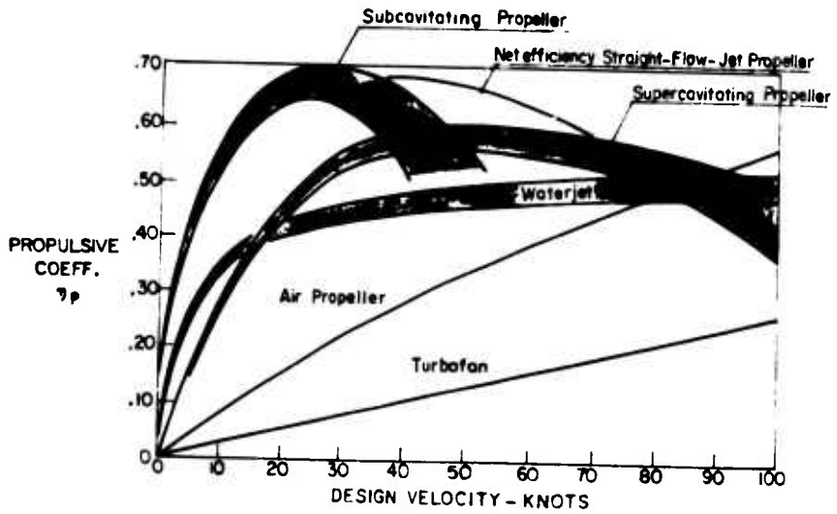


Fig. 1 Practical propulsive coefficient comparison

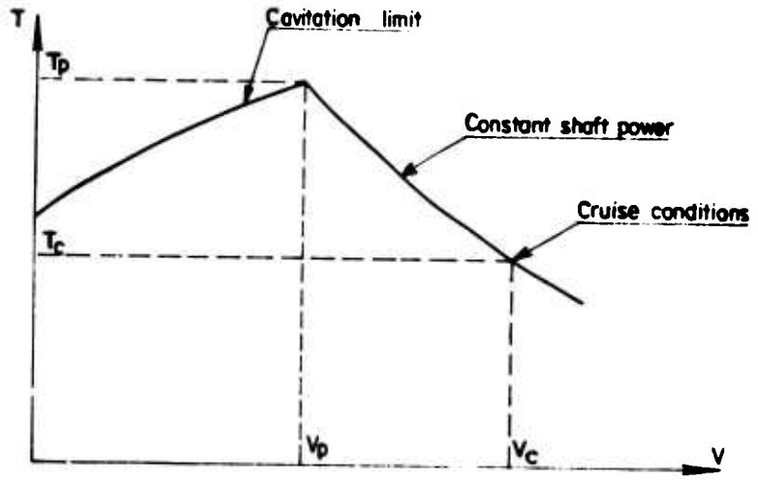


Fig. 2 Definition of peak thrust ratio

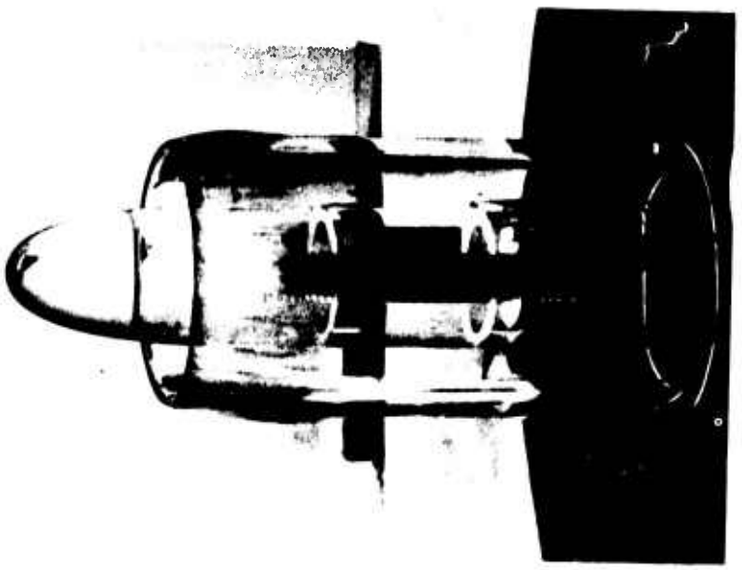


Fig. 3 Scale model used in tunnel test on flow conditions at the inlet of an SFJP propulsion unit

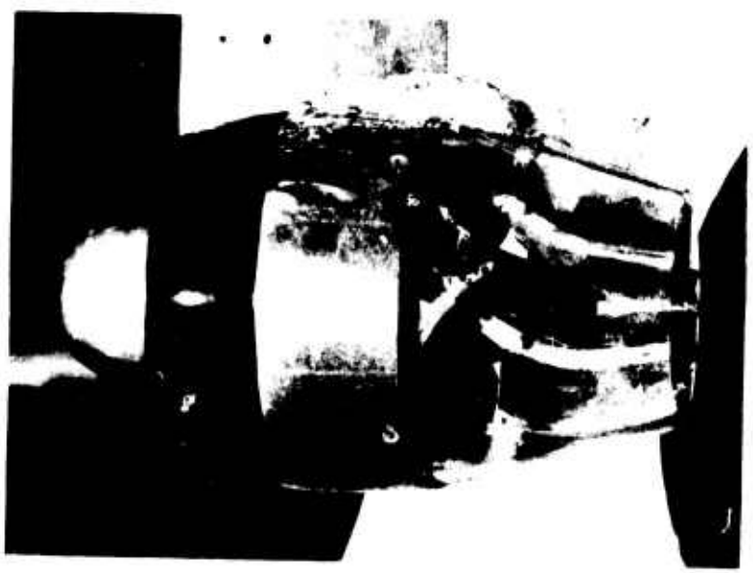


Fig. 4 Scale model test in tunnel of SFJP propulsion unit external circuit

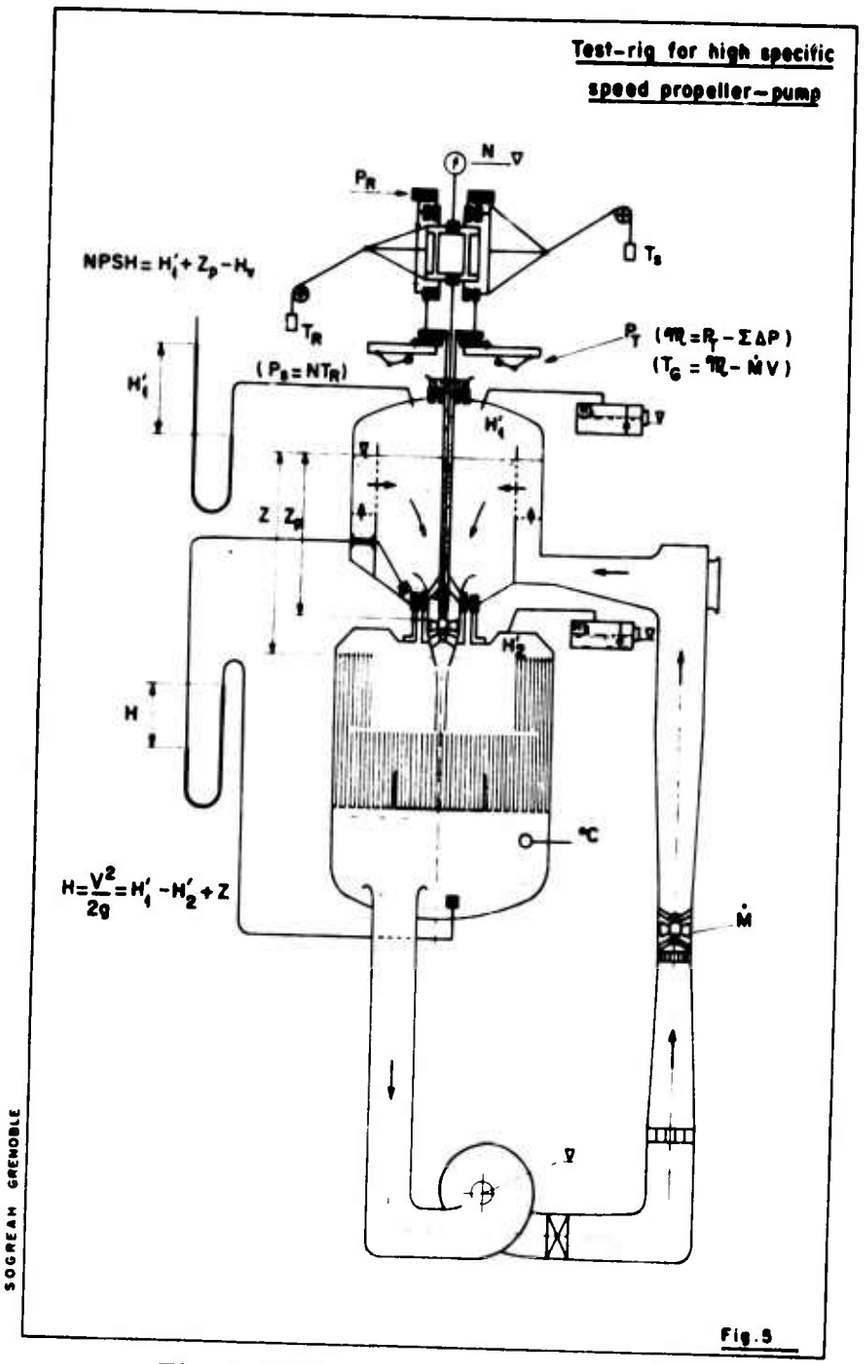


Fig. 5 SFJP propulsion unit test rig

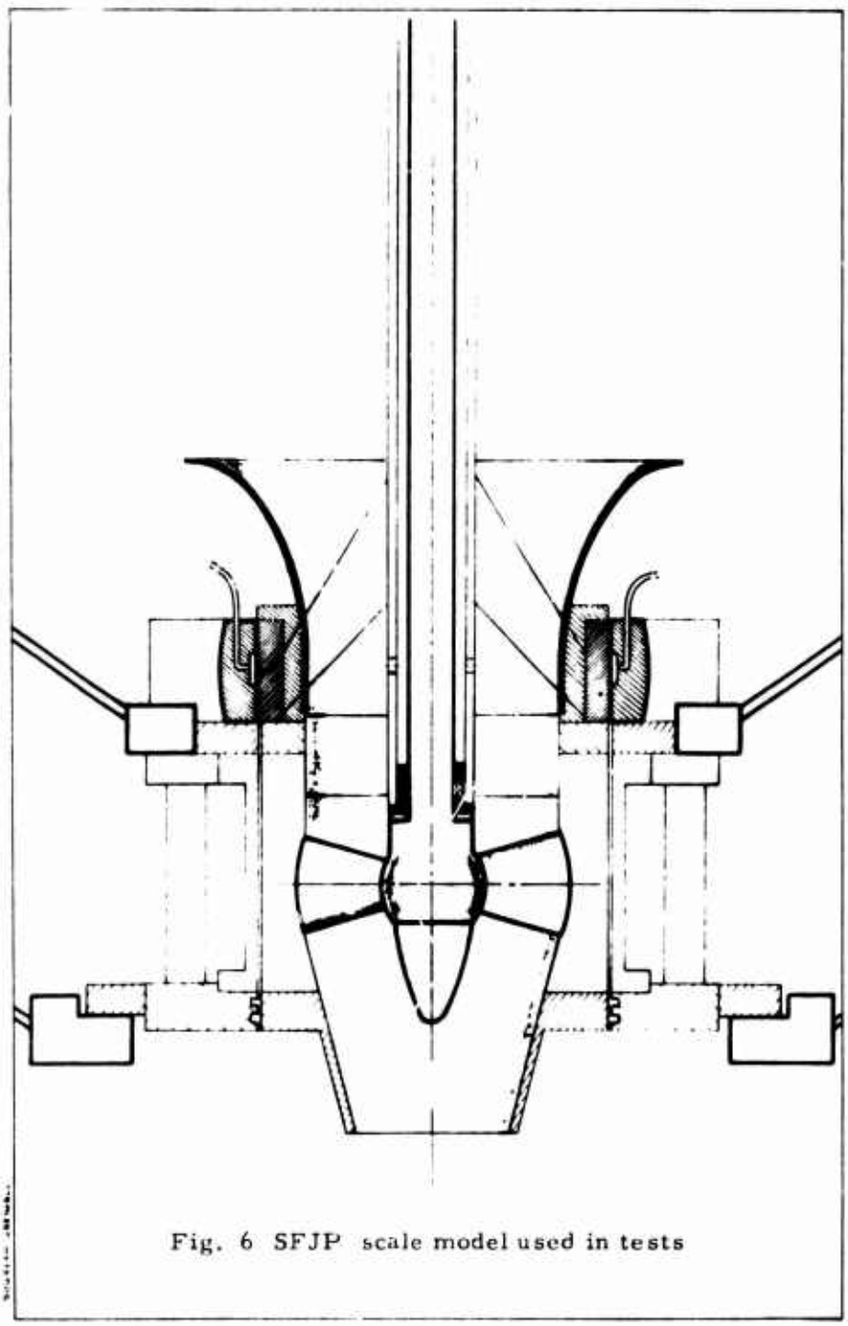


Fig. 6 SFJP scale model used in tests

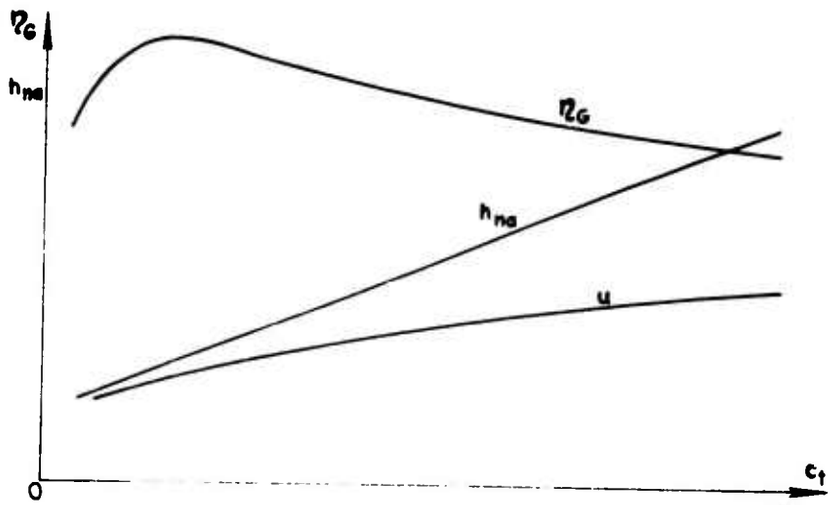


Fig. 7 SFJP Rig tests results

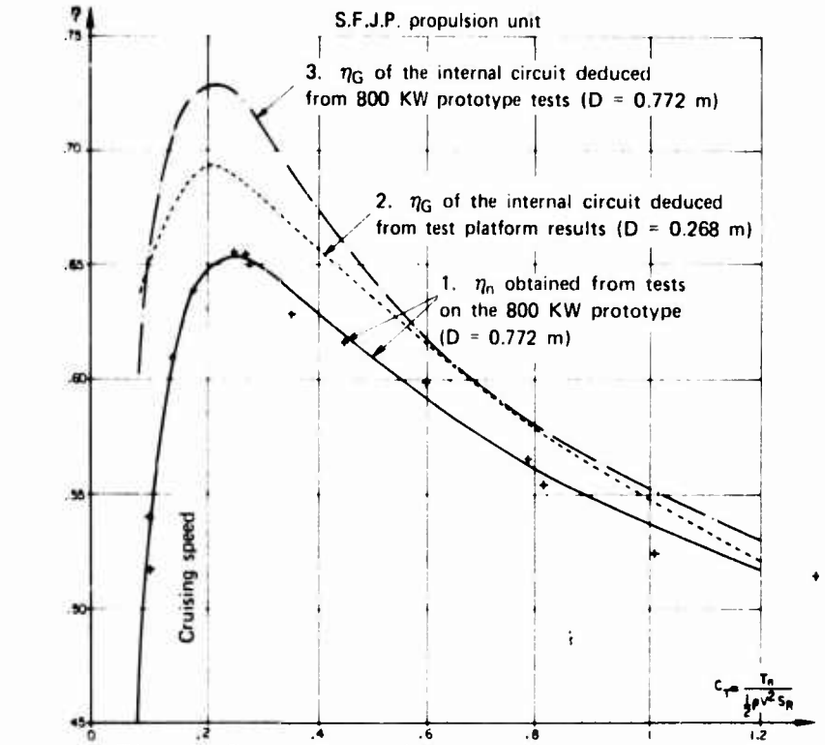


Fig. 8 Comparison of the test results

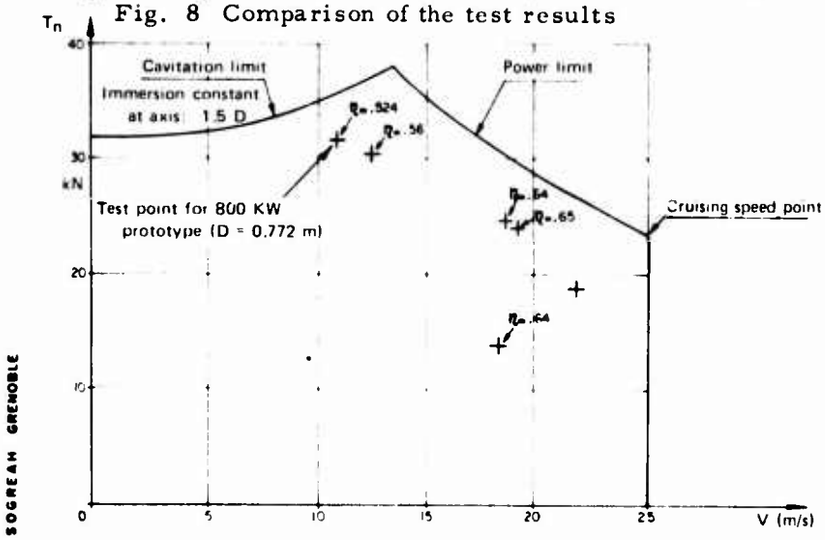


Fig. 9 Range of characteristics of the 800 kw prototype (D = 0.772 m) deduced from test rig results (D = 0.268 m)

DISCUSSION

William B. Morgan
Naval Ship Research and Development Center
Bethesda, Maryland, U.S.A.

The propulsion device discussed by the authors would more appropriately be called a ducted propeller. The term water-jet is usually reserved for a propulsion device where a pump is located in a long pipe and the pump does not induce a drag around the duct. The device shown in Figure 4 is a ducted propeller of the decelerating-flow type. Since the authors do not give any references it is not clear whether they are familiar with the vast amount of literature which is available. I thought that it has been conclusively shown that it is possible to consider the duct separately from the impeller and to perform tests on the inlet, Figure 3, and the interior flow, Figure 6, separately. In the duct shown in Figure 4, the impeller would induce a circulation about the duct which, in case of the decelerating-flow, would cause a drag increase. I do not believe it is possible to separate the internal and external flow as you have done.

In Figure 1, you have purportedly shown a comparison between the efficiencies of various propulsion devices. This figure was not valid when it was published nor is it valid today. Also one should consider the partially-submerged propeller. This propeller is not applicable to hydrofoil craft but can be a very efficient means of propulsion where there is a flat bottom at the stern.

REPLY TO DISCUSSION

Jacques Duport
SOGREAH
Grenoble, France

Thank you, Dr. Morgan for your comments. About the discussion on denominations, I think we have also to find names in

French, for instance for "Z flow" or "straight flow" propeller units.

Regarding the information contained in Figure 1 we know that it may be obsolete to some extent, since we mention the date of the source (1965). This discussion might be a good opportunity to collect recent characteristics of propeller devices applicable to fast surface ships. These informations should include not only the efficiency at cruise condition but also some other parameters as the one we have proposed (or equivalent) dealing with the "intermediate-speed" performance and the weight-balance of the propeller unit.

We agree with Dr. Morgan that the "partially submerged propeller" should be included in the comparison, while keeping in mind that it is suitable only when no important relative movement between the ship body and the water surface can occur.

The authors are well aware of the literature available on ducted propellers, even if they are not familiar with all the methods used in this field. For the sake of simplicity of experimental approach they decided to carry out a "separate flow approach" as it has been described in the paper. They agree that this is justified only if the drag of the duct is properly taken into account, which is the case with the method used. However they recognize that the justification has not been clearly and sufficiently explained in the paper and they plan to complement the present reply to Dr. Morgan in an appendix to their paper.

APPENDIX
TO THE PAPER BY J. DUPORT, M. VISCONTI AND J. MERLE
"Water-Jet Propulsion for High-Speed Surface Ships"

This appendix is complementing the reply to Dr. J. W. Morgan's discussion. The authors also take the opportunity of bringing complementary information on the test of the 800 kW prototype of the "Isère" propeller.

The authors have written that "the hydrodynamics of internal flow can be to a large extent analysed separately from the external

flow analysis". This does not mean that each flow can be considered as independent from the other ; particularly the circulation around the duct and the negative thrust on this part of the propeller are properly taken into account.

The authors were probably wrong not to explain clearly enough that the so-called "separate flow approach" is preceded by a "complete flow approach (i. e. dealing with both flows together) which serves the purpose of determining the respective "limit conditions" (i. e. boundary conditions) of each flow.

Before coming back to this "complete flow approach "which, in the case of the "Isère" design studies, was a simplified one - we feel it advisable to emphasize :

(i) that either internal or external flow is entirely determined as soon as the "limit conditions" are fixed. For the internal flow, these conditions are (see Figure 10) :

. the "flow tube" separating both flows, upstream as well as downstream of the propeller, and the internal solid boundaries ;

. pressure (which is equal to p_∞) at each remote cross-section Si and Sj ;

. velocity distribution in each of these sections. Each flow can then be analysed from these limit conditions (as soon as they are known) without further reference to the other part of the complete flow.

(ii) predetermination of the "complete flow" need presetting of

- the circulation around the duct (or equivalently the internal rate of flow)
- the radial load distribution of the impeller (or equivalently the normal velocity distribution in section Sj .

Once these figures are preset, the profiles (and r. p. m.) of the impeller (stator and rotor) have to be designed in accordance with them ; it is enough for that to apply to the impeller design the limit conditions proper to the internal flow.

(iii) in a "inviscid flow approach" as the one considered presently, the thrust of the propeller (including the duct) can be derived from the internal flow description alone. This is an obvious result of the momentum equation applied to the complete flow.

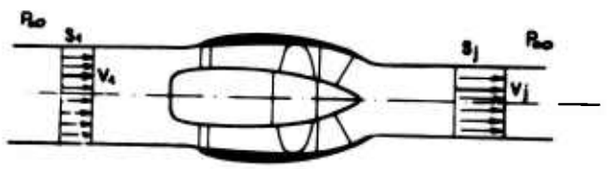


Fig. 10

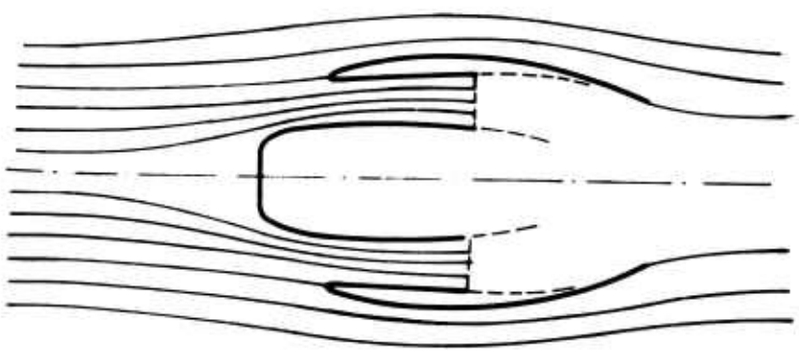


Fig. 11

As a result of this :

- presetting of the figures mentionned in (ii) here above takes account directly of the required thrust ;

- the propeller thrust can be derived from the thrust measured on the "internal flow" model as described in paragraph VI of our paper.

As already mentionned the "complete flow approach" was a simplified one which appeared to be applicable due to the reduced contraction between the nozzle outlet and the jet diameter. (Diameter ratio .95).

According to this the downstream separating flow tube was assumed to be the same as the "free-jet" flow surface. As indicated in the paper, the slight discrepancy might be corrected through a limited nozzle diameter adaptation if required. It must be noted here that the "complete flow" test on the prototype did not give any evidence of such effect, and no correction had to be applied.

The determination of the "upstream separating surface was made through the "potential flow approach" described in paragraph V. 2. a and illustrated in Figure 11 attached to this annex.

To conclude we would like to insist on the fact that the accordance between the "expected performances" (for instance thrust versus r.p.m. etc) and the measured performances of the prototype is quite satisfactory in the whole range of parameters. This, as well as the relative simplicity of the approach, is, may be, the best justification for the way we followed.

The tests in Toulouse have been continued through an improvement of the trailing edge of the nozzle (which was formerly unduly thick) the efficiency has been raised by more than 1%, the net efficiency is then now a little more than 66,5% .

* * *

THE FORCES ON AN AIR-CUSHION VEHICLE EXECUTING AN UNSTEADY MOTION

Lawrence J. Doctors
University of New South Wales
Sydney, Australia

ABSTRACT

This paper treats the theoretical problem of an air-cushion vehicle (ACV) travelling over water of uniform finite or infinite depth, with an arbitrary motion. The ACV is modelled by a pressure distribution applied to the free surface of an inviscid incompressible fluid and the boundary conditions on the free surface are linearized.

Numerical results are presented firstly for accelerated motion from rest. In deep water, the hump condition is delayed to a higher Froude number, while in finite depth, the hump resistance is appreciably reduced - even by moderate levels of acceleration.

The effect of tank walls on these results when carrying out model tests is next examined. The side walls of the tank alter the resistance by less than one per cent in accelerated motion, if the tank width is greater than four times the model beam.

Finally, calculations of the side force acting on a yawing ACV are presented. For super-hump speeds, the side force is of the same order as the wave resistance and favorably aids the turn. It is also shown that the steady-state forces are realized when the craft has travelled a distance of less than two vehicle lengths after a manoeuver.

Preceding page blank

I. INTRODUCTION

I. 1. Background

Havelock (1909, 1914 and 1926) was the first to study the theoretical problem of the wave resistance of a pressure distribution. His interest lay in a desire to represent the disturbance from a ship. As a result, the pressure distributions that he chose to analyze were very smooth and were not typical of the pressure underneath an air-cushion vehicle (ACV). However, later on, Havelock (1932) derived the general expression for a pressure distribution travelling at a constant speed of advance. In this paper, he also showed that, under the assumption of a small disturbance, the action of the pressure was equivalent to a source distribution on the undisturbed free surface. The relation was :

$$\sigma = \frac{c}{\rho g} \frac{\partial p}{\partial x} \quad , \tag{1}$$

where σ and p are the source intensity and pressure at the same point, c is the velocity in the x direction, ρ is the density of the fluid and g is the acceleration due to gravity.

Lunde (1951a) extended the theoretical treatment to include the case of an arbitrary distribution moving over finite depth. Numerical calculations which are directly applicable to the ACV have been carried out by other workers. For example, Newman and Poole (1962) considered the two cases of a constant pressure acting over a rectangular area, and over an elliptical area. The most striking feature of their results is the very strong interaction between the bow and stern wave systems. The resistance curves displayed a series of humps and hollows - particularly for the rectangular distribution (where the interaction would be greater). A hump is produced when the bow and stern wave systems are in phase and combine to give a trailing wave of a maximum height. A hollow occurs when the two wave systems are out of phase by half a wavelength so that the combined amplitude is a minimum.

The interference effects are found to be stronger for large beam to length ratios, as would be expected from this argument, since the wave motion becomes more nearly two-dimensional. The humps are found to occur at Froude numbers given approximately by

$$F = 1 / \sqrt{(2n - 1)\pi} \qquad \text{for } n = 1, 2, 3, \ldots \tag{2}$$

and the hollows occur approximately when

$$F = 1/\sqrt{2\pi n} \qquad \text{for } n = 1, 2, 3, \ldots \tag{3}$$

In the limit of infinite beam (a two-dimensional pressure band), the humps and hollows are given precisely by Eqs (2) and (3). This result was found by Lamb (1932).

In water of finite depth, the main, or "last", hump ($n = 1$) is shifted to a lower Froude number, and for sufficiently shallow water, occurs at a depth Froude number, F_d, equal to unity (that is, at the depth critical speed). Similar calculations were given by Barratt (1965).

Newman and Poole also considered the effect of a restricted waterway, such as a canal. In such a case, the wave pattern is constituted from wavelets of discrete frequencies only, which can exist in the tank, whereas in laterally unrestricted water a continuous distribution of frequencies exists. As the speed is increased past the critical speed, the transverse wave component can no longer occur, and as a result there is a discontinuity in the wave resistance curve. This sudden drop in resistance is given by

$$\Delta R = \frac{3W^2}{2\rho g B d^2} \tag{4}$$

where W is the weight of the ACV, B is the width of the tank and d is the water depth.

Havelock (1922) also presented some results for a very smooth pressure distribution moving over water of finite depth. These too, showed the shift of the main hump and the increase in its magnitude in shallower water. Havelock's curves displayed only the main hump. The secondary ($n = 2$) and other humps did not occur because of his choice of pressure distribution.

In recent years, a number of experiments have been carried out in order to check the above-mentioned theoretical results. These have been performed in particular by Everest (1966a, 1966b, 1966c and 1967) and Hogben (1966). The fundamental question pointed out in these papers is the resolution of the total drag on the ACV into its components. Apart from the wave resistance, the forces acting on the craft are aerodynamic drag and wetting drag.

In these experiments, the total drag was usually measured with a dynamometer. The aerodynamic drag was then estimated from the drag coefficient on the model, and the momentum drag was obtained from the mass flow into the cushion. The agreement between theory and experiment was found to be best at speeds greater than hump. At lower speeds, nonlinear and viscous effects become important and there was a large scatter in the data.

To avoid the troublesome wetting drag, Everest (1966a) attempted to eliminate it using a thin polythene sheet floating on the water surface. The resistance breakdown is further discussed by Hogben (1966). The experiments only indicated the presence of the first two (n = 1, 2) and possibly there (n = 3) humps. Hogben (1965) showed that this result fitted in with the idea that the maximum ratio of wave height to length is about one seventh. That is, wave breaking prevents the occurrence of the additional humps.

Further experimental work by Everest, Willis and Hogben (1968 and 1969) dealt with an ACV at an arbitrary angle of yaw. This problem was also studied numerically by Murthy (1970). In the experiments, the wave resistance was measured directly from a wave pattern survey, using the transverse cut method. There was considerably less scatter in the data using this method, since the rather doubtful technique of estimating the wetting drag was eliminated. Indeed, the agreement was found to be somewhat better, particularly for the lower of the two cushion pressures tested.

In an attempt to get better agreement with experiments at lower speeds, Doctors and Sharma (1970 and 1972) used a pressure distribution which essentially acted on a rectangular area but had a controlled amount of smoothing - both in the longitudinal (x axis) and in the transverse (y axis) direction. The distribution used was :

$$p(x,y) = \frac{1}{4} p_o \left[\tanh\{\alpha(x+a)\} - \tanh\{\alpha(x-a)\}\right] \times \left[\tanh\{\beta(y+b)\} - \tanh\{\beta(y-b)\}\right], \qquad (5)$$

where p_o is the nominal cushion pressure, and a and b are the nominal half-length and half-beam respectively. The rate of pressure fall-off at the edges is determined by the parameters α and β. This function is shown in Fig. 1. As a special case, $\alpha, \beta \to \infty$ is equivalent to a uniform pressure acting on a rectangular area $2a \times 2b$.

In practice, of ourse, the pressure at the edge of an ACV

does fall-off at a finite rate, corresponding approximately to $\alpha a = \beta a = 40$. Nevertheless, it was found that only by selecting $\alpha a = \beta a = 5$, could the humps in the resistance curve above the third be essentially eliminated. Thus clearly, viscosity and non-linearity are important at low speeds. Some of these calculations are reviewed in this paper.

Another problem of practical interest is the wave resistance during accelerated motion, as one is frequently concerned with the ability of a heavily-laden craft to overcome the hump resistance in order to reach the cruising speed.

The problem of accelerated motion for a ship has been treated by Sretensky (1939), Lunde (1951b, 1953a and 1953b) and Shebalov (1966). Wehausen (1964) made numerical calculations for a particular motion of a ship model starting from rest. His results consisted of asymptotic expressions valid for large values of the time after a steady speed was obtained.

Djachenko (1966) derived an expression for the resistance of an arbitrary pressure distribution moving with a general acceleration pattern in deep water. He also presented some results for a two-dimensional distribution.

Doctors and Sharma found that the main effect of accelerated motion on an ACV is to shift the main hump to a higher Froude number, and in finite depth to reduce the magnitude of the hump quite significantly. These results are partially presented in this paper.

I.2. Present Work

The basic theory for the wave resistance of a time varying pressure distribution will first be given. Then the results will be applied to the case of an ACV executing rectilinear motion in a horizontally unrestricted region.

The work will then be extended to the case of an ACV moving along the centerline of a rectangular channel. From these calculations it is possible to determine the effect of the tank walls on the wave resistance.

Finally, the case of a yawing ACV will be examined. In particular, the induced side force acting on the craft will be determined, so that its importance during a manoeuver may be assessed.

II. BASIC THEORY

II. 1. Problem Statement

We represent the ACV by a pressure distribution $p(x, y, t)$ acting on the free surface, and travelling with the speed of the craft. Two right-handed coordinate systems (reference frames) will be used, and are shown in Fig. 2. A third coordinate system that rotates with the craft during a yawing motion will be introduced later. The axis system ξyz is fixed in space, and the system xyz moves with the craft, z being vertically upwards while x and ξ are in the direction of the rectilinear motion. The relation between the coordinates is then given by

$$\begin{aligned} x &= \xi - s(t) \\ &= \xi - \int_0^t c(\tau)\, d\tau \end{aligned} \tag{6}$$

where s is the distance that the craft has moved. The pressure in the stationary reference frame is denoted by $p^s(\xi, y, t)$. The velocity potential in the stationary frame, ϕ (such that the velocity is its positive derivative), satisfies the Laplace equation, so that

$$\nabla^2 \phi = 0 \tag{7}$$

The kinematic boundary condition on the free surface requires that a particle of fluid on the surface remains on it (for example, see Stoker (1957)), so that

$$\frac{D}{Dt}\left[z - \zeta(\xi, y, t)\right]_{z=\zeta} = 0$$

where ζ is the elevation of the free surface. Now we have the substantial derivative :

$$\frac{D}{Dt} = \frac{\partial}{\partial t} + \phi_\xi \frac{\partial}{\partial \xi} + \phi_y \frac{\partial}{\partial y} + \phi_z \frac{\partial}{\partial z}$$

so that the exact kinematic condition becomes

$$\left[\phi_z - \phi_\xi \zeta_\xi - \phi_y \zeta_y\right]_{z=\zeta} - \zeta_t = 0 \tag{8}$$

The linearized kinematic condition is obtained by dropping the second

order terms, and then writing the remaining terms as a Taylor expansion about the point $z = 0$. After dropping the higher order terms again, we obtain simply

$$\left[\phi_z\right]_{z=0} - \zeta_t = 0 \tag{9}$$

The dynamic condition on the surface - the Bernoulli equation - in the stationary frame is

$$\left[\phi_t + \frac{1}{2}(\phi_\xi^2 + \phi_y^2 + \phi_z^2)\right]_{z=\zeta} + \frac{p^s}{\rho} + g\zeta = f, \tag{10}$$

where f is an arbitrary function of time, which may be put to zero without loss of generality. Eq. (10) is now linearized to give

$$\left[\phi_t\right]_{z=0} + \frac{p^s}{\rho} + g\zeta = 0 \tag{11}$$

The combined free surface condition is obtained from Eqs. (9) and (11) by eliminating ζ :

$$\left[\phi_{tt} + g\,\phi_z\right]_{z=0} = -\frac{1}{\rho}\,p^s{}_t \tag{12}$$

The final boundary condition needed states that there should be no flux through the water bed :

$$\left[\phi_z\right]_{z=-d} = 0 \tag{13}$$

II. 2. The Potential

The solution of this set of equations can be obtained by an application of the double Fourier transform pair :

$$F(w, u) = \frac{1}{2\pi}\int_{-\infty}^{\infty} dx \int_{-\infty}^{\infty} dy\, f(x, y) \exp\left\{-i(wx + uy)\right\}$$

and

$$f(x, y) = \frac{1}{2\pi}\int_{-\infty}^{\infty} dw \int_{-\infty}^{\infty} du\, F(w, u) \exp\left\{i(wx + uy)\right\}, \tag{14}$$

and the Laplace transform pair :

$$\mathcal{L}\{f(t)\} = \int_0^\infty f(t)\exp(-qt)\,dt$$

and

$$f(t) = \frac{1}{2\pi i}\int_{\delta-i\infty}^{\delta+i\infty} \mathcal{L}\{f(t)\}\exp(qt)\,dt \qquad (15)$$

δ being a positive constant.

The Fourier transform of Eq. (7) is first taken, giving

$$\Phi_{zz} - k^2\Phi = 0 \qquad (16)$$

where Φ is the Fourier transform of ϕ, and

$$k^2 = w^2 + u^2 \qquad (17)$$

The solution of Eq. (16) subject to the transformed bed condition, Eq. (13), is

$$\Phi(w, u; z, t) = A(w, u; t) \cdot \cosh\{k(z + d)\} \qquad (18)$$

Eq. (18) is now substituted into the Fourier transform of the free surface condition, Eq. (12), giving

$$A_{tt} + \gamma^2 A = -\frac{1}{\rho}\,\mathrm{sech}(kd)\,P_t \qquad (19)$$

where P is the Fourier transform of p^5 and

$$\gamma^2 = gk \cdot \tanh(kd) \qquad (20)$$

We now take the Laplace transform of Eq. (19):

$$(q^2 + \gamma^2)\,\mathcal{L}\{A\} = -\frac{1}{\rho}\,\mathrm{sech}(kd)\left[q\,\mathcal{L}\{P(w, u;t)\} - P(w, u;0)\right]$$

The inverse Laplace transform is taken, using the convolution theorem on the first term:

$$\Phi(w,u;z,t) = \frac{\cosh\{k(z+d)\}}{\rho \cdot \cosh(kd)}\left[-\int_0^t P(w,u;\tau)\cdot\cos\{\gamma(t-\tau)\}d\tau \right.$$
$$\left. \ldots + \frac{\sin(\gamma t)}{\gamma} P(w,u;0)\right]$$

We express P by means of the Fourier transform, and then the inverse Fourier transform is taken :

$$\phi(\xi,y,z,t) = -\frac{1}{4\pi^2\rho}\iint_{S'} dS' \int_0^t d\tau \int_{-\infty}^{\infty} dw \int_{-\infty}^{\infty} du\ p^s(\xi',y',\tau)\ldots$$
$$\ldots \frac{\cosh\{k(z+d)\}}{\cosh(kd)}\cdot\cos\{\sqrt{gk\cdot\tanh(kd)}\cdot(t-\tau)\}$$
$$\cdot\exp\{i(w(\xi-\xi')+u(y-y'))\} + \frac{1}{4\pi^2\rho}\iint_{S'} dS' \int_{-\infty}^{\infty} dw \ldots$$
$$\ldots \int_{-\infty}^{\infty} du\ p^s(\xi',y',0)\ \frac{\cosh\{k(z+d)\}}{\cosh(kd)}$$
$$\cdot\frac{\sin(\sqrt{gk\cdot\tanh(kd)}\cdot t)}{\sqrt{gk\cdot\tanh(kd)}}\exp\{i(w(\xi-\xi')+u(y-y'))\} \quad (21)$$

where $p^s = p^s(\xi',y',\tau)$, defined over the area S', while ξ' and y' are dummy variables in the stationary reference frame.

Eq. (21) is the potential for an arbitrary time-varying pressure distribution starting at $t = 0$. Thus the solution for the general motion of an ACV is obtained. In the following sections, we shall consider special motions of a pressure distribution which is non-time varying with respect to axes rigidly attached to the vehicle.

III. RECTILINEAR MOTION IN HORIZONTALLY UNRESTRICTED WATER

III.1. The Potential

We now consider motion of a craft starting from rest at $t = 0$. The expression for the potential, Eq. (21), may be simplified by partial integration of the five-fold integral with respect to τ :

$$\phi(\xi, y, z, t) = -\frac{1}{4\pi^2\rho}\iint_{S'} dS' \int_0^t d\tau \int_{-\infty}^{\infty} dw \int_{-\infty}^{\infty} du\, p^s_\tau(\xi', y', \tau)$$
$$\cdots \frac{\cosh\{k(z+d)\}}{\cosh(kd)} \cdot \frac{\sin\{\gamma(t-\tau)\}}{\gamma} \cdots$$
$$\cdots \exp\{i(w(\xi - \xi') + u(y - y'))\} \qquad (22)$$

The pressure distribution, p^s , as measured in the stationary reference frame is a function of time. It is related to the pressure in the moving frame, p , by the following equation :

$$p^s(\xi, y, t) = p(x, y)$$
$$= p(\xi - s(t), y) \qquad (23)$$

III. 2. The Wave Resistance

The resistance of the pressure distribution is defined as the longitudinal component of the force acting on the free surface, and is therefore given by

$$R(t) = \int_S p^s(\xi, y, t)\ \zeta_\xi\ d\xi\ dy \qquad (24)$$

Substituting Eq. (11), we obtain

$$R = -\frac{1}{g}\int_S p^s \left(\left[\phi_{t\xi}\right]_{z=0} + p^s{}_\xi/\rho\right) d\xi\ dy$$

The second term in this expression contributes nothing to the integral providing the pressure drops to zero at $\xi = \pm\infty$. The result for ϕ , Eq. (22), is now used. If one expresses the pressure in terms of the moving frame by Eq. (23), then the wave resistance becomes :

$$R = \frac{1}{4\pi^2\rho g}\iint_S p\, dS \iint_{S'} p'dS' \int_0^t c(\tau)\, d\tau \int_{-\infty}^{\infty} dw \int_{-\infty}^{\infty} du\, w^2 \cos\{\gamma(t-\tau)\}$$
$$\exp\{i(w(x - x' + s(t) - s(\tau)) + u(y - y'))\}$$

The real part of the integrand is now expanded. Then it is simplified by invoking properties of even and odd functions. The final result is :

$$R = \frac{1}{2\pi^2 \rho g} \int_0^t c(\tau)\, d\tau \int_0^\infty dw \int_{-\infty}^{\infty} du\, w^2 \,.\, (P^2 + Q^2) \,.$$

$$. \cos\left\{\sqrt{gk \cdot \tanh kd}\cdot (t - \tau)\right\} \cdot \cos\left\{w(s(t) - s(\tau))\right\}, \quad (25)$$

where

$$\begin{matrix} P(w,u) \\ Q(w,u) \end{matrix} = \iint_S p(x,y) \begin{matrix} \cos \\ \sin \end{matrix} (wx + uy)\, dx\, dy \qquad (26)$$

The range of the u integration in Eq. (25) may be halved for a pressure symmetric about the x axis.

Eq. (25) is similar to that for a thin ship obtained by Lunde (1951b). His formula included an additional integral which was simply proportional to the instantaneous acceleration. This extra term is zero if the singularity distribution (Eq. (1)) lies on the free surface - as for a pressure distribution.

The steady-state wave resistance can be derived from Eq. (25) by allowing the velocity of the craft to be constant for a long time. If the velocity is suddenly established at a value c, then one obtains

$$R = \frac{c}{4\pi^2 \rho g} \int_0^\infty w^2\, dw \int_{-\infty}^{\infty} du\, (P^2 + Q^2) \left[\frac{\sin\{(\gamma + wc)t\}}{\gamma + wc} + \frac{\sin\{(\gamma - wc)t\}}{\gamma - wc}\right]$$

As $t \to \infty$, the oscillations in the integrand increase so that there is only a contribution from the second term, and this occurs when

$$\gamma - wc = 0 \qquad (27)$$

This is the relationship between the transverse and longitudinal wave numbers for free waves travelling at the speed of the craft. The analysis is simplified if we use polar coordinates :

$$w = k \cos\theta$$

and

$$u = k \sin\theta \qquad (28)$$

where k is the circular wave number and θ is the wave direction. The limit process is carried out for a similar case by Havelock

(1958), and the final result is

$$R = \frac{1}{2\pi\rho g}\left[\int_{-\pi/2}^{-\theta_1} + \int_{\theta_1}^{\pi/2}\right] \frac{k^3 \cos\theta}{1 - k_o d.\sec^2\theta.\operatorname{sech}^2(kd)} \cdot$$
$$\cdot\left\{P^2(k\cos\theta, k\sin\theta) + Q^2(k\cos\theta, k\sin\theta)\right\} d\theta \qquad (29)$$

in which

$$k_o = g / c^2 \qquad (30)$$

and k is the non-zero solution of Eq. (27), that is, of

$$k - k_o \sec^2\theta \cdot \tanh(kd) = 0 \qquad (31)$$

The lower limit for θ is taken as θ_1, the smallest positive value of θ satisfying Eq. (31) for a real k. It is given by :

$$\theta_1 = 0 \qquad \text{for } k_o d > 1 \quad \text{(subcritical speed)}$$
$$\theta_1 = \arccos\sqrt{k_o d} \qquad \text{for } k_o d < 1 \quad \text{(supercritical speed)} \qquad (32)$$

III. 3. Results

Some results previously published (Figs. 3 to 7) are now presented to show some of the effects of the choice of pressure distribution given by Eq. (5). For this choice, it was shown that

$$P(w,u) = p_o \frac{\pi \cdot \sin(aw)}{\alpha \cdot \sinh(\pi w/2\alpha)} \cdot \frac{\pi \cdot \sin(bu)}{\beta \cdot \sinh(\pi u/2\beta)}$$

and

$$Q(w,u) = 0 \qquad (33)$$

while the weight supported by the pressure is just

$$W = 4\, p_o\, ab \qquad (34)$$

For convenience the wave resistance is expressed as a dimensionless coefficient :

$$R_c = \frac{R}{W} \cdot \frac{\rho g a}{p_o} \tag{35}$$

Fig. 3a shows the wave resistance of a distribution with a beam to length ratio of 1/2. The variable used for the abscissa is $A = 1/2\ F^2$. This has the effect of expanding the horizontal scale at low Froude numbers. Curve 1, with $_{\alpha}a = \beta a = \infty$, displays the unrealistic low-speed oscillations which are characteristic of the sharp-edged distribution and were referred to previously. It is seen, that with increasing degrees of smoothing (smaller values of αa and βa), the low-speed humps and hollows may be eliminated. The case with $\alpha a = \beta a = 5$ results in only about three humps, more in keeping with experiments. Fig. 3b presents results for finite depth water for three different distributions. The chief difference now is that the main hump is shifted to the right and occurs near the critical depth Froude number. It is seen that Curve 2 has smoothing applied only at the bow and stern -equivalent to a sidewall ACV. The result is similar to the case for smoothing all around, showing that the wave pattern is essentially produced by the fore and aft portions of the cushion and not the sides. The resistance in the region of the main hump is hardly affected by the smoothing.

The result of varying the depth of water is displayed in Fig. 4. The peak resistance increases in magnitude as the depth decreases, and occurs in each case at a depth Froude number slightly less than unity. The location of the other humps is also affected, but to a lesser degree.

Beam to length ratio is varied in Fig. 5. The general effect of increasing the beam is to increase the maxima and to decrease the minima in the wave resistance curve. This is due to the transverse waves assuming greater importance as the two-dimensional case is approached. A secondary effect is a shift in the locations of the oscillations to the right, so that in the limit of infinite beam, they occur at Froude numbers given precisely by Eqs (2) and (3).

We now turn to the effect of constant levels of acceleration of the craft from rest. Fig. 6a applies to a smooth ($\alpha a = 5$) two-dimensional pressure band moving over deep water. A general displacement of the oscillations to higher Froude numbers occurs. This shift is greater for the higher acceleration. In addition, most of the low-speed oscillations apparent in steady-state motion do not occur in accelerated motion. The resistance of a smooth band over finite depth water is shown in Fig. 6b. Here the reduction of the peaks is

even more dramatic than in deep water. More striking, however, is that for this and for all other two-dimensional cases studied, the wave resistance becomes negative beyond a certain velocity in finite depth. The resistance then asymptotically approaches zero. (The ordinate in this figure is plotted on an arsinh scale.) The depth Froude number at which the negative peak resistance occurs in shallow water has been found to be

$$F_d = 1 + 2\sqrt{\dot{a}c/gd} \tag{36}$$

The resistance of an accelerating three-dimensional pressure distribution is shown in Fig. 7a (deep water) and Fig. 7b (finite depth). In deep water, the wave resistance shows similar, but less marked, effects due to acceleration as does the corresponding two-dimensional case (Fig. 6a). In finite depth, there is again a strong reduction in the main peak as well as an elimination of nearly all the low-speed oscillations. However, there is no region of negative wave resistance -thus indicating the influence of the diverging wave pattern.

IV. RECTILINEAR MOTION IN A TANK

IV. 1. The Potential

We now consider the problem of an ACV moving along the centerline of a rectangular tank of length L and width B. The initial distance at $t = 0$ between the starting end of the tank and the coordinate axes xyz fixed to the model is taken as σ. This problem is crucial to the testing of models, as one must know the effect of tank walls. For instance, during steady motion in an infinitely long tank, Newman and Poole showed that the effect of tank width in the neighborhood of unit depth Froude number to be importance (see Eq. (4)).

We utilize Eq (22) for the potential in a horizontally unbounded region, and satisfy the additional condition of no flux through the four tank walls, by employing a system of image ACVs as shown in Fig. 8. We consider first only the array of distributions on the tank centerline, and later on apply the boundary condition on the tank sidewalls. The potentials for the individual distributions, $\phi^{(n)}$, are related to the primary potential, ϕ, as follows :

$$\phi^{(n)}(\xi, y, z, t) = \phi(\xi - nL, y, z, t) \qquad \text{for } n \text{ even,}$$

$$\phi^{(n)}(\xi, y, z, t) = \phi(-\xi + (n+1)L - 2\sigma, y, z, t) \text{ for } n \text{ odd.}$$

We add ϕ to $\phi^{(-1)}$, $\phi^{(1)}$ to $\phi^{(-2)}$, $\phi^{(2)}$ to $\phi^{(-3)}$, and so on. This only alters the exponential factor in Eq. (22), which now becomes :

$$\text{factor} = 2\exp\{i(w(-\sigma - \xi') + u(y - y'))\} \cdot \cos\{w(\sigma + \xi)\} \sum_{n=-\infty}^{\infty} \exp(2inwL)$$

The integral with respect to w of this factor in Eq. (22) can be simplified using the Poisson summation formula to give

$$\phi(\xi, y, z, t) = -\frac{1}{2\pi\rho L} \iint_{S'} dS' \int_0^t d\tau \sum_{n=-\infty}^{\infty} \int_{-\infty}^{\infty} du\, p^s_\tau(\xi', y', \tau) \ldots$$

$$\ldots \frac{\cosh\{k_n(z+d)\}}{\cosh(k_n d)} \cdot \frac{\sin\{\gamma_n(t-\tau)\}}{\gamma_n} \cos\{w_n(\sigma + \xi)\}$$

$$\cdot \exp\{i(w_n(-\sigma - \xi') + u(y - y'))\},$$

where

$$w_n = \pi n / L$$

$$k_n^2 = w_n^2 + u^2$$

and

$$\gamma_n^2 = g k_n \cdot \tanh(k_n d) \tag{37}$$

We now satisfy the condition on the side walls of the tank by including the image ACVs on lines parallel to the tank centerline. The procedure is similar to that just carried out, and if we assume that the pressure distribution is symmetric about the x axis, then

$$\phi(\xi, y, z, t) = -\frac{4}{\rho BL} \iint_{S'} dS' \int_0^t d\tau \sum_{n=0}^{\infty} \epsilon_n \sum_{m=0}^{\infty} \epsilon_m\, p^s_\tau(\xi', y', \tau) \ldots$$

$$\ldots \frac{\cosh\{k_{mn}(z+d)\}}{\cosh(k_{mn} d)} \cdot \frac{\sin\{\gamma_{mn}(t-\tau)\}}{\gamma_{mn}} \cos\{w_n(\sigma + \xi)\}$$

$$\cdot \exp\{i(w_n(-\sigma - \xi') + u_m(y - y'))\}, \tag{38}$$

where

$$u_m = 2\pi m/B \quad , \tag{39}$$

$$k_{mn}^2 = w_n^2 + u_m^2 \quad , \tag{40}$$

$$\gamma_{mn}^2 = g k_{mn} \cdot \tanh(k_{mn} d) \quad , \tag{41}$$

and

$$\epsilon_o = 1/2, \qquad \epsilon_n = 1 \qquad \text{for } n > 0$$

IV.2. The Wave Resistance

The method of obtaining the wave drag is the same as in the previous section and utilizes Eqs (24) and (38). After some algebra, one obtains :

$$R = \frac{2}{\rho g B L} \int_0^t c(\tau)\, d\tau \sum_{n=0}^{\infty} \epsilon_n \sum_{m=0}^{\infty} \epsilon_m\, w_n^2 \cdot \cos\left\{\sqrt{g k_{mn} \cdot \tanh(k_{mn} d)} \cdot (t - \tau)\right\} \cdot$$

$$\cdot \Big[P_{mn}^2 \left\{\cos(w_n(s(t) - s(\tau))) - \cos(w_n(s(t) + s(\tau) + 2\sigma))\right\} + \ldots$$

$$+ Q_{mn}^2 \left\{\cos(w_n(s(t) - s(\tau))) + \cos(w_n(s(t) + s(\tau) + 2\sigma)) + \ldots\right.$$

$$\left. + 2 P_{mn} Q_{mn} \sin(w_n(s(t) + s(\tau) + 2\sigma))\right] \quad , \tag{42}$$

where

$$P_{mn} = P(w_n, u_m)$$

and

$$Q_{mn} = Q(w_n, u_m)$$

It is clear that the fluid motion in the tank consists only of wavelets whose wavenumbers are given by Eqs (37) and (39), and that in the limit of $L \to \infty$ and $B \to \infty$, the result for a longitudinally and laterally unbounded region is recovered. The terms containing σ are due to reflections off the starting end of the tank, and as $\sigma \to \infty$ they contribute nothing to the wave resistance.

The wave resistance for steady motion in an endless tank may be obtained from Eq. (29) by setting up a laterally disposed array of images. The result, derived by Newman and Poole, in the present notation, is

$$R = \frac{2k_o}{\rho g B} \sum_{m=0}^{\infty} \epsilon_m \frac{k_m^2 \cdot \tanh(k_m d) \left\{P_m^2 + Q_m^2\right\}}{2k_m - k_o \tanh(k_m d) - k_m k_o d \cdot \operatorname{sech}^2(k_m d)} , \qquad (43)$$

in which u_m is given by Eq. (39) and w_m by

$$k_m^2 = w_m^2 + u_m^2$$

The circular wave number, k_m, is the solution of

$$k_m - k_m k_o \tanh(k_m d) = u_m^2 \qquad (44)$$

(The value of k_m when $m = 0$ is distinct from, and generally not equal to, k_0, the fundamental wave number.)

IV. 3. Results

The wave resistance of a smoothed rectangular distribution moving in a tank is shown in Fig. 9. In deep water (Fig. 9a), it is seen that the effect of the walls is small for $B/a = 2$. For $B/a > 4$ (tank width greater than four times model width), the resistance coefficient differs from the infinite width value by less than 0.01. It may be pointed out here that for the special case of $B/a = 1$, that is, the tank width equal to the nominal beam of the model, the pressure carries approximately 7% of the weight of the ACV beyond the tank walls. However, it can be shown that this case is mathematically equivalent to a two-dimensional pressure band spanning the width of the channel.

In finite depth (Fig. 9b) the influence of the tank walls in the region of unit depth Froude number is considerably greater, as was shown by Newman and Poole. The drop in wave resistance (Eq. (4)) at the critical speed does not depend on smoothing. Even when $B/a = 64$, so that the tank width is sixty-four times the model beam there is a discontinuity in resistance coefficient of 0.188. Thus steady-state experiments in this speed range are difficult.

The effect of side walls of an endless tank on the wave resistance of an accelerating ACV is displayed in Fig. 10. Two different levels of acceleration in both deep water and finite depth were calculated. In all cases the wave resistance is a smooth function of the tank width. For the low-speed range, increasing tank width generally decreases the wave resistance. On the other hand, this trend is reversed for high speeds (greater than the hump speed).

The case of infinite tank width is not plotted, in order to avoid confusion with the case of $B/a = 4$, with which it is almost identical. This difference in wave resistance coefficient for the cases calculated is less than 0.01, so that one might consider that a tank width equal to four times the model beam to be essentially infinite.

Even in finite depth there is no sudden change in resistance as the model accelerates through the critical depth Froude number. (A depth Froude number of unity is passed when $t\sqrt{g/a} = 14.14$ if $\dot{c}/g = 0.05$, and when $t\sqrt{g/a} = 7.07$ if $\dot{c}/g = 0.1$.) This sharply contrasts the case of steady motion, in which the drop or discontinuity in wave resistance coefficient when $d/a = 0.5$ and $B/a = 4$ is 3.0!

The effect of the tank end walls was found to be slightly greater in finite depth, and thus only the former is shown, in Fig. 11. The case of an infinitely wide tank is presented in Fig. 11a for $\sigma/a = 1, 2$ and ∞. In the region near $t = 0$, there is a slight increase in the resistance when $\sigma/a = 1$ only. Incidentally, when $\sigma/a = 1$, part of the pressure "extends" beyond the starting end wall, so one must expect some interference. When $\sigma/a = 2$, the clearance from the starting end wall is half a craft length and there is no noticeable interference.

The two curves for the finite values of σ were calculated for a tank length $L/a = 20$. There is no perceptible effect from the far end wall until the model "passes" through its image - as indicated by one or two oscillations in the curves near $t\sqrt{g/a} = 20$.

The case of $B/a = 1$ (that is, a two-dimensional pressure band) is shown in Fig. 11b. For the case of no nominal separation of the craft from the starting end wall at $t = 0$, there is now a slightly greater effect on the wave resistance.

V. FORCES ON A YAWING ACV

V.1. The Potential

We now consider the special case of an ACV travelling for a long time in the longitudinal or x direction. The craft is either fixed in a steady yaw position, or it starts a yawing motion after initial transients have died away. We may therefore use Eq. (21) for the potential, and drop the second term which will approach zero as $t \to \infty$

V.2. The Forces

The wave resistance is defined by Eq. (24), and the side force by

$$S(t) = \iint_S p^s(\xi, y, t) \quad \zeta_y \quad d\xi \quad dy \tag{45}$$

Thus the side force is the positive force to port (the y direction) required to hold the craft on a straight course.

The analysis for the two forces now continues, as in the case for rectilinear unyawed motion in horizontally unrestricted water. The forces are :

$$\frac{R}{S} = -\frac{i}{4\pi^2\rho g} \int_0^t d\tau \iint_S p(x, y, t)\, dS \iint_{S'} p(x', y', \tau)\, dS' \int_{-\infty}^{\infty} dw' \int_{-\infty}^{\infty} du \left(\frac{w}{u}\right) \cdot \gamma \cdot$$

$$\cdot \sin\{\gamma(t - \tau)\} \cdot \exp\{i(w(x - x' + s(t) - s(\tau) + u(y - y'))\}.$$

And after some simplification:

$$\frac{R}{S} = \frac{1}{2\pi^2\rho g} \int_0^{\infty} d\tau \int_0^{\infty} dw \int_{-\infty}^{\infty} du \left(\frac{w}{u}\right) \cdot \gamma \cdot \sin\{\gamma(t - \tau)\} \cdot$$

$$\cdot \left[(QP' - PQ') \cdot \cos\{w(s(t) - s(\tau))\} + (PP' + QQ') \cdot \sin\{w(s(t) - s(\tau))\}\right], \tag{46}$$

in which

$$P = P(w, u, t),$$

$$Q = Q(w, u, t),$$

$$P' = P(w, u, \tau)$$

and

$$Q' = Q(w, u, \tau) \ .$$

It is convenient to calculate the P and Q functions using an axis system $x^* y^* z$ that rotates with the craft rather than the xyz system, in which the x axis lies in the direction of motion. This is illustrated in Fig. 12. The yaw angle $\epsilon(t)$ is taken positive for clockwise rotation of the craft, when looking down on it. If w^* and u^* are the induced wavenumbers relative to these craft axes, then

$$w^*(t) = w \cos\{\epsilon(t)\} - u \sin\{\epsilon(t)\} = k \cos\{\theta + \epsilon(t)\}$$

and

$$u^*(t) = w \sin\{\epsilon(t)\} + u \cos\{\epsilon(t)\} = k \sin\{\theta + \epsilon(t)\} \ . \qquad (47)$$

Then it may be shown that

$$\begin{matrix} P(w, u, t) \\ Q(w, u, t) \end{matrix} = \int_S p^*(x^*, y^*) \begin{matrix} \cos \\ \sin \end{matrix} (w^* x^* + u^* y^*) \, dx^* \, dy^*, \qquad (48)$$

analogous to Eq. (26).

For the pressure distribution given by Eq. (5), it immediately follows from Eq. (33) that

$$P(w, u, t) = p_o \ \frac{\pi \cdot \sin(aw^*)}{\alpha \cdot \sinh(\pi w^*/2\alpha)} \ \frac{\pi \cdot \sin(bu^*)}{\beta \cdot \sinh(\pi u^*/2\beta)}$$

and

$$Q(w, u, t) = 0 \qquad (49)$$

We now consider a craft travelling at a constant velocity at a fixed angle of yaw from time $-T$ to 0, and then allowed to yaw up to time t. The τ integral in Eq. (46) for just the first phase of the motion is

$$I = \int_{-T}^{0} \sin\{\gamma(t - \tau)\} \cdot \Big[(QP' - PQ') \cos\{wc(t - \tau)\} + \ldots$$
$$\ldots + (PP' + QQ') \sin\{wc(t - \tau)\} \Big] \, d\tau$$

$$= \frac{1}{2}\{Q(w,u,t)\ P(w,u,-0) - P(w,u,t)\ Q(w,u,-0)\} \cdot$$

$$\cdot\left[\frac{\cos\{(\gamma+wc)t\}}{\gamma+wc} - \frac{\cos\{(\gamma+wc)(t+T)\}}{\gamma+wc} + \frac{\cos\{(\gamma-wc)t\}}{\gamma-wc} - \frac{\cos\{(\gamma-wc)(t+T)\}}{\gamma-wc}\right] \ldots$$

$$\ldots + \frac{1}{2}\{P(w,u,t)\ P(w,u,-0) + Q(w,u,t)\ Q(w,u,-0)\} \cdot$$

$$\cdot\left[\frac{\sin\{(\gamma+wc)t\}}{\gamma+wc} - \frac{\sin\{(\gamma+wc)(t+T)\}}{\gamma+wc} - \frac{\sin\{(\gamma-wc)t\}}{\gamma-wc} + \frac{\sin\{(\gamma-wc)(t+T)\}}{\gamma-wc}\right]$$

We consider first the case when $t = 0$ and $T \to \infty$ (that is, a steady state). The four terms containing the cosine factors, and the first and third sine factors are zero. The fourth sine term is the only one that gives a non-zero result in the wu integral of Eq. (46) as $T \to \infty$. The steady-state forces may be obtained in the same manner as the limit of Eq. (25) for large time :

$$\frac{R}{S} = \frac{1}{2\pi\rho g}\left[\int_{-\pi/2}^{-\theta_1} + \int_{\theta_1}^{\pi/2}\right] \frac{k^3 \cdot \begin{pmatrix}\cos\theta \\ \sin\theta\end{pmatrix}}{1 - k_o d \cdot \sec^2\theta \cdot \operatorname{sech}^2(kd)} \cdot$$

$$\cdot\{P^2(k\cos\theta,\ k\sin\theta) + Q^2(k\cos\theta,\ k\sin\theta)\}\ d\theta, \quad (50)$$

where k, k_o and θ_1 are given by Eqs (30), (31) and (32).

If we now assume that the ACV starts yawing at $t = 0$, then as $T \to \infty$, the second and fourth cosine terms, and the second sine term contribute nothing to the wu integral in Eq. (46). The expression for the forces after $t = 0$ becomes :

$$\frac{R}{S} = \frac{1}{2\pi\rho g}\left[\int_{-\pi/2}^{-\theta_1} + \int_{\theta_1}^{\pi/2}\right] \frac{k^3 \cdot \begin{pmatrix}\cos\theta \\ \sin\theta\end{pmatrix}}{1 - k_o d \cdot \sec^2\theta \cdot \operatorname{sech}^2(kd)} \cdot$$

$$\cdot\{P(w,u,t)\ P(w,u,-0) + Q(w,u,t)\ Q(w,u,-0)\}\ d\theta + \ldots$$

(cont'd over)

$$\ldots + \frac{1}{4\pi^2 \rho g} \int_0^{\infty} dw \int_{-\infty}^{\infty} du \left(\frac{w}{u}\right) \cdot \gamma \cdot \{Q(w,u,t)\, P(w,u,-0) \quad - \ldots$$

$$\ldots - P(w,u,t)\, Q(w,u,-0)\} \cdot \left[\frac{\cos\{(\gamma + wc)t\}}{\gamma + wc} + \frac{\cos\{(\gamma - wc)t\}}{\gamma - wc}\right] + \ldots$$

$$\ldots + \frac{1}{4\pi^2 \rho g} \int_0^{\infty} dw \int_{-\infty}^{\infty} du \left(\frac{w}{u}\right) \cdot \gamma \cdot \{P(w,u,t)\, P(w,u,-0) + \ldots$$

$$\ldots + Q(w,u,t)\, Q(w,u,-0)\} \cdot \left[\frac{\sin\{(\gamma + wc)t\}}{\gamma + wc} - \frac{\sin\{(\gamma - wc)t\}}{\gamma - wc}\right] + \ldots$$

$$\ldots + \frac{1}{2\pi^2 \rho g} \int_0^{t} d\tau \int_0^{\infty} dw \int_{-\infty}^{\infty} du \left(\frac{w}{u}\right) \cdot \gamma \cdot \sin\{\gamma(t - \tau)\} \cdot \qquad (51)$$

$$\cdot \left[\{Q(w,u,t)\, P(w,u,\tau) - P(w,u,t)\, Q(w,u,\tau)\} \cdot \cos\{w(s(t) - s(\tau))\} + \ldots\right.$$

$$\left. \ldots + \{P(w,u,t)\, P(w,u,\tau) + Q(w,u,t)\, Q(w,u,\tau)\} \cdot \sin\{w(s(t) - s(\tau))\}\right] \cdot$$

V.3. Results

The (steady-state) wave resistance of a yawed ACV is shown in Fig. 13. Fig. 13a indicates the marked effect of smoothing the pressure fall-off on a rectangular cushion, for a Froude number of unity. This is accentuated for yaw angles in the neighborhood of 10° and 85° . The peaks would seem to be caused by interference between short wavelets - as short wave components are not produced by a smoothed distribution. The slopes of the curves are zero at yaw angles of 0° and 90° - as required by symmetry.

The variation of wave resistance of a smoothed distribution with yaw angle for a series of different Froude numbers is displayed in Fig. 13b. At super-hump speeds, yawing the vehicle increases the effective Froude number so that the resistance drops a little. On the other hand, yawing at a sub-hump speed (for example, $F = 0.4$) can bring the craft onto the hump (at constant speed of advance), and thereby increase the resistance.

The wave-induced side force is shown in Fig. 14. It is non-dimensionalized in the same manner as the wave resistance in Eq.(35)

The effect of smoothing on side force (Fig. 14a) is seen to be even more vivid than on resistance (Fig. 13a). Increase in sharpness has a considerable effect on the side force for very small, or for very large, yaw angles - even at this relatively high speed. At the same Froude number, the effect of sharpness on unyawed wave resistance (Fig. 3a) was considerably less. The linear theory predicts a peak dimensionless side force of 2.63 in contrast to a dimensionless wave resistance of 0.73 at zero yaw angle. It seems that nonlinear and viscous effects would preclude the development of such large side forces in practice.

Different Froude numbers are considered in Fig. 14b. The side force (for $\alpha a = \beta a = 5$) is seen to be positive for super-hump speeds, and therefore favorable during a coordinated turn. It reaches a maximum at a yaw angle of about 30° . Thus there is an optimum sideslip angle for generating the maximum side force. For sub-hump speeds, there is a range of yaw angle in which the side force is negative.

Unsteady yawing motion is now considered. The side force for different rates of constant rotational speed after travelling at zero yaw angle for a long time is presented in Fig. 15. The abscissa is the yaw angle, and is proportional to the time after the initiation of the manoeuver. The general effect of increasing the yaw rate is to decrease the available side force. However, as typical average yaw rates are in the vicinity of 5° per unit time, it is clear that the unsteady influence is of secondary importance. The side force qualitatively follows the same trends at the two speeds considered, namely $F = 0.6$ (fig. 15a) and $F = 1.0$ (Fig. 15b).

Finally, in Fig. 16, a manoeuver is studied, in which the yaw angle is instantaneously changed from zero to 5°, 10°, 15° and 20°. The distance the ACV must travel before the steady-state side force is achieved is slightly greater for larger manoeuvers. Nevertheless, this effect is small. Almost the full steady-state side force is generated after the vehicle has moved one craft length at $F = 0.6$ (Fig. 16a), and after 1.25 craft lengths at $F = 1.0$ (Fig. 16b).

A favorable side force is developed immediately after this sudden yaw manoeuver, and then increases slowly at first. It may be shown that for a small jump in yaw angle, the initially generated side force is just one half of the final steady-state side force. This feature is evident in the curves, particularly for the smaller manoeuvers.

VI. CONCLUDING REMARKS

VI. 1. Present Work

Turning firstly to the case of Rectilinear Motion in a Tank, it is clear that the problem of interference from the side walls during accelerated motion in finite depth water is considerably less than that during steady motion. Model tests under such unsteady conditions would be much easier to perform as a tank width equal to four times the model beam essentially simulates the laterally unrestricted case.

With regard to the yawing ACV, the great dependence of side force at super-hump speeds on smoothing was an unexpected result. So much so, that it would be unrealistic to model the pressure under the craft with a sharp distribution. Even assuming practical values of $\alpha a = \beta a = 40$ (which has a negligible effect on unyawed wave resistance) reduces the maximum predicted induced side force by almost one half. A study of the expression for the steady-state forces, Eq. (50), reveals that this difference is due to the high frequency oscillations in the integral for θ just less than $\pi/2$. The effect is worst for a yawed sharp distribution when the oscillations decay very slowly and is further emphasized in the integral for side force which contains a $\sin\theta$ factor, rather, than the integral for wave resistance which contains a $\cos\theta$ factor. A particularly large number of subdivisions in the integration is therefore required under these conditions. This probably explains the small discrepancies found at small non-zero yaw angles and yaw angles just below 90°, when attempting to verify the theoretical wave resistance calculated by Murthy (1970) and Everest (1969).

In practice, these high frequency wavelets probably break due to excessive theoretical steepness, and other practical effects such as cushion air flow.

The induced side force has nevertheless been found to be significant, being of similar magnitude to the wave resistance. It clearly plays a role in the control of ACVs. This force has been experienced by drivers of air-cushion vehicles, who usually refer to it as "keel effect".

During a typical manoeuver, it has been found that the induced side force is almost equal to the steady-state value at the same instantaneous yaw angle.

VI.2. Future Work

It would be interesting to verify some of the above-mentioned theoretical results by experiment. In particular, one would like to know how accurately the induced side force is predicted - or what the equivalent smoothing would be. Such an experiment would have to take into account aerodynamic and momentum side forces as well as skirt contact, which might be significant.

Numerical work can be extended in various areas. Further test cases, including the effect of finite depth might be examined. Incidentally, many manoeuvers are carried out in finite depth near the terminals. This aspect is therefore important.

Possibilities for theoretical work include an investigation into the yawing moment acting on the vehicle about the vertical axis. Some experiments by Everest indicated that the craft is generally stable in yaw.

ACKNOWLEDGEMENTS

The writer is grateful to the Office of Naval Research, Washington for their support of part of this work under Contract No. N00014-67-A-0181-0018 Task No. NR 062-420, which was carried out during 1969 and 1970 in the Department of Naval Architecture and Marine Engineering at the University of Michigan in Ann Arbor, Michigan. This work is briefly covered in the section on Rectilinear Motion in Horizontally Unrestricted Water. For a more detailed account, the reader is referred to Doctors and Sharma (1970 and 1972).

The Section on Rectilinear Motion in a Tank represents some calculations performed for research supported by the Australian Research Grants Committee during 1972.

The writer also wishes to acknowledge valuable suggestions pertaining to this paper made by Professor P. T. Fink, Dean of the Faculty of Engineering at the University of New South Wales in Sydney.

NOMENCLATURE

a	**half length of craft**
A	$1/2F^2$
b	**half beam of craft**
B	**width of tank**
c	**velocity of craft**
d	**water depth**
F	**Froude number** $= c/\sqrt{2ga}$
F_d	**depth Froude number** $= c/\sqrt{gd}$
g	**acceleration due to gravity**
k	**circular wave number** $= \sqrt{w^2 + u^2}$
k_o	**fundamental wave number** $= g/c^2$
L	**length of tank**
n, m	**indices for longitudinal and transverse wavenumbers in a tank**
p	**cushion pressure measured in the moving reference frame xyz**
p^s	**cushion pressure measured in the stationary frame** ξyz
p_o	**nominal cushion pressure**
P, Q	**functions defined by Eq. (26) or (48)**
R	**wave resistance**
R_c	**wave resistance coefficient defined by Eq. (35)**
s	**distance travelled by craft**
S	**induced side force, or area of pressure distribution**

S_c	side force coefficient, analogous to R_c
t	time
w, u	induced longitudinal and transverse wavenumbers
W	weight of craft
x, y, z	coordinate system travelling with craft, but not rotating with it
α	longitudinal cushion pressure fall-off parameter
β	transverse cushion pressure fall-off parameter
γ	$\sqrt{gk' \tanh (kd)}$
ϵ	yaw angle of vehicle relative to x axis (see Eq. (47))
ζ	free surface elevation
θ	wave direction with respect to the x axis
ξ	longitudinal coordinate in the stationary reference frame
ρ	water density
σ	initial position of model in the tank
τ	dummy time variable
ϕ	velocity potential in the stationary reference frame, such that the velocity is its positive derivative

Superscripts

$*$	variable reffered to axis system moving and rotating with craft
$'$	dummy variable
$\cdot$	time differentiation

* * *

REFERENCES

Barratt, M.J. : "The Wave Drag of a Hovercraft", J. Fluid Mechanics, 22, Part 1 pp 39-47 (1965)

Djachenko, V.K. : "The Wave Resistance of a Surface Pressure Distribution in Unsteady Motion", Proc. Leningrad Shipbuilding Inst. (Hydrodynamics and Theory of Ships Division) English Translation : Dept. Naval Architecture and Marine Engineering, University of Michigan, Ann Arbor, Michigan, Report 44, 12 pp (1966)

Doctors, L.J. and Sharma, S.D. : "The Wave Resistance of an Air-Cushion Vehicle in Accelerated Motion", Dept. Naval Architecture and Marine Engineering, University of Michigan, Ann Arbor, Michigan, Report 99, 104 pp + 92 figs (1970)

Doctors, L.J. and Sharma, S.D. : "The Wave Resistance of an Air Cushion Vehicle in Steady and Accelerated Motion", J. Ship Research, 16,4, pp. 248-260 (1972).

Everest, J.T. : "The Calm Water Performance of a Rectangular Hovercraft", National Physical Laboratory (Ship Division), Report 72, 12 pp + 29 figs (1966)

Everest, J.T : "Shallow Water Wave Drag of a Rectangular Hovercraft", Ibid., Report 79, 8 pp + 19 figs (1966)

Everest, J.T. : "Measurements of the Wave Pattern Resistance of a Rectangular Hovercraft", Ibid., Tech. Mem. 147 (1966)

Everest, J.T. and Hogben, N : "Research on Hovercraft over Calm Water", Trans. Royal Inst. Naval Architects, 109, pp 311-326 (1967)

Everest, J.T. and Willis, R.C. : "Experiments on the Skirted Hovercraft Running at Ang. s of Yaw with Special Attention to Wave Drag", National Physical Laboratory (Ship Division) Report 119, 8pp + 15 figs (1968)

Everest, J.T. and Hogben, N. : "A theoretical and Experimental Study of the Wavemaking of Hovercraft of Arbitrary Planform and Angle of Yaw", Trans. Royal Inst. Naval Architects, 111, pp 343-365 (1969)

Havelock, T.H. : "The Wave-Making Resistance of Ships : A Theoretical and Practical Analysis", Proc. Royal Soc. London, Series A, 82, pp 276-300 (1909)

Havelock, T. H. : "Ship Resistance : The Wave-Making Properties of Certain Travelling Pressure Disturbances", Ibid., 89, pp 489-499 (1914)

Havelock, T. H. : "The Effect of Shallow Water on Wave Resistance", Ibid., 100, pp 499-505 (1922)

Havelock, T. H. : "Some Aspects of the Theory of Ship Waves and Wave Resistance", Trans. North-East Coast Inst. Engineers and Shipbuilders, 42, pp 71-83 (1926)

Havelock, T. H. : "The Theory of Wave Resistance", Proc. Royal Soc. London, Series A, 138, pp 339-348 (1932)

Havelock, T. H. : "The Effect of Speed of Advance upon the Damping of Heave and Pitch", Trans. Royal Inst. Naval Architects 100, pp 131-135 (1958)

Hogben, N. : "Wave Resistance of Steep Two-Dimensional Waves", National Physical Laboratory (Ship Division), Report 55, 9 pp + 5 figs (1965)

Hogben, N. : "An Investigation of Hovercraft Wavemaking", J. Royal Aeronautical Society, 70, pp 321-329 (1966)

Lamb, H. : Hydrodynamics, New York, Dover Pubs., 738 pp (1945). Originally : Cambridge, Cambridge University Press (1932)

Lunde, J.K. : "On the Linearized Theory of Wave Resistance for a Pressure Distribution Moving at Constant Speed of Advance on the Surface of Deep or Shallow Water", Skipsmodelltanken, Norges Tekniske Høgskole, Trondheim, Medd. 8, 48pp, in English (1951)

Lunde, J.K. : "On the Linearized Theory of Wave Resistance for Displacement Ships in Steady and Accelerated Motion", Trans. Soc. Naval Architects and Marine Engineers, 59, pp 25-85 (1951)

Lunde, J.K. : "The Linearized Theory of Wave Resistance and its Application to Ship-Shaped Bodies in Motion on the Surface of a Deep, Previously Undisturbed Fluid", Skipsmodelltanken, Norges Tekniske Høgskole, Trondheim, Medellelse 23 (1953). Translation : Soc. Naval Architects and Marine Engineers, Tech. and Research Bulletin 1 - 8, 70pp (1957)

Lunde, J.K. : "A Note on the Linearized Theory of Wave Resistance for Accelerated Motion", Skipsmodelltanken, Norges Tekniske Høgskole, Trondheim, Medellelse 27, 14 pp (1953)

Murthy, T. K. S. : "The Wave Reistance of a Drifting Hovercraft", Hovering Craft and Hydrofoil, 9, pp 20-24 (1970)

Newman, J. N. and Poole, F. A. P. : "The Wave Resistance of a Moving Pressure Distribution in a Canal", Schiffstechnik, 9, pp 21-26, in English (1962)

Shebalov, A. N. : "Theory of Ship Wave Resistance for Unsteady Motion in Still Water", Proc. Leningrad Shipbuilding Inst. (Hydromechanics and Theory of Ships Division). English Translation : Dept. Naval Architecture and Marine Engineering, University of Michigan, Ann Arbor, Michigan, Report 67, 14 pp (1966)

Sretensky, L. N. : "On the Theory of Wave Resistance" Trudy Tsentral. Aero-Gidrodinam. Inst., 348, 28 pp, in Russian (1939)

Stoker, J. J. : "Water Waves", 4 of Pure and Applied Mathematics, Interscience Publishers Inc., New York, 567 pp (1957)

Wehausen, J. V. : "Effect of the Initial Acceleration upon the Wave Resistance of Ship Models", J. Ship Research, 7, 3, pp 38-50 (1964)

* * *

LIST OF FIGURES

1. Pressure Distribution Used

2. The Two Coordinate Systems

3. Wave Resistance for Different Amounts of Smoothing
   (a) Deep Water
   (b) Finite Depth

4. Wave Resistance for Different Depths

5. Wave Resistance for Different Beam to Length Ratios

6. Unsteady Two-Dimensional Wave Resistance
   (a) Deep Water
   (b) Finite Depth

7. Unsteady Three-Dimensional Wave Resistance
   (a) Deep Water
   (b) Finite Depth

8. Image System Used to Represent Tank Walls

9. Wave Resistance in an Endless Tank
   (a) Deep Water
   (b) Finite Depth

10. Unsteady Wave Resistance for Different Widths of an Endless Tank
   (a) Deep Water, $c/g = 0.05$
   (b) Deep Water, $c/g = 0.1$
   (c) Finite Depth, $c/g = 0.05$
   (d) Finite Depth, $c/g = 0.1$

11. Unsteady Wave Resistance for Different Locations of Tank Ends in Finite Depth
   (a) Infinitely Wide Tank
   (b) Two-Dimensional Pressure Band

12. Axis System Fixed to Craft

13. Wave Resistance in Deep Water while Yawed
   (a) For Different Amounts of Smoothing
   (b) For Different Froude Numbers

14. Side Force in Deep Water while Yawed
   (a) For Different Amounts of Smoothing
   (b) For Different Froude Numbers

15. Unsteady Side Force in Deep Water while Yawing
   (a) $F = 0.6$
   (b) $F = 1.0$

16. Unsteady Side Force in Deep Water After a Step Change in Yaw Angle
    (a) F = 0.6
    (b) F = 1.0

* * *

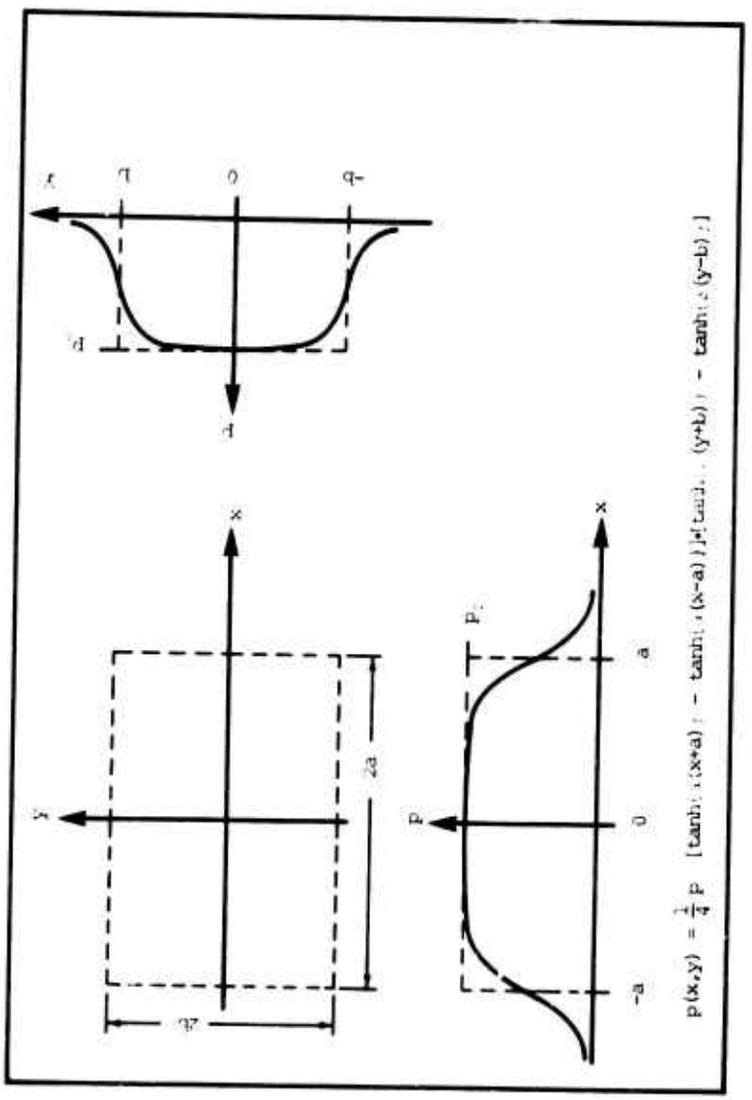


Figure 1. Pressure distribution used

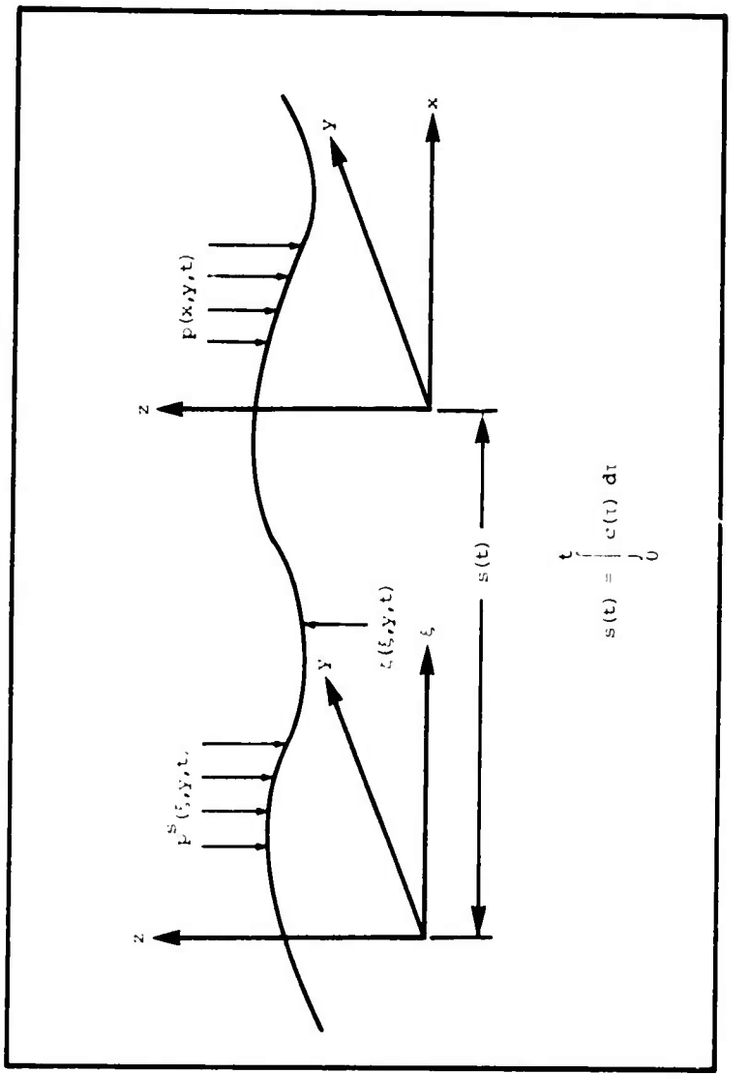


Figure 2. The two coordinate systems

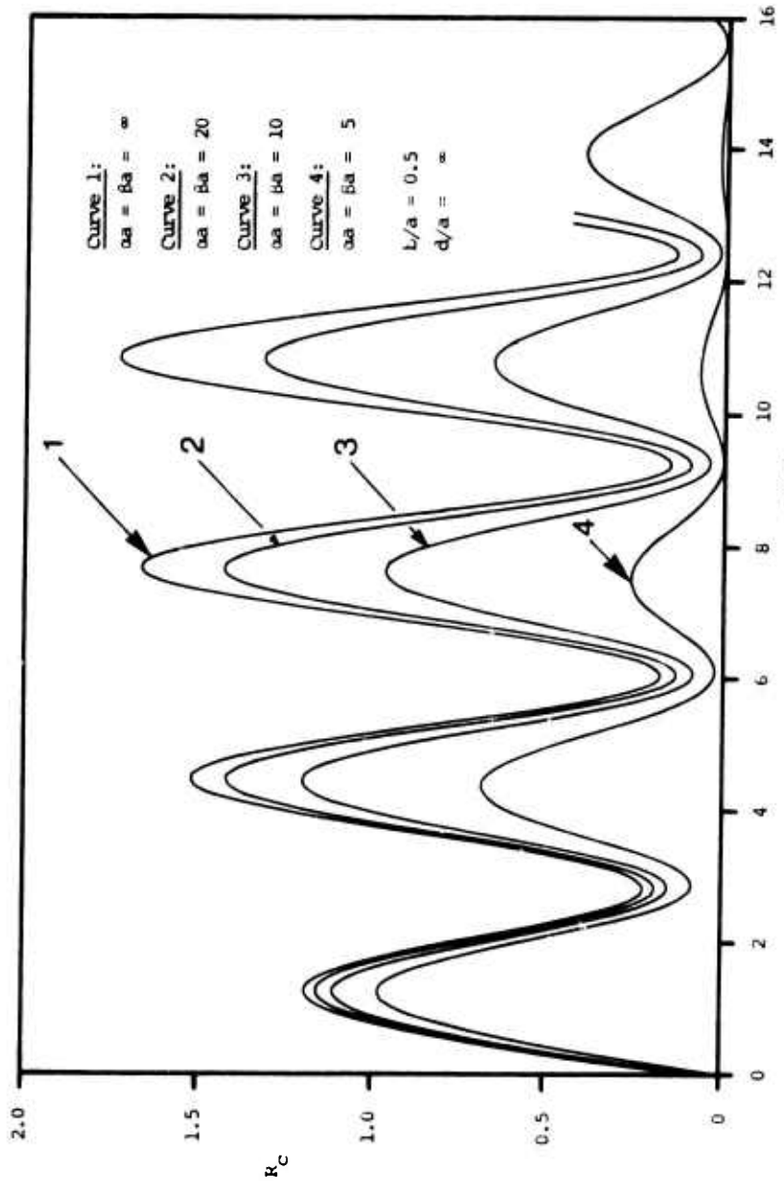


Figure 3. Wave resistance for different amounts of smoothing, (a) deep water

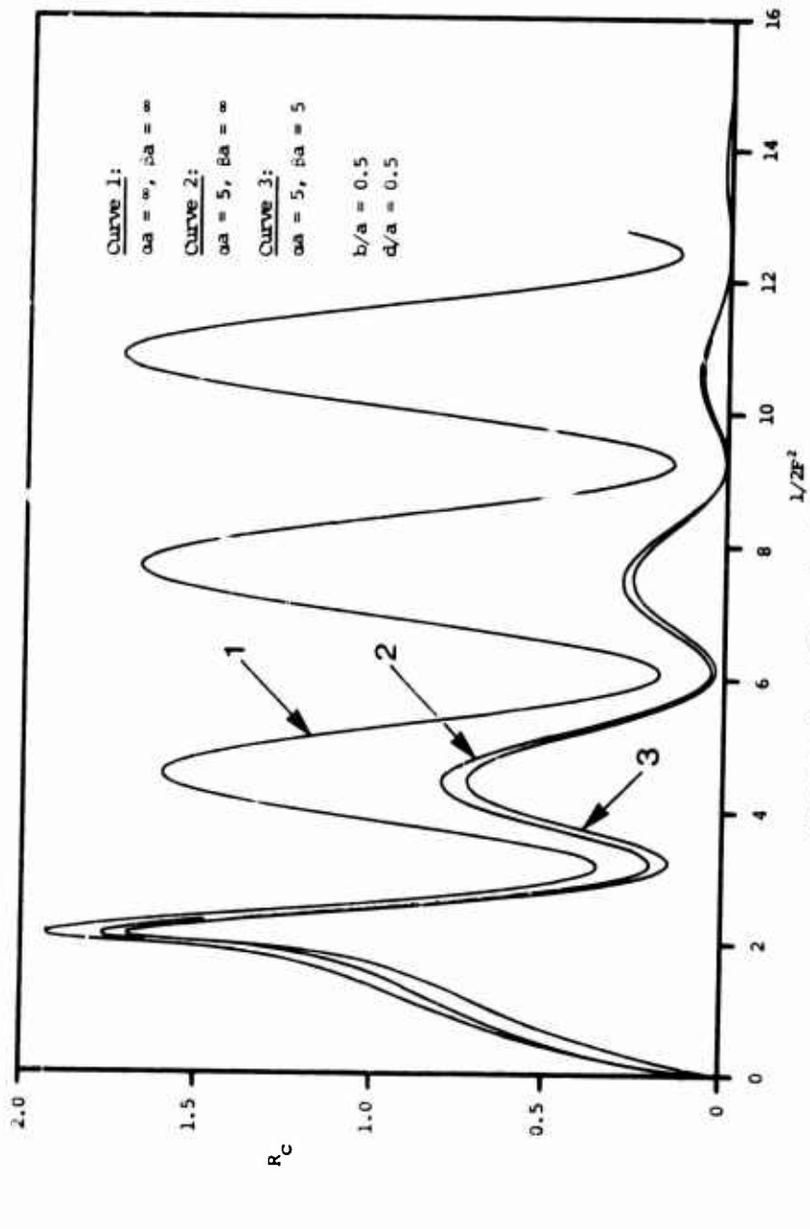


Figure 3. (Cont.) (b) finite depth

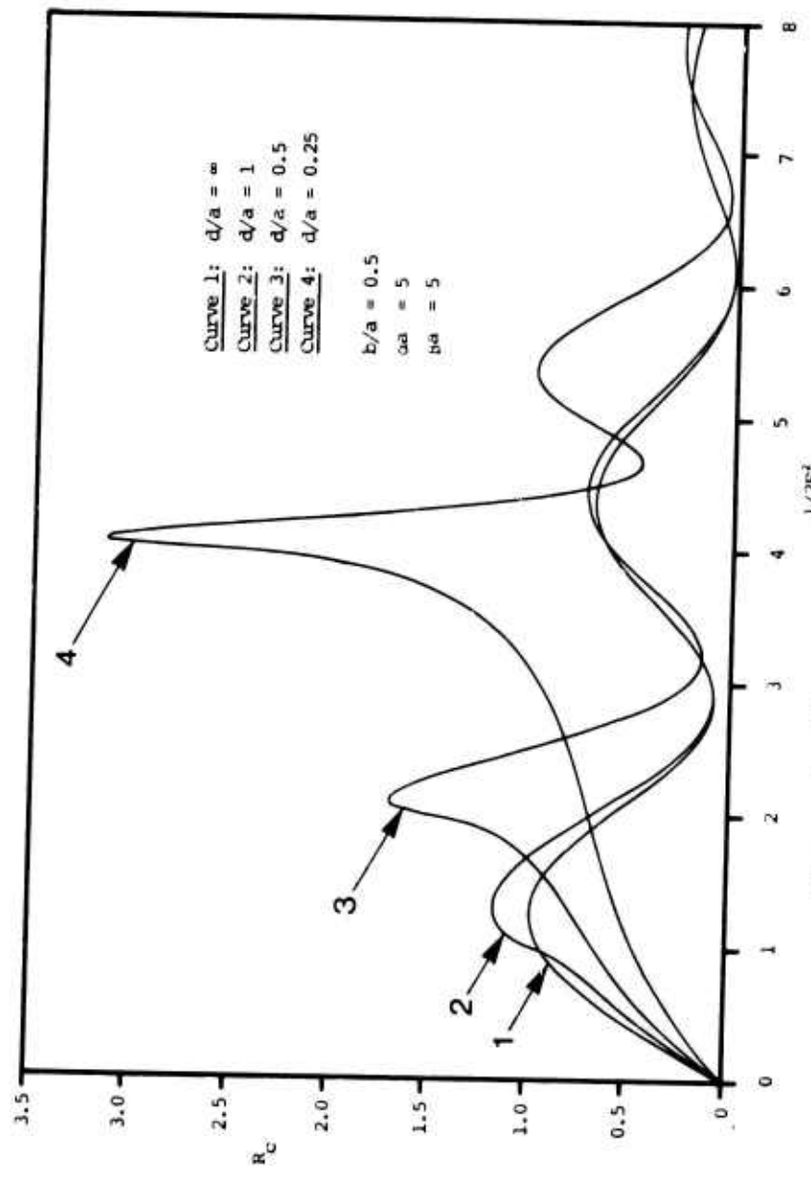


Figure 4. Wave resistance for different depths

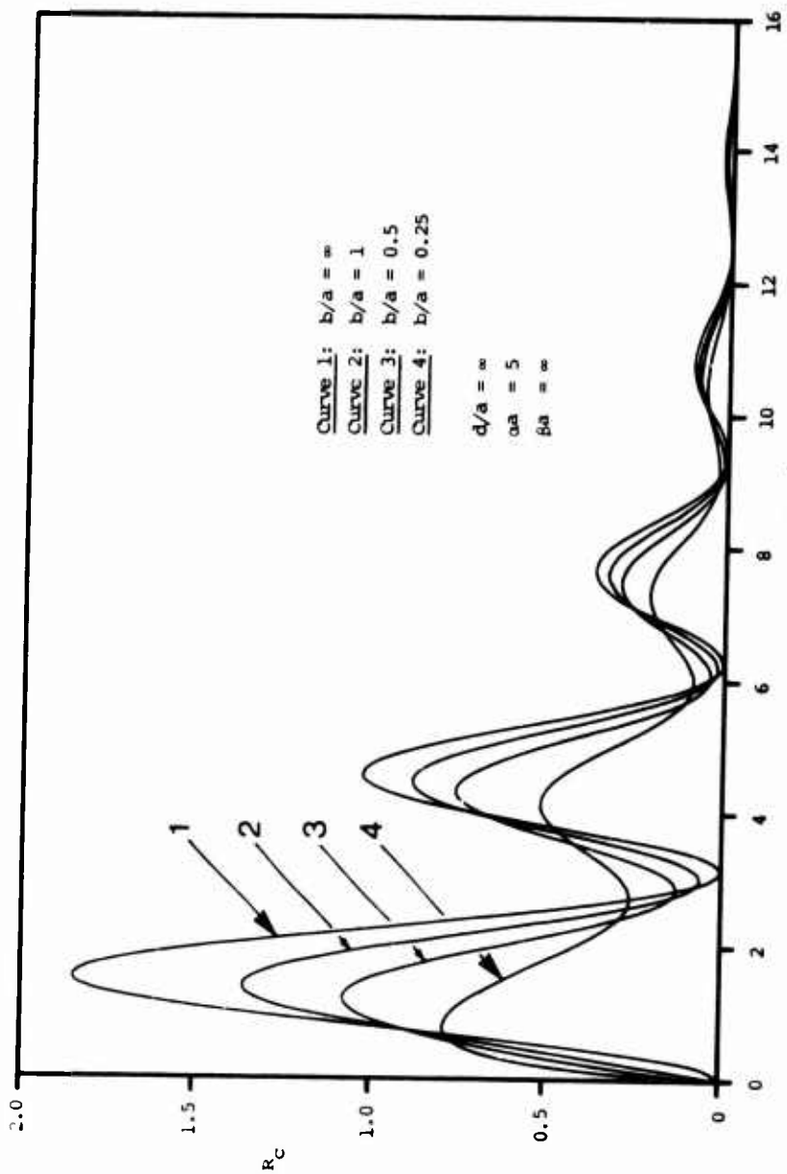


Figure 5. Wave resistance for different beam to length ratios

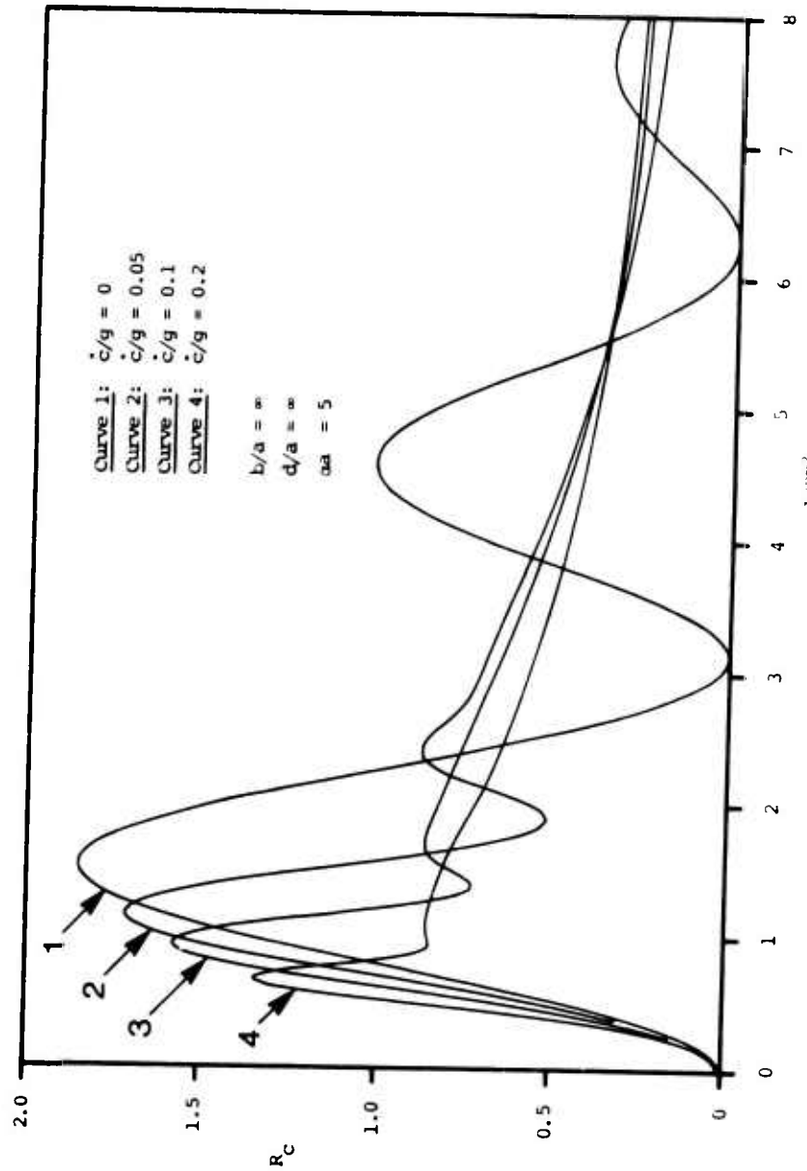


Figure 6. Unsteady two-dimensional wave resistance, (a) deep water

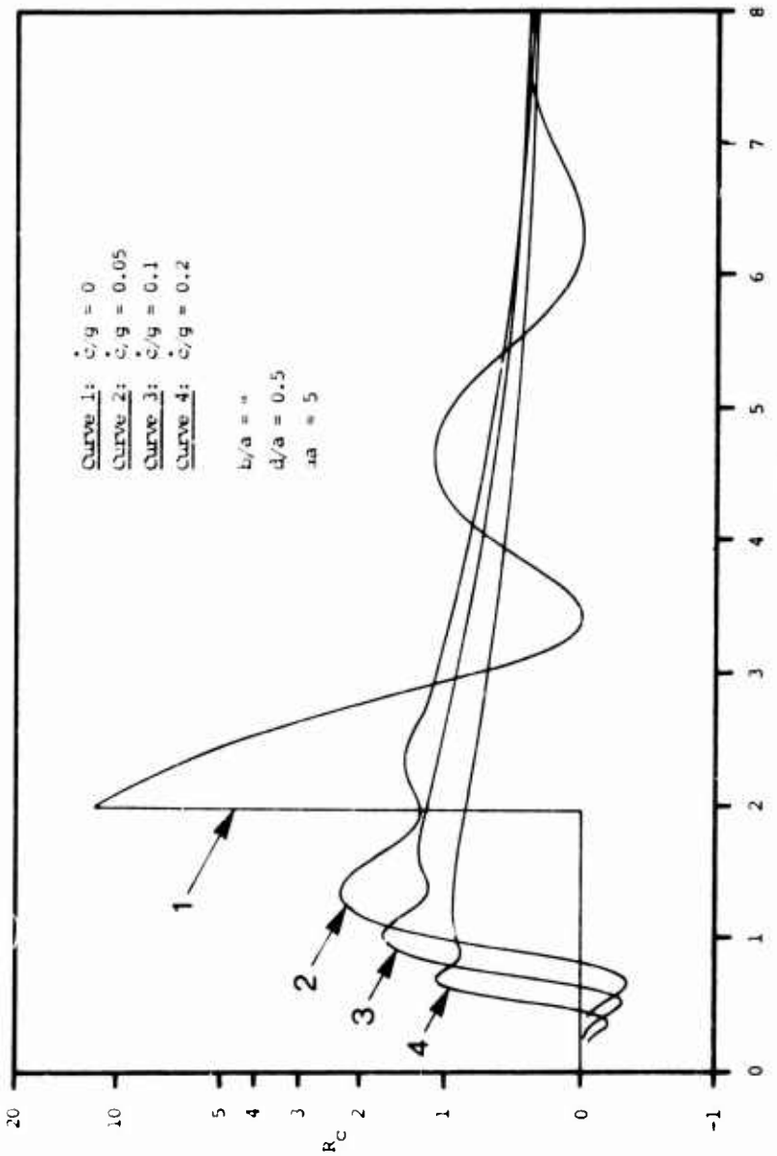


Figure 6. (Cont.) (b) finite depth

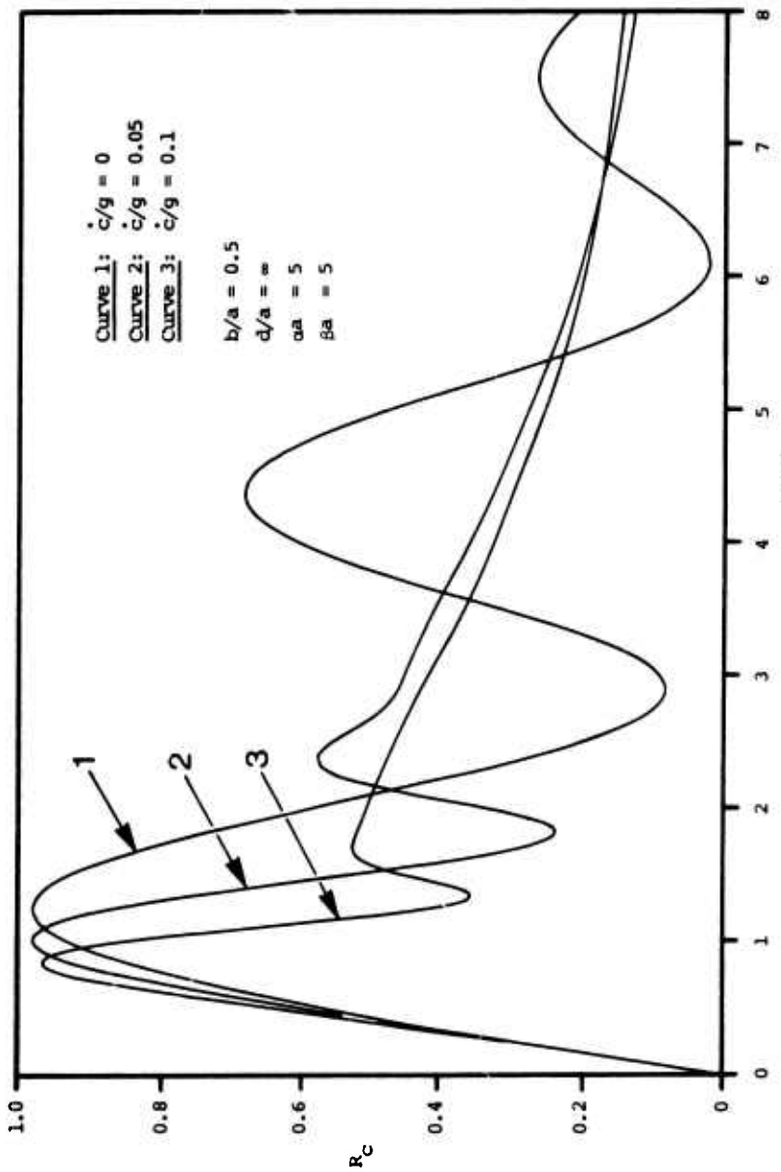


Figure 7. Unsteady three-dimensional wave resistance, (a) deep water

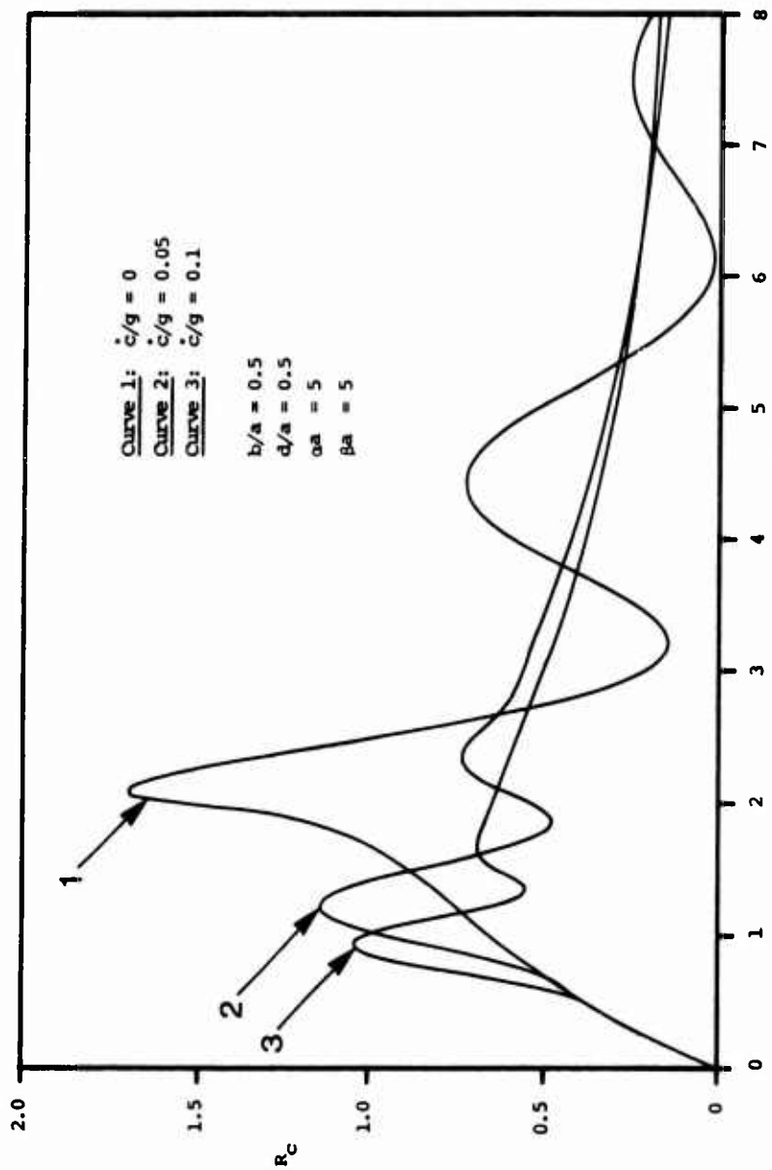


Figure 7. (Cont.) (b) finite depth

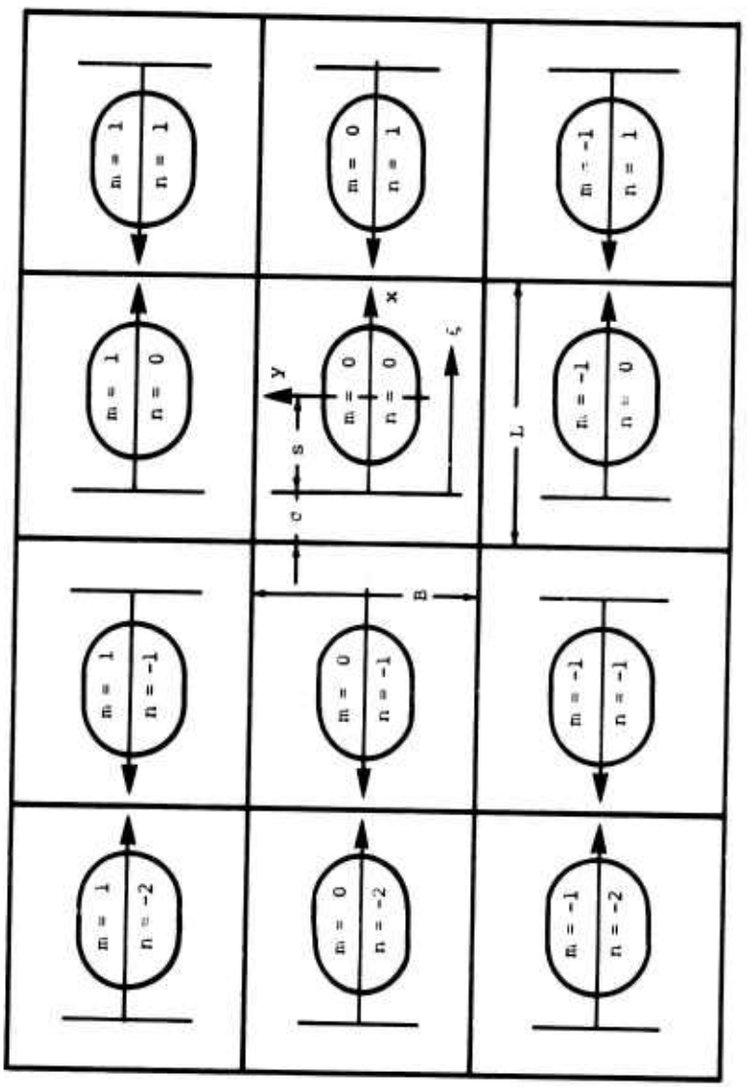


Figure 8. Image system used to represent tank walls

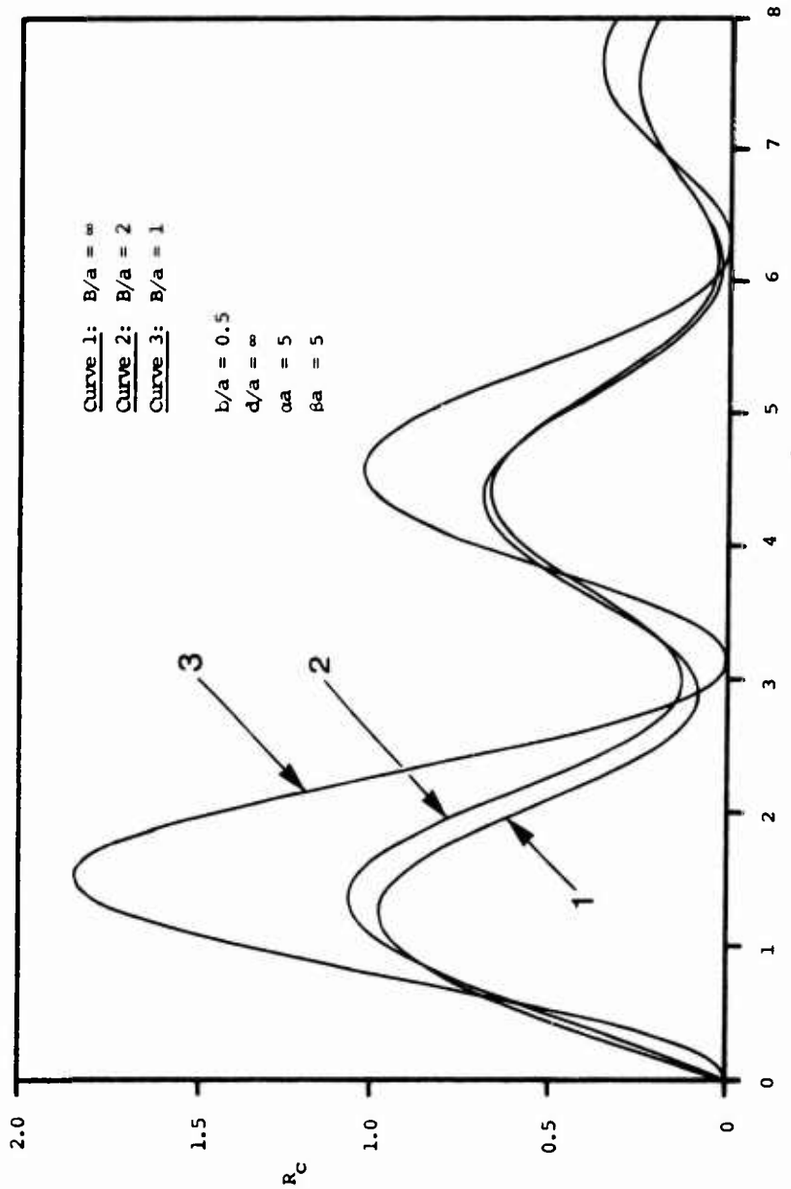


Figure 9. Wave resistance in an endless tank, (a) deep water

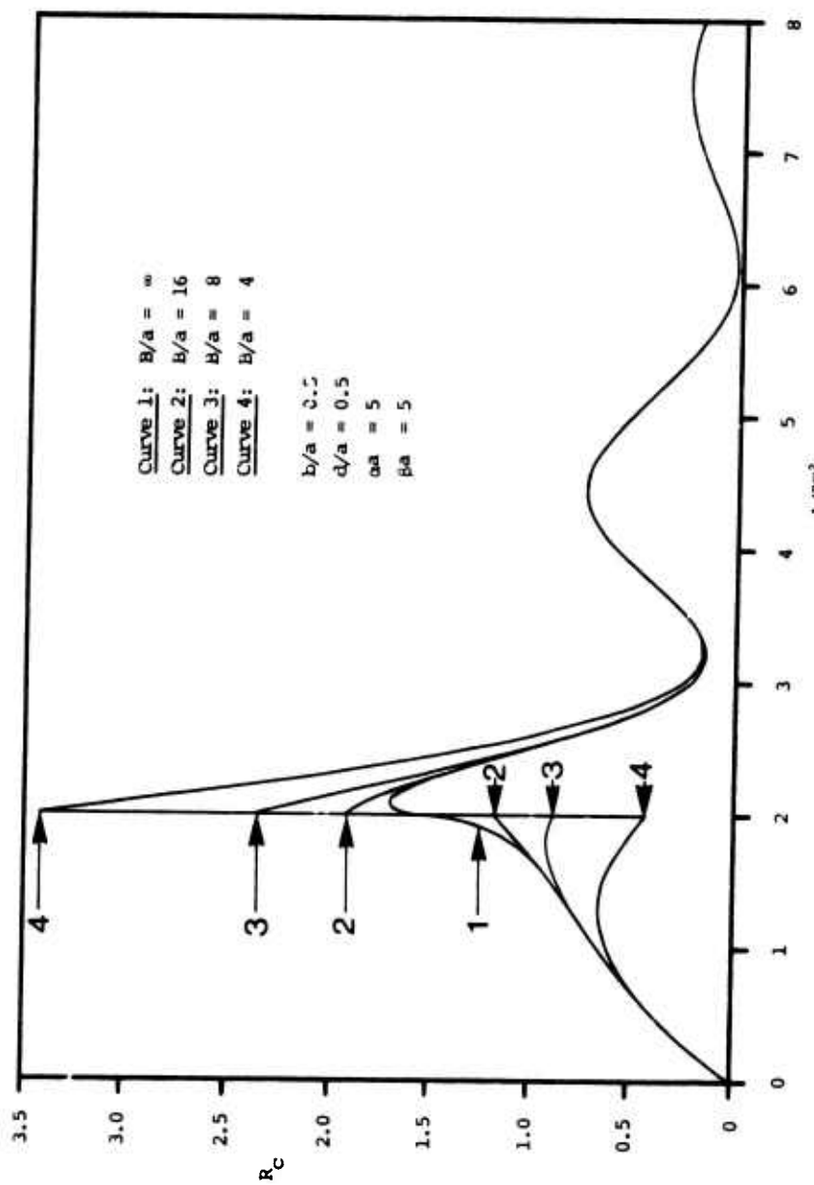


Figure 9. (Cont.) (b) finite depth

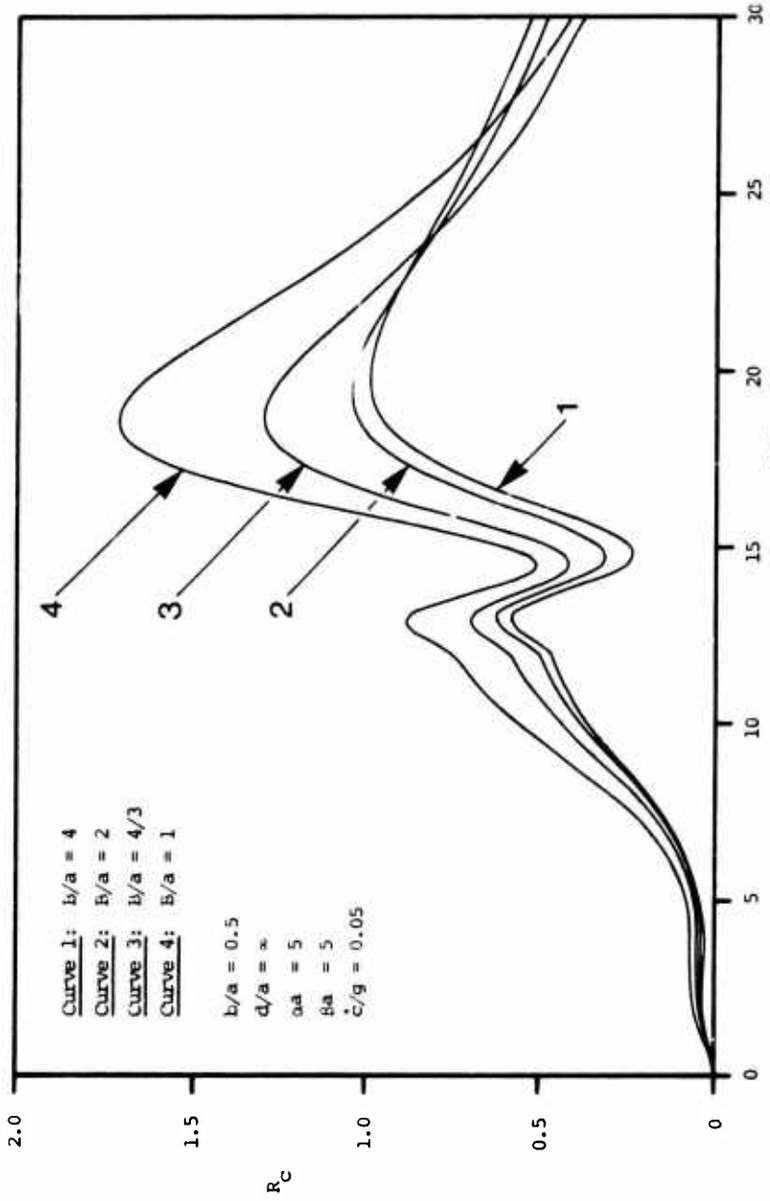


Figure 10. Unsteady wave resistance for different widths of an endless tank, (a) deep water, $c/g = 0.05$

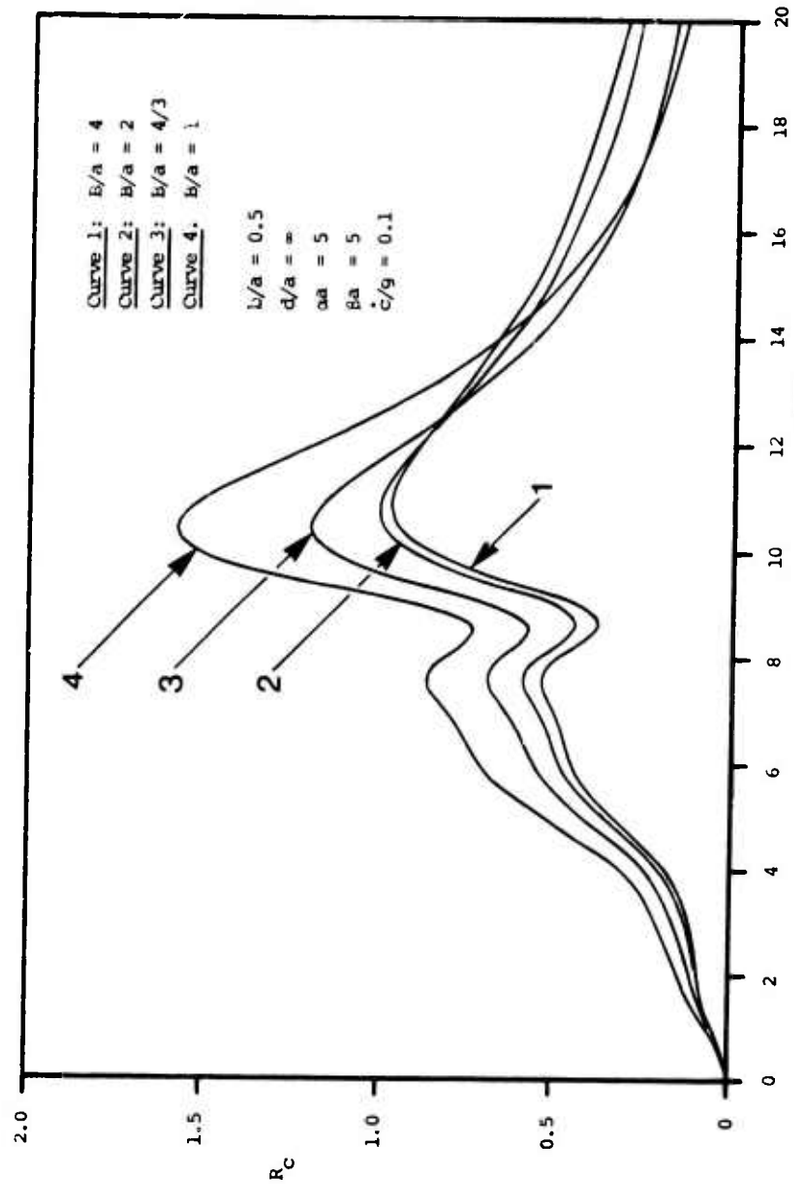


Figure 10. (Cont.) (b) deep water, $\dot{c}/g = 0.1$

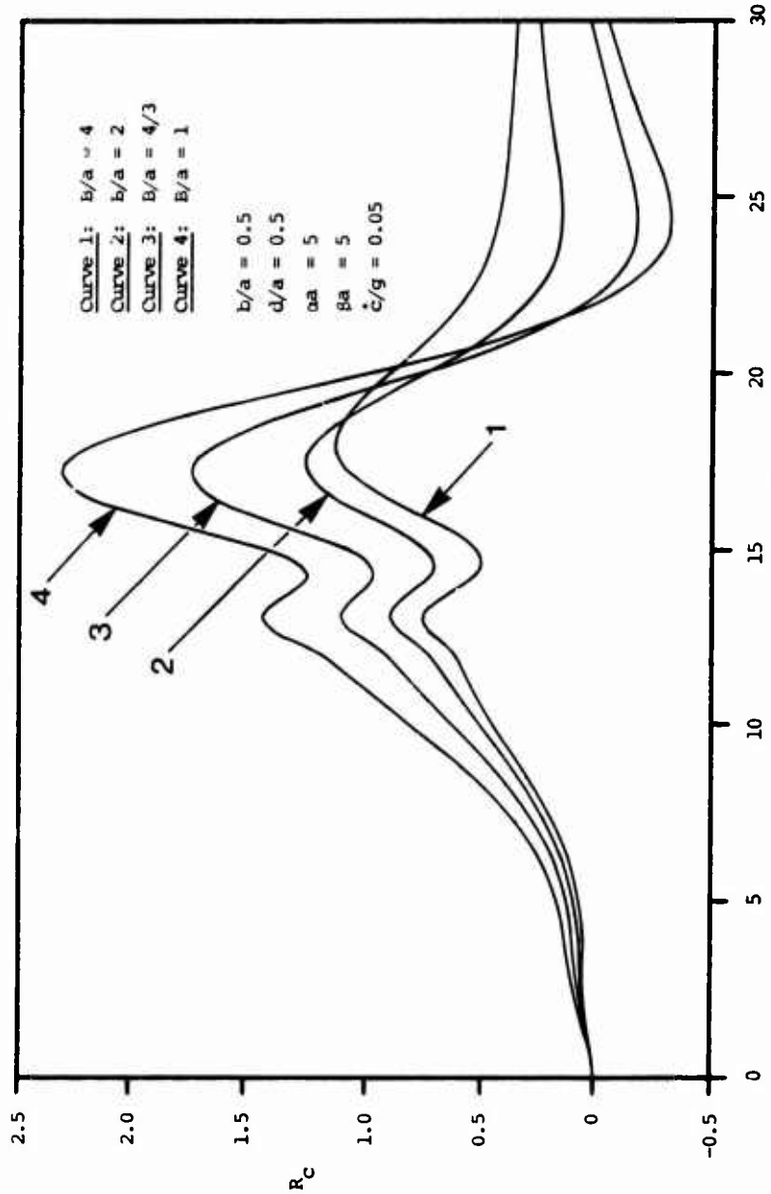


Figure 10. (Cont.) (c) finite depth, $\dot{c}/g = 0.05$

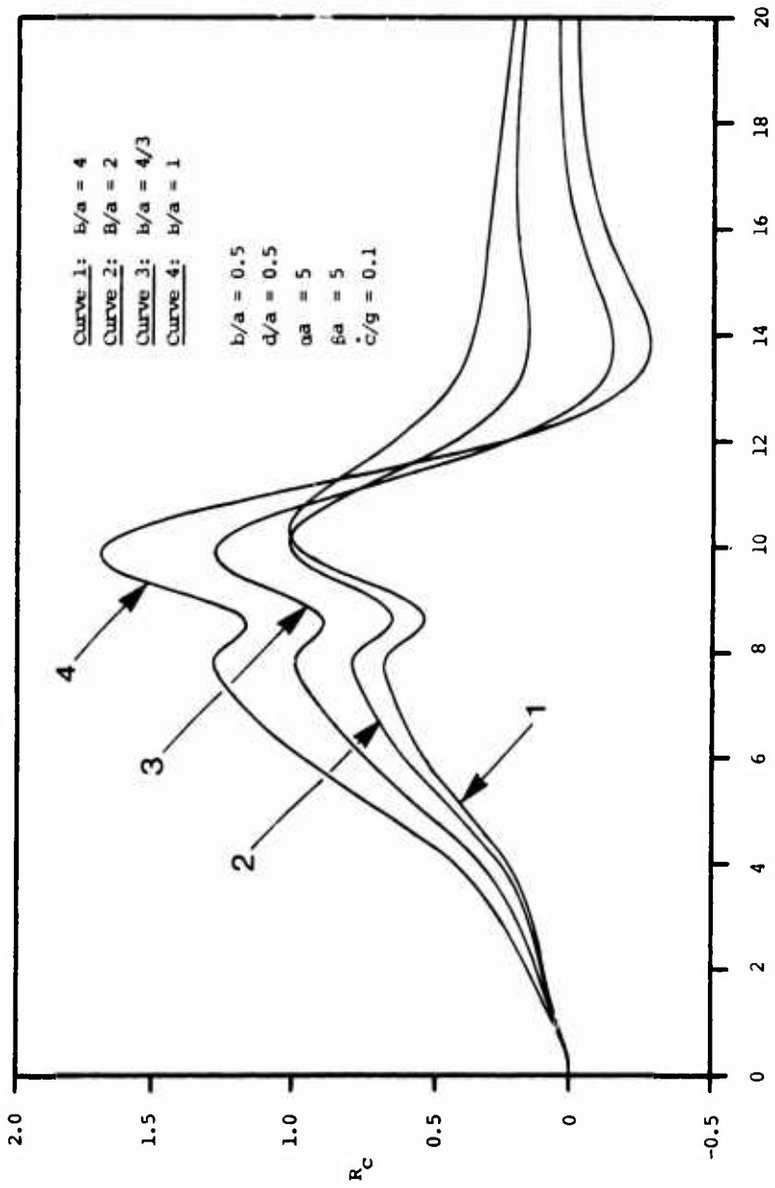


Figure 10. (Cont.) (d) finite depth, $\dot{c}/g = 0.1$

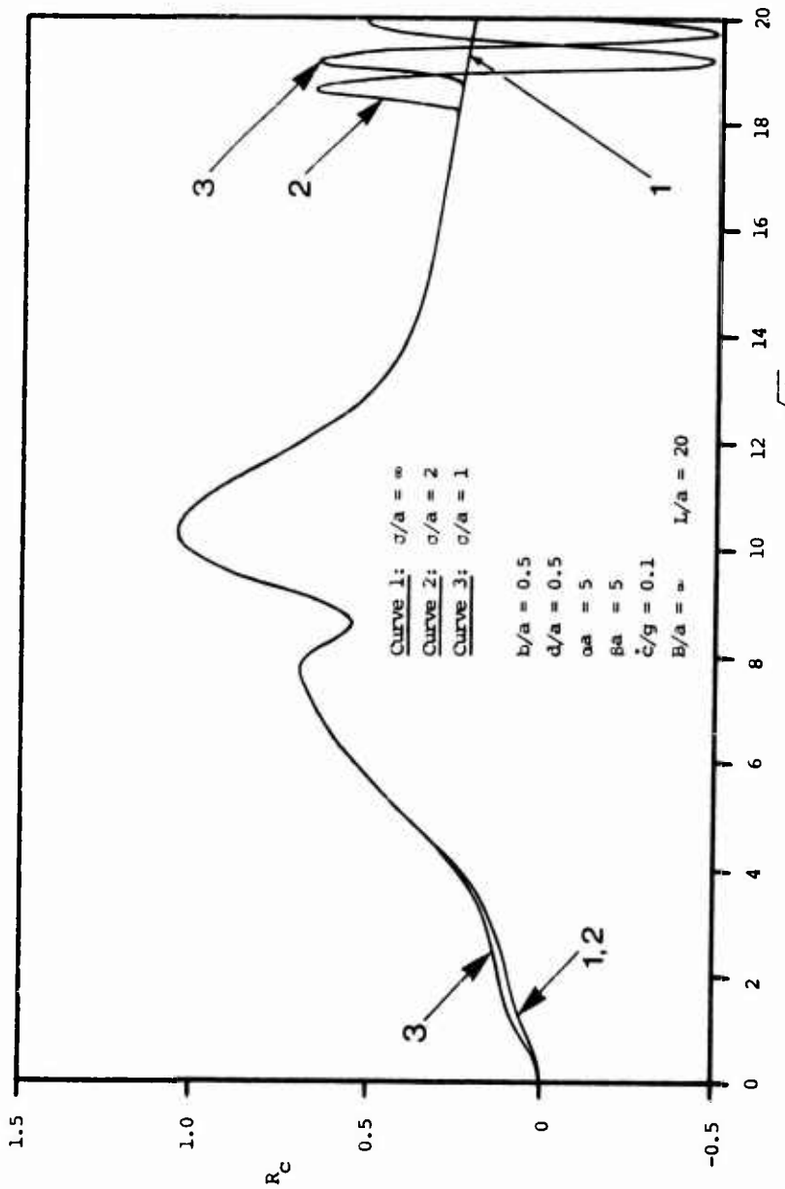


Figure 11. Unsteady wave resistance for different locations of tank ends in finite depth, (a) infinitely wide tank

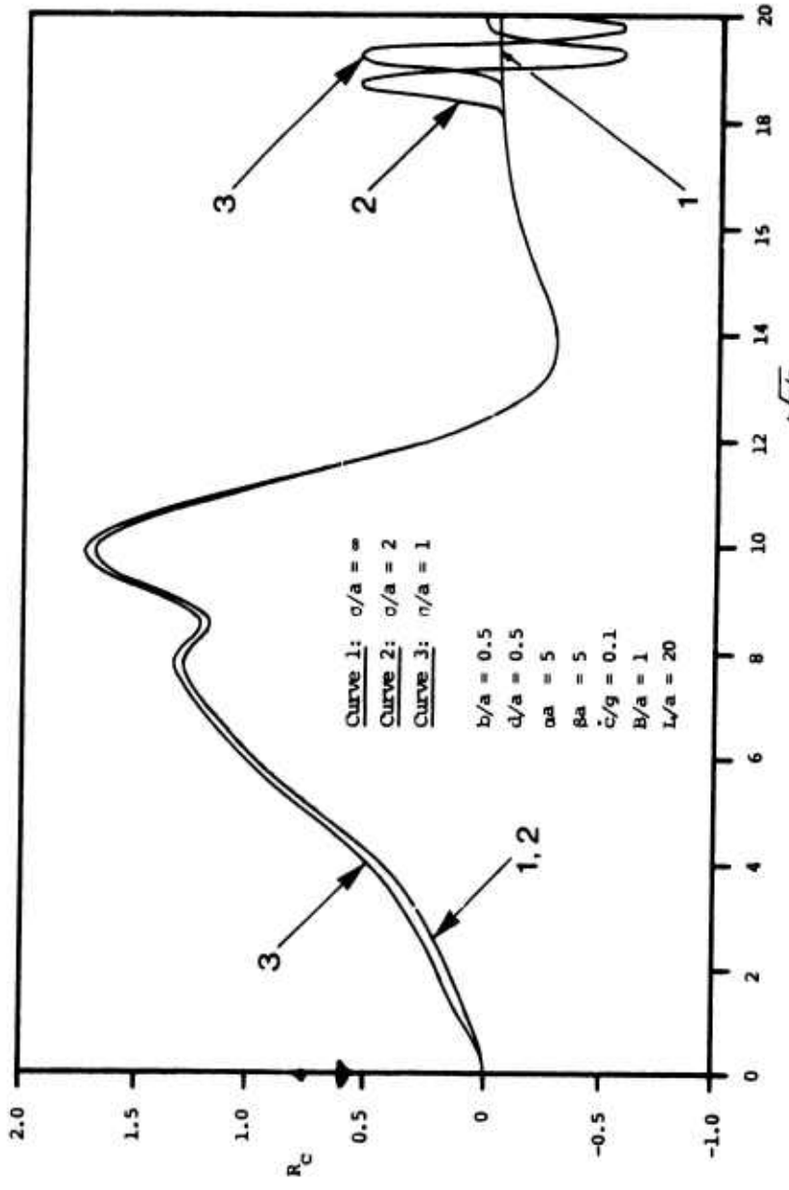


Figure 11. (Cont.) (b) two-dimensional pressure band

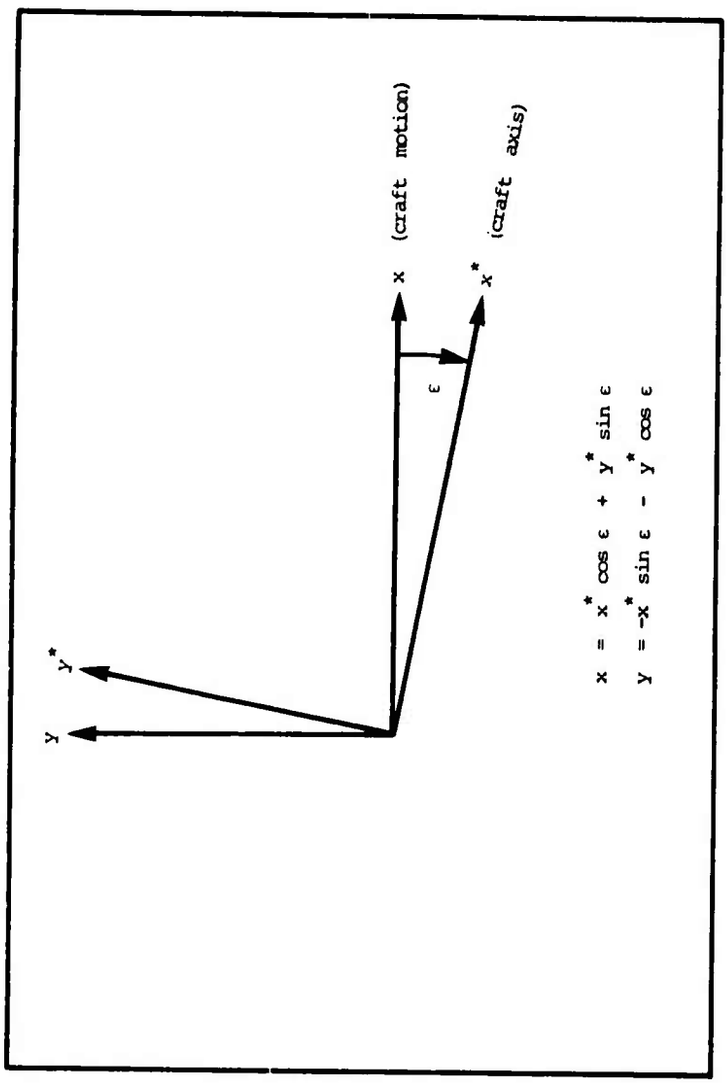


Figure 12. Axis system fixed to craft

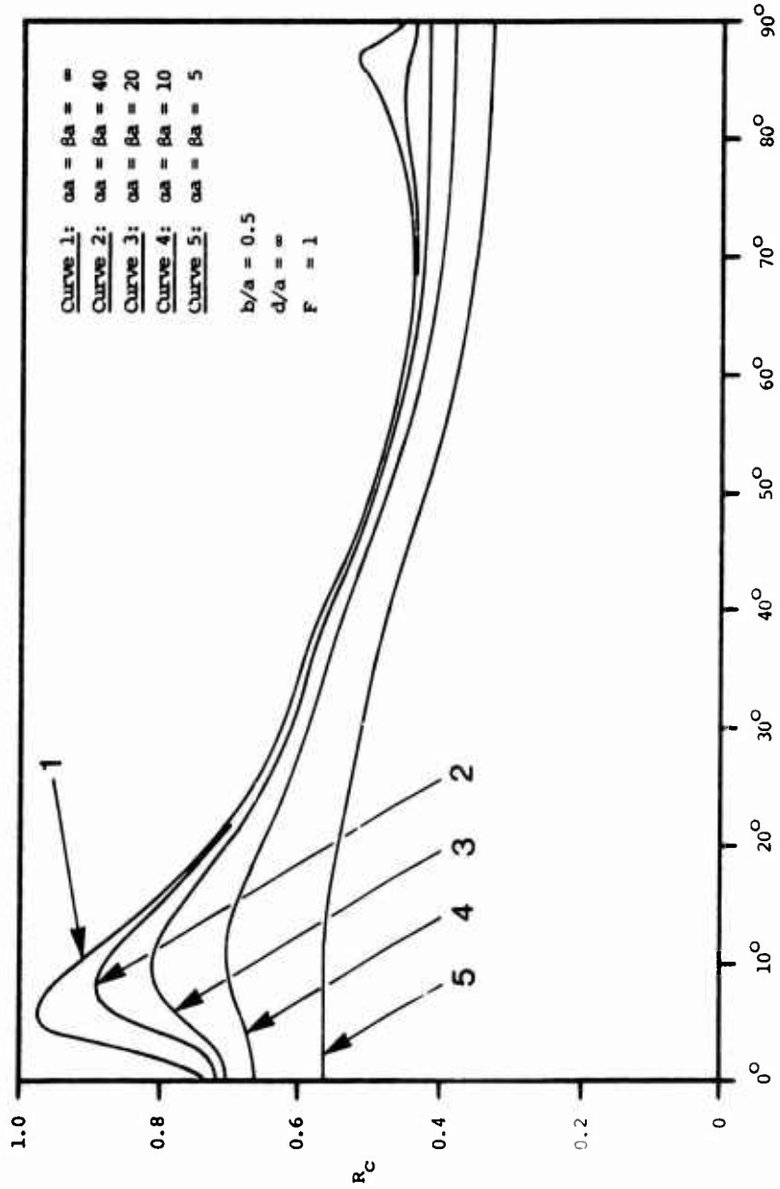


Figure 13. Wave resistance in deep water while yawed, (a) for different amounts of smoothing

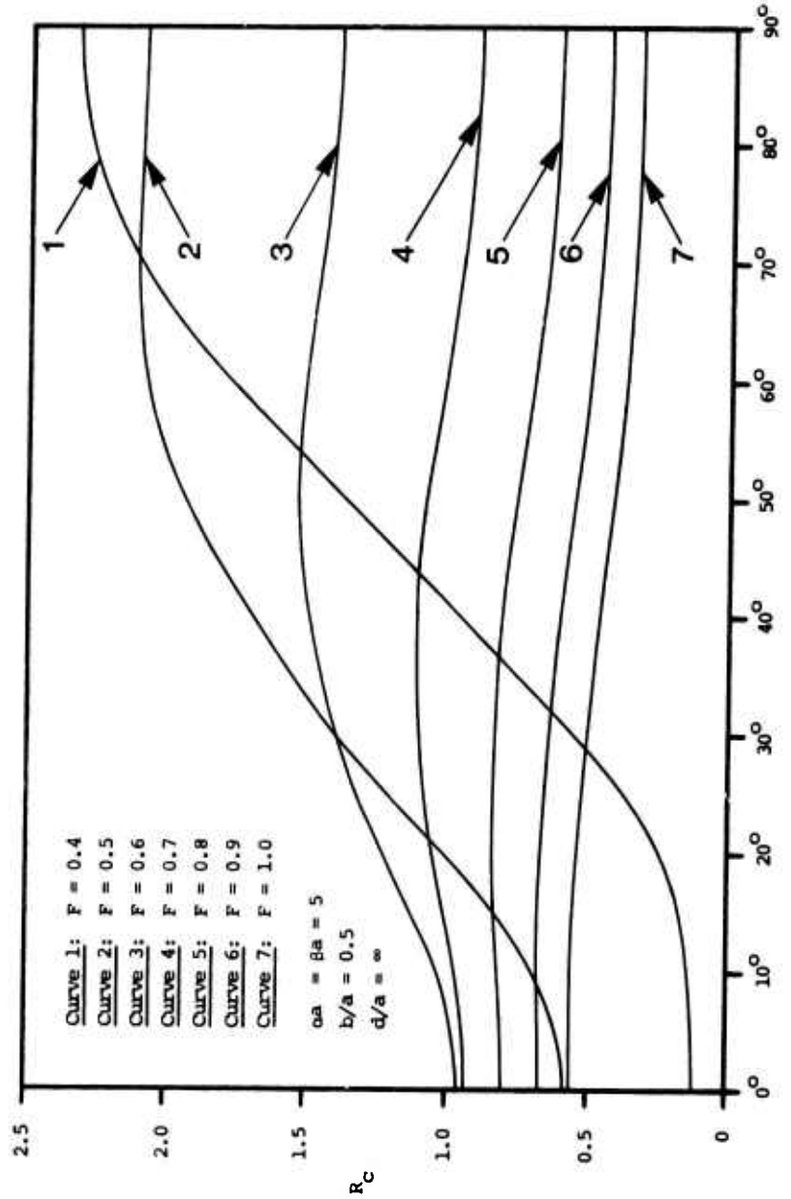


Figure 13. (Cont.) (b) for different Froude numbers

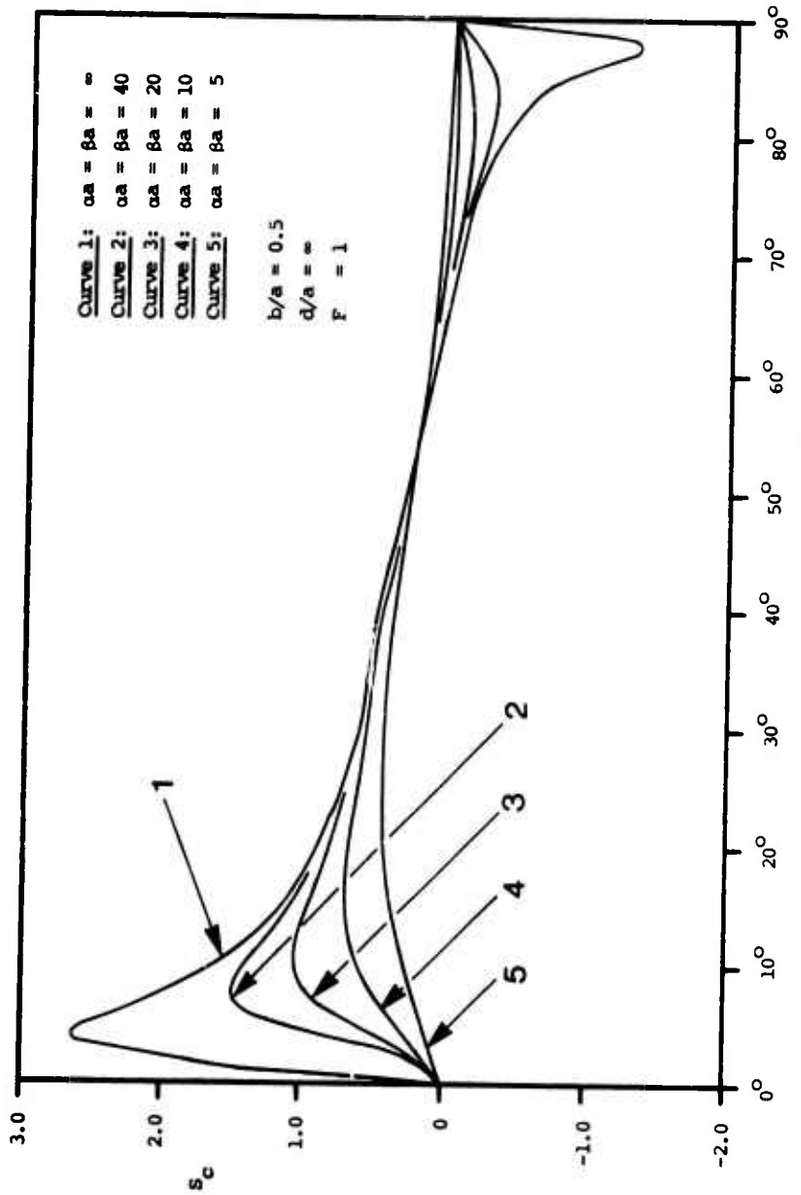


Figure 14. Side force in deep water while yawed, (a) for different amounts of smoothing

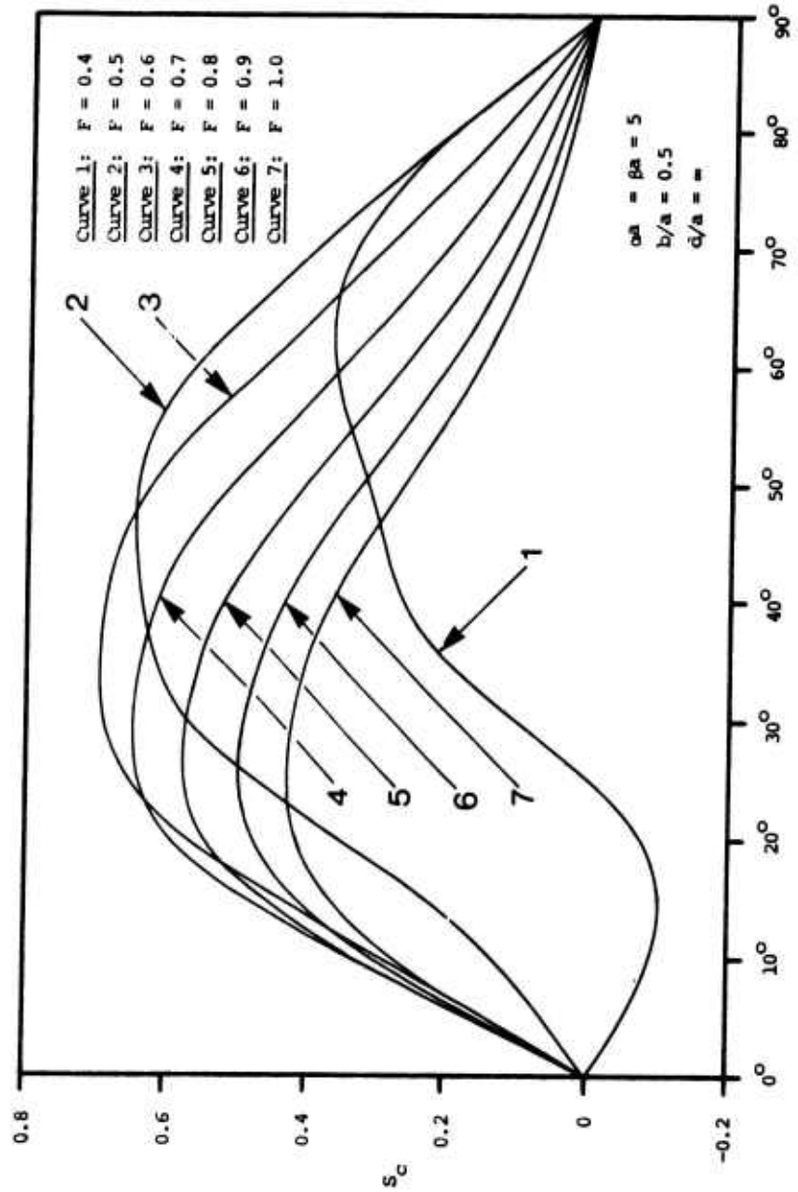


Figure 14. (Cont.) (b) for different Froude numbers

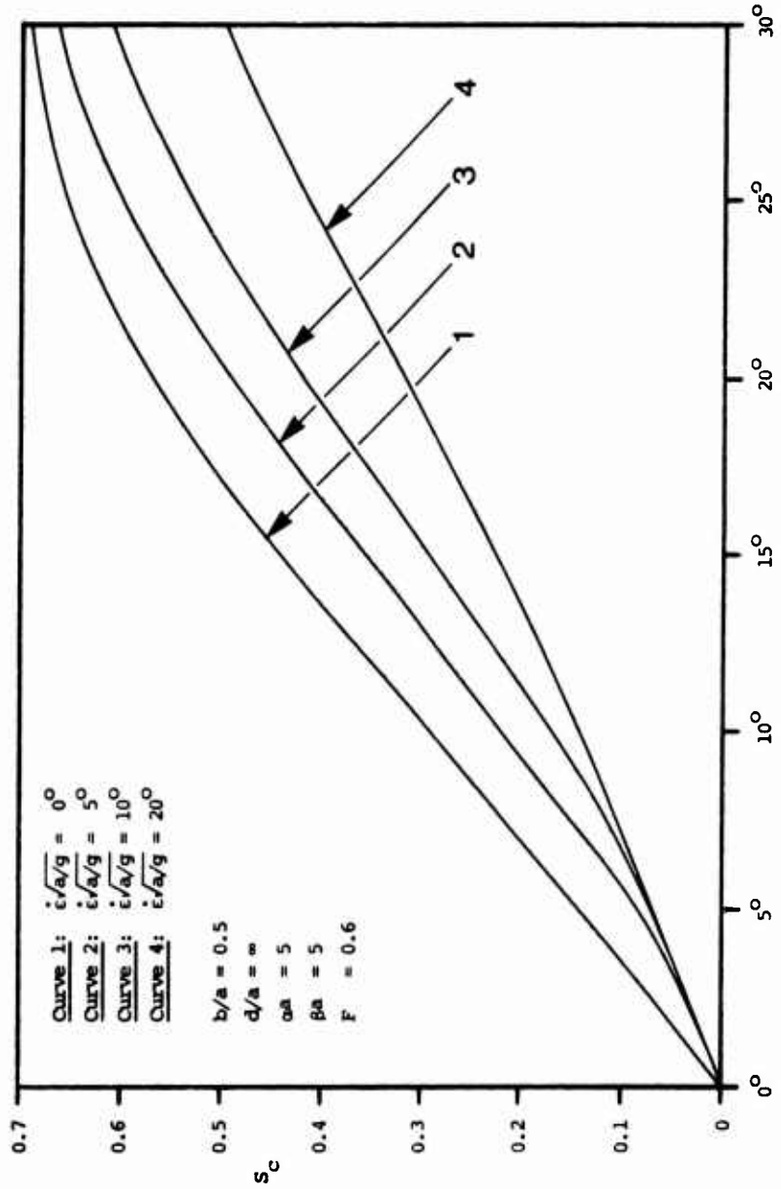


Figure 15. Unsteady side force in deep water while yawing, (a) F = 0.6

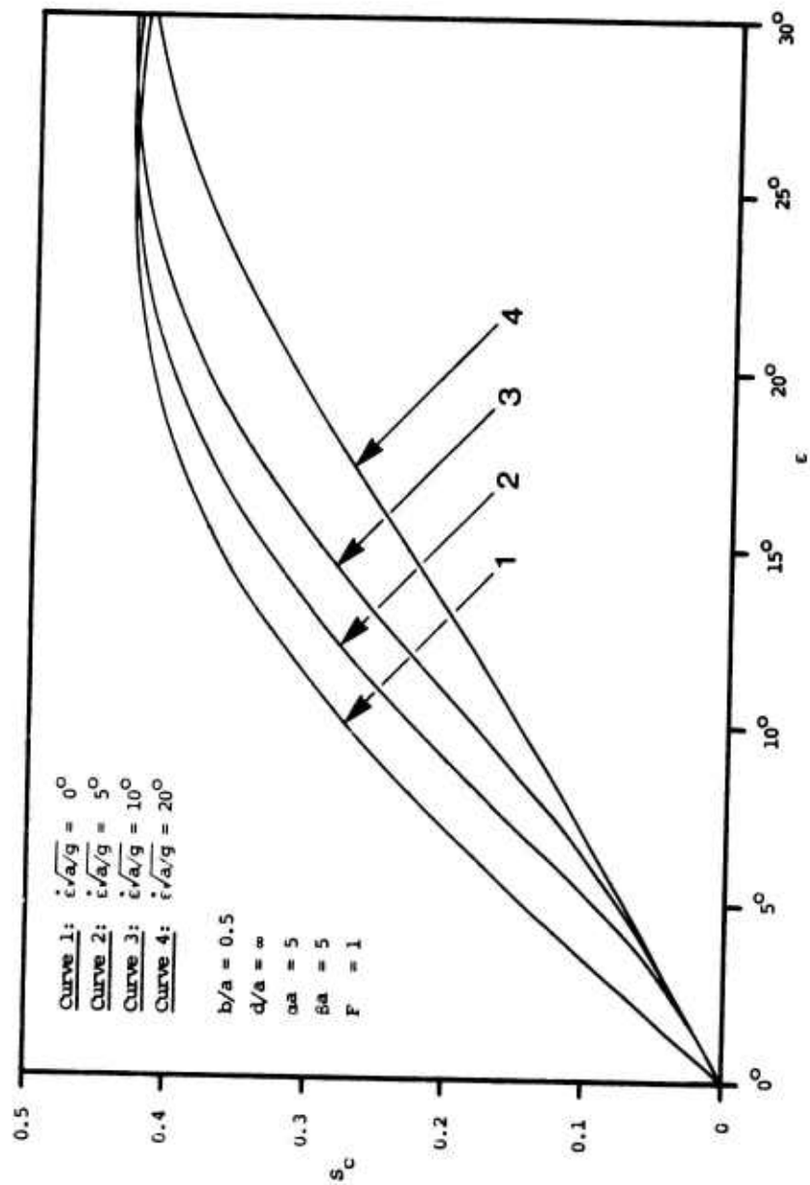


Figure 15. (Cont.) (b) F = 1.0

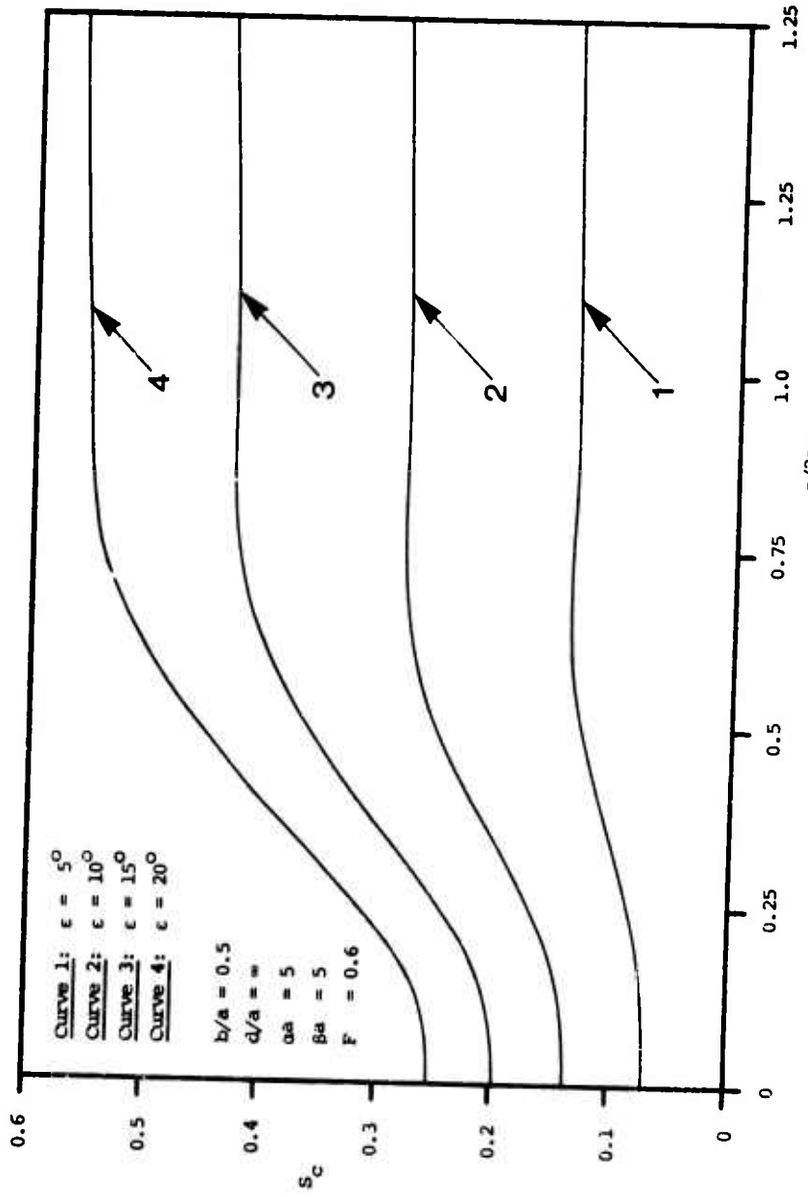


Figure 16. Unsteady side force in deep water after a step change in yaw angle, (a) F = 0.6

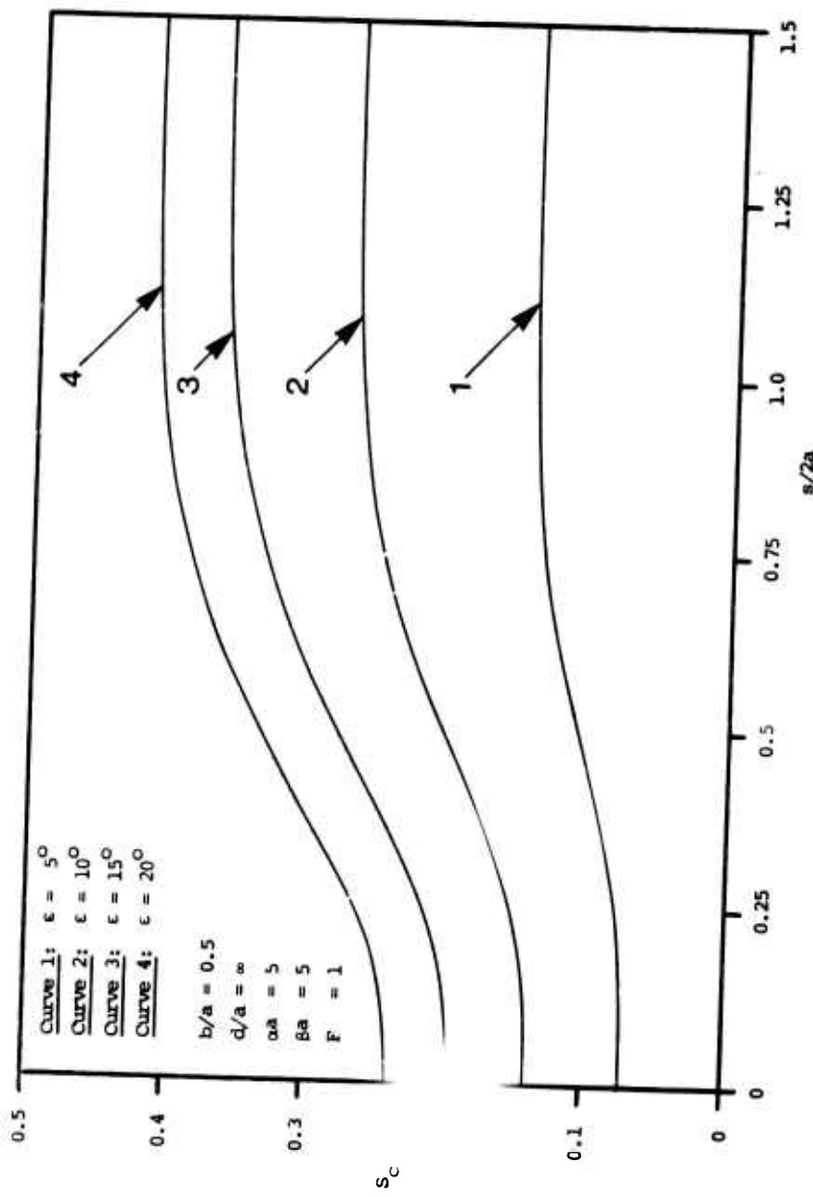


Figure 16. (Cont.) (b) F = 1.0

DISCUSSION

Jorgens Strom-Tejsen

Naval Ship Research and Development Center
Bethesda, Maryland, U.S.A.

I should like to take the opportunity to ask Dr Doctors a few questions about the work he has carried out. Dr Doctors has shown in his paper that by smoothing the pressure distribution some of the very pronounced humps and hollows in the resistance curve disappear. This is the case in particular at the lower Froude numbers, whereas at the higher Froude numbers the last hump seemed to have been affected very little. I would like to ask Dr Doctors if he has any similar experience when rounding the corners of the surface of a big shift ? One would expect that rounding the corner, actually using the right angle, a pressure platform would be round the corner, and in a similar way the humps and hollows at the lower Froude numbers would disappear.

This brings me to another question. Actually, the linearised wave resistance theory being used, we can only expect it to be accurate at the highest Froude numbers, whereas going down to the lower Froude numbers, on the assumptions we make, namely, that the wave slope is low is not valid any longer. Has it any importance at all, this smoothing or rounding away of the corner ? If this is not so at the lower Froude numbers, the wave resistance theory would not hold at all any how.

We saw some rather interesting figures showing the effect when the surface effect shift was at the yaw angle or drift angle. In some cases the side force was negative and in other cases it was positive. This means that in certain cases the surface effect shift would heel to one side and in other cases it would heel to the other side. I wonder if Dr Doctors could clarify this sine convention, and give us an idea about whether it is heeling away, or in what way it is heeling, relative to the drift angle he has been using.

Finally, I would like to indicate that at the Naval Ship Research and Development Center we have made some somewhat similar computations, using pressure distribution, not smooth but actually using a staircase variation so that the pressure distribution is varied from

its full value down to a zero value in a staircase fashion rather than in a smooth way. We found, in the same way as in Dr Doctors' case, a certain effect at lower Froude numbers and very little effect at higher Froude numbers. Again, it appeared that it is only in the case of using a very large smoothing area that it had any real effect. I wonder if Dr Doctors could comment on what the alpha and beta really mean in physical terms ?

REPLY TO DISCUSSION

Lawrence J. Doctors
University of New South Wales
Sydney, Australia

I thank Dr. Strom-Tejsen for his questions. In answer to the first question regarding the shape of the planform, I have not made numerical studies of this parameter myself. Other workers, mentioned in the paper, have studied shapes which include elliptical and triangular ones. At high Froude numbers (i. e. in the region of the hump speed, and above), smoothing of the planform shape has a similar effect to decreasing the rate of pressure fall-off at the edges. That is, the wave resistance is reduced a little. These two types of smoothing have, however, different effects at low Froude numbers.

For example, the sharp-edged rectangular distribution has a wave resistance coefficient which oscillates between 0 and 2 at asymptotically low speeds, while the smooth rectangular distribution has a resistance which approaches zero (see Fig. 3). On the other hand, the wave resistance coefficient of a sharp-edged circular area appears to have a behaviour somewhat intermediate to these two (see Barratt (1965)).

With regard to the second question, the limitation to the application of the linear theory is basically the slope of the waves generated by the pressure distribution. Thus, for typical ACV's, only the main or secondary hump have been realised in practice. On the other hand, by using models with a smaller nominal pressure (more precisely : $p_o/\rho ga$), more low speed humps and hollows may be measured. My thesis supervisor at the University of Michigan, Dr. S. D. Sharma, initially suggested the method of smoothing in the manner described. We found that smoothing in the transverse direc-

tion has very little effect, and that smoothing in the longitudinal direction, simulated by $\alpha a = 5$, gave reasonable agreement with experimental results. Since this value of αa does not produce an excessively steep wave system (for the usual range of $p_o/\rho ga$), linear theory would be valid in this case. On the other hand, actual measurements of the pressure drop-off indicate that $\alpha a = 40$ (i. e. eight times as smooth) would be more realistic. Thus, we found that nonlinearity and viscous action was the main cause of the discrepancy at low speeds. However, we pursued the use of such large amounts of smoothing, since it gave us an adequate model at low speeds, and allowed us to compute the unsteady wave resistance of an ACV starting from rest.

Finally, with regard to the sign convention during yaw motion; side force on the craft and yaw to starboard were considered positive. In most cases the side force had the same sign as the yaw angle, indicating that this effect favourably aids the turn. In a couple of instances at low speeds, principally subhump speeds, the opposite was true.

* * *

A LINEARIZED POTENTIAL FLOW THEORY FOR THE MOTIONS OF AMPHIBIOUS AND NON AMPHIBIOUS AIR CUSHION VEHICLES IN A SEAWAY

Dr. T. K. S. Murthy
Portsmouth Polytechnic
Portsmouth, U.K.

ABSTRACT

The problem of the motions in a seaway of an ACV supported by an air cushion which is bounded by flexible extensions at the front and the rear and by rigid hulls immersed in the water along the si es is first formulated in the most general sense just to show how impossible it is to obtain a solution without some form of acceptable linearization. Four perturbation parameters are therefore selected relating to the cushion pressure, the width of the side hulls, the amplitude of the oscillations and the slope of the incident waves. The velocity potential for the motion of the side hulls is derived in the form of an integral representation, but it has been found possible to derive only an integral equation for the potential due to the motion of the air cushion. This could, however, be reduced to an integral representation under certain additional assumptions, such as that the side hulls are slender

The steady motion and forced oscillation of the ACV in calm water are first discussed. The expressions for the forces and moment show clearly the separate effects of the air cushion and the side hulls together with the interaction between the two which may enable the optimization of the overall configuration to be made. An investigation of the free oscillation in regular waves yields expressions for the response functions which may

Preceding page blank

be used to obtain an estimate of the motions of the ACV in irregular seas within the limits of the theory of linear superposition.

I - INTRODUCTION AND SUMMARY.

The purpose of this study is to develop ultimately a comprehensive hydrodynamic theory for the general motion of an Air Cushion Vehicle (denoted, in short, by ACV and alternatively referred to as hovercraft) in an arbitrary seaway. This general non-linear problem will be formulated presently and, as may be expected, it will soon become apparent that the solution will have to be carried through in various successive stages, with some form of acceptable linearization adopted at each stage in order to render the mathematical solution tractable and to keep the algebraic work within reasonable bounds. Practical results can, however, be obtained from calculations based on the lower order theory which can be relatively simple and a comparison can then be made with the results of full-scale trials and model test data so that any differences pointing perhaps to a deficiency in the theory may possibly be reconciled by invoking the higher order theory.

In a previous work (1970) the author[1] has considered the case of an "ideal" hovercraft as a starting point for the larger study. This amphibious craft is completely separated from the water surface during its motions and oscillations and was assumed to be travelling under a constant longitudinal thrust at a uniform speed in a unidirectional seaway composed of regular waves with their long crests normal to the direction of motion. Although the hovercraft was assumed to be clear of the water surface, practical expressions for the wave resistance and side force in longitudinal and drifting motion over calm water, the restoring forces and moments due to forced oscillation over calm water and the response functions for free oscillation in a regular seaway have been derived. The effects of the compartmentation of the cushion and the overall cushion stiffness on the motion have also been presented. The mean increased resistance over waves and the added mass and damping of water can also be calculated. In order to keep the algebra simple, the hovercraft was assumed to undergo coplanar motion in the longitudinal plane with freedom in pitch, heave and surge only.

This restriction of the motion to a plane, although not a strict requirement of the linearized theory, was considered as the only type of motion which was likely when the craft was operating for a long

time (long enough for the transients to have died away) in a regular seaway with a uniform speed in a direction normal to the wave crests and also capable of showing the essential features of a more general type of motion. The extension of the theory to longitudinal or drifting motion in a direction oblique to the regular seaway with six degrees of freedom is straightforward and no major revision of the theory is required as the beam/length ratio of present day hovercraft is of the order of unity and the disturbance of the water surface due to the motion of the craft in the longitudinal or beamwise direction may be considered to be of similar order providing that no water contact takes place. The situation therefore is quite different from the case of conventional displacement vessels. Also, the extension of the theory to motion in an arbitrary course such as that during manoeuvering, to accelerated motion in starting from rest and to motion in shallow and restricted off-shore coastal waters can all be undertaken with suitable modification of the results. The prediction of the motion in an irregular, multi-directional, seaway can also be made by the method of spectral analysis on the basis of the theory of linear superposition.

The amphibious hovercraft free from water contact may be considered as a special case of a more general type of ACV which we take up as the subject of our present study. The ACV is now assumed to be borne on air cushion contained by peripheral skirts at the bow and the stern and by the side hulls which extend below the hard structure along the sides of the craft and which remain permanently immersed in the water during the motion and oscillations of the craft (see fig. 1).

It is however, assumed that the flexible extensions do not contact the water surface during the motions and oscillations of the ACV, but an extension of the present theory to take into account skirt contact is straightforward if it is assumed that the flexible extensions are rigid enough to retain their shape when contacting the water. A later extension would be to cover the case of compliance to the pressure of the water.

It is assumed that the air cushion is bounded by thin hulls along the sides and the air jets (or plenum air escape) at the front and the rear. The theory can also be suitably revised to cover the case of hulls (or skegs) which are located inboard of the lateral boundary, the whole air cushion then being enclosed within peripheral skirts. This configuration is sometimes adopted when water propulsion is used. The side hulls are assumed to be "thin" with different "semi-widths" on either side. A vertical plane is sometimes used on the inboard side of the hulls because of the relative simplicity in

production, but we have covered the possibility of having different off-sets on the two hull surfaces on either side of a longitudinal plane. We are, however, assuming that the surfaces on the outer sides of the two hulls and those on the inner sides are respectively of the same shape in order to have lateral symmetry very essential to the motion in a straight line we shall be considering.

The ACV is considered as a freely hovering (but partially floating) rigid body in motion under the action of given external forces (such as those due to wind, propeller thrust, etc.) together with the hydrostatic and hydrodynamic forces arising out of the "ground effect" of the air cushion in depressing the water surface and from the immersed part of the side hulls. The equations of motion for the most general type of motion in six degrees of freedom will include in addition to the external forces and the forces due to ground effect, some types of internal forces peculiar to ACVs, such as momentum drag, forces arising from the uneven escape of momentum due to the leakage of the air cushion through the air curtain at the front and the rear and, possibly, even through the troughs of the induced waves which may make part of the side hulls run dry unless the hulls are of suitable draught. There is also the pneumatic effect of the "wave pumping" of the air in the cushion due to the passage through progressive waves. We shall assume, however, that the only force which enables the uniform translation of the ACV is the longitudinal thrust, leaving due account to be taken of all the other factors when the occasion arises.

In the earlier study, the hovercraft was replaced by its equivalent mathematical model, namely a "travelling pressure disturbance" with a basic "hull form" for the craft dictated by the planform of the air cushion and the two-dimensional distribution of pressure on the water surface consituting the lower boundary of the cushion. All the results were derived on this basis and without enquiring into the actual mechanism employed for the generation and retention of the air cushion, i.e. whether a peripheral jet system or plenum chamber with or without compartmentation was used. This model will be retained for the present study with a separate examination of the effect of the side hulls and the possible interaction between the two.

It may be taken for granted that hull design has arrived at a stage of perfection due to the efforts of naval architects over the centuries, but a basic requirement for developing the hydrodynamic theory of the motions of the composite ACV, i.e. with the air cushion enclosed along the sides by the hulls is a knowledge of the hull form of the air cushion which plays usually the major role in supporting the ACV above the water with a small contribution from the buoyancy of the side hulls. It is commonly assumed for want of a more precise

knowledge that the pressure in the cushion at all points is uniform and that the pressure on the water surface is also uniform and of the same value. This kind of stepped cushion with an abrupt drop between the pressure within the cushion and the ambient pressure outside will have a hull in the form of a right cylinder with vertical sides and, in our case will resemble a rectangular box. It is obvious that this type of hull will be totally unsuitable for a fast planing type of displacement vessel. It will appear during the course of this study that the mathematical work is considerably simplified if it can be assumed that the pressure is diffused continuously from a maximum value at the centre in such a manner that it becomes zero at the boundary and, preferably, with a zero gradient in the direction of motion. The purpose will be equally served if the pressure is uniform in the main part of the cushion and diffused over an annular region close to the boundary. It is interesting to note that this type of diffusion of pressure selected with the object of mathematical expediency in obtaining an easier solution of the problem on hand gives a hull shape for the air cushion with an aesthetic appeal and with a reasonable dead rise and flare at the bow and at the stern which may be considered by the naval architect as very acceptable for planing motions in the displacement mode.

The actual mechanism by which the above pressure distribution may be generated in the case of practical ACVs considered as hardware is merely an engineering matter, although in the present state of the art not much progress has been made in this direction, presumably because no investigation as so far been made as to the direction in which to proceed or, wether it is necessary to proceed in any direction at all towards perfecting a "tailor made" cushion. This could probably be achieved by suitable compartmentation of the cushion and by introducing auxiliary flows in the (supposedly) quiescent air in the cushion. It is only a question of accentuating the entrainment of air and trapped vertices known to exist in the vicinity of the boundary. Assuming that such a manipulation of the pressure distribution is feasible (and there is no reason to doubt this), we are indeed in a fortunate position with hovercraft for without altering the deck space, it seems possible to give the ACV an arbitrary cushion hull shape by a simple manipulation of cushion aerodynamics.

The analytical methods used in this study are essentially those first used in the classic work of Peters and Stoker [2] and later followed by Newman [3][4], Joosen [5] and others. These works constitute a rational approach to the unsteady motion of ships, but a solution has so far been obtained only for thin ships and slender ships.

Peters and Stoker (2) have indeed considered a flat planing type of hull and a yacht type of hull which is a combination of a thin vertical hull and a thin horizontal hull. However, the utmost that has been achieved in these cases is the derivation of integral equations for the potential with singularities at the edges of the hull. No method of solution of the singular integral equations, or even the possibility of a solution has been indicated, as the equations contain singular kernels and are therefore not of the classic Fredholm type.

In the case of an amphibious hovercraft, however, we had managed to derive an explicit integral representation for the potential in the form of a source singularity distribution over the free surface directly below the cushion opening together with a distribution of line sources and line doublets along the boundary of this region. This happy position had come about because the two boundary conditions for this boundary value problem for amphibious hovercraft free from water contact were of identical nature, both relating to the pressure on the free surface, and therefore constituting a Dirichlet problem. In the case of bodies floating on the water surface there is a pressure condition on the free surface not occupied by the floating body, namely that the pressure is constant (taken as zero for convenience) and a velocity condition on the immersed part of the hull, namely that the normal velocity of the hull and of the contiguous water particles are equal. In other words, the flow is tangential to the hull when boundary layer effects are ignored. There are, of course, the usual conditions at infinity and at the ocean bottom. This is therefore a Neumann problem.

In the case of the ACV we are now considering, having an air cushion of the type previously studied but with the addition of a pair of parallel side hulls of arbitrary immersion, the boundary conditions are of a mixed nature. The two pressure conditions for a freely hovering air cushion are still present together with the normal velocity condition for floating bodies just discussed. It will be seen presently that an explicit integral representation for the potential due to the hulls is possible on the assumption that they are "thin" (a common and necessary assumption in the theory of ship motions) and with a sufficiently large separation so that the effects of mutual interference may be ignored. However, it has been found possible only to derive an integral equation for the potential due to the air cushion with the kernel containing the "jumps" in the potential across the boundary. Although the presence of the air cushion does not appear to affect the potential for the motion and oscillations of the side hulls in calm water, the influence of the side hulls on the potential of the air cushion

cannot be ignored by simply setting the parameter representing the width of the hulls equal to zero, for although the wave-making effects of the hulls are thereby eliminated, they nevertheless provide a vertical barrier for the fluid flow. However, on the assumption that the immersion of the side hulls is of a small order (say, of the same order as their width) the integral over the longitudinal planes of the hulls can be ignored and if the cushion pressure is also assumed to be diffused in such a manner that it is zero at the front and rear of the cushion where air leakage occurs, it is possible to obtain a simple integral representation for the potential. This procedure enables practical results to be derived pending a rigorous solution of the integral equation.

The problem is first formulated in the most general terms in Section 2, just to show how impossible it is to obtain a general solution. If the problem is difficult to solve in the case of displacement ships, it will certainly be more so in the case of ACVs, where the laws of cushion aerodynamics relating to ground effect enter with an extremely complicated relationship between the pressure distribution and the relative distance between a point on the hemline of the flexible skirts at the bow and stern and the elevation of the water surface directly below.

It is therefore clear that the problem has to be linearized in a suitable manner if its solution is to be rendered mathematically tractable. The usual method of solution in problems of this nature is the assumption of a basic slenderness parameter representing geometrical restrictions on the body. Thus, for example, in "thin ship" theory, the slenderness parameter is the beam/length ratio which is assumed to tend to zero. Similarly, in "flat ship" theory it is the draught/length ratio and in "slender body" theory both the beam and the draught are assumed to be small compared with the length. These restrictions are necessary for the validity of the linearized theory which assumes that the ship reduces to a thin vertical or horizontal disc or a thin straight line and that it can then have a translatory motion with finite velocity parallel to the plane of the disc or along the longitudinal axis without creating waves of finite amplitude. The squares of the perturbation velocities of the water particles can then be neglected and the problem becomes linear. This then is the objective, namely, that the wave making of the vessel in steady motion shall be negligible. In the case of an amphibious ACV, it would appear that the geometrical dimensions are not directly relevant to the problem so long as the craft is not immersed in the water. It is the cushion pressure, i.e. the total weight of the craft divided by the cushion

area which determines the wave making at any particular speed. A large planform area is therefore desirable (for a given weight) and as the popular value for beam/length ratio of present-day hovercraft is about 2/3, it appears that the geometrical dimensions are to be unrestricted for hovercraft in order so that the theory may be successfully applied.

In the case of a rigid sidewall ACV, the total weight of the craft is usually supported mainly by the air cushion with a smaller contribution of the order of 10% from the buoyancy of the immersed side hulls. We shall select δ as the small parameter representing the thin width of the side hulls and β to denote the smallness of the cushion pressure. We shall not make any a priori assumptions as to the fractional weights supported by the air cushion and by the hulls so that we shall not stipulate the relative orders of magnitude of δ and β . As stated above, the smallness of β is ensured by having a large length and a large beam for the cushion and as the latter implies a wide separation for the hulls the effects of mutual interference between the two hulls may be considered negligible. The solution of the problem therefore becomes easier. At a later stage we may have to stipulate that the draught of the hulls should also be small (thus, in effect, treating them as slender hulls) so that an integral representation for the cushion potential may be derived from the integral equation. This stipulation makes the buoyancy contribution from the side hulls to the support of the ACV of a smaller order than the "cushion lift" and is probably in keeping with present-day practice.

The other two parameters selected are those indicating the smallness of the oscillations of the ACV and the small slope of the incident wave. Having selected these perturbation parameters, the procedure would be to expand all the physical variables relating to the motion of the fluid, the boundary conditions and the motion of the ACV in terms of these parameters. Perturbation expansions are thus obtained in the form of a series comprising powers of the perturbation parameters and when terms of the same order are collected together, the result is a sequence of linear boundary-value problems which are, in the general case, more readily solved because the boundary conditions can then be imposed on fixed domains. Thus, for example, the free surface boundary conditions can be satisfied on the known plane $z = 0$ instead of the unknown surface $z = \zeta$.

On the basis of the equations of motion developed in Appendix III of Reference 1, expressions for the forces and moments are derived in Section 5 in the form of surface integrals over the steady posi-

tion of the lower boundary of the cushion on the undisturbed water surface and over the steady position of the longitudinal planes of the hulls below the load water plane. Some of the expressions also include a line integral along the load waterline of the hulls. These expressions may appear very complicated, but they could be progressively simplified when the air cushion has longitudinal symmetry (as well as lateral symmetry, which is implied throughout this analysis) and when the cushion pressure is taken to be strictly uniform throughout the cushion (as is commonly assumed) or when the pressure is diffused to zero at the boundaries along the front and the rear and particularly for a rectangular cushion. The surface integrals over the hull can be expressed in closed form when the hulls are mathematically defined and, particularly, when they are "polynomial simple ships". However, with the advent of present-day high speed computers the solution from a general table of off-sets need not present any serious problems.

The steady motion of an ACV in calm water is discussed in Section 6. Expressions have been derived for the sinkage and trim, for the wave resistance in longitudinal motion and for the side force on a drifting amphibious ACV. As may be expected, the expression for the wave resistance combines with exact agreement the well-known Michell integral for the wave resistance of a thin ship and the result for a surface pressure distribution given by Havelock [6]. In addition we have derived for the first time two additional terms denoting respectively the interference of the air cushion on the side hull and that of the side hulls on the air cushion.

The above expressions involve the steady potential for motion in calm water derived in Appendix V. The potential for the motion of the side hulls is given in the form of an integral representation, but the potential of the air cushion is given by an integral equation in the form of a source distribution on the free surface of water directly below the cushion opening in its steady position and a distribution of line sources and line doublets oriented longitudinally along the boundaries at the front and the rear of strength equal respectively to the "jump" in the velocity and "jump" in the potential itself across the boundaries. The line distribution may however be ignored in the case of a diffused cushion. We have also, in addition, a distribution of doublets oriented laterally along the longitudinal planes of the two side hulls with strength equal to the "jump" in the potential across the planes. Pending a rigorous solution the resulting integral equation (if possible at all), the surface integral over the longitudinal planes may be ignored if the immersion of the hulls is considered to be small

for then the integral will be of a higher order. The expression for the interference potential, namely, the potential representing the interference between the air cushion and the side hulls have not been derived here, as it is only required in the higher order theory, but a brief sketch of the method of its solution is indicated in Appendix V.

The restoring forces and moment acting on ACV which is forced to oscillate in calm water are discussed in Section 7. In the lowest order they contain inertial and hydrostatic terms only as the dynamic pressure of the water represented by the steady and unsteady potentials enter only in the higher order. The expression for the higher order forces and moment could be used for the calculation of the mean increased wave resistance due to the oscillations and the added mass and damping of water by the appropriate combination of the real and imaginary parts of the oscillatory potentials with those of the oscillatory displacements.

The free oscillation of an ACV moving with uniform speed into a regular train of sinusoidal waves is discussed in Section 8. The lowest order exciting forces and moment are again of a hydrostatic nature. The pitch and heave response functions can be obtained from the expressions presented in this section so that a statistical prediction of the performance of the craft in an irregular seaway can be made if it can be assumed that the behaviour of the craft is linear in small waves. There appears to be no positive experimental evidence in this respect at the moment.

The accelerations in surge, heave and pitch which can be calculated from the expressions derived in Section 8 will combine together in different forms at various locations in the craft and dictate the level of passenger comfort at that point during a ride in a seaway. The optimization of the shape of the side hulls could be carried out by well established methods, but it would be interesting to ascertain the effect of different shapes for the cushion hull on the motions and accelerations.

The potentials representing the disturbance of the incident waves by the side hulls (the diffracted wave) and the corresponding potential representing disturbance by the air cushion have not been derived here. These potentials enter only in the higher order forces and moment, but they will have to be derived if the added mass and damping of water, the mean increased resistance in waves and other similar quantities are to be calculated.

The neglect of these potentials here is tantamount to invoking the classic Froude - Kriloff hypothesis, namely that the waves affect the ACV, but that the ACV does not affect the waves. Sufficient information regarding the motion of the ACV can, however, be gathered by studying the lowest order forces.

The theory presented here is concerned solely with the hydrodynamic contribution to the motions of the ACV which is translating in a straight line with a uniform speed V under the action of a constant thrust T. Other internal and external forces could also be taken into account with a suitable modification of the results. A typical quantity for inclusion will be the pneumatic effect of the wave-pumping of the air cushion by the progressive waves.

This theory must also be used with caution in dealing with the actual motion of ACVs over water. In order to satisfy the assumptions made in linearizing the problem, the results can be only applied when the cushion pressure is low and the side hulls thin. Extrapolation of these results with the object of predicting the motions in an irregular seaway has also to be done with care since there is no positive experimental evidence to show that ACV motions are not non-linear.

Although the expressions for the potentials and the forces and moment derived here appear to be extremely complicated, their solution by numerical methods with the use of present-day high speed digital computers need not present any serious problems. It is very likely that the new technique provided by the Finite Element Method (FEM) may prove to be a very useful and powerful tool in this respect and particularly for the solution of the singular integral equations. This is being investigated.

II. GENERAL FORMULATION OF THE PROBLEM

We start with the consideration of the general case of an ACV moving on the surface of water at a mean speed V in its course, which is defined as the vertical projection of the path of the centre of gravity of the craft on the undisturbed surface of water. We may also assume that the ACV has a small angular velocity ω about a vertical axis.

II. 1 Co-ordinate Systems

Three rectangular co-ordinate systems are employed. The first is a fixed system, or inertial frame of reference (X, Y, Z), with the X, Y- plane in the horizontal position of equilibrium of the undis-

turbed free surface of water and the Z-axis taken vertically downwards. The second is a moving co-ordinate system (x, y, z) with the x, y-plane coinciding with the X, Y-plane, i. e. also lying in the undisturbed free surface and the x-axis having the instantaneous direction of the horizontal component of the velocity of the C. G. The x-axis is therefore along the tangent to the course of the craft. The z-axis is taken positive downwards and contains the C. G. (on the negative side, in the case of ACVs). As we have assumed that the ACV has an angular velocity in the horizontal plane, the x-axis will be continually rotating away from the X-axis (see figure2).

A third co-ordinate system fixed in the ACV and moving with it will be introduced in the next section.

The following equations for the transformation of co-ordinates from the (X, Y, Z) system to the (x, y, z) system and vice versa are easily derived :

$$X = X_G + x\cos\alpha - y\sin\alpha \qquad x = (X - X_G)\cos\alpha + (Y - Y_G)\sin\alpha$$

$$Y = Y_G + x\sin\alpha + y\cos\alpha \qquad y = (Y - Y_G)\cos\alpha - (X - X_G)\sin\alpha$$

$$Z = z \qquad z = Z \qquad (1\text{-}1)$$

where X_G and Y_G are the co-ordinates of the C. G. in the fixed system and α is the angle by which the x-axis has rotated from the X-axis at any instant.

$$\text{i. e.} \qquad \alpha = \int_0^t \omega(\tau)\, d\tau \qquad (1\text{-}2)$$

II. 2 Laplace's Equation

The water is assumed to be inviscid and incompressible. It is also assumed to be incapable of sustaining surface tension so that the pressure of the water particles on the free surface may be equated directly to the air pressure thereon. There exists therefore a velocity potential for the motion of the water $\Phi(X, Y, Z{:}t)$ satisfying Laplace's equation

$$\nabla^2 \Phi \equiv \Phi_{XX} + \Phi_{YY} + \Phi_{ZZ} = 0$$

in the domain occupied by water, i.e. for all $Z > 0$ in the case of deep water of infinite extent or in the domain

$$d(X, Y) > Z > 0$$

in the case of shallow water of infinite extent.

In the moving co-ordinate system the velocity potential may be written

$$\bar{\Phi}(X, Y, Z : t) = \bar{\Phi}(X_G + x\cos\alpha - y\sin\alpha,\ Y_G + z\sin\alpha + y\cos\alpha,\ z;t)$$

$$= \phi(x, y, z;t), \text{ say.}$$

It is then easy to derive from (1-1) the following equations for the transformation of various derivatives between the two systems :

$$\bar{\Phi}_X = \Phi_x \cos\alpha - \Phi_y \sin\alpha, \quad \bar{\Phi}_{XX} = \Phi_{xx}\cos^2\alpha - 2\Phi_{xy}\sin\cos\alpha + \Phi_{yy}\sin^2\alpha$$

$$\bar{\Phi}_Y = \Phi_x \sin\alpha + \Phi_y \cos\alpha, \quad \bar{\Phi}_{YY} = \Phi_{xx}\sin^2\alpha + 2\Phi_{xy}\sin\alpha\cos\alpha + \Phi_{yy}\cos^2\alpha$$

$$\bar{\Phi}_Z = \Phi_z \qquad \bar{\Phi}_{ZZ} = \Phi_{zz} \tag{1-3}$$

so that

$$\left[\nabla\bar{\Phi}(X, Y, Z;t)\right]^2 = \left[\nabla\Phi(x, y, z;t)\right]^2 \tag{1-4}$$

and

$$\nabla^2\bar{\Phi}(X, Y, Z;t) = \nabla^2\Phi(x, y, z;t) \tag{1-5}$$

It follows that Φ is a harmonic function in the (x, y, z) system in the same way as $\bar{\Phi}$ is un the (X, Y, Z) system.

II. 3 Bernoulli's Equation

The compressibility of water may be ignored even at the high speeds attained by ACVs at present and we may write Bernoulli's law as

$$\frac{p}{\rho} - gZ + \frac{1}{2}\left[\nabla\Phi\right]^2 + \Phi_t = \text{constant} \qquad (1\text{-}6)$$

where the constant on the right-hand side is independent of the space variables and, as is usually done, may be set equal to zero, it being understood that Φ_t is suitably adjusted.

Now, Φ_t can be expressed in a manner similar to the other derivatives in (1-3) as

$$\Phi_t = (\omega y - V)\Phi_x - \omega x \Phi_y + \Phi_t \qquad (1\text{-}7)$$

where the speed V of the ACV in its course is an arbitrary function of the time for accelerating motion.

The relation between the pressure $p(x, y, z;t)$ and the velocity potential $\Phi(x, y, z;t)$ may therefore be written

$$\frac{p}{\rho} - gz + \frac{1}{2}(\nabla\Phi)^2 + (\omega y - V(t))\Phi_x - \omega x \Phi_y + \Phi_t = 0 \qquad (1\text{-}8)$$

II. 4 Conditions on Boundary Surfaces

If $F(X, Y, Z : t) \equiv f(x, y, z;t) = 0$

is a boundary surface, which may be fixed or moving, the kinematic condition on such a surface is

$$\frac{dF}{dt} \equiv \Phi_X F_X + \Phi_Y F_Y + \Phi_Z F_Z + F_t = 0$$

Using the relations (1-3) and (1-7) the corresponding condition in the (x, y, z) system becomes

$$\Phi_x f_x + \Phi_y f_y + \Phi_z f_z + (\omega y - V) f_x - \omega x f_y + f_t = 0 \qquad (1\text{-}9)$$

The free surface of water given by the equation

$$z - \zeta(x, y;t) = 0$$

is a boundary surface, fluctuating with respect to time, and the kinematic condition on this surface may therefore be written

$$\Phi_x \zeta_x + \Phi_y \zeta_y + \Phi_z \zeta_z + (\omega y - V)\zeta_x - \omega x \zeta_y + \zeta_t = 0 \qquad (1\text{-}10)$$

to be satisfied for $z = \zeta$. This condition applies both to the external free surface (EFS) and the internal free surface (IFS) defined and discussed in the Introduction.

The dynamic conditions on the free surface $z = \zeta$ are obtained from (2-8) by setting $p = 0$ for the EFS and $p = p_s(x, y)$, the surface pressure applied by the air cushion on the IFS, respectively.

The kinematic condition (1-9) is also applicable to the instantaneous position of the moving (and oscillating) side hulls of the ACV and to the lower edges of the flexible extensions immersed below the surface of water.

II. 5 The General Non-Linear Problem

The strict formulation of a very general type of ACV problem would be on the following lines. A rigid body in the form of an ACV is supported above the water surface partly by the air cushion (containing air at a pressure higher than atmospheric) and partly by the buoyancy of the immersed part of the side hulls. In the position of "static hovering", i.e. at zero speed ahead, the steady pressure applied by the air cushion to the IFS may be assumed to have a distribution of the form

$$p_s = p_o(x, y)$$

over a region S_o of the water surface which is the vertical projection of the cushion opening on the water surface. This region is therefore bounded by the inner sides of the side hulls and the curves representing the vertical projection of the hemline of the skirts at the bow and at the stern. The "cushion hull form" is thus determined by the plan form of S_o and the pressure distribution thereon. It may be assumed as an approximation that the latter is unaltered during steady forward motion in the horizontal plane. However, the water surface will now be disturbed due to the generation of surface waves by the air cushion and by immersed side hulls (with perhaps a complicated kind of coupling between the two as will be shown later). The steady disturbance will travel with the same speed as the ACV but will cause a steady variation of the shape of the IFS i.e. of the cushion hull form. If the ACV now performs oscillations during steady translation, which may be forced oscillations in calm water or wave excited oscillations in a seaway, the pressure distribution on the water surface will no longer be steady or of the basic form. This is because the region S over which the pressure is apllied is now a fluctuating domain, as it is the instantaneous position of the vertical projection of the cushion opening

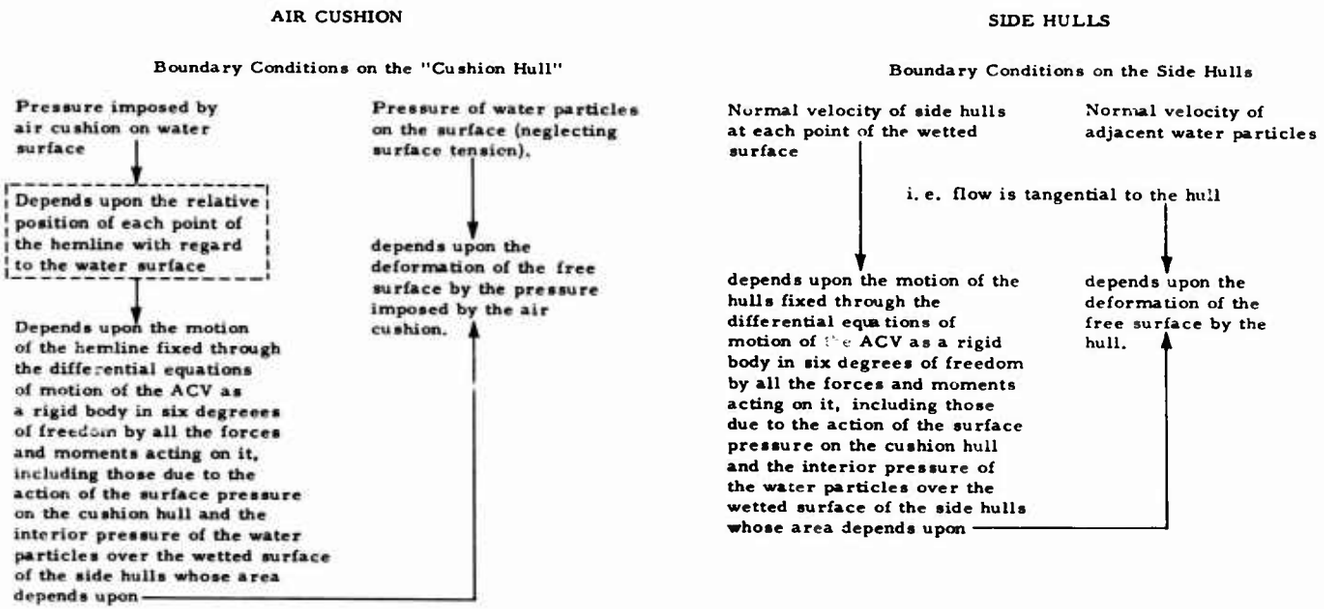
on the water surface and its shape and location in space will be therefore dependent on the oscillations of the craft in all modes expect, perhaps, in heave. The actual pressure distribution during oscillations will also be different from the basic distribution on account of the cushion and peripheral jet (or plenum chamber) characteristics peculiar to hovercraft which dictate the pressure in the cushion in terms of the local clearance between any point of the periphery and the elevation of the water surface directly below it. In our case, the pressure variations will be initiated in annular regions adjacent to the bow and stern skirts, but the perturbation pressures will no doubt be transmitted to the interior due to induced flows and entrainment of external air with the result that the distribution over the entire region may be substantially altered.

The basic problem is essentially that of determining the velocity potential $\Phi(x, y, z; t)$ as a harmonic function satisfying Laplace's equation in the domain $z \geq \zeta(x, y; t)$ for all time $t > 0$ when the initial position and velocity of the ACV and of the water particles are prescribed at time $t = 0$. A singularity has to be accepted for the solution of Φ at the boundary of the region S if the applied pressure is discontinuous there, i.e. if the pressure is different from atmospheric. The velocity potential can be used to calculate the elevation and slope of the IFS on which the pressure is applied by the air cushion. The forces and moments on the ACV considered as a rigid body are in part due to the action of the applied pressure on the IFS which is the cushion hull and can therefore be determined in terms of the applied pressure and the slope of the disturbed water surface. It is appreciated that in common with other surface wave problems the elevation and slope at individual points of the region S cannot be determined accurately from the potential due to interference effects although the evaluation will be corrected at some distance away from the pressure field. However, we only require the total integral effect of the applied pressure and for this purpose the potential can be used to obtain practical results.

The other contribution to the forces and moments on the ACV arises from the action of the pressure of the water particles acting on the instantaneous position of the immersed portion of the side hulls. The boundary conditions dictate that the relative velocity of the water particles at each point in a direction normal to the instantaneous position of the oscillating side hulls is zero. The pressure on the free surface is also prescribed as zero. But both the immersed hulls and the free surface of water are moving boundaries of the domain in which the velocity potential is to be determined. A coupling between the motion of the side hulls and that of the water therefore exists. As

stated above, this coupling between the motion of the ACV and that of the water introduces an additional complication in the case of the air cushion due to the laws of cushion aerodynamics.
Also, the IFS is a moving boundary on which the potential is to be determined.

This complicated situation is illustrated in the block diagram below


AIR CUSHION
Boundary Conditions on the "Cushion Hull"
Pressure imposed by air cushion on water surface
Depends upon the relative position of each point of the hemline with regard to the water surface
Depends upon the motion of the hemline fixed through the differential equations of motion of the ACV as a rigid body in six degreees of freedom by all the forces and moments acting on it, including those due to the action of the surface pressure on the cushion hull and the interior pressure of the water particles over the wetted surface of the side hulls whose area depends upon
Pressure of water particles on the surface (neglecting surface tension),
depends upon the deformation of the free surface by the pressure imposed by the air cushion.
SIDE HULLS
Boundary Conditions on the Side Hulls
Normal velocity of side hulls at each point of the wetted surface
Normal velocity of adjacent water particles
i.e. flow is tangential to the hull
depends upon the motion of the hulls fixed through the differential equations of motion of the ACV as a rigid body in six degrees of freedom by all the forces and moments acting on it, including those due to the action of the surface pressure on the cushion hull and the interior pressure of the water particles over the wetted surface of the side hulls whose area depends upon
depends upon the deformation of the free surface by the hull.

It is clear from the above that the situation in respect of the ACV leads to a very complicated non-linear problem. The position of the free surface is not known a priori and the velocity potential has therefore to be determined in a fluctuating and unknown domain. The boundary conditions are of a mixed type. These relating to the air cushion are stipulated in terms of pressure and those relating to the side hulls in terms of velocity. Appropriate boundary conditions at infinity may be imposed from physical considerations in order to obtain a unique solution of the problem, but it is doubtful whether this general non-linear problem will be mathematically tractable. It will be observed that the motions of the ACV are not given in advance (except in the case of forced oscillations of a pre-determined kind), but are unknown functions of the time to be determined as part of the solution. The motions vary the pressure distribution on the IFS and therefore dictate the appropriate elevation slope of the water surface which together with the pressure distribution determine the forces and moments on the ACV due to the air cushion. Similarly, the motions vary the wetted surface of the side hulls and the pressure of the water particles both of which determine the forces and moments due to the side hulls. This highly non-linear problem has therefore to be linearized in a suitable manner if a practical solution is to be achieved and this we shall endeavour to do in the next section.

III. THE LINEARIZED PROBLEM

As the general non-linear problem has been shown to be highly complicated, we shall not attempt the solution of the single boundary value problem, but consider instead a sequence of linear boundary-value problems which result when all the relevant physical variables relating to the motions of the ACV and of the water are expanded in terms of say, four small perturbation parameters, δ , β , α and ϵ , describing respectively the orders of magnitude of the width of the side hulls, the cushion pressure, the amplitude of the unsteady motions and the slope of the incident waves in the regular seaway. The reasons for the choice of these parameters are explained in the Introduction.

The solution of the sequence of linear boundary-value problems is relatively simple and all relevant quantities determining the motion are obtained in the form of a power series in the perturbation parameters. An approximate solution of the general non-linear problem can thus be obtained up to any desired degree of accuracy.

We shall now consider the problem of an ACV that has been operating at sea for a long time under a constant propulsive thrust. This problem is simpler and more of practical interest than that where the ACV starts from rest and moves over water under the action of given forces, such as these due to wind, control setting, etc., in an arbitrary seaway. After the lapse of a sufficiently long time, all the transients would have disappeared, and if the propulsive thrust is the only force acting on the ACV, it would be moving at a steady speed of translation. The linear displacement of the centre of gravity of the ACV from its equilibrium position of steady translation may be represented by components along three axes fixed in the craft (this system of axes will be described presently), namely, surge, sway and heave. Similarly, the angular displacements of the craft may be represented by components along these axes, namely, roll, pitch and yaw. It is expected that each component of displacement will consist of two terms, one independent of time and representing the steady displacement that would exist during motion with uniform velocity in calm water and the other an oscillatory term simple harmonic in the time due to the excitation by the incident waves coming from infinity. If the ACV is symmetrical about a longitudinal axis, it may be expected that the motion in calm water will produce non-zero displacements only in pitch and heave (and, possibly, in surge, which is trivial, since the steady surge displacement can be absorbed in the forward motion). The complete solution of our linearized problem depends then on the determination of the forward speed for a given thrust (or thrust required for a given forward speed), the steady pitch and heave displacements (usually known as trim and sinkage) and the six oscillatory components of displacement.

An irregular, but long crested, seaway may be assumed to be composed of a system of simple harmonic progressive waves, each of a given frequency. Any irregular wave train may therefore be expanded as a Fourier series with respect to time. In the linearized theory, we may assume that the ACV responds to each wave component as though it existed independently of the others. By the theory of linear superposition the motion of the ACV will be composed of the same Fourier components. Similarly, in the case of forced oscillation in calm water, any arbitrary type of oscillation may be represented by a Fourier series with respect to time. It is therefore only necessary to consider a single sinusoidal component for our solution. The results can then be generalised by spectral analysis.

We shall presently be expanding all the physical variables describing the motion of the ACV and that of the water in powers of the perturbation parameters. Taking the velocity potential of the water as an example, the correct expansion would be

$$\Phi(x, y, z; \delta; \beta; \alpha; \epsilon; t) = \mathrm{Re} \sum_{k, l, m, n, p} \delta^k \beta^l \alpha^m \epsilon^n e^{i\sigma pt} \Phi_{klmn}(x, y, z)$$

Corresponding to excitation by waves with frequencies

$$\sigma, 2\sigma, 3\sigma, \text{------}$$

However, as the algebra will become extremely complex, the whole solution can first be carried through for one frequency component with say, $p = 1$. The final result can then be extended to any number of Fourier components in the wave system. It may be observed in this connection that in simulating an irregular seaway in a towing tank a finite number (of the order of ten) Fourier components is usually selected. In this case, when we desire a verification of the theory from experimental results, the solution should cover the same number of Fourier components.

III. 1 Coplanar Motion

The analysis will be restricted to a study of the ACV moving in a longitudinal plane. This is by no means a requirement of the linearized problem, but this simpler study will reveal clearly the general features of arbitrary motion in all six degrees of freedom.

III. 2 Body-fixed Axes

The third co-ordinate system mentioned in section II. 1 is the (x', y', z') system fixed in the ACV. The origin o' coincides with the origin o of the moving system when there are no oscillations. Also, the z'-axis (like the z-axis) contains the C.G. (on the negative side) and the x', z'-plane (like the x, z-plane) is the fore-and-aft plane of lateral symmetry of the ACV.

It is clear that the x', y'-plane is the load waterplane (LWP) of the side hulls when the ACV is on its air cushion.

All the three systems of axes are illustrated in Figure 2.

III. 3 Transformation of Co-ordinates

It is easy to derive the following equations for the transformation of co-ordinates between the moving system (x, y, z) and the body-fixed system (x' , y' , z').

$$x = \bar{x} + x' \cos\theta + (z' - z_G) \sin\theta \qquad x' = (x - \bar{x}) \cos\theta + (\bar{z} + z_G) \sin\theta$$

$$y = y' \qquad y' = y$$

$$z = \bar{z} + z_G + (z'-z_G) \cos\theta - x'\sin\theta \qquad z' = (x - \bar{x}) \sin\theta - (\bar{z}+z_G-z)\cos\theta + z_G \qquad (2-1)$$

where $\bar{x}, \bar{z}$ and θ are the surge, heave and pitch displacements

III. 4 Perturbation Expansions

We will now expend some of the physical variables representing the motion of the ACV and that of the water in powers of four perturbation parameters δ, β, α and ϵ defined below.

δ = $\frac{\text{semi-width}}{\text{length}}$ ratio of the side hulls.

β = $\frac{\text{draught}}{\text{length}}$ ratio of the air cushion (i. e. $\frac{\text{cushion pressure}}{\rho\, g\, L}$)

α = amplitude of small motion (and oscillation)

ϵ = $\frac{\text{amplitude}}{\text{length}}$ ratio of the incident waves.

The first two parameters have been selected from the requirement of the linearized theory that the amplitude/length ratio of the waves induced by the side hulls and the air cushion due to the motion of the ACV should be small. The amplitudes of the induced waves may be assumed to be proportional to the beam of the side hulls and the cushion pressure (in head of water) and the length is proportional to F_n^2. It is therefore clear that the speed of the ACV should be sufficiently large.

The linearized theory is therefore inapplicable to very low speeds on account of the unacceptable steepness of the induced waves.

The third parameter need not be specifically defined at this stage, but one criterion is that this parameter should be sufficiently small so that the water contact of the flexible extensions does not take place at the bow and at the stern. It will be shown later that this parameter is of the same order as that of the incident wave.

The fourth small parameter (like the first two) ensures that the orbital velocities of the water particles in the incident wave are sufficiently small so that the squares of the perturbation velocities may be neglected in the linearized theory.

All the four parameters are assumed to be sufficiently small to ensure the convergence of the perturbation series which follow.

Assuming that the motion is periodic of frequency σ, we may write the following perturbation expansions for the motion of the water and of the ACV considered as a rigid body. It will be assumed that the unsteady flow of water is produced by the periodic forced oscillation of the craft. Since we shall only consider the linearized problem, the motion for arbitrary periodic oscillations may be deduced by the method of Fourier transforms.

Basic "Hull Form" of the air cushion $p_c\ (x, y) = \beta\, p_o\ (x, y)$

Hull surface of the side hulls

S_{1+}	Starboard side of starboard hull	$y' - b = \delta\, h_1\ (x',\ z')$
S_{1-}	Port side	$y' - b = -\delta\, h_2\ (x',\ z')$
S_{2+}	Starboard side of port hull	$y' + b = \delta\, h_2\ (x',\ z')$
S_{2-}	Port side	$y' + b = -\delta\, h_1\ (x',\ z')$

Surface pressure distribution due to the air cushion

$$p_s\ (x, y; t; \delta; \beta; \alpha; \epsilon) = \mathrm{Re} \sum_{k,l,m,n} e^{i\sigma t} \delta^k \beta^l \alpha^m \epsilon^n\, p_{klmn}\ (x, y)$$

Velocity potential

$$\Phi\ (x, y, z; t; \delta, \beta, \alpha, \epsilon) = \mathrm{Re} \sum_{k,l,m,n} e^{i\sigma t}\, \delta^k \beta^l \alpha^m \epsilon^n\, \Phi_{klmn}\ (x, y, z)$$

Water elevation

$$\zeta(x, y; t; \delta, \beta, \alpha, \epsilon) = \mathrm{Re} \sum_{k,l,m,n} e^{i\sigma t} \delta^k \beta^l \alpha^m \epsilon^n \zeta_{klmn}(x, y)$$

Surge displacement

$$\bar{x}(t; \delta; \beta; \alpha) = \mathrm{Re} \sum_{k,l,m} e^{i\sigma t} \delta^k \beta^l \alpha^m \bar{x}_{klm}$$

Heave displacement

$$\bar{z}(t; \delta; \beta; \alpha) = \mathrm{Re} \sum_{k,l,m} e^{i\sigma t} \delta^k \beta^l \alpha^m \bar{z}_{klm}$$

Pitch displacement

$$\theta(t; \delta; \beta; \alpha) = \mathrm{Re} \sum_{k,l,m} e^{i\sigma t} \delta^k \beta^l \alpha^m \theta_{klm} \qquad (2\text{-}2)$$

The frequency σ is that of forced oscillation in calm water or equal to the encountered frequency σ_e of the waves in a regular seaway. The displacement parameters are not expanded in powers of ϵ for, by definition, α is the order of the displacement due wave excitation of the order of forced displacements in the absence of waves. The quantities relating to the motion of the water contain, however, all the four parameters. A phase lag between the displacements is not explicitly shown in the above expressions. However, if for example, $\bar{z}_{klm}$ and θ_{klm} are considered as complex quantities a phase lag is implicit between heave and pitch.

The steady displacements of the type

$$\bar{x}_{110} \qquad \bar{z}_{110} \quad \text{and} \quad \theta_{110}$$

relate to motion in calm water and the oscillatory displacements

$$\bar{x}_{klm} \qquad \bar{z}_{klm} \quad \text{and} \quad \theta_{klm}$$

are restricted to the first order in α, i.e. with $m = 1$ since we shall be evaluating forces and moments up to a maximum order of $\delta^2 \alpha\epsilon$, $\delta\beta\alpha\epsilon$ and $\beta^2 \alpha\epsilon$ and for this purpose displacement of the first



order will be sufficient. In a similar manner the surface pressure during oscillations will also be restricted to the same order.

We may now write down the expansions we shall actually be using in the subsequent work.

$$\Phi(x,y,z;t;\delta;\beta;\alpha;\epsilon) = \delta\Phi_{1000} + \beta\Phi_{0100} + \delta\beta\Phi_{1100} + \text{Re } e^{i\sigma t}\left[\delta\alpha\Phi_{1010} + \beta\alpha\Phi_{0110} + \epsilon\Phi_{0001} + \delta\epsilon\Phi_{1001} + \beta\epsilon\Phi_{0101}\right] + 0(\delta^2,\beta^2,\delta\alpha^2,\beta\alpha,\epsilon^2)$$

$$\bar{x}(t;\delta;\beta;\alpha) = \delta\bar{x}_{100} + \beta\bar{x}_{010} + \text{Re}\,.\,\alpha e^{i\sigma t}\left[\bar{x}_{001} + \delta\bar{x}_{101} + \beta\bar{x}_{011}\right] + \delta\beta\bar{x}_{110} + 0(\delta^2,\beta^2,\delta\beta\alpha,\alpha^2)$$

$$\bar{z}(t;\delta;\beta;\alpha) = \delta\bar{z}_{100} + \beta\bar{z}_{010} + \text{Re}\,.\,\alpha e^{i\sigma t}\left[\bar{z}_{001} + \delta\bar{z}_{101} + \beta\bar{z}_{011}\right] + \delta\beta\bar{z}_{110} + 0(\delta^2,\beta^2,\delta\beta\alpha,\alpha^2)$$

$$\theta(t;\delta;\beta;\alpha) = \delta\theta_{100} + \beta\theta_{010} + \text{Re}.\alpha e^{i\sigma t}\left[\theta_{001} + \delta\theta_{101} + \beta\theta_{011}\right] + \delta\beta\theta_{110} + 0(\delta^2,\beta^2,\delta\beta\alpha,\alpha^2) \qquad (2\text{-}3)$$

The linearization of our problem is achieved by substituting the above expansions in Laplace's equation and in the boundary conditions and collecting terms of the same order. The result is a sequence of linear boundary value problems for the potentials Φ_{klmn}. Having derived the potentials, the pressure of the water particles on the side hulls and the shape of the cushion hull can be calculated. The forces and moments on the ACV considered as a rigid body can thus be evaluated.

IV. DEVELOPMENT OF BOUNDARY CONDITIONS

In the case of a conventional displacement vessel there are two types of boundary conditions for the velocity potential

Φ (x, y, z;t). These are (i) the kinematic and dynamic conditions on the free surface of water on all sides exterior to the immersed part of the hull and (ii) the conditions on the immersed part of the hull itself. The latter condition takes the form of the equality of the normal velocity of the fluid and that of the hull, i.e. that the flow is purely tangential to the hull surface when boundary layer effects are ignored. This is therefore a Neumann problem. Also, when dealing with an ideal amphibious hovercraft as in the previous study (1970) which was assumed completely separated from the water surface at all times both conditions relate to the free surface of water, one on the external free surface (EFS) and the other on the internal free surface (IFS) which is the vertical projection of the cushion opening (i.e. of the hemline of the skirts) on the water surface directly below the craft. Both these conditions relate to the pressure on the free surface giving a Dirichlet problem.

In the case of the general type of ACV now under consideration, there will be three types of conditions :

(i) The kinematic and dynamic conditions on the EFS

(ii) A normal velocity condition on the immersed parts of the side hulls which separate the EFS from the IFS

(iii) A pressure condition on the IFS which forms the lower boundary of the cushion.

This is therefore a mixed boundary condition problem.

IV. 1 Conditions on the External Free Surface (EFS)

The kinematic free surface condition applicable to the EFS and IFS has been derived in Section II in the form

$$\Phi_x \zeta_x + \Phi_y \zeta_y + \Phi_z \zeta_z + (\omega y - V)\, \zeta_x - \omega x\, \zeta_y + \zeta_t = 0 \qquad (4\text{-}1)$$

on $z = \zeta$. On the EFS the pressure is zero and substituting $p = 0$ in Bernoulli's equation (1-8) we derive

$$\zeta = \frac{1}{g}\left[\Phi_t + (\omega y - V)\Phi_x - \omega x \Phi_y + \frac{1}{2}(\nabla\Phi)^2\right] \qquad (4\text{-}2)$$

also on $z = \zeta$

As the position of the free surface denoted by $z = \zeta$ is unknown we will endeavour to eliminate the derivatives of ζ from (4-1) by using (4-2) in order to derive an explicit equation for Φ. Denoting the terms on the right-hand side of (4-2) by R, for the time being, and noting that R is a function of z and t and that its value is to be taken when $z = \zeta$, the derivatives of ζ are evaluated and substituted in (4-1) giving the condition

$$\left(\frac{\partial}{\partial t} - V\frac{\partial}{\partial x}\right) R + \omega(y R_x - x R_y) + \nabla\Phi . \nabla R - \Phi_z = 0 \qquad (4-3)$$

where R is, of course,

$$R = \frac{1}{g}\left[\Phi_t - V\Phi_x + \omega(y\Phi_x - x\Phi_y) + \frac{1}{2}(\nabla\Phi)^2\right]$$

and eliminating the derivatives of R, we derive finally,

$$\left(\frac{\partial}{\partial t} - V\frac{\partial}{\partial x}\right)^2 \Phi + 2\nabla\Phi . \nabla(\Phi_t - V\Phi_x) + \frac{1}{2}\nabla\Phi . \nabla\left[(\nabla\Phi)^2\right] - g\Phi_z = S \qquad (4-4)$$

where S is an algebraic expression of a complicated nature each term of which has, however, ω or ω^2 as a factor. This condition can therefore be simplified when ω is set equal to zero and in the case of our coplaner motion in a straight course,

$$\left(\frac{\partial}{\partial t} - V\frac{\partial}{\partial x}\right)^2 \Phi - g\Phi_z + 2\nabla\Phi . \nabla(\Phi_t - V\Phi_x) + \frac{1}{2}\nabla\Phi . \nabla\left[(\nabla\Phi)^2\right] = 0 \qquad (4-5)$$

This is the exact free surface condition. We have made no approximations so far, but the condition is only applicable on the actual free surface $z = \zeta$. Although we have elimanated ζ from the equation itself, we are still in some difficulty as we do not know the position of the free surface for the application of the condition thereon. We will therefore attempt to derive a condition, even if it is an approximate one, which can be imposed on the known surface $z = 0$. This, in effect, is the first stage in the linearization of the problem.

Assuming that the potential may be continued analytically from the actual free surface $z = \zeta$ to the plane $z = 0$, we may expand it in the form of Taylor's series

$$\Phi(x, y, z; t) = \Phi(x, y, o; t) + \zeta\frac{\partial\Phi}{\partial z}\Big|_{z=0} +$$

The expansion in series may safely be expected to be convergent for Φ is of small order $\left[0\,(\delta, \beta)\right]$ and the derivatives of Φ may also be assumed to be of the same small order. It is clear from (4-2) that ζ is also of small order and may therefore be treated as a small constant for the purpose on the expansion.

Substituting the above series in (4-5), we get

$$\left(\frac{\partial}{\partial t} - V\frac{\partial}{\partial x}\right)^2 \phi + \zeta \frac{\partial}{\partial z}\left(\frac{\partial}{\partial t} - V\frac{\partial}{\partial x}\right)^2 \Phi - g\Phi_z - g\,\zeta\phi_{zz}$$

$$+ 2\,\nabla(\Phi + \zeta\Phi_z) \cdot \nabla\left[\Phi_t - V\Phi_x + \zeta\frac{\partial}{\partial z}\,(\Phi_t - V\Phi_x)\right] + 0(\Phi^3) = 0$$

on $z = 0$.

Now, from (4-2) with $\omega = 0$

$$\zeta = \frac{1}{g}\,(\Phi_t - V\Phi_x) + 0\,(\Phi^2)$$

so that we have an approximate condition

$$\phi_{tt} - 2V\Phi_{xt} + V^2\Phi_{xx} - g\Phi_z + 2\,\nabla\Phi.\nabla\,(\Phi_t - V\Phi_z)$$

$$+\frac{1}{g}(\Phi_t - V\Phi_x)\frac{\partial}{\partial z}\,(\Phi_{tt} - 2V\Phi_{xt} + V^2\Phi_{xx} - g\Phi_z) + 0\,(\Phi^3) = 0$$

on $z = 0$. (4-6)

IV. 2 Conditions on the Internal Free Surface (IFS)

If there is a distribution of surface pressure $p_s\,(x, y; t)$ on the IFS, we have from Bernoulli's equation (1-8) with $\omega = 0$,

$$\zeta = \frac{1}{g}\left[\Phi_t - V\Phi_x + \frac{1}{2}\,(\nabla\Phi)^2\right]_{z\,=\,\zeta} + \frac{p_s\,(x, y; t)}{\rho\, g}$$

with x, y in the IFS.

The kinematic condition is the same as that on the EFS and given by (4-1) with $\omega = 0$,

$$(\Phi_x - V)\,\zeta_x + \Phi_y\,\zeta_y - \Phi_z\,\zeta_z + \zeta_t = 0$$

also on $z = \zeta$.

Eliminating ζ as before, we derive

$$\left(\frac{\partial}{\partial t} - V\frac{\partial}{\partial x}\right)^2 \Phi - g\Phi_z + 2\nabla\Phi.\ \nabla(\Phi_t - V\Phi_x) + \frac{1}{2}\nabla\Phi.\nabla\left[(\nabla\Phi)^2\right]$$

$$+\frac{1}{\rho}\left[\left(\frac{\partial}{\partial t} - V\frac{\partial}{\partial x}\right) p_s\,(x,y) + \Phi_x p_{s_x}\,(x,y) + \Phi_y p_{s_y}\,(x,y)\right] = 0$$

This is the exact free surface condition on $z = \zeta$ and the approximate condition on $z = 0$ is obtained as before by a Taylor expansion of Φ, giving the final result

$$\Phi_{tt} - 2V\Phi_{xt} + V^2\Phi_{xx} - g\Phi_z + 2\nabla\Phi.\ \nabla(\Phi_t - V\Phi_x)$$

$$+\frac{1}{g}\left(\Phi_t - V\Phi_x + \frac{p_s}{\rho}\right)\frac{\partial}{\partial z}\left(\Phi_{tt} - 2V\Phi_{xt} + V^2\Phi_{xx} - g\Phi_z\right)$$

$$+\frac{1}{\rho}\left[\left(\frac{\partial}{\partial t} - V\frac{\partial}{\partial x}\right) p_s + \Phi_x p_{s_x} + \Phi_y p_{s_y}\right]$$

$$+\frac{1}{\rho g} V p_{s_x}\frac{\partial}{\partial z}(\Phi_t - V\Phi_x) + 0(\Phi^3) = 0 \qquad (4\text{-}7)$$

IV. 3 Conditions on the Hull Surfaces

Setting $\omega = 0$ in (1-9) the kinematic condition applicable to the wetted hull surfaces is

$$(\Phi_x - V)\,H_x + \Phi_y H_y + \Phi_z H_z + H_t = 0$$

i.e. $\nabla\Phi.\nabla H + \left(\frac{\partial}{\partial t} - V\frac{\partial}{\partial x}\right) H = 0$

where the hull surface is given in the moving co-ordinate system by an equation of the form

$$H(x, y, z; t) = 0$$

The above condition stipulates that the normal velocity of the hull at each point is equal to that of the contiguous fluid particle, i.e. that

the flow is tangential when viscous effects are ignored.

Now, the fluid velocity normal to the hull surface is

$$\frac{\partial \Phi}{\partial n} = \hat{n} . \nabla \Phi$$

where $\hat{n}$ is the unit normal vector drawn into the hull given by

$$\hat{n} = \frac{H_x \hat{i} + H_y \hat{j} + H_z \hat{k}}{\left[H_x^2 + H_y^2 + H_z^2 \right]^{\frac{1}{2}}} = \frac{\nabla H}{|\nabla H|}$$

so that

$$\frac{\partial \Phi}{\partial n} = \frac{\nabla \Phi . \nabla H}{|\nabla H|} = -\frac{\left(\frac{\partial H}{\partial t} - V \frac{\partial H}{\partial x} \right)}{|\nabla H|} \qquad (4-8)$$

Now, the equation of the hull surfaces is naturally given in the body fixed system (x' , y' , z') in the form

$$\begin{aligned} H(x, y, z; t) &= \delta h_1 (x' , z') - (y' - b) = 0 && \text{on } S_{1+} \\ &= \delta h_2 (x' , z') + (y' - b) = 0 && \text{on } S_{1-} \\ &= \delta h_2 (x' , z') - (y' + b) = 0 && \text{on } S_{2+} \\ &= \delta h_1 (x' , z') + (y' + b) = 0 && \text{on } S_{2-} \end{aligned} \qquad (4-9)$$

We will therefore have to evaluate $\frac{\partial \Phi}{\partial \hat{n}}$ given by (4-8) in the (x' , y' , z') system the transformation of co-ordinates between the (x, y, z) system and the (x' , y' , z') system being given by (4-1).

Considering first the surface S_{1+}

$$\frac{\partial H}{\partial t} = \frac{\partial}{\partial t} \left[\delta h, (x' , z') - (y' - b) \right]$$

where

$$x' = (x - \bar{x}) \cos\theta + (\bar{z} - h_G - z) \sin\theta$$

$$y' = y$$

and

$$z' = (x - \bar{x}) \sin\theta - (\bar{z} - h_G - z) \cos\theta - h_G$$

so that x' and z' are functions of x, z and the displacement parameters $\bar{x}, \bar{z}, \theta$ which are themselves simple harmonic functions of the time. However, y' is always equal to y in coplaner motion and does not depend upon t.

We may therefore write,

$$\frac{\partial H}{\partial t} = \delta \frac{\partial}{\partial t} h_1 (x', z')$$

$$= \delta \left[\frac{\partial x'}{\partial t} \frac{\partial h_1}{\partial x'} + \frac{\partial z'}{\partial t} \frac{\partial h_1}{\partial z'} \right]$$

$$= \delta \left[\left\{ \dot{z} \sin\theta - \dot{x} \cos\theta - (z' - z_G) \dot{\theta} \right\} \frac{\partial h_1}{\partial x'} + \left\{ x' \dot{\theta} - \dot{x} \sin\theta - \dot{z} \cos\theta \right\} \frac{\partial h_1}{\partial z'} \right]$$

Also

$$\frac{\partial H}{\partial x} = \delta \frac{\partial}{\partial x} h_1 (x', z') = \delta \left[\frac{\partial x'}{\partial x} \frac{\partial h_1}{\partial x'} + \frac{\partial z'}{\partial x} \frac{\partial h}{\partial z'} \right]$$

$$= \delta \left[\cos\theta \frac{\partial h_1}{\partial x'} + \sin\theta \frac{\partial h_1}{\partial z'} \right]$$

$$\frac{\partial H}{\partial y} = \frac{\partial H}{\partial y'} = -1$$

$$\frac{\partial H}{\partial z} = \delta \frac{\partial}{\partial z} h(x', z') = \delta \left[\frac{\partial x'}{\partial z} \frac{\partial h_1}{\partial x'} + \frac{\partial z'}{\partial z} \frac{\partial h_1}{\partial z'} \right]$$

$$= \delta \left[-\sin\theta \frac{\partial h_1}{\partial x'} + \cos\theta \frac{\partial h_1}{\partial z'} \right]$$

so that

$$\frac{\partial \Phi}{\partial n} = -\frac{\left(\frac{\partial H}{\partial t} - V\frac{\partial H}{\partial x}\right)}{|\nabla H|}$$

$$= \delta\left[\left\{\dot{x}\cos\theta - \dot{z}\sin\theta + (z' - z_G)\dot{\theta} + V\cos\theta\right\}\frac{\partial h_1}{\partial x'}\right.$$

$$\left. + \left\{\dot{x}\sin\theta + \dot{z}\cos\theta - x'\ddot{\theta} + V\sin\theta\right\}\frac{\partial h_1}{\partial z'}\right]$$

$$\left[1 + \delta^2\left(\frac{\partial h_1}{\partial x'}\right)^2 + \delta^2\left(\frac{\partial h_1}{\partial z'}\right)^2\right]^{-1/2} \qquad (4\text{-}10)$$

This applies to the surface S_{1+}. On the surface S_{2-} the hull function h_1 is the same, but $\partial H/\partial y'$ will be $+1$ instead of -1. The expression $\partial \Phi/\partial n$ will be unaltered for $|\nabla H|$ will be the same.

Thus (4-10) expresses the normal velocity for the two outer hull surfaces S_{1+} and S_{2-}

In the case of the two inner hull surfaces S_{1-} and S_{2+} we simply replace the hull function h_1 by h_2.

V. THE FORCES AND MOMENTS

It is shown in the earlier work (Appendix III of Reference 1) that the forces and moments acting on the ACV as a rigid body may be written in the form

$$\vec{F} = X\hat{i} + Y\hat{j} + Z\hat{k} = \vec{F}_P + \vec{F}_R$$

and

$$\vec{M} = L\hat{i} + M\hat{j} + M\hat{k} = \vec{M}_P + \vec{M}_R$$

where, taking into account the side hulls in addition to the cushion hull which was the subject of the previous study, we may write for the pressure force

$$\vec{F}_P = \vec{F}_{P_C} + \vec{F}_{P_H} = -\iint_S p_s\,\hat{n}\,dS - \iint_{S_1+S_2} p\,\hat{n}\,dS \qquad (5\text{-}1)$$

and for the pressure moment.

$$\vec{M}_P = \vec{M}_{P_C} + \vec{M}_{P_H} = -\iint_S p_s\,(\vec{r}' \times \hat{n})\,dS \; - \iint_{S_1+S_2} p\,(\vec{r}' \times \hat{n})\,dS \qquad (5\text{-}2)$$

The surface integrals are taken over the displaced position of the effective hull, S, of the air cushion, i.e. the instantaneous position of the IFS and the instantaneous wetted surfaces S_1 and S_2 of the side hulls.

$\vec{r}'$ is the position vector of an element of area dS with o' as origin and the unit normal $\hat{n}$ is taken out of the water and into the cushion hull and the side hulls. Also, p_s is the surface distribution of pressure acting on the cushion hull ($z = \zeta$) and p the pressure of water at an interior point ($z > \zeta_+$) of the immersed surface of the side hulls.

The rigid body force and moment are

$$\vec{F}_R = \iiint_V (\dot{\vec{U}} - g\hat{k})\,dm \qquad (5\text{-}3)$$

and

$$\vec{M}_R = \iiint_V r' \times (\dot{\vec{U}} - g\hat{k})\,dm \qquad (5\text{-}4)$$

where $\vec{r}'$ is the position vector of an element of mass dm of the ACV with absolute velocity $\vec{U}$, and the triple integral is taken throughout the volume of the ACV contained by matter.

These are the forces and moments acting at and about the C.G. of the ACV due to its inertia and the pressure of the water on the effective hull of the air cushion and on the side hulls.

The above expressions are written partly in the moving (x, y, z) system and partly in the fixed (x', y', z') system, but it is obviously to be preferred that we should study the motion of the craft in the steady (x, y, z) system particularly in view of the fact that the pressure distribution on the water surface and the motion of the water are given in this system.

The detailed derivation of the forces and moments are carried out in Appendix, II, III, and IV where the forces and moments on the cushion hull, those on the side hulls and the rigid body forces and

moments are separately evaluated. The forces and moments of the same order may be added together and if, following Newman's[4] notation we write the total forces and moment in the form :

$$X = X_{P_C} + X_{P_H} + X_R = \delta X_{1000} + \beta X_{0100} + \delta^2 X_{2000}$$

$$+ \delta\beta X_{1100} + \beta^2 X_{0200} + \delta\alpha X_{1010} + \delta\epsilon X_{1001} + \beta\alpha X_{0110}$$

$$+ \beta\epsilon X_{0101} + \qquad (5\text{-}5)$$

with similar expansions for Z and M, we have the following results :

Longitudinal Force

$$0(\delta) \quad X_{1000} = 0$$

$$0(\beta) \quad X_{0100} = 0$$

$$0(\delta^2) \quad X_{2000} = -2\rho V \iint_{\bar{S}_{1_o}} \Phi_{1000_{x'}}(x', b, z') \frac{\partial h}{\partial x'} \, dx'dz'$$

$$0(\delta\beta) \quad X_{1100} = -\frac{V}{g} \iint_{\bar{S}_o} p_o \, \Phi_{1000_{xx}}^{(x, y, o)} \, dxdy$$

$$- 2\rho V \iint_{S_{1_o}} \left[\Phi_{0100_{x'}}^{(x', b + z')} \frac{\partial h_1}{\partial x'} + \Phi_{0100_{x'}}(x', b-, z') \frac{\partial h_2}{\partial x'} \right] dx'dz'$$

$$0(\beta^2) \quad X_{0200} = \frac{1}{g} \iint_{\zeta_o} \left[\frac{1}{\rho} p_o p_{o_x} - V p_o \, \Phi_{0100_{xx}}^{(x, y, o)} \right] dxdy$$

$$0(\delta\alpha) \quad X_{1010} = -\left(\frac{m_2}{\delta}\right) \sigma^2 \bar{x}_{001} \, e^{i\sigma t}$$

$$0(\beta\alpha) \quad X_{0110} = -\left(\frac{m_1}{\beta}\right) \sigma^2 \bar{x}_{001} \, e^{i\sigma t}$$

$$0(\delta^2\alpha)\ X_{2010} = -2\rho e^{i\sigma t}\iint_{\bar{S}_{1_o}}\Big[V\Big\{\bar{x}_{001}\frac{\partial h}{\partial x'} + \bar{z}_{001}\frac{\partial h}{\partial z'} + \theta_{001}\,(\overline{z' + h_G}\,\frac{\partial h}{\partial x'} - x'\frac{\partial h}{\partial z'})\Big\}\Phi_{1000_{x'x'}} + (V\phi_{1010_{x'}} - i\sigma\Phi_{1010})\frac{\partial h}{\partial x'}\Big]dx'dz' - \left(\frac{m_2}{\delta}\right)\sigma^2\bar{x}_{101}e^{i\sigma t}$$

$$0(\beta^2\alpha)\ X_{0210} = \frac{1}{g}e^{i\sigma t}\iint_{\bar{S}_o}\Big[p_o\,(i\sigma\Phi_{0110_x} - V\Phi_{0110_{xx}}) + (\bar{x}_{001} + h_G\,\theta_{001})\Big\{\frac{1}{\rho}(p_o p_{o_{xx}} + p_{o_x}^2) - V\,(2p_{o_x}\Phi_{0100_{xx}} + p_o\Phi_{0100_{xxx}})\Big\}\Big]dxdy - \left(\frac{m_1}{\rho}\right)\sigma^2\,\bar{x}_{011}\,e^{i\sigma t}$$

$$0(\delta\beta\alpha)\ X_{1110} = -2e^{i\sigma t}\rho\iint_{\bar{S}_{1_o}}\Big[V\Big\{\bar{x}_{001}\frac{\partial h_1}{\partial x'} + \bar{z}_{001}\frac{\partial h_1}{\partial z'} + \theta_{001}\,(\overline{z' + h_G}\,\frac{\partial h_1}{\partial x'} - x'\frac{\partial h_1}{\partial z'})\Big\}\Phi^{+}_{0100_{x'x'}} + (V\Phi^{+}_{0110} - i\sigma\Phi^{+}_{0110})\frac{\partial h_1}{\partial x'} + V\Big\{\bar{x}_{001}\frac{\partial h_2}{\partial x'} + \bar{z}_{001}\frac{\partial h_2}{\partial z'} + \theta_{001}\,(\overline{z' + h_G}\,\frac{\partial h_2}{\partial x'} - x'\frac{\partial h_2}{\partial z'})\Big\}\Phi^{-}_{0100_{x'x'}} + (\bar{V}\Phi^{-}_{0110_{x'}} - i\sigma\Phi^{-}_{0110})\frac{\partial h_2}{\partial x'}\Big]dx'dz' + \frac{1}{g}e^{i\sigma t}\iint_{\bar{S}_o}\Big[p_o\,(i\sigma\Phi_{1010_x} - V\Phi_{1010_{xx'}}) - V\,(\bar{x}_{001} + h_G\theta_{001})(2p_{o_x}\Phi_{1000_{xx}} + p_o\Phi_{1000_{xxx}})\Big]dxdy - \Big[\frac{m_1}{\beta}\sigma^2\bar{x}_{101} + \left(\frac{m_2}{\delta}\right)\sigma^2\,\bar{x}_{011}\Big]e^{i\sigma t}$$

$$0(\delta\epsilon)\ X_{1001} = 2\rho\, e^{i\sigma_e t}\iint_{\bar{S}_{1_o}} (i\sigma_e \Phi_{0001} - V\Phi_{0001_{x'}})\ \frac{\partial h}{\partial x'}\ dx'dz'$$

$$0(\beta\epsilon)\ X_{0101} = \frac{1}{g}\, e^{i\sigma_e t}\iint_{\bar{S}_o} p_o\,(i\sigma_e \Phi_{0001_x} - V\Phi_{0001_{xx}})\ dxdy \qquad (5\text{-}6)$$

Vertical Force

$$0(\delta)\ Z_{1000} = 2\rho g\iint_{\bar{S}_{1_o}} h(x', z')\ dx'dz' - \left(\frac{m_2}{\delta}\right)g = 0$$

$$0(\beta)\ Z_{0100} = -\iint_{\bar{S}_o} p_o\ dx\ dy - \left(\frac{m_1}{\beta}\right)\ g = 0$$

$$0(\delta^2)\ Z_{2000} = -2\rho V\iint_{\bar{S}_{1_o}} \Phi_{1000_{x'}}\ \frac{\partial h}{\partial z'}\ dx'dz' + 2\rho g\int_L (\bar{z}_{100} - x'\theta_{100})\ h(x', o)\ dx'$$

$$0(\delta\beta)\ Z_{1100} = -2\rho V\iint_{\bar{S}_{1_o}} \left(\Phi^{+}_{0100_{x'}}\ \frac{\partial h_1}{\partial z'} + \Phi^{-}_{0100_{x'}}\ \frac{\partial h_2}{\partial z'}\right) dx'dz' + 2\rho g\int_L (\bar{z}_{010} - x'\theta_{010})\ h(x', o)\ dx' - 2(\bar{x}_{100} + h_G\ \theta_{100})\iint_{\bar{S}_o} p_{o_x}\ dxdy$$

$$0(\beta^2)\ Z_{0200} = -2(\bar{x}_{010} + h_G\,\theta_{010})\iint_{\bar{S}_o} p_{o_x}\ dxdy$$

$$0(\delta\alpha)\ Z_{1010} = -\left(\frac{m_2}{\delta}\right)\sigma^2 \bar{z}_{001} e^{i\sigma t} + 2\rho g e^{i\sigma t}\int_L (\bar{z}_{001} - x'\theta_{001})\ h(x', o)\ dx'$$

$$0(\beta\alpha)\ Z_{0110} = -e^{i\sigma t}(\bar{x}_{001} + h_G\,\theta_{001})\iint_{\bar{S}_o} p_{o_x}\ dxdy - \left(\frac{m_1}{\beta}\right)\sigma^2\,\bar{z}_{001}\, e^{i\sigma t}$$

$$0(\delta^2\alpha)\, Z_{2010} = -2\rho\, e^{i\sigma t} \iint_{\bar{S}_{1_o}} \Big[\Big\{ V(\bar{x}_{001} + \overline{z' + h}_G\, \theta_{001})\, \Phi_{1000_{x'x'}} + V(\bar{z}_{001} - x'\theta_{001})\, \Phi_{1000_{x'z'}} + V\Phi_{1010_{x'}} - i\sigma\Phi_{1010} \Big\} \frac{\partial h}{\partial z'} - V\theta_{001}\, \Phi_{1000_{x'}} \frac{\partial h}{\partial x'} \Big]\, dx'dz' + 2\rho\, e^{i\sigma t} \int_{L} \Big[g(\bar{z}_{101} - x'\theta_{101})\, h(x', o) - V(\bar{z}_{001} - x'\theta_{001})\, \Phi_{1000_{x'}} \frac{\partial h}{\partial z'} \Big]\, dx' - \left(\frac{m_2}{\delta}\right) \sigma^2 \bar{z}_{101}\, e^{i\sigma t}$$

$$0(\beta^2\alpha)\, Z_{0210} = -e^{i\sigma t} \iint_{\bar{S}_o} \Big[\bar{r}_{010} \cdot s_{001} + \bar{r}_{001}\, s_{010} + 2\bar{r}_{011}\, p_{o_x} + 2\bar{r}_{010}\bar{r}_{001}\, p_{o_{xx}} \Big]\, dxdy - \left(\frac{m_1}{\beta}\right) \sigma^2 \bar{z}_{011}\, e^{i\sigma t}$$

$$0(\delta\beta\alpha)\, Z_{1110} = -2e^{i\sigma t\rho} \iint_{\bar{S}_{1_o}} \Big[\Big\{ V(\bar{x}_{001} + \overline{z' + h}_G\, \theta_{001})\, \Phi^{+}_{0100_{x'z'}} + V(\bar{z}_{001} - x'\theta_{001})\Phi^{+}_{0100_{x'z'}} + V\phi^{+}_{0110_{x'}} - i\sigma\phi^{+}_{0110} \Big\} \frac{\partial h_1}{\partial z'} - V\theta_{001}\, \Phi^{+}_{0100_{x'}} \frac{\partial h_1}{\partial x'} + \Big\{ V(\bar{x}_{001} + \overline{z' + h}_G\theta_{001})\Phi^{-}_{0100_{x'x'}} + V(\bar{z}_{001} - x'\theta_{001})\, \Phi^{-}_{0100} + V\Phi^{-}_{0110_{x'}} - i\sigma\Phi^{-}_{0110} \Big\} \frac{\partial h_2}{\partial z'} - V\theta_{001}\, \Phi^{-}_{0100} \frac{\partial h_2}{\partial x'} \Big]\, dx'dz' + 2\rho e^{i\sigma t} \int_{L} \Big[g(\bar{z}_{011} - x'\theta_{011})\, h(x', o) - V(\bar{z}_{001} - x'\theta_{001}) \Big(\Phi^{+}_{0100} \frac{\partial h_1}{\partial z'} + \Phi^{-}_{0100} \frac{\partial h_2}{\partial z'} \Big) \Big] dx' - e^{i\sigma t} \iint \Big[\bar{r}_{100} s_{001} + \bar{r}_{001} s_{100} + 2\bar{r}_{101}\, p_{o_x} + 2\bar{r}_{100}\bar{r}_{001}\, p_{o_{xx}} \Big]\, dxdy$$

$$-\left[\left(\frac{m_1}{\beta}\right)\sigma^2 z_{101} + \left(\frac{m_2}{\delta}\right)\sigma^2 \bar{z}_{011}\right] e^{i\sigma t}$$

$$0(\delta\epsilon)\ Z_{1001} = 2\rho e^{i\sigma_e t}\iint_{\bar{S}_{1_o}} (i\sigma_e \Phi_{0001} - V\Phi_{0001_{x'}})\frac{\partial h}{\partial z'}\ dx'dz'$$

$$0(\beta\epsilon)\ Z_{0101} = 0 \qquad (5-7)$$

Pitching Moment

$$0(\delta)\ M_{1000} = -2\rho g\iint_{\bar{S}_{1_o}} x'\ h(x', z')\ dx'dz'$$

$$0(\beta)\ M_{0100} = \iint_{\bar{S}_o} x\ p_o\ dxdy$$

$$0(\delta^2)\ M_{2000} = -2\rho\iint_{S_{1_o}}\left[V\left(z'\frac{\partial h}{\partial x'} - x'\frac{\partial h}{\partial z'}\right)\Phi_{1000_{x'}} + g\theta_{100}z'h(x', z')\right]$$

$$dx'dz' - 2\rho g\int_L (\bar{z}_{100} - x'\theta_{100})\, x'\, h(x', o)\ dx' -$$

$$-\left(\frac{m_2}{\delta}\right) g h_G \theta_{100}$$

$$0(\delta\beta)\ M_{1100} = -2\rho\iint_{S_{1_o}}\left[V\left\{\left(z'\frac{\partial h_1}{\partial x'} - x'\frac{\partial h_1}{\partial z'}\right)\Phi^{+}_{0100_{x'}}\right.\right.$$

$$\left.\left.\left(z'\frac{\partial h_2}{\partial x'} - x'\frac{\partial h_2}{\partial z'}\right)\Phi^{-}_{0100_{x'}}\right\} + g\theta_{010}z'h(x', z')\right] dx'dz'$$

$$-2\rho g\int_L (\bar{z}_{010} - x'\theta_{010})\, x'\, h(x', o)\ dx' + 2(\bar{x}_{100} + h_G\theta_{100})$$

$$\iint_{\bar{S}_o} x\ p_{o_x}\ dxdy - \left[\frac{m_1}{\beta}\theta_{100} + \left(\frac{m_2}{\delta}\right)\theta_{010}\right] gh_G$$

$$0(\beta^2)\ M_{0200} = 2(\bar{x}_{010} + h_G\theta_{010})\iint_{\bar{S}_o} x\ p_{o_x}\ dxdy -$$

$$-\left(\frac{m_1}{\beta}\right) g h_G \theta_{010}$$

$$0(\delta\alpha)\ M_{1010} = -2\rho g \theta_{001} e^{i\sigma t} \iint_{S_{1_o}} z' h(x', z')\, dx'dz' -$$

$$- 2\rho g e^{i\sigma t} \int_L (\bar{z}_{001} - x'\theta_{001})\, x' h(x', o)\, dx' +$$

$$+ \left[\left(\frac{m_2}{\delta}\right) h_G (\sigma^2 \bar{x}_{001} - g\theta_{001}) - \frac{I_2}{\delta} \sigma^2 \theta_{001}\right] e^{i\sigma t}$$

$$0(\beta\alpha)\ M_{0110} = 2(\bar{x}_{001} + h_G \theta_{001}) e^{i\sigma t} \iint xp_{o_x}\, dxdy +$$

$$+ \left[\left(\frac{m_1}{\beta}\right) h_G (\sigma^2 \bar{x}_{001} - g\theta_{001}) - \left(\frac{I_1}{\beta}\right)\sigma^2 \theta_{001}\right] e^{i\sigma t}$$

$$0(\delta^2\alpha)\ M_{2010} = -2\rho e^{i\sigma t} \iint_{S_{1_o}} \Big[\Big\{ V(x_{001} + \overline{z' + h_G}\theta_{001}) \Phi_{1000_{x'x'}}$$

$$+ V(\bar{z}_{001} - x\theta_{001}) \Phi_{1000_{x'z'}} + V\Phi_{1010_x} - i\sigma\Phi_{1010} \Big\}$$

$$\left(z' \frac{\partial h}{\partial x'} - x' \frac{\partial h}{\partial z'}\right) + g\theta_{101} z' h(x', z') \Big]\, dx'dz' +$$

$$+ 2\rho e^{i\sigma t} \int_L \Big[V(\bar{z}_{001} - x'\theta_{001}) \Phi_{1000_x}, \frac{\partial h}{\partial \bar{z}'} - g(\bar{z}_{101} -$$

$$- x'\theta_{101})\, h(x', o) \Big]\, x'dx' + \left[\left(\frac{m_2}{\delta}\right) h_G \sigma^2 (\bar{x}_{101} -$$

$$- \bar{z}_{001}\theta_{100}) - g\theta_{101} - \left(\frac{I_2}{\delta}\right)\sigma^2 \theta_{101}\Big] e^{i\sigma t}$$

$$0(\beta^2\alpha)\ M_{0210} = e^{i\sigma t} \iint_{\bar{S}_0} \Big[x(\bar{r}_{010} s_{001} + \bar{r}_{001} s_{010} + 2\bar{r}_{011} p_{o_x} +$$

$$+ \bar{r}_{010}\bar{r}_{001} (3xp_{o_{xx}} - 2p_{o_x}) - \frac{1}{g} p_o \bar{z}_{001} \left(\frac{1}{\rho} p_o -$$

$$- V\Phi_{0100_{xx}}) \Big]\ dxdy + \left[\left(\frac{m_1}{\beta}\right) h_G \sigma^2 (\bar{x}_{011} - \bar{z}_{001}\theta_{010}) -$$

$$- g\theta_{011} - \left(\frac{I}{\beta}\right) \sigma^2 \theta_{011}\right] e^{i\sigma t}$$

$$0(\delta\beta\alpha)\quad M_{1110} = -2\rho e^{i\sigma t}\iint_{\xi_{1_\delta}}\Big[\Big\{V(\bar{x}_{001} + \overline{z' + h_G}\,\theta_{001})\Phi^{+}_{0100_{x'x'}} + V(\bar{z}_{001} - x'\theta_{001})\Phi^{+}_{0100_{x'z'}} + V\Phi^{+}_{0110_{x'}} - i\sigma\Phi^{+}_{0110}\Big\}(z'\frac{\partial h_1}{\partial x'} - x'\frac{\partial h_1}{\partial z'}) + \Big\{V(\bar{x}_{001} + \overline{z' + h_G}\,\theta_{001})\Phi^{-}_{0100_{x'x'}} + V(\bar{z}_{001} - x'0_{001})\Phi^{-}_{0100_{x'z'}} + V\Phi^{-}_{0110_{x'}} - i\sigma\Phi^{-}_{0110}\Big\}(z'\frac{\partial h_2}{\partial x'} - x'\frac{\partial h_2}{\partial z'}) + g\,\theta_{011}\,z'\,h(x',z')\Big]dx'dz' +$$

$$+ e^{i\sigma t}\iint_{\xi_0}\Big[x(\bar{r}_{100}s_{001} + \bar{r}_{001}s_{100} + 2\bar{r}_{101}p_{o_x}) + 2\bar{r}_{100}\bar{r}_{001}(xp_{o_{xx}} - p_{o_x}) + \frac{1}{g}\,V\,p_o\,\bar{z}_{001}\,\Phi_{1000_{xx}}\Big]dxdy + \Big[\Big(\frac{m_1}{\beta}\Big)h_G\Big\{\sigma^2(\bar{x}_{101} - \bar{z}_{001}\,\theta_{100}) - g_{101}\Big\} - \Big(\frac{I_1}{\beta}\Big)\sigma^2\,\theta_{101} + \Big(\frac{m_2}{\delta}\Big)h_G\Big\{\sigma^2(\bar{x}_{011} - \bar{z}_{001}\,\theta_{010}) - g\theta_{011}\Big\} - \Big(\frac{I_2}{\delta}\Big)\sigma^2\theta_{011}\Big]e^{i\sigma t} + 2\rho e^{i\sigma t}\int_{L}\Big[V(\bar{z}_{001} - x'\theta_{001})(\Phi^{+}_{0100_{x'}}\frac{\partial h_1}{\partial z'} + \bar{\Phi}_{0100_x}\frac{\partial h_2}{\partial z'}) - g(\bar{z}_{011} - x'\theta_{011})\,h(x',o)\Big]x'dx'$$

$$0(\delta\epsilon)\quad M_{1001} = 2\rho e^{i\sigma_e t}\iint_{\xi_{1_0}}(i\sigma_e\,\Phi_{0001} - V\Phi_{0001_{x'}})(z'\frac{\partial h}{\partial x'} - x'\frac{\partial h}{\partial z'})\,dx'dz'$$

$$0(\beta\epsilon)\quad M_{0101} = 0$$

(5-8)

VI. STEADY MOTION IN CALM WATER

When the ACV moves at a uniform speed in a longitudinal direction under the action of a constant propulsive thrust the motions of the craft and of the fluid are independent of time. The waves induced by the air cushion and by the side hulls travel with the same speed as the craft and there is therefore no periodic disturbance. Although it is not expected that the ACV would develop periodic oscillations, it is quite conceivable that it will take up a steady state trim on account of the steady disturbance of the water surface appropriate to the forward speed.

Let us assume that the steady displacements of the ACV are :

$$\text{Surge} \quad \bar{x} = \delta\bar{x}_{100} + \beta\bar{x}_{010} + \delta\beta\bar{x}_{110}$$

$$\text{heave} \quad \bar{z} = \delta\bar{z}_{100} + \beta\bar{z}_{010} + \delta\beta\bar{z}_{110}$$

$$\text{pitch} \quad \theta = \delta\theta_{100} + \beta\theta_{010} + \delta\beta\theta_{110} \qquad (6\text{-}1)$$

These are the displacements at and about the C.G. of the vehicle. The first set of terms denote the displacement due to the motion of the side hulls, the second due to the air cushion and the third due to the interference between the motions of the air cushion and of the side hulls.

The only force acting on the ACV apart from its weight is the thrust T which may be assumed to act in a direction parallel to the deck of the ACV at a height h_T above the C.G. This is on the assumption that air propulsion is employed. In the case of water propulsion, the thrust line will be below the C.G. and also, possibly, oblique to the deck surface, but the principle of the discussion which follows will be the same.

The thrust is adjusted in such a manner that it is just sufficient to overcome wave resistance as this is the only horizontal force (apart from skin friction, which is not considered in this study, for the fluid has no viscosity) to enable uniform progression. When the craft takes up a pitch trim the components of thrust along the x and z axes will be $T\cos\theta$ and $-T\sin\theta$ respectively, so that these should equal respectively the longitudinal and vertical forces at the C.G. of the ACV arising out of the action of the fluid pressure due

to the uniform motion and steady displacements. Also, the moment of the thrust about the C. G.

$$- h_T \quad T$$

must be equal to the moment due to the fluid pressure.

Using the expansion (5-5) for the longitudinal force and similar expansions for the vertical force and pitching moment, we may write

$$T \cos\theta = \left[1 + 0\,(\delta^2, \beta^2, \delta\beta)\right] \; T = \delta X_{1000} + \beta X_{0100} + \delta^2 X_{2000} + \beta^2 X_{0200} + \delta\beta X_{1100} + 0(\delta^2\beta, \delta\beta^2) \tag{6-2}$$

$$T \sin\theta = \left[\delta\theta_{100} + \beta\theta_{010} + \delta\beta\theta_{110}\right] \; T = \delta Z_{1000} + \beta Z_{0100} + \delta^2 Z_{2000} + \beta^2 Z_{0200} + \delta\beta Z_{1100} + 0\,(\delta^2\beta, \delta\beta^2) \tag{6-3}$$

$$- h_r T = \delta M_{1000} + \beta M_{0100} + \delta^2 M_{2000} + \beta^2 M_{0200} + \delta\beta M_{1100} + 0\,(\delta^2\beta, \delta\beta^2) \tag{6-4}$$

It will be noted that we have not used terms containing α or ϵ as we are considering steady motion in calm water.

Referring to (5-6) and (5-7) we see that

$$X_{1000} = 0 \qquad \text{and} \quad X_{0100} = 0$$

and, similarly,

$$Z_{1000} = 0 \qquad \text{and} \quad Z_{0100} = 0$$

from conditions of equilibrium in the hydrostatic case. Similarly, during static hovering, i. e. at zero speed ahead, the total moment about the C. G, of the pressure on the cushion hull and that on the side hulls should be zero for equilibrium

$$\text{i. e.} \qquad \delta M_{1000} + \beta M_{0100} = 0$$

$$\text{i.e.} \quad -2\rho g \iint_{\bar{S}_{l_o}} x' . \delta h\,(x', z')\, dx'dz' + \iint_{\bar{S}_o} x\, \beta p_o \quad dxdy = 0$$

which specifies the distance of the centre of buoyancy of the side hulls and that of the centre of pressure of the air cushion from the C.G. If these distances are x_B and x_p respectively

$$- x_B m_2 g - x_p m_1 g = 0$$

$$\text{i.e.} \quad m_2 x_B = - m_1 x_p$$

a result which is obvious.

We may therefore delete the lowest order terms of $0(\delta, \beta)$ from (6-2) (6-3) and (6-4). The first equation then shows that T is of $0(\delta^2, \beta^2, \delta\beta)$

$$T = \delta^2 X_{2000} + \beta^2 X_{0200} + \delta\beta X_{1100} \qquad (6\text{-}5)$$

and since the left-hand side of (6-3) now becomes of $0(\delta^3, \delta^2\beta, \delta\beta^2, \beta^3)$ we conclude that

$$\delta^2 Z_{2000} + \beta^2 Z_{0200} + \delta\beta Z_{1100} = 0 \qquad (6\text{-}6)$$

and we may also write

$$- h_T \; T = \delta^2 M_{2000} + \beta^2 M_{0200} + \delta\beta M_{1100} \qquad (6\text{-}7)$$

The wave resistance is given exactly by (6-5) for $T = - R_W$ and this will be discussed in detail presently.

Some general remarks can be made without the actual solution of the surface integrals for the forces and moment in (6-5), (6-6) and (6-7).

Let us consider the integrals

$$\iint_{\bar{S}_o} p_{o_x} \, dxdy = \oint_{L_C} p_o \, dy$$

$$\iint_{\bar{S}_o} x\, p_{o_x} \, dxdy = \oint_{L_C} x\, p_o \, dy - \iint_{\bar{S}_o} p_o \, dxdy$$

$$\text{and} \iint_{\bar{S}_o} p_o \, p_{o_x} \, dxdy = \frac{1}{2} \oint_{L_C} p_o^2 \, dy$$

where the contour L_C is the boundary of the cushion

$$L_C = L_B + L_{1-} + L_S + L_{2+}$$

discussed in Appendix V. Since L_{1-} and L_{2+} differ from the longitidinal planes $y = \pm b$, by the semi-width of the hulls i.e. by $0(\delta)$ we may indeed set

$$dy = 0 + 0(\delta)$$

along L_{1-} and L_{2+} and the line integral may be taken over the bow and stern sections L_B and L_S only.

In the case of a uniform cushion with p_o = constant throughout the cushion, the first and last line integrals vanish. The line integrals also vanish in the case of a non-uniform cushion with the pressure reduced to a zero or non-zero uniform value at the front and rear boundaries and generally, in the case of any non-uniform cushion with fore-and-aft symmetry both in the pressure distribution and in the plan form of the cushion. The line integrals will only survive when the pressure along the front and rear boundaries have different values, say, in the case of compartmented cushions.

VI.1 Sinkage and Trim

Let us now consider (6-6) which shows that each term should be separately equal to zero as the three terms are of different orders and substituting for these terms from (5-7).

$$-2\rho V \iint_{\bar{S}_{1_o}} \Phi_{1000_{x'}} \frac{\partial h}{\partial z'} \, dx'dz' + 2\rho g \int_L (\bar{z}_{100} - x'\theta_{100}) \, h \, (x', o) \, dx' = 0 \qquad (6\text{-}8)$$

$$2(\bar{x}_{010} + h_G \theta_{010}) \iint_{\bar{S}_{1_o}} p_{o_x} \, dxdy = 0 \qquad (6\text{-}9)$$

and

$$- 2\rho V \iint_{\bar{S}_{1_o}} \left(\Phi^{+}_{0100_{x'}} \frac{\partial h_1}{\partial z'} + \Phi^{-}_{0100_{x'}} \frac{\partial h_2}{\partial z'}\right) dx'dz' +$$

$$+ 2\rho g \int_L (\bar{z}_{010} - x'\theta_{010})\, h(x', o)\, dx' -$$

$$- 2(\bar{x}_{100} + h_G \theta_{100}) \iint_{\bar{S}_o} p_{o_x}\, dxdy = 0 \qquad (6\text{-}10)$$

In the case of an arbitrary non-uniform cushion without fore-and-aft symmetry and with different pressures along the front and rear boundaries

$$\iint_{\bar{S}_o} p_{o_x}\, dxdy$$

will have a non-zero value as has just been established. In this case, therefore, (6-9) gives

$$\bar{x}_{010} + h_G \theta_{010} = 0$$

In the case of other types of cushion just discussed i.e. in the case of a uniform cushion or non-uniform cushion with fore-and-aft symmetry, the surface integral in (6-9) vanishes and the set of three equations becomes degenerate.

In the general case, however, we have three equations above for the six unknowns determining the surge displacement, sinkage and trim of the ACV during steady motion, namely

$$\bar{x}_{100}, \bar{x}_{010}, \bar{z}_{100}, \bar{z}_{010}, \theta_{100} \text{ and } \theta_{010}$$

The other three equations will be provided by the equations for the moment which we shall now consider.

Substituting for T on the left-hand side of (6-7) from (6-5) and equating terms of the same order given by (5-6) and (5-8) we have the three equations :

$$- 2\rho \iint_{\bar{S}_{1_0}} \left[V \left(z' \frac{\partial h}{\partial x'} - x' \frac{\partial h}{\partial z'} \right) \Phi_{1000_{x'}} + g\theta_{100}\, z'\, h(x', z') \right] dx'dz'$$
$$- 2\rho g \int_L (\bar{z}_{100} - x'\theta_{100})\, x'\, h(x', o)\, dx' - \left(\frac{m_2}{\delta}\right) g h_G \theta_{100}$$
$$= 2\rho V h_T \iint_{\bar{S}_{1_0}} \Phi_{1000_{x'}} \frac{\partial h}{\partial x'}\, dx'dz' \qquad (6\text{-}11)$$

$$2(\bar{x}_{010} + h_G \theta_{010}) \iint_{\bar{S}_0} x\, p_{o_x}\, dxdy - \left(\frac{m_1}{\beta}\right) g h_G \theta_{010}$$
$$= -\frac{1}{g} h_T \iint_{\bar{S}_0} \left[\frac{1}{\rho}\, p_o\, p_{o_x} - V p_o \Phi_{0100_{xx}}(x, y, o) \right] dxdy \qquad (6\text{-}12)$$

$$- 2\rho \iint_{\bar{S}_{1_0}} \left[V \left\{ \left(z' \frac{\partial h_1}{\partial x'} - x' \frac{\partial h_1}{\partial z'} \right) \Phi^{+}_{0100_{x'}} + \left(z' \frac{\partial h_2}{\partial x'} - x' \frac{\partial h_2}{\partial z'} \right) \Phi^{-}_{0100_{x'}} \right\} + g\theta_{010}\, z'\, h(x', z') \right] dx'dz' -$$
$$- 2\rho g \int_L (\bar{z}_{010} - x'\theta_{010})\, x'\, h(x', o)\, dx' +$$
$$+ 2(\bar{x}_{100} + h_G \theta_{100}) \iint_{\bar{S}_0} x\, p_{o_x}\, dxdy - \left\{ \left(\frac{m_1}{\beta}\right) \theta_{100} + \left(\frac{m_2}{\delta}\right) \theta_{010} \right\} g h_G = 2\rho V h_T \iint_{\bar{S}_{1_0}} \left[\Phi^{+}_{0100_{x'}} \frac{\partial h_1}{\partial x'} + \Phi^{-}_{0100_{x'}} \frac{\partial h_2}{\partial x'} \right] dx'dz' + \frac{V}{g} h_T \iint_{\bar{S}_0} p_o\, \Phi_{1000_{xx}}(x, y, o)\, dxdy \qquad (6\text{-}13)$$

We may simplify equations (6-8) to (6-13) using the following relations.

$$2\delta \int_L h(x', o)\, dx' = A$$
$$2\delta \int_L x'\, h(x', o)\, dx' = A\, x_A$$
$$2\delta \int_L x'^2\, h(x', o)\, dx' = I_A$$
$$2\rho g \delta \iint_{\bar{S}_{1_0}} z'\, h(x', z')\, dx'dz' = m_2\, g\, z_B$$

$$\beta \iint_{\bar{S}_0} x\, p_{o_x}\, dxdy = \rho \int_{L_c} x_{p_o}\, dy + m_1 g$$

We thus have the set of equations :

$$\bar{z}_{100} - x_A \theta_{100} = \frac{2V\delta}{gA} \iint_{\bar{S}_{1_0}} \Phi_{1000_{x'}}(x', b, z')\, \frac{\partial h}{\partial z'}\, dx'dz' \qquad (6\text{-}14)$$

$$\bar{x}_{010} + h_G \theta_{010} = 0 \quad \text{if} \iint_{\bar{S}_0} p_{o_x}\, dx\, dy \neq 0 \qquad (6\text{-}15)$$

$$\bar{z}_{010} - x_A \theta_{010} = \frac{2V\delta}{gA} \iint_{\bar{S}_{1_0}} \left(\Phi^{+}_{0100_{x'}} \frac{\partial^{h_1}}{\partial z'} + \Phi^{-}_{0100_{x'}} \frac{\partial^{h_2}}{\partial z'}\right) dx'dz' + \frac{2\delta}{\rho gA} \left(\bar{x}_{100} + h_G \theta_{100}\right) \iint_{\bar{S}_0} p_{o_x}\, dxdy \qquad (6\text{-}16)$$

$$\bar{z}_{100} + \frac{m_2 (h_G + z_B) - \rho I_A}{\rho A x_A} \theta_{100} = -\frac{2\delta}{gAx_A} \iint_{S_{1_0}} \left[V \left\{ (z' + h_T) \frac{\partial h}{\partial x'} - x' \frac{\partial h}{\partial z'} \right\} \Phi_{1000_{x'}}\right] dx'dz' \qquad (6\text{-}17)$$

$$2 (x_{100} + h_G \theta_{100}) \int_{L_B + L_S} x p_o\, dy + (2\bar{x}_{100} + h_G \theta_{100}) \left(\frac{m_1}{\beta}\right) g = -\frac{h_T}{2\rho g} \int_{L_c} p_o^2\, dy + \frac{V}{g} h_T \iint_{\bar{S}_0} p_o \Phi^{(x, y, o)}_{0100_{xx}}\, dxdy \qquad (6\text{-}18)$$

$$2 (\bar{x}_{100} + h_G \theta_{100}) \int_{L_B + L_S} x\, p_o\, dy + (2\, \bar{x}_{100} + h_G \theta_{100}) \left(\frac{m_1}{\beta}\right) g + g \theta_{010} \left\{\rho \left(\frac{I_A}{\delta}\right) - \left(\frac{m_2}{\delta}\right) (h_G + z_B)\right\} - \rho g\, \bar{z}_{010} \left(\frac{A}{\delta}\right) x_A = 2\rho \iint_{\bar{S}_{1_0}} \left[V \left\{ (z' + h_T) \frac{\partial^{h_1}}{\partial x'} - x' \frac{\partial^{h_1}}{\partial z'} \right\} \Phi^{+}_{0100_{x'}} + V \left\{ (z' + h_T) \frac{\partial^{h_2}}{\partial x'} - x' \frac{\partial h_2}{\partial z'} \right\} \Phi^{-}_{0100_{x'}} \right] dx'dz' + \frac{V}{g} h_T \iint_{\bar{S}_0} p_o \Phi_{1000_{xx}}(x, y, o)\, dxdy \qquad (6\text{-}19)$$

It will be readily observed from the above equations that when $x = 0$ i.e. when the C.G. of the waterplane area of the side hulls lies below the C.G. of the ACV, the pitch and heave displacements are uncoupled.

The above equations are applicable to arbitrary non-uniform cushions. From (6-15) and (6-18) we readily obtain

$$\beta x_{010} = -h_G(\beta\theta_{010}) = -\frac{h_T}{2\rho g^2 m_1}\int_{L_B+L_S}(\beta p_o)^2\,dy + \frac{Vh_T}{m_1 g^2}\iint_{\bar{S}_o}(\beta p_o)(\beta\Phi_{0100_{xx}})\,dxdy \qquad (6\text{-}20)$$

so that the steady surge and pitch displacements of $0(\beta)$ are zero of the thrust line passes through the C.G.

The other four displacements can be obtained from the four equations (6-14), (6-16), (6-17) and (6-19).

The displacements in the lowest order

$$\delta\bar{x}_{100} + \beta\bar{x}_{010}$$

$$\delta\bar{z}_{100} + \beta\bar{z}_{010}$$

and

$$\delta\theta_{100} + \delta\theta_{010}$$

have thus been solved. The higher order displacement of $0(\delta\beta)$ can also be obtained by considering the higher order forces and moment.

In the case of uniform cushions or non-uniform cushions with fore-and-aft symmetry,

$$\iint_{\bar{S}_o} p_{o_x}\,dxdy = 0$$

and equation (6-15) does not exist. We could obtain $\bar{x}_{100}$, $\bar{z}_{100}$, and θ_{100} from (6-14), (6-17) and (6-19), but there are only two remaining equations for solving $\bar{x}_{010}$, $\bar{z}_{010}$ and θ_{010}.

We could, however, make the additional assumption that $\bar{x}_{010}$ and $\bar{x}_{100}$ are both zero, for the steady surge displacement is not a useful quantity and can, in any case, be absorbed in the co-ordinate system. In this manner the sinkage (heave displacement) and trim (pitch displacement) can be calculated.

VI . 2 The Steady Potential

It is shown in Appendix V that the potential in steady motion can be derived in the form

$$\Phi(x, y, z) = \delta\Phi_{1000} + \beta\Phi_{0100}$$

where

$$\Phi_{1000} = \frac{V}{4\pi}\iint_{\bar{S}_{1_0}} \frac{\partial h}{\partial \xi'}\left[G(x, y, z; \xi', b, \zeta') + G(x, y, z; \xi', -b, \zeta')\right] d\xi' d\zeta'$$

and

$$\begin{aligned}\Phi_{0100} = {} & \frac{V}{4\pi\rho g}\iint_{\bar{S}_0} \frac{\partial P_o}{\partial \xi}\; G(x, y, z; \xi, \eta, o)\; d\xi\, d\eta + \ldots \\ & + \frac{V^2}{4\pi\rho g}\oint_{L_B^+ L_S}\Big[\Big[\Phi_{0100}(\xi, \eta, o)\Big]_{EFS}^{IFS}\; \frac{\partial}{\partial \xi}\; G(x, y, z; \xi, \eta, o) - \\ & - \Big[\frac{\partial}{\partial \xi}\; \Phi_{0100}(\xi, \eta, o)\Big]_{EFS}^{IFS}\; G(x, y, z; \xi, \eta, o)\Big]\; d\eta - \\ & - \frac{1}{4\pi}\iint_{\bar{S}_{10}}\Big[\Phi_{0100}(\xi', b-, \zeta') - \Phi_{0100}(\xi', b+, \zeta')\Big] \ldots \\ & \Big[\frac{\partial G(x, y, z; \xi', \eta', \zeta')}{\partial \eta'}\Big|_{\eta'=b} - \frac{\partial G(x, y, z; \xi', \eta', \zeta')}{\partial \eta'}\Big|_{\eta'=-b}\Big]\Big] \qquad d\xi' d\zeta' \end{aligned} \tag{6-21}$$

As indicated in Appendix V, we have only derived an integral equation for Φ_{0100}, although Φ_{1000} has been explicitly solved in the form of an integral representation on the assumption that the separation between the side hulls is sufficiently large for the interference effects between the hulls to be considered negligible. In this case there will be no "jump" in the potential between the two sides of each hull

and an explicit solution is possible.

The velocity potential due to the air cushion now derived can be shown to be of the same general form as that previously obtained for the acceleration potential of an amphibious ACV in Reference 1. There is, however, an additional term now in the form of a surface integral over the longitudinal planes of the hulls which provide a vertical barrier along the lateral sides of the cushion.

The Green's function to be used for steady motion is

$$\bar{G}(x,y,z;\xi,\eta,\zeta) = \left[(x-\zeta)^2 + (y-\eta)^2 + (z-\zeta)^2\right]^{-1/2} - \left[(x-\xi)^2 + (y-\eta)^2 + (z+\zeta)^2\right]^{-1/2} + \frac{4g}{\pi} \operatorname{Re} \int_0^{\pi/2} \int_M \frac{e^{-p(z+\zeta)+ip(x-\xi)\cos\theta} \cos p(y-\eta)\sin\theta}{g - pV^2\cos^2\theta} \, dp\, d\theta \qquad (6\text{-}22)$$

where M is the contour along the real axis of the complex p-plane passing above the point

$$p = p_o = \frac{g}{V^2} \sec^2\theta$$

The integrand in (6-22) is complex, but as we are interested only in the real part of the integral, we must seek the contribution from the real part along the real p-axis and that of the imaginary part along the semi-circle above the simple pole

$$p = k_o \sec^2\theta$$

where $k_o = g/V^2$. We thus obtain after evaluating the residue

$$\bar{G}(x,y,z;\xi,\eta,\zeta) = \left[(x-\xi)^2 + (y-\eta)^2 + (z-\zeta)^2\right]^{-1/2} - \left[(x-\xi)^2 + (y-\eta)^2 + (z+\zeta)^2\right]^{-1/2} - 4k_o \int_0^{\pi/2} e^{-k_o(z+\zeta)\sec^2\theta} \sin\left[k_o(x-\xi)\sec\theta\right]$$

$$\cos\left[k_o(y-\eta)\sec^2\theta\sin\theta\right]\sec^2\theta\,d\theta - \frac{4k_o}{\pi}\int_0^{\pi/2}\sec^2\theta\,d\theta$$

$$\oint_0^\infty \frac{e^{-p(z+\zeta)}\cos\left[p(x-\xi)\cos\theta\right]\cos\left[p(y-\eta)\sin\theta\right]}{p - k_o\sec^2\theta}\,dp \qquad (6\text{-}23)$$

where $\oint$ indicates that the Cauchy principal value is to be taken.

VI. 3 Wave Resistance

The wave resistance is given by

$$R_W = -\delta^2 X_{2000} - \beta^2 X_{0200} - \delta\beta X_{1100}$$

and substituting for the longitudinal forces from (5-6), we may write

$$R_W = 2\rho V\delta^2 \iint_{\bar{S}_{1_0}} \Phi_{1000_{x'}}(x', b, z')\,\frac{\partial h}{\partial x'}\,dx'dz' -$$

$$-\frac{1}{g}\beta 2\iint_{\bar{S}_0}\left[\frac{1}{\rho}\,p_o\,p_{o_x} - V\,p_o\,\Phi_{0100_{xx}}(x,y,o)\right]dxdy +$$

$$+ 2\rho V\,\delta\beta\iint_{\bar{S}_{1_0}}\left[\Phi_{0100_{x'}}(x', b+, z')\frac{\partial h_1}{\partial x'} + \Phi_{0100_{x'}}(x', b-, z')\frac{\partial h_2}{\partial x'}\right]$$

$$dx'dz' + \frac{V}{g}\delta\beta\iint_{\bar{S}_0} p_o\,\Phi_{1000_{xx}}(x,y,o)\,dxdy \qquad (6\text{-}23A)$$

The first term on the RHS, is the wave resistance due to the side hulls in calm water. It is assumed that the separation between the side hulls is sufficiently large to avoid the necessity of evaluating the potential on the two separate sides of $\bar{S}_{1_0}$ due to possible interference between the two hulls. The second term gives the wave resistance of the air cushion and the two remaining terms represent the interference effects of the air cushion on the side hulls and of the side hulls on the air cushion respectively. These terms may be evaluated separately and then added together to give the combined wave resistance of the entire system moving in calm water.

Considering first the hull resistance and substituting for the potential from (6-21), we have

$$\frac{1}{\delta^2} R_{W\ hulls} = \frac{\rho V^2}{2\pi} \iint_{S_{1_0}} \frac{\partial h}{\partial x'} dx' dz' \iint_{S_{1_0}} \frac{\partial h}{\partial \xi'} d\xi' d\zeta' \left[G_{x'}(x', b, z'; \xi', b, \zeta') + G_{x'}(x', b, z'; \xi', -b, \zeta') \right] \tag{6-24}$$

Now

$$\frac{\partial G(x', b, z'; \xi', b, \zeta')}{\delta x'} = -\frac{x' - \xi'}{\left[(x' - \xi')^2 + (z' - \zeta')^2\right]^{3/2}} + \frac{x' - \xi'}{\left[(x' - \xi')^2 + (z' + \zeta')^2\right]^{3/2}} - 4k_o^2 \int_0^{\pi/2} e^{-k_o(z' + \zeta')\sec^2\theta} \cos\left[k_o(x' - \xi')\sec\theta\right] \sec^3\theta \, d\theta + \frac{4k_o}{\pi} \int_0^{\pi/2} \sec\theta \, d\theta \int_0^{\infty} \frac{p e^{-p(z' + \zeta')} \sin\left[p(x - \xi)\cos\theta\right]}{p - k_o \sec^2\theta} dp \tag{6-25}$$

and

$$\frac{\partial G(x', b, z'; \xi', -b, \zeta')}{\partial x'} = -\frac{x' - \xi'}{\left[(x' - \xi')^2 + 4b^2 + (z' - \zeta')^2\right]^{3/2}} + \frac{x' - \xi'}{\left[(x' - \xi')^2 + 4b^2 + (z' + \zeta')^2\right]^{3/2}} - 4k_o^2 \int_0^{\pi/2} e^{-k_o(z' + \zeta')\sec^2\theta} \cos\left[k_o(x' - \xi')\sec\theta\right] \cos\left[2k_o b \sec^2\theta \sin\theta\right] \sec^3\theta \, d\theta + \frac{4k_o}{\pi} \int_0^{\pi/2} \sec\theta \, d\theta \int_0^{\infty} \frac{p e^{-p(z' + \zeta')} \sin\left[p(x' - \xi')\cos\theta\right] \cos\left[2pb\sin\theta\right]}{p - k_o \sec^2\theta} dp \tag{6-26}$$

We may write (6-24) in the form

$$\frac{1}{\delta^2} R_{W_{hulls}} = \frac{\rho V^2}{2\pi} \iint_{\bar{S}_{1_0}} \frac{\partial h(x', z')}{\partial x'} \, dx'dz' \iint_{\bar{S}_{1_0}} \frac{\partial h(\xi', \zeta')}{\partial \xi'} \, d\xi' \, d\xi'$$
$$\left[f_1 (x', z' ; \xi', \zeta') + f_2 (x', z' ; \xi' \; \zeta') \right]$$

where f_1 and f_2 are given by (6-25) and (6-26) respectively.

The above equation may also be written

$$\frac{1}{\partial^2} R_{W_{hulls}} = \frac{\rho V^2}{2\pi} \iint_{\bar{S}_{1_0}} \frac{\partial h(\xi', \zeta')}{\partial \xi'} \, d\xi' \, d\zeta' \iint_{\bar{S}_{1_0}} \frac{\partial h(x', z')}{\partial x'} \, dx'dz'$$
$$\left[f_1 (\xi', \zeta' ; x', z') + f_2 (\xi', \zeta' ; x', z') \right]$$

by interchanging x' with ξ' and z' with ζ'

$$\text{i.e.} \quad = \frac{\rho V^2}{4\pi} \iint_{\bar{S}_{1_0}} \frac{\partial h(x', z')}{\partial x'} \, dx'dz' \iint_{\bar{S}_{1_0}} \frac{\partial h(\xi', \xi')}{\partial \xi'} \, d\xi' \, d\xi'$$
$$\left[f_1 (x', z' ; \xi', \zeta') + f_1 (\xi', \zeta' ; x', z') + f_2 (x', z' ; \xi', \zeta') + \right.$$
$$\left. + f_2 (\xi', \zeta' ; x', z') \right]$$

by the addition of the above two expressions and taking half the value.

It will be seen that the first, second and fourth terms on the RHS of (6-25) and (6-26) are odd functions of $(x' - \xi')$ so that they cancel respectively with each other when we take the sum

$$f_1 (x', z' ; \xi', \zeta') + f_1 (\xi', \zeta' ; x', z')$$

and

$$f_2 (x', z' ; \xi', \zeta') + f_2 (\xi', \zeta' ; x', z')$$

but the third term is an even function and gives a contribution to the sum by doubling itself in each case so that we have

$$\frac{1}{\delta^2} R_{W_{hulls}} = -\frac{4\rho V^2 k_o^2}{\pi} \iint_{S_{1_0}} \frac{\partial h(x', z')}{\partial x'} dx'dz' \iint_{S_{1_0}} \frac{\partial h(\xi', \zeta')}{\partial \xi'} d\xi' d\zeta'$$
$$\int_0^{\pi/2} e^{-k_o (z'+\zeta') \sec^2\theta} \cos\left[k_o (x' - \xi') \sec\theta\right]$$
$$\left[1 + \cos 2 k_o b \sec^2\theta \sin\theta\right] \sec^3\theta \, d\theta \qquad (6\text{-}27)$$

If we use the expansions

$$\cos\left[k_o (x' - \xi') \sec\theta\right] = \cos (k_o x' \sec\theta) \cos (k_o \xi' \sec\theta) +$$
$$+ \sin (k_o x' \sec\theta) \sin (k_o \xi' \sec\theta)$$

and

$$1 + \cos (2 k_o b \sec^2\theta \sin\theta) = 2 \cos^2 (k_o b \sec^2\theta \sin\theta)$$

and write

$$P(\theta) = \cos (k_o b \sec^2\theta \sin\theta) \iint_{S_{1_0}} \frac{\partial h(x', z')}{\partial x'} e^{-k_o z' \sec^2\theta}$$
$$\cos (k_o x' (\sec\theta) \, dx'dz'$$

and

$$Q(\theta) = \cos (k_o b \sec^2\theta \sin\theta) \iint_{S_{1_0}} \frac{\partial h(x', z')}{\partial x'} e^{-k_o z' \sec^2\theta}$$
$$\sin (k_o x' \sec\theta) \, dx'dz' \qquad (6\text{-}28)$$

we have for the absolute value of the wave resistance

$$\frac{1}{\delta^2} R_{W_{hulls}} = \frac{8\rho g^2}{\pi V^2} \int_0^{\pi/2} (P^2 + Q^2) \sec^3\theta \, d\theta \qquad (6\text{-}29)$$

When the quantity b representing one half of the separation between the two hulls is set equal to zero we get the result for two superimposed hulls which is the limiting condition of two contiguous hulls with the width doubled and as the resistance can be seen from (6-28) and (6-29) to be proportional to the square of the width of the hull, we will have to take one quarter of the above value for a single

hull

$$\frac{1}{\delta^2} R_{W_{hull}} = \frac{2\rho g^2}{\pi V^2} \int_0^{\pi/2} (P_o^2 + Q_o^2) \sec^3\theta \, d\theta \qquad (6\text{-}30)$$

where

$$P_o + iQ_o = \iint_{S_{10}} \exp(-k_o z' \sec^2\theta + ik_o x' \sec\theta) \, dx'dz'$$

which is the familiar Michell integral for the steady state wave resistance of a single hull. The constant 2 is usually given as 4 in Michell's formula, but we have taken h to be the total width of the hull and not the semi-width.

We will now consider the wave resistance of the air cushion

$$\frac{1}{\beta^2} R_{W_{cushion}} = -\frac{1}{g} \iint_{S_o} \left[\frac{1}{\rho} p_o p_{o_x} - V p_o \Phi_{0100_{xx}}(x, y, o) \right] dxdy$$

where the potential is given by (6-21). This is an integral equation and attempts are being made to solve this, but we can obtain a simple integral representation for the potential of the form

$$\Phi_{0100} = \frac{V}{4\pi\rho g} \iint_{S_o} \frac{\partial p_o(\xi, \eta)}{\partial \xi} G(x, y, z; \xi, \eta, o) \, d\xi d\eta$$

if we make the following assumptions.

(i) The pressure in the cushion is diffused in such a manner that it becomes zero at the front and rear boundaries where the plenum air escape with air entrainment from the atmosphere and the generation of trapped vortices will probably ensure that this is so in practice. If this assumption is valid, the "jumps" in the potential and in the longitudinal velocity of the water particles will vanish and the line integral in (6-21) may be ignored.

(ii) Although a discontinuity in the potential may be assumed not to exist at the front and rear boundaries, a discontinuity will certainly be present across the vertical barriers imposed by the side hulls as there is no air escape across these boundaries to alleviate a discontinuity of the pressure. However, if the depth of immersion of the side hulls is small and of the same order, say, as that of the hull width, the surface integral over $\overline{S}_{1_o}$ will be of $0(\delta)$ higher

than that of the potential and may therefore be ignored.

As stated above, the above assumptions may be made pending a rigorous solution of the integral equation for the potential so that practical results can be achieved even if they are approximate ones.

Also, under assumption (i) above,

$$\iint_{S_o} p_o \, p_{o_x} \, dxdy = \oint_{L_C} p_o^2 \, dy = 0$$

and we may write simply

$$\frac{1}{\beta^2} R_{W_{cushion}} = \frac{V}{g} \iint_{S_o} p_o \, \Phi_{0100_{xx}}(x, y, o) \, dxdy$$

$$= \frac{V}{g} \oint_{L_C} p_o \, \Phi_{0100_x} \, dy - \frac{V}{g} \iint_{S_o} p_{o_x} \, \Phi_{0100_x} \, dxdy$$

The line integral is again zero and

$$\frac{1}{\beta^2} R_{W_{cushion}} = -\frac{V}{g} \iint_{S_o} p_{o_x} \, \Phi_{0100_x} \, dxdy$$

$$= -\frac{V^2}{4\pi\rho g^2} \iint_{S_o} \frac{\partial p_o(x, y)}{\partial x} \, dxdy \iint_{S_o} \frac{\partial p_o(\xi, \eta)}{\partial \xi} \, d\xi \, d\eta$$

$$\left[G_x(x, y, o; \xi, \eta, o) \right] \qquad (6\text{-}31)$$

This is almost exactly of the same form as the expression (6-24) for the hull wave resistance with p_o instead of h.

Now

$$\frac{\delta G(x, y, o; \xi, \eta; o)}{\partial x} = -4k_o^2 \int_0^{\pi/2} \cos\left[k_o(x-\xi) \sec\theta\right]$$

$$\cos\left[k_o(y-\eta) \sec^2\theta \sin\theta\right] \sec^3\theta \, d\theta + \frac{4k_o}{\pi} \int_0^{\pi/2} \sec\theta \, d\theta$$

$$\int_0^{\infty} \frac{p \sin\left[p(x-\xi)\cos\theta\right]\cos\left[(y-\eta)\sin\theta\right]}{p - k_o \sec^2\theta} \, dp$$

Substituting in (6-31) and noting that the second term on the RHS makes no contribution to the double surface integrals, we have

$$\frac{1}{\beta^2} R_{W_{cushion}} = \frac{1}{\pi\rho V^2} \iint_{S_o} \frac{\partial p_o(x,y)}{\partial x} \, dxdy \iint_{S_o} \frac{\partial p_o(\xi,\eta)}{\partial \xi} \, d\xi d\eta$$
$$\int_0^{\pi/2} \cos\left[k_o(x-\xi)\sec\theta\right]\cos\left[k_o(y-\eta)\sec^2\theta\sin\theta\right] \sec^3\theta \, d\theta$$

It is easy to reduce this as before to the form

$$\frac{1}{\beta^2} R_{W_{cushion}} = \frac{1}{\pi\rho V^2} \int_0^{\pi/2} \left[P^2(\theta) + Q^2(\theta)\right] \sec^3\theta \, d\theta \qquad (6\text{-}32)$$

where now

$$\begin{Bmatrix} P(\theta) \\ Q(\theta) \end{Bmatrix} = \iint_{S_o} \frac{\partial p_o(x,y)}{\partial x} \begin{Bmatrix} \cos \\ \sin \end{Bmatrix} \left[k_o(x\cos\theta + y\sin\theta)\sec^2\theta\right] \, dxdy \qquad (6\text{-}33)$$

These expressions may be compared with (6-28) and (6-29) for the hull wave resitance.

It is clear from (6-33) that we may write by the use of Stokes' theorem,

$$\begin{Bmatrix} P(\theta) \\ Q(\theta) \end{Bmatrix} = \oint_{L_C} p_o(x,y) \begin{Bmatrix} \cos \\ \sin \end{Bmatrix} \left[k_o(x\cos\theta + y\sin\theta)\sec^2\theta\right] \, dy -$$
$$- k_o \sec\theta \iint_{S_o} p_o(x,y) \begin{Bmatrix} -\sin \\ \cos \end{Bmatrix} \left[k_o(x\cos_\theta + y\sin_\theta)\sec^2\theta\right] dxdy$$

The line integral vanishes and we have

$$\frac{1}{\beta^2} R_{W_{cushion}} = \frac{k_o^2}{\pi\rho V^2} \int_0^{\pi/2} \left[P_1^2(\theta) + Q_1^2(\theta)\right] \sec^5\theta \, d\theta \qquad (6\text{-}34)$$

where

$$\begin{Bmatrix} P_1(\theta) \\ Q_1(\theta) \end{Bmatrix} = \iint_{\bar{S}_0} p_o(x, y) \begin{Bmatrix} \cos \\ \sin \end{Bmatrix} \left[k_o (x\cos\theta + y\sin\theta) \sec^2\theta \right] \quad dxdy \tag{6-35}$$

These results agree exactly with those given by Havelock [6] for a surface pressure distribution which is continuous and is zero at the outer boundaries.

We now come that part of the wave resistance which is due to the interference between the air cushion and the side hulls.

Referring to (6-23A) we shall not attempt to evaluate the integral over $\bar{S}_{1_o}$ for under the assumption made previously (i. e. with small side hull immersion) the integral will be of $0(\delta^2\beta)$. The interference of the air cushion on the side hulls may therefore be neglected.

The effect of the interference of the side hulls on the air cushion is given by

$$\frac{1}{\delta\beta} R_{W_{interference}} = \frac{V}{g} \iint_{\bar{S}_0} p_o \, \Phi_{1000xx}(x, y, o) \, dxdy =$$

$$= -\frac{V}{g} \iint_{\bar{S}_0} \frac{\partial p_o}{\partial x} \, dxdy \iint_{\bar{S}_{1_o}} \frac{\partial h}{\partial \xi'} \, d\xi' d\zeta' \left[G_x(x, y, o; \xi', b, \zeta') + \right.$$

$$\left. + G_x(x, y, o; \xi', -b, \zeta') \right] \tag{6-36}$$

It does not appear that this double surface integral could be reduced to the simple form of a single integral as in the case of the hull resistance and the cushion resistance.

VI . 4 Drifting Amphibious ACV

The case of an amphibious hovercraft drifting in calm water has been discussed in section 7 of Reference 1 and a solution for the wave resistance in closed form has been obtained in the form

$$\frac{1}{\beta^2} R_{W_{cushion}} = \frac{k_o^2}{2\pi\rho V^2} \int_{-\pi/2}^{\pi/2} \left[P^2(\theta, \beta) + Q^2(\theta, \beta) \right] \quad \sec^5\theta \, d\theta$$

with

$$\begin{Bmatrix} P(\theta, \beta) \\ Q(\theta, \beta) \end{Bmatrix} = \iint_{\xi_0} p_o(x, y \begin{Bmatrix} \cos \\ \sin \end{Bmatrix} \left[k_o \left(x\cos(\theta+\beta) + y\sin(\beta+\theta) \right) \sec^2\theta \right] \, dxdy \tag{6-37}$$

where β is the angle of drift on the right-hand side.

The side force $\vec{F}_S$ in drifting motion has also been obtained in Reference 1

$$\frac{1}{\beta 2} F_S = \frac{k_o^2}{2\pi\rho V^2} \int_{-\pi/2}^{\pi/2} \left[P^2(\theta, \beta) + Q^2(\theta, \beta) \right] \sec^6\theta \sin(\beta + \theta) \, d\theta$$

It is not worth attempting to find a solution for a drifting ACV with side hulls since the lateral motion will induce a disturbance of the water which will not be consistent with the basic assumptions of this linearized theory.

VII. FORCED OSCILLATION IN CALM WATER

Let us now consider the case of an ACV which is forced to oscillate in calm water during steady translation. Obviously, we have in mind the forced oscillation of an ACV model during towing tank tests. We will now derive the oscillatory forces and moment acting on the craft when the motion and oscillations are confined to the longitudinal plane. Such a motion can be deliberately imparted to the model by a mechanical oscillator such as the Planar Motion Mechanism (PMM). The added mass and damping of water can be determined by experiments of this nature in calm water.

In the case of an amphibious ACV free from water contact, the discussion of the motion in the longitudinal plane can be applied directly to motion in the lateral plane for the disturbance of the water would be comparable in both cases, the beam/length ratio of present day hovercraft being of the order of unity. The discussion of surge, heave and pitch in this section will then apply also to sway, heave and roll in beamwise motion.

VII. 1 The Unsteady Potential

The potential can be expressed in the form

$$\Phi(x, y, z; t; \delta; \beta; \alpha) = \delta\Phi_{1000} + \beta\Phi_{0100} + \\ + e^{i\sigma t}\left[\delta\alpha\Phi_{1010} + \beta\alpha\Phi_{0110} + \quad\right]$$

The displacements will consist of the steady terms constituting the trim of the ACV in calm water together with the oscillatory terms :

$$\bar{x} = \delta\bar{x}_{100} + \beta\bar{x}_{010} + \alpha e^{i\sigma t}\bar{x}_{001} + \delta\alpha e^{i\sigma t}\bar{x}_{101} + \beta\alpha e^{i\sigma t}\bar{x}_{011} +$$

with similar expressions for $\bar{z}$ and θ.

In the above expansions σ is the frequency of forced oscillation. The discussion in this section will apply equally to free oscillation due to wave excitation in which case σ will be the frequency of encounter of the waves. This is discussed in the next section.

The steady potentials Φ_{1000} and Φ_{0100} have been discussed in the preceding section. The oscillatory potentials Φ_{1010} and Φ_{0110} are derived in Appendix V with an explicit integral representation for the former and an integral equation for the latter which could, however, be simplified and an explicit solution obtained under certain assumptions similar to those outlined in the last section.

VII. 2 Lowest Order Restoring Forces and Moments

The lowest order restoring forces and moments are obtained from (5-6), (5-7) and (5-8) and after simplification reduce to :

$$e^{i\sigma t}(\delta\alpha X_{1010} + \beta\alpha X_{0110}) = -\alpha m \sigma^2 \bar{x}_{001} e^{i\sigma t}$$

$$e^{i\sigma t}(\delta\alpha Z_{1010} + \beta\alpha Z_{0110}) = \alpha e^{i\sigma t}\left[\rho g A(\bar{z}_{001} - x_A \theta_{001}) - \right.$$

$$\left. - \sigma^2 m \bar{z}_{001} - (\bar{x}_{001} + h_G \theta_{001}) \iint_{\zeta_0} \beta P_{o_x} \, dxdy\right]$$

$$e^{i\sigma t}\left(\delta\alpha M_{1010} + \beta\alpha M_{0110}\right) = \alpha e^{i\sigma t}\Big[mh_G\left(\sigma^2\bar{x}_{001} - g\theta_{001}\right) +$$

$$+ \left(\rho g I_A - m_2 g z_B - \sigma^2 I\right)\theta_{001} - \rho g \bar{z}_{001}\, Ax_A +$$

$$+ 2\left(\bar{x}_{001} + h_G\,\theta_{001}\right)\iint_{\bar{S}_0} \beta x\, p_{o_x}\, dxdy\Big] \qquad (7\text{-}1)$$

These expressions give the restoring forces and moment acting on the craft when it is given oscillatory displacements in surge, heave and pitch of a forced nature. The longitudinal force contains the inertia term only, but the vertical force and pitching moment contain in addition, the contributions due to hydrostatic pressure. The velocity potential of the water does not enter in the forces and moment of this order and we cannot therefore expect to find such effects as the added mass and damping of water which are of a hydrodynamic nature and of a higher order.

VII. 3 Higher Order Restoring Forces and Moment Added Mass and Damping Effects

The higher order forces and moment can also be written down from (5-6), (5-7) and (5-8) in the same manner as (7-1). These second order forces and moment include the added mass and damping effects of water as the potentials Φ_{1010} and Φ_{0110} enter into these expressions in addition to the steady potentials and the steady displacements as the steady disturbance of the water persists during the oscillations. The pitch and heave stiffness of the air cushion also play their part in determining the forces and moments of this order.

It is clear that the steady potentials Φ_{1000} and Φ_{0100} (which are real) will be in phase with the displacements and will not therefore yield any damping contribution. The only contribution will be from the unsteady potentials Φ_{1010} and Φ_{0110} which have a real part and an imaginary part, so that when the product with $e^{i\sigma t}$ is taken there will be components of force in phase and in quadrature with the displacements giving rise to added mass and damping effects.

It will have to be remembered that we are discussing only hydrodynamic effects here. The damping due to aerodynamic and pneumatic effects in the air cushion will also have to be taken into account.

VIII. FREE OSCILLATION IN WAVES

We will now consider the case of an ACV moving at a constant speed in a seaway composed of regular waves with their crests normal to the course of the craft. It is assumed that the craft has been operating for a long time so that all the transients would have subsided. The craft would then undergo periodic oscillations in pitch, heave and surge with the same frequency as that at which the progressive waves are encountered. It is assumed for the purpose of this initial study that the seaway is composed of a single system of simple harmonic waves of a particular frequency. An extension to motion in an irregular seaway can then be made by using the methods of spectral analysis.

The velocity potential of the water will now be composed of several terms as follows :

$$\phi(x, y, z; t; \delta, \beta, \epsilon) = \delta\Phi_{1000} + \beta\Phi_{0100} + \mathrm{Re.}\, e^{i\sigma_e t}$$

$$\left[\epsilon\phi_{0001} + \delta\epsilon\Phi_{1001} + \beta\epsilon\Phi_{0101} + \quad\right]$$

where Φ_{1000} and Φ_{0101} are the steady potentials for motion in calm water discussed in Section 6;

Φ_{0001} is the potential of the incident wave;

Φ_{1001} is the potential of the wave diffracted from the side hulls;

Φ_{0101} is the potential of the wave representing the disturbance of the incident wave by the air cushion;

and σ_e is the encountered frequency of the regular waves.

VIII. 1 Incident Wave Potential

It has been shown in Reference 1 that the velocity potential of a regular wave of amplitude a_w, circular frequency σ and progressing along the negative x-axis may be written in the form

$$\Phi = \frac{a_w}{\lambda}\left(\frac{g}{\sigma}\right)\left(\frac{2\pi}{k}\right)\exp\left[-kz + i(kx + \sigma_e t + \gamma)\right]$$

where the wave length

$$\lambda = \frac{2\pi}{k}$$

and the wave number

$$k = \frac{\sigma^2}{g}$$

The frequency of encounter

$$\sigma_e = \sigma + kV$$

and γ is the phase angle of the wave.

As we have denoted the amplitude/length ratio of the incident waves by the small perturbation parameter ϵ, we may write

$$\Phi = \epsilon \frac{2\pi g}{\sigma k} \exp \left[-kz + i(kx + \sigma_e t + \gamma)\right]$$

so that in our notation

$$\Phi_{0001} = \frac{2\pi g}{\sigma k} \exp \left[-kz + i(kx + \gamma) \right] \qquad (8\text{-}1)$$

VIII. 2 Lowest Order Exciting Forces

We are now in a position to compute the lowest order exciting force in the longitudinal direction from (5-6)

$$\delta\epsilon X_{1001} + \beta\epsilon X_{0101} = 2\delta\epsilon\rho e^{i\sigma_e t} \iint_{\bar{S}_{1_0}} (i\sigma_e \Phi_{0001} - V\Phi_{000_{1_{x'}}}) \frac{\partial h}{\partial x'} \, dx'dz'$$

$$\ldots + \frac{1}{g} \beta\epsilon e^{i\sigma e t} \iint_{\bar{S}_0} (i\sigma_e \Phi_{0001_x} - V\Phi_{0001_{xx}}) \, p_o \, dxdy$$

and substituting for the derivatives of Φ_{0001} from (8-1) we get

$$\delta\epsilon X_{1001} + \beta\epsilon X_{0101} = \delta\epsilon \frac{4\pi i\rho g}{k} e^{i\sigma e t}$$

$$\iint_{\bar{S}_{1_0}} \exp \left[- kz' + i(kx + \gamma) \right] \frac{\partial h}{\partial x'} \, dx'dz' -$$

$$- 2\pi \beta\epsilon e^{i\sigma e t} \iint_{\bar{S}_0} \exp \left[i(kx + \gamma) \right] \, p_o \, dxdy \qquad (8\text{-}2)$$

The vertical force and pitching moment due to wave excitation arise mainly from the side hulls as the air cushion provides no contribution and we have

$$\delta\epsilon Z_{1001} = \delta\epsilon \frac{4\pi i\rho g}{k} e^{i\sigma et} \iint_{\bar{S}_{1_0}} \exp\left[-kz' + i(kx + \gamma)\right] \frac{\partial h}{\partial z'} \, dx'dz' \tag{8-3}$$

and

$$\delta\epsilon M_{1001} = \delta\epsilon \frac{4\pi i\rho g}{k} e^{i\sigma et} \iint_{\bar{S}_{1_0}} \exp\left[-kz' + i(kx + \gamma)\right] \left[z' \frac{\partial h}{\partial x'} - x' \frac{\partial h}{\partial z'}\right] dx'dz' \tag{8-4}$$

It will be noted that these forces and moment are purely of a hydrostatic nature.

VIII. 3 Free Oscillation

When the ACV responds freely in waves taking up displacements appropriate to the excitation, restoring forces are developed on account of the displacements. It is assumed, of course, that there are no external forces acting on the craft apart from the constant thrust. It has been shown earlier in Section 6 that the small displacement in pitch will not provide a restoring force in the longitudinal or vertical directions although the thrust line is displaced in space. There will also be no restoring moment available in pitch on this account as the contribution is of a higher order. As the ACV is in equilibrium under the action of the restoring forces due to the displacements caused by the exciting forces, we may set

$$\text{Restoring} \begin{Bmatrix} \text{Force} \\ \text{Moment} \end{Bmatrix} + \text{Exciting} \begin{Bmatrix} \text{Force} \\ \text{Moment} \end{Bmatrix} = 0$$

$$\text{i.e.} \quad \delta\alpha \begin{Bmatrix} X \\ Z \\ M \end{Bmatrix} + \beta\alpha \begin{Bmatrix} X \\ Z \\ M \end{Bmatrix} + \text{higher order restoring forces} +$$

$$+ \delta\epsilon \begin{Bmatrix} X \\ Z \\ M \end{Bmatrix} + \beta\epsilon \begin{Bmatrix} X \\ Z \\ M \end{Bmatrix} + \text{higher order exciting forces} = 0$$

It is clear from the above system of equations that the order of the displacement caused by the incident wave has to be the same as the order ϵ of the waves themselves.

Using the expressions derived in Section 7 for the restoring forces and moment, we can now write the following set of equations :

$$X_{1010} + X_{1001} = -\left(\frac{m_2}{\delta}\right)\sigma_e^2 \bar{x}_{001} e^{i\sigma_e t} + \frac{4\pi i\rho g}{k} e^{i\sigma_e t} \iint_{\bar{S}_{1_0}} \exp\left[-kz' + i(kx + \gamma)\right] \frac{\partial h}{\partial x'}\, dx'dz' = 0$$

$$X_{0110} + X_{0101} = -\left(\frac{m_1}{\beta}\right)\sigma_e^2 \bar{x}_{001} e^{i\sigma_e t} - 2\pi e^{i\sigma_e t} \iint_{\bar{S}_o} \exp\left[i(kx + \gamma)\right] p_o\, dxdy = 0$$

$$Z_{1010} + Z_{1001} = -e^{i\sigma_e t}\left[\rho g\left(\frac{A}{\delta}\right)(\bar{z}_{001} - x_A \theta_{001}) - \left(\frac{m_2}{\delta}\right)\sigma_e^2 \bar{z}_{001}\right] + \frac{4\pi i\rho g}{k} e^{i\sigma_e t} \iint_{\bar{S}_{1_0}} \exp\left[-kz' + i(kx + \gamma)\right] \frac{\partial h}{\partial z'}\, dx'dz' = 0$$

$$Z_{0110} + Z_{0101} = -e^{i\sigma_e t}(\bar{x}_{001} + h_G \theta_{001}) \iint_{\bar{S}_o} p_{o_x}\, dxdy - \left(\frac{m_1}{\beta}\right)\sigma_e^2 \bar{z}_{001} e^{i\sigma_e t} = 0$$

$$M_{1010} + M_{1001} = e^{i\sigma_e t}\left[\left(\frac{m_2}{\delta}\right) h_G (\sigma_e^2 \bar{x}_{001} - g\theta_{001}) + \left\{\rho g\left(\frac{I_A}{\delta}\right) - \left(\frac{m_2}{\delta}\right) g z_B - \sigma_e^2\left(\frac{I_2}{\delta}\right)\right\}\theta_{001} - \rho g\, \bar{z}_{001}\left(\frac{A}{\delta}\right) x_A\right] + \frac{4\pi i\rho g}{k} e^{i\sigma_e t} \iint_{\bar{S}_{1_0}} \exp\left[-kz' + i(kx + \gamma)\right]\left[z'\frac{\partial h}{\partial x'} - x'\frac{\partial h}{\partial z'}\right] dx'dz'$$

$$M_{0110} + M_{0001} = 2(\bar{x}_{001} + h_G \theta_{001}) e^{i\sigma_e t} \iint_{\bar{S}_o} x p_{o_x}\, dxdy + \left[\left(\frac{m_1}{\beta}\right) h_G (\sigma_e^2 \bar{x}_{001} - g\theta_{001}) - \left(\frac{I_1}{\beta}\right)\sigma_e^2 \theta_{001}\right] e^{i\sigma_e t} = 0 \qquad (8\text{-}5)$$

The lowest order displacements in surge, heave and pitch are given by $\alpha\bar{x}_{001} e^{i\sigma_e t}$, $\alpha\bar{z}_{001} e^{i\sigma_e t}$ and $\alpha\theta_{001} e^{i\sigma_e t}$ and it may appear from (8-5) that there are six equations for these three unknown quantities. However, these should be reduced to a set of three equations, by setting the total longitudinal force, vertical force and pitching moment equal to zero. This step is suggested by the fact that although $\left(\frac{m_1}{\beta}\right)$ and $\left(\frac{m_2}{\delta}\right)$, the masses supported by the air cushion

and side hulls respectively, are known from design considerations, it is not possible to separate the total inertia

$$I = \beta\left(\frac{I_1}{\beta}\right) + \delta\left(\frac{I_2}{\delta}\right)$$

into separate components $\left(\frac{I_1}{\beta}\right)$ and $\left(\frac{I_2}{\delta}\right)$.

We thus obtain the set of equations :

$$m\sigma_e^2 \bar{x}_{001} = 2\pi \iint_{\bar{S}_0} \beta p_o \exp i(kx + \gamma)\, dxdy - \frac{4\pi i\rho g}{k} \iint_{\bar{S}_{1_0}} \exp\left[-kz' + i(kx + \gamma)\right] \frac{\partial\left[\delta h(x', z')\right]}{\delta x'}\, dx'dz'$$

$$m\sigma_e^2 \bar{z}_{001} - \rho g A(\bar{z}_{001} - x_A \theta_{001}) - \frac{4\pi i\rho g}{k} \iint_{\bar{S}_{1_0}} \exp\left[-kz' + i(kx + \gamma)\right] \frac{\partial\left[\delta h(x', z')\right]}{\partial x'}\, dx'dz' + (\bar{z}_{001} + h_G \theta_{001}) \iint_{\bar{S}_0} \beta p_{o_x}\, dxdy = 0$$

$$mh_G(\sigma_e^2 \bar{x}_{001} - g\theta_{001}) + (\rho g I_A - m_2 g z_B - \sigma_e^2 I)\theta_{001} - \rho g \bar{z}_{001} Ax_A + \frac{4\pi i\rho g}{k} \iint_{\bar{S}_{1_0}} \exp\left[-kz' + i(kx + \gamma)\right] \left[z' \frac{\partial\left[\delta h(x', z')\right]}{\partial x'} - x' \frac{\partial\left[\delta h(x', z')\right]}{\partial z'}\right] dx'dz' + 2(\bar{x}_{001} + h_G \theta_{001}) \iint_{\bar{S}_0} \beta x p_{o_x}\, dxdy = 0 \qquad (8\text{-}6)$$

The first of the above equations gives the oscillatory surge displacement explicitly. The left-hand side is actually the surge acceleration and this is independent of speed for the term σ_e which depends upon the speed of motion is absent on the right-hand side.

The other two equations enable the solution of the heave and pitch oscillatory displacements. As before, these displacements are

uncoupled if $x_A = 0$.

When we set the parameter δ denoting the thickness of the side hulls equal to zero and also the water plane area A equal to zero we get the results for an amphibious ACV which are discussed in great detail in Section 9 of Reference 1.

Having calculated the oscillatory displacements and thereby the accelerations in the three modes we can estimate the ride comfort in waves by combining these accelerations in the appropriate forms at various locations in the ACV.

The higher order displacements can also be derived by considering the higher order forces and moment.

The response functions in surge pitch and heave can be computed for a specific ACV configuration and motion predictions in an irregular seaway can be made by the use of spectral analysis within the limits of the theory of linear superposition.

IX . DISCUSSION AND CONCLUSIONS

The assumptions underlying this theoretical investigation of the motions of an ACV in a seaway and some of the results obtained here have been discussed in the Introduction and Summary. Attention is confined in this study to coplanar motion in the longitudinal plane with freedom in surge, pitch and heave only. Results for the amphibious ACV free from water contact can be obtained from the general results by setting the hull parameter $\delta = 0$ and omitting the surface integral over the longitudinal plane of the hull and the line integral over the waterline occurring in the integral representation for the potential due to the air cushion. These results can then be applied equally well for beamwise motion in the lateral direction as the beam/length ration is generally of the order of unity and the disturbance of the water due to longitudinal, drifting or purely lateral motion will be of the same order. Obviously, this does not apply to an ACV with immersed side hulls.

The primary results are contained in the horizontal and vertical forces and for the pitching moment derived at the end of Section 5. As may be expected, the lowest order forces and moment are purely of inertial and hydrostatic nature. The hydrodynamic pressure of the water does enter in the higher order and it is possible to calculate the added mass and damping of water, the mean increased resistance due to forced oscillation in calm water and due

to the free oscillation in waves etc. The evaluation of these quantities and the derivation of the higher order potentials such as those due to the interference between the air cushion and the side hulls, the diffraction of the incident wave by the side hulls and the disturbance of the incident wave by the air cushion are not carried out here, but the simpler results such as the steady trim taken up by the craft during uniform translation in calm water and the expression for the wave resistance which combines the well-known results of Michell and Havelock and also introduces an additional term representing the effects of interference between the air cushion and the side hulls show that our method of approach to the solution of the problem is a practical one. The expression for the side force on a drifting amphibious ACV and the response functions for the amphibious and non-amphibious ACV (for which expressions have been derived although not explicitly solved here) will also have practical applications. The ride comfort in waves can also be estimated by combining the levels of acceleration in surge, pitch and heave in an appropriate manner depending on the location in the ACV. It would, however, be premature to suggest that these response functions can be used for the prediction of the performance of the ACV in an irregular seaway by the application of the theory of linear superposition in the absence of experimental results confirming the linearity of the motions in waves of small amplitude.

The method of solution presented here can also be used in the case of the water contact of the flexible extensions and even in the case of immersion in water if the flexible extensions are assumed to be of a fixed shape. A later extension could cover the case of flexible extensions compliant to the water pressure.

It cannot be stressed too highly that the theory presented here must be used with a certain amount of caution when applied to the actual operation of an ACV over water. The underlying assumptions for the linearized theory are that the cushion pressure is small, that the hull is "thin" and that the speed of translation is moderate or large. The slope of the induced wave may then be considered to be small. Also, the oscillatory displacements and the slope of the incident wave should also be small quantities.

It is needless to add that the theoretical results derived here should be confirmed (or corrected) by experimental work such as that with a mechanical oscillator of the PMM type and also by full scale trials so that the scale effect can also be established. Apart from the configuration of the side hulls, which can no doubt be per-

fected by the naval architect, the "hull form" of the air cushion appears to play an important part in the performance of the ACV. It is commonly assumed for want of more precise knowledge that the pressure is uniform within the cushion. It is obvious that this cannot to so unless the flexible extensions are also immersed in the water in the same manner as the side hulls. There seems to be some evidence to show that the pressure is reduced to atmospheric at the front and rear boundaries of the cushion where there is leakage of air. This renders the mathematical work slightly easier and enables practical results to be obtained. This also gives the ACV cushion a "hull form" with an acceptable deadrise and flare which may be considered by the naval architect as very suitable for fast planing motions.

It is also necessary to point out that we have gone into some detail to study the hydrodynamic (including hydrostatic) effects on the motions of the ACV. It is assumed for this purpose that the aerodynamic effects are known including, in particular, the stiffness and damping of the peripheral-jet or plenum type of cushion. It may be thought that such effects as that due to "wave pumping" should have been taken into account, but this is purely a pneumatic effect as the compression (or rarefaction) of the air cushion is due to the form of the progressive wave underneath it and not due to the pressure of the disturbed water and as such has not been treated here. No doubt this important aspect will have to be taken into account along with other aerodynamic effects in arriving at an overall picture of the motions of the ACV in a seaway.

The higher order expressions for the forces and moment derived in this study are extremely complicated but their solution by numerical methods with the aid of present-day high speed digital computers need not present any serious problems. The finite element method (FEM) which is receiving increasing attention in recent years may prove to be valuable and powerful tool for the solution of problems of this nature.

* * *

X. ACKNOWLEDGEMENTS

The author is indebted to the President of Portsmouth Polytechnic for the facilities provided for the preparation of this study and is personally grateful to Dr. D.C. Chandler, Head of Department of Mechanical Engineering and Naval Architecture for his interest and encouragement of this work.

Special thanks are also due to Professor G.M. Lilley, Head of the Department of Aeronautics & Astronautics, University of Southampton, for his continuing interest in this development of the previous work carried out at the University.

The assistance provided by Mrs. Ann Martyn in the patient and careful preparation of the manuscript is also very much appreciated.

* * *

XI LIST OF SELECTED REFERENCES

1 Murthy T.K.S. A Linearized Potential Flow Theory for the Motions of Air Cushion Vehicles in a Seaway Univeristy of Southampton, Department of Aeronautics & Astronautics, A.A.S.U. Report N° 299, June 1970, (240 pages, including 5 appendices; 12 figs)

2 Peters A.S. and Stoker J.J The Motion of a Ship, as a Floating Rigid Body, in a Seaway. Comm. Pure and App. Maths., vol. 10, N° 3, 1957, pp 399-490

3 Newman J.N. The Damping and Wave Resistance of a Pitching and Heaving Ship. Journal of Ship Research, vol. 3, N° 1, June 1959, pp 1-19.

4 Newman J.N. A Linearized Theory for the Motion of a Thin Ship in Regular Waves. Journal of Ship Research, vol. 5, N° 1, June 1961, pp 34-55.

5 Joosen W.P.A. Slender Boby Theory for an Oscillating Ship at Forward Speed. Fifth Symposium on Naval Hydrodynamics. U.S. Office of Naval Research, Department of the Navy, ACR - 112, pp 167-183.

6 Havelock T.H. The Theory of Wave Resistance. Proc. Roy. Soc. A. vol. 138, 1922, pp 339-348.

A complete list of 40 references will be found in Reference 1.

• • •

APPENDIX I

DISTRIBUTION OF SURFACE PRESSURE DURING OSCILLATIONS

Let the pressure distribution on the IFS due to the air cushion be of the basic form

$$p_s = p_o\ (x, y)$$

during "static hovering", i.e. at zero speed ahead. This distribution determines the basic "hull form" of the air cushion. We may assume that the same distribution prevails even during steady translation. The motion of the side hulls through the water will generate an induced wave, but this will only cause a pressure variation in the interior of the fluid leaving conditions on the surface unaltered. This will also be true of the incident waves whose surface pressure is equal to that of the atmosphere, but the action of the waves in altering the cushion pressure due to "wave pumping" should be taken into account. This requires separate treatment. In other words, the surface pressure distribution is dictated only by the motion and oscillations of the air cushion and will remain of the basic form if the relative vertical and angular positions of the air gap at the bow and stern are the same as those when the ACV is stationary.

We are, however, allowing for oscillatory displacements in surge, heave and pitch during uniform translation. The surge displacements will not directly affect the pressure distribution, but the displacements in pitch and heave will certainly cause a variation of the design "daylight clearance" along the bow and stern sections of the air cushion and a different distribution of pressure on the water surface will result. The situation is fully discussed in Appendix II of Reference 1 where the result for the revised pressure distribution is derived in the form

$$p_s(x, y) = p_o(x, y) + \left[\bar{x} + h_G\theta + o(\theta)^2\right]\left[\frac{\partial p_o(x, y)}{\partial x} + \theta\left.\frac{\partial f_1(x', y')}{\partial x'}\right|_{x'=x} + \ldots\right.$$

$$\ldots + \bar{z}\left.\frac{\partial f_2(x', y')}{\partial x'}\right|_{x'=x} + 0(\theta^2, z^2)\Big] \ldots +$$

$$\ldots + \frac{1}{2}\left[\bar{x} + h_G\theta + 0(\theta^2)\right]^2\left[\frac{\partial^2 p_o(x, y)}{\partial x} + \theta\left.\frac{\delta^2 f_1(x', y')}{\partial x'^2}\right|_{x'=x} \ldots\right.$$

$$+ \bar{z} \left. \frac{\partial^2 f_2(x', y')}{\partial x'^2} \right|_{x'=x} + 0\,(\theta^2, \bar{z}^2)\Big] + 0\,(\bar{x} + h_G\theta)^3$$

where h_G is the height of the C. G. above the undisturbed water surface and f_1 and f_2 are the pitch and heave stiffness functions of the air cushion.

It will be seen from (2-2) that the basic hull form is assumed to be of $0(\beta)$. The pitch and heave stiffness functions are therefore also of $0(\beta)$ and we may write

$$\beta p_o(x, y) \text{ for } p_o(x, y)$$

$$\beta f_1(x', y') \text{ for } f_1(x', y')$$

and

$$\beta f_2(x', y') \text{ for } f_2(x', y')$$

we may also substitute from (2-3)

$$\bar{x} = \delta\bar{x}_{100} + \beta\bar{x}_{010} + \delta\beta\,\bar{x}_{110} + \mathrm{Re.}\alpha e^{i\sigma t}(\bar{x}_{001} + \delta\bar{x}_{101} + \beta\bar{x}_{011}) +$$

$$+ 0\,(\delta^2\beta^2, \delta\beta\alpha, \alpha^2)$$

with similar expansions for $\bar{z}$ and θ and derive finally

$$p_s(x, y) = \beta p_o(x, y) + \beta^2\bar{r}_{010}p_{o_x} + \delta\beta\bar{r}_{100}p_{o_x} + \beta\alpha e^{i\sigma t}\bar{r}_{001}p_{o_x} +$$

$$+\delta\beta\alpha e^{i\sigma t}(\bar{r}_{100}s_{001} + \bar{r}_{001}s_{100} + \bar{r}_{101}p_{o_x} + \bar{r}_{001}\bar{r}_{100}p_{o_{xx}}) +$$

$$+\beta^2\alpha e^{i\sigma t}(\bar{r}_{010}s_{001} + \bar{r}_{001}s_{010} + \bar{r}_{011}p_{o_x} + \bar{r}_{010}\bar{r}_{001}p_{o_{xx}}) +$$

$$+\delta\beta^2(\bar{r}_{100}s_{010} + \bar{r}_{010}s_{100} + \bar{r}_{110}p_{o_x} + \bar{r}_{100}\bar{r}_{010}p_{o_{xx}}) +$$

$$+\delta^2\beta(\bar{r}_{100}s_{100} + \frac{1}{2}\bar{r}^2_{100}p_{o_{xx}}) +$$

$$+ 0 (\delta^3, \delta^2\beta , \delta\beta^2\alpha \ \delta^2\alpha, \alpha^2) \qquad (I-1)$$

It may be as well to point out that the terms of $0(\delta^2\beta,\delta\beta^2 \ \beta^2\alpha)$ are slightly in deficit due to the forcible linearization implied in writing

$$x - x' = \bar{x} + h_G \theta + 0 (\theta^2)$$

where the $0 (\theta^2)$ terms cannot be explicitly written down.

We have written above

$$\bar{r}_{klm} \equiv \bar{x}_{klm} + h_G \theta_{klm}$$

for the coupled displacement parameter and

$$s_{klm} \equiv f_{1_{x'}} \theta_{klm} + f_{2_{x'}} \bar{z}_{klm}$$

for the coupled stiffness function.

It will be seen that the pitch and heave stiffness functions enter only in the higher order terms. Also, if the cushion is truly uniform in the longitudinal direction such that

$$p_{o_x} = 0 \ , \quad p_{o_{xx}} = 0$$

the variation of pressure distribution due to the oscillations is of a very high order.

* * *

APPENDIX II

PRESSURE FORCES AND MOMENTS ON THE CUSHION HULL

The force due to the action of the surface pressure on the cushion hull is form (5-1)

$$\vec{F}_{P_C} = -\iint_S p_s \, \hat{n} \, dS$$

where S is the instantaneous position of the IFS and $\hat{n}$ is the unit normal drawn out of the water surface and into the lower boundary of the cushion.

The equation of the IFS is given by

$$\zeta(x, y) - z = 0$$

so that the outward drawn normal is

$$\hat{n} = \frac{\zeta_x \hat{i} + \zeta_y \hat{j} - \hat{k}}{\left[1 + \zeta_x^2 + \zeta_y^2\right]^{1/2}}$$

and

$$dS = -\left[1 + \zeta_x^2 + \zeta_y^2\right]^{1/2} \, dxdy$$

where the negative sign has been used on the right-hand side since dS is an element of the cushion hull positive on the upper side of the free surface, whereas in our co-ordinate system the element of area dxdy is positive along the z-direction which is vertically downwards.

We therefore have

$$\hat{n} \, dS = -(\zeta_x \hat{i} + \zeta_y \hat{j} - \hat{k}) \, dxdy$$

and ζ is given on the IFS by Bernoulli's equation (1-8) with $\omega = 0$

$$\zeta = \frac{1}{g}\left[\Phi_t - V\Phi_x + \frac{1}{2}(\nabla\Phi)^2\right]\Bigg|_{z=\zeta} + \frac{p_s(x, y; t)}{\rho g}$$

where the potential has the value on $z = \zeta$, i.e. with the argument (x, y, ζ) but may be continued analytically from the surface to the

plane $z = 0$ in the form

$$\Phi(x, y, \zeta; t) = \Phi(x, y, 0; t) + \zeta \left.\frac{\partial \Phi}{\partial z}\right|_{z=0} +$$

Since ζ may be assumed to be of the same order as Φ, we may retain only the first term in the above expansion and write

$$\zeta = \frac{1}{g}\left[\Phi_t - V\Phi_x + \frac{1}{2}(\nabla\Phi)^2\right]\Bigg|_{Z=0} + \frac{p_s(x, y; t)}{\rho g}$$

We therefore have

$$\overrightarrow{F_p} = \iint_{S_o} p_s \left(\zeta_x \hat{i} + \zeta_y \hat{j} - \hat{k}\right) dxdy$$

and substituting for the derivations of ζ

$$\overrightarrow{F_p} = \iint_{S_o} p_s \left[\frac{1}{g}\left(\Phi_{xt} - V\Phi_{xx} + \nabla\Phi \cdot \nabla\Phi_x + \frac{1}{\rho} p_{s_x}\right)\hat{i} + \right.$$

$$\left. \ldots + \frac{1}{g}\left(\Phi_{yt} - V\Phi_{xy} + \nabla\Phi \cdot \nabla\Phi_y + \frac{1}{\rho} p_{s_y}\right)\hat{j} - \hat{k}\right] dxdy$$

where the potential has now the argument $(x, y, 0)$ and the integration has thus been reduced to S_o which is the instantaneous position of the part of the plane $z = 0$ contained within the vertical projection of the hemline of the skirts at the bow and the stern and between the inner surfaces of the side hulls.

The components of the pressure force are therefore

$$X_{P_C} = \frac{1}{g}\iint_{S_o} p_s \left(\Phi_{x_t} - V\Phi_{xx} + \nabla\Phi \cdot \nabla\Phi_x + \frac{1}{\rho} p_{s_x}\right) dxdy$$

$$Y_{P_C} = \frac{1}{g}\iint_{S_o} p_s \left(\Phi_{yt} - V\Phi_{xy} + \nabla\Phi \cdot \nabla\Phi_y + \frac{1}{\rho} p_{s_y}\right) dxdy$$

and

$$Z_{P_C} = -\iint_{S_o} p_s \, dxdy \qquad \text{(II. 1)}$$

From the symmetry of the motion with displacements in the longitudinal plane it may be concluded that the lateral force Y_{P_C} is zero. This could in fact, be established as follows :

Since

$$Y_{P_C} = \iint_{S_o} p_s \quad \frac{d\zeta}{dy}\, dxdy$$

and p_s may be assumed to be an even function of y as indeed p_o no doubt is, as may be seen from (I. 1) and ζ is also an even function of y (i. e. $d\zeta/dy$ an odd function), there are surface element pairs on oppposite sides of the longitudinal axis where the integrand is of equal but opposite sign. The surface integral therefore vanishes on account of the symmetry of the domain of integration about the longitudinal axis.

We are therefore left only with the longitudinal force and the vertical force.

We may substitute for Φ from (2. 3) and for p_s from (I. 1)

$$\Phi = \delta\Phi_{1000} + \beta\Phi_{0100} + \delta\beta\Phi_{1100} + \mathrm{Re.}\, e^{i\sigma t} (\delta\alpha\Phi_{1010} +$$

$$+ \beta\alpha\Phi_{0110} + \epsilon\Phi_{0001} + \delta\epsilon\Phi_{1001} + \beta\epsilon\Phi_{0101})$$

and

$$p_s = \beta p_o + \beta^2 \bar{r}_{010} p_{o_x} + \delta\beta \bar{r}_{100} p_{o_x} + \beta\alpha e^{i\sigma t} \bar{r}_{001} p_{o_x} +$$

$$+ \delta\beta\alpha e^{i\sigma t} (\bar{r}_{100} s_{001} + \bar{r}_{001} s_{100} + \bar{r}_{101} p_{o_x} + \bar{r}_{100}\bar{r}_{001} p_{o_{xx}})$$

$$+ \beta^2\alpha e^{i\sigma t} (\bar{r}_{010} s_{001} + \bar{r}_{001} s_{010} + \bar{r}_{011} p_{o_x} + \bar{r}_{010}\bar{r}_{001} p_{o_{xx}})$$

$$+ \delta\beta^2 (\bar{r}_{100} s_{010} + \bar{r}_{010} s_{100} + \bar{r}_{110} p_{o_x} + \bar{r}_{100}\bar{r}_{010} p_{o_x})$$

$$+ \delta^2\beta (\bar{r}_{100} s_{100} + \frac{1}{2} \bar{r}_{100}^2 p_{o_{xx}})$$

The integrals in (II. 1) are to be taken over the instantaneous position

S_o and if this domain is subdivided into

$$S_o = \overline{S}_o + S'_o$$

where $\overline{S}_o$ is the equilibrium configuration and S'_o is the oscillating strip, it is shown in Appendix V that an integral of the form

$$\iint_{S_o} f(x, y)\ dxdy$$

is equivalent to an integral over the known steady surface

$$\iint_{\overline{S}_o} \left[f(x, y) + (\bar{x} + h_G\theta)\ \frac{\partial f(x, y)}{\partial x} \right] dxdy$$

Substituting for Φ and p_s in (II. 1) and making the above correction for the domain of integration we derive finally after simplification the following results.

Longitudinal Force.

$$\begin{aligned} X_{P_C} = \frac{1}{g} \iint_{\overline{S}_o} dxdy \quad & \Big[\delta\beta(-Vp_o \Phi_{1000_{xx}}) + \\ & + \beta^2 \left(\frac{1}{\rho}\ p_o p_{o_x} - Vp_o \Phi_{0100_{xx}}\right) + \delta\beta^2 \Big\{ -Vp_o \Phi_{1100_{xx}} + \\ & + p_o \left(\nabla\Phi_{1000} \cdot \nabla\Phi_{0100_x} + \nabla\Phi_{1000_x} \cdot \nabla\Phi_{0100} \right) - \\ & - V(\bar{x}_{010} + h_G\theta_{010})(2p_{o_x} \Phi_{1000_{xx}} + p_o \Phi_{1000_{xxx}}) - \\ & - V(\bar{x}_{100} + h_G\theta_{100})(2p_{o_x} \Phi_{0100_{xx}} + p_o \Phi_{0100_{xxx}}) \Big\} + \\ & + \delta^2\beta \Big\{ p_o\ \nabla\Phi_{1000} \cdot \nabla\Phi_{1000_x} - \\ & - V(\bar{x}_{100} + h_G\theta_{100})(2p_{o_x} \Phi_{1000_{xx}} + p_o \Phi_{1000_{xxx}}) \Big\} + \\ & + \delta\beta\alpha e^{i\sigma t} \Big\{ p_o (i\sigma\Phi_{1010_x} - V\Phi_{1010_{xx}}) - \end{aligned}$$

$$
\begin{aligned}
&- V\left(\bar{x}_{001} + h_G\theta_{001}\right)\left(2p_{o_x}\Phi_{1000_{xx}} + p_o\Phi_{1000_{xxx}}\right)\Big\} + \\
&+ \beta^2\alpha\, e^{i\sigma t}\Big\{p_o\left(i\sigma\Phi_{0110_x} - V\Phi_{0110_{xx}}\right) + \\
&+ \left(\bar{x}_{001} + h_G\theta_{001}\right)\left[\frac{1}{\rho}\left(p_o p_{o_{xx}} + p_{o_x}^2\right) - \right. \\
&\left. - V\left(2p_{o_x}\Phi_{0100_{xx}} + p_o\Phi_{0100_{xxx}}\right)\right]\Big\} + \\
&+ \beta\epsilon e^{i\sigma t}\Big\{p_o\left(i\sigma\Phi_{0001_x} - V\Phi_{0001_{xx}}\right)\Big\} + \\
&+ \delta\beta\epsilon e^{i\sigma t}\Big\{p_o\left(i\sigma\Phi_{1001_x} - V\Phi_{1001_{xx}}\right) + \\
&+ p_o\left(\nabla\Phi_{1000}\cdot\nabla\Phi_{0001_x} + \nabla\Phi_{1000_x}\cdot\nabla\Phi_{0001}\right) + \\
&+ \left(\bar{x}_{100} + h_G\theta_{100}\right)\Big[2p_{o_x}\left(i\sigma\Phi_{0001_x} - V\Phi_{0001_{xx}}\right) + \\
&+ p_o\left(i\sigma\Phi_{0001_{xx}} - V\Phi_{0001_{xxx}}\right)\Big]\Big\} + \\
&+ \beta^2\epsilon\, e^{i\sigma_e t}\Big\{p_o\left(i\sigma\Phi_{0101_x} - V\Phi_{0101_{xx}}\right) + \\
&+ p_o\left(\nabla\Phi_{0100}\cdot\nabla\Phi_{0001_x} + \nabla\Phi_{0100_x}\cdot\nabla\Phi_{0001}\right) + \\
&+ \left(\bar{x}_{010} + h_G\theta_{010}\right)\Big[2p_{o_x}\left(i\sigma\Phi_{0001_x} - V\Phi_{0001_{xx}}\right) + \\
&+ p_o\left(i\sigma\Phi_{0001_{xx}} - V\Phi_{0001_{xxx}}\right)\Big]\Big\} + \\
&+ \beta\alpha\epsilon e^{2i\sigma_e t^*}\Big\{\left(\bar{x}_{001} + h_G\theta_{001}\right)\Big[2p_{o_x}\left(i\sigma\Phi_{0001_x} - V\Phi_{0001_{xx}}\right) \\
&+ p_o\left(i\sigma\Phi_{0001_{xx}} - V\Phi_{0001_{xxx}}\right)\Big]\Big\}\Big] \qquad \text{(II. 2)}
\end{aligned}
$$

Lateral Force

$$Y_{P_C} = 0$$

Vertical Force

$$Z_{P_C} = -\iint_{S_o} dxdy \quad \Big[\beta p_o + 2\delta\beta \quad (\bar{x}_{100} + h_G\theta_{100})\, p_{o_x}$$

$$+ 2\beta^2 (\bar{x}_{010} + h_G\theta_{010})\, p_{o_x}$$

$$+ \delta\beta^2 \left(\bar{r}_{100}s_{010} + \bar{r}_{010}s_{100} + 2\bar{r}_{110}p_{o_x} + 3\bar{r}_{100}\bar{r}_{010}p_{o_x}\right) +$$

$$+ \delta^2\beta \quad (\bar{r}_{100}s_{100} + \frac{3}{2}\ \bar{r}_{100}^{\ 2}\ p_{o_{xx}})$$

$$+ \beta\alpha e^{i\sigma t} (\bar{r}_{001}\ p_{o_x})$$

$$+ \delta\beta\alpha e^{i\sigma t} \left(\bar{r}_{100}s_{001} + \bar{r}_{001}s_{100} + 2\bar{r}_{101}p_{o_x} + 2\bar{r}_{100}\bar{r}_{100}p_{o_{xx}}\right)$$

$$+ \beta^2\alpha\epsilon e^{i\sigma t} (\bar{r}_{010}s_{001} + \bar{r}_{001}s_{010} + 2\bar{r}_{011}\ p_{o_x} +$$

$$\cdot\ 2\bar{r}_{010}\bar{r}_{001}\ p_{o_{xx}})\Big] \qquad \text{(II. 3)}$$

It is of course understood that the real part of the complex quantities on the right-hand side are to be taken, although the symbol "Re" , has not been explicitly indicated. But, in view of the possible confusion in the case of terms with $e^{2i\sigma t}$ *as a factor, the following convention may be established. The factor $e^{i\sigma t}$ occurs both with respect to the displacements which are assumed to be simple harmonic (and of the same frequency as the wave) and with respect to the wave potential which is also simple harmonic. As the displacements and the potentials could be complex, the real part of these quantities multiplied by $e^{i\sigma t}$ is to be taken. In the case of terms containing $e^{2i\sigma t}$ *as a factor, the correct procedure would be to assign a factor of $e^{i\sigma t}$ to the displacement and take the real part, assign another

factor of $e^{i\sigma t}$ to the terms containing the potential and again take the real part. The two real parts are then multiplied together. This procedure is implicitly understood when a factor of $e^{2i\sigma t}$ * is indicated by an asterisk.

It will be seen that the cushion stiffness terms denoted by the parameter s_{klm} enters in the higher order vertical force of $0(\delta^2\beta, \delta\beta^2, \delta\beta\alpha, \beta^2\alpha)$ although the longitudinal force of these orders is free from this effect. In actual fact, the effect of stiffness is contained in the longitudinal force of $0(\delta\beta\alpha\epsilon, \beta^2\alpha\delta)$ although these forces have not been written down.

Also, it may appear a little surprising that the dynamic pressure of the water obtained from the potential Φ does not enter in the expression for the vertical force at all, whereas the horizontal force contains the potential in all orders. This is due to the approximation contained in our expression

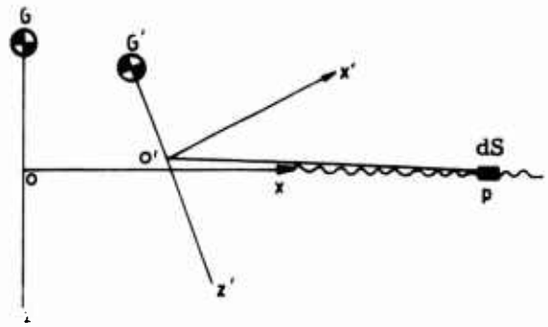
$$\hat{n}\, dS = -(\zeta_x \hat{i} + \zeta_y \hat{j} - \hat{k})\, dxdy$$

which is valid only for an infinitesimal slope of the water surface in the x- and y-directions . It appears, therefore, that the actual shape of the IFS determined by Φ is irrelevant as far as the vertical force is concerned so long as the slope is very small. The situation is therefore much the same as over wavy ground as the hydrodynamic properties of the water surface do not seem to matter for small slopes. On the other hand, in the case of the horizontal force, which is proportional to the actual slope, however small, the dynamic pressure determined by the motion of the water is very relevant. This also applies to the moment as will be seen presently.

Turning now to the moment due to the action of the surface pressure on the cushion hull

$$\overrightarrow{M_{P_C}} = -\iint_S p_s\, (\overrightarrow{r}' \times \hat{n})\, dS$$

and since the position vector with respect to o' of an element dS of the IFS at P (see sketch) may be written



$$\overrightarrow{r'} = (x_p - x_o)\,\hat{i} + (y_p - y_o)\,\hat{j} + (z_p - z_{o'})\,\hat{k}$$

where

$$x_o' = x_{G'} - z'_{G'} = \bar{x} + h_G \sin\theta$$

$$y_o' = 0$$

$$z_o' = z_{G'} - z'_{G'} \cos\theta = \bar{z} - h_G (1 - \cos\theta)$$

and if (x, y, ζ) are the co-ordinates of P

$$\overrightarrow{r'} = (x - \bar{x} - h_G \sin\theta)\,\hat{i} + y\,\hat{j} + \left[\zeta - \bar{z} + h_G (1 - \cos\theta)\right]\,\hat{k}$$

and therefore

$$\overrightarrow{M}_{P_C} = \iint_{S_o} p_s \left[(x - \bar{x} - h_G \sin\theta)\,\hat{i} + y\,\hat{j} + \left[\zeta - \bar{z} + h_G (1 - \cos\theta)\right]\,\hat{k}\right] \left[\zeta_x\,\hat{i} + \zeta_y\,\hat{j} - \hat{k}\right] dxdy$$

where the cross denotes the vector product

$$\text{i.e. } \overrightarrow{M}_{P_C} = \iint_{S_o} p_s \left[-\left\{ y + \left[\zeta - \bar{z} + h_G (1 - \cos\theta)\right]\zeta_y \right\}\hat{i} + \left\{ x - \bar{x} - h_G \sin\theta + \left[\zeta - \bar{z} + h_G (1 - \cos\theta)\right]\zeta_x \right\}\hat{j} + \left\{ (x - \bar{x} - h_G \sin\theta)\,\zeta_y - y\,\zeta_x \right\}\hat{k} \right] dxdy$$

we may now linearize this by setting

$$\sin\theta = \theta \qquad \text{and} \quad \cos\theta = 1 + 0(\theta^2)$$

bearing in mind that p_s is of $0(\beta)$, ζ is of $0(\delta,\beta)$ and θ^2 is of $0(\delta^2,\delta\beta,\beta^2,\delta\alpha,\beta\alpha,\alpha^2)$. The linearization will certainly be valid for the moments of the order we are considering and therefore

$$\overrightarrow{M}_{P_C} = \iint_{S_o} p_s \left[-\left\{ y + (\zeta - \bar{z})\zeta_y \right\} \hat{i} + \left\{ x - \bar{x} - h_G\theta + (\zeta - \bar{z})\zeta_x \right\} \hat{j} + \left\{ (x - \bar{x} - h_G\theta)\ \zeta_y - y\ \zeta_x \right\} \hat{k} \right] dxdy$$

As the motion is confined to the longitudinal plane we may conclude as before that for this symmetrical motion p_s, ζ and ζ_x are even functions of y whilst ζ_y is an odd function so that the integrals of all the terms containing ζ_y may be set equal to zero and for the same reason

$$\iint_{S_o} p_s\, y\, dxdy = 0$$

and

$$\iint_{S_o} p_s\, \zeta_x\, y\, dx\, dy = 0$$

The $\hat{i}$ and $\hat{k}$ integrals therefore vanish and we are left only with the $\hat{j}$ component or the pitching moment

$$M_{P_C} = \iint_{S_o} p_s \left[x - \bar{x} - h_G\theta + (\zeta - \bar{z})\ \zeta_x \right] dxdy$$

This result is obvious as there cannot be a rolling moment or yawing moment in symmetrical motion in the longitudinal plane normal to the crests of the waves.

Substituting for p_s and for ζ in terms of Φ and carrying out the correction implied in replacing S_o by $\bar{S}_o$ as before, the final result is :

$$
\begin{aligned}
M_{P_C} = \iint_{S_o} dxdy \; \Big[& \beta x p_o + 2\delta\beta \; (\bar{x}_{100} + h_G \theta_{100}) \, x p_{o_x} \\
& + 2\beta^2 \, (\bar{x}_{010} + h_G \theta_{010}) \, x p_{o_x} \\
& + \delta\beta^2 \Big\{ x \, (\bar{r}_{100} s_{010} + \bar{r}_{010} s_{100} + 2\bar{r}_{110} p_{o_x} \\
& + 2\bar{r}_{100} \bar{r}_{010} p_{o_{xx}}) - 2\bar{r}_{100} \bar{r}_{010} \, p_{o_x} \\
& + \frac{V^2}{g^2} \, p_o \, (\Phi_{1000_x} \Phi_{0100_{xx}} + \Phi_{1000_{xx}} \Phi_{0100_x}) \\
& - \frac{V}{\rho g^2} \, p_o \, (p_o \Phi_{1000_{xx}} + p_{o_x} \Phi_{1000_x}) - \frac{1}{\rho g} p_o \, \bar{z}_{100} \, p_{o_x} \\
& + \frac{V}{g} \, p_o \, (\bar{z}_{100} \Phi_{0100_{xx}} + \bar{z}_{010} \Phi_{1000_{xx}}) \Big\} \\
& + \delta^2\beta \Big\{ x \, (\bar{r}_{100} s_{100} + \frac{1}{2} \, \bar{r}_{100}^2 \, p_{o_{xx}}) \, \bar{r}_{100}^2 \, p_{o_x} \\
& + \frac{V^2}{g^2} \, p_o \, \Phi_{1000_x} \Phi_{1000_{xx}} + \frac{V}{g} p_o \, \bar{z}_{100} \, \Phi_{1000_{xx}} \Big\} \\
& + 2\beta\alpha \, e^{i\sigma t} \, (\bar{x}_{001} + h_G \theta_{001}) \, x \, p_{o_x} \\
& + \delta\beta\alpha e^{i\sigma t} \Big\{ x (\bar{r}_{100} s_{001} + \bar{r}_{001} s_{100} + 2\bar{r}_{101} p_{o_x} \\
& + 2\bar{r}_{100} \bar{r}_{001} p_{o_{xx}}) - 2\bar{r}_{100} \bar{r}_{001} p_{o_x} + \frac{V}{g} \, p_o \, \bar{z}_{001} \Phi_{1000_{xx}} \Big\} \\
& + \beta^2\alpha \, e^{i\sigma t} \Big\{ x (\bar{r}_{010} s_{001} + \bar{r}_{001} s_{010} + 2\bar{r}_{011} \, p_{o_x} \\
& + 3\bar{r}_{010} \bar{r}_{001} \, p_{o_{xx}}) - 2\bar{r}_{010} \bar{r}_{001} \, p_{o_x}
\end{aligned}
$$

$$
\left. - \frac{1}{g} p_o \bar{z}_{001} \left(\frac{1}{\rho} p_o - V \Phi_{0100_{xx}} \right) \right\}
$$

$$
+ \delta\beta\alpha e^{i\sigma e t} \left\{ - \frac{V}{g^2} p_o \left[\left(i\sigma \Phi_{0001_x} - V \Phi_{0001_{xx}} \right) \Phi_{1000_x} \right. \right.
$$

$$
\left. + \left(i\sigma \Phi_{0001} - V \Phi_{0001_x} \right) \Phi_{1000_{xx}} \right]
$$

$$
\left. - \frac{1}{g} p_o \bar{z}_{100} \left(i\sigma \Phi_{0001_x} - V \Phi_{0001_{xx}} \right) \right\}
$$

$$
+ \beta^2 \epsilon e^{i\sigma e t} \left\{ - \frac{V}{g^2} p_o \left[\left(i\sigma \Phi_{0001_x} - V \Phi_{0001_{xx}} \right) \Phi_{0100_x} \right. \right.
$$

$$
\left. + \left(i\sigma \Phi_{0001} - V \Phi_{0001_x} \right) \Phi_{0100_{xx}} \right]
$$

$$
- \frac{1}{g} p_o \bar{z}_{010} \left(i\sigma \Phi_{0001_x} - V \Phi_{0001_{xx}} \right)
$$

$$
+ \frac{p_o}{\rho g^2} \left[p_{o_x} \left(i\sigma \Phi_{0001} - V \Phi_{0001_x} \right) \right.
$$

$$
\left. \left. + p_o \left(i\sigma \Phi_{0001_x} - V \Phi_{0001_{xx}} \right) \right] \right\}
$$

$$
+ \beta\alpha\epsilon e^{2i\sigma e t^*} \left\{ - \frac{1}{g} p_o \bar{z}_{001} \left(i\sigma \Phi_{0001} - V \Phi_{0001_x} \right) \right\}
$$

(II. 4)

* * *

APPENDIX III
PRESSURE FORCES AND MOMENTS ON THE SIDE HULLS

The force on the ACV due to the action of the pressure of the fluid on the immersed side hulls is from (5. 1)

$$\overrightarrow{F_{P_H}} = -\iint_{S_1+S_2} p\,\hat{n}\,dS$$

where the pressure of the water particles on and below the surface of the fluid on either side of each hull is given by Bernoulli's equation (1- 8) with $\omega = 0$

$$p(x, y, z;t) = -\rho\left[\Phi_t - V\Phi_x + \frac{1}{2}(\nabla\Phi)^2 - gz\right]$$

The pressure is therefore given in the moving (x, y, z)-system , but the domain of integration, namely, the instantaneous position of the wetted surfaces of the moving and oscillating hulls is however, given in the body-fixed (x', y', z') system by the hull functions (4 -9) below the free surface $z = \zeta$.

This difficulty did not arise in the case of the cushion hull since the domain of integration in that case was that part of the plane $z = 0$ lying within the instantaneous boundary of the cushion.

The unit normal into the hulls is discussed in section (IV. 3) and we may write

$$\hat{n}\,dS = (H_x\,\hat{i} + H_y\,\hat{j} + H_z\,\hat{k})\,dxdz$$

$$= \left[\delta\left(\frac{\partial h_1}{\partial x'}\cos\theta + \frac{\partial h_1}{\partial z'}\sin\theta\right)\hat{i}\right.$$

$$\left. - \hat{j} + \delta\left(\frac{\partial h_1}{\partial z'}\cos\theta - \frac{\partial h_1}{\partial x'}\sin\theta\right)\hat{k}\right]dx'dz'$$

This applies to the hull surface S_{1+} . In the case of the other hull surfaces the above expression has to be modified slightly. The scheme is set out below.

Hull Surface	Hull function	j-component
S_{1+}	h_1	- 1
S_{1-}	h_2	+ 1
S_{2+}	h_2	- 1
S_{2-}	h_1	+ 1

It will be noted that we have replaced the element of area dxdz by dx'dz' since the Jacobian of the transformation,

$$\frac{\partial(x, z)}{\partial(x', z')}$$

is unity. Also we have altered the domain of integration from the hull surface to the longitudinal planes

$$y = y' = \pm b$$

and we will therefore have to express the pressure in the (x', y', z') system and use its value on both sides of the longitudinal planes in view of the possibility of a discontinuity across the planes. This could arise because of the singularity of the potential discussed in Appendix V.

We may now replace the surface of S_1 by

$$S_1 = S_{1_{o+}} + S_{1_{o-}}$$

where $S_{1_{o+}}$ is the side of the plane $y' = b$ facing the +ive y' - axis and $S_{1_{o-}}$ is the side facing the -ive y' - axis with a similar notation for the other hull,

$$S_2 = S_{2_{o+}} + S_{2_{o-}}$$

It will be remembered that these surfaces which are both sides of the

longitudinal planes of the hulls are to be taken in their instantaneous position when evaluating the surface integral for the pressure force.

The pressure of water may be assumed to be an even function of y and therefore of y'

$$\text{i.e.} \qquad p_{S_1}{}_{o+} = p_{S_2}{}_{o-}$$

and

$$p_{S_1}{}_{o-} = p_{S_2}{}_{o+}$$

and in integrating over S_1 and S_2 we may combine the integrals over

$$S_1{}_{o+} + S_2{}_{o-}$$

and

$$S_1{}_{o-} + S_2{}_{o+}$$

where the hull functions are the same for each group. The j-component is however, of a different sign in each group and therefore the lateral force vanishes.

We thus have

$$X_{P_H} = -2\delta \iint_{S_{1o}} \left[\left(p^+ \frac{\partial h_1}{\partial x'} + p^- \frac{\partial h_2}{\partial x'} \right) \cos\theta + \left(p^+ \frac{\partial h_1}{\partial z'} + p^- \frac{\partial h_2}{\partial z'} \right) \sin\theta \right] dx'dz'$$

$$Y_{P_H} = 0$$

$$Z_{P_H} = -2\delta \iint_{S_{1o}} \left[\left(p^+ \frac{\partial h_1}{\partial z'} + p^- \frac{\partial h_2}{\partial z'} \right) \cos\theta \right.$$

$$- \left(p^{+} \frac{\partial h_1}{\partial x'} + p^{-} \frac{\partial h_2}{\partial x'} \right) \sin\theta \Bigg] \, dx'dz' \qquad \text{(III. 1)}$$

where we have combined all the four sides of the two longitudinal planes whose immersed parts are geometrically similar, except that the profile of the disturbed water surface will be dissimilar on the inner and outer sides of each plane. This wave elevation, however, introduces a very high order correction, as will be seen presently, and for our present purposes we may indeed consider that all the four sides are equivalent. The integration is now over one side of a longitudinal plane, but the different pressures on the two sides are to be taken into account.

We will now have to express the pressure on both sides of the longitudinal plane of a hull in the (x', y', z') system. The pressure is given in the (x, y, z) system in terms of the potential in the form

$$p(x, y, z; t) = - \rho \left[\Phi_t - V\Phi_x + \frac{1}{2}(\nabla\Phi)^2 - gz \right]$$

and inserting the expansion for Φ

$$\Phi = \delta\Phi_{1000} + \beta\Phi_{0100} + \delta\beta\Phi_{1100} + e^{i\sigma t} \left(\delta\alpha\Phi_{1010} + \beta\alpha\Phi_{0110} + \epsilon\Phi_{0001} + \delta\epsilon\Phi_{1001} + \beta\epsilon\Phi_{0101} \right)$$

we have

$$p(x, y, z; t) = \delta\rho V\Phi_{1000_x} + \beta\rho V\Phi_{0100_x} + \delta\beta\rho \left(V\Phi_{1100_x} - \nabla\Phi_{1000} \cdot \nabla\Phi_{0100} \right) - \beta^2 \cdot \frac{1}{2}\rho\nabla\Phi_{0100} \cdot \nabla\Phi_{0100}$$

$$- \delta\alpha\rho e^{i\sigma t} (i\sigma\Phi_{1010} - V\Phi_{1010_x}) -$$

$$- \beta\alpha\rho e^{i\sigma t} (i\sigma\Phi_{0110} - V\Phi_{0110_x}) -$$

$$- \epsilon\rho e^{i\sigma t} (i\sigma\Phi_{0001} - V\Phi_{0001_x}) -$$

$$- \delta\epsilon\rho e^{i\sigma t}\left(i\sigma\Phi_{1001} - V\Phi_{1001_x} + \nabla\Phi_{1000}\cdot\nabla\Phi_{0001}\right)$$

$$- \beta\epsilon\rho e^{i\sigma t}\left(i\sigma\Phi_{0101} - V\Phi_{0101_x} + \nabla\Phi_{0100}\cdot\nabla\Phi_{0001}\right)$$

$$- \delta\alpha\epsilon\rho e^{2i\sigma t^*}\ \nabla\Phi_{1010}\cdot\ \nabla\Phi_{0001}$$

$$- \beta\alpha\epsilon\rho e^{2i\sigma t^*}\ \nabla\Phi_{0110}\cdot\ \nabla\Phi_{0001} + \rho gz \qquad \text{(III. 2)}$$

where the argument to be used for the potentials is $(x, b+, z)$ and $(x, b-, z)$ for p^+ and p^- respectively.

To obtain the pressure in the (x', y', z') system we may expand the potentials in the form of a Taylor series. In view of the singularity of the potential at $y' = b$, separate expansions will have to be used for the two sides.

Thus, in the case of $S_{1_{o+}}$

$$\Phi+_{1000}(x, y, z) = \Phi_{1000}(x', b+, z') + (x-x')\,\Phi_{1000_{x'}}(x', b+, z')$$

$$+ (y-b)\,\Phi_{1000_{y'}}(x', b+, z')$$

$$+ (z-z')\,\Phi_{1000_{z'}}(x', b+, z')$$

where

$$x - x' = \bar{x} + (z' + h_G)\,\theta = \delta r_{100} + \beta r_{010} + \alpha e^{i\sigma t} r_{001}$$

$$y - b = y' - b = \delta h_1\,(x', z')$$

and

$$z - z' = \bar{z} - x'\theta = \delta r'_{100} + \beta r'_{010} + \alpha e^{i\sigma t} r'_{001}$$

but the normal derivative $\Phi_{1000\,y'}$ i. e. the velocity across the plane may be considered equal to zero, so that

$$\delta\rho V \Phi^{+}_{1000_x}(x, y, z) = \delta\rho V \Phi_{1000_{x'}}(x', b+, z')$$

$$+ \delta\beta\rho V \left(r_{010}\Phi_{1000_{x'x'}} + r'_{010}\Phi_{1000_{x'z'}}\right) +$$

$$+ \delta\alpha e^{i\sigma t}\rho V \left(r_{001}\Phi_{1000_{x'x'}} + r'_{001}\Phi_{1000_{x'z'}}\right)$$

when $0(\delta^2)$ is neglected.

The expansion on the inner side i. e. on S_{1_0}- will be identical but the argument of the potential will now be (x', b-, z').

Similar expansions can be written down for the other terms in (III. 2) giving finally

$$p(x, y, z;t) = \delta\rho V\Phi_{1000_{x'}} + \beta\rho V\Phi_{0100_{x'}}$$

$$+ \beta^2\rho\left\{ V\left(r_{010}\Phi_{1010_{x'x'}} + r'_{010}\Phi_{1010_{x'z'}}\right)\right.$$

$$\left. - \frac{1}{2}\nabla'\Phi_{0100}\cdot\nabla'\Phi_{0100}\right\}$$

$$+ \delta\beta\rho\left\{V\left(r_{010}\Phi_{1000_{x'x'}} + r'_{010}\Phi_{1000_{x'z'}}\right.\right.$$

$$\left. + r_{100}\Phi_{0100_{x'x'}} + r'_{100}\Phi_{0100_{x'z'}} + \Phi_{1100_{x'}}\right)$$

$$\left. - \nabla'\Phi_{1000}\cdot\nabla'\Phi_{0100}\right\}$$

$$+ \delta\alpha e^{i\sigma t}\rho\left\{V\left(r_{001}\Phi_{1000_{x'x'}} + r'_{001}\Phi_{1000_{x'z'}}\right.\right.$$

$$\left. + \Phi_{1010_{x'}}\right) - i\sigma\Phi_{1010}\Big\}$$

$$+ \beta\alpha e^{i\sigma t}\rho\left\{V\left(r_{001}\Phi_{0100_{x'x'}} + r'_{001}\Phi_{0100_{x'z'}}\right.\right.$$

$$+ \Phi_{0110_{x'}}) - i\sigma\Phi_{0110}\Big\} \; - \epsilon e^{i\sigma t}\rho(i\sigma\Phi_{0001} - V\Phi_{0001_{x'}})$$

$$- \delta\epsilon e^{i\sigma t}\rho\Big\{r_{100}\left(i\sigma\Phi_{0001_{x'}} - V\Phi_{0001_{x'x'}}\right)$$

$$+ r'_{100}\left(i\sigma\Phi_{0001_{z'}} - V\Phi_{0001_{x'z'}}\right)$$

$$+ i\sigma\Phi_{1001} - V\Phi_{1001_{x'}} + \nabla'\Phi_{1000}\cdot\nabla'\Phi_{0001}\Big\}$$

$$- \beta\epsilon e^{i\sigma t}\rho\Big\{r_{010}(i\sigma\Phi_{0001_{x'}} - V\Phi_{0001_{x'x'}})$$

$$+ r'_{010}(i\sigma\Phi_{0001_{z'}} - V\Phi_{0001_{x'z'}})$$

$$+ i\sigma\Phi_{0101} - V\Phi_{0101_{x'}} + \nabla'\Phi_{0100}\cdot\nabla'\Phi_{0001}\Big\}$$

$$- \alpha\epsilon e^{2i\sigma t^*}\rho\Big\{r_{001}\left(i\sigma\Phi_{0001_{x'}} - V\Phi_{0001_{x'x'}}\right)$$

$$+ r'_{001}\left(i\sigma\Phi_{0001_{z'}} - V\Phi_{0001_{x'z'}}\right)\Big\}$$

$$+ \rho g\left\{\bar{z} + z'\cos\theta - x'\sin\theta - h_G(1 - \cos\theta)\right\} \qquad \text{(III. 3)}$$

The argument of the potentials in the above expression is $(x', b+, z')$ for p^+ and $(x', b-, z')$ for $\bar{p}$. The corresponding potentials may then be denoted by Φ^+ and Φ^- .

We may now substitute for p^+ and p^- in (III. 1), but before doing so we will reduce the domain of integration from the unknown region S_{1_o} to a known region with a correction term.

We may write

$$S_{1_o} = \bar{S}_{1_o} + S'_{1_o} + S''_{1_o}$$

where $\bar{S}_{1_o}$ is the equilibrium position below the load water plane $z' = 0$ which is known from design considerations, S'_{1_o} is the strip between $z' = 0$ and the undisturbed water surface $z = 0$ and S''_{1_o} is the additional strip between $z = 0$ and the actual free surface $z = \zeta$.

Let us first consider the contribution of the last term in (III. 3) which represents the hydrostatic pressure of the water to the horizontal and vertical forces given by (III. 1). This pressure is the same on both sides of the longitudinal plane so that we may combine h_1 and h_2 , and considering first the horizontal force

$$- 2\delta\rho g \iint_{\bar{S}_{1_o}+S'_{1_o}} \left[\bar{z} + z'\cos\theta - x'\sin\theta - h_G(1-\cos\theta)\right] \cdot \left[\frac{\partial h}{\partial x'}\cos\theta + \frac{\partial h}{\partial z'}\sin\theta\right] dx'dz'$$

which may be transformed by Stokes' theorem into

$$- 2\delta\rho g\cos\theta \oint_C h(x',z') \left[\bar{z} + z'\cos\theta - x'\sin\theta - h_G(1-\cos\theta)\right] dz'$$

$$- 2\delta\rho g\sin\theta\cos\theta \iint_{\bar{S}_{1_o}+S'_{1_o}} h(x',z')\, dx'dz'$$

$$- 2\delta\rho g\sin\theta \oint_C h(x',z') \left[\bar{z} + z'\cos\theta - x'\sin\theta - h_G(1-\cos\theta)\right] dx'$$

$$+ 2\delta\rho g\sin\theta\cos\theta \iint_{\bar{S}_{1_o}+S'_{1_o}} h(x',z')\, dx'dz'$$

where the line integrals are taken along the boundary of the region $\bar{S}_{1_o} + S'_{1_o}$, i. e. the line of intersection of the plane $y = b$ with the plane $z = 0$ and along a line from the stem to the stern running along the keel.

Along the upper boundary, i. e. along the waterline,

$$\bar{z} + z'\cos\theta - x'\sin\theta - h_G(1-\cos\theta) = z = 0$$

and along the lower boundary

$$h(x', z') = 0$$

as the hull may be assumed to have a pointed keel. The line integrals along C are therefore both zero and the surface integrals cancel with each other so that the net result is zero.

Now, on the strip S''_{1_o} the integral may be written

$$-2\delta\rho g \int dx' \int_{z=o}^{z=\zeta} z\left(\frac{\partial h}{\partial x'} \cos\theta + \frac{\partial h}{\partial z'} \sin\theta\right) dz'$$

and expanding the integral about its value when $z' = 0$ the inner integral becomes

$$\int_{z=o}^{z=\zeta} z' \frac{\partial z}{\partial z'}\left[\frac{\partial h}{\partial x'} \cos\theta + \frac{\partial h}{\partial z'} \sin\theta\right]_{z'=o} dz'$$

and since

$$\frac{dz}{dz'} = \cos\theta = 1 + 0(\theta^2)$$

the integral becomes

$$\left[\frac{\partial h}{\partial x'} \cos\theta + \frac{\partial h}{\partial z'} \sin\theta\right]_{z'=o} \left[\frac{1}{2} z'^2\right]_{z=o}^{z=\zeta} = \frac{1}{2} \frac{\partial h}{\partial x'} \zeta^2$$

on linearizing with respect to θ and noting that

$$z'^2 = z^2 + 0(\theta^2) .$$

The surface integral over S''_{1_o} therefore becomes

$$-\delta\rho g \int_L \frac{\partial h(x', z')}{\partial x'} \zeta^2 dx'$$

and writing $\zeta = \delta\zeta_{100} + \beta\zeta_{010} + \epsilon e^{i\sigma t}\zeta_{001} +$

the result is

$$-2\rho g e^{i\sigma t}\int_L \left(\delta^2\epsilon\,\zeta_{100}\cdot\zeta_{001} + \delta\beta\epsilon\,\zeta_{010}\,\zeta_{010}\right)\frac{\partial h}{\partial x'}\,dx'$$

the integration being along the load waterline L i.e. along the x' axis. The contribution is therefore of a much higher order.

Similarly the contribution of the hydrostatic pressure to the vertical force may be evaluated. In this case,

$$-2\delta\rho g\iint_{\bar{\zeta}_{1_0}+\zeta'_{1_0}}\left[\bar{z} + z'\cos\theta - x'\sin\theta - h_G(1-\cos\theta)\right]\left[\frac{\partial h}{\partial z'}\cos\theta - \frac{\partial h}{\partial x'}\sin\theta\right]dx'dz'$$

$$= -2\delta\rho g\cos\theta\oint_C h(x'z')\left[\bar{z} + z'\cos\theta - x'\sin\theta - h_G(1-\cos\theta)\right]dx'$$

$$+ 2\delta\rho g\cos^2\theta\iint_{\bar{\zeta}_{1_0}+\zeta'_{1_0}} h(x', z')\,dx'dz'$$

$$+ 2\delta\rho g\sin\theta\oint_C h(x', z')\left[\bar{z} + z'\cos\theta - x'\sin\theta - h_G(1-\cos\theta)\right]dz'$$

$$+ 2\delta\rho g\sin^2\theta\iint_{\bar{\zeta}_{1_0}+\zeta'_{1_0}} h(x', z')\,dx'dz'$$

As before, the line integrals are each zero and the surface integrals combine together to give

$$2\delta\rho g\iint_{\bar{\zeta}_{1_0}+\zeta'_{1_0}} h(x', z')\,dx'dz'$$

which is simply the displacement of the two hulls below $z = 0$. We may write the above integral in the form

$$2\delta\rho g\iint_{\zeta_{1_0}} h(x', z')\,dx'dz' + 2\delta\rho g\iint_{\zeta'_{1_0}} h(x', z')\,dx'dz'$$

The first integral is the known force due to the displacement below the load waterline i. e. $m_2 g$. The second integral will however, have to be evaluated. This is discussed below.

As regards the strip S''_{1_0} , the integral becomes by expanding the integrand about $z' = 0$ and carrying out the integration as before

$$- 2 \rho g e^{i\sigma t} \int_L \left(\delta^2 \epsilon \, \zeta_{100} \cdot \zeta_{001} + \delta \beta \epsilon \zeta_{010} \, \zeta_{001} \right) \frac{\partial h}{\partial z'} \, dx'$$

We will now evaluate the correction for the hydrodynamic pressure terms when substituted in (III. 1). We will replace the integration over S_{1_0} by that on the known surface $\bar{S}_{1_0}$ together with a correction denoting the integral over S'_{1_0} . The evaluation of the integral over S''_{1_0} will be unnecessary as this raises the order by $\delta\epsilon$ or $\beta\epsilon$.

The integrals are all of the form

$$\iint_{S_{1_0}} f(x', z') \frac{\partial h}{\partial x'} \, dx'dz'$$

or

$$\iint_{S_{1_0}} f(x', z') \frac{\partial h}{\partial z'} \, dx'dz'$$

Now,

$$\iint_{S'_{1_0}} f(x'z, \frac{\partial h}{\partial x'} \, dx'dz' = \int dx' \int_{z=0}^{z'=0} f(x', z') \frac{\partial h}{\partial x'} \, dz'$$

and when $z = 0$

$$z' = x'\theta - \bar{z} + 0(\bar{x}\,\theta, \theta^2)$$

so that in view of the smallness of the range of integration, we may replace the integrand by its value when $z' = 0$ giving

$$\int (\bar{z} - x' \theta) \left[f(x', z') \frac{\partial h}{\partial x'} \right]_{z'=0} dx'$$

which becomes an integration by parts

$$\left[h(x', z')\,(\bar{z} - x'\theta)\,f(x', z')\right]_{\text{stern}}^{\text{stem}} - \int_{\text{stern}}^{\text{stem}} h(x', 0)\frac{\partial}{\partial x'}\left[(\bar{z} - x'\theta)\,f(x', z')\right]_{z'=0} dx'$$

The first term vanishes at both ends on the waterline, and the second integral is taken along the +ives x' direction so that this term becomes

$$\int_{\text{Stem}}^{\text{Stern}} h(x', 0)\,\frac{\partial}{\partial x'}\left[(\bar{z} - x'\theta)\,f(x', z')\right] dx'$$

To this integral may be added the integral of zero value along the keel from the stern back to the stem as $h(x', z')$ is zero everywhere along this line giving

$$\oint_C h(x', z')\,\frac{\partial}{\partial x'}\left[(\bar{z} - x'\theta)\,f(x', z')\right] dx'$$

which is taken around the boundary of $\bar{S}_{1_o}$.

This may be transformed by Stokes' theorem into

$$\iint_{\bar{S}_{1_o}} -\frac{\partial h}{\partial z'}\,-\frac{\partial}{\partial x'}\left[(\bar{z} - x'\theta)\,f(x', z')\right] dx'dz' + \iint_{\bar{S}_{1_o}} h(x', z')\,\frac{\partial^2}{\partial z'\partial x'}\left[(\bar{z} - x'\theta)\,f(x'z')\right] dx'dz'$$

The second surface integral may be written

$$\iint_{\bar{S}_{1_o}} h(x', z')\,\frac{\partial}{\partial x'}\left[(\bar{z} - x'\theta)\,\frac{\partial f}{\partial x'}\right] dx'dz' =$$

$$= \oint_C h(x', z')\,(\bar{z} - x'\theta)\,\frac{\partial f}{\partial z'}\,dz' - \iint_{\bar{S}_{1_o}} \frac{\partial h}{\partial x'}\,(\bar{z} - x'\theta)\,\frac{\partial f}{\partial z'}\,dx'dz'$$

The line integral is obviously zero, since

$$h(x', z') = 0 \quad \text{for } z' \neq 0$$

and we may combine the second surface integral with the first giving the result

$$\iint_{S'_{1_0}} f(x'z') \frac{\partial h}{\partial x'} dx'dz' = \iint_{\bar{S}_{1_0}} \left[\frac{\partial h}{\partial z'} \frac{\partial}{\partial x'} \left[(\bar{z} - x'\theta) f(x', z') \right] - \frac{\partial h}{\partial x'} (\bar{z} - x'\theta) \frac{\partial f}{\partial z'} \right] dx'dz'$$

$$= \iint_{\bar{S}_{1_0}} \left[(\bar{z} - x'\theta) - \left[\frac{\partial h}{\partial z'} \frac{\partial f}{\partial x'} - \frac{\partial h}{\partial x'} \frac{\partial f}{\partial z'} \right] - \theta \frac{\partial h}{\partial z'} f(x', z') \right] dx'dz'$$

In the case of $\iint_{S_{1_0}} f(x', z') \frac{\partial h}{\partial z'} dx'dz'$

the integral may be written

$$\int dx' \int_{z=0}^{z'=0} f(x', z') \left(-\frac{\partial h}{\partial z'} \right) dz'$$

which can be approximated as before to

$$\int (\bar{z} - x'\theta) \left[f(x', z') \frac{\partial h}{\partial z'} \right]_{z'=0} dx'$$

i. e. $$\int_L (\bar{z} - x'\theta) f(x', 0) \frac{\partial h}{\partial z'} dx'$$

It does not seem easily possible to convert this into a surface integral for merging with the main integral over $\bar{S}_{1_0}$ as has just been done in the previous case.

Substituting for p^+ and p^- in terms of the potentials and reducing the integration to the known surface $\bar{S}_{1_0}$ after correcting for the strips S'_{1_0} and S''_{1_0} we have the following results for the longitudinal force and the vertical force.

It is assumed here that the potentials Φ_{1000} and Φ_{1010} will be continuous across the longitudinal planes for these are the potentials of the side hulls in the absence of the air cushion. The

wave potential Φ_{0001} and the hydrostatic pressure will, of course, be the same on both sides. The hull functions h_1 and h_2 have therefore been combined in these cases to give the total width h. In the case of the potentials involving the cushion pressure namely, Φ_{0100} and Φ_{0101}, the two sides are considered separately.

The final result is :

$$
\begin{aligned}
X_{P_H} = \iint_{\xi_{1_0}} \Bigg[& -2\delta^2 \rho V \Phi_{1000_{x'}}(x', b, z') \frac{\partial h}{\partial x'} \\
& - 2\delta\beta\rho V \left\{ \Phi_{0100_{x'}}(x', b+, z') \frac{\partial h_1}{\partial x'} + \Phi_{0100_{x'}}(x', b-, z') \frac{\partial h_2}{\partial x'} \right\} \\
& - 2\delta^2 \alpha e^{i\sigma t} \rho \Bigg[V \left\{ \bar{x}_{001} \frac{\partial h}{\partial x'} + \bar{z}_{001} \frac{\partial h}{\partial z'} \right. \\
& \left. + \theta_{001} \left(\overline{z' + h_G} \frac{\partial h}{\partial x'} - x' \frac{\partial h}{\partial z'} \right) \right\} \Phi_{1000_{x'x'}} \\
& + (V\Phi_{1010_{x'}} - i\sigma\Phi_{1010}) \frac{\partial h}{\partial x'} \Bigg] - \\
& - 2\delta\beta\alpha e^{i\sigma t} \rho \Bigg[V \left\{ \bar{x}_{001} \frac{\partial h_1}{\partial x'} + \bar{z}_{001} \frac{\partial h_1}{\partial z'} \right. \\
& \left. + \theta_{001} \left(\overline{z' + h_G} \frac{\partial h_1}{\partial x'} - x' \frac{\partial h_1}{\partial z'} \right) \right\} \Phi^{+}_{0100_{x'x'}} \\
& + (V\Phi^{+}_{0110_{x'}} - i\sigma\Phi^{+}_{0110}) \frac{\partial h_1}{\partial x'} + \dots \\
& + V \left\{ \bar{x}_{001} \frac{\partial h_2}{\partial x'} + \bar{z}_{001} \frac{\partial h_2}{\partial x'} \right\} + \\
& + \theta_{001} \left(z' + h_G \frac{\partial h_2}{\partial x'} - x' \frac{\partial h_2}{\partial x'} \right) \Phi^{-}_{0100_{x'x'}} \\
& + (V\Phi^{-}_{0110_{x'}} - i\sigma\Phi^{-}_{0110}) \frac{\partial h_2}{\partial x'} \Bigg] .
\end{aligned}
$$

$$+ 2\delta\epsilon\, e^{i\sigma t} \quad \rho\left(i\sigma\Phi_{0001} - V\Phi_{0001_{x'}}\right) \quad \frac{\partial h}{\partial x'}$$

$$+ 2\delta^2\,\epsilon\, e^{i\sigma t}\rho\Bigg[\Bigg\{\bar{x}_{100} \quad \frac{\partial h}{\partial x'} + \bar{z}_{100} \quad \frac{\partial h}{\partial z'}$$

$$+ \theta_{100}\left(\overline{z' + h}_G \quad \frac{\partial h}{\partial x'} - x' \quad \frac{\partial h}{\partial z'}\right)\Bigg\} \quad \left(i\sigma\Phi_{0001_{x'}} - V\Phi_{0001_{x'x'}}\right)$$

$$+ \left(i\sigma\Phi_{1001} - V\Phi_{1001_{x'}} + \nabla'\Phi_{1000} \cdot \nabla'\Phi_{0001}\right) \frac{\partial h}{\partial x'}$$

$$+ \theta_{100} \quad \nabla'\Phi_{1000} \cdot \nabla'\Phi_{0001} \quad \frac{\partial h}{\partial z'}\Bigg]$$

$$+ 2\delta\beta\epsilon\, e^{i\sigma t}\rho\Bigg[\Bigg\{\bar{x}_{010} \quad \frac{\partial h}{\partial x'} + \bar{z}_{010} \quad \frac{\partial h}{\partial z'}$$

$$+ \theta_{010}\left(\overline{z' + h}_G \quad \frac{\partial h}{\partial z'} - x' \quad \frac{\partial h}{\partial z'}\right)\Bigg\} \quad \left(i\sigma\Phi_{0001_{x'}} - V\Phi_{0001_{x'x'}}\right)$$

$$+ \left(i\sigma\Phi^{+}_{0101} - V\Phi^{+}_{0101_{x'}} + \nabla'\Phi^{+}_{0100} \quad \nabla'\Phi_{0001}\right) \quad \frac{\partial h_1}{\partial x'}$$

$$+ \left(i\sigma\Phi^{-}_{0101} - V\Phi^{-}_{0101_{x'}} + \nabla'\Phi^{-}_{0100} \quad \nabla'\Phi_{0001}\right) \quad \frac{\partial h_2}{\partial x'}$$

$$+ \theta_{010} \quad \nabla'\Phi_{1000} \cdot \nabla'\Phi_{0001} \quad \frac{\partial h}{\partial z'}\Bigg]$$

$$+ 2\delta\alpha\epsilon e^{2i\sigma t^*}\rho\Bigg[\Bigg\{\bar{x}_{001} \quad \frac{\partial h}{\partial x'} + \bar{z}_{001} \quad \frac{\partial h}{\partial z'} +$$

$$+ \theta_{001}\left(\overline{z' + h}_G \quad \frac{\partial h}{\partial x'} - x' \quad \frac{\partial h}{\partial z'}\right)\Bigg\}$$

$$\left\{i\sigma\Phi_{0001_{x'}} - V\Phi_{0001_{x'x'}}\right\}\Bigg]\Bigg] \quad dx'dz'$$

$$- 2\delta^2 \epsilon \rho g \int_L \zeta_{100} \; \zeta_{001} \frac{\partial h}{\partial x'} \; dx'$$

$$- 2\delta \beta \epsilon \rho g \int_L \zeta_{010} \; \zeta_{001} \frac{\partial h}{\partial x'} \; dx' \qquad \text{(III. 4)}$$

$$Z_{P_H} = \iint_{\zeta_{1_0}} \Big[2\delta \rho g \, h(x', z') - 2\delta^2 \rho V \Phi_{1000_{x'}} \frac{\partial h}{\partial z'}$$

$$- 2\delta \beta \rho V \left(\Phi^{+}_{0100_{x'}} \frac{\partial h_1}{\partial x'} + \Phi^{-}_{0100_{x'}} \frac{\partial h_2}{\partial x'} \right)$$

$$- 2\delta^2 \alpha \, e^{i\sigma t} \rho \Big[\Big[V \Big\{ (\bar{x}_{001} + h_G \theta_{001}) \Phi_{1000_{x'x'}}$$

$$+ (\bar{z}_{001} - x' \theta_{001}) \Phi_{1000_{x'z'}} \Big\} + V \Phi_{1010_{x'}}$$

$$- i\sigma \Phi_{1010} \Big] \frac{\partial h}{\partial z'} - V \theta_{001} \Phi_{1000_{x'}} \frac{\partial h}{\partial x'} \Big]$$

$$- 2\delta \beta \alpha e^{i\sigma t} \rho \Big[\Big[V \Big\{ (\bar{x}_{001} + \overline{z' + h_G} \, \theta_{001}) \Phi^{+}_{0100_{x'x'}}$$

$$+ (\bar{z}_{001} - x' \theta_{001}) \Phi^{+}_{0100_{x'z'}} \Big\} + V \Phi^{+}_{0100_{x'}}$$

$$- i\sigma \Phi^{+}_{0100} \Big] \frac{\partial h_1}{\partial z'} - V \theta_{001} \Phi^{+}_{0100_{x'}} \frac{\partial h_1}{\partial x'}$$

$$+ \Big[V \Big\{ (\bar{x}_{001} + \overline{z' + h_G} \, \theta_{001}) \Phi^{-}_{0100_{x'x'}}$$

$$+ (\bar{z}_{001} - x' \theta_{001}) \Phi^{-}_{0100_{x'z'}} \Big\} + V \Phi^{-}_{0100_{x'}}$$

$$- i\sigma \Phi^{-}_{0100} \Big] \frac{\partial h_2}{\partial z'} - V \theta_{001} \Phi^{-}_{0100_{x'}} \frac{\partial h_2}{\partial x'} \Big]$$

$$+ 2\delta\epsilon\, e^{i\sigma t}\ \rho\,(i\sigma\Phi_{0001} - V\Phi_{0001_{x'}})\ -\frac{\partial h}{\partial z'}$$

$$+ 2\delta^2\epsilon\, e^{i\sigma t}\ \rho\Bigg[\Bigg\{(\bar{x}_{100} + \overline{z' + h}_G\,\theta_{100})\,(i\sigma\Phi_{0001_{x'}} - V\Phi_{0001_{x'x'}})$$

$$+ (\bar{z}_{100} - x'\theta_{100})\,(i\sigma\Phi_{0001_{z'}} - V\Phi_{0001_{x'z'}})$$

$$+ i\sigma\Phi_{1001} - \Phi_{1001_{x'}} + \nabla'\Phi_{1000}\cdot\nabla'\Phi_{0001}\Bigg\}\frac{\partial h}{\partial z'}$$

$$- \theta_{100}\,(i\sigma\Phi_{0001} - V\Phi_{0001_{x'}})\ \frac{\partial h}{\partial x'}\Bigg]$$

$$+ 2\delta\beta\epsilon\, e^{i\sigma t}\ \rho\Bigg[\Bigg\{(\bar{x}_{010} + \overline{z' + h}_G\,\theta_{010})\,(i\sigma\Phi_{0001_{x'}} - V\Phi_{0001_{x'x'}})$$

$$+ (\bar{z}_{010} - x'\theta_{010})\,(i\sigma\Phi_{0001_{z'}} - V\Phi_{0001_{x'z'}})\Bigg\}\frac{\partial h}{\partial z'}$$

$$+ (i\sigma\Phi^{+}_{0101} - V\Phi^{+}_{0101_{x'}} + \nabla'\Phi^{+}_{0101}\cdot\nabla'\Phi_{0001})\ \frac{\partial h_1}{\partial z'}$$

$$+ (i\sigma\Phi^{-}_{0101} - V\Phi^{-}_{0101_{x'}} + \nabla'\Phi^{-}_{0101}\cdot\nabla'\Phi_{0001})\ \frac{\partial h_2}{\partial z'}$$

$$- \theta_{010}\,(i\sigma\Phi_{0001} - V\Phi_{0001_{x'}})\ \frac{\partial h}{\partial x'}\Bigg]$$

$$+ 2\delta\alpha\epsilon e^{2i\sigma t}\,\rho^{*}\Bigg[\Bigg\{(\bar{x}_{0001} + \overline{z' + h}_G\,\theta_{001})$$

$$(i\sigma\Phi_{0001_{x'}} - V\Phi_{0001_{x'x'}}) + (\bar{z}_{001} - x'\theta_{001})$$

$$(i\sigma\Phi_{0001_{z'}} - V\Phi_{0001_{x'z'}})\Bigg\}\frac{\partial h}{\partial z'}$$

$$- \theta_{001} \left(i\sigma\Phi_{0001} - V\Phi_{0001_{x'}} \right) \frac{\partial h}{\partial x'} \Bigg] \Bigg] \, dx'dz'$$

+ line integrals which follow (III. 5)

Line integrals to be added to surface integrals for vertical force Z_{P_H}

$$+ \int_L \Big[2\delta^2 \rho g \left(\bar{z}_{100} - x'\theta_{100} \right) h(x', o)$$

$$+ 2\delta\beta \rho g \left(\bar{z}_{010} - x'\theta_{010} \right) h(x', o)$$

$$+ 2\delta\alpha \, e^{i\sigma t} \rho g \left(\bar{z}_{001} - x'\theta_{101} \right) h(x', o)$$

$$+ 2\delta^2\alpha \, e^{i\sigma t} \Big\{ \rho g \left(\bar{z}_{101} - x'\theta_{101} \right) h(x', o)$$

$$- \rho V \left(\bar{z}_{001} - x'\theta_{001} \right) \Phi_{1000_{x'}} \frac{\partial h}{\partial z'} \Big\}$$

$$+ 2\delta\beta\alpha e^{i\sigma t} \rho \Big\{ g \left(\bar{z}_{011} - x'\theta_{011} \right) h(x', o)$$

$$- V \left(\bar{z}_{001} - x'\theta_{001} \right) \left(\Phi^{+}_{0100_{x'}} \frac{\partial h_1}{\partial z'} + \Phi^{-}_{0100_{x'}} \frac{\partial h_2}{\partial z'} \right) \Big\}$$

$$+ 2\delta^2\epsilon \, e^{i\sigma t} \rho \Big\{ \left(\bar{z}_{100} - x'\theta_{100} \right) \left(i\sigma\Phi_{0001} - V\Phi_{0001_{x'}} \right) \frac{\partial h}{\partial z'}$$

$$- g\zeta_{100} \zeta_{001} \frac{\partial h}{\partial z'} \Big\}$$

$$+ 2\delta\beta\epsilon \, e^{i\sigma t} \rho \Big\{ \left(\bar{z}_{010} - x'\theta_{010} \right) \left(i\sigma\Phi_{0001} - V\Phi_{0001_{x'}} \right) \frac{\partial h}{\partial z'}$$

$$- g\zeta_{010} \zeta_{001} \frac{\partial h}{\partial z'} \Big\}$$

$$+ 2\delta\alpha\epsilon \, e^{2i\sigma t^*} \rho \left(\bar{z}_{001} - x'\theta_{001} \right) \left(i\sigma\Phi_{0001} - V\Phi_{0001_{x'}} \right) \frac{\partial h}{\partial z'} \Big] dx' \quad \text{(III. 6)}$$

We will now turn our attention to the moment on the ACV due to the action of the pressure of the water particles on the hulls given by (5.2)

$$\overrightarrow{M_{P_H}} = -\iint_{S_1+S_2} p\,(\overrightarrow{r'} \times \hat{n})\ dS$$

and as $\overrightarrow{r'}$ may be written in terms of the components along the $\hat{i}$, $\hat{j}$, $\hat{k}$ axis.

$$\overrightarrow{r'} = (x' \cos\theta + y' \sin\theta)\,\hat{i} + y'\,\hat{j} + (z' \cos\theta - x' \sin\theta)\,\hat{k}$$

and

$$\hat{n}\,dS = \left[\delta\left(\frac{\partial h_1}{\partial x'} \cos\theta + \frac{\partial h_1}{\partial z'} \sin\theta\right)\hat{i} \mp \hat{j} + \delta\left(\frac{\partial h_1}{\partial z'} \cos\theta - \frac{\partial h_1}{\partial x'} \sin\theta\right)\hat{k}\right] dx'dz'$$

we have

$$(\overrightarrow{r'} \times \hat{n})\,dS = \left[\left\{\delta y'\left(\frac{\partial h_1}{\partial z'} \cos\theta - \frac{\partial h_1}{\partial x'} \sin\theta\right) \pm (z' \cos\theta - x' \sin\theta)\right\}\hat{i}\right.$$

$$+ \delta\left(z' \frac{\partial h_1}{\partial x'} - x' \frac{\partial h_1}{\partial z'}\right)\hat{j}$$

$$\left. + \left\{\mp(\bar{x}'\cos\theta + z' \sin\theta) - \delta y'\left(\frac{\partial h}{\partial x'} \cos\theta + \frac{\partial h}{\partial z'} \sin\theta\right)\right\}\hat{k}\right] dx'dz'$$

the upper and lower signs referring to the hull surfaces S_{1+} and S_{2-} with h_2 replacing h_1 in the case of S_{2+} and S_{1-}

The integration is now performed on the outer sides of the longitudinal planes of the hulls and combining $S_{1_{O}+}$ and $S_{2_{O}-}$ together as before, the integration may be confined to $S_{1_{O}+}$ with the integrands added together.

The combined $\hat{i}$-moment on the two hull surfaces is therefore

$$-\delta \iint_{S_{1_O}} py' \left(\frac{\partial h_1}{\partial z'} \cos\theta - \frac{\partial h_1}{\partial x'} \sin\theta\right) dx'dz'$$

which vanishes as p, $\frac{\partial h_1}{\partial x'}$ and $\frac{\partial h_1}{\partial z'}$ are even functions of y'.

The $\hat{k}$-component also vanishes and both components similarly vanish on the inner hull surfaces for the same reason.

We are therefore left only with the pitching moment

$$M_{P_H} = -2\delta \iint_{S_{1_o}} \left[p^+ \left(z' \frac{\partial h_1}{\partial x'} - x' \frac{\partial h_1}{\partial z'} \right) + p^- \left(z' \frac{\partial h_2}{\partial x'} - x' \frac{\partial h_2}{\partial z'} \right) \right] dx'dz'$$

and using the expression for p^+ and p^- given in (III. 3) we derive finally the following result for the pitching moment where the integration is reduced as before to $\bar{S}_{1_o}$ incorporating the correction terms where necessary.

$$\begin{aligned}
M_{P_H} = \iint_{S_{1_o}} \Bigg[& - 2\delta \rho g x' h(x', z') \\
& - 2\delta^2 \rho \left\{ V \Phi_{1000_{x'}} \left(z' \frac{\partial h}{\partial x'} - x' \frac{\partial h}{\partial z'} \right) + g\theta_{100} z' h(x', z') \right\} \\
& - 2\delta\beta\rho \Bigg\{ V \left[\Phi^+_{0100_{x'}} \left(z' \frac{\partial h_1}{\partial x'} - x' \frac{\partial h_1}{\partial x'} \right) \right. \\
& \left. + \Phi^-_{0100_{x'}} \left(z' \frac{\partial h_2}{\partial x'} - x' \frac{\partial h_2}{\partial x'} \right) \right] + g\theta_{010} z' h(x', z') \Bigg\} - \\
& - 2\delta\alpha e^{i\sigma t} \rho g \theta_{001} z' h(x', z') \\
& - 2\delta^2 \alpha e^{i\sigma t} \rho \Bigg[\Bigg\{ V \left(\bar{x}_{001} + \overline{z' + h_G} \theta_{001} \right) \Phi_{1000_{x'x'}} \\
& + \left(\bar{z}_{001} - x'\theta_{001} \right) \Phi_{1000_{x'z'}} \Bigg]^+ \\
& + V\Phi_{1010_{x'}} - i\sigma\Phi_{1010} \Bigg\} \left(z' \frac{\partial h}{\partial x'} - x' \frac{\partial h}{\partial z'} \right)
\end{aligned}$$

$$+ g\theta_{101}\, z'\, h\,(x', z') \Big]$$

$$- 2\delta\beta\alpha\, e^{i\sigma t}\rho\Bigg[\Bigg\{V\Big[(\bar{x}_{001} + \overline{z' + h}_G\theta_{001})\,\Phi^{+}_{0100_{x'x'}}$$

$$+ (\bar{z}_{001} - x'\theta_{001})\,\Phi^{+}_{0100_{x'z'}}\Big] + V\Phi^{+}_{0110_{x'}}$$

$$- i\sigma\Phi^{+}_{0110}\Bigg\}\quad (z'\,\frac{\partial h_1}{\partial x'} - x'\,\frac{\partial h_1}{\partial z'})$$

$$+\Bigg\{V\Big[(\bar{x}_{001} + \overline{z' + h}_G\theta_{001})\,\Phi^{-}_{0100_{x'x'}}$$

$$+ (\bar{z}_{001} - x'\theta_{001})\,\Phi^{-}_{0100_{x'z'}}\Big] + V\Phi^{-}_{0110_{x'}}$$

$$- i\sigma\Phi^{-}_{0110}\Bigg\}\quad (z'\,\frac{\partial h_2}{\partial x'} - x'\,\frac{\partial h_2}{\partial z'})$$

$$+ g\theta_{011}\, z'\, h(x', z')\Big]$$

$$+ 2\delta\epsilon\, e^{i\sigma t}\,\rho\,(i\sigma\Phi_{0001} - V\Phi_{0001_{x'}})\,(z'\,\frac{\partial h}{\partial x'} - x'\,\frac{\partial h}{\partial z'})$$

$$+ 2\delta^2_{\epsilon}\, e^{i\sigma t}\rho\Big[(\bar{x}_{100} + \overline{z' + h}_G\theta_{100})\,(i\sigma\Phi_{0001_{x'}} - V\Phi_{0001_{x'x'}})$$

$$+ (\bar{z}_{100} - x'\theta_{100})\,(i\sigma\Phi_{0001_{z'}} - V\Phi_{0001_{x'z'}})$$

$$+ i\sigma\Phi_{1001} - V\Phi_{1001_{x'}} + \nabla'\Phi_{1000}\cdot\nabla'\Phi_{0001}\Big]\Big[z'\,\frac{\partial h}{\partial x'} - x'\,\frac{\partial h}{\partial z'}\Big]$$

$$\ldots + 2\delta\beta\epsilon\, e^{i\sigma t}\rho\Big[\Big\{(\bar{x}_{010} + z' + h_G\theta_{010})\,(i\sigma\Phi_{0001_{x'}} - V\Phi_{0001_{x'x'}})$$

$$+ (\bar{z}_{010} - x'\theta_{010}) (i\sigma\Phi_{0001_{z'}} - V\Phi_{0001_{x'z'}}) \Big\} (z'\frac{\partial h}{\partial x'} - x'\frac{\partial h}{\partial z'})$$

$$+ (i\sigma\Phi^{+}_{0101} - V\Phi^{+}_{0101_{x'}} + \nabla'\Phi^{+}_{0100} \cdot \nabla'\Phi_{0001})$$

$$(z' \frac{\partial h_1}{\partial x'} - x' \frac{\partial h_1}{\partial z'}) + (i\sigma\Phi^{-}_{0101} - V\Phi^{-}_{0101_{x'}}$$

$$+ \nabla'\Phi^{-}_{0100} \cdot \nabla'\Phi_{0001}) (z' \frac{\partial h_2}{\partial x'} - x' \frac{\partial h_2}{\partial z'})$$

$$+ 2\delta\alpha\epsilon\, e^{2i\sigma t^*} \rho\Big[(\bar{x}_{001} + \overline{z' + h}_G \theta_{001}) \quad (i\sigma\Phi_{0001_{x'}}$$

$$- V\Phi_{0001_{x'x'}}) + (\bar{z}_{001} - x'\theta_{001})$$

$$(i\sigma\Phi_{0001_{z'}} - V\Phi_{0001_{x'z'}}) \Big] \quad dx'dz' \Big]$$

$$+ \text{line integrals which follow} \qquad \text{(III. 7)}$$

Line integrals to be added to surface integrals for pitching moment $\overline{M_{P_H}}$

$$\int_L \Big[-2\delta^2 \quad \rho g (\bar{z}_{100} - x'\theta_{100}) x' h(x', 0)$$

$$-2\delta\beta \quad \rho g(\bar{z}_{010} - x'\theta_{010}) x' h(x', 0)$$

$$-2\delta\alpha \quad e^{i\sigma t} \rho g \quad (\bar{z}_{001} - x'\theta_{001}) x' h (x', 0)$$

$$+ 2\delta^2\alpha\, e^{i\sigma t} \rho \Big\{ V (\bar{z}_{001} - x'\theta_{001}) \Phi_{1000_{x'}} \frac{\partial h}{\partial z'}$$

$$- g(\bar{z}_{101} - x'\theta_{101}) h (x', 0) \Big\} x'$$

$$+ 2\delta\beta\alpha e^{i\sigma t}\rho\left\{V(\bar{z}_{001} - x'\theta_{001})\,(\Phi^{+}_{0100_{x'}}\,\frac{\partial h_1}{\partial z'} + \Phi^{-}_{0100_{x'}}\,\frac{\partial h_2}{\partial z'})\right.$$

$$\left. - g(\bar{z}_{011} - x'\theta_{011})\,h\,(x',0)\right\}\,x'$$

$$+ 2\delta^2\epsilon\, e^{i\sigma t}\,\rho\left\{g\zeta_{100}\,\zeta_{001}\,\frac{\partial h}{\partial z'} - (\bar{z}_{100} - x'\theta_{100})\right.$$

$$\left.(i\sigma\Phi_{0001} - V\Phi_{0001_{x'}})\,\frac{\partial h}{\partial z'}\right\}\,x'$$

$$+ 2\delta\beta\epsilon e^{i\sigma t}\,\rho\left\{g\zeta_{010}\,\zeta_{001}\,\frac{\partial h}{\partial z'} - (\bar{z}_{010} - x'\theta_{010})\right.$$

$$\left.(i\sigma\Phi_{0001} - V\Phi_{0001_{x'}})\,\frac{\partial h}{\partial z'}\right\}\,x'$$

$$-2\delta\alpha\epsilon e^{2i\sigma t^{*}}\,\rho(\bar{z}_{001} - x'\theta_{001})\,(i\sigma\Phi_{0001} - V\Phi_{0001_{x'}})\frac{\partial h}{\partial z'}\,x'\Big]dx'$$

(III. 8)

APPENDIX IV
RIGID BODY FORCES AND MOMENTS

The rigid body force due to the weight and inertia of the ACV is from (5. 3)

$$\vec{F}_R = \iiint_V (\dot{\vec{U}} - g\hat{k})\,dm$$

where $\vec{U}$ is the absolute velocity of an element of mass dm contained within the body V of the ACV.

It is easy to show that

$$\iiint_V (\dot{\vec{U}} - g\hat{k})\,dm = m\,(\dot{\vec{U}}_G - g\hat{k})$$

where m is the total mass of the ACV and $\vec{U}_G$ the absolute velocity of its C. G.

$$\vec{U}_G = (V + \dot{\bar{x}})\hat{i} + \dot{\bar{y}}\hat{j} + \dot{\bar{z}}\hat{k}$$

and this reduces to

$$\dot{\vec{U}}_G = \ddot{\bar{x}}\,\hat{i} + \ddot{\bar{z}}\,\hat{k}$$

for the coplanar motion we are considering.

We therefore have

$$\vec{F}_R = m\left[\ddot{\bar{x}}\,\hat{i} + (\ddot{\bar{z}} - g)\,\hat{k}\right]$$

and substituting for the displacements, we derive for the components of the rigid body force

$$X_R = -m\sigma^2\,\alpha e^{i\sigma t}\,(\bar{x}_{001} + \delta\bar{x}_{101} + \beta\bar{x}_{011})$$

and (IV. 1)

$$Z_R = -m\sigma^2\,\alpha e^{i\sigma t}\,(\bar{z}_{001} + \delta\bar{z}_{101} + \beta\bar{z}_{011}) - mg$$

As regards the moment, we have from (5.4)

$$\vec{M}_R = \iiint_V \vec{r}' \times (\dot{\vec{U}} - g)\,\hat{k}\,dm$$

where the absolute velocity $\vec{U}$ at the point (x, y, z) of the body is

$$\vec{U} = (V + \dot{x})\,\hat{i} + \dot{y}\,\hat{j} + \dot{z}\,\hat{k}$$

reducing to

$$\dot{\vec{U}} = \ddot{x}\,\hat{i} + \ddot{z}\,\hat{k}$$

for coplanar motion and since

$$x = \bar{x} + x'\cos\theta + (z' + h_G)\sin\theta$$

and

$$z = \bar{z} + z'\cos\theta - x'\sin\theta - h_G(1 - \cos\theta)$$

we have

$$\ddot{x} = \ddot{\bar{x}} + \left[(z' + h_G)\cos\theta - x'\sin\theta\right]\ddot{\theta} - \left[x'\cos\theta + (z' + h_G)\sin\theta\right]\dot{\theta}^2$$

and

$$\ddot{z} = \ddot{\bar{z}} - \left[x' \cos\theta + (z' + h_G) \sin\theta\right]\ddot{\theta} + \left[x' \sin\theta - (z' + h_G) \cos\theta\right]\dot{\theta}^2$$

Also, since

$$\overrightarrow{r'} = (x' \cos\theta + y' \sin\theta)\,\hat{i} + y'\,\hat{j} + (z' \cos\theta - x' \sin\theta)\,\hat{k}$$

we derive after substitution and carrying out the vector product

$$\begin{aligned}
\vec{M}_R = \iiint_V \Big[& y' \Big\{ -g + \ddot{\bar{z}} - \left[x' \cos\theta + (z' + h_G) \sin\theta\right]\ddot{\theta} \\
& + \left[x' \sin\theta - (z' + h_G) \cos\theta\right]\dot{\theta}^2 \Big\}\hat{i} \\
& + \Big\{ (z' \cos\theta - x' \sin\theta)\Big[\ddot{\bar{x}} + \Big\{(z' + h_G) \cos\theta - x' \sin\theta\Big\}\ddot{\theta} \\
& - \Big\{x' \cos\theta + (z' + h_G) \sin\theta\Big\}\dot{\theta}^2\Big] \\
& - (x' \cos\theta + z' \sin\theta)\ \Big[-g + \ddot{\bar{z}} - \Big\{x' \cos\theta + (z' + h_G) \sin\theta\Big\}\ddot{\theta} \\
& + \Big\{x' \sin\theta - (z' + h_G) \cos\theta\Big]\ \dot{\theta}^2\Big]\Big\}\hat{j} \\
& - y' \Big\{ \ddot{\bar{x}} + \left[(z' + h_G) \cos\theta - x' \sin\theta\right]\ddot{\theta} \\
& + \left[x' \cos\theta - (z' + h_G) \sin\theta\right]\ \dot{\theta}^2 \Big\}\ \hat{k}\ \Big]\, dm
\end{aligned}$$

Now, we have the following results :

(i) $\iiint_V z'\, dm = m\, z'_{G'} = -m\, h_G$

i.e. $\iiint_V (z' + h_G)\, dm = 0$

(ii) $\iiint_V x'\, dm = m\, x'_{G'} = 0$

(iii) $\iiint_V y'\, dm = m\, y'_{G'} = 0$

} since the z'-axis passes through the C. G.

(iv) $\iiint_V x'\, y'\, dm = 0, \iiint_V y'\, z'\, dm = 0$ due to the lateral symmetry

and

$$(v) \qquad \iiint_V (x'^2 + z'^2)\, dm = I_{y'y'}$$

where $I_{y'y'}$ is the moment of inertia of the ACV in pitch about a lateral axis through o' .

When these results are used, the $\hat{i}$ and $\hat{k}$ integrals in the above expression vanish (a result not unexpected) and after simplification the final result for the pitching moment is

$$M_R = I\ddot{\theta} - mh_G \left[(\ddot{\bar{x}} \cos\theta + (g - \ddot{\bar{z}}) \sin\theta\right]$$

where

$$I = I_{y'y'} + mh_G^2$$

is the moment of inertia of the ACV about a lateral axis through the C. G.

This expression may be linearized for small values of θ and introducing the perturbation expansions for $\bar{x}$, $\bar{z}$ and θ , the final result is

$$\begin{aligned} M_R = &- \delta mgh_G\, \theta_{100} - \beta mgh_G\, \theta_{010} - \delta\beta mgh_G\, \theta_{110} \\ &+ \alpha e^{i\sigma t} \left\{ mh_G (\sigma^2 \bar{x}_{001} - g\theta_{001}) - \sigma^2 I \theta_{001} \right\} \\ &+ \delta\alpha e^{i\sigma t} \left\{ mh_G \left[\sigma^2 (\bar{x}_{101} - \bar{z}_{001}\, \theta_{100}) - g\theta_{101}\right] - \sigma^2 I\theta_{101} \right\} \\ &+ \beta\alpha e^{i\sigma t} \left\{ mh_G \left[\sigma^2 (\bar{x}_{011} - \bar{z}_{001}\, \theta_{010}) - g\theta_{011}\right] - \sigma^2 I\theta_{011} \right\} \\ &- \delta\beta\alpha e^{i\sigma t} \left\{ mh_G\, \sigma^2 (\bar{z}_{001}\, \theta_{110} + \bar{z}_{101}\, \theta_{010} + \bar{z}_{011}\, \theta_{100}) \right\} \\ &- \delta^2\alpha\, e^{i\sigma t}\ mh_G\, \sigma^2 \bar{z}_{101}\, \theta_{100} \\ &- \beta^2\alpha\, e^{i\sigma t}\ mh_G\, \sigma^2 \bar{z}_{011}\, \theta_{010} \end{aligned} \qquad (IV.2)$$

We have taken the mass of the ACV to be m which may be split up into

$$m = m_1 + m_2$$

where $m_1 g$ is that part of the weight of the ACV which is supported by the air cushion and $m_2 g$ the other part supported by the buoyancy of the side hulls. As the cushion pressure is taken to be of $0(\beta)$ and the cushion area may be considered to be of order zero it is clear that m_1 is of $0(\beta)$

$$\text{i.e.} \qquad m_1 = \beta\left(\frac{m_1}{\beta}\right)$$

where $\frac{m_1}{\beta}$ is now of order zero. In a similar manner, the width of the side hulls is taken to be of small order δ and the length and draught being of order zero, m_2 is of $0(\delta)$

$$\text{i.e.} \qquad m_2 = \delta\left(\frac{m_2}{\delta}\right)$$

where again $\frac{m_2}{\delta}$ is of order zero.

Also,

$$I = m k^2$$

where k is the radius of gyration in pitch (of order zero), so that

$$I = \beta\left(\frac{m_1}{\beta} k^2\right) + \delta\left(\frac{m_2}{\delta} k^2\right)$$

$$= \beta\left(\frac{I_1}{\beta}\right) + \delta\left(\frac{I_2}{\delta}\right)$$

where I_1 and I_2 are the moments of inertia of the partial masses supported by the cushion and the side hulls respectively.

Assigning the correct orders of magnitude to m and I in (IV. 1) and (IV. 2) we derive the following results :

$$X_R = -e^{i\sigma t}\left[\delta\alpha\left(\frac{m_2}{\delta}\right)\sigma^2\bar{x}_{001} + \beta\alpha\left(\frac{m_1}{\beta}\right)\sigma^2\bar{x}_{001} + \right.$$

$$+ \delta^2\alpha\left(\frac{m_2}{\delta}\right)\sigma^2\bar{x}_{101} + \beta^2\alpha\left(\frac{m_1}{\beta}\right)\sigma^2\bar{x}_{011} +$$

$$\left. + \delta\beta\alpha\left\{\left(\frac{m_1}{\beta}\right)\sigma^2\bar{x}_{101} + \left(\frac{m_2}{\delta}\right)\sigma^2\bar{x}_{011}\right\}\right] \qquad \text{(IV. 3)}$$

$$Z_R = -\delta\left(\frac{m_2}{\delta}\right)g - \beta\left(\frac{m_1}{\beta}\right)g -$$

$$-e^{i\sigma t}\left[\delta\alpha\left(\frac{m_2}{\delta}\right)\sigma^2\bar{z}_{001} + \beta\alpha\left(\frac{m_1}{\beta}\right)\sigma^2\bar{z}_{001} + \right.$$

$$+ \delta^2\alpha\left(\frac{m_2}{\delta}\right)\sigma^2\bar{z}_{101} + \beta^2\alpha\left(\frac{m_1}{\beta}\right)\sigma^2\bar{z}_{011} +$$

$$\left. + \delta\beta\alpha\left\{\left(\frac{m_1}{\beta}\right)\sigma^2\bar{z}_{101} + \left(\frac{m_2}{\beta}\right)\sigma^2\bar{z}_{011}\right\}\right] \qquad \text{(IV. 4)}$$

$$M_R = -\delta^2\left(\frac{m_2}{\delta}\right)gh_G\theta_{100} -$$

$$-\delta\beta\left\{\left(\frac{m_1}{\beta}\right)\theta_{100} + \left(\frac{m_2}{\delta}\right)\theta_{010}\right\}gh_G -$$

$$-\beta^2\left(\frac{m_1}{\beta}\right)gh_G\theta_{010} -$$

$$-\delta\beta^2\left(\frac{m_1}{\beta}\right)gh_G\theta_{110} -$$

$$-\delta^2\beta\left(\frac{m_2}{\delta}\right)gh_G\theta_{110}$$

$$+\delta\alpha e^{i\sigma t}\left[\left(\frac{m_2}{\delta}\right)h_G\left(\sigma^2\bar{x}_{001} - g\theta_{001}\right) - \left(\frac{I_2}{\delta}\right)\sigma^2\theta_{001}\right] +$$

$$+\beta\alpha e^{i\sigma t}\left[\left(\frac{m_1}{\beta}\right) h_G\left(\sigma^2 \bar{x}_{001} - g\theta_{001}\right) - \left(\frac{I_1}{\beta}\right)\sigma^2\theta_{001}\right] +$$

$$+\delta\beta\alpha e^{i\sigma t}\left[\left(\frac{m_1}{\beta}\right) h_G\left\{\sigma^2\left(\bar{x}_{101} - \bar{z}_{001}\,\theta_{100}\right) -\right.\right.$$

$$\left.\left. - g\theta_{101}\right\} - \left(\frac{I_1}{\beta}\right)\sigma^2\theta_{101} +\right.$$

$$\left. + \left(\frac{m_2}{\delta}\right) h_G\,\sigma^2\left(\bar{x}_{011} - \bar{z}_{001}\theta_{010}\right) - g\theta_{011} - \left(\frac{I_2}{\delta}\right)\sigma^2\theta_{011}\right] +$$

$$+\delta^2\alpha e^{i\sigma t}\left(\frac{m_2}{\delta}\right) h_G\left\{\sigma^2\left(\bar{x}_{101} - \bar{z}_{001}\theta_{100}\right) -\right.$$

$$\left. - g\theta_{101}\right\} - \left(\frac{I_2}{\delta}\right)\sigma^2\theta_{101} +$$

$$+\beta^2\alpha e^{i\sigma t}\left(\frac{m_1}{\beta}\right) h_G\left\{\sigma^2\left(\bar{x}_{011} - \bar{z}_{001}\theta_{010}\right) -\right.$$

$$\left. - g\theta_{011}\right\} - \left(\frac{I_1}{\beta}\right)\sigma^2\theta_{011} \qquad \text{(IV. 5)}$$

APPENDIX V
DERIVATION OF INTEGRAL REPRESENTATION FOR VELOCITY POTENTIAL

The boundary value problem for the harmonic function ϕ has been formulated in Section III. The classical method of dealing with such problems is the application of Green's theorem in conjunction with appropriate Green's functions giving the following integral equation for Φ :

$$\Phi(x, y, z; t) = \frac{1}{4\pi}\iint_{\Sigma}\left[G(x, y, z; \xi, \eta, \zeta)\,\frac{\partial\Phi}{\partial n} - \right.$$

$$\left. - \Phi(\xi, \eta, \zeta; t)\,\frac{\partial G}{\partial n}\right] . \, dS \qquad \text{(V. 1)}$$

where the Green's function $G(x, y, z, \xi, \eta, \zeta)$ is a harmonic function in the lower half-space $z > 0$, $\zeta > 0$, except near the point $(x = \xi,\ y = \eta,\ z = \zeta)$ where it behaves like a unit source with a singularity of the type $1/r$,

$$\text{i.e.} \qquad \nabla^2 \left(G - \frac{1}{r}\right) = 0$$

with

$$r = \left[(x - \xi)^2 + (y - \eta)^2 + (z - \zeta)^2\right]^{\frac{1}{2}}$$

The surface integral and normal derivatives are taken with respect to the dummy variables (ξ, η, ζ) which have the same disposition as (x, y, z) . The integration is performed over an arbitrary closed surface $\sum$ which completely surrounds the point (x, y, z) at which the potential is to be determined and the derivatives are evaluated in the direction of the normal out of $\sum$.

The potential Φ is assumed to be composed of potentials of various orders (see (2.3)) :

$$\begin{aligned}\Phi(x, y, z; t) = {} & \delta \Phi_{1000}(x, y, z) + \beta \Phi_{0100}(x, y, z) + \delta\beta \Phi_{1100}(x, y, z) + \\ & + \delta\alpha e^{i\sigma t} \Phi_{1010}(x, y, z) + \beta\alpha e^{i\sigma t} \phi_{0110}(x, y, z) + \\ & + \epsilon e^{i\sigma_e t} \Phi_{0001}(x, y, z) + \delta\epsilon e^{i\sigma_e t} \Phi_{1001}(x, y, z) + \\ & + \beta\epsilon e^{i\sigma_e t} \Phi_{0101}(x, y, z) \qquad \text{(V. 2)}\end{aligned}$$

where

Φ_{1000} is the potential due to the motion of the side hulls in calm water,

Φ_{0100} is the potential due to the motion of the air cushion over calm water,

Φ_{1100} is the potential due to the interference between the side hulls and the air cushion in calm water,

Φ_{1010} and Φ_{0110} are the potentials due to the forced oscillation of the side hulls and the air cushion respectively in calm water,

Φ_{0001} is the potential of the incident wave,

and Φ_{1001} and Φ_{0101} are the potentials denoting the interference between the side hulls and the incident wave (the diffracted wave) and between the air cushion and the incident wave (the disturbed wave) respectively.

We shall only derive the lower order potentials

$$\Phi_{1000}\ ,\ \Phi_{0100},\ \Phi_{1010} \text{ and } \Phi_{0110}$$

in this study as these will be sufficient to evaluate the forces and moment of low order. The method of derivation of the interference potential Φ_{1100} will also be briefly indicated without actually carrying out the solution.

The potential of the incident wave is readily written down. The diffracted wave potential and that of the wave of disturbance are only required in the higher order theory.

Boundary Conditions.

The boundary conditions satisfied by the potential are :

(i) $\nabla^2 \Phi = 0$

This applies to potentials of all orders.

(ii) On the EFS $(z = 0)$ the condition (4. 6) is

$$\Phi_{tt} - 2V\Phi_{xt} + V^2\Phi_{xx} - g\Phi_z + 2\nabla\Phi.\nabla\,(\Phi_t - V\Phi_x) +$$

$$+\frac{1}{g}\,(\Phi_t - V\Phi_x)\,\frac{\partial}{\partial z}\,(\Phi_{tt} - 2V\Phi_{xt} + V^2\Phi_{xx} - g\Phi_z) = 0$$

which reduces to the following conditions :

$0(\delta)$ $\quad V^2\Phi_{1000_{xx}} - g\Phi_{1000_z} = 0$

$$0(\beta) \qquad V^2\Phi_{0100_{xx}} - g\Phi_{0100_z} = 0$$

$$0(\delta\alpha) \qquad V^2\Phi_{1010_{xx}} - 2i\sigma V\Phi_{1010_x} - \sigma^2\Phi_{1010} - g\Phi_{1010_z} = 0$$

$$0(\beta\alpha) \qquad V^2\Phi_{0110_{xx}} - 2i\sigma V\Phi_{0110_x} - \sigma^2\Phi_{0110} - g\Phi_{0110_z} = 0$$

$$0(\delta\beta) \qquad V^2\Phi_{1100_{xx}} - g\Phi_{1100_z} = 2V\left(\nabla\Phi_{1000}\cdot\nabla\Phi_{0100_x} + \nabla\Phi_{0100}\cdot\nabla\Phi_{1000_x}\right) + \frac{V}{g}\left[\Phi_{1000_x}\frac{\partial}{\partial z}\left(V^2\Phi_{0100_{xx}} - g\Phi_{0100_z}\right) + \Phi_{0100_x}\frac{\partial}{\partial z}\left(V^2\Phi_{1000_{xx}} - g\Phi_{1000_z}\right)\right] \qquad (V.3)$$

It will be noted that the first four equations are homogeneous, whereas the equation for the interference potential is an inhomogeneous one.

If we denote by Ψ the time-independent part of the oscillatory potential Φ (i.e. without the factor $e^{i\sigma t}$), the first four of the above equations reduce to the form

$$V^2\Psi_{xx} - 2i\sigma V\Psi_x - \sigma^2\Psi - g\Psi_z = 0 \qquad (V.4)$$

In the case of the steady potentials σ is, of course, set equal to zero.

(iii) On the IFS ($z = 0$) the condition (4-7) is

$$\Phi_{tt} - 2V\Phi_{xt} + V^2\Phi_{xx} - g\Phi_z + 2\nabla\Phi.\ \nabla(\Phi_t - V\Phi_x) + \frac{1}{g}\left(\Phi_t - V\Phi_x + \frac{p_s}{\rho}\right)\frac{\partial}{\partial z}\left(\Phi_{tt} - 2V\Phi_{xt} + V^2\Phi_{xx} - g\Phi_z\right) +$$

$$+\frac{1}{\rho}\left[\left(\frac{\partial}{\partial t} - V\frac{\partial}{\partial x}\right) p_s + \Phi_x p_{s_x} + \Phi_y p_{s_y}\right] +$$

$$+\frac{1}{\rho g} V p_{s_x} \frac{\partial}{\partial z} (\Phi_t - V\Phi_x) = 0$$

The surface pressure distribution is given by (I. 1) in the form

$$p_s(x, y) = \beta p_{010} + \delta\beta \cdot p_{110} + \beta\alpha e^{i\sigma t} p_{011} +$$

where

$$p_{010} = p_o(x, y)$$

$$p_{110} = \bar{r}_{100} p_{o_x}(x, y) = (\bar{x}_{100} + h_G \theta_{100}) p_{o_x}(x, y)$$

and

$$p_{011} = \bar{r}_{001} p_{o_x}(x, y) = (\bar{x}_{001} + h_G \theta_{001}) p_{o_x}(x, y)$$

and the conditions satisfied by the various potentials are

$$0(\delta) \quad V^2\Phi_{1000_{xx}} - g\Phi_{1000_z} = 0$$

$$0(\beta) \quad V^2\Phi_{0100_{xx}} - g\Phi_{0100_z} = \frac{V}{\rho} p_{010_x}$$

$$0(\delta\alpha) \quad V^2\Phi_{1010_{xx}} - 2i\sigma V\Phi_{1010_x} - \sigma^2\Phi_{1010} - g\Phi_{1010_z} = 0$$

$$0(\beta\alpha) \quad V^2\Phi_{0110_{xx}} - 2i\sigma V\Phi_{0110_x} - \sigma^2\Phi_{0110} - g\Phi_{0110_z} =$$

$$= \frac{1}{\rho} (V p_{011_x} - i\sigma p_{011})$$

$$0(\delta\beta)\ V^2\Phi_{1100_{xx}} - g\Phi_{1100_z} = 2V(\nabla\Phi_{1000}\cdot\nabla\Phi_{0100_x} + \nabla\Phi_{0100}\cdot\nabla\Phi_{1000_x})$$

$$+\frac{V}{g}\,\Phi_{1000_x}\,\frac{\partial}{\partial z}\,(V^2\Phi_{0100_{xx}} - g\Phi_{0100_z})$$

$$-\frac{1}{g}\left(\frac{1}{\rho}\,p_{010} - V\Phi_{0100_x}\right)$$

$$\frac{\partial}{\partial z}(V^2\ \ 1000_{xx} - g\ \ 1000_z) +$$

$$\frac{V^2}{\rho g}\ \ p_{010_x}\,\Phi_{1000_{xz}} + \frac{V}{\rho}\ \ p_{010_x} -$$

$$\cdot\frac{1}{\rho}(\Phi_{1000_x}\,p_{010_x} +$$

$$+\Phi_{1000_y}\ \ p_{010_y}) \qquad (V.5)$$

The first four of the above equations may be written in the form

$$V^2\Psi_{xx} - 2i\sigma V\Psi_x - \sigma^2\Psi - g\Psi_z = \frac{1}{\rho}\,(V\bar{p}_{s_x} - i\sigma\bar{p}_s) \qquad (V.6)$$

where $\bar{p}_s$ is the time-independent part of p_s

(iv) On the side hulls the condition (4.10) is

$$\frac{\partial\Phi}{\partial\eta} = \delta\left[\left\{\dot{x}\cos\theta - \dot{z}\sin\theta + (z' + h_G)\,\dot{\theta} + V\cos\theta\right\}\frac{\partial h_1}{\partial x'} +\right.$$

$$\left. + \left\{\dot{x}\sin\theta + \dot{z}\cos\theta - x'\,\dot{\theta} + V\sin\theta\right\}\frac{\partial h_1}{\partial z'}\right]$$

$$\left[1 + \delta^2\left(\frac{\partial h_1}{\partial x'}\right)^2 + \delta^2\left(\frac{\partial h_1}{\partial z'}\right)^2\right]^{-1/2}$$

which reduces to

$$0(\delta) \qquad \frac{\partial \Phi_{1000}}{\partial n} = V \frac{\partial h_1}{\partial x'}$$

$$0(\beta) \qquad \frac{\partial \Phi_{0100}}{\partial n} = 0 \qquad \text{Condition does not apply.}$$

$$0(\delta\alpha) \qquad \frac{\partial \Phi_{1010}}{\partial n} = i\sigma r_{001} \frac{\partial h_1}{\partial x'} + (i\sigma r'_{001} + V\theta_{001}) \frac{\partial h_1}{\partial z'}$$

$$0(\beta\alpha) \qquad \frac{\partial \Phi_{0110}}{\partial n} = 0 \qquad \text{no condition}$$

$$0(\delta\beta) \qquad \frac{\partial \Phi_{1100}}{\partial n} = V\theta_{010} \frac{\partial h_1}{\partial z'} \qquad \text{(V. 7)}$$

These conditions relate to the outer hull surfaces. In the case of the inner surfaces the hull function h_1 should be replaced by h_2 .

The first four conditions may be represented in the form

$$\frac{\partial \Psi}{\partial n} = \delta \left[(\alpha i\sigma r_{001} + V) \frac{\partial h_1}{\partial x'} + \alpha (i\sigma r'_{001} + V\theta_{001}) \frac{\partial h_1}{\partial z'} \right] \qquad \text{(V. 8)}$$

(v) Radiation and Boundedness Conditions.

We may assume that the potentials of all orders satisfy the conditions

$$\Phi \longrightarrow 0 \quad , \quad \text{i. e.} \quad \Psi \longrightarrow 0$$

and

$$\frac{\partial \Phi}{\partial z} \longrightarrow 0 \quad , \quad \text{i. e.} \quad \frac{\partial \Psi}{\partial z} \longrightarrow 0$$

as $z \longrightarrow \infty$ at the bottom of the ocean. We may also assume that the potentials and their derivatives satisfy suitable radiation conditions as

$$x^2 + y^2 \longrightarrow \infty$$

These conditions will be specifically stipulated in due course.

Singularity of the Potential.

It will be seen from (V. 3) and (V. 5) that the potentials Φ_{1000} and Φ_{1010} relating to the steady motion and forced oscillation of the side hulls of an ACV in the full displacement mode (i. e. without an air cushion) in calm water satisfy identical conditions both on the EFS et IFS. However, they have to satisfy additional boundary conditions on the hull surfaces given by (V. 7). On the other hand, the potentials Φ_{0100} and Φ_{0110} relating to the air cushion of an amphibious ACV (without the side hulls) satisfy different conditions on the EFS and on the IFS unless the basic pressure distribution is truly uniform in the longitudinal direction such that

$$p_{o_x} = 0 \quad \text{and} \quad p_{o_{xx}} = 0$$

throughout the length of the cushion. However, this would imply a discontinuity in the pressure at the boundary along the bow and the stern where the pressure drops suddenly from the uniform cushion pressure to the atmospheric. A discontinuity in the value of the potential at the boundary is therefore to be expected.

It is also to be noted that the cushion potentials Φ_{0100} and Φ_{0110} do not have to meet any specific conditions on the hull surfaces and that the interference potential Φ_{1100} satisfies different boundary conditions on the EFS and IFS and also a condition on the hull surface.

The Green's Function.

Let us now choose a Green's function $G(x, y, z; \xi, \eta, \zeta)$ such that

$$\nabla^2 G = G_{xx} + G_{yy} + G_{zz} = -4\pi\, \delta(x - \xi)\ \delta(y - \eta)\ \delta(z - \zeta)$$

where δ is the Dirac delta-function. This ensures that G is a harmonic function in $z > 0$ with a singularity of the type $\frac{1}{r}$ at $x = \xi$, $y = \eta$, $z = \zeta$.

Let C also be such that

$$V^2 G_{\xi\xi} + 2i\sigma V G_\xi - \sigma^2 G - gG_\zeta = 0, \quad \text{on } \zeta = 0 \qquad (V.9)$$

It will be observed that this free surface condition we have stipulated for G is the same as that satisfied by the potentials in (V.4) with the difference that V is replaced by -V so that the second term on the left hand side is of a different sign. The reason for this will be apparent presently.

We may also assume that

$$\lim_{\zeta \to \infty} G = 0$$

and

$$\lim_{\xi \to \infty} \frac{\partial G}{\partial \zeta} = 0$$

A suitable radiation condition is also imposed on G for large $(\xi^2 + \zeta^2)^{\frac{1}{2}}$ and fixed ζ in order to obtain a unique solution of the problem.

The radiation conditions for ϕ and G are fully discussed in Appendix V of Reference 1.

The Domain of Integration.

We may subdivide the closed surface Σ into the following separate regions :

$$\Sigma = \Sigma_o + \Sigma_1 + \Sigma_2 + \Sigma_3$$

where Σ_o is a surface of small depth below the undisturbed water surface which just encloses the immersed part of the side hulls of the ACV in its interior and which intersects the EFS in a closed curve L_4 (see Figure 3). This curve will therefore contain in its interior the actual boundary L_H of the ACV on $z = 0$, i.e. the closed curve formed by the intersections of the outer surfaces of the hulls on $z = 0$ and the vertical projection thereon of the hemline of the skirts at the bow and stern.

Σ_1 is the lateral surface and Σ_2 the base of a large circu-

lar cylinder with its axis along the z-axis and extending downwards to the bottom of the deep ocean. The radius and depth of this vertical cylinder are assumed to be very large. If the intersection of this cylinder with the plane $z = 0$ is the circle L_3, it is obvious that L_4 (and therefore L_H) will be contained well within it. Also, $\sum_3$ is the ring-shaped domain on $z = 0$ lying between the circle L_3 and the closed curve L_4.

We may now apply Green's theorem to the closed domain in $z > 0$ bounded by $\sum$, i.e. by $\sum_o + \sum_1 + \sum_2 + \sum_3$, with (x, y, z) lying within $\sum$

$$\Psi(x, y, z) = \frac{1}{4\pi} \iint_{\sum_o + \sum_1 + \sum_2 + \sum_3} \left[G \frac{\partial \Psi}{\partial n} - \Psi \frac{\partial G}{\partial n} \right] dS \qquad (V.10)$$

The boundary conditions satisfied by Ψ are given by (V.4), (V.6), and (V.8).

Considering first the integral over $\sum_2$ the base of the large cylinder, the integrand tends to zero in view of the assumed behaviour of Φ (and therefore of Ψ) and of G as $\zeta \to \infty$. The integral over the lateral surface $\sum_1$ is also zero as the radius $r \to \infty$ since the radiation conditions are specially selected (and considered physically reasonable) to ensure that this is so. A full discussion of this matter will be found in Appendix V of Reference 1.

We are therefore left only to deal with the integrals over $\sum_o$ and $\sum_3$. As regards the later,

$$\frac{1}{4\pi} \iint_{\sum_3} \left(G \frac{\partial \Psi}{\partial n} - \Psi \frac{\partial G}{\partial n} \right) dS = \frac{1}{4\pi} \iint_{\sum_3} \left(\Psi \frac{\partial G}{\partial \zeta} - G \frac{\partial \Psi}{\partial \zeta} \right) d\xi\, d\eta$$

and on substituting for Ψ_ζ from (V.9) the integral becomes,

$$\frac{1}{4\pi g} \iint_{\sum_3} \left[\Psi(V^2 G_{\xi\xi} + 2i\sigma V G_\xi - \sigma^2 G) - G(V^2 \Psi_{\xi\xi} - 2i\sigma V \Psi_\xi - \sigma^2 \Psi) \right] d\xi\, d\eta$$

$$= \frac{1}{4\pi g} \iint_{\sum_3} \left[V^2 (\Psi G_{\xi\xi} - G \Psi_{\xi\xi}) + 2i\sigma V (\Psi G_\xi + G \Psi_\xi) \right] d\xi\, d\eta$$

$$= \frac{1}{4\pi g} \iint_{\sum_3} \frac{\partial}{\partial \xi} \left[V^2 (\Psi G_\xi - G \Psi_\xi) + 2i\sigma V \Psi G \right] d\xi\, d\eta$$

$$= \frac{1}{4\pi g} \oint_{L_3} \left[V^2 (\Psi G_\xi - G\Psi_\xi) + 2i\sigma V \Psi G \right] d\eta +$$

$$+ \frac{1}{4\pi g} \oint_{L_4} \left[V^2 (\Psi G_\xi - G\Psi_\xi) + 2i\sigma V \Psi G \right] d\eta$$

where the line integrals are taken in the clockwise direction (viewed from above) along L_3 and in the counter-clockwise direction along L_4 in order to keep the domain of integration to the left, bearing in mind that the positive side of the element of area $d\xi d\eta$ is along the z-axis i.e. below the free surface. This is in accordance with the usual convention.

It is important to note that the above substitution for Ψ_ξ from (V.4) is only valid for potentials of $0(\delta, \beta, \delta\alpha$ and $\beta\alpha)$. It is not valid for the potential of $0(\delta\beta)$.

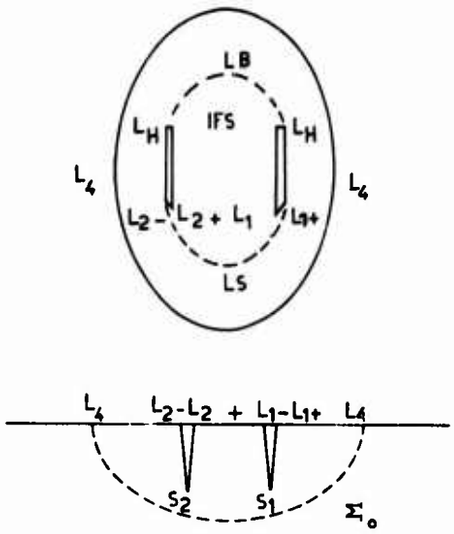
It can be shown that the line integral along L_3 also vanishes under the assumed radiation conditions.

We have then,

$$\Psi(x, y, z) = \frac{1}{4\pi} \iint_{\Sigma_o} \left(G \frac{\partial \Psi}{\partial n} - \Psi \frac{\partial G}{\partial n} \right) dS +$$

$$+ \frac{V^2}{4\pi g} \oint_{L_4} \left(\Psi G_\xi - G\Psi_\xi + \frac{2i\sigma}{V} \Psi G \right) d\eta \qquad (V.11)$$

We may now contract the surface Σ_o surrounding the ACV on the water surface to the actual boundary of the craft composed of the immersed hulls S_1 and S_2 and the internal free surface S. The curve L_4 will then tend to the curve L_H in the limit.



Thus we may write,

$$\Psi(x,y,z) = \frac{1}{4\pi}\iint_{S_1+S_2}\left(G\,\frac{\partial\Psi}{\partial n} - \Psi\,\frac{\partial G}{\partial n}\right)dS + \frac{1}{4\pi}\iint_{S_o}\left(\Psi\frac{\partial G}{\partial \zeta} - G\,\frac{\partial\Psi}{\partial\zeta}\right)d\xi\,d\eta + \frac{V^2}{4\pi g}\;\underset{L_4\to L_H}{\mathrm{Lt}}\;\oint_{L_4}\left(\Psi G_\xi - G\Psi_\xi + \frac{2i\sigma}{V}\Psi G\right)d\eta \qquad (V.12)$$

where we have denoted by S_o the part of the plane $z = 0$ contained within the IFS.

It will be recalled that L_H is the boundary of the ACV on the water surface. This curve may be sub-divided as follows :

$$L_H = L_{1+} + L_B + L_{2-} + L_S$$

where L_{1+} and L_{2-} are the intersections of the outer hull surfaces

with the plane $z = 0$ and L_B and L_S are the vertical projections of the hemlines of the skirts at the bow and the stern. All these curves are to be traversed in the same direction as L_4, i.e. in the counter-clockwise direction.

The surface integral over S_o may be transformed by the application of Stokes' theorem :

$$g \iint_{S_o} \Psi G_\zeta \, d\xi d\eta = \iint_{S_o} \Psi(V^2 G_{\xi\xi} + 2i\sigma V G_\xi - \sigma^2 G) \, d\xi d\eta$$

$$= V^2 \oint_{L_C} \Psi \, G_\xi d\eta - V^2 \iint_{S_o} \Psi_\xi G_\xi \, d\xi d\eta +$$

$$+ 2i\sigma V \oint_{L_C} \Psi \, G \, d\eta - 2i\sigma V \iint_{S_o} \Psi_\xi G \, d\xi d\eta -$$

$$- \sigma^2 \iint_{S_o} \Psi G \, d\xi d\eta$$

and since

$$\iint_{S_o} \Psi_\xi \, G_\xi \, d\xi d\eta = \oint_{L_C} \Psi_\xi G \, d\eta - \iint_{S_o} \Psi_{\xi\xi} G \, d\xi d\eta$$

we may combine all these integrals together and write

$$\frac{1}{4\pi} \iint_{S_o} (\Psi \frac{\partial G}{\partial \zeta} - G \frac{\partial \Psi}{\partial \zeta}) \, d\xi d\eta = \frac{1}{4\pi g} \iint_{S_o} (V^2 \Psi_{\xi\xi} - 2i\sigma V \Psi_\xi - \sigma^2 \Psi -$$

$$- g\Psi_\zeta) G \, d\xi d\eta + \frac{V^2}{4\pi g} \oint_{L_C} (\Psi G_\xi -$$

$$- \Psi_\xi G + \frac{2i\sigma}{V} \Psi G) \, d\eta$$

where, now, L_C is the boundary of the IFS

$$L_C = L_{1-} + L_B + L_{2+} + L_S ,$$

L_{1-} and L_{2+} being the intersections of the inner hull surfaces with $z = 0$ and L_B and L_S as defined previously in connection with L_H.

All these curves are to be traversed in the clockwise direction in order to keep the positive side of S_o (which is below the free surface) to the left.

We may now write (V. 12) in the form

$$\Psi(x,y,z) = \frac{1}{4\pi}\iint_{S_1+S_2}\left(G\ \frac{\partial\Psi}{\partial n} - \Psi\frac{\partial G}{\partial n}\right) dS +$$

$$+\frac{1}{4\pi g}\iint_{S_o}\left(V^2\Psi_{\xi\xi} - 2i\sigma V\Psi_\xi - \sigma^2\Psi - g\Psi_\zeta\right) G\ d\xi d\eta$$

$$+\frac{V^2}{4\pi g}\oint_{L_C}\left(\Psi G_\xi - G\Psi_\xi + \frac{2i\sigma}{V}\Psi G\right) d\eta +$$

$$\frac{V^2}{4\pi g}\ \lim_{L_4 \to L_H}\oint_{L_4}\left(\Psi G_\xi - G\Psi_\xi + \frac{2i\sigma}{V}\Psi G\right) d\eta$$

Now, the function of Ψ and its derivatives in the integrand of the surface integral over S_o is given exactly by the free surface condition (V. 6) on the IFS applicable to potentials of $0(\delta, \beta, \delta\alpha, \beta\alpha)$, namely,

$$\frac{1}{\rho}\left(V\bar{p}_{s_\xi} - i\sigma\bar{p}_s\right)$$

Substituting this value and combining the line integrals, we may write

$$\Psi(x,y,z) = \frac{1}{4\pi}\iint_{S_1+S_2}\left(G\frac{\partial\Psi}{\partial n} - \frac{\partial G}{\partial n}\right) dS +$$

$$+\frac{1}{4\pi\rho g}\iint_{S_o}\left(V\bar{p}_{s_\xi} - i\sigma\bar{p}_s\right) G\ d\xi d\eta +$$

$$+\frac{V^2}{4\pi g}\left[\oint_{L_H} + \oint_{L_C}\right]\left[\Psi G_\xi - G\Psi_\xi + \frac{2i\sigma}{V}\Psi G\right] d\eta \qquad (V.13)$$

It will be noted that the contour L_H and L_C have in common the curves L_B and L_S at the bow and stern which are taken in different directions. Choosing the clockwise direction for the integration, the combined line integral may be written

$$\frac{V^2}{4\pi g} \oint_{L_B + L_S} \left[[\Psi] G_\xi - G [\Psi_\xi] + \frac{2i\sigma}{V} [\Psi] G \right] d\eta +$$

+ (line integrals along the hull intersection L_{1+}, L_{1-}, L_{2+} and L_{2-})

where $[\Psi]$ and $[\Psi_\xi]$ denote the "jumps" in these functions across the cushion boundary in crossing from a point on the EFS outside to a point on the IFS just within. These jumps will exist due to the singularity of the potential at the boundary of the cushion indicated earlier. We are, of course, assuming that G is continuous across the boundary.

The line integrals along the hull surfaces need not be discussed in detail as their order will be $0(\delta)$ higher than that of the potential under investigation. This is because the total width of each hull is of $0(\delta)$ and the line integral is taken with respect to η on the hull surfaces. On the other hand, the line integrals along L_B and L_S will be of the same order as the potential as η can now take a value up to the semi-width of the ACV on either side. However, the line integrals around the hulls will have to be taken into account when evaluating Ψ_{110} by including the contribution of $0(\delta\beta)$ arising from the integration of the potential Ψ_{010} of $0(\beta)$.

It may be added that the line integral along the cushion boundary will vanish if there is no discontinuity of Ψ at the boundary. As the discontinuity arises mainly because of a pressure distribution within the IFS higher than atmospheric, a suitable distribution of pressure will remove the discontinuity and the need for evaluating the line integral. This will be discussed presently.

The surface of integration S_0 is that part of the plane $z = 0$ contained within the instantaneous position of the IFS, which is a fluctuating region oscillating about the steady state position $\bar{S}_0$ say. As the instantaneous position S_0 is unknown and has to be solved as part of the problem, we will reduce the surface of integration to the known region $\bar{S}_0$.

The instantaneous surface S_o may be assumed to be composed of the steady surface $\bar{S}_o$ together with an additional strip of area S'_o arising out of the oscillations.

The strip corresponding to an element of area $d\bar{\xi}d\eta$ extends from the point L on the boundary of $\bar{S}_o$ to L' on the boundary of S_o. If ξ_L and $\xi_{L'}$ are the longitudinal co-ordinates of L and L' respectively,

$$\xi_L = \xi_{L'}$$

in the undisturbed condition when L and L' coincide.

In the disturbed condition points on S_o are obtained by the vertical projections of points lying in the $\xi'\eta'$ plane within the displaced position of the cushion boundary in that plane. Thus, setting $\zeta' = 0$ in equation (3.1) for transformation of co-ordinates, we obtain after linearization with respect to θ

$$\xi_{L'} = \xi'_L + (\bar{x} + h_G)\theta$$

$$= \xi_L + (\bar{x} + h_G)\theta$$

since the geometry of the cushion boundary in the $\xi'\eta'$-plane is unchanged by the displacement.

We may now write

$$\iint_{S_o} f(\xi\eta)\, d\xi d\eta = \iint_{\bar{S}_o} f(\xi\eta)\, d\xi d\eta + \iint_{S'_o} f(\xi\eta)\, d\xi d\eta$$

The integral over S'_o may be written

$$\int d\eta \int_{\xi_L}^{\xi_{L'}} f(\xi\eta)\, d\xi$$

and as the length of the strip is small, we may replace the inner integral by

$$(\xi_{L'} - \xi_L)\left[f(\xi\eta)\right]_{\xi=\xi_L}$$

so that the surface integral over S_o' becomes the line integral

$$\oint_{L_C} (\xi_{L'} - \xi_L) \quad f(\xi,\eta) \quad d\eta$$
$$= (\bar{x} + h_G\theta) \oint_{L_C} f(\xi,\eta)\, d\eta$$

which may be re-written as a surface integral by Stokes' theorem

$$(\bar{x} + h_G\theta) \iint_{S_o} \frac{\partial f}{\partial \xi} \quad d\xi d\eta$$

We have, therefore, generally,

$$\iint_{S_o} f(\xi,\eta)\, d\xi d\eta = \iint_{\bar{S}_o} \left[f(\xi,\eta) + (\bar{x} + h_G\theta) \frac{\partial f(\xi,\eta)}{\partial \xi} \right] d\xi\, d\eta$$

It is obvious that there is no additional correction term required when $f(\xi,\eta)$ is uniform throughout $\bar{S}_o$ or when it has a zero value at the boundary.

Applying this result to the integral over S_o in (V.13) we may write

$$\Psi(x,y,z) = \frac{1}{4\pi} \iint_{S_1+S_2} \left(G \frac{\partial \Psi}{\partial n} - \Psi \frac{\partial G}{\partial n}\right) dS +$$
$$+ \frac{1}{4\pi\rho g} \iint_{S_o} \Big[(V\bar{p}_{s_\xi} - i\sigma \bar{p}_s)\, G + (\bar{x} + h_G\theta)$$
$$\frac{\partial}{\partial \xi} \left[(V\bar{p}_{s_\xi} - i\sigma \bar{p}_s)\, G \right] \Big] d\xi\, d\eta +$$
$$+ \frac{V^2}{4\pi g} \oint_{L_B+L_S} \left[[\Psi]\, G_\xi - G[\Psi_\xi] + \frac{2i\sigma}{V} [\Psi]\, G \right] d\eta \qquad (V.14)$$

We will now proceed to discuss the integral over the hull surfaces.

Considering first

$$\iint_{S_1+S_2} \Psi \frac{\partial G}{\partial n} \, dS ,$$

since

$$\frac{\partial G}{\partial n} = \hat{n} . \nabla G$$

where $\hat{n}$, the unit normal out of Σ, i. e. into the hull, is given by

$$\hat{n} = \frac{\nabla H}{|\nabla H|}$$

we may write,

$$\frac{\partial G}{\partial n} dS = \frac{\nabla G . \nabla H}{|\nabla H|} \, dS$$

$$= \nabla G . \nabla H \quad d\xi' \quad d\zeta'$$

$$= \left[\delta \left(\frac{\partial h_1}{\partial \xi'} \cos\theta + \frac{\partial h_1}{\partial \zeta'} \sin\theta \right) \frac{\partial G}{\partial \xi} \mp \frac{\partial G}{\partial \eta} + \right.$$

$$\left. + \delta \left(\frac{\partial h_1}{\partial \zeta'} \cos\theta - \frac{\partial h_1}{\partial \xi'} \sin\theta \right) \frac{\partial G}{\partial \zeta} \right] d\xi' d\zeta'$$

on the outer hull surfaces S_{1+} and S_{2-} as discussed in Section IV.3 In the case of the inner hull surfaces S_{2+} and S_{1-} we replace h_1 by h_2 .

On linearizing with respect to θ ,

$$\frac{\partial G}{\partial n} dS = \left[\delta \left(\frac{\partial h_1}{\partial \xi'} + \theta \frac{\partial h_1}{\partial \zeta'} \right) \frac{\partial G}{\partial \xi} \mp \frac{\partial G}{\partial \eta} + \delta \left(\frac{\partial h_1}{\partial \zeta'} - \theta \frac{\partial h_1}{\partial \xi'} \right) \frac{\partial G}{\partial \zeta} \right] d\xi' d\zeta'$$

Now, the terms containing θ have δ as a factor and as θ is of $0(\delta, \beta, \alpha, \delta\alpha, \beta\alpha)$ these terms will actually be of $0(\delta^2, \delta\beta, \delta\alpha)$. Also

$\frac{\partial G}{\partial n}$ has Ψ as a factor and these terms will therefore become of a much higher order. We may therefore ignore the terms containing θ and write simply

$$\frac{\partial G}{\partial n} \; dS = \xi \left[\mp \frac{\partial G}{\partial \eta} + \delta \left(\frac{\partial h_1}{\partial \xi'} \frac{\partial G}{\partial \xi} + \frac{\partial h_1}{\partial \zeta'} \frac{\partial G}{\partial \zeta} \right) \right] \quad d\xi' d\zeta'$$

It should be noted that the derivatives of G on the actual hull surface should be used although we have reduced the domain of integration to the longitudinal plane of the hulls. We will therefore have to expand the derivatives from the hull surface to the longitudinal plane.

Let

$$G = G_r + \frac{1}{r}$$

where G_r is the regular part of G and

$$r = \left[(x - \xi)^2 + (y - \eta)^2 + (z - \zeta)^2 \right]^{1/2}$$

Then, using Taylor's theorem for the expansion of regular functions

$$\frac{\partial G_r}{\partial n}\bigg|_{\eta - b = \delta h_1(\xi'\zeta')} = - \frac{\partial G_r}{\partial \eta}\bigg|_{\eta = b_+} + \delta \left[\frac{\partial h_1}{\partial \xi'} \frac{\partial G_r}{\partial \xi} + \frac{\partial h_1}{\partial \zeta'} \frac{\partial G_r}{\partial \zeta} \right]_{\eta = b_+}$$

$$+ \delta \; h_1(\xi'\zeta') \left[- \frac{\partial^2 G_r}{\partial \eta^2} + \right.$$

$$\left. \delta \left\{ \frac{\partial h_1}{\partial \xi'} \frac{\partial^2 G_r}{\partial \xi \partial \eta} + \frac{\partial h_1}{\partial \zeta'} \frac{\partial^2 G_r}{\partial \eta \partial \zeta} \right\} \right]$$

$$= - \frac{\partial G_r}{\partial \eta}\bigg|_{\eta = b_+} + \delta \left[\frac{\partial h_1}{\partial \xi'} \frac{\partial G_r}{\partial \xi} + \frac{\partial h_1}{\partial \zeta'} \frac{\partial G_r}{\partial \zeta} - \right.$$

$$\left. - h_1(\xi'\zeta') \frac{\partial^2 G_r}{\partial \eta^2} \right]_{\eta = b_+} + O(\delta^2)$$

This is on the outer hull surface S_{1+} . In the case of the other surface S_{2-} the expansion would be

$$\left.\frac{\partial G_r}{\partial n}\right|_{\eta+b=-\delta h_1(\xi'\zeta')} = \left.\frac{\partial G_r}{\partial \eta}\right|_{\eta=-b_-} + \delta\left[\frac{\partial h_1}{\partial \xi'}\frac{\partial G_r}{\partial \xi} + \frac{\partial h_1}{\partial \zeta'}\frac{\partial G_r}{\partial \zeta}\right]_{\eta=-b_-} - \delta h_1(\xi'\zeta')\left.\frac{\partial^2 G_r}{\partial \eta^2}\right|_{\eta=-b_-} + 0(\delta^2)$$

$$= \left.\frac{\partial G_r}{\partial \eta}\right|_{\eta=-b_1} + \delta\left[\frac{\partial h_1}{\partial \xi'}\frac{\partial G_r}{\partial \xi} + \frac{\partial h_1}{\partial \zeta'}\frac{\partial G_r}{\partial \zeta} - h_1(\xi'\xi')\frac{\partial^2 G_r}{\partial \eta^2}\right]_{\eta=-b_-}$$

Similar expansions with h_2 instead of h_1 will apply to the two inner hull surfaces S_{2+} and S_{1-} .

The normal derivarive has thus been reduced to the derivative in the lateral direction across the longitudinal planes with the addition of $0(\delta)$ terms which are only required when we have to evaluate the $0(\delta\beta)$ potential.

Let us now consider the singular part of G , namely $1/r$. As in the case of G_r

$$\frac{\partial}{\partial n}\left(\frac{1}{r}\right) = \mp\frac{\partial}{\partial \eta}\left(\frac{1}{r}\right) + \delta\left[\frac{\partial h_1}{\partial \xi'}\frac{\partial}{\partial \xi}\left(\frac{1}{r}\right) + \frac{\partial h_1}{\partial \zeta'}\frac{\partial}{\partial \zeta}\left(\frac{1}{r}\right)\right]$$

If the point (x, y, z) at which the potential is to be determined is far removed from (ξ, η, ζ) which is confined to the hull surfaces for the purposes of integration, there is no difficulty, for $1/r$ is then regular and may be considered as part of G_r in the above expansion. We shall, however, be actually interested in the case when (x, y, z) also lies on the hull surfaces for the determination of the potential and thereby the pressure thereon which causes the forces and moment. A closer examination of the normal derivative is therefore necessary in this case in view of the possible singularity at $(x = \xi\ ,\ y = \eta\ ,\ z = \zeta)$.

Now

$$\frac{\partial}{\partial \xi}\left(-\frac{1}{r}\right) = \frac{x-\xi}{r^3}, \frac{\partial}{\partial \eta}\left(\frac{1}{r}\right) = \frac{y-\eta}{r^3}, \frac{\partial}{\partial \zeta}\left(\frac{1}{r}\right) = \frac{z-\zeta}{r^3}$$

so that

$$\frac{\partial}{\partial n}\left(\frac{1}{r}\right) = \mp \frac{y-\eta}{r^3} + \delta\left(\frac{x-\xi}{r^3}\frac{\partial h_1}{\partial \xi'} + \frac{z-\zeta}{r^3}\frac{\partial h_1}{\partial \zeta}\right)$$

and considering first S_{1+} with

$$\eta = \eta' = b + \delta\, h_1 \quad (\xi'\zeta')$$

we have

$$\frac{\partial}{\partial n}\left(\frac{1}{r}\right)_{S_{1+}} = \frac{-y + b + \delta h_1(\xi'\zeta') + \delta(x-\xi)\frac{\partial h_1}{\partial \zeta'} + \delta(z-\zeta)\frac{\partial h_1}{\partial \zeta'}}{\left[(x-\xi)^2 + \left\{y - b - \delta\, h_1\,(\xi'\zeta')\right\}^2 + (z-\zeta)^2\right]^{3/2}}$$

Assume now that (x, y, z) lies just outside S_1 so that

$$y = b + \delta\, h_1\,(x'z') + \epsilon$$

where ϵ is a small positive quantity $\ll \delta$

Then

$$\frac{\partial}{\partial n}\left(\frac{1}{r}\right) = \frac{-\delta h_1(x', z') - \epsilon + \delta h_1(\xi'\zeta') + \delta(x-\xi)\frac{\partial h_1}{\partial \xi'} + \delta(z-\zeta)\frac{\partial h_1}{\partial \xi'}}{\left[(x-\xi)^2 + \left[\delta\, h_1(x'z') + \epsilon - \delta h_1(\xi'\zeta')\right]^2 + (z-\xi)^2\right]^{3/2}}$$

which is of $0(\delta)$ as $\epsilon \longrightarrow 0$, unless $x \longrightarrow \xi$ and $z \longrightarrow \zeta$ when it is of $0\left(\frac{1}{\epsilon^{\frac{1}{2}}}\right)$.

In the limiting case when δ also $\longrightarrow 0$ it can be shown that

$$\frac{\partial}{\partial n}\left(\frac{1}{r}\right) \longrightarrow 2\pi\delta\ (x-\xi)\ \delta\ (z-\xi) + 0(\delta)$$

where the operator δ stands for the Dirac delta-function.

Similarly, in the case of S_{2-}, the normal derivative is of $0(\delta)$ or

$$-\frac{\partial}{\partial n}\left(\frac{1}{r}\right) \longrightarrow -2\pi\delta(x-\xi)\quad \delta(z-\zeta) + 0(\delta)$$

and results for S_{1-} and S_{2+} could also be written down in the same manner.

We may therefore write, neglecting the $0(\delta)$ terms.

$$\begin{aligned}
\iint_{S_1+S_2} \Psi\frac{\partial G}{\partial n}\,dS = \iint_{S_{1_o}+S_{2_o}} \Bigg[& \Psi_{\eta=b+}\left\{\left.\frac{\partial G}{\partial \eta}\right|_{\eta=b+} + 2\pi\delta(x-\xi)\,\delta(z-\zeta)\right\} + \\
& + \Psi_{\eta=b-}\left\{\left.\frac{\partial G}{\partial \eta}\right|_{\eta=b-} - 2\pi\delta(x-\xi)\,\delta(z-\zeta)\right\} + \\
& + \Psi_{\eta=-b+}\left\{\left.\frac{\partial G}{\partial \eta}\right|_{\eta=-b+} + 2\pi\delta(x-\xi)\,\delta(z-\zeta)\right\} + \\
& + \Psi_{\eta=-b-}\left\{\left.\frac{\partial G}{\partial \eta}\right|_{\eta=-b-} - 2\pi\delta(x-\xi)\,\delta(z-\zeta)\right\}\Bigg]\,d\xi'd\zeta' \\
= \iint_{S_{1_o}+S_{2_o}} \Bigg[& \left\{\Psi_{b-} - \Psi_{b+}\right\}\left\{\left.\frac{\partial G}{\partial \eta}\right|_{\eta=b} - 2\pi\delta(x-\xi)(z-\zeta)\right\} + \\
& + \left\{\Psi_{-b+} - \Psi_{-b-}\right\}\left\{-\left.\frac{\partial G}{\partial \eta}\right|_{\eta=-b} + \right. \\
& \left. + 2\pi\delta(x-\xi)\,\delta(z-\zeta)\right\}\Bigg]\,d\zeta'd\zeta'
\end{aligned}$$

where S_{1_o} and S_{2_o} denote one side each of the immersed part of the longitudinal planes of the hulls. We have assumed here that G and G_η are continuous across the longitudinal planes, but allowed for a discontinuity in the value of the potential across the planes. The values of G_η at $\eta = b$ and $\eta = -b$ will, of course, be different.

As explained earlier this discontinuity in the potential is due to the pressure in the cushion and may therefore be assumed to be of $0(\beta)$.

Now $\Psi(x, y, z)$ is an even function of y , i. e. $\Psi(\xi, \eta, \zeta)$ is an even function of η , so that

$$\Psi b_+ = \Psi\text{-}b_-$$

and

$$\Psi_{b_-} = \Psi_{-b_+}$$

The "jumps" in the potentials from the IFS to the EFS across the hulls

$$\left[\Psi\right]_b = \Psi_{b_-} - \Psi_{b_+}$$

and

$$\left[\Psi\right]_{-b} = \Psi_{-b_+} - \Psi_{-b_-}$$

will therefore be the same at corresponding points (ξ', ζ') on the longitudinal planes.

The terms involving the delta-functions will therefore cancel with each other, but such a cancellation will not be possible in the case of the "jump" terms as the value of $\frac{\partial G}{\partial \eta}$ will be different on the two longitudinal planes $\eta = \pm b$, so that

$$\iint_{S_1+S_2} \Psi \frac{\partial G}{\partial n}\, dS = \iint_{S_{1o}} \left[\Psi_{b-} - \Psi_{b+}\right] \left[\left.\frac{\partial G\,(x, y, z; \xi, \eta, \zeta)}{\partial \eta}\right|_{\eta = b} - \left.\frac{\partial G\,(x, y, z; \xi, \eta, \zeta)}{\partial \eta}\right|_{\eta = -b}\right] d\xi' d\zeta' \qquad \text{(V. 15)}$$

where the integration is now reduced to one side of the longitudinal plane of S_1, which is geometrically similar to that of S_2 .

The domain of integration is given in the body-fixed system. The Green's function, however, is given in the moving system, but can be expressed on the longitudinal planes in the (x', y', z') system by a Taylor series

$$G(x, y, z, \xi, \eta, \zeta) = G(x, y, z; \xi', b, \zeta') + (\xi - \xi') \left.\frac{\partial G}{\partial \xi}\right|_{(\xi', b, \zeta')} +$$

$$+ (\eta - b) \left.\frac{\partial G}{\partial \eta}\right|_{(\xi', b, \zeta')} + (\zeta - \zeta') \left.\frac{\partial G}{\partial \zeta}\right|_{(\xi', b, \zeta')}$$

It is assumed that this expansion is permissible even for the singular part of G. A similar expansion has been carried out for the potential in Appendix III for the evaluation of the pressure in the (x', y', z') system. As the potential is expressed in terms of G, this implied an expansion of G. It may be hoped that the singular terms arising from the two expansions will either cancel with each other or become of a higher order than that we are concerned with at the moment.

Now,

$$\xi - \xi' = \bar{x} + (\zeta' + h_G)\,\theta + O(\theta^2)$$

$$\eta - \eta' = \delta h_1 \quad (\xi', \zeta') \quad \text{in the case of } S_1$$

and

$$\zeta - \zeta' = \bar{z} - \xi'\theta + O(\theta^2)$$

and as $\frac{\partial G}{\partial \eta}$ has Ψ as a factor and we are only concerned with potentials of $(\delta, \beta, \delta\alpha, \beta\alpha)$ we may use only the $0(\alpha)$ term in the expansion for G

$$G(x, y, z; \xi, \eta, \zeta) = G(x, y, z; \xi', b, \zeta') + \alpha e^{i\sigma t} \left[r_{001} \frac{\partial G}{\partial \xi'} + r'_{001} \left.\frac{\partial G}{\partial \zeta'}\right|_{\eta' = b} \right]$$

so that

$$G_\eta(x, y, z; \xi, \eta, \zeta) = G_\eta(x, y, z; \xi', b, \zeta') +$$

$$+ \alpha e^{i\sigma t} \left[r_{001} \left.\frac{\partial^2 G}{\partial \xi' \partial \eta'}\right|_{\eta' = b} + \left.\frac{\partial^2 G}{\partial \eta' \partial \zeta'}\right|_{\eta' = b} \right.$$

where we have written

$$\frac{\partial G}{\partial \xi} = \frac{\partial G}{\partial \xi'}$$

and

$$\frac{\partial G}{\partial \zeta} = \frac{\partial G}{\partial \zeta'}$$

when terms of a higher order are neglected and , of course,

$$\frac{\partial G}{\partial \eta} = \frac{\partial G}{\partial \eta'}$$

A similar result will hold for S_2 with $(\xi', -b, \zeta')$ as the argument of the Green's function.

We therefore have

$$\iint_{S_1+S_2} \Psi \frac{\partial G}{\partial n} dS = \iint_{S_{1_0}} \left[\Psi_{b-} - \Psi_{b+}\right] \left[\frac{\partial G(x, y, z; \xi', \eta, \zeta')}{\partial \eta'}\bigg|_{\eta'=b} - \frac{\partial G(x, y, z; \xi', \eta, \zeta')}{\partial \eta}\bigg|_{\eta'=-b}\right]$$

$$+ \alpha e^{i\sigma t} \left\{ r_{001} \left[\frac{\partial^2 G}{\partial \xi' \partial \eta'}\bigg|_{\eta'=b} - \frac{\partial^2 G}{\partial \xi' \partial \eta'}\bigg|_{\eta'=-b} \right] + \right.$$

$$\left. + r'_{001} \left[\frac{\partial^2 G}{\partial \eta' \partial \zeta'}\bigg|_{\eta'=b} - \frac{\partial^2 G}{\partial \eta' \partial \zeta'}\bigg|_{\eta'=-b} \right] \right\} \Bigg] \, d\xi' d\zeta' \qquad \text{(V. 16)}$$

we have finally to evaluate

$$\iint_{S_1+S_2} G \frac{\partial \Psi}{\partial n} \, dS$$

Now, $\frac{\partial \Psi}{\partial n}$ is given exactly by the linearized boundary condition (V. 8) on the hull

$$\frac{\partial \Psi}{\partial n} = \delta V \frac{\partial h_1}{\partial \xi'} + \delta\alpha \left\{ i\sigma \left(r_{001} \frac{\partial h_1}{\partial \xi'} + r'_{001} \frac{\partial h_1}{\partial \zeta'} \right) + V\theta_{001} \frac{\partial h_1}{\partial \zeta'} \right]$$

applicable to S_{1+} and S_{2-} with a similar expression for S_{1-} and S_{2+} where h_2 replaces h_1 . Inserting these expressions, using the expansion derived above for G and combining S_{1_0} and S_{2_0} we have

$$\iint_{S_1+S_2} G\frac{\partial \Psi}{\partial n}\,dS = \iint_{S_{1_o}} \Bigg[\delta V \frac{\partial h}{\partial \xi'}\left[G(x,y,z;\xi',b,\zeta') + G(x,y,z;\xi',-b,\zeta') \right] +$$

$$\delta\alpha \Bigg[\Bigg\{ i\sigma \left(r_{001}\frac{\partial h}{\partial \xi'} + r'_{001}\frac{\partial h}{\partial \zeta'} \right) + V\theta_{001}\frac{\partial h}{\partial \xi'} \Bigg\} \left[G_b + G_{-b} \right]$$

$$+ V\frac{\partial h}{\partial \zeta'} e^{i\sigma t} \Bigg\{ r_{001}\frac{\partial}{\partial \xi'}\left(G_b + G_{-b} \right) +$$

$$+ r'_{001}\frac{\partial}{\partial \zeta'}\left(G_b + G_{-b} \right) \Bigg\} \Bigg] \, d\xi'\, d\zeta' \qquad \text{(V. 17)}$$

We may now combine (V. 17) with (V. 16) noting that the integration is to be performed on the instantaneous position of one side of the longitudinal plane of one of the hulls. As the instantaneous position is unknown, we will reduce the integration to the known equilibrium position.

We may write as in Appendix III

$$S_{1_o} = \bar{S}_{1_o} + S'_{1_o}$$

where S_{1_o} is one side of the longitudinal plane immersed below the free surface $\zeta = 0$, $\bar{S}_{1_o}$ is the steady part of this plane below the load waterplane $\zeta' = 0$ and S'_{1_o} is the oscillating strip between $\zeta = 0$ and $\zeta' = 0$. From the discussion in Appendix III where we evaluated the pressure force and moment over the strip S'_{1_o}, the correction for the first term in the integrand of (V. 17) is an additional integral over the basic surface $\bar{S}_{1_o}$

$$\delta V \iint_{S'_{1_o}} \left[G_b + G_{-b} \right] \frac{\partial h}{\partial \xi'}\, d\xi' d\zeta' = \delta\alpha e^{i\sigma t} \iint_{\bar{S}_{1_o}} \Bigg[(\bar{z}_{001} - \xi'\theta_{001}) \Bigg\{ \frac{\partial h}{\partial \zeta'}\frac{\partial}{\partial \xi'}\left[G_b + G_{-b} \right]$$

$$- \frac{\partial h}{\partial \xi'}\frac{\partial}{\partial \zeta'}\left[G_b + G_{-b} \right] \Bigg\}$$

$$- \theta_{001} \cdot \frac{\partial h}{\partial \zeta'}\left[G_b + G_{-b} \right] \Bigg] d\xi' d\zeta'$$

We need not correct the second term in the integrand for the integral will be $0(\delta^2\alpha, \delta\beta\alpha, \delta\alpha^2)$.

A correction is similarly to be made for only the first term in the integral of (V. 16). This takes the form of a line integral

$$\alpha e^{i\sigma t}\int_{L}(\bar{z}_{001} - \xi'\theta_{001})\left[\Psi_b - \Psi_{b+}\right]_{\zeta'=o}\left[\frac{\partial G(x, y, z; \xi', \eta', 0)}{\partial \eta'}\Big|_{\eta'=b} - \frac{\partial G(x, y, z; \xi', \eta', 0)}{\partial \eta'}\Big|_{\eta'=b}\right] d\xi'$$

As we have defined Ψ as the time-independent part of Φ, we may suppress the factor $e^{i\sigma t}$ in (V. 16), (V. 17) and the correction terms. This factor arose from the expansion of the Green's function and in deriving the correction terms, but may be suppressed for the time being so long as it is understood that we use this factor always along with α when we derive the time-dependent potential Φ .

Combining (V. 16) with (V. 17) and taking into account the correction terms we have, after simplification

$$\begin{aligned}
\iint_{S_1+S_2}\left(G\frac{\partial \Psi}{\partial n} - \Psi\frac{\partial G}{\partial n}\right) dS = {} & \iint_{\xi_1 o}\delta V\frac{\partial h}{\partial \xi'}\left[G(x, y, z; \xi', b, \zeta') + G(x, y, z; \xi', -b, \zeta')\right] \\
& + \delta\alpha\left\{\left(r_{001}\frac{\partial h}{\partial \xi'} + r'_{001}\frac{\partial h}{\partial \zeta'}\right)\left(i\sigma + V\frac{\partial}{\partial \xi'}\right)\left(G_b + G_{-b}\right)\right\} - \\
& - \left[\Psi_b\right]\left[\frac{\partial G}{\partial \eta'}\Big|_{\eta'=b} - \frac{\partial G}{\partial \eta'}\Big|_{\eta'=-b}\right] + \\
& + \alpha\left\{r_{001}\left(\frac{\partial^2 G}{\partial \xi' \partial \eta'}\Big|_{\eta'=b} - \frac{\partial^2 G}{\partial \xi' \partial \eta'}\Big|_{\eta'=-b}\right) + \right. \\
& \left. + r'_{001}\left(\frac{\partial^2 G}{\partial \eta' \partial \zeta'}\Big|_{\eta'=b} - \frac{\partial^2 G}{\partial \eta' \partial \zeta'}\Big|_{\eta'=-b}\right)\right] d\xi' d\zeta' - \\
& - \alpha\int_{L} r'_{001}\left[\Psi\right]_{\substack{\eta'=b \\ \zeta'=o}}\left[\frac{\partial G(x, y, z; \xi', \eta', o)}{\partial \eta'}\Big|_{\eta'=b} - \frac{\partial G(x, y, z; \xi', \eta', o)}{\partial \eta'}\Big|_{\eta'=-b}\right] d\eta'
\end{aligned} \tag{V. 18}$$

We may now use (V. 18) in (V. 14) to derive an integral representation for Ψ , but before doing so the integrand in the integral over $\bar{S}_o$ in (V. 14) will be re-written by using the expansion for p_s .

$$p_s(\xi,\eta) = \beta p_o(\xi,\eta) + \beta\alpha e^{i\sigma t}(\bar{x}_{001} + h_G\theta_{001})\, p_{o_\xi}$$

i. e.

$$V\bar{p}_{s_\xi} - i\sigma\bar{p}_s = \beta V p_{o_\xi} + \beta\alpha(\bar{x}_{001} + h_G\theta_{001})(V p_{o_{\xi\xi}} - i\sigma p_{o_\xi})$$

so that the integral over $\bar{S}_o$ becomes

$$\iint_{S_o}\left[\beta V p_{o_\xi} G + \beta\alpha(\bar{x}_{001} + h_G\theta_{001})\left\{2V p_{o_{\xi\xi}} G + p_{o_\xi}(V\frac{\partial}{\partial\xi} - i\sigma)G\right\}\right] d\xi\, d\eta$$

We therefore have finally,

$$\begin{aligned}
\Psi(x,y,z) = {} & \frac{1}{4\pi}\iint_{S_{1_o}}\left[\delta V\frac{\partial h}{\partial\xi'}\left[G(x,y,z;\xi',b,\zeta') + G(x,y,z;\xi',-b,\zeta')\right] + \right. \\
& \left. + \delta\alpha\left\{(r_{001}\frac{\partial h}{\partial\xi'} + r'_{001}\frac{\partial h}{\partial\zeta'})(i\sigma + V\frac{\partial}{\partial\xi'})(G_b + G_{-b})\right\}\right] d\xi' d\zeta' \\
& - \frac{1}{4\pi}\iint_{S_{1_o}}\left[\Psi\right]_b\left[\frac{\partial G}{\partial\eta'}\Big|_b - \frac{\partial G}{\partial\eta'}\Big|_{-b} + \alpha\left\{r_{001}\left(\frac{\partial^2 G}{\partial\xi'\partial\eta'}\Big|_b - \frac{\partial^2 G}{\partial\xi'\partial\eta'}\Big|_{-b}\right)\right.\right. \\
& \left.\left. + r'_{001}\left(\frac{\partial^2 G}{\partial\eta'\partial\zeta'}\Big|_b - \frac{\partial^2 G}{\partial\eta'\partial\zeta'}\Big|_{-b}\right)\right\}\right] d\xi' d\zeta' - \\
& - -\frac{\alpha}{4\pi}\int_L r'_{001}\left[\Psi\right]_{\substack{\eta'=b\\ \zeta'=o}}\left[\frac{\partial G(x,y,z;\xi',\eta',o)}{\partial\eta'}\Big|_{\eta'=b} - \frac{\partial G(x,y,z;\xi',\eta',o)}{\partial\eta'}\Big|_{\eta'=-b}\right] d\xi' \\
& + \frac{1}{4\pi\rho g}\iint_{S_o}\left[\beta V p_{o_\xi} G + \beta\alpha(\bar{x}_{001} + h_G\theta_{001})\right. \\
& \left.\left\{2V p_{o_{\xi\xi}} G + p_{o_\xi}(V\frac{\partial}{\partial\xi} - i\sigma)G\right\}\right] d\xi\, d\eta +
\end{aligned}$$

$$+\frac{V^2}{4\pi g}\oint_{L_{B+L_S}}\left[[\Psi]\ G_\xi - G\,[\Psi_\xi] + \frac{2i\sigma}{V}[\Psi]G\right]\ d\eta \qquad (V.19)$$

The potentials of various orders may now readily be written down by equating terms of the same order on both sides of (V. 19) with the assumption that the "jumps" in the potential relate only to the cushion and not to the side hulls. This has been discussed above.

We thus derive the following expressions for the potentials :

$$0(\delta)\Phi_{1000}(x,y,z) = \frac{V}{4\pi}\iint_{\xi_{1o}}\frac{\partial h}{\partial \xi'}\left[G(x,y,z;\xi',b,\zeta') + G(x,y,z;\xi',-b,\zeta')\right]\ d\xi'\,d\zeta'$$

$$0(\delta\alpha)\Phi_{1010}(x,y,z) = \frac{1}{4\pi}\iint_{\xi_{1o}}\left\{\left(\bar{x}_{001} + (\zeta'+h_G)\,\theta_{001}\right)\frac{\partial h}{\partial \xi'} + \right.$$

$$\left. + (\bar{z}_{001} - \xi'\theta_{001})\frac{\partial h}{\partial \zeta'}\right\}\left[i\sigma + V\frac{\partial}{\partial \xi'}\right]\left[G_b + G_{-b}\right]\ d\xi'\,d\zeta'$$

$$0(\beta)\Phi_{0100}(x,y,z) = \frac{V}{4\pi\rho g}\iint_{\xi_o} p_{o_\xi}\ G(x,y,z;\xi,\eta,o)\ d\xi\,d\eta +$$

$$+\frac{V^2}{4\pi g}\oint_{L_{B+L_S}}\left[\Phi_{0100}(\xi,\eta,o)\right]\ G_\xi(x,y,z;\xi,\eta,o) -$$

$$-\left[\frac{\partial}{\partial \xi}\Phi_{0100}(\xi,\eta,o)\right]G(x,y,z;\xi,\eta,o)\ d\eta -$$

$$-\frac{1}{4\pi}\iint_{\xi_{1o}}\left[\Phi_{0100}(\xi,b-,\zeta') - \Phi_{0100}(\xi',b+,\zeta')\right]$$

$$\left[\frac{\partial G(x,y,z;\xi',\eta',\zeta')}{\partial \eta'}\Big|_{\eta'=b} - \frac{\partial G(x,y,z;\xi',\eta',\zeta')}{\partial \eta}\Big|_{\eta'=-b}\right]\ d\xi'\,d\zeta'$$

$$0(\beta\alpha)\Phi_{0110}(x,y,z) = \frac{(\bar{x}_{001} + h_G\theta_{001})}{4\pi\rho g}\iint_{\xi_o}\left[(2Vp_{o_{\xi\xi}} - i\sigma p_{o_\xi})G(x,y,z;\xi,\eta,o)\right.$$

$$\left. + Vp_{o_\xi}\ G_\xi(x,y,z;\xi,\eta,o)\right]\ d\xi\,d\eta$$

$$+\frac{V^2}{4\pi g}\oint_{L_B+L_S}\left[\left[\Phi_{0110}(\xi,\eta,o)\right]\left[G_\xi(x,y,z;\xi,\eta,o)+\right.\right.$$

$$\left.\left.+\frac{2i\sigma}{V}\,G(x,y,z;\xi,\eta,o)\right]-\right.$$

$$-\left[\frac{\partial}{\partial\xi}\Phi_{0110}(\xi,\eta,o)\right]\,G(x,y,z;\xi,\eta,o)\Big]\,d\eta-$$

$$-\frac{1}{4\pi}\iint_{\bar{S}_{1_o}}\left[\left\{\Phi_{0100}(\xi',b-,\zeta')-\Phi_{0100}(\xi',b+,\zeta')\right\}\right.$$

$$\left\{(\bar{x}_{001}+(\zeta'+h_G)\theta_{001})\left(\frac{\partial^2 G(x,y,z;\xi',\eta',\zeta')}{\partial\xi'\partial\eta'}\Big|_{\eta'=b}\right.\right.-$$

$$\left.-\frac{\partial^2 G(x,y,z;\xi',\eta',\zeta')}{\partial\xi'\partial\eta'}\Big|_{\eta'=-b}\right)+(\bar{z}_{001}-\xi'\theta_{001})$$

$$\left(\frac{\partial^2 G(x',y,z;\xi',\eta',\zeta')}{\partial\eta'\partial\zeta'}\Big|_{\eta'=b}-\frac{\partial^2 G(x,y,z;\xi',\eta',\zeta')}{\partial\eta'\partial\zeta'}\Big|_{\eta'=-b}\right)\Big\}+$$

$$+\left\{\Phi_{0110}(\xi',b-,\zeta')-\Phi_{0110}(\xi',b+,\zeta')\right\}$$

$$\left.\left\{\frac{\partial G(x,y,z;\xi',\eta',\zeta')}{\partial\eta'}\Big|_{\eta'=b}-\frac{\partial G(x,y,z;\xi',\eta',\zeta')}{\partial\eta'}\Big|_{\eta'=-b}\right\}\right]d\xi'\,d\zeta'-$$

$$-\frac{1}{4\pi}\int_L(\bar{z}_{001}-\xi'\theta_{001})\left[\Phi_{0100}(\xi',b-,o)-\right.$$

$$\left.-\Phi_{0100}(\xi',b+,o)\right]\left[\frac{\partial G(x,y,z;\xi',\eta',o)}{\partial\eta'}\Big|_{\eta'=b}-\right.$$

$$- \left. \frac{\partial G(x, y, z; \xi', \eta', o)}{\partial \eta'} \right|_{\eta' = -b} \Bigg] d\xi' \qquad (V.20)$$

It will be observed that we have derived an integral representation for the hull potentials in the form of a source singularity distribution over the two longitudinal planes of strength equal to the normal velocity in the case of steady motion (the classical Michell potential) and a source distribution of density equal to the normal oscillating velocity together with a distribution of doublets oriented longitudinally and of strength equal to the product of the normal oscillating displacement and the forward velocity.

In the case of the air cushion, we have derived integral equations for the potentials and an explicit integral representation is only possible under some additional assumptions.

During steady motion there is a primary distribution of sources over the steady position of the lower boundary of the cushion with a strength equal to the longitudinal gradient of the basic pressure distribution with an additional line distribution of sources, doublets and quadrupoles along the bow and the stern, the strength being equal respectively to the "jump" in the longitudinal velocity of the water particles and the "jump" in the potential itself. As these jumps are caused by the discontinuity in the pressure it may be assumed that the line distribution will vanish if the cushion pressure is such that it is diffused to a zero value at the boundary and with a zero value of the longitudinal gradient there. In addition, there is a distribution of doublets oriented laterally over the longitudinal planes of the side hulls of strength equal to the jump in the potential across the planes. The oscillatory potential is given by a similar distribution of sources and doublets over the IFS, along the boundaries of the cushion, over the longitudinal planes, and along the waterline.

These potentials are discussed in further detail in Sections 6 and 7.

The Interference Potention Φ_{1100}

The derivation of the interference potential Φ_{110} is slightly more involved as all terms of $0(\delta\beta)$ have now to be taken into account. The method depends upon finding first a particular solution of Laplace's equation satisfying the inhomogeneous equation represented by the boundary condition (V. 3). The homogeneous function denoting the difference between the actual potential Φ_{1100} and this

particular solution will then satisfy the homogeneous form of (V. 3) and can be solved in the same manner as Φ_{1000} or Φ_{0100} .

The Green's Function.

The potential of a source of maximum unit strength and pulsating with frequency σ while moving with uniform velocity V along the x-axis at a depth ζ below the undisturbed water surface satisfies the conditions stipulated for the Green's function in connection with this problem. This function is given in different forms by various authors, but we shall use the representation derived by Peters and Stoker [2] .

$$G(x,y,z;\xi,\eta,\zeta) = \left[(x-\xi)^2 + (y-\eta)^2 + (z-\zeta)^2\right]^{-1/2} -$$

$$- \left[(x-\xi)^2 + (y-\eta)^2 + (z+\zeta)^2\right]^{-1/2} +$$

$$+\frac{2g}{\pi}\int_0^{\gamma}\int_0^{\infty} \frac{pe^{-p(z+\zeta)+ip(x-\xi)\cos\theta}\cos p(y-\eta)\sin\theta}{gp-(\sigma+pV\cos\theta)^2}\,dp\,d\theta +$$

$$+\frac{2g}{\pi}\int_{\gamma}^{\pi/2}\int_{M_1} \frac{pe^{-p(z+\zeta)+ip(x-\xi)\cos\theta}\cos p(y-\eta)\sin\theta}{gp-(\sigma+pV\cos\theta)^2}\,dp\,d\theta$$

$$+\frac{2g}{\pi}\int_{\pi/2}^{\pi}\int_{M_2} \frac{pe^{-p(z+\zeta)+ip(x-\xi)\cos\theta}\cos p(y-\eta)\sin\theta}{gp-(\sigma+pV\cos\theta)^2}\,dp\,d\theta$$

where

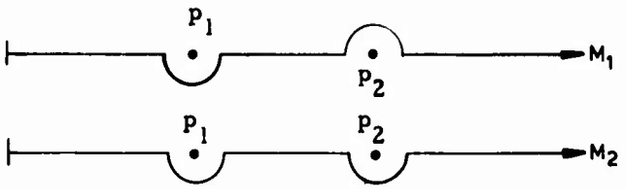
$$\gamma = \begin{cases} 0 & \text{if } 1 < g/4\sigma V \\ \arccos g/4\sigma V & \text{if } g/4\sigma V \leq 1 \end{cases}$$

p_1, p_2 are the real zeros of the denominator in the integrand

$$\begin{Bmatrix} \sqrt{p_1} \\ \sqrt{p_2} \end{Bmatrix} = \frac{\sqrt{g} \pm \sqrt{g - 4\sigma V \cos\theta}}{2V \cos\theta} \quad \text{when } \gamma \leq \theta < \pi/2$$

$$\begin{Bmatrix} \sqrt{p_1} \\ \sqrt{p_2} \end{Bmatrix} \frac{\mp \sqrt{g} - \sqrt{g - 4\sigma V \cos\theta}}{2V \cos\theta} \quad \text{when} \quad \pi/2 < \theta < \pi$$

and M_1 and M_2 are the contours of integration in the complex p-plane



(V.21)

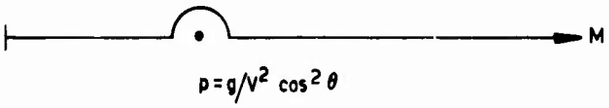
In the case of the steady potentials Φ_{1000} and Φ_{0100} we may use the steady Green's function $\bar{G}$ obtained by setting $\sigma = 0$ above, i.e.

$$\bar{G}(x, y, z; \xi, \eta, \zeta) = \left[(x - \xi)^2 + (y - \eta)^2 + (z - \zeta)^2\right]^{-1/2} -$$

$$- \left[(x - \xi)^2 + (y - \eta)^2 + (z + \zeta)^2\right]^{-1/2} +$$

$$+ \frac{4g}{\pi} \operatorname{Re} \int_0^{\pi/2} \int_M \frac{e^{-p(z+\zeta) + ip(x-\xi)\cos\theta} \cos p(y-\eta)\sin\theta}{g - pV^2\cos^2\theta} \, dp\, d\theta$$

where M is now the contour of integration



(V.22)

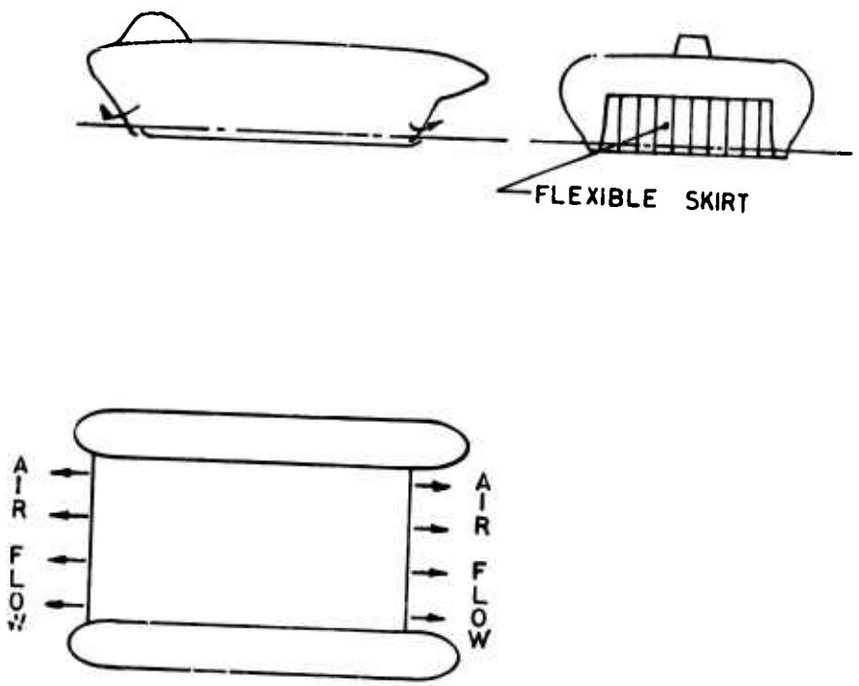


Fig. 1 Sidewall ACV configuration

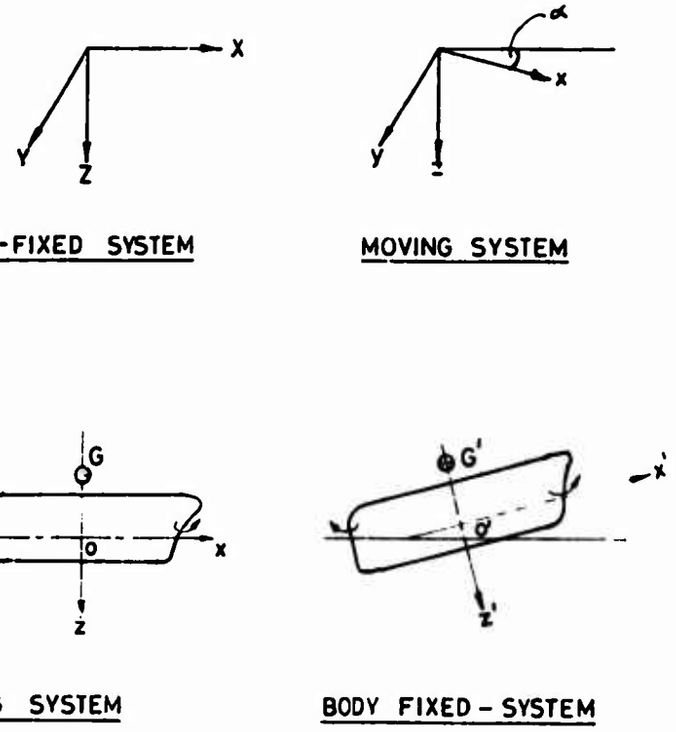


Fig. 2 Co-ordinate systems

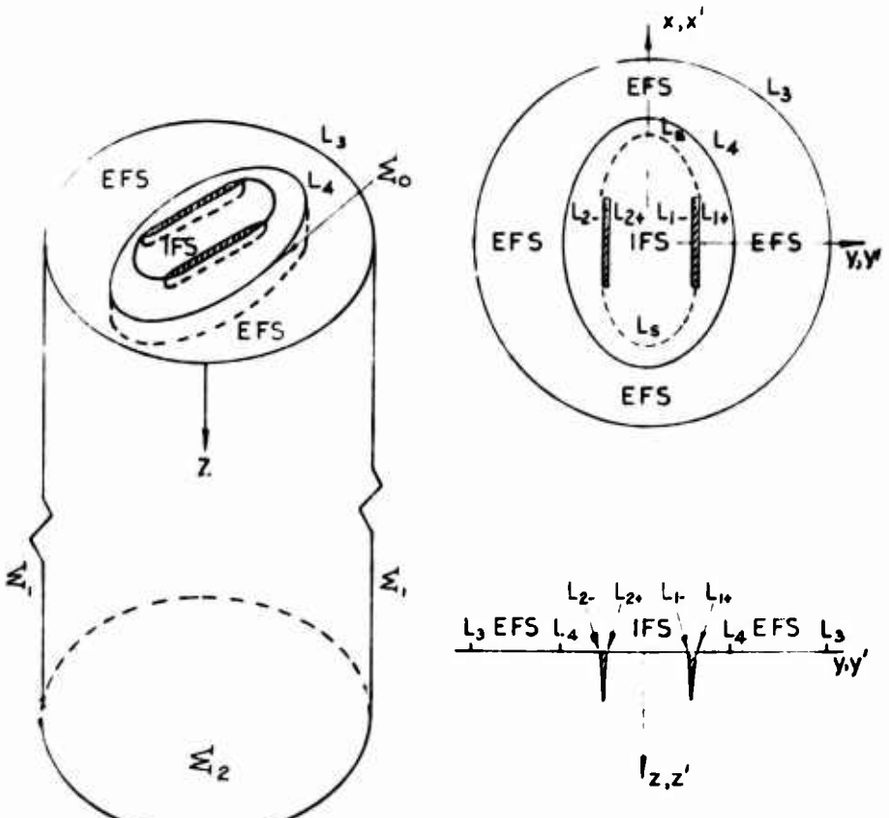


Fig.3 Domain of integration in Green's theorem

NOMENCLATURE

ACV	air cushion vehicle.
EFS	external free-surface - free surface of water of infinite extent outside the immersed part of the side hulls and the vertical projection of the flexible extensions at the front and rear of the air cushion.
IFS	internal free surface - free surface of water contained between the inner sides of the immersed part of the side hulls and the vertical projection of the flexible extensions at the front and rear of the air cushion.
A	total waterplane area of the two side hulls at zero speed ahead.
a_w	amplitude of the regular incident waves.
b	one half of the separation between the two side hulls.
$\vec{F}$	external force vector acting at the C. G. of the ACV.
$\vec{F}_P$	pressure force vector.
$\vec{F}_{P_C}$	pressure force vector (cushion hull).
$\vec{F}_{P_H}$	pressure force vector (side hulls).
$\vec{F}_R$	rigid body force vector.
$\vec{F}_S$	side force on an amphibious ACV in drifting motion.
f_1	pitch stiffness function of the air cushion.
f_2	heave stiffness function of the air cushion.
$\overline{G}$	steady Green's function.
G	unsteady Green's function.
G	equilibrium position of C. G. during steady translation.
G'	instantaneous position of C. G. during oscillations.
g	acceleration due to gravity.
H	hull function in (x, y, z) system.
h	total width of side hulls at (x', z')
h_1, h_2	hull function in (x', y', z') system on the starboard/port side of S_1 and port/starboard side of S_2 .

h_G height of C. G. above undisturbed water surface at zero speed ahead.

h_T height of the thrust line above C. G

I moment of inertia of ACV about lateral axis through C. G ($= I_{y'y'} + m\, h_G^2$)

I_A moment of inertia of waterplane area of both side hulls about lateral axis through the origin o' .

$I_{y'y'}$ moment of inertia of ACV about lateral axis through o' .

$\hat{i}, \hat{j}, \hat{k}$ unit vectors along axis in (x, y, z) - system .

$\hat{i}', \hat{j}', \hat{k}'$ unit vectors along axes in (x', y', z') - system.

k, l, m, n as superscripts refer to the powers of perturbation parameters in perturbation expansions.
as subscripts refer to the component terms of the perturbation expansions.

k wave number of incident wave ($= \sigma^2/g$).

k_o related to speed of translation ($= g/V^2$).

L, M, N, components of moment vector.

L load waterline on the longitudinal planes of the side hulls.

L_B vertical projection of hemline of the flexible extension at the front of the cushion on the plane $z = 0$.

L_C lower boundary of air cushion on the undisturbed water surface.

L_H boundary of ACV on undisturbed water surface.

L_S vertical projection of the hemline of the flexible extension at the rear of the cushion on the plane $z = 0$.

L_1, L_2, L_3, L_4 as defined in Appendix V.

$\vec{M}$ moment vector.

$\vec{M}_P$ pressure moment vector.

$\vec{M}_{P_C}$ pressure moment vector (cushion hull).

$\vec{M}_{P_H}$ pressure moment vector (side hulls).

$\vec{M}_R$ rigid body moment vector.

m total mass of ACV.

m_1 partial mass of ACV supported by air cushion.

m_2 partial mass of ACV supported by the buoyancy of the side hulls.

$\hat{n}$ unit normal vector.

0 origin of co-ordinate system fixed in space.

o origin of co-ordinate system translating in space with uniform speed V in a straight line.

o' origin of co-ordinate system fixed in the ACV.

p variable of integration.

p, p_c cushion pressure (excess over ambient).

$p_o(x, y)$ basic hull form of the air cushion.

p_s surface pressure on IFS.

$\bar{p}_s$ time-independent part of p_s

R_W wave resistance

r distance between (x, y, z) and (ξ, η, ζ).

$\vec{r}$ position vector of element of mass of ACV or element of area of IFS with o' as origin.

r_{klm} coupled displacement parameter $= \bar{x}_{klm} + (z' + h_G)\,\theta_{klm}$

$\bar{r}_{klm}$ coupled displacement parameter $= \bar{x}_{klm} + h_G\,\theta_{klm}$

S, S_o surfaces of integration.

S instantaneous position of IFS during oscillations.

S_o instantaneous position of the part of the plane $z = 0$ contained within IFS.

$\bar{S}_o$ steady position of S_o.

S'_o oscillating strip denoting the difference between S_o and $\bar{S}_o$

S_1 starboard hull.

S_2 port hull.

S_{1+}, S_{1-} starboard/port side of starboard hull.

S_{2+}, S_{2-} starboard/port side of port hull.

S_{1_o}, S_{2_o} longitudinal planes of S_1, S_2 in their instantaneous position.

$S_{1_o}^{\pm}$ $S_{2_o}^{\pm}$ starboard/port side of S_{1_o} , S_{2_o}

$\bar{S}_{1_o}$ $\bar{S}_{2_o}$ steady positions of S_{1_o} , S_{2_o} below the load waterplane $z' = 0$

S_{1_o}' S_{2_o}' strip of the longitudinal planes between $z' = 0$ and $z = 0$.

S_{1_o}'' S_{2_o}'' strip of the longitudinal planes between $z = 0$ and $z = \zeta$

s_{klm} coupled stiffness function = $f_{1_x}\ \theta_{klm} + f_{2_x}\ \bar{z}_{klm}$

T forward thrust of ACV propulsion system.

t time

$\vec{U}$ absolute velocity of element of mass of ACV

V mean forward speed of ACV.

X, Y, Z rectangular co-ordinate system fixed in space.

X, Y, Z components of force vector.

X_P, Y_P, Z_P components of pressure for e vector.

X_{p_c} , Y_{p_c} , Z_{p_c} components of pressure force vector (cushion hull).

X_{p_h} , Y_{p_h} , Z_{p_h} components of pressure force vector (side hulls).

X_R, Y_R, Z_R components of rigid body force vector.

x, y, z rectangular co-ordinate system translating in space with uniform velocity V .

x', y', z' rectangular co-ordinate system fixed in the ACV.

$\bar{x}$ surge displacement.

$\bar{z}$ heave displacement.

x_A x-coordinate of C. G. of waterplane area of the side hulls.

x_B, z_B x, z-coordinates of the centre of buoyancy of the side hulls.

x_p x-coordinate of the centre of pressure of the air cushion.

α motion perturbation parameter denoting the small order of the amplitude of the motions due to forced oscillation or due to wave excitation.

β cushion pressure perturbation parameter denoting the small order of the cushion pressure.

γ the phase angle of the incident waves.

δ side hulls perturbation parameter denoting the small order of the semi-width of the side hulls on either side of the longitudinal plane.

ϵ incident wave perturbation parameter denoting the small order of the wave slope (ratio of the amplitude to the length of the wave).

ξ, η, ζ dummy co-ordinate system having the same disposition as the (x, y, z) system -source point co-ordinates.

θ angular co-ordinate ; variable of integration.

θ pitch displacement.

λ wave length of the incident wave.

ρ fluid density.

$\sum$ control surface (comprising $\sum_0$ $\sum_1$ $\sum_2$ and $\sum_3$) $\sum_0 \sum_1 \sum_2 \sum_3$ as defined in Appendix V.

σ frequency of incident wave relative to space.

σ_e encountered frequency of incident wave ($= \sigma + kV$)

Φ velocity potential of water in frame of reference fixed in space.

Φ velocity potential of water in frame of reference moving in space with velocity V .

Ψ time-independent part of velocity potential.

ζ elevation of water surface.

ω angular velocity of ACV about a vertical axis.

A dot denotes differentiation with respect to time.

Derivatives are noted by subscripts when not written in explicit form.

Special Note.

In the case of terms containing $e^{i\sigma t}$ as a factor, it is naturally understood that the real part of the complex quantity is to be taken. This exponential factor denoting harmonic variation with respect to time occurs both in the case of the oscillatory displacements and in the case of the unsteady potential. When a factor of

$e^{2i\sigma t}$ is given it is implied that a factor of $e^{i\sigma t}$ should be taken with the displacements and a similar factor with the potential. The real parts of each are separately taken and then combined together. This convention is specifically indicated by the asterisk.

* * *

DISCUSSION

Lawrence J. Doctors
University of New South Wales
Sydney, Australia

I find this paper very interesting, because the response of an aircushion vehicle to a seaway is an important factor in the operation of these craft. Violent motions are to be avoided from the points of view of both the passengers, and of the craft structure, i. e. safety. In addition, it is desirable to maintain a minimum operating speed, which is not always possible in waves of a large amplitude.

I would like to ask some questions about the analysis used by the author. Firstly, I can see no place in the paper, where the fan characteristics are involved. Surely, the interaction between fan pressure and volume flow would affect the dynamics of the craft. In other words, this is an additional parameter in the coupling between the motion of the ACV and the response of the water surface.

Secondly, one would expect the timewise varying air gap between the skirt hemline and the water to be an important factor. Has this in fact been considered, for the air gap affects the pressure drop under the skirt ?

I am also interested in the way the pitch stability of the amphibious craft is modelled. For example, does the author compartment the air cushion with a transverse skirt ? Incidentally, this would introduce a nonlinearity under certain conditions.

My final question is this : Has Dr. Murthy carried out any numerical calculations, or does he consider that computer time would be too excessive ?

* * *

REPLY TO DISCUSSION

T. K. S. Murthy
Portsmouth Polytechnic
Portsmouth, U.K.

Dr. Doctors is quite right. I missed mentioning these things in my hurried talk. I would refer you to page 167 where I have clearly stressed that we have gone into some detail to study the hydrodynamic, including hydrostatic, effects on the motions of the ACV. It is only a short paragraph and I will read it :

"It is assumed for this purpose that the aerodynamic effects are known including, in particular, the stiffness and damping of the peripheral-jet or plenum type of cushion. It may be thought that such effects as that due to "wave pumping" should have been taken into account..."

Of course, that includes the question of fan characteristics as well. These are assumed to be known and they can be fed into the equations. I am only assuming that the ACV is moving under the action of a constant thrust. I am assuming that the pressure distribution is known. The expressions involve the pitch and heave stiffness of the air cushion itself, which are assumed to be known ; they are the functions f_1 and f_2 given in the text of the paper, which take into account the air gap of the cushion and the stiffness and damping of the air cushion due to variations in the gap.

The third point is concerned with stability. In my work I am not concerned with the actual cushion ; I only want to know what the pressure distribution is. People think, rather naively, that the cushion is uniform. It is very easy to construct a uniform cushion within a rectangular boundary but one can see very easily that this type of cushion will be unsuitable for high speed motion because if you translate it into shipping terms a uniform rectangular cushion will have a hull form in the shape of a vertical cylinder with a vertical bow and stern, and no naval architect would use this type of hull form for a fast bearing planing vessel.

It is also made clear in the expressions that the distribution of pressure, particularly the diffusion of the pressure - what Dr. Doctors has been calling "smoothing" at the boundaries - is very

important as far as the motions are concerned. So one has to look a bit more deeply into the actual pressure distribution in the cushion and we can, it appears, have a tailormade cushion for each job we have in mind, whether we want a cargo ACV or a very fast ACV. It depends on the role the craft has to play and you can design a suitable distribution of pressure. As to how it is done, you can accentuate the entrance entrainment of the air from the atmosphere and produce a non-uniform cushion of a suitable shape for the role the vehicle has to play in actual operation.

The last point raised was whether a numerical computation was made. That was meant as my third apology when I started. No results are given here. The work was done purely as a private venture. It was not sponsored by any Government or any agency. Calculations involve the use of a computer, which costs money. But the expressions are available here and can be applied to any specific configuration, and quite realistic results can be obtained. I am also considering the feasibility of applying the finite element method which may be the only answer to problems of this kind, because some of these integral equations are singular and there may not be any easy way of solving them without the use of the FEM technique. This I am studying now. So, once again, I am sorry I have no results here because results cost money, but they can be obtained probably at some later stage.

DISCUSSION

Roger Brard

Bassin d'Essais des Carènes
Paris, France

You just said that you deal with singular equations. I suppose you mean equations whose kernel is singular ?

REPLY TO DISCUSSION

T.K.S. Murthy

Portsmouth Polytechnic
Portsmouth, U.K.

Yes.

DISCUSSION

Paul Kaplan
Oceanics Inc.
Plainview, New-York, U.S.A.

I certainly agree as regards the importance of pressure. This is a craft which by definition is an air-cushion vehicle with 90 to 100 per cent of its weight supported by air pressure. A deviation in the equilibrium pressure of 50 per cent, which could easily occur and could be computed for simple "wave pumping" by waves commensurate with the length of the craft (without such great height that would violate linearity) will show changes of pressure of the order of 50 per cent of the equilibrium pressure. Therefore accelerations of 1/2g immediately are possible. In order to account for this you do not just say that the equation contains a damping coefficient and stiffness coefficient that represent pressure effects. Pressure is a degree of freedom which must be added into any equation system. Therefore you have heave, pitch, surge, and pressure is also a state variable ; it couples with the others and it is the most important element. That introduces the fan as well as the Plenum geometry and the wave pumping. The end result of this is that if you neglect anything with the air pressure in the manner shown here, then motion responses are erroneous. I would suggest that this paper is very useful in many respects for determining hydrodynamic forces, but the title is somewhat erroneous. I would suggest it be changed somewhat and there it would still maintain utility. The paper should be called "A linearised potential flow theory for the hydrodynamic forces associated with the motions of air-cushion-vehicles in a sea-way".

Now here are some positive contributions to balance what I have said before. The aspect of linearity is important and the resulting ability to predict motions in irregular seas even more so. There has been published recently some results for motions in regular waves which include equations which also have this pressure degree of freedom. The agreement with experiments, while not perfect, is more than adequate. The predictions based on the application of spectral analysis to predict RNS values of accelerations in irregular seas agrees quite well also. Therefore, not only is there an aspect of utility of the theory for getting hydrodynamic forces ; there also is a virtue in linearity, so that is a benefit as well.

REPLY TO DISCUSSION

T. K. S. Murthy

Portsmouth Polytechnic
Portsmouth, U.K.

I quite agree with Dr. Kaplan. I have made it clear that I am only concerned with the hydrodynamic part of the study and I have put various riders in the results saying that these are only the hydrodynamic effects. These appear throughout the paper in various places. I have mentioned cushion pumping and cushion stiffness and compartmentation. These are naturally to be added to the results here. I agree with what Dr. Kaplan has said.

* * *

ON THE DETERMINATION OF AEROHYDRODYNAMIC PERFORMANCE OF AIR CUSHION VEHICLES

S.D. Prokhorov, V.N. Treshchevsky, L.D. Volkov
Kryloff Ship Research Institute
Leningrad, U.S.S.R.

ABSTRACT

Experimental and theoretical methods of determination of hydro-and-aerodynamical characteristics necessary for air cushion vehicles dynamic calculations are discussed. The influence of ship form on mentioned characteristics corresponding to steady and unsteady motion is analysed.

The estimation of propulsive performance and manoeuverability characteristics of ACVs while designing these vehicles can be based on tests carried out with self-propelled models and simulation of various operational conditions for these models. It is obvious that the model behaviour is governed in this case by the total aerohydrodynamic loads which are different in nature. At the same time separate definition of aero-and-hydrodynamic forces of various nature is of interest, specifically, for the analysis of the effect some components of these forces have upon the ACVs performance and dynamics.

The forces acting on ACVs can be classified into the following categories :
a) aerodynamic forces due to the oncoming flow around the hull, flexible skirt, stabilizing fins and controls;
b) aerodynamic forces due to the air cushion and interaction between the latter and counter air flow;
c) hydrodynamic forces due to the contact of the flexible skirt with water surface and interaction between the air cushion and water surface;
d) hydrodynamic forces due to the effect of waves.

The cruising conditions of ACVs are characterized by the active interaction of the structural elements with both water and air

Preceding page blank

environments. The difficulties in simulating the aerohydrodynamic effect and the necessity of analysing the data obtained make one carry out the experiments in the towing tanks and wind tunnels independently. In the last few years the central place in such experiments belonged to obtaining the steady and non-steady characteristics necessary for the calculation of transient processes and estimating the ACV seakeeping qualities.

This paper gives a brief description of the most typical, in the authors' opinion, methods of defining the above characteristics. The description of these methods is illustrated by the measurement results concerned with schematized models of ACV s with different bow form.

I. DEFINITION OF AERODYNAMIC CHARACTERISTICS

As is known, the character of ACV movement in the longitudinal plane depends mainly on the air cushion parameters and also on hydrodynamic interaction between the flexible skirt and water surface. The ACV movement in the horizontal plane depends, to a great extend, on aerodynamics of external flow around the vehicle

There are two main problems relating to the study of external flow around the ACV, viz., the decrease in air resistance and the achievement of predetermined maneuverability and stability. The first problem can be solved only on the basis of the rational choice of the hull form. The second one is usually solved by mounting the system of stabilizers. For the ACV s with the length-to-breadth ratio of 1.5 to 2.5 the resistance as well as side forces are determined by the distribution of normal pressure over the perimeter of the hull; so the studies of both problems are closely connected with each other.

The experimental investigation of the aerodynamic forces and moments which are due to the external flow is generally carried out on rigid models because slight deformations of the flexible skirt have little effect on its aerodynamic characteristics. A six-component balance is used for this purpose Water surface is simulated by a flat ground board.

The nature of aerodynamic factors can be revealed from the results of the experiment with schematized models carried out for the study of the effect the hull form has the ACV s aerodynamic characteristics. Table 1 lists the values of geometric characteristics of the models tested, their resitance factors and the derivatives of

side force and yawing moment with respect to the yaw angle β for $\beta = 0$ which are necessary for the calculation of ACV movement in the horizontal plane. The aerodynamic forces are related to the product of the velocity head q and centerplane area S, while the moment is related to qSL where L is the model length. The moment is calculated with respect to the middle of the hull length.

As is seen from the Table 1, the resistance is mainly influenced by the forebody form. With the change of relationship $\frac{LH}{L}$ from 0.5 to 2 the resistance factor decreases by 30-40 per cent. The influence of the stern form on the resistance is less important, which is due to separation effects and the formation of the dead zone at the stern. The angle of run ranging from $\frac{LK}{L} = 0$ to 2 leads to a decrease in resistance only by 10 per cent.

It is known that the heave stability of the ACV s mainly depends on the sign and value of the derivative m_y^{β}. The minimum value of the derivative m_y^{β} which is favourable from the viewpoint of stability of motion occurs for the models 7 and 8 with the smallest values of angles of run and entrance. As is seen from the Table, the bow elongation results in increasing the destabilizing moment m_y, so the requirements of minimum values for the coefficients of resistance and yawing moment are rather inconsistent. Since the required value of the derivative m_y^{β} can always be obtained due to the fitting of vertical stabilizers without noticeable increase in resistance, the hulls with elongated bows and blunt sterns appear to be the most advantageous.

For the approximate estimates of the ACV s aerodynamic characteristics at the initial stages of designing the theoretical methods are of interest. The method is developed for the calculation of both the total and distributed aerodynamic characteristics of ACV hulls with flat sterns at different yaw angles and angular velocity ω_y depending upon the forebody forms and paramenters $\frac{H}{L}$ and $\frac{B}{L}$.

The method is based on replacing the hull of the ACV by a vortex surface which extends beyond the hull for modelling the vortex trace effect (figure 1). The free water surface is simulated by an image body so that in fact consideration is given to a model with a double height H. The transverse vortices are directed parallel to the lines forming the flat stern contour. The longitudinal vortex which leaves the body from stern contour corners has the density equal to the difference between the densities of vertical and horizontal vortices replacing the contour. Longitudinal vortices arranged in the deck plane are parallel to the longitudinal axis of the hull. Calculations

were carried out for the finite number of discrete vortices spaced equally from the control points where the boundary condition is satisfied. The density of all vortices is defined from the system of equations characterizing the boundary condition on the body surface at control points. For the proper choice of the value of circulation around the body, as with the known Joukowski condition in the wing theory, a supplementary condition is introduced, viz. the density of the trace vortices in all the points of the vortex sheet is the same and equals to the density of the vortex shedding from the contour of separation at the stern. Then the system of equations for defining the densities $\Gamma_1, \Gamma_2, \Gamma_3 \ldots \Gamma_n$ takes the form :

$$\sum_{k=1}^{n} \Gamma_k \left[\sum_i Fi\,(Si, Sj) + \sum_p F_p\,(Sp, Sj) \right] = F\,(Sj, \beta, \omega_y) \qquad (1)$$

where F_i and F_p = induced velocities corresponding to transverse and longitudinal vortices,

F = normal component of the free stream velocity,

ω_y = angular velocity of yaw.

Figure 2 shows the pressure distribution over the contour of intersuction of the model and the basic plane obtained by the calculation method for model 2 with the angle $\beta = 10°$. The test results on defining the pressure distribution at the same section of the model are also plotted in the same figure. As is seen, there is a fairly good agreement between the theory and experiment.

As noted above, the aerohydrodynamic forces due to the air cushion are the decisive factors for the longitudinal motion of the ACV. One of the methods used for defining the steady and non-steady aerodynamic forces is based on the measurement of forces acting upon the model which performs the harmonic oscillations. When carrying out these tests in a wind tunnel the forces are evaluated which are connected with the qualities of an air cushion and deformation of flexible skirts above the ground board simulating the water surface. In some cases the results of such tests can be used, for the calculations of the ACV movement above the ice surface.

Non-steady aerodynamic characteristics of ACV models with built-in fans and flexible skirts are determined by using the experimental plant shown in figure 3. The principle of operation of this plant consists in generating the definite harmonic oscillations for the model and measuring the loads acting on this model with the consequent determination of the lift and lateral moment derivatives according to the kinematic parameters of motion. The plant is equipped

with a mechanism of compensating for the model inertia forces and with an electric harmonic analyzer for automatically defining and recording the signal constant components which are proportional to the required rotational and translational derivatives. The model is mounted upside-down (figure 3) on two supporting pillars which make reciprocating oscillations with arbitrary shift in phases with respect to each other. Each pillar is supplied with a strain gauge which serves as a connecting link between the model and the oscillating pillar.

The distances to the ground board h; the trim angle Ψ and their first-order and second-order time derivatives $\dot{h}, \dot{\psi}$, $\ddot{h}$, $\ddot{\psi}$ are adopted as kinematic parameters defining the model aerodynamic characteristics in the longitudinal plane. In linear approximation the expansion of the vertical force or longitudinal moment as a series in kinematic parameters has the form

$$R = R_o(h_o,\Psi_o) + R^{h}(h_o, \Psi_o) \cdot h + R^{\Psi}(h_o, \Psi_o)\Psi + R^{\dot{h}}(h_o,\Psi_o)\dot{h} \ldots$$
$$\ldots + R^{\dot{\Psi}}(h_o, \Psi_o)\dot{\Psi} + R^{\ddot{h}}(h_o, \Psi_o)\ddot{h} + R^{\ddot{\Psi}}(h_o, \Psi_o)\ddot{\Psi} \qquad (2)$$

where h_o Ψ_o are mean values of height and trim in respect of which the values h and ψ are changed.

The tests are carried out for two types of motion : translatory and angular harmonic oscillations of the model where, with the results of the model static tests also used, all the derivatives entering into equation (2) can be determined. The values of rotatory and translatory derivatives of the vertical force and the longitudinal moment are determined and they are transformed to a dimensionless form through dividing these by the model weight G or by the product GL.

$$C_y = \frac{y}{G} \qquad M_z = \frac{M_z}{GL} \qquad (3)$$

As the dimensionless kinematic parameters the following factors are used :

$$\bar{h} = \frac{h}{L}; \qquad \bar{\Psi} = \frac{\Psi^o}{57,3}; \qquad \bar{\dot{h}} = \frac{\dot{h}\cdot Q_o}{L^3 g}$$
$$\bar{\dot{\Psi}} = \frac{\dot{\Psi}\ Q_o}{L^2 g} \qquad \bar{\ddot{h}} = \frac{\ddot{h}\ Q^2_o}{L^5\ g^2} \qquad \bar{\ddot{\Psi}} = \frac{\ddot{\Psi}\ Q^2_o}{L^4\ g^2} \qquad (4)$$

where Q_o = air flow rate corresponding to the parameters

$$h_o, \qquad \psi_o \quad (m^3/sec)$$

g = acceleration of gravity (m/sec^2)

The value $Sh_* = \frac{\omega \cdot Q_o}{L^2 g}$ should be adopted as the dimensionless criterion of similarity which is similar to the known Strouhal number (ω = angular frequency of oscillations). Then the dimensionless values of parameters $\overline{h}$, $\overline{\psi}$, $\overline{\dot{h}}$, $\overline{\dot{\psi}}$ in equations (4) are the products of the dimensionless amplitude of vertical and angular oscillations and Strouhal number Sh_* or Sh_*^2.

Using the procedure described the tests were carried out for three schematized models of ACV s with built-in fans. The scheme of the sectional flexible skirt mounted on the models is shown in the sketch (figure 3). The geometric characteristics of models are given in Table 2. Figures 4-5 show some of the results obtained. The curves in figure 4 illustrate the character of changing the factors $C_y^{\dot{h}}$, $m_z^{\dot{h}}$, $m_z^{\dot{\psi}}$ versus the dimensionless parameter Sh_* at different values of pressure factor $K_p = \frac{P_p}{P_n}$ (P_p , P_n = pressures in the receiver and air-cushion, respectively) and air flow rate Q. It is typical that the external air velocity effect on the non-steady characteristics is practically absent in the range of the examined actual relationships of the contrary velocity head and the cushion pressure (Fig. 5). The curve in Figure 5 shows the influence of the bow form at the fixed values of frequency and pressure factor upon the same characteristics. It is obvious that the bow form influences mainly the moment characteristics.

The non-steady aerodynamic characteristics necessary for the study of the ACV maneuvering in the horizontal plane are also defined in the wind tunnel by the method of harmonic oscillations of the model around its vertical axis and measuring the yaw damping moment influencing the model. In this case the procedure of measurements is similar to that described above. The experiments show that the principal role in generating the damping moment belongs to the vertical stabilizers and the hull effect on this moment is not significant. It is observed that in some cases the damping moment on the hull-stabilizer system decreases due to the adverse effect of the hull on the stabilizers.

II . DETERMINATION OF HYDRODYNAMIC CHARACTERISTICS

In the towing tanks the tests are carried out to determine

the main hydrodynamic characteristics of ACV s. In this case the model is usually subjected to the action of both the hydro-and-aerodynamic forces. Then, depending on the test conditions, account is made of either the results directly obtained by measurements, or the aerodynamic components are to be excluded with the use of data on the blowings of the model in the wind tunnel.

The most typical tests carried out in the towing tanks are those with the towed models exhibiting the freedom of heaving and trim; during these tests the resistance and kinematic parameters are measured in the longitudinal plane in calm water and in waves. The purpose of such tests is not only in obtaining the propulsive performance data but it is largely connected with the evaluation of dynamic properties of these vehicles. Thus the measurements carried out at different positions of the centre of gravity along the model make it possible to plot the positional curves against the trim angle and to judge about the static stability depending upon the conditions of motion. The same type of towing tests is the basis for determining the regions of steady motion in the longitudinal plane defined by the influence of the waves and speed.

Such experiments were carried out specifically on a series of models with the particulars given in Table 2. In this case the resistance and kinematic parameters were changed up to the critical conditions preceding the development of plough-in. The curves in figure 6 show the effect of the bow planeform on the relative resistance $\frac{x}{G}$ depending upon the running trim angle which is defined by a given position of the center of gravity. It is seen from the curve plotted for a cruising regime that the effect in question is observed only with trim by the bow; in this case model N° 2 appears to be preferable. The advantages of a semi-round bow planeform manifest themselves in waves too, as is seen from the curve of figure 7 where the relative gain in resistance is presented for all three models in waves.

The air flow rate effect examined on model N° 2 is typical for this experiment. The curve in figure 8 shows the effect of the dimensionless factor of air rate upon the relative resistance in waves

$$\overline{Q} = \frac{Q}{Sn\sqrt{\frac{2\,Pn}{\rho}}}$$

where Q = air rate, m/sec;
Sn = area of the air cushion, m^2
Pn = pressure in the cushion, kg/m^2

It is seen that practically in all the cases the increase in the flow air rate results in a decrease of resistance; in this case the supply of air into the forward part of the air cushion, is the most favourable.

The curve of figure 9 serves as an example of plotting the regions of stable motion. The relationships shown are the result of processing the model N° 2 test data according to the evaluation of the limiting regimes when plough-in is developing with the consequent loss in stability. The curve shows the favourable influence of increase in the air flow rate at the bow centering, making it possible to delay the setting of the critical regimes.

The definition of the non-steady hydrodynamic characteristics which are necessary specifically for carrying out the calculations of ACV heaving and pitching is based on the same methods used in a similar case for displacement vessels. The linear character of the restoring forces $Y^h = \frac{\partial Y}{\partial h}$ and moments $M_z^{\Psi} = \frac{\partial M_z}{\partial \Psi}$ defined experimentally in the working range of the flying heights h and trim angle Ψ for ACV with a flexible skirt gives grounds as a first approximation to proceed from the linear theory premises while defining the non-steady characteristics. The tests are carried out on a plant which makes is possible to perform in calm water the forced heaving and pitching motions of the model; the plant is equipped with strain gauges and provides the recording of kinematics of motion. To define, for example, the coefficients of inertia and damping forces by the test results, the equation of the forced heaving motions is written in the following way :

$$(M + Y^{\ddot{h}})\,\ddot{y} + Y^{\dot{h}}\,\dot{y} + \frac{\partial Y}{\partial h}\,y = C\,(\tau \cos \sigma_k t - y),$$

where M = model mass,
C = rigidity of spring,
τ = amplitude of disturbances,
σ_k = frequency of disturbing force

Having experimentally defined the parameters of the forced motions of the model in the form

$$y = A_y e^{i(\sigma_k t - \delta_y)}$$

where A_y = amplitude of oscillations of the model centre of gravity,

δ_y = phase shift between the translation of the model and the disturbing force,

one can find the coefficients $Y^{\ddot{h}}$ and $Y^{\dot{h}}$ and similarly the moment coefficients characterizing the pure pitching motions $M_z^{\ddot{\psi}}$ and $M_z^{\dot{\psi}}$. The definition of factors characterizing the influence of pitching upon heaving is possible provided that the vertical translations of the center of gravity are recorded.

The experimental plant scheme and some of the results obtained are given in figures 10-11. Depending upon the type of rope-and-block connections provision is made for the translational vertical (var. 1) or angular (var. 2) motions of the model and for recording kinematic parameters on the oscillograph tape. In figure 11 the coefficients of inertia forces obtained by the above method are plotted against frequency.

It is necessary to note that the aerodynamic characteristics corresponding to flight over the water surface are different from similar characteristics of the model over the ground board. The difference is obviously due to the influence of the water surface deformations and mass forces; it minimizes as the Froude number increases.

The experimental plant described was also used for the definition of damping and inertia characteristics which manifest themselves at non-steady motion of the model along the longitudinal axis; the plant is switched on according to variant 3. As the test results show, the forces determining the above loads are negligible for ACV models.

In the cases when during the tests in a towing tank the aerodynamic components are so important (in comparison to hydrodynamic forces) that they cannot be neglected, it is necessary to consider that the aerodynamic effect upon the model tested is not fully simulated. This introduces some infinity in the results obtained due to both the distorbed aerodynamic action and the effect of this action upon the position of the freely towed model and consequently upon its hydrodynamic characteristics in the total forces and moments measured. In such cases the aerodynamic components are excluded from tests in the towing tank and are determined in a wind tunnel. The procedure of carrying out the experiments of such kind is as follows : the model is rigidly fastened to the dynamometer which measures the lift, drag and longitudinal moment of the model at the fixed values of height and trim of the model. During the tests the measurements are carried out in a prescribed regime. Then according to the same program the tests are conducted on a model equipped with a working fan over the ground board fixed under the model in a close vicinity to water

surface and transported together with the model. The aerodynamic forces to be excluded are determined as the difference between the results of the measurements carried out over the board both underway and at a speed equal to zero in flight.

The specific behaviour of the ACV with a flexible skirt makes difficult in some cases the use of traditional methods in calculating the maneuvering qualities, dynamic stability and so on in terms of the solution of equations of motion. The complexity and considerable amount of tests necessary for defining the coefficients of the equations makes one use other methods of study. The determination of transfer functions according to the required parameters in terms of the experimentally defined frequency characteristics is considered to be reasonable. These functions make it possible, as is known, to calculate normal maneuvers of the object according to linear theory. Besides it is important to have the possibility of directly evaluating the behaviour of models in certain conditions, specifically, in damage situations. The tests with the both aims in view are carried out on the experimental plant making it possible to simulate, in the main, the conditions of the model free movement and in some cases to eliminate the necessity of carrying out the expensive tests with self-propelled models.

The basic diagram of the plant is shown in figure 12. During the tests the model is towed along the towing tank; it displays five degrees of freedom, i. e. vertical emergence, side displacement, heeling, yawing and trimming angles; all the kinematic parameters are recorded. In case of side displacement the model is relieved of inertia and friction forces in movable units of the plant by means of a special servo-system. The significant element of the plant is the system bringing the towing force into coincidence with the model centre line irrespective of the position of model relative to the tank axis. Finally, in case it is difficult to arrange the drives of controls on the model, the electric systems are provided for the plant which are capable to imitate the action of the controls, particularly, side force controls, by prescribing the side force, yawing moment and heeling moment in accordance with the required law.

Some test data obtained on the plant described are given below. The studies were carried out on the ACV schematized model N° 2 for the purpose of evaluating its course stability (with vertical stabilizers mounted) and checking its other dynamic characteristics. Figure 13 shows the relationship between the amplitude frequency characteristic of the model for yawing angle at different speeds. It

is seen that with the increase in Froude number the response of the model increases up to the values Fr = 1.10. The same figure shows the variation of the relative amplitude of the model yawing angle at fixed frequency and speed as dependent on the pressure factor of the air cushion K_p.

Some damage situations with the same model were studied, particularly, the transition process at first instants after suddenly applying the yawing moment, which may be the consequence of a spontaneous reverse or failure of propellers at one side of the model. It is seen from figure 14 how kinematic parameters of motion are changing after the instantaneous application of the rolling moment (induced for example, by the breaking of the flexible skirt along the side) until the steps are taken to keep the ship in the upright position. This experimental plant makes it possible to simulate the maneuver of course-keeping in this condition by applying the counter yawing moment imitating the action of controls. It is typical for this case to set the model in a steady motion with a drift to the inclined side.

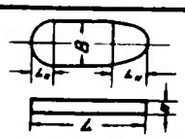
The condition that the towing carriage speed should always be constant makes it impossible to simulate to the full extent the full scale performance of the vehicle. However, this restriction is no barrier to solving a wide variety of practical problems; in this case the error is directed to the safe side.

* * *

Table 1

$\frac{L}{B} = 2.5$

$\frac{B}{H} = 2.4$



$\bar{V}$

Nos.	$\frac{L}{B}$	$\frac{L_н}{B}$	$\frac{L_к}{B}$	C_{x_1}	$C_{z_1}^{\beta}$	$m_{y_1}^{\beta}$
1	2,5	0,25	0	0,162	0,97	0,20
2	2,5	0,50	0	0,140	0,97	0,20
3	2,5	1,00	0	0,118	1,03	0,22
4	2,5	0,25	0,50	0,163	1,03	0,21
5	2,5	0,50	0,50	0,137	1,03	0,21
6	2,5	1,00	0,50	0,120	1,03	0,23
7	2,5	0,25	0,25	0,166	1,03	0,17
8	2,5	0,50	0,25	0,137	1,03	0,18
9	2,5	1,00	0,25	0,123	1,03	0,23
10	2,5	0,25	1,00	0,150	0,92	0,23
11	2,5	0,50	1,00	0,125	0,92	0,23
12	2,5	1,00	1,00	0,110	0,92	0,23
13	1,5	0,50	0	-	1,44	0,18
14	2,0	0,50	0	-	1,26	0,20
15	3,0	0,50	0	-	1,10	0,23

Table 2

Particulars	Designation	Model		
		No.1	No.2	No.3
Planeform of air cushion	———	elliptical 	round 	rectangular 
Length of the same	$L_{n,м}$	1,98	2,11	2,04
Breadth of the same	$B_{n,м}$	1,0	1,0	1,0
Area of the same	$S_{n,м}$	1,72	2,0	2,0
Coefficient of air cushion area	$\varphi = \frac{S_n}{L_n B_n}$	0,90	0,925	0,985

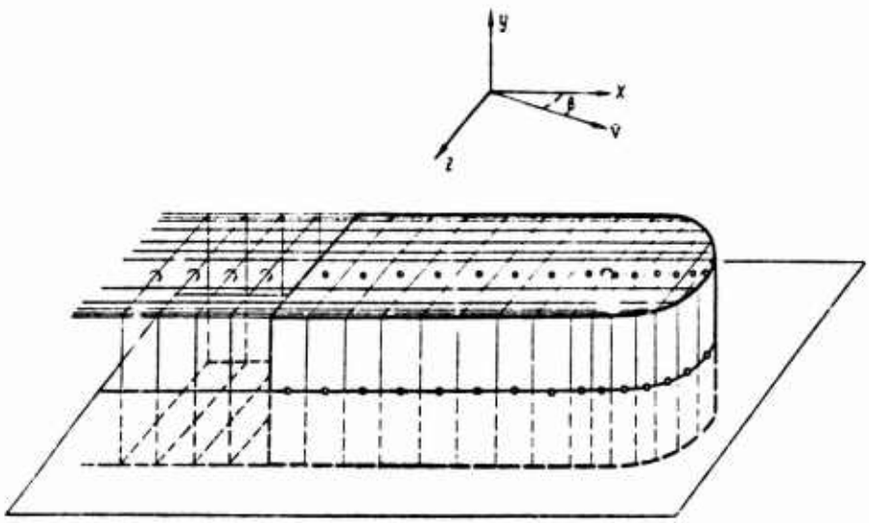


Figure 1 Vortex system of ACV's hull.

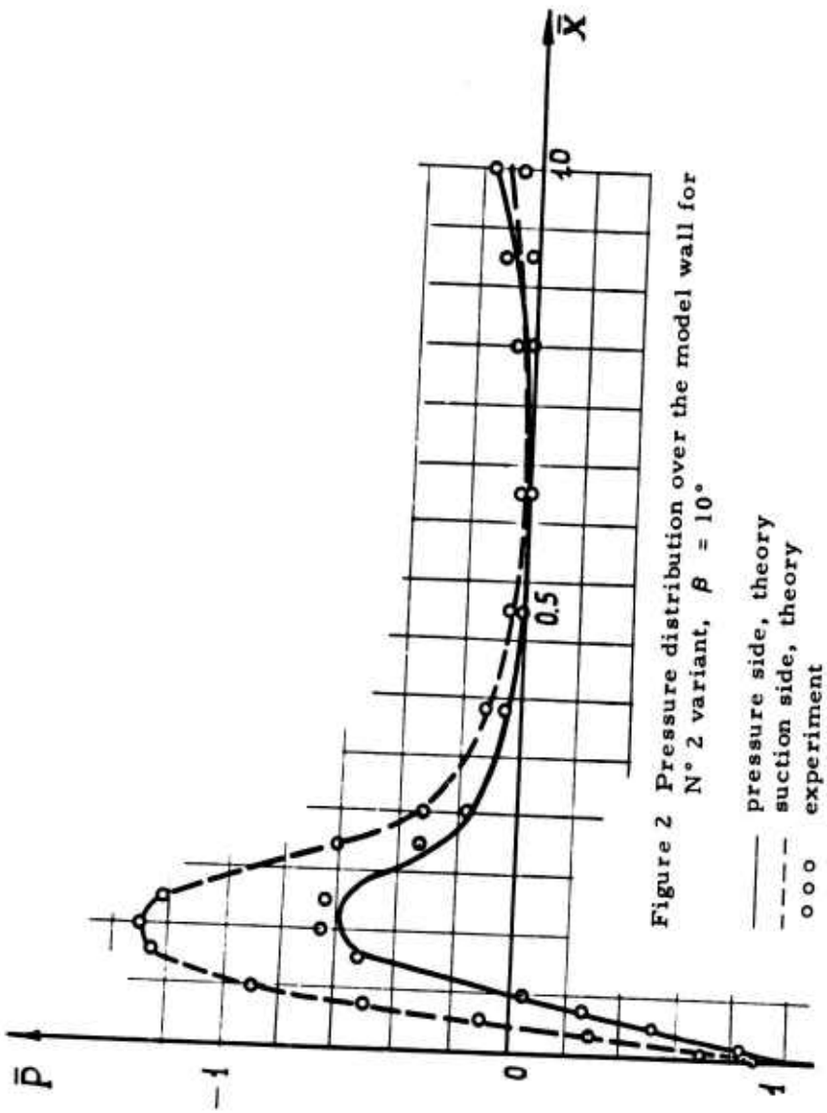


Figure 2 Pressure distribution over the model wall for N° 2 variant, $\beta = 10°$

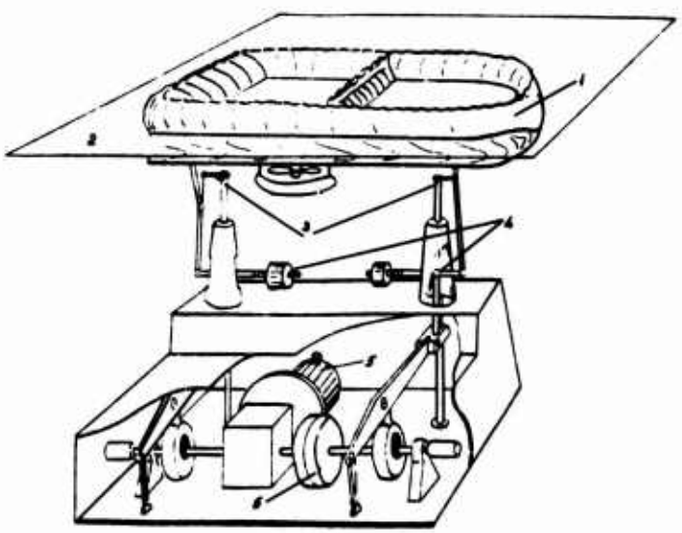


Figure 3 Scheme of the plant for determining the aerodynamic performance of ACV models.

1 - model
2 - ground board
3 - strain gauges
4 - mechanism of compensating for inertia forces
5 - electric motor
6 - phase shift regulation coupling

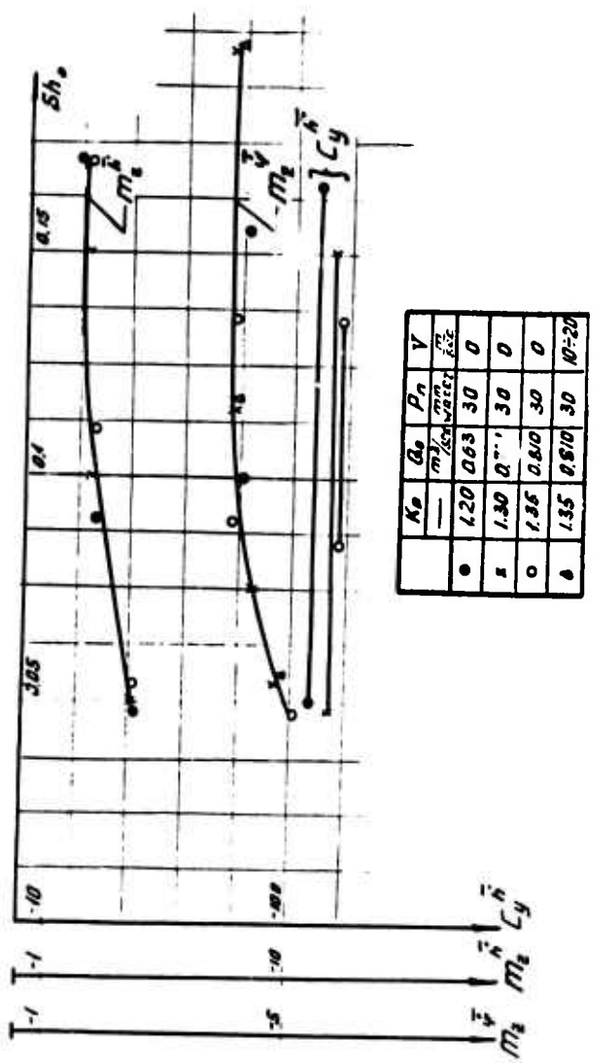


Figure 4 Coefficients $C_y^{\bar{v}}$, $m_z^{\bar{v}}$, $m_z^{\dot{\psi}}$ versus Sh_* number
(Model N° 1)

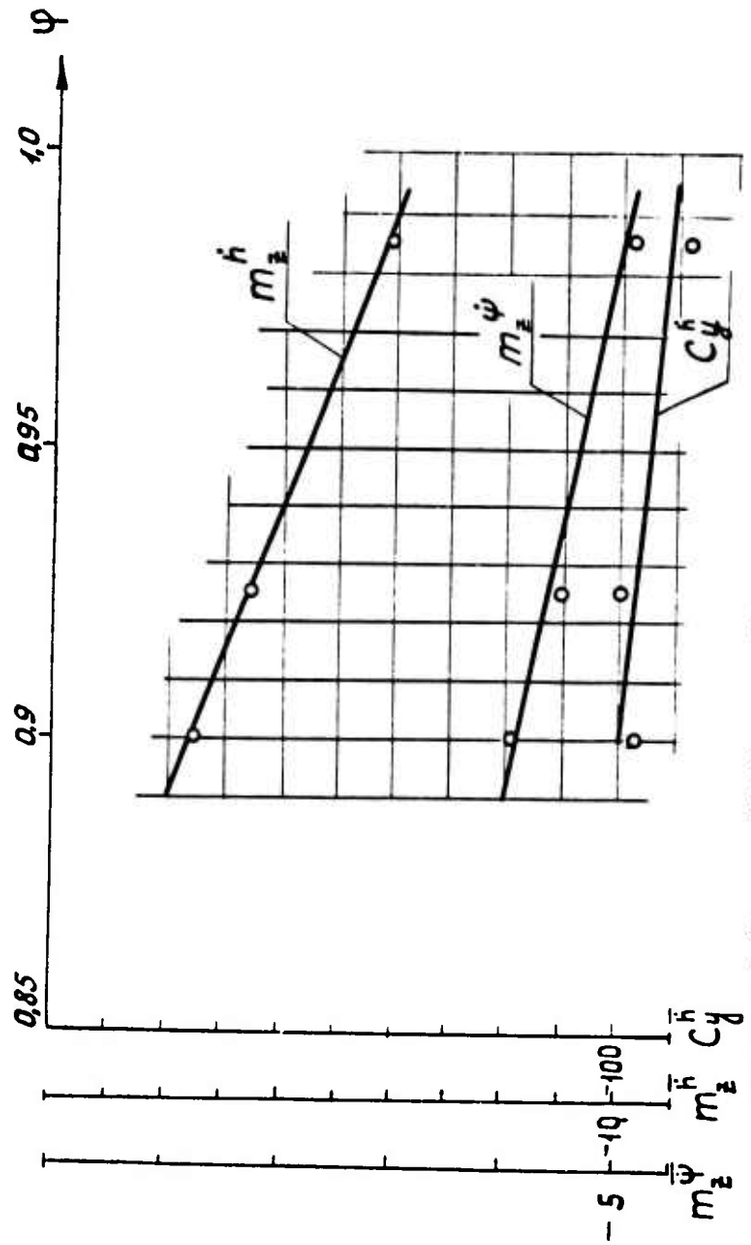


Figure 5 Influence of fullness coefficient φ upon coefficients C_y^h, m_z^h, $m_z^{\dot{\psi}}$.

$Sh_* = 0.1$ $K_p = 1.3$ $Q_o = 0.73\ m^3/sec$

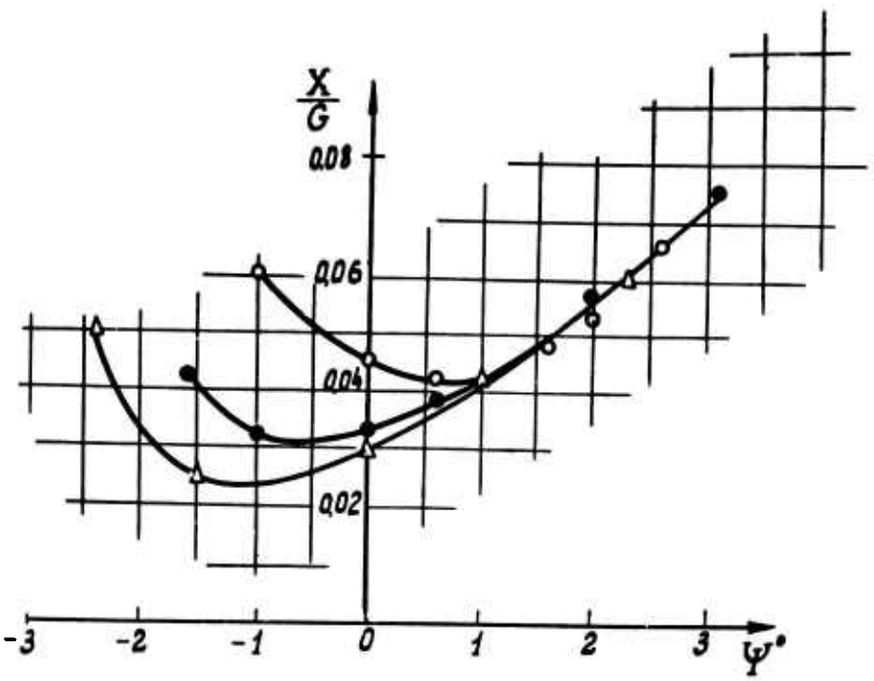


Figure 6 Relative resistance versus running trim angle in calm water

$$F_r = \frac{V}{\sqrt{gL}} = 1.1$$

● ● ● model N° 1
△△△ model N° 2
o o o model N° 3

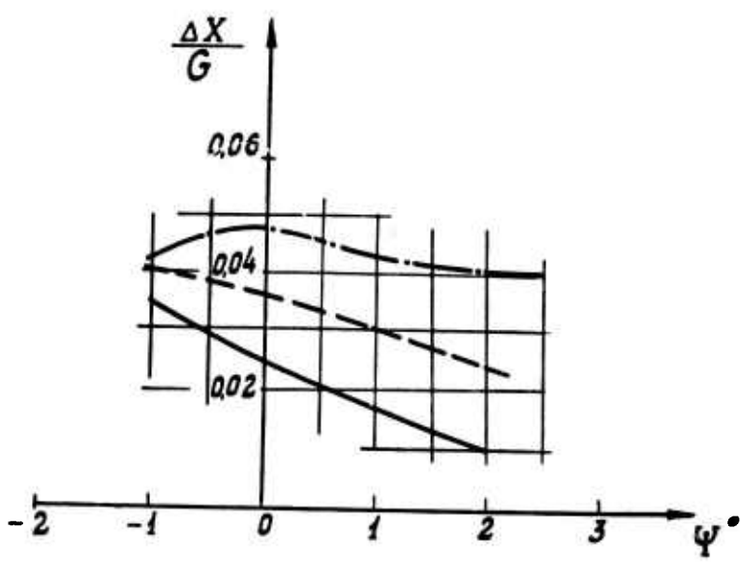


Figure 7 Influence of the running trim angle upon the gain in resistance in waves (wave length λ = 2.2 m, wave height h = 0.08 m)

---- model N° 1
——— model N° 2
—·—· model N° 3

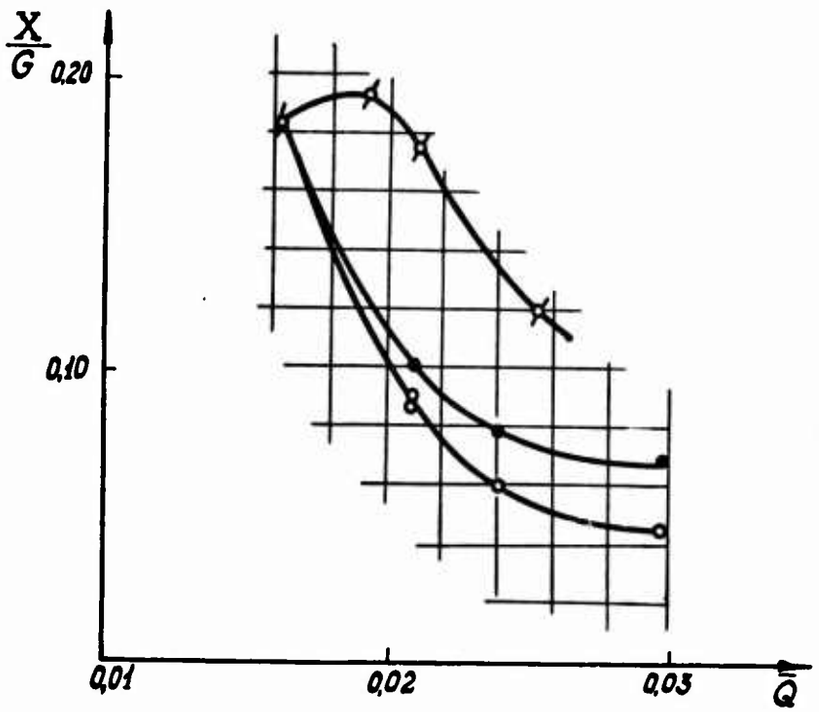


Figure 8 Relative resistance in waves against the air flow rate for different methods of the additional air supply (wave length λ = 3.1 m, wave height h = 0.08m) Fr = 1.10

ooo additional air supply into the forward part
ø ø ø air supply into the after part
••• air supply along the perimeter of air cushion

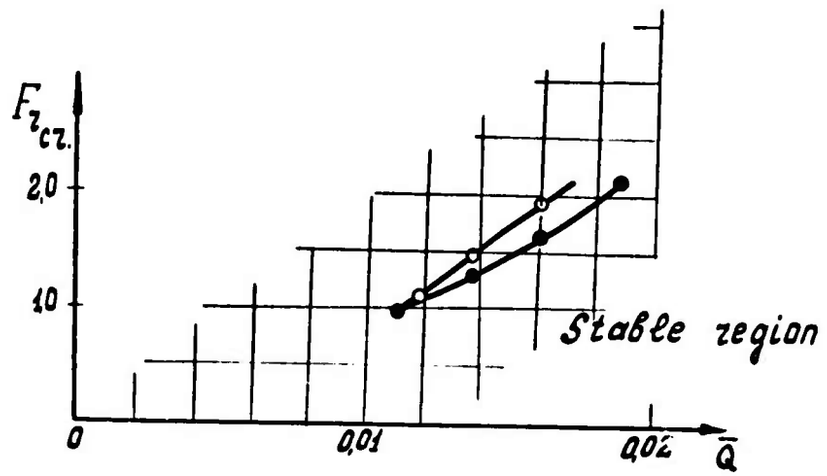


Figure 9 Influence of the relative air flow rate upon the longitudinal stability of motion (Fr_{cr} - onset of plough-in of the flexible skirt) for two positions of the center of gravity along the model length (wave length λ = 3.1 m wave height h = 0.08 m; G = 80 kg; K_p = 1.25)

ooo $\frac{M_z}{GL}$ = 0.012 ••• $\frac{M_z}{GL}$ = 0.019

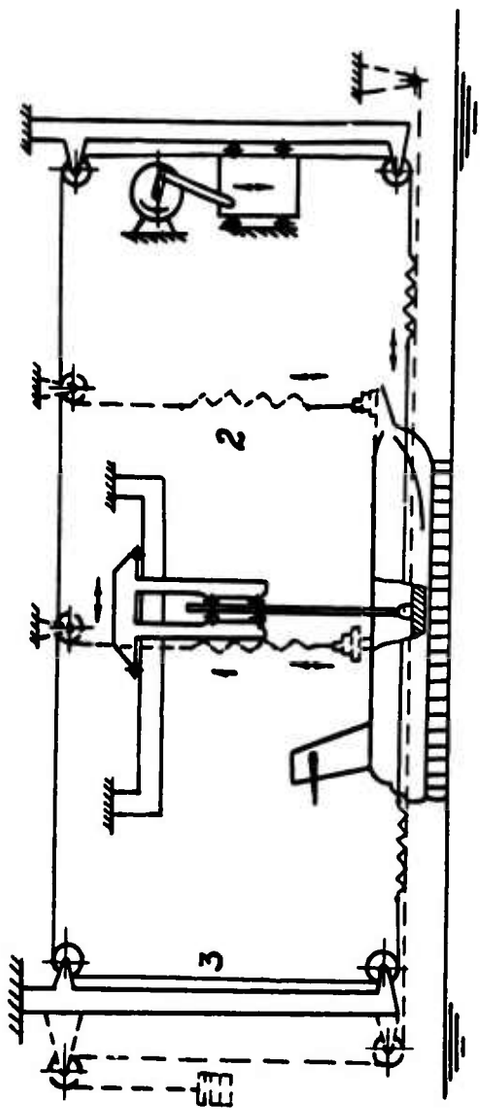


Figure 10 Experimental plant for the determination of non-steady hydrodynamic performance in longitudinal plane.

1 - scheme of switching on for heaving studies; 2 - scheme of switching on for pitching studies; 3 - scheme of switching on for the study of translatory motion along the longitudinal axis.

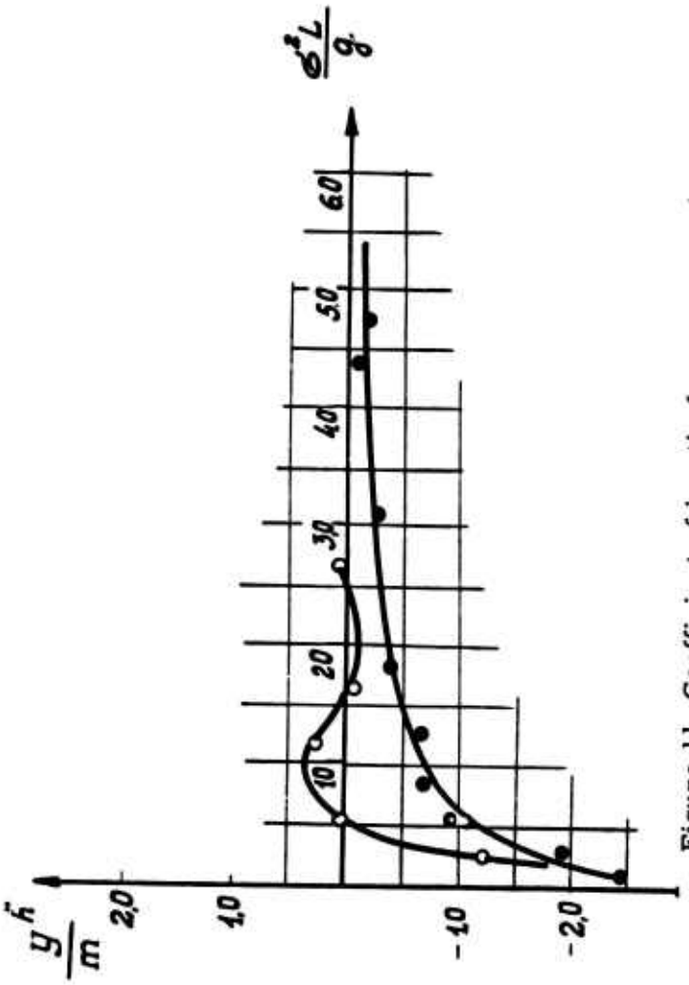


Figure 11 Coefficient of inertia forces versus frequency of vertical oscillations for the schematized model of ACV

ooo Fr = 0.0 ●●● Fr = 1.5

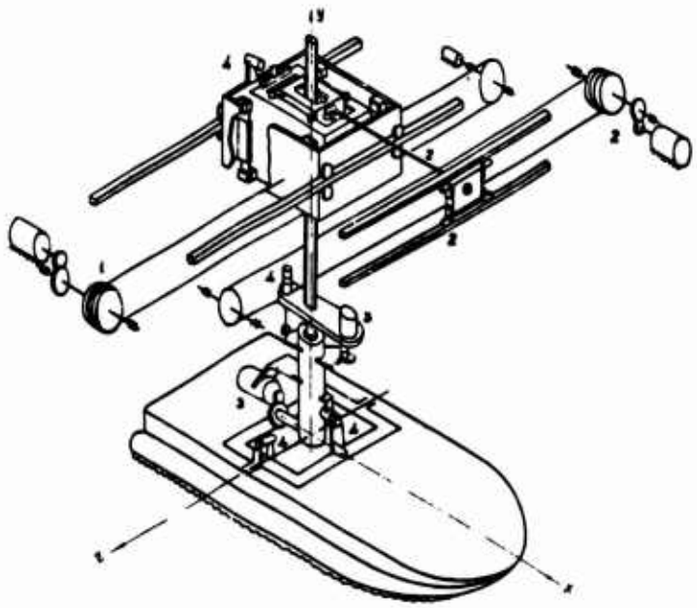


Figure 12 Experimental plant for dynamic tests with the ACV towed models in the towing tank.

1- system of unloading the movable units; 2 - system of bringing the towing force into coincidence with a model centre line 3- system of imitating the external forces; 4- strain gauges for recording the kinematic parameters.

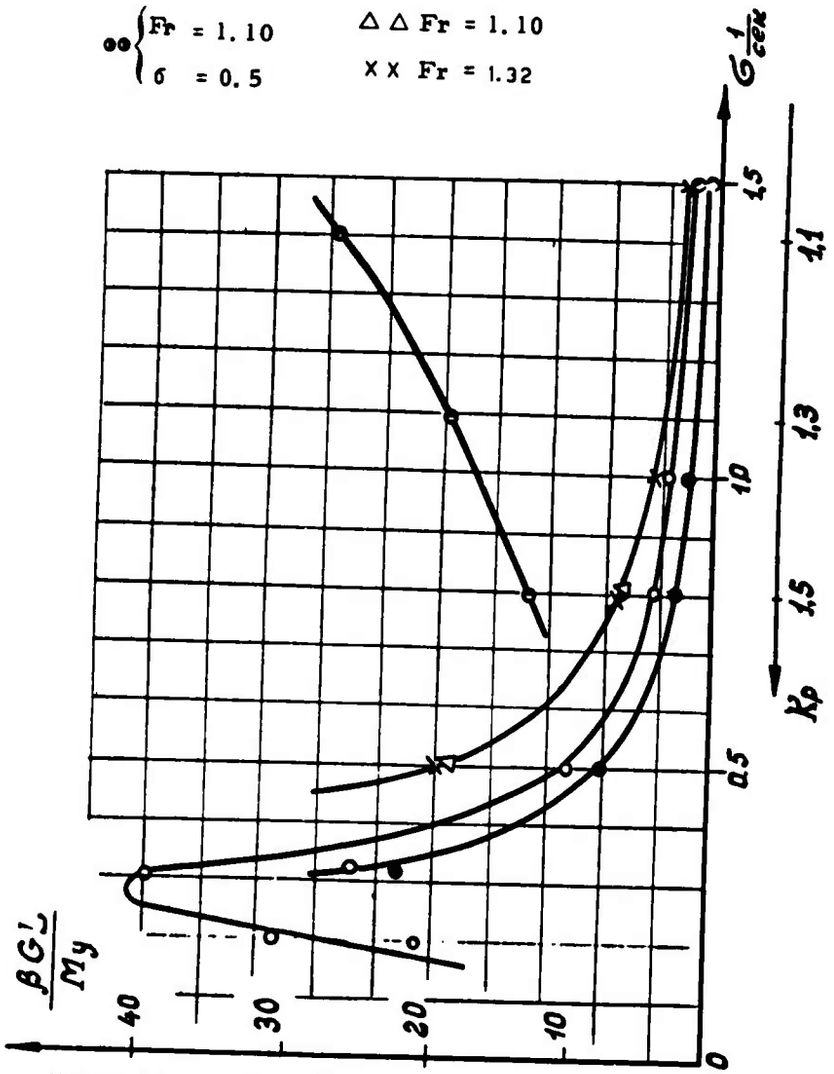


Figure 13 Relationship between the amplitude-frequency characteristic of the model for yawing angle at different speeds and pressure factors of the air cushion.

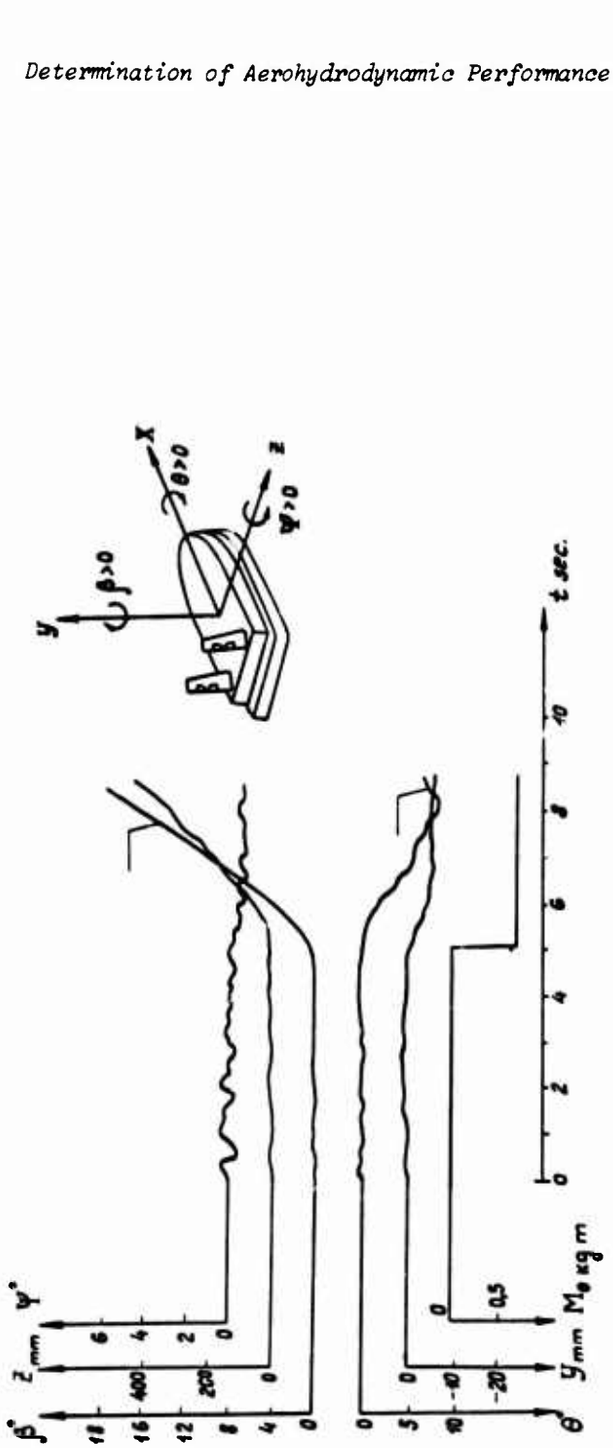


Figure 14 Transition process at the instantaneous application of the rolling moment.

DISCUSSION

P. Kaplan
Oceanics Inc.
Plainview, New York, U.S.A.

I think my comments with regard to experiments contain some helpful information and also provide a warning with regard to any expectation of prediction of dynamic performance of air cushion vehicles from ordinary experiments in towing tanks. For one thing, referring to the particular case, in which you used forced oscillation, the equation given on page 12 deals with the single degree of freedom of heave motion. There is a pressure variation here and if you actually wrote the equations involving both pressure and heave motion coupled together, you would find that there is an effective mass entering the system. The effective mass is dependent upon the geometry of the plenum system and certain aspects of the pressure ratios, etc. The net result is that you have some reduction in the effective mass. That is why you find what people are referring to as a negative aided mass for ACVs, which may not be quite so. There is a real physical mass, and there may be some hydrodynamic effective mass since the frequency dependence in Fig. 11 may be indicative of that, but it also depends on how you look at the water surface behaviour at low frequency and at high frequency and also at low speed and at high speed. But that is not the point. The main thing is that the pressure is influential, and that it should be accounted for ; it should be measured and the equations for the system should include it. Analyse that and then look at your resulting inertia and the other terms. Correlate the results, and that is the way you will understand what is happening with these vehicles.

Secondly, with regard to model tests, let us look at how you scale. All naval architects are accustomed to scaling dynamic phenomena in terms of Froude scaling and that is because certain parameter scales in that way. What is the most fundamental parameter that determines the behaviour of any vehicle in response to a seaway disturbance ? There are two, mainly : the natural frequency and the damping. The natural frequency can be derived for any type cushion system for an air cushion vehicle. It involves pressure ratios, i. e. atmospheric to normal pressure that supports the system, and the geometric height of the plenum.

Pressure scales linearly, and the height scales linearly ; atmospheric pressure is not scaled in any facility, at least it is not scaled at speeds appropriate for ACV. The situation is such that if you consider this effect, the natural frequency of the system is scaled linearly while for Froude scaling it varies as the square root of your scale ratio. Therefore you have shifted natural frequency coincidence well out of proportion, depending upon your scale ratio. In addition, the relative damping, that is the matter of so-called relative to critical damping, also changes due to scaling because of the operation pressure system. The resulting question is, what consequence does this have upon the motion ?

Some results have been obtained based on analysis and simulation work, and have been published in the open literature, on this particular point. It shows the following. You can predict the vertical acceleration responses from tests in waves at model scale at atmospheric pressure. Unfortunately the prediction is unconservative. You think you are getting by with a certain acceleration, and if you work out the equations which you validated by your original procedure to correlate with your testing at non-scaled atmospheric pressure, you then scale the atmospheric pressure to simulate real life and your accelerations are larger. However I do not say that there is no business for towing tanks in getting information for ACV. I do say there is business for theoreticians, together with towing tanks, to get the right information.

REPLY TO DISCUSSION

Vjacheslav N. Treshchevsky
Kryloff Research Institute
Leningrad, U.S.S.R.

I am grateful to you for your comment. I would say that the problems of scale effect which you mention are taken into acount and special experiments have been and are being made in order to exclude wide errors connected with the scale effect in various types of experiments.

You mentioned the negative value of the term corresponding to mass which is on one of the illustrations. It is difficult to explain it quite correct, I think the reason of the phenomena is in the inter-

action between the ACV hull, the air cushion and water surface. I may add that this is stable experimental data and I have seen the correlating results in a German paper.

I can add that frequency characteristic shown on Figure 11 being derived experimentally includes the influence of all the factors mentioned by Mr Kaplan (variable pressure, ACV's geometry). The possibility of exact theoretical calculation of this characteristic seems to be doubtful.

The use of model data in ACV dynamics isn't the subject of the paper. Nevertheless the assumption of the linear character of the natural frequency versus scale dimension is not obvious. As for similarity criterion, the Froude number and dimensionless frequency were used among others. The natural frequency and damping are ACV's characteristics, determined by flight conditions.

* * *

UNCONVENTIONAL SHIPS

Monday, August 21, 1972

Afternoon Session

Chairman : R. Leopold
Naval Ship Engineering Center, U.S.A.

	Page
Hydrodynamics and Simulation in the Canadian Hydrofoil Program. R. T. Schmitke, E. A. Jones (Defence Research Establishment Atlantic, Canada).	293
Bending Flutter and Torsional Flutter of Flexible Hydrofoil Struts. P. K. Besch, Y. N. Liu (Naval Ship Research and Development Center, U. S. A.).	343
On the Design of the Propulsion Systems with "Z" Drives for Hydrofoil Ships. A. A. Rousetsky (Kryloff Research Institute, Leningrad, U. S. S. R.).	401
Hydrodynamic Development of a High Speed Planing Hull for Rough Water. D. Savitsky (Stevens Institute of Technology), J. K. Roper (Atlantic Hydrofoils, inc.), L. Benen (Naval Ship Systems Command), (U. S. A.).	419
Motion and Resistance of a Low-Waterplane Catamaran. P. C. Pien, C. M. Lee (Naval Ship Research and Development Center, U. S. A.)	463

HYDRODYNAMICS AND SIMULATION IN THE CANADIAN HYDROFOIL PROGRAM

R. T. Schmitke and E. A. Jones
Defence Research Establishment Atlantic
Dartmouth, N.S. Canada

ABSTRACT

Hydrodynamic aspects of the Canadian hydrofoil program are discussed, with particular reference to HMCS BRAS D'OR. Associated simulation studies are described and key results of BRAS D'OR seakeeping trials are presented.

I. INTRODUCTION

For more than a decade the Canadian hydrofoil program has been synonymous with the design, construction and trials of HMCS BRAS D'OR[1] (Figure 1). The recent suspension of trials and subsequent mothballing of the ship make this an appropriate time for a comprehensive review of design experience in the light of trials observations. This paper is particularly concerned with the hydrodynamics of the hydrofoil system and associated simulation studies.

Factors governing foil system configuration and hydrodynamic design are described, with some details of development experience at the model scale and a thorough discussion of full scale trials observations. The mathematical models used in simulation studies are then presented, and predictions of steady state and dynamic performance are compared with trials data. The paper concludes with an analysis of BRAS D'OR seakeeping trials.

II. FOIL SYSTEM HYDRODYNAMICS

System Configuration

Since its inception the Canadian hydrofoil program has been

Preceding page blank

based on passively stable surface-piercing hydrofoil systems, thereby complementing U. S. effort on automatically controlled fully-submerged systems. The principal relative merits of each type are listed below [2] . Fully-submerged systems offer :

a) a smoother ride in moderate to heavy seas,

b) higher lift-drag ratio,

c) lower foil system weight,

d) greater foilborne manoeuvrability,

e) retraction capability,

Surface-piercing systems offer :

a) inherent stability,

b) a wider range of foilborne speeds,

c) better sea-keeping at hullborne speeds,

d) higher potential for remaining foilborne in extreme seas,

e) greater tolerance to off-design loads, such as those imposed by towed sonar.

Successful contouring of large waves requires that the bow foil respond rapidly to changes in immersion depth ; for satisfactory following sea operation, the bow foil must also be reasonably insensitive to wave orbital velocities. Together these requirements dictate that the bow foil combine high rate of change of lift with draft, $\frac{\partial L}{\partial h}$, with low rate of change of lift with angle, $\frac{\partial L}{\partial \alpha}$.

The after foil, on the other hand, must have high $\frac{\partial L}{\partial \alpha}$ to provide adequate damping of seaway-induced motions. Furthermore, $\frac{\partial L}{\partial h}$ must be lower than at the bow foil in order that downward heave displacements cause upward trim. Since foil efficiency generally increases with $\frac{\partial L}{\partial \alpha}$, a canard configuration is the logical result, with the bow foil carrying as little weight as dynamically feasible.

A secondary but significant advantage of the canard configuration is that it lends itself to a hull with very fine bow lines. This is necessary for reduced pounding due to wave impact when foilborne and is particularly important for the Canadian rôle with its emphasis

on good hullborne performance and seakeeping.

The Sub-Cavitating Main Foil

In addition to providing adequate heave damping through high $\frac{\partial L}{\partial \alpha}$, the main foil unit must provide roll stiffness without undue heave stiffness. The BRAS D'OR unit (Figure 2) accomplishes this by use of anhedral and dihedral surface-piercing elements at either end of a fully-submerged main foil unit. The latter serves as the primary lifting element and, combined with the dihedrals, provides the required characteristics with high efficiency. The upper anhedral panels are highly cambered and twisted to develop high lift at take-off. The anhedral tips are incidence-controlled to augment roll stability at low foilborne speeds and improve turning performance.

The theoretical tools required for hydrodynamic design of a subcavitating foil system have been obtained by adding free surface corrections to methods borrowed from subsonic aerodynamics. The prevention of cavitation is the chief hydrodynamic constraint in section design, and cavitation-free operation above 40 knots necessitates a departure from conventional low speed aerofoils to delayed-cavitation sections such as illustrated in Figure 3. The design of the particular sections used in BRAS D'OR is described in [3]. They are highly efficient and provide an approximately uniform pressure distribution when operating over a wide range of angle-of-attack in close proximity to the free surface. The practical upper limits of the delayed-cavitation regime are approximately 60 knots in calm water and 50 knots in rough seas - the design speeds for BRAS D'OR.

Full scale trials showed that in general the BRAS D'OR main foil unit has successfully met its design requirements for high efficiency, low $\frac{\partial L}{\partial h}$ and high $\frac{\partial L}{\partial \alpha}$. The only significant hydrodynamic problems encountered were associated with emergence of the anhedral-dihedral foil intersections at about 45 knots, which resulted in lateral jerkiness even in calm water. There were two specific problems. The first was caused by intermittent ventilation of the dihedral foils and anhedral tips and was countered by installing additional anti-ventilation fences. The second was fundamental to the main foil geometry and was more difficult to solve. It was due to increased roll and heave stiffness below the intersections, when both the anhedral tips and the dihedral foils become surface-piercing. It was alleviated by reducing the mean angle-of-attack of the anhedral tips by 2°. This increased main foil immersion and delayed the emergence of the anhedral-dihedral intersections to approximately 50 knots. The net result was a significant increase in riding comfort in

small to moderate waves at speeds up to 50 knots.

Main foil cavitation was never observed during calm water trials, even at 62 knots, indicating that section design met all expectations in this very important respect. No problems arose from hydrodynamic interference between individual foil elements. However, both full scale trials and model tests at the National Physical Laboratory showed that bow foil wake reduces main foil lift by approximately 10% .

The Super-Ventilated Bow Foil

Operating conditions for the bow foil are demanding. At foil-borne speeds in rough seas the bow foil is subject to wide and rapid changes of both immersion and angle-of-attack. The hydrofoil system is wholly area-stabilized longitudinally and the lightly-loaded depth-sensitive bow foil is the primary source of control, so that smooth lift vs. immersion and lift vs. angle-of-attack characteristics are essential. Sub-cavitating hydrofoil sections are prone to ventilation in rough water and the resulting sharp losses in lift at the primary longitudinal control element cause an unacceptable diving tendency[4] . Superventilated sections are therefore used for the bow foil, despite their lower efficiency. In this case, occasional suppression of ventilation gives sharp lift increases, but unlike the converse situation with subcavitating sections this is an inherently safe effect.

The BRAS D'OR bow foil is of diamond configuration (Figure 4) with a sub-cavitating centre strut and super-ventilated dihedral and anhedral elements. Tulin Two-Term lower surfaces[5] were chosen for the super-ventilated sections (Figure 5) because these appeared to offer the best compromise between hydrodynamic efficiency and structural strength. Design incidence is nominally 5° above zero lift (as established by model tests), and rake angle of the unit is adjustable in flight to permit operation at optimum incidence for the prevailing sea condition.

Little information was available on the practical operation of surface-piercing super-ventilated hydrofoils, so that extensive experimental development was necessary. Model size had to be as large as practical to minimize scale effects : consequently, the bulk of the work was done at quarter scale, taxing the limits of available towing tank facilities. The same bow foil was also used as part of a complete quarter scale manned model of the system. A great strength of the development program lay in the ability to test the same model both in the controlled environment of towing tanks and as a functional unit in realistic seaways.

A major concern of the experimental program was upper surface design, with the objective of inhibiting and controlling intermittent flow reattachment. The leading edge was made as fine as practicable and, to enforce reattachment to occur in stages and hence reduce the severity of accompanying lift increases, two additional break points were incorporated in the upper surface, at 66% and 87% chord. A major problem of the initial manned model trials was that the anhedral foils served as fences to inhibit the spread of ventilation down the dihedrals, leading to cyclic pitching at speeds close to intersection emergence. This was overcome by adding another large upper surface spoiler to the anhedral sections in the neighbourhood of the intersection.

The most comprehensive set of quarter scale towing tank data was obtained at the National Physical Laboratory (NPL) under Froude-scaled conditions, providing good definition of bow foil characteristics. (Figures 6 and 7). Data points have been coded to show the spanwise extent of leading edge ventilation down the dihedral foils from the upper surface. (For all test conditions of interest, the cavities behind the midback spoilers remained consistently ventilated.) Spanwise extent of leading edge ventilation is indicated by the degree of openness of the points, e.g. :

100 %	fully open	0
50 %	50% open	◐
0%	fully closed	●

Figure 9 shows that the lift-curve slope decreases gradually with increasing rake angle as ventilation spreads down the leading edge of the dihedrals.

The most interesting quarter scale tank tests took place at the Lockheed Underwater Missile Facility (LUMF), where both cavitation and Froude numbers were scaled. Cavitation scaling was found to have no significant effect on flow state, lift or drag. An equally significant finding was that lift values obtained at NPL were much higher than at LUMF (Figure 8). These differences were later shown to be due in large part to deterioration of the foil surfaces and leading edges during the time interval between the two series of tests.

It was possible to estimate full scale bow foil lift characteris-

tics by direct observation of depth of immersion. Figure 9 shows the steady state lift coefficient (based on horizontally projected immersed area) of the bow foil unit over the foilborne speed range. The full scale lift coefficient falls within limits established by quarter scale model tests at NPL and LUMF except at low speeds. For these, leading edge ventilation extended only partially down the span of the dihedral foils at quarter scale but was complete at full scale, giving lower lift but more stable flow.

The inhibiting effect of the outboard intersections was clear at quarter scale. The dihedral foils ventilated from the mid-back spoilers under most conditions, but the intersections, acting as fences, prevented the initiation of leading edge ventilation until they emerged. It almost invariably occurred on one foil at a time since the associated loss of lift caused the intersections to re-immerse, inhibiting the second dihedral more strongly. At full scale, initial establishment of leading edge ventilation on the dihedrals still appeared to be associated with emergence of the intersections, but invariably occurred simultaneously on both dihedral foils. Effects were less clear but full scale ventilation certainly occurred more readily and more strongly than indicated even by LUMF quarter scale tests at correctly scaled Froude and cavitation numbers. This was due at least in part to the fact that full scale trials were seldom held under really calm conditions, the practical limit for "calm" water being set at waves 3 feet in height. Occasionally, during take-off in exceptionaly smooth seas, leading edge ventilation was delayed until ship speed approached 40 knots ; during this interim period, pitch angles of up to 9° were observed. This situation was easily overcome by increasing speed or bow foil incidence until leading edge ventilation occurred.

Bow foil rake angle optimization trials showed that a strong and persistent ventilated cavity was achieved in calm water at the design rake angle setting (0°). In rough water optimum rake angle varied with heading to the sea ; suitable flow and ship motion characteristics were generally achieved in head, beam and following State 5 seas at rake angles of -1°, 0° and 1 1/2° respectively.

In short, steep seas, flow re-attachment sometimes occurred on the bow foil dihedrals during deep immersion at the face of larger waves. The resulting discontinuous increase in lift gave added impetus to bow up pitch motion. As depth of immersion decreased at the rear wave slope, ventilated flow was re-established, accompanied by a sudden decrease in lift. Oscillograph records of vertical acceleration during these periods exhibit a sharp positive and negative spike followed by a return to normal acceleration levels as the ship encoutered waves of more typical size and normal ventilated flow was re-

established. Because these vertical acceleration spikes were an important source of motional discomfort, an objective of future development must be to improve ventilation stability at extreme depths of immersion.

Foilborne sea time has not been sufficient to enable firm and quantitative conclusions to be drawn regarding the suitability of bow foil $\frac{\partial L}{\partial h}$ and $\frac{\partial L}{\partial \alpha}$ for rough water operation. However, the ship never experienced difficulty in following seas, while pitch response to head and bow seas was high. It seems probable that a reduction in $\frac{\partial L}{\partial h}$ of about 20% would result in lower vertical accelerations without compromising stability.

A high drag penalty is paid for using super-ventilated sections. The philosophy adopted during BRAS D'OR design was that this condition could be tolerated since the bow foil is primarily a control element carrying only 10% of total ship weight. However, trials and model test data indicate that approximately 30% of total foilborne drag is due to the bow foil. In addition, the high bow foil drag makes fuel consumption, and hence range and endurance, extremely sensitive to longitudinal C. G. location.

BRAS D'OR sea trials have therefore specified three objectives for future super-ventilated bow foil development : reduction of drag, optimization of $\frac{\partial L}{\partial h}$ and $\frac{\partial L}{\partial \alpha}$ for rough sea operation, and improvment in ventilated flow stability. These are important considerations, but are secondary to the demonstrated success of the super-ventilated bow foil unit in stabilizing, controlling and steering the ship over a wide range of speed and sea conditions.

III. SIMULATION

Hydrofoil simulation in Canada began with the extensive and comprehensive studies carried out by the DeHavilland Aircraft of Canada Ltd. in support of BRAS D'OR design [6] . These studies were subsequently supplemented at the Defence Research Establishment Atlantic [7,8] , with the objective of achieving simple methods applicable to all surface-piercing hydrofoil systems. It is largely upon the latter work that this section of the paper is based. Four topics are treated : the general equations of motion for surface-piercing hydrofoil vessels, prediction of steady state performance, analysis of calm water stability and analog simulation of random seas. Because of the close similarity to aircraft practice, descriptive material is kept to a minimum.

Equations of Motion for Surface-Piercing Hydrofoil Ships

The equations of motion listed below are written with respect to the axis system illustrated in Figure 10. The origin is at the C.G. and in the reference condition of steady symmetric flight in calm water at speed U_o, the x-axis is directed horizontally forward, the z-axis vertically upward and the y-axis to port. The pitch angle is positive for downward rotation of the bow.

$$\text{Pitch}: \quad I_Y \ddot{\theta} = \Sigma (-L_i x_i \cos\Gamma_i - D_i z_i + M_i \cos\Gamma_i) - \\ - T (x_T \sin\gamma - z_T \cos\gamma) \tag{1}$$

$$\text{Heave}: \quad m (\dot{w} - U_o \dot{\theta}) = \Sigma L_i \cos\Gamma_i + T \sin\gamma - W \tag{2}$$

$$\text{Surge}: \quad m (\dot{u} - g\theta) = T \cos\gamma - \Sigma D_i \tag{3}$$

$$\text{Sideslip}: \quad m (\dot{v} + U_o r + g\phi) = - \Sigma L_i \sin\Gamma_i \tag{4}$$

$$\text{Roll}: \quad I_x \ddot{\phi} = \Sigma L_i (y_i \cos\Gamma_i + z_i \sin\Gamma_i) \tag{5}$$

$$\text{Yaw}: \quad I_z \dot{r} = \Sigma (D_i Y_i - L_i x_i \sin\Gamma_i + M_i \sin\Gamma_i) \tag{6}$$

where summation of lift (L_i), drag (D_i) and pitching moment (M_i) is over all foil and strut elements, individually located at (x_i, y_i, z_i). W is all-up-weight and the line of action of thrust (T) passes through (x_T, z_T). The following sign convention is adopted for dihedral and anhedral angles :

for a port dihedral foil of angle Γ_{DP}, $\Gamma_i = \Gamma_{DP}$

for a stbd. dihedral foil of angle Γ_{DS}, $\Gamma_i = \Gamma_{DS}$

for a port anhedral foil of angle Γ_{AP}, $\Gamma_i = -\Gamma_{AP}$ (7)

for a stbd. anhedral foil of angle Γ_{AS}, $\Gamma_i = \Gamma_{AS}$

L_i, D_i and M_i may be evaluated by the methods of References [9], [10], [11] and [12].

Steady State Performance

In the steady state, equations (1) to (3) become

$$\Sigma(L_i x_i \cos\Gamma_i + D_i z_i - M_i \cos\Gamma_i) + (x_T \cot\gamma - z_T)$$

$$\Sigma D_i = 0 \qquad (8)$$

$$\Sigma L_i \cos\Gamma_i + \cot\gamma \Sigma D_i = W \qquad (9)$$

Since dynamic pressure is constant L_i, D_i and M_i are functions of immersion depth (h) and angle-of-attack (α) alone. For an all-fixed foil system, furthermore, knowledge of h and α for a single foil element enables all other h's and α's to be determined. Hence (8) and (9) contain only two unknowns : h and α of a reference foil element. Because of the non-linear nature of these equations the solution must be obtained by an iterative technique.

Figure 11 illustrates the accuracy obtainable using the above procedure. Predicted curves of BRAS D'OR trim, keel clearance and weight- drag ratio are presented, along with trials measurements of these quantities. Estimated measurement accuracies are $\pm 1/4°$ for trim, $\pm$ 1 ft. for keel clearance and $\pm$ 1.5 for W/D. The accuracy of the resistance prediction is of particular importance ; the fact that measured drag is higher than predicted is probably due largely to the one to three foot waves encountered during most calm water trials.

Calm Water Stability

Foilborne stability in calm water is most easily assessed by

solving the linearized equations of ship motion. Linearization of (1) to (6) results in the following two sets of three coupled linear ordinary differential equations :

Longitudinal

$$\text{Pitch}: \quad I_Y \ddot{\theta} = M_u u + M_z z + M_w \dot{z} + (M_\theta + U_o M_w)\theta + M_{\dot{\theta}} \dot{\theta} \tag{10}$$

$$\text{Heave}: \quad m\ddot{z} = Z_u u + Z_z z + Z_w \dot{z} + (Z_\theta + U_o Z_w)\theta + Z_{\dot{\theta}} \dot{\theta} \tag{11}$$

$$\text{Surge}: \quad m(\dot{u} - g\theta) = X_u u + X_z z + X_w \dot{z} + (X_\theta + U_o X_w)\theta + X_{\dot{\theta}} \dot{\theta} \tag{12}$$

Lateral

$$\text{Sideslip}: \quad m(\dot{v} + U_o r + g\phi) = Y_v v + Y_r r + Y_{\dot{\phi}} \dot{\phi} + Y_\phi \phi \tag{13}$$

$$\text{Roll}: \quad I_x \ddot{\phi} = K_v v + K_r r + K_{\dot{\phi}} \dot{\phi} + K_\phi \phi \tag{14}$$

$$\text{Yaw}: \quad I_z \dot{r} = N_v v + N_r r + N_{\dot{\phi}} \dot{\phi} + N_\phi \phi \tag{15}$$

where

$$z = \int_o^t (w - U_o \theta)\, dt \tag{16}$$

and the stability derivatives M_u , M_z etc. are listed in the Appendix.

The longitudinal modes of motion characteristic of passively-stabilized surface-piercing hydrofoil ships consist of a lightly damped oscillation governed by ship pitching characteristics, a heavily damped oscillation related to heave and a simple convergence arising from surge-heave-pitch coupling. These are termed the pitch, heave

and coupled subsidence modes, respectively. For canard configurations, the coupled subsidence mode is always stable, but in airplane configurations instability may result from adverse heave-pitch coupling. Neither the pitch nor the heave modes are significantly influenced by surge.

Root locus plots showing the effect on BRAS D'OR's longitudinal modes of varying speed are presented in Figure 12. Longitudinal dynamics are dominated by the lightly-damped pitch mode in which the damping ratio decreases and natural frequency increases with increasing speed ; this mode's characteristics are a direct result of the bow foil's design, which combined high $\frac{\partial L}{\partial h}$, with low $\frac{\partial L}{\partial \alpha}$. Similarly, the characteristics of the heave mode follow from the combination of low $\frac{\partial L}{\partial h}$ with high $\frac{\partial L}{\partial \alpha}$ in the main foil.

Generally speaking, three modes of lateral motion may be distinguished for passively-stabilized surface-piercing hydrofoil ships (Figure 13) : a rapid convergence of little importance, an oscillation governed by ship rolling characteristics, and a slow convergence arising from sideslip-roll-yaw coupling.

Simulation of Random Seas

In Equations (1) to (6) a seaway acts as a forcing function through the variation of foil immersion depth and angle-of-attack with wave elevation and orbital velocity. The simulation of these seaway variables is now discussed.

The Pierson-Moskowitz spectral form is chosen as a model of the sea [13] . The equation for the wave elevation power spectral density is :

$$\Phi(\omega) = \frac{.0081 g^2}{\omega^5} \exp\left\{-.74 \left(\frac{g}{V\omega}\right)^4\right\} \qquad (17)$$

where V is wind speed. Significant wave height is given by :

$$\bar{h}_{1/3} = 1.86 \left(\frac{V}{10}\right)^2 \qquad (18)$$

for V in knots.

Consider now the case where a hydrofoil ship is travelling at speed U_o into a head sea. The wave elevation spectrum, expressed in terms of frequency of encounter, is

$$\Phi'(\omega') = \frac{\Phi(\omega)}{1 + \frac{2U_o\omega}{g}} \tag{19}$$

with a similar expression holding for the transformed orbital velocity spectrum, $\Phi'_w(\omega')$.

$$\omega' = \omega + \frac{\omega^2 U_o}{g} \tag{20}$$

is the angular frequency of encounter. Φ' and Φ'_w are plotted in Figures 14 and 15 for U_o = 50 knots and V = 24 knots (Sea State 5).

The white noise technique for simulating a random head sea will now be described. The basis of this method is that a signal with a prescribed spectrum can be generated by passing white noise of spectral density Φ_o through a linear filter so designed that the square of its frequency response, $H(\omega)$, has the desired shape. Filter output is, then,

$$\Phi(\omega) = \left|H(\omega)\right|^2 \Phi_o \tag{21}$$

In particular, the generation of waves with spectrum Φ' can be accomplished using a filter network consisting of three high pass filters and two integrators ; the approximation to Φ' which is thus obtained is shown in Figure 14. Taking the vertical orbital velocity to be the input to the last integrator multiplied by a suitable constant results in the approximation to Φ'_w shown in Figure 15. Proper phasing between wave elevation and orbital velocity has been achieved, while also obtaining good approximations to the spectra.

In head seas the waves seen by the main foil lag those at the

bow foil by

$$\Delta\zeta = \frac{\omega^2 \ell}{g} \tag{22}$$

where ℓ is the foil base length. Over the frequency range of interest, $\Delta\zeta$ can be very well approximated by a time lag and constant phase lead (Figure 16) :

$$\Delta\zeta = T\omega' - \Delta\phi \tag{23}$$

A block diagram of the head sea simulation system is shown in Figure 17. Results derived from simulating BRAS D'OR foilborne motions in rough water are presented in the next section ; surge was neglected in this simulation in order to simplify the problem and also because it was felt that neglecting surge should give conservative results. (Consider the case where the bow foil encounters a steep high wave, leading to a rapid increase in bow foil immersion depth. In practice a speed reduction of several knots occurs, and the attendant dynamic pressure decrease results in lower lift and accelerations than on the simulated, constant speed ship.)

IV. BRAS D'OR FOILBORNE SEA-KEEPING TRIALS

BRAS D'OR rough water trials were less comprehensive than desired, but enough data were obtained to enable comparison of measured characteristics with predictions and to reach general conclusions about sea-keeping ability. Data will be presented for three key trials, two in Sea State 4 and one in Sea State 5. The wave elevation power spectral densities measured during these trials are shown in Figure 18 and are compared with the Pierson-Moskowitz theoretical spectra for Sea States 4 and 5 (significant wave heights of 7' and 10'). Wave measurements were made by a buoy equipped to measure vertical accelerations and are admittedly inaccurate, due partly to limitations of the buoy itself and partly to the practical difficulty of making a single measurement representative of rapidly changing conditions in a trials area close to the coast.

The variation of root mean square values of longitudinal ship motion parameters with heading to the sea is shown in Figure 19 for an average speed of 39 knots. These values do not exhibit the systematic increase with sea height that one would expect, probably because

of different sea energy distributions. For all three seaways there are similar trends with change of heading : vertical accelerations are highest in head and bow seas and lowest in following seas, while pitch angle shows the opposite trend.

The longitudinal distribution of vertical accelerations is indicated in Figure 20, the points representing average root mean square values for the three sea trials. The most interesting feature of these plots is the comparatively small change in vertical acceleration along the length of the ship, illustrating the well-controlled pitch response of this canard configuration, with its special bow foil.

Figure 21 compares predicted and measured root mean square vertical accelerations at the bow. The predictions were derived from analog simulation of pitch and heave motions in a theoretical head Sea State 5 with significant wave height of 10.7 feet, while the measurements were obtained during head and bow sea runs in Sea States 4 and 5. Predicted acceleration levels are higher than measured, reflecting the higher theoretical sea state and perhaps to some degree, supporting the intuitive argument that neglect of surge is a conservative simplification of the simulation problem.

Figure 22 presents typical power spectral density plots of vertical acceleration at the bow and pitch angle for head sea runs at speeds of 34 and 42 knots. Also given are the corresponding spectra for the encountered seaway, derived from the nominal Sea State 5 plot of Figure 18. There are two dominant seaway frequencies, and although the effects of both are clearly apparent in the pitch angle plots, pitching is associated mainly with the lower frequency. Pitch response falls off with increasing speed, particularly at the lower frequencies. Bow vertical acceleration peaks at the higher seaway frequency ; the magnitude of this peak increases with speed and there is also a shift in the energy distribution toward higher frequencies.

The response transforms of Figures 23 and 24 quantitatively characterize BRAS D'OR's pitch and heave response to random head seas at speeds of 35 and 40 knots. Although the experimental results are scattered, reflecting inaccuracy of sea state measurement, system non-linearity and limited statistical confidence, they nevertheless furnish a reasonable indication of mean ship response, as given by the dashed lines in the Figures. Pitch response peaks at approximately .2 Hz, in agreement with the prediction of pitch natural frequency obtained from linear stability analysis. Bow vertical acceleration response is fairly flat above .2 Hz, but falls off rapidly below this frequency.

Agreement between simulated and measured response transforms is very good. These predictions were obtained by analog simulation of pitch and heave motions in regular waves of small amplitude - a procedure equivalent to linearization. The predictions of Fig. 21, on the other hand, were obtained by simulating ship motions in a random State 5 sea generated as described in Section 3. The regular wave technique was adopted for response transform prediction because it enabled more accurate modelling of the effects of circulation delay and wave orbital velocity on main foil angle-of-attack. Bow foil flow re-attachment and emergence of the main foil anhedral-dihedral intersections, both of which occurred occasionally during trials but never in the simulation, are probably the cause of the only notable discrepancy, under-prediction of pitch response below .3 Hz at 35 knots.

Roll and sway characteristics are presented in Figure 25 in terms of rms values for lateral acceleration and roll angle, for the three seaways of Figure 18. Lateral accelerations are given at two ship stations, the CG and the Control Information Centre, located comparatively high in the ship in the upper deck superstructure. As with the pitch-heave characteristics given earlier, there seems to be little effective difference between the state 4 and 5 seas. Roll angle is very dependent on direction to the seaway, increasing greatly for seas on and abaft the beam. The lateral accelerations exhibit a much smaller dependence because the roll frequency decreases for beam and stern seas.

The effect of heading on the frequency distribution is shown by the power spectral density plots of Figure 26. These show lateral acceleration at the CIC for head and following sea runs at 39 knots in Sea State 5. The first peak is at the main rolling frequency and is due to accelerometer tilt. For the head sea, in addition to the increase in frequency of the main acceleration component, there is an increase in level in the 1 to 2 Hz range. This is significant because lateral "jerkiness" was considered the most uncomfortable feature of the ride, especially at higher speeds and for higher stations in the ship.

The effect of increased speed is shown in Figure 27 by comparing lateral acceleration at the CIC for head sea runs of 34 and 42 knots in the same Sea State 5. The effect of increased height within the ship is particularly marked and is illustrated by Figure 28 which compares lateral accelerations at the CG and CIC with the corresponding roll angle plot for 39 knots in head Sea State 5. A very small amount of roll angle energy above 0.5 Hz seems responsible for really significant lateral acceleration at the CIC. The problem of lateral acceleration amplification with height is clearly deserving of attention

in large hydrofoil ship design.

It is difficult to relate seakeeping data directly to habitability or to compare the capability of different systems, other than subjectively. The behaviour of the BRAS D'OR canard system was well up to expectation in seaways encountered, both for straight runs and turns. There was a complete absence of slamming and motions were modest, particularly in pitch and heave. Motions were almost certainly greater for BRAS D'OR than for a comparable fully-submerged system but less than for other types of craft with surface-piercing foils. There were no particular problems for the crew when seated. Personnel moving about and standing, tired quickly, mainly because of the roll motions, but this situation would not arise in an operational ship.

For BRAS D'OR, a deciding factor in the choice of foil system was the exceptional hullborne seakeeping offered by the canard surface-piercing arrangement. For the tasks envisaged, the habitability is more important under hullborne cruise conditions than for short periods of foilborne operation. Experience with BRAS D'OR supports the contention that foilborne motions are acceptable for continuous periods of several hours and has confirmed the promise of exceptionally good hullborne seakeeping [2]

V. CONCLUSION

The Canadian hydrofoil program has significantly advanced both the performance and the fundamental understanding of surface-piercing hydrofoil systems designed for open ocean operation ; the development of a successful super-ventilated bow foil unit is especially noteworthy. As regards simulation, the extension of aerodynamic methods into the hydrofoil field has proved reasonably successful, yielding satisfactory predictions of both steady state and dynamic performance ; of particular importance is the good characterization of BRAS D'OR pitch and heave response derived from a linear mathematical model.

NOTATION

C_D	drag coefficient
C_L	lift coefficient
C_M	pitching moment coefficient
D	drag
H	frequency response

I_x	rolling moment of inertia
I_y	pitching moment of inertia
I_z	yawing moment of inertia
K	rolling moment
L	lift
M	pitching moment
N	yawing moment
S	immersed foil area
T	thrust, also time lag
U_o	ship steady state speed
V	wind speed
W	ship all-up weight
X	surging force
Y	swaying force
Z	heaving force
c	chord
g	acceleration due to gravity
$\bar{h}_{1/3}$	significant wave height
ℓ	foil base length
m	mass
q	dynamic pressure
r	yawing velocity
u	surging velocity
v	swaying velocity
w	heaving velocity
(x_i, y_i, z_i)	foil coordinates
z	heave
Γ	dihedral angle
$\Delta\phi$	constant phase lead
$\Delta\zeta$	phase lag
Φ	spectral density

A	sweep angle
α	angle-of-attack
γ	inclination of thrust line to horizontal
ϕ	roll angle
η	wave elevation
ρ	density
θ	pitch angle
ω	wave frequency
ω'	frequency of encounter

REFERENCES

1 EAMES, M. C. and JONES, E. A., "HMCS BRAS D'OR - An Open Ocean Hydrofoil Ship", Journal R. I. N. A., Vol. 1, No. 1, April 1971.

2 EAMES, M. C. and DRUMMOND, T. G., "HMCS BRAS D'OR -Sea Trials and Future Prospects", presented at R. I. N. A. Spring Meeting, April 1972.

3 RICHARDSON, J. R., "Hydrofoil Profiles with Wide Cavitation Buckets", Engineering Research Associates, Toronto (Prepared for DeHavilland Aircraft of Canada Ltd.) September 1961.

4 JONES, E. A., "Rx Craft, A Manned Model of the RCN Hydrofoil Ship "BRAS D'OR" ", J. Hydronautics, Vol. 1, No. 1, July 1967.

5 TULIN, M. P. and BURKART, M. P., "Linearized Theory for Flow about Lifting Foils at Zero Cavitation Number", David Taylor Model Basin, Report C-638, February 1955.

6 OATES, G. L., and DAVIS, B. V., "Hydrofoil Motions in a Random Seaway," 5th Symposium on Naval Hydrodynamics, Bergen, August 1964.

7 SCHMITKE, R. T., "Longitudinal Simulation and Trials of the Rx Hydrofoil Craft", CAS Journal, Vol. 16, No. 3, March 1970.

8 SCHMITKE, R. T., "A Computer Simulation of the Performance and Dynamics of HMCS BRAS D'OR (FHE-400)", CAS Journal, Vol. 17, No. 3, March 1971.

9 DIEDERICH, F. W., "A Plan-Form Parameter for Correlating Certain Aerodynamic Characteristics of Swept Wings", NASA Tech. Note 2335, April 1951.

10 WADLIN, K. L. and CHRISTOPHER, K. W., "A Method for Calculation of Hydrodynamic Lift for Submerged and Planing Rectangular Lifting Surfaces", NASA Tech. Report R-14, 1959.

11 AUSLAENDER, J., "The Linearized Theory for Supercavitating Hydrofoils Operating at High Speeds Near a Free Surface", Hydronautics Technical Report 001-5, June 1961.

12 JOHNSON, V. E., " Theoretical and Experimental Investigation of Supercavitating Hydrofoils Operating Near the Free Water Surface" NASA Tech. Report R-93, 1961.

13 PIERSON, W. J. and MOSKOWITZ, L., "A Proposed Spectral Form of Fully Developed Wind Seas Based on the Similarity Theory of S. A. Kitaigorodski." J. of Geophysical Research, Vol. 69, November 1964.

* * *

APPENDIX

STABILITY DERIVATIVES

Stability derivatives are listed below for a single foil element, using the sign convention of equation (7) . Summation of a given expression over all foil elements gives the total ship stability derivative.

Longitudinal

$$X_u = -\frac{3}{2}\ \rho U_o\ SC_D$$

$$X_z = q\left(C_D\ \frac{\partial S}{\partial h} + S\ \frac{\partial C_D}{\partial h}\right)$$

$$X_w = \frac{\rho U_o}{2}\ S \cos\Gamma\ (C_{D_\alpha} - C_L)$$

$$X_\theta = -q\ x_i\ \left(C_D\ \frac{\partial S}{\partial h} + S\ \frac{\partial C_D}{\partial h}\right)$$

$$X_{\dot\theta} = \frac{\rho U_o}{2}\ S\ \left[C_D\ (z_T + 2\ z_i) + x_i \cos\Gamma\ (C_{D_\alpha} - C_L)\right]$$

$$Z_u = \rho U_o\ SC_L\ \cos\Gamma$$

$$Z_z = -q\ \left(C_L\ \frac{\partial S}{\partial h} + S\ \frac{\partial C_L}{\partial h}\right)\ \cos\Gamma$$

$$Z_w = -\frac{\rho U_o}{2}\ S\ (C_{L_\alpha}\ \cos^2\Gamma + C_D)$$

$$Z_\theta = q\left(C_L\ \frac{\partial S}{\partial h} + S\ \frac{\partial C_L}{\partial h}\right)\ x_i\ \cos\Gamma$$

$$Z_{\dot\theta} = \frac{\rho U_o}{2}\ S\ \left[2\ C_L z_i \cos\Gamma + x_i(C_{L_\alpha}\ \cos^2\Gamma + C_D)\right]$$

$$M_u = - \rho U_o \, SC_D \, z_i - Z_u x_i$$

$$M_z = X_z z_i - Z_z x_i - q \left(cS \frac{\partial C_M}{\partial h} + C_M \frac{\partial (cS)}{\partial h} \right) \cos \Gamma$$

$$M_w = X_w z_i - Z_w x_i$$

$$M_\theta = X_\theta z_i - Z_\theta x_i + q x_i \left(c S \frac{\partial C_M}{\partial h} + C_M \frac{\partial (cS)}{\partial h} \right) \cos \Gamma$$

$$M_{\dot{\theta}} = - \frac{\rho U_o}{2} S \left[2 C_D z_i + x_i \cos \Gamma \left(C_{D_\alpha} - C_L \right) \right] z_i - Z_{\dot{\theta}} x_i$$

where the derivation of X_u and $X_{\dot{\theta}}$ assumes constant thrust horsepower.

Lateral

$$Y_v = - \frac{\rho U_o}{2} S \left(C_{L_\alpha} \sin^2 \Gamma + C_D \right)$$

$$Y_{\dot{\phi}} = \frac{\rho U_o}{2} S \left(C_{L_\alpha} \hat{y}_i \sin \Gamma + C_D z_i - C_L y_i \tan \Lambda \right)$$

$$Y_r = \frac{\rho U_o}{2} S \left(2 C_L y_i \sin \Gamma - C_{L_\alpha} x_i \sin^2 \Gamma - C_D x_i \right)$$

$$Y_\phi = - q \sin \Gamma \left(C_L \frac{\partial S}{\partial \phi} + S \frac{\partial C_L}{\partial \phi} \right)$$

$$K_v = -Y_v z_i + \frac{\rho U_o}{2} S \left(C_L y_i \tan \Lambda + C_{L_\alpha} y_i \sin \Gamma \cos \Gamma \right)$$

$$K_{\dot{\phi}} = - Y_{\dot{\phi}} z_i - \frac{\rho U_o}{2} S \left(C_D y_i^2 + C_L y_i z_i \tan \Lambda + C_{L_\alpha} y_i \hat{y}_i \cos \Gamma \right)$$

$$K_r = -Y_r z_i + \frac{\rho U_o}{2} S \left[C_L x_i y_i \tan \Lambda + y_i \cos \Gamma \right.$$

$$\left. (C_{L_\alpha} x_i \sin \Gamma - 2 C_L y_i) \right]$$

$$K_\phi = -Y_\phi z_i + q \left[y_i \cos \Gamma (C_L \frac{\partial S}{\partial \phi} + S \frac{\partial C_L}{\partial \phi}) \right.$$

$$\left. + S C_L \frac{\partial \hat{y}_i}{\partial \phi} \right]$$

$$N_v = Y_v x_i - \frac{\rho U_o}{2} S y_i \sin \Gamma (C_L - C_{D_\alpha})$$

$$N_{\dot{\phi}} = Y_{\dot{\phi}} x_i + \frac{\rho U_o}{2} S y_i \hat{y}_i (C_L - C_{D_\alpha})$$

$$N_r = Y_r x_i - \frac{\rho U_o}{2} S y_i \left[(C_L - C_{D_\alpha}) x_i \sin \Gamma + 2 C_D y_i \right]$$

$$N_\phi = Y_\phi x_i + q C_D (y_i \frac{\partial S}{\partial \phi} + S \frac{\partial y_i}{\partial \phi})$$

where S is immersed foil area, Λ is sweep angle and

$$\hat{y}_i = y_i \cos \Gamma + z_i \sin \Gamma$$

* * *

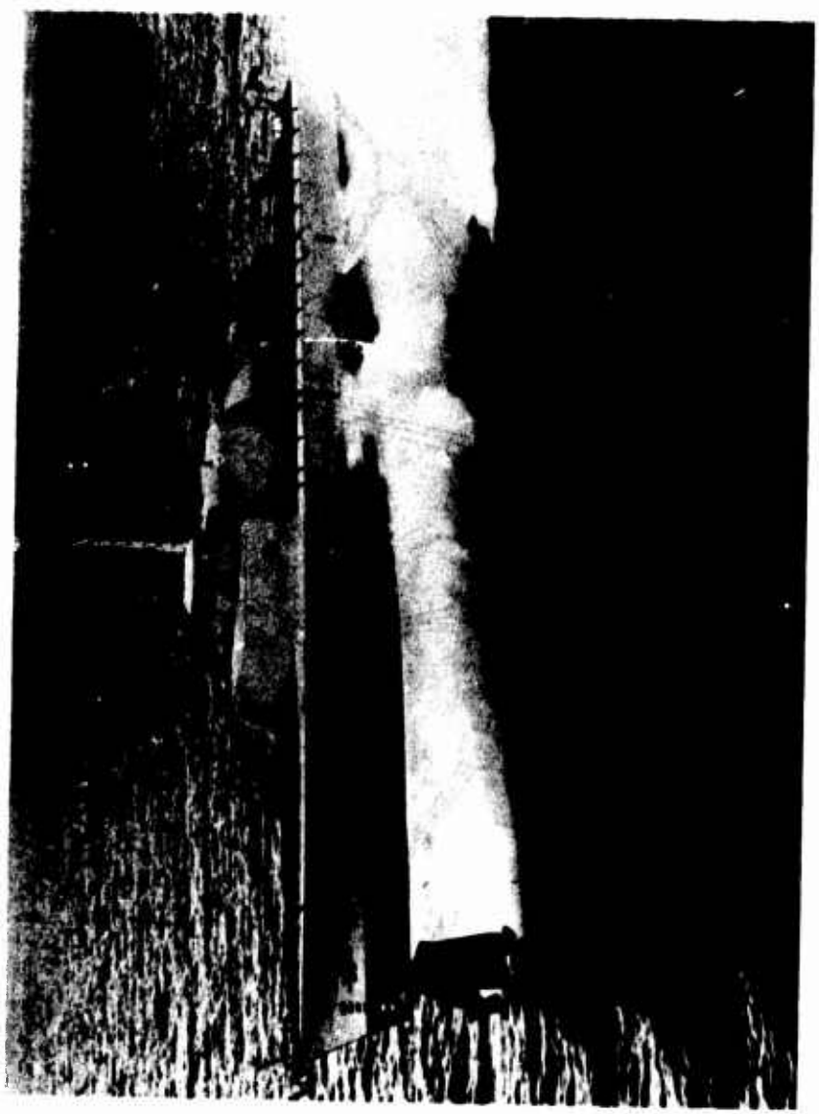


Figure 1 HMCS BRAS D'OR (Canadian Forces Photo)

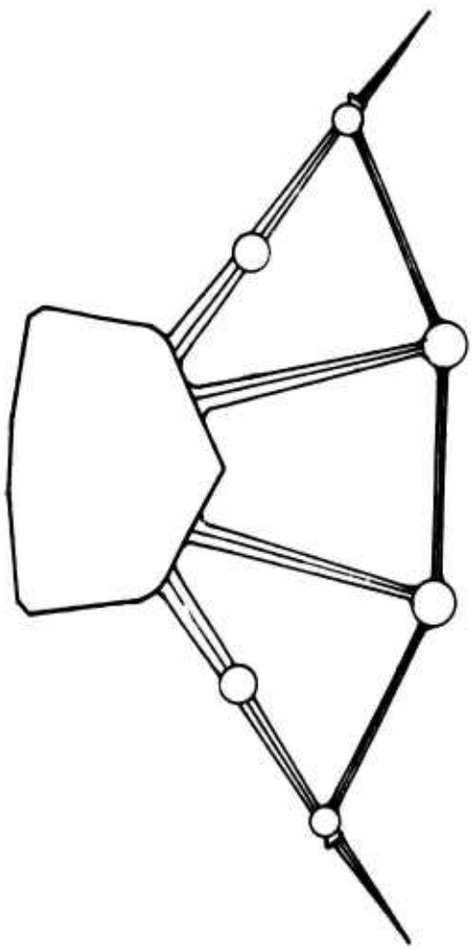


Figure 2 BRAS D'OR main foil unit



Figure 3 Delayed cavitation section

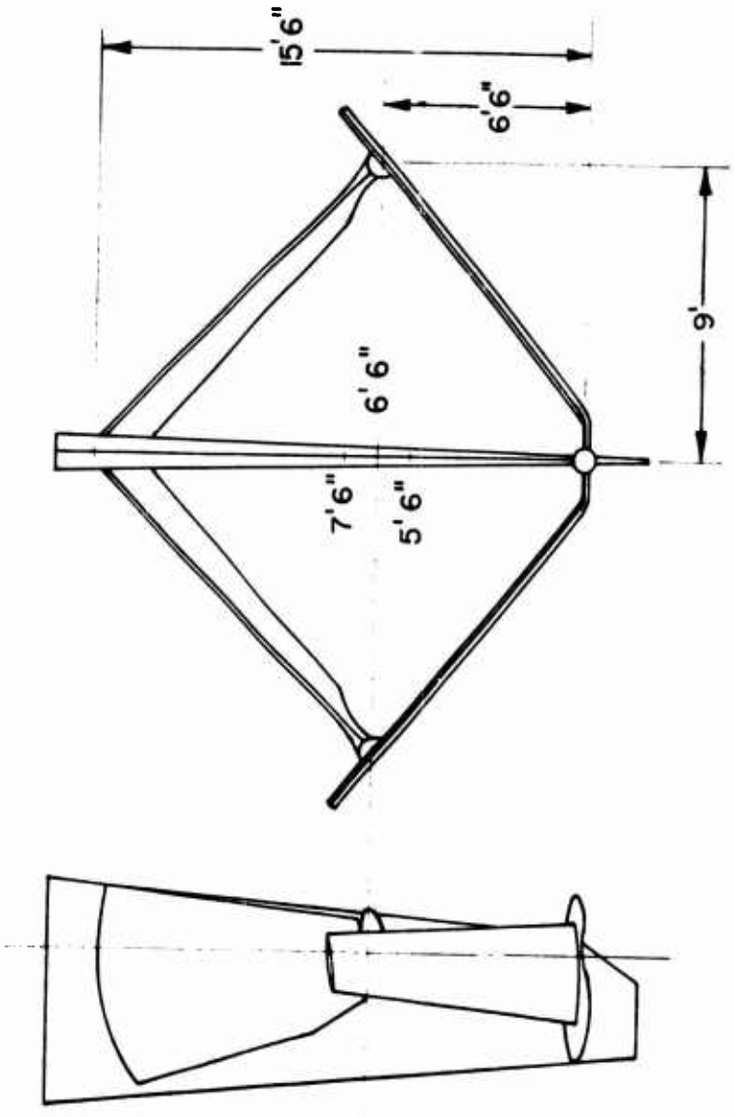


Figure 4 BRAS D'OR bow foil unit

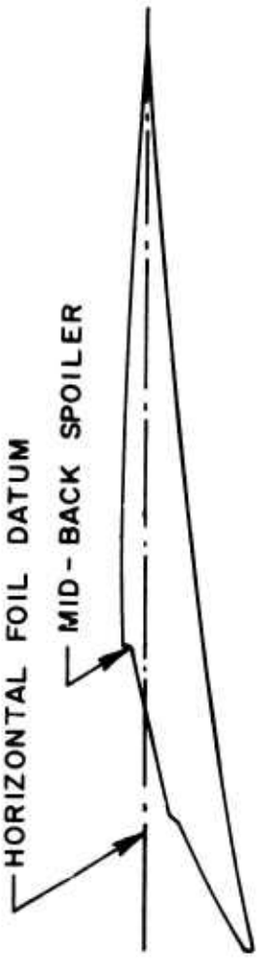


Figure 5 Superventilated section

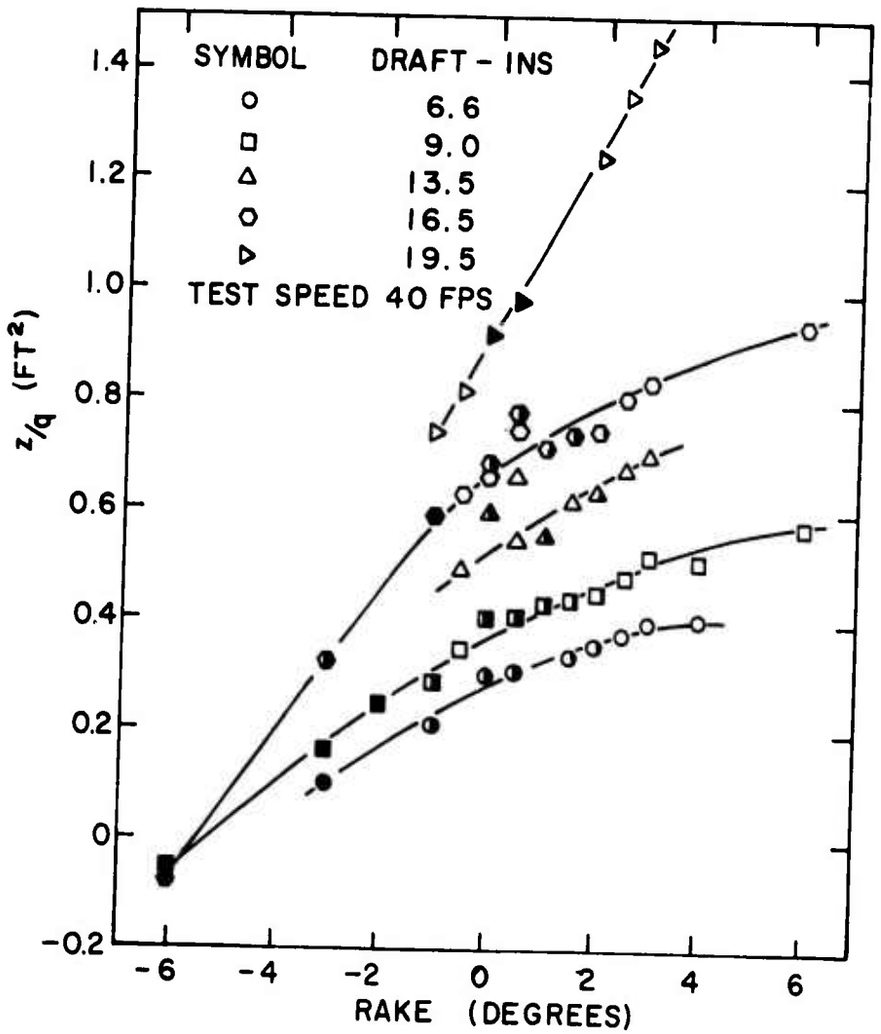


Figure 6 Quarter scale lift data (NPL)

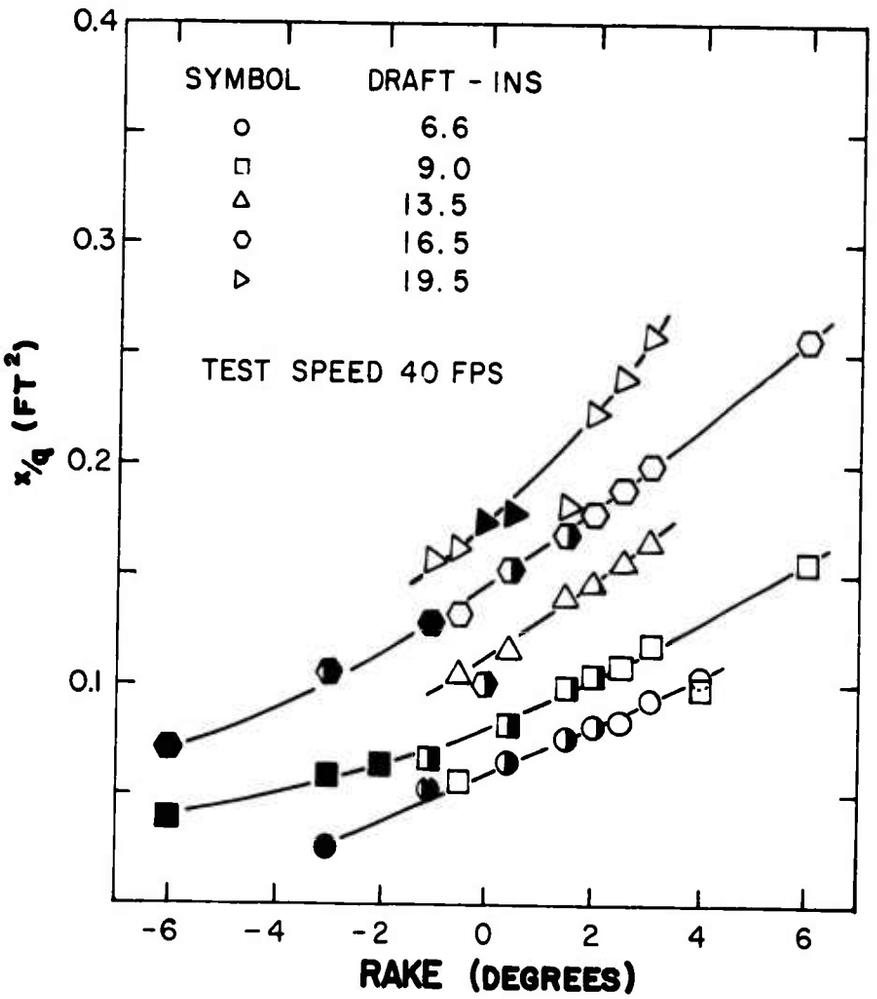


Figure 7 Quarter scale drag data (NPL)

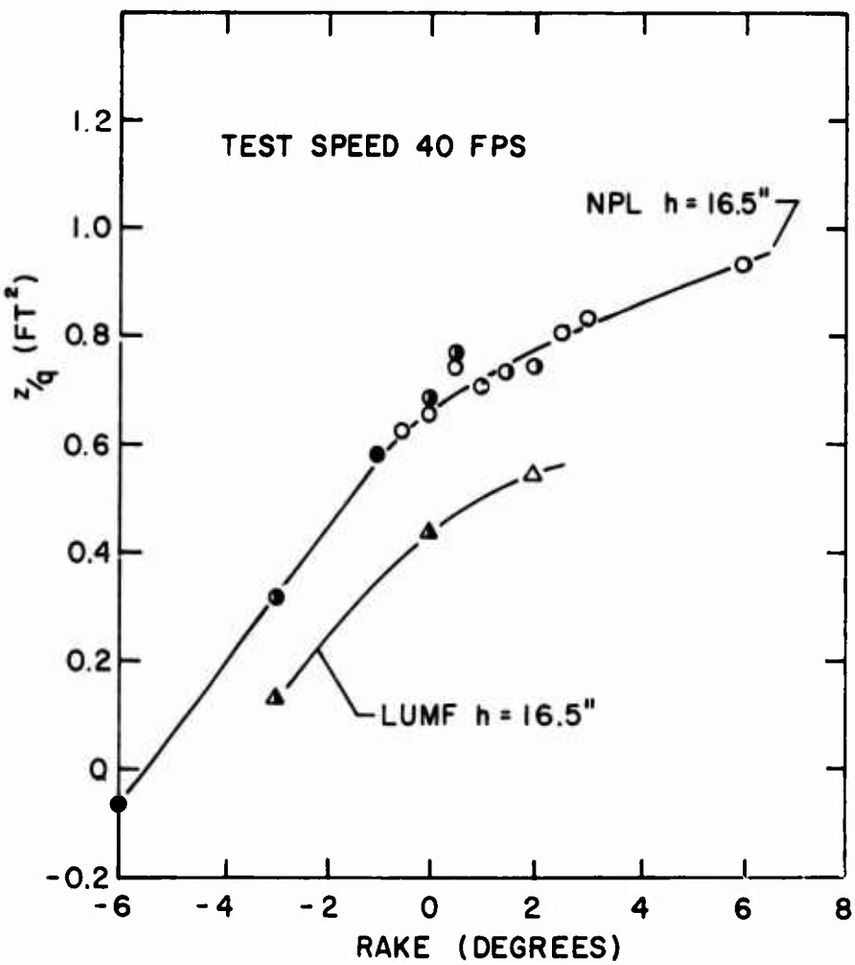


Figure 8 Comparison of NPL and LUMF lift data

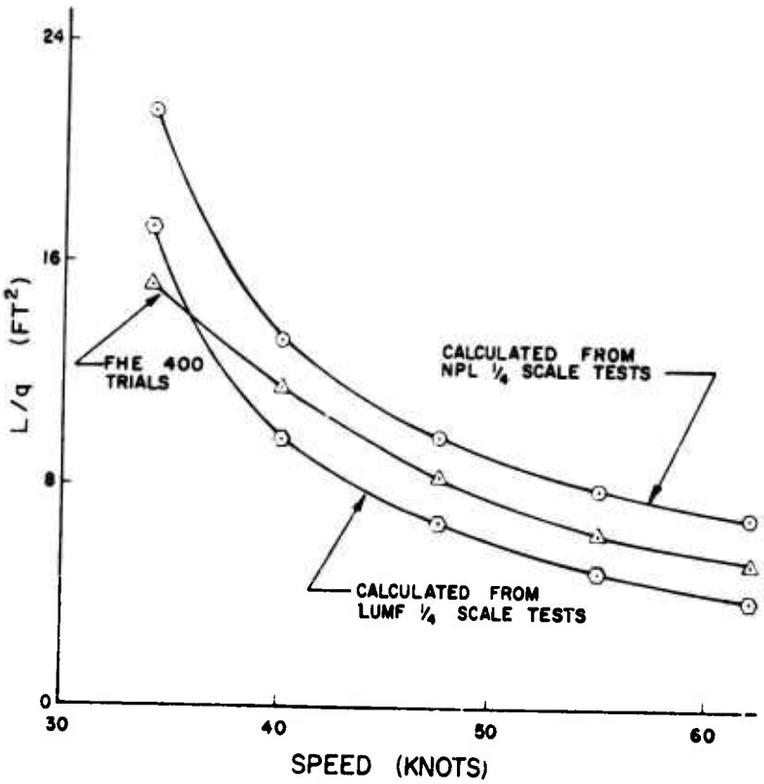


Figure 9 BRAS D'OR bow foil lift coefficient

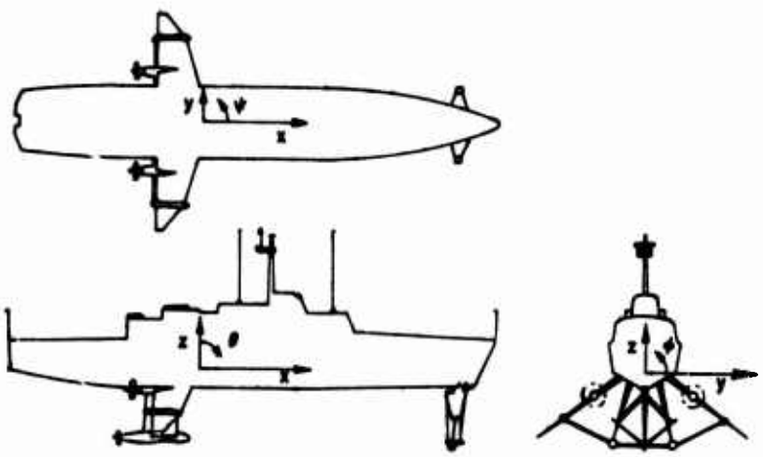


Figure 10 Axis system

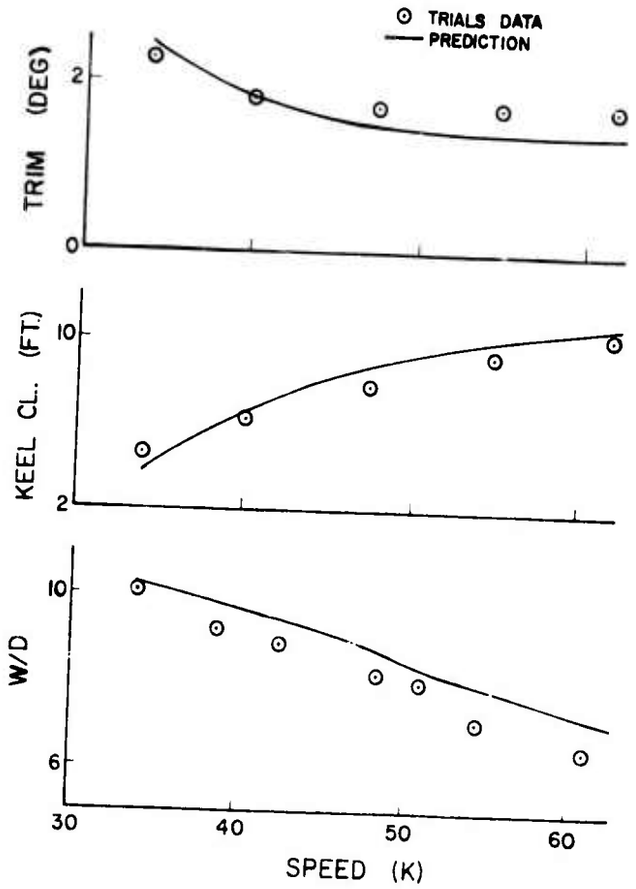


Figure 11 BRAS D'OR trim, rise and W/D

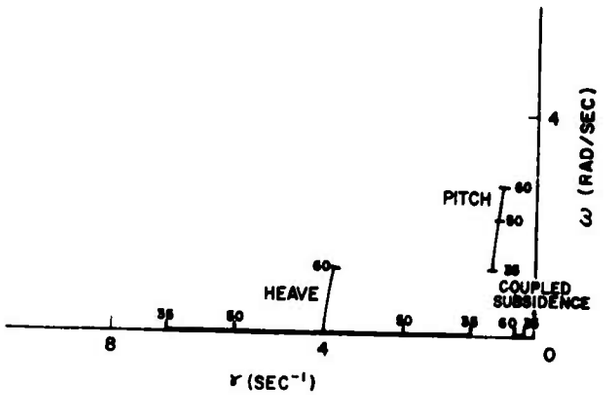


Figure 12 BRAS D'OR longitudinal root loci, 35-60 K

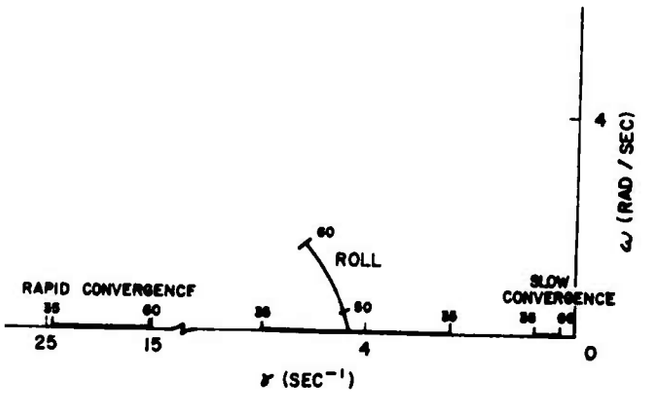


Figure 13 BRAS D'OR lateral root loci, 35-60 K

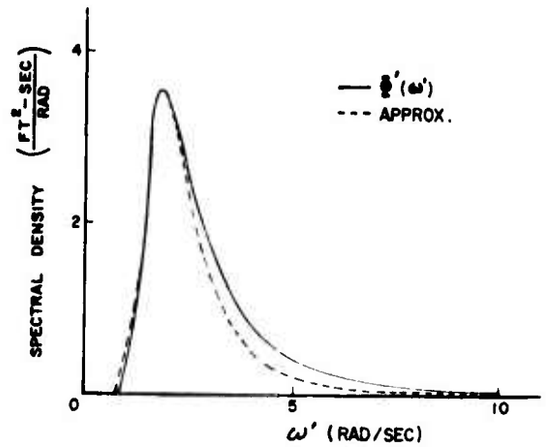


Figure 14 Wave elevation spectrum, head sea state 5, 50 K

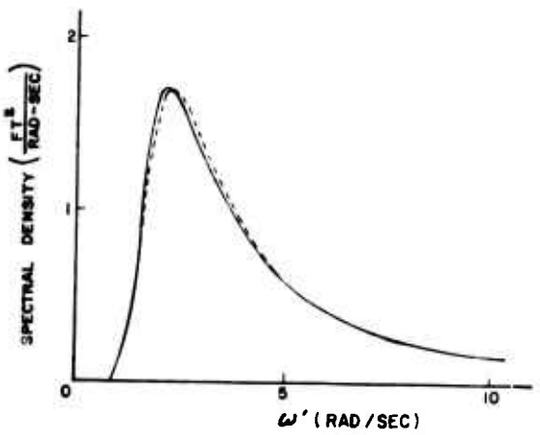


Figure 15 Wave orbital velocity spectrum, head sea state 5, 50 K

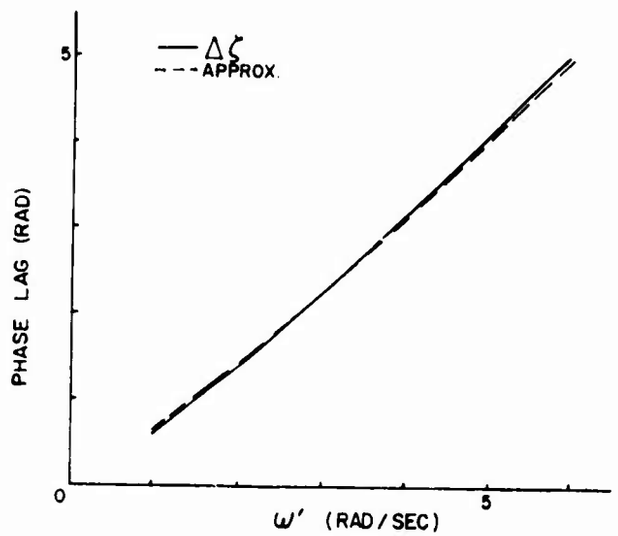


Figure 16 Phase lag

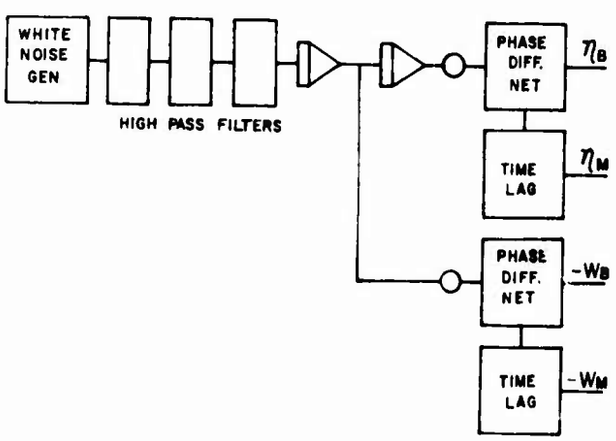


Figure 17 Head sea simulation diagram

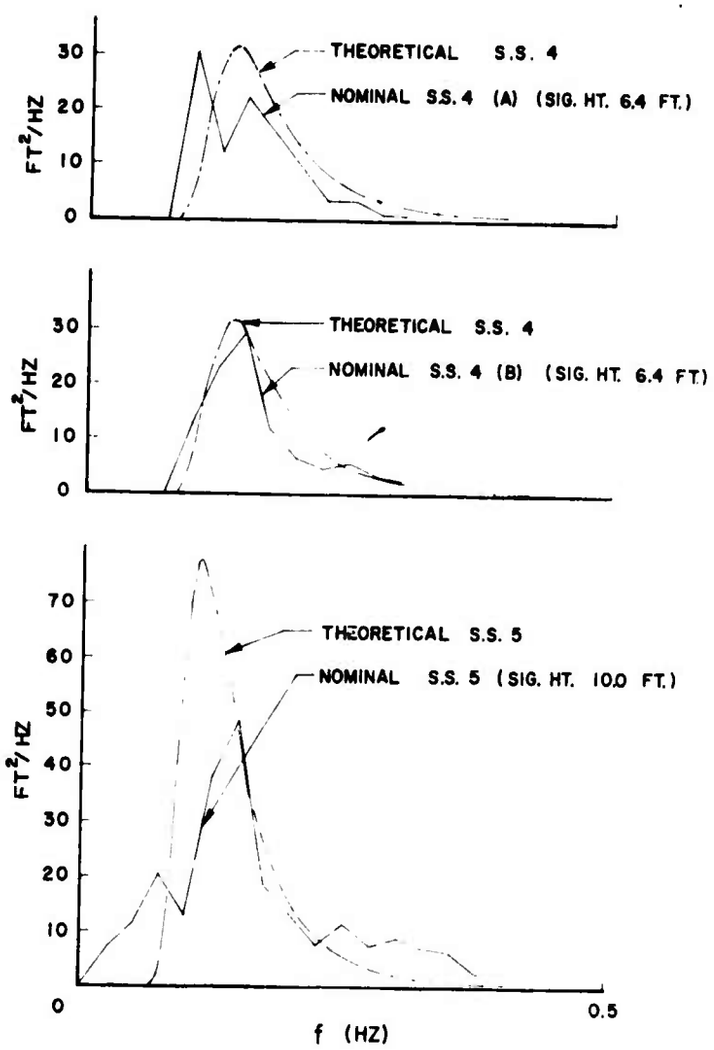


Figure 18 Trials wave elevation spectra

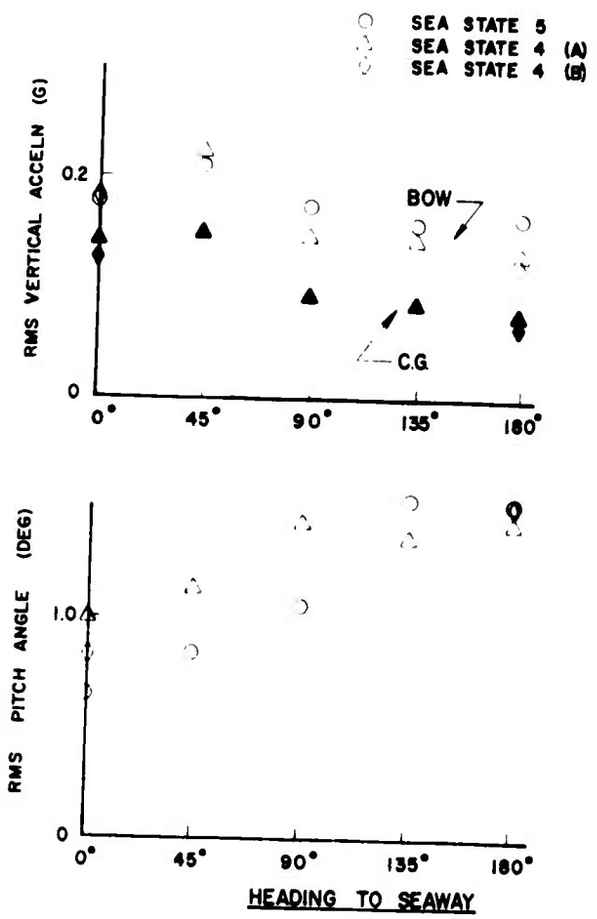


Figure 19 Pitch angle and vertical accelerations, 39 knots

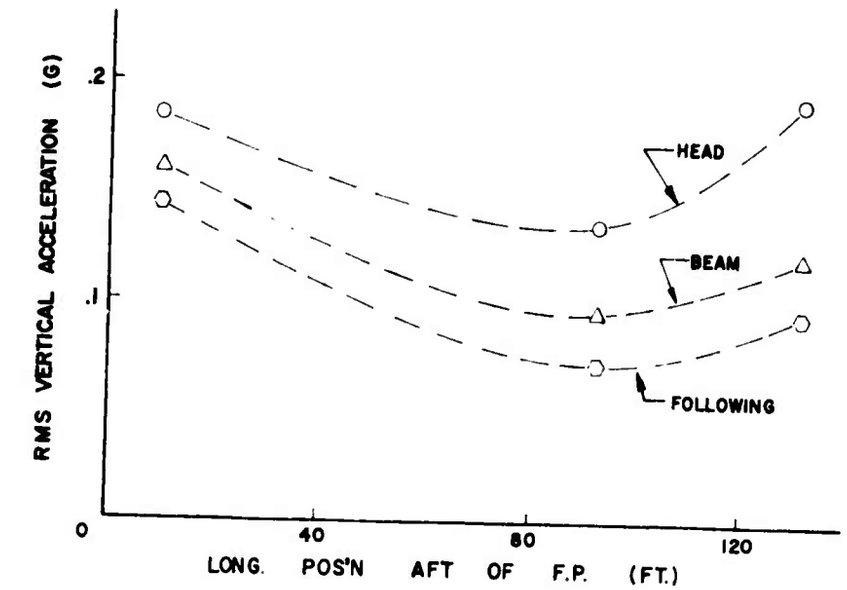


Figure 20 Longitudinal distribution of vertical accelerations, 39 knots

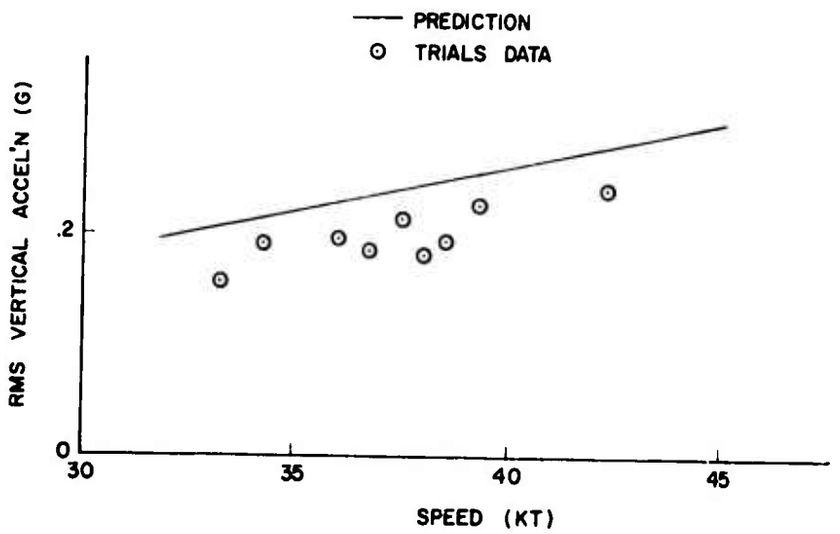


Figure 21 Vertical acceleration at bow - predicted and measured

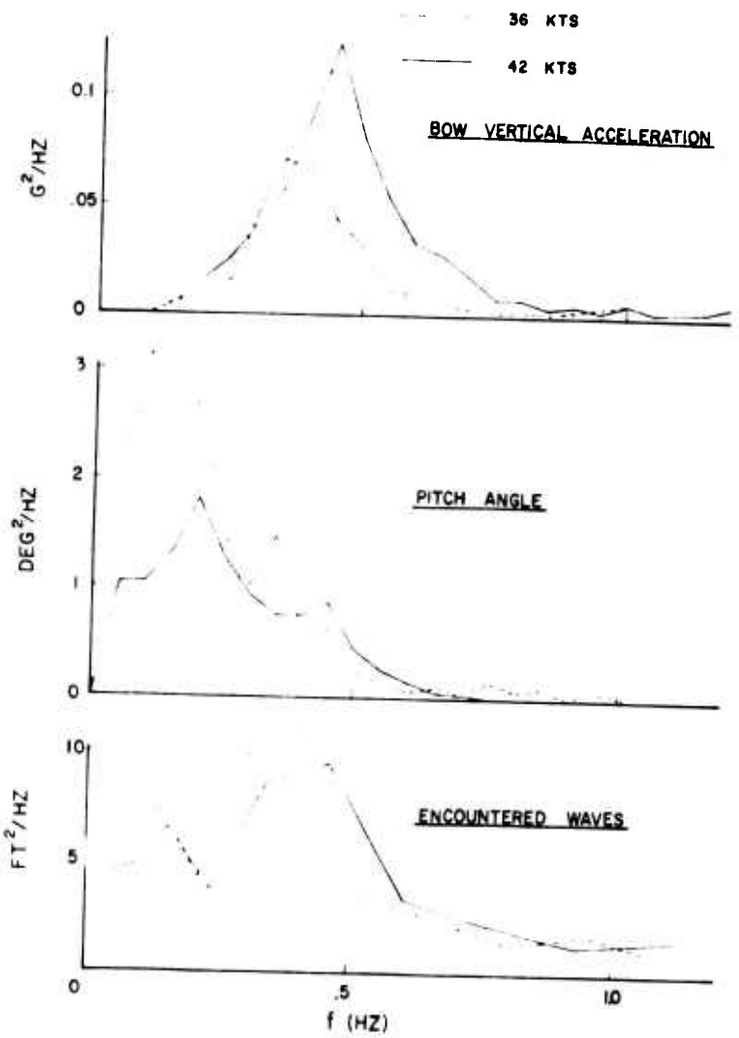


Figure 22 Power spectral densities, sea State 5

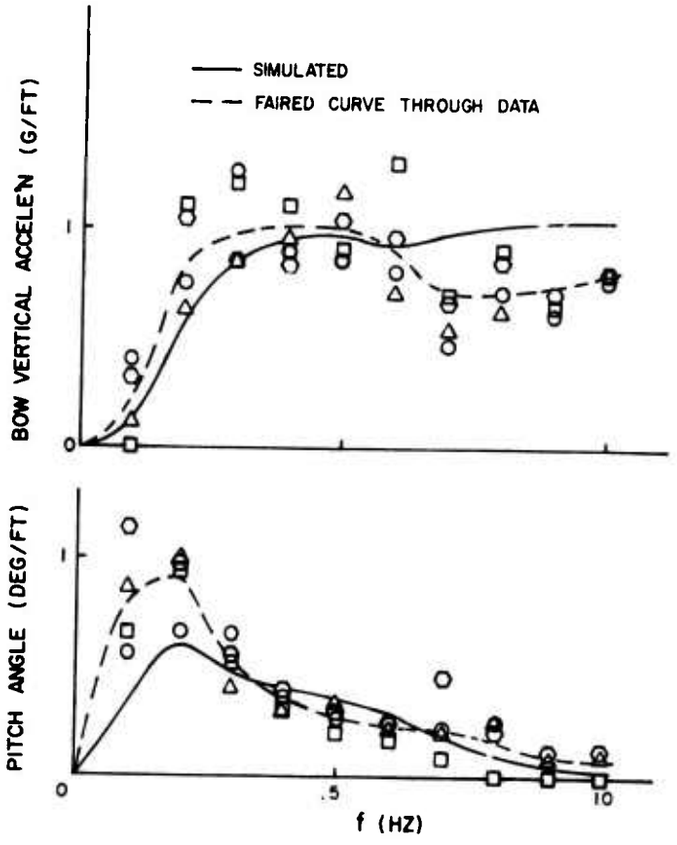


Figure 23 BRAS D'OR head sea response transforms, 35 K

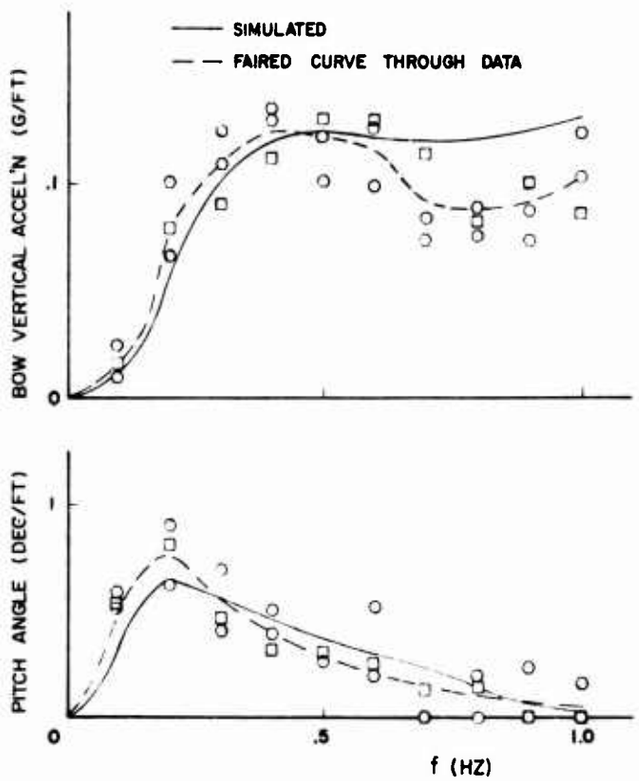


Figure 24 BRAS D'OR head sea response transforms, 40 K

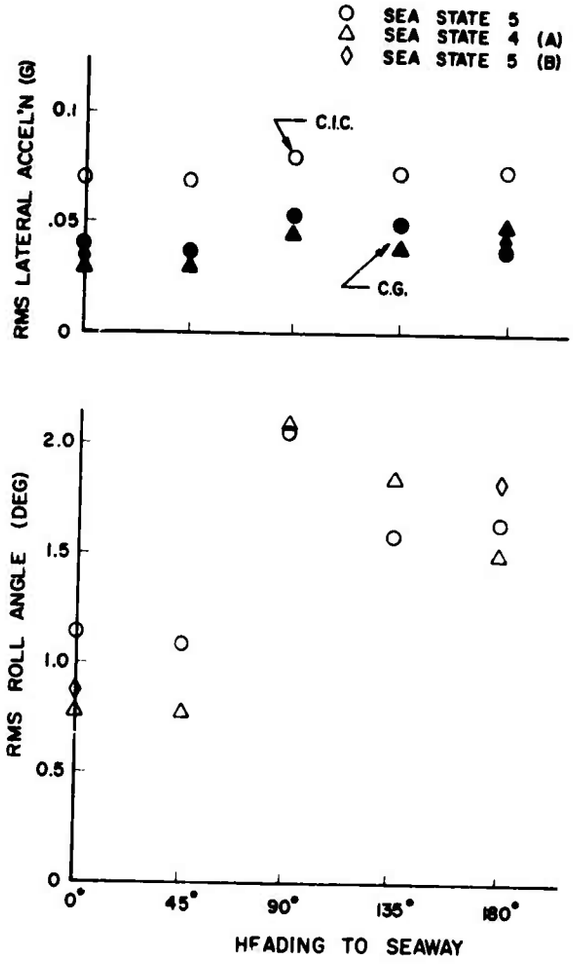


Figure 25 Roll angle and lateral accelerations, 39 knots

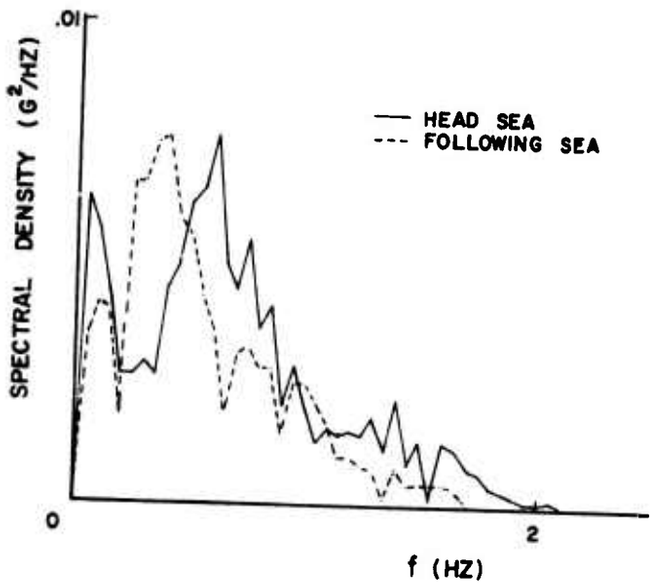


Figure 26 CIC lateral acceleration spectra, sea State 5

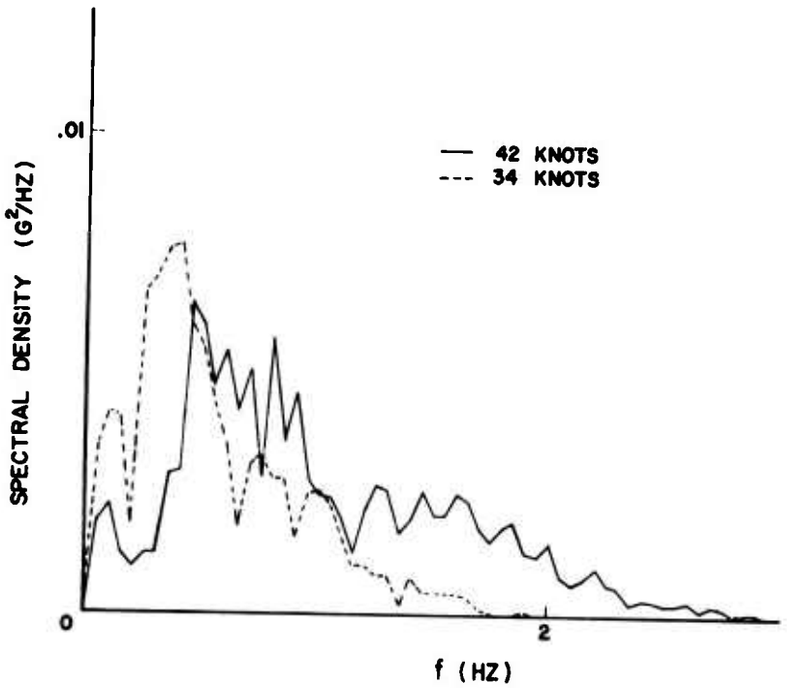


Figure 27 CIC lateral acceleration spectra, head sea State 5

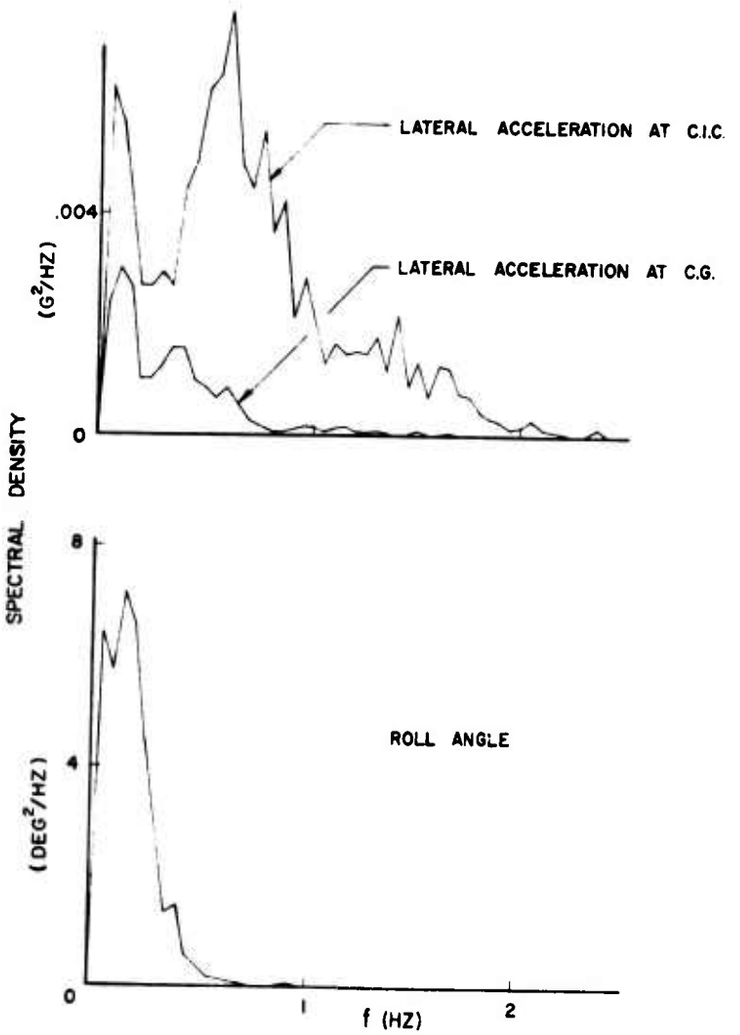


Figure 28 Lateral acceleration and roll spectra, head sea state 5, 39 K

DISCUSSION

Christopher Hook
Hydrofin
Bosham, Sussex, U.K.

I listened to the two papers by Michael Eames given recently at the Royal Institute of Naval Architects in London and I make no apology for repeating here the specific question I put to Eames at the end of his second Paper.

In the discussion of hydrofoils in England there has been a lot of talk about resonance and I asked Mr. Eames specifically if in the course of the development work on the Canadian boat they had ever encountered any resonance phenomena, because whether the damping system be a diamond foil working basically on the Grunberg principle or a mechanically highly damped system, the resonance effects are going to be directly connected with the amount of damping. If the speaker would enlarge on this I think it would be of interest to all the listeners.

REPLY TO DISCUSSION

Rodney T. Schmitke
Defence Research Establishment Atlantic
Dartmouth, Nova Scotia, Canada

Figures 23 and 24 show that BRAS D'OR's pitch response peaks at approximately .2Hz, the natural frequency of the ship in pitch. Response is fairly broad, however, and the peak is not pronounced (low Q), so there is no resonance problem.

DISCUSSION

Reuven Leopold
U.S. Navy Naval Ship Engineering Center
Hyattsville, Maryland, U.S.A.

I have some comments and questions. Could a marginally stable configuration be predictable to be stable by not accounting for surge and thus lead to a bad foil configuration design choice ? The Paper states on page 16 :

> "... surge was neglected in this simulation in order to simplify the problem and also because it was felt that neglecting surge should give conservative results."

In a paper titled "The effect of surge, added mass and unsteady lift on the motion of a hydrofoil boat in a seaway", which I wrote about 10 years ago, I showed that foil configurations which were stable became unstable once the surge was taken into account.

REPLY TO DISCUSSION

Rodney T. Schmitke
Defence Research Establishment Atlantic
Dartmouth, Nova Scotia, Canada

In answer to the question, the surge was taken into account in doing stability analysis and the configuration was found to be stable (Figure 12). Furthermore, in all my work on this type of configuration I find that the only contribution of surge is a very slow subsidence and it does not seem to couple into the pitch and heave motions significantly.

DISCUSSION

Reuven Leopold
U.S. Navy Naval Ship Engineering Center
Hyattsville, Maryland, U.S.A.

Page 2 states that the bow foil, as the main control mechanics, leads to high $\partial L/\partial h$ for contouring of large waves ; however, high lift versus depth slope for rough seas results in high vertical acceleration. For the purpose of not losing momentary control in rough seas and cause diving, the superventilating bow sections are used, which in turn introduce additional drag. The question is this : while reduction of drag and the improvement in ventilated flow stability are definite objectives in all operating conditions, the requirements for $\partial L/\partial h$ are different at low frequency - that is calm seas - than at high frequency - that is high sea states. The gain on $\partial L/\partial h$ is fixed for a constant speed and could not be modulated unless automatically controlled surfaces were introduced. How does the author propose to optimize $\partial L/\partial h$ for rough seas without compromising calm seas operations ?

REPLY TO DISCUSSION

Rodney T. Schmitke
Defence Research Establishment Atlantic
Dartmouth, Nova Scotia, Canada

The essential compromise is not between rough sea and calm water operation, but rather between head seas and following seas. Optimization of $\partial L/\partial h$ for head sea operation must of course be subject to the constraint of providing adequate stability in following seas. This constraint indeed limits the extent to which $\partial L/\partial h$ may be altered, but we feel that at least a slight reduction is feasible and will result in improved motions. We should point out that $\partial L/\partial h$ at a given speed may be adjusted, albeit not greatly, by changing bow foil incidence. Thus in head seas the bow foil is trimmed down, lowering $\partial L/\partial h$,

while in following seas incidence is increased, increasing $\partial L/\partial h$. This technique was employed quite successfully during BRAS D'OR sea trials.

* * *

BENDING FLUTTER AND TORSIONAL FLUTTER OF FLEXIBLE HYDROFOIL STRUTS

Peter K. Besch and Yuan-Ning Liu
Naval Ship Research and Development Center
Bethesda, Maryland, U.S.A.

ABSTRACT

A large body of experimental and theoretical flutter results for hydrofoil struts were analyzed to determine significant characteristics. Flutter was found to occur in two different structural mode shapes, corresponding to a predominantly bending mode and a predominantly torsional mode, respectively. The flutter mode shape was related to the vibration mode shapes and the generalized mass ratio of the strut at zero speed. The behavior of the hydroelastic modes of typical struts as a function of speed was investigated using a strip theory with three-dimensional loading modifications. Flutter predictions for struts which underwent flutter in the torsional mode were usually conservative and predicted the correct mode shape. However, flutter predictions for struts which underwent flutter in the bending mode were unreliable in predicting the mode of flutter because of an extreme sensitivity to the loading modification used. Strut-foil systems of the inverted-T configuration typical of full-scale hydrofoil craft appear to undergo either bending flutter or torsional flutter, depending on pod and foil characteristics.

I. INTRODUCTION

The high speeds associated with many unconventional ships will require a better understanding of flutter and other hydroelastic phenomena than has been available for design of existing ships.

Prominent among unconventional ships are hydrofoil craft and surface effect ships. Flutter is a recognized problem for the strut-foil systems of hydrofoil craft. The rudders contemplated for surface effect ships may be similarly vulnerable.

Much research has been done on the flutter of strut models analogous to the above systems. The initial demonstration of strut flutter was made by Hillborne[1] in 1958. Further experimental work has often been accompanied by difficulties, including models that wouldn't flutter, models that were destroyed by flutter or divergence, and facility limitations. Numerous theoretical analyses have been produced, but none has been successful in predicting all experimental results conservatively.

Out of these efforts have come many clues to the nature of strut flutter. By combining previous results with some recent experimental and theoretical work we have produced a concept of flutter involving two different flutter regions. This paper will discuss existing flutter data from the standpoint of two flutter regions, and will present calculations which indicate the origin of the two regions. The expected accuracy of flutter speed predictions within each region will be described.

Existing data deals with a large number of simple struts, and a small number of struts with tip pods, some with foils forming an inverted-T configuration. A sample configuration is shown in Figure 1. All tested configurations have been small-scale models. Most discussion will be devoted to simple struts and struts with pods. One strut with foils has been included.

All struts were cantilever supported from an effectively rigid foundation, so that the structural characteristics of the system were those of a cantilever beam in which both bending and twisting could occur. Because of the relatively high aspect ratio and thin profile of the struts, bending consisted of displacements perpendicular to the plane of the strut, while twisting occurred about a spanwise elastic axis. Vibration modes of the struts consisted of a series of modes which could usually be identified as predominantly bending or predominantly twisting or torsion.

The mode shapes of the struts at flutter inception could also be characterized as predominantly bending or torsion. In most cases, struts displayed either bending or torsional oscillations at flutter.

[1] References are listed on page 393

This was the basis for dividing flutter phenomena into two regions. Flutter in one region occured in a predominantly bending mode shape, and will be referred to as bending flutter. Flutter in the other region occurred in a predominantly torsional mode shape, and will be referred to as torsional flutter.

It appears that all hydrofoil struts, including those with pods and foils attached, undergo either bending flutter or torsional flutter. The type of flutter characteristic of a given strut can be determined by examining its vibration modes, except in a transition region where strong coupling of structural modes occurs. Most available data can be readily placed into the appropriate flutter regions.

Experimental results from each flutter region were examined separately. The two flutter regions corresponded to two ranges of generalized mass ratio. In the bending flutter region, struts had low values of generalized mass ratio, while struts in the torsional flutter region had high values of generalized mass ratio. Flutter speed varied differently in each region as a function of mass ratio or strut submergence, a related parameter.

Calculated flutter characteristics show substantial qualitative agreement with observed characteristics. Flutter was found to occur in a different hydroelastic mode in each flutter region. Predicted flutter inception speeds for torsional flutter were conservative for most struts, with many predictions being overconservative. Unfortunately, flutter speed predictions for bending flutter were not usable because two flutter modes were often predicted to be unstable in the bending flutter region, with the wrong mode predicted to be the least stable. This discrepancy was related to an extreme sensitivity of the flutter calculation to hydrodynamic loading modification in the bending flutter region.

II. EXPERIMENTAL FLUTTER CHARACTERISTICS

II.1. Bending-Type and Torsion-Type Struts

The flutter mode of a strut is strongly correlated with the nature of the vibration modes of the strut in air or in water. It is therefore convenient to define a method for classifying struts according to important differences in vibration modes. Strut mode shapes are those of a cantilever beam, with bending displacements perpendicular to the plane of the strut and torsional rotations about a spanwise elastic axis. Mode shapes are designated by their similarity to the uncoupled mode shapes of a cantilever beam. Some uncoupled mode shapes are shown in Figure 2, numbered in order of increasing frequency.

All struts exhibit a fundamental (lowest frequency) vibration mode shape resembling first bending. Struts show a marked difference in their second modes, however, permitting struts to be divided into two groups. The second mode of any strut will consist of a second bending mode coupled with a first torsion mode, with one usually predominating. Predominance is determined by the relative linear displacements produced by bending and torsion, which provide an indication of nodal line characteristics. If the second vibration mode is predominantly second bending, the strut is a bending-type strut. If the second vibration mode is predominantly first torsion, the strut is a torsion-type strut.

Struts having little or no tip weighting are usually bending-type struts. Struts having relatively heavy pods are usually torsion-type struts. A transition region exists in which the second vibration mode of a strut is equally due to a second bending mode shape and a first torsion mode shape, with neither predominating. Struts in this transition region have moderately weighted pods or medium to large foils. The effect of foils in coupling second bending and first torsion is very pronounced when the foils are submerged due to the large rotary inertia effect at the tip of the strut. When such strong coupling occurs, it is impossible to classify the strut as bending-type or torsion-type.

In most cases the third vibration modes of bending-type struts are first torsion, while torsion-type struts have a third vibration mode resembling second bending. This observation indicates that a change in strut type usually involves a reversal in the order of the second and third mode shapes.

Most struts have the same mode order in air and in water. If there is a difference, the mode order in water should be used for classifying a strut. Either measurement or calculation can be used to determine the required mode shapes.

II. 2. Flutter Mode Shapes

The flutter mode shapes of bending-type struts are radically different from those of torsion-type struts. Bending-type struts undergo flutter in a predominantly first bending mode shape, while torsion-type struts undergo flutter in a predominantly first torsion mode shape. In accordance with the flutter mode shapes, flutter of bending-type hydrofoils will be referred to as bending flutter, and flutter of torsion-type hydrofoils will be referred to as torsional flutter.

The two types of flutter mode shapes have not been quantitatively measured, but were discovered because the very striking dif-

ferences in mode shape usually observed. Differences in flutter mode shapes were reported by Huang [2] as a result of flutter testing a strut with and without a heavy pod. The bending amplitude of the strut alone was reported to be considerably larger than the torsional amplitude which was also present. When the pod was added, the torsional amplitude became larger than bending.

A similar result was obtained in an experiment performed at the Naval Ship Research and Development Center (NSRDC) in which a bending-type strut and a torsion-type strut were flutter tested. Both struts had been previously tested but mode shapes were not reported. Motions of the struts were visually observed and recorded on video tape. The bending-type strut, Model A of Reference 3, underwent large first bending oscillations with little evident twisting. In constrast, the torsion-type strut, Model 2T of Reference 4, displayed first torsion oscillations with no visible bending.

In addition to a change in mode shape, a change in frequency would be expected when the flutter mode changes. Several pod configurations for Model 2T were flutter tested [4], and a significant change in flutter frequency occured when the strut changed from bending-type to torsion-type. Flutter data for this strut are plotted in Figure 3. As the pod mass was increased and the pod center of gravity was moved aft, an abrupt increase in frequency occured between pod configurations A and B. Vibration modes calculated in water identify pod configuration A as a bending-type model, while pod configuration B gives strongly coupled second bending and first torsion modes for both its second and third modes and therefore falls in the transition region between bending-type and torsion-type struts. Pod configuration C was a torsion-type strut.

Although mode shapes have been observed in only a small number of cases, other aspects of flutter data exhibit a dual nature corresponding to differences in mode shape. The effects of generalized mass ratio and of strut submergence vary according to the flutter region. These effects will be discussed below.

II. 3. Generalized Mass Ratio

Generalized mass ratio is a parameter which indicates the relative importance of structural and fluid inertia in determining the motion of a strut. Both structural and fluid inertia are related to the vibration mode shape (and therefore to the elastic properties) of the strut. This relationship is included in the most general form of the parameter, which can be expressed in terms of matrix elements as

$$\mu_{generalized} = \frac{\begin{Bmatrix} H_i \\ \Theta_i \end{Bmatrix}^T [M] \begin{Bmatrix} H_i \\ \Theta_i \end{Bmatrix}}{\begin{Bmatrix} H_i \\ \Theta_i \end{Bmatrix}^T [M^*] \begin{Bmatrix} H_i \\ \Theta_i \end{Bmatrix}}$$

This expression reduces to the mass ratio traditionally used in flutter analysis when pure bending motion of uniform amplitude is assumed. A similar simplification occurs when pure torsional motion is assumed. These assumed motions provide suitable approximations to the mode shapes of bending and torsional flutter. Exact flutter mode shapes are of course not available. Therefore simplified expressions for mass ratio were used in analyzing experimental flutter results.

It was found that bending flutter occurs at low values of mass ratio, and that torsional flutter occurs at high values of mass ratio. Other than this generalization, comparisons involving mass ratio will not be made between struts having different flutter modes. Such comparisons would require extensive calculations involving exact flutter mode shapes, which are not available. Calculations presented later indicate that bending flutter and torsional flutter involve entirely different vibration modes and do not represent different mass ratio ranges of the same mode. Mass ratio will be used as a parameter for comparing flutter results of similar mode. Each flutter region will be discussed separately.

Bending Flutter Region

In the bending flutter region, generalized mass ratio can be approximated by dividing total strut mass by the mass of a cylinder of water circumscribing the strut. The cylinder of water should have a diameter equal to the strut chord and a length equal to the submerged span of the strut. This cylinder of water approximates the added mass of the strut for the first bending mode shape associated with bending flutter. Bending mass ratio may be written symbolically as

$$\mu_{bending} = \frac{mL + M_{pod}}{\pi \rho b^2 \ell + M^*_{pod}}$$

Flutter speeds obtained from bending-type struts are plotted as a function of bending mass ratio in Figure 4. Values of bending mass ratio range from 0.1 to 0.66. The flutter speeds fall into two

groups. The higher flutter speeds correspond to strut models which are geometrically larger by a factor of approximately 4 than strut models represented in the lower group. Within each group, the flutter speeds are sensitive to mass ratio and a sweep parameter κ . The sweep paremeter [5, 6] combines sweep angle and unswept aspect ratio into a single parameter. Numerical values of κ are given for the data points in Figure 4. For similar size models, the data can be fairly consistently divided into families based on similar values of κ as shown. An increase in sweep angle therefore increases the flutter speed, while an increase in aspect ratio decreases the flutter speed. Lines of constant κ value approach zero as mass ratio decreases in a manner which could be approximated by a square root dependence on mass ratio, a relation which has previously been observed [3] for low mass ratio struts. Similar trends have been predicted in the lower mass ratio region when sweep angle was included in the analysis [6, 7, 8] . Groups of different sized models can be correlated by dimensional analysis. It has been shown [9] that the flutter speeds are related according to the square root of bending or torsional stiffness.

Torsional Flutter Region

Generalized mass ratio for torsional motion can be represented by the ratio of the total moment of inertia of a strut and the added moment of inertia of the submerged portion of the strut. In the present work, rotation was assumed to occur about the elastic axis of the strut. The resulting torsional mass ratio may be written

$$\mu_{\text{torsion}} = \frac{I_\alpha}{\pi\rho b^4 (1/8 + a^2)\,\ell + I^*_{\alpha,\,\text{pod}}}$$

Available flutter speeds for torsion-type struts are plotted as a function of torsional mass ratio in Figure 5. A substantial amount of data is shown which was obtained at NSRDC and has not been previously published. All strut models in this group had pods and were similar in size to the struts described in Reference 4. A complete description of this data will be published in the near future.

As shown in Figure 5, torsional flutter has been obtained at values of torsional mass ratio between 0.61 and 6.2 . Flutter speeds generally decrease as mass ratio increases. The wide variation in flutter speed results at least in part from wide variation in strut characteristics. In an attempt to adjust flutter speeds for differences in geometric size and torsional frequency, the data has been replotted

in Figure 6 after normalization by the factor $b\omega_\alpha$. This normalization was successful for values of mass ratio between 2.0 and 6.2, but large variations still exist at values below 2.0. Parameters that differ among the lower mass ratio models include the elastic axis location, profile, sweep angle, and submergence of the struts, and the size and inertial characteristics of pods attached to the struts. The effects of strut profile have recently been investigated at NSRDC, and results for three different profiles are indicated in Figure 6. At speeds high enough to produce ventilation over the entire chord of the strut, a ventilated cavity originating from a blunt leading edge on a strut substantially destabilizes the system. The effects of strut submergence will be discussed later.

The reduced flutter speeds for torsional flutter exhibit the characteristics found in classical hydrofoil flutter. The flutter speed parameter gradually decreases to a minimum value as mass ratio decreases, and then increases rapidly for related series of strut models at lower values of mass ratio. Minimum values occur approximately between mass ratios of 2.0 to 3.0. The effect of mass ratio on torsional flutter speeds is similar to that predicted by classical two-dimensional flutter theory and also to that predicted in the higher mass ratio region in finite sweep angle analyses [6, 7, 8].

II.4. Strut Submergence

The effects of strut submergence on flutter speed are closely related to the effects of generalized mass ratio. When the simplified forms of mass ratio are used, the two parameters are inversely proportional to one another. The close relationship is evident in experimental flutter results in which submergence has been varied without changing other strut characteristics. These results, shown in Fig. 7, constitute a replotting of data contained in Figures 4 through 6 but are given to illustrate the effects of submergence directly.

Flutter speeds for bending-type struts decrease as strut submergence increases, with minimum flutter speeds occurring at full submergence. The increase in submerged length produces a decrease in mass ratio and therefore a decrease in flutter speed. Torsion-type struts show a local minimum in flutter speed at approximately 50 % submergence. This local minimum would be expected to occur if the strut configuration passed through intermediate values of mass ratio, and will not necessarily correspond to 50 percent submergence. An increase in flutter speed will of course occur as the submergence becomes very small regardless of the mass ratio. The effect of submergence on the strut model with pod and foils is similar to that observed for struts without foils in the bending flutter region and at high

values of mass ratio in the torsional flutter region.

Strut submergence also affects the vibration mode shapes of struts, and has a particularly large effect on the second bending mode. As a result, a strut could change from a bending-type strut to a torsion-type strut during changes in submergence. Because of the occurrence of minimum flutter speeds at different depths for different modes, and the possibility of different flutter modes occuring at different depths, it is conceivable that a strut could undergo bending flutter at one depth and torsional flutter at another depth.

III. THEORETICAL FLUTTER CHARACTERISTICS

The dual nature of experimental flutter results also appears in theoretical results. Bending flutter and torsional flutter correspond to instabilities in different hydroelastic modes. Transition from bending flutter to torsional flutter occurs when the torsional flutter mode becomes less stable than the bending flutter mode.

The frequency and mode shape characteristics of the hydroelastic modes involved in flutter are predicted accurately in the flutter analysis. However, damping characteristics, and, consequently, flutter speeds are not predicted accurately. In the bending flutter region, flutter speed predictions are not usable because a second mode is also predicted to be unstable which does not correspond to experimental results. Flutter speed predictions in the torsional flutter region correctly indicate the unstable mode but are generally overconservative. Calculated hydroelastic modes of a strut with attached foils indicate that the strut underwent torsional flutter at a speed which was overconservatively predicted.

III. 1. Flutter Theory

Understanding of the differences between bending flutter and torsional flutter requires consideration of the behavior of the hydroelastic modes [12], or resonances, of the strut systems over a wide range of speeds, and not merely a calculation of each strut's speed of neutral stability. This approach was in fact used in a paper [8] presented at the Fourth Symposium on Naval Hydrodynamics. This earlier paper described the hydroelastic modes of bending-type struts only. The present paper extends the earlier results to include a description of the hydroelastic modes of torsion-type struts as well.

Hydroelastic modes are the vibration modes of the strut-fluid system and correspond to eigenvalues and eigenvectors of the velocity-dependent equations of motion. The equations of motion were generated

by assuming a lumped parameter representation for the strut, with elastic and inertial properties lumped at discrete points along a straight elastic axis. This procedure is well established as an accurate means of predicting vibration mode shapes and frequencies of elongated structures in air. The hydrodynamic forces on the strut were also lumped at stations along the axis. Values of structural parameters and hydrodynamic forces at spanwise stations were assigned by dividing the strut into strips normal to the elastic axis. A numerically converged solution was obtained when 10 strips were used.

Displacements were assumed to occur in bending normal to the plane of the strut and in torsion about the strut elastic axis. The equations of motion for the entire system written in matrix form are

$$\left[M\right]\begin{Bmatrix}\ddot{h}_i\\ \ddot{\theta}_i\end{Bmatrix} + \left[C\right]\begin{Bmatrix}\dot{h}_i\\ \dot{\theta}_i\end{Bmatrix} + (1 + jg)\left[K\right]\begin{Bmatrix}h_i\\ \theta_i\end{Bmatrix} = \left\{F_i\right\}$$

The hydrodynamic force F was expressed in terms of the physical displacements and their time derivatives, permitting the structural and hydrodynamic expressions to be combined. Further simplification is achieved by representing strut motion as a series of standing waves in the form

$$h_i = H_i e^{st} \qquad \text{and} \qquad \theta_i = \Theta_i e^{st}$$

The resulting system of linear equations for the hydroelastic system is

$$\left(s^2\left[M'\right] + s\left[C'\right] + \left[K'\right]\right)\begin{Bmatrix}H_i\\ \Theta_i\end{Bmatrix} = \left\{0\right\}$$

Solutions to the above equations are the complex eigenvalues of s, which may be written

$$s = -\zeta\omega \pm j\sqrt{1 - \zeta^2}\,\omega$$

in terms of the damping ratio ζ and the undamped natural frequency ω. Each eigenvalue of s corresponds to a mode of oscillation of the strut-fluid system. Flutter occurs at the lowest speed for which the real part of one of the eigenvalues becomes zero.

Eigenvalues for selected speeds were obtained by a digital computer calculation based on Muller's quadratic method [13]. Flutter speeds were determined by interpolation among damping values across the zero damping axis. Eigenvectors were also obtained, giving the vibration mode shapes in standing-wave form.

The most general form of strut motion is composed of travelling waves as well as standing waves. Further calculations were therefore made to determine whether travelling-wave oscillations were occurring. Travelling waves were found in connection with bending motion and will be described later.

III. 2. Hydrodynamic loading

Hydrodynamic loading on discrete sections of the strut was calculated with a strip theory. The theory was formulated to allow spanwise variation of the loading so that the effects of three-dimensional flow could be investigated.

The lift and moment expressions used were

$$-P_i = p_i \pi \rho b_i^2 \left[\ddot{h}_i - V_n \dot{\theta}_i + V_n \dot{\sigma}_i \tan \Lambda_{ea} + b_i a_i \left(\ddot{\theta}_i + V_n \dot{\tau}_i \tan \Lambda_{ea} \right) \right] - C \ell_{\alpha,i} \rho V_n b_i \, C(k) \, w_i$$

$$-M_i = p_i \pi \rho b_i^4 (1/8 + a_i^2) \left(\ddot{\theta}_i + V_n \dot{\tau}_i \tan \Lambda_{ea} \right) + p_i \pi \rho b_i^2 V_n \left(\dot{h}_i + V_n \sigma_i \tan \Lambda_{ea} \right) + p_i \pi \rho b_i^3 a_i \left(\ddot{h}_i + V_n \dot{\sigma}_i \tan \Lambda_{ea} \right) - p_i \pi \rho b_i^2 V_n^2 \left(\theta_i - a_i b_i \tau_i \tan \Lambda_{ea} \right) + 2 \pi \rho V_n b_i^2 \left[\frac{1}{2} p_i - (a_i - a_{c,i}) \frac{C(k) \cdot C \ell_{\alpha,i}}{2\pi} \right] w_i$$

where

$$w_i = -\dot{h}_i + V_n \theta_i - V_n \sigma_i \tan \Lambda_{ea} + b_i \left(\frac{C \ell_{\alpha,i}}{2\pi} + a_{c,i} - a_i \right) \left(\dot{\theta}_i + V_n \tau_i \tan \Lambda_{ea} \right)$$

In this formulation, spanwise loading variations were introduced separately for circulatory and noncirculatory loading. The loading

due to circulatory flow was varied by inserting steady values of lift slope C_{ℓ_α} and aerodynamic center a_c obtained by a separate calculation. This approach was originated by Yates [14]. The noncirculatory terms were varied by inclusion of a multiplicative factor p. The factor permitted reducing the magnitude of the noncirculatory loading below that associated with two-dimensional flow. This modification was introduced by the authors [15], in accordance with a suggestion by Yates [16]. Spanwise distributions for p will be discussed later.

The given expressions correspond to two-dimensional hydrodynamic loading when a lift slope of 2π, an aerodynamic center location at quarter chord, and a noncirculatory modification factor of unity are used. Three-dimensional loading requires that appropriate spanwise distributions of these quantities be used. In a number of flutter calculations presented later, the effects of three-dimensional flow were studied by varying the above quantities but keeping all spanwise values equal.

Spanwise distributions of lift slope and aerodynamic center were obtained from lifting surface theory [17]. The distributions were calculated using a uniform angle of attack along the span of the strut, and an antisymmetric loading boundary condition at the free surface.

Two different distributions of noncirculatory modification factor were used, one for low frequencies and one for high frequencies [15]. At low frequencies, the factor consisted of the three-dimensional added mass of the strut, expressed as a fraction of the two-dimensional added mass, outboard of the spanwise position being considered. The free surface was treated as a reflecting plane. At high frequencies, the spanwise distribution of added mass on a surface-piercing strut decreases to zero at the free surface. This condition was approximated by assuming the midspan of the submerged portion of the strut to be a reflecting plane and using the low frequency distribution on either side.

Values of the nondimensional frequency, $\ell\omega^2/g$, were used to distinguish between low frequency and high frequency conditions, indicating that the generation of gravity waves was involved in the boundary condition. The low frequency condition exists for values of $\ell\omega^2/g$ of 1 or less, while high frequency loading corresponds to values of $\ell\omega^2/g$ of 10 or greater.

III. 3. Bending Flutter

The hydroelastic modes of several bending-type struts were calculated. In general, two unstable modes were predicted for each strut. One of the unstable modes showed fair correlation with experimental flutter occurrences, while the second unstable mode did not correlate well with experimental results. It therefore appears that one unstable mode corresponded to the experimentally observed instabilities for all of the struts, while the other unstable mode was incorrectly predicted to be unstable. The incorrect prediction was, in fact, found to occur only for limited ranges of spanwise loading inputs, suggesting that the prediction was caused by a slightly inaccurate loading formulation in a highly sensitive calculation.

The mode in which bending flutter occurred had a first bending mode shape, and had the lowest frequency among the existing modes at the experimental flutter speed. At speeds below flutter, the mode was highly damped. Its damping decreased rapidly in a short speed interval prior to flutter. Values of damping were predicted nonconservatively.

These results will be illustrated by presenting detailed characteristics of the hydroelastic modes of a typical bending-type strut, Model 2 of Reference 4. The structural characteristics and three-dimensional loading parameters for Model 2 are given in the Appendix. Several hydroelastic modes calculated for Model 2 are shown as functions of speed in Figures 8 and 9. The damping ratio ζ was plotted without structural damping because no experimental values were available. Predominant mode shapes are indicated on the frequency curves. Predicted instabilities must be compared with an experimental flutter speed of 81 knots and a frequency of 4.1 Hz at that speed. The mode shape at flutter was observed to be predominantly first bending in a motion picture of the experiment.

Flutter is predicted to occur at 83 knots in the presence of two-dimensional loading, as shown in Figure 8. The instability occurs in a mode which first appears, fully damped, at a speed of 30 knots and decreases in stability as speed increases until neutral stability is reached at 83 knots. Although the unstable mode appears at a speed near that at which mode 1 damps out, the two modes coexist over a small speed range. Therefore the unstable mode is considered to be a new mode rather than mode 1. The frequency and mode shape of the new mode show good agreement with experiment. Mode 3 is stable and increases in frequency as speed increases.

The predicted instabilities are much different, and less

accurate, when three-dimensional loading modifications are included. Despite the theoretically improved loading expression, the flutter speed predicted for the new mode is a highly nonconservative 147 knots. Mode 3 is unstable over the entire speed range, except at low speeds where inclusion of structural damping would produce a positive damping ratio. Both unstable modes have a first bending mode shape in the vicinity of the experimental flutter speed. The frequency of mode 3 now decreases rapidly with speed, but nevertheless does not decrease sufficiently to agree with experiment at 81 knots . On the other hand, the frequency of the new mode shows fairly good agreement with experiment at 81 knots . In this case and in general, frequencies of hydroelastic modes are predicted more accurately than damping characteristics, and are less sensitive to variation in hydrodynamic loading. It is concluded that flutter occurred experimentally in the new mode, and that mode 3 is not unstable below 81 knots .

Each of the loading modification parameters was varied independently to determine its effect on predicted flutter instabilities. Equal loading was used at all spanwise positions. The resulting flutter speeds for the new mode and mode 3 are shown in Figure 10. Mode 3 becomes unstable when any of the three modification parameters is changed sufficiently from two-dimensional values. A three-dimensional value of lift slope produces greater instability in mode 3 than three-dimensional values of the other parameters. Interactions among parameters and variations in strut configuration also affect the stability of mode 3. The behavior of hydroelastic modes 1 and 2 was not significantly affected by the variation of applied loading.

The nature of the oscillations experienced by Model 2 at flutter was further investigated in order to determine whether the oscillations consisted of standing or traveling waves. Calculations by Dugundji, et al.[18] and Prasad, et al.[19] had indicated a bending flutter condition occurring in the form of travelling waves for low mass ratio wings. The present complex eigenvalue calculation restricted oscillations to a series of standing waves in which nodal lines remained stationary and all displacements in each mode maintained their relative distributions at all times. Travelling waves are characterized by nodal lines which traverse the entire surface of the strut during a cycle of oscillation.

A direct solution to the equations of motion was attempted, using a finite difference technique in the time domain[20]. The method of solution yields a time history of the transient motion following an initial excitation of finite duration. Flutter inception occurs when oscillations change from decreasing to increasing amplitude. Neutral stability should occur at the same speed using either method of solution.

Calculations were performed by a digital computer program which required that hydrodynamic force expressions be real. Because of this restriction, the imaginary part of the Theodorsen circulation function was omitted from the loading used.

Unsatisfactory results were obtained from the direct method of solution. The predicted flutter speed did not agree with that predicted by the eigenvalue calculation. Furthermore, values of negative damping above flutter inception were so large that no oscillation occurred. As a result, the presence of travelling waves could not be detected. The discrepancies between the two methods of solution may have resulted from the difference in hydrodynamic loading used. It is evident that further investigation of this method of calculation is required.

The hydroelastic mode characteristics of Model 2 are typical of three other bending-type struts that were analyzed. Flutter predictions using two-dimensional loading were often fairly accurate. The mode 3 instability appeared in two of the three additional calculations using three-dimensional loading. The flutter inception speeds for the new mode were again nonconservative, and less accurate than those obtained using two-dimensional loading. Frequencies predicted for the new mode agreed well with frequencies observed at flutter, while those for mode 3 did not agree well. Frequency predictions were equally accurate for both types of loading. Predicted mode shapes for the new mode were predominantly first bending. This agrees with mode shapes observed for bending flutter.

The damping behavior of the new mode as a function of speed shows qualitative agreement with experimental results. In an experiment performed at NSRDC, damping was found to be extremely high for a bending-type strut at all speeds below flutter inception. At flutter inception, damping decreased sufficiently to permit flow-excited oscillations of large amplitude. This behavior would be expected of an instability occurring in the new mode, which decreases in damping from a highly damped condition at intermediate speeds.

In view of the more accurate frequency correlations of the new mode, and its high damping characteristics at intermediate speeds, it is concluded that bending flutter occurs in the mode designated as the new mode. Measurements of damping of strut modes at various speeds are needed to confirm this conclusion. The appearance of a calculated instability in mode 3 is probably caused by extreme sensitivity of the calculated damping to load variation. The present flutter calculation can be used to indicate a possible occurrence of bending flutter, but cannot be used for estimating flutter speeds. Design

calculations should be performed with both two-dimensional and three-dimensional loading so that all potential instabilities will be discovered.

III. 4. Torsional Flutter

The calculated hydroelastic modes of torsion-type struts exhibit more simple behavior than those of bending-type struts. Only one mode is unstable. It is the mode with the second-lowest frequency, and therefore with a predominantly first torsion mode shape, at zero speed. Low damping is predicted in this mode at all speeds below flutter, in contrast to the high damping predicted in the bending flutter mode. Observed characteristics of torsional flutter correlate well with the characteristics of this hydroelastic mode. A mode analogous to the new mode previously described appears for some torsion-type struts, but it is stable throughout the speed range of interest. Three-dimensional loading modifications have very little effect on the qualitative characteristics of the hydroelastic modes of torsion-type struts, but do change the predicted flutter speeds.

Predicted torsional flutter speeds ranged from 59 percent conservative to 36 percent nonconservative when three-dimensional loading was used. The predicted flutter speeds were nonconservative for struts with extremely heavy pods, and became increasingly conservative as the struts decreased in mass ratio and approached the bending flutter region.

As an example of hydroelastic modes for torsion-type struts, the modes for Model 2T of Reference 4 are shown in Figure 11. The structural characteristics of Model 2T are identical to those of Model 2 except for the addition of a long, slender pod to the strut tip. The pod is described in the Appendix. The damping ratio includes the value of structural damping measured at zero speed. One value of damping ratio and frequency was reported in Reference 4, and the others were measured at NSRDC by deflecting the strut with an attached line and cutting it during the test runs. A flutter speed of 18.1 knots was obtained at NSRDC, and a frequency of 6.4 Hz was observed at that speed. The vibration mode shape prior to and at flutter was predominantly first torsion.

Flutter is predicted to occur in mode 2 at 14.1 knots when two-dimensional loading is used. This prediction is conservative by 22 percent. The calculated damping values are lower than the experimental values, but show a similar variation with speed. Frequencies of the hydroelastic modes remain relatively constant as a function of speed, and agree well with available data. The mode shape of the unstable mode, mode 2, changes from first torsion to first bending prior

to the predicted flutter inception, so that flutter is incorrectly predicted to occur with a first bending mode shape.

Slight changes occur in the hydroelastic modes when three-dimensional loading modifications are included. The three-dimensional loading used for Model 2 was also used for Model 2T. The damping of mode 2 increases, remaining below the experimental values for part of the speed range below flutter inception but yielding a flutter speed of 18.8 knots, which is very close to the experimental value but is slightly nonconservative. The flutter mode shape is predicted to be predominantly first torsion, which is the mode shape that was observed.

The good agreement between experimental and theoretical characteristics of mode 2 clearly establishes that the instability has been correctly predicted. Identification of the unstable mode is easier than for Model 2 because sufficient data are available and the modes are unambiguous in predicting instability.

The effects of independent variation of the loading modification parameters on predicted flutter speeds for Model 2T are shown in Figure 12. Equal values of loading were used at all spanwise stations. The calculation is conservative and reasonably accurate using two-dimensional loading, and is unaffected by loading modifications except when lift slope is reduced below 70 percent of the two-dimensional value. While the calculation is sensitive only to lift slope for the conditions shown, strong interactions occur among the modifying parameters when they are varied simultaneously. This interaction is demonstrated by the 18.8 knot flutter speed prediction obtained when three-dimensional values are used for all modifying parameters.

No mode corresponding to the new mode described for Model 2 appears in the speed range shown for Model 2T. Such a mode does appear at higher speeds, however, but remains stable at all speeds for which calculations were made.

An indication of travelling wave motion was found in the flutter mode of Model 2T. However, a discrepancy in calculated flutter speed similar to that found for Model 2 prevents full confidence in the results. The direct method of calculation yielded increasing and decreasing oscillations above and below a different flutter speed from that obtained by eigenvalue calculation. Calculated mode shapes in bending and torsion at flutter are shown in Figure 13 as functions of time. The bending oscillations are travelling waves, while the torsional oscillations are standing waves. Strut deflections due to torsion were approximately twice as large as those due to bending. Therefore the flutter oscillations were predominantly standing waves, although travelling waves

were not insignificant.

Flutter characteristics calculated for several other torsion-type struts using three-dimensional loading were similar to those of Model 2T. Flutter invariably occurred in mode 2 . Calculated flutter speeds, which are compared with experimental values in Figure 14, ranged from 59 percent conservative for very light pods to 36 percent nonconservative for very heavy pods. Frequency predictions showed good agreement with measured values at the experimental flutter speeds. Flutter mode shapes were predicted to be first torsion, with occasionally significant amounts of first bending or second bending. These mode shape predictions agreed with visually observed mode shapes.

Examples of predicted flutter characteristics of both bending-type and torsion-type struts, as well as a strut in the transition region (pod configuration B), are shown in Figure 3. The increasingly conservative torsional flutter speed predictions are evident as pod inertia decreases, until bending flutter occurs with pod configuration A. In view of the good correlation between theoretical and experimental frequency and mode shape in the torsional flutter region, it is concluded that torsional flutter is an instability of hydroelastic mode 2 for torsion-type struts.

A new mode similar to that of Model 2 and Model 2T also appears in the hydroelastic modes of other torsion-type struts. This mode appears at lower speeds for struts with lighter pods. The stability of the new mode decreases as strut pods become lighter and strut configurations shift from torsion-type to bending-type. Bending flutter appears to originate when the new mode becomes unstable at a lower speed than the mode which is unstable in torsional flutter. A shift in the mode shapes of the second and third modes occurs as part of this transition. It is perhaps not coincidental that the mode which is unstable in the torsional region, and the mode which is incorrectly predicted to be unstable in the bending region, both originate as first torsion modes.

Calculations made for struts with large pods included an approximate correction for hydrodynamic forces acting on the pod. The correction, added to the tip of the strut, consisted of the linearized lift and moment due to the unsteady motion of a pod-sized slender body, and is described on page 417 of Reference 12. This correction produced much lower flutter speeds than using pod added mass alone, particularly for heavy pods.

III. 5. Struts with Foils

Successful flutter analysis of strut-foil systems is of considerable practical importance, because struts will generally be used in combination with load-bearing foils. Only inverted-T strut-foil configurations have been considered in the present work, in view of the interest of the U. S. Navy in such configurations. It is clear that for such systems foils have a sizable effect on flutter characteristics. Flutter speeds obtained experimentally by Huang [2] showed an increase of as much as 146 percent when a pod was replaced by a pod and foil combination of equal mass. The parameters governing the effects of foils on flutter characteristics have only begun to be investigated. An early discovery has been that foil angle of attack is an important flutter parameter [2].

While experimental results are relatively scarce, much can be deduced about the flutter characteristics of struts with foils by considering the structural effects of adding foils. A strut with no tip attachment will usually be a bending-type strut, and a heavily tip-weighted strut will be a torsion-type strut. Therefore struts with foils will vary from bending-type to torsion-type, with many configurations being in the transition region, according to the size and weight of the foils. Other parameters will be important to the extent that they produce bending-type or torsion-type characteristics. The rotational inertia of the foils will affect the coupling between the second and third vibration modes, so that large or high aspect ratio foils will produce struts in the transition region. Large or heavy pods tend to produce torsion-type struts. These effects are related to the generalized mass ratio of the strut.

Flutter characteristics calculated for a strut with foils were consistent with these deductions. The strut had a large pod and full-sized foils. The calculated instability occurred in hydroelastic mode 2, the unstable mode in torsional flutter. The flutter speed prediction was overconservative. The second and third vibration modes at zero speed were composed equally of second bending and first torsion mode shapes, indicating that the strut was in the transition region.

The flutter analysis performed on the strut-foil model [2] will be described in detail to permit comparison with previous results. Structural characteristics of the model are given in the Appendix. Several approximations were made in obtaining a theoretical representation for the pod and foils. Structural properties of the pod and the foils were represented by adding equivalent masses and moments of inertia to the tip of the strut. Hydrodynamic loading on the pod and

foils was represented only by adding their added mass and moment of inertia to the structural components.

The effects of the pod and foils on the vibration mode shapes of the submerged strut are shown in Figure 15. It was necessary to use 67 percent of the published values for bending and torsional stiffness to achieve agreement with measured in-air frequencies. These stiffness values were used for in-water frequency calculations and hydroelastic mode calculations as well. The strut alone is a bending-type strut, and the strut with pod is a torsion-type strut. The second and third modes of the strut with pod and foils each exhibit both first torsion and second bending oscillations. Strong couplings due to the foils has also produced similar frequencies for these modes. The strut-foil model must be classified in the transition region. The effect of the foils is particularly striking because the pod-foil combination has the same mass as the pod used on the strut-pod model.

Flutter was found experimentally to depend on the angle of attack of the foil. Two flutter conditions were obtained : at 16.6 knots with an angle of attack of -4 deg , and at 18.1 knots with an angle of attack of -2 deg . Testing was halted prior to flutter at higher angles of attack because divergent deflections of the strut began to occur. Flutter mode shapes were described as equally large bending and torsional deflections. The bending deflections were seen to change from second bending to first bending, while the torsional deflections were consistently first torsion. Structural damping was not determined experimentally.

Calculated hydroelastic modes for the strut-foil model are shown in Figures 16 and 17. Both two-dimensional and three-dimensional loading yield a flutter instability in mode 2. The predicted flutter speed is overconservative at approximately 6 knots in both cases. An additional unstable mode is found which is different for the two types of loading. Two-dimensional loading yields an instability in the new mode, while three-dimensional loading yields an instability in mode 3. The frequencies predicted using three-dimensional loading for mode 2 at the observed flutter speeds agree well with the experimental frequencies, while those predicted for mode 3 do not agree well. On the basis of the usually reliable frequency calculation of three-dimensional loading, it is concluded that flutter occurred experimentally in mode 2. Additional damping data for individual modes is needed to confirm this conclusion.

Predicted mode shapes do not agree with observations. Mode 2 consisted of both second bending and first torsion oscillations at low

speeds, but showed almost exclusively first bending oscillations at the experimental flutter speed.

Experimental [2] and theoretical results were also obtained for the strut with a pod lighter than, and equal to, the weight of the pod with foils. Torsional flutter occurred in both cases, at 20.1 knots with the smaller pod weight and at 9.5 knots with the larger pod weight. The large decrease in flutter speed when weight was added to the pod would be expected at low values of torsional mass ratio, as may be seen in Figure 5. Converting part of the pod mass into foils has raised the flutter speed, and has had a similar effect to reducing the pod mass. The foils have reduced the generalized mass ratio of the strut. Calculations of generalized mass ratio are required in order to correlate experimental results with values of this parameter.

It is apparent that additional experimental and theoretical research is needed to adequately understand flutter of struts with foils. Experimental results can provide a reliable indication of the effects of foil-related parameters and can lead to accurate simulation of full-scale systems with reduced-scale models. Theoretical research is needed to improve the accuracy of flutter speed predictions.

IV. DISCUSSION

The primary deficiency of the present flutter analysis is its prediction of damping. This deficiency results in inaccurate predictions of flutter speed for most struts. In the torsional flutter region, the inaccuracy is strongly correlated with the value of torsional mass ratio of the strut. The relationship between experimental and theoretical flutter speeds has been illustrated in Figure 14. Predictions follow a fairly well-defined curve which is overconservative at low mass ratio, quite nonconservative at high mass ratio, and which crosses over experimental values at a mass ratio of slightly less than 2. It should be noted that the single very nonconservative prediction was strongly influenced by the presence of a large pod, and is therefore not strictly representative of flutter characteristics of simple struts.

The conservative predictions obtained at low values of torsional mass ratio are highly significant. Many previous studies of hydrofoil and airfoil flutter have shown a tendency for predicted flutter speeds to become nonconservative at low values of mass ration, leading to a loss of confidence in flutter predictions in this region. These studies have used two-dimensional loading without accounting for sweep angle. The present analysis, and a similar analysis [4] made previously, showed no tendency for predictions to become nonconser-

vative at low mass ratio for torsional flutter. It appears that the most significant difference in the two types of calculations is the inclusion of sweep angle as a parameter which couples structural and hydrodynamic effects. The present calculation should reliably indicate the presence of a flutter instability throughout the mass ratio range shown in Figure 14. Additional comparisons with existing flutter data can help to determine the accuracy of flutter speed prediction to be expected as a function of mass ratio.

Improvement in the accuracy of flutter speed prediction will require improvement in the hydrodynamic loading formulation. The sensitivity of calculated damping to small changes in loading, particularly for bending-type struts, suggests that hydrodynamic loading must be very accurately described in order to obtain accurate flutter speed predictions. Possible sources of inaccuracy in the loading formulation are the presence of cavitation, real fluid effects involving the boundary layer and wake, and inexact modification of the two-dimensional loading for three-dimensional flow. Rowe [21] has shown that large changes in calculated flutter speed result when the loading applied to struts is modified to simulate cavitation. Available observations are insufficiently detailed to confirm the existence of the assumed distributions of cavitation. It has been shown [22] that altering boundary layer characteristics with disturbance wires affects agreement between theoretical and experimental loading in two-dimensional flow. However, the results of such modification on flutter characteristics have not been investigated. Reliable measurements of three-dimensional strut loading which could be used to assess the accuracy of the strip theory employed in the present flutter analysis are not available.

The existence of two different unstable hydroelastic modes implies that future flutter experiments and calculations must be carried out in sufficient detail to distinguish between the modes. This will require measurement or calculation of hydroelastic mode characteristics as a function of speed. Measurements of damping characteristics at zero speed are important, particularly for struts which undergo torsional flutter, so that calculated damping can be adjusted to include structural damping.

Flutter research will be incomplete until hydroelastic mode characteristics of full-scale strut systems are measured. These measurements will provide comparisons with model data and calculations as well as indicate the stability of the actual struts.

V. DESIGN PROCEDURES

Design of inverted-T strut-foil systems to operate in subcavi-

tating flow can be based on the flutter-free performance of the existing U. S. Navy hydrofoil craft. In order to estimate the effect of variations in configuration, it would be helpful to calculate the hydroelastic mode characteristics and the generalized mass ratio of existing struts for comparison with parametric trends obtained from models. Further model testing may be required to establish stability criteria in areas where theory and present data are inadequate, such as in the presence of cavitating flow.

Additional information about hydroelastic stability can be obtained by flutter testing a reduced-scale model of a proposed design. The model should be dynamically and geometrically scaled, except for sweep angle. It has been found to be virtually impossible to obtain flutter in a low density strut model at small sweep angles prior to structural failure due to approaching divergence. Instead of testing the model at the small sweep angle usually found on full-scale struts, the model should be tested at several larger sweep angles, decreasing the angle until static deflections indicate proximity to divergence. Flutter speeds must then be extrapolated to the required value of sweep angle.

Damping and frequency measurements for individual hydroelastic modes of torsion-type struts have been readily obtained at NSRDC by implusive excitation. This technique involves inducing oscillation of the strut at the desired frequency, and determining damping and frequency from the resulting decaying oscillations. Excitation was obtained from a vibration generator rapidly swept over a narrow frequency interval including the desired resonance. The technique can be applied at small speed increments to permit a close approach to the flutter inception speed to be made safely. It has been found, however, that at speeds above flutter inception struts often exhibit amplitude-limited flutter over a varying speed range before large negative damping leads to large amplitude oscillations. Because of the difference in damping characteristics, amplitude-limited bending flutter occurs over a narrow speed range while amplitude-limited torsional flutter can occur over a wide speed range. This phenomenon probably resulted in the failure of Model 2T, pod configuration D, shown in Figure 3 at a speed far above flutter inception.

Development of flutter testing techniques for full scale craft would permit verification of the stability of a given design. Such techniques should be evaluated in models and on existing craft. Future designs could provide for the flutter testing system to be installed in all craft during construction to make underway flutter testing routine for hydrofoil vessels.

VI. CONCLUSIONS

Strut flutter occurs in two different hydroelastic modes. At low values of generalized mass ratio flutter occurs in a predominantly first bending mode shape with the qualitative characteristics of the "new mode" previously described. At higher values of generalized mass ratio, flutter occurs in a predominantly first torsion mode shape with the qualitative characteristics "mode 2" described in the text. The flutter mode of a strut can be determined by examining the mode shape of the second vibration mode of a strut in water, except in a transition region where strong coupling interferes with this identification.

Flutter speed predictions using the present analysis are generally inaccurate. In the bending flutter region, flutter is often predicted to occur in the wrong mode so that flutter speed predictions cannot be used. In the torsional flutter region, the accuracy of flutter speed predictions is dependent on the value of torsional mass ratio. Predicted mode shapes and frequencies are nearly always accurate when three-dimensional hydrodynamic loading is used.

Foils attached to a strut in an inverted-T configuration have a strong effect on the flutter characteristics of the strut. Further investigation of foil effects is needed.

NOTATION

a	nondimensional distance from midchord to elastic axis, measured perpendicular to elastic axis, positive aft as fraction of semichord b
a_c	nondimensional distance from midchord to local aerodynamic center (for steady flow) measured perpendicular to elastic axis, positive aft as a fraction of semichord b
b	semichord measured perpendicular to elastic axis
$[C]$	damping matrix of strut
$[C']$	effective damping matrix of the strut-fluid system
$C(k)$	complex Theodorsen circulation function
C_{ℓ_α}	local lift slope for a strip perpendicular to elastic axis in steady flow

EI	bending stiffness
F	hydrodynamic force
GJ	torsional stiffness
g	structural damping coefficient ; also, gravitational acceleration
H	amplitude of bending displacement h
h	linear displacement of strut at elastic axis
I_α	total mass moment of inertia of strut and tip attachments about elastic axis
$I^*_{\alpha, pod}$	added moment of inertia of pod about elastic axis, approximated by the added moment of inertia of a prolate spheroid.
j	$\sqrt{-1}$
$[K]$	stiffness matrix of strut
$[K']$	effective stiffness matrix of the strut-fluid system
L	strut length along elastic axis
ℓ	distance from free surface to tip of strut along elastic axis
M	oscillatory moment about elastic axis per unit span of strut, positive in direction of positive θ
M_{pod}	pod mass
M^*_{pod}	added mass of pod
$[M]$	mass matrix of strut
$[M^*]$	added mass matrix of strut
$[M']$	effective mass matrix of the strut-fluid system
m	mass per unit span along elastic axis

P	oscillatory lift per unit span of strut along elastic axis, positive in direction of positive h
p	spanwise modification factor for noncirculatory loading
r_α	nondimensional radius of gyration
s	complex eigenvalue
t	time
V	flow speed
w	downwash ; vertical component of flow velocity on foil, positive in direction of negative h
x_α	nondimensional distance from elastic axis to center of gravity, measured perpendicular to elastic axis, positive aft as fraction of semichord b
y	spanwise coordinate along elastic axis of strut
ζ	damping ratio, giving damping as a fraction of critical damping
Θ	amplitude of torsional displacement θ
θ	torsional displacement of strut about elastic axis, positive when leading edge moves in direction of positive h
κ	sweep parameter ; $(2b \tan \Lambda_{ea}) / L$
Λ_{ea}	elastic-axis sweep angle, positive for sweepback
$\mu_{bending}$	approximation to generalized mass ratio for bending motion
$\mu_{generalized}$	generalized mass ratio
$\mu_{torsion}$	approximation to generalized mass ratio for torsional motion
ρ	fluid density
σ	local bending slope of elastic axis $\partial h/\partial y$

τ	local rate of change of twist along elastic axis $\partial\theta/\partial y$
ω	circular frequency of oscillation
ω_α	circular frequency of first torsional vibration in air

SUBSCRIPTS

i	subscript to indicate that the parameter is associated with ith strip station on strut
n	subscript to indicate that the parameter is perpendicular to elastic axis

SUPERSCRIPT

$(\cdot)$	dot over a quantity indicates differentiation with respect to time

* * *

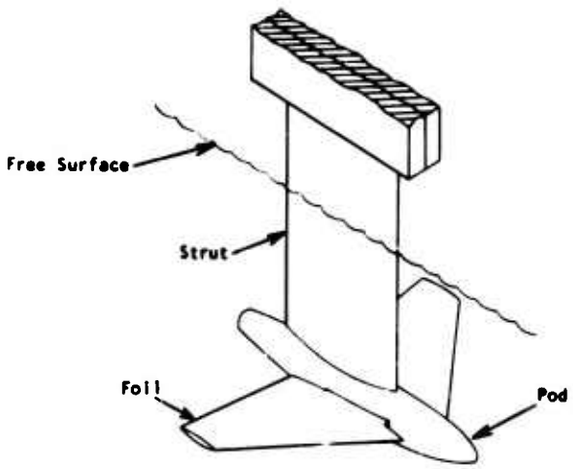


Figure 1. Typical strut-pod-foil system

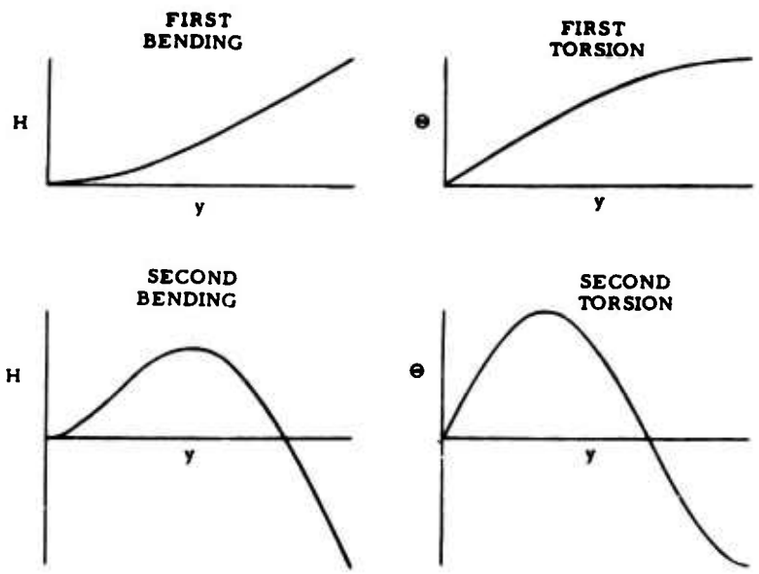


Figure 2. Uncoupled mode shapes of cantilever beam

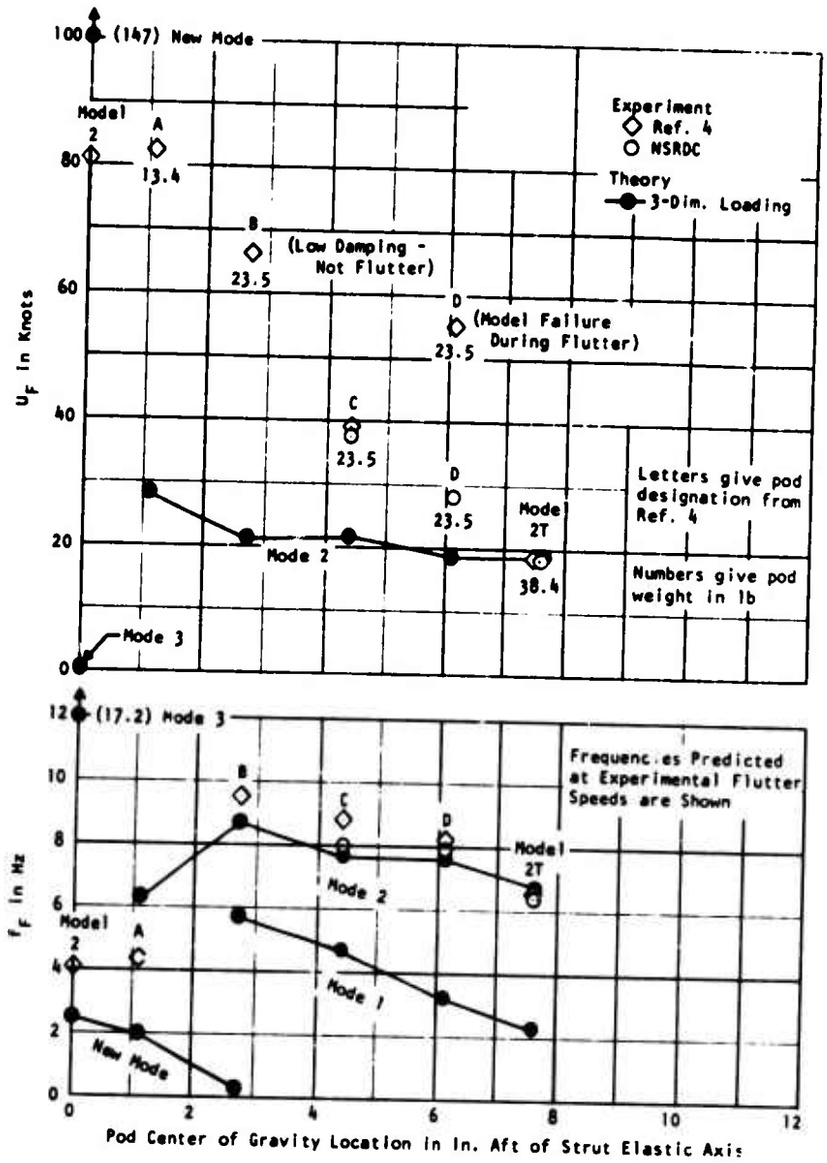


Figure 3. Effect of pod mass and center of gravity location on flutter speed U_F and flutter frequency f_F

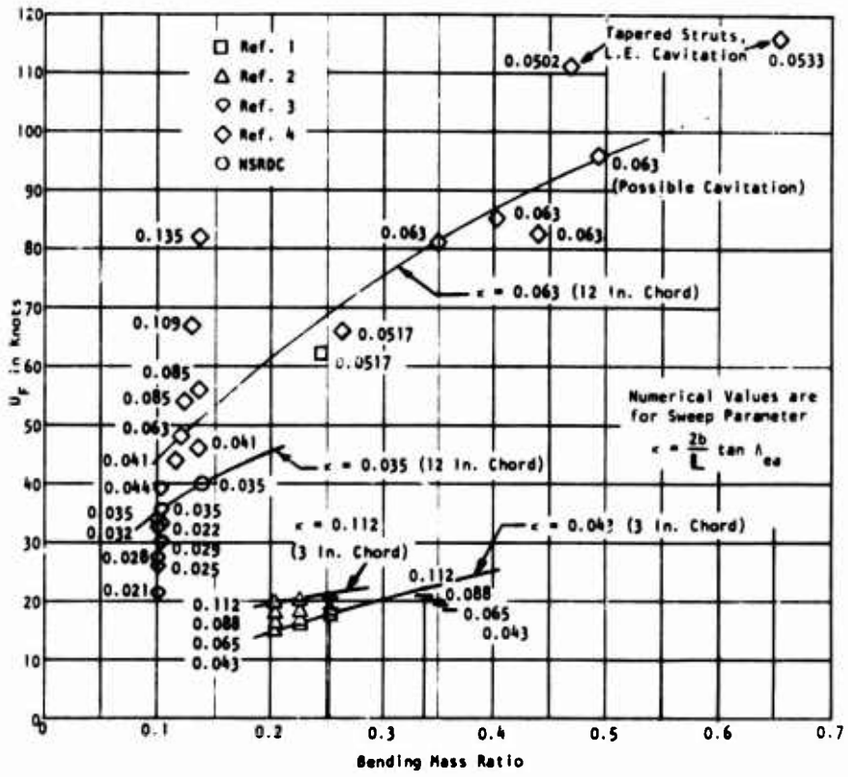


Figure 4. Experimental flutter speed U_F as a function of bending mass ratio for bending-type struts

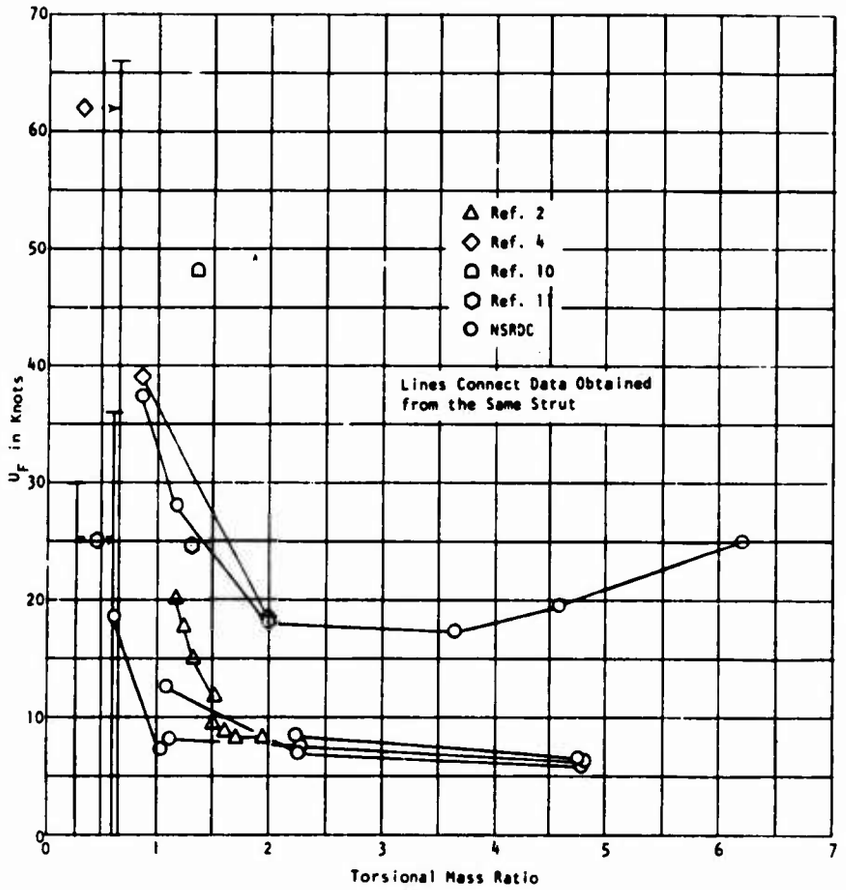


Figure 5. Experimental flutter speed U_F as a function of torsional mass ratio for torsion-type struts

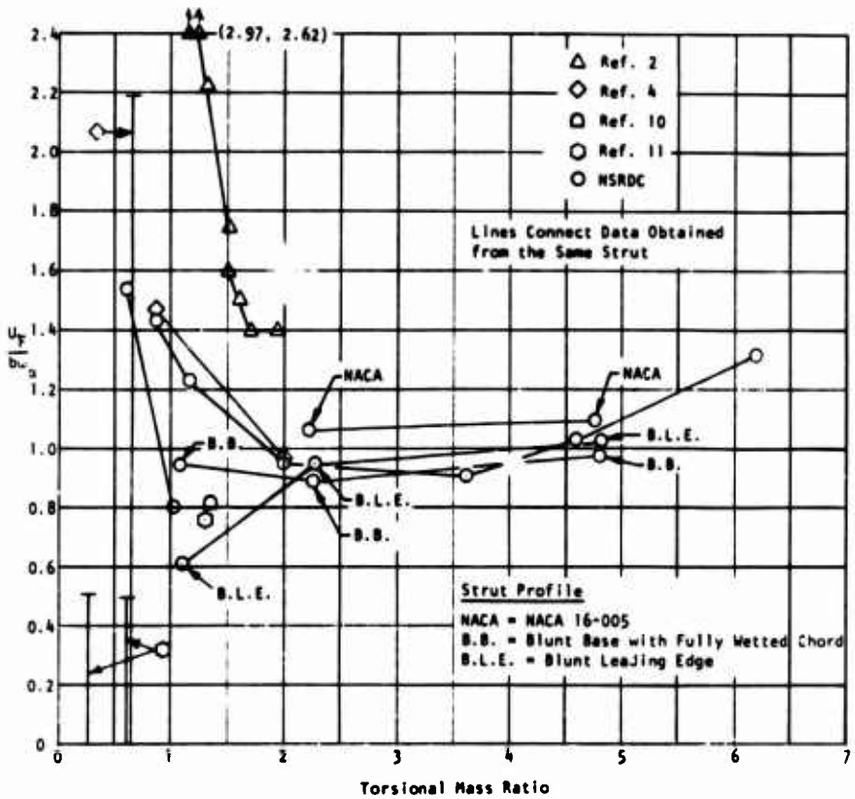


Figure 6. Reduced flutter speed $U_F/b\omega_\alpha$ as a function of torsional mass ratio for torsion-type struts

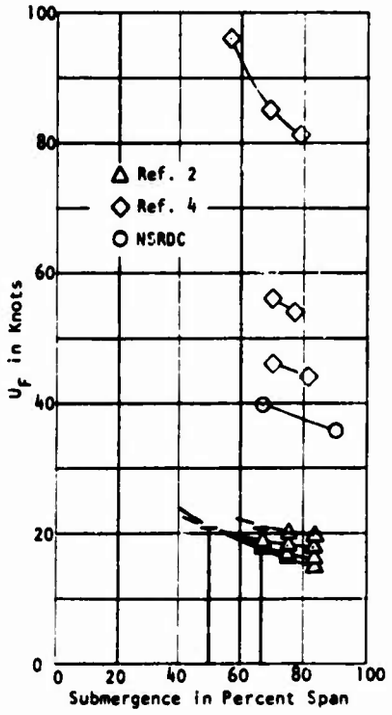


Figure 7a.
Strut models (bending-type)

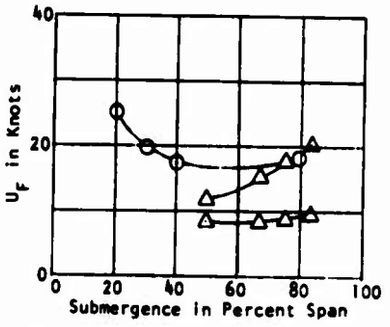


Figure 7b.
Strut-pod models (torsion-type)

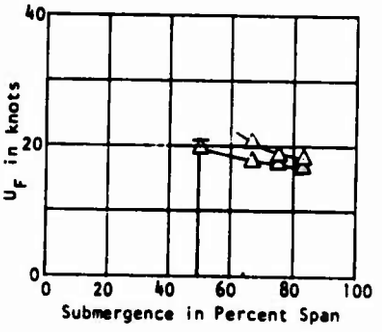


Figure 7c.
Strut with pod and foils

Note : Lines connect data obtained from the same strut

Figure 7. Comparison of the effect of strut submergence on flutter speed U_F for strut models with and without pods and foils

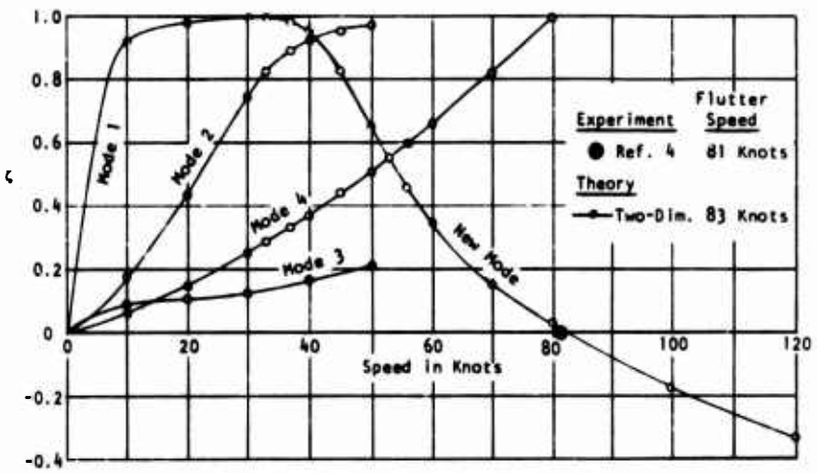


Figure 8a. Damping ratio ζ

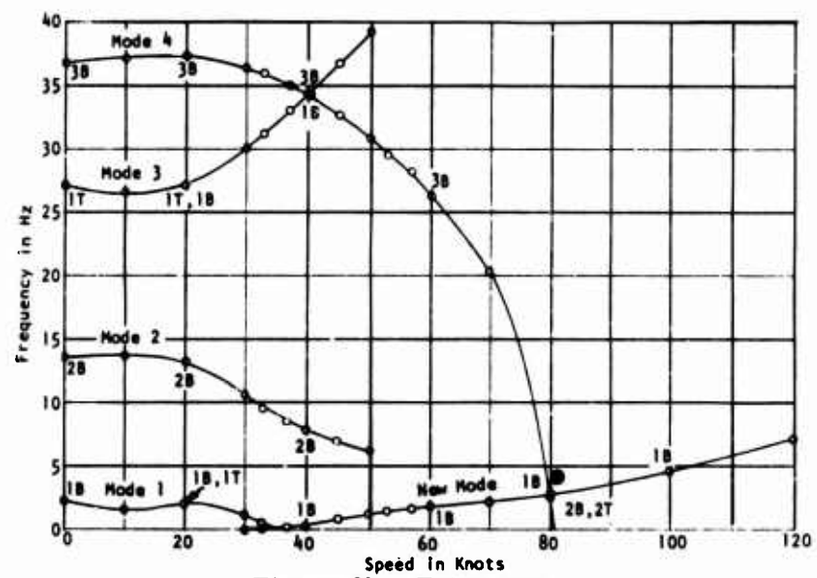


Figure 8b. Frequency

Figure 8. Hydroelastic mode characteristics for Model 2 (Two-dimensional loading calculation)

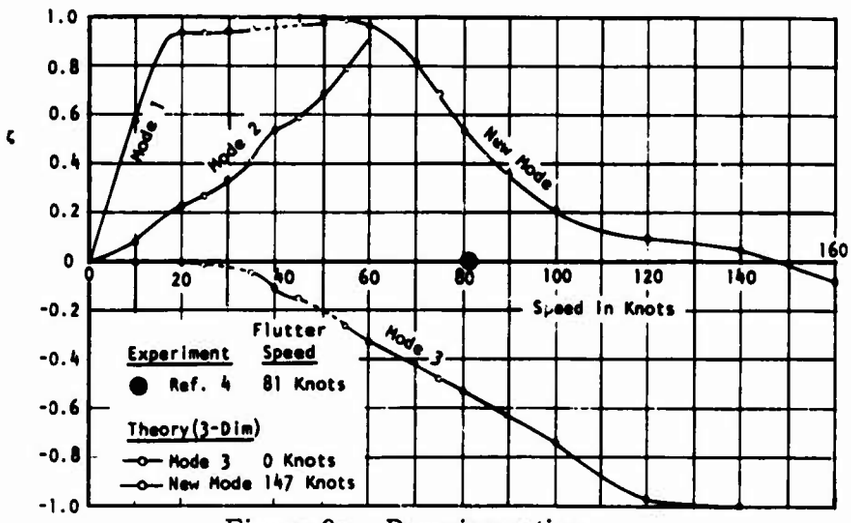


Figure 9a. Damping ratio ζ

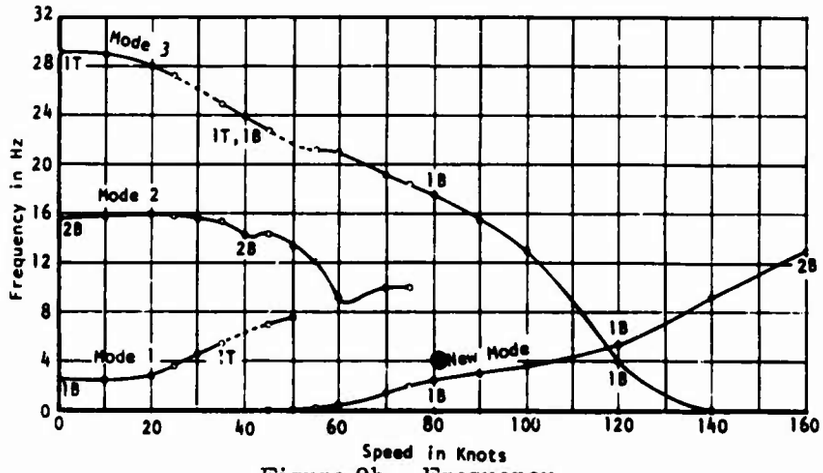


Figure 9b. Frequency

Figure 9. Hydroelastic mode characteristics for Model 2 (Three-dimensional loading calculation)

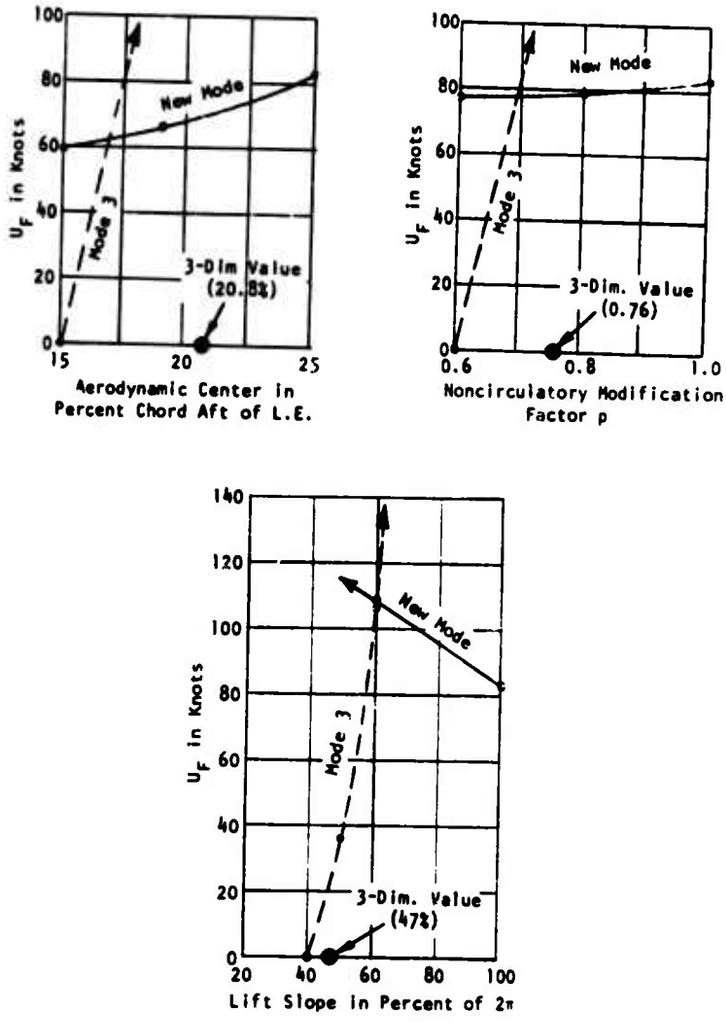


Figure 10. Effect of loading modifications on calculated flutter speed U_F for Model 2

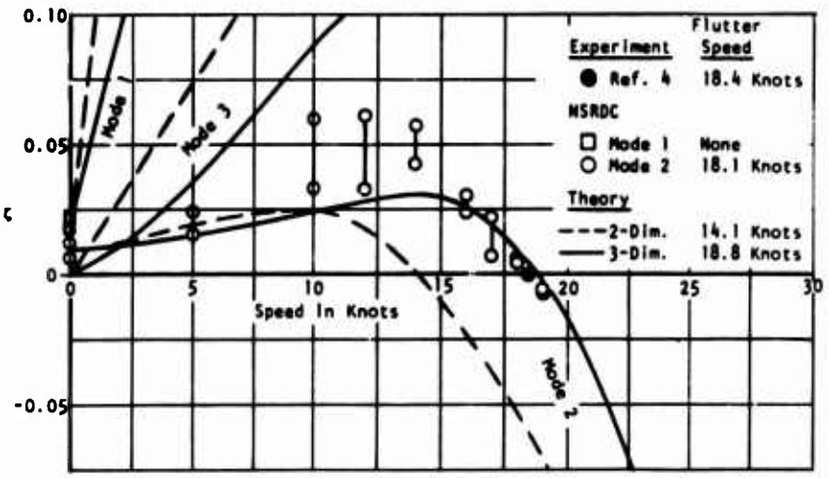


Figure 11a. Damping ratio ζ

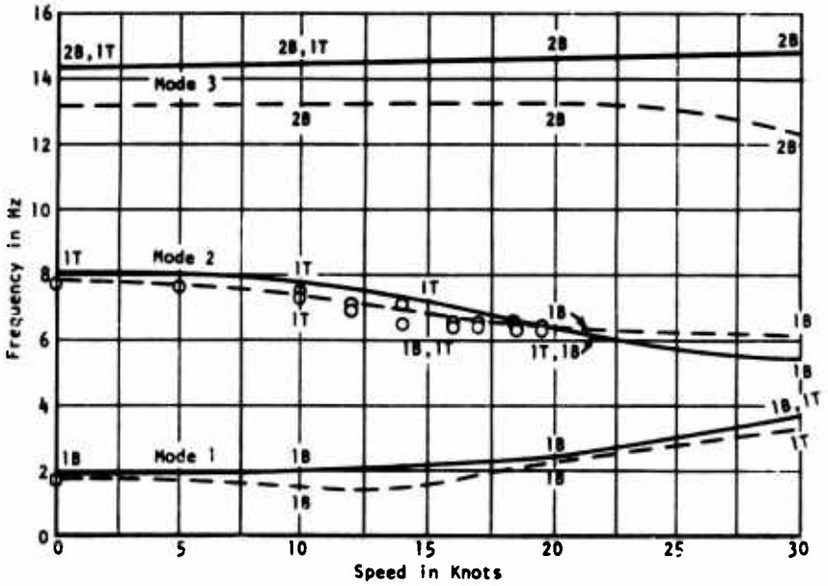


Figure 11b. Frequency

Figure 11. Hydroelastic mode characteristics for Model 2T

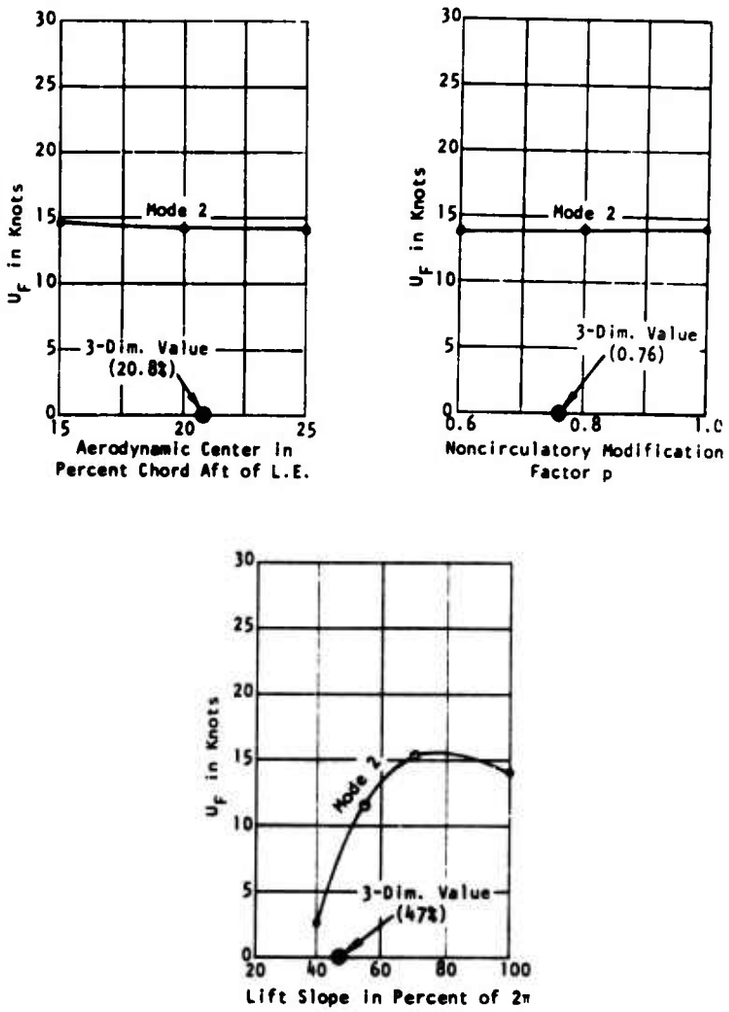


Figure 12. Effect of loading modifications on calculated flutter speed U_F for Model 2T

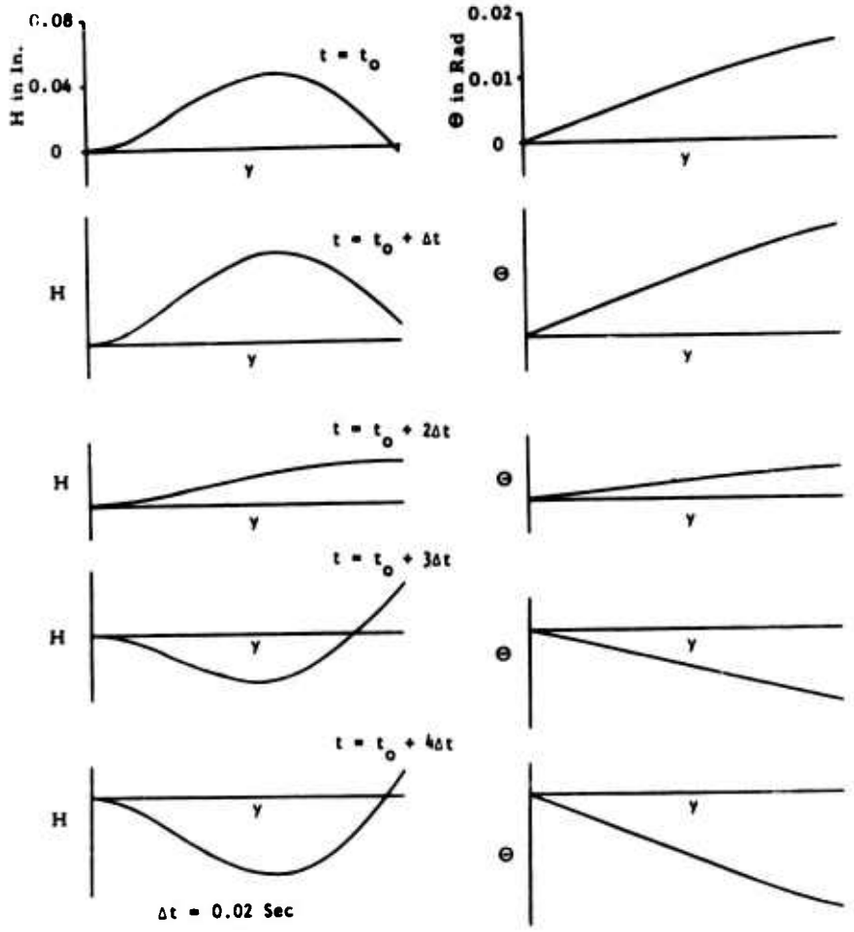


Figure 13. Calculated transient response for Model 2T at flutter

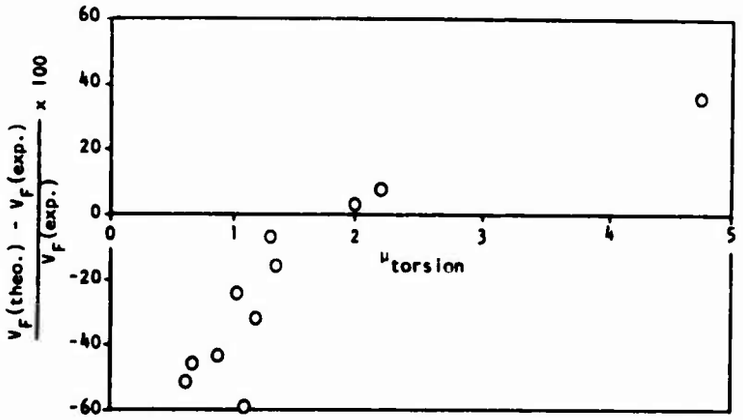


Figure 14. Comparison of experimental and theoretical flutter speeds for torsion-type struts without foils

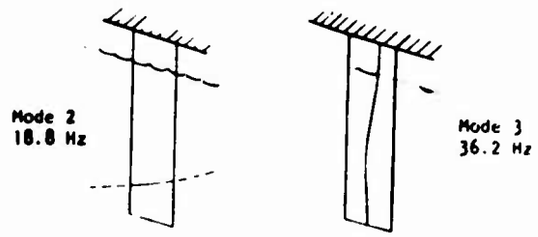


Figure 15a. Strut

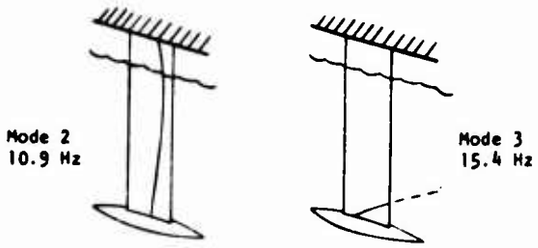


Figure 15b. Strut with pod

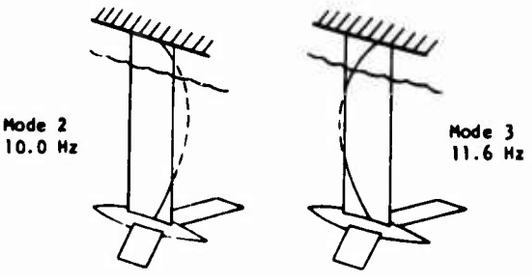


Figure 15c. Strut with pod and foils

Figure 15. Calculated nodal lines for strut of Reference 2 at 83 percent submergence in water

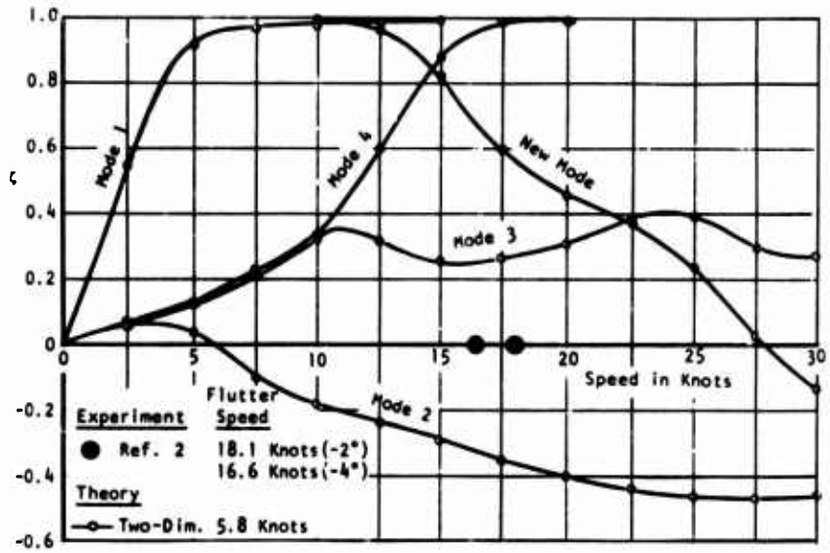


Figure 16a. Damping ratio ζ

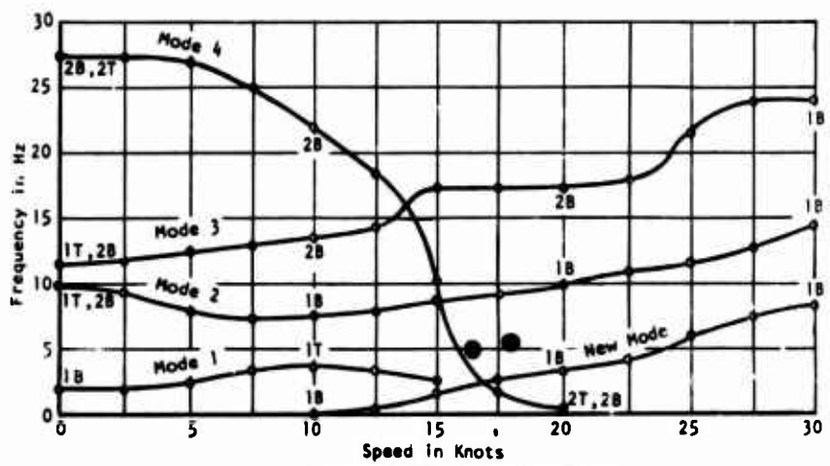


Figure 16b. Frequency

Figure 16. Hydrostatic mode characteristics for strut of Reference 2 with pod and foils (Two-dimensional loading calculation)

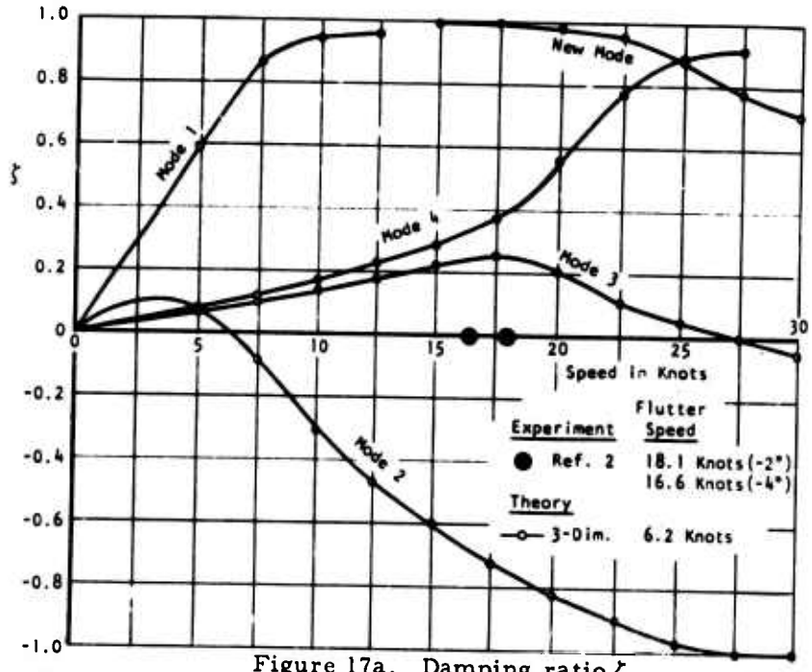


Figure 17a. Damping ratio ζ

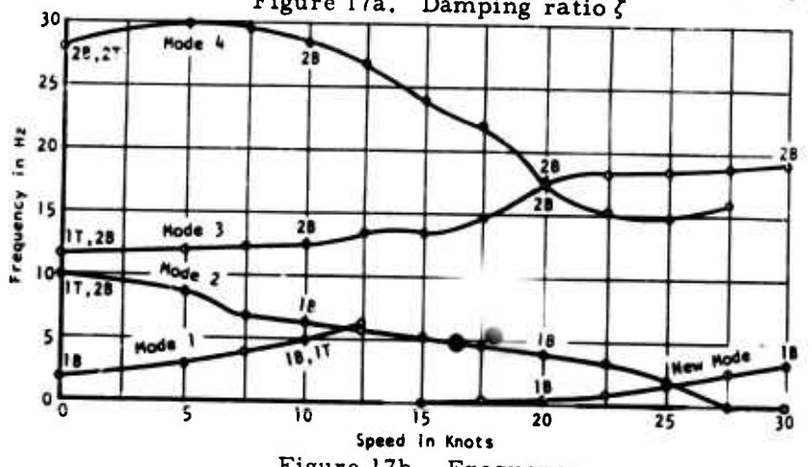


Figure 17b. Frequency

Figure 17. Hydroelastic mode[illegible]istics for strut of Reference 2 with po[illegible]s (Three-dimensional loading calculation

APPENDIX

DESCRIPTION OF STRUT MODELS

MODEL 2

Model 2 was a blunt-based strut [4] constructed of solid steel. Its dimensions are shown in Figure 18, and its structural characteristics are summarized in Table 1. Spanwise distributions of lift slope, aerodynamic center, and noncirculatory modification factor are shown in Figure 19.

MODEL 2 T

Model 2 T was constructed to the same specifications as Model 2, except that a 2-inch diameter pod was welded to its tip [4]. Pod dimensions are shown in Figure 20. Weights were placed in the body of the pod to produce different inertial configurations.

STRUT-FOIL MODEL

The strut [2] consisted of a solid bar of copper alloy covered with flexible silicone rubber. The leading edge of the strut was coated with a thin layer of plastic which was slit to reduce its stiffening effect. The strut profile closely resembled that of Models 2 and 2 T, except for a rounded leading edge. Strut dimensions are shown in Figure 21. Structural characteristics are given in Table 2. The three-dimensional loading curves for this strut were essentially the same as those for Model 2, differing only in sweep angle.

The pod and foils were machined from solid aluminium and were attached to the strut with bolts. Dimensions for these components are given in Figure 22.

* * *

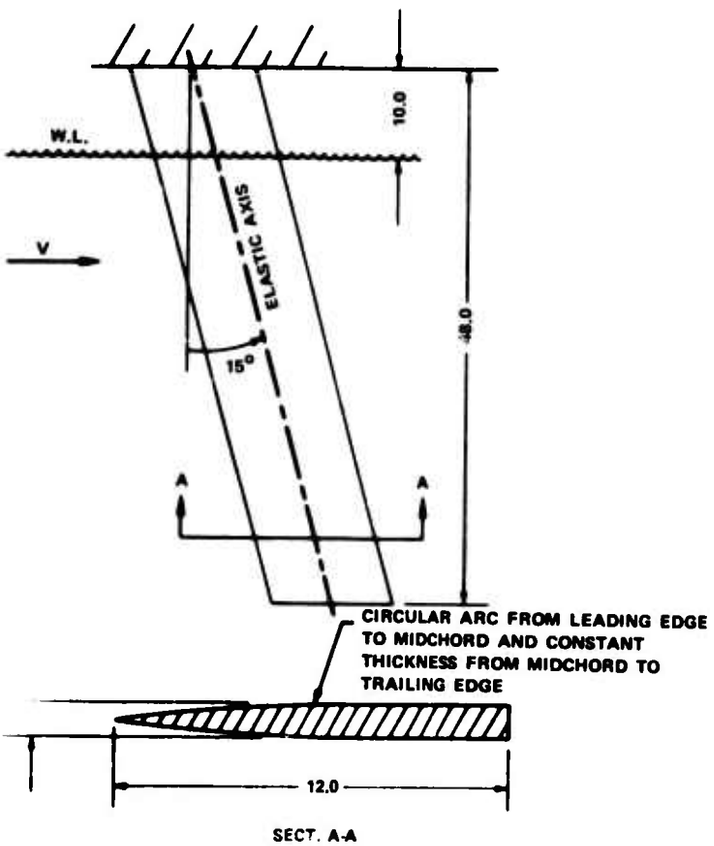


Figure 18. Mo ensions

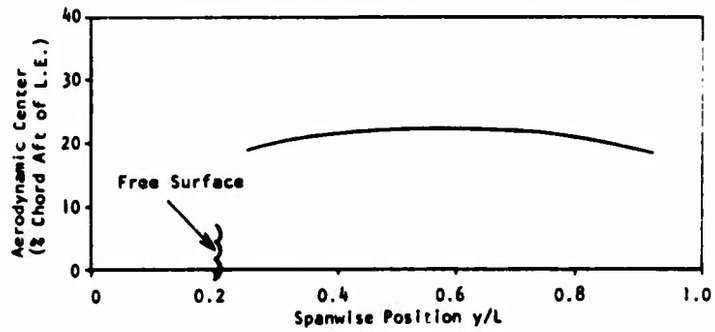


Figure 19a. Aerodynamic center location

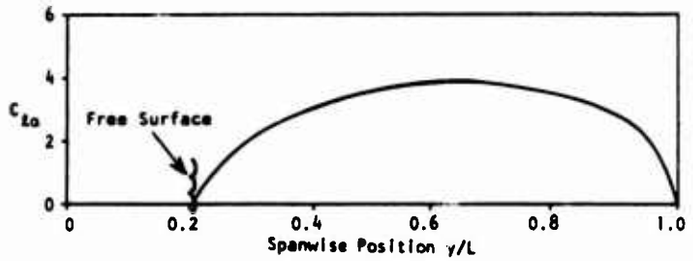


Figure 19b. Local lift coefficient slope C_{ℓ_α}

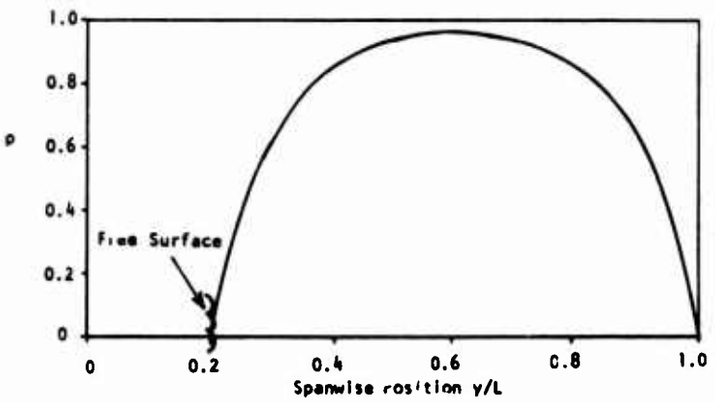


Figure 19c. Noncirculatory modification factor p

Figure 19.
Spanwise distributions of loading modification parameters

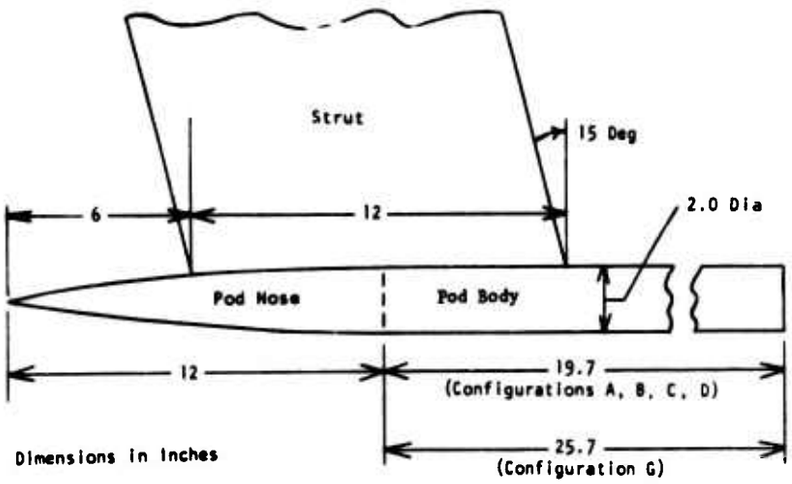


Figure 20. Pod used on Model 2T

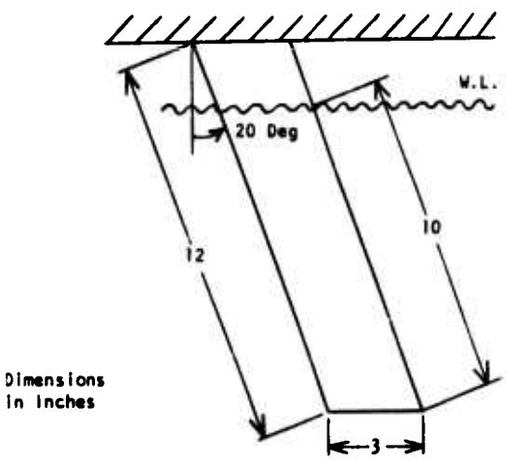


Figure 21. Strut used with pod and foils (Ref. 2)

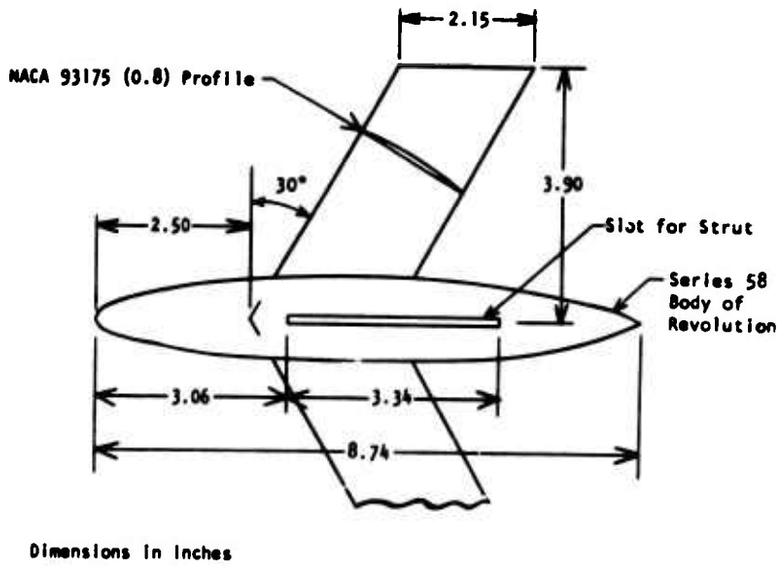


Figure 22. Pod and foil attachment for strut of Ref. 2

TABLE 1

Structural Characteristics of Model 2

Model Parameter	Value
L in in.	49.693
Λ_{ea} in deg.	15
b in in.	5.796
m in lb-sec^2/in.^{2}	0.00273
a	0.38
x_α	-0.214
I_α in lb-sec^2-in.	1.488
EI in lb-in.^{2}	1.293×10^6
GJ in lb-in.^{2}	2.070×10^6

TABLE 2

Structural Characteristics of Strut of Reference 2

Model Parameter	Value
L in in.	12
Λ_{ea} in deg.	15
b in in.	1.449
m in lb-sec^2/in.^{2}	1.0363×10^{-4}
Strut weight in lb.	0.48
Pod and foils weight in lb.	0.73
a	0.38
x_α	-0.214
I_α (strut) in lb-sec^2-in.	8.525×10^{-4}
EI* in lb-in.^{2}	383
GJ* in lb-in.^{2}	614

*Note : 0.67 of Ref. 2 value

REFERENCES

[1] HILLBORNE, D. V., "The Hydroelastic Stability of Struts", Admiralty Res. Lab Report No. ARL/R1/G/HY/5/3, 1958.

[2] HUANG, T. T., "Experimental Study of a Low Modulus Flutter Model for Strut-Foil-Pod Configurations", Hydronautics, Inc. Technical Report 459-2, Jul. 1967.

[3] SQUIRES, C. E., Jr., "Hydrofoil Flutter, Small Sweep Angle Investigation - Final Report", Grumman Aircraft Engineering Corporation Report DA Nonr-3989. 3 (Nov 1963).

[4] BAIRD, E. F., et al., "Investigation of Hydrofoil Flutter - Final Report", Grumman Aircraft Engineering Corporation Report DA 10-480-3, Feb. 1962.

[5] JORDAN, P. F., "On the Flutter of Swept Wings", Journal of the Aeronautical Sciences, Vol. 24, No. 3, pp. 203-210, 1957.

[6] CAPORALI, R. L., and E. J. BRUNELLE, "Hydrofoil Instability at Low Mass Density Ratios", Princeton University Aerospace and Mechanical Sciences Report No. 670, Mar. 1964.

[7] HERR, R. W., "A Study of Flutter at Low Mass Ratio with Possible Application to Hydrofoils", NASA TN-D-831, May 1961.

[8] SQUIRES, C. E., Jr., and E. F. BAIRD, "The Flutter Characteristics of a Hydrofoil Strut", Proceedings of the Fourth Symposium on Naval Hydrodynamics, pp. 739-759, 1962.

[9] HO, H. W., "The Development and Testing of Low Modulus Flutter Models of a Base-Vented Strut", Hydronautics, Inc. Technical Report No. 459-1, May 1965.

[10] ABRAMSON, H. N., and RANSLEBEN, G. E., Jr., "An Experimental Investigation of Flutter of a Fully Submerged Subcavitating Hydrofoil", Journal of Aircraft, Vol. 2, No. 5, pp. 439-442, 1965.

[11] BESCH, P.K., and LIU, Y.N., "Flutter and Divergence Characteristics of Four Low Mass Ratio Hydrofoils", Naval Ship Research and Development Center Report 3410, Oct. 1970.

[12] BISPLINGHOFF, R.L., and ASHLEY, H., "Principles of Aeroelasticity", John Wiley and Sons, Inc. New York, 1962, p. 235.

[13] WILKINSON, J.H., "The Algebraic Eigenvalue Problem", Oxford University Press, New York, 1965.

[14] YATES, E.C., Jr., "Calculation of Flutter Characteristics for Finite-Span Swept or Unswept Wings at Subsonic and Supersonic Speeds by a Modified Strip Analysis", NACA RM L57L10, 1958.

[15] LIU, Y.N., and BESCH, P.K., "Hydrofoil Flutter Analysis, Using a Modified Strip Theory", Naval Ship Research and Development Center Report 3624, Jul. 1971.

[16] YATES, E.C., Jr., "Flutter Prediction at Low Mass-Density Ratios with Application to the Finite-Span Noncavitating Hydrofoil", AIAA Third Marine Systems and ASW Meeting, Apr-May 1968.

[17] ASHLEY, H., et al. "New Directions in Lifting Surface Theory", AIAA Journal, Vol. 3, No. 1, pp. 3-16, 1965.

[18] DUGUNDJI, J. and GHAREEB, N., "Pure Bending Flutter of a Swept Wing in a High-Density, Low-Speed Flow", AIAA Journal, Vol. 3, No. 6, pp. 1126-1133, 1965.

[19] PRASAD, S.N., et al., "Bending-Torsional Flutter of a Swept Wing in a High-Density, Low-Speed Flow", AIAA Journal, Vol. 5, No. 2, pp. 316-321, 1967.

[20] PETERSON, L., "Theoretical Basis for SADSAM Computer Program", MacNeal-Schwendler Corporation Project Report, Dec 1970.

[21] ROWE, W.S., and MARVIN, T.G.B., "A Program of Theoretical Research on Hydroelastic Stability", The Boeing Company, Contract N00014-67-C-0248, Nov. 1968.

[22] GREIDANUS, J.H., et al., "Experimental Determination of the Aerodynamic Coefficients of an Oscillating Wing in Incompressible Two-Dimensional Flow, Part I, Wing with Fixed Axis of Rotation", Report F101, National Aeronautical and Astronautical Research Institute, Amsterdam, 1952.

DISCUSSION

Reuven Leopold
U.S. Navy Naval Ship Engineering Center
Hyattsville, Maryland, U.S.A.

Thank you, Mr. Besch. Besides the interesting paper we may congratulate you on finishing on time. The floor is open for discussion. If no-one has a question ready, I guess I will fill in. I have an awful lot of questions and I thought I would never get them in, but it looks as though I shall.

The tested configuration was designed as a cantilever beam. The analysis assumed the same, hence fixed at one end. In an actual design, fixity cannot be (or by design is not) achieved. For example the strut serves as a rudder, or is supported by a flexible foundation. How would this affect the flutter dominating mode shapes ?

REPLY TO DISCUSSION

Peter K. Besch
Naval Ship Research and Development Center
Bethesda, Maryland, U.S.A.

We can include motion of the hull and flexibility of the hull in our analysis, but we have not done so in this paper. Our paper merely consists of the analysis of existing results, and we admit that further analysis would be required for full-scale applications. The analysis requires further development in order to be able to treat model results successfully and these are firmly supported cantilever beams. It must further be remembered that no full-scale data is available of any type in this area, so further work must be done.

DISCUSSION

Reuven Leopold
U.S. Navy Naval Ship Engineering Center
Hyattsville, Maryland, U.S.A.

Thank you. I have a few more questions.

The authors stated that predicted mode shapesand frequencies are nearly always accurate when 3-D hydro-loading is used. Could they elaborate on the techniques used ? How many modes were extracted per typical model, and what is the cost and length of calculation time for such an effort ?

REPLY TO DISCUSSION

Peter K. Besch
Naval Ship Research and Development Center
Bethesda, Maryland, U.S.A.

We have extracted ten modes for each strut at each speed. The accuracy would normally only remain good through four or five modes. But we have found that it is only necessary to analyze the first four modes to conduct the stability analysis. Therefore the accuracy of higher modes would not be particularly important in our flutter analysis. The calculation is fairly efficient in that one detailed flutter analysis can be conducted in approximately ten minutes, on a CDC 6700 computer.

DISCUSSION

John P. Breslin
Stevens Institute of Technology
Hoboken, New Jersey, U.S.A.

If I understood correctly, Mr. Besch said that for the bending type of flutter the correlation achieved was much better when one used two-dimensional hydrodynamics than when one used three-dimensional. If that is so, it is surprising to me, and I wonder if he could tell us briefly what the three dimensional calculation included and what it excluded ?

REPLY TO DISCUSSION

Peter K. Besch
Naval Ship Research and Development Center
Bethesda, Maryland, U.S.A.

First of all, the two dimensional calculation consisted of Theodorsen loading with a modification to allow for coupling between bending and torsion due to the sweep angle. This is the NACA swept wing flutter theory ; it was further developed by Yates at NASA to include spanwise variation in the two-dimensional lift slope and in the two-dimensional aerodynamic centre location at each local position. The calculation was further extended by us to include the modification for spanwise variation of non-circulatory loading. So we have three quantities varying in a spanwise direction to permit simulation of three-dimensional flow. It seems that the first large improvement in accuracy is obtained by including sweep angle. Further modification which includes the load parameters I have just mentioned does not produce generally accurate results.

DISCUSSION

John P. Breslin
Stevens Institute of Technology
Hoboken, New Jersey, U.S.A.

What you are saying is that the two-dimensional method was modified to account for a spanwise variation. An unsteady three-dimensional theory from the outset was never applied. Is that right ?

REPLY TO DISCUSSION

Peter K. Besch
Naval Ship Research and Development Center
Bethesda, Maryland, U.S.A.

The lift slope and aerodynamic center modifications were derived from steady lifting-surface theory. The remainder of the loading was a fully unsteady formulation.

DISCUSSION

John P. Breslin
Stevens Institute of Technology
Hoboken, New Jersey, U.S.A.

You mean a three-dimensional analysis.

REPLY TO DISCUSSION

Peter K. Besch
Naval Ship Research and Development Center
Bethesda, Maryland, U.S.A.

The hydrodynamic analysis was not an unsteady three-dimensional theory in the sense of a lifting-surface theory. A two-dimensional unsteady strip theory was modified using three-dimensional steady lifting-surface theory.

The only parts of the three-dimensional loading formulation that were independent of frequency were the lift slope and aerodynamic center distributions. The reduced frequencies of the bending-type struts at flutter are welle below 0.1 , so the above approximation is valid for this region. Torsion-type struts have higher reduced frequencies at flutter, but the flutter calculation is more accurate for this region.

DISCUSSION

Reuven Leopold
U.S. Navy Naval Ship Engineering Center
Hyattsville, Maryland, U.S.A.

If there are no other questions, as we have a few more minutes, perhaps you would allow some of the designer in me to come out in a few comments. There are problems that come to the designer many times as design changes, since that is the name of the game. In the area where flutter is a consideration such changes pose difficult problems. It is evident from the Paper, and from other investigations, that the flutter evaluation is sensitive to small changes in the structural stiffness, weight distribution and geometry. During an actual design and fabrication many changes take place. A typical example is when skin thickness is designed to a minimum gauge, whereas in the actual fabrication a standard gauge is used. While such design changes are usually in the direction of lowering the static design stresses and deflections, the modification in structural characteristics may result in lowering the flutter speed. It is thus important to direct the flutter investigation effort towards sensitivity type evaluation of the various configurations to variations in the governing parameters. This will assist the designer in assessing the design adequacy from the hydro-

elasticity viewpoint - in other words, provide a tool for the designer, and that is something which sometimes research efforts do not culminate in.

That was merely a comment.

* * *

ON THE DESIGN OF THE PROPULSION SYSTEMS WITH «Z» DRIVES FOR HYDROFOIL SHIPS

A.A. Rousetsky
Kryloff Ship Research Institute
Leningrad, U.S.S.R.

ABSTRACT

The design features of propeller with "Z" power drive are described. The data on the velocity field produced by the propulsion pod are given and recommendations for choice of the elements of propeller and propulsion pod adapted to velocity field are given.

Information on the hydrofoil "Typhoon" propulsion system design are set forth.

The propeller powered through an inclined shaft is the most extensively employed propulsion system for hydrofoil ships. Such propulsion systems distinguished by simple design are used for most hydrofoil ships now in operation. However, this system has some disadvantages. The oncoming flow obliquity due to the propeller shaft inclination results in the periodic change of the incident angles of the propeller elements, the amplitude being increased with the decrease in the relative radius. The variation of the incident angles prevents from designing the optimum propeller, from the point of view of propulsion qualities, and forces the designers to make a certain compromise, while choosing the propeller elements, to avoid the intensive erosion damages on the propeller blades. The method of designing the propellers adapted to the oblique flow is described in papers [1], [2].

The experience obtained in calculating such propellers shows that with the oblique flow angles exceeding 14° - 15° the design of the ship propeller displaying satisfactory erosion characteristics has failed. At the same time the improvment of the hydrofoil ship seakeeping

qualities requires the increase in clearance between the ship bottom and free surface and this dictates the increase in the propeller shaft inclination . That is why the propulsion system known as "Z" drive came into use on seagoing hydrofoil ships . There are different va - riants for "Z"drives distinguished by the arrangement of ship propel- lers : (a) single propeller "Z" drive with one propeller at the forward end or at the after end of the propulsion pod and (b) twin propeller "Z" drive where one propeller is at the forward end of the propulsion pod and the other is at its after end . The disadvantages of the latter "Z" drive are due to the forward propeller effect upon the flow around "Z" drive and the after propeller operation . This effect can result in intensive erosion damages on Z-drive elements situated in the forward propeller wake . As a consequence such type of the propeller arrange- ment is used only for "Z" drive intended for high power transmission where the decrease in dimensions of the gear assembly and propulsion pod is required . From the point of view of providing the uniform velo- city field in the propeller disk , (a)-variant with a propeller at the for - ward end of the propulsion pod is preferable ; however , the propulsion efficiency of this "Z" drive is somewhat below the efficiency of "Z" drive with a propeller at the after end of the propulsion pod . Besides there is a danger of erosion damage on "Z" drive hull . Thus at pre - sent"Z" drive with a single after propeller is considered to be the most attractive ; a number of hydrofoil ships are equipped with such " Z " drives .

The design of propeller "Z" drive propulsion system involves a series of problems which can be divided into two groups : the first group deals with choosing the geometry of the propulsion pod and strut; the second group deals with designing ship propellers adapted to the velocity field generated by "Z" drive hull .

Generally the propulsion pod-and-strut cross sections are pre- determined taking into account the arrangement of the gear assembly and bearings of the vertical shaft . Since the increase in the wetted surface is unfavourable , from the point of view of resistance , the problem is reduced to the choice of minimum length-to-diameter ratio providing the absence of cavitation on these elements .

As the calculations and experiments show , length-to-diameter ratio providing the minimum resistance lies in the range of 4-5 ; in this case no cavitation occurs on the propulsion pod up to cavitation numbers 0.2-0.3 . Circular-arc cross sections for the propulsion pod are preferable provided that there are no structural impediments .

To preclude cavitation on the strut its maximum relative thickness in the first approximation may be determined according to the following empirical formula :

$$\delta_{max} \leq \frac{\sigma}{2,5}$$

where σ is the cavitation number .

This formula holds for the profiles with a fairly unique pressure distribution . Specifically , NACA-16 and Mandel profiles comply with these requirements . At the place of the strut-free surface intersection the strut profile usually has the form of a symmetric segment developing smoothly into the parent profile of the part immersed . The most critical element of "Z " drive is the junction of the pod with the strut because here , and particularly in its bow part , the cavitation inception is possible . The radius of the fillet at the place of junction is chosen so that the thickness-chord ratio should not exceed the value δ max .

It is obvious that with the proper choice of "Z " drive forms the cavitation can be avoided only in a comparatively narrow range of incident angles . The critical cavitation number versus the angle of incidence is shown in Fig. 1 .

For designing the propeller to be mounted on "Z " drive the knowledge of the hull-propeller interaction factors is necessary . The distinguishing feature of the propulsion system in question is the large value of D/d ratio where D is the propeller diameter , d is the pod diameter . In these conditions the decisive role in the formation of the nominal wake in way of propeller belongs to a potential component . Replacing the propulsion pod with a system of singularities makes it possible to calculate in the first approximation the value of nominal wake . It is of interest to note that in the range of diameter relation $(1.5 < \frac{D}{d} < 2.0)$ under discussion the wake value is practically independent of this relation . This is supported by the data in Fig. 2 where the values of the nominal wake are plotted against the pod length-to-diameter ratio at different $\frac{D}{d}$.

As is known , "Z "drive propellers operate at comparatively small load factor values σ_p ranging from 0.3 to 0.6 . It makes possible in practical calculations to consider the effective wake to be equal to the nominal one . To proceed from the assumption that the wake is potential , the thrust deduction factor can be calculated from the known formula .

$$t = \frac{2\,Wp}{1 + \sqrt{1 + 6p}} \qquad (2)$$

where Wp is the nominal potential wake factor .

The thrust deduction factors calculated by formula (2) hold , strictly speaking , for the perfect fluid only , however , the errors due to this assumption are essential but at very small load factors . The interaction factors can be refined through the tests in a cavitation tunnel . During the tests "Z" drive resistance and propeller performance curves are recorded . Apart from the refinement of the interaction factors , the tests make it possible to reveal the propeller cavitation effect upon the value of these factors . When analysing these experimental results the wake and thrust deduction factors may be determined by the following formulae :

$$W = 1 - \frac{\lambda p}{\lambda} \; , \; t = \frac{\Delta R}{P}$$

where λp - propeller advance ratio ,

λ - apparent advance ratio ,

P - propeller thrust ,

ΔR - gain in resistance of "Z" drive due to the presence of propeller .

The tests with various types of "Z" drives showed that the wake value was independent of the propeller loading . This gives grounds to consider that the wake value will neither be influenced by the propeller loading changes due to cavitation .

Therefore the wake value obtained by the comparison of the propeller performance curves for subcavitating regimes may be used in further calculations . For the agreement of the propeller performance curves in open water and downstream of "Z" drive under cavitation use is made of the correction factors taking into account the effects of the flow nonuniformity and pressure change in the propeller disk upon the propeller thrust and torque .

The dependence of the thrust deduction factor upon the propeller loading and cavitation number for the propulsion system with the pod length-to-diameter ratio $\frac{L}{d} = 5$ and $\frac{D}{d} = 1.5$ is shown in Fig. 3 . As is seen with the development of cavitation the thrust deduction factor decreases . This result is in qualitative agreement with the conclusions of the paper [3] .

By way of comparison the thrust deduction factor calculated by Eq. (2) is plotted on the same curve against propeller loading in the absence of cavitation . The value W_{pnom} for the propulsion system under study amounts to 0.045 .The agreement of t-values in the range of moderate and high loads is considered to be quite satisfactory .

The propeller mounted on "Z" drive operates in a radially nonuniform axial flow . Besides this the propeller oncoming flow exhibits circumferential nonuniformity due to the strut effect and sometimes due to the foils adjacent to the pod . For the purpose of adapting the propeller to the wake the results of the experimental investigation of the velocity field are used . The typical results of the measurements for "Z" drive with length-to-diameter ratio $\frac{L}{d} = 5$ are given in Fig. 4 (a) and (b) . It is of interest to note that the nominal wake factors obtained by integrating the diagrams of velocity distributions are in good agreement with the theoretical data and also with the design wake factor defined in terms of propeller characteristics .

In making calculations use is made of the wake values averaged over the circumference ; however , after the propeller design is finished it is necessary to verify the possibility of cavitation inception on the face of propeller blade in the positions corresponding to the minimum wake values . The most effective method of verification is the visual observation during the tests in a cavitation tunnel .

In choosing the optimum values of the propeller diameter and the number of revolutions for the propulsion systems with "Z" drives it should be taken into account that the increase in the number of revolutions makes it possible to decrease the dimensions of the reduction gear and consequently the propulsion pod dimensions and , as a result , to decrease "Z" drive resistance . In this case the number of revolutions may increase in comparison with the optimum number specific for an isolated propeller .

REFERENCES

1 I. V. TITOFF, A. A. ROUSETSKY, and E. P. GEORGIEVSKAYA, "Principles of cavitating propeller design and development on this basis of screw propellers with better resistance to erosion for hydrofoil vessels "Raketa" and "Meteor", Seventh Symposium on Naval Hydrodynamics, 1968, Rome.

2 E. P. GEORGIEVSKAYA. "Propeller cavitation erosion and methods of protection" (in Russian), Sudostroenie, 1970.

3 V. F. Bavin, I. J. MINIOVICH, "Experimental investigation of interaction between hull and cavitating propeller", 10 th ITTC, 1963, London.

* * *

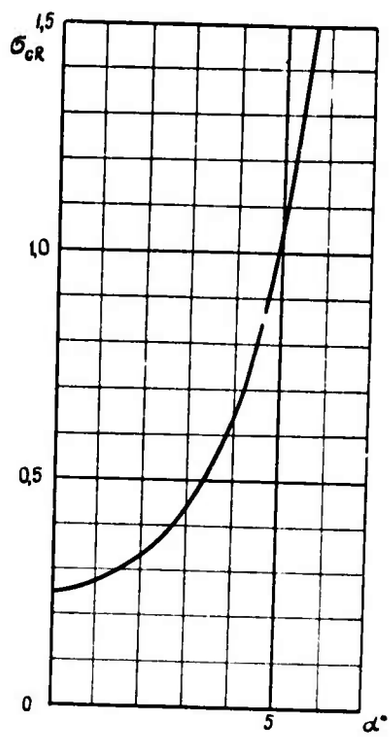


Fig. 1 . Critical cavitation number versus incident angle

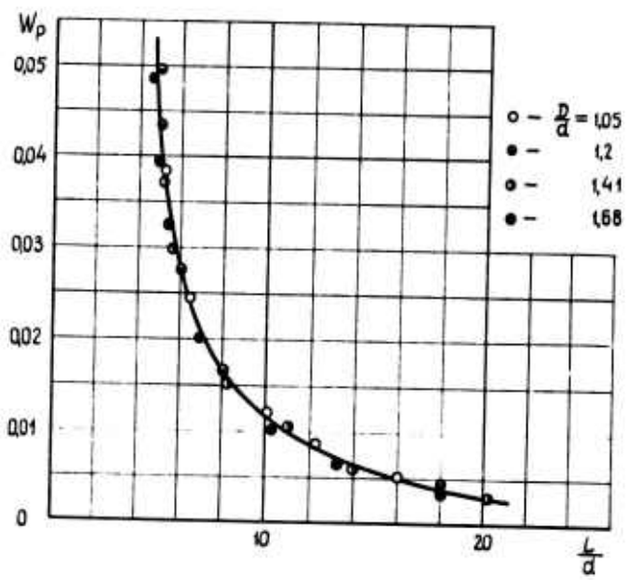


Fig. 2 . Nominal wake factor versus pod length-to-diameter ratio .

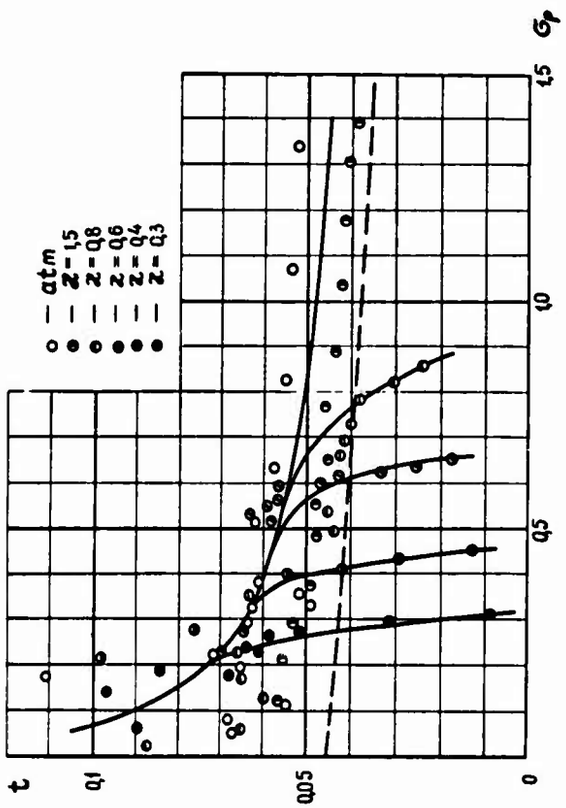
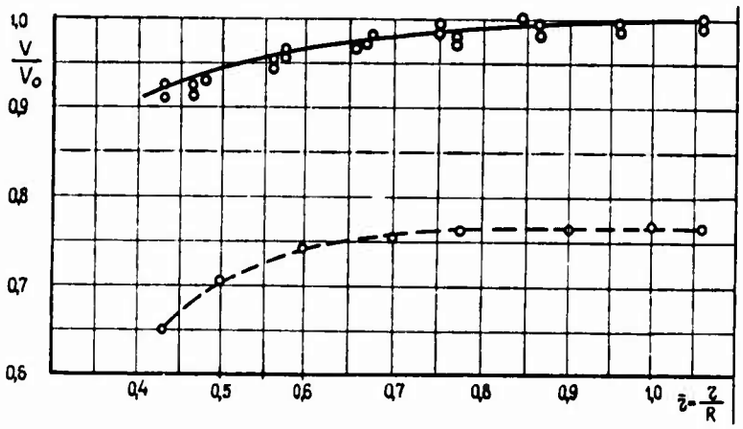
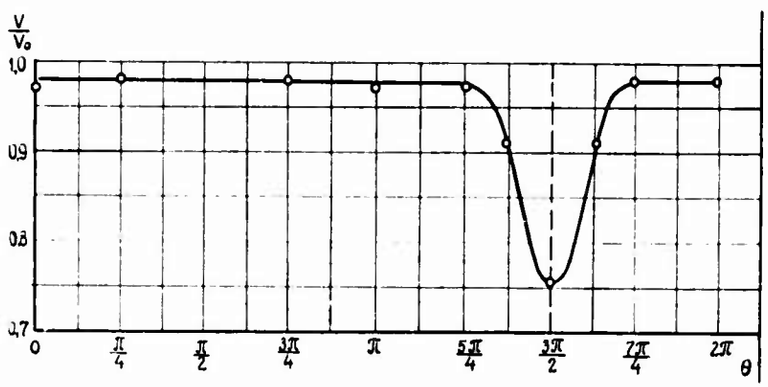


Fig. 3. Thrust deduction factor of the propeller situated at the after part of the propulsion pod.
------- calculation by formula (2)



(a) along the radius
- - - - - - - - in the strut plane



(b) along the circumference at the relative radius $\bar{r} = 0.7$

Fig. 4. Results of measuring the velocity field in way of propeller .

DISCUSSION

Henry M. Cheng
Office of the Chief of Naval Operation
U.S.A.

The author has discussed in the paper mostly what is involved in and the implications of a 'Z'-drive propulsion system. However the technical information presented is very sketchy. I wonder if he is purposely doing so to tease us. Figure 3, showing information on thrust reduction, as he defined it, is only applied to a particular configuration of the pod, that is the L over d equals 5, and the diameter of the propeller (D) to the diameter of the pod d is I.5. I wonder if any more work is being done with other configurations for different L over Ds and D over ds.

Secondly, in the conclusions the author alluded to the fact that the paper is to help us to choose the optimum designs among the parameters, and yet the information presented is incomplete to help us to accomplish this. If it is not already in the plan I am certainly hopeful that this work is going to be pursued.

The third point is that the title implies the whole propulsion system of a 'Z'-drive, whereas the discussion of the other elements of the system, which are very important and have pronounced effects on the selection of the pod, the proportions and the propeller itself, is done only briefly. The material presented is considered only a very small portion of the total system. I wonder if the paper is intended for a general discussion and some more information will be coming from the author ?

Lastly, the information presented is intended for hydrofoil ships application. To my knowledge there are very few, if any, hydrofoils with propulsion pod independent of or divorced from the foil. This brings me to my comment : whether this information is useful at all, if the pod is separated from the foil which is dependent of the loading and the other components of the total system that we call the propulsion system here.

REPLY TO DISCUSSION

Vjacheslav N. Treshchevsky
Kryloff Research Institute
Leningrad U.S.S.R.

I can say that the method described in the paper has been used in the design of several hydrofoils, so that considerations concerning the construction of hydrodynamical complex in general were taken into account.

DISCUSSION

Reuven Leopold
U.S. Navy Naval Ship Engineering Center
Hyattsville, Maryland, U.S.A.

I have a couple of questions relating to the L over D ratio. Has the author established the horsepower range in which pods of 4 to 5 are not over-large in relation to the gears they enclose ? Would not the pod of the higher L over D which enclosed the gears more efficiently be preferable ?

Secondly, the statement that the higher power 'Z'-drive led to a tandem propeller requirement should also be questioned. How would the author propose to avoid cavitation on the aft propeller resulting from flow distortions and vortices of the forward propeller ?

DISCUSSION

Jorgens Strom - Tejsen
Naval Ship Research and Development Center
Bethesda, Maryland U.S.A.

I should like to make a few comments to supplement what Henry Cheng has said.

The application of the propulsion pod has certainly many advantages, as pointed out by the author, in particular the fact it is possible to align the propulsion pod in such a way that the flow into the propeller becomes cleaner and more uniform. It is possible to reduce cavitation and vibration. On the other hand, the introduction of a 'Z'-drive with its complexity of gearing and so on has certainly discouraged its application by most. I would like to bring to your attention the fact that this year wa shall see the development of a superconducting motor which would make it possible to use the propulser pod eventually, at some time in the future. A simple conducting motor would make it possible to have the motor itself mounted down in the pod and still have a sufficiently small size so that the diameter of the propeller to the diameter of the pod would still be of the order of magnitude mentioned by the authors. To what extent is work of this nature being pursued in the Soviet Union today ? Looking through the literature on hull-propeller interaction or propulser-pod-propeller interaction, it is very clear it is difficult to find any really good information about wake and thrust deduction. We have a lot of information from submarines and torpedoes but for most of these cases the propeller diameter is much smaller than what we are talking about here. So I should like to compliment the authors for providing this information ; it is very valuable. The effect of cavitation on thrust deduction is extremely interesting. We have to realise that in the net thrust efficiency for a propulser pod combination the thrust deduction comes in as in any hull-propeller interaction with its full weight, so that unless we can predict the thrust deduction with accuracy we cannot predict this combination. Two or three points means quite a lot. Figure 3, for instance, shows very clearly how the effect of cavitation might change the thrust deduction from, say, .05 to .02. It is three percentage points.

I should like to add my plea to Henry Cheng's for additional

information. It is most important, because if we are going to put a right-angled drive, with its complexity of gears, shafts and double gears down in the pod, and so on, the real problem becomes, as Henry Cheng mentioned, a matter of optimising a system of the pod and the propulser. So long as we have a conventionally loaded or lightly loaded propeller there is really no problem in that the optimum combination can be found, this being very close to the optimum propeller or may be one could say it is a trade-off between weight and the propeller itself, but as we come to the very lightly loaded propeller, as we find them on these craft, hydrofoil boats and so on, it is necessary to take the total system into account in optimising the hydrodynamics. We have to have both the pod track in the picture and the propeller.

It turns out that the optimum combination is a trade-off between the two. It is not the optimum propeller but we have to have a much higher shaft rpm in order to get high efficiency. I wonder if the author has any comments or could add something about the kind of work being carried out in the Sovied Union today. I think this was also pretty similar to what Henry Cheng mentioned.

Finally, I should like to ask a question related to Figure 2. There we see the wake for the pod. Of course the wake is very small. It is suggested from this figure that the diameter of the propeller to the diameter of the pod is really of minor importance, and in a way I can only agree. On the other hand, I think it might well leave us with the impression that the diameter of the propeller is of no significance at all, and that is certainly not so. It is quite clear that as the propeller diameter to pod diameter increases we see the wake being reduced, and we ought to see a set of curves where the uppermost curve, for instance, can be for a smaller propeller diameter to pod diameter ratio and then other curves coming further down. So I am suggesting that the propeller diameter is a parameter that ought to have been in that curve and which will show up as soon as we cover a wider range of propeller diameter to pod diameter ratios. Are any curves available at present ? That is my last question.

DISCUSSION

William B. Morgan
Naval Ship Research and Development Center
Bethesda, Maryland, U.S.A.

1. Reference to Figure 3 what is the definition of $\sigma\rho$? Is æ on Figure 3 the cavitation number or does it have some other definition ? Were the experimental data presented in this figure obtained in the cavitation towing tank.

2. In 1963 at the 10th ITTC, results were presented from the Kryloff Shipbuilding Research Institute on a propeller which was vented with air and operating behind a ship's hull. The results were much the same as shown in Figure 3. However in 1969 at the 12th ITTC, results presented from the Kryloff Shipbuilding Research Institute on a cavitating propeller operating behind a hull in the cavitation towing tank. These results indicated that the thrust deduction might go up with increasing cavitation. Would the author please comment on the discrepancy between these results ?

DISCUSSION

Horst Nowacki
University of Michigan
Ann Arbor, Michigan, U.S.A.

I would appreciate clarification as to whether the definition of the wake fraction W_p used in connection with Figure 2 of the paper is actually the same as in equation (2) of the paper. In the context of equation (Z) one would expect the wake fraction on the propeller axis in the propeller plane to be used whereas in Figure 2 the volume average of the nominal wake fraction in the propeller plane might have been presented. Is this understanding correct ?

REPLY TO DISCUSSION

Vjacheslav N. Treshchevsky
Kryloff Research Institute
Leningrad U.S.S.R.

I am thankful to Mr. Strom-Tejsen for his comments. He is right pointing out that the wake must decrease with increasing D/d ratio. For instance, for L/D = 5 and D/d = 2,5 the value of the wake is about 0,02-0,025. But D/d = 2,5 is too large for practical realization, and Figure 2 corresponds to D/d ratios which are of interest for 'Z'-drive design. I also share Mr. Strom-Tejsen's point of view that taking into account the pod resistance and weight characteristics the efficiency of the whole complex is more important than the maximum fo the propeller efficiency. But the increase of the number of revolutions usually correlates with the loss of the effective thrust corresponding to take-off conditions. Thus when power is restricted these considerations cannot always be realised.

In connection with Mr. Leopold questions I can say that at a given pod diameter and assuming L/d > 5 we have as a consequence the decrease of efficiency. Increase of the L/d ratio may be necessary when speed increases and general design considerations are taken into account. As for better conditions for the after propeller of the two propeller 'Z'-drive construction the free vortex density of the forward propeller must be relaxed and the ratio D for/D aft > 1 chosen.

Answering Mr. Morgan's question concerning Figure 3, I am to tell that x means the cavitation number, $\sigma\rho = \frac{P}{\delta^2 F_p V^2}$ - the load factor. The increase of the thrust deduction due to propeller cavitation can take place only when after the propeller some construction elements are present.

I can also inform in connection with Mr. Novacki question that in formula (2) the effective potential wake, and on Figure 2 - the nominal one are used.

To conclude, I can say that the method described in the paper was used in design of hydrofoils, so that considerations concerning the construction of the hydrodynamic complex in general were taken into account. Information on one such hydrofoil - Typhoon was published

in our Shipbuilding magazine.

DISCUSSION

Reuven Leopold
U.S. Navy Naval Ship Engineering Center
Hyattsville, Maryland, U.S.A.

You mentioned that you have used this to desing an actual case. What is the power, if you have built one in actuality ?

REPLY TO DISCUSSION

Vjacheslav N. Treshchevsky
Kryloff Research Institute
Leningrad U.S.S.R.

I can mention one hydrofoil of that type built. It is called Bafun in Russian. All the details of the construction of this vessel were published in our suipbuilding magazine earlier this year, so you can find that. It is the largest vessel with 'Z'-drive in the Soviet Union.

* * *

HYDRODYNAMIC DEVELOPMENT OF A HIGH SPEED PLANING HULL FOR ROUGH WATER

Daniel Savitsky
Stevens Institute of Technology
Hoboken, New Jersey, U.S.A.
John K. Roper
Atlantic Hydrofoils, Inc.
Hancock, N.H. U.S.A.
Lawrence Benen
Naval Ship Systems Command
U.S. Navy, U.S.A.

ABSTRACT

The hydrodynamic development of a new planing craft intended for sustained high-speed operation in a seaway is discussed. The design philosophy is presented and then implemented to achieve optimum hull form and loading for both smooth and rough water operation of the craft. The resultant hull form is a high length-beam ratio, highly loaded, double chine configuration which provides greatly improved seakeeping, high speed and high maneuverability.

Extensive model tests were conducted to predict the SHP ; EHP ; seakeeping ; course-keeping stability ; and turning characteristics of the design. The extensiveness of the model test program and data analysis are unique for a planing craft. These results are presented in a form which should be of general interest to the designers of a high-speed planing craft.

INTRODUCTION

Although world navies are traditionally considered to be high sea state fleets with ocean-spanning capabilities, the small, high-

Preceding page blank

speed craft is an essential complement to this fleet. These small craft are called into service to assist in ASW operations ; to patrol in coastal and riverine environments ; and to act in concert with larger naval units. Although ubiquitous in numbers, small craft are not individually a high portion of total naval capability, cost, or personnel. In fact, on an equal cost basis, it appears that more units can be procured which can cover more areas than can larger ships. These features have made the small, high-speed craft attractive as the principal naval force for many small countries with large coastlines.

There are basically four different types of small, high-speed craft, i.e., round-bottom boats, hard-chine planing craft, hydrofoil boats, and various forms of air-supported vehicles. The most numerous of these craft is by far the hard-chine planing hull-especially when considering speed-length ratios in excess of approximately 2.0 where dynamic lifting forces are significant. Because they are equipped with large power, lightweight engines, it is not uncommon for planing craft to operate at speed-length ratios in excess of 5.0. Further, it is also not uncommon for these craft to operate sufficiently removed from the coastline so that moderate to high sea states are their normal environment. Thus, the small boat designer is faced with the formidable task of producing craft whose high speed potential is not seriously compromised in rough seas.

The purpose of the present paper is to describe the hydrodynamic development of a new planing craft intended for sustained high-speed operation in a seaway. The design philosophy is presented and then implemented to achieve optimum hull form and loading for both smooth and rough water operation of the craft. The resultant hull form is a high length-beam ratio (6.5), highly loaded (beam loading = 0.75), moderate deadrise (β = 20°), double chine configuration which provides good seakeeping, high speed, and large maneuverability. Extensive model tests were conducted to predict the SHP ; EHP ; seakeeping ; course-keeping stability ; and turning characteristics of the design. The extensiveness of the model test program and data analysis are unique for a planing craft. The present paper presents these results in a form which should be of general interest to designers of high-speed planing hulls.

POSTULATED PERFORMANCE OBJECTIVES

The design of any marine craft is based upon specifications which have been prescribed to achieve desired performance objectives. Among the more significant requirements which have a pronounced influence on hull form are : operational speeds ; dimensions and

weight of payload components ; sea state; tolerable "g" loadings in that sea state ; restrictions on draft, length, and beam, metacentric stability ; and maneuvering qualities. Certainly, special purpose craft have additional restrictions but these are not included in this study.

For the present paper, the following set of performance specifications are prescribed.

1. Full Load Displacement : 150,000 lbs.

A designer's experience is invaluable in making the first engineering estimate of full load displacement. Nevertheless, design studies and possible model tests are carried out at additional displacements of approximately 80% and 120% of the initial estimate.

2. Maximum Speed : In excess of 40 knots.

Interception and attack missions require high speeds. For the present study, a nominal speed of 45 knots is assumed.

3. Cruise Speed : Approximately 12 knots.

A patrol mission requires long endurance at slow search speeds. A cruise speed of 12 knots is selected.

4. Maximum Hull Draft : 3.5 ft.

5. Operational Sea State : 3.

It is desired that the craft operate at 45 knots in a state 3 head sea having a significant wave height of 4.6 ft.

6. Average Center-of-Gravity Impact Acceleration : $(\eta_{CG})_{avg} = 0.4g$

It is specified that the average center-of-gravity impact acceleration should not exceed 0.4g while running in a state 3 head sea at 45 knots.

7. Metacentric Stability : GM = 3.0 ft.

A GM of 3.0 ft. was selected to provide metacentric stability under conditions of high wind and severe super-structure icing.

The above set of requirements do not pre-specify the length or beam of the craft. There may, of course, be operations where

either of these dimensions must be fixed in advance. The design procedure developed in subsequent sections of this paper can be equally applied to those cases and will show the extent to which the pre-specified length, for example, may inhibit attainment of the performance requirements.

DESIGN PROCEDURES FOR BASIC HULL DIMENSIONS

In this section of the paper a methodology is developed for rationally selecting the length, beam, longitudinal center-of-gravity, nominal deadrise, and effective horsepower of the basic hull form which will satisfy the performance requirements previously specified. No attempt is made to optimize the hull design to attain, say, minimum resistance while satisfying the seakeeping requirements. This can be developed as a subsequent study using the basic design procedures developed herein.

The design procedure is primarily based upon a combination of smooth water prediction techniques such as given in References 1 and 2, and rough water prediction techniques such as given in Reference 3 . While both studies are concerned with prismatic planing hulls (constant beam, constant deadrise, buttocks parallel to the keel) these techniques have been successfully applied to actual hull forms by proper selection of an effective constant deadrise and beam.

Separate considerations are first given to relating hull dimensions to the following hydrodynamic characteristics

1. Hydrodynamic Impact in a Seaway
2. Hydrostatic Displacement
3. Smooth Water Planing (High Speed)
4. Smooth Water Operation (Low Speed)
5. Metacentric Stability

The results of these elemental studies are then combined to specify a hull form, overall dimensions, center of gravity, and effective horse-power to achieve the operational objectives.

Hydrodynamic Impact in a Seaway

In Reference 3 , Fridsma presents the results of a systematic study of the effects of deadrise, trim, loading, length-beam ratio, bow section shape, speed, and sea state on the performance of a series of prismatic planing models operating in irregular waves. A statistical analysis of the measurements of added resistance, heave motions, pitch motions and impact accelerations resulted in quantitative relations between these measured quantities and hull dimensions and operating conditions. The results of those parametric studies are summarized in design charts which enable full-scale performance predictions for planing craft. Using the procedures described by Fridsma, the average center of gravity acceleration is computed for a range of combinations of beam, length-beam ratio, deadrise and trim angle for a maximum speed of 45 knots in a state 3 head sea. To enter the design charts of Reference 3 , the following coefficients are evaluated :

C_Δ = Beam loading = $\frac{\Delta}{wB^3}$

$V_k/\sqrt{L}$ = Speed-length ratio

L/B = Length-beam ratio

$H_{1/3}/B$ = Significant wave height/beam = $H_{1/3}/B$

C_v = Speed coefficient = $V/\sqrt{gB}$

where

Δ = displacement = 150,000 lbs.

V_k = maximum speed = 45 knots

V = maximum speed = 76 ft/sec.

L = length between perpendiculars, ft.

B = average beam over aft 80% of hull, ft.

$H_{1/3}$ = significant wave in state 3 sea = 4.6 ft.

w = weight density of water = 64 lbs/ft^3

ρ = mass density of water = 2 lb-sec^2/ft^4

and

β = deadrise angle at station 5 , degrees

τ = trim angle of mean buttock line, degrees

$(\eta_{CG})_{avg}$ = average vertical acceleration at center of gravity "g"

$(\eta_{CG})_{1/10}$ = 1/10 highest vertical acceleration at center of gravity "g". From the statistical analysis of Reference 3 , $(\eta_{CG})_{1/10} = 3.3\ (\eta_{CG})_{avg}$

The previous coefficients are evaluated for a range of initially assumed values of beam :

B	C_Δ	$1/C_\Delta^2$	$H_{1/3}/B$	C_v
13 ft.	1.070	.86	.353	3.76
14	.856	1.36	.328	3.58
15	.695	2.06	.307	3.45
18	.402	6.10	.258	3.16

The following relations between initially assumed beam, assumed length-beam ratio, and speed-length ratio will also prove useful :

	B = 13 ft.		B = 14 ft.		B = 15 ft.		B = 18 ft.	
L/B	L	$V_k/\sqrt{L}$	L	$V_k/\sqrt{L}$	L	$V_k/\sqrt{L}$	L	$V_k/\sqrt{L}$
4	52 ft.	6.2	56 ft.	6.0	60 ft.	5.8	72 ft.	5.3
5	65	5.6	70	5.4	75	5.2	90	4.7
6	78	5.1	84	4.9	90	4.7	108	4.3

Referring to Figures 16, 17, and 18 of Reference 3 , which are reproduced as Figures 1, 2, and 3 of the present report, it is seen that the average value of center-of-gravity acceleration is obtained

directly from these design charts for arbitrary combinations of L/B, $1/C^2_\Delta$, $V_k/\sqrt{L}$, and $H^{1/3}/B$ such as listed above. It is to be noted that these results are for a trim angle of 4° and a deadrise angle of 20°. Corrections for other combinations of trim and deadrise angle will be described subsequently.

For each assumed value of beam, the average CG accelerations for 45 knots in a state 3 head sea is obtained from the design charts of Figures 1-3 and plotted on the right half of Figure 4 as a function of length-beam ratio. These results are obtained by extrapolations of the design charts as suggested in Reference 3 . The ordinate of the plot in Figure 4 is the quantity :

$$\eta_{CG\ (Average)} \left[\frac{\tau^\circ}{4} \left(\frac{5}{3} - \frac{\beta^\circ}{30} \right) \right]$$

which defines the dependence of acceleration upon trim and deadrise as developed in Reference 3. For $\tau = 4°$ and $\beta = 20°$, the quantity in the square brackets is unity so that η_{CG}(Average) as given in Figure 4, corresponds to the design charts of Reference 3 . Superposed on Figure 4 are curves of constant boat length for various combinations of beam and length-beam ratio.

The quantity $\tau°/4\ (5/3 - \beta°/30)$ is plotted on the left half of Figure 4 for ease of applying these results to arbitrary combinations of τ and β .

Some interesting observations can be made by an examination of the results in Figure 4 :

Effect of Beam on Hydrodynamic Impact :

All other conditions being equal, a reduction of hull beam leads to significant reductions in impact load. For example, a 28% reduction in beam (from 18 ft. to 13 ft.) results in a 69% reduction in impact accelerations (from 1.10g to 0.35g). Even a 1 ft. reduction in beam, from 15 ft. to 14 ft., decreases the impact acceleration by approximately 29%. This powerful effect of beam results from the large dependence of impact upon the inverse of beam loading coefficient $C_\Delta = \Delta/wB$. The effect of C_Δ has long been familiar to the designer of water-based aircraft (References 4 and 5) and has just recently been quantitatively identified by Fridsma[3] for the case of the planing hull.

$$(2)\quad K = \frac{.40\ g}{(\eta_{CG})_{avg}\ (\tau = 4^\circ,\ \beta = 20^\circ)} = \frac{\tau^\circ}{4}\left(\frac{5}{3} - \frac{\beta^\circ}{30}\right)$$

(3) τ = equilibrium trim angle to achieve $(\eta_{CG})_{avg} = 0.40\ g$ for

$\beta = 20^\circ$, $V_K = 45$; $\Delta = 150,000$ lb.

$$\tau = \frac{4K}{\left(\frac{5}{3} - \frac{20}{30}\right)} = 4K$$

Static Displacement Considerations

The block coefficient for planing hulls can vary between 0.40 and 0.50. Having fixed a draft of 3.5 ft. for the present design, the relations between length and beam will take on a more limited set of values than those previously developed from considerations of only hull impact.

$$C_B = \frac{\Delta}{L\ B\ d\ w}$$

where

Δ = 150,000 lbs.

L = length between perpendiculars, ft.

d = maximum draft, 3.5 ft.

w = weight density of water, 64 lbs/ft^3

B	C_B = 0.40 L	C_B = 0.45 L	C_B = 0.50 L
13 ft.	128 ft.	114 ft.	103 ft.
14	119	106	95
15	111	98	89
18	93	82	75

These combinations of length and beam are superposed on the plots of Figure 4. This results in a substantial reduction in length-beam combinations for further study.

Smooth Water Planing (45 knots)

A computational procedure for predicting the smooth water equilibrium conditions of a planing hull is given by Savitsky[1] . This procedure has been programmed for high-speed computers and is generally available to the small boat naval architect. In Reference 2 , Hadler extends this work to include the effects of propellers and appendages. Unfortunately, a computer program for this extended computation is not yet generally available to the small boat naval architect.

For the present study, which is intended to define the principal hull dimensions for preliminary design, the simplified computational procedure developed by Savitsky is considered adequate. A 20° deadrise hull is initially assumed and the equilibrium trim and wetted keel length are computed for values of beam between 13 ft. and 18 ft; for longitudinal center-of-gravity positions between 22 ft. and 44 ft. forward of the transom, for a planing speed of 45 knots and a displacement of 150,000 lbs. The results of this computation are plotted in Figure 5. For each value of beam, the trim angle required to achieve $(\eta_{CG})_{avg} = 0.4$ is also indicated.

Using the results of Figure 5, the following relation between beam, LCG , wetted keel length and suggested L (load waterline length) is obtained. These values are also plotted in Figure 6.

B	τ	LCG	L_k	L	C_B	$L/\nabla^{1/3}$
13 ft.	4.5°	32.5 ft.	62 ft.	68 ft.	.76	5.2
14	3.3	38.0	82	90	.53	6.8
15	2.2	42.5	96	106	.42	8.0
18	1.6	44.0	110	121	.31	9.2

The length L is load waterline length and is taken to be equal to 1.10 L_k. It has been found that this relation between L and L_k is most satisfactory. If L is less than 10% greater than L_k, there is substantial bow immersion at high speed resulting in a significant increase in smooth water resistance. When L is much larger than 1.10 L_k, the excessive hull length forward of L_k provides additional impact area when running in a seaway with resultant increasing impact loads.

Also included in the previous tabulation are the corresponding values of block coefficient C_B and slenderness ratio $L/\nabla^{1/3}$. These will be subsequently discussed.

Smooth Water Operation (Low Speeds)

Since one of the operational objectives for the craft is to cruise at 12 knots for extended periods, the hydrodynamic resistance should be minimized. For a displacement of 150,000 lbs., the volume Froude number

$$F_\nabla = \frac{V}{\sqrt{g\,\nabla^{1/3}}} = \frac{20.4}{\sqrt{32.2 \times (2350)^{1/3}}} = 1.0$$

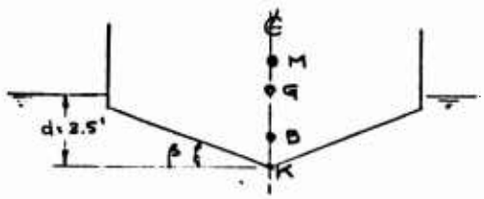
From a basic study of the resistance of planing hulls in the prehump speed region (Reference 6), it has been found that low speed resistance is primarily dependent upon slenderness ratio $L/\nabla^{1/3}$. Figure 7 of this report shows the variation of resistance-weight ratio of the Series 62 hull form (Reference 7) as a function of $L/\nabla^{1/3}$ for $F_\nabla = 1.0$. It is seen that, although the data points represent a wide range of hull loadings and length-beam ratios, they

are closely represented by a single curve relating the data to $L/\nabla^{1/3}$. Similar plots for other hull series are given in Reference 6 and also indicate the pronounced dependence of low speed resistance on slenderness ratio. Using these results as a guide, it is concluded that a value of $L/\nabla^{1/3}$ equal to at least 7.0 is essential for low resistance at pre-hump speeds. For a displacement of 150,000 lbs., this results in a minimum hull length of 92 ft.

Comparing this criteria with possible combinations of hull dimensions of page 429, it is seen that a hull beam should be at least equal to or greater than 14 ft. This limitation is also plotted on Figure 6.

Metacentric Stability

The specified requirement for metacentric stability is that the GM be equal to at least 3.0 ft. An engineering estimate of GM for a planing craft with deadrise is made using the following assumptions.



$$KB = \frac{2}{3} d = \frac{2}{3}(3.5) = 2.33 \text{ ft.}$$

$$I = \text{water plane moment of inertia} = .55\left(\frac{1}{12} L B^3\right)$$

Preliminary weight estimates for the present design showed that the vertical center of gravity of the craft, KG, is 6.2 ft. above the Keel. Considering a minimum boat lenght of 92 ft., as determined from the low speed requirement, the following values of GM are computed for each assumed beam.

B	I	BM	KM	GM
13 ft.	9,110 ft.^{4}	3.9 ft.	6.2 ft.	0.0 ft.
14	11,400	4.9	7.2	1.0
15	14,000	6.0	8.3	2.1
15.7	16,410	7.0	9.3	3.1
18	24,200	10.4	12.7	6.5

where

KG = 6.2 ft.

BM = I/V

V = 150,000/64 = 2,340 ft^3

KM = KB + BM

GM = KM - KG

A minimum beam of 15.7 ft. is required to attain the specified metacentric height of 3.0 ft.

Selection of Basic Hull Dimensions

The previous elemental hull studies developed the following restrictions on hull dimensions to satisfy the postulated operating conditions.

Low Speed Operation (V_k = 12 knots)

For low resistance in the cruise condition, the hull length should be equal to or greater than 92 ft.

Metacentric Stability (GM = 3.0 ft.)

For a hull length of 92 ft., the required hull beam is 15.7 ft.

Hydrodynamic Impact (η_{CG})$_{avg}$ = 0.4 g in state 3 head sea)

Two possible options are available for a 20° deadrise hull.

(1)

$\overline{B}$	=	15.7 ft.
L	=	116 ft.
LCG	=	43.5 ft.
C_B	=	.36

(2)

$\overline{B}$	=	14 ft.
L	=	92 ft.
LCG	=	38 ft.
C_B	=	.53

Option (1) satisfies all the hydrodynamic and operational requirements while Option (2) does not satisfy the basic metacentric height requirement. The 116 ft. boat lenght of Option (1) was considered excessive when compared with space requirements for internal arrangements. This excessive length would increase the cost of the boat without materially improving its performance.

As a compromise design, a double chine hull having a length of 92 ft. was selected. A mid-length section through this hull is shown in Figure 8. The inner chine beam is 14 ft. and the outer chine beam is 15.7 ft. In the static or low speed condition, the wetted beam is 15.7 ft. so that the metacentric stability requirement is satisfied by the combination of L = 92 ft. and b = 15.7 ft. At the 45-knot condition, the flow separates from the lower chine so that the 92 ft. long hull has an effective beam of 14 ft. This satisfies the high-speed impact requirements. The metacentric stability of the craft is now satisfied by considering the additional roll stabilizing moments developed by the dynamic loads generated at high speeds.

In summary then, the following basic hull dimensions and loadings are selected for preliminary design

L = 92 ft.

B_{outer} = 15.7 ft.

B_{inner} = 14 ft.

LCG = 38 ft.

β = 20° (Sta. 5)

Δ = 150,000 lbs.

At a smooth water planing speed of 45 knots, this craft is expected to run at a trim angle of 3.3° and develop $(\eta_{CG})_{avg}$ = 0.4 g in a State 3 head sea.

It will be noted that a nominal 20° deadrise hull has been selected. Considerations were also given to deadrise angles of 10° and 30°. The details of these calculations (which follow the previous procedures) will not be presented, but the results will be summarized. Figure 9 presents a plot of resistance-weight ratio (R/Δ) versus trim angle for deadrise angles of 10°, 20°, and 30°. These results follow from Reference 1. Superposed on Figure 9 are the maximum trim angles for combinations of deadrise and beam which will result in $(\eta_{CG})_{avg}$ = 0.4 g when the 150,000 lb. craft runs at 45 knots in a State 3 head sea.

Considering the 30° deadrise case, it is seen that a 14 ft. beam requires a trim angle equal to or less than 5° to satisfy the impact requirements. Further, the minimum drag-lift ratio for a 30° deadrise craft occurs at a trim angle of approximately 5°. This high trim angle could impair visibility during high-speed operation and was thus not considered acceptable. A reduction in trim angle to improve visibility would reduce the impact loads below the maximum acceptable value but, according to Figure 9, would significantly increase the drag-lift ratio to values substantially larger than for the 20° deadrise surface. Thus, the 30° deadrise case was not further considered.

A 10° deadrise surface having a beam of 14 ft. would be required to run at a trim angle of 2.4° so as not to exceed the design impact acceleration. For this case, the drag-lift ratio would be slightly less than that for the 20° deadrise surface. The boat length and LCG position for β = 10°, τ = 2.4°, b = 14 ft., Δ = 150,000 lbs. and V_k = 45 knots are computed from the monograph given in Figure 19 of Reference 1:

L_k = 69 ft.

LCG = 35 ft.

$L = 1.10 \times L_k = 76$ ft.

The boat length of 76 ft. is 20% less than the 92 ft. length required for low resistance at 12 knots and is thus not acceptable.

In summary then, the 20° deadrise hull was accepted as best meeting the design requirements of the craft.

Description of Final Hull Form

The lines are shown in Figure 10 and show that the principal dimensions of the craft are in substantial agreement with those developed by the design procedures presented herein.

Length, design waterline	92'-0"
Beam, lower chine (nominal)	14'-0"
Beam, upper chine (nominal)	15'-7"
Deadrise, station 5	20°
Deadrise, station 10	10°
Draft (full load)	3.5

It is seen that the craft is a hard, double-chine hull whose high-length beam ratio is favorable for low resistance and good seakeeping. Several detail design features are of interest and will be separately described. Koelbel (Reference 8) provides excellent design guidance in this regard.

Chine Configuration

It has been found that, for planing craft operating at speed-length ratios greater than approximately 2.0 - 2.5, a hard chine is required to assure complete separation of the flow from the bottom. At these speed-length ratios, a round bilge hull will prevent flow separation and result in significant side wetting and thus increase the hydrodynamic drag. The present 45-knot design condition corresponds to a speed-length ratio of 4.6 and clearly requires a hard chine

configuration.

In designing a double chine configuration, it is important that the upper chine location be within the cavity found by the boundary of the flow separation from the lower chine. As shown by Korvin-Kroukovsky (Reference 9), the trajectory of the free streamline representing the cavity of the boundary is a function of deadrise angle. Figure 11 of the present report, which is taken from Reference 9, plots the separation trajectory for various deadrise angles. It is seen that the width of the separation cavity increases with decreasing deadrise angle. If the upper chine is located outboard of this cavity boundary, the originally separated flow from the lower chine will reattach to the bottom somewhere between both chines and thus preclude complete flow separation from the lower chine. In the present design, the outer deadrise angle is 45° and the outer chine is approximately 0.80 ft. outboard of the inner chine. This is sufficient to clear the lower chine trajectory at station 5 and result in complete separation from the lower chine. Observations of the wetted bottom areas during model tests confirmed this prediction.

Section Shapes

The section shapes are slightly convex. This section pounds less than others of equal deadrise because there is less likelihood of instantaneous water contact over large bottom areas.

Planform Shape

At high planing speeds, when dynamic lift predominates, it is usual to narrow the beam towards the stern. This reduces bottom friction without a noticeable loss in lift. The narrow transom also avoids the possibility of reattachment of the separation cavity formed in the region of maximum beam. For the present design, the transom width was determined by considerations of space requirements for the auxiliary machinery in the stern area. This resulted in a slight reduction of beam towards the stern which, in the model tests, was found to be sufficient to avoid flow reattachment.

Bottom Warp

The increase in deadrise with length forward of the transom is referred to as bottom warp and is required to provide a relatively high deadrise in the bow regions. Brown (Reference 10) has shown that there is a slight reduction in planing efficiency for moderate values of warp. The slightly convex bottom sections, from keel to lower chine, used in the planing area aft of the high-speed stagnation line

are easily warped to result in increased deadrise and curvature in the bow sections. This combination reduces pounding and impact pressures in a seaway. The transverse section shape above the lower chine is increasingly more concave as the bow is approached. This upper "flare" is desirable to deflect the bow spray outboard of the deck and to provide additional buoyancy to reduce low-speed pitching in a seaway.

Spray Rails

Spray rails are provided along both chines to assure flow separation from the chines. The spray rail for the upper chine must not extend into the separated flow cavity formed by the lower chine. Otherwise flow reattachment will occur at high speeds. Separation from the upper chine occurs at a speed-length ratio between 2.0 to 2.5 while separation from the lower chine is expected to occur at a speed-length ratio of approximately 3.0.

Final Design

An artist's conception of the final design is given in Figures 12 and 13.

MODEL TESTS

Model tests were conducted at the Davidson Laboratory, Stevens Institute of Technology to evaluate the performance of the craft in smooth water and waves. A 1/11-scale model was used to determine EHP and SHP. A 1/16-scale model was used to investigate the seakeeping, maneuvering, and turning ability of the craft. Some of the principal results and test procedures are presented herein.

Resistance and Propulsion

Smooth Water Resistance

A 1/11-scale model was constructed according to the lines of Figure 10. To assure flow separation from the bottom, the upper and lower chines of the model were sharpened by the addition of mylar plastic strips which projected vertically a distance of 1/32 of an inch below each chine. Tests were made for a range of loadings and speeds. The test procedure simulated towing the model through the shaft axis. Measurements were made of the heave, trim, drag and wetted areas. For the purpose of the present paper, Figure 14 presents a comparison between values of trim and drag computed by

the procedures of Reference 1 and the results of model tests. The comparison is for a displacement of 150,000 lbs. with an LCG of 38 ft. In the computational procedure, the upper chine beam (15.7 ft.) is used for speeds up to 40 knots and the lower chine beam (14 ft.) is used for higher speeds. This was consistent with test results where complete flow separation from the lower chine was observed at speeds greater than approximately 40 knots (full-scale equivalent). An effective deadrise angle of 20° was used in the computations.

It is seen that the computed and measured results agree well enough to justify use of Reference 1 for engineering estimates of planing boat performance. At speeds below 20 knots, extensive bow immersion precluded application of the methods of Reference 1 which are restricted to prismatic-like planing hulls. Reference 6 will provide procedures for performance estimates at low speeds where bow immersion is significant.

It is interesting to note the complete absence of a "hump" trim in Figure 14. This is attributed to the high-length beam ratio hull which, for normal LCG positions, is constrained to run at low trim angles. The low trim is, of course, most beneficial to improved seakeeping.

Self-Propelled Tests

Self-propelled tests of the 1/11-scale model were carried out to determine propulsion characteristics, e.g. wake fraction, thrust deduction coefficient, relative rotative efficiency and, subsequently, predictions of delivered horsepower.

The test program included resistance tests of the partly appended model, open water tests of the stock propellers used in propulsion tests and self-propelled tests of the 1/11-scale model for overload and underload conditions (so-called "British" method) at a number of speeds and displacement conditions. The open-water tests were carried out with the shaft horizontal and with a shaft inclination of 12°. Self-propelled tests were made with all three propellers driving and instrumented.

The rudders were not fitted for these tests since they are located approximately 4 propeller diameters aft of the propellers, out-of-line with any of the propeller races and, consequently, could have little influence on propeller-hull interaction.

Three propeller dynamometers were installed in the model

for measuring thrust, torque and RPM. These were "reaction" type dynamometers having capacities of 10 lb. thrust, 5 in-lb. torque, RPM up to 10,000 and 0.50 HP. The averaging of the force and motion signals, as well as additional data processing, was accomplished using a PDP-8E computer on line. The computer has a built-in analog-to-digital converter and is programmed to carry out operations such as signal averaging, correcting for zero levels, and multiplying by calibration factors to obtain results in engineering units.

Davidson Laboratory uses the overload and underload testing procedure where a group of test runs are carried out at fixed speed with various rates of propeller rotation. This type of test provides information which may be applied for any desired assumptions concerning appendage drag, roughness allowance, scale ratio, air drag or rough water-drag increment.

Some typical propeller-hull interaction factors, derived from the test data for the model self-propulsion point (towing force = 0), are given for a speed corresponding to 45 knots and a displacement of 150,000 lbs.

$$\text{Wake fractions} = \begin{matrix} 1 - W_T = 0.99 \\ 1 - W_Q = 0.96 \end{matrix}$$

$$\text{Relative rotative efficiency} = {}_{RR} = Q_o/Q_B = 0.92$$

$$\text{Thrust deduction} = 1 - t = 0.94$$

These values of wake fraction, relative rotative efficiency and thrust deduction are used to select the particular propeller design which absorbs the installed power at the proper RPM and speed and has good efficiency even while operating under cavitating conditions.

It is interesting to note that the thrust wake fraction is 0.99 indicating an essentially undisturbed flow to the propeller. The thrust deduction is small, $1-t = 0.94$, indicating a small effect of propeller-induced flow on the hull resistance.

Rough Water Tests

The rough water performance was measured for several loads and LCG positions in a variety of sea states. Measured quantities included heave and pitch motions, vertical accelerations at the bow and CG, and mean resistance in waves. During each test run, the

data were processed by a PDP-8E computer on line. Each channel of data was analyzed at the rate of 200 scans per second and, at the conclusion of each test run, an ordered listing of the peaks and troughs of the pitch and heave motions and the accelerations at the bow and CG were printed out in addition to statistics such as 1/10, 1/3, and average values. This instantaneous output of processed data was extremely useful in interpreting the results.

A comparison between the computed average CG acceleration and the results of model tests is tabulated below for a displacement of 150,000 lbs., a speed of 45 knots and a range of LCG in a head State 3 sea.

	$(\eta_{CG})_{avg}$	
LCG	Computed	Measured
38	0.40 g	0.35 g
34	0.50 g	0.45 g
30	0.60 g	0.55 g

It is seen that the computed values are approximately 0.05g larger than the measured values. The average values are used in this comparison since, in random sea tests, the average statistics include considerably more impact peaks than do the 1/10 highest statistics. Thus, the comparison between measured and computed results are expected to be more reliable. It is interesting to note that a forward movement of LCG from 34 ft. to 38 ft. reduces the impact accelerations by nearly 35 %.

The measured pitch and heave motions and added resistance in waves are not presented in this paper, but are in substantial agreement with results computed by the methods of Reference 3 .

Coursekeeping Stability and Turning Performance

The calm water stability and maneuvering characteristics of the 1/16-scale model with appendages were investigated by means of straight course tests and by rotating arm tests. In both tests, the model was free to heave and pitch, but was restrained in yaw, roll, surge and sway. The restraining forces and moments were measured

in a body axis system having its origin at the center-of-gravity.

The straight course tests were made at port yaw angles up to 12° and at port roll angles up to 20°. Also, at zero yaw and roll the effects due to rudder deflection up to 35° were measured.

The rotating arm tests were made at port yaw angles up to 12°, port roll angles up to 20° with the boat making port turns at radii corresponding to 2.5 and 5.0 boat lengths.

The model was tested at a displacement of 120,000 lbs. at an LCG = 34 ft. and at speeds corresponding to 14 and 45 knots. The data obtained during the tests were processed on a digital computer and tables of drag, side force, yaw moment, roll moment, trim and heave were produced as a function of yaw angle and roll angle for each of the radii and speeds investigated. The reduced data were plotted and cross-faired as a function of yaw angle and radius for each of the speeds and roll angles. From these plots, which are not reproduced here, the coefficients needed for stability analysis were determined and are tabulated below. These include the rates of change of side force and yaw moment with yaw angle and radius at zero roll angle.

Hydrodynamic and Inertia Coefficients

Speed	N'_v	N'_r	Y'_v	Y'_r	n'_z	m'_y
14 knots	0.110	-.103	-.316	0.0293	1.00	0.651
45 knots	0.096	-.052	-.258	0.0084	1.00	0.651

where

$n'_z + I'_z = 2 I_z / \rho B^5$ $\qquad$ $m'_y = m' = 2 W / \rho g B^3$

$N' = N/qB^3$ $\qquad$ $Y' = Y/qB^2$

$q = \rho U^2/2$ $\qquad$ B = beam = 15.7 ft.

N = yaw moment, ft-lbs. $\qquad$ Y = side force, lbs.

W = 120,000 lbs.

Dynamic Course Stability

Dynamic stability relates to the track of a vessel following a small disturbance in, for example, heading angle when no corrective action is taken (i.e., controls fixed). A ship is said to be dynamically stable when, having suffered a disturbance from an initial straight path, it tends to take up a new straight path. The vessel may perform diminishing oscillations about the new track. The degree of stability is measured by the magnitude of a stability index which is negative if the vessel is stable and vice versa.

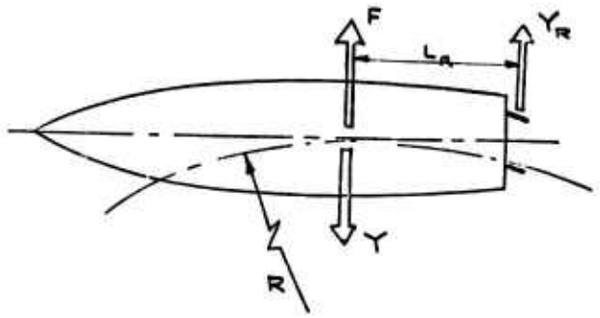
The course stability may be found from linear differential equations governing the craft's motion. The coefficients in these equations may be found from the forces and moments measured during steady state turns, as described above. At both 14 and 45 knots, the craft is statically stable, that is to say that when run at a constant yaw angle the yaw moment tends to reduce the yaw angle. Static stability is measured by the coefficient N'_v and is positive for static stability. However, the degree of static stability is not enough to impair maneuverability. Since it is statically stable, it follows that the craft is also dynamically stable, though oscillatory. These oscillations decay very rapidly, however, being damped to 40 % of the initial disturbance by the time the craft has traveled one boat length. The stability index has been calculated to be

Speed	Stability Index
14 knots	$\sigma = -0.29$
45 knots	$\sigma = -0.22$

Turning Performance

The straight course tests with the rudders deflected showed that the longitudinal position of the center of pressure coincided with the quarter chord point of the mean rudder chord and the vertical location coincided with the depth of the mean rudder chord. Thus, the effect of the rudders can be represented by a force acting at the aerodynamic center of the rudder. The magnitude of the rudder "lift force" was calculated from aerodynamic theory and confirmed by experiment to be represented by a lift curve slope of 0.0373 per degree.

The forces acting on the boat when making a steady turn to port are shown in the following sketch.



The equilibrium equations in side force and yaw moment are

$$Y = F + Y_R \qquad \text{and} \qquad N = \ell_R Y_R$$

which can be combined into

$$F = Y - N/\ell_R \tag{1}$$

The component of centrifugal force in the x, y plane when the craft has yaw and roll angle of β and ϕ is

$$F = (w/g)\ (V^2/R) \cos \beta \cos \varphi$$

For each speed and radius, the quantity $Y - N/\ell_R$ is plotted as a function of yaw angle for each roll angle and the yaw angles necessary to satisfy Equation (1) are found. At these intersections, the roll moment due to the rudder is found from

$$K_R = (Y - F)\, d_R$$

where d_R is the distance of the rudder mean chord below the craft VCG. This roll moment is superimposed on a plot of roll moment versus roll angle to give the roll angles at equilibrium.

The results of this calculation show that the craft turning diameter is less than 15 boat lengths and that it will roll inboard during turns.

CONCLUSIONS

A quantitative design procedure is described to determine the principal hull dimensions for planing craft intended to satisfy prescribed operational conditions. The method is applied to establish a hull form required to operate at high speeds in moderate sea states. Principal design features of this craft are described. Extensive model tests were conducted to predict the SHP, EHP, seakeeping, course-keeping stability and turning characteristics of the design. Some of these model test results are presented.

ACKNOWLEDGEMENTS

The authors would like to express their appreciation to Mr. Joseph G. Koelbel, Jr. and to Mr. G. Gordon Sammis for their invaluable assistance in all phases of the development of this new planing craft.

REFERENCES

1 SAVITSKY, Daniel, "Hydrodynamic Design of Planing Hulls" Marine Technology, SNAME, Vol. 1, No. 1, October 1964.

2 HADLER, J.B., "The Prediction of Power Performance of Planing Craft", SNAME Transactions, Vol. 74, 1966.

3 FRIDSMA, Gerard, "A Systematic Study of the Rough-Water Performance of Planing Boats, Irregular Waves - Part II" Davidson Laboratory, Stevens Institute of Technology Report No. 1495, March 1971.

4 MILWITZSKY, Benjamin, "Generalized Theory for Seaplane Impact" NACA Report 1103, 1952.

5 MIXSON, John S., "The Effect of Beam Loading on Water

Impact Loads and Motions", NASA Memo 1-5-596, 1959.

6 SAVITSKY, Daniel and MERCIER, J., "Resistance of Transom-Stern Craft in the Pre-Planing Regime", Davidson Laboratory, Stevens Institute of Technology. Report 5 IT-DL-73-1667. July 1973.

7 CLEMENT, E. P. and BLOUNT, D. L., "Resistance Tests of a Systematic Series of Planing Hull Forms", Transactions SNAME, Vol. 71, 1963.

8 KOELBEL, Joseph G., Jr., "The Detail Design of Planing Hull Forms", SNAME South East Section on Smallcraft Hydrodynamics, Miami, Florida, May 1966.

9 KORVIN-KROUKOVSKY, B. V. and CHABROW, F. R., "The Discontinuous Fluid Flow Past an Immersed Wedge" Davidson Laboratory, Stevens Institude of Technology Report 334, October 1948.

10 BROWN, P. W., "An Experimental Study of Planing Surfaces with Warp" Davidson Laboratory, Stevens Institute of Technology (Report to be published).

* * *

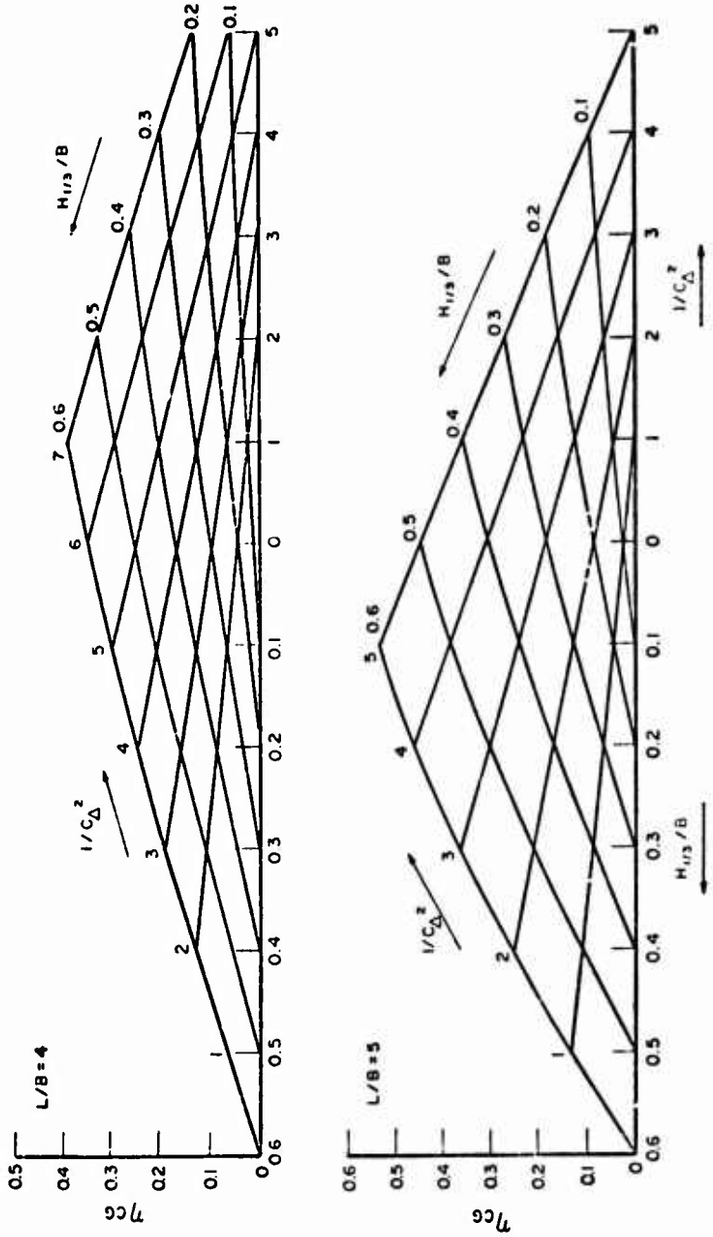


Figure 1. Average CG acceleration at $V/\sqrt{L} = 2$
($\tau = 4°$, $\beta = 20°$)

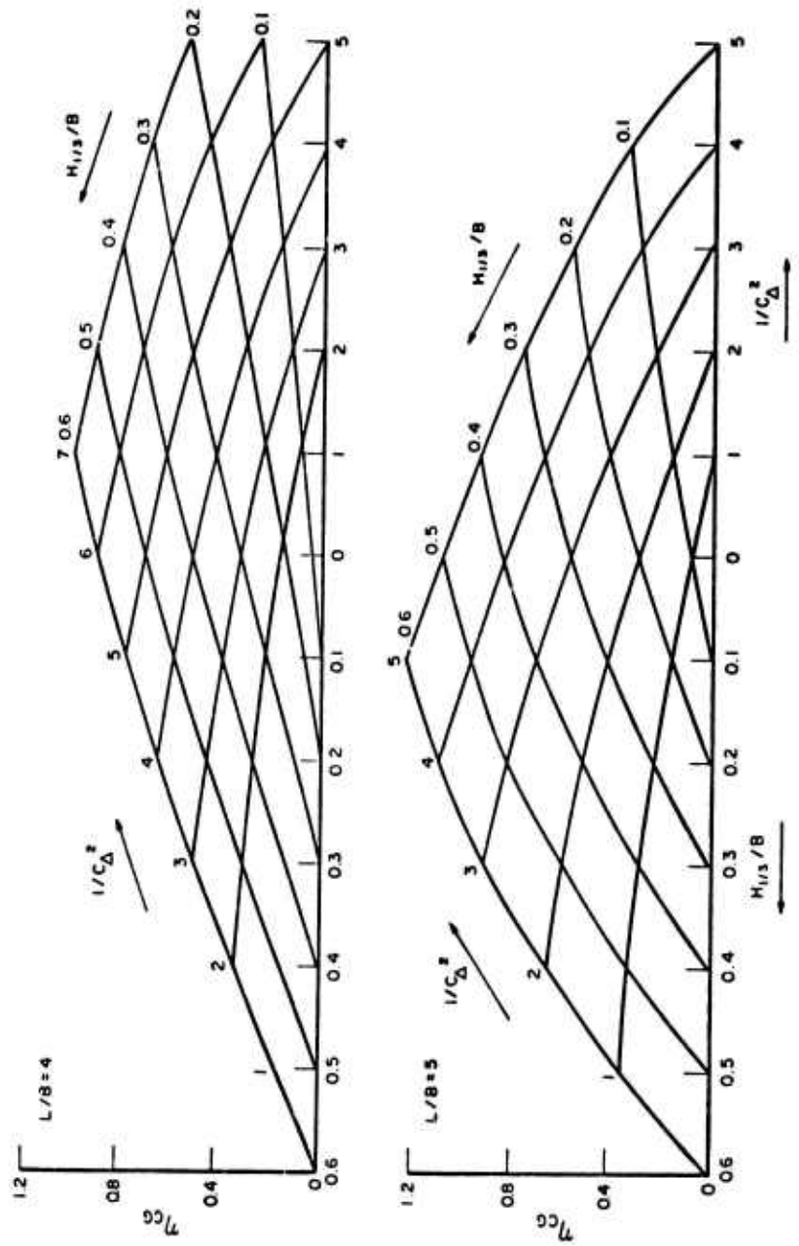


Figure 2. Average CG acceleration at $V/\sqrt{L} = 4$
($\tau = 4°$, $\beta = 20°$)

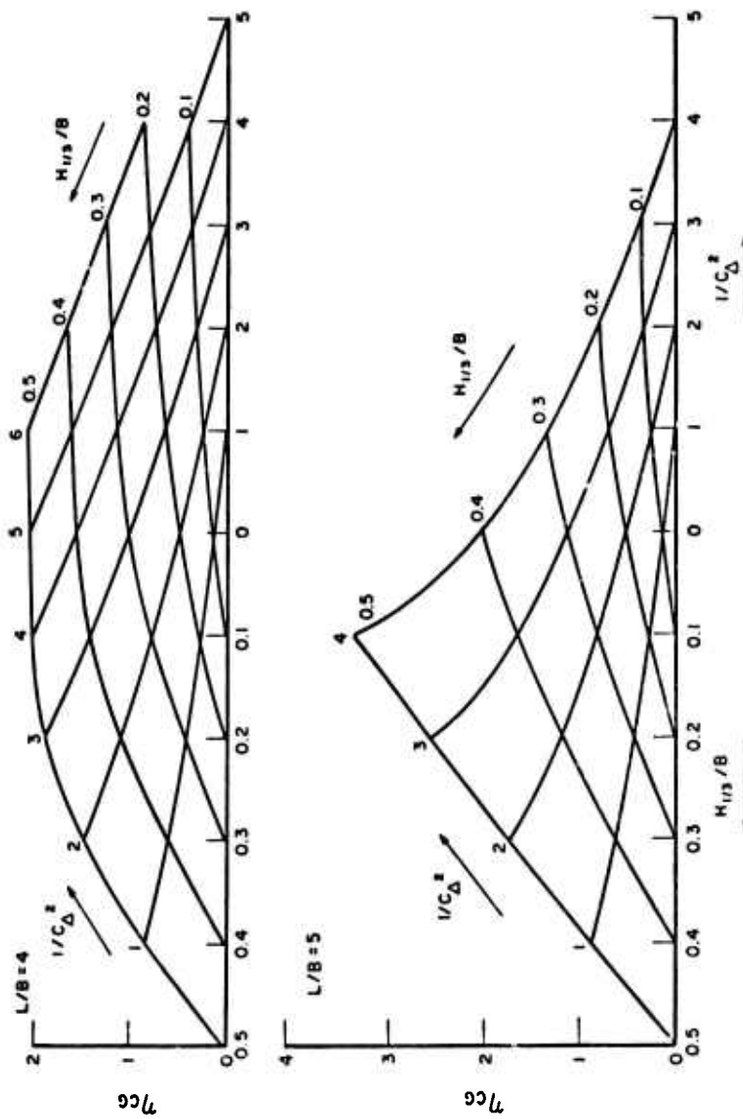


Figure 3. Average CG acceleration at $V/\sqrt{L} = 6$
($\tau = 4°$, $\beta = 20°$)

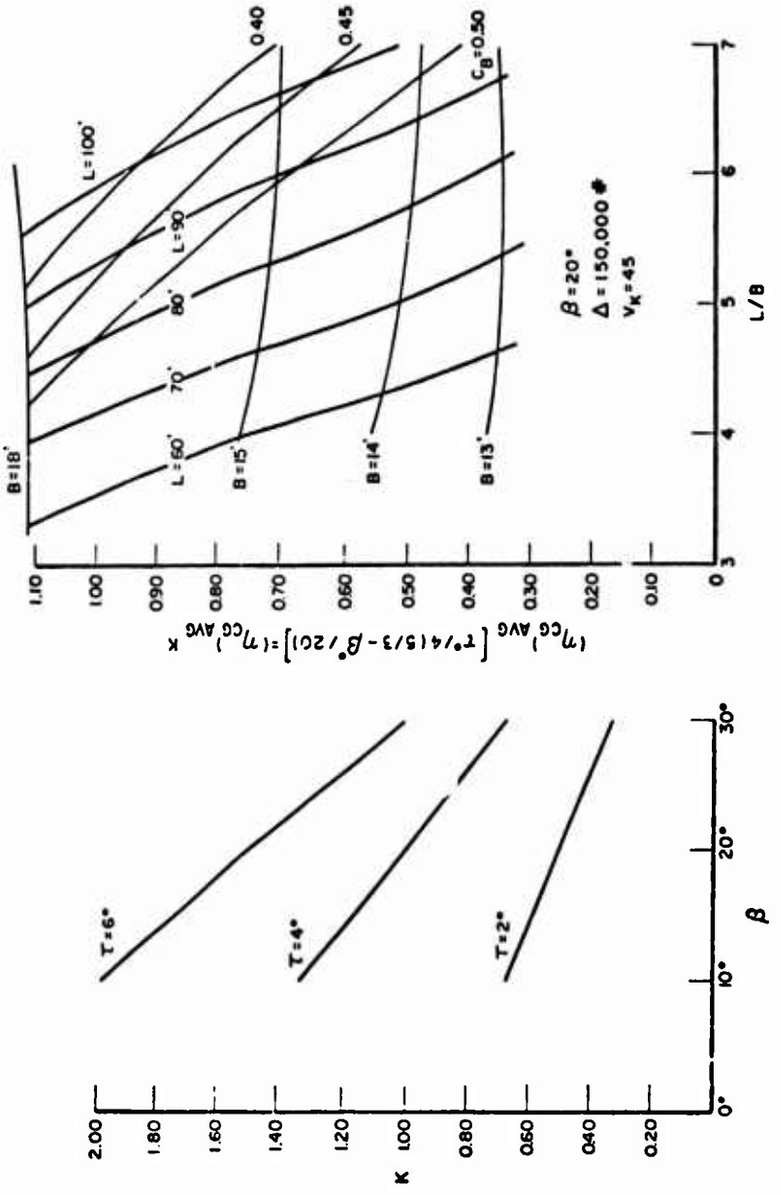


Figure 4. Average CG acceleration for various values of beam

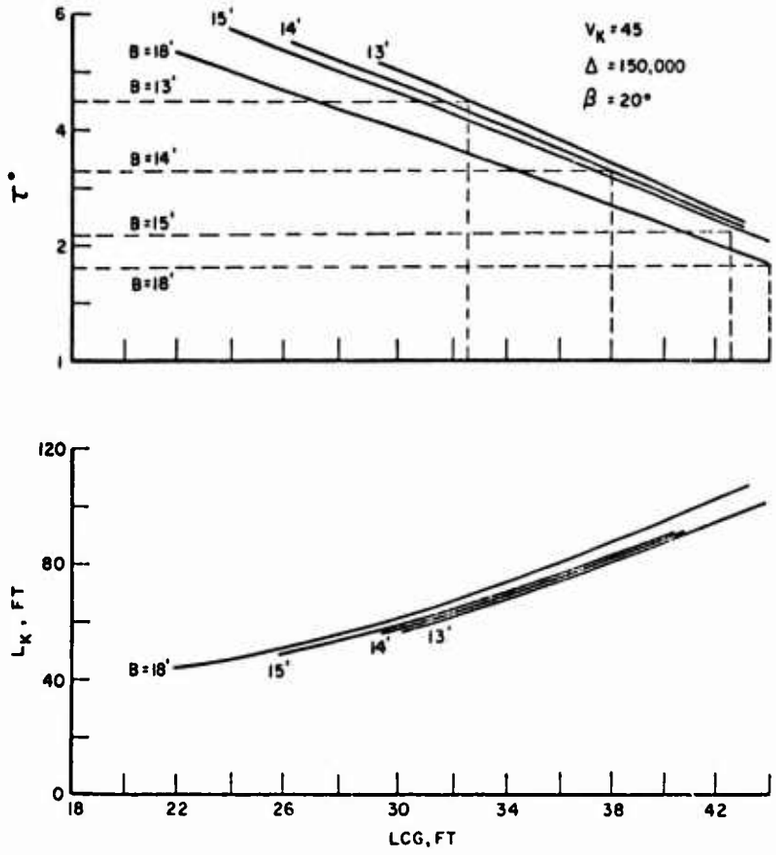


Figure 5. Equilibrium conditions in smooth water for various values of beam and LCG

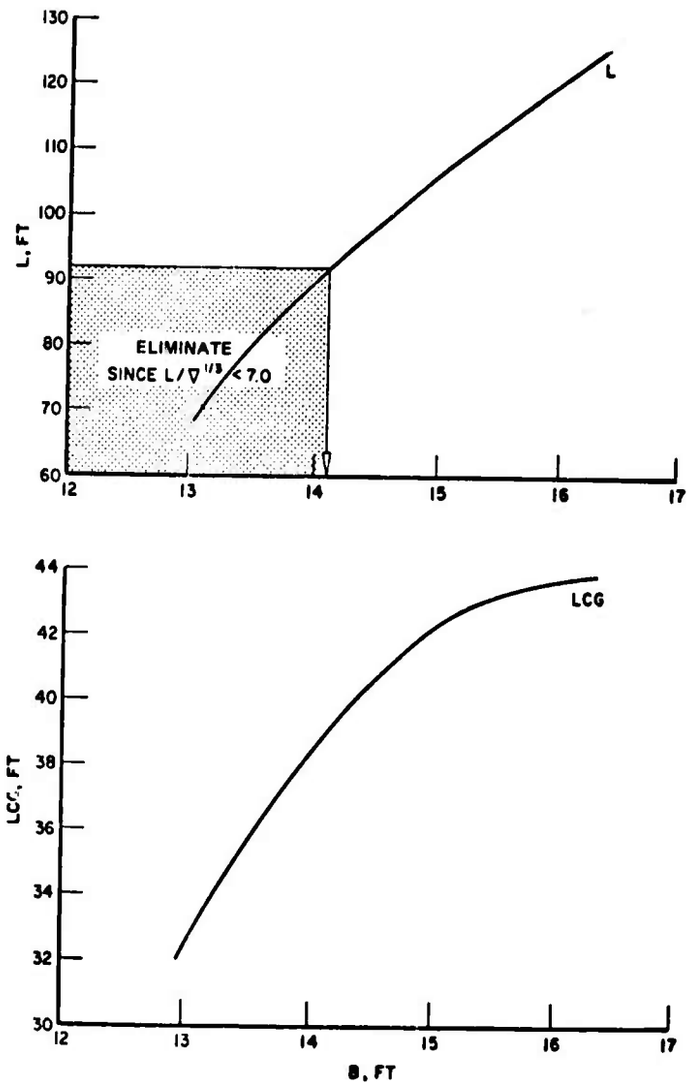


Figure 6. Relation between beam and length to achieve $(\eta_{CG})_{avg}$ = 0.4 g V_K = 45 knot Δ = 150,000 lb.

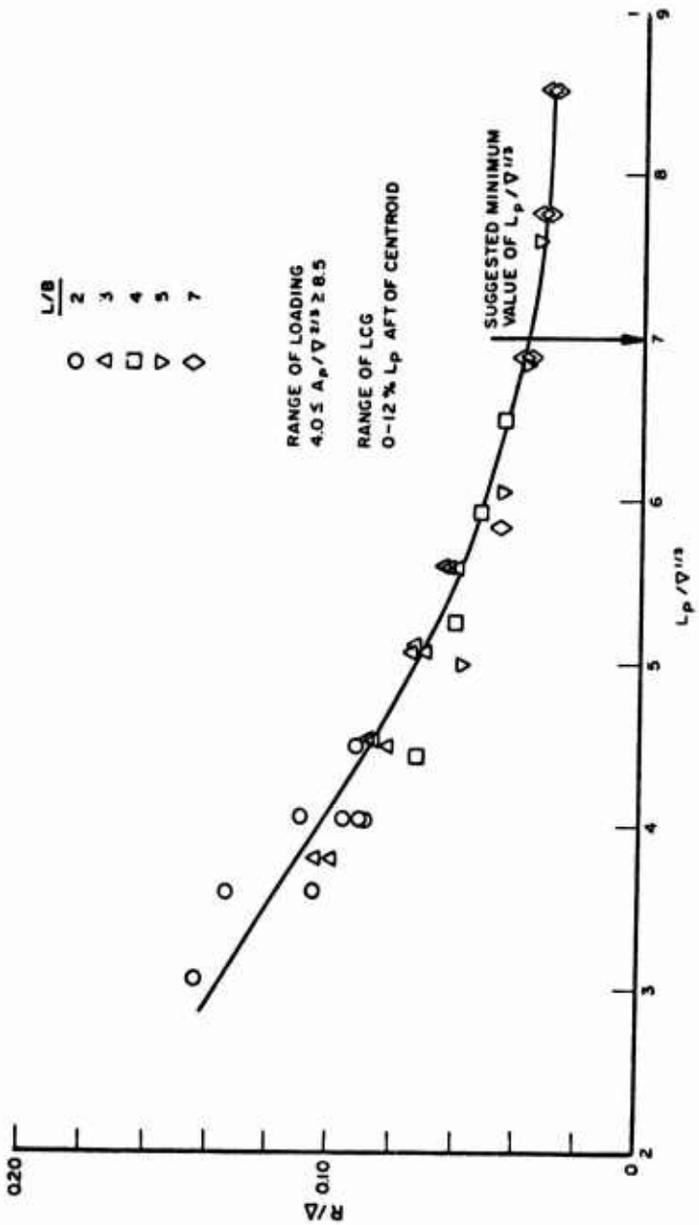


Figure 7. R/Δ for F_∇ = 1.0 series 62 hulls

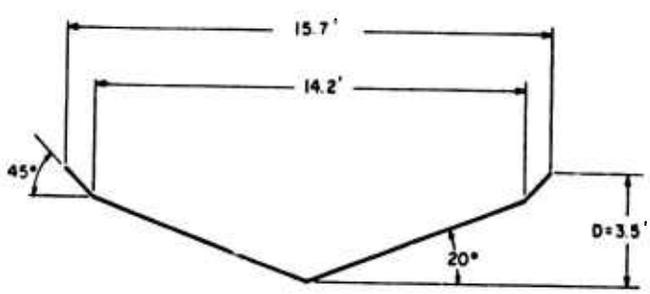


Figure 8. Double chine hull form selected for design

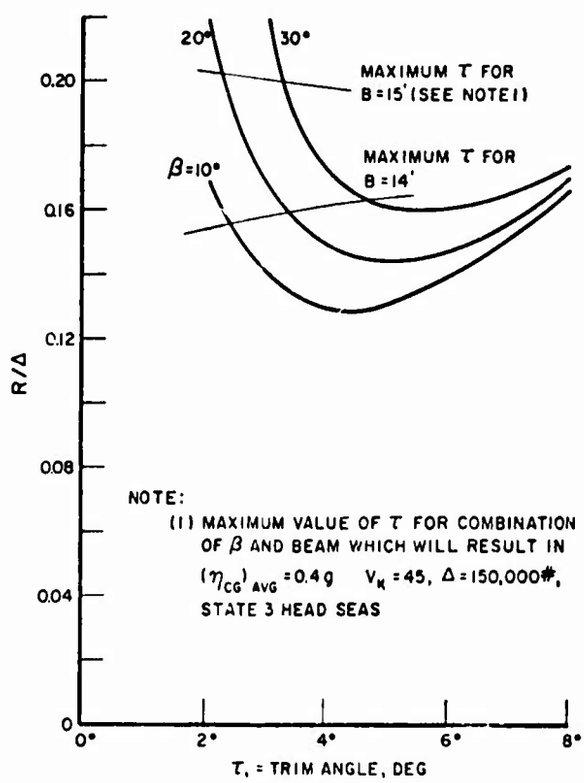


Figure 9. Variation of R/Δ for various τ and β

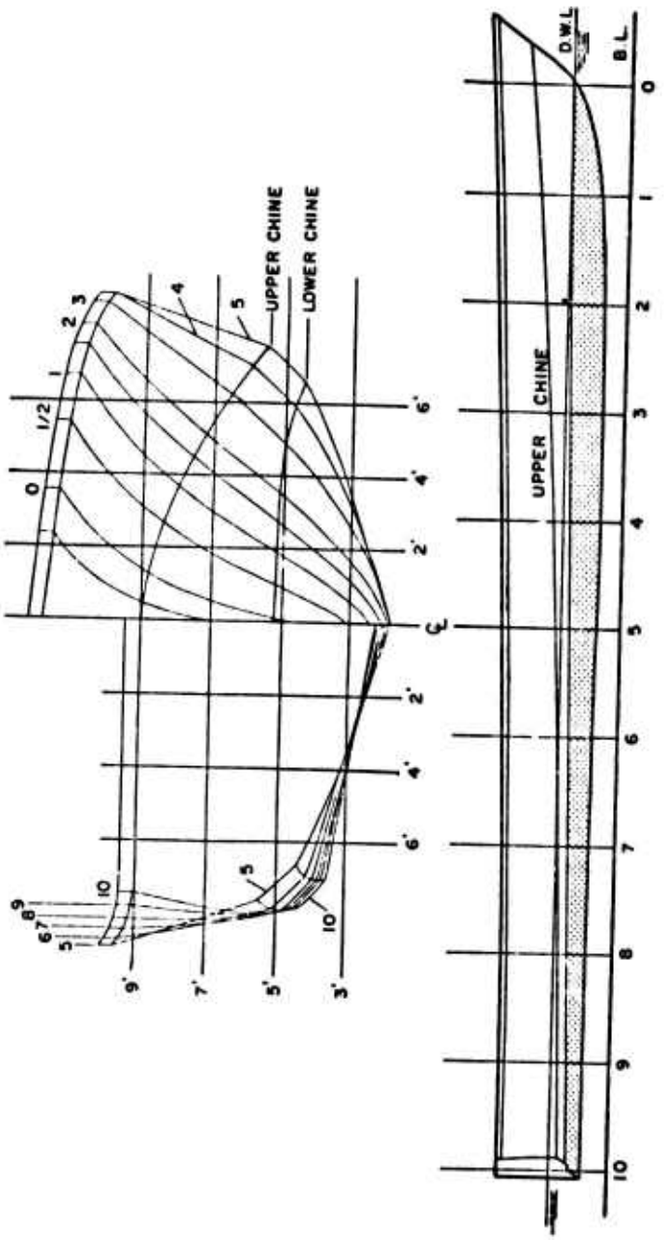


Figure 10. Line plan of final configuration

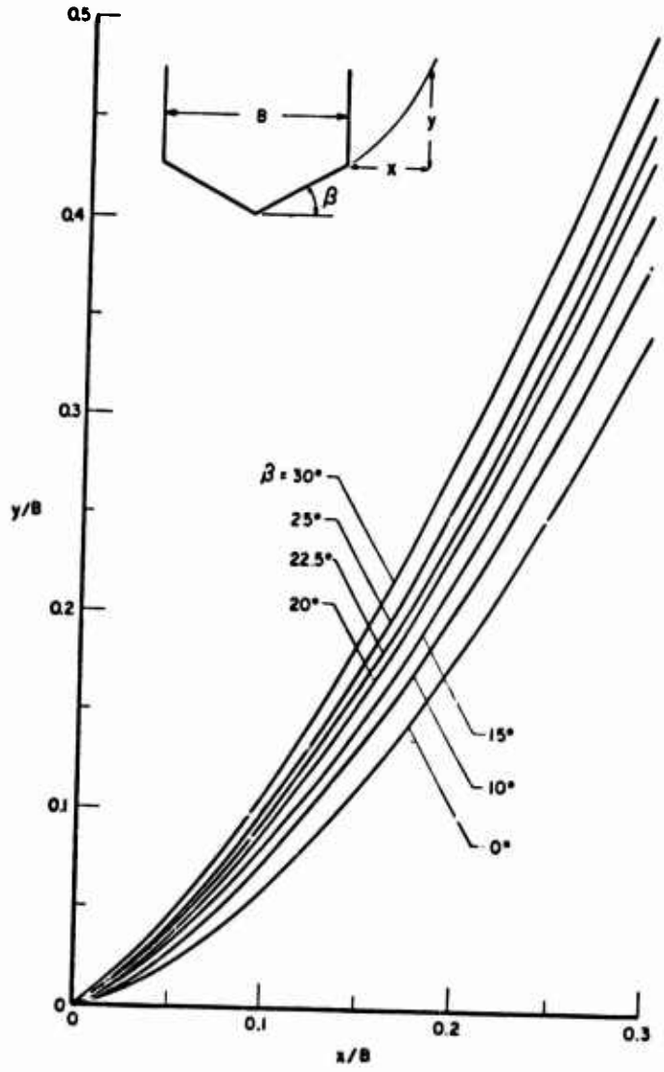


Figure 11. Shape of free streamline for immersed V-bottom

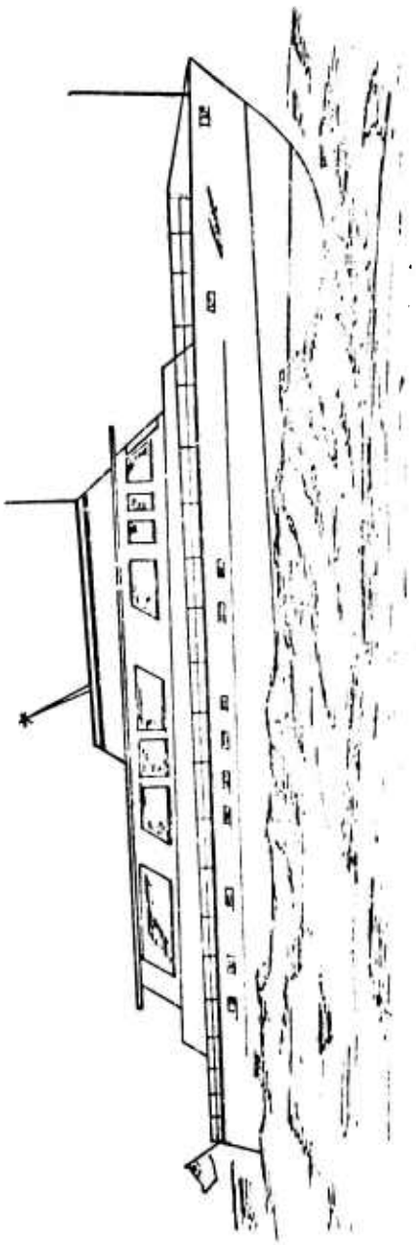


Figure 12. Final configuration

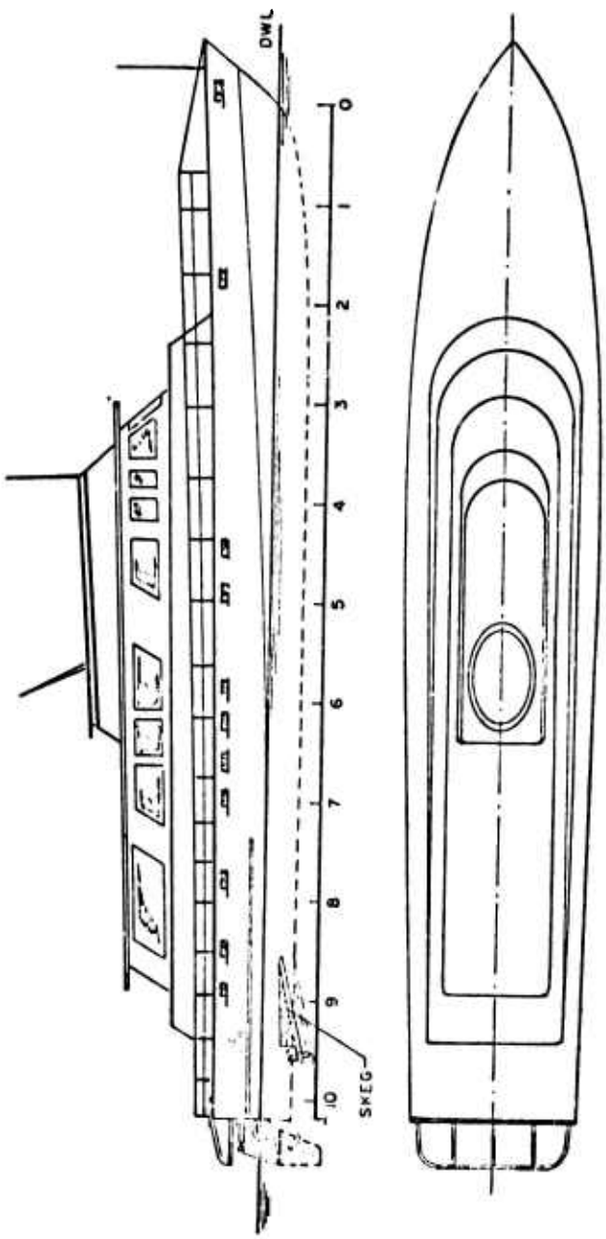


Figure 13. Outboard profile and plan view

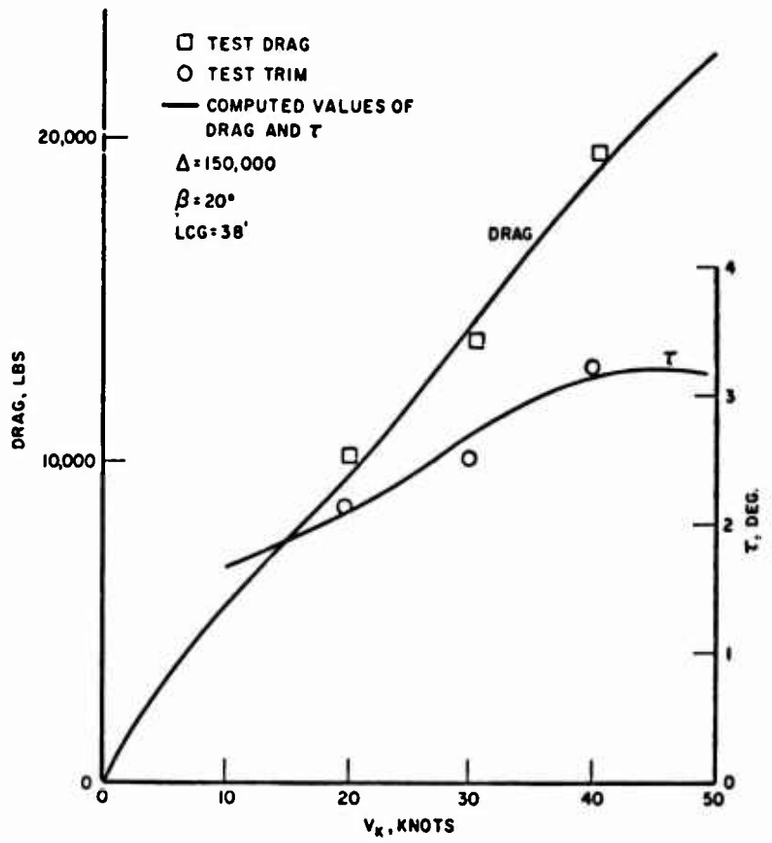


Figure 14. Computed and measured values of resistance and trim in smooth water

DISCUSSION

Manley Saint-Denis
University of Hawai
Honolulu, U.S.A.

I am very happy that seakeeping has been treated in this paper as the pre-eminent factor in the design of planing craft, for to the present, seakeeping has been introduced in the design of small craft hardly at all. Indeed it has been ignored except for raising the chine at the bow and narrowing the beam. And then the designers have simply put their trust in God, hoping that he would be kind to them and to the sea-beaten crews that would man in the open sea the craft they had designed. Therefore, I am grateful that something is being done because, waves being independent of the size of the vehicle that ventures over the surface of the sea, I suppose it is not a profound revelation to state that the smaller the craft the more she suffers. For a large vessel, even a heavy sea can be only an inconvenience, but for a small craft even a modest sea can lead to a very miserable experience. Therefore, starting the design of planing craft by considering the sea behaviour as the very first step in the process is the correct way to proceed, and I am glad to see the authors have done just this.

My second point relates to the authors' conclusion that if you narrow the beam, reduce the trim angle and up the dead-rise, things will be better rather than worse ; and while the exposition of the paper itself gives quite some insight into the sensivity of how impact, sea behaviour and other effects are related to the design features, the designers do not unfortunately go further into the matter.

I should like to point out that if all the authors wanted to do was to show how to develop a design to fulfil some very rigid specifications, such as the inflexible ones they have stated, the design process could be shortened considerably. In fact, one could develop a simple computer program that would yield an almost instantaneous answer, for the line of logic is simple and unambiguous in such a case. However, the point I should like to raise is that the specifications are not always quite as rigid as the authors have listed them, that indeed one has to play with them somewhat, giving up somewhat little here to gain somewhat more elsewhere : for example, take the problem of the transverse metacentric height, the metacentric height is reduce by

decreasing the beam, but this step also lessens the impact force, and so one might be better off. Is it worthwhile ? How much is it worthwhile ? The answer is not easy, of course, but such type of problems - so called trade-off problems - are not treated. The computer technique is in hand for coping very nicely with such problems and it is feasible to set up a programme that would yield a design, by satisfying in an optimum manner an imposed set of trade-off criteria. Therefore I humbly suggest that the authors, having been successful so far, should continue their quest for further success by applying themselves to this step.

DISCUSSION

Reuven Leopold
U.S. Navy. Naval Ship Engineering Center
Hyattsville, Maryland, U.S.A.

The importance of high endurance, and hence low resistance, at low -about 12 knots- cruising speeds is emphasised. Certainly a broad transom will have an adverse effect on resistance at these low speeds. This point is not discussed in the paper. Was the possibility of incorporating a method of trim control in a design to reduce or eliminate transom immersion at low cruising speeds considered in this design methodology ?

REPLY TO DISCUSSION

Daniel Savitsky
Stevens Institute of Technology
Hoboken, New Jersey, U.S.A.

Yes. Deliberate trim control was considered, but it is not presented here.

DISCUSSION

Reuven Leopold
U.S. Navy. Naval Ship Engineering Center
Hyattsville, Maryland, U.S.A.

The requirement to achieve 45 knots in state 3 seas is emphasized. However the effects of air drag and sea state on the power required to propel the craft at 45 knots is not discussed. Assuming that a state 3 sea is generated by a 15 knot wind, how much is the calm water 0 kn. relative wind resistance of the craft at 45 knots increased by the presence of a 60 knot relative wind and a state 3 sea ?

REPLY TO DISCUSSION

Daniel Savitsky
Stevens Institute of Technology
Hoboken, New Jersey, U.S.A.

It is important to emphasize that the present paper presents a methodology for rational design of planing hulls. The method has been applied to a particular set of design parameters to demonstrate its validity. It now remains to use this technique to develop optimum designs as suggested by Dr. Saint-Denis and Dr. Leopold.

MOTION AND RESISTANCE OF A LOW-WATERPLANE CATAMARAN

P. C. Pien and C. M. Lee
Naval Ship Research and Development Center
Bethesda, Maryland, U.S.A.

ABSTRACT

The unusually large, useful deck area is the advantage normally associated with catamarans. In addition, small-waterplane-area-twin-hull-ship (SWATHS) can exhibit good seaworthiness characteristics in rough seas but at the expense of high powering requirements due to the large wetted hull surface. A well-balanced design of such a craft must be the result of a compromise among motion, powering, and structural weight considerations. In this paper, however, only the hydrodynamic aspect of the design is discussed. It consists of two parts. The first part deals with ship motion, while the second part deals with resistance.

In the first part, a theoretical method of predicting the motion and hydrodynamic loads of catamarans in a seaway is given. Based on theoretical analysis, tolerable limits on hull characteristics are determined to ensure the desired motion characteristics. In the second part, a set of lines is developed within these limits such that the powering requirement is an optimum. This is done theoretically, based on existing wavemaking-resistance theory. Finally, a design example is given to show how hydrodynamic theories are used in designing a SWATHS.

Preceding page blank

INTRODUCTION

There are many types of naval ships which are volume-limited. In such cases, the proposition of using a catamaran hull configuration becomes very attractive because of its large deck area. A conventional catamaran, however, was found to have some bad motion characteristics and cannot offer a stable platform in heavy seas. Since the sea-excited ship motions can be reduced by submerging the hull, a small-waterplane-area-twin-hull-ship (SWATHS) has become a subject of great interest.

To explore the potential advantages of a SWATHS, a few experimental models were developed and tested for resistance as well as for motions. The expected favorable motion characteristics were generally confirmed. However, the resistance level was found to be unusually high, and the power requirement was much higher than expected. The percentage of structural weight to total weight of a SWATHS is also expected to be high. This, coupled with large machinery and fuel weights, greatly restricts its payload.

Before building a SWATHS which can accommodate a reasonable payload, it is necessary to reduce the power requirement by controlling the hull resistance, and to reduce the structural weight by controlling the hydrodynamic loading on the hull structure. Since the hydrodynamic loading depends upon the relative motions between the hull and the surrounding water, it is essential to control the ship motions in such a way that the hydrodynamic loading is minimized.

In attempt to solve this problem, an investigation of catamaran hydrodynamics was undertaken at the Naval Ship Research and Development Center. Research efforts in catamaran motions were made by the Ship Dynamics Division, while parallel efforts in catamaran resistance were made by the Ship Powering Division. Since the development of a successful catamaran design is contingent upon solving the motion and resistance problems simultaneously, the results of these efforts were incorporated, and are presented here as a single contribution.

This paper consists of two essentially independent parts written by two different authors; the first part by Lee, and the second part by Pien. In dealing with the motion problem, it was necessary to carry the theoretical work beyond that of solving the motion problem of a single hull. Since this additional theoretical work has not previously been published, it is discussed here in its entirety.

Several examples of comparisons between the theoretical predictions and the experimentally obtained motions are given.

In dealing with the resistance problem, it was found that, by using the concept of an effective hull form, the design problem of a catamaran and a conventional hull became the same. Hence, no additional theoretical development was necessary. Because of this, it was possible to devote this section exclusively to the catamaran design procedure and design examples.

Based on the motion work, the principal dimensions and hull coefficients which control ship motions in a given seaway can be specified. These specifications constitute part of the hull-form design conditions. Within all the design contraints, an optimum catamaran hull form based on powering considerations can be developed by following the design procedure. When this is done, a table of hull offsets is available which can be used to make a final check on ship motions. Since the hull characteristics required for ship motion considerations may conflict with those required for the optimum power requirement, a compromise between ship motion and ship powering is necessary. Based on the work given in this paper, a well-balanced design can be developed.

I - MOTION OF CATAMARAN.

I . 1 - Background.

One of the obvious advantages of a catamaran is the large available deck area. If this large deck area is to be efficiently utilized, it must behave as a stable platform. From a seaworthiness viewpoint there are some special features associated with twin-hull configurations.

First, an increase of overall beam results in a decrease in natural period in roll. A smaller natural period in roll makes catamarans very jerky ships. Most conventional monohull ships have a greater natural period in roll than in pitch. In case of catamarans, the pitch period may be slightly larger than that of monohull ships of equivalent length and displacement. This fact together with the decrease in the roll period for catamarans tends to bring the natural period for roll and pitch closer to each other. This could cause simultaneous excitation of large roll and pitch motions, which make very uncomfortable riding for the crews.

Second, the existence of a cross-deck structure between

then the motion x_o of the mass at the natural frequency ω_n can be expressed by

$$x_o = \frac{F}{\omega_n c}$$

In the case of ship motion, F corresponds to the wave exciting force and is proportional to $\sqrt{c}$ as shown by Newman (1962). Thus we have $x_o \sim C^{-\frac{1}{2}}$. This means that a reduction in damping at the natural frequency could result in a large motion. However, the natural period may be increased by proper design to such a magnitude that the corresponding wavelengths may not be frequently encountered by ships in the ocean. Furthermore, the concern for an expected high-peaked resonant motion resulting from a reduction of wave damping of the system may not be serious because of an augmentation of viscous damping due to an increased wetted surface on the LWP catamarans.

Although reduction of motions of catamarans may be accomplished through SWATHS configurations, such configurations present formidable structural problems. The decrease in waterplane area reduces the restoring buoyancy, and this, in turn, makes the LWP catamarans weight sensitive. The limited tolerance for additional weight requires a narrow margin for safety factors on structural weights. An additional complication to the structural problem is the lack of data for wave loading. The wave loading includes the contribution from impinging waves as well as from motion-generated inertial and hydrodynamic forces. To obtain an accurate wave loading the effect of the wave diffraction by two hulls and of the motion of the body should be taken into account in the theoretical analysis.

In this work an analytical method has been developed for predicting characteristics of motion and hydrodynamic loads of catamarans, either conventional or SWATHS. The equations of motion for catamarans are derived in the frequency domain under an assumption of linear excitation-response relationship. The hydrodynamic coefficients involved in the equations of motion are determined from strip theory, assuming slender geometry of each hull of the catamaran. The effect of forward speed on the hydrodynamic coefficients is treated as if there were no perturbation on the fluid due to a translation of the ship.

An apparent underestimation of damping by potential theory results in an unrealistically large motion amplitude at the resonant

frequency. Thus, introduction of supplemental damping into the equation of motion is needed to achieve a reasonable prediction of catamaran motions. The supplemental damping is introduced into the equations of motion in a form linearly proportional to the oscillation velocity. This damping is found to depend on the ratio of the ship speed to the celerity of motion-generated waves. This fact implies that the interaction between the wave systems, created by oscillation and forward speed, is important and should be included in the evaluation of damping.

Prediction of statistical averages of motion amplitudes for catamarans in irregular seas is made by using the frequency response-amplitude operator in conjunction with the Pierson and Moskowitz (1964) sea spectrum. The probable frequency of a water contact with the cross-deck structure is computed for given conditions such as height of the cross-deck structure from the waterline, significant wave height, and forward speed. The formula used is based on a truncated Rayleigh's probability distribution for slamming and is similar to the formula developed by Ochi (1964) for bow slamming of monohull ships.

The expressions are developed for various loadings contributed by inertial and hydrodynamic effects, such as bending and torsion moments and shear forces on both the cross-deck structure and the supporting strut (shear and bending only).

Presentation of the work on motion of catamarans is given in the following order. In section 2, the subjects covered are : formulation of equations of motion, derivation of the hydrodynamic coefficients and derivation of an expression to estimate the number of slammings of the cross-deck structure per given period in regular and irregular waves. In Section 3, the derivation of expressions for various hydrodynamic loads on catamarans is given. In Section 4, a presentation of comparisons of theoretical and experimental results is made, and concluding remarks are given.

I . 2 - Motion.

Equations of Motion

The assumptions or conditions made in this paper for studying motions of catamarans are as follows. A catamaran which is made of two symmetrical hulls is cruising with a constant speed, while it is experiencing an undulatory motion due to sea waves. The sea waves are assumed to be made of a linear sum of unidirectional

regular waves of different frequencies. The response of a catamaran to these waves is assumed linear in amplitudes and frequencies. The amplitudes of the waves and the motions are assumed to be small, and, consequently, the fluid disturbance generated by the motions of waves and ship is also assumed small. The depth of the ocean is assumed infinitely deep and the effects of wind and current on the motion are not considered.

Within a linear approximation of the motion and with the conditions prescribed in this work it is convenient to choose 0xyz, a coordinate system representing the mean position of the catamaran as the reference frame for which the equations of motion are to be formulated. When the catamaran has only steady translation, the 0xz plane coincides with the longitudinal plane of symmetry of the catamaran, the 0xy plane coincides with the calm water surface, the 0z axis is directed upward, the 0x axis is directed toward the bow, and the 0y axis is directed toward the port side. Since the wave excitation is assumed to be of harmonic nature in time, the equations can be formulated in a frequency domain.

With the conditions stated in the foregoing paragraph, the linearly coupled motion of a catamaran in six degrees of freedom can be written with the motion-generated displacements from the mean position denoted by ξ_i ; where the values of i represent 1 for surge, 2 for sway, 3 for heave, 4 for roll, 5 for pitch, and 6 for yaw, as

$$\sum_{k=1}^{6} \left\{ (M_{ik} + A_{ik}) \ddot{\xi}_k + B_{ik} \dot{\xi}_k + C_{ik} \xi_k = F_i^{(e)} e^{-j\omega t} \right. \quad (1)$$

for $i = 1, 2, \ldots, 6$. The equation shown above is a degenerate case of the equations of motion of floating bodies in waves, formulated in the time domain which has the form of integro-differential equations as shown by Cummins (1962) and Ogilvie (1964). In Equation (1) M_{ik} is the mass or moment of inertia of the catamaran, A_{ik} , the added inertia, B_{ik} , the damping, C_{ik} , the restoring constants, $F_i^{(e)}$, the wave excitation in the form of complex amplitude, and j is the imaginary unit associated only with a harmonic-time function.

The expression "added mass (or inertia)" which will be frequently referred to in this paper is used for mathematical convenience. Thus, it does not have the same meaning as the classical added mass which is an intrinsic property of the geometry of the body only and is independent of motion, frequency, and forward speed. The mathematical relation between the added mass of the classical definition given in Lamb's Hydrodynamics and the one referred to in this

paper is derived in, e. g., Wehausen (1971, pp. 243-245). To be compatible with the complex expression on the right side of Equation (1), the motion displacements ξ_k are assumed to be complex functions in the form of

$$\xi_k(t) = \mathrm{Re}_j \left[\xi_{ko} e^{-j\omega t} \right] = \mathrm{Re}_j \left[(\xi_{kc} + j\xi_{ks}) e^{-j\omega t} \right] \quad (2)$$

where Re_j means that the real part of a complex function in terms of the imaginary unit of j should be taken, and ξ_{kc} and ξ_{ks} are real functions.

Each hull of the catamaran is assumed to be slender so that the change of the surface normal in the length direction is small compared to the change in the transverse directions. This slenderness assumption together with the symmetry of the two hulls lead to decoupling motions into three independent groups of motion : (1) surge, (2) heave and pitch, and (3) sway, roll and yaw. In this work the surge motion will not be considered. The explicit forms of the remaining two groups of motion are given as follows. Heave and pitch equations :

$$(M + A_{33})\ \ddot{\xi}_3 + B_{33}\dot{\xi}_3 + C_{33}\xi_3 + A_{35}\ddot{\xi}_5 + B_{35}\dot{\xi}_5 + C_{35}\xi_5 = F_3^{(e)} e^{-j\omega t} \quad (3)$$

$$(I_5 + A_{55})\ \ddot{\xi}_5 + B_{55}\dot{\xi}_5 + C_{55}\xi_5 + A_{53}\ddot{\xi}_3 + B_{53}\dot{\xi}_3 + C_{33}\xi_3 = F_5^{(e)} e^{-j\omega t} \quad (4)$$

Sway, roll, and yaw equations :

$$(M + A_{22})\ \ddot{\xi}_2 + B_{22}\dot{\xi}_2 + (A_{24} - Mz_g)\ \ddot{\xi}_4 + B_{24}\dot{\xi}_4 + A_{26}\ddot{\xi}_6 + B_{26}\dot{\xi}_6 = F_2^{(e)} e^{-j\omega t} \quad (5)$$

$$(I_4 + A_{44})\ \ddot{\xi}_4 + B_{44}\dot{\xi}_4 + C_{44}\xi_4 + (A_{42} - Mz_g)\ \ddot{\xi}_2 + B_{42}\dot{\xi}_2 + A_{46}\ddot{\xi}_6 + B_{46}\dot{\xi}_6 = F_4^{(e)} e^{-j\omega t} \quad (6)$$

$$(I_6 + A_{66})\ \ddot{\xi}_6 + B_{66}\dot{\xi}_6 + A_{62}\ddot{\xi}_2 + B_{62}\dot{\xi}_2 + A_{64}\ddot{\xi}_4 + B_{64}\dot{\xi}_4 = F_6^{(e)} e^{-j\omega t} \quad (7)$$

In the previously given equations, M is the mass of the catamaran; I_4, I_5 and I_6 are mass moments of inertia about the $0x$, $0y$ and $0z$ axes, respectively; z_g is the z coordinate of the center of mass; and the restoring constants C_{33}, C_{35}, C_{55}, C_{53} and C_{44} are given by

$$C_{33} = \rho g A_w$$

$$C_{35} = C_{53} = - \rho g M_w$$

$$C_{55} = M_g (\overline{GM})_e$$

$$C_{44} = \rho g \forall (\overline{GM})_t$$

Here A_w is the waterplane area at the mean position of the catamaran, M_w the area moment of the waterplane about the $0y$ axis, $(\overline{GM})_e$ and $(\overline{GM})_t$ the restoring moment arm in pitch and roll respectively.

The major task in solving the equations of motion shown previously lies in determining the hydrodynamic coefficients, A_{ik} B_{ik} and $F_i^{(e)}$; i, k = 2, 3, ... 6. They are functions of hull geometry, wave frequency, and forward speed. The method of determining these coefficients is described in Appendix A, and the results are presented in Table 1. The lowercase letters a_{ik} and b_{ik} shown in Table 1 are sectional added mass and damping, and U is the forward velocity. These are obtained by solving two-dimensional boundary-value problems for velocity potentials representing the fluid motion generated by an oscillation of infinitely long twin cylinders. The cylinders are semisubmerged horizontally, have a certain separation distance between, and are rigidly connected together from above. The twin cylinders have a uniform cross section which is identical to the cross section at any given location along the length of the catamaran.

The method of distribution of pulsating sources along the sumberged contours of the cylinders is employed in solving the velocity potential; see Lee, Jones, and Bedel (1971). The method used is similar to the one developed by Frank (1967) for single cylinders.

Table 1 - Strip approximations of hydrodynamic coefficients *

$$A_{22} = \int_{-\ell_1}^{\ell_2} a_{22}(x)\,dx$$

$$B_{22} = \int b_{22}\,dx$$

$$A_{24} = \int a_{24}\,dx$$

$$B_{24} = \int b_{24}\,dx$$

$$A_{26} = \int x\,a_{22}\,dx + \frac{U}{\omega^2} B_{22}$$

$$B_{26} = \int x\,b_{22}\,dx - U A_{22}$$

$$A_{33} = \int a_{33}\,dx$$

$$B_{33} = \int b_{33}\,dx$$

$$A_{35} = -\int x\,a_{33}\,dx - \frac{U}{\omega^2} B_{33}$$

$$B_{35} = -\int x\,b_{33}\,dx + U A_{33}$$

$$A_{44} = \int a_{44}\,dx$$

$$B_{44} = \int b_{44}\,dx$$

$$A_{42} = A_{24} = \int a_{24}\,dx$$

$$B_{42} = B_{24} = \int b_{24}\,dx$$

$$A_{46} = \int x\,a_{24}\,dx + \frac{U}{\omega^2} B_{24}$$

$$B_{46} = \int x\,b_{24}\,dx - U A_{42}$$

$$A_{55} = \int x^2 a_{33}\,dx + \frac{U^2}{\omega^2} A_{33}$$

$$B_{55} = \int x^2 b_{33}\,dx + \frac{U^2}{\omega^2} B_{33}$$

$$A_{53} = -\int x\,a_{33}\,dx + \frac{U}{\omega^2} B_{33}$$

$$B_{53} = -\int x\,b_{33}\,dx - U A_{33}$$

$$A_{66} = \int x^2 a_{22}\,dx + \frac{U^2}{\omega^2} A_{22}$$

$$B_{66} = \int x^2 b_{22}\,dx + \frac{U^2}{\omega^2} B_{22}$$

$$A_{62} = \int x\,a_{22}\,dx - \frac{U}{\omega^2} B_{22}$$

$$B_{62} = \int x\,b_{22}\,dx + U A_{22}$$

$$A_{64} = \int x\,a_{24}\,dx - \frac{U}{\omega^2} B_{24}$$

$$B_{64} = \int x\,b_{24}\,dx + U A_{24}$$

* Lowercase letters mean two-dimensional hydrodynamic coefficients; integrals are from the aft to the fore perpendicular.

Since

$$\xi_k(t) = \mathrm{Re}_j \left[\xi_{ko} \, e^{-j\omega t} \right]$$

$$= \mathrm{Re}_j \left[(\xi_{kc} + j \, \xi_{ks}) \, e^{-j\omega t} \right]$$

as defined in Equation (2), we have

$$\dot{\xi}_k = -j\omega \xi_{ko} \, e^{-j\omega t}$$

$$\ddot{\xi}_k = -\omega^2 \xi_{ko} \, e^{-j\omega t}$$

in which we have dropped Re_j for the sake of brevity; however, it will be understood in the sequal that the real part is meant whenever a term is involved with $e^{-j\omega t}$. Substitution of the foregoing results into Equations (3) through (7) yields two sets of complex algebraic equations of the form

$$A_1 x_1 = B_1$$

$$A_2 x_2 = B_2 \tag{8}$$

where

$$x_1 = \begin{bmatrix} \xi_{30} \\ \xi_{50} \end{bmatrix} \qquad x_2 = \begin{bmatrix} \xi_{20} \\ \xi_{40} \\ \xi_{60} \end{bmatrix}$$

$$B_1 = \begin{bmatrix} F_3^{(e)} \\ F_5^{(e)} \end{bmatrix} \qquad B_2 = \begin{bmatrix} F_2^{(e)} \\ F_4^{(e)} \\ F_5^{(e)} \end{bmatrix}$$

$$A_1 = \begin{bmatrix} -\omega^2 (M + A_{33}) + C_{33} - j\omega B_{33} & -\omega^2 A_{35} + C_{35} - j\omega B_{35} \\ -\omega^2 A_{53} + C_{53} - j\omega B_{53} & -\omega^2 (I_5 + A_{55}) + C_{55} - j\omega B_{55} \end{bmatrix}$$

and

$$A_2 = \begin{bmatrix} -\omega^2 (M + A_{22}) - j\omega B_{22} & -\omega^2 (A_{24} - Mz_g) - j\omega B_{24} & -\omega^2 A_{26} - j\omega B_{26} \\ -\omega^2 (A_{42} - Mz_g) - j\omega B_{42} & -\omega^2 (I_4 + A_{44}) + C_{44} - j\omega B_{44} & -\omega^2 A_{46} - j\omega B_{46} \\ -\omega^2 A_{62} - j\omega B_{62} & -\omega^2 A_{64} - j\omega B_{64} & -\omega^2 (I_6 + A_{66}) - j\omega B_{66} \end{bmatrix}$$

After an inversion of the matrix in Equation (8), we can obtain the absolute motion amplitudes by

$$\xi_k^o \equiv \left| \xi_{ko} \right| = \left\{ (\xi_{kc})^2 + (\xi_{ks})^2 \right\}^{\frac{1}{2}} \qquad (9)$$

$k = 2, 3, \ldots, 6$

and the phase angle with respect to the wave motion at the origin 0 by

$$\alpha_k = \tan^{-1} \left\{ - \xi_{ks} / \xi_{kc} \right\} \qquad (10)$$

$k = 2, 3, \ldots 6$

Once the motion amplitudes ξ_k^o are obtained as previously described as a function of wave frequency, we can obtain various statistical averages of the displacement and velocity of the ship, using the method introduced by St. Denis and Pierson (1953). We can show that the statistical averages of the short-term response of ships to sea waves can be given by

$$(\xi^o_k)_{\text{stat ave}} = C \sqrt{E_d}$$

$$(\dot{\xi}^o_k)_{\text{stat ave}} = C \sqrt{E_v}$$

$k = 2, 3, \ldots, 6$

where

$$C = \begin{cases} 1.253 & \text{for mean average} \\ 2.0 & \text{for one-third highest average} \\ 2.546 & \text{for one-tenth highest average} \end{cases}$$

$$E_d = \int_0^\infty \left(\xi_k^o(\omega_o) / A(\omega_o) \right)^2 S(\omega_o)\, d\omega_o = \text{Variance of motion} \quad (11)$$

$$E_V = \int_0^\infty (\omega_o\ \xi_k^o / A)^2\, S(\omega_o)\, d\omega_o = \text{Variance of velocity} \quad (12)$$

where A is the wave amplitude and $S(\omega_o)$ is the sea-energy spectrum. The sea-energy spectrum in this work is that introduced by Pierson and Moskowitz (1964), which is given by

$$S(\omega_o) = \frac{C_1}{\omega_o^5}\ e^{-C_2/\omega_o^4} \quad (13)$$

where ω_o is the wave frequency and C_1 and C_2 are constants which are given by

$$C_1 = 0.0081\ g^2 \text{ and } C_2 = 33.56\ /(\text{significant wave height in feet})^2$$

The dimension of $S(\omega_o)$ is $[\ L^2\ T\ ]$, and the scaling unit is governed by that used for the gravitational acceleration g.

Absolute and Relative Vertical Motion.

One of the important aspects to be examined in catamaran motion is the chance of slamming the bottom of the cross-deck structure. To avoid slamming, it might be desirable to raise the cross-deck structure as high as possible. However, for various reasons such as roll instability, wind resistance, structural problems, and problems caused by a high freeboard, e.g., recovery operations of divers or objects from the sea, a high cross-deck may be undesirable. Hence, the first criterion in determining the height of the cross-deck should be the acceptable minimum deck height from a slamming standpoint.

To find out the chance of slamming, we first have to know the magnitude of the relative vertical displacement and velocity of the ship with respect to the wave surface. Specifically, we would like to know the vertical amplitude and phase of the forward portion of the cross-deck structure with respect to the motion of the free

surface beneath it. The relative velocity will also be needed to determine the threshold velocity for slamming.

Let us consider a situation in which a ship is perfectly contouring with the wave so that no chance of slamming may occur. When it comes to the working efficiency of the ship crew, contouring performance of the catamaran may not necessarily be the favorable condition because frequent oscillation of a ship can be quite a deterrent to easy movement. In this respect, we would like to reduce the absolute vertical motion with respect to the calm water level. Thus, a study on both absolute and relative vertical motions along the length of catamarans is important.

Among various sea conditions that most unfavorable one to a ship would be a periodic swelled sea, having an encountering period lying in the resonance band of the ship. Although sinusoidal waves may not correctly represent the swell condition, an application of sinusoidal waves for a qualitative study of slamming characteristics of a catamaran cross-deck will be made; then the study will be extended to irregular sea conditions.

The absolute vertical displacement of a station at x is obtained by

$$\xi_{30}^{(A)} = \xi_{30} - x\,\xi_{50} \tag{14}$$

where ξ_{30} and ξ_{50} are the complex motion amplitudes of heave and pitch, respectively, and the pitch angle is positive when the bow is down. The relative vertical displacement of the same station with respect to the incoming wave surface[3] is given by

$$\xi_{30}^{(R)} = \xi_{30}^{(A)} - \zeta_{w0} \tag{15}$$

where the free-surface elevation ζ_{w0} is given by

---

[3] Deformation of the free surface is caused not only by the incoming waves but also by the ship-generated waves. An evaluation of local free-surface disturbance due to an oscillating ship with a forward speed is an extremely difficult task to achieve. The difficulty is more so for the region between the two hulls of a catamaran. Thus, the present analysis should be regarded as a gross estimate.

$$\zeta_{w0} = A\, e^{jK_o (x \cos\beta - y \sin\beta)}$$

where A is the wave amplitude, β is the wave heading angle with respect to the positive x-axis, and $K_o = \omega_o^2/g$ is the wave number. If we choose the midspan of the cross structure to be the location of our interest, then

$$\zeta_{w0} = A\, e^{jK_o x \cos\beta}$$

Amplitudes of vertical displacement are obtained by taking the absolute values of $\xi_{30}^{(A)}$ and $\xi_{30}^{(R)}$, i.e., $\left|\xi_{30}^{(A)}\right|$ and $\left|\xi_{30}^{(R)}\right|$. If we denote the height of the bottom of the cross structure from the calm water level at x by c_o, then we know that when $\left|\xi_{30}^{(R)}\right| \geq c_o$, a water contact on the bottom of the cross structure can be made. The water contact establishes only the necessary condition for slamming. The sufficient condition is the magnitude of the relative velocity between the structure and the free surface "period". The criterion of the relative velocity for which the phenomenon of slamming is realized is often called "threshold velocity", denoted by W^*; see Ochi (1964). The threshold velocity is a function of geometry of the ship, and no analytical means seems to exist except some empirical values for certain types of monohulls.

The vertical velocity of the cross structure at x can be obtained by multiplying the vertical displacement by $(-j\omega)$. Thus, absolute and relative vertical velocities are given, respectively, by

$$W_{30}^{(A)} = -j\omega\, \xi_{30}^{(A)} \tag{16}$$

$$W_{30}^{(R)} = -j\omega\, \xi_{30}^{(R)} \tag{17}$$

Hence, if the following two conditions

$$\left|\xi_{30}^{(R)}\right| \geq c_o \tag{18}$$

and

$$\left|W_{30}^{(R)}\right| \geq W^* \tag{19}$$

are met, we may anticipate slamming of the cross-deck structure.

Extension of such an anlysis to irregular seas for monohulls was made by Ochi (1964). If we let

$$E_d^{(R)} = \int_0^\infty \left(\left| \xi_{30}^{(R)} \right| / A \right)^2 S(\omega_o)\, d\omega_o \tag{20}$$

and

$$E_v^{(R)} = \int_0^\infty \left(\omega \left| \xi_{30}^{(R)} \right| / A \right)^2 S(\omega_o)\, d\omega_o , \tag{21}$$

we can show that the numbers of probable water contact and slamming of the bottom of the cross structure during n hours are obtained by

$$N_W = \frac{1800\, n}{\pi} \sqrt{\frac{E_v^{(R)}}{E_d^{(R)}}}\; e^{-\frac{c_o^2}{2 E_d^{(R)}}} \tag{22}$$

for water contact, and

$$N_s = \frac{1800\, n}{\pi} \sqrt{\frac{E_v^{(R)}}{E_d^{(R)}}}\; e^{-\frac{c_o^2}{2 E_d^{(R)}}} \; - \frac{W^{*2}}{2 E_v^{(R)}} = N_W\, e^{-\frac{W^{*2}}{2 E_v^{(R)}}} \tag{23}$$

for slamming.

I . 3 - Hydrodynamic Loads.

In this section we will analyze the dynamic loads exerted on ship structure by the oscillatory motions of a ship and the fluid surrounding the ship. Other hydrodynamic loads contributed by maneuvering operations of a ship will not be included.

Contributing sources for the dynamic loading can be conveniently separated into two parts. One part is the mass inertial effect due to the acceleration of the ship, and the other is the hydrodynamic effect. The hydrodynamic effect is further divided into two parts; one is contributed by the change of pressure distribution caused by incoming and diffracted waves, and the other is contributed by

the change of pressure distribution due to the oscillatory motion of the ship. We assume that the motion displacements $\xi_i(t)$, i = 1, 2, . . . , 6 are already known, and for brevity we will dispense hereafter with the term $e^{-j\omega t}$ with the understanding that the time dependence of the loading quantities to be studied is harmonic.

The types of loading to be considered can be divided into three major parts; these are :

Shear Forces (figure 1a)

a. Transverse shear in the 0yz plane (V_2)
b. Vertical shear in the 0yz plane (V_3)
c. Transverse shear in the 0xy plane (V_4)
d. Vertical shear in the 0xz plane (V_5)

Bending Moments (figure 1b)

a. Transverse bending (M_1)
b. Horizontal bending (M_2)
c. Longitudinal bending (M_3)

Torsion Moments (figure 1c)

a. Yaw torsion moment (T_2)
b. Pitch torsion moment (T_3)

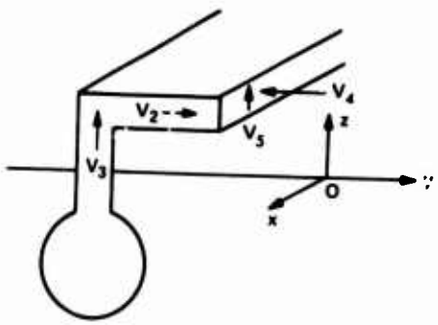
In the sequel the symbols in the parentheses shown previously will be used to denote the specific types of loading.

If we let f_2 and f_3 denote, respectively, the sectional heave and sway forces due to the mass inertia, and R_2 and R_3 denote the horizontal and vertical restoring forces, then the shear forces at section x can be expressed by

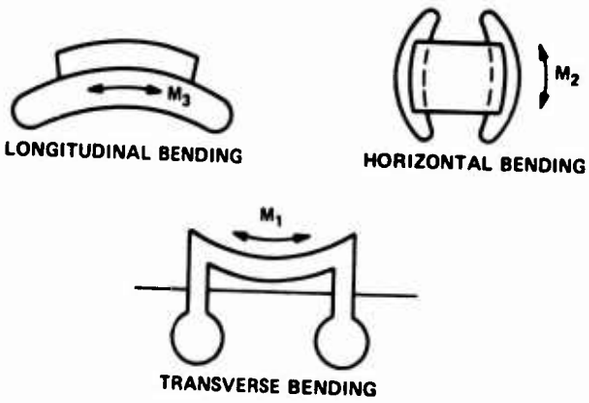
$$V_i(x) = \int_{-\ell_1}^{\ell} f_i(s)\,ds - \int_{-\ell_1}^{x} ds \int_{C(s)} p\,n_i\,d\ell - R_i \qquad (24)$$

for i = 2, 3

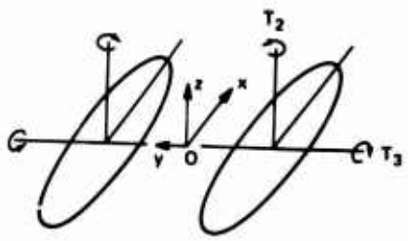
$$f_2(s) = -\omega^2 m(s)\,(\xi_{20} + s\,\xi_{60} - \bar{z}(s)\,\xi_{40}) \qquad (25)$$



a. Shear Forces



b. Bending Moments



c. Torsion Moments

Figure 1 Description of types of loading

$$f_3(s) = -\omega^2 m(s)(\xi_{30} - s\,\xi_{50}) \tag{26}$$

$$R_2 = 0$$

$$R_3 = -\rho g \int_{-\ell_1}^{x} b(s)(\xi_{30} - s\,\xi_{50})\,ds \tag{27}$$

where $m(s)$ is the sectional mass; $\bar{z}(s)$ is the vertical coordinate of the sectional mass center; $b(s)$ is the sectional beam at $x = s$; $-\ell_1$ is the x coordinate of the aft perpendicular of the ship; and $c(s)$ implies a contour integral in the counterlockwise direction over the immersed portion of the section. The hydrodynamic pressure p is obtained from the Bernoulli equation by

$$p = \rho\left(j\omega + U\frac{\partial}{\partial x}\right)\left(\phi_I + \phi_D + \sum_{k=2}^{6} \xi_{ko}\,\phi_k\right)$$

where ϕ_I is the velocity potential for the incoming waves; ϕ_D, for the diffracted waves; and ϕ_k, for the motion-generated disturbance in the fluid; see Appendix A for a more detailed explanation for these potentials. Employing procedures similar to those used in deriving Equations (72) and (73) in Appendix A, we can show that

$$\begin{aligned}\int_{-\ell_1}^{x} ds \int_{C(S)} pn_i\,d\ell = {} & \rho\int_{-\ell_1}^{x} ds \int_{C(S)} \left(j\omega_o\, n_i + \phi_i \frac{\partial}{\partial n}\right)\phi_I\,d\ell \\ & - \frac{\rho U}{j\omega}\int_{C(\omega)} \phi_i\,\phi_{In}\,d\ell - \rho\sum_{k=2}^{6}\xi_{ko}\int_{-\ell_1}^{x} ds \\ & \int_{C(S)} \phi_k\,\phi_{In}\,d\ell + \frac{\rho U}{j\omega}\sum_{k=2}^{6}\xi_{ko}\int_{C(S)}\phi_k\phi_{in}\,d\ell\end{aligned} \tag{28}$$

for $i = 2, 3$

where ϕ_{In}, for instance, means $\frac{\partial \phi_I}{\partial n}$ and the last term corresponds to the last term of Equation (68).

If we let

$$-\rho\int_{-\ell_1}^{x} ds \int_{C(S)} \phi_k\,\phi_{in}\,d\ell \equiv \omega^2 A_{ik}(x) + j\omega\,B_{ik}(x) \tag{29}$$

for $i = 2, 3$, and substitute this expression into Equation (28), we get

$$\int_{-\ell_1}^{x} ds \int_{C(S)} p\, n_i\, d\ell = \rho \int_{-\ell_1}^{x} ds \int_{C(S)} \left(j\,\omega_o\, n_i + \phi_i \frac{\partial}{\partial n}\right) \phi_i\, d\ell$$
$$- \frac{\rho\, U}{j\omega} \int_{C(x)} \phi_i\, \phi_{In}\, d\ell + \sum_{k=2}^{6} \left(\omega^2 A_{ik}(x) + j\omega\, B_{ik}(x)\right)$$
$$+ U \sum_{k=2}^{6} \xi_{ko} \left(j\,\omega\, a_{ik}(x) - b_{ik}(x)\right) \qquad (30)$$

where $a_{ik}(x)$ and $b_{ik}(x)$ are the sectional added mass and damping of the cross section at x. The expressions of $A_{ik}(x)$ and $B_{ik}(x)$ in terms of sectional added inertia and damping are almost identical to those for A_{ik} and B_{ik} shown in Table 1, except that the integrals in the table should be replaced by $\int_{-\ell_1}^{x}$, and A_{ik} and B_{ik} should be replaced by $A_{ik}(x)$ and $B_{ik}(x)$. For instance,

$$A_{35}(x) = -\int_{-\ell_1}^{x} s\, a_{33}(s)\, ds - \frac{U}{\omega^2} B_{33}(x)$$

where

$$B_{33}(x) = \int_{-\ell_1}^{x} b_{33}(s)\, ds$$

Returning to Equation (24), we can now write

$$V_2(x) = -\omega^2 \int_{-\ell_1}^{x} m(s) \left(\xi_{20} + s\,\xi_{60} - \bar{z}(s)\,\xi_{40}\right) ds$$
$$- \rho \int_{-\ell_1}^{x} ds \int_{C(S)} \left(j\,\omega_o n_2 + \phi_2 \frac{\partial}{\partial n}\right) \phi_I\, d\ell$$
$$- \frac{j\,\rho\, U}{\omega} \int_{C(x)} \phi_2 \phi_{In}\, d\ell - \left(\omega^2 A_{22}(x) + j\,\omega\, B_{22}(x)\right) \xi_{20}$$
$$- \left(\omega^2 A_{24}(x) + j\,\omega\, B_{24}(x)\right) \xi_{20} - \left(\omega^2 A_{26}(x) + j\,\omega\, B_{26}(x)\right) \xi_{60}$$
$$+ U \sum_{k=2}^{6} \xi_{ko} \left(j\,\omega\, a_{2k}(x) - b_{2k}(x)\right) \qquad (31)$$

in which

$$a_{23}(x) = a_{25}(x) = b_{23}(x) = b_{25}(x) = 0$$

$$a_{26}(x) = x\, a_{22}(x) \qquad b_{26}(x) = x\, b_{22}(x)$$

$$\begin{aligned} V_3(x) = &- \omega^2 \int_{-\ell_1}^{x} m(s)\,(\xi_{30} - s\,\xi_{50})\,ds \\ &- \rho \int_{-\ell_1}^{x} ds \int_{C(S)} (j\omega_o n_3 + \Phi_3 \frac{\partial}{\partial n})\,\Phi_I \; ds \\ &+ \frac{j\rho U}{\omega} \int_{C(S)} \Phi_3 \Phi_{In}\, d\ell - (\omega^2 A_{33}(x) + j\omega B_{33}(x))\,\xi_{30} \\ &- (\omega^2 A_{35}(x) + j\omega B_{35}(x))\,\xi_{50} + U \Big\{ (j\omega a_{33}(x) - b_{33}(x))\,\xi_{30} \\ &+ (j\omega a_{35}(x) - b_{35}(x))\,\xi_{50} \Big\} + \rho g \int_{-\ell_1}^{x} b(s)\,(\xi_{30} - s\,\xi_{50})\,ds \end{aligned} \tag{32}$$

in which

$$a_{35}(x) = -x\, a_{33}(x) \qquad b_{35}(x) = -x\, b_{33}(x)$$

The horizontal bending moment M_2 and the longitudinal bending moment M_3 can be obtained by

$$M_2(x) = \int_{-\ell_1}^{x} V_2(s)\,ds \tag{33}$$

$$M_3(x) = \int_{-\ell_1}^{x} V_3(s)\,ds \tag{34}$$

The previously described loadings V_2, V_3, M_2 and M_3 are obtained in exactly the same way as for monohull ships. However, to obtain the remaining loadings, the loadings on each hull should be separately studied. We would like to obtain the shear forces and bending moment at the various locations over a transverse cross section. The loadings V_4, V_5 and M_1 fall in this category.

Let us consider the right half of a cross section, located x from the origin. The structural members of this section will be divided into three parts : the cross-deck, the strut, and the main hull -

which will be denoted by A, B and C respectively, as shown in figure 2. First we will consider V_4, V_5 and M_1 at the left edge of the member A, which is the longitudinal centerline section of the catamaran.

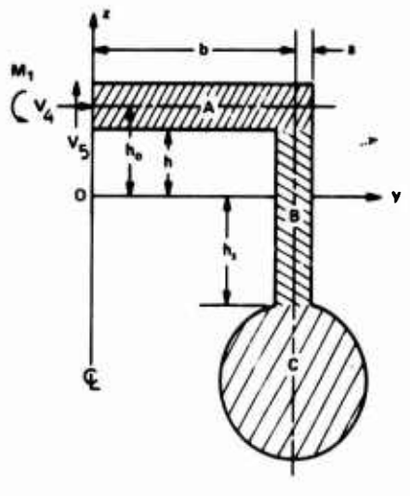


Figure 2 - A simplified cross section for loading analysis

The expressions for these loadings can be given in the form of

$$V_{i+2}(0) = f_i' - \int_{C_R} p\, n_i\, d\ell - R_i' \tag{35}$$

for i = 2, 3.

$$M_1(0) = M_1' - \int_{C_R} p \left\{ y n_3 + (h_o - z)\, n_2 \right\} d\ell - R_1' \tag{36}$$

Here f_i' are the inertial forces contributed by the mass of one-half of the cross section, C_R means the line integral in counterclockwise direction along the immersed contour of the right half of the cross section at its mean position, the subscripted R's are the restoring forces and moment, M_1' is the mass inertial moment, and h_o is as shown in figure 2. We can show that

$$f_2' = - \omega^2 m' \left\{ \xi_{20} + x \xi_{60} - \bar{z}' \xi_{40} \right\} \tag{37}$$

$$f'_3 = -\omega^2 m' (\xi_{30} - x \xi_{50} + \bar{y}' \xi_{40}) \tag{38}$$

$$M'_1 = -\omega^2 m' \{ \bar{y}' \xi_{30} - (\bar{z}' - h_o) \xi_{20} \} - \omega^2 [I'_x + m' \{ (\bar{z}' - h_o)^2 + (\bar{y}')^2 \}] \tag{39}$$

where m' is the mass of the half section, I'_x is the mass moment of inertia of roll about the center of mass of the half cross section, and $(\bar{y}', \bar{z}')$ is the coordinate of the mass center of the half section. The restoring forces and moment are given by

$$R'_1 = -2\rho g a b (\xi_{30} - x \xi_{50}) - \rho g S'_A \overline{GM}' \xi_{40} \tag{40}$$

where b and a are as shown in figure 2, S'_A is one-half of the immersed total sectional area, and $\overline{GM}'$ is the transverse metacentric height from the mass center.

$$R'_2 = 0 \tag{41}$$

$$R'_3 = -2\rho g a (\xi_{30} - x \xi_{50} + b \xi_{40}) \tag{42}$$

The pressure p at any point on the immersed contour of the right half section is given by

$$p = \rho (j\omega + U \frac{\partial}{\partial x}) (\phi_I + \phi_D + \sum_{k=2}^{6} \xi_{ko} \phi_k) \tag{43}$$

Then

$$\int_{C_R} p n_i \, d\ell = j\rho\omega_o \int_{C_R} \phi_I n_i \, d\ell + j\rho\omega \int_{C_R} \phi_D n_i \, d\ell + j\rho\omega \sum_{k=2}^{6} \xi_{ko} \int_{C_R} \phi_k n_i \, d\ell \tag{44}$$

for $i = 2, 3, 4$, where n_2 and n_3 are respectively the y and z components of the unit normal vector on the body surface and $n_4 = yn_3 - zn_2$.

Note that we can no longer apply Haskind's relation (1957) to express the diffracted wave force for a half cross section in terms of ϕ_{In} and ϕ_k as shown in Appendix A. This means that we

---

4 To be strictly true, the application of Haskind's relation in strip approximation is incorrect. Faltinsen (1971) has shown a three-dimensional diffraction effect.

have to obtain the solution of Φ_D before we can evaluate complete hydrodynamic loadings. In Append x B, the method of solving Φ_D by source distribution similar to that used in solving the motion potentials Φ_k is given. We shall not attempt to reduce the last integral of the right side of Equation (44) to added inertias and dampings. However, attention should be paid to the fact that decoupling between the motions of the vertical and horizontal planes can no longer be made in this integral. This is because we are dealing only with one hull for which there exists asymmetric pressure distribution even for a symmetric demihull, due to the blockage effect of the other hull. Thus, every term of the summation in Equation (44) would survive.

Applying the foregoing results into Equations (35) and (36), we obtain the following expressions

$$\begin{aligned} V_4(0) = &- \omega^2 m' (\xi_{20} + x \xi_{60} - \bar{z}' \xi_{40}) \\ &+ \rho \sum_{k=2}^{6} \xi_{ko} \int_{C_R} \Phi_{2n} \phi_k \, d\ell - j\rho \int_{C_R} (\omega_o \Phi_I + \omega \Phi_D) n_2 d\ell \end{aligned} \tag{45}$$

$$\begin{aligned} V_5(0) = &- \omega^2 m' (\xi_{30} - x \xi_{50} + \bar{y}' \xi_{40}) \\ &- j\rho \int_{C_R} (\omega_o \Phi_I + \omega \Phi_D) n_3 \, d\ell \\ &+ \rho \sum_{k=2}^{6} \xi_{ko} \int_{C_R} \Phi_{3n} \Phi_k \, d\ell \\ &+ 2\rho g a (\xi_{30} - x \xi_{50} + b \xi_{40}) \end{aligned} \tag{46}$$

$$\begin{aligned} M_1(0) = &- \omega^2 \left[I'_x + m' \left\{ \bar{y}^2 + (\bar{z} - h_o)^2 \right\} \right] \xi_{40} \\ &- \omega^2 m' \left\{ \bar{y} \xi_{30} - (\bar{z} - h_o) \xi_{20} \right\} \\ &- j\rho \int_{C_R} (\omega_o \Phi_I + \omega \Phi_D) \left\{ y n_3 + (h_o - z) n_2 \right\} d\ell \\ &+ \rho \sum_{k=2}^{6} \xi_{ko} \int_{C_R} \Phi_{4n} \Phi_k \, d\ell \\ &+ 2 \rho g a b (\xi_{30} - x \xi_{50}) + \rho g S'_A \overline{GM}' \xi_{40} \end{aligned} \tag{47}$$

Once the loadings at the centerline section of the cross-deck member are known, we can find the loadings at any section of the structural members in the following way.

For $-h_s \leq z \leq h$

$$V_4(z) = V_4(0) + \omega^2 m_A \left\{\xi_{20} + x\ \xi_{60} - h_o \xi_{40}\right\} + \omega^2 \int_z^h m''_B(\xi) \left\{\xi_{20} + x\ \xi_{60} + (\overline{z} - \zeta)\ \xi_{40}\right\} d\zeta$$

$$+ \rho \sum_{k=2}^{6} \xi_{ko} \left\{\int_z^o (\Phi_{2y}\, \Phi_k\big|_{y=b-a} + \Phi_{2y}\, \Phi_k\big|_{y=b+a})\, d\zeta\right\} - j\rho \int_Z^o \left\{(\omega_o \Phi_I + \omega\ \Phi_D)\big|_{y=b-a} + (\omega_o \Phi_I + \omega\ \Phi_D)_{y=b+a}\right\} ds\,\zeta \quad (48)$$

where m_A is the mass of the member A, and $m''_B(\zeta)$ is the mass distribution of the member B. If $z \geq 0$, the expression below the dotted line should be discarded.

$$M_1(z) = M_1(0) - \omega^2 m' (b^2 + z^2 - h_o^2 + 2h_o\overline{z} - 2b\overline{y} - 2z\overline{z}) - V_4(0)(h_o - z) - V_5(0)\, b + \omega^2 \int_o^{b+a} m''_A(\eta)(b - \eta)(\xi_{30} - x\ \xi_{50} + y\ \xi_{40})\, d\eta + \omega^2 \int_z^h (\zeta - z)\left\{\xi_{20} + x\ \xi_{60} + (\overline{z} - \zeta)\ \xi_{40}\right\} d\zeta$$

$$+ \rho \sum_{k=2}^{6} \xi_{ko} \int_Z^o (\Phi_{4x}\, \Phi_k\big|_{y=b-a} + \Phi_{4x}\, \Phi_k\big|_{y=b+a})\, d\zeta - j\rho \int_Z^o \left\{(\omega_o \Phi_I + \omega\Phi_D)\big|_{y=b-a} + (\omega_o \Phi_I + \omega\ \Phi_D)\big|_{y=b+a}\right\} (\zeta - z)\, d\zeta \quad (49)$$

where $m''_A(\eta)$ is the mass distribution of the member A. If $z \geq 0$, the expression below the dotted line should be discarded.

For $0 \leq y \leq b + a$

$$V_5(y) = V_5(0) + \omega^2 \int_o^y m''_A(\eta)(\xi_{30} - x\ \xi_{50} + y\ \xi_{40})\, d\eta \quad (50)$$

$$M_1(y) = M_1(0) - V_5(0)\, y - \omega^2 \int_0^y m''_A(\eta)(y-\eta)(\xi_{30} - x\,\xi_{50} + \eta\,\xi_{40})\, d\eta \quad (51)$$

Let us proceed to derive the expressions for the torsion moments T_2 and T_3. We assume that the twist center is located at the center of mass of the catamaran. The torque T_2 and T_3 are induced by out-of-phase hydrodynamic moments of yaw and pitch acting on the two hulls of a catamaran. From the equilibrium law, each hull should exercise equal magnitude but opposite torque load on the cross-deck structure. Thus, we can determine T_2 and T_3 by considering the yaw and pitch moment contributed by dynamic effects on one hull.

Utilizing the expressions derived earlier, we can write

$$T_2 = \frac{1}{2}\int_{-\ell_1}^{\ell_2} x\, f_2(x)\, dx - \int_{-\ell_1}^{\ell_2} x\, dx \int_{C_R} p\, n_2\, d\ell \quad (52)$$

and

$$T_3 = -\frac{1}{2}\int_{-\ell_1}^{\ell_2} x\, f_3(x)\, dx + \int_{-\ell_1}^{\ell_2} x\, dx \int_{C_R} p\, n_3\, d\ell + \frac{1}{2}\rho g \int_{-\ell_1}^{\ell_2} x\, b(x)\,(\xi_{30} - x\,\xi_{50})\, dx \quad (53)$$

where $-\ell_1$ and ℓ_2 are the locations of the aft and fore perpendiculars; $f_2(x)$ and $f_3(x)$ are given by Equations (25) and (26), respectively; c_R is the contour integral of a half cross section; p the hydrodynamic pressure and the expressions for $\int_{C_R} p\, n_i\, d\ell$ for $i = 2, 3$ are given by Equation (44); and $b(x)$ is the half beam of the cross section at x.

I . 4 - Results and Discussion.

Numerical results from the theory developed in the preceeding sections are compared with available experimental results. The presentation of the results is made in the following order. The first part deals with the two-dimensional hydrodynamic coefficients. The second part deals with the three-dimensional hydrodynamic coefficients. The third part deals with the heave and pitch motions of three catamaran models. Two of the models are of conventional-catamaran configuration and the other one is of a SWATHS configuration. The description of these three catamarans is given in Table 2 and figure 5

The strip approximations employed in our analysis of motions and hydrodynamic loadings are based on a two-dimensional approximation of the fluid motion at each transverse cross section. A solution for the velocity potential associated with heaving, swaying, or rolling twin cylindrical bodies of arbitrary but uniform cross sectional forms has been developed by the method of source distribution. Lee, Jones, and Bedel (1971) show good agreement between theoretical and experimental values of heave added mass and damping of four different types of twin cylinders. Figure 3 compares heave added mass and damping in nondimensional forms $a_{33}/(\rho\forall)$ and $b_{33}/(\rho\forall\omega)$ where $\forall$ is the immersed volume at the mean position versus the frequency number $\frac{\omega^2 a}{g}$ for twin rectangular cylinders. The dotted lines in Figures 3a and b are the theoretical results for one cylinder only. If the separation distance between the two cylinders is large, one would expect that the added mass and damping coefficients for the twin cylinders approach those for the single cylinder. Thus the difference between the solid and dotted curves in these two figures can be regarded as the measure of a hydrodynamic interaction between the two hulls. The added mass reflects the local behavior of the fluid motion near the body, whereas the damping is sensitive only to the far-field behavior of the fluid motion. Here in figures 3a and b we can observe that both local and far-field behavior of fluid motions generated by a single cylinder is quite different from the behavior of twin cylinders.

Two types of singular solutions may occur at certain frequencies in the problem of oscillating twin cylinders. One is associated with a mutual blockage effect between two cylinders, and the other is associated with the method of singularity distributions; see John (1950). The former is of both mathematical and physical origin; the latter is strictly of mathematical origin and applies to both single and twin cylinders. The former type of singular behavior is shown in figure 3c at the frequency number of about unity. The experimental results seem to confirm the singular behavior. The frequencies at which such singular behavior occurs can be determined by

$$\frac{\omega^2 a}{g} = \frac{n\pi}{(b/a - 1)} \qquad \text{for } n = 1, 2, \ldots \tag{54}$$

where the definition of a and b is as shown in figure 3a.

The second type of singular behavior is shown in figure 3d by the solid curve. This type of singular behavior results from the break down of the solution of the Fredholm-type integral equation at

certain eigen frequencies.

Existence of such singular behavior in the solution of sectional hydrodynamic coefficients can present troubles in applying strip approximations to three-dimensional hydrodynamic coefficients. Removal of the second type of singular behavior has been achieved by imposing a rigid wall condition, i.e., $\phi_z = 0$ or a pressure relief condition, i.e., $\phi = 0$, on the line $z = 0$ inside cylinders.[5] A mathematical proof of legitimacy for employing this technique will be published in the future. Figure 3d shows heave added mass of a rectangular cylinder obtained with and without the additional interior boundary in the solution of the boundary-value problem.

Removal of the other type of singularity may not be possible unless a full threee-dimensional solution of the problem is achieved. However, for catamarans having the inner hull separation distance on the order of the beam of one hull, the lowest frequency at which this singularity occur may lie out of the practical range of interest in ship motions. For example, if we take $b/a = 2$, the longest critical wave length λ_c which can be encountered in head waves can be obtained by

$$\lambda_c = \frac{4\pi U^2}{g\left(1 + \sqrt{1 + 4U^2\sqrt{\frac{\pi}{ag}} + 2U\sqrt{\frac{\pi}{ag}}}\right)} \tag{55}$$

For $a = 15'$, we have

U (knots)	λ_c (ft)
10	17.8
20	77.2
30	124.1

Comparison of theoretical results with experimental results of three-dimensional added mass and damping for NSRDC Model 5061, the description of which is given in Table 2 and figure 5, is shown in figure 4 for Froude numbers $F_n = 0$ and 0.253 (10 knots). The three-dimensional added mass and damping are obtained from the two-dimensional added mass and damping by the strip approximation as

[5] Employment of this technique was first made by Paul Wood of the University of California at Berkeley.

shown in Table 1. The results in figure 4 are extracted from Jones (1972) and are nondimensional values defined by

$$\overline{A}_{33} = \frac{A_{33}}{M} \qquad \overline{B}_{33} = \frac{B_{33}}{M\sqrt{g/L}}$$

$$\overline{A}_{35} \text{ or } \overline{A}_{53} = \frac{A_{35} \text{ or } A_{53}}{M\,L} \qquad \overline{B}_{35} \text{ or } \overline{B}_{53} = \frac{B_{35} \text{ or } B_{53}}{M\sqrt{gL}}$$

$$\overline{A}_{55} = \frac{A_{55}}{ML^2} \qquad \overline{B}_{55} = \frac{B_{55}}{ML\sqrt{gL}}$$

$$\overline{\omega} = \omega\sqrt{\frac{L}{g}}$$

The experimental results are taken at several amplitudes of oscillation. Agreement between the theoretical and the experimental results is good for the zero-speed case, whereas some discrepancies can be observed for the case of $F_n = 0.253$.

Comparison of theoretical and experimental values of nondimensional heave amplitude ξ_3^o/A and pitch amplitude $\xi_5^o\lambda/(2\pi A)$ versus wavelength λ/L for the catamarans shown in figure 5 are presented in figures 6 through 8. A is the wave amplitude, λ is the wavelength, and L is the ship length. Most of the results shown in these figures are from Jones (1972).

Unrealistically high-spiked theoretical values of heave and pitch amplitudes for 30 knots shown in figure 8 imply that damping values obtained from theory have been underestimated. The deficiency of theory may be traced to several assumptions or approximations made in the present analysis: the ideal-fluid assumption, the strip approximation of three-dimensional hydrodynamic coefficients, and the assumption of neglecting the second-order effect of coupling between the steady and oscillatory perturbation potentials. None of these assumptions can be removed without undergoing major renovations in the analytical procedures.

Nevertheless, an attempt to introduce supplemental damping in the equations of motion has been made by using a trial-and-error approach. The first approach attempted was to express the

sectional heave-damping force in the form of

$$F_d = b_{33} W(t) + c_1 U W + c_2 |W| W \qquad (56)$$

where $W(t) = \dot{\xi}_3 - x \dot{\xi}_5$, and c_1 and c_2 are constants. An expression similar to Equation (56) is given in Thwaites (1960) for a slender body for a moderate angle of incidence in an unbounded fluid. The second term of the right side of Equation (56) is called viscous lift and the third term is called cross-flow drag. From the model test results, it was found that the damping obtained from theory for the case of zero speed seemed adequate. Thus, addition of the cross-flow drag which is independent of speed was considered unnecessary. However, the viscous-lift term, which depends on forward speed, seemed proper to be retained. Use of the test results for c_1, given in Thwaites (1960, pp. 415-416), and a modification of the sectional heave damping obtained by adding $c_1 U$ to b_{33}, has not been successful. From this trial-and-error approach, it was learned that additional damping seemed to depend on a parameter $\omega U/g$. This parameter is the ratio of ship speed to the celerity of motion-generated waves. When the ratio is less than one-fourth, there can be generated a chain of ring waves propagating ahead of the ship; see Wehausen and Laitone (1960, p 494). Dependence of the supplemental damping on this parameter implies that the hitherto neglected interaction effect between two wave systems, one produced by oscillation and the other by translation of ship, is important.

The strip approximation may exaggerate the effect of the hydrodynamic interaction between the two hulls. When a catamaran sails with a forward speed so that $\omega U/g > 1/4$, the motion-generated waves will be swept back by the forward speed. Especially between the two hulls, the steady horizontal flow can be accelerated by a channel effect which leaves less chance for the oscillation-generated waves by the two hulls to interact in this region. To examine whether the foregoing postulation is true, the heave damping and heave and pitch amplitudes of Model 5061 and the demihull of this model are compared in figure 9 together with experimental results for twin hulls. There seems little change in the motion results between the twin and the demi-hulls except at the resonant wavelengths. At the shorter wavelengths, the heave damping of the demihull shows a better agreement with the experimental values. However, a similar comparison to that previously described for the heave and pitch amplitudes of 5266 at 30 knots revealed that the demihull has higher motion amplitudes at the resonant wavelengths than the twin hulls do. This seems to imply that for LWP catamarans, the underestimation

of damping does not necessarily arise from an over-estimation of the mutual hydrodynamic interaction effects of the two hulls by the strip approximation.

The dotted curves in figure 8 are obtained with modified heave and pitch damping values. These are obtained by modifying the sectional heave damping by $b_{33}^*(x) = b_{33}(x) + \alpha\rho\omega S_A(x)\frac{\omega U}{g}$ where $b_{33}(x)$ is the old heave damping at a cross section at x, ρ is the density of water, $S_A(x)$ is the sectional area and $\alpha = 3.0$ for Model 5266. The constant α is a function of ship geometry and is obtained at present from the comparison of the theoretical and the experimental results of motion. The hydrodynamic coefficients affected by this change are B_{33}, A_{35}, A_{53}, and B_{66} (Table 1). A further investigation to remove the discrepancy of the motion prediction at the resonant wavelengths by better techniques seems to be definitely necessary.

The absolute and relative vertical motions of Model 5266 at a speed of 30 knots, which are computed with the modified damping, are shown in figure 10. If we assume the height of the cross-deck of Model 5266 from the designed waterline is 30 feet, the water contact could be made when a sinusoidal incoming wave having an amplitude of 27 feet is encountered with an interval period of 18 seconds as the ship runs at 30 knots. The irregular-sea computation showed that the chance of water contact of the cross-deck of Model 5266 is zero to a significant wave height of 20 feet at 30 knots.

The results presented in this section cover only part of the analysis made in part 1. Numerical results for the sway, roll and yaw motions and the hydrodynamic loads were not available at the time of this writing.

I.5 - Concluding Remarks on the Prediction of Motion of Catamarans.

1. The strip approximation seems to yield a satisfactory motion prediction, except at the resonant wavelengths. The shortcoming of the strip approximation is considered to arise from inability to account for the correct forward speed effect on the hydrodynamic coefficients over the range of resonant frequencies. The area to be improved in the theory seems to be the evaluation of the damping coefficients. Proper incorporation of the interaction effect between the waves generated by the forward speed and the body oscillation is considered to be the most important factor to be investigated.

2. Although an improvement of the analytical prediction at

the resonant wavelengths should be made, with proper supplemental damping the prediction method can be utilized for parametric study of catamaran hull geometry with respect to seaworthiness characteristics.

II - HULL FORM RESISTANCE AND DESIGN PROCEDURE.

II . 1 - A General Discussion of Catamaran Hull Resistance.

A SWATHS is a special category of catamarans. First it will be appropriate to discuss a general catamaran. The resistance problem for a catamaran hull configuration is far more complex than that of a monohull. This complexity arises from two interference effects between the demihulls : a surface wave, which is familiar phenomenon, and the flow curvature, induced by the displacement of each demihull. This displacement interference exists even in the absence of a free surface.

The pressure distribution over a single hull towed alone is different from that when one hull is towed alongside another hull in that the hydrodynamic property is significantly changed. To predict the combined resistance of two ship models towed side-by-side would be rather difficult, even if we knew all the hydrodynamic properties of each model when towed alone. In the first place, the stagnation points would be altered, and the flow on both sides of each hull would no longer be the same. As a result, a crossflow and a side force would be produced. Such a crossflow would increase eddying, and the side force would have additional resistance similar to the induced drag of a lifting body or lifting surface.

For these reasons, the surface wave of each model is also altered due to the presence of another hull. Indeed, for a catamaran hull configuration, we are not only confronted with the added complexity in wavemaking resistance and viscous resistance but also with a new problem of induced drag. Faced with this situation, it seems very tempting to obtain a catamaran model series for prediction of resistance. Such a series, however, would be very expensive to accomplish. Furthermore, its usefulness would be very limited because the interference effect depends not only upon the hull distance but also upon the hull geometry. The interference effects obtained from a catamaran model series could not be applied to a catamaran having a hull geometry that was different from that of the series. A catamaran series would only be useful if it had good resistance performance and if it were possible to confine our catamaran hull designs within the series Then we would be faced with the same problem in designing a catamaran hull forms with good resistance performance. This is the subject

of this part of the paper.

II . 2 - Design Procedure.

Designing a catamaran hull form with good resistance qualities is a much easier problem than predicting the resistance of a given hull form. For instance, for the purpose of reducing the resistance, the crossflow around each demihull is eliminated. Hence, in a design problem, we have to deal only with the hull form without crossflow, and we need not be concerned with the complications crossflow would create. Since the basic flow around a demihull is not straight but is curved due to the presence of another demihull, the geometry of a demihull cannot have symmetry with respect to both sides if the crossflow is to be avoided. The amount of asymmetry depends upon the geometry of, as well as the distance between, the demihulls. Since hull geometry and hull distance are the objectives of the design problem for a catamaran hull form, it is very difficult to solve the problem in one step. To simplify the situation, a concept of an effective hull form is introduced as follows.

Concept of an Effective Hull Form.

We define a monohull in a straight uniform flow to be an effective hull for a demihull in a curved flow, if the flow relative to the hull is the same in both cases. If a demihull were towed alone and then towed with another demihull, a different effective hull form would result, even though its physical geometry had been kept the same. To maintain the same effective hull form, changes must be introduced to the hull geometry. Whenever the distance between demihulls is varied, a corresponding variation in hull geometry is also needed.

Since the geometrical difference between a demihull and its effective hull can be determined after the effective hull geometry and the hull distance are given, it is rather logical to divide the design problem into two steps. In the first step an effective hull form is developed, and in the second step the geometry of the demihull is determined.

Designing an Effective Hull Form for the Demihull of a Catamaran.

The viscous drag and the free wave system of a demihull are considered to be the same as those of its effective hull form. Hence, the resistance of a catamaran can be optimized by developing an optimum effective hull form. Since effective and geometric hull

forms are the same in a straight uniform flow, the design of an effective hull form is equivalent to the design of a monohull. Therefore, the concept of an effective hull form enables us to link together the design problems of a single hull and a catamaran. This link is an important step in the future development of catamaran technology. With this link, it becomes possible to utilize all the knowledge and information of single hull form design to the design of catamaran hull forms.

In designing a single hull form, there are two possible approaches. One is the empirical approach, based on model series work and successful ships built in the past. The other approach is theoretical, the essential foundation of which is the wavemaking-resistance theory. With the first approach, many good hull forms have been developed. However, since it is not possible to know what makes good hull forms, this approach is very difficult when designing unusual hull forms for which there is very little available information. On the other hand, due to the oversimplification of a theory, the second approach cannot always produce satisfactory results. Perhaps the most rewarding approach would be a combination of the two and a great deal of intuition. At this point, we shall presume that a good monohull can be developed one way or another, so we shall not discuss the design of a single hull form further, except to make a few remarks pertinent to demihull design.

The attractive feature of a catamaran hull configuration, as far as wavemaking resistance is concerned, is the added freedom in the displacement-volume distribution. In the case of a monohull, the required transverse stability limits the freedom of the displacement-volume distribution in the vertical direction. The benefit of wave cancellation can mainly be achieved by the proper longitudinal distribution of the displacement-volume. In the case of a catamaran, the transverse stability does not depend solely on the waterplane area of each demihull. Hence, we can have more freedom in distributing the displacement-volume in the vertical direction. It then becomes possible to have cancellation between waves produced by displacement volume at various depths. In the case of a SWATHS , for instance, it is possible to have wave cancellation between a strut and a submerged body. Since the distance between two demihulls can be varied to a certain extent, another freedom of displacement-volume distribution is obtained. As a result, a far greater degree of wave cancellation is possible for a catamaran hull configuration than for a monohull. In designing an effective hull form for a demihull, the advantage of greater wave cancellation should be achieved.

If the effective hull form is to be chosen from a group of existing monohull forms with good resistance qualities, the one with the lowest resistance value at design condition is not necessarily the best choice for the effective demihull form. The one with the lowest resistance at the design speed may not give the best wave cancellation between the two demihulls. The wave cancellation at a given Froude number and a given hull distance depends upon the free wave amplitude-spectrum distribution of each demihull. The wavemaking resistance of a catamaran depends not only upon the level of the free wave amplitude curve, but also upon the shape of such a curve. Before the best choice can be made, it is necessary to obtain the amplitude-spectrum curve of each monohull, either experimentally or theoretically. Experimental methods are available for obtaining wave "cuts" from which a wave amplitude-spectrum curve can be deduced. By using the Douglas program and the existing wavemaking resistance theory, the wave amplitude-spectrum curve of a monohull can also be computed. If the possibility of obtaining the wave amplitude-spectrum curve does not exist, hull forms with pronounced hollows and humps in their C_r curves should be avoided, even though the C_r values at the design speed are relatively low.

If a theoretical approach is used in designing an effective hull form, two singularity distributions, one for each demihull, are placed the desired distance apart. On the basis of linearized wavemaking resistance theory, the surface wave of a catamaran is a linear superposition of the waves produced by the demihulls. Within the constraints of design conditions, the optimum singularity distribution is obtained by minimizing the wavemaking resistance of a catamaran. The final design, of course, has to be chosen on the basis of total resistance rather than on the basis of wavemaking resistance alone. By tracing a number of streamlines generated by one of the singularity distributions in a uniform flow, the hull geometry of an effective hull is obtained.

Based on theoretical insight and whatever practical information is available, we assume that the design of an effective hull for a demihull can be carried out successfully. Our remaining task is to find a way of obtaining the geometry of a demihull from the geometry of its effective hull form. This will be discussed in the next section.

Developing the Geometry of a Demihull from its Effective Hull Form.

Before discussing the procedure for obtaining the geometry of a demihull from the geometry of its effective hull form, let us first consider a two-dimensional, thin, symmetrical section. In a straight

uniform flow, there is no circulation on this symmetrical section. However, if we place this section in a curved flow, we have to curve the section in such a way that its original plane of symmetry coincides with the flow in order to maintain the stagnation points and thus avoid the creation of circulation on this section. Similarly, we have to modify the single-hull geometry in the presence of another demihull so that there is no shift in the stagnation points. In this case, however the beam of each demihull is relatively large in comparison with the distance between the demihulls. The flow curvatures on two sides of a demihull are quite different, and the usual practice of adding thickness distribution to a mean cambered surface may not always be applied here. Instead, we have chosen the following procedure.

The Douglas program, used to compute the source distribution, has been extended to trace offbody streamlines. Our objective is to obtain the distortion in the effective hull form placed at the location of one demihull in the presence of another for the purpose of obtaining its final geometry. We shall measure the distortion of the effective hull form due to the flow curvature with respect to the midship section. In other words, the midship section of the demihull is identical to that of its effective hull form. Let us consider an afterbody plan of the effective hull form placed at the midship section. If a number of points along a given station of this body plan are chosen as starting points of streamline tracing, all streamlines are parallel in a uniform flow in the absence of the other demihull, and the station section defined by these points will not be distorted. Due to the presence of the other demihull, however, the streamlines so traced will no longer be parallel but will be distorted according to the flow curvatures due to the other demihull. The points obtained by intersecting these distorbed streamlines by a cross plane at the corresponding longitudinal location will then define the required hull cross section of the demihull. In this manner the afterbody of the demihull is obtained. Similarly, by placing a forebody plan at the midship section and by reversing the direction of the uniform flow at infinity, we can obtain the forebody of the demihull.

A computing program has been developed, using the existing Douglas program as a starting point for computing the body plan of a demihull. Using the offsets of the effective hull form as input data, the required offset table of the demihull is generated by this computing program. By using this computer program, an existing single hull can easily be converted into a demihull of a catamaran without changing its hydrodynamic properties.

II. 3. - Design Examples - SWATHS.

Remarks Pertinent to SWATHS Hull Form Design.

The design procedure previously described can easily be followed in designing a SWATHS . In this case, a theoretical approach is necessary since there is very little information available. Due to the relatively simple geometry of a demihull, its singularity representation can be much simpler in comparison with that of a usual monohull. A thin wall-sided strut can be approximately represented by a surface singularity distribution on a vertical plane with density varying longitudinally but not vertically. The depth of such a distribution is the same as the strut draft. In addition, vertical line source and line doublet can be included to represent a strut bulb. A submerged hull is represented by a line-source distribution which generates a body of revolution in an infinite fluid with uniform flow. If the main body is not exactly a body of revolution, it is approximated by a line-source distribution which would generate a body of revolution having the same sectional area curve as the main hull.

For a surface and a line singularity distribution on a common vertical plane, the body generated in a uniform flow with a free surface would be symmetrical with respect to the vertical plane. The strut horizontal section would vary with depth, and the submerged main hull would sag in the middle. To retain the wall sidedness of the strut and to prevent the main hull from sagging, an additional singularity distribution is necessary. Since the main objective of a theoretical analysis is developing a hull form with good resistance performance rather than achieving an accurate resistance prediction, such an additional singularity has been ignored. In other words, each demihull is represented by a surface singularity distribution on a central plane and a longitudinal line-source distribution.

First Design Example - A 100,000-Ton, 30-Knot, SWATHS Model 5266.

Singularity Distributions and the Theoretical Wavemaking Resitance. Within the limits of constraints imposed on the hull geometry, an optimum singularity distribution of an effective hull form for both demihulls was determined. These constraints were specified based on functional requirements on ship displacement and space as well as ship motion. The optimization was done on the wavemaking resistance first, and then the total resistance was computed. Within

the desig constraints, hull parameters which influenced the wetted surface most were varied. The optimization of wavemaking resistance and the conputation of total resistance were repeated. After a few such repetitions, a final singularity distribution was chosen.

The theoretical analysis was performed with the aid of an existing wavemaking reistance computer program. Since the sub merged main-hull length was different from the strut length, some difficulty was encountered in using this program. For this reason, discrete source points, rather than a continuous line source, were used for a main hull. The final singularity distribution of this design is given as follows.

Submerged main body:

x	y	-z	m
1.1275	.295	.1411	.000470
1.1250	.295	.1411	.000470
1.1150	.295	.1411	.000470
1.1000	.295	.1411	.000470
1.0800	.295	.1411	.000470
1.0550	.295	.1411	.000470
1.0250	.295	.1411	.000470
.9900	.295	.1411	.000470
.9500	.295	.1411	.000470
.9050	.295	.1411	.000470
.8550	.295	.1411	.000470
.8000	.295	.1411	.000470
.7400	.295	.1411	.000470
.6750	.295	.1411	.000470
.6050	.295	.1411	.000470
.5300	.295	.1411	.000470
-.3300	.295	.1411	-.000235
-.3832	.295	.1411	-.000235
-.4363	.295	.1411	-.000235
-.4895	.295	.1411	-.000235
-.5300	.295	.1411	-.000235
-.5426	.295	.1411	-.000235
-.5958	.295	.1411	-.000235
-.6050	.295	.1411	-.000235
-.6490	.295	.1411	-.000235
-.6750	.295	.1411	-.000235
-.7021	.295	.1411	-.000235
-.7400	.295	.1411	-.000235
-.7553	.295	.1411	-.000235
-.8000	.295	.1411	-.000235
-.8084	.295	.1411	-.000235
-.8550	.295	.1411	-.000235
-.8620	.295	.1411	-.000235
-.9050	.295	.1411	-.000235
-.9148	.295	.1411	-.000235
-.9500	.295	.1411	-.000235
-.9679	.295	.1411	-.000235
-.9900	.295	.1411	-.000235

x	±y	-z	m
-1.0211	.295	.1411	-.000235
-1.0254	.295	.1411	-.000235
-1.0554	.295	.1411	-.000235
-1.0742	.295	.1411	-.000235
-1.0854	.295	.1411	-.000235
-1.1054	.295	.1411	-.000235
-1.1154	.295	.1411	-.000235
-1.1254	.295	.1411	-.000235
-1.1274	.295	.1411	-.000235
-1.1274	.295	.1411	-.000235

where x, y, z are coordinates of a source point, and m is the point-source strength. The origin is taken at the midship section in the center of a catamaran at the undisturbed free surface.

Strut :

$$m(x) = 2.8283x - 18.3987x^2 + 46.3879x^3 - 50.5260x^4 + 19.8121x^5$$

for forebody with $0 \leq x \leq 1$

$$-m = 2.3116|x| - 14.7986|x|^2 + 39.3606|x|^3 - 45.2937|x|^4 + \ldots$$
$$\ldots + 18.4201|x|^5$$

for afterbody with $-1 \leq x \leq 0$

In addition, there is a line source of 0.01 at $x = 1$ and a line sink of the same strength at $x = -1$. The singularity strength is normalized on the base of a unit of forward ship speed and the strut singularity distribution length as two units. The depth of the previously described surface and line singularity distribution is 0.099.

The wavemaking resistance coefficient C_w is normalized by wetted surface rather than the length square of the strut. For the purpose of direct comparison with the experimental residual resistance coefficient C_r , it is plotted against $V/\sqrt{L}$; where L is related to the main hull length. The theoretical wavemaking resistance curve is shown in figure 11 .

Model Experimental Results The experimental hull form

of each demihull was obtained in two steps. In the first step, an effective hull form was derived from its singularity distribution bv the method of double-model or zero-Froude-number technique. Further simplification was introduced here by obtaining strut and main-hull geometries separately. A load waterline for the strut was computed from the strut singularities alone, and all the other waterlines were the same as the load waterline. The main-hull geometry was obtained by tracing a streamline generated by the line source points in an infinite medium. Then the strut and main-hull were joined together with the proper fillet. In the second step, the demihull geometry was computed from its effective hull form, and the singularity distribution of the other demihull properly located. Due to the small width of the strut as compared with the flow curvature induced by the other demihull, the load waterplane was cambered by computing the distortion of its centerline. To maintain the wall sidedness of the strut, this camberline was used at all the depths. Furthermore, it was also used to camber the submerged main-hull.

For the purpose of internal functional arrangement and twin-screw propulsion arrangement, the main-hull cross sections were changed gradually from circular to elliptical sections, and a beavertail was formed at the stern. To increase propeller submergence, the tail end was slightly bent downward. Figure 12 shows the lines of this model, and figure 13 gives the hull characteristics.

A 16-ft model was built and tested for resistance and powering. The C_r values were also plotted in figure 11 for comparison.

Second Design Example - Model 5276.

Singularity Distributions and Theoretical Wavemaking Resitance. This design represents a 4000-ton, 30-knot ship. The singularity distribution for each main-hull was chosen to be the same as that of Model 5266. However, the main-hull geometry was kept as a body of revolution. The operating Froude number was much higher than that of Model 5266. Struts were redesigned to give better performance at operating condition.

At low Froude number, it is possible to achieve great beneficial wave interference between struts and main-hulls. The theoretical wavemaking resistance of a SWATHS way have lower wavemaking resistance with than without struts, despite the added strut-displacement volumes, as for Model 5266. At high Froude number beyond the last hump, it is difficult to achieve such great

beneficial wave interference between struts and main-hulls. After a number of computations, the following singularity distributions for each demihull strut were chosen :

Forebody

Surface Source

$$m(x) = 9.4498x - 69.5632x^2 + 189.4110x^3 - 213.4796x^4 + 83.5701x^5$$

Surface Doublet

$$D(x) = 1.1375\,(x - .4)^3 - 1.1375\,(x - .4)^4$$

with $.4 \leq x \leq 1$

The doublet was in the x-direction. Singularity distributions for the afterbody were such that a symmetrical strut was obtained. The depth of these distributions was 0.118.

Model Experimental Results. The offsets of the effective hull form were obtained in the same manner as in the case of Model 5266. In this case, it was decided to keep the demihull geometry the same as that of its effective hull geometry for two purposes : first, to be able to test a demihull alone without the complications of camber, and, second, to have a gross assessment as to the penalty of having no camber. By comparing the theoretical and experimental resistance results of a catamaran and a demihull, it might be possible to estimate the added resistance due to displacement interference effects. Figure 14 shows the lines of this model, and figure 15 gives the hull characteristics of this design.

Comparison Between Theoretical Wavemaking Resistance Coefficient C_w and Experimental Residual Resistance C_r . The theoretical predictions and experimental results are given in figure 16 . The C_r curves are much higher than expected both for a catamaran configuration and a single hull. In view of the good agreement between C_w and C_r curves for Model 5266, the cause of the disagreement for this model is not clear. In view of this, additional tests with modified struts were carried out.

Additional Results from One Demihull Tested Alone. It was speculated that the blunt strut endings followed by rapid curvature changes might have caused flow separation. If separation did occur, the testing model would have been modified and would not have been

the same as built. With this in mind, struts were modified to remove the cause of flow separation. This was done simply by cutting off the blunt endings in order to save time and effort in the shop. The corresponding source distribution was as follows :

$$m(x) = 3.4533x^2 - 54.2007x^3 + 287.262x^4 - 702.9402x^5 + 1106.1540x^6 + 1642.7120x^7 - 1586.4090x^8 + 477.3101x^9$$

for forebody.

The afterbody singularity distribution was such that a symmetrical strut was obtained. Figure 17 gives the waterplane of the modified strut. The modified demihull was tested alone in the captive condition, i.e., restricted from heaving and pitching. Figure 18 shows the comparison between C_w and C_r curves and, again, the agreement is quite good.

The strut was further modified to regain the waterplane area lost in the first modification. Figure 19 shows the strut waterplane after the second modification. The corresponding source distribution is given as follows :

$$m(x) = 22.8204x^3 - 447.7026x^4 + 3276.9175x^5 - 11883.5996x^6 + 23318.8100x^7 - 23199.7132x^8 + 5282.0771x^9 + 11396.8366x^{10} - 10699.5081x^{11} + 2933.4272x^{12}$$

for forebody.

The strut was again kept symmetrical with respect to the middle length. Figure 20 shows the comparison between C_w and C_r . The agreement is also good.

At the present time, a SWATHS with proper camber is under construction. The strut with the second modification, Model 5276-E, is used for the catamaran configuration. At a later date, another demihull without camber will be built and tested in a catamaran configuration in combination with Model 5276-E. After these additional experimental results are obtained, the influence of camber on resistance can be assessed.

Figure 21 gives the resistance comparison between two single hulls, Model 5276-C and Model 5276-E, at a 32-ft draft. To

assess the contribution of the main hull to the total wavemaking resistance of a catamaran, the C_w curve of a single main hull without a strut was also computed and is plotted in Figure 21. This curve was computed on the assumption that the main hull alone had the same displacement volume as Model 5276-E. In other words, the diameter was increased but its centerline depth was not changed. To facilitate a direct comparison of wavemaking resistance, this C_w curve was computed by using the wetted surface of Model 5276-E rather than that of the main hull form. This C_w curve gives the limit as the size of a strut is reduced to zero while the total displacement volume is kept constant. Figure 22 gives the same information at a 28-ft draft.

It is important to note that, at high Froude number, the wavemaking resistance of a submerged main hull cannot be ignored. The wavemaking resistance of a SWATHS can be greatly reduced by diminishing the strut size while the total displacement volume is kept the same.

II.4. - Concluding Remarks about the Catamaran Hull Form Design Procedure.

Based on the concept of an effective hull form, the problem of designing a catamaran essentially becomes the same as that of designing a conventional single hull. The direct link between these two design problems is a computer program developed to obtain offsets of a demihull form offsets of its effective hull at a specified hull distance. By using this computer program, a pair of monohulls can be converted into a pair of demihulls of a catamaran without altering the original hydrodynamic properties.

In general, the SWATHS is a special case of catamaran configuration. Due to the simplicity of its hull geometry, designing a SWATHS theoretically is much simpler than designing a conventional catamaran. Two design examples for SWATHS were given. Except in the case of a strut with blunt endings and quick curvature reversals, comparisons of theoretical C_w curves with experimental C_r curves showed good agreement.

How low the resistance level of a catamaran hull form can be designed depends both upon our ability to design a conventional single hull and on the design constraints imposed. To enhance the good resistance performance of a catamaran, restrictions imposed on the hull geometry should be kept to a minimum. For developing a specific type of catamaran, the major effort should be directed toward developing an effective hull form first, rather than toward developing a catamaran hull form directly. In so doing, not only would the expense

be reduced, but the information so obtained would also be more basic and useful.

III - CONCLUSION

The selection of catamaran hull forms which possess good hydrodynamic characteristics should be the result of the best compromise among motion, powering, and sea-load considerations.

In the first part of this work, analytical methods of predicting motion and sea-loads of catamarans are presented. In the second part, a hull form design procedure which provides a set of ship lines with good resistance characteristics is presented.

It is anticipated that the utilization of the methods described in this work will contribute a useful, basic input in the preliminary design of a SWATHS.

* * *

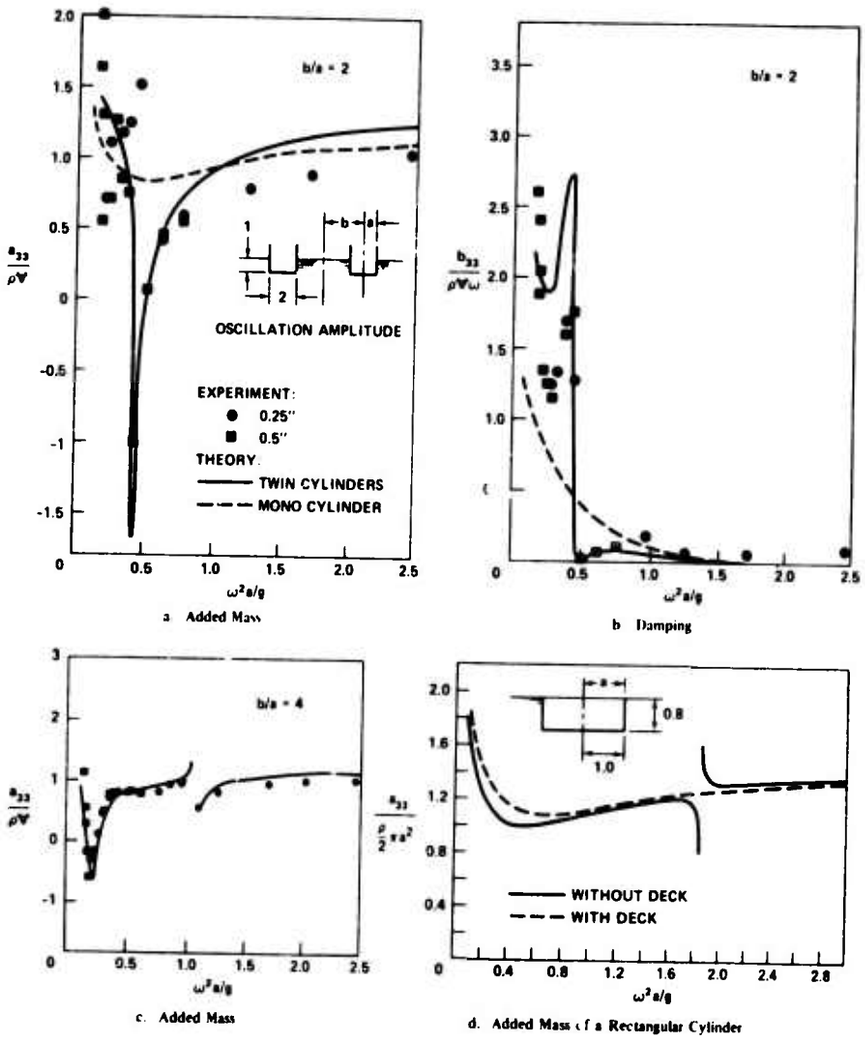


Figure 3 Two-dimensional heave added mass and damping coefficients.

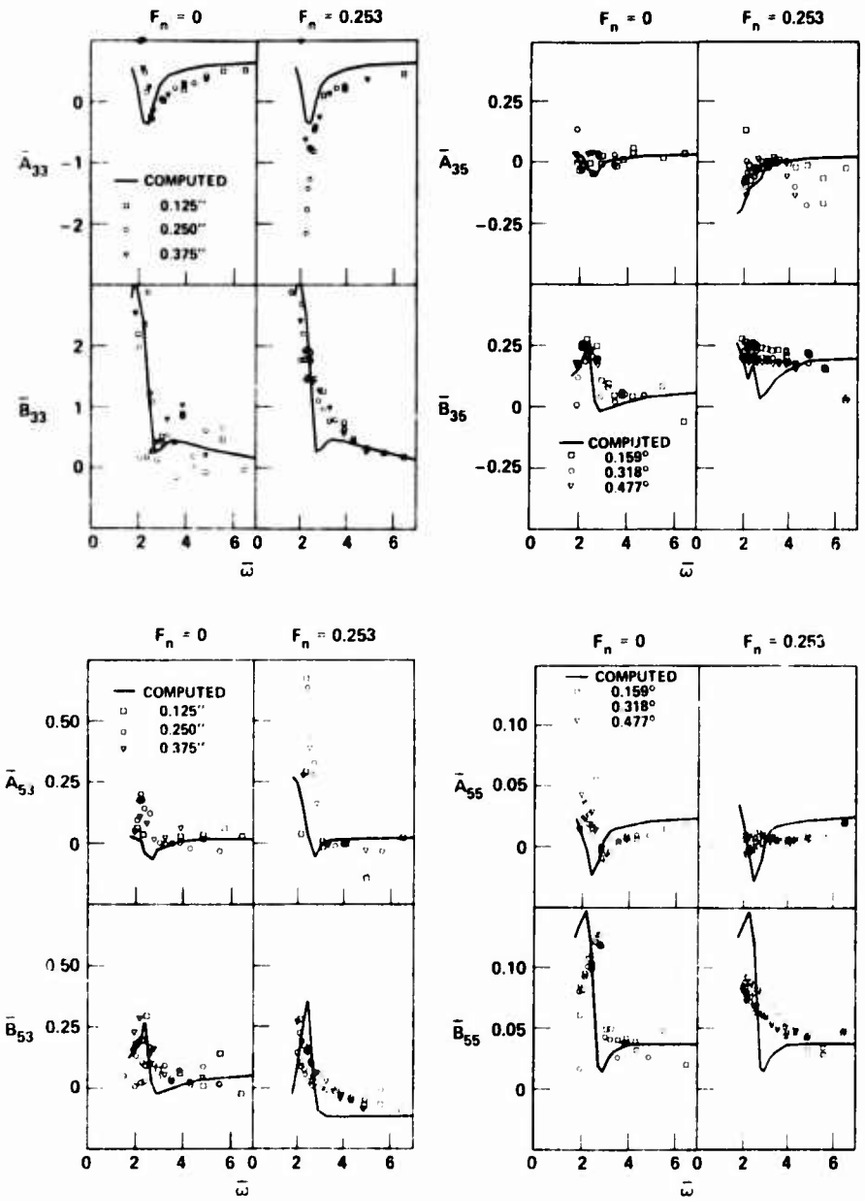


Figure 4 Added mass and damping coefficients of Model 5061

TABLE 2 – Particular Dimensions

NSRDC Model Number	5182	5061	5266
Beam (Each Hull) in Feet at the Waterline	38.0	24.0	30.42
Draft in Feet (Station 10)	17.0	18.0	69.5
Length in Feet at the Waterline	550.0	210.0	850.0
Displacement of Each Hull in Long Tons	14,000 (S.W.)*	1386 (S.W.)	50,500 (S.W.)
Hull Spacing in Feet**	30.0	38.0	207
Longitudinal Center of Gravity Aft of F. P. in Feet	285.3	105.6	420
Longitudinal Radius of Gyration in Feet	0.24L	0.233L	0.26L
Block Coefficient	0.72	0.55	0.964
Scale Ratio	24.78	16.89	50.0
Diameter in Feet	–	–	–

*Salt Water
**Between the inner hulls

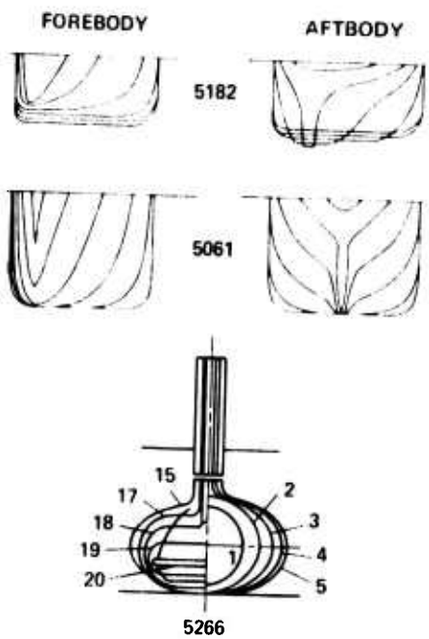


Figure 5 Body plans

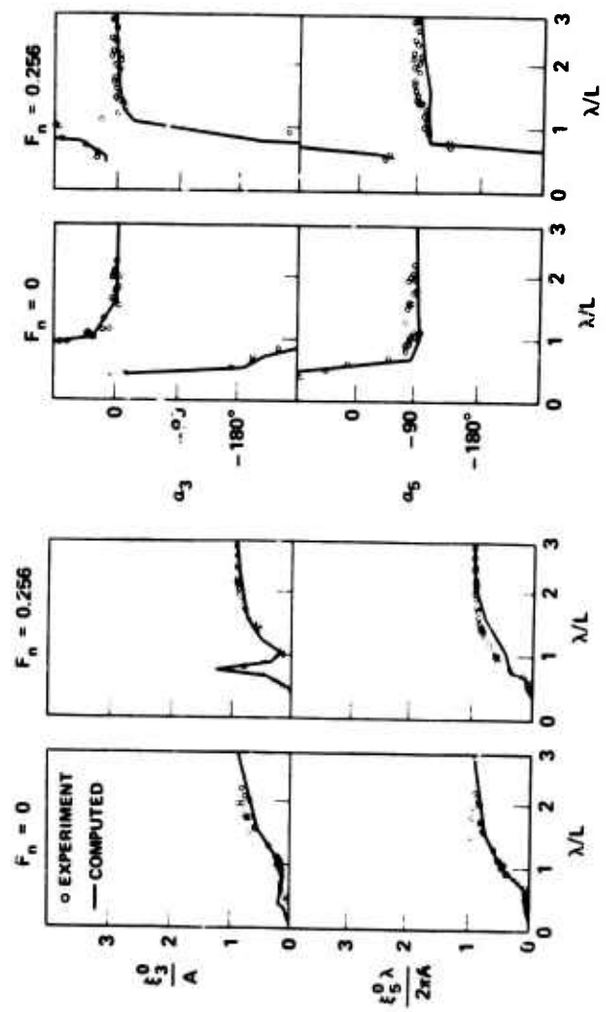


Figure 6 Heave and pitch motions of Model 5182

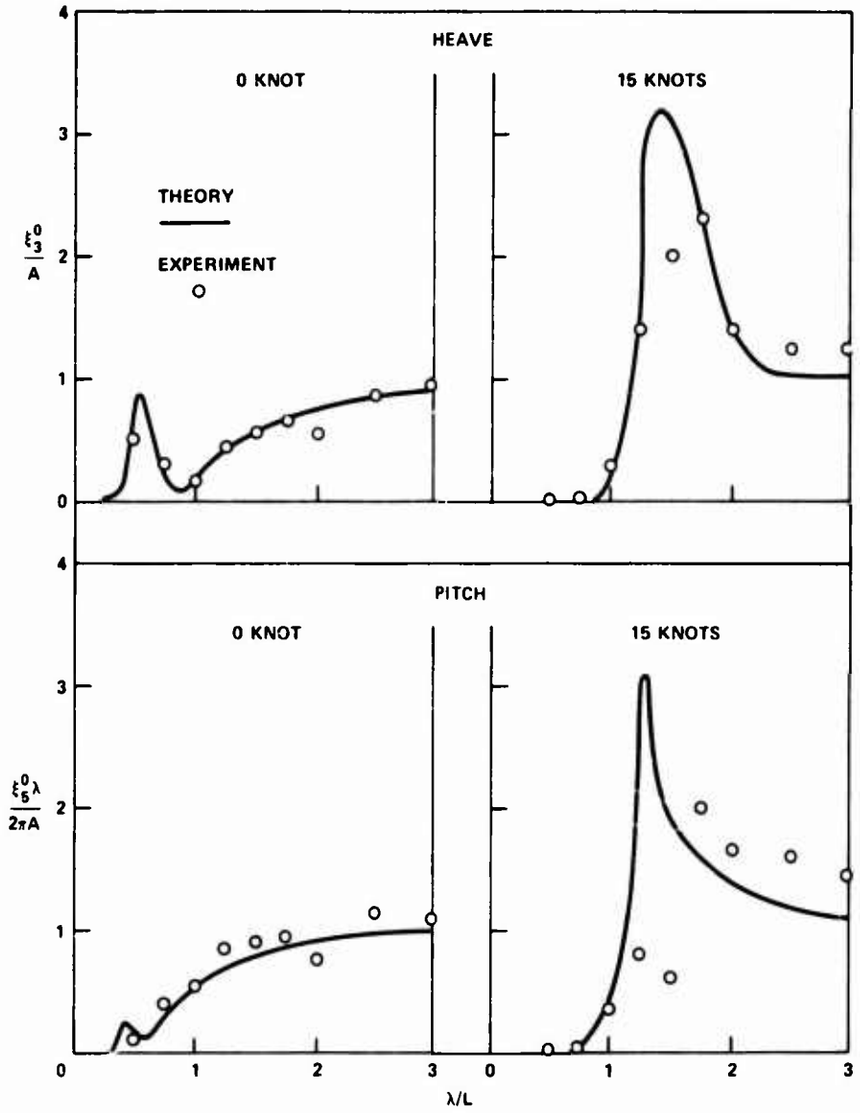


Figure 7 Heave and pitch motions of Model 5061

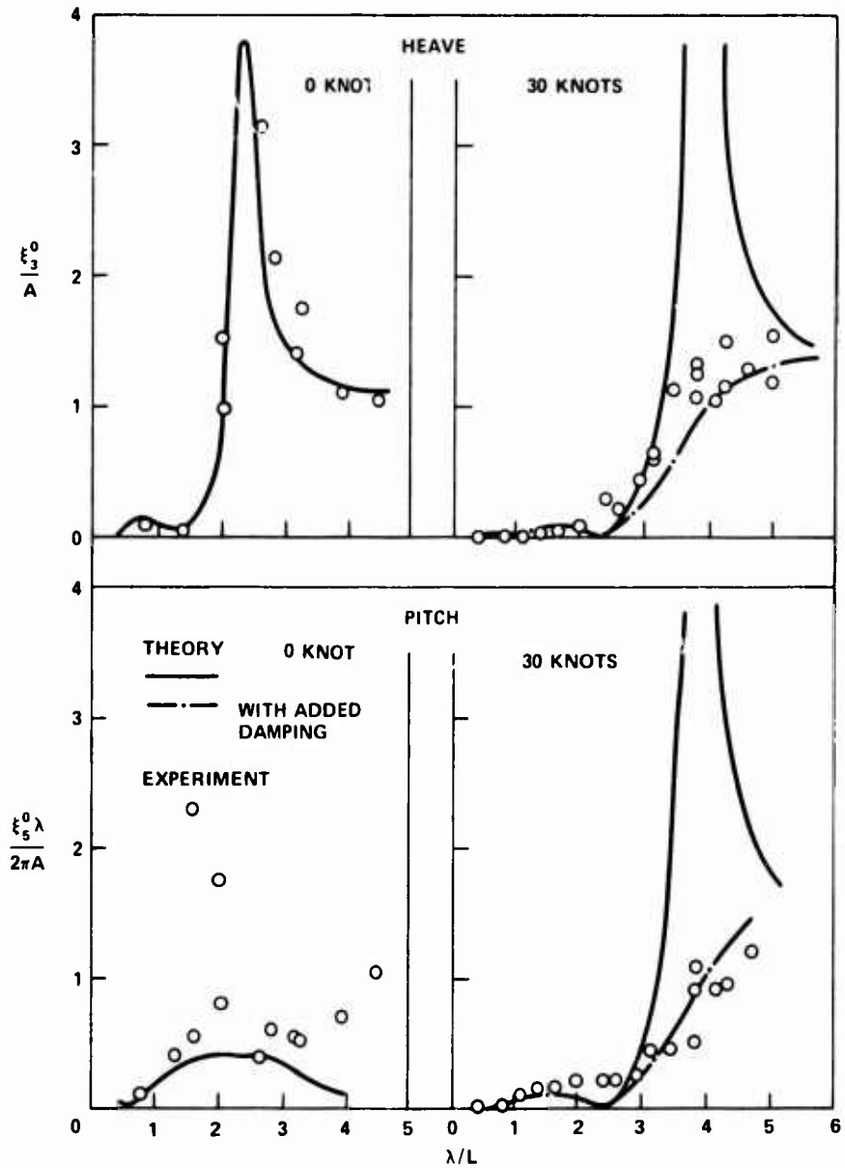


Figure 8 Heave and pitch motions of Model 5266

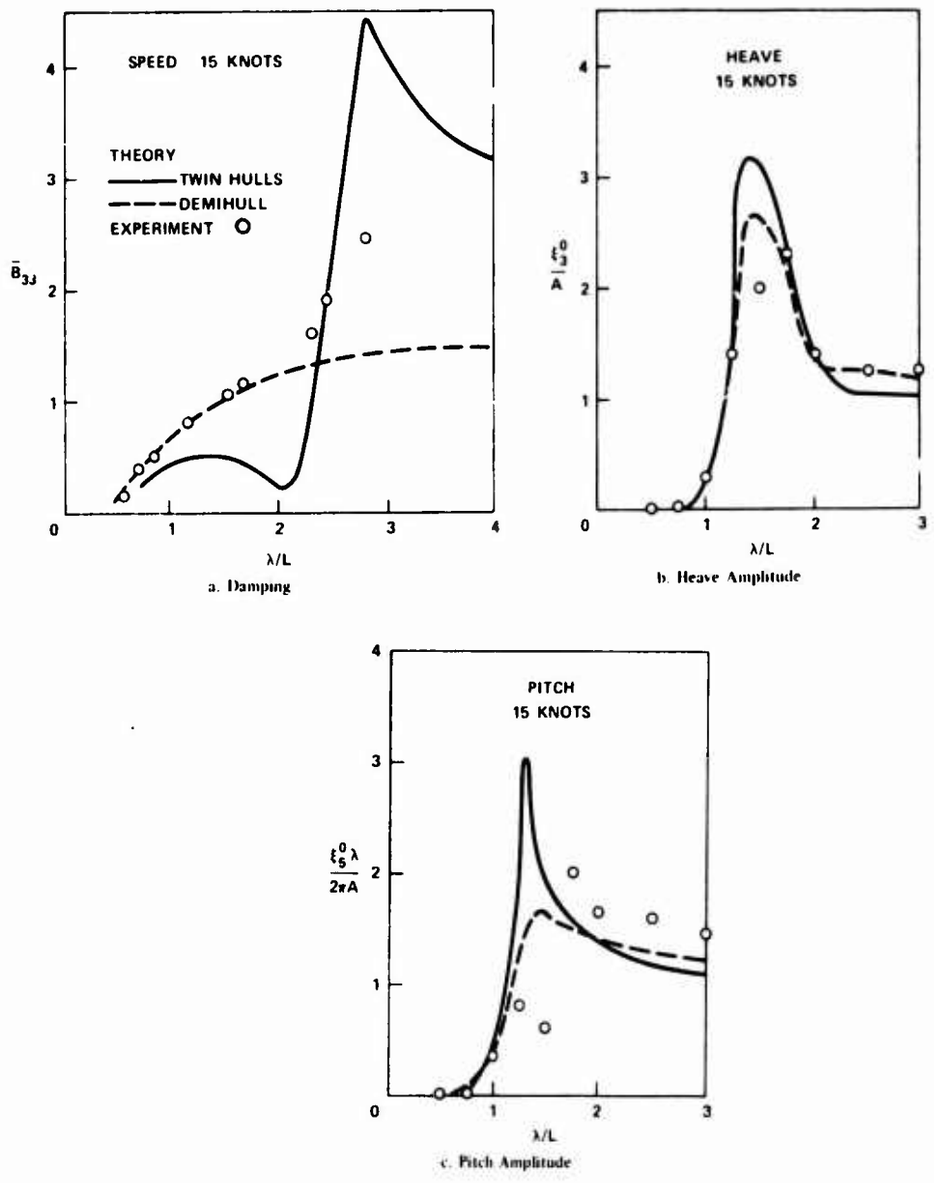


Figure 9 Comparison between twin hulls and demihull of Model 5061

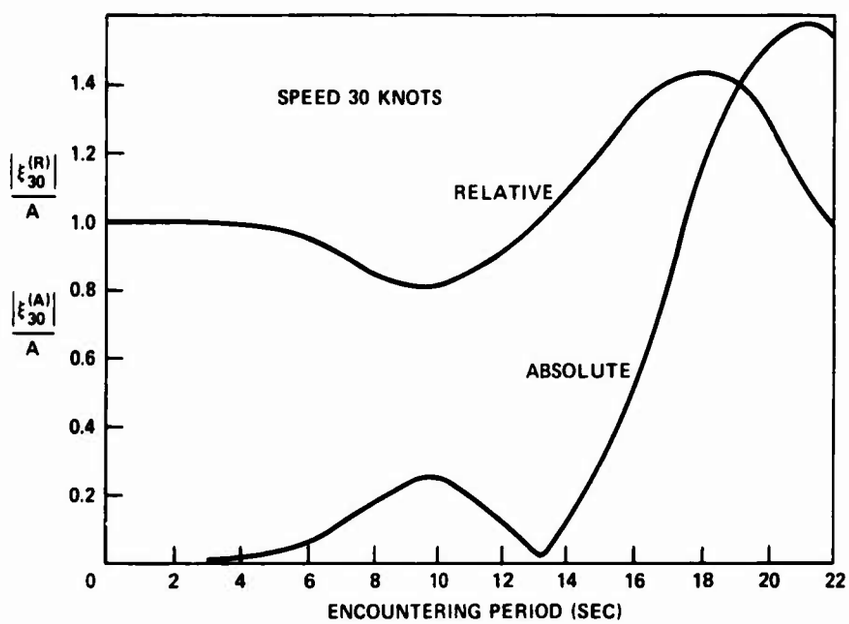


Figure 10 Absolute and relative vertical motion of the front edge of cross-deck of Model 5266

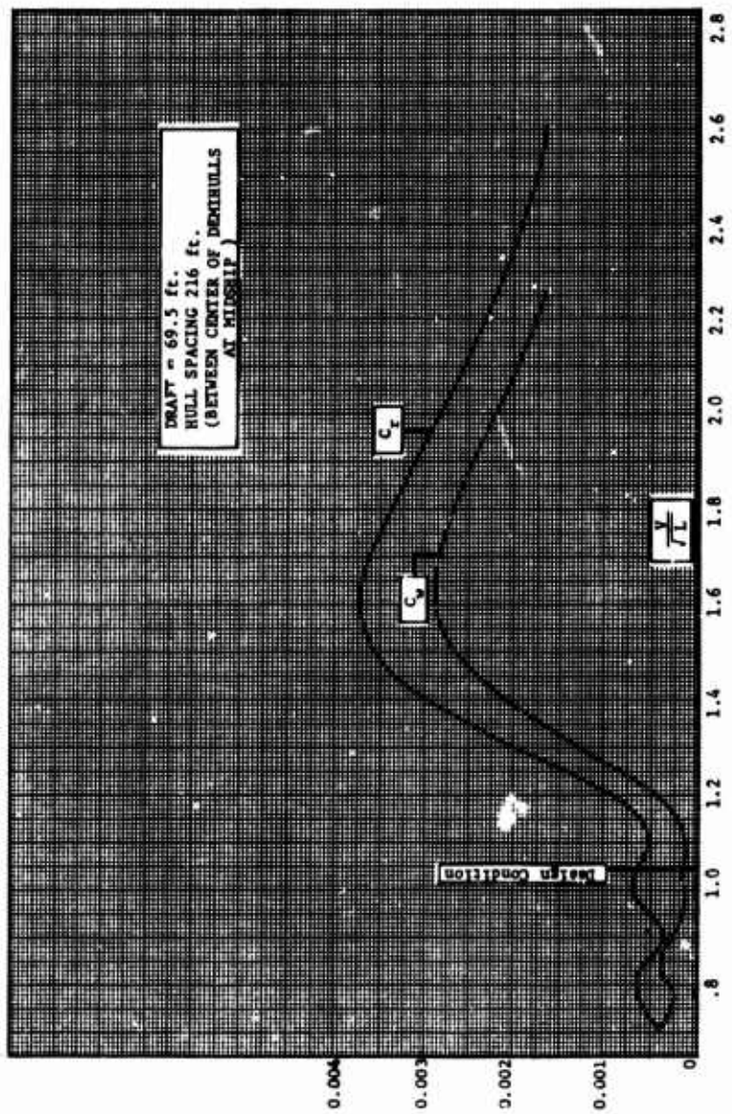


Figure 11 Catamaran C_w and C_r curves for Model 5266

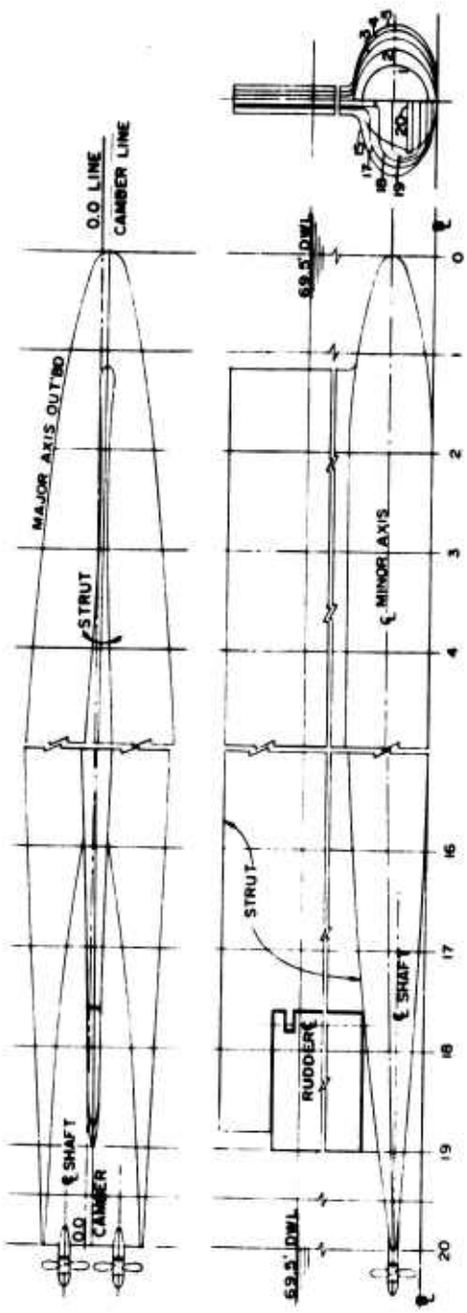


Figure 12 Abbreviated lines and body plan for LWP catamaran represented by Model 5266

APPENDAGES: None

	DIMENSIONS* SHIP	MODEL			LOA COEFFICIENTS*	
Length (LOA) FT	850	17.0	C_B	0.616	C_{WF}	0.82
Length (LBP) FT	—	—	C_P	0.776	C_{WA}	0.88
Beam (B_{IX}) FT	70	1.4	C_X	0.794	L_E/L	0.50
Draft (H) FT	38	0.76	C_W	0.846	L_P/L	0.0
Displ.in Tons	39790S.W.	0.310F.W.	C_{PF}	0.80	L_R/L	0.50
Wetted Surf.Sq Ft	117097	46.84	C_{PA}	0.75	L/B_{IX}	12.14
Design V in Kts	30	4.24	C_{PE}	0.80	B_{IX}/H	1.84
LCB_{LOA} 0.491	.ft of F. End		C_{PR}	0.75	$\Delta/(0IL)^3$	64.79
LCF_{LOA} 0.517	Aft of F. End		C_{PV}	0.73	$S/\sqrt{\Delta L}$	20.13
λ = 50.0	$V/\sqrt{L_{EFF}}$ = 1.040		C_{PVA}	0.68		
Ⓚ = 2.995	Ⓟ = 0.872		C_{PVF}	0.78		

LINES: NSRDC Shop Plans, Model 5266

*NOTE: The coefficients and dimensions presented above are for that portion of a single hull that is below the 38 ft waterline. This draft corresponds to the total height (minor axis) of the largest elliptical body section. The total full-scale displacement, wetted surface, and draft, for a single hull, are 50,500 tons S.W., 164,780 sq ft, and 69.5 ft, respectively. That portion of the full-scale hull above the 38 ft waterline (strut) has a waterline length (LWL) of 757.5 ft, a beam (B_X) of 30.4 ft, and a waterplane coefficient (C_W) of 0.515.

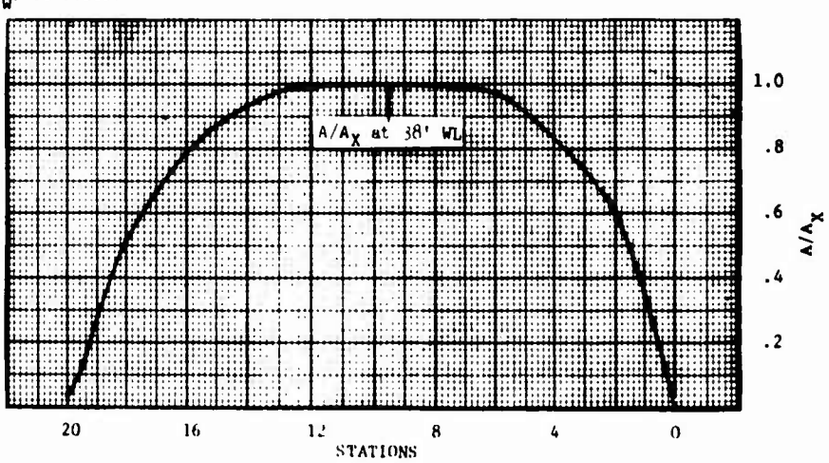


Figure 13 Ship and model data for a LWP catamaran represented by Model 5266

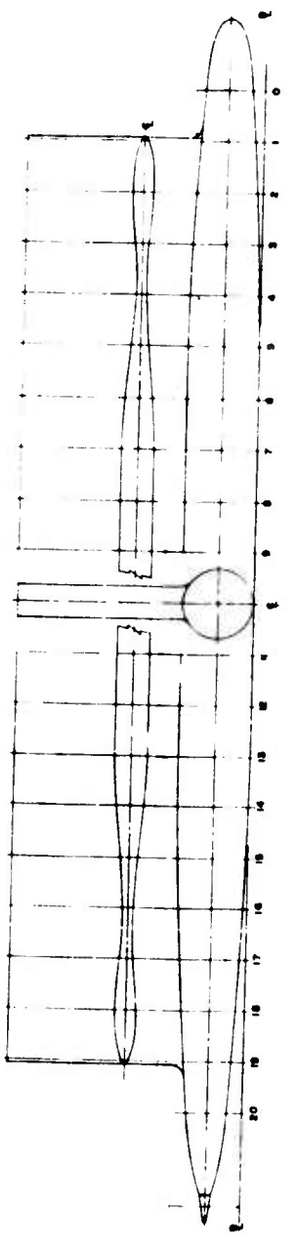


Figure 14 Profile and strut section for an LWP catamaran demihull represented by Model 5276

PHOTOGRAPH LAY-UP SHEET NSRDC-1070B/1e (6140)

SHIP AND MODEL DATA
FOR
A LWP CATAMARAN REPRESENTED BY

MODEL 5276

APPENDAGES: NONE

DIMENSIONS *	SHIP	MODEL
LENGTH (LOA) FT	287	14.07
LENGTH (LBP) FT		
BEAM (B_X) FT	17.3	0.85
DRAFT (H) FT	17.3	0.85
DISPL IN TONS	1486 S.W.	0.170 W
WETTED SURF SQ FT	12481	29.99
DESIGN V IN KTS	32	7.08
LCB_{LOA} = 0.479	AFT OF F. End	
LCF_{LOA} = 0.486	AFT OF F. End	
WL ENTRANCE HALF ANGLE :		
λ = 20.4	$V/\sqrt{L_{EFF}}$ = 1.962	
(K) = 5.525	(P) = 1.619	
LINES		

LOA COEFFICIENTS *	
C_B 0.602	C_{WF} 0.88
C_P 0.758	C_{WA} 0.81
C_X 0.795	L_E/L 0.36
C_W 0.847	L_P/L 0.22
C_{PF} 0.80	L_R/L 0.42
C_{PA} 0.71	L/B_X 16.55
C_{PE} 0.73	B_X/H 1.0
C_{PR} 0.66	$\Delta/(0IL)^3$ 62.9
C_{PV} 0.71	$S/\sqrt{\Delta L}$ 19.12
C_{PVA} 0.72	f
C_{PVF} 0.73	t
LBP COEFFICIENTS	
C_B	L/B_X
C_P	$\Delta/(0IL)^3$

*NOTE: 1, The coefficients and dimensions presented above are for that portion of a single hull that is below the 17.3 ft waterline. This draft corresponds to the total height at the top of the body of revolution. The total full-scale displacement, wetted surface, and draft, for a single hull, are 2026 tons S.W., 19197 sq. ft., and 32 ft., respectively. That portion of the full-scale hull above the 17.3 ft. waterline (strut) has a waterline length (LWL) of 226.5 ft., a beam (B_X) of 8.0 ft., and a water plane coefficient (C_W) of 0.709.

2, Sectional area curve same as Model 5266

For detail see Figure 2-3

Figure 15 Ship and model data for a LWP catamaran represented by Model 5276

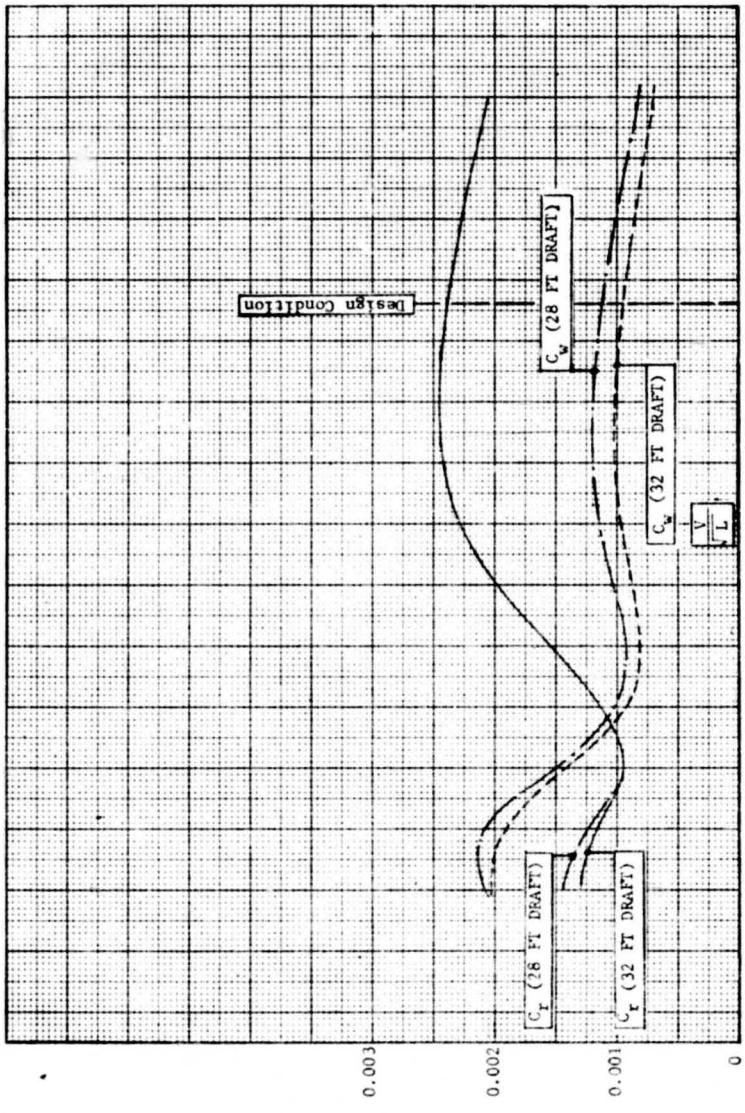


Figure 16 C_w and C_r curves for Model 5276 tested as a single hull

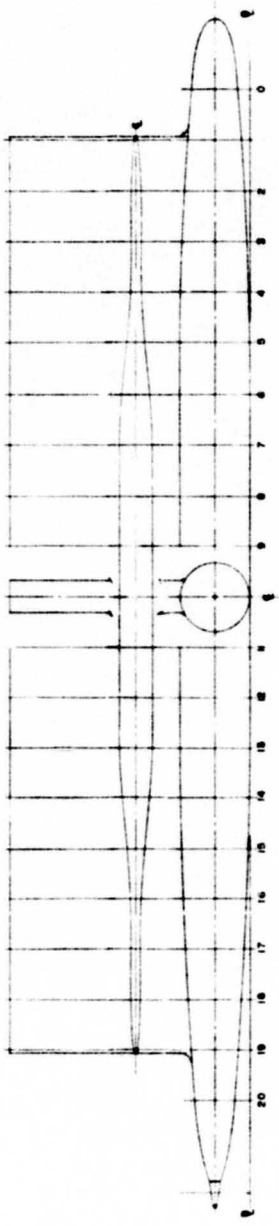


Figure 17 Profile and strut section for a single hull, Model 5276-C

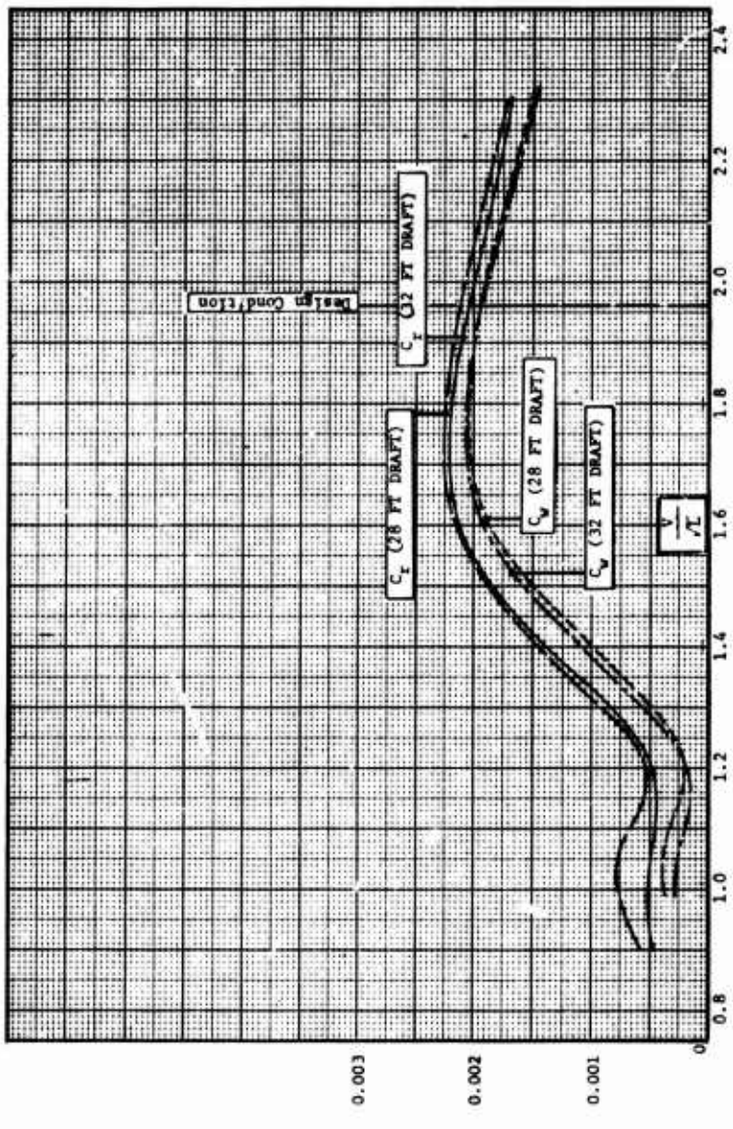


Figure 18 C_w and C_r curves for Model 5276-C tested as a single hull

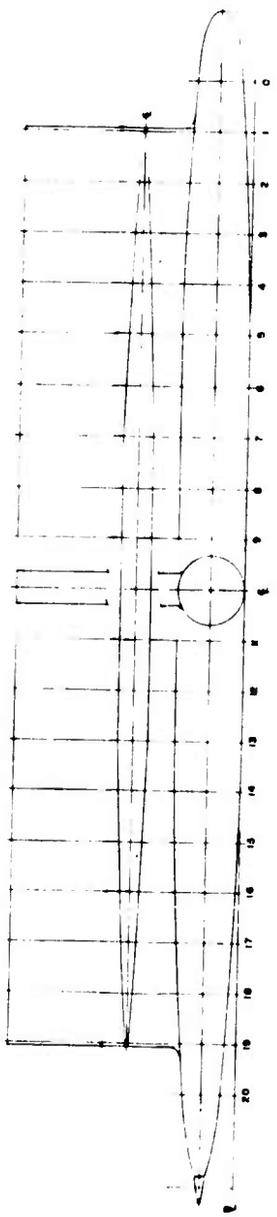


Figure 19 Profile and strut section for a single hull, Model 5276-E

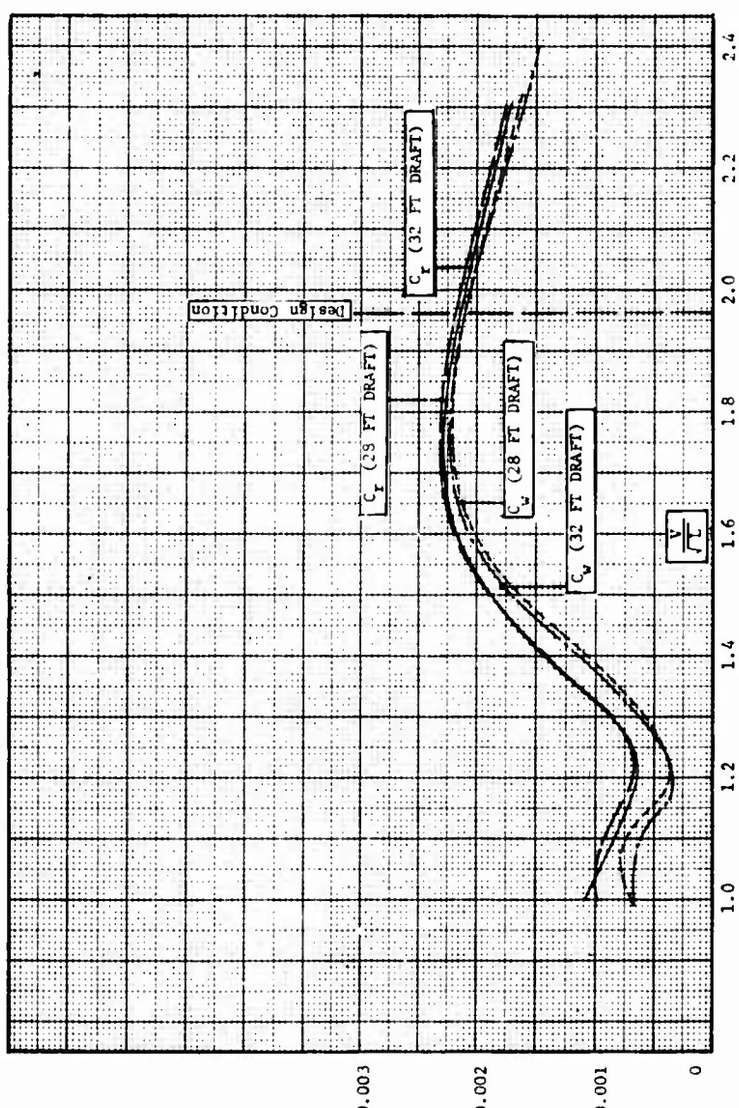


Figure 20 C_w and C_r curves for Model 5276-E tested as a single hull

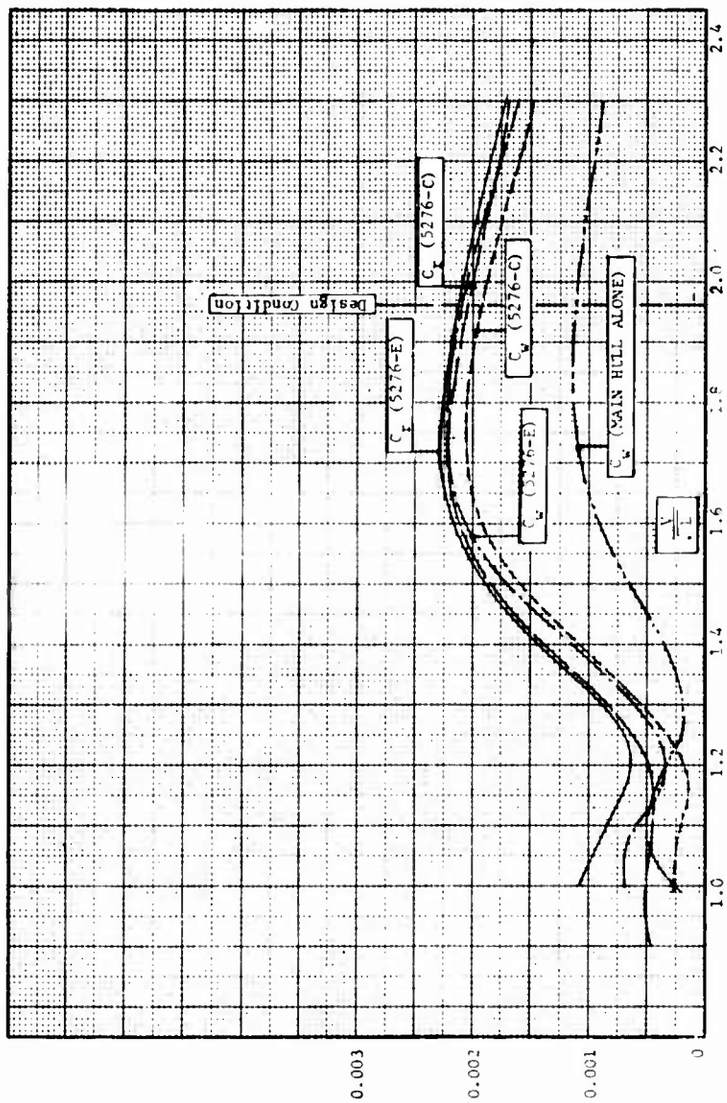


Figure 21 Comparisons of C_W and C_F curves between Model 5276-C, Model 5276-E and a main hull at 32-ft draft

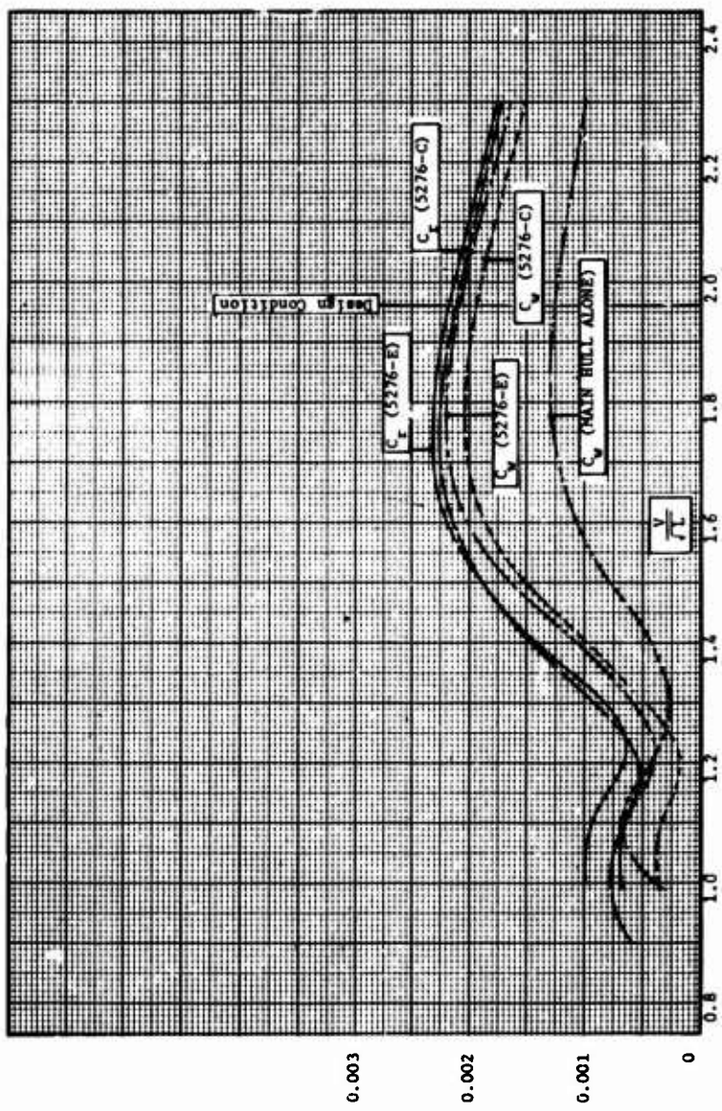


Figure 22 Comparisons of C_W and C_F curves between Model 5276-C, Model 5276-E and a main hull at 28-ft draft

APPENDIX A - DETERMINATION OF HYDRODYNAMIC COEFFICIENTS.

If we assume that the fluid surrounding a catamaran has irrotational motion, we can introduce a velocity potential $\Phi(x, y, z, t)$ in the fluid region. The velocity potential should satisfy, in addition to the Laplace equation, the following boundary conditions

$$\left(\frac{\partial}{\partial t} - U\frac{\partial}{\partial x}\right)^2 \Phi(x, y, z, t) + g\,\Phi_z = 0 \qquad \text{on } z = 0 \tag{57}$$

where g is the gravitational acceleration,

$$\nabla\Phi \cdot \underline{n} = V_n \qquad \text{on } S_o \tag{58}$$

where $\underline{n}$ is the unit normal vector on the body surface pointing into the body, V_n is the normal component of the velocity of the body surface, and S_o is the mean position of the body,

$$\Phi_z(x, y, -\infty, t) = 0 \tag{59}$$

and a physically appropriate far-field condition for $(x^2 + y^2)^{\frac{1}{2}} \longrightarrow \infty$ to make the problem well posed.

Assuming the flow disturbance to be a small perturbation from uniform flow, we can express Φ in the form

$$\Phi = -Ux + \phi_s(x, y, z) + \phi_o(x, y, z)\, e^{-j\omega t} \tag{60}$$

where U is the forward velocity of the ship; ϕ_s is the steady potential, representing the wavemaking disturbance due to the forward velocity; and $\phi_o = \phi_{oc} + j\,\phi_{os}$ is the potential associated with the oscillatory fluid disturbance. We can further divide ϕ_o into three distinct origins of the oscillatory fluid disturbance as

$$\phi_o = \phi_I + \phi_D + \phi_M \tag{61}$$

The incoming wave potential, ϕ_I is given by

$$\phi_I = \frac{Ag}{\omega_o}\, e^{K_o(z + j\,x\cos\beta - j\,y\sin\beta)} \tag{62}$$

where β is the wave-heading angle with respect to the positive

x-axis, ω_o is the wave frequency, K_o is the wave number given by ω_o^2 / g, and A is the wave amplitude. The wave diffraction is represented by Φ_D and the fluid disturbance caused by the motion of the body in initially calm water is represented by Φ_M . Within a linear approximation to the solution of the velocity potential Φ_M we can let

$$\Phi_M = \sum_{k=2}^{6} \xi_{ko} \Phi_k \tag{63}$$

where Φ_k is another set of velocity potentials, and $\xi_{ko}, k = 2, \ldots, 6$ are the complex amplitudes of the displacement of the body from its mean position in sway, heave, roll, pitch, and yaw modes, respectively. The pressure at any point of the hull is obtained from Bernoulli's equation by

$$p = \frac{\rho}{2} U^2 - \rho(\Phi_t + g\, z(t) + \frac{1}{2} | \nabla \Phi |^2) \tag{64}$$

At this point, we will establish the following conditions : (1) the motion of the body is small, so that the pressure at a point on the body surface at any instant can be obtained via Taylor's expansion of the pressure at the mean position of the body; (2) the terms of Φ (Φ_s^2 , $\Phi_s \Phi_o$, Φ_o^2 , $\xi_{ko} \Phi_s$, $\xi_{ko} \Phi_D$, ξ_{ko}) will be discarded in the evaluation of the pressure; (3) only those components of the pressure which have harmonic time dependence will be considered, and (4) the static-pressure component and the component which contributes to the static restoring force or moment of the body will not be included in evaluation of the pressure.[6]

With the foregoing conditions, the complex amplitude of the pressure at a point on the body surface can be expressed by

$$\begin{aligned} p &= \rho (j\omega + U \frac{\partial}{\partial x}) \Phi_o \\ \rho &= (j\omega + U \frac{\partial}{\partial x}) (\Phi_I + \Phi_D + \sum_{k=2}^{6} \xi_{ko} \Phi_k) \end{aligned} \tag{65}$$

evaluated at the mean position of the body.

---

[6] These conditions are also applied to monohull ships by Salvesen, Tuck and Faltinsen (1970).

Integration of the pressure over the wetted surface of a catamaran should yield the hydrodynamic forces and moments. Thus, we have

$$F_i^{(H)} = \iint_{S_o} p\, n_i\, ds$$

$$= \rho \iint_{S_o} n_i \left(j\omega + U\frac{\partial}{\partial x}\right)(\phi_I + \phi_D + \sum_{k=2}^{6} \xi_{ko}\, \phi_k)\, ds$$

for $i = 2, 3, \ldots, 6$, where n_2 and n_3 are respectively the y and z components of the unit normal vector and $n_4 = yn_3 - zn_2$, $n_5 = -xn_3$, $n_6 = xn_2$.

We can further decompose the hydrodynamic force into two parts i.e.

$$F_i^{(H)} = F_i^{(e)} + F_i^{(m)}$$

where

$$F_i^{(e)} = \text{wave-excited force}$$

$$= \rho \iint_{S_o} n_i \left(j\omega + U\frac{\partial}{\partial x}\right)(\phi_I + \phi_D)\, ds \qquad (66)$$

and

$$F_i^{(m)} = \text{motion-excited force}$$

$$= \rho \sum_{k=2}^{6} \xi_{ko} \iint_{S_o} n_i \left(j\omega + U\frac{\partial}{\partial x}\right) \phi_k\, ds \qquad (67)$$

Applying the results of Ogilvie and Tuck (1969) to the simplified case in this work, we can show for any differentiable scalar function ϕ with the usage of Kronecker's delta function that

$$\iint_S n_i \phi_x\, ds = \iint_S (n_3\ \delta_{i5} - n_2\ \delta_{i6})\phi\, ds - \iint_{C(x)} n_i\ \phi\, d\ell \qquad (68)$$

where S is the immersed hull surface forward of the cross section at x, and c(x) is the line integral along the contour of the cross section. Utilization of Equation (68) in Equation (66) yields

$$F_i^{(e)} = \rho \iint_{So} n_i \left(j\omega + U\frac{\partial}{\partial x}\right)(\phi_I + \phi_D)\, ds$$

$$= \rho \iint_{So} j\, n_i \left(\omega + U K_o \cos\beta\right) \phi_I\, ds$$

$$+ \rho \iint_{So} (j\omega\, n_i + U n_3\, \delta_{i5} - U n_2\, \delta_{i6})\, \phi_D\, ds \qquad (69)$$

where the line integral at the stern section is neglected.

Within the accuracy of the order of approximation in this work and together with a slenderness assumption of each hull of the catamaran, we can derive from Equation (58) and (61) that

$$\phi_{Mn} = -j\omega\ (\underline{\xi}_o + \underline{\alpha}_o \times \underline{\Lambda}) \cdot \underline{n} - U(\underline{\alpha}_o \times \underline{e}_1) \cdot \underline{n} \quad \text{on } S_o \qquad (70)$$

where

$$\underline{\xi}_o = (\xi_{10}, \xi_{20}, \xi_{30})$$

$$\underline{\alpha}_o = (\xi_{40}, \xi_{50}, \xi_{60})$$

$$\underline{\Lambda} = (x, y, z)$$

and $\underline{e}_1$ is the unit vector in the x direction. Substitution of Equation (63) into Equation (70) yields

$$\phi_{in} = -j\omega\ n_i + U n_3\ \delta_{i5} - U n_2\ \delta_{i6} \qquad (71)$$

on S_o for $i = 2, 3, \ldots, 6$,

Using Equation (71) and the relation

$$\omega + U K_o \cos\beta = \omega_o$$

in Equation (69), we get

$$F_i^{(e)} = j\rho\omega_o \iint_{S_o} n_i \Phi_I \, ds$$

$$- \rho \iint_{S_o} (\Phi_{in} + \frac{2U}{j\omega} \Phi_{3n} \delta_{i5} - \frac{2U}{j\omega} \Phi_{2n} \delta_{i6}) \Phi_D \, ds$$

Since

$$\iint_{S_o} \Phi_{in} \Phi_D \, ds = \iint_{S_o} \Phi_{Dn} \Phi_i \, ds$$

by Green's theorem and

$$\Phi_{In} = - \Phi_{Dn} \qquad \text{on } S_o$$

from the kinematic boundary condition, we can show that

$$F_i^{(e)} = \rho \iint_{S_o} \left\{ j\omega_o n_i + (\Phi_i + \frac{2U}{j\omega} \Phi_3 \delta_{i5} - \frac{2U}{j\omega} \Phi_2 \delta_{i6}) \frac{\partial}{\partial n} \right\} \Phi_I \, ds \tag{72}$$

The above procedure for eliminating the diffraction potential Φ_D from the expression for the wave-exciting force and moment was first shown by Haskind (1957) for zero speed and later it was extended by Newman (1965) for the case of forward speeds and is referred to as the Haskind-Newman relation.

Similarly, we can derive

$$F_i^{(m)} = \rho \sum_{k=2}^{6} \xi_{ko} \iint_{S_o} (j\omega n_i + Un_3 \delta_{i5} - Un_2 \delta_{i6}) \Phi_k \, ds \tag{73}$$

$$= - \rho \sum_{k=2}^{6} \xi_{ko} \iint_{S_o} (\Phi_{in} + \frac{2U}{j\omega} \Phi_{3n} \delta_{i5} - \frac{2U}{j\omega} \Phi_{2n} \delta_{i6}) \Phi_k \, ds$$

If we express $F_i^{(m)}$ in the form

$$F_i^{(m)} = \sum_{k=2}^{6} \xi_{ko} (\omega^2 A_{ik} + j\omega B_{ik})$$

where A_{ik} are the so-called added mass quantities, and B_{jk} are the damping quantities, we find from Equation (73) that

$$A_{ik} = \mathrm{Re}_j \left\{ - \frac{\rho}{\omega^2} \iint_{S_o} (\Phi_{in} + \frac{2U}{j\omega} \Phi_{3n} \delta_{i5} - \frac{2U}{j\omega} \Phi_{2n} \delta_{i6}) \Phi_k \, ds \right\} \tag{74}$$

$$B_{ik} = \mathrm{Im}_j \left\{ -\frac{\rho}{\omega} \iint_{S_o} \left(\Phi_{in} + \frac{2U}{j\omega} \Phi_{3n} \delta_{i5} - \frac{2U}{j\omega} \Phi_{2n} \delta_{i6} \right) \Phi_k \, ds \right\} \quad (75)$$

Using Newton's second law, we can show that the equations of motion can be expressed in the form

$$-\omega^2 \sum_{k=2}^{6} M_{ik} \xi_{ko} = F_i^{(e)} + F_i^{(m)} + F_{ik}^{(s)} \quad (76)$$

where

$$M_{ik} = \begin{bmatrix} M & 0 & -Mz_g & 0 & 0 \\ 0 & M & 0 & 0 & 0 \\ -Mz_g & 0 & I_4 & 0 & 0 \\ 0 & 0 & 0 & I_5 & 0 \\ 0 & 0 & 0 & 0 & I_6 \end{bmatrix}$$

z_g is the z-coordinate of the center of mass, and

$F_{ik}^{(s)}$ = Hydrostatic restoring force

$$= \begin{bmatrix} 0 & 0 & 0 & 0 & 0 \\ 0 & -C_{33} & 0 & -C_{35} & 0 \\ 0 & 0 & -C_{44} & 0 & 0 \\ 0 & -C_{53} & 0 & 0 & -C_{55} \\ 0 & 0 & 0 & 0 & 0 \end{bmatrix}$$

Thus, the equations reduce to the algebraic equation :

$$\sum_{k=2}^{6} \left\{ -\omega^2 (M_{ik} + A_{ik}) - j\omega B_{ik} + C_{ik} \right\} \xi_{ko} = F_i^{(e)} \quad (77)$$

where A_{ik} , B_{ik} and $F_i^{(e)}$ are frequency and speed dependent.

For slender catamarans we can assume that no coupling exists between the motions on the horizontal and vertical planes so that

$$A_{ik} = B_{ik} = 0$$

for the following combinations of i and k

$$i = 2, 4, 6 \qquad \text{for } k = 3, 5$$

or

$$i = 3, 5 \qquad \text{for } k = 2, 4, 6$$

As has been seen previously, the hydrodynamic coefficients appearing in the equations of motion can be obtained, if the solution of the velocity potentials Φ_i (i = 2, . . . , 6) are known. In the solution of Φ_i , the flow around each transverse section is assumed to be two-dimensional, and, thus, the variable x enters as a parameter in the expressions for Φ_i . A correct mathematical development to lead to such an approximation from the slender-body theory is given by Ogilvie and Tuck (1969), and a comprehensive review of this approximation is given in Newman (1970).

Approximation of three-dimensional flow by two-dimensional flow as described previously is often called the strip approximation. The strip approximation of the hydrodynamic coefficients has been quite successful in the prediction of motions of monohull ships. Regardless of the possibility that the two-body interference of the flow between the hulls may weaken the two-dimensional approximation, the strip approximation is applied in this work to check both the reliability of the approximation and the areas which might be improved should the approximation prove unreliable.

The assumption of linear excitation-response relationship and the strip approximation lead finally to determination of the hydrodynamic coefficients shown in Table 1. The solution of two-dimensional added inertia and damping is obtained by using the method of source distribution. The description of the method for heave added mass and damping is given in Lee, Jones, and Bedel (1971).

For illustration, the derivation of A_{53} , B_{53} and B_{26} will be shown here. From Equation (74) and the strip approximation, we have

$$A_{53} = -\frac{\rho}{\omega^2} \mathrm{Re}_j \int_L dx \int_{C(x)} \left(\Phi_{5n} + \frac{2U}{j\omega} \Phi_{3n}\right) \Phi_3 \, d\ell$$

where $\int_L$ means an integral over the length of the body from the aft to the fore perpendicular. From Equation (71) we have

$$\Phi_{5n} = -j\omega n_5 + U n_3 = j\omega n_3 \left(x + \frac{U}{j\omega}\right) = -\left(x + \frac{U}{j\omega}\right) \Phi_{3n}$$

Thus,

$$\begin{aligned} A_{53} &= -\frac{\rho}{\omega^2} \mathrm{Re}_j \int_L dx \int_{C(x)} \left(-x + \frac{U}{j\omega}\right) \Phi_{3n} \Phi_3 \, d\ell \\ &= -\int_L x \, dx \left\{-\frac{\rho}{\omega^2} \mathrm{Re}_j \int_{C(x)} \Phi_3 \Phi_{3n} \, d\ell \right\} \\ &\quad + \frac{U}{\omega^2} \left\{-\frac{\rho}{\omega} \mathrm{Im}_j \int_L dx \int_{C(x)} \Phi_3 \Phi_{3n} \, d\ell \right. \\ &= -\int_L x \, a_{33}(x) \, dx + \frac{U}{\omega^2} B_{33} \end{aligned}$$

where

$$a_{33}(x) = -\frac{\rho}{\omega^2} \mathrm{Re}_j \int_{C(x)} \Phi_3 \Phi_{3n} \, d\ell$$

Similarly, we can show, using Equation (75), that

$$\begin{aligned} B_{53} &= -\frac{\rho}{\omega} \mathrm{Im}_j \int_L dx \int_{C(x)} \left(\Phi_{5n} + \frac{2U}{j\omega} \Phi_{3n}\right) \Phi_3 \, d\ell \\ &= -\frac{\rho}{\omega} \mathrm{Im}_j \int_L dx \int_{C(x)} \left(-x + \frac{U}{j\omega}\right) \Phi_{3n} \Phi_3 \, d\ell \\ &= -\int_L x \, b_{33}(x) \, dx - U \left\{-\frac{\rho}{\omega^2} \mathrm{Re}_j \int_L dx \int_{C(x)} \Phi_3 \Phi_{3n} \, d\ell \right\} \\ &= -\int_L x \, b_{33}(x) \, dx - U A_{33} \end{aligned}$$

where

$$b_{33}(x) = -\frac{\rho}{\omega} \mathrm{Im}_j \int_{C(x)} \Phi_3 \Phi_{3n} \, d\ell$$

From Equation (75) we have

$$B_{26} = -\frac{\rho}{\omega} \mathrm{Im}_j \int_L dx \int_{C(x)} \phi_{2n} \phi_6 \, d\ell$$

Since by inspection we can deduce of Equation (71) that

$$\phi_6 = (x + \frac{U}{j\omega}) \phi_2$$

we can show that

$$B_{26} = \int_L dx \left\{ -\frac{\rho}{\omega} \mathrm{Im}_j \int_{C(x)} \phi_2 \phi_{2n} \, d\ell - U \left\{ -\frac{\rho}{\omega^2} \mathrm{Re}_j \int_L dx \int_{C(x)} \phi_2 \phi_{2n} \, d\ell \right\} \right.$$

$$= \int_L x \, b_{22}(x) \, dx - U A_{22}$$

APPENDIX B - SOLUTION OF DIFFRACTION POTENTIAL

In the following, the solution of the diffraction potential ϕ_D will be obtained in the Oyz plane.

The boundary-value problem for ϕ_D is described as

$$\left(\frac{\partial^2}{\partial y^2} + \frac{\partial^2}{\partial z^2} \right) \phi_D(y, z) = 0$$

$$\phi_{Dz}(y, 0) - K_o \phi_D = 0 \tag{78}$$

where

$$K = \omega^2 / g$$

$$\phi_{Dn}\Big|_{c_o} = -\phi_{In}\Big|_{c_o} \tag{79}$$

where c_o is the contour of the immersed portion of a catamaran cross section located at x, and the incoming wave potential ϕ_I is given by

$$\phi_I = \frac{Ag}{\omega_o} e^{jK_o x \cos\beta} e^{K_o (z - jy \sin\beta)} \tag{80}$$

where

$$K_o = \omega_o^2 / g$$

Since the variable x enters into this problem as a parameter, we take $e^{jk_o x \cos\beta}$ as a constant term and let it be denoted by c.

$$\phi_{Dz}(y, -\infty) = 0$$

$$\phi_D \sim B e^{Kz + jK_o|y|} \quad \text{as} \quad |y| \to \infty \tag{81}$$

where B is a constant.

Substituting Equation (80) into Equation (79), we obtain

$$\phi_{Dn}\Big|_{c_o} = -\omega_o AC(-j n_2 \sin\beta + n_3) e^{K_o(z - jy\sin\beta)} \tag{82}$$

where n_2 and n_3 are the y and z components of the unit normal vector on c_o. For brevity, we let

$$y' = y \sin\beta$$

$$n_2' = -n_2 \sin\beta$$

$$A' = -\omega_o AC$$

We have from Equation (82)

$$\phi_{Dn}\Big|_{c_o} = A' e^{K_o z}(n_3 \cos K_o y' - n_2' \sin K_o y') - jA' e^{K_o z}(n_2' \cos K_o y' + n_3 \sin K_o y') \tag{83}$$

Since we assume that catamarans are made of two symmetrical hulls, we know that n_2 is odd, and n_3 is even, with respect to y. Then, it is clear that the real part of the right side of Equation (83) is an even function, and the imaginary part is an odd function. Now, we let

$$\phi_D = \phi_e + \phi_o$$

where Φ_e and Φ_o are even and odd functions in y, respectively, and satisfy the following body boundary conditions

$$\Phi_{en}\Big|_{c_o} = A' e^{K_o z}(n_3 \cos K_o y' - n_2' \sin K_o y') \qquad (84)$$

$$\Phi_{on}\Big|_{c_o} = -jA' e^{K_o z}(n_2' \cos K_o y' + n_3 \sin K_o y') \qquad (85)$$

The potentials Φ_e and Φ_o also independently satisfy the remaining conditions prescribed for Φ_D. With this arrangement, we can easily relate Φ_e to the problem of heaving twin cylinders and relate Φ_o to the problem of swaying twin cylinders with the only trivial difference being the magnitudes on the right side of Equations (84) and (85).

The solution for oscillating twin cylinders can be obtained by using the method of source distribution along the contour C_o. The expression for the source is given by

$$\begin{pmatrix} G_e \\ G_o \end{pmatrix} = \frac{1}{4\pi}\left[\ell n \frac{\{(y-\eta)^2 + (z-\zeta)^2\}}{\{(y+\eta)^2 + (z+\zeta)^2\}} \pm \ell n \frac{\{(y+\eta)^2 + (z-\zeta)^2\}}{\{(y+\eta)^2 + (z+\zeta)^2\}}\right.$$

$$+ \frac{1}{\pi}\int_0^\infty \frac{e^{k(z+\zeta)}}{K_o - k}\left\{\cos k(y-\eta) \pm \cos k(y+\eta)\right\} dk$$

$$\left. - j e^{K_o (z+\zeta)}\left\{\cos K_o (y-\eta) \pm \cos K_o (y+\eta)\right\}\right] \qquad (86)$$

where the plus sign corresponds to heave (G_e) and the minus sign corresponds to sway (G_o), and $\int_0^\infty$ means Cauchy's principal-value integral.

Let

$$\Phi_e = \int_{C_R} Q_e G_e \, d\ell \qquad (87)$$

$$\Phi_o = \int_{C_R} Q_o G_o \, d\ell \qquad (88)$$

where C_R is the integral along the immersed contour of the right-half of the cross section, and Q_e and Q_o are the unknown source strengths. Applying the boundary conditions given by Equations (84) and (85) to Equations (87) and (88), respectively, and solving the integral equations for Q_e and Q_o, we obtain the solutions of Φ_e

and ϕ_D and, hence, the solution of ϕ_D

ACKNOWLEDGMENTS.

The authors would like to express their thanks to Mr. J. B. Hadler for his encouragement and support of this work. The authors are also indebted to those who have contributed their experimental results to guide the analytical developments described in this work.

The authors would further like to acknowledge the funding support received from the following programs during the course of their work : The in-house Independent Research Program of the Naval Ship Research and Development Center, and the Research, Development, Test and Evaluation Program and the General Hydromechanics Research Program of the Naval Ship Systems Command.

* * *

REFERENCES

Cummins, W. E., "The Impulse Response Function and Ship Motions", Schiffstechnik, Vol. 9 (1962) pp 101-109; reprinted as NSRDC Report 1661.

Faltinsen, O., "A Rational Strip Theory of Ship Motions; part II ," Report 113, College of Engineering, University of Michigan (1971).

Frank, W., "Oscillation of Cylinders In or Below the Freee Sur - face of Deep Fluids", NSRDC Report 2375 (1967).

Haskind, M. D., "The Exciting Forces and Wetting of Ships in Waves" Isvestia Akademic Nauk SSSR, Otdelenie Teknicheskikh Nauk, No. 7 (1957); NSRDC T-307 (1962).

John, F., "On the Motion of Floating Bodies : II. Simple Harmonic Motions," Communications of Pure and Applied Mathematics, Vol. 3 (1950) pp. 45-101.

Jones, H. D., "Catamaran Motion Predictions in Regular Waves", NSRDC Report 3700 (1972).

Lee, C. M., Jones, H., and Bedel, J. W., "Added Mass and Damping Coefficients of Heaving Twin Cylinders in a Free Surface," NSRDC Report 3695 (1971).

Motora, S. and Koyama, T., "Wave-excitationless Ship Forms ," The Sixth Naval Hydrodynamic Symposium, Washington, D. C. (1966) pp. 383-411.

Newman, J. N., "The Exciting Forces on Fixed Bodies in Waves", Journal of Ship Research, Vol. 6, No. 3 (1962) pp. 10-17.

Newman, J. N., "Applications of Slender-Body Theory in Ship Hydrodynamic", Annual Review of Fluid Mechanics, Annual Reviews, Inc. Palo Alto, U. S. A., Vol. 2, (1970) pp. 67-94.

Newman, J. N., "The Exciting Forces on a Moving Body in Waves", Journal of Ship Research, Vol. 9, No. 3 (1965), pp. 190-199.

Ochi, M. K., "Prediction of Occurrence and Severity of Ship Slamming at Sea", The fifth Naval Hydrodynamics Symposium, Bergen, Norway (1964) pp 543-595

Ogilvie, T. F. and Tuck, E. O., "A Rational Strip Theory of Ship Motions; Part 1" Report 013, College of Engineering, University of Michigan (1969).

Ogilvie, T. F., "Recent Progress Toward the Understanding and Prediction of Ship Motion", The Fifth Naval Hydrodynamics Symposium, Bergen, Norway (1964).

Pierson, J. W. and Moskowitz, L. "A Proposed Spectral Form for Fully Developed Wind Seas, Based on the Similarity Theory of S. A. Kitaigarodskii", Journal of Geophysical Research, Vol. 69, No. 24 (1964) pp. 5181-5190.

Salvesen, N., Tuck, E. O. and Faltinsen, O., "Ship Motions and Sea Loads", The Society of Naval Architects and Marine Engineers Transactions Vol. 78 (1970) pp. 250-287.

St. Denis, M. and Pierson, W. J., "On the Motion of Ships in Confused Seas", Transactions of the Society of Naval Architects and Marine Engineers, Vol 61 (1953).

Thwaites, B., "Incompressible Aereodynamics", Oxford Press, England, (1960).

Wehausen, J. V., and Laitone, E. V., "Surface Waves", Encyclopedia of Physics, Vol. 9; Springer-Verlag, Berlin, (1960) pp. 446-778.

Wehausen, J. V., "The Motion of Floating Bodies", Annual Review of Fluid Mechanics, Annual Review, Inc., Palo Alto U. S. A., Vol. 3 (1971) pp. 237-268.

* * *

DISCUSSION

J. N. Newman
Massachusetts Institute of Technology
Cambridge, Massachusetts, U.S.A.

(Discussion read by Professor Beck)

Drs. Lee and Pien have applied up-to-date hydrodynamic techniques to the prediction of catamaran motions and wave resistance, and while they have each experienced isolated cases of poor agreement with experiments, the overall success in both problems is quite striking. My remarks will be focused on the principal discrepancy experienced in the seakeeping portion of this paper; namely, the substantial overprediction of pitch and heave, with forward speed, at a critical wavelength. It seems clear that this is associated with the presence of near-zero heave damping at zero forward speed, and the use of the zero-speed hydrodynamic coefficients in a strip-theory manner. This problem does not show up for conventional hull forms, even when (zero-damping) bulbous sections are present locally such as in the bow. But for a body such as Model 5266 where bulbous sections are dominant, the total heave damping coefficient will be more seriously affected and, in view of the strong coupling due to forward speed, both the pitch and heave motions will be exaggerated as shown in figure 8.

To be more specific, let us consider the case of a thin-body section, so that the explicit results of thin-ship theory are applicable. Then it is known that the two-dimensional damping coefficient for a section with offsets $y = \pm f(z)$ is proportional to the square of the integral

$$\int_0^T e^{-Kz} \frac{df}{dz} dz$$

or to the Laplace transform of the hull slope in the vertical direction. Here T is the ship's draft, and K is the wavenumber. Clearly, for a bulbous form where df/dz changes sign, the above integral will vanish for suitable combinations of the wavenumber and hull shape. Now in three dimensions and with zero speed, the same conclusion

will apply, for suitable shapes f (x, y), essentially because here the damping ccefficient depends on an integral, with respect to the waveangle θ , of the square of the surface integral.

$$\int_0^T \int_{-L/2}^{L/2} e^{-Kz + iKx \cos\theta} \frac{\partial f(x, z)}{\partial z} \, dxdz$$

and since the wavenumber K is independent of the parameter θ , the above integral will vanish for cylindrical vessels having the appropriate two-dimensional shape. Based on this argument, we can conclude that zero damping can occur not only in two dimensions but also in three, provided the forward speed is zero.

Finally, let us consider the case of forward speed. Then, as shown, for example, in my paper in the June 1959 issue of the Journal of Ship Research the threee-dimensional damping coefficient is again proportional to the square of a surface integral similar to that shown above, but now the wavenumber K is no longer a single constant, but, depending on the value of the Brard parameter $\omega U / g$, takes on either two or four discrete values, each of which depends on θ . Thus, since the square of the surface integral is integrated over a continuous spectrum of K ; the probability of zero damping is greatly reduced. The three-dimensional theory which I presented in 1959 was eclipsed by the subsequent success of the simpler strip theories, which could be more easily refined to account for the effects of finite beam. But Dr. Lee has discovered a situation where the three-dimensional and forward-speed effects may be more important, and I hope to have the opportunity to pursue this matter further, by resurrecting my 1959 theory and applying it to the catamaran configuration.

DISCUSSION

Robert F. Beck
University of Michigan
Ann Arbor, Michigan, U.S.A.

Personally, I am wondering if you have done any non-head-sea calculations. What you have shown in the paper is just for pitch

and heave in head seas. It would seem to [illegible] the non-head-sea case may be more critical for certain co[illegible]ons of ship speed and wave heading angles. If you have calculated these modes of motions, did you consider any viscous effects, particularly roll-damping, as Salvesen, et. al. had in their paper when they included an empirical viscous damping term.

REPLY TO DISCUSSION

Choung M. Lee
Naval Ship Research and Development Center
Bethesda, Maryland, U.S.A.

I will answer Professor Newman's discussion first. As I discussed in the paper, the under-estimation of the damping is expected to come from the deficiency of the strip theory which cannot take care of a three-dimensional flow when a catamaran has forward speed. I agree with Professor Newman's viewpoint that the forward speed effect on the motion of LWP catamarans could well be represented by a thin-ship approach. The difficult part is to incorporate the three-dimensional wave interference between the two hulls.

As to Professor Beck's question, I have pointed out that I formulated for five degrees of freedom [illegible]notion. The only numerical results we have obtained so far is up to coupled heave and pitch motion in head seas. As to roll damping, I suspect that we may have to introduce a similar kind of supplemental damping to the one introduced in the heave and pitch motion for LWP catamarans. However, at the present stage we are not sure if the supplemental damping should necessarily be governed by viscous effect alone as treated by Salvesen, Tuck and Faltinsen in their SNAME paper of 1970. More significant factor governing the damping could be the forward speed effect. I hope that our future investigation on this subject would clarify the question.

DISCUSSION

T. K. S. Murthy
Portsmouth Polytechnic
Portsmouth, U.K.

I have not had occasion so far to read the paper which Dr. Pien and Dr. Lee have presented, but from the presentation and the discussion I can see that they have used strip theory with two-dimensional damping values and that they have also made the assumption that the waves are not disturbed by the catamaran. These are perhaps two shortcomings in the work but it is obvious from the talk I gave this morning that if we put the parameter beta equals zero - we have chosen four parameters - delta, beta, alpha and epsilon - if we put beta relating to the cushion pressure equal to zero we get all the results we require for a catamaran.

In my treatment I did not start from the equations of motion, as is normally done. I have not specifically used added mass and damping values, but these are implicit in the equations. The strip theory is always suspect, particularly at forward speeds, and it is better not to use it. Although my theory is applicable only to the thin hulls of the conventional catamaran, it can also be applied to circular cylinders well below the free surface, whatever the dimensions might be, because then the wavemaking could be considered fairly negligible. I would strongly recommend that Dr. Pien and Dr. Lee use the method talked about this morning to see how it compares with their results. We should be very glad to collaborate with them in this respect and do some work at the University if required for confirmation of their results. This is a different approach. It does not make any explicit assumptions and we get the same results by a different approach. I strongly recommend some sort of collaboration between NSRDC and the University.

REPLY TO DISCUSSION

Choung M. Lee
Naval Ship Research and Development Center
Bethesda, Maryland, U.S.A.

Dr. Murthy's suggestion of using three-dimensional singularity distribution is well understood. In principle we can always use the method of singularity distribution to obtain the solution of a linear boundary-value problem in the three-dimensional space. The only difficulty is in the evaluation of the hydrodynamic quantities, which takes much more time than the two-dimensional solution does. This is the main reason why we have relied on the strip theory. Owing to the short time at my disposal I did not explain too well, but when I said that the presence of body did not disturb the incoming wave this was applicable only to the case of obtaining relative motion. In obtaining ship motion the wave diffraction effect due to the presence of body is incorporated in the wave-exciting term by use of the Haskind relation.

* * *

UNCONVENTIONAL SHIPS

Tuesday, August 22, 1972

Morning Session

Chairman : A. Castera
Bassin d'Essais des Carènes, Paris

	Page
Hydrodynamic Design of an S^3 Semi-Submerged Ship. T.G. Lang (Naval Undersea Research and Development Center, U.S.A.).	549
Propeller Excitation, and Response of 230 000 TDW Tankers. C.A. Johnsson (Statens Skeppsprovningsanstalt, Sweden). T. Søntvedt (Det Norske Veritas, Norway).	581
Motions of Moored Ships in Six Degrees of Freedom. I. Ming Yang (Tetra Tech. Inc., U.S.A.).	671
Analysis of Ship-Side Wave Profiles, with Special Reference to Hull's Sheltering Effect. K. Mori, T. Inui, H. Kajitani (University of Tokyo, Japan).	687

Preceding page blank

HYDRODYNAMIC DESIGN OF AN S^3 SEMI-SUBMERGED SHIP

Thomas G. Lang, PhD
Naval Undersea Research and Development Center
San Diego, California U.S.A.

ABSTRACT

The S^3 semisubmerged ship concept is described, and hydrodynamic characteristics are presented. Variations of the basic form are discussed and results of model tests and theory are presented on static and dynamic stability, drag and power, motion in waves and effectiveness of an automatic control system for motion reduction. The results show that an S^3 is inherently stable at all speeds, well damped in all modes, and should provide a near-level ride in high sea states if equipped with an automatic control system. Furthermore, an S^3 should have less drag than a monohull at the higher design speeds.

INTRODUCTION

Military and commercial users of ships are continuously searching for new design concepts which would provide improved speed, range, payload ratio, seaworthiness, or reliability. Such improvements are preferably to be attained at reduced cost, although cost tradeoffs are the general rule. Since monohulls have long been the most widely used hull form, it is generally accepted that their lead position is not easily challenged.

The large monohulls can carry a very large payload ratio, they have a long range at moderate-to-high ship speeds, and they offer good seaworthiness at a relatively low initial and operating cost per unit of payload. The small monohulls, on the other hand, have

Preceding page blank

other advantages, such as : low unit cost, more flexible utilization resulting from greater numbers for a given total cost, more frequent scheduling, less net cost when small payloads are required, and less target value in the case of military applications.

Unusual ship designs such as hydrofoils and various types of air-supported vehicles have already taken over some of the missions performed earlier by monohulls. These types of craft are high performance vehicles, and tend to be used when higher speed is important, such as certain passenger craft and special military applications. These craft require considerable power, are more complex in design, and are therefore more costly than monohulls.

There is a need for a new type of small displacement ship which has low cost, has all the desirable features of small ships, and yet has many of the desirable features of large ships.

One new type of displacement ship which has been receiving considerable attention lately, especially in the oil drilling industry, is called a semisubmersible. Typically, semisubmersibles are low-speed ships having two or more submerged cylindrical hulls with several vertical cylinders supporting a platform well above the water. These craft have been found to withstand very high sea states and winds, and exhibit small motion in waves relative to monohulls.

The term S^3 refers to a certain class of related semisubmerged ship designs and their characteristics. The S^3 semisubmerged ship concept discussed in Reference 1, and shown in Figure 1, belongs to the family of semisubmersibles ; however, it is designed to provide low drag at higher speeds, and to have good seaworthiness not only at rest, but underway. An S^3 tends to fill a gap in ship design since it can be small, having all of the advantages of small ships, and yet have the speed, deck space, and seaworthiness of large ships.

The S^3 concept stemmed from designs of the writer dating back to the 1950's. This concept was introduced at the Naval Undersea Center (NUC) in 1968, where it has been under active investigation ever since. The S^3 is not the only higher-speed semisubmerged ship concept, however. Several other types have been designed, as discussed in Reference 1, including a single-hull version conceived by Lundborg dating back to 1880, a multihulled version described by Blair in 1929, a twin-hulled version by Creed in 1945, the Trisec by Leopold at Litton Systems in 1969 (Ref 2), and more recent versions called Modcats designed by Pien at Naval Ship

Research and Development Center (NSRDC) (Ref 3)

DESCRIPTION

The typical design of an S^3 semisubmerged ship, shown in Figure 1, consists of two parallel torpedo-like hulls which support an above-water platform by means of four well-spaced streamlined vertical struts. Stabilizing fins attached to the aft portions of the hulls provide pitch stability at higher speeds. The water plane area and spacing of the struts provide static stability in both roll and pitch. Small controllable fins called canards may be placed near the hull noses. These canard fins can be used in conjunction with controllable stabilizing fins at the rear to provide motion control over heave, pitch and roll. If rudders are placed in each of the four struts, motion control over yaw and sway can be obtained, especially when an S^3 travels obliquely to waves. It should be noted that an S^3 design is inherently stable at all speeds, without the use of control surfaces.

Some of the advantages of the S^3 hull type relative to a monohull are : greatly improved seaworthiness, both at rest and underway; reduced wave drag at higher speeds , greater deck area and internal volume ; certain advantages of the unusual hull shape for placement of a central well, mounting sonars, carrying small craft, placement of propulsors, and potential for modular construction ; improved propulsive efficiency and greater cavitation resistance ; greater topside weight capacity; and the potential for a near-level ride in high sea states.

These advantages are to be weighed against the disadvantages. The primary disadvantage is the increased structural weight due to its relatively dispersed design form. Other possible disadvantages include the large draft, and the need for ballast control over trim.

Many variations of the typical design shown in Figure 1 are possible. The strut thickness and chord lengths can vary, the hull lengths and diameters can change, the hull cross-sectional shape can vary, the rudders can be located behind the propellers, the sizes and positions of the stabilizing and control fins can be varied, and the ship can be propelled by means other than propellers, such as pumpjets. Still other S^3 variations from the typical design form are presented in Figure 2; these include a two-strut and a six-strut, twin-hulled design, and several types of single-hulled designs. There is no "best" S^3 hull form, since the form will vary as a function of size, mission, and design constraints.

The primary objective of this paper is to describe the basic characteristics of an S^3 so that it can be compared with other types of ships for various types of applications. To do this, the drag and power, stability, motion in waves, and automatic control characteristics will be discussed.

DRAG AND POWER

In calm water, ship speed is a function of drag, and is therefore limited by the installed power. The maximum speed may be less in the higher sea states, since speed may be limited either by ship motion or by increased drag due to waves. In the case of monohulls, speed limitations in the higher sea states can be severe.

In order to compare the drag and power of a wide variety of ship forms, sizes, and speeds, the following equations are used :

$$\text{drag coefficient} = C_D = \frac{D}{\nabla^{2/3} \frac{\rho}{2} V^2} = C_{D_f} + C_{D_r}$$

$$\text{power} = P = \frac{D \cdot V}{\eta} = C_D \nabla^{2/3} \frac{\rho}{2} V^3 / \eta$$

$$\text{displacement Froude number} = F_\nabla = \frac{V}{\sqrt{g \nabla^{1/3}}} = \frac{V \rho^{1/6}}{g^{1/3} \Delta^{1/6}}$$

$$\text{hull efficiency} = E = \frac{\Delta \cdot V}{P} = \frac{\Delta}{D} \cdot \eta$$

$$\text{range} = R = \frac{\Delta_f}{\Delta} \cdot \frac{\Delta}{D} \cdot \eta \cdot \frac{1}{SFC} = \frac{\Delta_f}{\Delta} \cdot E \cdot \frac{1}{SFC}$$

where D = drag, ∇ = displaced volume, ρ = mass density of water, V = speed, η = propulsive efficiency, g = acceleration of gravity, $\Delta = \nabla \rho g$ = displaced weight, Δ_f = weight of fuel, and SFC = specific fuel consumption = weight of fuel consumed per unit power per unit time. The units used may be any consistent set. The term C_{D_f} is the frictional drag coefficient, and is assumed to be purely a function of Reynolds number ; the term C_{D_f} reduces as the size or speed increases. The term C_{D_r} is the residual drag coefficient ; it includes the wave drag and all other sources of drag except frictional drag, and is assumed to be purely

a function of F_∇ .

Figure 3 is reproduced from Reference 1, and shows the approximate hull efficiency E at maximum speed for a variety of ship types as a function of displacement Froude number F_∇ in calm water. Hull efficiency is an important parameter since the equation shows that it is directly proportional to range. Note that the hull efficiency of an S^3 is somewhat less than that of a monohull at low F_∇ , but somewhat greater than that of a monohull at high F_∇ where monohull wave drag becomes large. The reason for this result is that an S^3 has a greater frictional drag than a monohull due to its increased wetted surface area, but has less wave drag at higher speed due to its unusual hull form. A C_D of 0.05 and an η of 0.80 have been used for the S^3 curve in Figure 3 at F_∇ = 2.0, with C_D/η reducing slightly at lower F_∇ , and increasing slightly at higher F_∇ to reflect reduced propulsive efficiency. The propulsive efficiency η is somewhat greater for an S^3 than for monohulls since the boundary layer inflow to the propulsors will be more axially symmetric ; therefore, the S^3 propulsors can be more completely wake adapted, as in the case of torpedoes where propulsive efficiencies of 85% to 90% are not uncommon. The line shown in Figure 3 for monohulls is the locus of the highest measured values of E. In rough water, the value of E for monohulls will reduce considerably, as shown later, while E for an S^3 ship will not change appreciably.

The dashed lines in Figure 4 show the measured C_D from model tests. The model data relate to a small-craft S^3 design. The solid lines are the estimated drag coefficients for several 3000-ton ships, including an improved low-wave-drag four-strut S^3 , and the estimated C_D of an improved two-strut design taken from Ref 3. Notice that the values of C_D for the 3000-ton ships are significantly lower than those of the small models, primarily due to the Reynold's number effect on frictional drag and the use of thinner struts. The wave drag portion of the estimated value for the S^3 ship was calculated by Dr. R.B. Chapman of NUC using linearized thin ship theory in which all strut-strut, strut-hull, and hull-hull interactions were included. This same theory has provided excellent agreement with a large number of tests conducted on various struts, strut-hull combinations, and complete S^3 models. Reference 4 by Dr. Chapman contains data for estimating the spray drag of surface-piercing struts at high speeds.

Figure 5 shows the ratio of the drag in waves to the drag in calm water for tests on a 5-foot model of a DE-1006 destroyer

(Reference 5), and for tests on a 5-foot model of an S^3. The drag of the destroyer model increases by factors of five or more in waves, while waves are shown to have no significant effect on the drag of the S^3 model.

Figure 6 shows the power required for a 3000-ton, four-strut S^3 compared with the estimated power requirements for a hydrofoil, a high-speed surface effect ship and a destroyer. The results show that the S^3 requires significantly less power than either a hydrofoil or SES at speeds up to around 50 knots.

A photograph of a model of a 3000-ton S^3 is shown in Figure 7, together with a list of some of its estimated characteristics.

STABILITY

A wide variety of model tests have shown that the S^3 is inherently both statically and dynamically stable. In regard to static stability, the metacentric height in roll can be calculated from the equation

$$GM = \frac{I}{\nabla} - BG$$

where $I = \frac{b^2}{4} A$ = moment of inertia of the total waterplane area A,

b = strut center-line spacing,

∇ = displaced volume

BG = is the distance upward from the center of buoyancy to the center of gravity.

Large topside loads can be carried, even with a small waterplane area, due to the substantial transverse and longitudinal strut spacing.

Tests in large waves and high simulated winds have shown that GM in roll should be around 3/4 of the hull diameter (alternatively, approximately 8% of the beam), although values as little as 1/4 of the hull diameter are acceptable. Tests indicate that motion in beam waves reduces as the roll GM increases, contrary to some monohull results. However, since both wave drag and structural weight increase as the strut waterplane area and spacing increase, the roll GM should be made no larger than necessary.

The metacentric height in pitch is calculated from the same equation as for roll, except I now refers to the longitudinal area moment of inertia. Tests to date on S^3 models have shown that motion in waves reduces as the pitch GM increases. In other words, the struts should be well-spaced in the longitudinal direction. This is one of several reasons why the four-strut configuration was selected as a typical (but not the only) design form for an S^3 .

Figure 8 shows typical waterplane areas for a monohull, a catamaran ship, a two-strut low waterplane ship, and a four-strut S^3 . Note that the S^3 has the greatest static stability in both roll and pitch per unit waterplane area because the waterplane area is concentrated in the four corners of the ship where it is most effective. Another advantage of the four-strut configuration is that it has less virtual mass in the transverse direction than the two strut design, and therefore will have less motion and hydrodynamic loading in beam seas.

One of the first questions explored in a series of S^3 model tests conducted in 1969 concerned the dynamic stability of an S^3 . Figure 9 shows pitch data obtained on several 5-foot model configurations tested in calm water in the General Dynamics Aeromarine Test Facility model towing basin in San Diego, California. The hull diameters were 4 inches. Figure 9 shows that all models were stable at all test speeds except the non-S^3 model designated C + N which had no stabilizing fins. Thus, these tests showed that the S^3 stabilizing fins were necessary for dynamic stability at F_∇ greater than about 0.9. This result was in good agreement with S^3 design theory which shows that the dynamic instability of bare hulls will overcome the static stability provided by the struts above some critical speed unless stabilizing fins are incorporated.

A very useful device to further investigate the dynamic stability of an S^3 is the 5-foot radio-controlled model shown in Figure 10, which was tested in 1970. This model was stable under all test conditions and controlled well. All motions were well damped at rest and highly damped when underway. It operated well in waves and wind at all angles, although the greatest motion occurred in large following waves. Figure 11 shows an 11-foot model built and tested at the Naval Ship Research and Development Center in 1971. This model performed similar to the 5-foot model suggesting that model tests and the known scaling relationships are valid.

MOTION IN WAVES

During the 1969 towing tests, various S^3 model configurations were tested in 4-inch X 80-inch waves in head and following seas. The non-dimensional pitch and heave amplitudes for two S^3 models in head seas are shown in Figure 12 together with the pitch and heave amplitudes of a 5-foot model of a C-4 monohull ship. Note that the motion of the S^3 models is significantly less than that of the monohull model. The S^3 models were also tested in a variety of wave lengths, and no resonance was found in head seas.

The test results in following waves showed significantly more motion, as seen in Figure 13. The monohull was not tested in following waves. The wave height was equal to the hull diameters, so the waves were relatively high. Tests in 2-inch waves showed considerably less motion. Data taken on the lift force and pitching moment indicated that small control surfaces and an automatic control system would significantly reduce motion in following seas.

Tests at rest in beam seas showed that the roll of the S^3 models was significantly less than that of the monohull model, and no resonance occurred at any of the wavelengths tested.

AUTOMATIC CONTROL SYSTEM

The combined use of horizontal canard control fins near the noses of the hulls, and controllable stabilizing fins near the aft end of the hulls, provides motion control over heave, pitch and roll in high sea states.

Figure 14 presents computer results obtained by Dr D. T. Higdon of NUC showing the reduction of heave and pitch in head waves which is achievable by automatic stabilization of an S^3 ship similar in shape to the radio-controlled model of Figure 10. The already small motions are reduced by a factor of four or more.

Figure 15 shows the computer results for motion reduction in following waves. In this case, the result is much more dramatic. Heave is reduced by factors of twenty or more, and pitch is reduced by factors of five to ten.

SUMMARY

A considerable number of model tests, theoretical studies, and design studies have been conducted on the S^3 concept. The results show that the S^3 is highly stable and seaworthy (both at rest and underway), more efficient at higher speeds than conventional ships, and will provide a near-level ride if automatically controlled in high sea states. Also, many advantages result from its unusual hull form for various kinds of military and non-military applications.

REFERENCES

1 LANG, T.G., "S^3 New Type of High-Performance Semisubmerged Ship", American Society of Mechanical Engineers, Paper No. 71-WA/UnT-1, Winter Annual Meeting, Nov 28 - Dec 2, 1971.

2 LEOPOLD, R., "A New Hull Form for High-Speed Volume-Limited Displacement-Type Ships", Society of Naval Architects and Marine Engineers, Paper No. 8, Spring Meeting, May 21 - 24, 1969.

3 STEVENS, R.M., "New Dimensions in Naval Catamarans", American Society of Naval Engineers, ASNE Day Meeting, May 4 - 5, 1972.

4 CHAPMAN, R.B., "Spray Drag of Surface-Piercing Struts", Naval Undersea Research and Development Center, TP-251, Sep 1971.

5 SIBUL, O.J., "Ship Resistance in Uniform Waves", Institute of Engineering Research, University of California, Berkeley, California, Report No. NA-64-1, Jan 1964. AD # 606272.

* * *

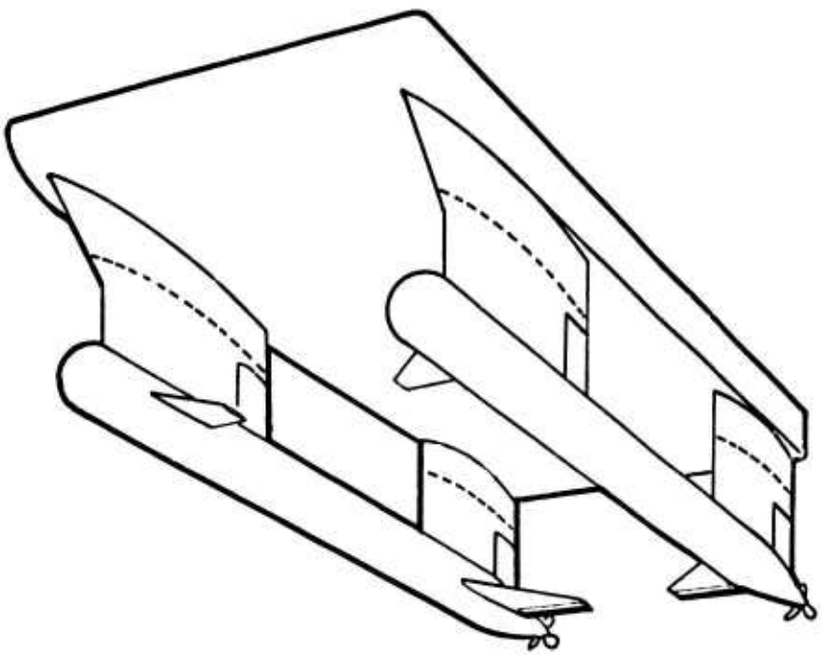


Figure 1. Basic S^3 semisubmerged ship concept

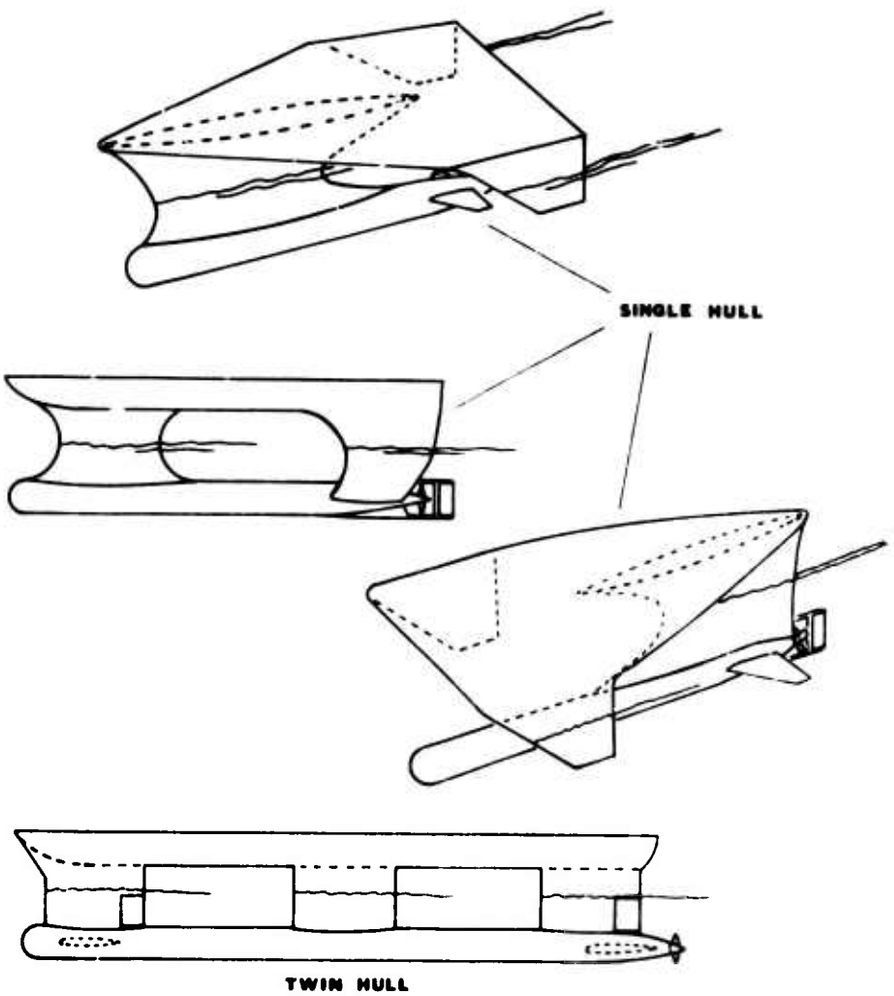


Figure 2. Alternative designs of the S^3 concept

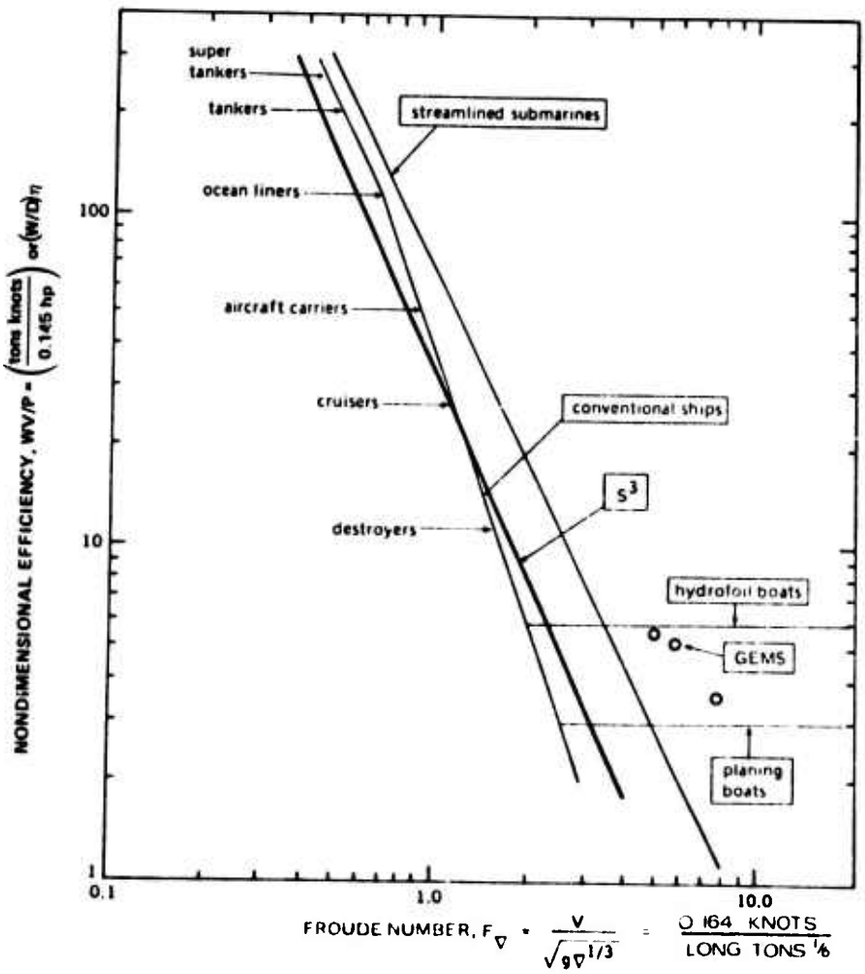


Figure 3. Hull efficiency of various ship types

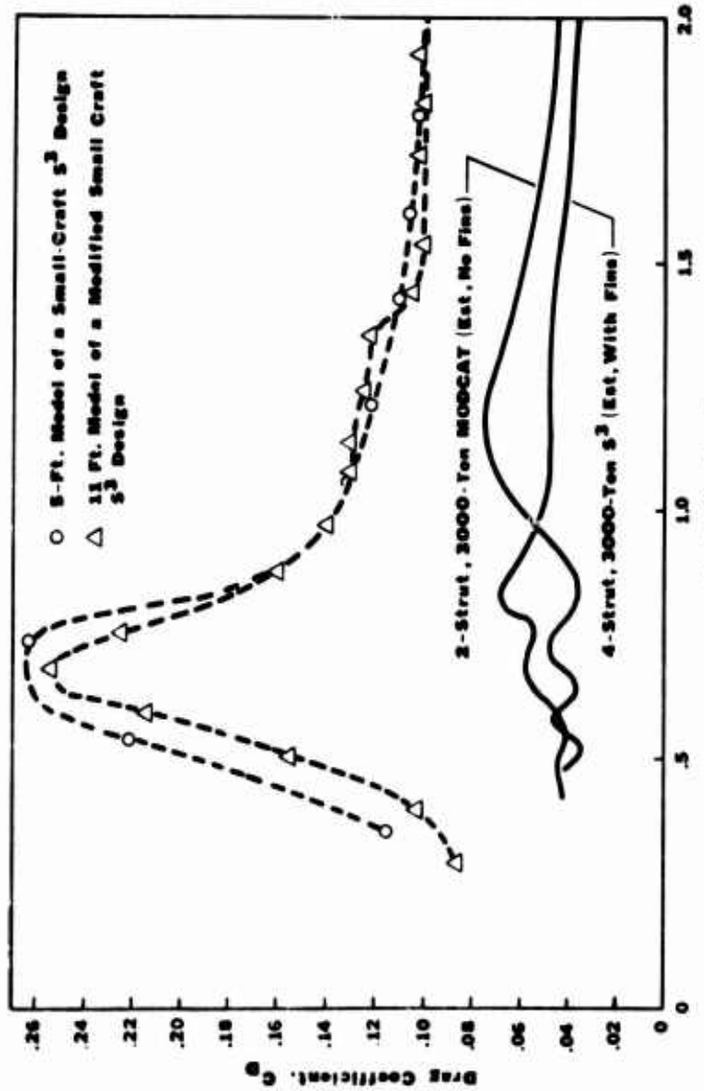


Figure 4. Drag coefficients of various S^3 models and 3000-ton ship designs

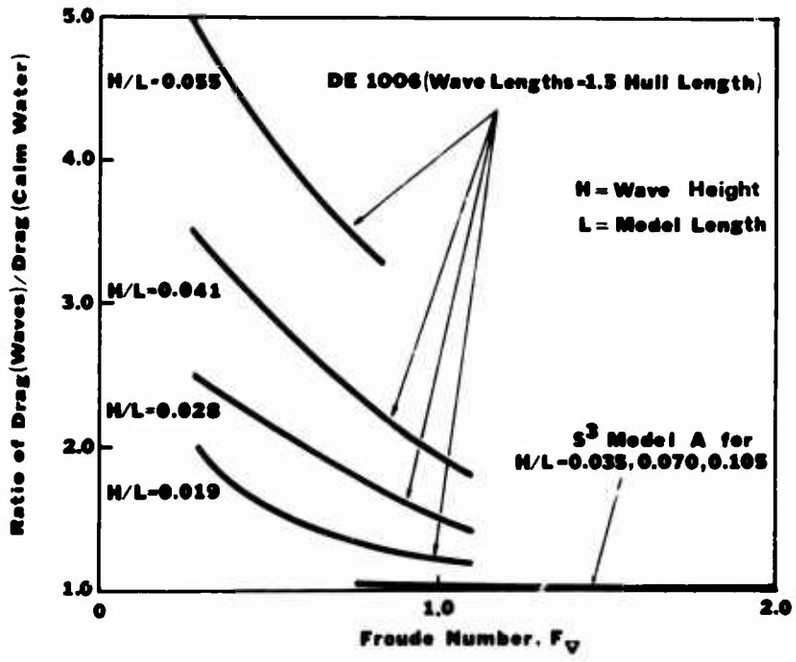


Figure 5. Effect of waves on the drag of five-foot destroyer and S^3 models

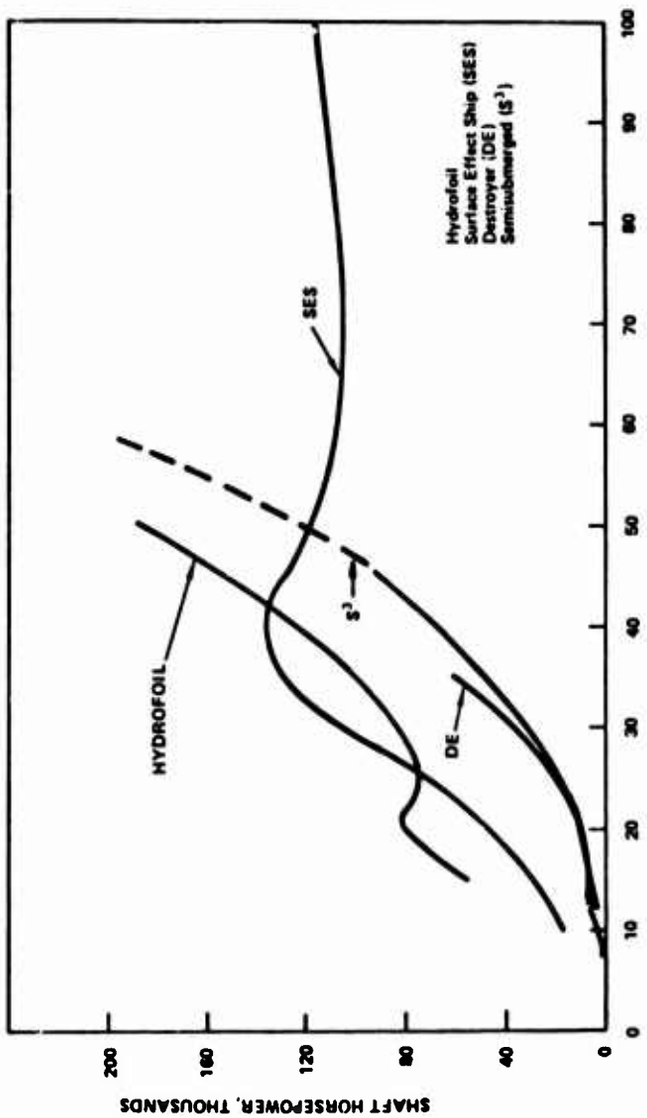


Figure 6. Power requirements for various kinds of 3000-ton ship designs



Figure 7. Model of a 3000-ton S^3 ship

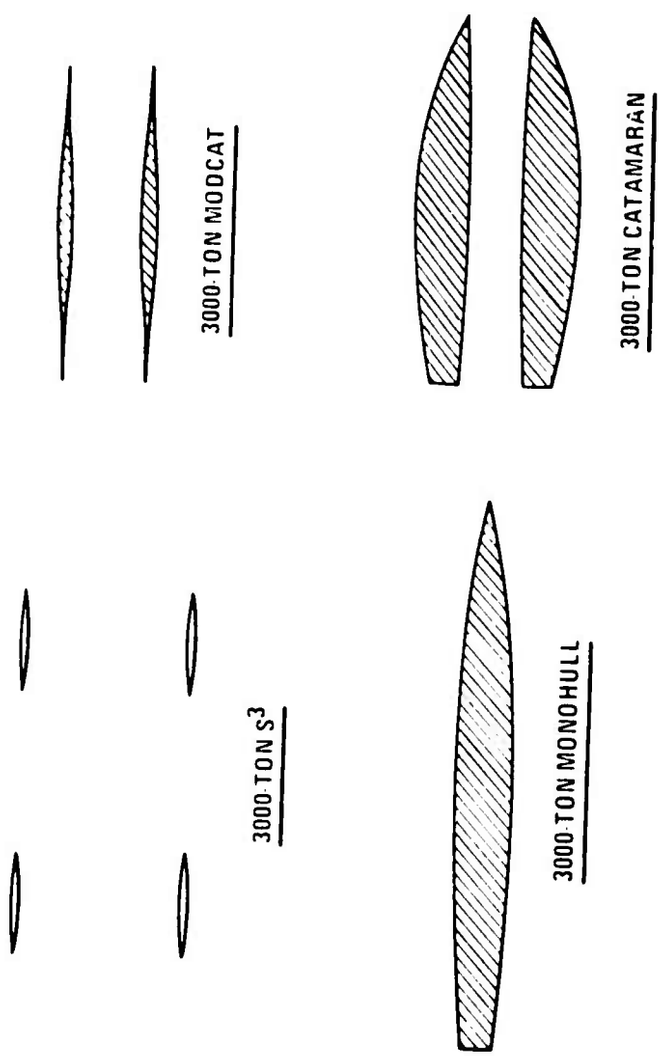


Figure 8. Waterplane areas of various ship types

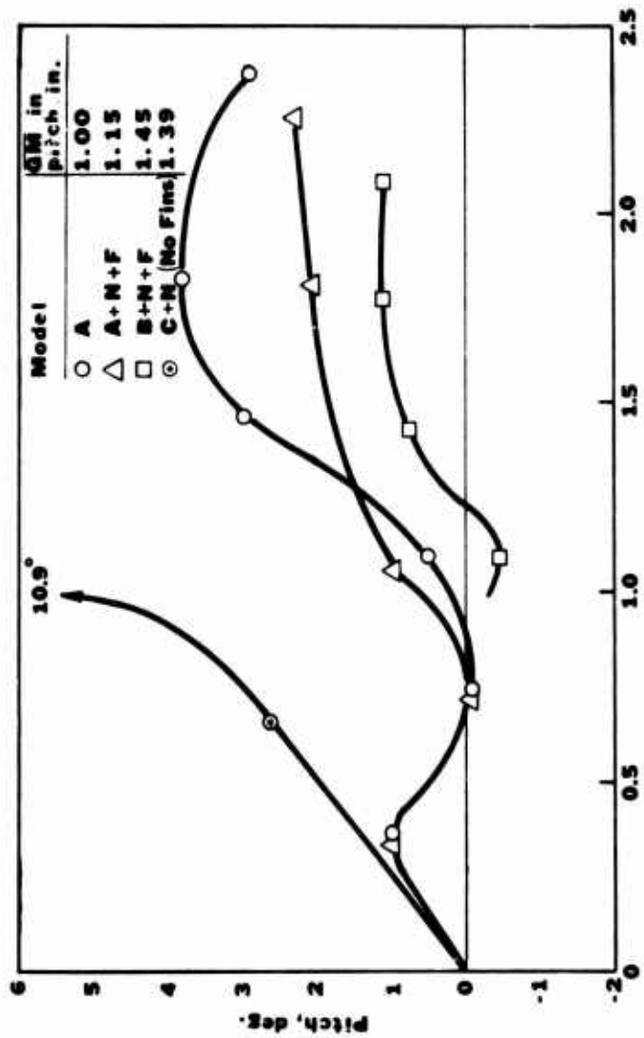


Figure 9. Pitch in calm water of S^3 models as a function of displacement Froude number

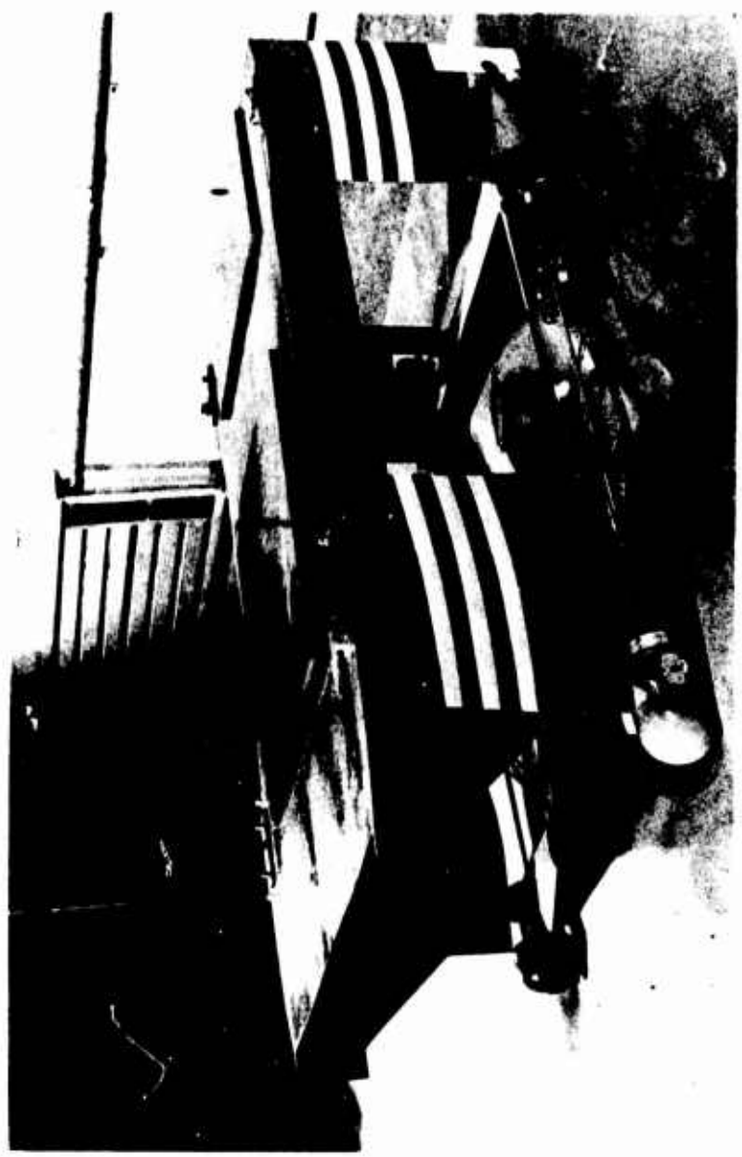


Figure 10. Five-foot radio-controlled S^3 model

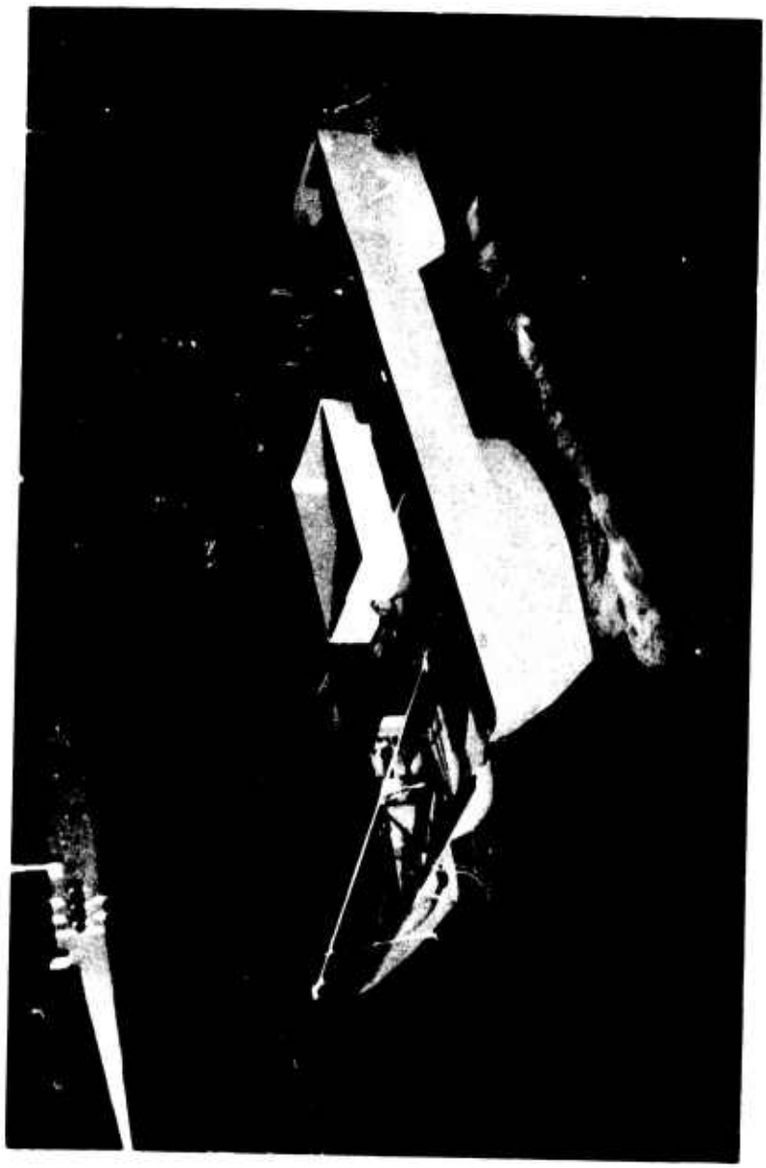


Figure 11. Eleven-foot self-propelled NSRDC model

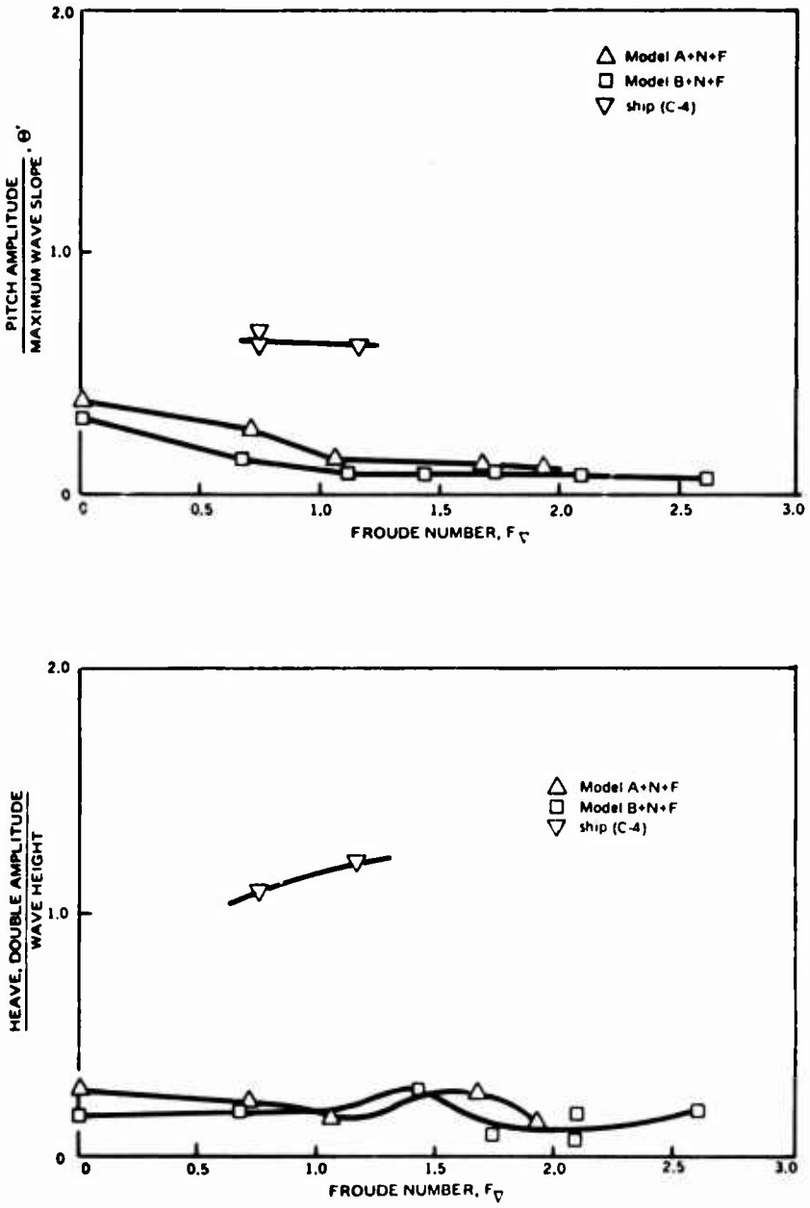


Figure 12. Pitch and heave of S^3 models in head seas

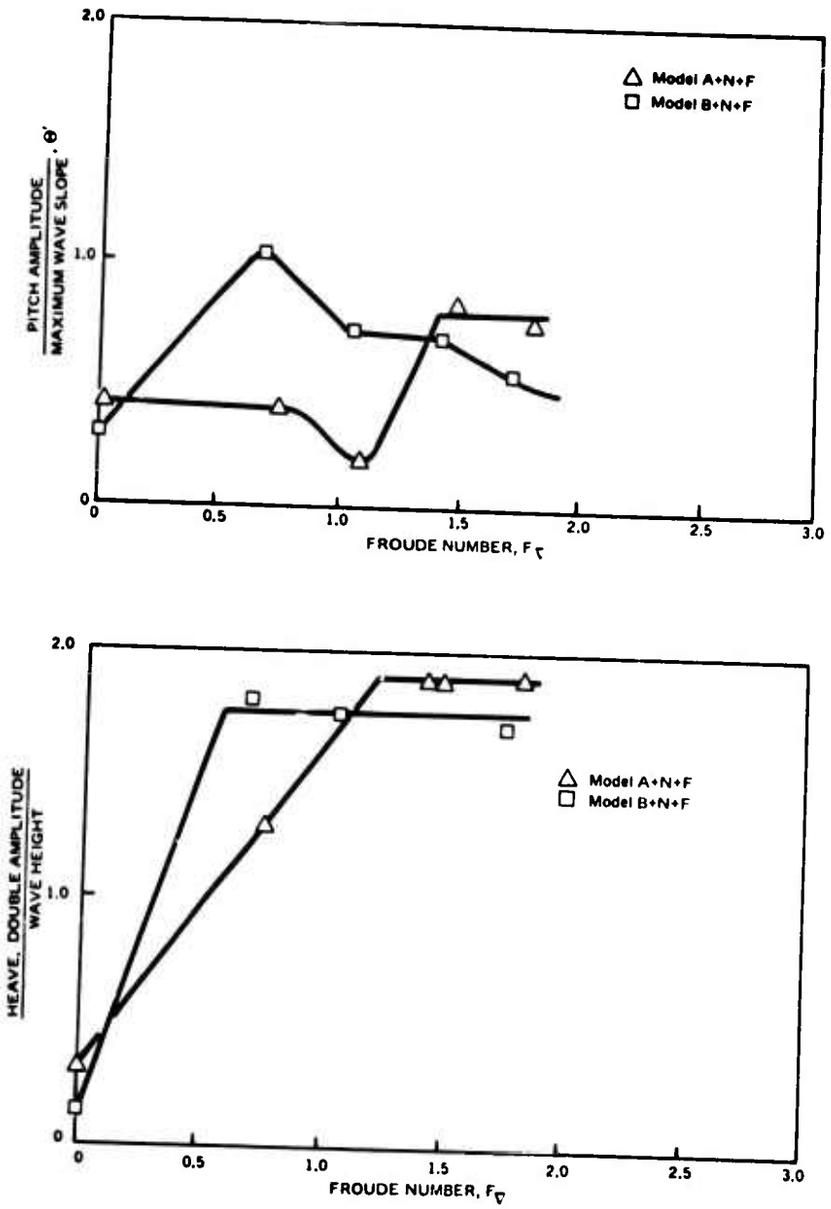


Figure 13. Pitch and heave of S^3 models in following seas

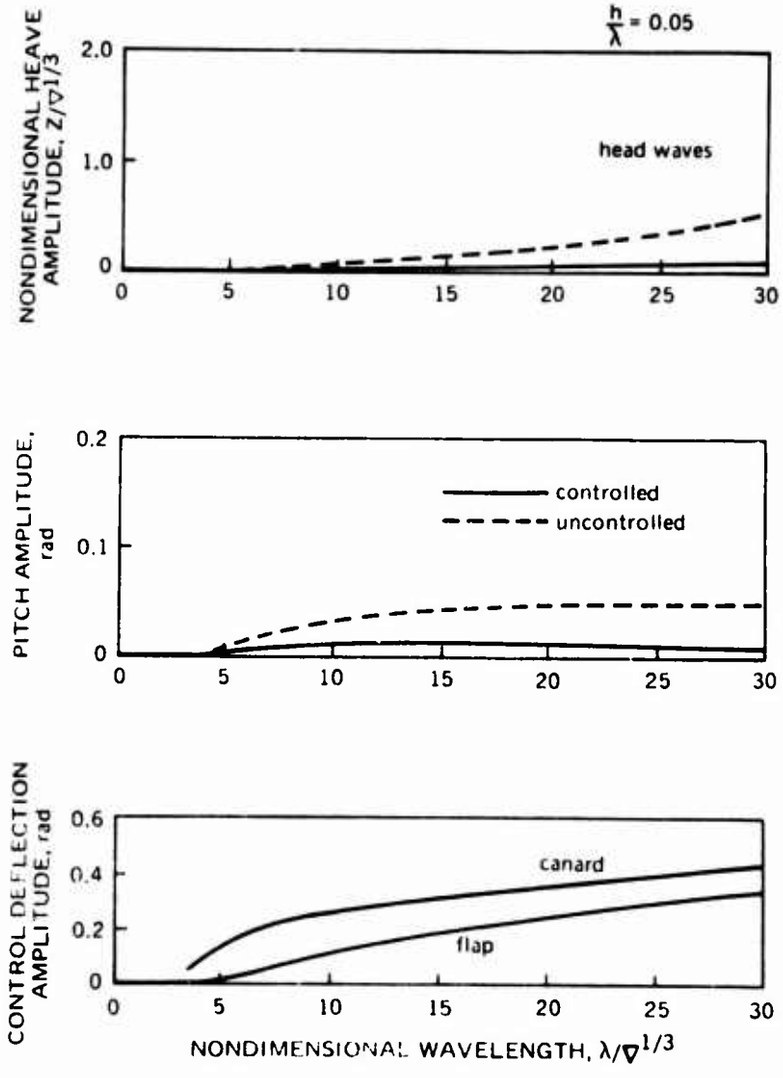


Figure 14. Effectiveness of automatic control in head seas at $F_{\nabla} = 1.65$

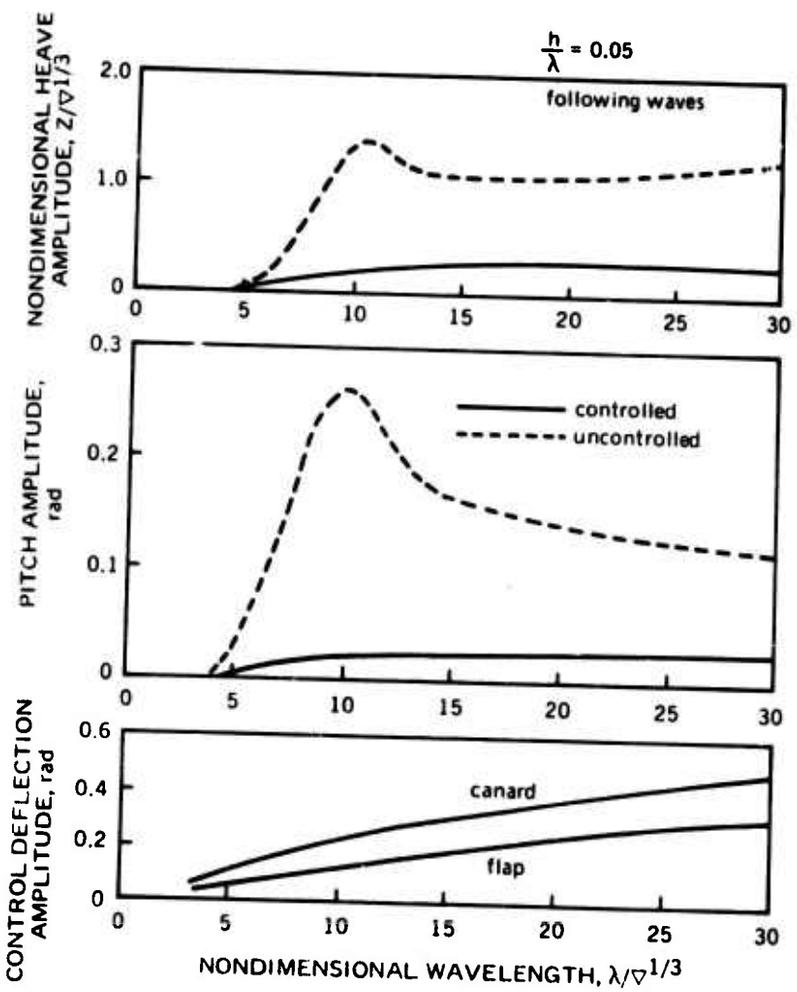


Figure 15. Effectiveness of automatic control in following seas at $F_\nabla = 1.65$

DISCUSSION

Gerald E. Bellows
Universität Hamburg, Institut für Schiffbau
Hamburg, Germany

I would like to thank Dr. Lang for an excellent presentation. It is evident that this type of ship has extremely good seakeeping properties. This is perhaps its major advantage over the monohull. I have studied ships of this type and have found that, with the cargo loaded on the deck, it is difficult to obtain sufficient GM in both the longitudinal and transverse directions. I wonder if Dr. Lang could give us a weight breakdown, including the structure, fuel, and cargo (or payload). I also would like to know what type of power plant would be used and if it would be located in the underwater hulls. I would like to know if it is possible to alter the draft by ballasting. Dr. Lang has mentioned in his report that the draft could be a problem, but this could be overcome by using ballast to alter the draft when entering port.

REPLY TO DISCUSSION

Thomas G. Lang
Naval Undersea Research and Development Center
San Diego, California, U.S.A.

To answer the first question, the metacentric height (GM) increases a little faster than the square of the distance between the waterplane areas. Thus by concentrating the waterplane area near the four corners of the platform through using four struts we obtain a maximum GM for a given waterplane area in both roll and pitch. As a result, it is possible to have a GM that is on the order of three or four times that of the conventional monohull in roll, and a GM which is much less than a monohull in pitch but yet one that gives very good pitch response. The result, as seen in the film, is an acceptable metacentric height in both roll and pitch.

As far as the ratios of the various weights are concerned, our preliminary calculations indicate a structural weight to total weight ratio on the order of 40 per cent for a moderately sized ship, if the ship is made out of aluminium. Thus, we are proposing that a ship of this type be made of aluminium to help to solve the weight problem.

In regard to the power plant, we would propose that the power plant on small craft be located in the top cross structure, with some type of a drive mechanism to transmit the power down to the propeller. In ships of a few thousand tons or greater, we would propose that the power plants be located in the tailcones of submerged hulls, with direct drive to the propeller through a gearbox. Alternatively, a cryogenically cooled electric power system
We are proposing gas turbines for power because of their light weight and efficiency, especially in the larger size range.

In answer to the last question, on ballasting, we do have provision for ballasting in all the proposed designs. In very shallow water ports, the loaded ship minus fuel provides a draft about equivalent to that of a monohull ; therefore such a ship could be fully loaded at the dock and the fuel topped off in the deeper region of the harbor.

DISCUSSION

Nils Salvesen
Naval Ship Research and Development Center
Bethesda, Maryland, U.S.A.

I have recently made an investigation of the seakeeping characteristics of low-water-plane catamarans and I found it a very interesting subject, Reference 1. What makes it so much more interesting than for conventional ships is that the seakeeping characteristics of catamarans and in particular LWP catamarans are extremely sensitive to changes in the hull geometry. For conventional monohulls, on the other hand, large changes in the hull parameters are required in order to produce any substantial effects on the seakeeping characteristics.

It is recognized that as far as the seakeeping is concerned, the major advantage of the LWP catamaran over conventional hulls is that they have a very low natural frequency due to their small water-

plane area. Therefore, in head seas, the maximum heave and pitch motions are usually at wave lengths approximately five times the length of the hull. This means that a long LWP catamaran (say longer than 300 feet) will only experience large pitch and heave motions in extremely severe sea conditions. On the other hand, a 100-foot catamaran will experience in ocean operation maximum pitch and heave motions a large percentage of the time.

This aspect of the motion responses of LWP catamarans is well-known ; however, it is less recognized that the added mass and damping coefficients as well as the exciting forces are all much smaller than for conventional hulls and that the maximum pitch and heave motions are extremely sensitive to small changes in these quantities. In particular, it is important to recognize that the damping coefficient for certain catamaran configurations can be so small that it results in pitch and heave motions several times larger than for conventional hulls as shown in Reference 1.

Another seakeeping aspect which deserves attention is the pitch and heave motions in following seas. Some of the LWP catamarans have about twice as much pitch motions in following seas than conventional monohulls and the maximum pitch motions occur at wave lengths of the order of magnitude of ship length (see Reference 1). Dr. Lang has demonstrated that these vertical motions in following seas can be considerably reduced by use of automatic control surfaces. I would like to ask Dr. Lang if he is of the opinion that LWP catamarans in general will need automatic control surfaces in order to have acceptable motions in following seas.

---

1 SALVESEN, N., "Seakeeping Characteristics of Small-Water-Area-Twin-Hull Ships", presented at AISS, SNAME, USN Advanced Marine Vehicles Meeting, Annapolis, Maryland, 17-19 July 1972, and published in the Journal of Hydronautics, Vol. 7 No. 1, Jan 1973.

REPLY TO DISCUSSION

Thomas G. Lang
Naval Undersea Research and Development Center
San Diego, California, U.S.A.

In answer to the first comment, we have not seen in our experiments any of the head sea resonance problems that Dr. Salvesen mentioned. As you saw in the motion picture, the S^3 model has extremely high damping when under way, in both roll and pitch. This large damping is provided largely by the canard fins at the front, and the stabilizing fins at the back. It is probable that the differences from Dr. Salvesen's results are due to differences in design form from the S^3 model. We have found relatively good comparisons between experiment and theory ; in general, the experimental results tended to show less motion than theory would predict, especially in the following sea case.

As far as automatic control is concerned, all of the tests you saw in the motion picture were without automatic control, so it is seen that the craft can operate effectively without automatic control.

In the case of following seas there is no motion problem until the waves reach a certain height. When not using automatic control, large craft motion in the very highest waves in a following seas can be alleviated by slowing down approximately the wave speed, or less.

* * *

DISCUSSION

Edmund P. Lover
Admiralty Experiment Works
Haslar, Gosport, Hants, U.K.

I have a point to make concerning this most interesting paper, and a question to ask.

Firstly, in Figure 3 of the paper a comparison is made between the S^3 form and conventional ships. I would like to make the point that the "hull efficiency" $WV/P\eta$ conventional monohulls can be improved significantly above that shown by increasing the length to displacement ratio. These longer vessels would also have improved seakeeping characteristics as well as the Froude number of crossover above which the S^3 shows to advantage.

My question is this. Was any simulation made during the model experiments of an emergency crash situation and, if so, did this exhibit any problems with maintenance of trim ?

REPLY TO DISCUSSION

Thomas G. Lang
Naval Undersea Research and Development Center
San Diego, California, U.S.A.

I agree with your comment of reduced drag for the larger length-beam ratio monohulls designed for higher speeds. In the nondimensional graph of hull efficiency, this effect is already included to a certain extent since the line for monohulls represents the maximum value of existing monohulls wherein the higher-speed monohulls already have a larger length-beam ratio. Thus, the monohull line represents the best of the known data, so the majority of monohulls will lie below that line as far as efficiency is concerned.

Regarding the question of a crash situation, the radio-con -

trolled model was used to test light crack avoidance and the problem of hull flooding in case a crack cannot be avoided. The model was operated at top speed and suddenly given full reverse thrust. In no case did the bow submerge or was there water over the deck. The main reason for this good behavior is that the relatively low waterplane area has been concentrated near the front and the back of the craft by making use of four struts. Thus, the metacentric height in pitch is a maximum for a given waterplane area. This metacentric height is adequate to prevent excessive pitch in the case of full reverse thrust from a condition of top forward speed. In the case of hull flooding, the control surfaces were adequate to raise the platform to trim conditions as speed increased. Trim at rest could be adjusted by blowing water ballast or fuel on the damaged side and/or counterflooding on the opposite side.

DISCUSSION

Hans Edstrand
Statens Skeppsprovningsanstalt
Göteborg, Sweden

I have not read Dr. Lang's paper, but when I looked at the beautiful film I wanted to ask a question. The model size seems to me to be enormous compared with the tank dimensions, and I should like to know if Dr. Lang has checked his results in a larger tank and if he has used the measurement for quantitative development.

REPLY TO DISCUSSION

Thomas G. Lang
Naval Undersea Research and Development Center
San Diego, California, U.S.A.

The model size is slightly large for the tank it was tested in. The model hull diameter was 4 inches and the model was 5 feet long; the tank was 6 feet deep, 12 feet wide, and 300 feet long. The ratio

of hull diameter to tank depth was 1/16. Dr. Chapman's analysis of drag indicates that the model drag would increase at most a few percent, depending on speed ; corrections for tank size have been made in the model tests. There is no evidence that tank depth has an effect on motion. One reason why tests were conducted in the larger model basin at Escondido, California, and in San Diego Bay was to verify that there were no significant effects of tank size on performance. The results on the 11-foot model at NSRDC showed essentially equivalent results. Thus to date, we have seen no significant effect of tank size on the model characteristics

DISCUSSION

Christopher Hook
Hydrofin
Bosham, Sussex, U.K.

This extremely interesting paper by Dr. Lang I must disagree with on the matter of his comparisons as given in Figure 6. If we refer to Figure 14 of the Silverleaf 42nd Thomas Gray Lecture (paper) given to the Institution of Mechanical Engineers and entitled "Developments in High Speed Marine Craft" we see that whereas the SES or amphibious Hovercraft shows higher speeds and better η (L/D) values in calm water than the Hydrofoil, this situation is reversed in even moderate sea conditions and we get : Hovercraft η (L/D) = 2 to 3 against submerged Hydrofoils approximately 6, and surface piercing hydrofoils 3 to 6 .

Now since the whole point of the raised platform is to eliminate wave effects as much as possible, it follows that it is unfair to present SES curves based on performances restricted to calm water and progressing right off the graph to the right, i. e. to a speed range which is far from having ever been demonstrated. I am informed on the best authority that until new skirt techniques have been developed, 100 knot speeds remain out of the question.

To be specific, in Figure 6 Dr. Lang appears to claim some 10 knot more speed for a given power than for a hydrofoil but that is not what he claimed verbally in this presentation. Surely there is a mistake here.

REPLY TO DISCUSSION

Thomas G. Lang
Naval Undersea Research and Development Center
San Diego, California U.S.A.

As pointed out by Mr. Hook, vehicle efficiency sould be compared in both calm water and rough water. The objective of the paper, however, was the semisubmerged ship concept ; consequently, full comparisons were not made between hydrofoils and SES.

In regard to Mr. Hook's comment on Figure 6, it should be recalled that all curves in this figure pertain to 3,000-ton vehicles. Conventional hydrofoils of this size are generally considered impractical ; hydrofoil weight tends to be high, and the design Froude number tends to be too low. Design tradeoffs for a conventional 3,000-ton hydrofoil between structures, cavitation, and hydrodynamic drag would tend ro result in reduced hydrodynamic efficiency of the order shown in Figure 6. On the other hand, the value of η L/D for semisubmerged ships, and displacement hulls in general, increase with displacement, for a given speed. This result should in no way detract from the good efficiency exhibited by small, high-speed hydrofoils and their excellent performance in rough water.

* * *

PROPELLER EXCITATION AND RESPONSE OF 230 000 TDW TANKERS

C.A. Johnsson
The Swedish State Shipbuilding Experimental Tank, Göteborg, Sweden

T. Søntvedt
Det norske Veritas, Oslo, Norway

ABSTRACT

In cooperation between Uddevallavarvet AB(UV), the Swedish State Shipbuilding Experimental Tank (SSPA) and Det norske Veritas (DnV) a comprehensive investigation concerning propulsion, cavitation and vibration has been carried out on two 230 000 TDW tanker ships. The results with reference to propulsion, propeller cavitation and erosion have been reported at the 1972 Spring Meeting of the Royal Institution of Naval Architects [4].

In the present report the results concerning vibration are reported. Full scale measurements of propeller induced pressure fluctuations at different positions on the stern, static and dynamic thrust and torque in the shaft, as well as vibratory response in different parts of the structure have been carried out.

In model scale the experiments of primary interest in this connection are the measurements of propeller induced pressure fluctuations in the stern, carried out under cavitating and non-cavitating conditions, the transducers being placed in the same positions as in full scale. These tests were carried out in the new cavitation tunnel at SSPA, allowing the use of the same ship model for the cavitation tests as for

the tests in the towing tank.

The results of the full scale and model experiments for different ship-propeller-configurations (five-and six-bladed propellers, hull with and without stern fins) have been analysed and compared.

Included in the comparison are results of theoretical calculations of the extent of cavitation over the propeller blades, different kinds of shaft vibrations and propeller induced hull pressure fluctuations from cavitating propellers.

I. INTRODUCTION

The ships included in the present investigation are the first two in a series of tankers of about 230 000 tons deadweight, which are to be delivered from Uddevallavarvet AB(UV) within the next few years. The first ship, T/T "Thorshammer", was delivered in December 1969, being equipped with a five-bladed propeller.

The model tests in the towing tank indicated very good propulsive performance, which was confirmed by the results of the speed trials with the first ship.

At the trials with this ship extensive measurements of vibratory response and pressure fluctuations on the hull near the sternpost were carried out by Det norske Veritas (DnV) together with recordings of different kinds of shaft vibrations [1]. The results of these measurements indicated that the levels of the pressure fluctuations registered by some of the transducers were very high ; in addition a loud pattering noise could be heard in the aft part of the ship. The vibration levels recorded were, however, not annoying.

At the docking of the ship, shortly after the trials, erosion was detected on four of five blades. The blades were modified but after one voyage to the Persian Gulf and back, erosion was again observed.

The high level of the pressure fluctuations was attributed to significant development of various forms of unstable cavitation and it was felt that there was a risk that the structure of the stern might be damaged. A proposal was made to fit the ship with streamline fins on the afterbody above the propeller and after extensive model testing of different alternatives in the towing tank the ship was fitted with fins,

as shown in Figure 1, and new full scale measurements of vibrations and pressure fluctuations were carried out [2]. The results of these measurements were promising. The pressure fluctuations, as well as the noise and vibration levels, were lower. Further the service reports confirmed the results of the model tests, indicating no increase of the power consumption. The problem of erosion of the propeller blades was, however, not solved, although some improvement could be noticed.

The main modification applied to the second ship was that fins (somewhat different from those of the first ship, see Figure 1) were fitted during construction. In addition, a six-bladed propeller was fitted, having a radial load distribution different from the original five-bladed design.

Successful trials were carried out with this ship [3]. Further, the new propeller has so far worked without any trouble.

II. SCOPE OF THE PRESENT INVESTIGATION

When the project work was completed it was felt that, if complementary model tests and full scale measurements could be carried out with the second ship, an opportunity had arisen to obtain unique material showing the influence of different modifications on the model as well as on the full scale, whereby investigations concerning the correlation factors for propulsion, vibratory response and cavitation could be made.

Accordingly a research program was e[illegible]ished, which was carried out in close cooperation between Udde[illegible]arvet, SSPA and DnV.

Together with the investigations carried out on the first ship the full scale program included :

1. Speed trials with measurements of propeller thrust and thrust variations (second ship only)

2. Photographing of cavitation patter[illegible]ent propeller loadings and angular blade positions (second sh[illegible]

3. Inspection of the propellers with regard to cavitation erosion

4. Measurement of propeller induced hull pressure variations

5. Measurement of hull vibrations

Corresponding model experiments were carried out, including studies of propeller cavitation behind complete ship models. In addition the model investigations included measurements of wake patterns and static pressure with and without propeller in the towing tank as well as in the cavitation tunnel, special streamline tests and tests with a ducted propeller.

The present report will deal primarily with items 4 and 5 above. The results of the measurements under items 1-3 above were summarized in [4].

III. SHIP AND MODEL CONFIGURATIONS TESTED

The main dimensions of the ships are :

Length between perpendiculars	L_{pp}	= 1020'-0"	= 310.89 m
Breadth	B_M	= 157'-10"	= 48.10 m
Draught, fully loaded condition	T	= 67'-7/8"	= 20.44 m
Draught, ballast condition, fore	T_F	=	10.7 m
Draught, ballast condition, aft	T_A	=	13.0 m
Displacement	260 850 long tons		
Deadweight	228 250 long tons		
Block coefficient	δ_{pp}	= 0.844	
Capacity of cargo oil tanks	10 124 300 cft		
Clean water ballast CT No 3	836 900 cft		
Class Det norske Veritas + 1.A.1.	"Tankskip for oljelast, F, EO."		

Main engine, General Electric steam turbine, 32 420 SHP (metric) at 85 rpm

Model scale 1:43.5

The different ship and propeller configurations tested are summarized in Table 1.

Table 1

Ship			Propeller				
Name	Model No	Fins	Model No	Z	D m	A_D/A_0 %	P/D 0.7 R
Thorshammer	1600-A	Without	P1378	5	8.80	0.58	0.738[2]
	1600-B[1]	With		"			
Norse King	1600-C	With	P1493	6	8.50	0.64	0.795
-	1600-A	Without	P1416a[3]	4	8.25	0.50	1.08

1) Model No 1600-B (Thorshammer) has a slightly different fin (smaller) than 1600-C (Norse King). Model 1600-B was not tested.

2) Refers to the full scale propeller. The corresponding value for the model propeller was 2% lower, i.e. $P/D_{model} = 0.723$.

3) Nozzle propeller. Dimensions of nozzle, $D_{max} = 10.0$ m, $l = 4.13$m.

The two conventional propellers were designed using the vortex theory in accordance with the standard procedure used for merchant ship propellers at SSPA. Different radial circulation distributions were used for the two propellers, resulting in different radial camber and pitch distributions.

IV. FULL SCALE TESTS

IV. 1. Test Equipment and Test Conditions

On the first ship tests were carried out at two different occasions ; at the delivery trials and at trials arranged after the ship had been fitted with stern fins. On the second ship tests were carried out at the delivery trials and immediately after, the test on this ship including photographing of cavitation patterns on the propeller blades. The equipment for taking these photographs is indicated in Figure 1. It is further described in [4].

Speed, Number of Revs and Sea State

Most of the tests were carried out in connection with the speed trials but not at the runs on the measured mile. The speeds for the tests reported here were recorded with the log of the ship, which is not a very accurate method. Accurate registration of the number of revs was, however, carried out in connection with all measurements by using a photoelectric cell, mounted on the shaft. Most of the results in this paper are therefore related to number of revs instead of speed.

In the table below the sea state during various tests is presented.

Sea State during Trials

Ship	Fins	Z	Loading Condition	Wind Beaufort	Sea
Thorshammer	No	5	Loaded		
"	No	5	Ballast		
"	Yes	5	Loaded	2	2
"	Yes	5	Ballast	2-3	2-3
Norse King	Yes	6	Loaded	6	4
"	Yes	6	Ballast	6	4

Vibratory Response in the Structure of the Ship

Vibratory response was registered at about 20 points in the structure (wing tank), engine room and deck house with the use of velocity transducers manufactured by CEC. The positions of these transducers, which were fitted at least at two of the trials, are shown in Figure 1. The fins, when installed were fitted with accelerometers, positioned in the vicinity of the pressure transducers, see below.

Table II

Positions of Pressure Transducers in Full Scale

Ship	Fins	Transducer	Height above base line	Distance from Center line	A P	Side	Working	Corr transd model
			m	m	m			
Thorshammer	No	1	9.12	~0.8	1.2[1]	SB	2)	
		2	9.12	~0.5	0.9[1]	SB	2)	≅ A
		3	9.12	~0.3	0.6[1]	SB	Yes	≅ A
		4	9.12	~0.5	0.9[1]	P	Yes	≅ A
		5	10.12	~0.55	0.9[1]	SB	2)	≅ B
		6	10.12	~0.55	0.9[1]	P	No	≅ B
Thorshammer	Yes	1	11.10[3]	~3.5	10.0	SB	Yes	
		2	13.10[4]	~1.5	5.7	SB	Yes	
		3	11.10[3]	~1.5	5.7	SB	Yes	
		4	11.10[3]	~0.2	3.75	SB	Yes	≈D
		5	9.12	0.3	0.6[1]	SB	Yes	≅ A
		6	10.12	~0.55	0.9[1]	SB	No	≅ B
Norse King	Yes	1	11.10[3]	~0.5	3.3	SB	Yes	
		2	11.10[3]	0	3.3	CL	Yes	= D
		3	11.10[3]	~0.5	3.3	P	Yes	
		4	11.10[3]	~0.5	4.2	SB	Yes	
		5	11.10[3]	0	4.2	CL	Yes	= C
		6	11.10[3]	~0.5	4.2	P	Yes	
		7	9.85	~0.3	0.5[1]	SB	Yes	= B

1) From aft end of stern post at the height considered

2) Not working at fully loaded condition

3) Fin, bottom

4) Fin, top

Pressure Fluctuations in the Afterbody

Measurements of the pressure fluctuations were carried out at different points in the afterbody using semi-conductor strain gauge transducers (ENDEVCO), see Figure 2 and Table II, having a membrane diameter of 8 mm.

The circuits included low pass filters (32 Hz). Accelerometers were fitted to the hull close to the transducers, in order to record the influence of the hull vibrations on the propeller induced pressure field, [28].

Propeller Cavitation

The equipment used for observation of propeller cavitation is described in [4].

Noise Level in the Afterbody

A tape-recorder Tandberg TB 11P was positioned in the aft of the main engine room and in locations adjacent to the propeller (the emergency exit channel).

Thrust, Thrust Variations and Shaft Response were measured by strain gauges (Hottinger) on the thrust bearing fundament and shaft and the signals telemetered to a digital voltmeter (thrust) and a UV-recorder (thrust variations). Aslo this circuit included a low pass filter.

Further, axial shaft resonances were recorded by a spring transducer, working against the flange coupling between propeller and intermediate shaft.

IV.2. Test Results

Vibratory Response in the Structure of the Ship

The results of the measurements of the vibration levels at

different points in the deck house and in wing tank No 5 SB are shown in Figures 3 and 4. The levels are given as amplitudes. In Figure 3 some levels, indicating the degree of unpleasantness, are marked for comparison. They were calculated from the ISSC criteria, based on acceleration, by using the formula

$$y = a/(2\pi f)^2$$

where y = vibration amplitude

a = acceleration, vertical

f = frequency of vibration

The results from the measurements in the wing tank indicate weak resonance at certain shaft speeds. The results of Figure 4 are the largest values measured over the speed range.

The diagrams of Figures 3 and 4 show that the vibration amplitudes in the accomodation spaces were of reasonable magnitude. On the first ship without fins, the amplitudes measured in the wing tank were, however, considerable due to resonance at certain shaft speeds (in general not the normal service speed). Unfortunately no measurements were carried out in the wing tank on this ship, when fitted with fins. From the results of the measurements in the deckhouse at the different occasions it can, however, be concluded that the introduction of fins reduced the vibration level considerably, but that the replacement of the five-blades propeller with a six-bladed one caused no further reduction of the vibration level. (In this connection it should be remarked that the structures of the hull and deckhouse are identical for the two ships apart from the fact that the second ship was fitted with bilge keels).

Pressure Fluctuations on the Hull

The results of the measurements of the pressure fluctuations at different points in the stern are given in Figures 5-6. In Figure 5 the two versions of the first ship are compared at fully loaded and ballast conditions. The results shown were obtained with transducers Nos 3 and 5 respectively, approximately corresponding to measuring point A in model tests. The diagram shows faired mean values of the peak to peak values $2p$, obtained in the way shown in Figure 7, normalised as

$$K_p = \frac{2p}{\rho D^2 n^2}$$

These results show the beneficial influence of the fins and it is further evident that the amplitudes in ballast condition are larger than in fully loaded condition.

In Figure 6 the two ship configurations having five-bladed (first ship) and six-bladed (second ship) propellers are compared, both being fitted with fins. The results were obtained for the transducers 4 and 2 respectively, which were placed at the bottom of the fin, on the starboard side, close to the centerline of the ship. The positions were slightly different for the two ships, as is shown in Table II and Figure 2. The difference is, however, small enough to allow direct comparison of the results.

The positions correspond approximately to measuring point D in model scale. The diagram shows that the pressure fluctuations measured on the two ships are very similar, in spite of the fact that the first ship was equipped with a five-bladed and the second with a six-bladed propeller. In fully loaded condition the six-bladed propeller caused somewhat larger amplitudes than the five-bladed. (The fact that only the second ship was fitted with bilge keels is not considered when making this comparison).

A sample record, obtained at the full scale measurements, is shown in Figure 8.

Propeller cavitation

Some of the photographs taken during the trials with "Norse King" were reproduced and discussed in [4]. In the present report some sketches based on these photographs are given in Figures 14 and 17 together with the results of the measurements of the pressure fluctuations and the corresponding cavitation patterns, obtained at the model tests.

Noise Level in the Afterbody

The noise level in the afterbody of "Thorshammer" is of a transient type, varying directly as the vibratory response in the structure of the ship and the recorded pressure fluctuations. This observation is valid for the ship with and without fins installed.

The noise level onboard "Norse King" is stable (mainly pulses of short duration, occurence frequency equal to blade frequency) in the higher speed range (70-85 RPM).

Mean Thrust, Thrust Fluctuations and Shaft Response

Recordings of mean thrust are presented in [1], [3] and [4]. In Figure 9 results of calculations of the natural frequency in the axial mode for the two ships are shown, assuming different values of the thrust bearing stiffness. As shown in the Figure, the measured natural frequencies for the two cases correspond to almost the same value of the thrust bearing stiffness, indicating that recorded resonances of shaft vibration in the axial mode are predicted with fairly good accuracy by a method now in use at DnV [5]. The vibratory output from the shaft through the thrust bearings is of moderate magnitude for all ship - propeller configurations.

Propeller Blade Erosion

The results of erosion studies in full scale and model scale were given in [4] and will not be discussed in the present report. It should, however, be noted that the eroded areas were similar in model and full scale. Regarding the relative merits of the different configurations, the full scale, as well as the model tests, showed that the area of erosion was not reduced essentially by the introduction of fins on the first ship, but was eliminated by fitting the second ship with a six-bladed propeller of new design. On the propeller of the first ship the erosion was, however, less rapid after the introduction of fins.

V. MODEL TESTS

V. 1. Test Arrangements and Facilities

Cavitation Tunnel

The cavitation tests were carried out in the new, large cavitation tunnel of SSPA. This tunnel, see [6] and Figure 10, is powered by a 1 000 Hp motor and has two interchangeable test sections, one being circular, as the remaining part of the circuit. The other test section, which is of interest in this connection, is of rectangular shape with a breadth of 2.6 m , a height of 1.5 m and a length of about 10 m. The section is covered by a recess in which the ship model is placed. This model is the one used in the towing tank for the self propulsion tests and it is normally made of paraffin wax.

The vertical position of the model is adjusted in such a way that the waterline, corresponding to the level of the free water surface in the towing tank, is flush with the top of the test section. Individually cut wooden plates are then fitted to simulate the free surface, and

the test section and the recess are filled completely with water. Up to now flat plates have been used and no attempts have been made to simulate the wave system around the hull. The maximum water speed is 6.8 m/sec. An electric motor and a strain gauge dynamometer for measuring thrust and torque for the propeller are placed in a watertight cylinder in the model.

Measurement of Pressure Fluctuations on the Hull

For the measurements of the pressure fluctuations differential transducers were used, being of the strain gauge type, manufactured by Statham. The maximum range for the transducers, used at the tests in the cavitation tunnel is ± 25 psi, the natural frequency being about 9 kHz. The diameter of the membrane is 1/4" (6.35 mm). One end of the transducer was connected to the atmospheric pressure.

The signals were amplified and registered on an oscillographic recorder, two channels being used for each transducer. One channel was used for the original signals, on the other a filtered signal was registered, the filter being tuned on the blade frequency. The natural frequency of the galvanometers was 1 650 Hz (original signals) and 400 Hz (filtered signals). For obtaining higher harmonics a frequency analyser (manufacturer Brüel and Kjaer, type 2107) was used. The range 63-2 000 Hz was used, the total sweeping time being 6 min for this range. The band width is about 6% of the frequency registered.

No accelerometer was fitted to the model during the tests as, at earlier measurements of a similar kind, carried out at SSPA, only low levels of the accelerometer signals were obtained.

V.2. Test Conditions in the Cavitation Tunnel

The first condition to be fulfilled in order to obtain reasonable results with regard to cavitation patterns, erosion patterns and pressure fluctuations is to accomplish a realistic wake distribution behind the ship model in the cavitation tunnel. This problem was thoroughly discussed in [4] and it will only be stated here that, if the wake distribution in the towing tank is used as that to be aimed at, the agreement obtained in this case was very good, in particular in fully loaded condition, as is evident from Figure 11. Thus it has been demonstrated at these tests that a representative wake distribution can be realised without incorporating a free water surface. The comparison was made by using ordinary Prandtl-tubes. Recently, when using five-hole spherical pitot tubes on another, similar project, the same degree of agreement was obtained also for the tangential velocities and flow angles.

For these kinds of tests it is further required to define the loading cases for the propeller. In the present investigation two combinations of advance ratio J and cavitation number σ were tested, one corresponding to the values of J and effective wake w_T, obtained from the propulsion tests in the towing tank, the other corresponding to the predicted full scale values of J and w_{TS}. The prediction method used for obtaining the latter values was discussed in [4].

The desired combination of J and σ was realised in the tunnel by using thrust identity with the open water tests.

Most of the tests in the tunnel were carried out at a water speed of V = 4 m/s and an air content ratio of $\alpha / \alpha_s \approx 0.4$, but in some cases these parameters were varied.

Non-Cavitating Flow :

V.3. Test Results, Pressure Fluctuations in Non-Cavitating Flow, Comparison with Theoretical Calculations

In Figure 12 the first harmonics of the pressure fluctuations obtained for the model with fins, fitted with the six-bladed propeller, are shown in fully loaded, as well as ballast condition. Amplitudes, obtained in the following manner, are included in the diagram :

A) Measurements in the towing tank, model speed 1.2 - 1.5 m/sec. Amplitudes registered on oscillographic recorder, original signals. These curves give the mean values over the speed range 11-18 knots.

B) Measurements in the cavitation tunnel, water speed 4 m/sec. J-value = $J_{\text{towing tank}}$. Amplitudes registered on oscillographic recorder, filtered signals. Measuring accuracy about the same as in towing tank.

C) Theoretical calculations, carried out by SSPA. Wake influence considered. Method of calculation described in [7].

D) Theoretical calculations, carried out by DnV. Wake influence considered. Method of calculation described in [8-9].

From the diagram in Figure 12 it can be concluded that the agreement between the measurements in cavitation tunnel and towing tank is reasonably good. Also the agreement between calculation and experiment is satisfactory.

The influence of number of blades and fins on the pressure

fluctuations in non-cavitating flow is demonstrated in connection with the results in cavitating flow, see section 5.6.

Cavitating Flow :

V.4. Measurement of Pressure Fluctuations in Cavitation Tunnel. Variation of Test Parameters, Wall Effects

Apart from the wake distribution the two most important test parameters in the cavitation tunnel are water speed and air content. Both parameters are known to affect the extent of the cavitation. With regard to the air content α/α_s it is plausible that it might affect the damping of the water and thereby the level of the pressure fluctuations registered by the transducers.

In order to investigate this influence, four different combinations of water speed and air content (4 and 5 m/sec, α/α_s = 0.13 and 0.40) were investigated for one propeller - hull configuration (six-bladed propeller, model without fins). From the results, some of which are given in Figure 13, it can be concluded that the influence of these parameters on the amplitudes was considerable for the filtered signals but rather small for the maximum values of the non-filtered signals.

A problem, which should not be neglected in connection with this kind of measurements, is that of wall effect. This has been discussed by Huse in [10], from whom we quote :

> "The pressure signal recorded by the pressure transducers may be split into two parts,
>
> 1) the "direct pressure wave" induced by propeller and cavity, propagating directly to the field point (pressure transducer), and
>
> 2) the reflected pressure wave induced by propeller and cavity, propagating to the field point by one or more reflections at the tunnel walls. "

On the basis of some approximate calculations Huse concludes that for the combination of test section and propeller size used at his experiments

> "wall effects are of minor importance in the case of a non-cavitating propeller and also in the case of cavities of constant

volume during the propeller revolution. The pressure field due to volume variation, however, is reflected from the tunnel walls in such a way that the reflected amplitude may possibly be of the same magnitude or even higher than the direct wave amplitude."

In fact, for one of the field points investigated, the calculations gave reflected amplitudes 4 times larger than those of the direct pressure wave.

It could be expected that, in the much larger test section used for the experiments reported here, the wall effects are of less importance.

V. 5. Test Results, Comparison with Full Scale

In this paragraph some test results will be given, which illustrate the correlation obtained between the measurements of pressure fluctuations in the tunnel under cavitating conditions and the corresponding full scale results. Analogous problems in connection with cavitation patterns and erosion patterns were discussed in [4].

In [4] it was shown that the erosion patterns as well as the cavitation patterns in fully loaded condition agreed very well in model and full scale. In ballast condition, however, the extension of the cavitation, as observed in the cavitation tunnel, was somewhat smaller than in full scale. Some of these comparisons are shown in Figures 14 and 17 in connection with the comparisons of the pressure fluctuations.

Pressure fluctuations, measured in model scale and full scale, are compared in Figures 14-17. In all the diagrams the following kinds of results are given in non-dimensional form :

A) Model tests, filtered signals, mean values over about 10-20 revs.

B) Model tests, signals obtained without filters, max values during 10-20 revs.

C) Full scale results, max values obtained as shown in Figure 7. This kind of curve should correspond to results according to B for the model. (For the case shown in Figure 16 this kind of value was not available.)

D) Full scale results, mean values obtained as shown in Figure 7.

In Figures 14, 15 and 17 some values of the following kind are also shown :

E) Full scale results, mean values of the first harmonic of blade frequency, obtained from the energy spectrum (with the use of UV recorders, D-Mac curve follower, paper tape and a computer program, estimating the energy spectrum of stationary stochastic processes, see [29].

These results correspond approximately to results of type A from the model tests.

In Figures 14 and 17 also the cavitation patterns obtained in full scale and model scale are shown. The full scale patterns were obtained from photographs taken in connection with the speed trials, the model patterns were sketched directly when observing the cavitation in the tunnel, the position angle for the blade being 20° from upright position for the sketches in Figure 14 and 25° for Figure 17.

From Figures 14-16 it is evident that, in fully loaded condition, the agreement between the pressure fluctuations in model and full scale is reasonably good. This applies to the non-filtered signals as well as to the few cases where a comparison was made for the filtered signals. In ballast condition, however, the amplitudes were lower during the model tests, which seems to be due to the fact that the extension of the cavitation was smaller on the model propeller in this case. When the propeller was run at a lower J (J and σ corresponding to self propulsion tests in the towing tank) the level of the unfiltered signals increased, however, to values reasonably close to those measured in full scale.

V. 6. Test Results. Comparison between Different Propeller-Hull Configurations

In Figures 18-20 the four different configurations are compared in the fully loaded condition. In the diagrams the amplitudes for the measuring point B are shown for three combinations of advance ratio J and cavitation number σ which correspond to three different speeds for the full scale ship. In Figure 20 the cavitation patterns in the blade position 20° from upright are also shown. More detailed cavitation patterns for the propellers in different blade positions are shown in Figures 22-23 for the speed 16 knots.

In Figure 18 the mean values of the filtered signals are given, in Figure 19 the corresponding maximum values. Further the diagram in Figure 20 shows the maximum values of the non-filtered signals.

Examples of different kinds of signals are shown in Figure 21 for some of the runs (results from the frequency analyser are also included).

In Figure 18 the results obtained at atmospheric pressure correspond closely to non-cavitating conditions, although limited cavitation was present at some configurations. The diagram shows that, under non-cavitating conditions, the difference between the amplitudes for the different hull-propeller configurations is small.

The diagram in Figure 18 further shows that, if the filtered signals are taken as representative (they should correspond approximately to the first harmonic), the influence of cavitation on the amplitudes of the signals of the five-bladed propeller is very small and independent of the model being fitted with fins or not. Especially in the case of the model without fins the difference between the amplitudes of the five-and six-bladed propeller in cavitating condition is appreciable, in spite of the fact that the cavitation patterns are very similar, see Figures 22-23. This situation is not changed very much if, instead, the maximum values of the filtered signals are compared.

If, however, the maximum amplitudes, obtained without filter, are compared, a more reasonable relation is obtained between the different configurations, see Figure 20. This diagram shows the beneficial influence of the fins for the five-bladed as well as the six-bladed propeller, which has been confirmed in full scale, both by vibration measurements and measurements of pressure fluctuations. Both with and without fins the five-blades propeller is better that the six-bladed, in agreement with the tendency of the corresponding full scale measurements. According to the vibration measurements in full scale the two propellers should, however, be roughly equal.

The amplification of the signals, caused by cavitation, is appreciably higher for the six-bladed than for the five-bladed propeller. The same tendency, although less pronounced, was found at systematic tests carried out at Wageningen, using a dummy model [11]. The maximum amplification factors found at the present tests were 4 (filtered signals) and 17 (max non-filtered/filtered without cavitation).

Apart from being observed from the non-filtered signals, the difference between the five- and the six-bladed propeller can be seen in the diagrams obtained from the frequency analyser, see Figure 21. It is evident that the content of higher harmonics is larger for the five-bladed than for the six-bladed propeller. Results of comparisons of higher harmonics have not been included here as, in several cases, it was difficult to determine the amplitudes with reasonable accuracy.

From the diagrams in Figures 22 and 23 it is evident that the maximum extent of cavitation in different blade positions is rather similar for the different hull-propeller configurations.

The main difference between the cavitation patterns for the five- and six-bladed propellers seems to be that, for the five-bladed propeller, the extension of the cavitation was more fluctuating with time than for the six-bladed. This may be one explanation of the fact that the high pressure pulses from the five-bladed propeller were of such a short duration that they were not manifested on the registrations of the filtered signals. It should also be mentioned that rather small band widths were used when filtering the signals.

The extension of the cavitation was rather similar, whether the model was fitted with fins or not. In spite of this a beneficial influence of the fins could be noted on the amplitudes of the pressure fluctuations.

A type of cavitation, which is regarded as important in connection with fluctuating pressures on the hull, is the so called propeller - hull - vortex cavitation [10]. This type of cavitation was observed frequently during the tests, but to about the same extent for the two propellers. This kind of cavitation was probably present during the full scale trials with the first ship, see [12], but could not be observed on the second ship, when making visual observations in connection with the photographing of cavitation.

VI. CAVITATION PATTERNS AND PRESSURE FLUCTUATIONS, THEORETICAL CALCULATIONS AND COMPARISON WITH EXPERIMENTS

VI. 1. Calculation of Circulation Distributions

Proper results for hydrodynamic loading particulars require the solution of a complicated lifting surface problem. With boundary layer aspects included, the downwash surface integral equation for a twisted wing of finite span should ideally be completely solved.

The importance of obtaining a reliable method for prediction of external loading was strongly emphasized by various authorities some years ago. Research was then initiated in Scandinavia to meet this demand along the following lines of approach : A method of calculation was desired, which should be able to reproduce open water diagrams within experimental accuracy for all relevant values of J . By combining unsteady effects, effects of curved flow and interaction with the inlet wake field one should then be able to simulate experi-

mental results from tests in grid wakes, as well as in the actual behind conditions. Two parallel methods of approach have been outlined :

1. Unsteady lifting line technique
2. Unsteady lifting surface technique

The steady part of 1, i.e. study of open water performance has been completed [13, 27]. For 14 propellers tested the method described in [13] reproduced recorded open water characteristics within experimental accuracy for all values of advance ratio. The method employs results from an experimental study of pressure distribution across a propeller surface [14] as the basic empirical "tool" for obtaining a realistic lift distribution along a lifting line.

Preliminary results from use of 2(unsteady lifting surface theory) for open water work indicate that the method works poorly for off design cases (low advance ratios) [15].

Combined with effects indicated above, the lifting line technique in use at DnV has been advanced to a stage where it has been possible to reproduce the experimental results in behind condition for the relatively few experimental results available. In Figure 24 is shown how both the lifting line and lifting surface technique may work poorly, when interaction between propeller and hull wake field is not considered. The propeller model in question works behind a 220 000 TDW tanker. Clearly, our method of approach, which includes interaction corrections, based on simple continuity of flow, reproduces the experiments "within experimental accuracy" [16].

Local advance ratios, as may be experienced in the tip region of the blade when passing a wake peak, will lead to a significantly nonlinear $C_L - \alpha$ relationship. This effect has been approximated by use of results of experiments for low aspect ratio wings described in [17] and [18].

To decrease the risk for a "happy coincidence to occur" we have performed other comparisons with experiments. Thus in Fig. 25 results from a one-blade dynamometer test are compared with calculated values, obtained by using our approach ; the calculations being based on the nominal wake field and the detailed propeller geometry. As far as we understand, the practical implications of the observations given above, are the following :

1. The wake survey should be performed in the propeller plane of the

towed model - from the shaft CL to at least 1.3 x R (R = propeller radius).

2. It is important to include both the axial and tangential wake field in the analysis.

3. It is possibly necessary to extend the lifting surface theory to include non-linearity and effects of interaction with nearby boundaries.

The resea.ch now initiated will continue in the 1972-1974 period.

VI. 2. Calculation of Radial and Chordwise Pressure Distributions

The corresponding detailed pressure distributions are then found, applying a method presented in [14] and [19] and briefly outlined in Appendix A. In Figures 26 and 27 detailed pressure distributions calculated in accordance with the said appendix are shown to correlate well with Høiby's experiments (see [14], Figure 21, J = 0.1068).

VI. 3. Calculation of Cavity Formation

For the ships considered in this report, the pressure distributions for the propeller blades in upwards vertical position (ϕ = 0) and corresponding extent of cavitation are given as follows :

Figure 28 illustrates the calculated extent of cavitation on the full scale propeller mounted onboard T/T "Thorshammer" with observed erosion on the blades included. In [4] it is concluded that model and full scale erosion patterns are similar (Figures 31-32- corresponding pressure distribution - calculated). Figure 29 gives the observed versus calculated amount of cavitation in loaded condition onboard T/T "Norse King". Figure 30 illustrates a similar comparison in the ballasted condition for RPM = 66, V_S = 12.5 knots. More interesting are the theoretical/full scale correlation and the tehoretical/model correlation presented in Figures 33 and 34 respectively. (Figures 35-36- corresponding pressure distribution). Assuming no scale effect on the cavitation tunnel wake field, we observe that the calculated difference in radial variation of the dynamic pressure relative to the static pressure is actually experienced by visual cavitation observations. Some difficulties reported with exact simulation of velocity, number of revs and tunnel pressure may also explain some of the discrepancies between model and full scale observations.

Details connected with determination of type and extent of cavitation are described in [19] and briefly outlined in Appendix B.

Applying symmetrical hysteresis effect, (although non-symmetrical in the tip region) and assuming that time dependent factors, such as inertia and duration of transient pressure, do not influence the onset of cavitation, a simple "maximum bubble radius" concept has been used to establish the extent of cavitation. Further, it has been assumed that the degree of turbulence of the inlet flow is so large that no laminar separation occurs. Also when ignoring effects of sudden charges of angle of incidence and several other effects, we find that, for several cases considered, the quality of the results obtained, when operating in behind condition, is satisfactory for engineering purposes [19].

The thickness of the sheet of cavities at 0.95 r/R is found by estimating the height of the tip vortex, as described in [18]. The radial thickness distribution is then found by linear interpolation, as the radial inception point is already determined. The method is briefly outlined in Appendix B.

VI.4. Calculation of Pressure Fluctuations on the Hull

Finally, in this section we will illustrate how simple mathematical models may be used in this case to approximate the complicated transfer function, giving rise to a fluctuating hull pressure field, during the formation of unstable cavities.

The acceleration potential caused by the cavity formation may be found by solution of the Volterra integral equation, if the formation be accurately represented at any time during growth and collapse. The vapour/liquid mixture representing a pulsating volume cannot be said to constitute a surface of known shape. Consequently, an ideal mathematical model of moderate complexity should be employed, together with empirical corrections found by experiments.

The mathematical model now in use at DnV [20] is described in some detail in Appendix C. The cavitation patterns observed onboard T/T 'Norse King", simulated as shown in Figures 37 and 38, have been used to obtain the results, presented in Figure 39. Clearly, the calculated values for blade frequency pressures on the hull closely resemble full scale values recorded. Also twice blade frequency components, as calculated, correspond approximately with values recorded, see Figure 40.

VII. SUMMARY AND CONCLUSIONS

The most important conclusions to be drawn from the results of the present investigation can be summarised as follows :

1. From the vibration measurements in full scale it can be conciuded that the introduction of afterbody fins lowered the level of the blade frequency hull vibrations. No further improvement seems to have been achieved by replacing the original five-bladed propeller on the first ship by a six-bladed propeller of different design on the second ship. For all configurations the amplitudes were somewhat larger in ballast than in fully loaded condition.

2. The conclusions drawn above were confirmed in general by the results of the measurements of hull pressure fluctuations in different points of the stern, made simultaneously with the vibration measurements. In fully loaded condition the amplitudes of the pressure fluctuations were, however, larger for the six-bladed than for the five-bladed propeller over most of the speed range, the vibration levels being about the same, as mentioned above.

3. Under non-cavitating conditions reasonable agreement was obtained between cavitation tunnel, towing tank and theoretical calculations for the amplitudes of the blade frequency harmonic of the pressure fluctuations. The pressure fluctuations obtained were similar for the different hull-propeller configurations.

4. The amplitudes of the pressure fluctuations in full scale and those obtained in the cavitation tunnel under cavitating conditions showed reasonably good agreement. This applies to the maximum peak to peak values, as well as the first harmonic for the fully loaded condition. In the ballast condition the amplitudes were smaller in model scale.

When judging the relative merits of the five- and six-bladed propellers from the vibration point of view on the basis of pressure fluctuations, measured in the cavitation tunnel under cavitating conditions, the results have to be analysed very carefully. Thus, in the present case, a relation between the different hull-propeller configurations, agreeing with the tendency of the full scale experiences, was obtained only when the maximum peak to peak values were used for comparison. Apparently, the pressure signals, recorded for the five-bladed propeller, were of pulse nature with rather unstable phase shifting. Consequently they did not affect the levels of the filtered signals, obtained in non-cavitating flow.

In the cases considered the amplification of the amplitudes of the pressure fluctuations, caused by cavitation, was larger for the six-bladed than the five-bladed propeller. Results reported in [11] show the same tendency.

5. The type and extension of the cavitation, as observed on the full scale ship (six-bladed propeller) and in the cavitation tunnel, are reasonably similar for the fully loaded condition. In the ballast condition, however, cavitation is more extensive on the ship than on the model propeller.

6. The observed type and extent of cavitation were confirmed with reasonable accuracy by the calculations illustrated in the present paper.

7. The pressure impulses of both blade and twice blade frequency, recorded onboard the ship, correlated well with those calculated with the use of the method developed for the calculation of pressure fluctuations from cavitating propellers.

VIII. ACKNOWLEDGEMENT

The investigation was carried out in close cooperation between the initiator, Uddevallavarvet AB, the Swedish State Shipbuilding Experimental Tank and Det norske Veritas. The work has been sponsored partly by the Swedish Board for Technical Development and partly by the shipyard and the shipowner companies involved, i.e. A/S Thor Dahl, Sandefjord and Odd Godager and Co, Oslo.

The authors would like to express their sincere thanks to all those members of the staffs of the above-mentioned establishments and companies, who have taken part in the investigations and contributed to the analysis of the material.

LIST OF SYMBOLS

A_D/A_0 = developed blade area ratio

C_L = $dL/\frac{1}{2}\rho c\, db\, V^2$ = lift coefficient

C_p = $(p-p_o)/\frac{1}{2}\rho V^2$ = pressure coefficient

c = blade chord

D = propeller diameter

dL = lift of profile

J = V_A/nD = advance ratio for propeller

K_p = $2p/\rho D^2 n^2$ = non-dimensional coefficient for blade frequency amplitude

K_T = $T/\rho D^4 n^2$ = thrust coefficient

k_α = correction factor for ideal angle of incidence, due to lifting surface effect

k_t = correction factor for angle of incidence, due to thickness effect

n = number of revolutions

P = propeller pitch

p = static pressure

p_o = static pressure in undisturbed flow

p_c = cavitation pressure

p_v = vapor pressure

r = radius of propeller blade section

T = thrust

t = maximum thickness of profile

V_A = advance velocity of propeller

V_s = ship speed

w = local wake

w_T = effective wake from thrust identity

x = non-dimensional chordwise coordinate, measured from leading edge

z = number of blades

α/α_s = air content

ρ = density of water

σ = $(p - p_v)/\frac{1}{2}\rho V_A^2$ = cavitation number for propeller

REFERENCES

[1] NESS, L. M., "T/T Thorshammer, Uddevallavarvets b nr 226, Vibrasjonsmalinger", DnV Report No 70-31-0, Oslo, May 1970 (in Norwegian).

[2] JØRGENSEN, Ø., "T/T Thorshammer, Uddevallavarvets b nr 226", DnV Report No 70-46-0, Oslo, April 1970 (in Norwegian).

[3] JØRGENSEN, Ø., "T/T Norse King, Uddevallavarvets b nr 234", DnV Report No 71-20-0, Oslo, Febr 1971 (in Norwegian).

[4] LINDGREN, H., JOHNSSON, C-A., SIMONSSON, E., "Propulsion and Cavitation Investigation on 230 000 tons dwt Tankers - Full Scale and Model Experiments", The Royal Institution of Naval Architects, Spring Meetings 1972, Paper No 8.

[5] "Computer program NV517 : Holzer Tabulation of Axial Vibrations in Straight Marine Shaft Systems"

[6] EDSTRAND, H., "Kavitationslaboratoriet vid Statens Skeppsprovningsanstalt (The Cavitation Laboratory at SSPA)", Swedish State Shipbuilding Experimental Tank Circular No 26, Göteborg 1970 (in Swedish).

[7] JOHNSSON, C-A., "Pressure Fluctuations Around a Marine Propeller. Results of Calculations and Comparison with Experiment", Swedish State Shipbuilding Experimental Tank Publ. No 69, Göteborg 1971.

[8] HUSE, E., "The Magnitude and Distribution of Propeller-Induced Surface Forces on a Single-Screw Ship Model", Norwegian Ship Model Experiment Tank Publ. No 100, Trondheim 1968.

[9] RAESTAD, A.E., "Computer Program NV538 : The Free Stream Pressure Field Induced by the Propeller", DnV Report No 70-22-M, Oslo 1970.

[10] HUSE, E., "Pressure Fluctuations on the Hull Induced by Cavitating Propellers", Norwegian Ship Model Experiment Tank Publ. No 111, Trondheim, March 1972.

[11] VAN OOSSANEN, P., VAN DER KOOY, J., "Vibratory Hull Forces Induced by Cavitating Propellers", The Royal Institution of Naval Architects, Spring Meetings 1972, Paper No 9.

[12] SØNTVEDT, T., "Propeller Induced Excitation Forces", DnV Publ. No 74, Oslo, Jan. 1971.

[13] SØNTVEDT, T., "Theoretical Calculations of Hydrodynamic Loading on the Marine Propeller. Part I. Open Water Performance. Progress Report No. 2", DnV Report No 71-64-M, Oslo 1971.

[14] HØIBY, O.W., "Three-Dimensional Effects in Propeller Theory", Norwegian Ship Model Experiment Tank, Publ. No 105, Trondheim, May 1970.

[15] KUIPER, C., "Unsteady Lifting Surface Theory", Design and Economical Considerations on Shipbuilding and Shipping, Rep of the Post Graduate Course, May 1969, pp 125-149, (Royal Institution of Engineers), Wageningen, Holland 1970.

[16] RAESTAD, A.E., "Estimation of a Marine Propeller's Induced Effects on the Hull Wake Field", DnV Report No 72-3-M, Oslo 1972.

[17] KUCHEMANN, D., "A Simple Method for Calculating the Span and Chordwise Loading on Straight and Swept Wings of any Given Aspect Ratio at Subsonic Speed", Aeronautical Research Council, R and M, no 2935, London 1956.

[18] KUCHEMANN, D., KETTLE, D.F., "The Effect of Endplates on Swept Wings", Royal Aircraft Establishment, Farnborough, Report No Aero 2429, June 1951.

[19] HOLDEN, K., "Type and Extent of Cavitation on Hydrofoils and Marine Propeller Blades", DnV Report No 72-2-M, Oslo 1972.

[20] HOLDEN, K., SØNTVEDT, T., "Propeller Cavitation as a Source to Vibration", DnV Report No 72-5-M, Oslo 1972.

[21] SCHOLTZ, N., "Strömungsuntersuchungen an Schaufelgittern", VDI-Forschungsheft 442, Düsseldorf 1954.

[22] SCHLICHTING, H., "Berechnung der Reibungslosen inkompressiblen Strömung für ein vorgegebenes Schaufelgitter", VDI-Forschungsheft 447, Düsseldorf 1955.

[23] POLLARD, D., WORDSWORTH, J., "A Comparison of Two Methods for Predicting the Potential Flow around Arbitrary Airfoils in Cascade", Aeronautical Research Council, C P No 618, London 1963.

[24] MORGAN, W.B., SILOVIC, V., DENNY, S., "Propeller Lifting Surface Corrections", Trans Society of Naval Architects and Marine Engineers, Vol. 76 (1968).

[25] STRASBERG, M., "The Influence of Air-Filled Nuclei on Cavitation Inception", David Taylor Model Basin Rep 1078, Washington D C, 1957.

[26] JOHNSSON, C-A., "On Theoretical Predictions of Characteristics and Cavitation Properties of Propellers", SSPA Publ. No 64, Göteborg 1968.

[27] HUSE, E., "Hull Vibration and Measurements of Propeller-Induced Pressure Fluctuations", Proc. 12th Int Towing Tank Conference, Rome, Sept. 1969.

[28] DENOOIJ, F.E., "Auto-Correlation Functions and Energy Spectrum of Stationary Stochastic Processes", DnV Report No 69-37-S, Oslo 1969.

[29] WEBER, J., "The Calculation of the Pressure Distribution over the Surface of Two-Dimensional and Swept Wings with Symmetrical Aerofoil Sections", Aeronautical Research Council, R and M, No 2918, London 1956.

* * *

APPENDIX A

CHORDWISE PRESSURE DISTRIBUTION, METHOD OF CALCULATION

From [14] and [19] we have for the contributions to the induced velocities :

1. Velocity distribution due to blade thickness distribution.

$$\frac{\Delta u_t(x,z)}{U_{N0}} = \frac{\tau \cdot \left(S^{(1)}(x) - \mu_T \cdot f(\Omega) \cdot \frac{S^{(2)}(x)}{S^{(7)}(x)}\right) \cdot \cos(\mu_T \Omega)}{S^{(7)}(x)} \qquad (1)$$

$$S^{(7)}(x) = \sqrt{1 + \left[\frac{S^{(2)}(x) + S^{(5)}(x)}{\cos(1-\mu_T)\Omega}\right]^2}$$

$$S^{(1)}(x) = \frac{1}{\pi} \int_0^1 \frac{dz(x')}{dx'} \frac{dx'}{x-x'}$$

$$S^{(2)}(x) = \frac{dz}{dx} \qquad S^{(5)}(X) = \pm \frac{dz_s}{dx}$$

z = profile thickness ordinates

z_s = camber ordinates

$U_{N0} = U_0 \cdot \cos\alpha \cdot \cos\Omega$

Ω = effective skew angle

τ = correction factor due to blade thickness taper

μ_T and $f(\Omega)$ = factors taking account of the effect of the centre section and the tip region

U_0 = resultant inflow velocity = $\sqrt{(\omega r+V_T)^2 + V_A^2 + V_R^2}$

2. Angle of incidence

$$\frac{\Delta u_\alpha (x,z)}{U_{z0}} = \pm \frac{1}{S^{(7)}(x)} \cdot \left(\frac{1-x}{x}\right)^n \cdot \left(1 + \frac{S^{(3)}(x)}{\cos(1-\mu_T)\Omega}\right) \qquad (2)$$

$$U_{z0} = U_0 \cdot \sin\alpha \cdot \cos\gamma$$

$$S^{(3)}(x) = \frac{1}{\pi} \int_0^1 \frac{dz(x')}{dx'} - \frac{2z(x')}{1-(1-2x')^2} \quad \frac{dx'}{x-x'}$$

γ = rake angle

$$n = 1 - \frac{1 - \frac{\Omega\mu_T}{\pi/2}}{2\left\{1 + \left(\frac{a_0 \cdot \cos\Omega\mu_T}{\pi A}\right)^2\right\}^{1/4}}$$

3. Mean Line Camber

$$\frac{\Delta u_c (x,z)}{U_0} = \frac{\gamma_b(x)}{2U_{N0}} = \frac{\mu_T \cdot \tan\Omega}{1+\mu_T^2 \cdot \tan^2\Omega} \cdot \frac{dz_s(x)}{dx} + \frac{1}{1+\mu_T^2 \cdot \tan^2\Omega} \cdot \left(\frac{1-x}{x}\right)^\Theta \cdot \qquad (3)$$

$$\frac{1}{\pi} \int_0^1 \frac{dz_s(x')}{dx'} \left(\frac{x'}{1-x'}\right)^\Theta \cdot \frac{dx'}{x-x'}$$

$$\Theta = 1 - \frac{1}{2\pi} \cdot \arccos \frac{\mu_T^2 \cdot \tan^2\Omega - 1}{\mu_T^2 \cdot \tan^2\Omega + 1}$$

4. Thickness of the Other Blades

The cascade effects are obtained as shown by O. Høiby [14], Scholz [21], Schlichting [22] and Pollard and Wordsworth [23].

$$\frac{u_c(x)}{U_{N0}} = \frac{k_2}{s} \int_0^1 \frac{dz_t(x')}{dx'} \cdot R(\phi, s, x')\, dx' \qquad (4)$$

u_c = chordwise induced velocity

$s = \dfrac{D \cdot \pi \cdot r'}{Z \cdot \text{chord}}$

$r' = 0.825\, r + 0.105$

$k_2 = \dfrac{dC_L}{d\alpha} / 2\pi$

$$R = \frac{2}{\pi} \cdot \left(\frac{x-x'}{s}\right) \sum_{n=1}^{Z/2} \frac{\left(\frac{x-x'}{s}\right) + n^2 \cdot \cos 2\phi}{\left(\frac{x-x'}{s}\right)^4 + n^4 + 2n^2 \cdot \cos 2\phi \left(\frac{x-x'}{s}\right)^2}$$

$\phi = \pi/2 - \psi$

ψ = pitch angle

5. Bound Vortices on Other Blades.

$$\frac{u_p(x)}{U_{N0}} = \frac{1}{U_{N0}} \cdot \int_{r_b}^{1} \sum u'_p \cdot \Gamma(\rho, Z)\, d\rho \qquad (5)$$

u_p = chordwise induced velocity

$\Gamma(\rho, Z)$ = circulation

$$u'_p = \frac{r \cdot \sin\psi(r) \cdot \sin(\phi - \Theta + \delta_k) - (\psi(r)\Theta - \psi(\rho)\phi)\cos(\phi - \Theta - \delta_k) \cdot \cos\psi(r)}{4\pi \left\{ (\psi(r)\Theta - \psi(\rho)\phi)^2 + r^2 + \rho^2 - 2r\rho \cos(\phi - \Theta + \delta_k) \right\}^{3/2}}$$

$\delta k = \dfrac{2\pi(k-1)}{Z}$, $k = 2, Z$, u'_p = chordwise induced velocity due to a bound vortex of unit strength at (δ_k, ρ, ϕ)

The angle of incidence is found from the following expressions :

$$\frac{dC_L}{d\alpha} = \frac{C_L}{\alpha_e + \alpha_i}$$

$$\alpha_e = \frac{C_L}{a} + (2n-1)(\beta_i \cdot 9) - C_L\left(\frac{1}{a} - \frac{1}{a_o}\right) - \int_o^1 \frac{V(x)}{U_{N0}}\, dx \qquad (6)$$

where C_L, β_i and β are obtained from lifting line calculations

$$a = a_o \cdot \frac{\cos \mu_T \Omega}{\sin \pi n_o} \cdot \frac{2n}{1 - \pi n(\cot \pi n - \cot \pi n_o)}$$

$$n_o = \frac{1}{2}\left(1 + \mu_T \frac{\Omega}{\pi/2}\right)$$

$$a_o = 0.9\left(1 + 0.8\frac{t}{c}\right) \cdot 2\pi$$

$$\frac{V(x)}{U_{N0}} = \frac{1}{U_{N0}} \cdot \int_{r_b}^{1} \sum_{k=2}^{Z} V'(x) \cdot \Gamma(\rho, Z) \cdot d\rho$$

$V(x)$ = induced velocity normal to the chord line

$$V'(x) = \frac{-r \cos\psi(r) \cdot \sin(\phi - \theta + \delta_k) + (\psi(r)\theta - \psi(\rho)\phi)\cos(\phi - \theta + \delta_k) \cdot \sin\psi(r)}{4\pi\left\{(\psi(r)\theta - \psi(\rho)\phi)^2 + r^2 + \rho^2 - 2r\rho\cos(\phi - \theta + \delta_k)\right\}^{3/2}}$$

$V'(x)$ = induced velocity normal to the chord line, due to a vortex of unit strength

$$\alpha_i = \beta_i - \beta + \int_o^1 \frac{Vc(x)}{U_{N0}}\, dx$$

$$\frac{Vc(x)}{U_{N0}} = \frac{k_2}{s} \cdot \int_o^1 \frac{dz_t(x')}{dx'} \cdot I(\phi, s, x')\, dx'$$

$V_c(x)$ = induced velocity normal to the chord line due to thickness of the other blades

$$I = \frac{2}{\pi}\left(\frac{x-x'}{s}\right) \cdot \sum_{n=1}^{Z/2} \frac{n^2 \cdot \sin 2\phi}{\left(\frac{x-x'}{s}\right)^4 + n^4 + 2n^2 \cdot \cos 2\phi \psi \left(\frac{x-x'}{s}\right)^2}$$

$$\alpha = (\psi - \beta + \alpha_o) \frac{dC_L}{d\alpha} / \frac{dC_L}{d\alpha_e} - \alpha_o - (\alpha_{i3} - \alpha_{i2})$$

α = effective angle of incidence, corrected for lifting surface effects

$$\alpha_{i3} = \alpha_{i2} \cdot k_\alpha + k_t \cdot \frac{t}{D}$$

where k_α and k_t are found from lifting surface theory [24].

From [14] we quote :

" For a swept wing Weber [30] has shown that a flow parallel to the span must be added, so that the total pressure distribution is given as :

$$C_p(x) = 1 - \left(\frac{V_L(x)}{U_0}\right)^2 - \cos^2\alpha \sin^2\Omega$$

$$V_L(x) = U_0 + \Delta u_t(x) + \Delta u_\alpha(x) + \Delta u_c(x) + u_c(x) + u_p(x)$$

APPENDIX B

CAVITY FORMATION, METHOD OF CALCULATION

1. Extent of Cavitation

When the detailed blade pressure distribution is known, the amount of cavitation may be determined, see [26, 27]

$$\int_{x_1}^{x_2} T_1 \sqrt{\frac{dp}{p}} = k \int_{x_2}^{x_3} T_2 \sqrt{\frac{dp}{p}} \qquad (1)$$

where

x_1 = the point at which the local pressure falls below the cavitation pressure $p_c \sim p_{vapor}$

x_2 = the point at which the local pressure has increased and reached the cavitation pressure

T_1 = the time when $p_{local} \leq p_{cav}$

p = local pressure

dp = $p_{cav} - p$

T_2 and x_3 are found by an iteration process

$x_1 + x_3$ = extent of cavitation

For symmetrical hysteresis k is equal to unity. In the tip region the hysteresis will be non-symmetrical and the factor k is below unity. The radial distribution of k is found from propeller cavitation tests in homogeneous flow, see [26].

2. Thickness

The diameter of the tip vortex obtained when separation takes place at the tip may be determined by the expression

$$\frac{h}{b} = \frac{\alpha - \alpha_s}{2} \cdot \frac{C_T}{\bar{C}} \cdot \frac{1}{A} \qquad (2)$$

where

h = diameter of the tip vortex

b = blade length

α = $\phi - \beta$

ϕ = pitch

β = advance angle

C_T = blade section length at 0.95 R

$\bar{C}$ = mean blade section length

A = aspect ratio

α_s = angle of incidence for separation at tip (relative to β). Based on experiments in [17] $\alpha = 8°$ in this report

The pressure in the centre of the vortex :

$$p_c = p_o - \frac{\rho (\Gamma_F)^2}{8\pi^2 (\frac{h}{2})^2} \qquad (3)$$

p_o = pressure at the radial section close to the boundary of the vortex

Γ_F = $\frac{\partial' \Gamma'_\beta}{\partial r}$. dr free vortex strength

Γ_β = bound circulation

Two cases A and B must be considered :

A. $p_o \leq p_{cav}$

The maximum cavitation thickness will be equal to the tip vortex diameter. The radial thickness distribution is found from observed shapes of thickness along the radius terminating at the radial inception point (calculated or observed).

B. $p_o > p_{cav} > p_c$

The diameter of the cavitating tip vortex is found from the pressure distribution across the tip vortex radius assuming symmetrical hysteresis as outlined in point 1 above.

APPENDIX C

PRESSURE FLUCTUATIONS ON THE HULL, METHOD OF CALCULATION

The velocity potential caused by a pulsating cavity may be found by solution of the Volterra equation if the cavity formation be accurately represented at any time during growth and collapse. The vapour/liquid mixture representing a pulsating volume cannot be said to constitute a surface of known shape. Consequently, an ideal mathematical model of moderate complexity should be employed together with empirical functions found by experiments.

The net velocity potential ϕ at any field point (x_f, y_f, z_f) caused by the small volume source $\Delta r \, \Delta x \, \Delta r$:

$$4\pi\phi = \frac{U_\tau}{d}\frac{\partial x}{\partial t}\Delta\tau\Delta x + \frac{U_r}{d}\frac{\partial \tau}{\partial r}\Delta x\ \Delta r + \frac{U_x}{d}\frac{\partial \tau}{\partial x}\Delta x\ \Delta r + \frac{1}{d}\frac{\partial \tau}{\partial t}\Delta x\ \Delta r + \frac{1}{d}\frac{\partial x}{\partial t}\Delta r\ \Delta\tau + \frac{1}{d}\frac{\partial r}{\partial t}\Delta x\Delta\tau \quad (1)$$

where

d = distance between volume source and field point

$\Delta\tau$ = thickness of volume

Δx = length of volume along helix

Δr = length of volume along radius

t = time

$U_{\tau, x, r}$ = velocity of advance of volume source

The first part of the right hand side of the equation is due to the motion of cavities and derivatives of τ, x and r with respect to time are zero. The last part is due to volume variation of cavities.

For unsteady, irrotational flow the fluctuating pressure p field at a field point :

$$\frac{p}{s\rho} = \frac{\partial\phi}{\partial t} - \frac{1}{2}U^2 \approx \frac{\partial\phi}{\partial t}$$

where

ρ = density of fluid

s = solid boundary factor [10]

U = velocity at the field point, negligible at the hull surface

Assuming $U_r = U_\tau = 0$ and combining eqs. (1) and (2) :

$$\frac{4\pi p}{s\rho} = \left[\frac{\partial}{\partial t}\left(\frac{1}{d}\right)\frac{\partial\tau}{\partial x}U_x + \frac{\partial}{\partial t}\left(\frac{1}{d}\right)\frac{\partial\tau}{\partial t} + \frac{1}{d}\frac{\partial^2\tau}{\partial t^2}\right]\Delta x\Delta r + \left[\frac{\partial}{\partial t}\left(\frac{1}{d}\right)\frac{\partial x}{\partial t} + \frac{1}{d}\frac{\partial^2 x}{\partial t^2}\right]\Delta r\ \Delta\tau + \left[\frac{\partial}{\partial t}\left(\frac{1}{d}\right)\frac{\partial r}{\partial t} + \frac{1}{d}\frac{\partial^2 r}{\partial t^2}\right]\Delta x\ \Delta\tau + \frac{2}{d}\frac{\partial\tau}{\partial t}\frac{\partial x}{\partial t}\Delta r + \frac{2}{d}\frac{\partial\tau}{\partial t}\frac{\partial r}{\partial t}\Delta x + \frac{2}{d}\frac{\partial x}{\partial t}\frac{\partial r}{\partial t}\Delta\tau \quad (3)$$

$$d^2 = (x_f - x_o)^2 + (y_f - y_o)^2 + (z_f - z_o)^2 \quad (4)$$

where

x_o, y_o, z_o = coordinate of volume source

$$\frac{\partial}{\partial t}\left(\frac{1}{d}\right) = \frac{2\pi rn}{d^3}\left[(x_f - x_o)\sin\phi - (y_f - y_o)\cos\phi\right] = e \quad (5)$$

where

n = RPS

ϕ = angular position of volume source

$$U_x \approx 2\pi rn/\cos\beta$$

where β = geometric pitch angle

We assume that the cavity formation at time t displaces a volume of liquid bound by the helicoidal blade surface and the plane P parallel to the shaft (Z_o-axis) (Figure 41).

In accordance with Figure 42 the thickness distribution in the x-direction :

$$\tau(x, r, t) = \tau(r, t) \cdot f(x) \quad (6)$$

Admittingly, the proposed distribution has been designed to suit mathematical interpretation of the extremely complex "shape" of the vapour/liquid formation.

The chordwise extent of the volume at any time when periodicity may be assumed a valid assumption :

$$x_t = x_o + \sum_{m=1}^{\infty} x_m \sin\left[\frac{4\pi^2 n\, mt}{\phi_t - \phi_o} + \Theta_m\right] \quad (7)$$

where

Θ_m = phase angle

n = RPS

m = harmonic order

ϕ_t = angular position for collapse of cavitation

ϕ_o = angular position for inception of cavitation

Dividing equation (3) by n^2D^2 and making use of derived quantities in given eqs. :

$$C_p = \frac{p}{\rho n^2 D^2} = \sum_1^z \left[\int_{r_i}^{r_t} \int_o^{x_t} I_1 \, dx \, dr + \int_{r_i}^{r_t} (I_2 \bar{\tau} + I_4) dr + \int_o^{x_t} (I_3 \bar{\tau}_{max} + I_5) \, dx + I_6 \bar{\tau}_{max} \right] \quad (8)$$

where

$x_{t\,max}$ = max. length of cavity along radius

$\bar{\tau}_{max}$ = max. thickness of cavity along radius

z = number of propeller blades

If we assume that $f = 1$ in equation (6)

$$I_1/K = u_x f' e \bar{\tau} + e \dot{\bar{\tau}} + \frac{1}{d} \ddot{\bar{\tau}} \quad (9)$$

$$I_2/K = e \dot{x} + \frac{\ddot{x}}{d} \quad (10)$$

$$I_3/K = e \dot{r} + \frac{\ddot{r}}{d} \quad (11)$$

$$I_4/K = (u_x + 2 \dot{x}) \frac{\dot{\bar{\tau}}}{d} \quad (12)$$

$$I_5/K = \frac{u_x f' \bar{\tau} \dot{r}}{d} + \frac{2}{d} \dot{\bar{\tau}} \dot{r} \quad (13)$$

$$I_6/K = \frac{2}{d} \dot{r} \dot{x} \quad (14)$$

The expressions for some of the variables in the above equations are finally listed :

$$\ddot{\tau} = -\left(\frac{4\pi^2 n}{\phi_t - \phi_o}\right)^2 \sum_{m=1}^{\infty} m^2 \bar{\tau}_m \sin\alpha \quad (15)$$

$$\ddot{x} = -\left(\frac{4^2 n}{\phi_t - \phi_o}\right)^2 \sum_{m=1}^{\infty} m^2 x_m \sin\alpha \quad (16)$$

where

$$\alpha = \frac{2\pi(\phi - \phi_o)m}{\phi_t - \phi_o} + \theta_m$$

A = aspect ratio of the cavitating body

k = reduced frequency

$$K = \frac{S}{4\pi n^2 D^2}$$

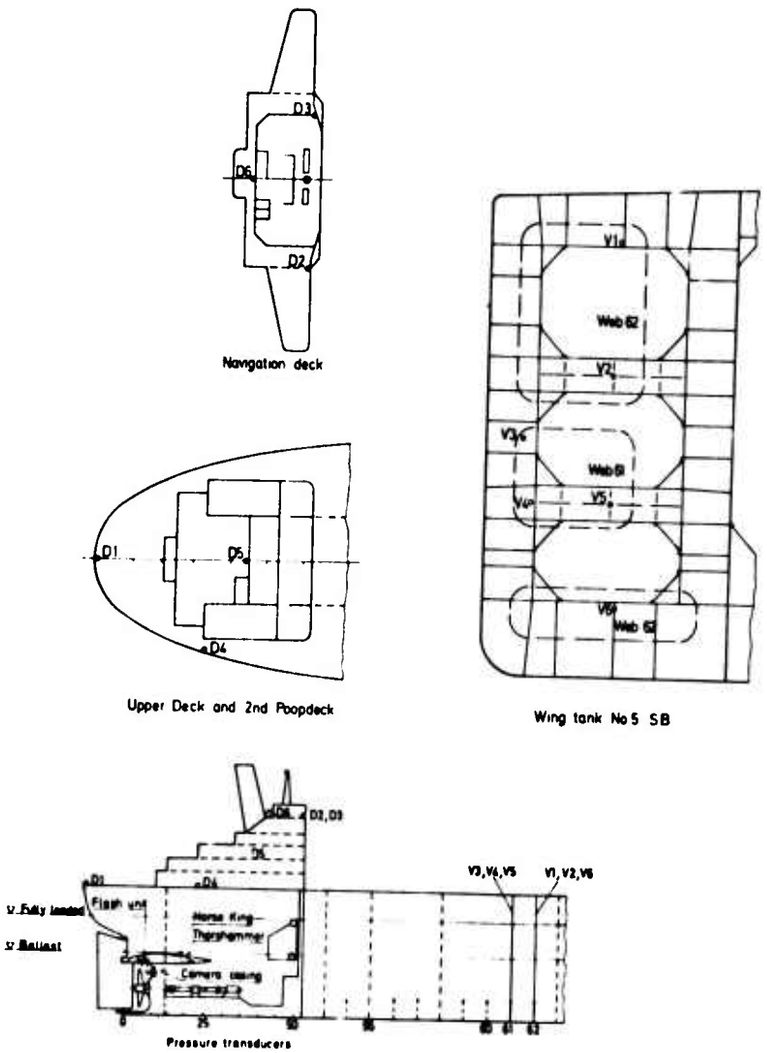


Figure 1 General arrangement and positions of vibration pickups

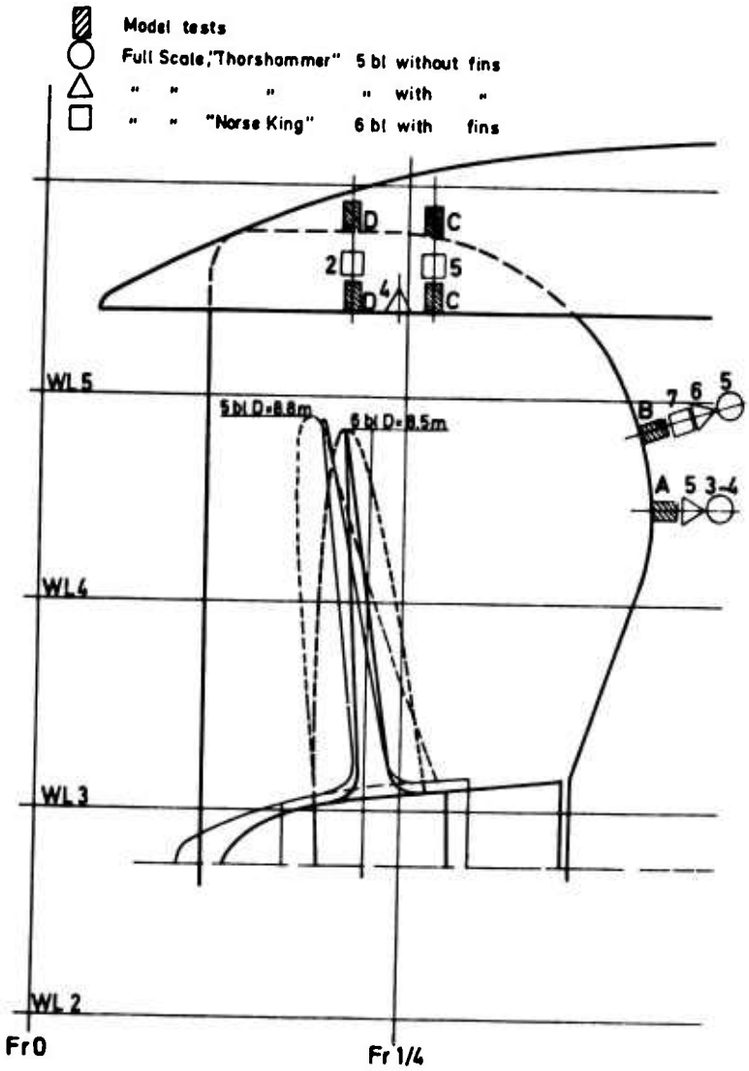


Figure 2 Positions of transducers for measuring pressure fluctuations on the model and full scale ship. For exact positions of transducers in full scale, see Table II. In model tests all transducers in centerline of model

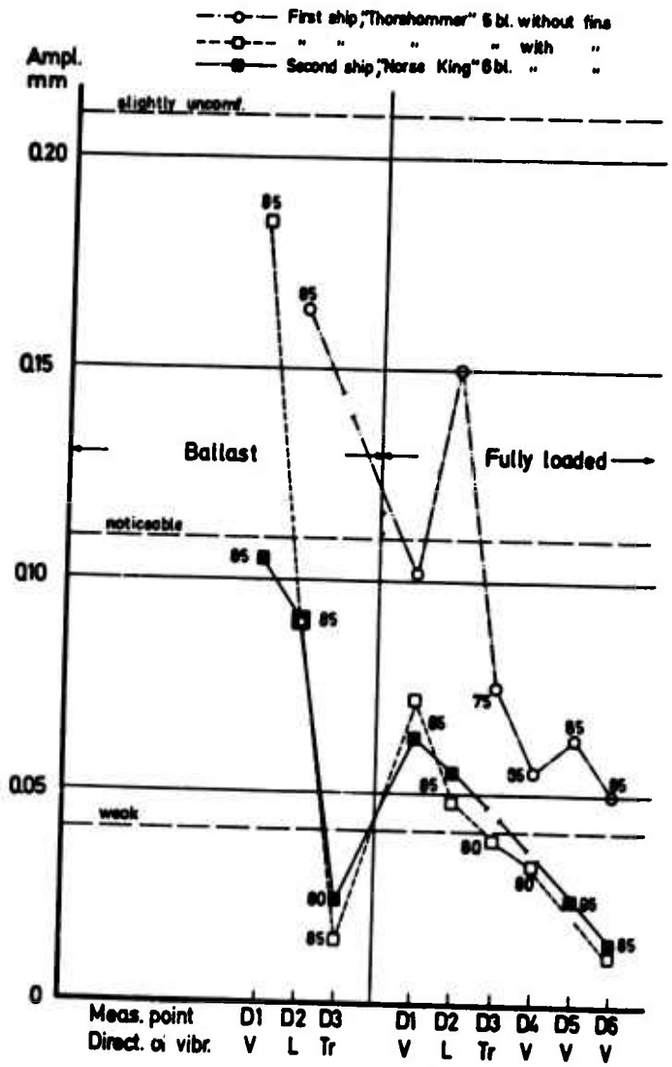


Figure 3 Vibration levels in deck house. For positions of pickups, see Figure 1. Numbers indicate approximate number of revs per min.

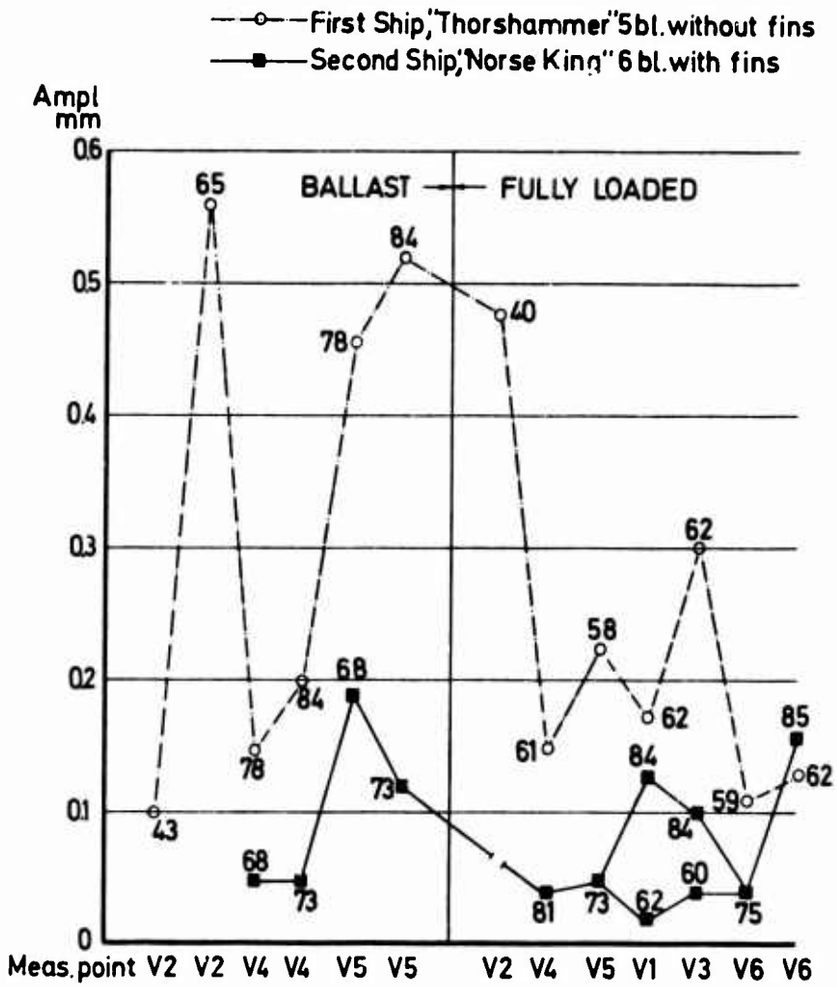


Figure 4 Vibration levels in wing tank No 5, SB. For positions of pickups, see Figure 1. Numbers indicate approximate number of revs per min.

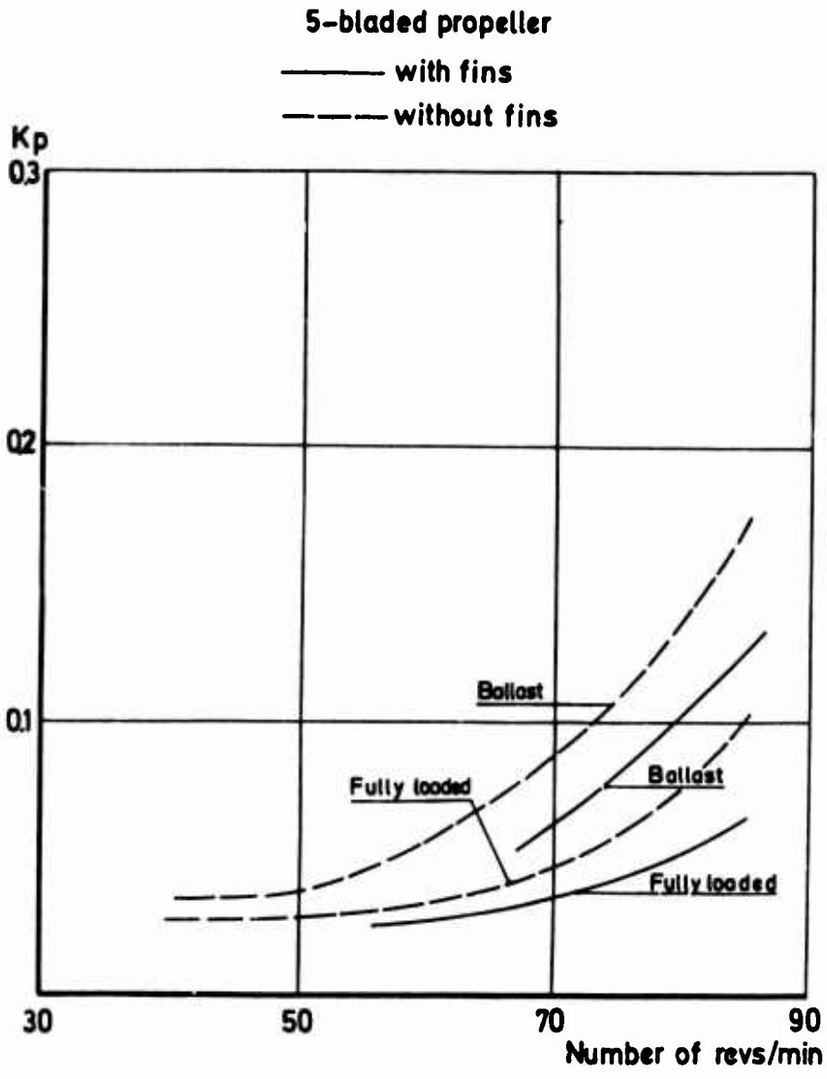


Figure 5 Pressure fluctuations in full scale. "Thorshammer" (first ship) with and without fins. Transducers 3 and 5 resp (measuring point A, see Table II and Figure 2)

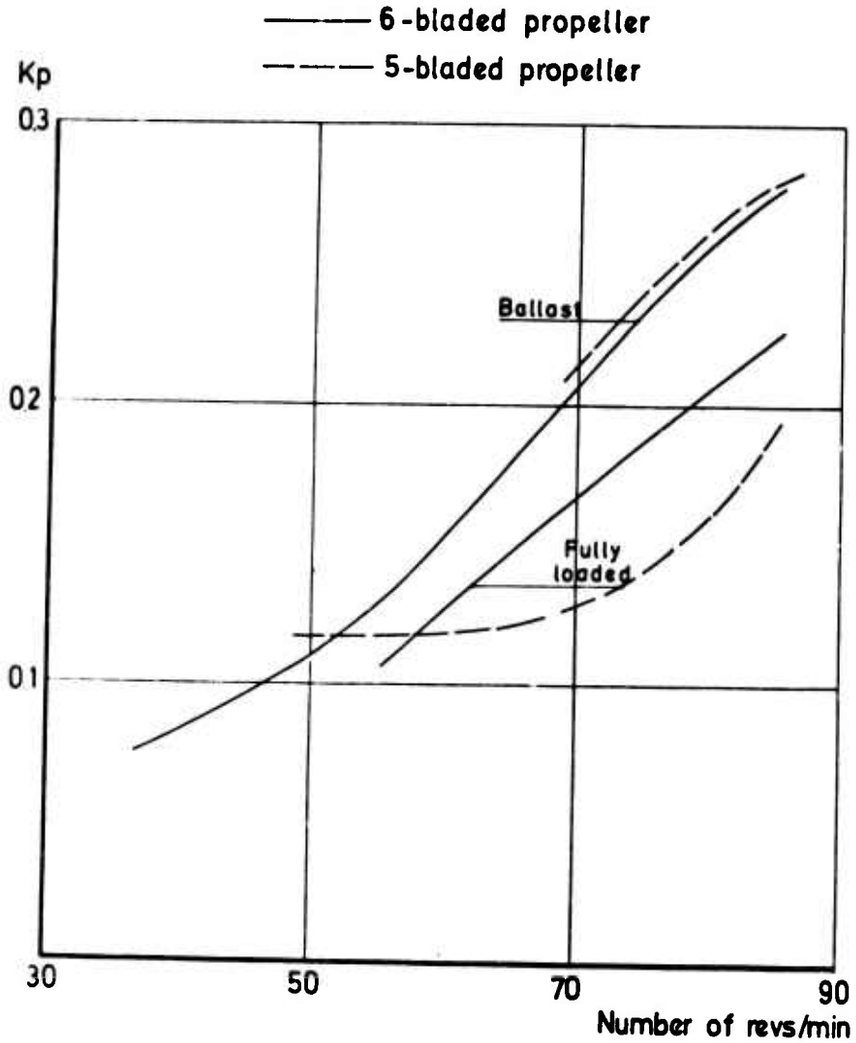


Figure 6 Pressure fluctuations in full scale. First and second ship (5- and 6-bladed propeller) with fins. Transducers 4 and 2 resp (measuring point D, see Table II and Figure 2). K_p-values based on diameter of 6-bladed propeller

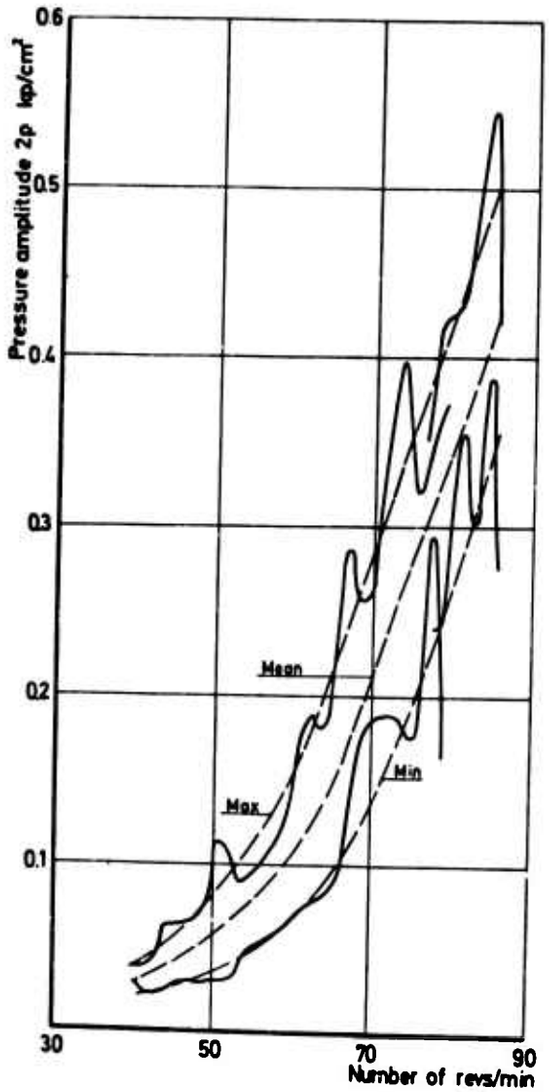
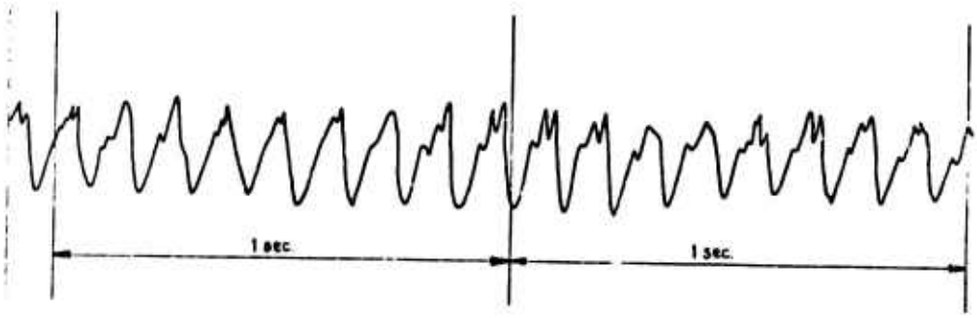


Figure 7 Pressure fluctuations in full scale. "Norse King" (with fins, 6-bladed propeller). Measuring pointD. Ballast condition

T/T "NORSE KING"
BALLAST
RPM = 85.4
VS = 17.8 knots



RECORD FROM SHIP MEASUREMENTS, CELL 2 (D)

ENERGY SPECTRUM

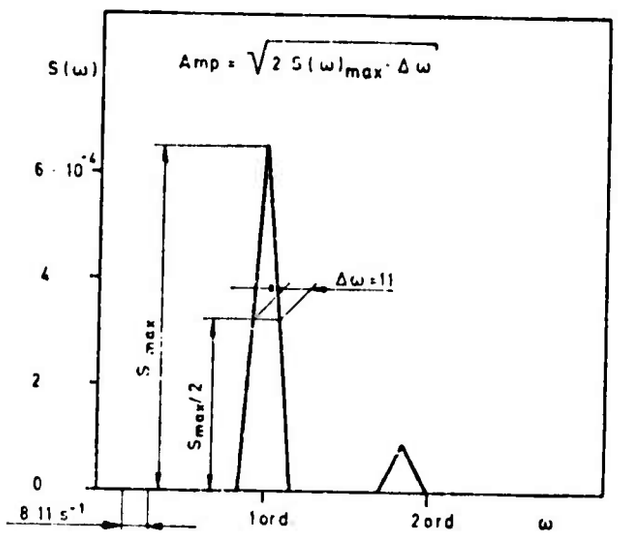


Figure 8 Pressure fluctuations in full scale. Sample of energy spectrum

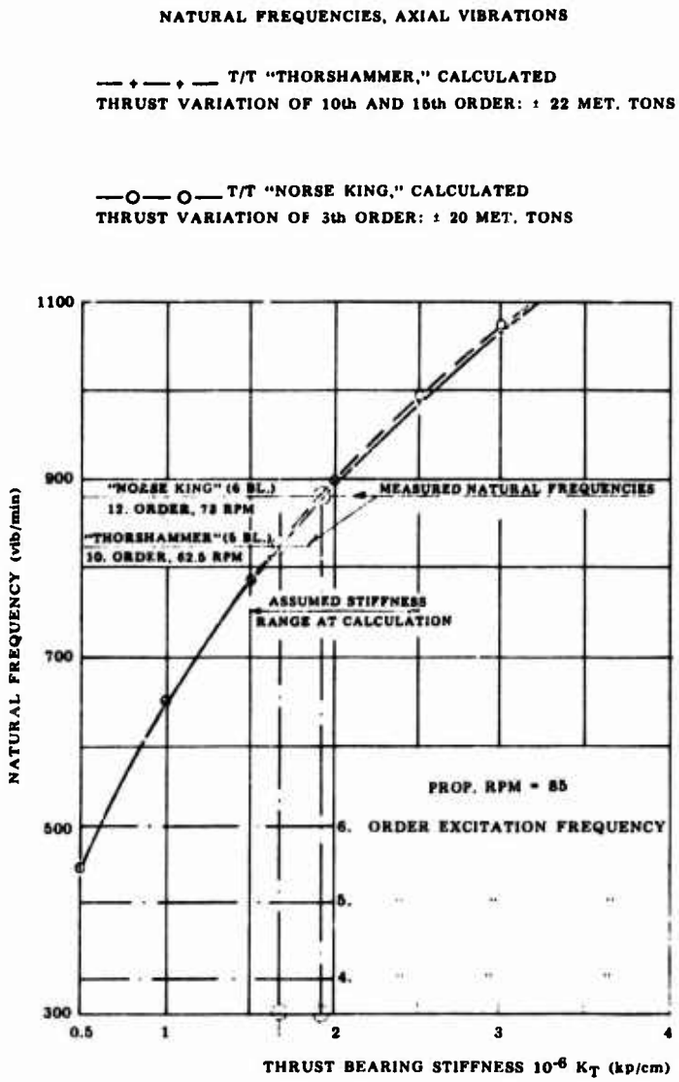


Figure 9 Axial mode of shaft vibration. Natural frequency of actual vibrations

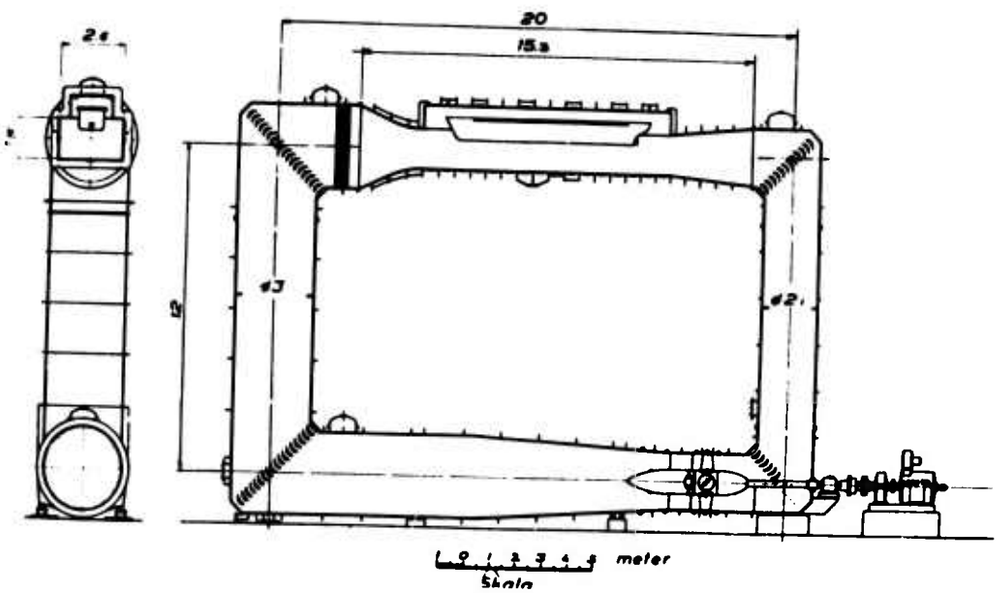


Figure 10 SSPA Cavitation Tunnel No 2. Large test section in place

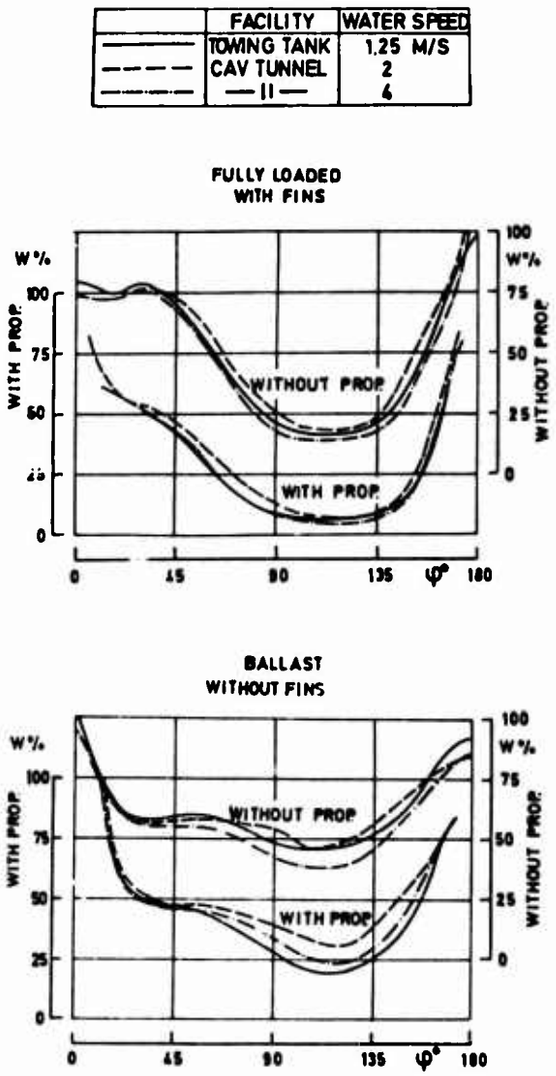


Figure 11 Wake patterns in towing tank and cavitation tunnel

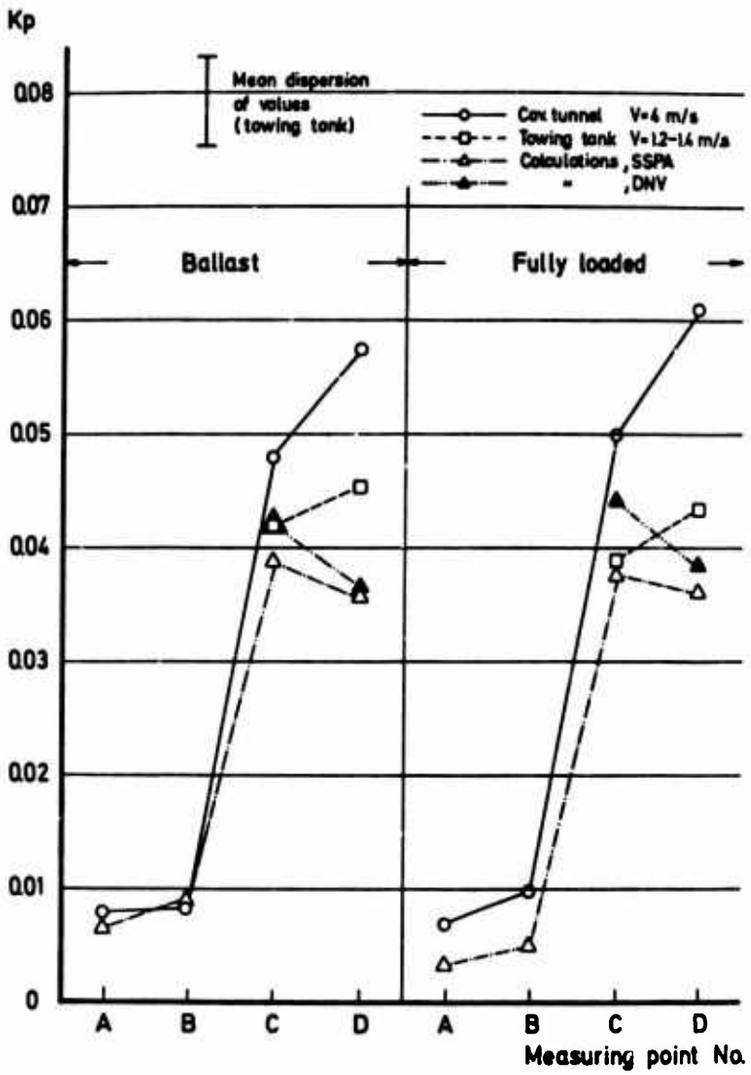


Figure 12 Pressure fluctuations in model scale. Non-cavitating flow. Model with fins, 6-bladed propeller

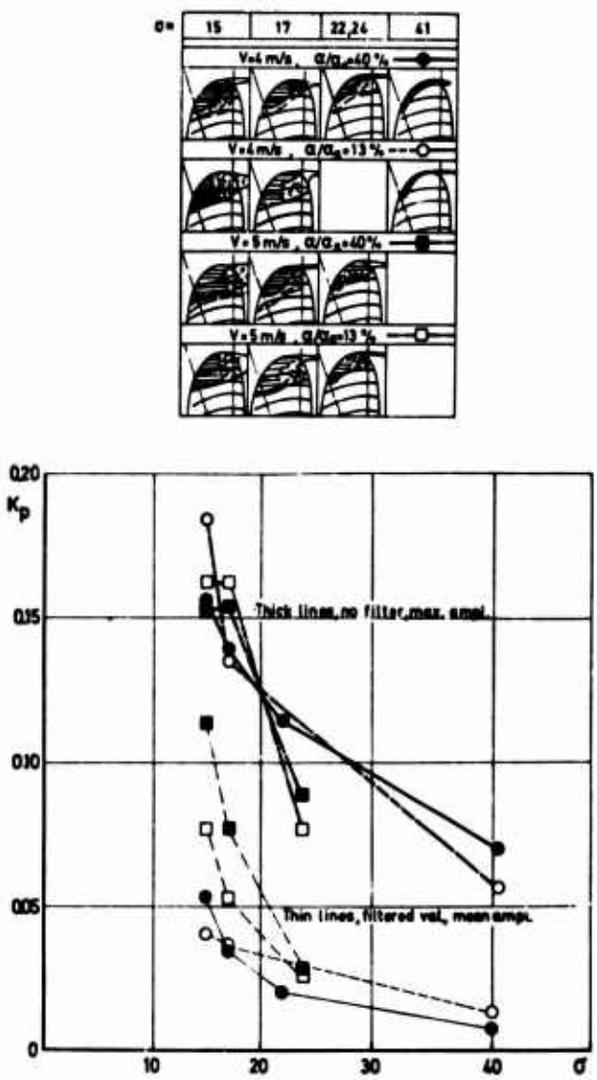


Figure 13 Pressure fluctuations in model scale. Influence of water speed and air content

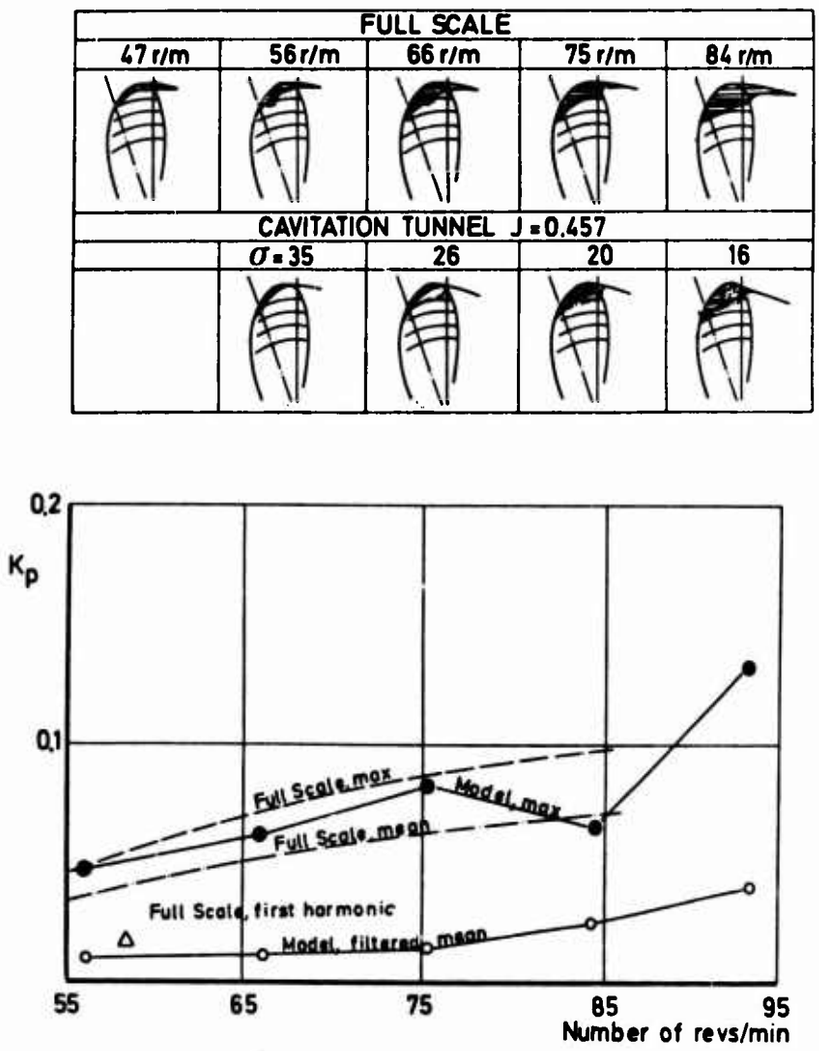


Figure 14 Pressure fluctuations and cavitation patterns in model and full scale. "Norse King (with fins, 6-bladed propeller). Measuring point B, fully loaded condition

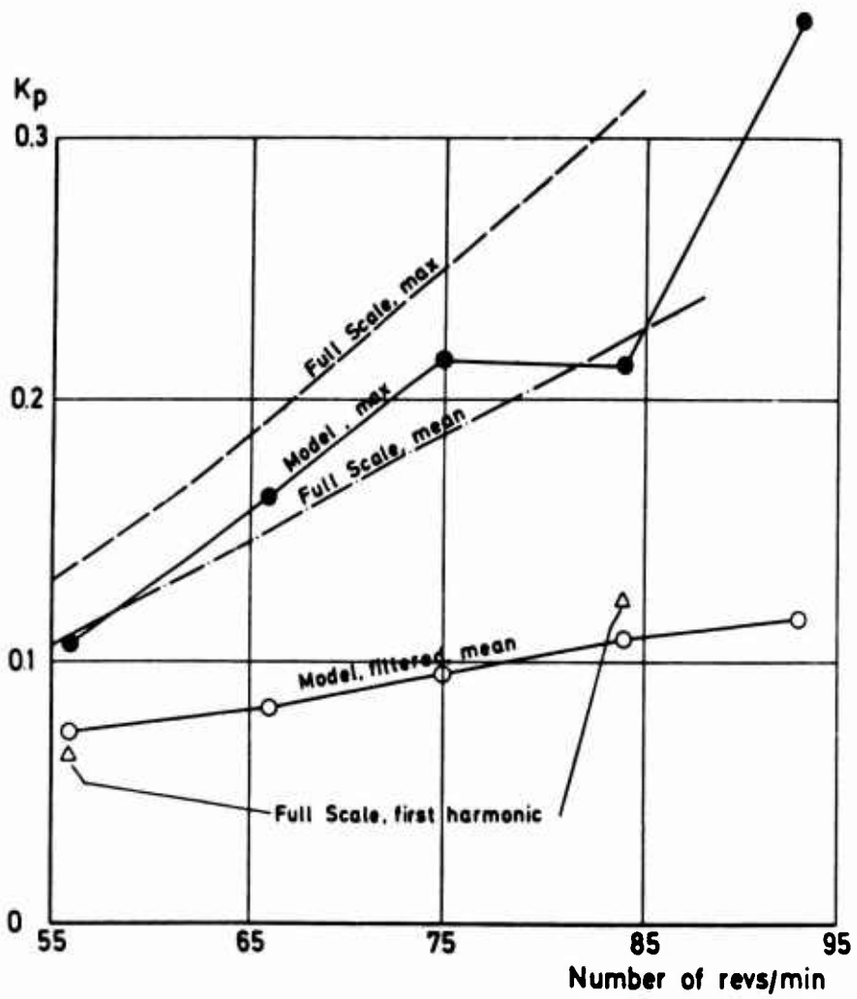


Figure 15 Pressure fluctuations in model and full scale. "Norse King" (with fins, 6-bladed propeller). Measuring point D, fully loaded condition.

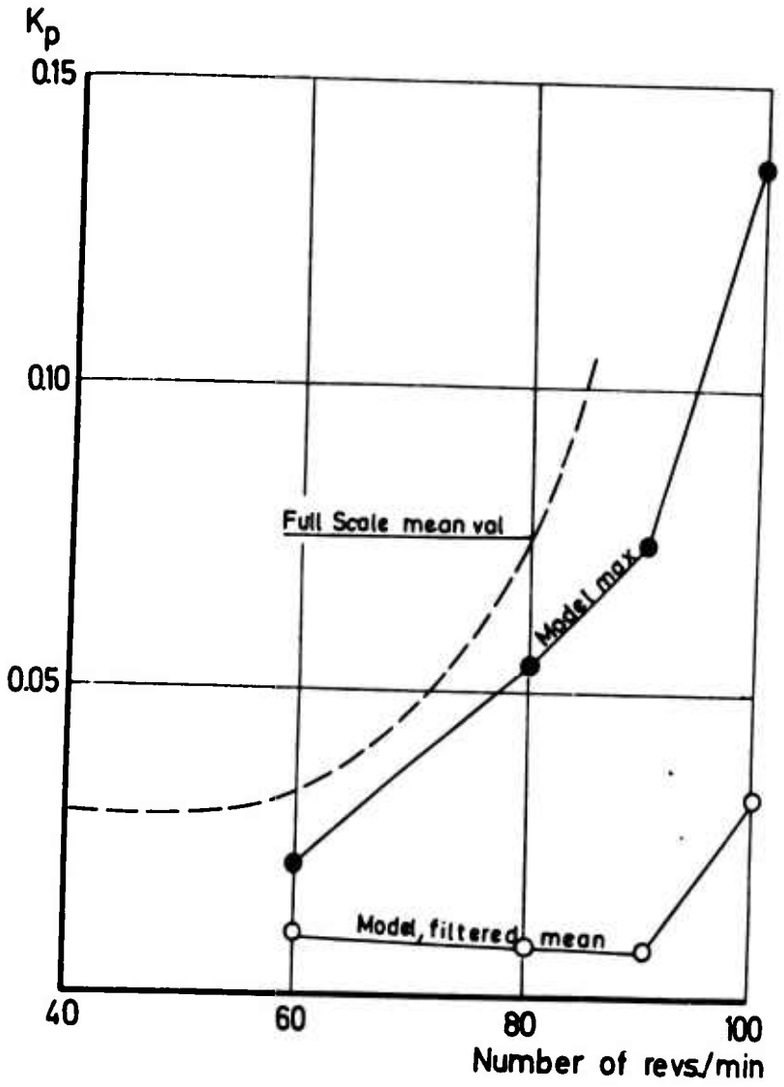


Figure 16 Pressure fluctuations in model and full scale, "Thorshammer" without fins (5-bladed propeller). Measuring point A. Fully loaded condition

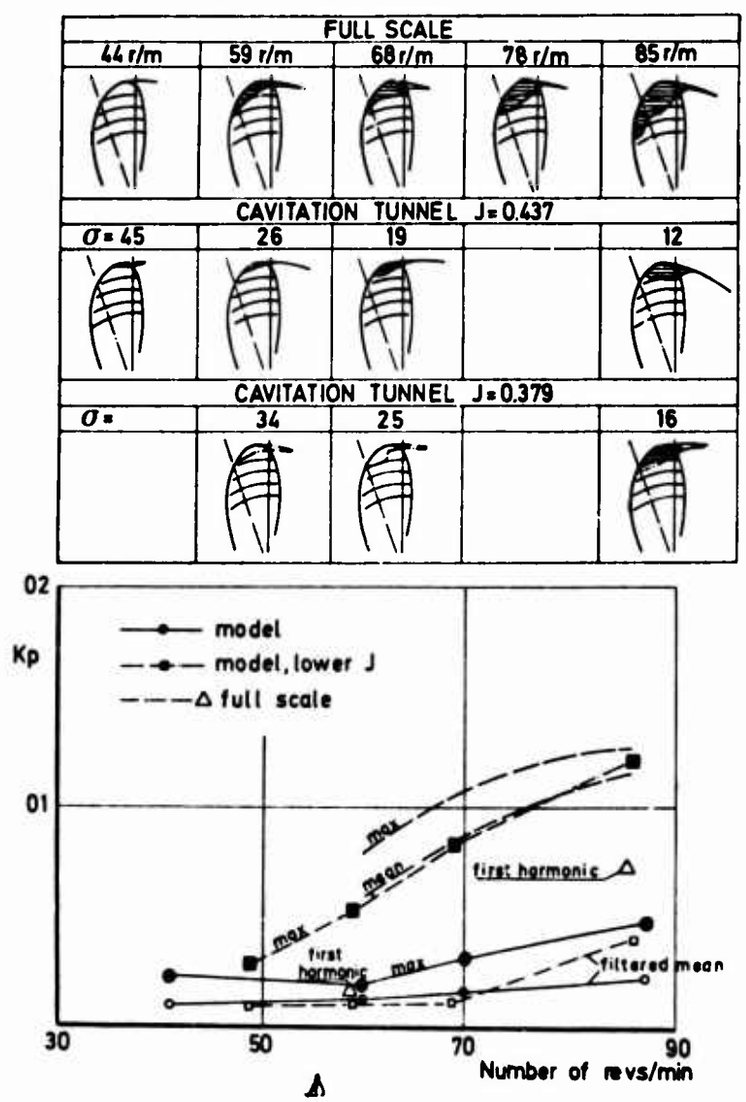


Figure 17 Pressure fluctuations and cavitation patterns in model and full scale. "Norse King" (with fins, 6-bladed propeller). Measuring point B. Ballast condition

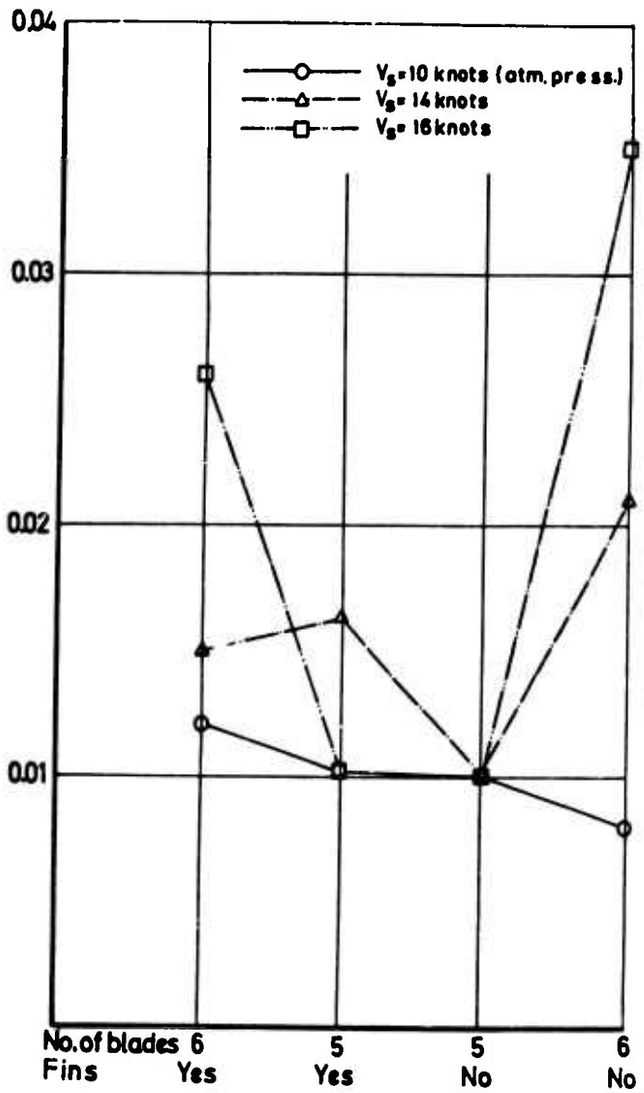


Figure 18 Pressure fluctuations in cavitation tunnel. Different hull - propeller configurations. Measuring point B. Filtered signals, mean values

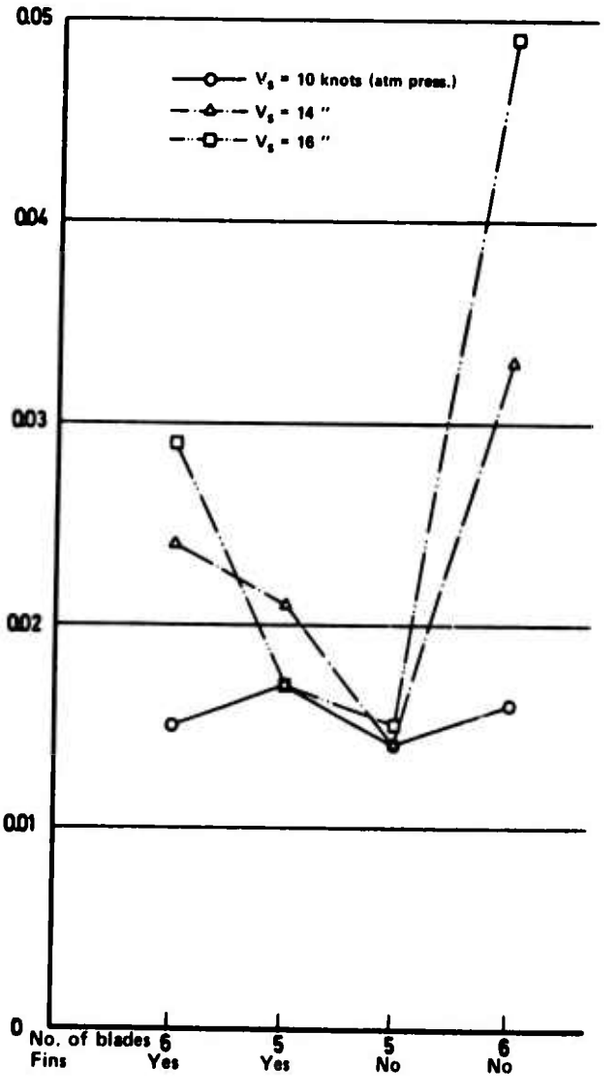


Figure 19 Pressure fluctuations in cavitation tunnel. Different hull - propeller configurations. Measuring point B. Filtered signals, maximum values

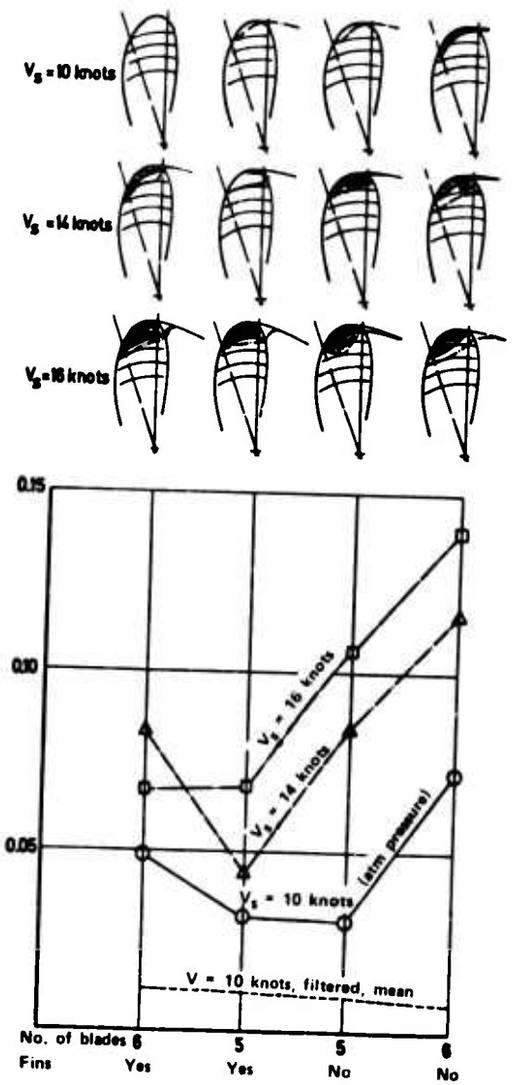


Figure 20 Pressure fluctuations in cavitation tunnel. Different hull - propeller configurations. Measuring point B. Non-filtered signals, maximum values

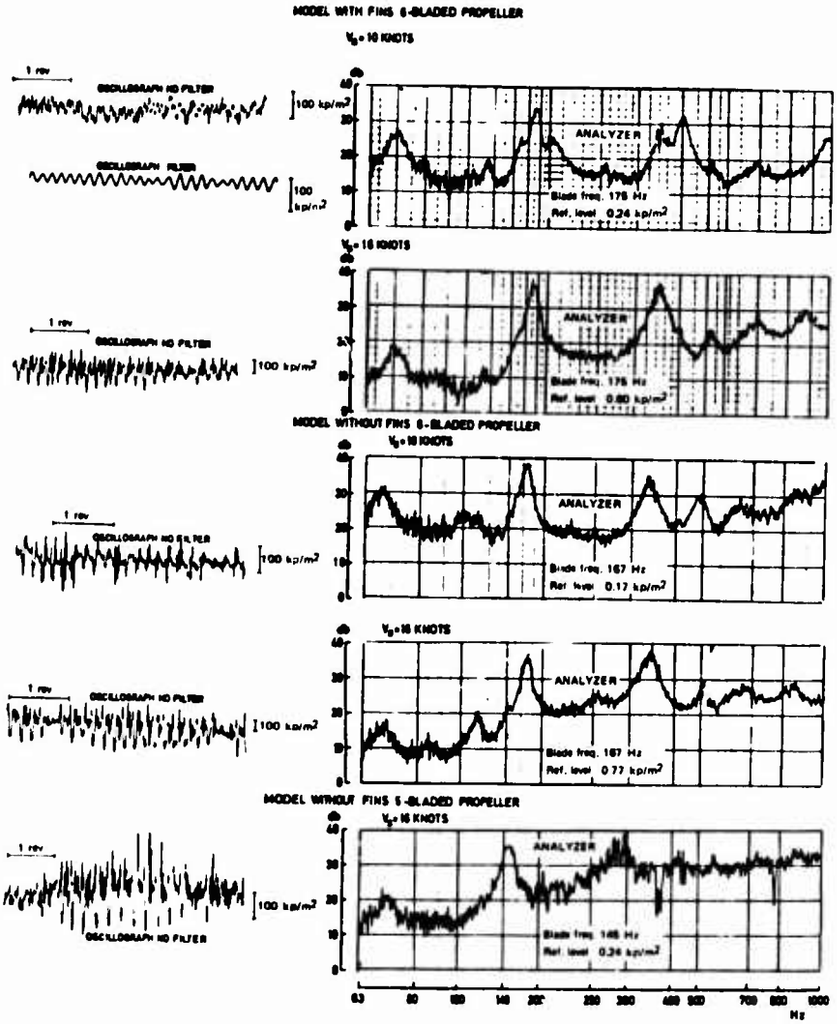


Figure 21 Pressure fluctuations in cavitation tunnel. Different kinds of signals. Oscillographic recorder and frequency analyser

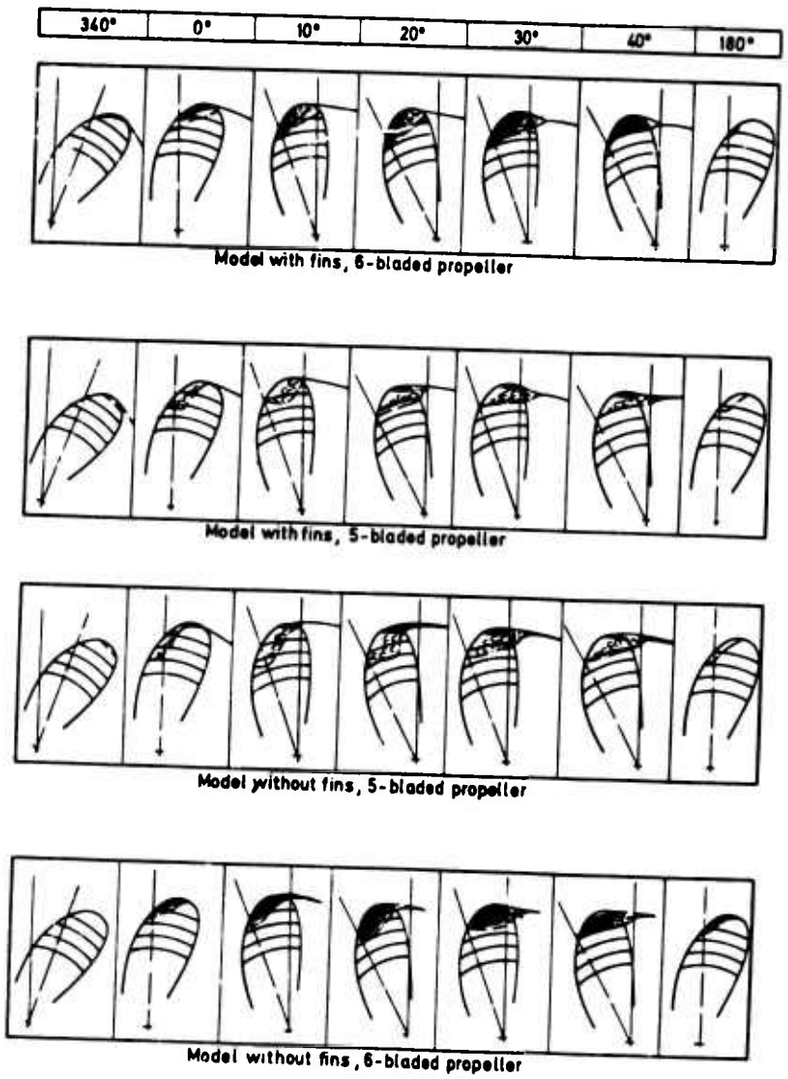


Figure 22 Tests in cavitation tunnel. Cavitation patterns in different blade positions. Different hull - propeller configurations. Fully loaded condition, 16 knots

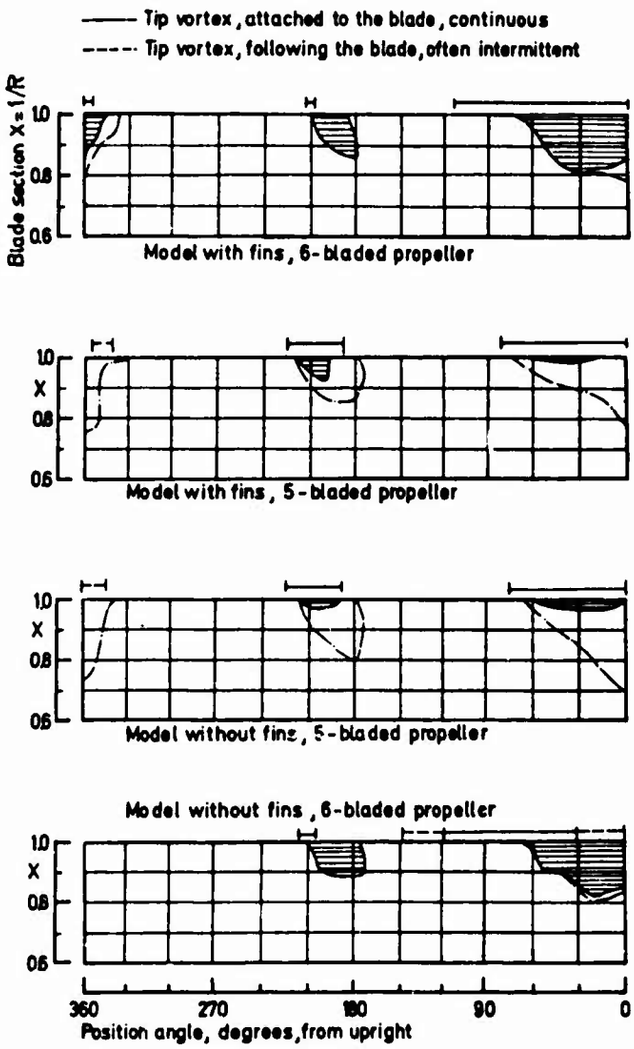


Figure 23 Tests in cavitation tunnel. Radial extension of cavitation in different blade positions. Different hull-propeller configurations. Fully loaded condition, 16 knots

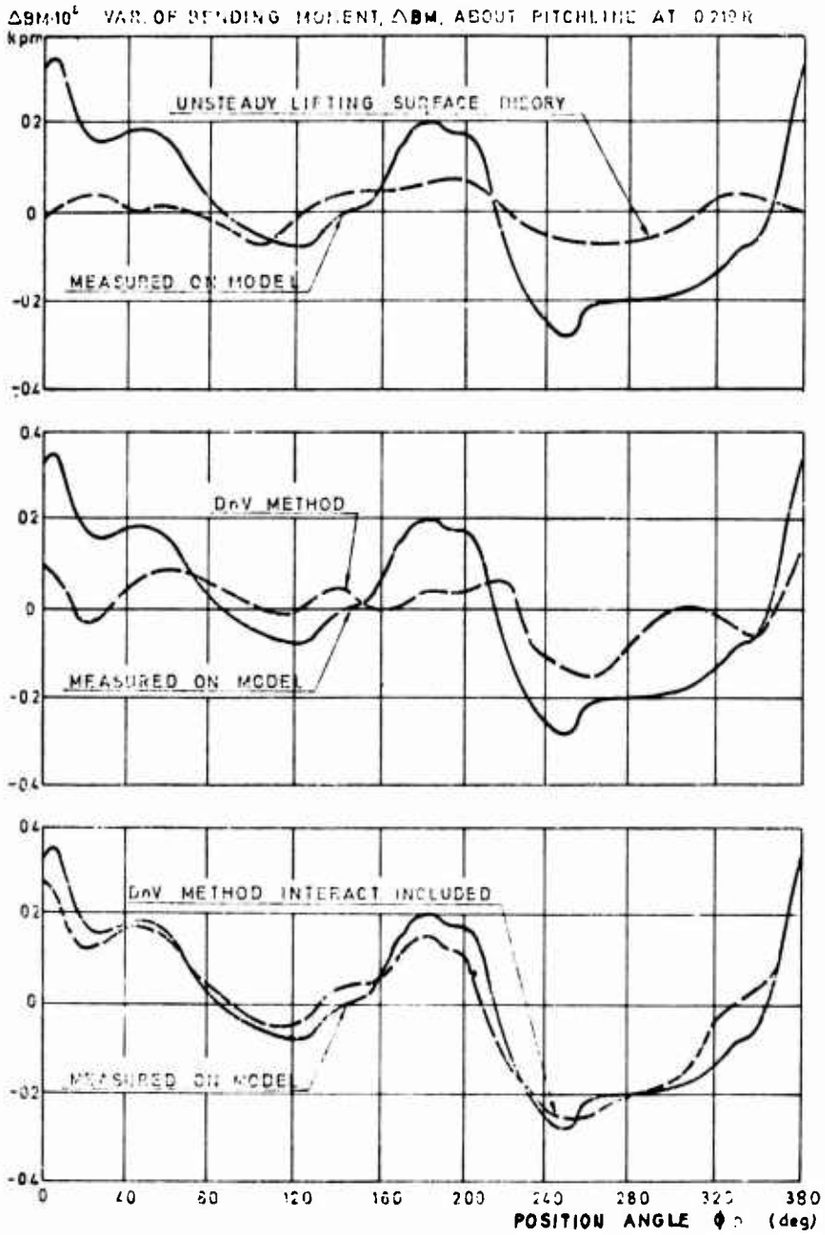


Figure 24 Variation of bending moment on a tanker propeller in a wake. Experiments and calculations

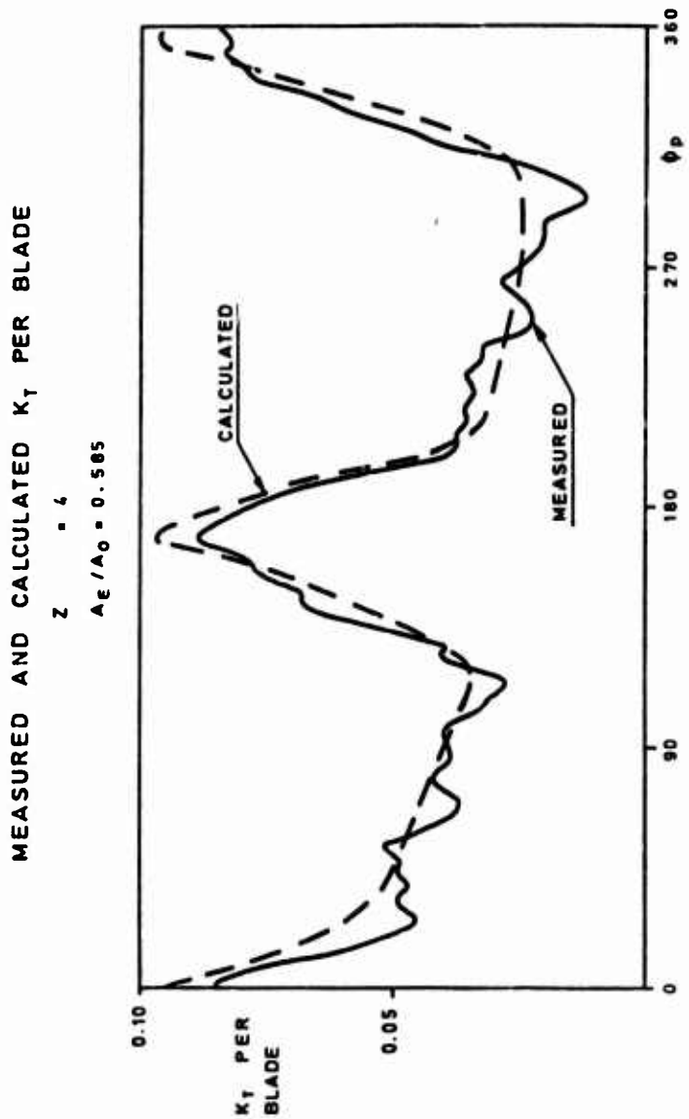


Figure 25 Thrust variation of model propeller in a wake. Experiments and calculations

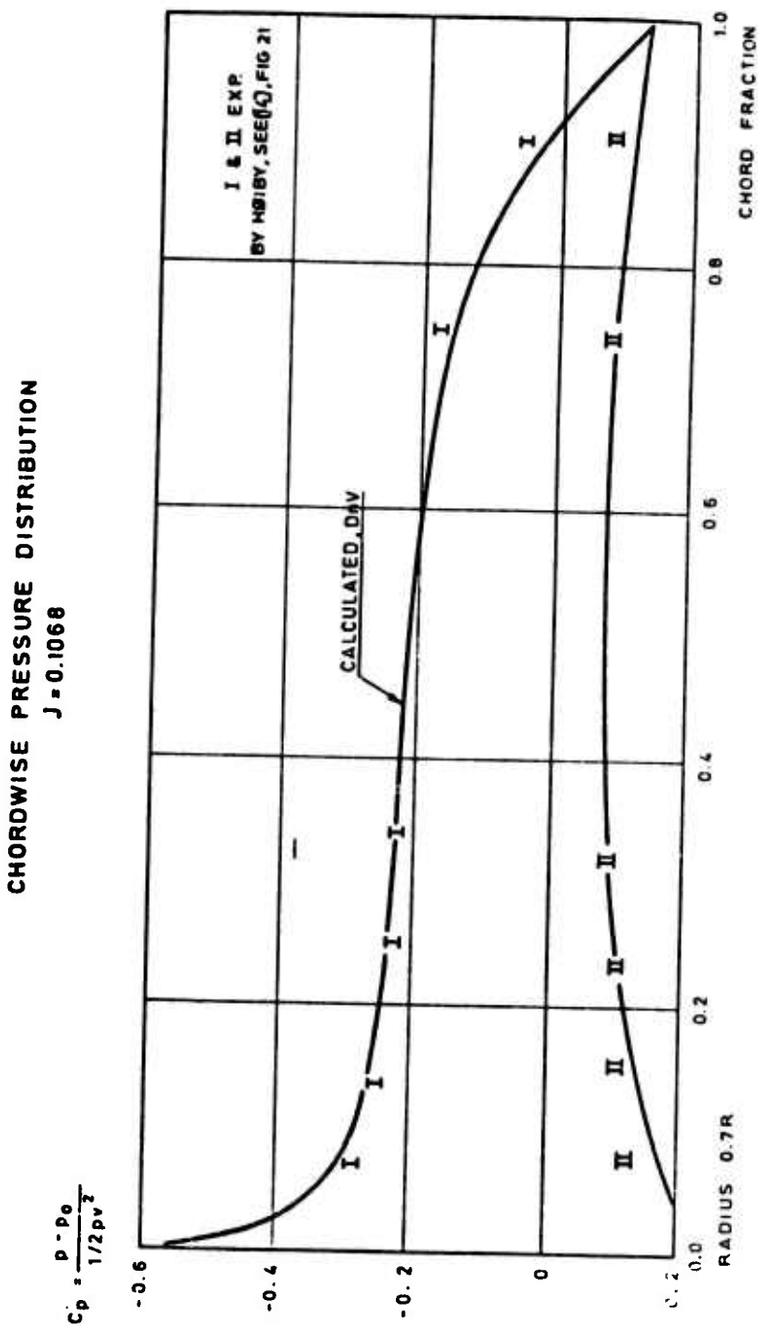


Figure 26 Chordwise pressure distribution of a propeller blade section. Experiments and calculations

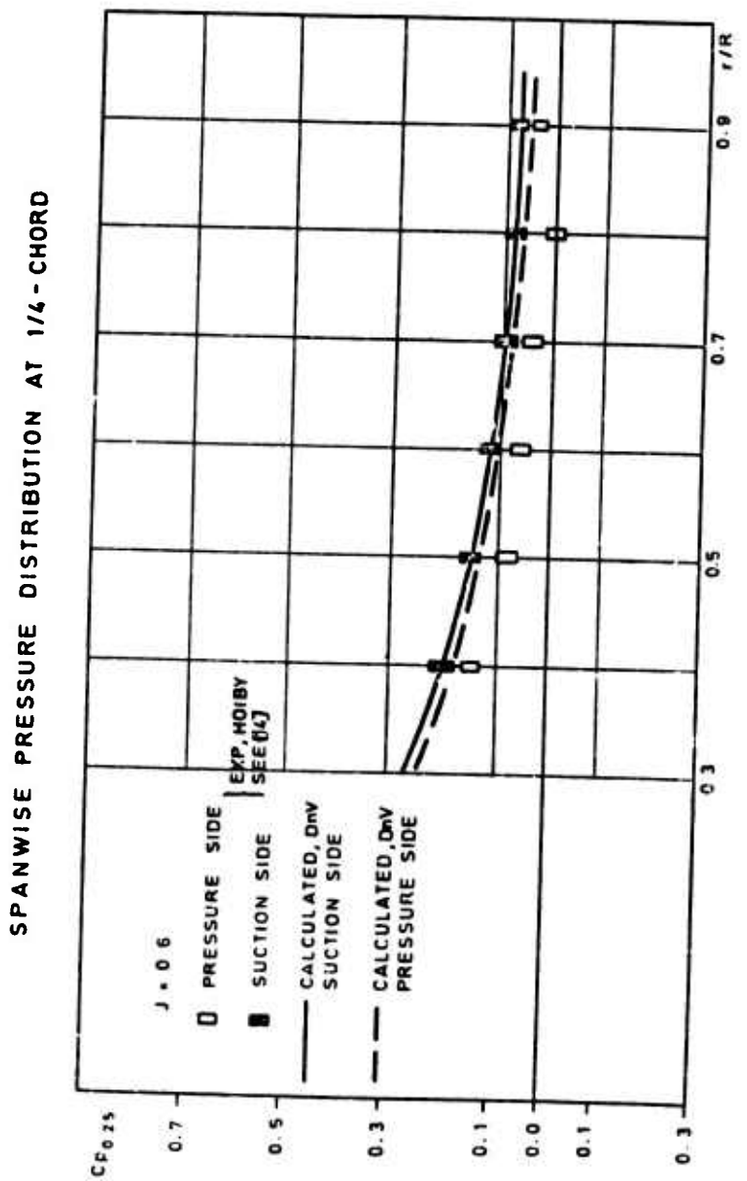


Figure 27 Spanwise pressure distribution of propeller blade. Experiments and calculations

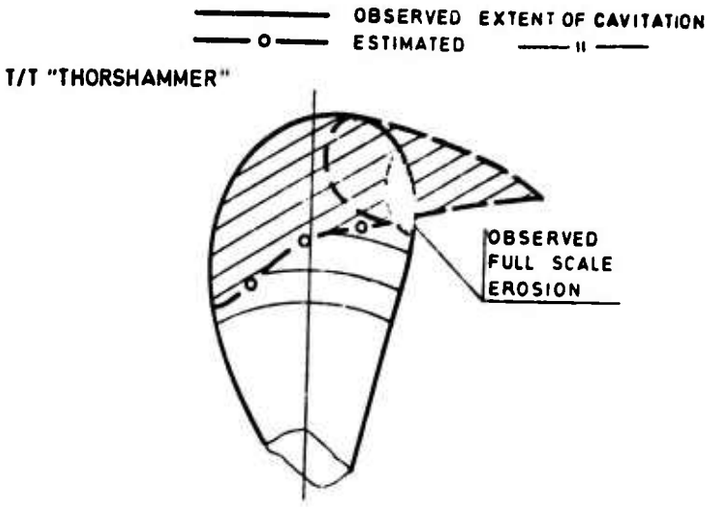


Figure 28 Calculated propeller cavitation
Ballast condition
RPM = 86, V_s = 18.1kts, Z = 5, ϕ = 0°

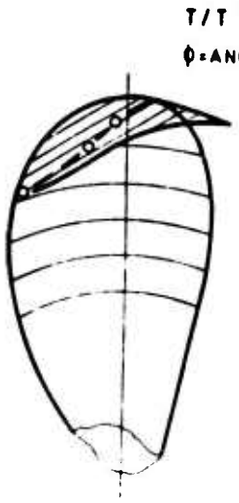


Figure 29
Loaded condition
full scale, 230 000 t.dw
RPM 84.5, V_s = 16.1kts,
Z = 5, ϕ = 0°

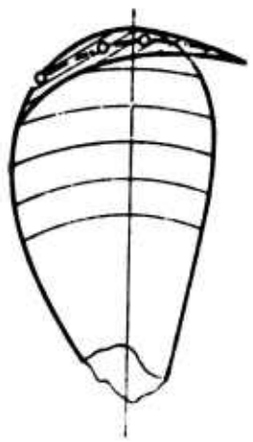


Figure 30
Ballast condition
full scale, 230 000 t.dw
RPM = 66, V_s = 12.5kts,
Z = 6, ϕ = 0°

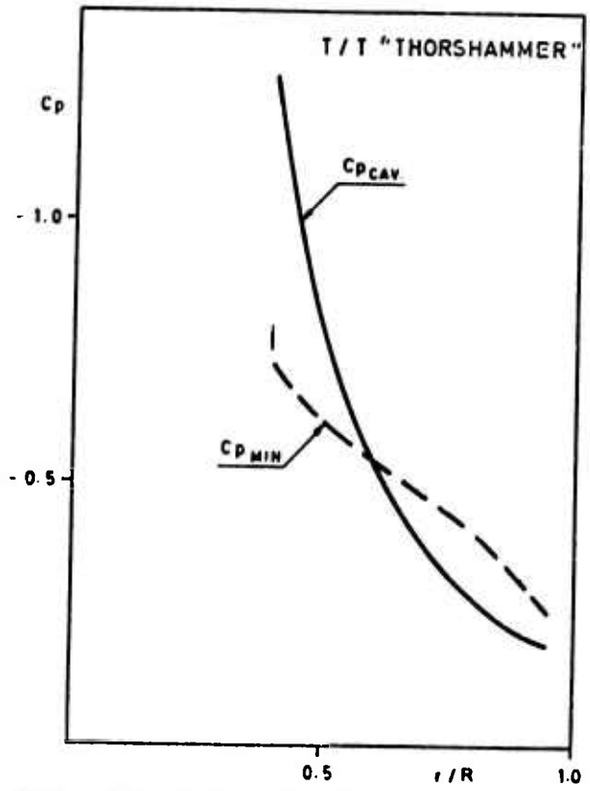


Figure 31 Radial distribution of minimum local pressure versus cavitation pressure (Ø = 0°) corresponding to Fig. 28

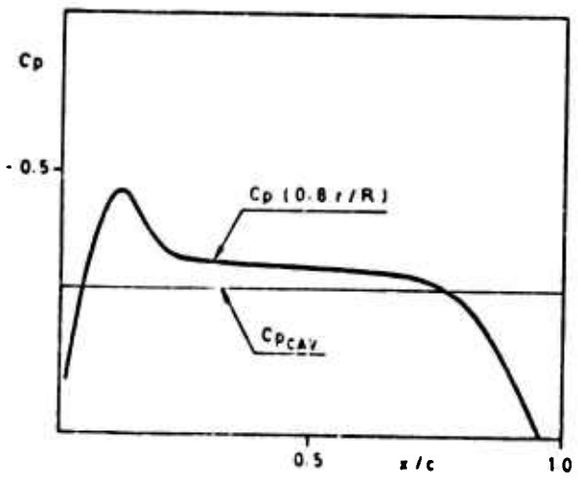


Figure 32 Chordwise pressure distribution at 0.8 R (Ø = 0°) corresponding to Figure 28

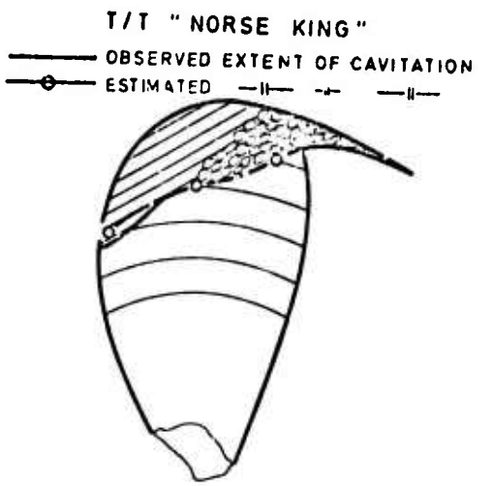


Figure 33 Full scale, ballast condition
RPM = 85.4 , V_s = 17.8 kts , Z = 6 , $\emptyset$ = 0°

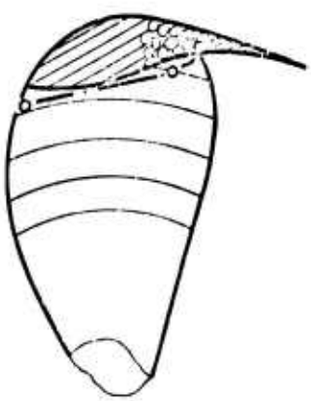


Figure 34 Model, ballast condition corresponding to full scale
RPM = 85.4 , V = 17.8 kts ; Z = 6 , $\emptyset$ = 0°

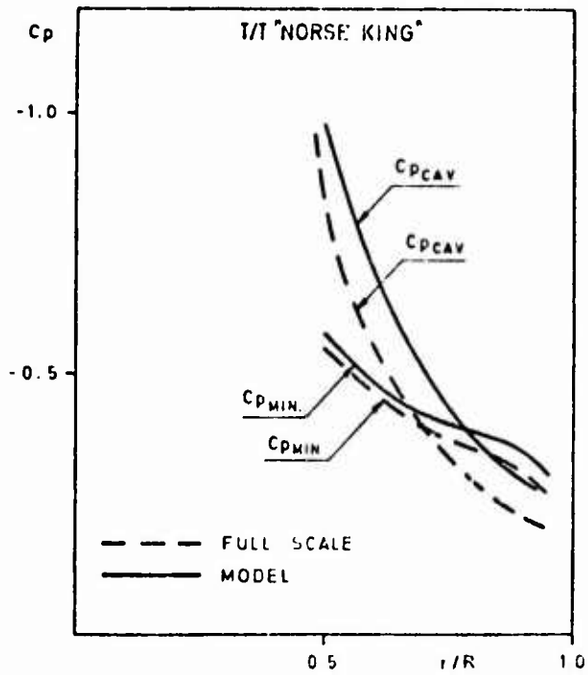


Figure 35 Radial distribution of minimum local pressure versus cavitation pressure (Ø = 0°) corresponding to Figure 33-34

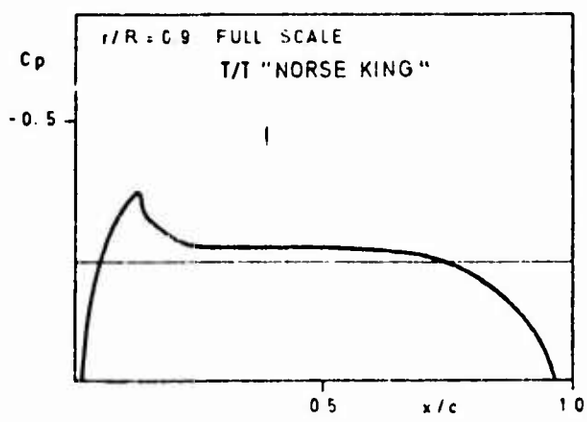


Figure 36 Chordwise pressure distribution at 0.9 R (Ø = 0°) corresponding to Figure 33

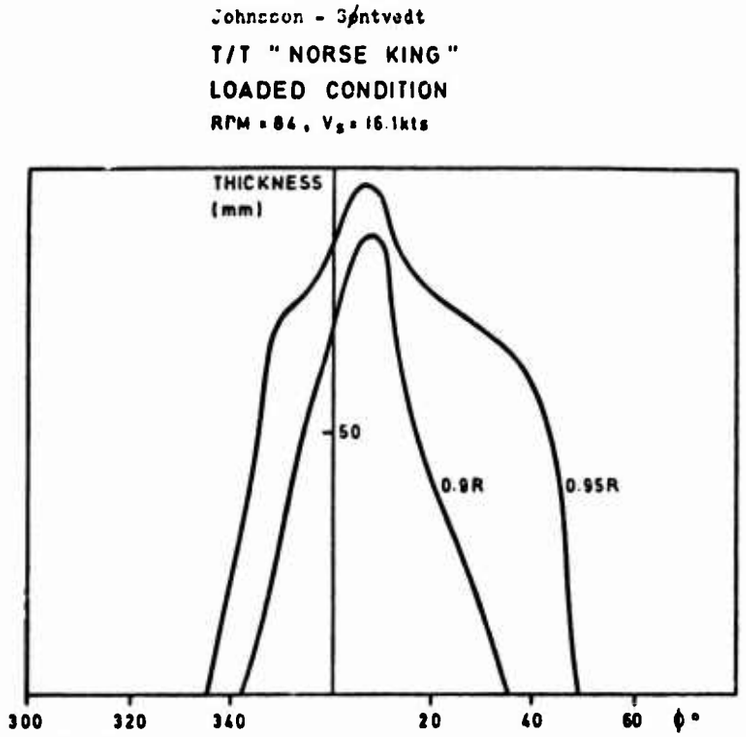


Figure 37 Estimated cavitation patterns. Full scale, fully loaded condition. Thickness distribution of cavitation bubble.

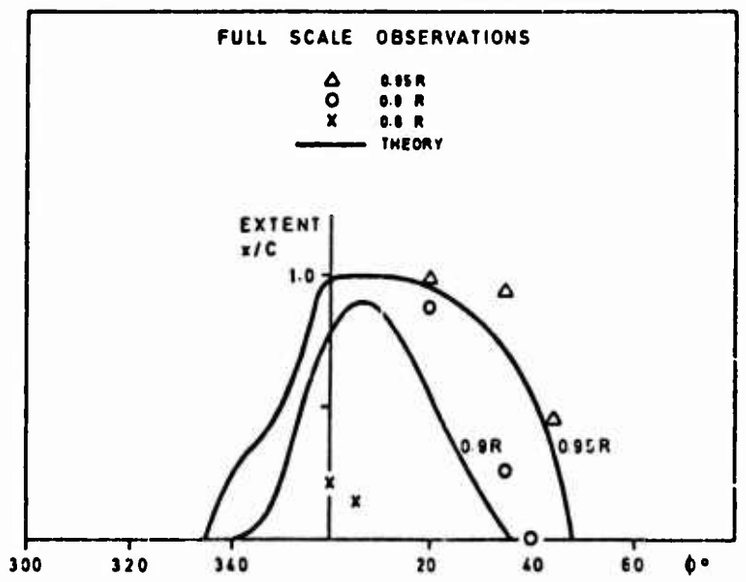


Figure 38 Estimated cavitation patterns. Full scale, fully loaded condition. Extent of cavitation bubble.

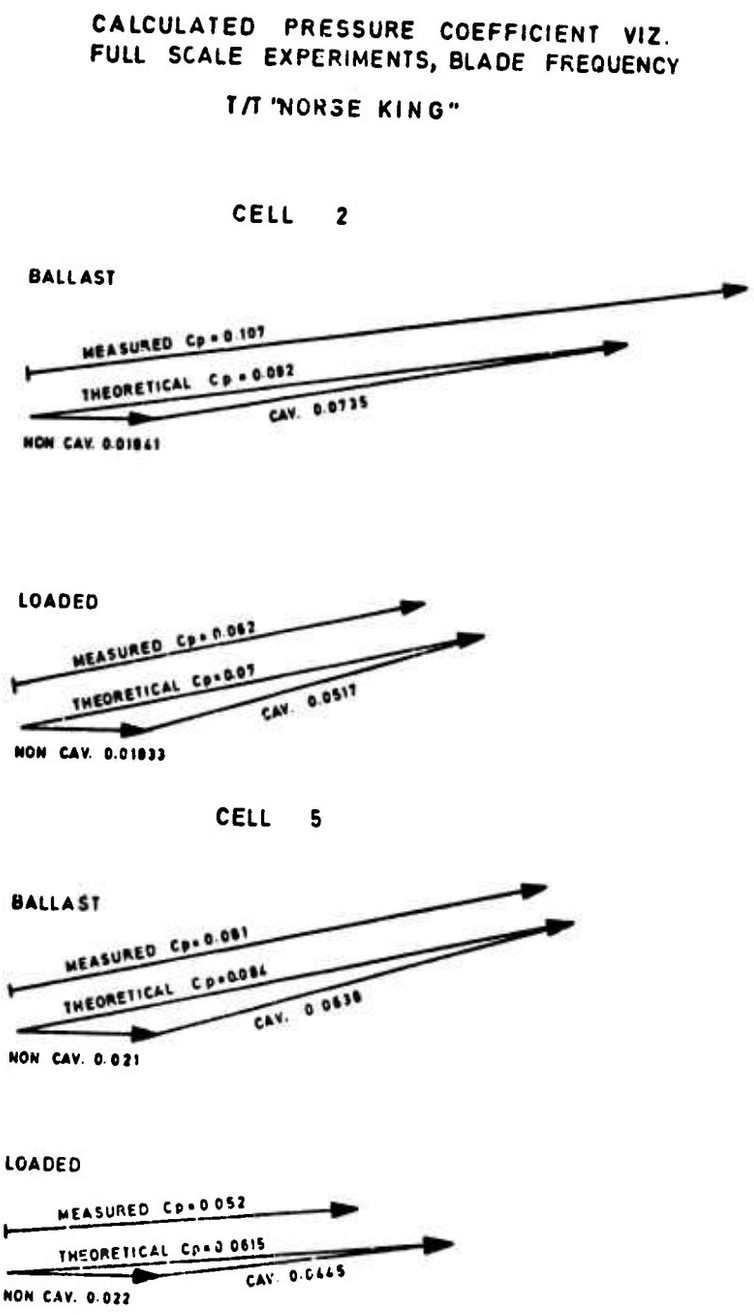
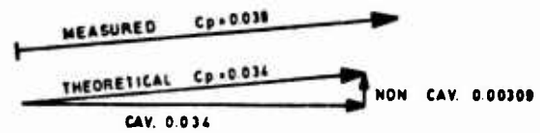


Figure 39 Calculated pressure coefficients. Full scale, blade frequency

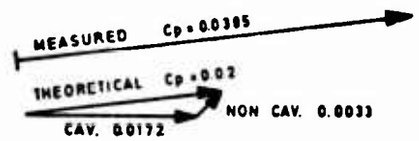
CALCULATED PRESSURE COEFFICIENT VIZ.
FULL SCALE EXPERIMENTS, TWICE BLADE FREQUENCY
T/T 'NORSE KING'

CELL 2

BALLAST

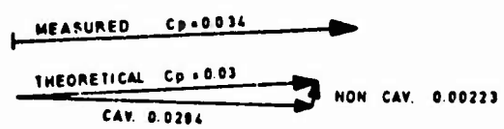


LOADED



CELL 5

BALLAST



LOADED

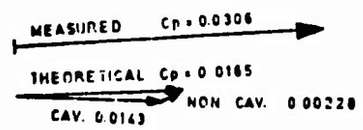


Figure 40 Calculated pressure coefficients. Full scale, twice blade frequency

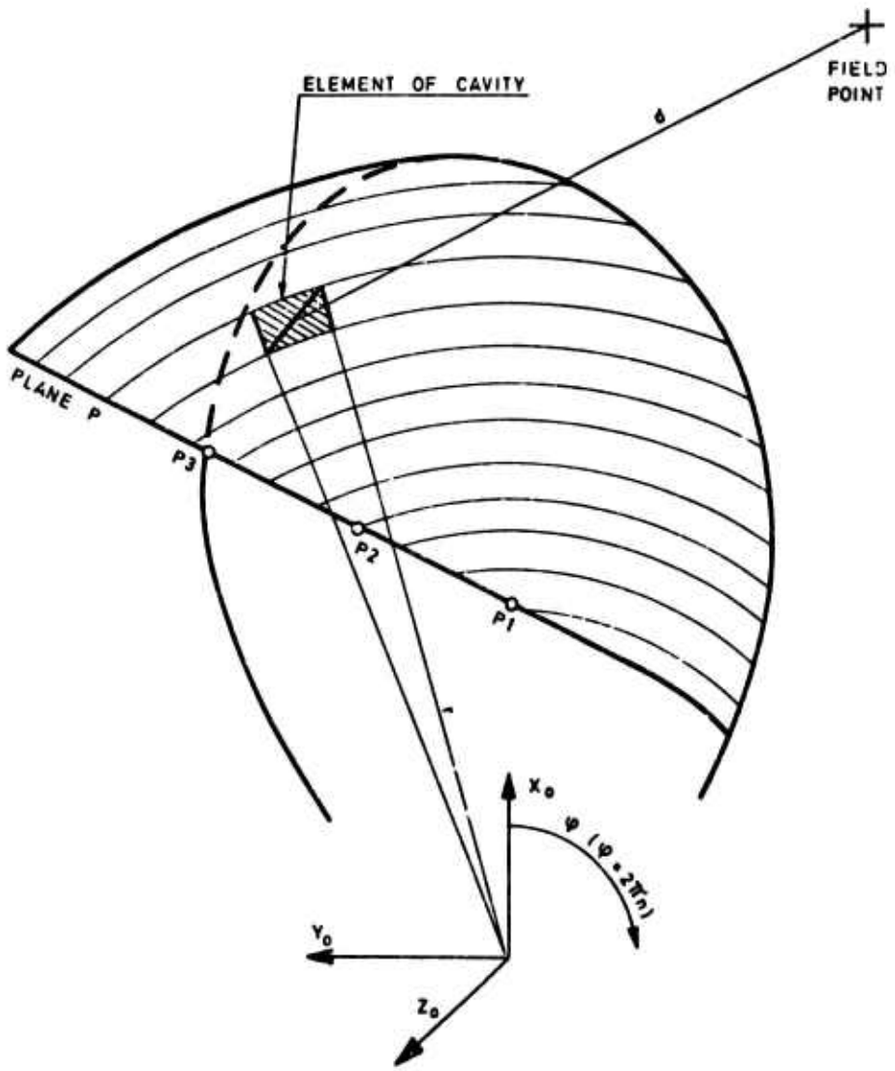


Figure 41 Geometry of cavity, assumed at calculations

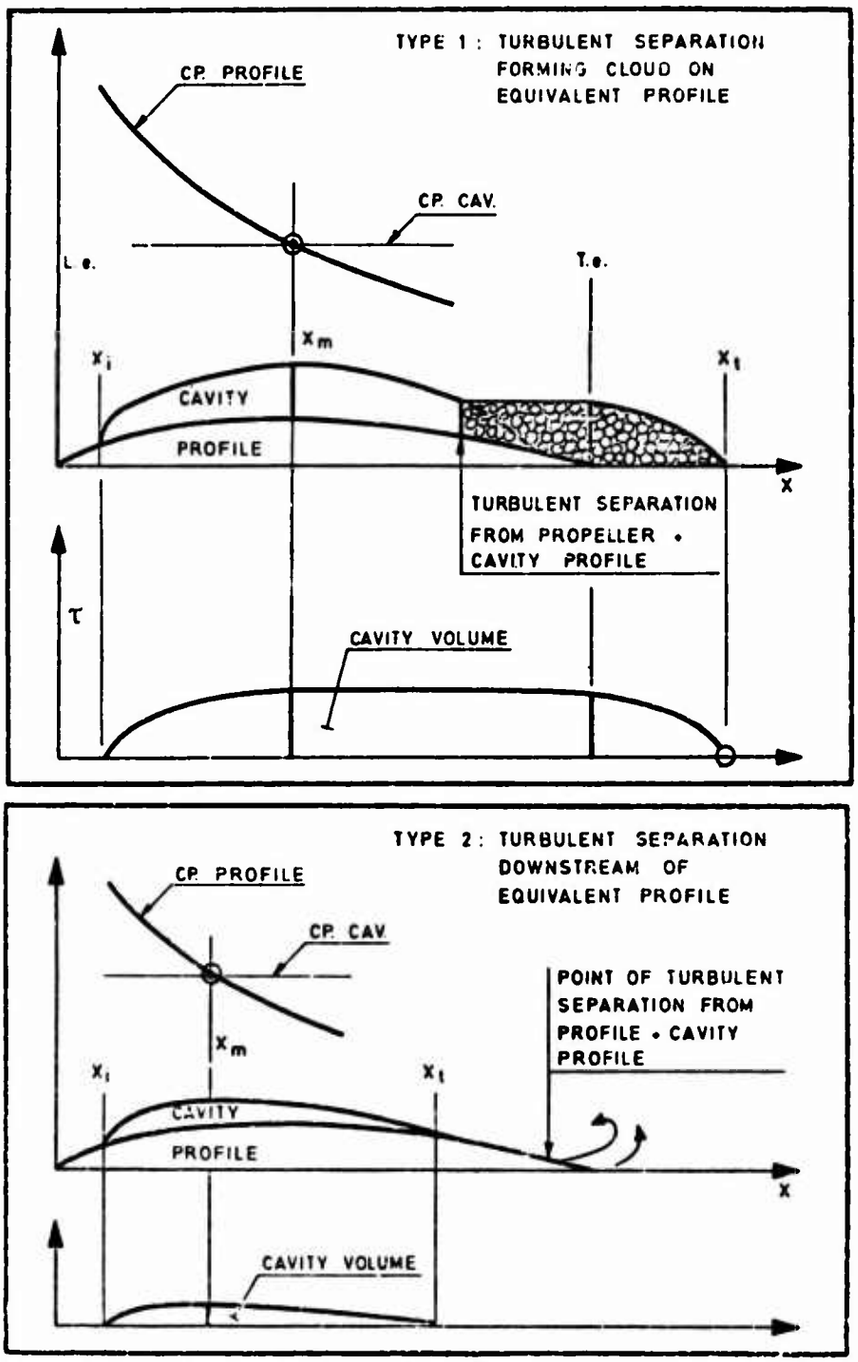


Figure 42 Simplified repr. of cavity volumes

DISCUSSION

William B. Morgan
Naval Ship Research and Development Center
Bethesda, Maryland, U.S.A.

The paper presents very interesting comparisons between model and full-scale pressure measurements. The agreements are reasonable, which is no doubt due to the carefulness with which the experiments were carried out. One would not expect much better agreement because of the relative sizes and locations of the transducers and the influence of ship motions on these pressures.

I was a bit confused by the discussion in the paper concerning the model mean pressures. It appears that the model mean pressures were not in quite as good an agreement with full scale values as the maximum amplitude of the pressures were, but when I read the paper more carefully I found that this was probably the way the data were analyzed. I would like to know whether or not the poor comparison is due to the way the data were analyzed.

In Section 6 the authors discuss the theoretical calculations and comparisons between theory and experiment. I find this discussion very confusing. The comparison between lifting line and lifting surface theory shown in Figure 24 is completely contrary to our experience. We have had generally very good experience with lifting surface theory and not too good with lifting line theory, when the propeller does not influence the wake. I would think that the comparison you have made merely indicates the inadequacy of your lifting surface calculations, not of lifting surface theory in general.

The observation that for this type of ship the propeller influences the wake is a very important one, I believe. However, from the description in the paper, I do not understand how you corrected the wake. Was this an unsteady correction ? If it was not, I do not understand why you got an increase in amplitude. If it was, I do not understand how you could make the correction by simple momentum theory.

Also, I do not understand your comment about extending the lifting surface theory to include non-linearity and effects of interaction with nearby boundaries in light of your results. In the first

place, you could have corrected the wake by the method you used for your lifting line calculations and, in the second place, it is not apparent that including non-linearity would improve the comparisons, since it would seem to me that non-linearities would cut off the peaks of the amplitudes. I am not saying we should not include non-linearities in the theory, but in the light of your results, I do not see how you can draw this conclusion.

I am also disappointed that ... paper of this kind, since a brief discussion was given of the effect of the propeller on the wake, nothing was said about scale effect on wake, which may be much more important than the effect of the propeller on the wake. The data in Figure 11 from the tunnel where you ran two different speeds indicates that this effect might be enormous. Do the authors have any comments on the scale effect on wake on high block ships when the scale ratio is so high ?

REPLY TO DISCUSSION

Carl-Anders Johnsson
Statens Skeppsprovningsanstalt
Göteborg, Sweden

Regarding the model and full scale pressure fluctuations it is concluded from the results in Figures 14-17 that they agree well in fully loaded condition. This applies to the maximum peak to peak values, as well as the first harmonic, values of the latter, however, being available in full scale only for the six-bladed propeller. In ballast condition the amplitudes were smaller in model scale.

The lifting surface method used for the theoretical calculations, the results of which are shown in Figure 24, is that of Tsakonas. The aim of this Figure is to show the importance of including the interaction between the propeller and the wake in the calculations. This is done in a simple manner assuming continuity along a streamline, the method being similar to that used when designing contra-rotating propellers. It must, however, be confessed that the effect of such a correction is unusually pronounced in the present case, the reason being that there is a rather rapid change in the radial and peripherical wake distributions just outside the propeller disk.

Comparisons between the method described and several one-blade dynamometer test (4 degr. of freedom) results serve to illustrate that the method in question is satisfactory for engineering purposes unless being faced with a very sharp wake peak.

Including successive radial displacements of wake grids we have observed that a large radial velocity variation, as experienced behind some ships, is accompanied by a corresponding change of hydrodynamic loading /1/. In fact no method for calculation including the effect of start vortices (or not) will respond correctly to the situation demonstrated unless extending the boundary to positions well outside the propeller disc.

The non-linear effects referred to in the paper are produced by separated flow near to the blade tip together with other tip effects all related to boundary layer flow. Full scale observations have clearly demonstrated that cavitating flows across the tips will account for the main portion of the unstable cavity volume. Hence, we must draw attention to the tip region - in particular - when predicting pressure impulses from propeller cavities. Thus we discuss a region of the blade in the present paper which cannot be considered to-day by other means than experiments and corresponding emperical "separation angles".

Regarding the importance of the wake scale effect on the wake distribution we will not speculate very much (the scale effect on mean wake is considered when determining the values of J and σ defining the loading case). We will only mention that for a tanker research project, now being tested in the large tunnel of SSPA, an attempt is made to estimate the influence of Reynold's number by repeating the tests with the same model, part of the parallel length having been cut away.

Records of blade stresses and fluctuating bearing forces on a large tanker which are reported in /2/, illustrate that model and full scale fluctuating stresses/forces are surprisingly similar.

DISCUSSION

Marinus Oosterveld
Netherlands Ship Model Basin
Wageningen, Netherlands

I should like to make some comments on this very interesting paper.

From model tests and structural calculations it has frequently been found that an increase of the excitation of the hull occurs when the propeller RPM approaches the service RPM. Explanations for the increase in excitation are :

- from an economic point of view, most of the screw designs are such that at service speed the propeller cavitates. For a proper designed screw this cavitation does not give problems with respect to erosion. However, as clearly shown in the paper, due to cavitation the propeller generated hydrodynamic forces may increase substantially.

- the lowest natural frequencies of the transversal and axial shaft vibrations of large tankers lie often in the blade frequency region at service speed. Consequently the shaft vibrations and bearing reaction forces are enlarged a great deal.

- a proper analysis of the whole vibrations therefore requires a determination of the propeller generated hydrodynamic hull and shaft forces, and a determination of the response of the shafting.

That brings me to my first question. Have calculations of the shaft vibrations been carried out in order to determine the magnification effect due to the resonance of the shaft ? These calculations may have influenced the choice of the number of the blades of the screw propeller.

Secondly, the introduction of the afterbody fins lowered the level of the pressure fluctuations on the ship's hull. Are large differences found in the wake field, and especially in the tangential component of the wake field due to the introduction of these fins ? It is a pity that the results of the wake field measurements are not given in the paper, as these are a base for the analysis, I suggest that the authors

add these data to the paper.

Finally, by testing the ship model at ballast condition in the cavitation tunnel the afterbody fins more or less coincide with the upper wall of the cavitation tunnel. Due to this fact, no differences in the wake pattern with and without fins will be found. Is this accordance with the measurement results found in the model basin ?

REPLY TO DISCUSSION

Carl-Anders Johnsson
Statens Skeppsprovningsanstalt
Göteborg, Sweden

Calculations of different kinds of shaft resonances including magnification effects were carried out for the two ships at the design stage and were decisive when determining the number of blades of the propeller.

Comparative curves of the wake distributions with and without fins were given in the first report on this investigation [4] and it was not considered necessary to include them again. These curves show that there was a considerable difference between the wake values obtained with and without fins in the 12 o'clock position, in particular in fully loaded condition where the measurements in the towing tank indicated highly separated flow without fins. This difference was very well reproduced in the tunnel, also in ballast condition, although the agreement between tunnel and towing tank was slightly better in fully loaded condition. This applies to the measurements carried out without propeller as well as those performed with rotating propeller. So we think the differences with full-scale what we call cavitation patterns cannot be entirely linked together with the wake distribution. There must be some other factors. We have discussed the question of the definition of loading cases. We all know that the definition of loading cases is a much more tricky business for ballast conditions. It is not entirely logical compared to what we use in fully loaded condition. May be we can get some useful information from the new vacuum tank regarding what happens to the efficiency and interaction factors under cavitating conditions.

DISCUSSION

Edmund V. Telfer
R.I.N.A.
Ewell, Surrey, U.K.

I had the privilege in the spring of discussing Mr Johnsson's paper before the Institution of Naval Architects and I went into the history of such fins, and there is no need for me to go into that again. All I would like to ask on this occasion is this : granted that the real effect of the fins in minimising cavitation vibration must emanate from the starboard fin and not the port fin, has the author tested everything he has done so far for both fins also only with the starboard fin in position ? I feel that is where the progress is to be made, and I would suggest that the port fin is quite unnecessary. I should like to have the author's reaction to that suggestion.

REPLY TO DISCUSSION

Carl-Anders Johnsson
Statens Skeppsprovningsanstalt
Göteborg, Sweden

In connection with the project, no single fin version has been tested and I do not think we have ever used that concept. Of course it is an interesting idea, but maybe we will lose one of the merits of the fin, that is the propulsion merit. Of course, the main effect of the fins, in this case at least, was that they reduced separation and accordingly, in the model test at least, more than compensated for the increase in frictional resistance. Probably that effect will not be so complete if we have only one fin, but from the research point of view it is a good idea and should be tried.

DISCUSSION

Harrison Lackenby
British Ship Research Association
Wallsend, Northumberland, U.K.

The paper is concerned primarily with the fluctuating pressure forces acting on the hull surface. These are also, of course, the unsteady forces and moments caused by the uneven wake distribution which act on the stern bearing and also contribute to propeller excited vibration.

Figure 5 gives one of these, namely, the fluctuating thrust, but there are also the fluctuating torque and the side forces and moments.

I should like to ask the authors whether they considered these and wether measurements or calculations of them were made.

Would they also care to express an opinion on the relative importance of the hull-surface pressure fluctuations as against the bearing forces and movements as affecting propeller excited vibration ?

REPLY TO DISCUSSION

Carl-Anders Johnsson
Statens Skeppsprovningsanstalt
Göteborg, Sweden

Calculations of different bearing forces were made at an early stage of the project but reliable measurements were only made of the thrust variations (and the mean thrust).

The relative importance of the bearing and surface forces has been discussed for many years and the investigations made indicate that, in the non-cavitating case, they are of the same magnitude.

Figure 37 and other Figures in the present paper show, however, the striking influence of cavitation on the surface forces in the present case. As an influence of cavitation of similar magnitude is not expected for the bearing forces our conclusion is that, in cases where the volume variation of the cavitation is important, the surface forces will be predominant.

DISCUSSION

Finn C. Michelsen
Norges Tekniske Høgskole
Trondheim, Norway

I do not know how far back my historical recollection goes. I was not at the London meetings, so I do not know what our colleague Professor Telfer said, but I do know that the fin has been used on Great Lakes carriers for some 20 years and that in fact, a paper was published on the subject in the Transactions of the Society of Naval Architects and Marine Engineers around 1950 by Professor Baier and Professor Ormondroyd. I believe the authors obtained a patent on this fin. The success of the fin is demonstrated clearly by the fact that these fins are still being installed on Great Lakes carriers, especially when they are repowered, so there is nothing new in that respect. I wish, however, that proper reference had been made to in the present paper to the work by Baier and Ormondroyd. I do not know whether Baier was the first inventor but he was at least a successful applicator of the fin. There is one phenomenon I should like to mention in connection with these fins, something that was said to occur on the Great Lakes carriers. The vibration level on these ships prior to installation of fins is usually not steady. It seems to build up a peak level about every 10 seconds, followed by somewhat of a lull. On a model we have discovered vortices that attach to the model on one side or the other and would sort of peel off into the wake, and this is apparently associated with these high level vibrations. The fin seems to affect the flow around the stern in a very large or significant way through the elimination of such vortices. I wonder if that is the phenomenon we are faced with there. The fact that the authors do not see any difference in the cavitation patterns in five bladers, six bladers and so forth may be an indication of this.

I should also say that the measurements on the Great Lakes

carriers performed by Ormondroyd indicated that the vibration level could drop to one quarter of the original level after the installation of fins.

Another thing that the vortices seem to affect is the course stability of the ship. These large vortices that are building up on one side or the other seem to produce a circulation around the rudder and the entire hull, and this tend to turn the ship which you then have to correct by giving helm. The ship will experience an added resistance due to this. On Great Lakes carriers a gain of a couple of knots has been realized after the installation of fins. I think that also is significant. I wonder if the authors have found anything similar on their ships ?

REPLY TO DISCUSSION

Carl-Anders Johnsson
Statens Skeepsprovningsanstalt
Göteborg, Sweden

After having listened to the discussion we are now fully aware of the disadvantage of writing two papers on the same investigation. We are, however, happy to be able to say that the reference which Professor Michelsen asks for is in the first paper [4] so we think that we have given full credit to Baier and Ormondroyd. We also feel sorry for Professor Michelsen that he missed the fine lecture that Professor Telfer gave in London on some earlier English experiences with fins.

Referring to the last part of Professor Michelsen's remarks, we can inform him that, during the model tests, we observed vortices springing between the propeller and the stern. In full scale they could, however, not be observed. It can, however, not be excluded that they were present, as the equipment used was more suited for photographing than for making visual observations.

A detailed discussion of the results of the resistance and propulsion tests with and without fins, as well as a discussion of the full scale tests was given in the first paper. Model tests indicated a gain in power of 6% in ballast and 1% in fully loaded condition when fins were fitted.

DISCUSSION

John P. Breslin
Stevens Institute of Technology
Hoboken, New Jersey, U.S.A.

Unfortunately, I read this paper late last evening and have not been able to prepare a written discussion. I wish first of all to defend the unsteady lifting surface theory which is castigated by the authors (on p. 599) on the unexplained comparison shown on Figure 24. Here it is shown that the variation of blade bending moment with blade position is seriously over predicted by the unsteady lifting surface u. l. s. theory whereas the model measurements are very well fitted by the DnV. calculations. The u. l. s. theory was found for this application to yield excessively high values of the mean thrust and mean torque, although the unsteady force and moment components were found to be quite close to experimental results available to DnV. (This point is not at all mentioned by the authors). We subsequently furnished DnV. with an engineering correction for the mean loading distribution which together with the unsteady components placed the resulting bending moment variation much closer to the measured variation. The correction was based on the use of the thrust and torque coefficients from Troost's charts which for the mean wake value (obtained without the propeller) agreed very closely with the values provided by DnV. from the self-propulsion test. This agreement of coefficients made it difficult for the discussor to believe that the propeller was seriously affecting the wake. In view of this subsequent effort I must strenuously object to this comparison which unfairly costs grave doubts on the usefulness on the u. l. s. program developed at Davidson Laboratory. Had the authors only informed us of this intended comparison we would have provided a still latter result obtained by application of a more exact theory. The results were recently provided by DnV., and they show excellent agreement of both measured and vibratory forces were found to be virtually equal to those from the less exact, earlier calculation.

It is very gratifying to learn that Mr. Huse and researchers at NSMB have realized that the influence of intermittent cavitation on blade frequency pressures predominantly arises from the time variation of the cavity volumes. I have been espousing this mechanism for some time in the USA where it has been rebutted by the idea that it is due to the thickening of the blade sections in steady-state fashion. At

the distances of interest from the cavity volumes an asymptotic representation of these by pulsating point sources should be quite exact. Thus I find the principal contribution to be due to the second-time derivative of the cavity volume and "the secondary" term arising from convection to be proportional to the first time derivative of the cavity volumes. The basic problem of first magnitude is to calculate these derivatives. Essentially I think they should be measured from three-view high speed photographs.

Finally, I hope that the authors will detail their method for accounting for the induction effects on the ship wake since their comparison with the measurements exhibited in Figure 24 is certainly fantastic !

REPLY TO DISCUSSION

Carl-Anders Johnsson
Statens Skeppsprovningsanstalt
Göteborg, Sweden

We think that most of the points raised by Professor Breslin are covered by our answer to Dr Morgan.

However, we certainly do not want to attack the unsteady lifting surface program developed at Davidson Laboratory. We are fully aware of its capabilities in dealing with wake components of order enabling force transfer to the shaft for most grid wakes available. We like to repeat that no method can work correctly with wrong boundary conditions e.g. the inlet wake containing no radial variations of the wake outside the propeller disc and the slip stream assumed to have constant radius and moving in axial direction.

By application of momentum theory the change in propeller load may be illustrated to be large. The authors cannot agree with Professor Breslin's word "fantastic" and hope that we have succeeded in illustrating a simple physical concept used in the theory.

DISCUSSION

Erling Huse
Ship Research Institute of Norway
Trondheim, Norway

First of all I would like to congratulate the authors on a very interesting and valuable contribution to our knowledge of cavitation as a source to ship vibration. This is, I think, an aspect of vibration excitation which deserves considerable attention. The work presented by the authors is therefore of great value in our efforts towards better methods of predicting and reducing propeller induced excitation forces.

In connection with the oscillating pressure measurements in the cavitation tunnel I would like to comment on the magnitude of the wall effect mentioned by the authors. At the Ship Research Institute of Norway we have recently determined experimentally this wall effect in our two cavitation tunnels. I would like to show you how we do it and some results.

Let us first recall that the pressure field induced by the cavities on the propeller blades is mainly the sum of two components. First we have the pressure field due to the cavity motion. This is in principle a "dipole field" whose amplitude decays rapidly with increasing distance from the propeller. Therefore one may expect the wall effect for this pressure field to be relatively small. This we have also confirmed experimentally. The experimental procedure is first to measure in the cavitation tunnel the pressure amplitude on the hull model surface with the propeller running with no cavitation and at zero thrust. (The pressure field is in this case mainly due to blade thickness and thus of the same type as that of cavity motion). The same measurement is next carried out in the towing basin where there are no tunnel walls in the vicinity of the propeller. The difference in pressure amplitude measured on the hull in the cavitation tunnel and in the towing basin is due to reflections from the tunnel walls and thus represents the wall effect.

The second and most important contribution to the total pressure field is that due to the volume variation of the cavities. This effect produces a pressure field which is in principle a "pole field". Since its amplitude decays relatively slowly with increasing distance it will be subject to a more pronounced wall effect that the pressure

field due to cavity motion. The main problem in measuring wall effect in this case is to design a transmitter to produce the required oscillating pressure pole field. Figure 2 shows the principle of the pressure wave transmitter that we have developed in Trondheim. A signal generator feeds an AC current to the coil winding. This makes the rubber membranes oscillate, producing an effective volume variation. The amplitude of the volume variation itself is measured by measuring the pressure fluctuation in the closed air volume inside the transmitter by means of a pressure transducer.

Now we first fit the afterbody model in the cavitation tunnel with this pressure wave transmitter instead of the propeller as shown in Figure 1. We adjust the volume variation to a certain level and measure the pressure amplitude on the hull. This procedure is then repeated in the towing basin with exactly the same volume variation. The difference in pressure amplitude on the hull in the two cases represents the wall effect.

In our larger tunnel of 1200 mm diameter test section we have in this way determined the wall effect for one particular afterbody model with a 240 mm diameter propeller. On the hull directly above the propeller the wall effect was found to be less than measurement accuracy, i.e. less than 10 percent, in a frequency range up to 300 cps. Hence this tunnel seems to be acceptable for pressure measurements on the afterbody model. In our second and much smaller cavitation tunnel, however, where we have tried to measure pressure fluctuations on a plate above the propeller, we have found the wall effect to be unacceptably high, amounting to a factor of up to 2.

From investigations in our own tunnels, and by considering the test section dimensions of the SSPA tunnel, I feel confident that the wall effect has been negligible in the case of the tunnel measurements described by the authors.

Finally I have a direct question regarding the damping of the acceleration potential mentioned by the authors. I find it hard to understand what physical phenomenon the authors are referring to, and I find it even harder to understand how they have been able to make corrections for it. Could the authors please tell us the magnitude of the damping coefficient they have applied in their calculations, and also explain the theoretical basis of this correction.

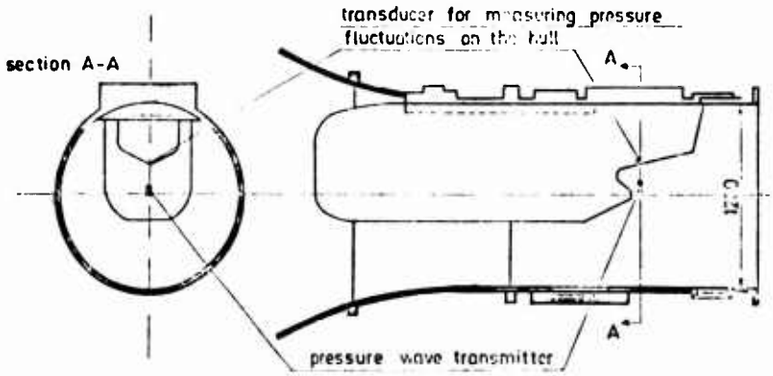


Figure 1 Afterbody model in tunnel test section

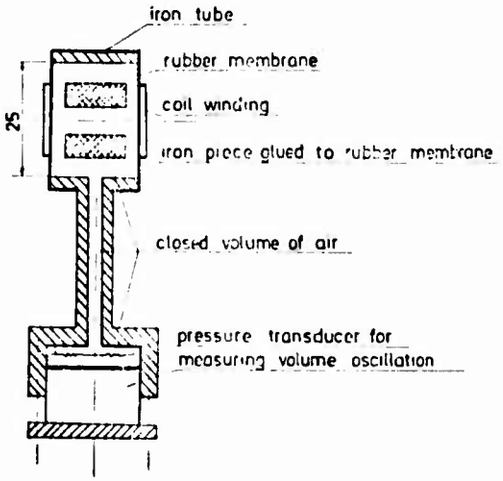


Figure 2 Pressure wave transmitter

REPLY TO DISCUSSION

Carl-Anders Johnsson
Statens Skeppsprovningsanstalt
Göteborg, Sweden

Thank you, Mr Huse, for your comments. We read your contribution with interest and also with some relief, to get, without paying for it, a good investigation of the wall effect of a tunnel of similar dimensions as that of SSPA.

On trials we have several times observed that pressure fluctuations certain up to 5-6 times blade frequency. Preliminary, it was required to study the mechanism by which such components could be included.

The m^2 term in Equations (15) and (16) of Appendix C however, leads to large magnitudes of the component of that frequency, as the corresponding inaccuracies in the Fourier term become significant. Consequently, empirical damping of the signal was required ; for convenience the reduced frequency/oscillating blade relationship was chosen as the "building brick". Presently, we terminate computations at twice blade frequency and can neglect the method originally included in the paper.

* * *

MOTIONS OF MOORED SHIPS IN SIX DEGREES OF FREEDOM

I -Min Yang
Tetra Tech, Inc.
Pasadena, California U.S.A.

ABSTRACT

The equations of motions of a moored ship having six degrees of freedom were formulated. The mooring force is nonlinear and asymmetrical. A new approach is developed to solve the resulting nonlinear and asymmetrical problem.

INTRODUCTION

Recently the development of large ships has attracted many investigators to study motions of moored ships. The introduction of container ships and the increase of oil exploration in deeper water depths make it necessary to have a through understanding of motions of moored structures. For container ships, the operation of loading and unloading containers are controlled by land based huge cranes, extensive ship motion may greatly reduce container loading and unloading rate. Oil exploration in deep sea needs to drill through the ocean floor from a moored ship (or other moored structures), large motions of the ship may hinder drilling operation. Another related problem is that of a moored buoy system. The effective design and development of such system also require an ability to predict its oscillatory motions.

The study of motions of a moored ship is usually limited to the

Preceding page blank

surge motion [1]*, that is, the moored ship is considered as having only one degree of freedom, and it is known that the force-elongation relationship of a mooring line is highly nonlinear [2]. Kaplan and Putz [3], and Muga [4] have investigated moored structures in six degrees of freedom. In their study, the force-elongation relationship of mooring lines is assumed to be linear, thus the problem is linear and the solution can be readily obtained. In this paper, we consider a more general six degree of freedom problem. The mooring force is a nonlinear function of elongation ; since a ship can not be symmetrically moored, and fenders are only at one side of the ship, motions of the ship are asymmetric. An approach has been developed to generate an approximate steady-state solution to this nonlinear asymmetric problem.

FORMULATION

The motion of a moored ship in waves is an oscillating system with six degrees of freedom corresponding to surge, heave, sway, roll, pitch, and yaw. The ship is considered as a rigid body and its deformation is neglected. Usually the length of a ship is much longer than its beam, and the slender body theory can be applied to find the hydrodynamic properties of a moored ship. According to this theory, for an elongated body where lateral dimensions are small compared to its length, the flow field at any cross-section is independent of that at any other sections. Hence, the flow field of an elongated body, like a ship, is reduced to a two dimensional problem of its cross-sections. The total hydrodynamical properties is found by integrating over the length of the body.

The six dynamic variables surge, sway, heave, roll, pitch, and yaw of a ship are expressed in terms of two right-hand cartesian coordinate systems. A moving systems which is fixed in the ship, and a fixed system which is fixed in space. The moving system (y_1, y_2, y_3) has its origin at the center of gravity of the ship and its three axes (y_1, y_2, y_3) coincident with the three principal axes of the ship. The y_1-axis is positive toward the bow, the y_2-axis is positive to port and the y_3-axis is positive upward. This system will move with the ship and the angular displacements about the three axes are respectively, the roll, the pitch and the yaw of the ship. They are positive for rotations about the positive directions of y_1, y_2 and y_3 in a counterclockwise direction. The fixed systems (x_1, x_2, x_3) is chosen such that the two coordinate systems are coincident when the ship is at rest. Then the

* Numbers in brackets designate References at the end of the paper.

three components of translational motion of the origin of the moving system relative to the fixed system are defined as the surge, the sway, and the heave of the ship. The positive directions of forces and moments are defined in the same way as their corresponding displacements.

The forces and moments on a moored ship can be divided into four categories : inertia, damping, restoring and exciting forces and moments. The details of determining these forces and moments are discussed in [5] , and only a brief discussion will be given below.

The inertia forces and moments arise from change of velocities of the ship and water particles around it. Although the change of velocity of water particles depends on their position in relation to the ship, it can be assumed that a certain amount of water behaves as if integral with the ship and moves with it. The amount of entrained water is different for different components of motion and the mass or the moment of inertia of such entrained water is called the added mass or added moment of inertia. By applying the slender body theory, the inertia force or moment on a section of the ship is then equal to the product of the virtual mass (the sum of natural mass and added mass) or the virtual moment of inertia (the sum of natural moment of inertia and added moment of inertia) and acceleration. The added mass and added moment of inertia depend on wave frequency, water depth, shape of ship sections and the clearance between ship sections and side walls.

Damping forces and moments arise from wave generation and are proportional to the relative velocity between the ship and water particles. The proportional constants are called the damping coefficients and depend on wave frequency, water depth, shape of ship sections and the clearance between ship sections and side walls.

Restoring forces and moments come from three different origins and will be discussed separately in the following.

Hydrostatic restoring forces and moments are due to the buoyancy effect resulting from ship displacement. The total hydrostatic restoring force has only one component in the vertical direction and the hydrostatic restoring moments has components in the roll and pitch direction.

The second restoring forces and moments come from mooring lines. The behavior of a mooring line under tension has been investigated by Wilson [2] . The relationship between force and elongation is highly nonlinear and in general can be represented in

the following form :

$$T = c\left(\frac{\Delta L}{L}\right)^n \quad \text{if} \quad \Delta L > 0$$

$$= 0 \qquad \text{if} \quad \Delta L \leq 0$$

where L is the moored length of a mooring line, the change in length due to a tensile force T is ΔL, and c and n are two constants depending on the type of mooring lines. The total restoring force and moment due to all mooring lines have components in all three directions of translation and rotation.

Another restoring forces and moments come from fenders which will be in action only when they are in contact with the ship. The total restoring force has only one component in the sway direction and the total restoring moment has components in the roll and yaw directions.

Finally there are the exciting forces and moments due to water waves. The waves are assumed to be sinusoidal standing or progressive waves and have a unique frequency, then forces and moments on ship sections can be obtained from certain wave potential.

The six equations of motion for a moored ship are obtained by balancing the various forces and moments discussed above and may be represented in the following matrix form :

$$M\ddot{\bar{x}} + C\dot{\bar{x}} + K_o\bar{x} + \bar{f}(\bar{x}) = \bar{g}(t) \qquad (1)$$

where

M = virtual mass and moment of inertia matrix

C = damping matrix

K_o = stiffness matrix due to linear restoring forces and moments

$\bar{f}(\bar{x})$ = force vector due to nonlinear restoring forces and moments

$\bar{g}(t)$ = force vector related to water waves
$= q_i \cos(\omega t + \psi_i), \quad i = 1, \ldots, 6$

$\bar{x}$ = $(x_1, x_2, x_3, \theta_1, \theta_2, \theta_3)$

The first three elements x_1 , x_2 , x_3 in the displacement vector $\bar{x}$ represent the surge, the sway and the heave of the moored ship, and the next three elements θ_1, θ_2, and θ_3 represent respectively the roll, the pitch and the yaw of the ship. The force vector $\bar{f}(\bar{x})$ is nonlinear. If its argument $\bar{x}$ is replaced by $-\bar{x}$, $\bar{f}(-\bar{x})$ will in general differ from $\bar{f}(\bar{x})$ in magnitude as well as in sign. Hence $\bar{f}(\bar{x})$ is asymmetric. The quantities ω, q_i and ψ_i represent wave frequency, force or moment amplitude and phase angle for the ith element of the vector $\bar{g}(t)$.

METHOD OF SOLUTION

Since the excitation vector is harmonic, we assumed that an approximate steady-state solution for the response of the system (1) may take the following form :

$$x_i = z_i + y_i \tag{2}$$

$$= z_i + \gamma_i \cos(\omega t + \varphi_i) \qquad i = 1\ldots,6 \tag{3}$$

z_i is a constant introduced to account for the asymmetry of $\bar{f}(\bar{x})$ in (1). If $\bar{f}(\bar{x})$ is symmetric, then z_i will vanish. y_i is a harmonic function whose amplitude and phase are γ_i and φ_i.

Consider a linear system defined by

$$M\ddot{\bar{y}} + C\dot{\bar{y}} + (K_o + K)\bar{y} = \bar{g}(t) \tag{4}$$

where K is an unknown matrix. If K is known, this linear system can readily be solved to give :

$$\gamma_i = \sqrt{w_i^2 + w_{i+6}^2} \qquad i = 1,\ldots,6 \tag{5}$$

$$\varphi_i = \tan^{-1}\frac{w_{i+6}}{w_i} \tag{6}$$

where w_i's are given by

$$\begin{pmatrix} w_1 \\ \cdot \\ \cdot \\ \cdot \\ \cdot \\ \cdot \\ \cdot \\ w_{12} \end{pmatrix} = \begin{bmatrix} V_1 - V_2 & & \\ & & \\ & & \\ & & \\ & & \\ & & \\ & & V_2 - V_1 \end{bmatrix}^{-1} \begin{pmatrix} q_1 \cos \psi_1 \\ \cdot \\ \cdot \\ q_6 \cos \psi_6 \\ q_1 \sin \psi_1 \\ \cdot \\ \cdot \\ q_6 \sin \psi_6 \end{pmatrix} \tag{7}$$

in which

$$V_1 = K + K_o - M\omega^2 \tag{8}$$

$$V_2 = C\omega \tag{9}$$

and the superscript -1 for a matrix denotes its inverse.

If the exact solution for the linear system is used as an approximate solution for the nonlinear system, direct substitution gives

$$\bar{\epsilon}(z_i, k_{ij}) = \bar{f}(\bar{x}) - K\bar{y} + K_o\bar{z} \tag{10}$$

where k_{ij} are the (i, j) element of K and $\bar{\epsilon}$ denotes the error vector. The unknowns k_{ij} are chosen in such a way that the average mean-square error over one cycle defined by the integral

$$\epsilon_a = \frac{1}{2\pi}\int_0^{2\pi} \sum_{i=1}^{6} \epsilon_i^2 \, d\theta, \qquad \theta = \omega t \tag{11}$$

is a minimum. This leads to

$$\frac{\partial \epsilon_a}{\partial k_{ij}} = 0 \qquad i, j = 1, \ldots, 6 \tag{12}$$

However, it can be shown that not all k_{ij}'s are independent. In order to avoid this difficulty, we choose in this case,

$$k_{ij} = 0 \qquad \text{if } i \neq j \tag{13}$$

Then, k_{ii} can be uniquely determined as follows :

$$k_{ii} = \frac{1}{\pi Y_i} \int_0^{2\pi} f_i \cos(\theta + \varphi_i)\, d\theta \tag{14}$$

Six more equations are furnished to determine z_i by averaging the nonlinear equations over one cycle which leads to

$$2\pi K_o \bar{z} + \int_0^{2\pi} \bar{f}(\bar{x}) d\theta = 0 \qquad i = 1, \ldots, 6 \tag{15}$$

Thus the solution of the nonlinear system is reduced to the solution of Equations (5) - (7), (14) and (15). They are nonlinear algebraic equations but can be solved numerically by the following iteration approach. First, set $z_i = 0$ and assume a set of values k_{ii}. Then Equation (7) can be solved by simple matrix inversion and Y_i and φ_i are determined from Equations (5) and (6). Now a new set of values of k_{ii} and z_i are calculated from (14) and (15). This procedure can be repeated until required accuracy is reached.

SUMMARY AND DISCUSSION

An approach to the determination of an approximate solution for the steady-state response of moored ships in six degrees of freedom has been formulated. This approach can be applied to moored structures in open sea as well as moored ships in harbors. In this paper, the degrees of freedom of the system is specified as six. However, this approach is still valid for degrees of freedom other than six.

The accuracy of an approximate analysis is difficult to predict in general. A different version of this approach where $\mathbf{f}(\bar{x})$ is symmetric has been employed to problems which possess known exact solution [6] , it shows that the accuracy of this approach is well within the limits of practical engineering usefulness.

REFERENCES

[1] WILSON, B.W., "The Energy Problem in the Mooring of Ships Exposed to Waves", Proceedings of Princeton Conference on Berthing and Cargo Handling in Exposed Locations, October, 1958.

[2] WILSON, B.W., "Elastic Characteristics of Moorings", Journal of the Waterways and Harbors Division, ASCE, WW4, November, 1967.

[3] KAPLAN, P., and PUTZ, R.R., "The Motions of a Moored Construction-Type Barge in Irregular Waves and Their Influence on Construction Operation", Contract NBy-32206, an investigation conducted by Marine Advisers, Inc., La Jolla, California for U.S. Naval Civil Engineering Laboratory, Port Hueneme, California, 1962.

[4] MUGA, B.J., "Hydrodynamic Analysis of a Spread-Moored Platform in the Open Sea", U.S. Naval Civil Engineering Laboratory, Port Hueneme, California, August, 1966.

[5] HWANG, L.S., YANG, I., DIVOKY, D. and YUEN, A., "A Study of Wave and Ship Behavior at Long Beach Harbor with Application to a Modern Container Ship", an investigation conducted by Tetra Tech. Inc., Pasadena, California for the Port of Long Beach, Long Beach, California, 1972.

[6] YANG, I., "Stationary Random Response of Multidegree-of-freedom Systems", California Institute of Technology, Dynamic Laboratory, Report No. DYNL-100, June, 1970.

* * *

DISCUSSION

Manley Saint-Denis

University of Hawai
Honolulu, Hawai, U.S.A.

I am afraid I must begin by begging the author's forgiveness and the indulgence of the audience for the critical remarks I am about to make on this paper. Perhaps this is the wrong way to start a discussion, but if it is not the right way, it is at least a diplomatic one. However I must confess with some alacrity that my remarks are going to be rather suggestive and tentative and not at all forceful or categorical. This is due in part, perhaps, to the manifest voids in the paper which have led me to infer, perhaps mistakenly, what might be the full development. Having provided sufficient cushioning for my criticism, it is time that I voice it. I have five specific comments and one general recommendation.

The first is this : I have been unable to discover anything new in the paper. Lack of originality is not in itself condemnable, of course, if the paper contains other rewards, such as elegance of development or an efficient computer programme, etc... But these I find not to be present.

My second comment is that the paper appears to consist of two parts : an adequate introduction and a short conclusion ; but of the essential development that should be the core of the presentation there is only a hint. It is this parsimony of the essential that I have found to be rather distressing. To rest the paper on reports that, if not proprietary, are not generally available militates against an appreciation of it.

My third comment relates to the author's statement that the solution is valid for a ship moored alongside a dock, a condition that introduces an asymmetric non-linearity in the restoration but this is, in principle at least, a grave insufficiency, for the proximity of the rigid boundary, which is the dock, affects also the hydrodynamic mass, the damping reaction and the acceleration and velocity terms of the excitation, so that all these are non-linear, and the non-linearities are not readily written off as negligible. Indeed, they are quite powerful.

My fourth comment is that the equation of motion reveals an excitation that consists of a single component related to wave displacement. This is correct only so long as the excitation is linear (in which case its amplitude is frequency dependent), but not when the excitation is non-linear (in which case its amplitude is a function of both frequency and amplitude of motion).

My fifth comment relates to the conclusion that the accuracy of the approximate approach is well within the limits of practical engineering usefulness. But comparison is against another computational method and not against measured reality, and such a comparison leads to an appreciation of the validity of the approximation, not of the basic method.

The paper raises a large number of stimulating questions but it provides a paucity of answers to them, and my recommendation is quite simple. I suggest that the author complete his paper and add thereto whatever experimental or trial data he can adduce in support of the technique described. Only then will it be possible to appreciate the paper and to comment constructively on its intrinsic merits, which at present stand unrevealed.

REPLY TO DISCUSSION

I-Min Yang
Tetra Tech, Inc.
Pasadena, California, U.S.A.

From the comments made by the discusser, it seems to me that he has some misunderstanding about the definition of nonlinear differential equations. Hence he can not find any originality in this paper. In equation (1), the independent variable is the time t, and the dependent variables are the components of the displacement vector $\bar{x}$. Since it is assumed that $\bar{f}(\bar{x})$ is a nonlinear vector function of $\bar{x}$, the differential equation (1) is therefore nonlinear. The frequency ω in this equation is just a parameter, that is, for a particular case, it is a constant. The hydrodynamic coefficients (virtual masses and damping coefficients), and amplitude and phase angles of wave forces depend on ω and the dock in a very complicated manner, but for a fixed ω, they are just constants. Thus they have nothing to do with the nonlinearity of differential equations. (For

example, in equation (1), if $\bar{f}(\bar{x})$ is a linear function of $\bar{x}$, then equation (1) is always linear.) Many papers have been published in determining hydrodynamic coefficients and wave forces and since the main purpose of this paper is to present an approach to solve the nonlinear, asymmetrical problem due to the presence of mooring lines, I did not even try to explain how to find these coefficients in this paper.

The explanation of the approach is quite complete. If one reads this paper carefully, he will find that, although it is a quite short paper, it contains all information about the approach.

It is true as the discusser pointed out I failed to compare the results with measured data. However, the comparison with an exact solution does indicate how good the approach is. If the hydrodynamic coefficients and the representation of mooring lines are adequate, then this approach will give very reasonable and practical results.

DISCUSSION

Paul Kaplan
Oceanics Inc.
New-York, U.S.A.

My comments are somewhat similar to those of Dr Saint-Denis but perhaps they are motivated by different reasons. In some ways, when I looked at the paper and considered the content of it I was reminded of a modern song that was popular a couple of years ago by Miss Peggy Lee. It is called "Is that all there is". If you think about the song, it starts out on a sad tone and that is the way I felt initially, but the song proceeds by careful consideration to some sort of positive outlook. Perhaps if you bear with me and my discussion and some interchange between the author and myself, the same result may be achieved.

My interest in this particular subject is indicated by the fact that there is a reference to the paper I wrote ten years ago dealing with the motions of a moored ship with six degrees of freedom, and it was linear. Two years ago at the last Naval Hydrodynamics Symposium I presented a similar subject which was just concerned with a few problems in the whole general area of mooring and positioning ships at

sea. Therefore I am concerned about some aspects of that is in this paper and how they modify what may be considered as some results of my own some time ago, and therefore raise questions. For one thing, this being a naval hydrodynamic symposium, there is no indication as to what is unique in the paper from a hydrodynamic point of view. There are walls and there is a mention by the author of the fact that the added mass and damping are affected by the presence of the walls. However, how did you take account of it ? What mathematical procedures, what techniques, what approaches were used ? This is the sort of information that we professionals could make some use of and would like to hear about so that if we have an apposing point of view or something interesting to say there can be some interchange in regard to it.

Another point is that this was applied, we are told, to a container ship. Was there anything unique about the container ship ? Was it a standard ship ? Was it one that also had barges perhaps ? Was it an unusual form, like a Lash or a Seabee ? This makes a difference in the type of ship computation per se.

On the question of non-linearity, what kind of non-linearities do we have ? I can imagine something with fenders. A fender will only provide a force, and it is one-sided, when you press against it ; when you go off, there is nothing. I would make an analogy with the so-called linear detector in electronics, which is one-sided in its variation. If you do that, you have a mathematical structure of what a non linearity looks like. Similarly with regard to other aspects of the non-linearity that comes from the mooring cable. For example, you made a particular assumption in your mathematical procedure which raises a very significant question in my mind. Equation 13 in the paper, which you alluded to also on your slide, said that you made the assumption that the Kij terms are zero. This means you are only using diagonal terms in the K matrix. The implication of that is very interesting. It means that you just take account of what I consider to be self-mode non-linearities - that is, non-linearities in each mode separately, like x^2, x^3, y^2, y^3 . Moored ships certainly have interactions of a non-linear nature because the bow and the stern when you yaw together with sway have some $xx\,y + x$ sine and $y - x$ sine at either end. Non-linearity reflects itself differently in different products. In fact, if you have similar mooring cables you can use the fact that the cross product term is opposite sines and this will allow you to get some information, something useful, and not as restricted as it is here. It is a suggestion. I do not know what you have perhaps done in considering that which led you to the conclusion of a reduced number of terms.

Similarly, you are dealing with a case of a sine wave here which I do not think is quite apropos, but nevertheless it is an analytical exercise that has its utility. How different are the results for the case you have obtained here with the non-linearity included as compared to the linear theory ? There must have been some results. Is there any significant difference ? Does it occur when in a certain region we have certain wave amplitudes ? This will certainly be useful to us.

Similarly, if you have an application to a real condition, even though it is a harbour and has a very narrow tune system, there are swells that come in and you have to treat the problem as one for a random system. There are techniques known as describing functions which you can use. and I am sure you can use them. Your reference says your thesis dealt with this problem area. It would be a natural and wonderful extension of this procedure. The question then is what are the theoretical results and how would they compare with the case of linearity ?

In concluding, I want to say something that is similar to the statement Dr Saint-Denis made. There is a statement which I used to hear years ago and perhaps it is applicable to my own delivery sometimes, but it is of oriental origin. It is essentially that one picture is worth a thousand words. I think we ought to make a little inversion here and put some more words together with some pictures, and the end product comes cut really two years from now. This is a tremendous opportunity to make a substantial contribution, and I should greatly like to see it.

REPLY TO DISCUSSION

I-Min Yang
Tetra Tech, Inc.
Pasadena, California, U.S.A.

(1) The discusser said, "...you just take account of what I consider to be self mode nonlinearities,...". This is not true. It is true that the matrix K is assumed to be diagonal, but if you read this paper carefully, you will find that k_{ij}'s are unknown quantities and their determination depends on all six modes of motion.

(2) Since the main purpose of this paper is to present an approach to find the nonlinear, asymmetrical motion of a moored ship, I have omitted the discussion of determining the hydrodynamic coefficients. In fact, I just used the data discussed in published papers.

(3) The effect of nonlinearity depends heavily on the nonlinear system. If the nonlinearity in the force-displacement relationship is very large, like the case of mooring lines, the resonant period determined by linear analysis is quite different from that determined by nonlinear analysis. For example, in one case I considered, it may shift from 20 seconds to 50 seconds.

(4) This paper discussed an analytical approach to investigate the motion of a moored ship. It seems to me that the lack of figures does not affect the understanding of this approach.

DISCUSSION

Ernest O. Tuck
University of Adelaide
Adelaide, Australia

I do not want to let one of Dr Saint-Denis's remarks pass. I forget which point number it was but it was the business about the exciting force being of only one type when he thought it ought perhaps to be of several types. I think this is quite erroneous. There is no reason to believe that the excitation is anything but the most general linear excitation in this particular problem. From my reading of the paper there is an input frequency-dependent phase as well as input amplitude, so I think that that particular point put by Dr Saint-Denis should not be allowed to stand.

Another point of his was that there is nothing new in this paper and I think that is quite wrong. I think myself that it is quite a good paper. I think Dr Yang explained about the matrix K_{ij}. The fact that it is diagonal does not necessarily mean that one is considering only self-linearities. I think that some of this criticism is simply misplaced and that the people making the criticism should read the paper a bit more carefully.

DISCUSSION

Grant Lewison
National Physical Laboratory
Feltham, Middlesex, U.K.

I should like to make one small point about the paper. The author has assumed that the response of the system is entirely fundamental mode -in other words, that there is only one harmonic present. This completely ignores the possibility of higher and lower mode harmonics which for many moored ships are well known to provide much bigger responses than the fundamental.

REPLY TO DISCUSSION

I-Min Yang
Tetra Tech, Inc.
Pasadena, California, U.S.A.

Thank you for the comments. Usually for a non-linear system there are some higher harmonical terms. But I compared the harmonic solution with the exact solution for some symmetric cases. The higher harmonical terms are not important.

DISCUSSION

Grant Lewison
National Physical Laboratory
Feltham, Middlesex, U.K.

What about the lower one - i.e. sub harmonic ?

REPLY TO DISCUSSION

I-Min Yang
Tetra Tech, Inc.
Pasadena, California, U.S.A.

If you want to have high harmonic or sub harmonic terms, of course you can do it by purely numerical integration. But note that near resonance, the solution is not unique and depends on initial conditions. The region of convergence for the peak solution is very narrow and therefore it is very difficult to obtain the most important results by numerical method. That is the main reason why I developed the approximate method for the harmonic case.

* * *

ANALYSIS OF SHIP-SIDE WAVE PROFILES, WITH SPECIAL REFERENCE TO HULL'S SHELTERING EFFECT

Kazuhiro Mori, Takao Inui,
and Hisashi Kajitani
University of Tokyo
Tokyo, Japan

ABSTRACT

Attempt is made to find out the effective wave-making source of a ship from the measurement of the hull-side wave profiles.

The integral equation of the source distribution function is simplified and solved numerically under the specific limitation, (a) rectangular, vertical central plane, and (b) draughtwise uniform.

Two Inuid models M 20 (B/L = 0.0746) and M 21 (B/L = 0.1184), whose hull-generating sources are optimized to give the minimum wave resistance at Fn = 0.2887(K_0L =12), are tank-tested and wave-analyzed.

The obtained source distribution $m(\xi)$ shows a clear discrepancy from the hull-generating source $m(\xi)$ in a similar way to the so-called μ-correction, or

$$\alpha(\xi) = m(\xi)/\bar{m}(\xi) = 1 - \mu(1 - |\xi|), \quad (\mu = 0.4)$$

Wave profiles, wave patterns and wave-making resistance are calculated in two ways, (a) from hull-generating source $\bar{m}(\xi)$, and (b) from wave-analyzed source $m(\xi)$.

The gap between experiment and calculation (a) is satisfactorily filled up by calculation (b).

From experimental results it is proved that the

design procedure where $\alpha(\xi)$ is taken into account is very significant.

The second order calculations for hull-surface condition as well as for free-surface condition are found not enough to give the theoretical basis for the correction function $\alpha(\xi)$, which suggests the importance of the hull's sheltering effect.

I. INTRODUCTION

The wave analysis has two objectives, i.e. (a) to determine wave-pattern resistance directly, and (b) to find out the actual wave-making mechanism of a ship-like floating body.

This paper deals with the problem (b) by means of the measurement of ship-side wave profiles rather than by free wave patterns in the rear of ships.

II. METHOD OF ANALYSIS

The co-ordinate system as shown in Figure 1 is adopted throughout the papers.

All quantities in the following equations are dimensionless, where ℓ (= L/2), half length of the ship, and U, the velocity of the uniform flow are taken as the units of length and speed, respectively.

Let us assume that the hydrodynamic singularity (source) is distributed on the surface

$$\eta = \eta(\xi, \zeta) \tag{1}$$

Then the perturbation velocity potential at an arbitrary control point P(x, y, z) is given by

$$\phi(x, y, z) = \frac{1}{4\pi} \iint_S m(\xi, \zeta)\, G(x, y, z; \xi, \eta, \zeta)\, dS \tag{2}$$

where U . $m(\xi,\zeta)$ denotes the source density at the point $Q(\xi,\eta,\zeta)$ on the distribution surface S . The Green function $G(x, y, z;\xi,\eta,\zeta)$ is

$$G(x, y, z;\xi, \eta,\zeta) = -\frac{1}{\gamma_1} - \frac{1}{\gamma_2} + H \tag{3}$$

where
$$\gamma_1^2 = (x-\xi)^2 + (y-\eta)^2 + (z-\zeta)^2$$
$$\gamma_2^2 = (x-\xi)^2 + (y-\eta)^2 + (z+\zeta)^2 \tag{4}$$

$$H = \frac{1}{\pi} \lim_{\mu \to 0} \int_{-\pi}^{\pi} d\theta \int_{o}^{\infty} \frac{k \exp\left[k(z+\zeta) + ik(\overline{x-\xi}\cos\theta + \overline{y-\eta}\sin\theta)\right]}{k - K_o \ell \sec^2\theta - i\mu\sec\theta} \, dk$$

By making use of the well-known free surface condition

$$\zeta(x, y) = -\frac{1}{K_o \ell} \frac{\partial \phi}{\partial x} \Bigg|_{z = 0} \tag{5}$$

the integral equation (2) can be converted to

$$\zeta(x, y) = -\frac{1}{4\pi K_o \ell} \iint_S m(\xi,\zeta) \frac{\partial}{\partial x} G(x, y, z;\xi, \eta,\zeta) \Big|_{z = 0} dS \tag{6}$$

where $\zeta(x, y)$ denotes the surface elevation in general.

For simplicity, let us confine ourselves to the specific limitations,

(a) the distribution surface is the rectangular, vertical central plane $(-1 \le \xi \le 1,\ -t \le \zeta \le 0)$

(b) the distribution function is draughtwise uniform.

Further, the ship-side wave profiles $\zeta_h(x, y)$ are selected as the given information of the wave elevation $\zeta(x, y)$.

Thus we have the fundamental integral equation

$$\zeta_h(x, y) = -\frac{1}{4\pi K_o \ell} \int_{-to}^{o} d\zeta \int_{-1}^{1} m(\xi) \frac{\partial}{\partial x} G(x, y, z;\xi, o,\zeta)_{z = 0} d\xi \tag{7}$$

For numerical solution of Equation (7), the modified Fourier expansions are introduced as follows

$$m(\xi) = \sum_{n=1}^{N} a_n \cos n\pi\xi' + \sum_{n=1}^{N} b_n \sin n\pi\xi' \quad (o \le \xi' \le 1) \tag{8}$$

where

$$\xi' = \frac{1}{2}(1+\xi) \qquad (-1 \le \xi \le 1) \tag{9}$$

Using above expression for $m(\xi)$, we divide the distribution plane into M number small meshes, and assume that within the meshes the source strength is constant, then the wave profiles are given by

$$\zeta_h(x,y) = \sum_{n=1}^{N} \left\{ a_n C_n(x,y) + b_n S_n(x,y) \right\} \tag{10}$$

with

$$C_n(x,y) = \sum_{i=1}^{M} \cos n\pi\xi_i' \cdot G_i(x,y;\bar{\xi}_i, to)$$

$$S_n(x,y) = \sum_{i=1}^{M} \sin n\pi\xi_i' \cdot G_i(x,y;\bar{\xi}_i, to) \tag{11}$$

where

$$G_i(x,y;\bar{\xi}_i, to) = -\frac{1}{4\pi K_o \ell} \int_{-to}^{o} d\zeta \int_{\xi_i}^{\xi_{i+1}} \frac{\partial}{\partial x} G(x,y,z;\xi,o,\zeta)_{z=0} d\xi \tag{12}$$

and

$$\bar{\xi}_i = \frac{1}{2}(\xi_i + \xi_{i+1})$$

By preliminary studies of Equations (8) and (10), five term truncation N = 5 are found suitable. Then 5 x 2 = 10 numerical coefficients $\{a_n\}$, $\{b_n\}$ $(n = 1, 2, \ldots, 5)$ are determined by the least square method.

Table 1 shows an example of such preliminary studies. Starting with the wave profiles which are calculated from the hull-generating source $m(\xi)$ of the model M21 at the speed of Fn = 0.2887 (K_oL = 12), the wave analyzed sources $m(\xi)$ are obtained for the cases N = 4, 5, 6 and 8.

Figures 2~4 also show the general features of the contribution function $G_i(x,y;\bar{\xi}_i, to)$ as expressed in Equation (12).

III. MODELS AND WAVE PROFILE MEASUREMENT

Among a variety of hull form characteristics, the beam-length ratio (B/L) is supposed as the leading parameter for the sheltering effect.

Therefore a set of two Inuid models M 20(B/L = 0.0746) and M 21(B/L = 0.1184) are prepared as shown in Table 2 and Figures 5~6 .

The hull generating sources $\overline{m}(\xi)$ of M 20 and M 21 are optimized to give the minimum wave resistance at the speed of K_oL = 12(Fn = 0.2887) under the following restraints:

$$\nabla_o' = 2 \int_{-t_o}^{o} d\zeta \int_{o}^{1} \xi \cdot \overline{m}(\xi)\, d\xi = \begin{cases} 0.018(\text{M 20}) \\ \\ 0.036(\text{M 21}) \end{cases} \qquad (13)$$

and

$$\overline{m}(\xi) = \sum_{i} a_i \xi^i \qquad (i = 1, 3, 5)$$

Three kinds of tank experiments, i.e. (a) towing test, (b) wave-profile measurement, and (c) wave pattern measurement, are carried out with M 20 and M 21 for the speed of K_oL = 7~20 (Fn = 0.3780 ~ 0.2236).

As the typical examples, the results of the wave-profile measurement at the speed of K_oL = 8, 12 and 16 are reproduced here in Figures 7~9 , where the two kinds of calculation, (a) from the hull-generating source $\overline{m}(\xi)$, and (b) from the wave-analyzed source $m(\xi)$, are also presented by dotted lines and by plots, respectively.

IV. ANALYSIS OF MEASURED WAVE PROFILES

The proposed method of analysis is applied to the measured

wave profiles of the two tested models M 20 and M 21 for the twelve speeds $K_oL = 7$ through $K_oL = 20$.

In this procedure, the measured wave profiles at twenty positions $x = -0.95, -0.85, \ldots, 0.95$ are adopted as the principal input data.

In addition, some selected readings of the wave recorder on the longitudinal cut line $y = 0.25$ ($x = 1.0 \sim 2.0$) are adopted as the supplemental input data, which are useful for the definite determination of the source around the stern.

Figures 10 ~ 12 show the wave-analyzed sources $m(\xi)$ of M 20 and M 21 for the three selected speeds $K_oL = 8$, 12 and 16, where the hull generating source $\overline{m}(\xi)$ is also given for comparison.

Because of a very low level of wave elevation, the accuracy of wave analysis is rather poor with the thin model M 20, particularly at the lower Froude number $Fn < 0.2887$ ($K_oL > 12$).

In Figures 13 and 14, the similar results at $K_oL = 10$, 11 and 12 are summarized with M 20 and M 21, respectively.

From Figures 10 through 14, a clear discrepancy, which is roughly proportional to the beam-length ratio of the models, is observed between the wave-analyzed source $m(\xi)$ and the hull-generating source $\overline{m}(\xi)$.

For the convenience of further studies including the effect of Froude number, the ratio of the two kinds of sources, or the correction function $\alpha(\xi) = m(\xi)/\overline{m}(\xi)$ is calculated with the wide model M 21.

The results are reproduced in Figures 15 ~ 17.

Here it must be remembered that the relative accuracy of $\alpha(\xi)$ is poor around midship, because of $\overline{m}(\xi)$ being null for $\xi = 0$.

With respect to the sheltering effect, the present authors [1] . [2] . [3] suggested a simple, empirical correction, like

$$\alpha(\xi) = 1 - \mu(1 - |\xi|) \tag{14}$$

with

$$\mu = 0.4 \qquad \text{for} \quad B/L = 0.12 \sim 0.15$$

In Figures 15 ~17, Equation (14), which we call μ- correction, is also given for comparison with the wave-analyzed result of M 21($B/L = 0.1184$).

It is noticeable that the general tendencies of the wave-analyzed correction function are of quite similar tendency to the simple, empirical relation (14), except the higher Froude number $Fn > 0.30$ ($K_0L < 11$).

At the higher speed range, the inclination of $\alpha(\xi)$ is getting steeper with increasing Froude number.

Therefore Equation (14) is modified here to a more general expression, like

$$\alpha(\xi) = a + b|\xi| \tag{15}$$

The results of the generalized straight line approximation, which is applied to the wave analyzed correction function of M 21, are given in Figure 18 together with the original proposal (14).

V. COMPARISON WITH TANK EXPERIMENT

Before entering the discussions on the theoretical basis for the obtained correction function $\alpha(\xi)$, its justification and usefulness are examined by comparison with tank experiments on four items, i.e. (i) wave profiles, (ii) wave patterns, (iii) wave-making resistance, and (iv) amplitude functions.

(i) Wave profiles

By direct integration, the model's side-wave profile is calculated from the wave-analyzed source distribution $m(\xi)$, which is reproduced by the plots in Figures 7 ~ 9.

Its satisfactory agreement with the measured wave-profile (full-lines) makes a striking contrast with the rather poor result of the existing theory (dotted lines).

A slight phase shift, however, is observed with the first wave crest of the wide model M 21, which appears to be attributable to the non-linear flow effects in close vicinity of the stem.

To find out the accuracy of approximation, similar calculation is also carried out with M 21 by adopting μ - correction ($\mu = 0.4$), whose result is also presented in Figures 7~9.

(ii) Wave Patterns

The measured wave contours of the tested two Inuid models M 20 and M 21 are obtained at a single speed Fn = 0.2887 (K_oL = 12) by cross fairing of the longitudinal cut wave recordings of every 5 cm intervals from y = 0.25 (close to the model's side) through y = 1.75 (tank side wall).

The final results are reproduced in Figures 19 (M 20) and 20 (M 21) respectively.

The corresponding calculations are carried out in three different ways.

(a) by existing theory, or from the hull-generating source $\overline{m}(\xi)$,

(b) from the wave-analyzed source $m(\xi)$,

(c) by μ - correction ($\mu = 0.4$)

These calculated wave patterns are presented in Figures 21 ~ 24.

The existing theory (a) (Figure 21) shows the poorest agreement with experiment. Particularly, the transverse waves are tremendously exaggerated in this calculation in accordance to the author's previous suggestions [1] .

The clear disagreement between existing theory (a) and experiment is again improved successfully by the present approach (b).

In fact, not only the general features but also the details of the measured wave patterns of the tested models M 20 (Figure 19) and M 21 (Figure 20) are beautifully reproduced in Figure 22 (M 20) and Figure 23 (M 21), respectively.

With respect to the effectiveness of the simple correction (c), Figure 24 shows its relative merits and demerits in comparison with (a) and (b).

(iii) Wave-Making Resistance

Ordinary towing tests are carried out with M 20 and M 21 by fitting the plate-stud stimulator at 0.05 L behind the stem.

The wave-making resistance coefficients

$$Cw = Rw / \frac{\rho}{2} U^2 L^2 \tag{16}$$

which are obtained by adopting Schoenherr-line with form factor K = 0.07 (M 20) and K = 0.15 (M 21), are presented in Figures 25 and 26.

In these Figures, the three kinds of calculations are also given for comparison with the experiment,

(a) Cw calculated by existing theory, or from the hull-generating source $\overline{m}(\xi)$,

(b) Cw calculated from the wave-analyzed source $m(\xi)$,

(c) Cw calculated by μ – correction ($\mu = 0.4$).

Calculation (b) again shows the best and the most satisfactory agreement with experiment in contrast to calculation (a) or (c).

(iv) Amplitude Function

Comparison is also made on the amplitude function of the total free waves for the speed of Fn = 0.2887 ($K_0L = 12$). Figures 27 (M 20) and 28 (M 21) show four kinds of amplitude function, i. e.

(a) Amplitude function calculated by existing theory,

(b) Amplitude function calculated from wave-analyzed source distribution,

(c) Amplitude function obtained from the measured free waves by longitudinal cut method,

(d) Amplitude function obtained from the measured free waves by transverse cut method.

As easily observed, the amplitude function (b) shows the highest average level of free wave amplitude, particularly in the transverse wave range. It appears that the difference between (b) and (c) or (d) may be partially explained by the wave-breaking resistance.

In Figures 25 and 26, Cw at the specific Froude number Fn = 0.2887, which is obtained from the longitudinal cut method (c), is also presented.

VI. SEARCH FOR THEORETICAL BASIS OF CORRECTION FUNCTION $\alpha(\xi)$

The practical usefulness as well as the experimental justification of the obtained correction function $\alpha(\xi)$ are clearly demonstrated in the preceding sections.

From a theoretical point of view, however, its hydrodynamical mechanism still remains open for further investigations.

From the standpoint of the boundary condition which is used to obtain velocity potential in Equation 2, two possible causes for the discrepancies between theoretical and wave-analyzed results can be mentioned. Namely, (a) finite Froude number effect for the hull-surface condition, (b) non-linear effect for the free-surface condition.

For the time being, preliminary calculations of these two higher order terms are carried out with respect to the amplitude functions.

VI. 1. Hull surface condition

Throughout the present paper, the hull-generating source $\overline{m}(\xi)$ is derived from the so-called double-model approximation which is correct only for limiting case $Fn \longrightarrow 0$ or $K_0L \longrightarrow \infty$.

To find out the effect of finite Froude number, the Green function $G(x, y, z ; \xi , \eta , \zeta)$ expressed in Equation (3) is rewritten as

$$G(x, y, z ; \xi , \eta , \zeta) = G_1 + G_2 + G_3 \tag{17}$$

where

$$G_1 = - \frac{1}{r_1} - \frac{1}{r_2} \tag{18}$$

$$G_2 = - 4 K_o \ell \int_{-\frac{\pi}{2} + \textcircled{H}}^{\frac{\pi}{2}} \sec^2\theta \, e^{K_o \ell (z + \zeta) \sec^2\theta} \sin(K_o \ell \, p \sec^2\theta) \, d\theta \tag{19}$$

$$G_3 = \frac{2 K_o \ell}{\pi} \int_{-\frac{\pi}{2} + \textcircled{H}}^{\frac{\pi}{2} + \textcircled{H}} d\theta \int_o^\infty k \, \frac{\sec^2\theta \cos(k K_o \ell \overline{z + \zeta}) - k \sin(k K_o \ell \overline{z + \zeta})}{k^2 + \sec^4\theta} \, e^{-k K_o \ell p} \, dk \tag{20}$$

$$p = (x - \xi) \cos\theta + (y - \eta) \sin\theta$$

$$\tan \textcircled{H} = (y - \eta) / (x - \xi) \tag{21}$$

In Equations (17) through (21), the second term G_2 denotes the free wave component which propagates oscillatorily to the rear of a ship, while $(G_1 + G_3)$ represents the local disturbance.

Differentiating Equation (17) as to x, y, z and integrating all over the distribution plane, the velocity components u, v, w are also written as

$$\begin{aligned} u &= u_1 + u_2 + u_3 \\ v &= v_1 + v_2 + v_3 \\ w &= w_1 + w_2 + w_3 \end{aligned} \tag{22}$$

In finite Froude number problem, the free wave terms u_2, v_2, and w_2 and a part of local disturbance u_3, v_3, and w_3 play important role which is shown in Figure 29 in the case of M 21 and $K_oL = 12$.

Based upon the "exact" hull-surface condition,

$$v - \frac{\partial f(x,z)}{\partial x} \quad u - \frac{\partial f(x,z)}{\partial z} \quad w = \frac{\partial f(x,z)}{\partial x} \tag{23}$$

where $y = f(x,z)$ denotes the half-breadth of the hull, the "exact" hull-generating sources for finite Froude number $K_oL = 12$ are obtained with M 21.

This result is presented in Figure 30 together with the double-model approximation $\overline{m}(\xi)$ and the wave-analyzed source $m(\xi)$.

The corresponding amplitude function is also given in Figure 31.

From Figures 30 and 31, it may be concluded that the effect of finite Froude number for the hull-surface condition can explain the cause of the correction function $\alpha(\xi)$ partially, but not completely.

VI. 2. Free-Surface Condition

Before discussing the problem (b), we assume that the second order term for the free-surface condition is independent of the higher contribution of the hull-surface condition (VI.1). The velocity

potential in Equation (2) is obtained from the linearized free-surface condition

$$\frac{U^2}{g} \frac{\partial^2 \phi}{\partial x^2} + \frac{\partial \phi}{\partial z} = 0 \Big|_{z=0} \tag{24}$$

Assuming that the second order term for the free-surface condition is independent of the hull-surface condition, the approximate calculations are carried out as follows.

Using small parameter ϵ (we can choose $\epsilon = B/L$), we can get the well-known expansions

$$\phi = \epsilon \phi_1 + \epsilon^2 \phi_2 + \epsilon^3 \phi_3 + \ldots \tag{25}$$

$$\zeta = \epsilon \zeta_1 + \epsilon^2 \zeta_2 + \epsilon^3 \zeta_3 + \ldots$$

Then the kinematical condition of free surface

$$(U + \frac{\partial \phi}{\partial x}) \frac{\partial \zeta}{\partial x} + \frac{\partial \phi}{\partial y} \frac{\partial \zeta}{\partial y} - \frac{\partial \phi}{\partial z} = 0 \Big|_{z=\zeta} \tag{26}$$

is written as

$$\epsilon \left\{ U \frac{\partial \zeta_1}{\partial x} - \frac{\partial \phi_1}{\partial z} \right\} + \epsilon^2 \left\{ U \frac{\partial \zeta_2}{\partial x} - \frac{\partial \phi_2}{\partial z} + \frac{\partial \phi_1}{\partial x} \frac{\partial \zeta_1}{\partial x} + \right.$$

$$\left. + \frac{\partial \phi_1}{\partial y} \frac{\partial \zeta_1}{\partial y} - \frac{\partial^2 \phi_1}{\partial z^2} \zeta_1 \right\} \tag{27}$$

$$+ \epsilon^3 \left\{ \ldots \right\} + \ldots = 0 \Big|_{z=0}$$

Similarly, the pressure condition

$$U \frac{\partial \phi}{\partial x} + \frac{1}{2} \left\{ \left(\frac{\partial \phi}{\partial x}\right)^2 + \left(\frac{\partial \phi}{\partial y}\right)^2 + \left(\frac{\partial \phi}{\partial z}\right)^2 \right\} + gz = 0 \Big|_{z=\zeta} \tag{28}$$

is expressed by

$$\epsilon \left\{ U \frac{\partial \phi_1}{\partial x} + g \zeta_1 \right\} + \epsilon^2 \left[U \frac{\partial \phi_2}{\partial x} + g \zeta_2 + U \frac{\partial^2 \phi_1}{\partial x \partial z} \zeta_1 \right.$$

$$\left. \mp \frac{1}{2} \left\{ \left(\frac{\partial \phi_1}{\partial x}\right)^2 + \left(\frac{\partial \phi_1}{\partial y}\right)^2 + \left(\frac{\partial \phi_1}{\partial z}\right)^2 \right\} \right] + \epsilon^3 \{ \ldots \} + \ldots \Big|_{z=0} \tag{29}$$

Paying attention to order of ϵ, we have following two equations as to ϵ and ϵ^2 respectively.

$$\frac{U^2}{g} \frac{\partial^2 \phi_1}{\partial x^2} + \frac{\partial \phi_1}{\partial z} = 0 \Big|_{z=0} \tag{30}$$

$$\frac{U^2}{g} \frac{\partial^2 \phi_2}{\partial x^2} + \frac{\partial \phi_2}{\partial z} + \frac{U}{g} \frac{\partial}{\partial x} \left\{ \left(\frac{\partial \phi_1}{\partial x}\right)^2 + \left(\frac{\partial \phi_1}{\partial y}\right)^2 + \left(\frac{\partial \phi_1}{\partial z}\right)^2 \right\}$$

$$- \frac{U}{g} \frac{\partial \phi_1}{\partial x} \left\{ \frac{\partial}{\partial z} \left(\frac{U^2}{g} \frac{\partial^2 \phi_1}{\partial x^2} + \frac{\partial \phi_1}{\partial z} \right) \right\} = 0 \Big|_{z=0} \tag{31}$$

Equation (31), which is the second order term of the free-surface condition, can be written as

$$\frac{U^2}{g} \frac{\partial^2 \phi_2}{\partial x^2} + \frac{\partial \phi_2}{\partial z} = \gamma 1(x, y) \tag{32}$$

where

$$\gamma_1(x,y) = -\frac{U}{g}\left[\frac{\partial}{\partial x}\varphi^2 - \frac{\partial \phi_1}{\partial x}\left\{\frac{\partial}{\partial z}\left(\frac{U^2}{g}\frac{\partial^2 \phi_1}{\partial x^2} + \frac{\partial \phi_1}{\partial z}\right)\right\}\right] \tag{33}$$

$$\varphi^2 = \left(\frac{\partial \phi_1}{\partial x}\right)^2 + \left(\frac{\partial \phi_1}{\partial y}\right)^2 + \left(\frac{\partial \phi_1}{\partial z}\right)^2 \tag{34}$$

The second order term of the velocity potential ϕ_2 is given in accordance with well-known Fourier double integral

$$\phi_2 = \frac{1}{4\pi}\int_{-\infty}^{\infty}\int_{o}^{\infty}\gamma_1(x',y')\,G(x,y,z\,;x',y',o)\,dx'\,dy' \tag{35}$$

where $G(x,y,z\,;x',y',o)$ is given in Equation (3) and (4.)

Once ϕ_1 is known, $\gamma_1(x,y)$ can be calculated by Equation (33) all over the $z = 0$ plane, then ϕ_2 is obtained by Equation (35) Equation (35) means that the velocity potential of second order term is just that of source distribution $\gamma_1(x,y)$ which is distributed over the free surface.

The second order amplitude function corresponding to ζ_2 is given as follows after some approximations.

$$C_2(\theta)/L = \frac{2}{\pi}\sec^2\theta\int_o^{\infty}\Big\{P(\theta,y')\cos(K_o\ell\sec^2\theta\sin\theta\,y') - Q(\theta,y')\sin(K_o\ell\sec^2\theta\sin\theta\,y')\Big\}\,dy'$$

contd.

$$S_2(\theta)/L = \frac{2}{\pi}\sec^2\theta \int_0^{\infty} \left\{ P(\theta, y') \sin(K_o \ell \sec^2\theta \sin\theta y') + Q(\theta, y') \cos(K_o \ell \sec^2\theta \sin\theta y') \right\} dy' \qquad (36)$$

where

$$P(\theta, y') = \frac{1}{2} K_o \ell \sec\theta \int_{-\infty}^{\infty} \delta^2 \sin(K_o \ell \sec\theta x') dx'$$

$$Q(\theta, y') = \frac{1}{2} K_o \ell \sec\theta \int_{-\infty}^{\infty} \delta^2 \cos(K_o \ell \sec\theta x') dx' \qquad (37)$$

Figure 32 shows the first order amplitude functions, $C_1(\theta)/L$, $S_1(\theta)/L$ of the model M21 at the speed of $K_oL = 12$ which are calculated in three different ways.

(a) by existing theory, or from $\overline{m}(\xi)$

(b) by wave-analyzed source $m(\xi)$

(c) by μ-correction ($\mu = 0.4$)

The difference between the result (a) and (b) is presented in Figure 33 together with the second order amplitude functions $C_2(\theta)/L$, $S_2(\theta)/L$ which are calculated Equation 36.

Figure 33 suggests that the second order correction for the free-surface condition is important only for the diverging wave range, where the wave-slope is predominant.

Consequently, it appears that the remarkable discrepancy which is observed in the transverse wave range cannot be explained by this kind of non-linear effect.

By summarizing the preceding discussions (VI. 1) and (VI.2) it may be safely concluded that the real mechanism of the sheltering effect $\alpha(\xi)$ should be investigated not only by the second order considerations but also from some different kind of approaches such as suggested by Brard [4] or Pien and Chang [5].

VII. APPLICATION TO HULL FOR M DESIGN

Although the theoretical basis of the sheltering effect still remains unsolved, the presently obtained results will be of practical use for the hull form design with least wave resistance.

As an example, an asymmetry Inuid model M 21-Modified is designed under the same geometrical restraints as M 21 except that

(a) The approximate correction function $\alpha(\xi)$ which is given in Figure 18 is applied in the process of minimization of wave resistance.

For example, at the designed Froude number Fn = 0.2887 ($K_oL = 12$), we have

$$\alpha(\xi) = \begin{cases} 0.3 + 0.8\,|\xi|\,, & \text{fore body} \\ 0.7 + 0.3\,|\xi|\,, & \text{aft body} \end{cases} \tag{38}$$

(b) The correction function $\alpha(\xi)$ being asymmetry fore and aft, the optimized hull form is also asymmetry under the following restraint,

$$\text{Total source} = W = \int_{-1}^{1} \bar{m}(\xi)\, d\xi = 0 \tag{39}$$

(c) The modified Fourier expansions are used for $\bar{m}(\xi)$.

It is expected that the modified asymmetry model M 21-M will be superior to the original model M 21 as far as wave resistance at the designed Froude number is concerned.

Figures 34 through 36 show the calculated results. i.e. (a) hull-generating source, (b) load water line, (c) amplitude function, respectively.

The towing tests of M 21-M were run on May 9th through 12th, 1972 and Figure 37 shows its result. As far as wave resistance is concerned, the agreement between experiment and the present theory is noticeable. Moreover, M 21-M is much less, as expected, than M 21 in wave-making resistance at the designed Froude number.

These results may suggest that the principal leading factors of the sheltering effect are B/L and the shape of water plane as discussed in the preceding sections. In this connection, it must also be remembered that the simple μ -correction of Equation (14) was originally proposed not with Inuid models but with Pienoid models.

Therefore, the correction function $\alpha(\xi)$ which is obtained with M 21(B/L = 0.1184) will be applicable not only to Inuids but also to more general hull forms with flat bottoms.

VIII. CONCLUSIONS

Analytical method for obtaining the effective wave-making source of a ship is developed, where the measurement of the hull-side wave profiles is adopted as input data, instead of the free wave patterns in the rear of a ship.

Two Inuid models with different beam-length ratio (B/L = 0.0746, 0.1184) are wave-analyzed.

Clear discrepancy is observed between the two kinds of sources, i.e. (a) hull-generating source $\overline{m}(\xi)$ based upon double-model assumption, and (b) effective wave-making source $m(\xi)$ analyzed from measured wave profiles by means of the proposed method.

The correction function $\alpha(\xi) = m(\xi)/\overline{m}(\xi)$ which is obtained from the wide model (B/L = 0.1184) is almost identical with the authors' proposal for the sheltering effect (1968),

$$\alpha(\xi) = 1 - \mu(1 - |\xi|), \qquad (\mu = 0.4)$$

The second order calculations for hull-surface condition as well as for free-surface condition are found insufficient to give the theoretical bases of the obtained correction function $\alpha(\xi)$, which suggests the importance of the hull's sheltering effect.

Considering $\alpha(\xi)$ as a correction function, M 21-M is designed under the same restraint condition as that of M 21. From towing test results, it is proved that M 21-M is much less that M 21 in wave-making resistance and such a design procedure is significant.

REFERENCES

[1] INUI, T., KAJITANI, H., FUKUTANI, N. and YAMAGUCHI, M., "On Wave Making Mechanism of Ship Hull Forms, Generated from Undulatory Source Distributions", Journ. Soc. Nav. Arch. Japan, Vol. 124, Dec. 1968.

[2] Do. : Selected Papers from Journ. Soc. Nav. Arch. Japan, Vol. 4, 1970.

[3] INUI, T. and KAJITANI, H., "Sheltering Effect of Complicated Hull Forms", Proc. 12th Int. Towing Tank Conference, Rome, 1969.

[4] BRARD, R., "The Neumann-Kelvin Problem for Surface Ships", Report 11CST, 1971.

[5] PIEN, P.C. and CHANG, M.S., "Potential Flow about a General Three-Dimensional Body", NSRDC Report 3608, 1971.

* * *

Table 1.

Analyzed source strength of M 21, based on calculated wave profiles

Remarks : $m(\xi)$ = wave-analyzed source

$\bar{m}(\xi)$ = hull-generating source

ξ	$\bar{m}(\xi)$	$m(\xi)$			
		N=4	N=5	N=6	N=8
-1.0	0.3207	0.3172	0.3159	0.2546	-0.0791
-0.9	0.2927	0.3015	0.2936	0.3112	0.2772
-0.8	0.3740	0.3796	0.3735	0.3712	0.3891
-0.7	0.4911	0.4980	0.4907	0.4979	0.4865
-0.6	0.5920	0.6042	0.5922	0.6036	0.5872
-0.5	0.6437	0.6595	0.6439	0.6442	0.6649
-0.4	0.6297	0.6444	0.6294	0.6291	0.5992
-0.3	0.5468	0.5577	0.5465	0.5611	0.5327
-0.2	0.4027	0.4108	0.4028	0.4219	0.4328
-0.1	0.2134	0.2218	0.2137	0.2123	0.1909
0.0	0.0000	0.0110	0.0001	-0.0231	-0.0434
0.1	-0.2134	-0.2007	-0.2136	-0.2281	-0.2153
0.2	-0.4027	-0.3911	-0.4029	-0.3863	-0.4881
0.3	-0.5468	-0.5376	-0.5466	-0.5198	-0.6691
0.4	-0.6297	-0.6197	-0.6294	-0.6324	-0.5650
0.5	-0.6437	-0.6254	-0.6438	-0.6717	-0.7467
0.6	-0.5920	-0.5578	-0.5922	-0.5853	-1.1521
0.7	-0.4911	-0.4410	-0.4910	-0.4251	-0.2983
0.8	-0.3740	-0.3198	-0.3740	-0.3400	-0.5465
0.9	-0.2927	-0.2514	-0.2936	-0.3322	-4.4894
1.0	-0.3207	-0.2909	-0.3138	0.1284	36.416

Table 2.
Principal particulars of M 20 & M 21

Item		M20	M21
L(m)		2.001	2.001
B(m)		0.1492	0.2368
D(m)		0.2055	0.2424
d(m)		0.1405	0.1724
$\nabla(m^3)$		0.0178	0.0347
$S(m^2)$		0.5390	0.6686
B/L		0.0746	0.1184
d/L		0.0702	0.0862
Designed Speed,		$K_sL=12$	
Condition of Restraint		$V_s'=0.018$	$V_s'=0.036$
Distribution Plane		T/L=0.04 (Inuid)	
Source Distribution	a_1	1.08722	2.17444
	a_3	-2.05643	-4.11286
	a_5	1.12955	2.25910

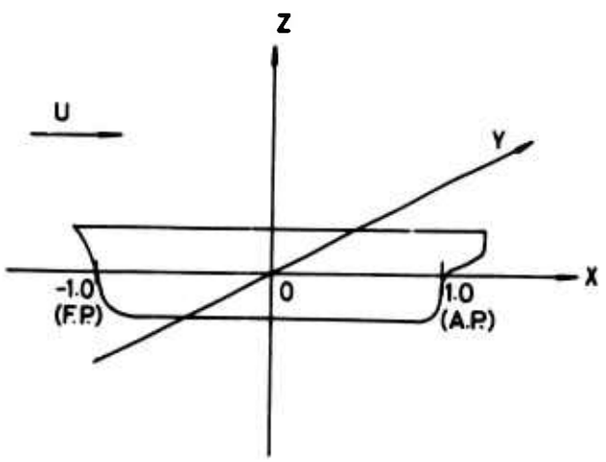


Figure 1. Co-ordinate system

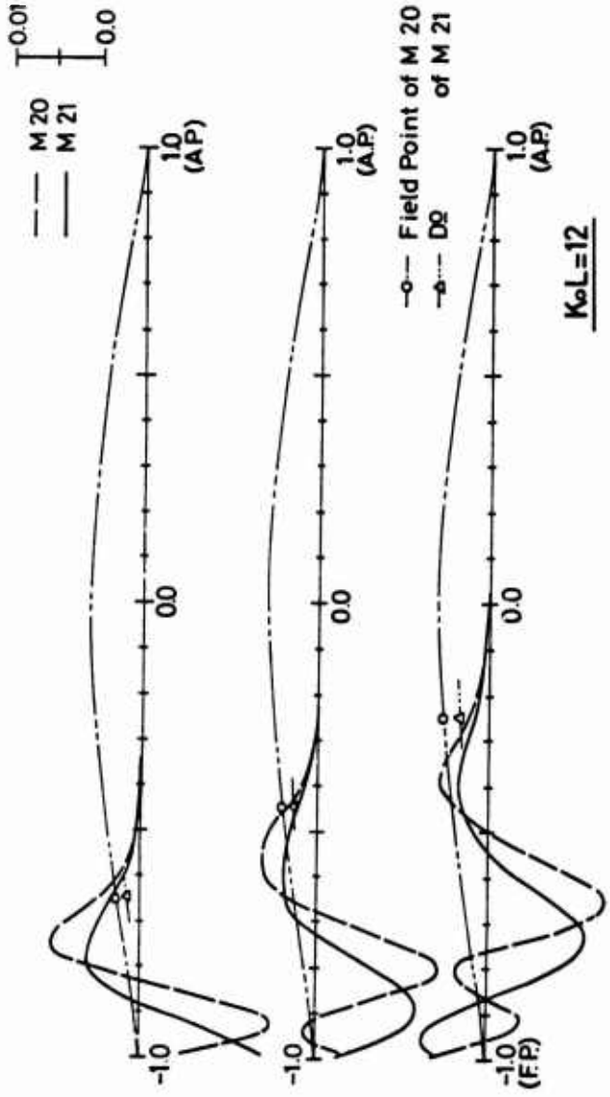


Figure 2. The effective wave height of finite sheet (1)

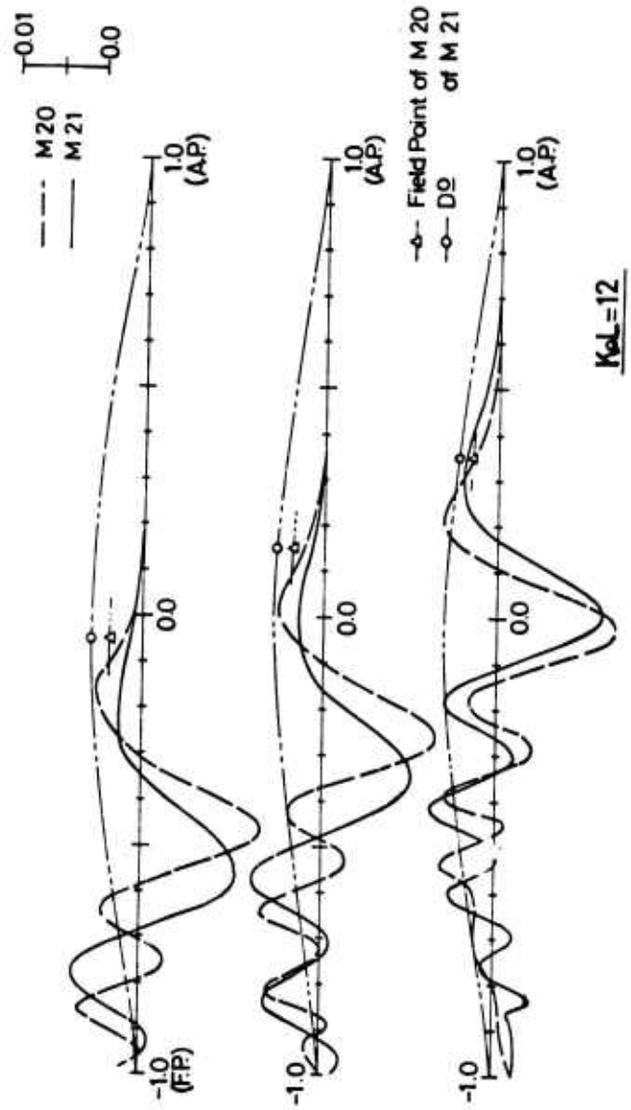


Figure 3. The effective wave height of finite sheet (2)

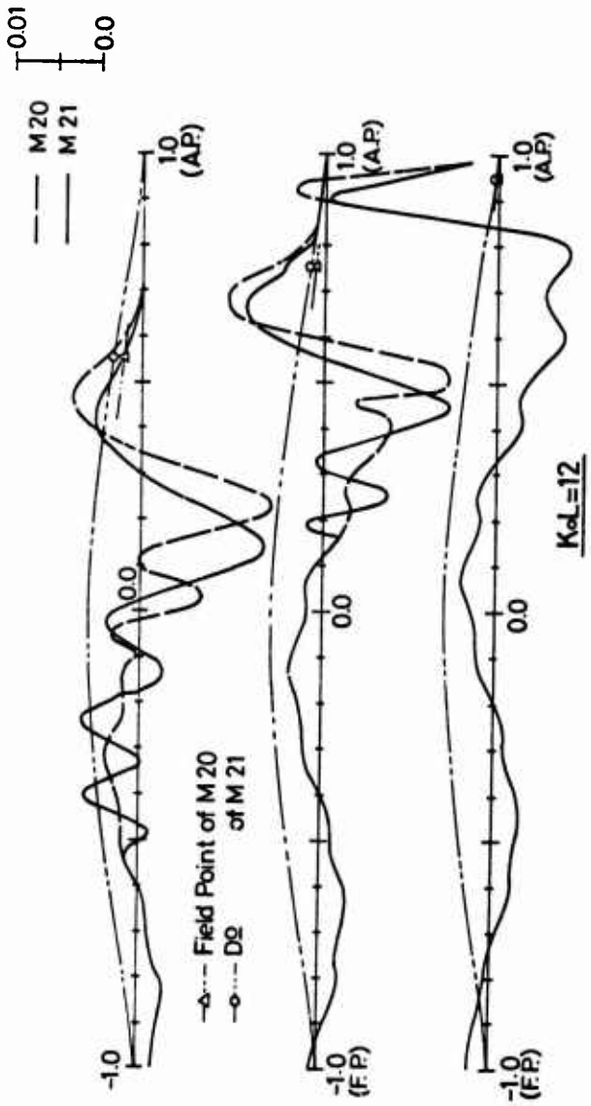


Figure 4. The effective wave height of finite sheet (3)

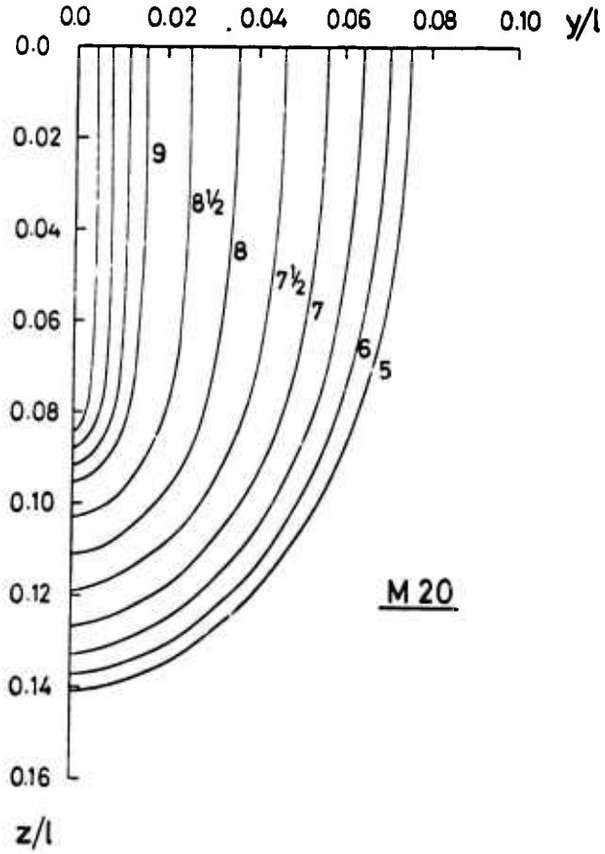


Figure 5. The body plan of M 20

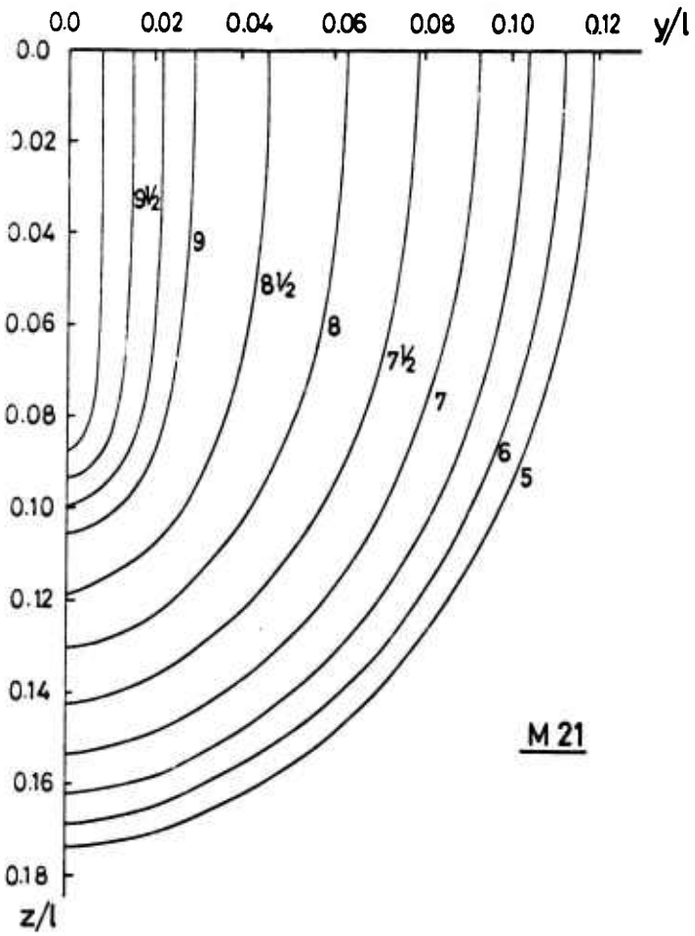


Figure 6. The body plan of M 21

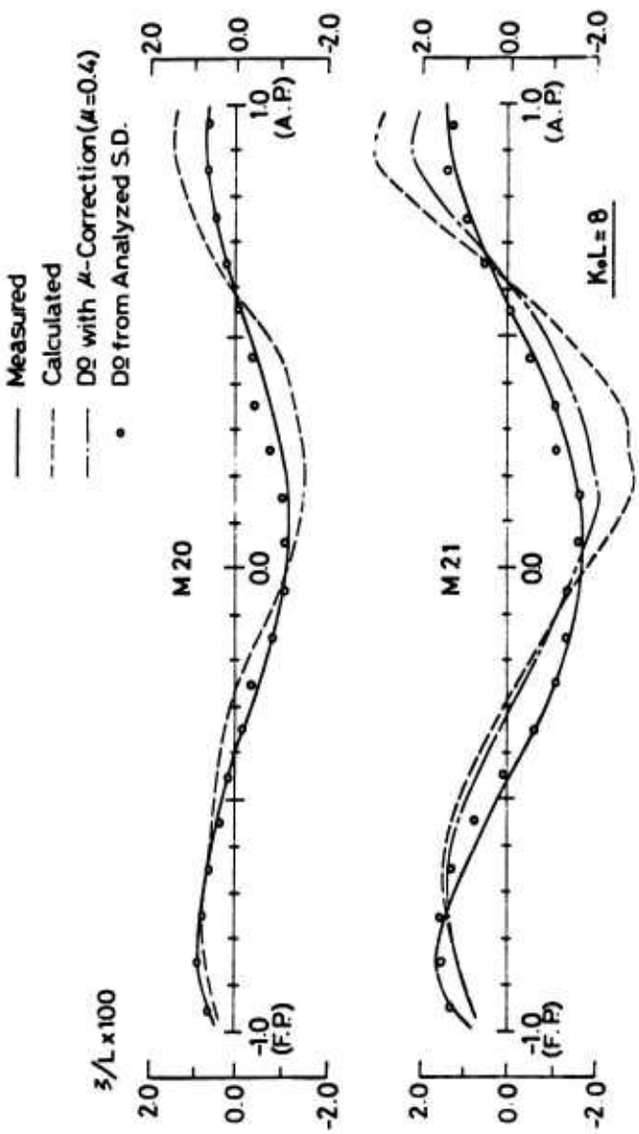


Figure 7. Wave profiles of M 20 & M 21 ($K_oL = 8$)

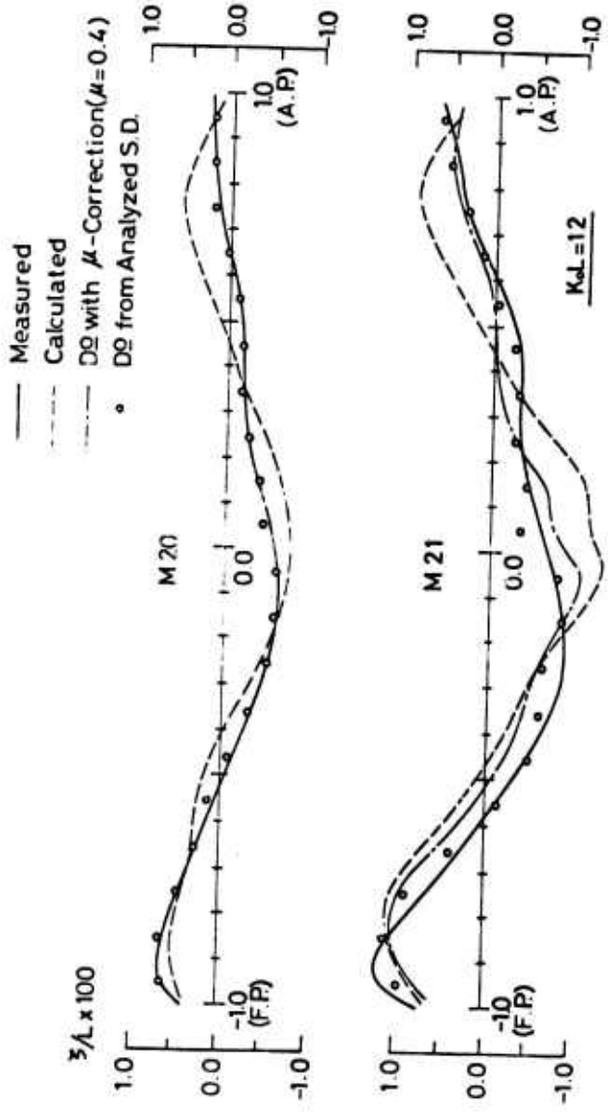


Figure 8. Wave profiles of M 20 & M 21 ($K_o L = 12$)

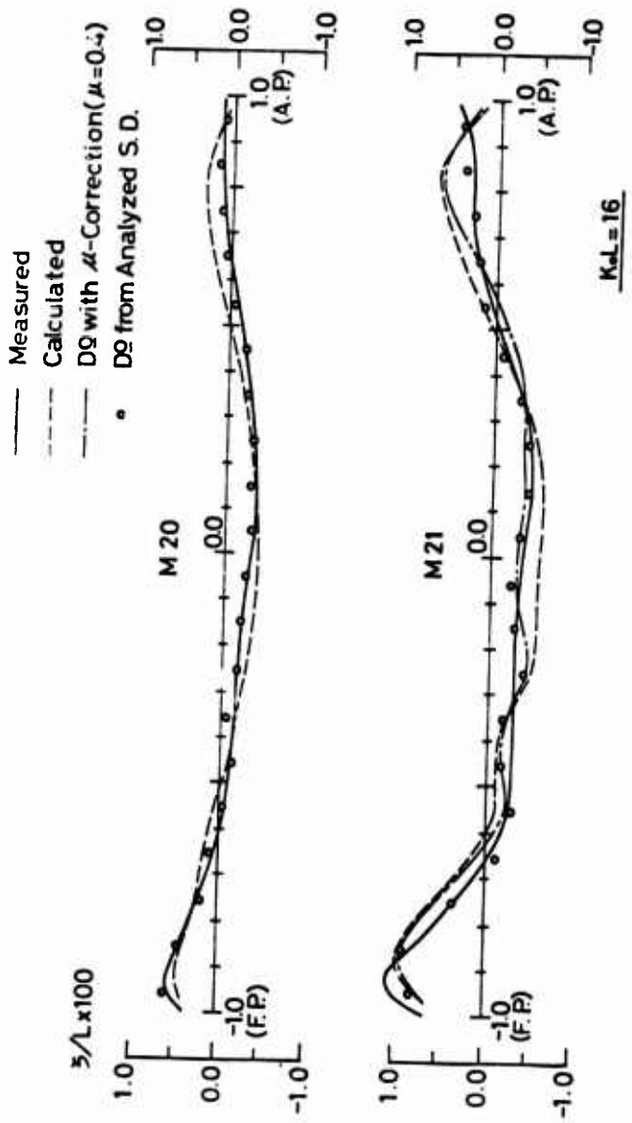


Figure 9. Wave profiles of M 20 & M 21 ($K_oL = 16$)

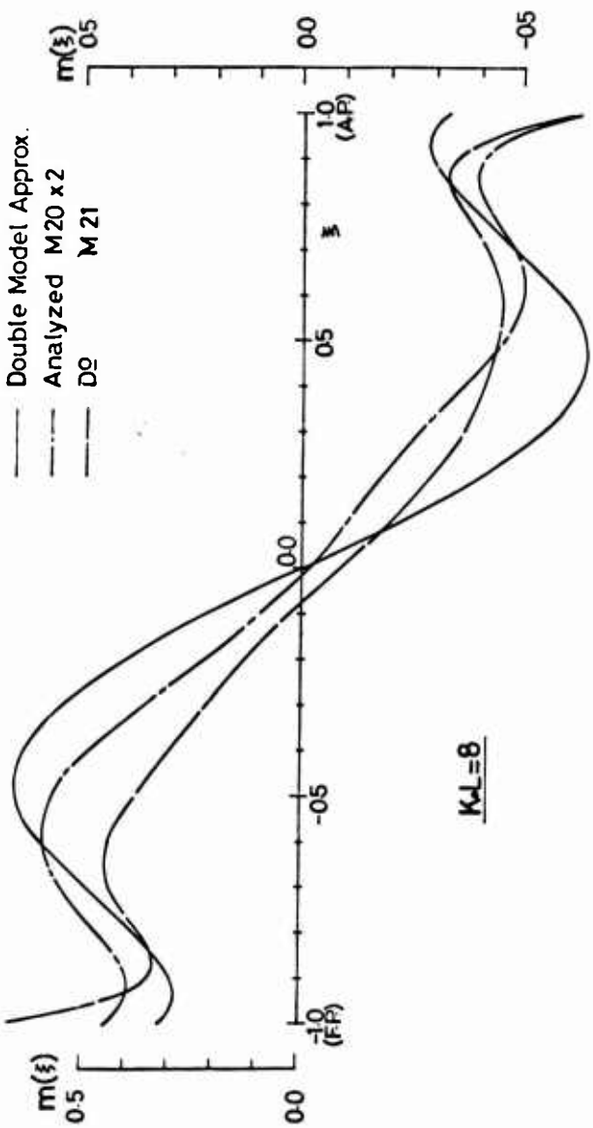


Figure 10. Wave-analyzed source distribution ($K_o L = 8$)

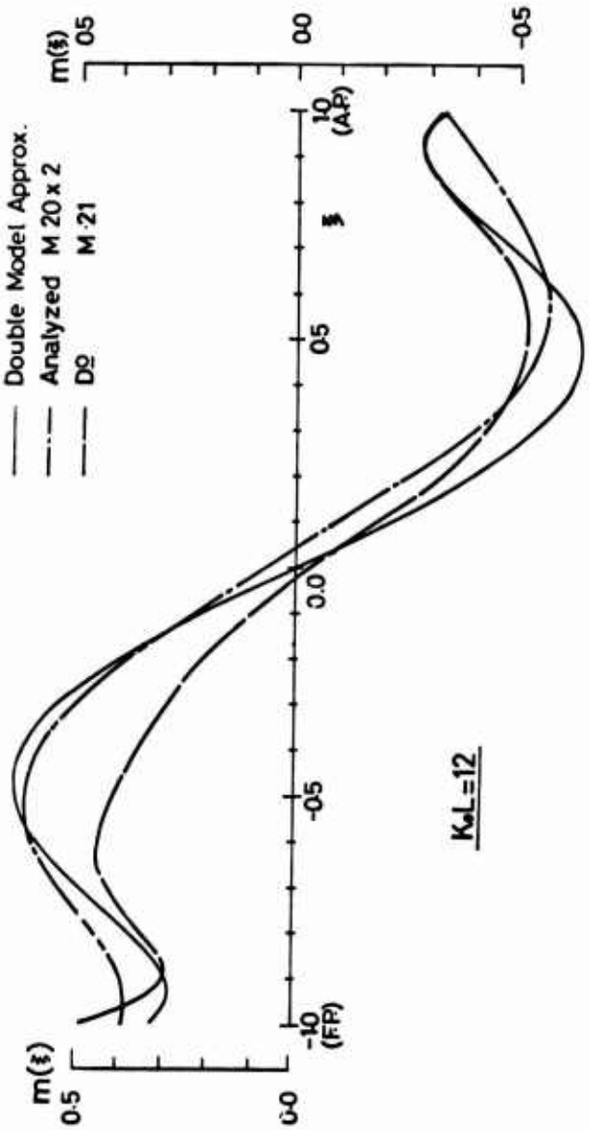


Figure 11. Wave-analyzed source distribution ($K_oL = 12$)

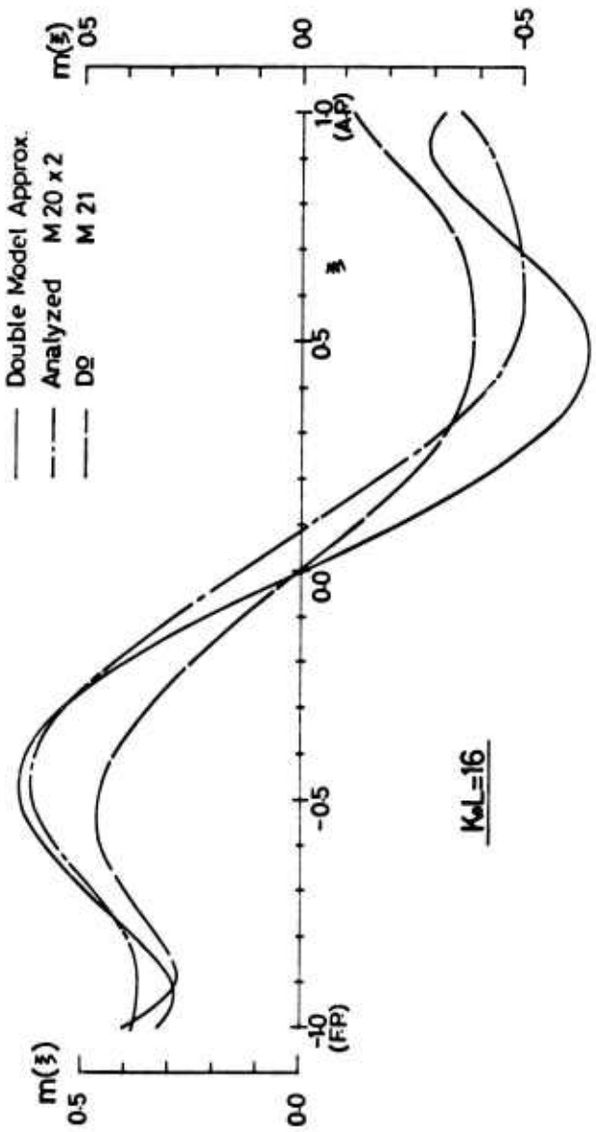


Figure 12. Wave-analyzed source distribution ($K_o L = 16$)

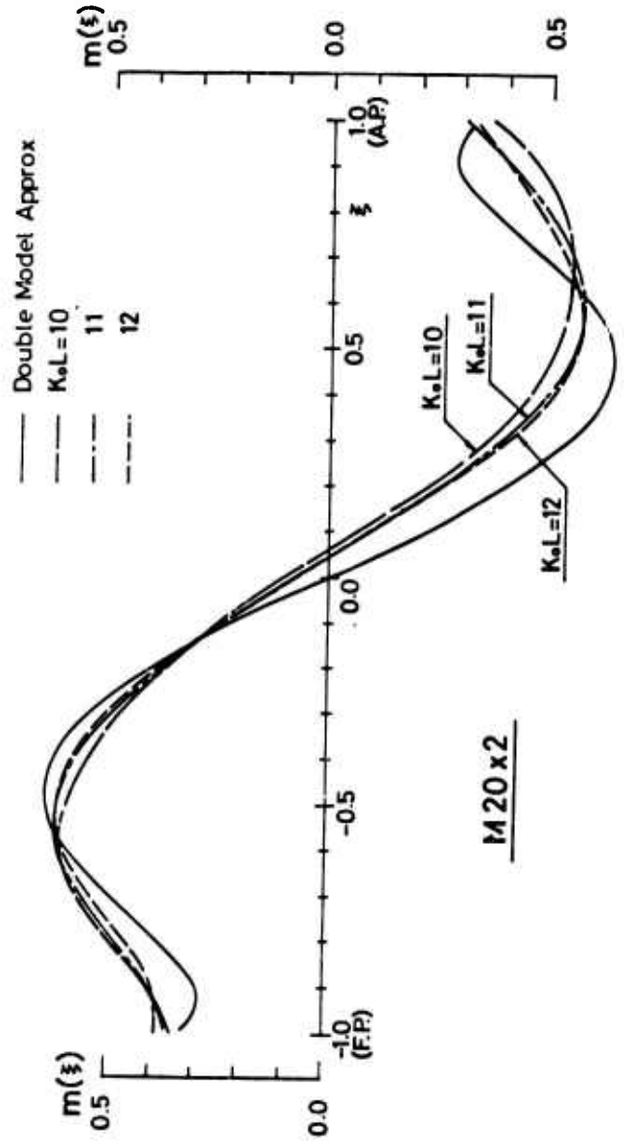


Figure 13. Wave-analyzed source distribution (M 20)

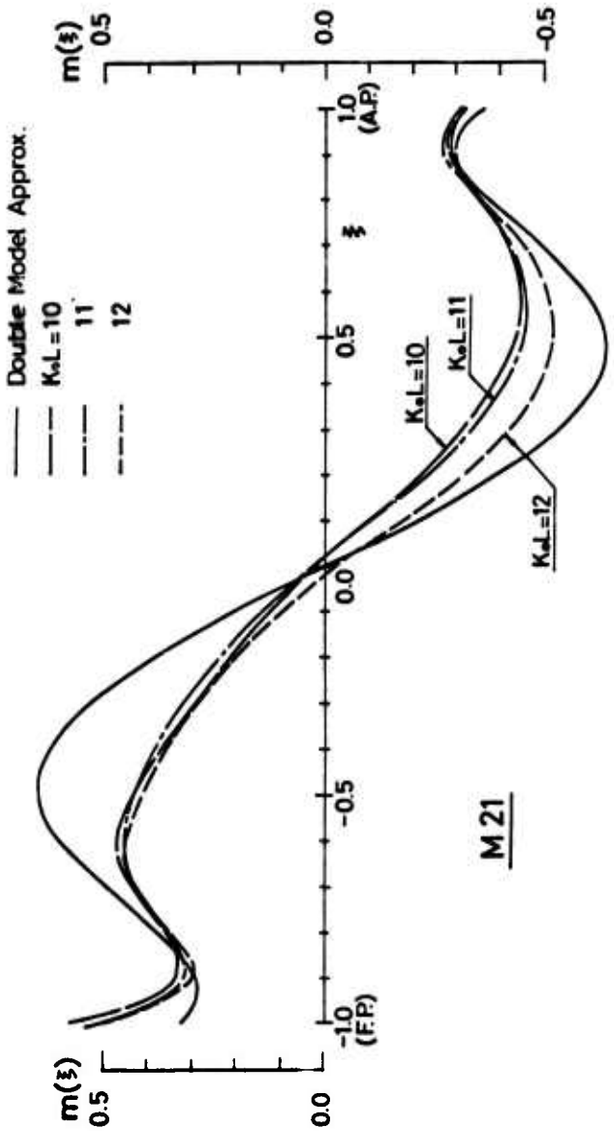


Figure 14. Wave-analyzed source distribution (M 21)

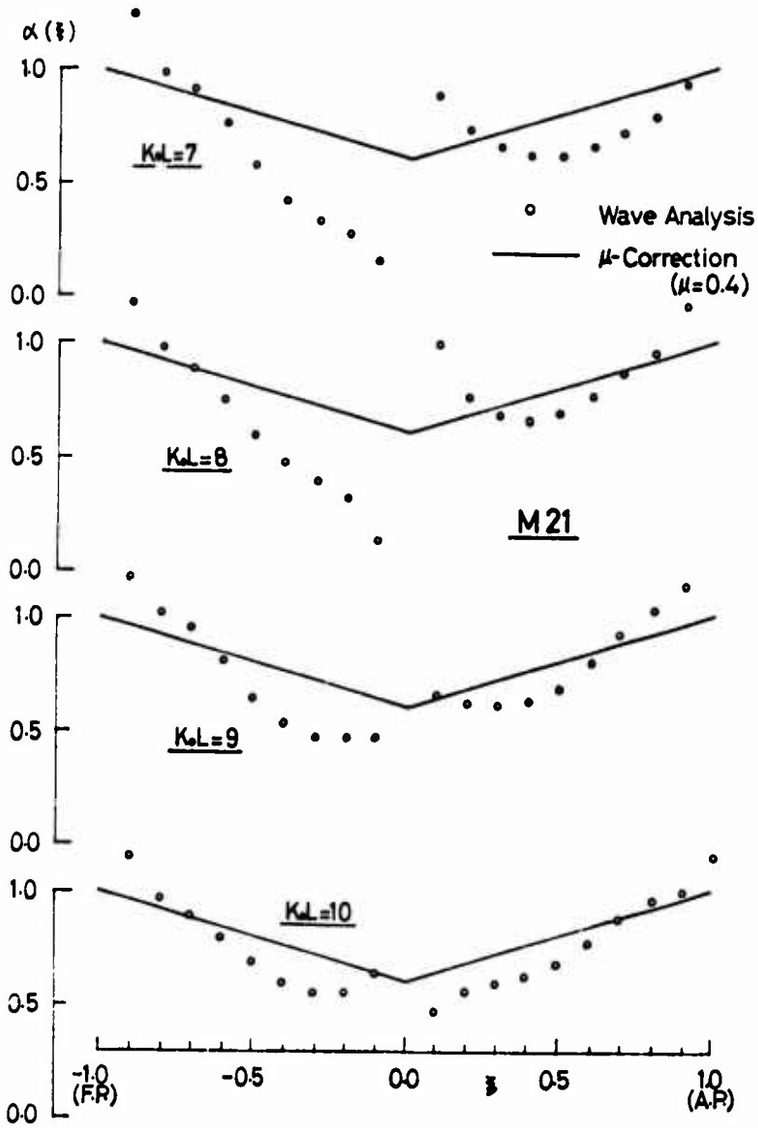


Figure 15. The ratio of $m(\xi)/\overline{m}(\xi)$ ($K_oL = 7 \sim 10$)

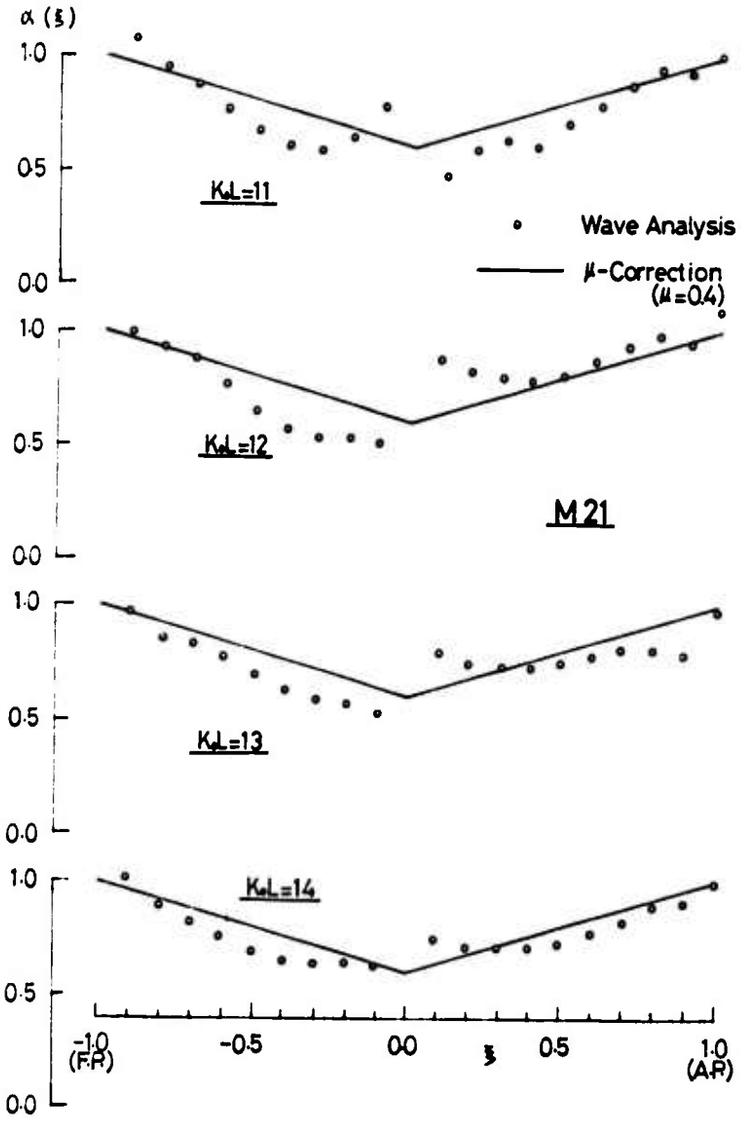


Figure 16. The ratio of $\overline{m}(\xi)/m(\xi)$ ($K_oL = 11 \sim 14$)

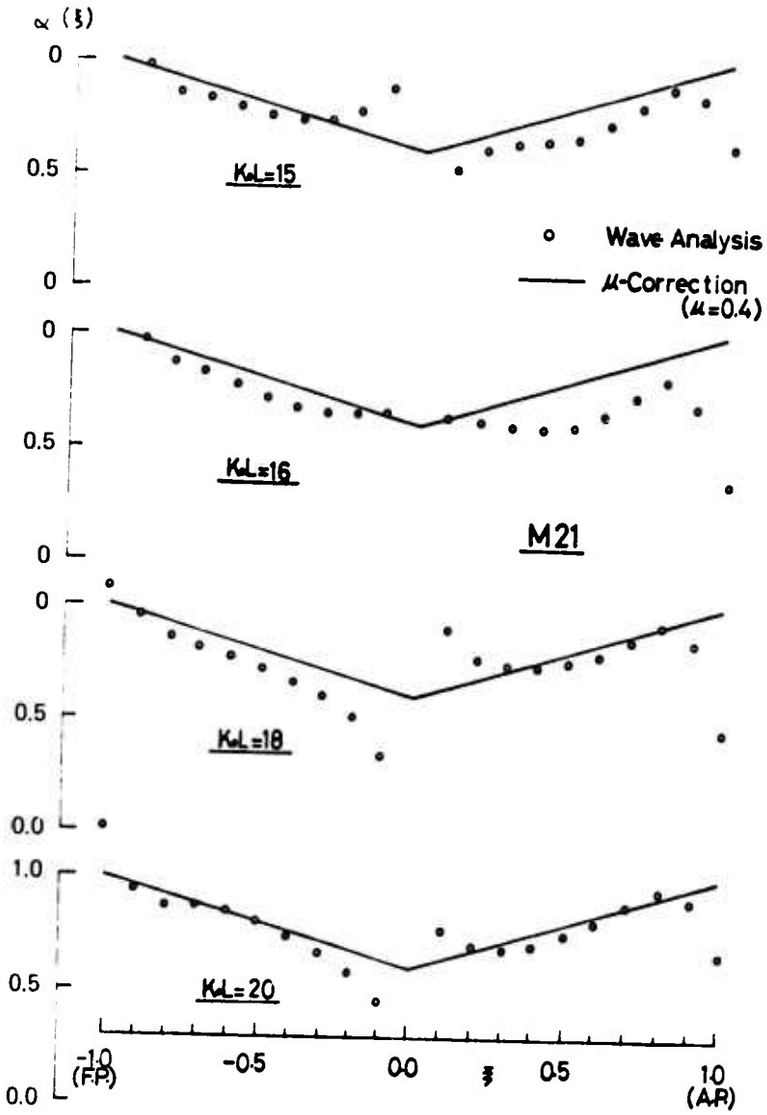


Figure 17. The ratio of $\bar{m}(\xi)/m(\xi)$ $(K_oL = 15 \sim 20)$

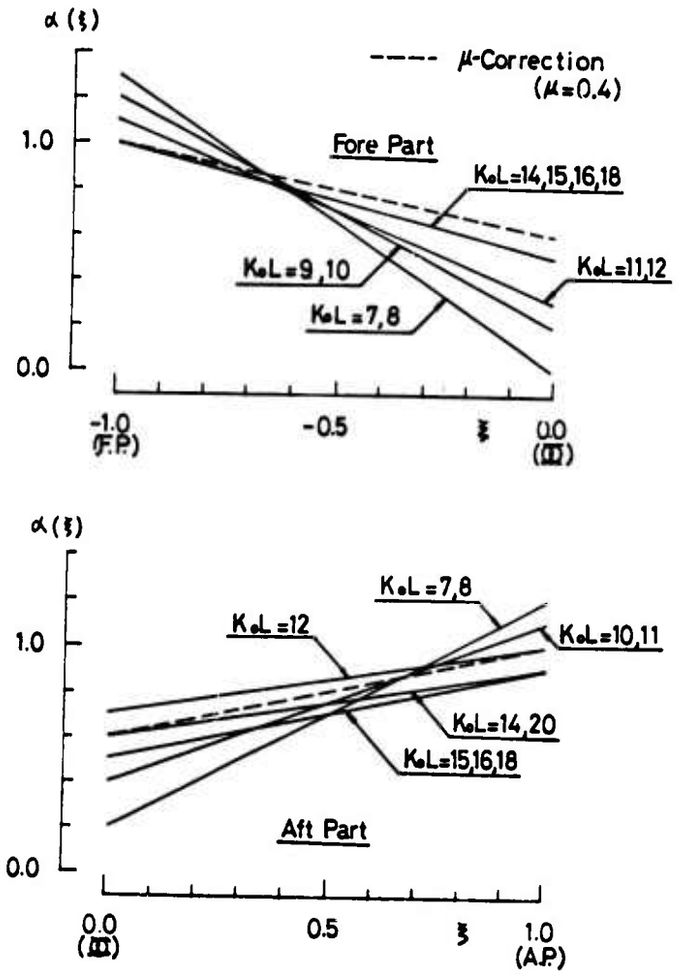


Figure 18. The correction function for M 21 type ships

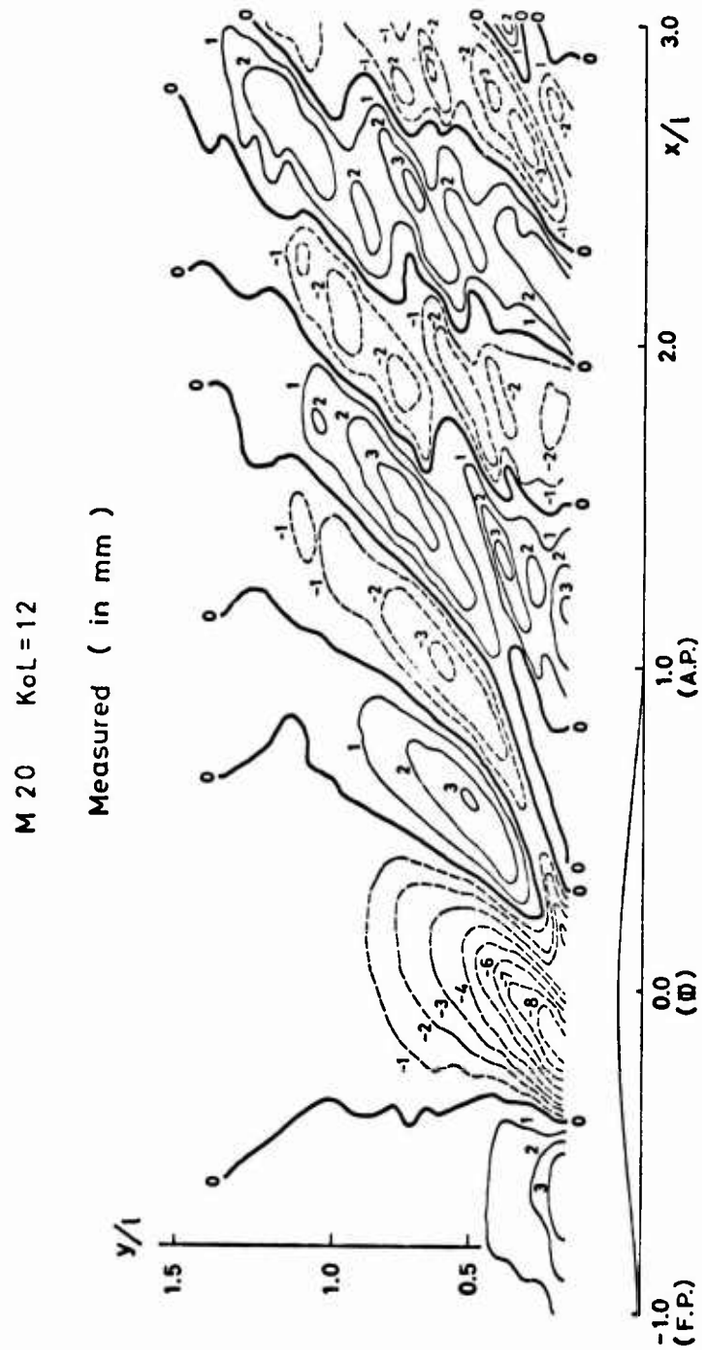


Figure 19. Measured wave pattern of M 20 ($K_oL = 12$)

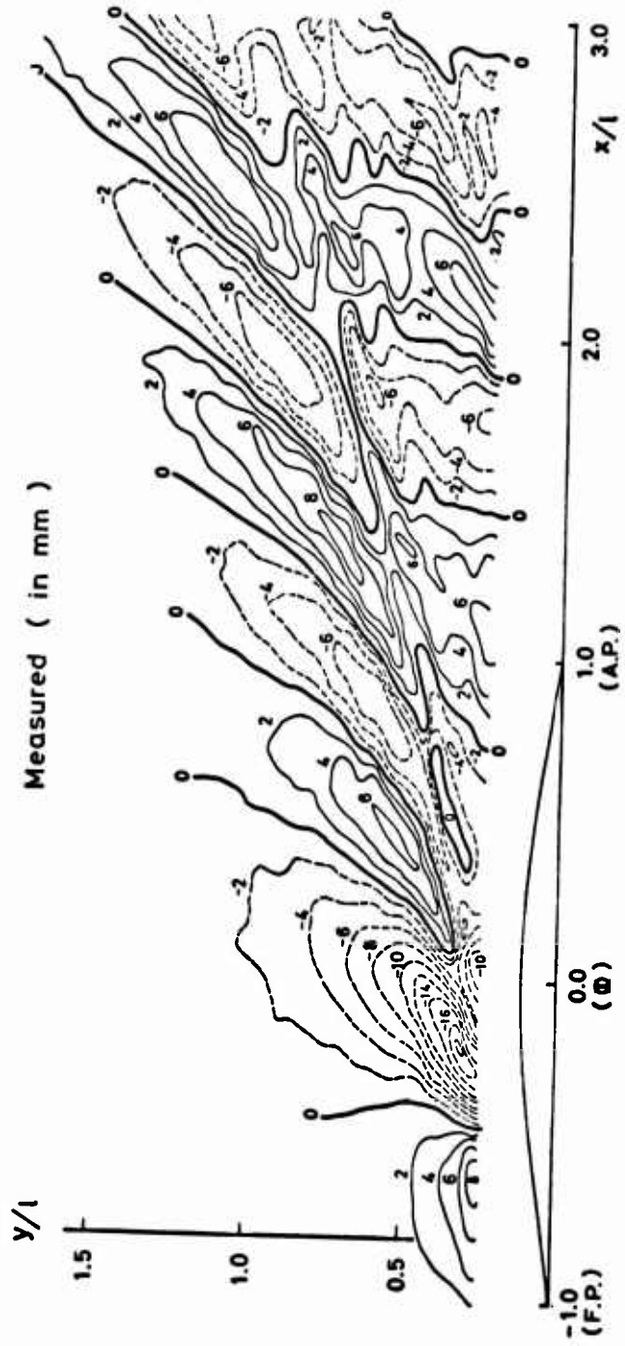


Figure 20. Measured wave pattern of M 21 ($K_oL = 12$)

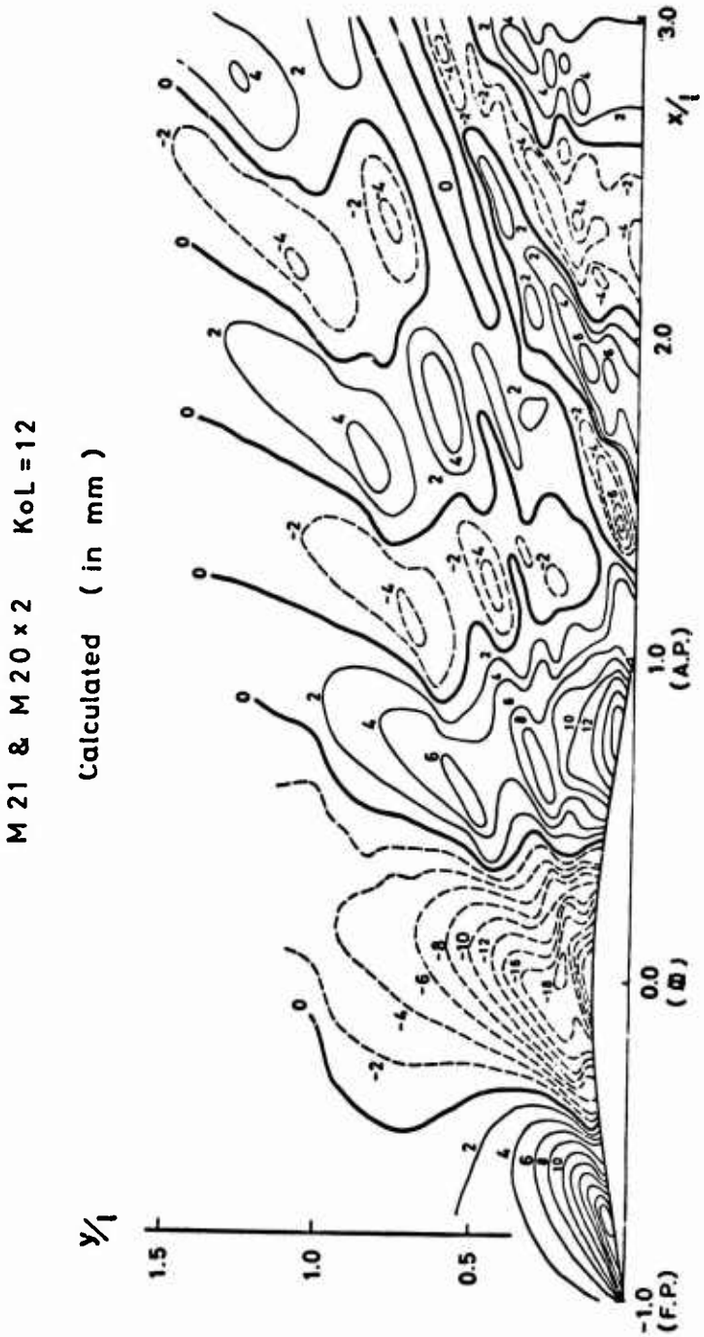


Figure 21. Calculated wave pattern of M 20 and M 21 ($K_oL = 12$)

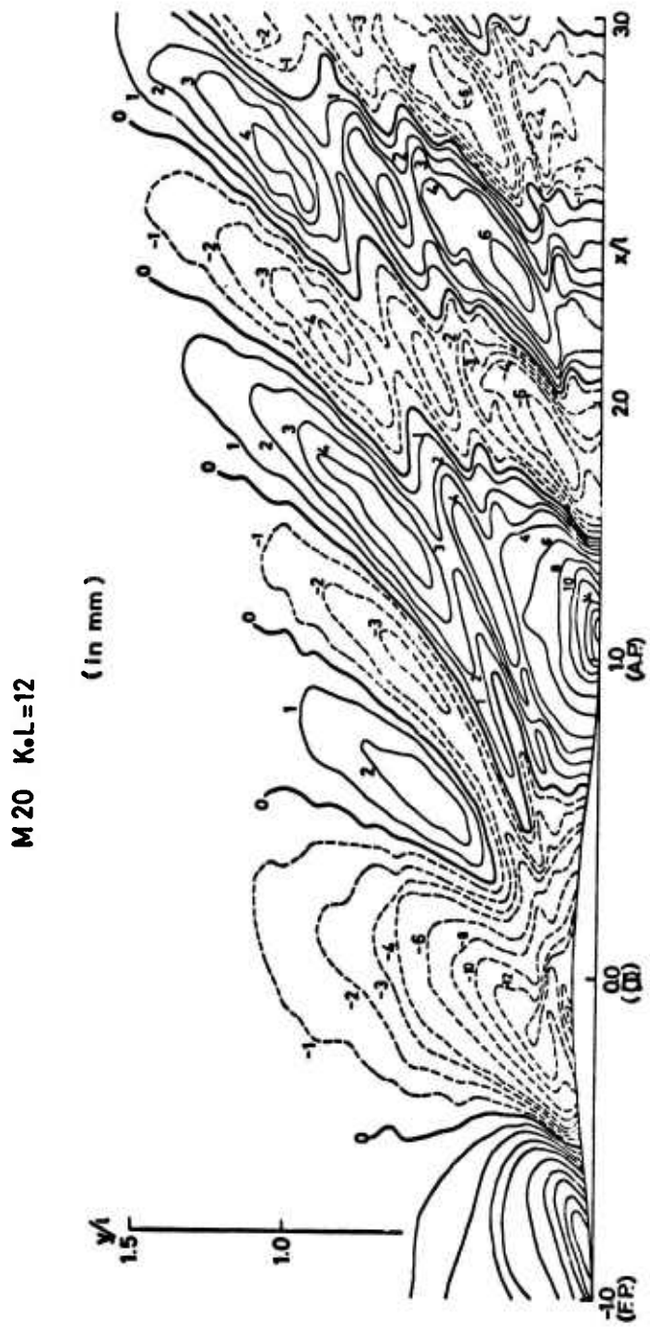


Figure 22. Calculated wave pattern from obtained wave-making source distribution $m(\xi)$ of M 20 ($K_0L = 12$)

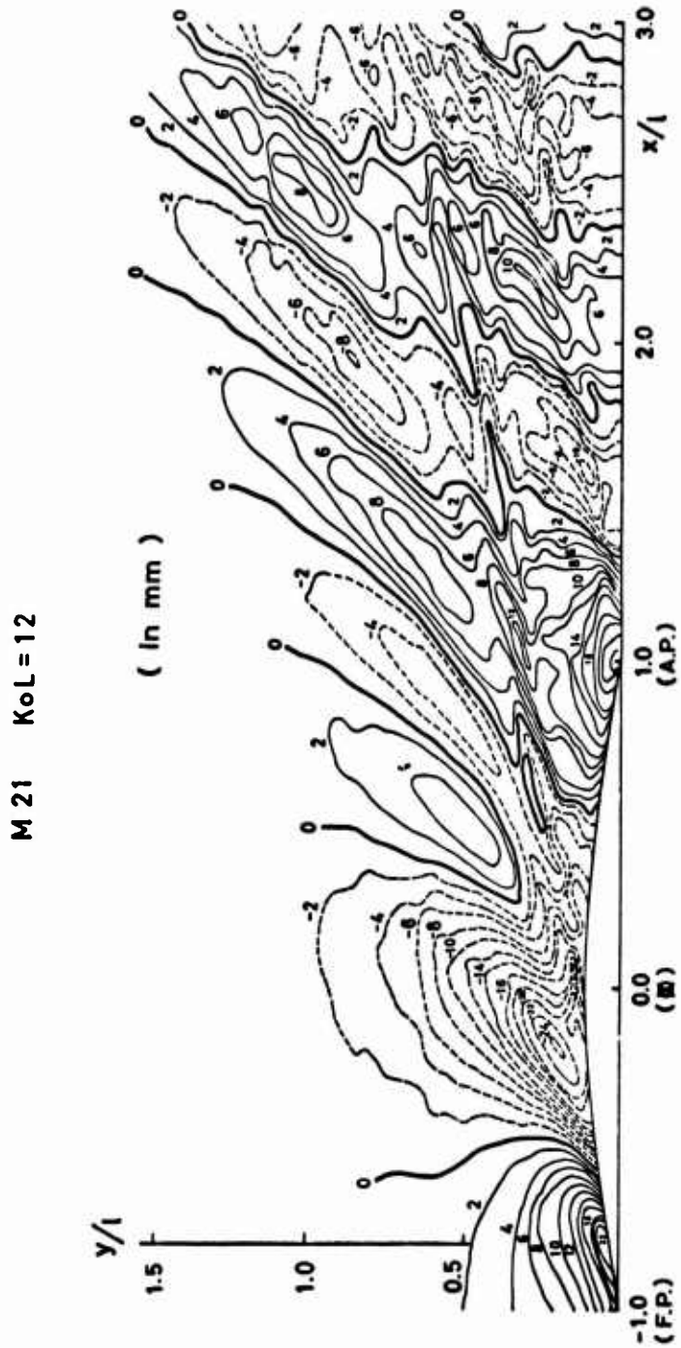


Figure 23. Calculated wave pattern from obtained wave-making source distribution m(ξ) of M 21 ($K_oL = 12$)

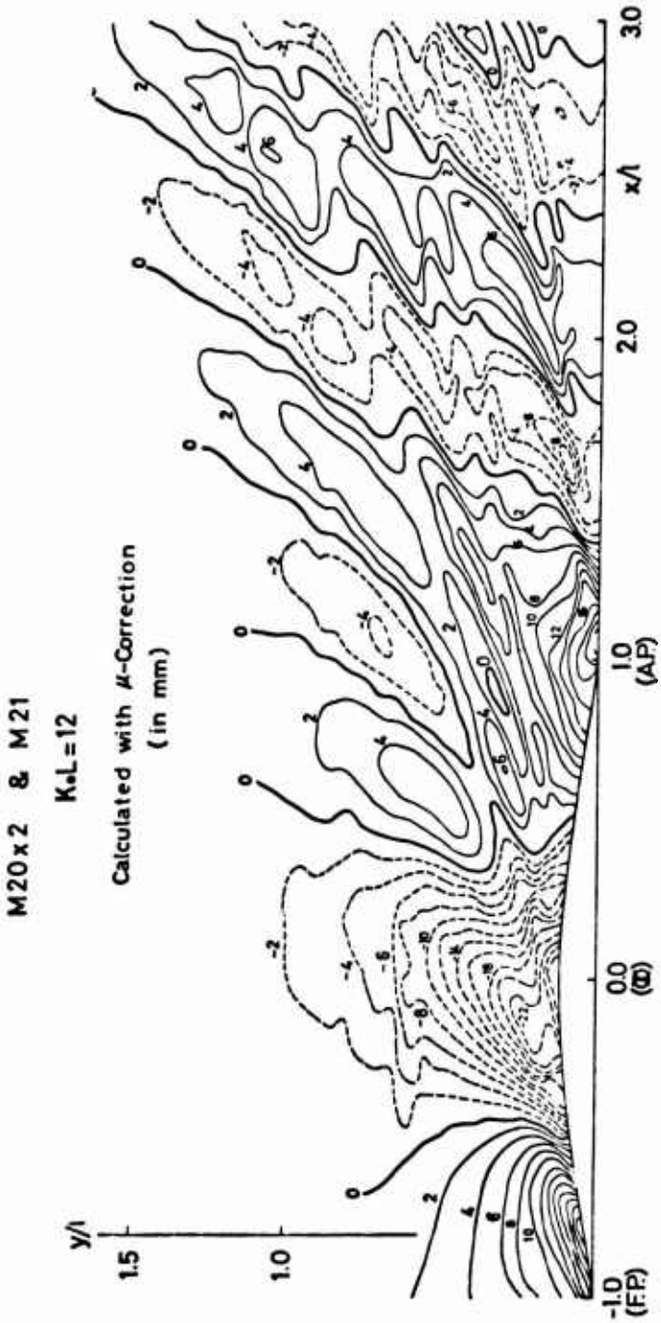


Figure 24. Calculated wave pattern of M 20 and M 21 with μ -correction ($\mu = 0.4$, $K_oL = 12$)

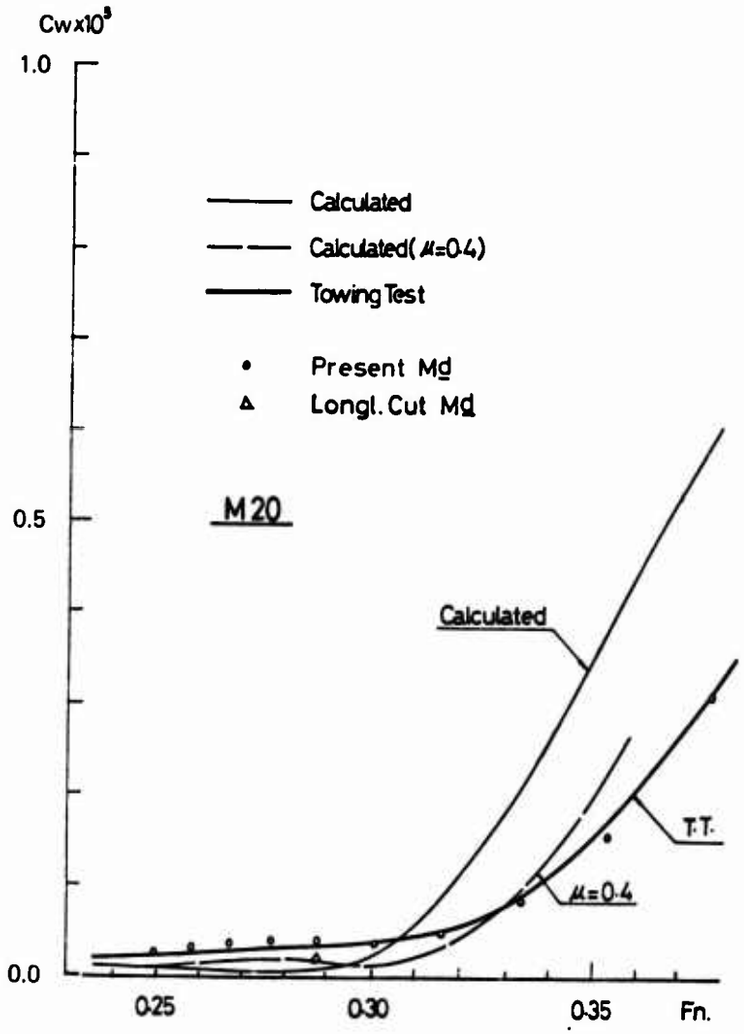


Figure 25. Wave-making resistance of M 20

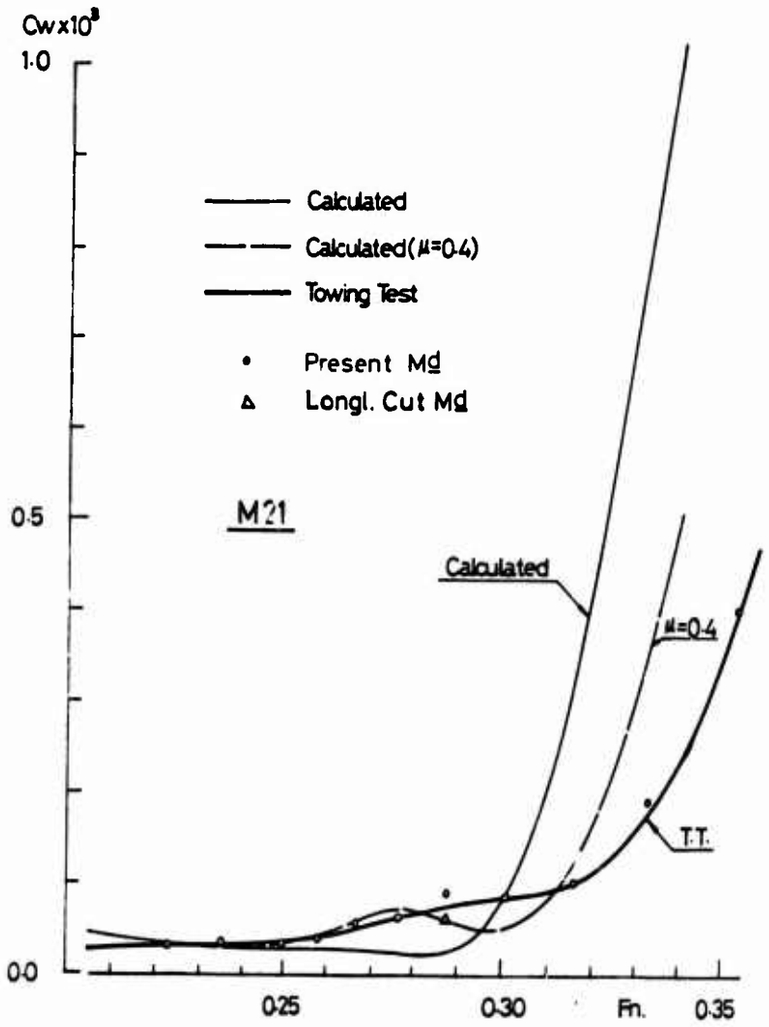


Figure 26. Wave-making resistance of M 21

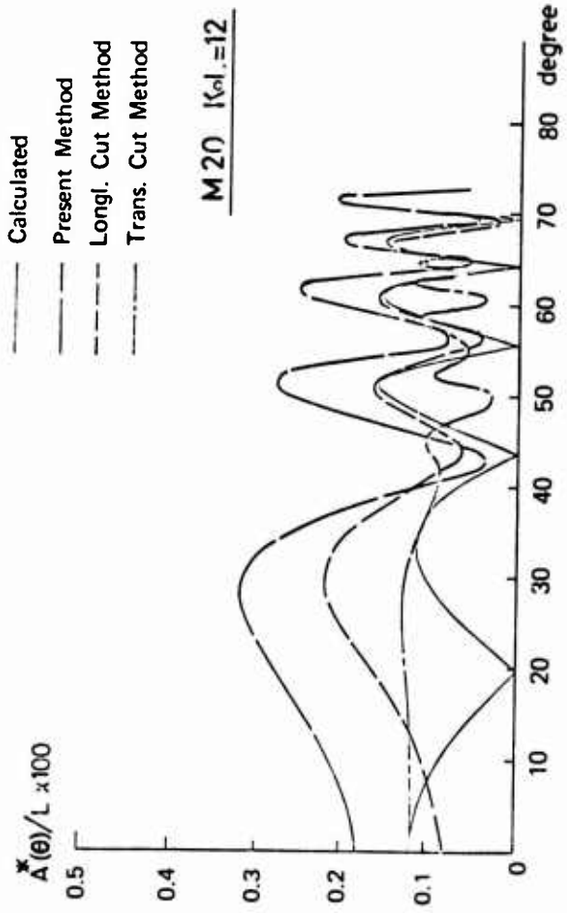


Figure 27. Wave-analyzed amplitude function by various method (M 20)

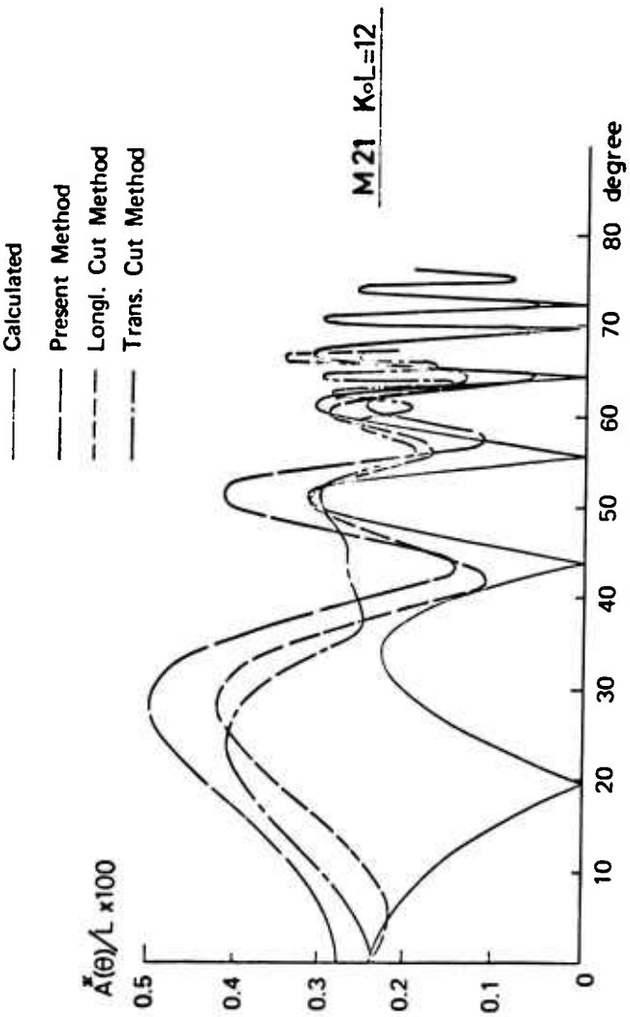


Figure 28. Wave-analyzed amplitude function by various method (M 21)

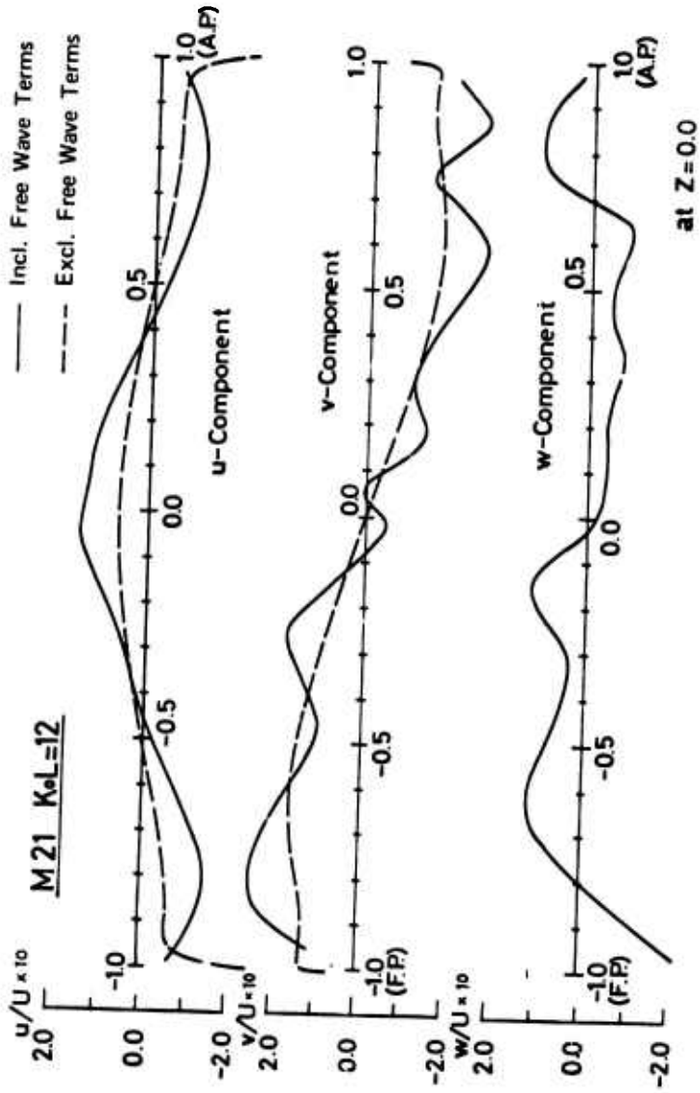


Figure 29. The velocity component of hull-surface (M 21)

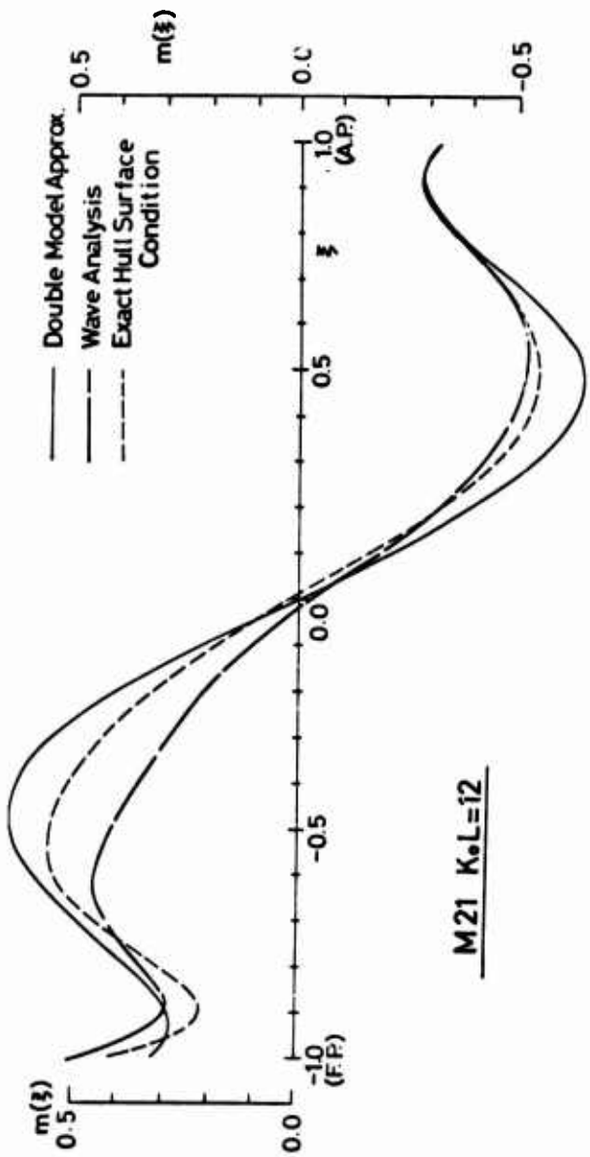


Figure 30. The source distribution obtained from exact hull-surface condition (M 21)

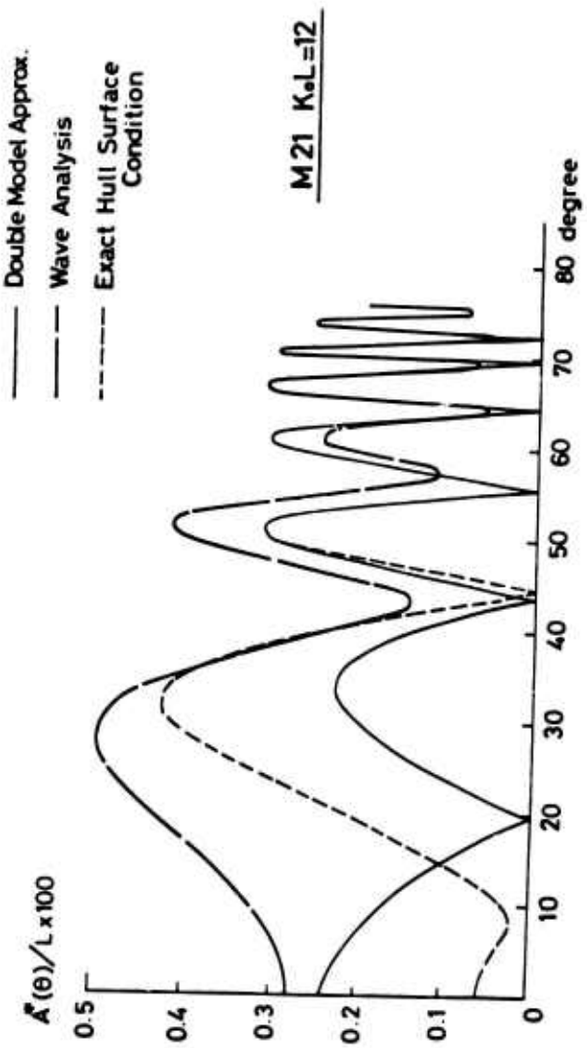


Figure 31. The amplitude function of the source distribution obtained from exact hull-surface condition (M 21)

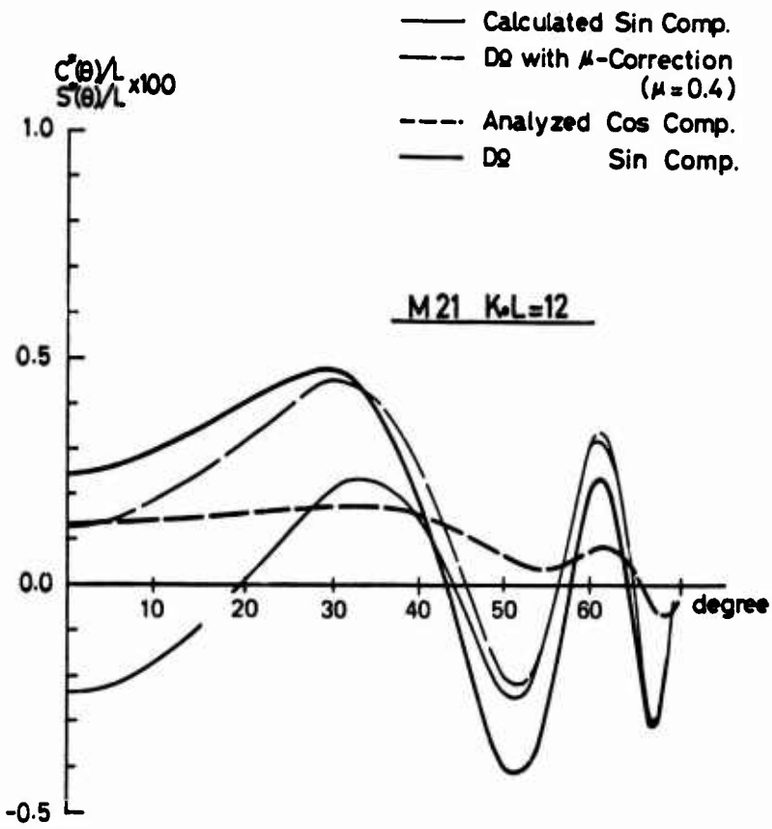


Figure 32. Wave-analyzed amplitude function of M 21 (K_oL = 12)

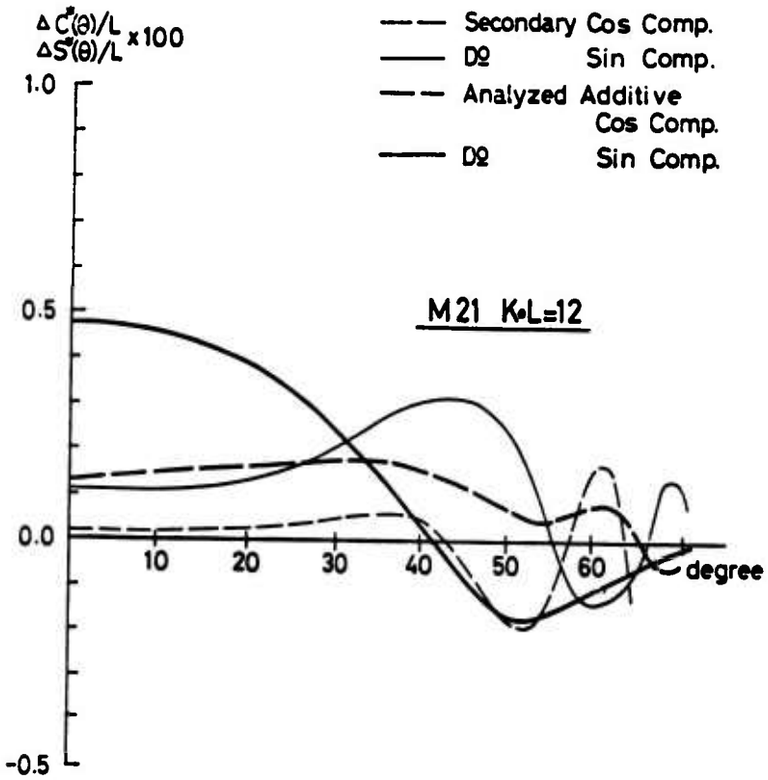
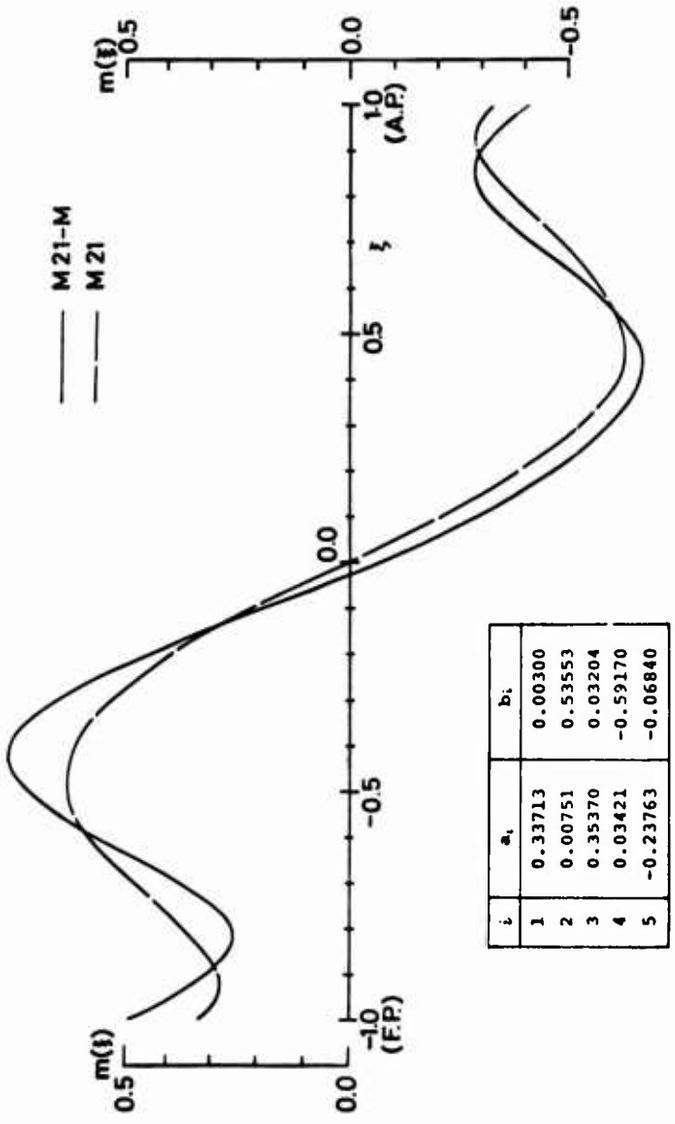


Figure 33. Comparison between wave-analyzed amplitude function and secondary contribution of free surface condition of M 21 ($K_o L = 12$)



i	a_i	b_i
1	0.33713	0.00300
2	0.00751	0.53553
3	0.35370	0.03204
4	0.03421	-0.59170
5	-0.23763	-0.06840

Figure 34. The source distribution of M 21-Modified (using correction function)

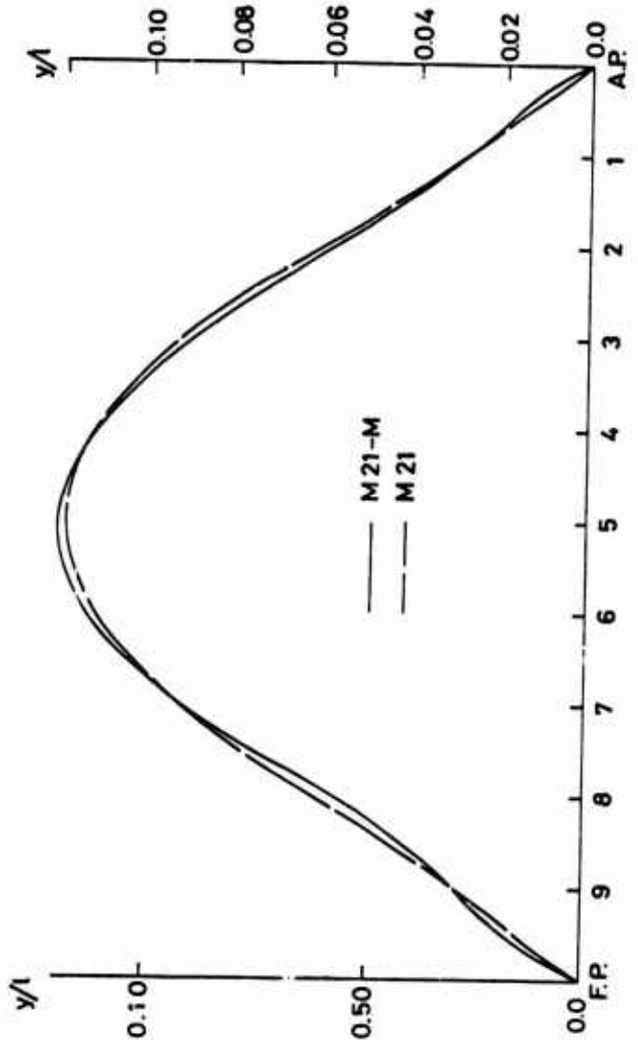


Figure 35. The water plane of M 21-Modified

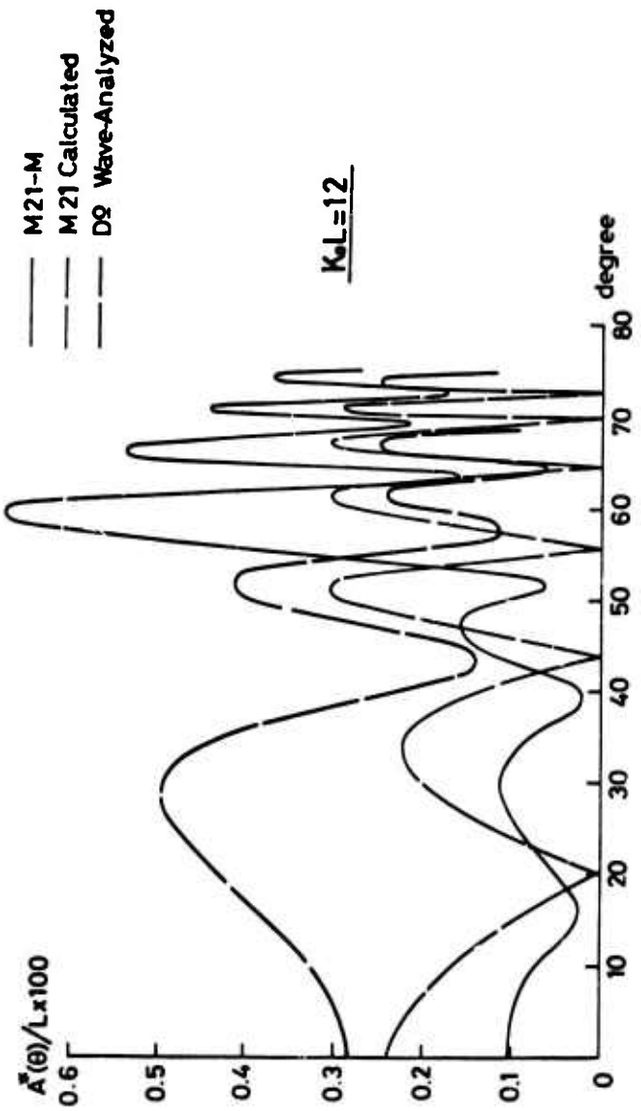


Figure 36. The amplitude function of M 21-Modified

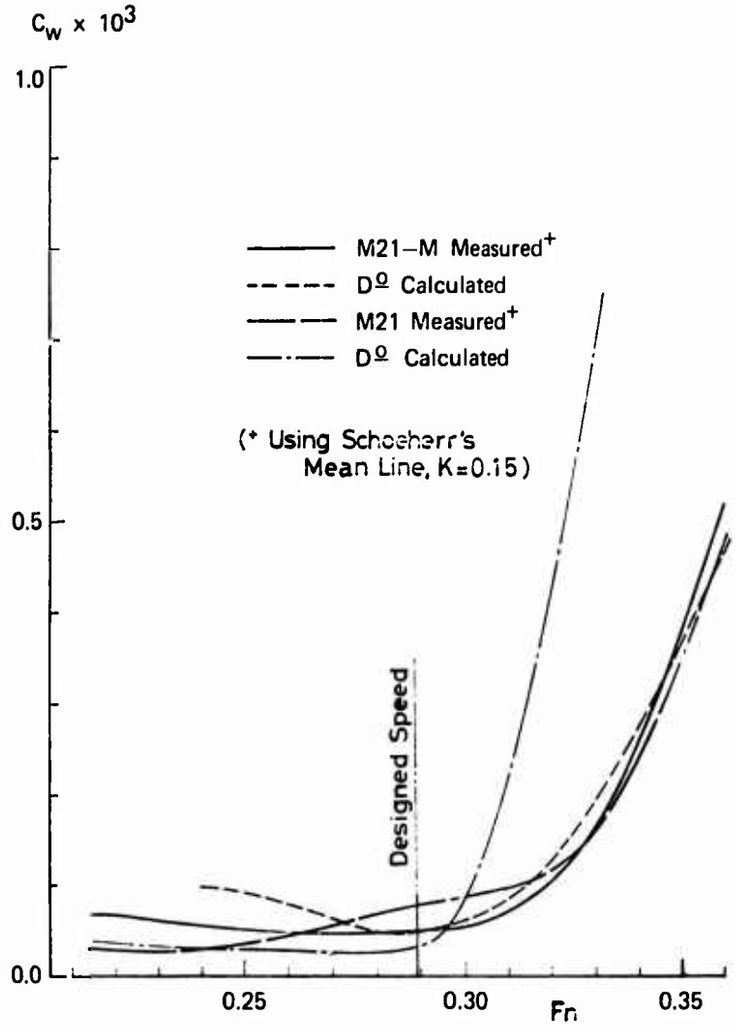


Figure 37. Wave-making resistance of M 21-Modified

DISCUSSION

Klaus W. Eggers

Institut für Schiffbau der Universität Hamburg
Hamburg, Germany

I feel that this paper deserves a very careful evaluation as well as comparison with concurrent approaches. I shall restrict my discussion to one remark only and two minor questions.

The authors deliberately do not display any physical assumptions regarding the effect covered by their correction, it may result from higher order effects of wave making theory for an ideal fluid or from viscousity or even from wave breaking. As far as the first method, called μ correction, is concerned, it retains the anti- symmetry of a source distribution for a symmetric ship and thus will not take account of viscous effects.

Now my questions : on Figure 12, I observe that the actual source density found from wave pattern survey deviates from this anti-symmetry, as could have been expected, but the deviation is smaller with the larger beam/length ratio. How can this be explained ?

Second, on Figure 25 there are represented different curves of wave resistance : from total drag, from wave pattern and from calculation using the method proposed. I would like to know from which Froude number measurement the underlying source distribution for the latter curve was taken and if there was any sensitive dependence found of wave resistance upon the Froude number selected for determining the source strength.

* * *

REPLY TO DISCUSSION

Kazuhiro Mori
University of Tokyo
Tokyo, Japan

Thank you, Professor Eggers, for your kind comments and questions, especially as to the μ -correction.

The comments of Professor Eggers about the results presented in Figure 12, the analysis of source distribution, are quite sound. There results concern a thiner model at a speed of KoL = 16, which is rather slow for which the amplitude of the absolute wave height is less than one centimetre. We measured the wave height by photo methods using scales drawn on the ship's surface, with a one-centimetre mesh. I am afraid the accuracy of the measured wave height is not enough, which explains the result of the analysis distribution in Figure 12.

Secondly, the wave making resistance coefficient is calculated from the analysied source distributions for each speed. The source strength is therefore not constant with speed.

DISCUSSION

Roger Brard
Bassin d'Essais des Carènes de la Marine
Paris, France

I should like first to congratulate warmly the authors for the valuable contribution to the ship wave theory that they have presented to this Symposium.

The idea of deriving the wave resistance from the surface elevation along the hull and not from the free waves is probably not quite new, since Guilloton, for instance, has attempted, some years ago, to take into account the surface elevation along the hull in the

computation of the wave resistance. Nevertheless, this idea is developed by the authors in a very original manner and they have done a considerable amount of theoretical and experimental work.

To obtain a ship form and a singularity distribution adapted to each other, one can start

- either from the ship hull and attempt to determine the singularity distribution to be associated with it,

- or from a given singularity distribution and determine the ship hull generated by that distribution.

The first path was first followed by Havelock. The sources are distributed in the longitudinal plane of symmetry and calculated by means of an approximate formula which implies the assumption that the length/beam ratio is considerably large and that the free surface behaves as a mirror. This first approach gives a solution which can be termed as Zero Froude number approximation for thin ship. At this stage, the theory is interesting from a scientific point of view only. The agreement between the measured wave resistance and the "residuary" resistance is too poor to be acceptable by naval architects. The Zero Froude number approximation transforms the real problem into a Neumann exterior problem. For solving that problem, in a rigorous manner, one can use a source distribution on the hull surface itself. Methods have been proposed by several authors - Hess and Smith [1], Landweber and Macagno [2] et al - in order to determine the source distribution. To my knowledge, it does not seem that the discrepancy between the measured resistance and the residuary resistance sensibly decreases ; it may even increase in some cases. It appears therefore that the Zero Froude condition may be one among the most important causes for discrepancy between theory and experiment.

The second path is that of Professor Inui and his School. The given source distribution is located in the plane of symmetry and completed by its image with respect to the plane of the free surface at rest. The ship form is obtained by integrating the system of differential equations for the streamlines of the relative motion. For the ship form so obtained the given source distribution can be considered as the rigorous solution of the Neumann problem related to the double model derived from that form. But this method does not permit to get over the drawback of the Zero-Froude number condition.

In their paper, the authors present a "wave-analyzed source distribution" such that the ship-side wave profile derived from this

new distribution be close to that yielded by the experiment. They show that the agreement between the wave amplitude functions calculated from the new distribution and those derived from a longitudinal cut remains unsufficiently good. They conclude that researches are to be pursued in one or two other directions. I just heard from Professor Inui that one obtains a very good agreement between the two kinds of wave amplitude functions if one adds to the effect of the sources that of a line integral which I had considered in a paper [3] submitted, for discussion, in June 1971, to my Colleagues of the I. T. T. C. Resistance Committee.

I consider as an interesting attempt the introduction of the wave profile on the hull into the calculation of the singularity distribution. One of the reasons why this does not provide a sufficiently good agreement with experiment may be the effect of viscosity and turbulence. The wave theory for inviscid fluid does not apply inside the boundary layer and wake. The longitudinal cut method does not give rise to this objection.

What is to be concluded from the effect of the line integral ? In the last months, Professor Landweber [4] has gone further that I did a year and half ago in the afore-mentioned paper on the Neumann-Kelvin problem. He has shown that, if the hull is represented by a source distribution the line integral can be transformed into a source distribution over the hull. Therefore one can solve the Neumann-Kelvin problem by using only a source distribution over the hull. But this requires the treatment of an integral equation with a kernel depending on the speed of the ship. However, if the first approximation is that obtained from the Zero Froude number condition, it can be shown that this approximation is certainly inaccurate when the Froude number decreases, and that the line integral expressed in term of that distribution should greatly improve the calculated wave resistance [5]. Hence, more detailed information on the procedure used by the authors for determining both "the wave-analyzed source distribution" and the line integral associated with it would be very much appreciated.

I would like to add that I am not convinced that wave breaking is responsible for the discrepancy between calculation and experiment, for the M-21 form is thin.

Much more important is undoubtedly the effect of the boundary layer and wake, not only because it entails a sensible loss of total head, but also because the boundary condition on the hull is altered. For this reason, I suggest that (it would be desirable that) the experiments of the authors be completed by a wake survey.

[1] SMITH, A.M.O., "Recent Progress in the Calculation of Potential Flows", Proceedings of the 7th ONR-Symposium on Naval Hydrodynamics, Roma, 1969.

[2] LANDWEBER, L., and MACAGNO, M., "Irrotational Flow About Ship Forms", Iowa Institute of Hydraulic Research, The University of Iowa, IIHR Report n° 123, december 1969.

[3] BRARD, R., "The Neumann-Kelvin Problem for Surface Ships", Bassin d'Essais des Carènes, Report 11 CST, January 1971 (unpublished).

[4] LANDWEBER, L., "Contributions on some Current Problems of Ship Resistance", May 1972, Paper prepared for the NSMB 40th Anniversary Symposium (August 1972).

[5] BRARD, R., "The Representation of a Given Ship Form by Singularity Distributions when the Boundary Condition on the Free Surface is Linearized", see Weinglum's issue of the Journal of Ship Research (March 1972).

REPLY TO DISCUSSION

Kazuhiro Mori
University of Tokyo
Tokyo, Japan

1. As to the empirical method

The so-called μ-correction has been proposed after quite same considerations as you have mentioned. If we were to use the kernel which depends on the speed of the ship, the calculations would get very complicated , such a method is quite useful,as shown in our paper, for hull form design.

2. As to the discrepancy in the amplitude functions

It is true that the B/L is not that large and wave-breaking may not occur. You pointed out as a main reason for the discrepancy, the effect of boundary layer, however we must remenber that the wave-making resistance obtained from analyzed source agrees with

that obtained from towing test (Figure 25 and Figure 26). So the discrepancy in amplitude functions between the present method and wave pattern analysis corresponds to the discrepancy between C_w obtained from towing test (C_w^T) and that given by wave pattern analysis (C_w^ω). In Figures 25 and 26, Δ denote C_w^ω.

As to the causes for this discrepancy between C_w^T and C_w^ω, we can mention first the failure of the wave pattern analysis method (longitudinal cut method) itself. The value of C_w^ω itself varies with y (the distance of the parallel cut line from the center line). Second, the magnitude of the discrepancy between C_w^ω and C_w^T is proportional to Fn^4, not to Fn^3, in medium speed range, this means that this discrepancy is related to some characteristic of the wave height. We thus mentioned the wave-breaking as one possible reason, together with the non-linear wave height reduction with distance in this term.

Of course the wake or boundary layer effect cannot be neglected, and should be considered in further studies.

3. As to line integral contribution

Our investigations made clear that the second order contribution of the boundary condition is not so large and we reach the conclusion that the line integral contribution must be taken into account.

From Green's theorem and free surface condition, the velocity potentiel Φ at P can be given as follows

$$\Phi(P) = \frac{1}{4\pi} \iint_{SM} \left\{ \Phi(P) \cdot \frac{\partial G}{\partial n}(P,Q) - G(P,Q) \frac{\partial}{\partial n} \Phi(Q) \right\} dS_o$$

$$+ \frac{1}{4\pi} \frac{1}{K_o} \int \left\{ \Phi(P) \cdot \frac{\partial}{\partial x} G(P,Q) - G(P,Q) \frac{\partial}{\partial x} \Phi(Q) \right\} dy \quad (A)$$

In the existing theory we take into account only the first term and neglect the second term which is the so-called line integration.

Figures 1 ~ 4 show the contribution of the second term

(1) the existing theory, namely the contribution of first term only ;

(2) the contribution of line integration, namely the second term ;

(3) (1) + (2) , namely the left hand side of Equation (A) ;

(4) wave analyzed result.

As to (2), Figures 1 and 2 present calculated results from theoretical wave height and Figures 3 and 4 are obtained from measured wave height.

The calculation is only a preliminary one and concerns only amplitude functions, but we can see striking agreements between (3) and (4). This suggests that the neglect of the contribution of the line integral was the most predominant cause of error.

* * *

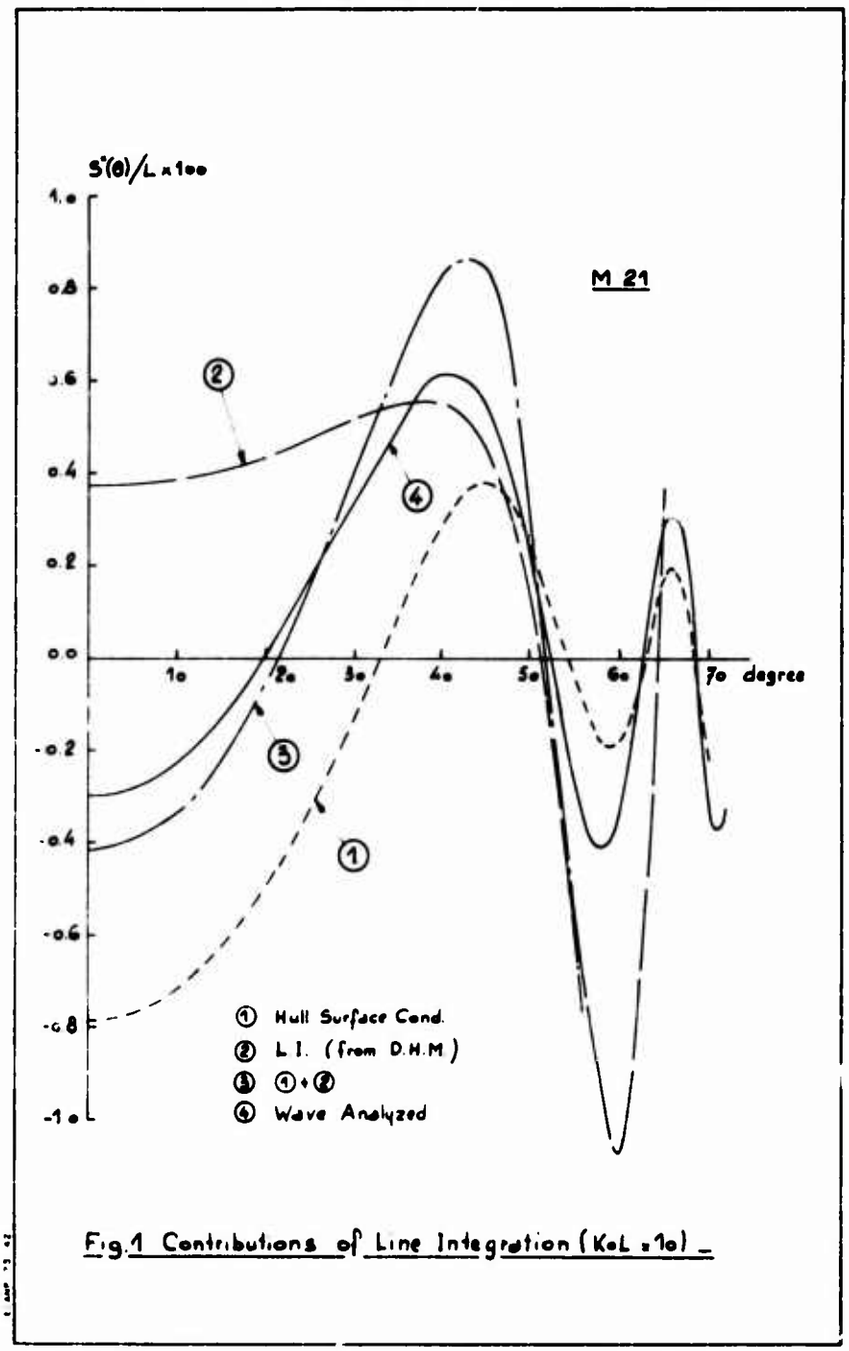


Fig.1 Contributions of Line Integration (KoL = 1o)

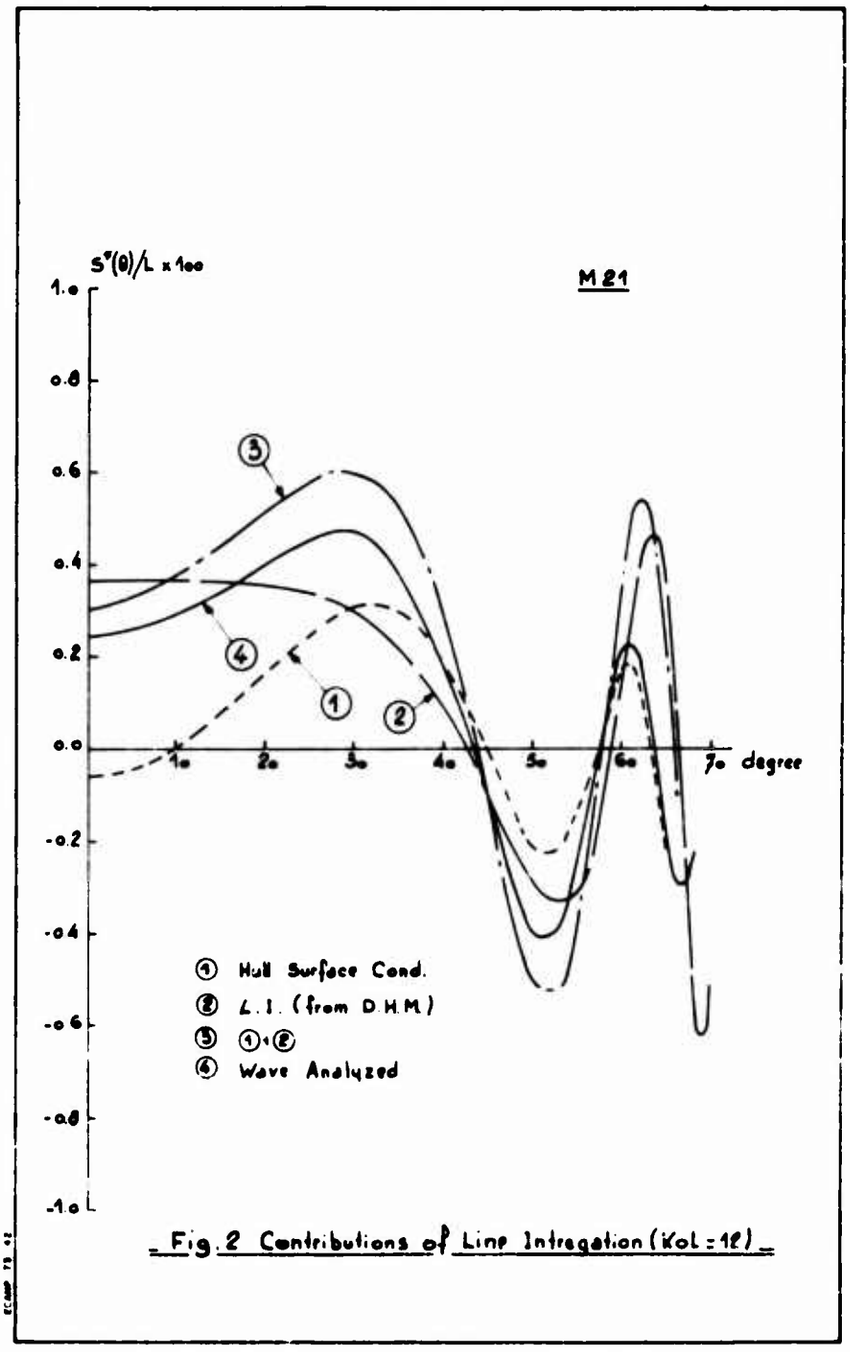


Fig. 2 Contributions of Line Intregation (Kol : 12)

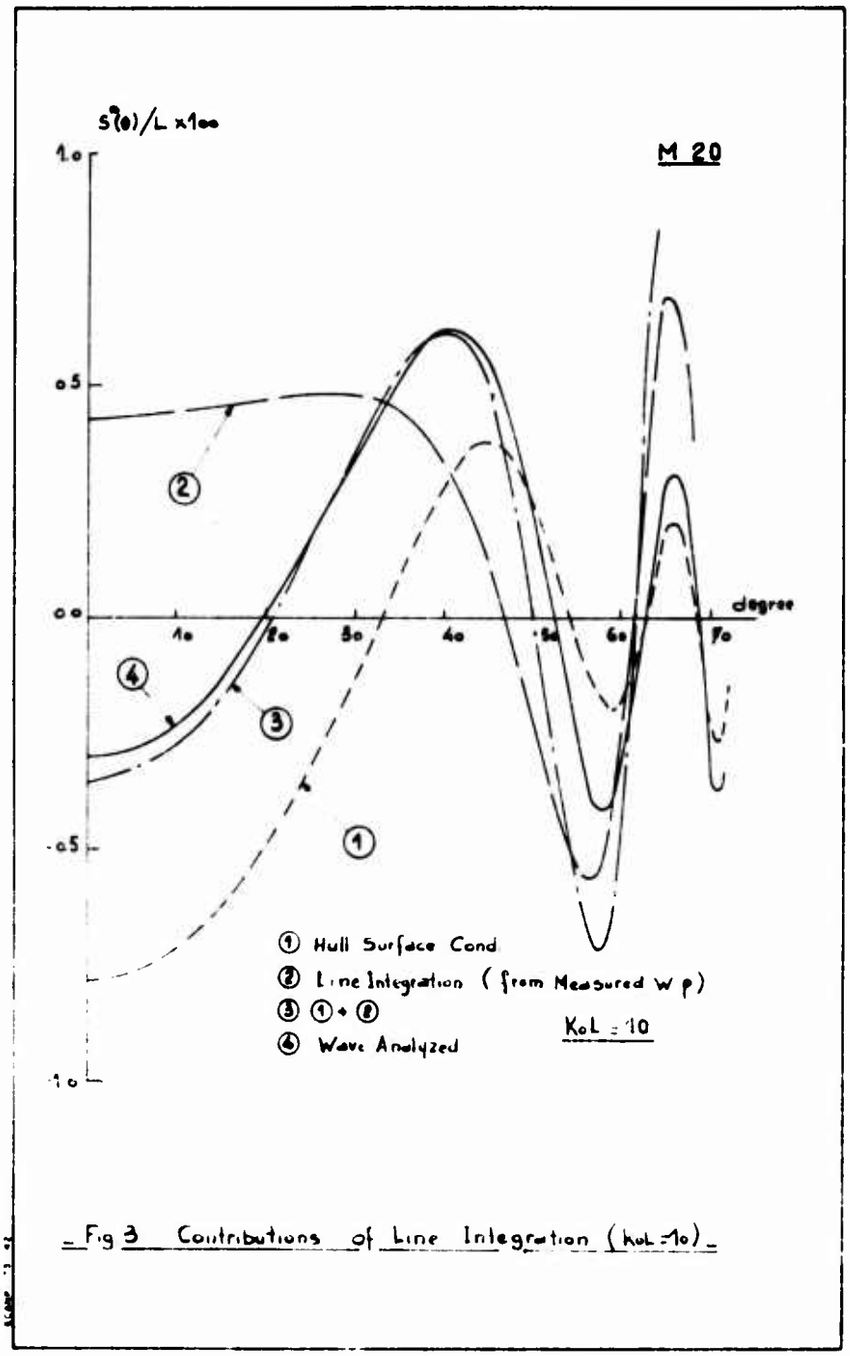


Fig 3 Contributions of Line Integration (KoL=10)

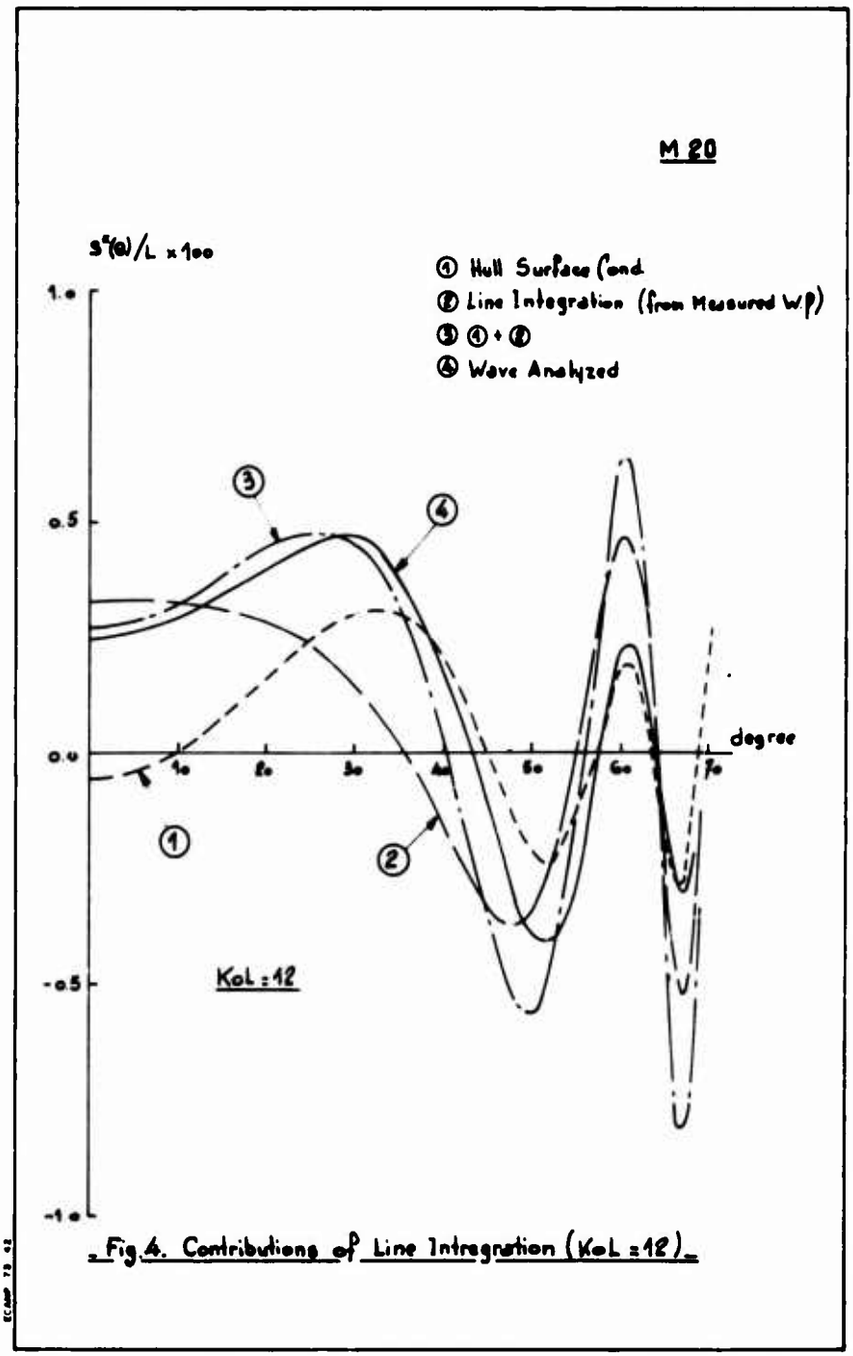


Fig.4. Contributions of Line Intregration (KoL = 12)

DISCUSSION

Louis Landweber
University of Iowa
Iowa City, Iowa, U.S.A.

The intensity of a ship's centerplane source distribution is related to the ship-side wave profile by an integral equation of the first kind. Since the strength of the source distribution is assumed to be independent of the depth coordinate, which is not true in general, the solution of the integral equation can yield only an approximation which matches well the ship-side wave profile, but not necessarily the far-field wave pattern, and hence the amplitude-distribution function and the wave resistance.

The assumption of thin-ship theory in the derivation of the integral equation seems unnecessary. It would be more accurate to apply the expression for the ship-side wave profile at the actual lateral coordinate of the hull than at the centerplane, as can equally well be done.

In their reply to Brard's discussion, the authors have shown that the agreement between the wave amplitude function from a longitudinal cut and from the ship-side wave profile is greatly improved by including the contribution from a line integral of singularities around the contour of the intersection of the hull with the free surface. Since the discussor has shown in his paper for the 40th Anniversary NSMB Symposium that this line integral can be transformed into an integral over the surface of the hull in such a way that the resulting system of singularities consists only of a source distribution on the hull surface, it would be interesting to know more precisely what singularities were assumed along the contour and how their strengths were obtained.

• • •

REPLY TO DISCUSSION

Kazuhiro Mori
University of Tokyo
Tokyo, Japan

It is true that the solution of the integral equation can yield only an approximation because the source density is assumed to be independent of the depth coordinate, but the wave pattern calculated from the obtained source (Figure 23) shows the rather well agreement with the measured one (Figure 20). Moreover the wavemaking resistance which is calculated in the same way agrees well with the results of the towing tank test (Figures 25, 26). This is the reason why the hull-side wave analysis is adopted here to find out the effective wavemaking source of a ship rather than far-field analysis. Besides it is conformed that the variation of the source to the depth direction is small.

As for the second comment, the ship-side wave profile, in this paper, is calculated at the actual lateral coordinate of the hull, as Professor Landweber has mentioned.

From the Green's theorem and the free surface condition, the velocity potential can be written,

$$\Phi(P) = \iint_S \left\{ \Phi(Q) \frac{\partial}{\partial n} G(P,Q) - G \frac{\partial \Phi}{\partial n} \right\} dS_o - \frac{1}{K_o} \int_C \left\{ \Phi \frac{\partial G}{\partial x} - G \frac{\partial}{\partial x} \Phi \right\} dy$$

here, S stands for the hull surface and C the real hull water line respectively. The second term is the line integration, which is composed by sources and doublets on $Z = 0$.

At the first step, assuming that the contribution of the first term is equivalent to the center plane source, the velocity potential of the first term is calculated. Next, using the first step values, the contribution of the second term can be calculated. This may be the iterative method to solve the integral equation. Figure A shows the results of this calculation. Though the iteration has done only once, the sum of the both terms shows the fairly well agreement compared with the results of the wave-analysis.

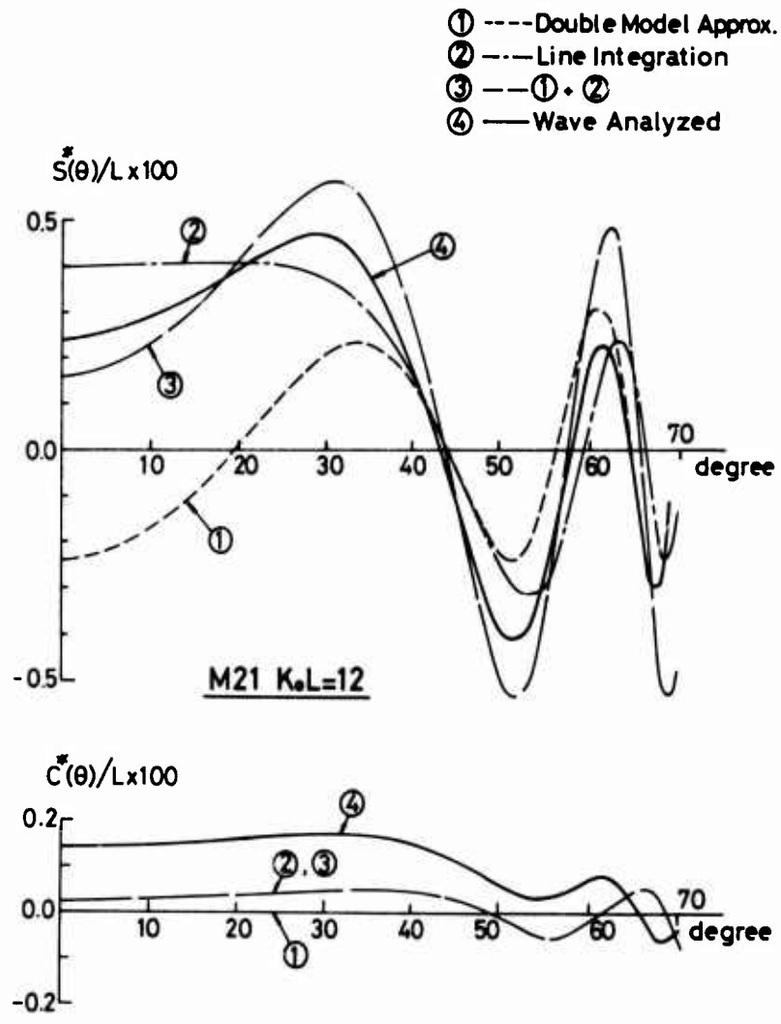


Fig. A The Amplitude Function of M21 (K_0L=12)

OCEAN ENGINEERING

Tuesday, August 22, 1972

Afternoon Session

Chairman : Pr. J.D. Van Manen
Netherlands Ship Model Basin,
Wageningen, Netherlands

	Page
Wave-Induced Eddies and Lift Forces on Circular Cylinders. R. L. Wiegel, R. C. Delmonte (University of California, U. S. A.).	761
Analyses of Multiple-Float-Supported Platforms in Waves. C. H. Kim, J. A. Mercier (Stevens Institute of Technology, U. S. A.).	793
Some Aspects of Very Large Offshore Structures. G. Van Oortmerssen (Netherlands Ship Model Basin).	957
Unstable Motion of Free Spar Buoys in Waves. J. C. Dern (Bassin d'Essais des Carènes, France).	1003
Auto-Oscillations of Anchored Vessels under the Action of Wind and Current. A. V. Gerassimov, R. I. Persnitz, N. N. Rakhmanin (Kryloff Research Institute, Leningrad, U. S. S. R.).	1079

WAVE-INDUCED EDDIES AND "LIFT" FORCES ON CIRCULAR CYLINDERS

R. L. Wiegel and R. C. Delmonte
University of California
Berkeley, California, U.S.A.

ABSTRACT

The frequency of eddies formed by and shed in the lee of bluff bodies in steady flow is well known, and to a lesser extent the associated "lift" forces have been studied and are reasonably well understood. The problem is more complicated in oscillatory flows such as exists in water waves. Results of studies are presented for the case of a vertical circular cylinder which pierces the water surface. The value of the Keulegan-Carpenter number (N_{CK}) in correlating the "lift" forces with the flow and cylinder parameters is shown. For higher values of N_{CK} it is found that the oscillatory flow tends to some extent to the steady state flow condition insofar as the "lift" forces are concerned. However, owing to the fact that in oscillatory flow the "wake" becomes the upstream flow, with eddies the same size as the cylinder, it is always more complicated. The "lift" forces are irregular for higher values of N_{CK} and should be described by a distribution function ; examples of such functions are given.

INTRODUCTION

The formation of eddies in the lee of a circular cylinder in uniform steady flow normal to the axis of the cylinder has been studi-

Preceding page blank

ed by a number of persons (see, for example, Laird, 1971). It has been found that the relationship among the frequency (cycles per second) of the eddies, f_e, the diameter of the cylinder D and the flow velocity V is given by the Strouhal number N_s,

$$N_s \left(1 - \frac{19.7}{N_R} \right) = \frac{f_e D}{V} \approx N_s \qquad (1)$$

where N_R is the Reynolds number, VD/ν, in which ν is the kinematic viscosity. Except in the range of laminar flow, the Reynolds number effect in this equation can be neglected. For flow in the sub-critical range (N_R less than about 2.0×10^5), there is a considerable variation of N_s; in fact, it is most likely that a spectrum of eddy frequencies exists (see Wiegel, 1964, p. 263 for a discussion of this). Extensive data on N_s at very high Reynolds numbers, as well as data on C_D (Figure 1) and the pressure distribution around a circular cylinder with its axis oriented normal to a steady flow, has been given by Roshko (1961) for steady flow. Few data are available on the resulting oscillating transverse forces. C_D is the coefficient of drag in the equation

$$F_D = \frac{1}{2} \rho C_D A V^2 \qquad (2)$$

where F_D is the drag force, ρ is the mass density of the fluid, A is the projected area of the cylinder and V is the speed of flow of fluid relative to the body.

What is the significance of N_s for the type of oscillating flow that exists in wave motion ? The horizontal component of water particle velocity is

$$u = \frac{\pi H}{T} \frac{\cosh 2\pi (y + d)/L}{\sinh 2\pi d/L} \cos \frac{2\pi t}{T} \qquad (3)$$

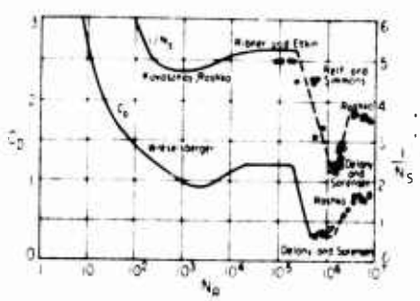


FIG. 1 DRAG COEFFICIENT AND RECIPROCAL OF STROUHAL NUMBER VERSUS REYNOLDS NUMBER
(From Roshko, 1961)

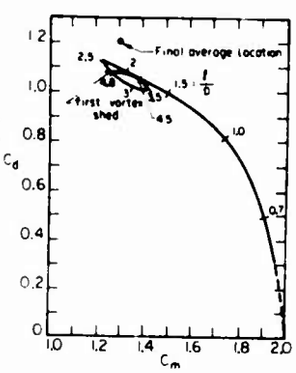
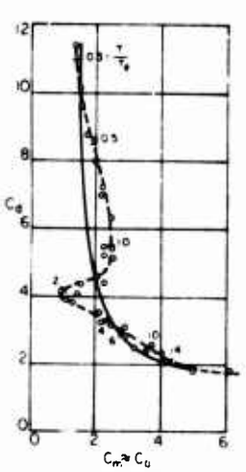
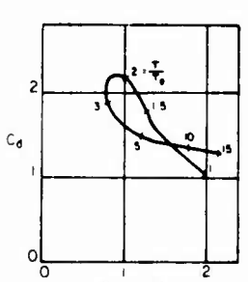


FIG. 2 CORRELATION OF DRAG AND INERTIA COEFFICIENTS
(From Sarpkaya and Garrison, 1963)



(a) PLATES



(b) CIRCULAR CYLINDERS

FIG. 3 INTER-RELATIONSHIP BETWEEN COEFFICIENTS OF COEFFICIENTS OF DRAG AND OF VIRTUAL MASS FOR (a) FLAT PLATES AND (b) CIRCULAR CYLINDERS (From Mc Nown and Keulegan, 1959)

For deep water the horizontal component of water particle velocity is approximately $u = (\pi H/T) \cos 2\pi t/T$ at $y = 0$. An average of u can be used to represent V; i.e., $V \approx u_{avg} \approx \pi H/2T$, where u_{avg} is the "average" horizontal component of water particle velocity due to a train of waves of height H and period T. For at least one pair of eddies to have time to form it can be argued that it is necessary for $T > 1/f_e \approx 2DT/\pi H N_s$, if $N_s \approx 0.2$, $H > 10D/\pi$.

Keulegan and Carpenter (1958) studied both experimentally and theoretically the problem of the forces exerted on a horizontal circular cylinder by an oscillating flow. In their experimental work the oscillations were of the standing water wave type, created by oscillating a tank of water. The cylinder was placed with its center in the node of the standing wave so that the water motion was simply back and forth in a horizontal plane. The axis of the cylinder was normal to the direction of flow (i.e., parallel to the wave front), and about half way between the water surface and the bottom. They found that C_D (and C_M) depended upon $u_{max} T/D$, (the Keulegan-Carpenter number N_{KC}), where $u = u_{max} \cos 2\pi t/T$. They observed that when N_{KC} was relatively small no eddy formed, that a single eddy formed when N_{KC} was about 15, and that numerous eddies formed for large values of the parameter. It is useful to note that this leads to a conclusion similar to the one above. For example, if one used the deep water wave equation for $u_{max} = \pi H/T$, then $u_{max} T/D > \pi H/D > 15$, and $H > 15D/\pi$ for one eddy to form.

It appears from the work described above that a high Reynolds number oscillating flow can exist which is quite different from that which occurs in high Reynolds number steady rectilinear flow, unless the wave heights are larger than the diameter of the circular cylinder. Even then, owing to the reversing nature of the flow, the "wake" during one portion of the cycle becomes the approaching flow during another portion of the cycle. It is likely that N_{KC} is of greater significance in correlating C_D and C_M with flow conditions than is N_R (Wiegel, 1964, p. 259), and that the ratio H/D should be held constant to correlate model and prototype results, or at least should be the appropriate value to indicate the prototype and model flows are in the same "eddy regime" (see Paape and Breusers, 1967, for similar results for a circular cylinder and for a flat plate oscillating in water).

In studying forces exerted by waves on circular cylinders one usually uses the equation developed by Morison, O'Brien, Johnson and Schaaf (1950). For a cylinder with its axial normal to the direction of wave advance the horizontal component of force per unit length of cylinder is given by

$$F_h = F_{Dh} + F_{Ih} \tag{4}$$

with

$$F_{Dh} = \frac{1}{2} \rho C_D D \left| u \right| u \tag{5}$$

and

$$F_{Ih} = \rho C_M \frac{\pi D^2}{4} \frac{\partial u}{\partial t} \tag{6}$$

where $\left| u \right| u$ is used rather than u^2 to account for direction of flow. F_{Dh} is the horizontal drag force per unit length of cylinder, F_{Ih} is the horizontal inertia force per unit length of cylinder, C_M is the coefficient of mass, C_D is the coefficient of drag, D is the cylinder diameter. $\partial u / \partial t$ is used in place of du/dt when the diameter of the cylinder is small compared with the wave length.

When the Keulegan-Carpenter number is sufficiently large that eddies form, an oscillating "lift" force will occur. For a vertical pile the "lift" (transverse) force will be in the horizontal plane normal to the direction of the drag force. Few data have been published on the coefficient of lift, C_L, for water wave type of flow (Chang, 1964 ; Bidde, 1970 ; 1971). In uniform rectilinear flows it can be as large as C_D, although there are few results available (Laird, 1961). The horizontal "lift" force per unit length of cylinder is given by

$$F_{Lh} = \frac{1}{2} \rho C_L D \left| u \right| u \tag{7}$$

where C_L is the coefficient of "lift".

Photographs taken of flow starting from rest, in the vicinity of a circular cylinder for the simpler case of a non-reversing flow, show that it takes time (the fluid particles must have time to travel a sufficient distance) for separation to occur and eddies to form (Rouse, 1946, p. 240). The effect of time on the flow, and hence on C_D and C_M has been studied by Sarpkaya and Garrison (1963 ; see also

Sarpkaya, 1963). A theory was developed which was used as a guide in analyzing laboratory data taken of the uniform acceleration of a circular cylinder in one direction. Figure 2 shows the relationship they found between C_D and C_M, which was dependent upon ℓ/d, where ℓ is the distance travelled by the cylinder from its rest position and D is the cylinder diameter. They indicated "steady state" (i.e., for large value of ℓ/D) values of $C_D = 1.2$ and $C_M = 1.3$.

The results shown in Figure 2 are different than those found by McNown and Keulegan (1959) for the relationship between C_D and C_M in oscillatory flow. They measured the horizontal force exerted on a horizontal circular cylinder placed in a standing water wave, with the cylinder being parallel to the bottom, far from both the free surface and the bottom, and with the axis of the cylinder normal to the direction of motion of the water particles. The axis of the cylinder was placed at the node of the standing wave so that the water particle motion was only horizontal (in the absence of the cylinder). Their results are shown in Figure 3. Here, T is the wave period and T_e is the period of a pair of eddies shedding in steady flow at a velocity characteristic of the unsteady flow. The characteristic velocity taken as the maximum velocity. They found that if T/T_e was 0.1 or less, separation and eddy formation were relatively unimportant, with the inertial effects being approximately those for the classical unseparated flow, and if T/T_e was greater than 10, the motion was quasi-steady.

"LIFT" FORCES EXERTED ON A VERTICAL PILE BY PROGRESSIVE WATER WAVES

Water Particle Motion and Eddies

Studies in the Hydraulic Laboratory of the University of California have been made by Bidde (1970, 1971) for the case of "deep water" and "transitional water" waves acting on a vertical "rigid"*

* The problems associated with a flexible pile are more complicated, owing to interaction of the pile motion and the formation of eddies. The reader is referred to the work of Price (1952) and Laird (1962, 1965) for details. The problem of an array, with the fluid flow - eddy interactions is also more complicated, and the reader is referred to papers by Laird and his colleagues for details on this subject (1960, 1963).

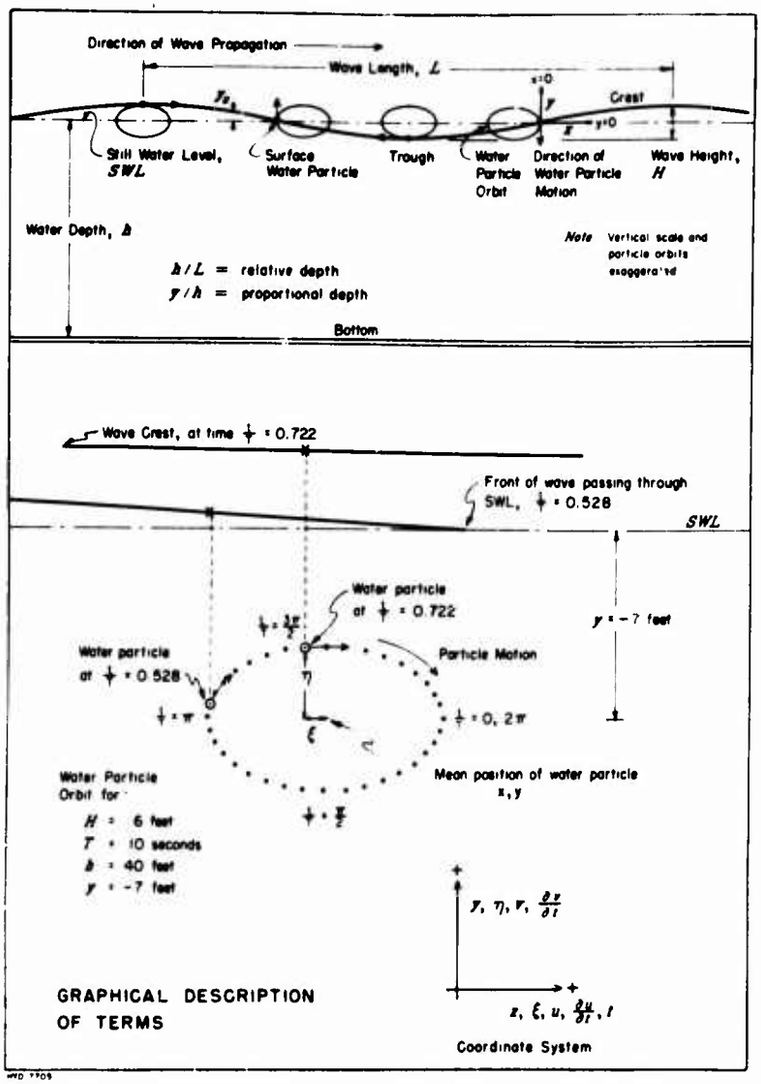


Figure 4. Water particle orbit due to waves (From Wiegel, 1964)

circular cylinder which extended from near the bottom through the water surface. For this case the undisturbed water particle motion was not simply a rectilinear back and forth motion, but the water particles moved in an elliptical orbit in a vertical plane, so that they were never at rest. Furthermore, any eddies that formed were affected by the free surface at the interface between the air and water. The horizontal component of water particle velocity is given by Equation (3), and the vertical component by

$$v = \frac{\pi H}{T} \frac{\sinh 2\pi (y + d)/L}{\sinh 2\pi d/L} \sin \frac{2\pi t}{T} \qquad (8)$$

In deep water the water particle speed, $q^2 = u^2 + v^2$, is given by

$$q = \pi H/T \qquad (9)$$

at the surface. Thus, the speed remains constant in deep water while the particle continuously changes direction. It is more complicated in transitional and shallow water. An example of the water particle path is shown in Figure 4. There is little reason to expect that eddies formed in such a flow would have the same characteristics as those formed in simple oscillating flow.

One of the most crucial factors in oscillating flow of this type is the fact that the wake formed during one portion of the cycle becomes the upstream flow in another portion of the cycle (the paper by Laird, Johnson and Walker, 1960, is useful in gaining some understanding of this problem), and little is known of the water particle motions under these conditions. When eddies, form, they appear to be of about the same size as the pile. In this regard it is interesting to refer to an observation made by Bacon and Reid (1923) in some studies of fluid forces on spheres. They found that if the scale of the turbulence was small compared with the diameter of the sphere, Reynolds number was a good criterion, but if the grain were coarse, then Reynolds number no longer served even as an indicator.

During the first stages of the study by Bidde, immiscible fluid particles with the same specific gravity as the water were made of a mixture of carbon tetrachloride and xylene, with some zinc oxide paste added to make the particles easily visible. The fluid was injected into the water by means of a long glass tube which had a rubber

bulb mounted at one end. The other end of the tube was heated and drawn to make the tip opening the desired size. Stereophotographic sets were taken of the trajectories of these tracer particles, and a computer program (Glaser, 1966) was used to calculate the space position of them. However, it was found to be too difficult and lengthy a job to pursue.

Owing to the difficulty described above, a description of the wake regime was developed by Bidde which was based upon his observations of the water surface characteristics, using magnesium powder sprinkled on the surface in the vicinity of the pile. An example of the relationship between the wake characteristic and the wave height, with the wave period being held constant is given in Table 1 together with the values of N_R and N_{KC}. Similar tables were constructed for a number of wave periods. The generalized results are shown in Figure 5. It was found that N_{KC} correlated reasonably well with the different regimes of the surface wake characteristics. When N_{KC} was about 3, one or two eddies formed, when its value was about 4 several eddies formed and shed, having the appearance of a von Karman vortex street, when it was 5-7 the wake started to become turbulent, and when it was larger than 7, the wake became quite turbulent, and the turbulent mass of water swept back and forth past the pile. Using the concept described previously, $H >$ about $3D/\pi$, that is, the wave height should be about equal to one pile diameter. As will be shown later, this was found to be the case for two piles, one about four times the diameter of the other.

The Reynolds number was between 4,000 and 7,000 for the values of the N_{KC} when the wake became quite turbulent with no detectable von Karman vortex street.

A similar phenomenon occurs in steady flow for N_R greater than 2,500, according to Rouse (1963). He states that for N_R greater than this value a trail as such can no longer be detected. Rouse further states that the body continues to be subjected to alternating "lift" forces, but that each vortex becomes progressively more unstable during its formation with a resulting wake that consists of a heterogeneous series of eddies.

"Lift" Forces (Bidde)

When eddies form, in addition to their effect on the longitudinal drag and inertial forces, "lift" forces are also exerted on the cylinder. For a vertical cylinder these lift forces act horizontally, but normal to the longitudinal forces (longitudinal being in the direction of wave motion), and should more properly be referred to as

Table 1. Observation of surface characteristics of eddies (From Bidde, 1970, 1971)

Water depth = 2.0 ft, cylinder diameter = 1-5/8", Wave period = 2.0 seconds

Run Number	Wave Height (feet)	Surface Reynolds Number	Surface Keulegan-Carpenter Number	Observations
1	0.028	850	0.9	No separation, no eddies (Amplitude of motion does not reach cylinder diameter)
2	0.04	1,220	1.3	
3	0.055	1,680	1.8	Small separation
4	0.07	2,140	2.3	Very weak von Karman street
5	0.08	2,450	2.7	Clear von Karman street
6	0.095	2,920	3.2	Wake of prior semicycle, when swept back gives rise to additional eddies
7	0.105	3,230	3.5	
8	0.120	3,700	4.0	
9	0.135	4,180	4.6	Eddies swept back by the time they are formed
10	0.155	4,810	5.2	
11	0.180	5,610	6.1	
12	0.20	6,250	6.8	
13	0.22	6,900	7.5	Becoming highly turbulent
14	0.24	7,550	8.2	
15	0.27	8,530	9.3	Extremely turbulent, no more eddies visible
16	0.30			
17	0.32			
18	0.34			
19	0.35	11,200	12.2	

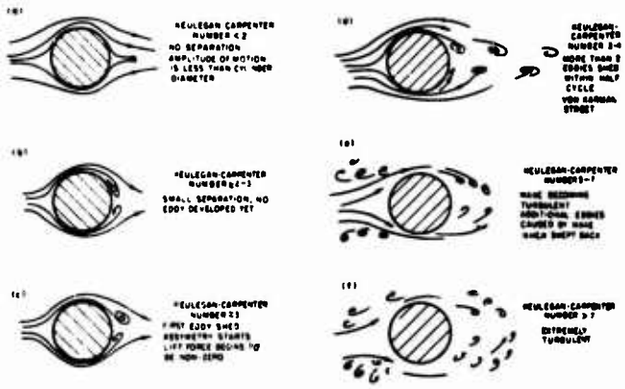


Figure 5. Wake characteristics as a function of the Keulegan-Carpenter number (Bidde, 1970)

transverse forces. Examples of waves, "lift" forces and longitudinal forces are shown in Figure 6 for three different values of N_{KC} (3.2, 6.2 and 10.2). The terms "top" and "bottom" associated with the lift and longitudinal forces refer to the forces measured by the top and bottom strain gages on the transducer ; the total "lift" and total longitudinal forces are the sums of the outputs of the top and bottom gages.

There is agreement between the visual observations described previously and the force measurements. Figure 6a shows a set of records for a N_{KC} of 3.2. The "lift" force has just begun to be non-zero. For this value of N_{KC} the first eddies develop and shed. The eddy strength is probably very small so that the "lift" force recorded is negligible. The "lift" forces for this case have a frequency which is about the same as the wave frequency. This might be due to the fact that the flow is not perfectly symmetrical. The horizontal component of velocity in one direction (wave crest) are slightly larger than those in the opposite direction (wave trough), and for the threshold condition the eddies only shed for one direction of the flow. The Keulegan-Carpenter number is 6.2 for the run shown in Figure 6b. The eddy is distinct, and the frequency of "lift" forces is approximately twice the frequency of waves. This shows that there is time only for two eddies to shed in each direction. The "lift" forces are about 25% of the longitudinal force. The wake is not yet completely turbulent, and the lift force records show a more or less regular pattern. The Keulegan-Carpenter number for the run shown in Figure 6c is 10.2. The wake is fully turbulent. The transvers ("lift") force record appears to be random. The ratio of maximum "lift" to maximum longitudinal force is about 40%.

An equation for "lift" forces is given by Equation (7). Use of this equation leads to difficulties as the time history of the force does not necessarily vanish when u goes through zero owing in part to the inertial force. Thus, very large values of C_L can be calculated from the laboratory measurements. This difficulty can be overcome partially by defining the relationship only for maximum values of the force as

$$(F_{Lh})_{max} = \frac{1}{2} \rho C_{L_{max}} (|u| u)_{max} D. \quad (8)$$

Chang (1964) found values of $C_{L_{max}}$ between 1.0 and 1.5 for value N_{KC} greater than about 10.

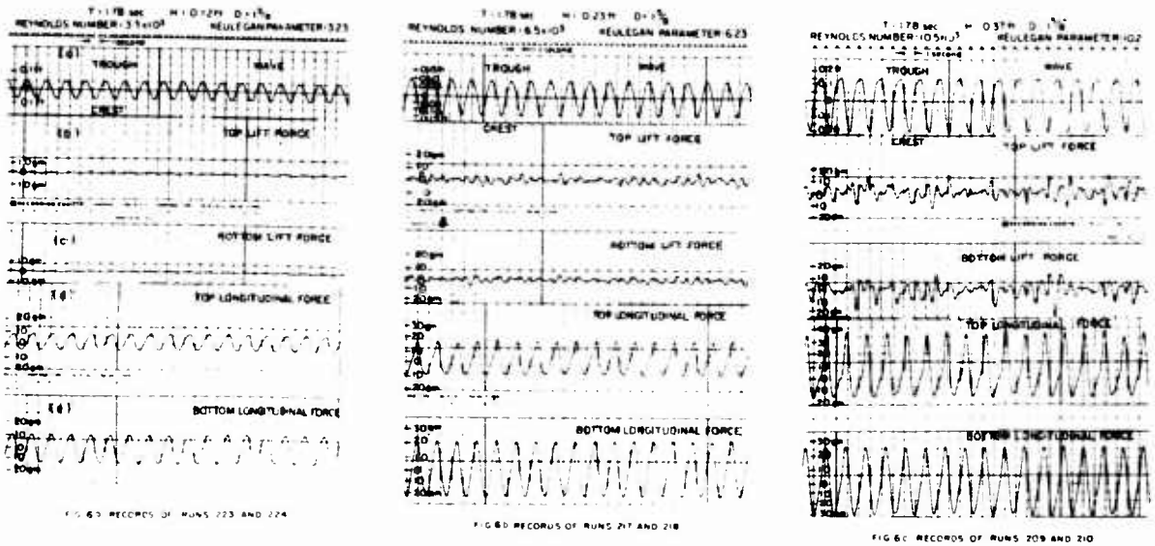


Figure 6. Sample wave and force records, uniform periodic (Bidde, 1970)

In the study by Bidde the ratio of "lift" to longitudinal force was used as a basic parameter rather than C_L as this parameter is comparatively less sensitive to any systematic errors in the instrumentation used to measure the forces, as similar errors would be present in both "lift" and longitudinal force measurements, and these errors would have a certain tendency to cancel out. Some of the data are shown in Figure 7 of the relationship between the wave height and the ratio of "lift" force to longitudinal force.

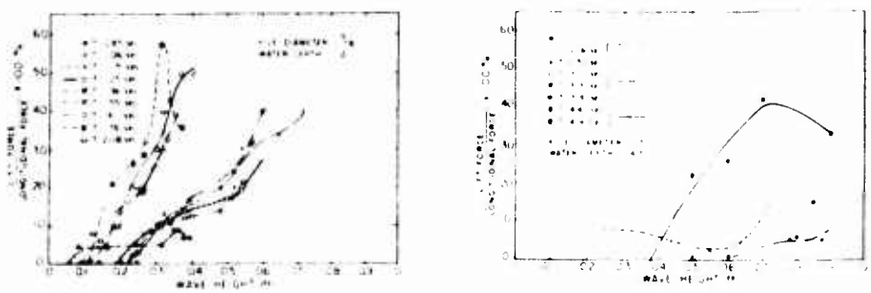


Figure 7. Relationship between ratio of lift to longitudinal force and wave height (Bidde, 1970, 1971)

The relationships between N_{KC} and N_R and the ratio of "lift" force to longitudinal force are shown in Figure 8. This graph indicates that the "lift" forces start at N_{KC} of about 15 the ratio of "lift" to longitudinal force shows a slight tendency to stop increasing.

As can be seen in Figure 6c the amplitude and frequency of the "lift" forces become irregular for larger values of N_{KC}, and it is necessary to specify what is measured. Bidde presented the ratios of average maximum "lift" forces to average maximum longitudinal forces. The longitudinal forces were uniform so that no problem existed in measuring and reporting them. Bidde drew a line by eye through the crests of the larger "lift" forces and another line through the throughs, and reported the "lift" force as the distance between the two lines. Furthermore, Bidde reported the ratio of the "lift" to longitudinal force as measured only by the bottom strain gages. An analysis of a few records showed that this ratio was the same as the ratio of the total forces.

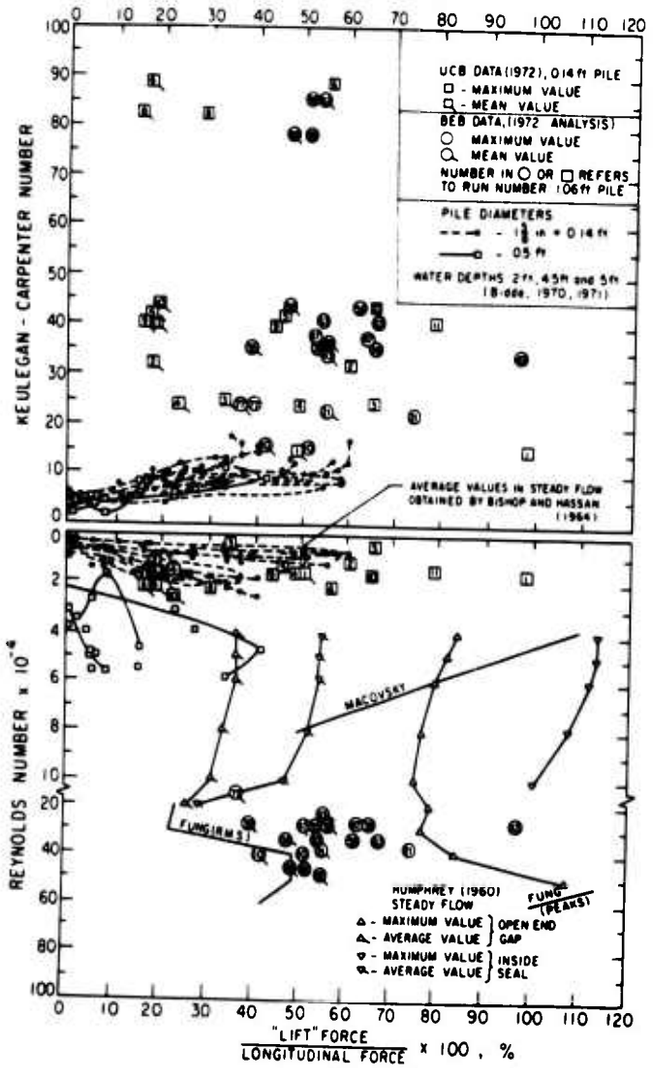


Figure 8. Ratio of "lift" force to longitudinal force (%) versus Keulegan-Carpenter number and Reynolds number

Bidde reported he was not able to compare his results directly with those of Chang (1964), as Chang gave his results graphically as $(C_L)_{max}$ vs N_{KC} and $(C_L)_{max}$ vs N_R with no values of $(C_D)_{max}$. However, Chang's graph of $(C_L)_{max}$ vs N_{RC} showed $(C_L)_{max}$ to approach zero for N_{KC} of about 5, and approach a value of 1.0 at about $N_{KC} = 20$.

"Lift" Forces (Present Study)

The work of Bidde described above was continued by the writers, to determine the effect of large values of N_{KC} on the ratio of "lift" forces to longitudinal forces. The results for the 1-5/8 inch (0.14 ft.) pile are reported herein. Tests were made for conditions that approximately modeled large scale tests which will be described subsequently. The pile was carefully checked to determine its sensitivity to direction and location of resultant force through a series of calibrations.

Aluminium powder and flour were sprinkled on the water surface to help in visualizing eddies. However, owing to the high values of N_{KC} (15 to 90) and high N_R, the wake was very turbulent and no distinct eddies were observed.

The crest to through distances for thirty consecutive "lift" forces were measured, while the crest to trough distances for only four consecutive longitudinal forces were measured as the longitudinal forces were quite uniform. The ratios of the averages of these two sets of data were plotted on Figure 8 (labeled UCB 1972), and tabulated in Table 2.

The Coastal Engineering Research Center (CERC ; formerly the Beach Erosion Board, BEB), U.S. Army Corps of Engineers, kindly lent to the writers the original records of forces exerted by waves on a vertical pile that were obtained by Ross * (1959) in their large wave tank (635 feet long by 15 feet wide by 20 feet deep). The active section of the test pile was 3.0 feet, with a dummy pile below and above the active section (Figure 9). The outside diameter of the pile was 1.06 feet. Data were not plotted in the form shown in Figure 7, as the minimum wave height used in these tests was greater

*Run numbers on original data rolls and those reported in T. M. 111 are not the same. See letter of 16 September 1971 from John C. Fairchild of CERC to Robert L. Wiegel of UCB for code.

TABLE 2. UCB 1972 DATA FOR 1-5/8 INCH (0.14 FT) O.D. PILE IN LARGE WAVE TANK

(1)	(2)	(3)	(4)	(5)	(6)	(7)	(8)	(9)	(10)	(11)	(12)	(13)
Run No.	Wave Height feet	Wave Period seconds	Water Depth feet	Average Total "Lift" Force grams	Average Total Longitudinal Force grams	50 Percentile Total "Lift" Force grams	(5)/(6) x 100 %	Maximum "Lift" / Longitudinal x 100 %	N_{KC} $\frac{(U_{max})_o T}{D}$	N'_{KC} $\frac{(U_{max})_c T}{D}$	N_R x 10^{-4} $(U_{max})_o D/\nu$	N'_R x 10^{-4} $(U_{max})_c D/\nu$
1	0.62	1.34	1.92	129	298	126	43	98	15	20	1.74	2.21
2	0.51	4.05	1.92	30	221	17	14	60	32	33	1.20	1.23
3	0.28	5.72	1.92	8	38	7	21	65	24	25	0.64	0.65
4	0.68	2.00	1.85	96	421	92	23	48	23	27	1.75	2.04
5	0.64	4.05	1.79	48	329	29	14	45	42	44	1.56	1.64
6	0.95	5.72	1.72	89	497	61	18	56	88	90	2.31	2.38
7 *	0.55	4.05	1.66	-	270	-	-	-	37	38	1.37	1.42
8	0.86	5.72	1.60	94	567	55	16	29	82	85	2.18	2.24
9	0.54	4.05	1.41	42	278	19	15	43	40	42	1.49	1.55
10	0.57	4.05	1.28	73	378	50	19	65	44	45	1.64	1.76
11	0.52	4.05	1.15	50	292	18	17	78	41	43	1.55	1.61

*Equipment did not work properly in Run 7, in regard to the "lift" force.

Notes: Linear wave theory used to calculate u_{max} (Eq. 3) for $\cos 2\pi t/T = 1$. $(u_{max})_o$ was calculated using $y = 0$, and $(u_{max})_c$ was calculated using $y = y_c$ (that is, the value of y at the wave crest). N_R and N'_R were calculated using ν at 60°F.

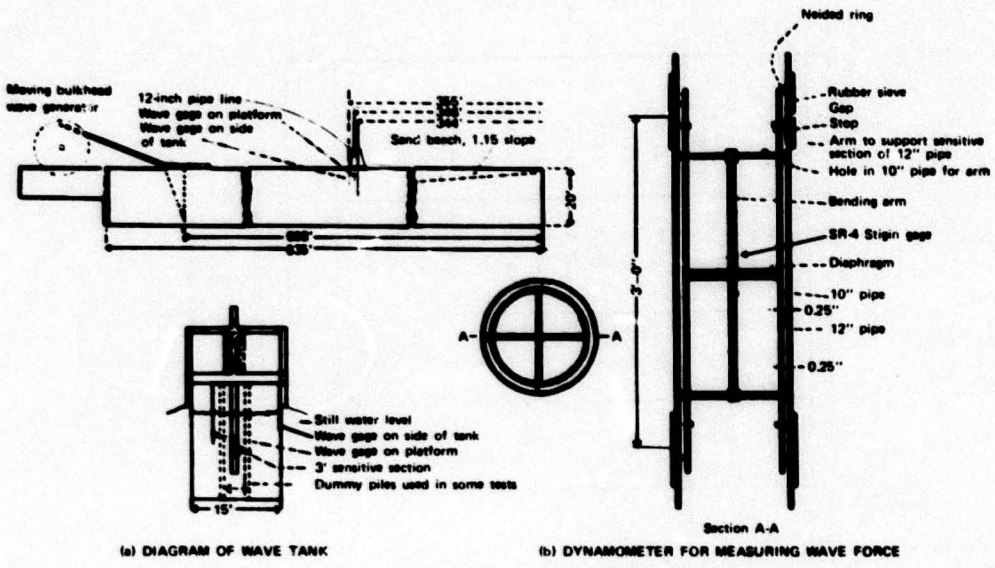


Figure 9. BEB arrangements (Ross, 1959)

than twice the pile diameter so that the "lift" forces were always substantial compared with the longitudinal forces. Longitudinal and "lift" forces were measured for waves with periods from 3.75 to 16.0 seconds and heights from 2.1 to 7.7 feet. The two sets of data labeled "BEB data, 1972 analysis" in Figure 8 are ratios of forces per unit length of pile, using the average of four consecutive waves for one set, and the maximum of the four waves for the second set. Representative examples of the BEB data are given in Table 3.

Owing to the manner in which Bidde analyzed and reported his data, it would be expected that they would lie between the maximum and mean values obtained by the writers for the same N_{KC}. If this is the case, it appears that Bidde reached the value of N_{KC} that divides the regime from a strong dependence of the ratio of lift to longitudinal force upon N_{KC} to one in which it is essentially independent of N_{KC}.

Bidde found for the smaller diameter ($1-\frac{5}{8}$ inch) pile that N_R

TABLE 3. BEB DATA (1972 ANALYSIS) FOR 1.06 FT O.D. PILE

(1)	(2)	(3)	(4)	(5)	(6)	(7)	(8)	(9)	(10)	(11)	(12)	(13)
Run* No.	Wave Height feet	Wave Period seconds	Water Depth feet	Average Total "Lift" Force pounds	Average Total Longitudinal Force pounds	50 Percentile Total "Lift" Force pounds	(5)/(6) x 100 %	Maximum "Lift" / Longitudinal x 100 %	N_{KC} / $(U_{max})_o T$ / D	N'_{KC} / $(U_{max})_c T$ / D	$N_R \times 10^{-4}$ / $(U_{max})_c D$ / ν	$N'_R \times 10^{-4}$ / $(U_{max})_c D$ / ν
10	5.0	3.75	15	3.5	5.5		42	72	17	20	40.9	51.1
35	4.4	11.3	15	1.4	4.1	6.8	39	56	35	36	29.1	29.9
77	2.2	16	15	0.7	2.7		35	77	25	26	14.3	14.6
21	5.3	5.6	14.5	4.3	7.8		55	43	23	27	37.7	44.5
39	4.2	11.3	14	3.0	5.8		54	63	35	36	28.5	29.4
92	7.2	16	13.5	5.2	9.2	11.7	54	67	85	88	49.3	50.9
43	4.0	11.3	13	3.2	6.4		55	100	34	35	28.1	29.0
88	6.3	16	12.5	3.3	7.5		47	82	77	80	44.7	46.3
47	3.9	11.3	11	3.0	7.2		52	53	37	38	29.9	31.0
58	4.5	11.3	10	2.1	5.7	9.1	46	106	44	46	36.0	37.4
63	4.0	11.3	9	3.2	7.4		54	63	41	43	33.7	35.3

*Run number in T.M. 111

Notes: Linear wave theory used to calculate u_{max} (Eq. 3) for $\cos 2\pi t/T = 1$. $(u_{max})_o$ was calculated using $y = 0$, and $(u_{max})_c$ was calculated using $y = y_c$ (that is, the value of y at the wave crest). N_R and N'_R were calculated using ν at 60°F. The forces reported in columns (5), (6) and (7) are the forces measured divided by 3 (the test section was 3 feet long) to obtain force per foot of pile.

appears to be as good a parameter for correlation purposes as N_{KC}. However, N_R fails to correlate well with the ratio of "lift" to longitudinal force when the values of the larger pile are compared with those of the smaller pile. For the smaller pile the minimum value of N_R at which eddies form is about 0.5×10^4, whereas it is 2.5×10^4 for the larger pile. For the same conditions the value of N_{KC} is 3 to 5 for both the piles. The UCB (1972) and BEB (1972 analysis) data reported herein seem to show an effect of N_R.

When the oscillating flow is such that the N_{KC} becomes large, one might expect the ratio fo "lift" to longitudinal forces would approach the values obtained for steady rectilinear flows. The writers were not able to find many data in the technical literature, however. The results they found have been plotted in Figure 8 (Bishop and Hassan, 1964 ; Humphrey, 1960 ; the two sets of curves labeled Fung and Macovsky were drawn from data attributed to them as they appeared in Humphrey's paper). These points were obtained by calculating the ratios of C_L to C_D from the values of the two coefficients given by the investigators.

Although it is evident that much work remains to be done before the problem is solved, it is clear that an engineer must consider a rather large "lift" force as well as a longitudinal force in his design.

If tests are made with piles of two different sizes, and complete geometric similarity conditions are met, and the Froude model law is adhered to, it can be shown that the "prototype" and "model" Keulegan-Carpenter numbers will be equal, but that the Reynolds numbers will not be equal. All geometric scale ratios must be the same, however. For example, in Figure 10 records obtained by Bidde of waves and forces for the 1.63 inch (0.14 ft.) and the 0.5 ft. diameter piles are reproduced. The wave height ratio is the same as the pile diameter ratio, and the wave period ratio is the square root of the pile diameter ratio. However, the water depth was the same in both cases, so that complete geometric similarity was not obtained. Note how different are the two sets of waves and forces. The records in this figure, and in Figure 11 show another interesting feature. There is not a "one to one" correlation of the wave to the "lift" force time series. Rather, the "lift" forces occur in bursts, with intervals of very small forces in between.

Comparative records are given in Figures 12-14 for the UCB 1972 and the BEB experiments. Froude modeling was used and complete geometric similarity was maintained. Owing to difficulties with the equipment, the ratio of wave heights was not quite correct for the

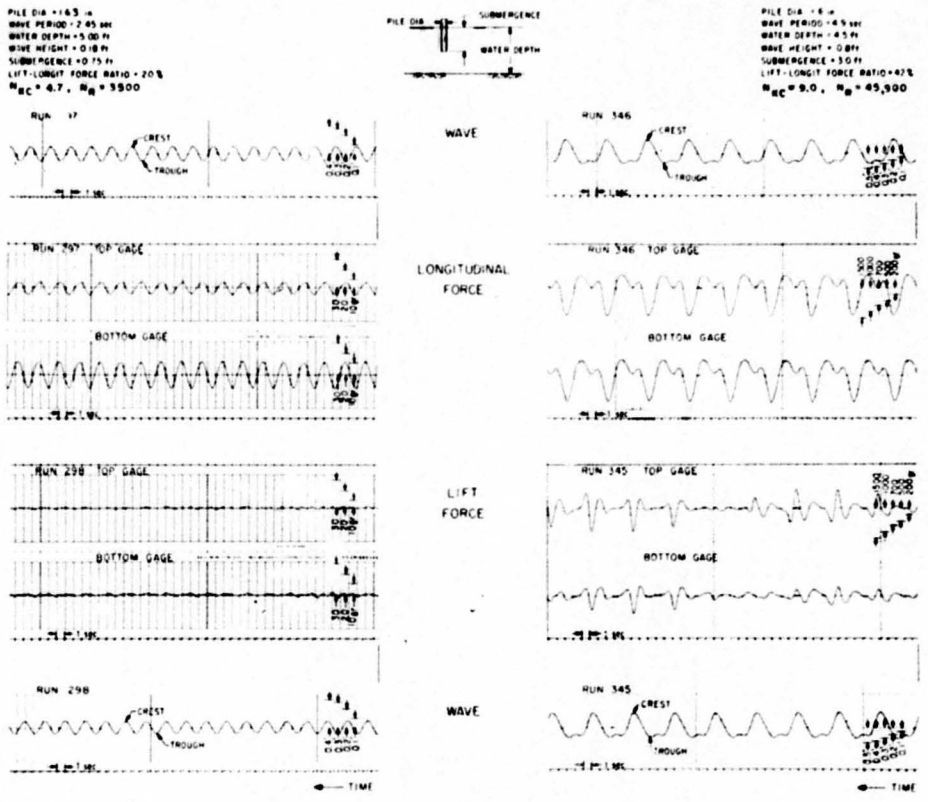


Figure 10. Comparison of longitudinal and lift forces, 6 in and 1.625 in. diameter piles

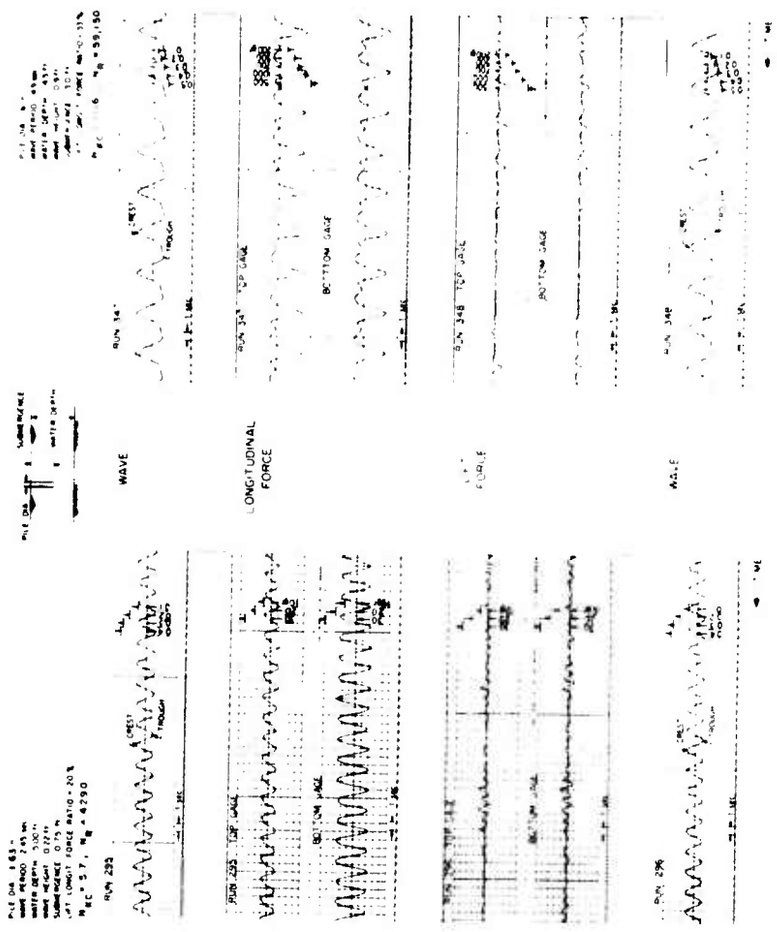


Figure 11. Comparison of longitudinal and lift forces, 6 in. and 1.625 in. diameter piles

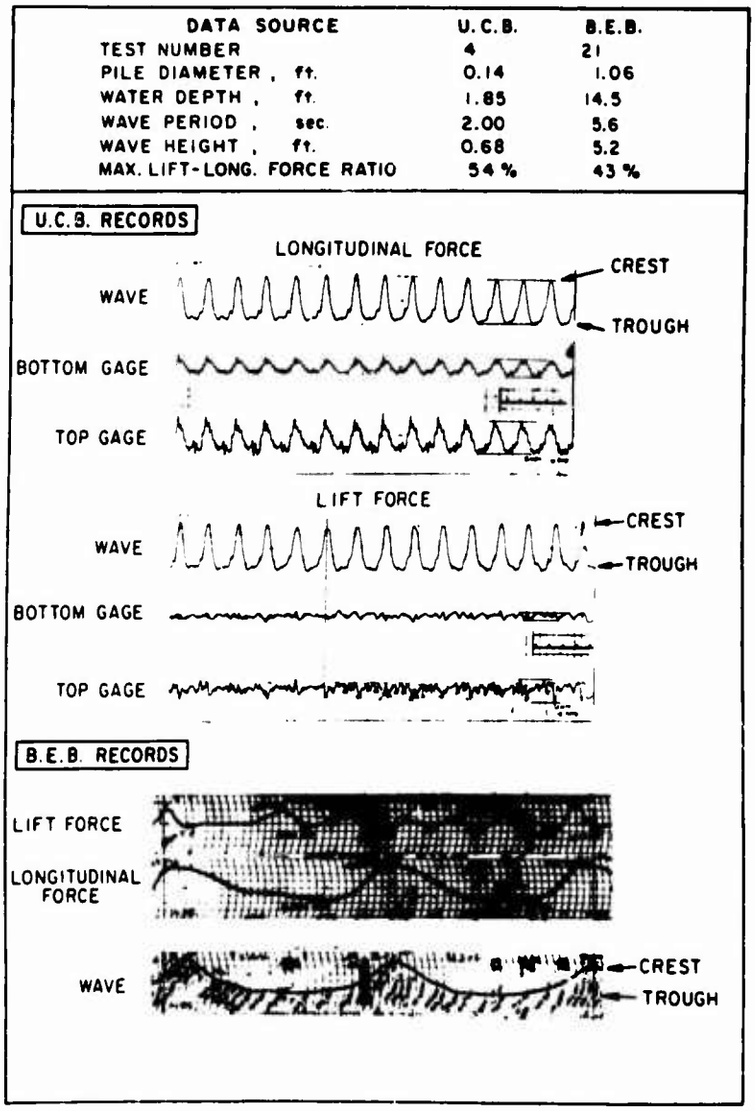


Figure 12. Comparison of UCB (1972) records and BEB records for N_{CK} of about 25

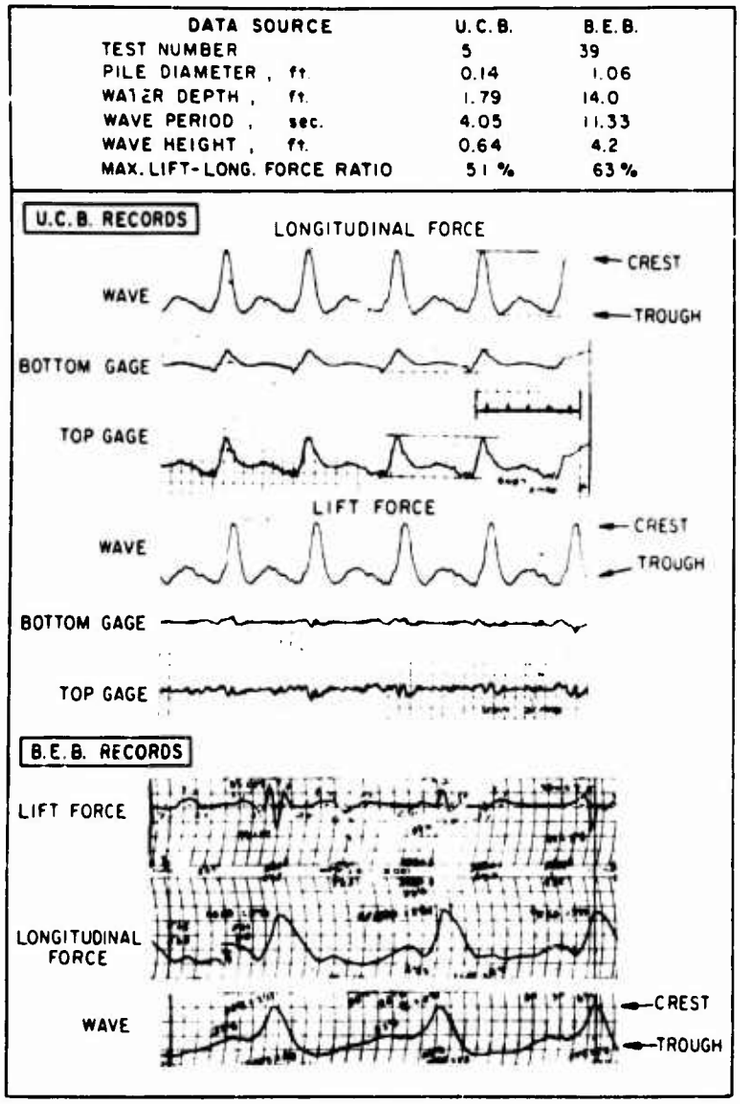


Figure 13. Comparison of UCB (1972) records and BEB records for N_{KC} of about 42 for the UCB and 35 for the BEB runs

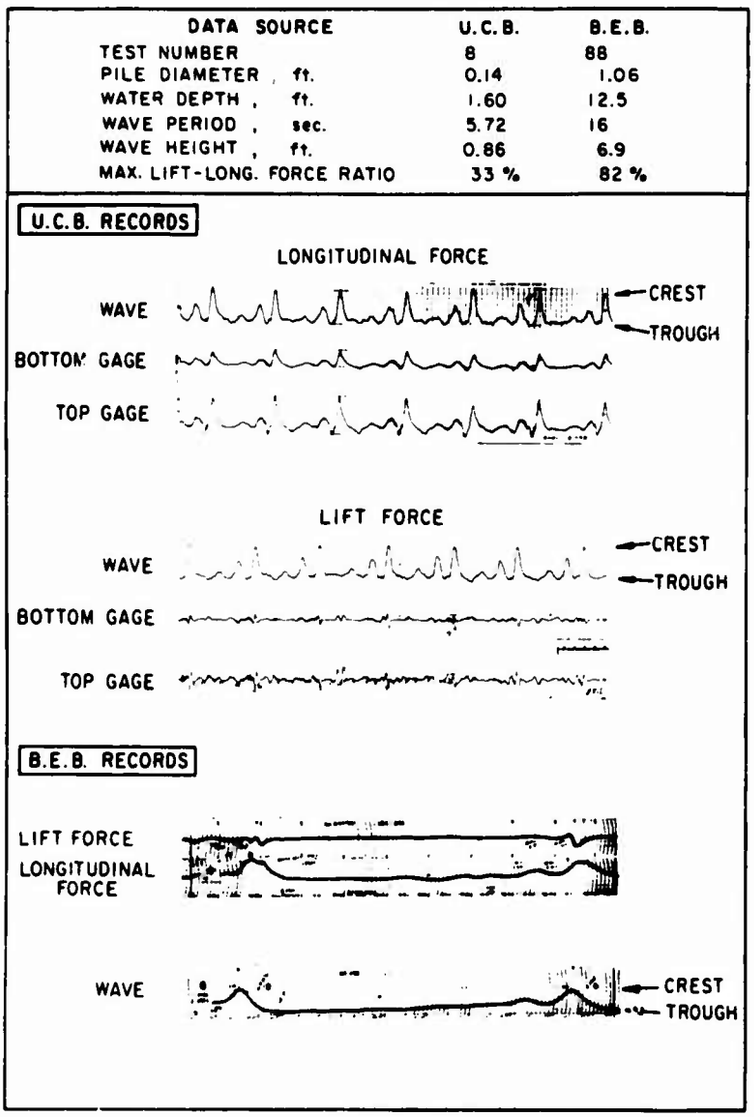


Figure 14. Comparison of UCB (1972) records and BEB records for N_{KC} of about 80

runs shown in Fig. 13, however. The lengths of the waves used in the runs shown in these figures were all rather long compared with the water depth, and were quite non-linear. The run shown in Figure 14 was chosen to show the worst comparison that was obtained, which was for the case of the most nonlinear wave tested.

"Lift" Force Distribution Function

Referring again to Figure 6c, it appeared to the writers that a "lift" force distribution function would be useful. Owing to this, some "lift" force records were analyzed in detail. The method by which this was done is shown in Figure 15. The "lift" forces for 30 consecutive force oscillations were measured for each of 10 runs. Total "lift" forces (the sum of the outputs of the top and bottom strain gages) were measured. The characteristics of the waves in these runs are given in Table 2. The characteristics of representative examples of the BEB data are given in Table 3. The distribution functions are shown in Figure 16.

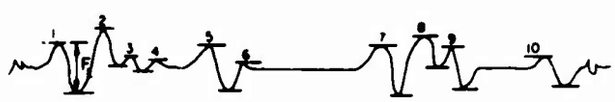


Figure 15. Method of analysis of "lift" force records, UCB 1972 force measured from crest to following trough

"Lift" Frequencies

Chang (1964) stated the frequency of the "lift" forces was twice the wave frequency. However, an examination of the sample records reproduced in his report showed that for a pile diameter of 0.083 foot, and a wave period of about two seconds, the "lift" force became irregular as the wave height was increased. One record showed the average "lift" frequency to be about three times the wave frequency. The writer's data showed that "lift" frequency to become quite irregular, as was the case of Bidde's data for a number of runs (see Figure 6c, for example). The BEB data showed the "lift" force frequencies varied from about 1.3 to 6 times the wave frequency.

Irregular Waves

Waves in the ocean are irregular. Irregular waves can be generated in the laboratory using a wave piston type generator. An example of such waves, together with the induced longitudinal and lift

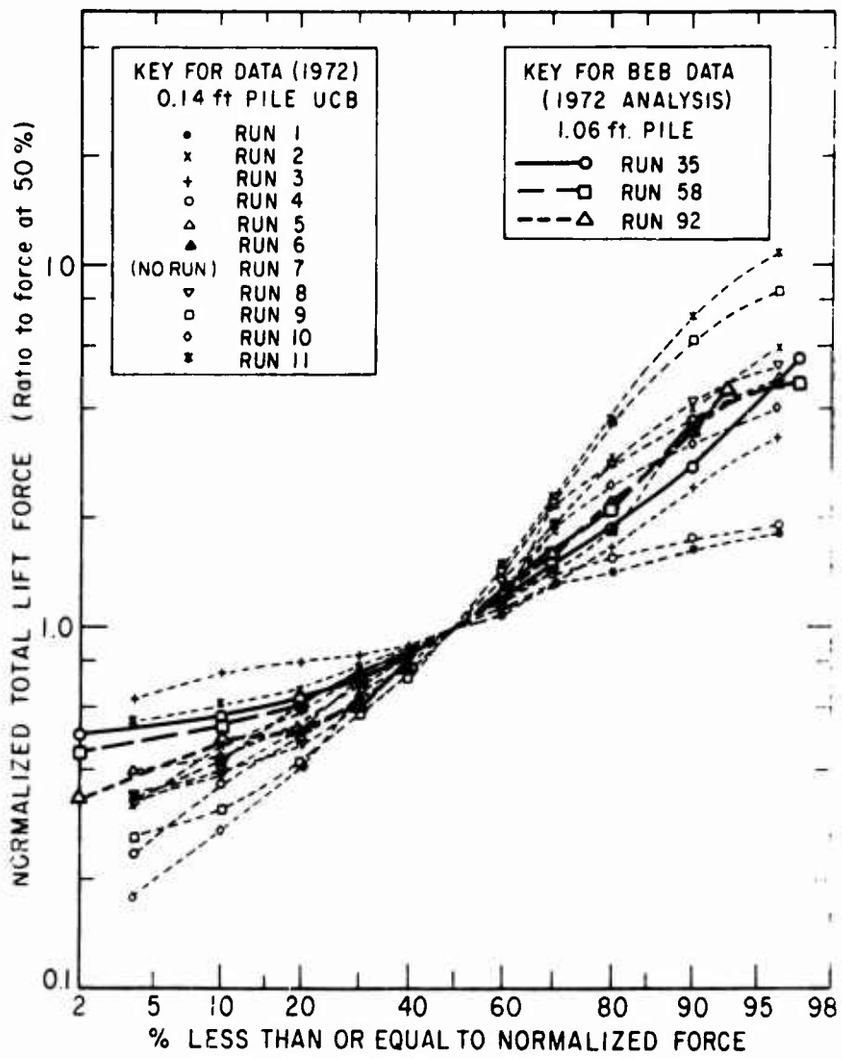


Figure 16. Total "lift" force distribution functions

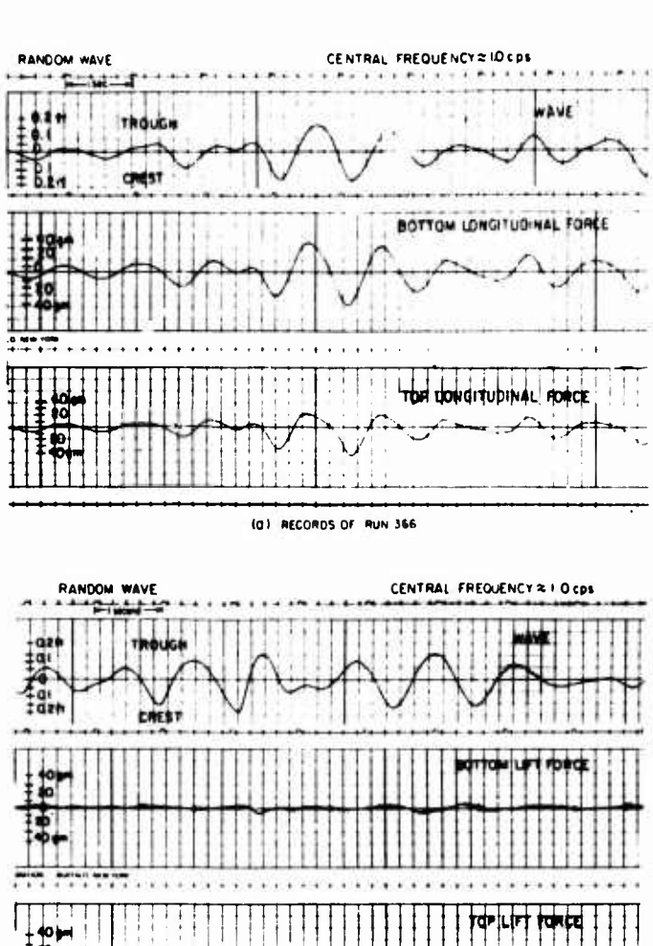


Figure 17. Sample wave and force records, irregular waves (Bidde, 1970)

forces is given in Figure 17 (Bidde 1970). It is suggested that as an approximation the case for regular waves can be extended to the case of two dimensional random waves. For example, the highest wave in Figure 17b has a height of 0.3 ft. Using linear theory, N_{KC} for this wave (the wave "period" is about 1.1 second) can be calculated, and is approximately 7.0. One would then estimate the ratio of "lift" to longitudinal force to be about 15 to 20%.

Waves in the ocean are three dimensional, having a directional wave spectrum. This presents a much more difficult problem than the case of an irregular system of two dimensional waves. Some work has been done in trying to analyse field studies made in the Gulf of Mexico by consortium of oil companies (Schoettle, 1962 ; Blank, 1969). The results of this attempt to analyze the field data to obtain information on "lift" forces was unsuccessful (Abdel-Aal and Wiegel, 1971).

CONCLUSIONS

The Keulegan-Carpenter Number appears to te a useful parameter to predict the ratio of "lift" to longitudinal wave induced forces in a regular system of two dimensional waves. For the case of a vertical pile piercing the water surface, "lift" forces start to occur for values of N_{KC} between 3 and 5, with the ratio of "lift" to longitudinal force increasing rapidly with increasing N_{KC} to a value of N_{KC} of about 15 to 20. The ratio then remains about constant, or perhaps decreases to some extent with increasing N_{KC}.

The value of the ratio of "lift" to longitudinal force, for N_{KC} greater than about 20 appears to be similar to the ratio of C_L/C_D for one directional steady flow.

For the higher values of N_{KC} the "lift" force becomes irregular and should be described by a distribution function.

ACKNOWLEDGEMENTS

The work presented herein was performed under Contract DACW-72-69-C-0001 between the Coastal Engineering Research Center, Corps of Engineers, U.S. Army, and the Univer. y of California.

REFERENCES

1 ABDEL-AAL, Farouk, and WIEGEL, R. L., "Preliminary Report on an Analysis of Project II Data (Wave Forces on a Pile), Hurricane Carla, Gulf of Mexico", University of California, Berkeley, California, Hydraulic Engineering Laboratory, Tech. Rept. HEL 9-18, June 1971, 40 pp.

2 BACON, David L., and REID, Elliott, G., " The Resistance of Spheres in Wind Tunnels and in Air, U.S. NACA, Ninth Annual Report, Rept. No. 479, 1923, pp. 471-487.

3 BIDDE, Devidas, "Wave Forces on a Circular Pile Due to Eddy Shedding, Ph. D. thesis, Department of Civil Engineering, University of California, Berkeley, California ; also, Tech. Rept. No. HEL 9-16, Hydraulic Engineering Laboratory June 1970, 141 pp.

4 BIDDE, Devidas, Laboratory Study Lift Forces on Circular Piles, Jour. Waterways, Harbors and Coastal Engineering Division, Proc. ASCE, Vol. 97, No. WW4, November 1971, pp. 595-614.

5 BISHOP, R. E. D., and HASSAN, A. Y., "The Lift and Drag Forces on a Circular Cylinder in a Flowing Fluid, Proc. Roy. Soc. (London), Ser. A., vol. 277, 1964, pp. 32-50.

6 BLANK, L. S., "Wave Project II, Users Guide," Chevron Oil Field Research Company, La Habra, California, 23 May 1969.

7 CHANG, K. S., "Transverse Forces on Cylinders Due to Vortex Sheding in Waves", M. S. Thesis, Mass. Inst. Tech.; January 1964, 94 pp.

8 GLASER, G. H., "Determination of Source Coordinates of Particles in Water by Stereophotogrammetry", M. S. Thesis, Dept. of Civil Engineering, University of California, Berkeley, California, 1966.

9 HUMPHREYS, John S., "On a Circular Cylinder in a Steady Wind at Transition Reynolds Number", Journ. Fluid Mechanics, Vol. 9, Part 4, 1960, pp. 603-612.

10 KEULEGAN, Garbis H., and CARPENTER, Lloyd H., "Forces on Cylinders and Plates in an Oscillating Fluid," Journal of Research of the National Bureau of Standards, Vol. 60, No. 5, May 1958, pp. 423-440.

11 LAIRD, A. D. K., "Eddy Forces on Rigid Cylinders", Jour. Waterways and Harbors Div., Proc. ASCE, vol. 87, No. WW4, November 1961, pp. 53-68.

12 LAIRD, A. D. K., "Water Forces on Flexible Oscillating Cylinders", Jour. Waterways and Harbors Div., Proc. ASCE, Vol. 88, No. WW3, August 1962, pp. 125-137.

13 LAIRD, A. D. K., "Forces on a Flexible Pile", Proceedings, Speciality Conference on Coastal Engineering, Santa Barbara, California, October 1965, ASCE, 1965, pp. 249-268.

14 LAIRD, A. D. K., "Eddy Formation Behind Circular Cylinders," Jour. Hydraulics Div., Proc. ASCE, Vol. 97, No. HY 6, June 1971, pp. 763-775.

15 LAIRD, A. D. K., JOHNSON, C. A., and WALKER, R. W., "Water Eddy Forces on Oscillating Cylinders, Jour. Hydraulics Div., Proc. ASCE, vol. 86, No. HY 9, Proc. Paper 2652, November 1960, pp. 43-54.

16 LAIRD, A. D. K., and WARREN, R. P., "Groups of Vertical Cylinders Oscillating in Water", Jour. Eng. Mechanics Div., Proc. ASCE, vol. 89, No. EM 1, Proc. Paper 3422, February 1963, pp. 25-35.

17 McNOWN, J. S., and KEULEGAN, G. H., "Vortex Formation and Resistance in Periodic Motion", Jour. Engineering Mechanics Division, Proc. ASCE, vol. 85, No. EM 1, January 1959, pp. 1-6.

18 MORISON, J. R., O'BRIEN, M. P., JOHNSON, J. W., and Schaaf, S. A., "The Force Exerted by Surface Waves on Piles," Petroleum Transactions, Vol. 189, TP 2846, 1950, pp. 149-154.

19 PAAPE, A., and BREUSERS, H. N. C., "The Influence of Pile Dimensions on Forces Exerted by Waves", Proc. Tenth Conf. on Coastal Engineering, Vol. II, ASCE, 1967, pp. 840-847.

20 PRICE, Peter, "Suppression of the Fluid-Induced Vibration of Circular Cylinders", Jour. Eng. Mech. Div., Proc. ASCE, vol. 82, No. EM 3, Proc. Paper 1030, July 1956, 22 pp.

21 ROSHKO, A., "On the Development of Turbulent Wakes From Vortex Streets", U.S. National Advisory Committee for Aeronautics, Tech. Rept. 1191, 1954, pp. 801-825.

22 ROSHKO, A., "Experiments on the Flow Past a Circular Cylinder at Very High Reynolds Numbers", Jour. Fluid Mechanics, vol. 10, Part 3, may 1961, pp. 345-356.

23 ROSS, Culbertson, W., "Large-Scale Tests of Wave Forces on Piling (Preliminary Report), U.S. Army Corps of Engineers, Beach Erosion Board, Tech. Memo. No. 111, May 1959.

24 ROUSE, HUNTER, "Elementary Fluid Mechanics, John Wiley & Sons, Inc., 1946, 376 pp.

25 ROUSE, HUNTER, " On the Role of Eddies in Fluid Motion", American Scientist, Vol. 51, No. 3, September 1963, pp. 285-314.

26 SARPKAYA, TURGET, "Lift, Drag and Added-Mass Coefficients for a Circular Cylinder Immersed in a Time-Dependent Flow", Jour. Applied Mechanics, vol. 30, Series E, No. 1, March 1963, pp. 13-15.

27 SARPKAYA, TURGET, and GARRISON, C.J., "Vortex Formation and Resistance in Unsteady Flow", Jour. Applied Mechanics, Vol. 30, Series E, No. 1, March 1963, pp. 16-24.

28 SCHOETTLE, V., "Design, Construction and Installation of Instrumentation for Wave Project II", Research Report 744, California Research Corporation, 1962.

29 WIEGEL, Robert L., "Oceanographical Engineering," Prentice-Hall, Inc., 1964, 532 pp.

* * *

DISCUSSION

Choung M. Lee
Naval Ship Research and Development Center
Bethesda, Maryland, U.S.A.

Perhaps I should direct this question to Keulegan anc Carpenter themselves, but since Professor Wiegel seems to have much experience in Keulegan number, I would like to ask one question. Keulegan number is formed by the maximum fluid velocity which is multiplied by the period of the flow and divided by the diameter of the circular cylinder. For a periodic fluid motion the maximum velocity can be simply converted into a product of the amplitude and the frequency which is equal to 2π times the amplitude over the period. Then the Keulegan number becomes the ratio of the amplitude of the oscillation of fluid to the diameter of the cylinder. This means that the Keulegan number is independent of frequency. It is a puzzle to me that all the forces acting on the circular cylinder only depend on the ratio of the amplitude of oscillation of fluid to the diameter of the circular cylinder. I believe that there must be a physical reason for such a phenomenon. I would appreciate Professor Wiegel's comment on this remark.

REPLY TO DISCUSSION

Robert L. Wiegel
University Of California
Berkeley, California, U.S.A.

One can make use of the wave equation, calculate the actual excursion of the water particle motion, and what one comes up with is a ratio of the distance that the water particle moves to the diameter of the pile. If you have water waves it is very simple to show that the controlling number there is probably only the ratio of wave height to the diameter. You are correct. I hope I put this in my Paper ; if not, I should have, because it is not really the time, it is the distance along the boundary that the fluid must move in order for the boundary layer to form and for the vortices to form, and so forth. So the time is really only used to calculate how far it has moved. I hope that has answered your question and I see that you indicate that it has.

ANALYSES OF MULTIPLE-FLOAT-SUPPORTED PLATFORMS IN WAVES

C.H. Kim and J.A. Mercier
Stevens Institute of Technology
Davidson Laboratory
Castle Point Station
Hoboken, New Jersey, U.S.A.

ABSTRACT

Results of several studies of the behavior of floating platforms in waves are presented. The contents of these studies may be briefly summarized :

MOTIONS RESPONSE OF A RELATED SERIES OF THREE AND FOUR FLOAT PLATFORMS

Transfer functions relating heave and pitch motions to incident waves have been used together with assumed (Pierson-Moskowitz) wave spectra to derive dimensionless spectral response information for these motions in waves as a function of significant wave height divided by (displaced volume)$^{1/3}$. The dependence on float slenderness, damping plate (or footing) size and metacentric height are presented in Figures and Tables.

SOME PROBLEMS OF THE HYDRODYNAMIC INTERACTION BETWEEN TWO FLOATING BODIES IN BEAM SEAS

An analysis is given of both wave- and motion-induced forces and moments on the individual bodies of a rigidly-connected twin-cylindrical body floating in beam seas. The influence of the hydrodynamic interaction effect on the sway-exciting force was found to be quite remarkable. The diffracted and radiated waves were evaluated and related to wave and damping forces and moments.

Numerical calculations were carried out of some hydrodynamic characteristics of interaction between two different cylindrical bodies floating in proximity in beam seas.

SLENDER VERTICAL FLOATS ISOLATED PERFORMANCE AND INTERACTION EFFECTS FOR LARGE ARRAYS

Relatively simple analytical procedures provide satisfactory description of the heave response of slender vertical floats to waves. It is found that viscous effects must account for most of the heave damping for such slender floats and that it is advisable to introduce specially-engineered damping devices to control resonant heaving motions.

Force and motion studies of a large array (210 elements) of slender floats reveal important interaction effects on wave-induced forces and, especially, heave motions. A satisfactory theoretical explanation of these effects is not yet available but a continuing empirical investigation is planned.

INTRODUCTION

This paper presents results for a somewhat "mixed-bag" of studies of the hydrodynamic performance of floating platforms in waves. The nature of these investigations range from systematic experimental determinations of the performance of multiple float supported platforms in irregular seas to rather sophisticated theoretical evaluations of the behavior of two cylindrical bodies in beam seas and to a combined theoretical and experimental study of an unusual concept for a large expandable floating platform.

The several studies are related because they all deal with floating configurations with zero nominal speed through the water. Two of the studies deal with the important problems of hydrodynamic interactions, although the nature and extent, as well as the modes of investigations of the interactions, differ significantly.

These studies represent a significant portion of the extensive research and development work which has been done on ocean platform behavior at Davidson Laboratory in recent years. They do not relate specifically to ad hoc testing and evaluation of drilling platforms and similar craft, but it is hoped (and anticipated) that the findings reported will prove to be useful for practical design purposes.

Each of the studies is prefaced by a section giving the background of the work done. A Brief summary of the investigations has been given in the Abstract of the paper.

Nomenclature for the three parts of the paper is, unavoidable, not completely uniform. The listings of symbols and their meanings, in the Nomenclature section, are separated into three parts, one for each of the studies.

The original model test program of the systematically-related float supported platforms was supported by the U.S. Naval Air Systems Command. Further analyses of the original data have been carried out by Davidson Laboratory.

The work on the theoretical evaluations of hydrodynamic behavior of two bodies in proximity was sponsored by the National Oceanic and Atmospheric Agencies Sea Grant Program Office as part of a continuing effort to improve prediction procedures for platform motions.

The study of large arrays of slender vertical floats was undertaken as a sub-contract to Goodyear Aerospace Corporation on a Project which is being technically monitored by the Office of Naval Research Ocean Technology Branch.

* * *

MOTIONS RESPONSE OF A RELATED SERIES OF THREE AND FOUR FLOAT PLATFORMS

BACKGROUND

In the early 1960's a substantial program of research and design analyses was undertaken on the concept of using slender vertical floats to support water-based aircraft, thus providing a comfortable and stable environment for crew and equipment. This work was supported by the United States Naval Air Systems Command under the cognizance of E.H.Handler, whose review article on "Tilt and Vertical Float Aircraft for Open Ocean Operations"* describes the progress of this concept up to 1966. Two early studies of particular significance established the validity of the concept. In one of these studies two PBM seaplanes [2] were tested in five-to-eight-foot high waves. One of these craft was supported avobe the water surface by vertical floats and was found to be quite comfortable while the crew of the conventional PBM soon became uncomfortable. The other investigation involved a one-man helicopter which was equipped with tiltable floats [3] and tested in heavy, choppy waves, reacting with slow and gentle motions. Earlier model tests of this vehicle at Davidson Laboratory [4] led to the introduction of horizontal plates at the lower end of the vertical floats, which are found to be a vital feature in the effective employment of this concept.

In order to provide systematic design information for the dynamic performance in waves of these types of craft, results of a series of vertical float configurations which have been model tested in irregular waves to determine their response characteristics have been described by Mercier [5] . Variations in the series include number of floats, float spacing and slenderness, size of damping plate and metacentric height, and heading of the vehicle relative to the waves. The information developed may also be useful for other types of craft, such as work platforms, research and range-tracking platforms, oil-drilling rigs and possibly buoys, which can be configured with vertical floats.

Float supported platforms may be envisioned with any number

---

* Superior numbers in text matter refer to similarly numbered references listed at the end of this paper.

of floats from one up. Single float platforms, such as the SPAR and FLIP research vehicles will not, however, be considered here. Only three and four-float supported platforms, applicable to air-sea craft, are treated in this report. The four-float configurations are arranged so that two of the floats support the main hull, and carry most of the weight while the other two floats are attached to the wings, producing a cruciform array. For the three-float configurations, all floats are of equal size in an equilateral triangular array.

The total displaced volume of the floats must equal the vehicle's weight and static pitch and roll stability must be provided. Static stability criteria usually follow naval architectural practice, measuring stability by metacentric height. From this consideration then, the float slenderness (waterplane area) and spacing are related to the vertical center of gravity of the craft.

Descriptions of the elementary fundamentals of the dynamic motions response of vertical float and "semi-submersible" platforms have been outlined by Barr [6], Julien and Carrive [7], and most recently and thoroughly by Hooft [8]. Considerations both of natural frequencies and of minimization of wave excitation forces and/or moments are of key importance in this regard. A more complete quantitative description of these considerations for heaving motions of isolated floats is given in the present paper as part of the discussion of the performance of closely-packed arrays of floats.

DESCRIPTIONS OF MODELS

Tests in irregular seas were conducted with variations of two basic model configurations. One represents a cruciform array of floats where two equal floats would attach to the aircraft fuselage and two to the wings. This type of system was investigated by Ling-Temco-Vought [9] for application to the XC-124A VTOL aircraft and by General Dynamics/Convair [10] for application to the P5A seaplane equipped with hydro-skis. The second configuration uses three equal floats in a triangular pattern. Such an arrangement has been planned by Boeing-Vertol [11] for application to the CH-46A helicopter.

Sketches illustrating the two basic configurations tested are shown in Figures 1 and 2. The basic frames, to which the floats are attached, are made of aluminum in a lightweight but rigid construction. The floats, which are interchangeable and have adjustable spacings, are made of low density (2 lbs per cu ft) closed-cell sytrofoam with 1/8-in thick aliminum plates on top to facilitate securing to the frame. All floats used have a circular cylindrical body shape with a

hemispherical end. Damping plates are attached, interchangeably, to the lower end of the float in way of the junction of the cylindrical float body and the hemispherical cap. These circular plates were made of 1/16-in. plexiglass with a 60-deg included angle bevel on the periphery. Model weight was selected to be 20-lb, resulting in model size suitable for the available apparatus.

The location of the gimbal-box is such that the center-of-rotation corresponds to the center-of-gravity of the model for a particular "average" set of floats and damping plates. It was felt that the influence on vertical center-of-gravity due to interchanging floats and damping collars would be negligible, being less than about 1/8 inch. Floats are designed so that the height of the gimbal-center is a constant distance above the stillwater level for all the float variants tested.

The model moments of inertia, about the pitch and roll axes, were fixed using the "average" sets of floats and damping plates. While changes in floats and float spacings may alter the model's pitch and roll inertias by amounts up to about 3 per cent, the small changes may be expected to approximate those which would be associated with corresponding design modifications for full-scale vehicles.

The geometric characteristics of the models are given in Table 1 for four-float (cruciform) configurations, and in Table 2 for three-float (triangular) configurations. Also shown in these tables are metacentric heights as computed according to the model design drawings and as measured in separate tests. The computed and measured values do not agree especially well, which is probably attributable to small discrepancies in the manufacture of the styrofoam floats, which would have an important effect on the waterplane inertias and, consequently, on GM (especially for the low values of GM used here). For a few cases where the GM was not measured, estimated values are entered in the table, and these are distinguished by being enclosed in parentheses.

The experiments were carried out in Davidson Laboratory Tank No. 2 which is 75-ft square with a water depth of 4.5 ft. The motions apparatus used to follow the model's motions and provide a means of recording the six components of motion with a minimum of interference has been described by Numata [12] in an appendix to his paper on "Hydrodynamic Model Tests of Offshore Drilling Structures." Tests were carried out in irregular waves with a significant height of 2 inches.

RESULTS

Figure 3 shows a sample oscillogram taken during a test run.

The information obtained from the tests of twenty-five variations in the configuration indicated in Tables 1 and 2 have been analyzed and are presented in two different ways.

The transfer functions, relating waves and motion, are presented in Reference 5 in a series of Tables, such as Table 3 given here, as a function of the non-dimensional frequency parameter, $\tilde{\omega}=\omega\sqrt{\nabla^{1/3}/g}$ where ω = frequency, ∇ = average displaced volume of the vehicle, and g is the acceleration of gravity. The displaced volume has been arbitrarily selected as a useful measure of size for non-dimensionalizing. These were derived by spectral analysis of the irregular sea model data using methods similar to those described in detail by Dalzell and Yamanouchi [13]. The sampling interval used for data analysis, 0.25 sec, was sufficiently low to assure unambiguous spectra, that is, no "aliasing."

Only those spectral results for which the answers appear reasonable are included in the tabulations. Generally, the measure of reasonableness is taken to be the coherency and it is preferred that this quantity should have a value of 0.8, or greater. In a few cases, and in some frequency ranges, the test results do not give such satisfactory values of coherency and a judgment concerning the adequacy of a sample of data has been made by a subjective interpretation of graphs of amplitude and phase versus frequency parameters. Examples of this type of graph are shown in Figure 4 for the results of Test Run 002 (the oscillogram for this run is shown in Figure 3). In this case the range of frequencies for which the coherencies may be considered good is rather wide, especially for the wave-heave correlation.

In Figure 4 and in the tables, the phase angles are positive when the motion lags the passage of the wave trough by the craft's center-of-gravity. Positive vehicle motions are taken as : surge forward, heave downwards, sway to starboard, pitch bow-up, roll starboard down and yaw bow to starboard, while the maximum positive wave elevation corresponds to a wave trough. Beam seas tests were conducted with waves approaching the craft from the starboard side while head seas tests, of course, have waves approaching from the bow.

The non-dimensional angular motion is presented as the ratio of motion (pitch or roll) to the maximum wave slope, as expressed by linear wave theory, $\omega^2\zeta/g$. This is felt to offer some advantage in interpolating the transfer function data for low frequencies - it being realized that for zero frequency (static conditions) the craft must assume the slope of the wave, and the amplitude ratio must then be unity. The phase of this motion is, however, reckoned relative to the wave amplitude measurement, and must correspond to +90° (i.e., phase

lag) for $\omega = 0$.

Impulse response functions were obtained as the Fourier transforms of the transfer functions in accordance with the theory first introduced in ship motions by Fuchs and MacCamy [14] , and more fully developed by Cummins [15] . Examples, again for Test Run 002, are shown in Figure 5. Tables, such as Table 4 given here, are given in Reference 5 for the twenty-five configurations tested. A comparison of measured and calculated heave and pitch motions for a cruciform model in head seas is given in Figure 6. The computations were carried out by the convolution integrals

$$z(\tilde{t}) = \int_{-\infty}^{\infty} k_z(\tilde{\tau})\zeta(\tilde{t}-\tilde{\tau})d\tilde{\tau}$$

and

$$\theta(\tilde{t}) = \frac{1}{\nabla^{1/3}} \int_{-\infty}^{\infty} k_\theta(\tilde{\tau})\zeta(\tilde{t}-\tilde{\tau})d\tilde{\tau} \qquad (1)$$

where k_z and k_θ are from Table 4.

DISCUSSION

Transfer Functions

A comparison of the results of several test runs indicates the influence of variations in the significant parameters. The transfer functions, particularly the amplitude ratio, afford a convenient graphical indication of the performance.

Heave responses for several cruciform models of Group A (Table 1) are shown in Figure 7. The amplitude ratios are plotted against the non-dimensional frequency parameter, $\tilde{\omega} = \omega\sqrt{\nabla^{1/3}/g}$. An auxiliary chart is arranged beneath the frequency parameter, in which the wave length corresponding to a particular craft displacement (long tons of sea water) and frequency parameter can be read. The displacement range covered extends both above and below the usual aircraft range, in case other types of platforms are to be considered. The heave-wave relations shown in Figure 7 all have similar shapes, having virtually no magnification or motion greater than wave elevation, and a sharp fall-off in response above a certain frequency. The damping plate size (which can be considered to be similar to the "footings" fitted to some drill rigs) appears to have the most influence on the heave response for these configurations, but it must be noted that greater variations in geometrical parameters could be adopted.

Pitch response for the models of Group A is given in Figure 8. The auxiliary wave-length-displacement chart is also shown beneath this figure. An additional scale of wave length/$\nabla^{1/3} = \lambda/\nabla^{1/3}$ is added to this Figure, which related to angular motions of the vehicle. This is incorporated for these cases because the wave exciting moment must be expected to be crucially dependent on the ratio of wave length to float spacing. If the wave forces which act on the floats were purely vertical, for instance, as is considered to be the case in the strip theory of ship motions, it would be found that when the wave length equalled the hull float spacing, the exciting moment would vanish since wave crests would occur at each of the floats simultaneously, etc. Table 1 shows the hull float spacing/$\nabla^{1/3}$ to be around 4, while the response curves of Figure 8 indicate practically null motion for $\lambda/\nabla^{1/3}$ in the range of 5.5 to 7. The apparent discrepancy is, of course, explained by noting that horizontal wave exciting forces on the floats contribute greatly to the moment about the center-of-gravity, which is quite high above the still waterline.

Short-term Statistics

While the transfer functions are interesting for making qualitative comparisons, especially because they are familiar, quantitative judgments of performance in realistic irregular waves require consideration of the spectra of the irregular response. For purposes of design and analysis, particular waves must be considered.

The 12th International Towing Tank Conference in Rome [16] adopted the following recommendation relative to wave spectra.

" The Conference recommends that wherever possible, use shall be made of information on wave conditions for the ship's service in presenting predicted ship behavior in waves. When information on typical sea spectra is not available, it is recommended that the following sea spectral formulation shall be used as an interim standard :

$$S_\zeta(\omega) = \frac{A}{\omega^5} e^{-B/\omega^4}$$

$S_\zeta(\omega)$ = spectral density, ft^2-sec

ω = circular frequency, rad/sec (2)

"If the only information available is significant wave height, $H_{1/3}$ ft

$$A = 8.10 \times 10^{-3} g^2 = 8.38 \text{ ft}^2\text{-sec}^{-4}$$

$$B = 33.56/(H_{1/3})^2$$

If statistical information is available on characteristic wave period and significant wave height

$$A = 173(H_{1/3})^2/T_1^4$$

$$B = 691/T_1^4$$

where $T_1 = 2\pi m_o/m_1$

m_o = variance or area under spectrum, ft^2

m_1 = first moment of spectrum about $\omega = 0$ axis, ft^2/sec

Data suggest that T_1 can be taken as the observed characteristic period. The Seakeeping Committee should study further the use of the proposed two parameter spectral formulation."

This formulation is based on work of Pierson and Moskowitz.[17]

The statistics of the response are related to the area under the response spectrum, where, assuming that the amplitudes of response records are narrow-banded and follow Rayleigh distributions, the average apparent response (crest-to-trough) is

$$\bar{x} = 2.5\sqrt{E_x} \tag{3}$$

the average of the one-third highest responses, or "significant" response, is

$$(\bar{x})_{1/3} = 4.0\sqrt{E_x} \tag{4}$$

and the average of the one-tenth highest responses is

$$(\bar{x})_{1/10} = 5.1\sqrt{E_x} \tag{5}$$

where

$$E_x = \int_0^\infty |\alpha_x(\omega)|^2 S_\zeta(\omega)d\omega \tag{6}$$

is the variance, or area under the spectral density curve, $\alpha_x(\omega)$ is the frequency response function (transfer function) describing response in the x^{th} mode of motion to a sinusoidal wave excitation, and $S_\zeta(\omega)$ is the input (wave) spectral density.

It is possible to express responses to the ITTC (or Pierson-Moskowitz) sea spectra in dimensionless form, applicable to any size

of configuration. Thus, if $\tilde{\alpha}_x(\tilde{\omega})$ is a non-dimensional ratio of response, x , to wave elevation, ζ , a non-dimensional variance may be obtained as

$$\tilde{E}_x = \frac{E_x}{\nabla^{2/3}} = \int_0^{\infty} |\tilde{\alpha}_x(\tilde{\omega})| \frac{2\times 0.0081}{\tilde{\omega}^5} e^{-\left(\frac{33.56}{\tilde{\omega}^4 g^2}\right)\left(\frac{\nabla^{2/3}}{H_{1/3}^2}\right)} d\tilde{\omega} \qquad (7)$$

where the spectral formulation with only significant wave height being available was chosen so that only one parameter ($\nabla^{1/3}/H_{1/3}$) would describe the relative intensity of the sea state.

Since wave elevation has dimensions of length, the response itself must have the same dimensions. This is, of course, the typical case for heave or surge but other examples of non-dimensional response are :

$$\alpha_\theta = \frac{\theta \nabla^{1/3}}{\zeta} \quad \text{for pitch angle} \qquad (8a)$$

$$\alpha_A = \frac{A}{g}\frac{\nabla^{1/3}}{\zeta} \quad \text{for acceleration} \qquad (8b)$$

$$\alpha_s = \frac{s}{\zeta} \quad \text{for relative motion} \qquad (8c)$$

$$\alpha_{\dot{s}} = \frac{\dot{s}\sqrt{\nabla^{1/3}/g}}{\zeta} \quad \text{for relative velocity} \qquad (8d)$$

$$\alpha_M = \frac{M}{\rho g \nabla \zeta} \quad \text{for bending moment} \qquad (8e)$$

$$\alpha_z = \frac{z}{\zeta} \quad \text{for heave} \qquad (8f)$$

and so forth.

The dimensionless presentation of spectral response was, to the authors knowledge, first introduced by Bennet [18] in 1966, who retained the two parameter (significant height and period) description of the irregular seas. This very useful form of presentation has been adopted by Lindgren and Williams [19] , among others, and deserves wider application. Fridsma [20] has exploited the useful scaling characteristics of the ITTC (Pierson-Moskowitz) spectra to present dimensionless results of motion and acceleration measurements carried out with planing model hulls in waves whose spectra corresponds with the ITTC recommendation. Thus, information for these highly non-linear responses can be given for craft of various sizes in realistic irregular seas.

The transfer functions previously presented by Mercier [5] have now been used to obtain spectral information on performance in irregular waves in accordance with Equation (7). Carpet plots showing significant (average of the one-third highest) heave and pitch responses as a function of significant wave height divided by (displaced volume)$^{1/3}$ and other parameters are shown in Figures 9 to 13. The device of carpet-plotting, which is common in aeronautical research and testing, permits cross plots to be presented on a single sheet of paper, and greatly facilitates performance comparisons and exhibiting dependencies of results on various parameters.

The effect of damping plate size on heave and pitch for a cruciform array of floats (test runs 002,012 and 018, Table 1) are shown in Figure 9. The same information is given in Figure 10 for platforms with a different distribution of displacement among the "hull" and "wing" floats ; hull float diam/wing float diam = 1.25 (rather than 1.5 for the results shown in Figure 9) (test runs 060,058 and 062, Table 1). In both cases, larger damping plates reduce heave response but increase pitch response. For three float configurations, having somewhat more slender floats, the corresponding results are given in Figure 11 (test runs 074,091, and 087) ; the influence on heave motions is similar but for pitching motions with low relative sea conditions, $H_{1/3}/\nabla^{1/3} \leq 0.7$, a suitable selection of damping plate size appears to lead to minimum pitch motions.

The effect of float slenderness on heave motions is exhibited in Fig. 12 for the cruciform (test runs 002,047 and 032) and triangular (test runs 074,096 and 083) float array models, both with damping plate diam/float diam = 1.6. Since the pitch response (but not the heave response) is strongly dependent on metacentric height, and since the tests with variations of float slenderness were not executed with uniform values of GM, the influence of float slenderness alone on pitch motions is not presented. It is interesting to note the distinctly different trends of heave response as a function of float draft-to-diameter ratio ; for the four-float configuration it appears that a maximum occurs for T/D_F between 2 and 2.5, while for the three-float array a minimum exists around $T/D_F = 5$. These different behaviors may be due to the different arrangements of floatation (three floats of four) as well as the different ranges of slendernesses investigated.

The influence of metacentric height on heave and pitch response is shown in Fig. 13 for a four-float configuration (test runs 002,005 and 006). As was stated above, the heave motion is not importantly affected by GM. On the other hand, the pitching motion is greatly affected by stability with excessively low metacentric height giving rise to large angular motions which are not characteristic of well-designed float-supported-platforms.

The results have been given for a range of dimensionless sea states $H_{1/3}/\nabla^{1/3}$ up to 1.0, so that for a craft of 30000 long tons displacement the corresponding significant wave height is 102 feet. This corresponds to a high Sea State 9 and, according to the recommendations of the ITTC [16], the approximate wind speed in the open ocean would be well above 80 knots. For a 10-ton craft, however, the significant height would be 7.05 feet, or Sea State 4.

Dimensionless statistical response data are presented in tabular form for all of the model tests reported by Mercier [5], in Tables 5a-5y. Large values of $H_{1/3}/\nabla^{1/3}$, up to 4.0 ($H_{1/3} \approx 75$ ft for a 3000-ton craft), are covered in these tables but because the transfer functions derived from the basic tests are not precisely defined at low frequencies, which are strongly excited by extremely high sea states, the results above $H_{1/3}/\nabla^{1/3} = 1.0$ are somewhat less reliable. This is especially true for the pitch motions which have very low but undefined natural frequencies. The transfer functions were extrapolated "by eye" to lower frequencies to permit these calculations for $1.0 < H_{1/3}/\nabla^{1/3} < 4.0$ to be undertaken.

Extreme Response

Ochi [21] has adapted order statistics with a given probability of being exceeded, for evaluating long-term statistical behavior which may be more appropriate for evaluating limiting sea state operating conditions. His equation, which is applicable to Rayleigh probability distributions, may be expressed non-dimensionally as

$$\frac{\hat{x}}{\nabla^{1/3}} = \sqrt{-2\,\tilde{E}_x\,\ell n\left\{1-(1-\text{Prob})^{1/N_o}\right\}} \qquad (9)$$

where $\hat{x}$ = extreme value (amplitude) (for examples : heave, $\hat{z}$; pitch, $\hat{\theta}\nabla^{1/3}$; acceleration, $(A/g)\nabla^{1/3}$, etc.)

$$N_o = \frac{3600}{\pi}\ \text{Time}\ \sqrt{\frac{g}{\nabla^{1/3}}}\ \sqrt{\dot{E}_x/\tilde{E}_x}$$

Time = Duration time in hours

Prob = Probability of computed value, $\hat{x}$, being exceeded

$\tilde{E}_x$ = Dimensionless response variance, Eq.(6)

$\tilde{\dot{E}}_x$ = Dimensionless response velocity variance

$$= \int_0^\infty \tilde{\omega}^2\,|\alpha_x(\tilde{\omega})|\,\frac{2\times 0.081}{\tilde{\omega}^5}\,e^{-\left(\frac{33.56}{\tilde{\omega}^4 g^2}\right)\left(\frac{\nabla^{2/3}}{H_{1/3}^2}\right)}\,d\tilde{\omega} \qquad (10)$$

For example, if a probability of being exceeded is 0.1, the expression implies that one platform in ten floating in the same area or statistical environment may experience a larger response than the estimated extreme value ($\hat{x}$) during the specified duration.

Because this type of response information is of interest for certain investigations the second moment of the response spectra, $\tilde{E}_{\dot{x}}$, have been calculated according to Equation (10) and included in Tables 5. It may be appropriate to note that a recent study by Dalzell [22] of the statistics of responses of systems with non-linearities suggests that applications which assume the Rayleigh distribution and involve order statistics and/or the estimation of extremes tend to over-predict. Since most platforms are subject to some extent of non-linear damping, at least for extreme sea states, Dalzell's observations should be borne in mind.

SOME PROBLEMS OF THE HYDRODYNAMIC INTERACTION BETWEEN TWO FLOATING BODIES IN BEAM SEAS

BACKGROUND

Ohsusu [23, 24] has theoretically evaluated the hydrodynamic forces and moments on two or more cylinders heaving, swaying and rolling on a calm water surface. Ohkusu and Takaki [25] have applied these analyses to evaluate the motions of multi-hull ships in waves. Wang and Wahab [26] have also studied the hydrodynamic forces on twin heaving cylinders on a calm water surface.

These investigators used the method of multipole expansion to determine the unknown velocity potential. In these analyses, the individual section must be symmetrical about its own vertical midplane and the two cylinders must be identical.

Lee, Jones and Bedel [27] have reported theoretical and experimental evaluations of the hydrodynamic forces on twin heaving cylinders on a calm water surface. Their theoretical analysis followed the method of source distribution over the immersed contours [28] of the cylinders. Consequently, cylinders of arbitrary cross-section, not necessarily symmetric about their vertical midplanes can be dealt with. This investigation also assumed the two cylinders to be symmetrically disposed with respect to each other.

All the above investigations [23-27] of multihull cylinders assumed that the cylinders are rigidly connected.

The present study also applies the close-fit source distribution method pioneered by Frank [28] . We assume two arbitrarily shaped bodies, which do not have to be either symmetrical about their vertical midplanes or to be symmetrically disposed with respect to each other. Furthermore, the two bodies may be unconnected or connected either rigidly or elastically.

This investigation, based on two-dimensional linearized theory, considers both the radiation and diffraction problems for two arbitrarily shaped cylindrical bodies floating in a train of beam waves ; the hydrodynamic inertial and damping forces and moments due to swaying, heaving and rolling of the cylinders on a calm water surface and the forces and moments induced by beam waves on the fixed cylinders are evaluated.

Brief descriptions will be given of the methods used to evaluate the unknown velocity potentials for the radiation and diffraction problems. Since the fundamental velocity potential of a two-dimensional pulsating source of unit intensity located below the free surface and satisfying the required hydrodynamic conditions inside and on the boundaries of the entire deep-water domain is a well-known solution stated by Wehausen and Laitone [29] , it is only necessary to discuss here the kinematical boundary conditions on the body contours.

Two applications of the theory will be considered in detail : 1) the analysis of the hydrodynamic forces on two rigidly connected cylinders and, 2) the relative heaving motions of two unconnected bodies in close proximity. Results of calculations for these cases will be presented and discussed. The case of a pair of three-dimensional, vertical body-of-revolution floats, in close proximity will be discussed on the basis of experimental results.

KINEMATIC BOUNDARY CONDITIONS

The Radiation Problem

Consider two arbitrarily shaped parallel cylinders oscillating in prescribed (arbitrary) modes of motion, with given amplitudes and phases, on or below the calm water surface in the form

$$[S]_a = S_a^{(m_a)} e^{-i\omega t}$$

$$[S]_b = S_b^{(m_b)} e^{-i(\epsilon_{S_a S_b} + \omega t)} \qquad (11)$$

where

$S_a^{(ma)}$, $S_b^{(mb)}$ = amplitudes of displacement in the mode of motion m_a and m_b, respectively (m_a or m_b = 2,3,4 correspond to sway, heave, roll)

$\epsilon_{S_a S_b}$ = phase difference between the motions of bodies a and b

For certain kinds of problems such as the relative heaving motions between adjacent bodies, it may be convenient to refer the phases of the motions to, for instance, the wave-exciting force.

The space coordinate system is defined in Figure 14a ; the y-axis lies on a calm water surface, the z-axis points vertically upward and the origin 0 is taken at the midpoint between the two walls of a and b .

The body contours C_a and C_b of a and b are approximately represented by polygons with a finite number of segments. A pulsating source of unknown strength is uniformly distributed on each segment to represent the flow induced by the motions of the two bodies. The velocity potential for the source of unit strength at (η, ζ) may be written [29] :

$$G(y,z;\eta,\zeta)e^{-i\omega t} \tag{12}$$

where (y,z) is the coordinate of a field point. The resultant velocity potential is represented as a sum of all of the discrete source segments of the polygonal approximation to the contours C_a and C_b ,

$$\varphi(y,z)^{(m_a, m_b, \epsilon_{S_a S_b})} = \sum_{j=1}^{N} Q_j \int_{S_{j_a}} G(y,z;\eta,\zeta)dS + \sum_{k=1}^{M} Q_k \int_{S_{k_b}} G(y,z;\eta,\zeta)dS \tag{13}$$

where S_{j_a}, S_{k_b} = j^{th} and k^{th} polygonal segments of a,b, respectively

Q_j, Q_k = (uniform) complex source intensity of the j^{th} and k^{th} polygonal segments of a,b, respectively

The unknown source intesities Q are determined numerically, satisfying the kinematic boundary conditions,

$$\frac{\partial \varphi}{\partial n}(y_a, z_a)^{(m_a, m_b, \epsilon_{S_a S_b})} = -i\omega u_n^{(m_a)}(y_a, z_a)$$

$$\frac{\partial \varphi}{\partial n}(y_b, y_b)^{(m_a, m_b, \epsilon_{S_a S_b})} = -i\omega u_n^{(m_b)}(y_a, z_a) e^{-i\epsilon_{S_a S_b}} \qquad (14)$$

with $u_n^{(m_a)}(y_a, z_a) = \sin\alpha_k$ for $m_a = 2$

$= -\cos\alpha_k$ 3

$= -(y_a \cos\alpha_k + z_a \sin\alpha_k)$ 4

for body a, and similarly for body b . The normal velocity $\frac{\partial \varphi}{\partial n}$ in Eq.(14) is taken to be the velocity induced on the k^{th} segment by all of the other segments. α_k = the orientation of the segment S_k in accordance with Ref. 28.

Two special cases of interest may be mentioned. If the bodies a and b are rigidly connected twin cylinders, Eq.(14) takes the form

$$\frac{\partial \varphi}{\partial n}^{(m)}(y_a, z_a) = -i\omega u_n^{(m)}(y_a, z_a)$$

$$\frac{\partial \varphi}{\partial n}^{(m)}(y_b, z_b) = -i\omega u_n^{(m)}(y_b, z_b) \qquad (14a)$$

while if body a is oscillated while body b is fixed, Eq.(14) reduces to

$$\frac{\partial \varphi^{(m)}(y_a, z_a)}{\partial n} = -i\omega u_n^{(m)}(y_a, z_a)$$

$$\frac{\partial \varphi^{(m)}(y_b, z_b)}{\partial n} = 0 \qquad (14b)$$

The Diffraction Problem

Consider an incident wave

$$h = ae^{i\nu y} \qquad (15)$$

where a = wave amplitude

ν = wave number

and the time factor $e^{-i\omega t}$ is omitted in this and subsequent sections. This wave encounters the fixed arbitrarily shaped bodies and is diffracted.

The velocity potential corresponding to the incident wave is

$$\varphi_I^{(o+e)} = -\frac{iga}{\omega} e^{\nu z} e^{i\nu y} \tag{16}$$

which can be expressed as odd and even function of y,

$$\varphi_I^{(o)} = -\frac{iga}{\omega} e^{\nu z} \sin \nu y$$

$$\varphi_I^{(e)} = -\frac{iga}{\omega} e^{\nu z} \cos \nu y \tag{17}$$

The odd function $\varphi_I^{(o)}$ corresponds to the part of the flow which is asymmetric about the z-axis, while the even function $\varphi_I^{(e)}$ corresponds to the symmetric flow.

The flows represented by the potentials $\varphi_I^{(o)}$ and $\varphi_I^{(e)}$ are disturbed in encountering the bodies. The disturbed flows corresponding to $\varphi_I^{(o)}$ and $\varphi_I^{(e)}$ are described by diffraction potentials, denoted $\varphi_D^{(o)}$ and $\varphi_D^{(e)}$, respectively. These potentials are represented in the same form as the radiation potentials [Eq. (13)], but with different source intensities, Q.

The unknown source densities are determined by satisfying the boundary conditions

$$\frac{\partial \varphi_D^{(\beta)}}{\partial n}(y_a, z_a) = -\frac{\partial \varphi_I^{(\beta)}}{\partial n}(y_a, z_a)$$

$$\frac{\partial \varphi_D^{(\beta)}}{\partial n}(y_b, z_b) = -\frac{\partial \varphi_I^{(\beta)}}{\partial n}(y_b, z_b) \tag{18}$$

where $\beta = o$ or e, on the straight-line segments representing the contours C_a and C_b. Thus there are two separate boundary conditions for the asymmetric and symmetric flows.

HYDRODYNAMIC FORCES AND MOMENTS

Relationship to Potentials

The linearized hydrodynamic pressure is given by

$$(\gamma) \quad = \quad ip\omega\varphi^{(\gamma)} \tag{19}$$

where, for the radiation problem $\varphi^{(\gamma)} = \varphi^{(m_a, m_b, \epsilon S_a S_b)}$, and for the diffraction problem $\varphi^{(\gamma)} = \varphi_I^{(o+e)} + \varphi_D^{(o+e)}$. Using the single superscript notation for the radiation or diffraction problem, the hydrodynamic forces and moments are given by

$$\begin{aligned} F_S^{(\gamma)} &= -\int_C p^{(\gamma)}\, dz \\ F_H^{(\gamma)} &= \int_C p^{(\gamma)}\, dy \\ F_R^{(\gamma)} &= \int_C p^{(\gamma)}\, (ydy + zdz) \end{aligned} \tag{20}$$

where C = body contour C_a or C_b.

Non-dimensional hydrodynamic moment arms for the sway and heave components of force, taking account that the pressure is complex, $p^{(\gamma)} = p_r^{(\gamma)} + ip_i^{(\gamma)}$, can be written

$$\begin{aligned} \ell_{S_r}^{(\gamma)} &= -\frac{1}{T}\frac{\int_C p_r^{(\gamma)}\, zdz}{\int_C p_r^{(\gamma)}\, dz} \\ \ell_{S_i}^{(\gamma)} &= -\frac{1}{T}\frac{\int_C p_i^{(\gamma)}\, zdz}{\int_C p_i^{(\gamma)}\, dz} \\ \ell_{H_r}^{(\gamma)} &= \frac{1}{T}\frac{\int_C p_r^{(\gamma)}\, ydy}{\int_C p_r^{(\gamma)}\, dy} \\ \ell_{H_i}^{(\gamma)} &= \frac{1}{T}\frac{\int_C p_i^{(\gamma)}\, ydy}{\int_C p_i^{(\gamma)}\, dy} \end{aligned} \tag{21}$$

where T = the maximum draft of the two bodies. The subscripts S, H, R indicate swaying and heaving forces and rolling moment, respectively.

The hydrodynamic force has real and imaginery parts, for instance

$$F_S^{(\gamma)} = F_{S_r}^{(\gamma)} + i F_{S_i}^{(\gamma)} \tag{22}$$

In the radiation problem, the real part of the hydrodynamic force (moment) is called the inertia force (moment while the imaginary part corresponds to a hydrodynamic damping force (moment). In the diffraction problem, the complex force defines the amplitude and phase of the wave-exciting force relative to the passage of the crest of the incident wave by the origin 0. The hydrodynamic moment arms also consist of inertial and damping parts in the radiation problem. In the diffraction problem, however, the moment arms of the real and imaginary components are identical because the force and moment maxima occur at the same instant.

Force and Moment Coefficients

Hydrodynamic interactions affect the pressure distributions and forces acting on the individual bodies. Certain components of these resultant forces and moments may be considered as internal forces for the evaluation of dynamic structural loading on rigidly connected cylinders. The hydrodynamic forces on individual bodies are useful and the individual bodies when they are elastically coupled or unconnected.

Table 6 defines the various force and moment components, in accordance with Eq.(20), and their corresponding dimensionless coefficients.

The first subscript denotes the mode of motion (in place of the parenthetical superscript used previously ; the forces, moments, and coefficients do, however, depend on the details of the modes and phases of motions), while the second subscript denotes the components of force (moment). For example,

$\omega^2 m''_{SR}$ = roll hydrodynamic inertial moment induced by swaying motion of unit amplitude of displacement

ωN_{RH} = the heave damping force induced by rolling motion of unit amplitude of displacement

The hydrodynamic moment arms, according to Eqs.(21), are presented in Table 7. The subscript notation is analogous to that used for Table 6, so that, for example, ℓ_{SS_r} indicates the moment arm for the hydrodynamic inertial sway force induced by sway motion.

The roll moments may be expressed in terms of the heave and sway forces and their respective levers as indicated in Table 8.

The wave-exciting forces and moments may be expressed in dimensionless form as shown in Table 9.

The wave-induced moment can, of course, be represented in terms of the sway and heave forces and corresponding moment arms in accordance with Eq.(21), in a manner similar to the motion-induced moments (Table 8). The separation of wave forces into odd and even parts will be shown to be useful for the case of the catamaran-type ship.

Rigidly Connected Twin Cylinders

All of the above formulas may be applied for bodies a, b and a+b, regardless of whether the bodies are similar (some care and consistency must be used in choosing and using relevant dimensions, draft and beam, for use in the dimensionless coefficients if the bodies are not twins). Based on a limited number of numerical calculation of twin cylinders, it is observed that the hydrodynamic forces, moment and moment arms due to oscillatory motions are entirely identical in magnitude for bodies a and b (see Table 10).

Consequently, the resultant hydrodynamic forces and moments may be given as shown in Tables 11 and 12, where the subscript (a+b) for the rigidly coupled bodies is omitted.

Since the bodies are twin and the incident wave flow consists of part which are symmetric and asymmetric with respect to the vertical z-axis, the odd and even components of the wave-exciting forces and moments on bodies a and b are equal in magnitude, whereas some forces on a,b act in opposite directions. (Table 12)

These relations which arise due to symmetry afford considerable simplications for evaluations of catamaran-type configurations. They are exhibited graphically in Figures 14a-d.

For convenience, the previously defined force and moment coefficients C, δ (Tables 6, 7) will be called the forces and moments. Figure 14a illustrates a typical force system, induced by the heaving motion of the twin bodies. The heaving motion induces both heaving and

swaying forces, $[C_{HH}]$, $[\delta_{HH}]$ and $[C_{HS}]$, $[\delta_{HS}]$, respectively, on the individual bodies a and b. The swaying forces $[C_{HS}]$, $[\delta_{HS}]$ on a and b are equal, opposite and colinear, hence, the resultant forces on the twin bodies (a+b) are only the heaving forces $2[C_{HH}]_a$ and $2[\delta_{HH}]_a$ (see Table 11). Figure 14b represents a typical force system induced by the swaying motion. This motion also induces both heaving and swaying forces on each body. The sway-induced heaving forces $[C_{SH}]$ and $[\delta_{SH}]$ on a as well as b set up a couple which contributes to the resultant rolling moments $2[C_{SR}]_a$ and $2[\delta_{SR}]_a$ (see Tables 8, 11). The sums of the swaying forces on the twin bodies (a+ b) are equal to $2[C_{SS}]_a$ and $2[\delta_{SS}]_a$, which also contribute to the resultant rolling moments $2[C_{SR}]_a$, $2[\delta_{SR}]_a$ (Tables 8, 11).

Another typical force system is that induced by the rolling motion, as illustrated in Figure 14c. The rolling motion induces the heaving forces $[C_{RH}]$, $[\delta_{RH}]$ and the swaying forces $[C_{RS}]$, $[\delta_{RS}]$ on each body. The heaving forces set up a couple and hence contribute to the resultant rolling moments C_{RR} , δ_{RR} on the twin bodies (a+b) (Tables 8, 11). The swaying forces on a and b are equal. Their resultants on (a+b) are equal to $2[C_{RS}]_a$ and $2[\delta_{RS}]_a$, and also contribute to the rolling moments C_{RR} , δ_{RR} (Tables 8, 11).

The non-dimensional expressions of the wave-exciting forces and moments are defined in Table 9. Referring to Figure 14d, first let us observe the typical wave-induced force system. The even and odd wave potentials induce both sway- and heave-exciting forces. The sway-exciting forces on a, b $[f_S^{(e)}]_a$, $[f_S^{(e)}]_b$ are equal, opposite and colinear, while the heave-exciting forces $[f_H^{(o)}]_a$, $[f_H^{(o)}]_b$ set up a couple.

We see from the figure that the resultant roll-exciting moment and the resultant sway-exciting force are due only to the odd wave potential, whereas the resultant heave-exciting force is due only to the even wave potential. (See Table 13).

The Radiated and Diffracted Waves

We consider at first the evaluation of the radiated and diffracted waves generated from a rigidly connected twin-cylinder floating in a regular beam wave.

The radiated and diffracted waves generated by a monohull cross section floating in a regular beam wave were evaluated in the previous work [30] . The radiated or the diffracted wave is the vector

sum of the far field waves induced by the pulsating sources $Q^{(\gamma)}$ distributed on the sectional contours, where $\gamma = m$ (mode number) for the radiation, and $\gamma = \beta(0+e)$ for the diffraction problem.

The asymptotic expression of the velocity potential $\varphi^{(\gamma)}$ at $y \to \pm\infty$ for both radiation ($\gamma = m$) and diffraction ($\gamma = \beta$) are identical in their forms

$$\varphi_{\pm}^{(\gamma)} = \frac{A_{\pm}^{\prime(\gamma)}}{\nu} e^{\nu z} e^{i(\pm \nu y \mp \epsilon_{\pm}^{\prime}(\gamma)} \tag{23}$$

where $\pm$ suffix refers to $y \to \pm\infty$.

It is to be noted that $\varphi_{\pm}^{(\gamma)}$ denotes both the potential per unit amplitude of displacement in forced oscillation for $\gamma = m$ and that per unit amplitude of the incident wave for $\gamma = \beta$, $A_{\pm}^{(\gamma)}$ and $\epsilon_{\pm}^{(\gamma)}$ are evaluated in a fashion similar to that given in Ref. 30 where the arbitrarily shaped geometry and both symmetric and asymmetric flow conditions will require that the term with $(-1)^m$ in the formula Eq. (25) of the above reference should be taken as zero. Hence,

$$A_{\pm}^{\prime(\gamma)} = \sqrt{C_{\pm}^{(\gamma)2} + D_{\pm}^{(\gamma)2}}$$

$$\epsilon_{\pm}^{\prime(\gamma)} = \tan^{-1}\left[\frac{D_{\pm}^{(\gamma)}}{C_{\pm}^{(\gamma)}}\right]$$

$$C_{\pm}^{(\gamma)} = \left\{\sum_{j=1}^{N} \pm Q_j^{(\gamma)} K_j + Q_{N+j}^{(\gamma)} L_j\right\}_a + \left\{\sum_{j=1}^{N} \pm Q_j^{(\gamma)} K_j + Q_{N+j}^{(\gamma)} L_j\right\}_b$$

$$D_{\pm}^{(\gamma)} = \left\{\sum_{j=1}^{N} \pm Q_j^{(\gamma)} L_j - Q_{N+j}^{(\gamma)} K_j\right\}_a + \left\{\sum_{j=1}^{N} \pm Q_j^{(\gamma)} L_j - Q_{N+j}^{(\gamma)} K_j\right\}_b \tag{24}$$

$$K_j = e^{\nu\zeta_{j+1}} \cos(\nu\eta_{j+1} + \alpha_j) - e^{\nu\zeta_j} \cos(\nu\eta_j + \alpha_j)$$

$$L_j = e^{\nu\zeta_{j+1}} \sin(\nu\eta_{j+1} + \alpha_j) - e^{\nu\zeta_j} \sin(\nu\eta_j + \alpha_j)$$

where

a, b = the suffixes indicating the terms of the bodies a and b, respectively

$Q_j^{(\gamma)}, Q_{N+j}^{(\gamma)}$ = the real and imaginary parts of the complex source strength, uniformly distributed over the elementary j^{th} segment of bodies a or b

(η_j, ζ_j), etc = the coordinates of the end points of the j^{th} segments

α_j = the slope of the j^{th} segment

The far field wave $h_{\pm}^{(\gamma)}$ is derived from the far field potential $\varphi_{\pm}^{(\gamma)}$ (Eq. 23) as

$$h_{\pm}^{(\gamma)} = \frac{iA_{\pm}^{'(\gamma)}}{\omega} e^{i(\pm\nu y \mp \epsilon_{\pm}^{'(\gamma)})} \tag{25}$$

Let the complex amplitude ratio be

$$A_{\pm}^{(\gamma)} = \frac{A_{\pm}^{'(\gamma)}}{\omega} e^{\mp i\epsilon_{\pm}^{'(\gamma)}} \; ; \; A_{\pm}^{(\gamma)} = \left|A_{\pm}^{(\gamma)}\right| e^{i\epsilon_{\pm}^{(\gamma)}} \tag{26}$$

The energy conservation law leads to the well known relation between the hydrodynamic damping coefficient $N^{(m)}$ and the radiated wave amplitude ratio $\left|A_{\pm}^{(m)}\right|$

$$N^{(m)} = \frac{eg^2}{\omega^3}\left|A_{\pm}^{(m)}\right|^2 \tag{27}$$

where

$\pm$ = suffix indicating the radiated wave at $y \to +\infty$ or $-\infty$.

It is to be noted that $\left|A_{\pm}^{(4)}\right|$ has the dimension of length ; in other words $\left|A_{\pm}^{(4)}\right|$ is not a non-dimensional, whereas the $\left|A_{\pm}^{(2)}\right|$, $\left|A_{\pm}^{(3)}\right|$ are.

By the Haskind-method [31,32] , one can also evaluate the wave-exciting forces and moments by the radiated wave amplitudes ; for the wave progressing to the positive end of the y-axis (Eq. 15), the wave-exciting forces are

$$f_S = \frac{A_-^{(2)}}{\nu B}$$

$$f_H = -\frac{A_-^{(3)}}{\nu B}$$

$$f_R = \frac{A_-^{(4)}}{\nu B \Gamma} \tag{28}$$

It is bo be noted that the wave-exciting forces and moments presented in Eq. (28) are the resultant values. In other words, we see by the Haskind-method that the exciting forces and moments on individual bodies a or b cannot be evaluated.

According to the theories by Haskind [33] and Maruo [34] , the mean wave force K is determined by the diffracted wave

$$\frac{K}{\frac{1}{2}\rho g a^2} = \left| A_- (o+e) \right|^2 \tag{29}$$

NUMERICAL CALCULATIONS

Added Mass and Damping Coefficients for Twin Cylinders

Figures 15, 16 and 17 exhibit the various hydrodynamic forces and moments on one of a pair of half-immersed circular cylindrical bodies as functions of the frequency parameter $\frac{\nu B}{2}$. The definitions of the various forces on this Body a are given in Tables 6, 7 and 8. The hydrodynamic forces on Body b are evaluated by employing the formulas in Table 10 with the aid of the information given in Fig. 15, 16 and 17. The resultant forces and moments on the twin Bodies (a+b) due to the swaying, heaving and rolling motions are evaluated by employing the formulas in Table 11 with the aid of the data in Fig. 15 16 and 17.

The Wave-Exciting Forces and Moments for Twin Cylinders

Figure 18 illustrates the behavior of the sway- and heave-exciting forces on Body a due to odd and even wave potentials as functions of the wave frequency. The vectorial sums of the forces such as $f^{(o+e)} = f^{(o)} + f^{(e)}$ on a, b, and (a+b) are shown in Figures 19 and 20. In this connection, refer to Tables 12 and 13.

The Haskind-method was applied to the evaluations of the resultant wave-exciting forces on the twin bodies and the results confirm exactly the corresponding values obtained by the present method. (See Figures 19, 20 and 21). A relevant discussion of this matter will be given in the following section.

It is interesting to observe the behavior of the sway-exciting forces on a and b (Figure 19). Ohkusu [35] recently reported on the hydrodynamic interaction between three vertical cylinders. His Fig. 13 on page 108 of Reference 35 shows behavior similar to that of the sway-exciting forces on Bodies a and b . A relevant discussion of this matter will be given in the following section.

The Radiated and Diffracted Waves

For the twin bodies, the radiated waves $\underline{A}^{(m)}$ and the diffracted waves $\underline{A}^{(o+e)}$ were evaluated according to the formulas in Eqs. (24 and 26) (see Figure 21). The radiated wave amplitudes $\underline{A}^{(m)}$ are very useful in evaluating the damping force coefficients $N^{(m)}$ or $\delta^{(m)}$ and the wave-exciting forces $f^{(o+e)}$ (see Eqs. 27, 28). By comparing Figures 15, 19, 20 and 21, one can readily confirm the validity of the formulas in Eqs. (27), (28). The diffracted wave amplitude ratio $\underline{A}^{(o+e)}$ is applied to estimating the mean wave force on the fixed twin bodies in the given incident wave, Eq. (15). The sudden drop of the value of $\underline{A}^{(o+e)}$ at frequency around 0.45 may be ascribed to the effect of the hydrodynamic interaction between the bodies in that close proximity.

The Wave-Exciting Forces on Some Semi-Submersible Cross Sections

We chose two simple cross sections : one submerged and the other surface piercing. Figures 22a and 22b represent the sway- and heave-exciting forces on the submerged circular cross section. It is seen from these figures that the interaction effects are negligibly small for the given frequency range. The wave-exciting forces on surface-piercing twin bodies are plotted against the wave frequency in Figures 23a, 23b. It is readily seen that the influence of the interaction effect on the sway-exciting forces is remarkable while the influence on

the heave-exciting forces is relatively small. Similar behavior was pointed out by Ohkusu [35] as described previously.

In connection with the present investigation, force measurements were made at Davidson Laboratory on twin Motora-type floats. These measurements are plotted in Figures 24a, 24b. Since the tests were carried in a relatively high frequency range, even a rough comparison with the present two-dimensional calculations cannot be made. However, the interaction effects appear to be quite small compared to the two-dimensional case, especially considering the very close spacing of the floats.

Interaction effects and the occurence of dramatic variations of force coefficients for particular, characteristic, frequencies should be expected to be weaker for three-dimensional than for two dimensional bodies. We have, however, noted an unusual flow pattern for waves passing a fixed toroidal body ; at a particular wave frequency a pulsating jet erupts in the center of the torus. Of course, the jet also exists for forced heaving oscillations in calm water at the same frequency. The shape of the torus corresponds to that of the profile of the twin cylinders of Figures 15-20 rotated about a vertical central axis, with $2S/B = 2$. The characteristic frequency described for this three-dimensional case corresponds to $\nu B/2 = 0.42$, rather close to the frequency shown in Figure 15 where C_{HH} and δ_{HH} vary dramatically.

Some Hydrodynamic Characteristics of Two Different Cylindrical Bodies Floating in Beam Seas

Some aspects of the hydrodynamic interaction between two arbitrarily shaped cylindrical floats were investigated numerically (see Figures 25a, 25b, 25c). First we evaluated the heaving added mass and damping coefficient C , δ on bodies a and b for heaving motions with unit amplitude and different phases. The results are plotted against the relative phase angle ϵ_b at two different frequencies $\nu(B_a+B_b)/2=0.45$ and 0.26 (Figure 25a). The results show significantly large effects on the hydrodynamic forces due to the hydrodynamic interactions between the two different cylinders floating freely with different phases.

As a special case of the above, we calculated the hydrodynamic forces on the swaying and heaving Body a in the presence of the fixed Body b (Figure 25b). Two draft ratios $T_b/T_a = 2$ and 15 were taken in order to observe the false wall effect on the hydrodynamic forces. The figure also shows the hydrodynamic inertial forces C_{HH} , C_{SS} on an isolated swaying and heaving Body a . It is seen that the increment of

the swaying added mass C_{SS} due to the increase of the depth of the false wall is nearly independent of the frequency.

The heaving added masses C_{HH} are remarkably dependent on the depth of the Body b , T_b/T_a , and the frequency.

The resultant heave-exciting forces $F_H^{(o+e)}$ on bodies a and b were calculated and plotted in Figure 25c. For comparison, the heave-exciting forces on isolated a and b are also plotted in the same figure.

SLENDER VERTICAL FLOATS : ISOLATED PERFORMANCE AND INTERACTION EFFECTS FOR LARGE ARRAYS

BACKGROUND

Column-stabilized floating ocean platforms used for oil exploration, research, or other applications, achieve low motions response to wave action by proper shape and spacing of rigidly-connected flotation elements. Another type of platform, which can also afford a useful working surface, might consist of an assemblage of resiliently-connected flotation elements, each of which individually has suitable motions response characteristics. Conceptual design studies for such a platform have been undertaken by engineers of Goodyear Aerospace Corporation (GAC). Davidson Laboratory of Stevens Institute of Technology has conducted a variety of hydrodynamic studies in connection with the design developments, some of which will be described in the present part of this paper.

An illustration of a concept for the array of floats and deck structure to be considered is depicted in Figure 26. The details of the deck panels and truss system are not important for the present hydrodynamic study : the structural restraint on body motions is assumed to be negligible (or, in a particular case, to be approximated by simple mechanisms). The effect of hydrodynamic interactions on the relatively closely spaced floats may, however, be important. Much of the presently described work, and work currently in progress, deals with these interactions.

An interesting feature of these multi-float platforms is that they are expandable. Modular construction is intended to permit convenient deployment of arrays with any number of floats from about 50

up (a minimum number are required to afford stability against capsizing). The resiliency of the structural components, including the floats themselves, which may be inflatable reinforced fabrics, pose certain interesting hydroelastic questions. Several hydroelastic aspects have been and are being studied but these will not be treated in this paper.

ANALYSIS OF VERTICAL FLOAT HEAVE MOTION

Elementary Equation of Motion

In the configuration depicted in Figure 26, the net buoyancy comes from the portion of the float above the hinge, which is located some distance below the stillwater level. The float shape, which is enlarged below the waterline, is intended to minimize the wave-induced vertical forces transmitted to the deck and structure, and thus minimize deck motions over a "sufficient" range of wave frequencies. The hinge is introduced to alleviate lateral loads in the float and in the structure : the wave-induced forces produce pendular motions of the lower part of the float (which is called an "attenuator") which relieve the elastic stresses and transmitted loads which would develop without the hinge.

Since the deck structure is assumed to be quite flexible, the (linearized) equation for the heave (z) motion, neglecting elastic restoring forces, can be expressed simply as

$$\rho\nabla\ddot{z} = - m'' \ddot{z} - Z_{\dot{z}}\dot{z} - Z_z z + Z_\zeta \zeta \qquad (30)$$

where

∇ = total displaced volume of float and attenuator

m'' = added mass

$Z_{\dot{z}}$ = damping force rate

Z_z = buoyant restoring-force rate = $\rho g A_w$

A_w = waterplane area

Z_ζ = wave-induced vertical force per unit wave elevation

ζ = wave elevation

If the deck's elastic restoring-force is to be taken into account, a term such as $EI\frac{\partial^4 z}{\partial x^4}$ must be incorporated to describe motion in

regular long-crested waves, such that the deck structure behaves like a beam (the more general case would have to represent the deck's elasticity as plate-like, or describe the details of the deck-truss structural behavior). These partial differential equations are considerably more complicated than the simpler equation (30). The deformation of the deck of a rectangular array of floats in regular "head" seas, assuming that no hydrodynamic interaction effects occur on the vertical forces on float elements, will be (at least in the case of linear response) a traveling wave with the same frequency and celerity as the incident water wave :

$$z_b = z_o \sin\left(\frac{2\pi x}{\lambda} - \omega t\right) \tag{31}$$

then

$$\frac{\partial^4 z_b}{\partial x^4} = \left(\frac{2\pi}{\lambda}\right)^4 z_b \tag{32}$$

or, since for water waves $2\pi/\lambda = \omega^2/g$,

$$\frac{\partial^4 z_b}{\partial x^4} = \frac{\omega^8}{g^4} z_b \tag{33}$$

The importance of a restoring force term like $EI\frac{\partial^4 z}{\partial x^4}$, compared to $\rho g A_w z$, increases as the frequency increases, or the wave length decreases. The design of the float-attenuator geometry is intended to produce vanishingly small wave-induced vertical force as frequency is increased. GAC structural analysts decided that the simple Eq.(30) is appropriate for analyses of the motions of the deck supported by a resiliently-connnected array of floats, such as is shown in Figure 26.

Coefficients of the Equation and Forces for Regular Waves

Elementary hydrodynamic theory can be applied to the estimation of the hydrodynamic coefficients and the wave-exciting forces for the equations of motion of slender vertical floats without external appendages. In the present instance, it is anticipated that external appendages will be required to assure sufficient heave damping and analyses of the hydrodynamic effects of the appendages must be approximate and quasi-empirical.

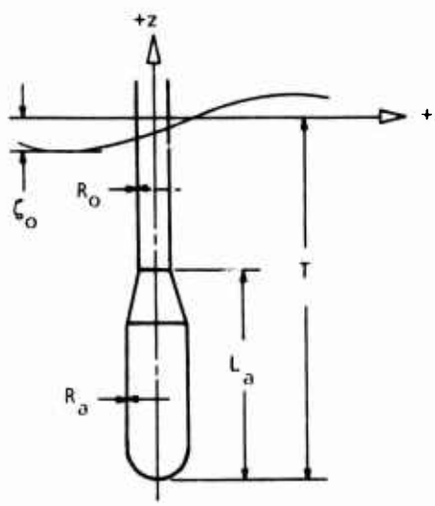
The buoyant force rate has already been expressed as $Z_z = \rho g A_w$.

The vertical wave-exciting force can be expressed as

$$Z_\zeta \zeta = \underbrace{\rho g \zeta S(0)}_{\text{Hydrostatic}} - \underbrace{\rho g \zeta \int_{-T}^{o} (1-e^{kz}) \frac{dS}{dz} dz}_{\text{"Smith" Correction}} - \underbrace{Z_{\dot\zeta} \frac{\partial \zeta_e}{\partial t}}_{\text{Damping}} - \underbrace{\sum m' \omega^2 \zeta e^{kz_e}}_{\text{Added mass}}$$

$$\underbrace{\qquad\qquad}_{\text{Froude-Krylov}} \qquad (34)$$

where



- S = sectional area of body
- k = wave number = $\omega^2/g = 2\pi/\lambda$
- λ = wave length
- $Z_{\dot\zeta}$ = damping coefficient
- ζ = wave elevation
- ζ_o = wave amplitude
- ζ_e = wave motion evaluated at depth corresponding to assumed damping source
- m' = element of effective added mass in vertical direction
- z_e = effective depth for evaluating wave acceleration for element of added mass

The Froude-Krylov force corresponds to that predicted by slender body theory and is the same as predicted by assuming that the presence of the body does not influence the wave's pressure field. For finite draft, T , the Froude-Krylov force decreases with increasing wave frequency (because of more rapid attenuation of wave pressure with depth) and, if the attenuator is shaped as in the sketch, may become opposed in sense to the wave elevation for sufficiently high frequencies.

The response of slender spar buoys to waves has been studied by Newman [36] , who performed a detailed slender-body analysis and by Rudnick [37] , who derived equations similar to Newman's [36] on the basis of a more elementary analysis, and who compared results of calculations with field measurements of the motions of the Flip platform. Newman notes that the slender-body theory applied to floats in waves loase its applicability at higher values of slenderness ratio than is the experience for aerodynamic analyses. Adee and Bai [38] have conducted experiments with cylindrical models having either flat or conical bottom ends and various draft-to-diameter ratios. They find that it is important to account for added mass effects even for quite slender floats. However, while they include added mass effects

on the inertial force (proportional to $\ddot{z}$), they appear to have neglected its effect on the vertical wave-induced force. For non-cylindrical floats, such as shown in the sketch, the inclusion of added mass effects is still more significant.

The added mass wave force results because the flow is unsteady and the presence of the body does modify the fluid acceleration patterns (contrary to the Froude-Krylov assumption) resulting in a pressure force in phase with the vertical wave acceleration. The added mass may be associated with two principal sources, the primary one being the enlarged attenuator at the lower end of the float. Externally-attached damping devices will also have associated added masses. The effective added mass from the primary source, the enlarge attenuator, may be estimated by assuming that the attenuator is similar to a prolate spheroid with a ratio of semi-major to semi-minor diameter, a/b equal to $L_a/2R_a$. Lamb [39] gives theoretical added mass coefficients for translation "end-on" that can be expressed as

$$m'_a = \frac{4}{3}\rho\pi R_a^3 k'_1 \tag{35}$$

where k'_1 can be taken from Table 14.

It has been found, of course, that the ideal fluid theory added mass is insufficient for slender craft such as airships and surface ships in monotonic rectilinear motion, presumably because of boundary layer influences (cf. Thompson and Kirschbaum [40] and Smith [41]). The reasons for the differences between theory and experience for these craft may not be relevant to the float-attenuator in the wave flow field so the tabulated theoretical values are recommended for use pending more complete experimental results. The wave acceleration can be evaluated at an effective depth, $z_e = T - L_a/2$.

The added mass associated with the damping devices, which probably would be attached to the float at the upper end of the conical transition above the attenuator (see sketch), is not derivable from familiar simplified cases. The interaction of the flow about the damping "collar" with the flow about the cylinder may be important and ought to be studied experimentally. For the purposes of the present analysis, the added mass of damping devices will be assumed to be a fraction of the added mass of the attenuator

$$m'_d = c'm'_a \tag{36}$$

where approrpiate values of c' should be obtained experimentally or simply assumed. The value of z_e to be used for evaluating the wave

acceleration for this component of force should be the depth corresponding to the damping source.

The total added mass, m'', is the sum of that associated with the attenuator shape plus that due to damping devices.

The heave damping force rate, $Z_{\dot{z}}$, is partly due to generation of radiated surface waves and partly to viscous influence associated with turbulent eddies around the float and damping plates and skin friction drag. It will be shown in the following section that the damping due to wave generation, which is strongly dependent on frequency, is quite small for slender vertical floats and, therefore, it is advantageous to provide additional viscous damping, which is likely to be independent of frequency. The damping coefficient will be expressed in terms of the ratio of the damping to the critical damping coefficient, (c/c_c), in the form

$$Z_{\dot{z}} = \left(\frac{c}{c_c}\right) \times (2\rho \nabla + m'')\omega_n \qquad (37a)$$

$$= \left(\frac{c}{c_c}\right) \times 2\rho A_w \sqrt{gTC_{vp}(1+C_{HH})} \qquad (37b)$$

where

C_{vp} = vertical prismatic coefficient, $\dfrac{\nabla}{A_w T}$

C_{HH} = added mass coefficient, $\dfrac{m''}{\rho \nabla}$

The viscous drag due to external damping devices will not, in general, be simply linearly proportional to velocity (although for small waves and motions it will be approximately so). The use of a linear coefficient may be justified on the bases that calculations based on such a simplification are instructive and that "equivalent" linearized coefficients may be derived for drag which is proportional to some other power of velocity in the way that Blagoveshchensky [42] and others have dealt with square-law damping.

Particular values of drag coefficients may be estimated for plates oscillating in a direction normal to their surfaces from results of significant investigations by Keulegan and Carpenter [43], McNown [44], McNown and Keulegan [45], Paape and Breusers [46], Martin [47], Ridjanovic [48], Brown [49], Henry [50], Woolam [51] and Tseng and Altman [52]. Additional investigations of the oscillating drag of ring-type damping collars around bodies of revolution will be

needed to provide information on the type of configuration being considered for these floats, as shown in Figure 26, where damping plate-body interaction effects may be significant.

The wave-exciting force associated with the damping devices, $Z_{\dot{\zeta}} \frac{\partial \zeta_e}{\partial t}$, may be estimated by taking $Z_{\dot{\zeta}} = Z_{\dot{z}}$, and $\frac{\partial \zeta_e}{\partial t}$ is the wave motion evaluated at the depth corresponding to the damping plate. Of course, since the oscillatory drag force on the damping devices is, in general, nonlinearly related to the relative velocity between the fluid and the plate, the detailed analysis of the motions would be rather more complicated than the simplified treatment given here. The effects of the nonlinearity of the drag may be expected to be important only for frequencies near the resonant frequency.

Responses

Although analyses have been presented by Newman [36] and others for wave-induced forces and motions of isolated spar-type floats, no results of systematic evaluations of the dependence of the forces and motions on geometric characteristics of floats are known to be available in published literature. Some results for the special case of floats like that shown in the sketch accompanying Eq.(34) will be presented here.

The influence of the ratio fo the diameters of the lower and upper cylindrical parts R_a/R_o, the ratio of the length of the lower cylinder to the overall draft, L_a/T, and the ratio of the draft to waterplane radius (slenderness ratio), T/R_o, will be shown. Wave forces and motions due to regular waves will be presented as a function of frequency, and spectral response information will be given as a function of significant wave height. The influence of the degree of damping on the responses will be described in a subsequent section.

Wave-Induced Force

The wave-induced vertical force, $Z_\zeta \zeta$, expressed as a function of the buoyant force, $\rho g S(o) \zeta$, is exhibited in Fig. 27 as a function of the dimensionless frequency parameter $\omega^2 T/g$, showing the influence of R_a/R_o. Other geometric parameters were held fixed for these results, viz., $L_a/T = 0.5$, $T/R_o = 30$; the assumed damping coefficient corresponds to a value of $c/c_c = 0.07$. Figure 28 shows the influence of L_a/T for $R_a/R_o = 1.8$, $T/R_o = 30$; again, $c/c_c = 0.07$. The influence of T/R_o is presented in Figure 29 for $R_a/R_o = 1.8$, $L_a/T = 0.5$ and $c/c_c = 0.07$. For all cases presented the damping

plate added mass, m'_d , is assumed to be $0.3\ m'_a$ and its effective depth $z_e = T - L_a$.

The results presented are typical : as frequency increases, the vertical forces decreases at first until it reaches a minimum value (which corresponds very closely to the "damping" component of the wave-induced force, Eq.(34), and then increases again when the components of force which are out-of-phase with wave elevation (due to pressure gradient and added mass) become important, followed by asymptotic attenuation to zero force for very short waves. Both R_a/R_o and L_a/T are seen to have important effects on the wave-induced force, T/R_o ; T/R_o is less important, in fact, the simplified theory (Newman [36]) neglecting added mass and damping indicates no dependence on T/R_o .

Transfer Functions

The ratio of heave motion to wave elevation can be derived from the solution of Eq.(30). This may be re-written in a form similar to that for the familiar simple harmonic oscillator.

$$\frac{z}{\zeta} = \frac{Z_\zeta \zeta / \rho g S(o) \zeta}{\sqrt{\left(1 - \frac{\omega^2}{\omega_n^2}\right)^2 + \left(2\left(\frac{c}{c_c}\right)\frac{\omega}{\omega^2}\right)^2}} \qquad (38)$$

where

$$\frac{\omega_n^2 T}{g} = \left[C_{vp}(1 + C_{HH})\right]^{-1} \qquad (39)$$

Only one set of transfer functions, exhibiting the dependence on R_a/R_o for $L_a/T = 0.5$, $T/R_o = 30$, $c/c_c = 0.07$, $m'_d = 0.3 m'_a$ and $z_e = 0.5$ (for damping plates), will be given in Figure 30. These results are, again, typical : the trends of the variation of motions with frequency follow the wave forces modified by the dynamic amplification factor. Note that the damping coefficient assumed, $c/c_c = 0.07$, results in values of the transfer function around 2.0 at resonance, and that the maximum value depends on the float shape as well as the relative damping.

Spectral Response

The statistics of the heave motion response may be derived for slender vertical floats using the transfer functions and the (dimensionless form of the) Pierson-Moskowitz wave spectrum, as was done in the first part of the paper for three- and four-float platforms. The significant dimension for use in non-dimensionalizing will be the draft for this case, instead of $\nabla^{1/3}$.

Some results showing the effect on "significant heave motion", $z_{1/3}/T$, of R_a/R_o, are given in Figure 31, with other particulars, the same as for Figure 27. The influence of L_a/T on the significant heave is shown in Figure 32 for the same cases as are considered in Figure 28. The effect of T/R_o on the statistical responses is small, as might be expected from the results for forces shown in Figure 29 - at least for floats which are sufficiently slender.

According to Figures 31 and 32, the "best" float shape is evidently a function of the design sea state or significant height : slender floats with displacement relatively uniformly distributed being better for mild sea conditions while higher values of R_a/R_o with the displacement concentrated near the bottom are better for more severe seas. An irregularity, or "bump", is discernible in some of the curves for values of $H_{1/3}/T$ at which an increase of sea state introduces a large increment of wave energy at the resonant frequency of the float.

It is interesting to note that the dependence on significant wave height of other heave-related spectral response characteristics may differ from that of heave. Figure 33 shows significant values of heave motion, vertical acceleration, and deck curvature $\frac{\partial^2 z}{\partial x^2}$, for a particular float having $R_a/R_o = 1.8$, $L_a/T = 0.5$, and $T/R_o = 30$. Since the transfer functions for acceleration and deck curvature depend on frequency in a different way than does heave, weighing high frequency more heavily, while attenuating low-frequency input, higher sea states do not produce as much increase of response as for heave. This is because an increase of sea state (according to the Pierson-Moskowitz spectra) adds significant energy in the low frequency range but not much at higher frequencies. For the case presented, the deck curvatures (and therefore the deck stresses) are very nearly proportional to the significant wave height, since

$$T\frac{\partial^2 z}{\partial x^2} \Big/ (H_{1/3}/T) \approx 0.3 \text{ over the range of } H_{1/3}/T \text{ values}$$

presented.

The Importance of Damping

The primary effect of an increase in the damping coefficient on the heave transfer functions is to reduce the maximum heave response, which occurs at a frequency slightly lesser than the resonant frequency, and to increase the minimum value which occurs for the frequency when the wave-induced force is due to the damping devices alone.

For design-analyses, the spectral response is most useful.

Figure 34 shows effect on significant heave motion of damping coefficient, c/c_c, for a particular float geometry. It is evident that damping is very useful to control motions in high sea states where some wave energy exists at frequencies corresponding to heave natural frequencies.

The damping which is available due to wave radiation can be obtained from the Kaskind-Newman relations [32], which gives the same result as Newman's slender-body analysis for the forces at resonance [36]. These give

$$Z_{\dot{z}_w} = \frac{k^2}{2\rho g\omega} \left|Z_\zeta\right|^2 \tag{40}$$

thus, at resonance $\omega = \omega_n$, the ratio of wave-damping to critical damping can be obtained as

$$\left(\frac{c}{c_c}\right) = \frac{Z_{\dot{z}_w}}{2\rho\nabla(1+C_{HH})\omega_n}$$

$$= \left|\frac{Z_{\zeta w}}{\rho g A_w}\right|^2 \frac{1}{4}\left(\frac{\omega_n^2 T}{g}\right)^2 \frac{A_w}{T^2} \tag{41}$$

and the corresponding transfer function

$$\frac{z}{\zeta} = \frac{\left|Z_{\zeta w}/\rho g A_w\right|}{2(c/c_c)_w} \tag{42}$$

contd.

$$= \frac{2T^2/A_w}{|Z_{\zeta w}/\rho g A_w| \left(\frac{\omega_n^2 T}{g}\right)^2} \qquad (42)$$

where $Z_{\zeta w}$ is the wave-induced vertical force evaluated without taking into account the damping term.

Since, at resonance, $|Z_{\zeta w}/\rho g A_w| < 1$, and for slender vertical floats $T^2/A_w \gg 1$ and $\frac{\omega_n^2 T}{g} < 1$, then $c/c_c \ll 1$ and $z/\zeta \gg 1$. For example, for $T/R_o = 30$, $R_a/R_o = 1.8$ and $L_a/T = 0.5$, the calculated "wave-damped" resonant heave motion z/ζ would be almost 8000 ! Wave-associated damping is inadequate for slender floats and viscous damping controls the resonant motion.

Results of tests on a 1/13th-scale model of a Manned Open Sea Experimentation Station (MOSES) reported by the Oceanic Institute, Waimanalo, Hawaii [53], showed that a ratio of damping to critical damping of 0.075 could be achieved. This was discovered in tests of the model with about 18 external rings attached to a slender shaft. The rings, which are intended to provide structural stiffening, have outside diameter about 15% larger than the shaft. Complementary tests were carried out with acetate sheet wrapped tightly around the rings to present a smooth, unbroken surface. With this shroud the damping was about 1% of critical.

Damping coefficients will, in general, be obtained most effectively by experiments, or will be estimated on the basis of empirical results. It has been known since Froude's investigations in 1874 [54] that the drag coefficient for an oscillating bluff body can be very different from that for the same body in steady flow. As in all model experimental work, it is important to be sure that the model conditions correspond to the full scale : thus, for dynamic similarity to exist, the model should be geometrically similar and the flow kinematically similar to the full size.

Certain experience from investigations of roll damping of ships with appendages can give insight into questions relevant to damping of platforms oscillating in waves. It is important to recognize that a small ambient current, due to oceanic circulation or induced by wind, can have an appreciable effect on energy dissipation, as has been found by many investigators into the rolling of ships [54-58]. This is because the model, in the course of its cyclical motion, must impart motion to fresh, previously unentrained water. Consider that for a current speed

of only one knot past a moored platform, the fluid which is 'entrained" by the motion of a platform may convect about 17 feet during a 10-sec period ; such a period is common for ocean waves, and the distance is about half of a typical column diameter for a large semi-submersible drill rig. Entrained fluid energy can be convected away at an appreciable rate by modest currents producing important effects on damping and, hence, resonant response.

Indeed, when the damping force is non-linear and, hence, superposition cannot be applied, it may be inappropriate to apply an oscillatory drag coefficient obtained for a particular structural element from tests with rectilinear oscillatory motion [43-45,47-51] to the somewhat different kinematic conditions of the orbital velocity pattern of waves. The differences may be modest but the question should be posed and, hopefully, investigated.

The question of scale effects is persistently present and model experimenters must be alert (and somewhat intuitive) to recognize when it may be appreciable. When phenomena are recognized to be predominantly viscous in origin, we are likely to suspect the possibility of scale effect. This is, of course, due in large part to the history and experience of testing ship models for resistance. Very little is known about scale effects on oscillatory hydrodynamic forces which may be relevant to platform motions testing and analysis. Some years ago, however, a program of experiments to study scale effects on roll damping of circular cylinders with and without appendages was undertaken by the Naval Ship Research and Development Center and Davidson Laboratory. While these studies were not directed to platform motions, the results are relevant to the phenomena of oscillatory damping in general and since they are the only results with which we are familiar which show the effect of model size, it may be useful to discuss them. Three cylinders with diameters of 6-in, 12-in and 24-in were suspended vertically in water by torsion springs. Three kinds of appendages were symmetrically attached to the models, as shown in Figure 35 for the smallest (6-in-diam) cylinder. Curves of decaying oscillation from various initial angular displacements were recorded and analyzed to obtain "square-law" damping moment coefficients of the form

$$C_m = \frac{\text{damping moment}}{(\rho/2)A\, R_{c.a.}^{\,3}\, \dot{\theta}I\dot{\theta}I} \qquad (43)$$

where A is the frontal area of both appendages and $R_{c.a.}$ is the radius from the axis of rotation to the center of area of the appendage. The results are tabulated in Table 15.

The 6-in and 12-in diameter models were tested at Davidson Laboratory by Mercier [59] , while the largest model was tested at the Naval Ship Research and Development Center by Gersten [60] .

The lessons of these test results are not entirely unexpected : sharp-edged geometric details produce high drag and little scale effect while well-rounded geometries produce lesser drag and are susceptible to perceptible scale effect. These results may provide qualitative guidance for other applications and configurations, such as for choosing a suitable scale ratio for a wave test of a floating platform with buoyant caisson-and-footing floatation elements.

Damping effects, while of principal importance for a fairly narrow band of frequencies near resonance, can have an appreciable effect on spectral response when there is appreciable wave energy at the resonant frequency. The nature of the damping and its dependence on geometric and flow features is as yet only imperfectly understood adn needs to be studied more vigorously.

ISOLATED FLOAT EXPERIMENTS

An experimental program was undertaken to determine hydrodynamic forces and moments and certain other features of performance for several floats. The results of these experiments may be used in conjunction with analytical work, such as described in the last section, to obtain empirically adjusted analytical procedures for performance evaluation. Certain results may also be compared with results of interaction tests, where several floats were placed in close proximity, to determine hydrodynamic interaction.

Models

Several types of models were built to evaluate the influence of various features on performance. Some of these models were selected on the basis of the analyses described in the previous section of this report. Some were also tested as part of an array of floats to evaluate nteraction effects. The scope of isolated float testing was curtailed when the extent and significance of interaction effects on wave-induced vertical floats was discovered. All models investigated in this test program were built to a scale ratio of 1:57.6.

Figure 36 illustrates the models which were tested. The deep cylinders (Figures 36-36) were planned to investigate the effect of

bending rigidity of the fabric attenuator on float forces and other performance features. Using classical vibration theory [61] , with an assumed bending rigidity $E = 15.268 \times 10^6$ lb-ft^2 for a six-foot diameter pressurized inflated float tube constructed of 3000 lb/in fabric, the computed lowest lateral bending frequency of the attenuator is 0.11 Hz, assuming hinged-free boundary conditions (corresponding to tests with the hinge, if the hinge is omitted, the lowest two cantilever natural frequencies are 0.025 Hz and 0.16 Hz). Since these frequencies are within the range of significant wave energy, it appeared to be important to study flexible model performance. The scale-equivalent flexural rigidity of the 1/57.6-scale model was provided by a central 0.45" x 0.06" plexiglas flat strip. The external shape of the float was simulated by cylindrical segments secured to the flexure strip by plexiglas bulkheads. A system of baffles and flow passages were used to inhibit flow passing from outside the model to inside it but which permits flow communication within the float. For shorter floats, the elastic laterla natural frequencies are higher and consequently, the influence of rigidity is lessened.

The slender float of Figure 36c was used in one set of interaction tests, while the full float of Figure 36d was used in the other set of float interaction tests and for the dynamic island tests. The float of Figure 36e is the same as that of Figure 36d except for the rounded bottom.

Apparatus

The apparatus used for these tests was an improved version of the equipment described by Mercier in published references [62,63] . Existing force balances and motion transducers were adapted for these tests.

A new data reduction procedure was applied for these tests. Electronic signals for forces, moments, waves and/or forced motion (heave, surge, pitch, sway, roll ; but not yaw) were recorded on analog magnetic tape as well as on oscillograms. For some of the tests, the signals were immediately processed by an on-line computer-controlled analog-to-digital converter and further evaluated by the computer (PDP-8E) to determine the Fourier coefficients of the signals. Other tests were "played-back" later during off-line processing. Sampling was carried out at the rate of eigher 20 or 50 samples per second, permitting accurate (and easy) interpretation of electronic-wave-forms which were sometimes relatively "noisy". Usually only the first harmonics of the wave forms were determined, but for several tests the second and third harmonics were also computer. Higher harmonics are of interest primarily for large amplitude waves or

motions where linearity of forces and moments is in question. Five to ten complete cycles of the wave forms were "averaged" in determining the Fourier coefficients except when the test period was very long, when no less than three cycles were used.

Forces oscillation tests were carried out by adjusting the crank offsets of the several motion-producing linkages so that either pure heave, surge, or pitch were produced. Yaw motion was not tested. A cosine potentiometer was coupled to the drive shaft of the mechanism. A constant (battery) voltage was applied to this potentiometer whose output was consequently proportional to the cosine of the shaft rotation angle and thus was suitable for use as a phase reference for the motion.

For some tests, both in waves and with forced oscillations, a hinge was used to permit the lower end of the attenuator to oscillate like a pendulum under the action of waves. In this way, the periodic side loads due to the waves are not completely transmitted to the floating base connecting structure by way of bending moments in the float but are rather absorbed by the pendulum-like motion of the attenuator. This reduces the strength requirements of the inflated float and, consequently, weight and cost.

A rotary variable differential transducer was connected to the attenuator by a system of strings to permit the measurement of angular motion.

Scaling

The periodic hydrodynamic forces and moments are assumed to follow Froude's scaling law. Thus the full-size force and moment are related to model quantities by

$$F_{\text{full size}} = F_{\text{model}} \times \frac{\rho_{\text{full size}}}{\rho_{\text{model}}} \times \lambda'^{3} \tag{44}$$

$$M_{\text{full size}} = M_{\text{model}} \times \frac{\rho_{\text{full size}}}{\rho_{\text{model}}} \times \lambda'^{4} \tag{45}$$

where

F = Force

M = Moment

ρ = Fluid density

λ' = Scale ratio

The corresponding frequ[illegible] f (cycles per second), for full scale and model, are also rela[illegible] roude's law

$$f_{f.s.} = \frac{1}{\sqrt{\lambda'}} \times f_m \tag{46}$$

Results

Vertical wave forces for the floats of Figures 36d and 36e are shown in Figure 37 along with a comparison with theoretical results according to Eq. (34) (except z_f was assumed negligible) and with the simplified Newman (or Froude-Krylov) theory which neglects that added mass type force. Model results are corrected to the full-size float in this and all subsequent figures. The effect of rounding of the bottom end of the float is insignificant and cannot be detected within the accuracy of the experiments. The phases between the wave and the heave force are not shown in the figures but, in general, for low frequencies the heave force is almost in-phase with the wave (maximum upward in way of a wave crest) while at high frequencies the force is nearly 180° out-of-phase with the wave. It may be noted that the agreement of test results with the complete predictive theory is quite good for this case. A comparison for a fuller float, which had been tested by Mercier [64] on a previous project, is shown in Figure 38. A computation procedure applied by Ochi, [65] based on two-dimensional strip theory is also shown. It is seen that the calculations are not as satisfactory for this rather fat float.

Tests with the attenuators attached to the upper part of the float through the hinge indicate that the vertical forces due to waves are not affected by the hinge, within the limits of experimental accuracy.

The side forces measured in waves are exhibited in Figure 39 for the full float of Figures 36d and 36e. Again, no influence of the rounded bottom is discernible. The phase of the force is approximately 90° with respect to the wave, indicating that the force is predominantly due to pressure gradient and inertia forces. The influence of wave amplitude on the forces and on the phase of the forces relative to the wave has been found to be small for the range of wave amplitudes used in the tests (corresponding to 1.1-ft to 10.0-ft, full size).

Side force due to waves for the slender float of Figure 36c is presented as a function of wave frequency in Figure 40. This information is presented in Figure 41 for the rigid and flexible cylindrical models of Figures 36a,b. Results for all models with the hinge in place are given in Figure 42 and the corresponding angular pitching

motions are given in Figure 43. The side forces are seen to be remarkably lower than the results without the hinge. The amount of angular motion, which is greatest for low frequencies of course, is about 3° per foot of wave elevation for a frequency of 0.07 Hertz. The resilient model exhibits a resonance-like behavior at a frequency of about 0.12 Hertz, somewhat higher than the calculated value of 0.11 hertz, as evidenced in both side force and pitch motions. This relatively modest amplification of response occurs at a frequency at which significant wave energy exists and is consequently considered disadvantageous.

A variety of other tests also were carried out, using several of these floats models and with various damping plates fitted. Besides wave tests, forced heave and surge oscillation tests were carried out. Results of these tests have not yet been analyzed in detail but are stored on magnetic tape for future processing.

INTERACTION EFFECT TESTS

Preliminary Wave Tests

Although in previous experience with floating platforms such as for drill rigs, hydrodynamic interaction between adjacent floats was found to be negligible, the large numbers of floats planned for the Floating Expandable Base are so closely packed in relation to their size that it was considered vital to investigate the interaction between floats at an early stage of this program.

Wave-induced forces were measured on individual floats in an array consisting of five rows of five floats each. The force-measuring balance could be moved so that forces on any one of the floats could be measured, as desired. The spacing of the floats was either three times the water-plane diameter or five times. Two sets of floats, shown in Figures 36c and 36d, having different proportions and drafts, were tested with and without damping plates.

Certain general findings of the tests can be given : the side forces and pitching moments acting on the floats due to waves are practically un-influenced by proximity ; the vertical wave-induced force is modified by an apparent increase in an added-mass type force component which is significant for higher frequencies and accounts for about a 30% increase above the isolated float results for the fatter of the two floats studied. Further, damping plates attached in way of the

fat lower parts of the floats may result in severe interaction influence on the drag-type force component but plates may be attached to the slender upper part of the float without important interaction. When the spacing of floats was five times the water-plane diameter, no measurable interaction influence was observed.

Some results for vertical (heave) force on the full float of figure 36d, both in the middle of the 25 float array and isolated, are exhibited in Figure 37, which shows the increase in force at high frequency. The introduction of a ten-foot diameter damping plate at the junction of the conical transition piece and the upper float produced only a minor increase in lift force at high frequency. Rather similar results were obtained with the deeper, more slender float of Fig. 36c; but when damping plates having 13.5-ft diameter were fitted to the lower end of the floats, the wave forces were dramatically increased, evidently because of a drag-type component in phase with the vertical wave velocity. The forces on the interior float elements of the array were found to be virtually the same as one another while the floats in the forward row (near the wave generator) and in the aft row were close to the results for isolated floats.

Horizontal forces measured on the full float of Figure 36d, isolated and in array, are shown in Figure 39. It is found (somewhat surprisingly) that little or no interaction occurs for this component of force and the floats in array experience essentially the same side force as the isolated floats.

Large-Array Investigations

A freely-floating model of a substantial segment of a Floating Expandable Base, having 35 rows of 6 floats each like those of Fig. 36d, with rows connected to each other by parallel motion linkages which are intended to permit freedom to heave while restraining against pitch motions, was tested in regular waves in Davidson Laboratory Tank No. 3, which is 300-ft long x 12-ft wide x 6-ft deep.

A particular, unexpected result of this model test program with the 35 by 6 array of floats (which have a nominal scale ratio of 1/57.6) was a "tail-wagging" phenomena where the heave motions increased from front to rear of model. This is an especially significant feature of the performance of arrays of large numbers of such floats. A variety of experiments have been carried out in order to study certain aspects of the hydrodynamic interaction observed in the motions response tests of the 35 by 6 array of floats. These include wave force

measurements on individual element rows of this large array to determine if the variation of wave force, with the model held fixed, is sufficient to produce the motions obtained in the previous test.

Possible scale effects were investigated briefly because of the possibility of viscous wake interaction due to vortex shedding, separated flow, etc., being dependent on Reynolds number. Since large scale model investigations are liable to be quite expensive, smaller scale tests were undertaken. Although it is not at all clear in what way the interaction effect in this unsteady flow situation depends on Reynolds number (this dependence can only be established by extensive experimentation), it has been found that for many flow situations a modest reduction in size, or Reynolds number, can have as much effect as a substantial increase in size. A model approximately one-third of the size of the 1/57.6-scale model, resulting in about one-fith of the Reynolds number, was employed.

Review of the wave-induced force measurements with the 1/57.6-scale model indicated that the variations in forces correspond reasonably with the variations in motions over the forward and middle part of the island but do not exhibit a continuous increase toward the trailing edge, which was felt to be called for to explain the tail-wagging. Since a suitable explanation in terms of elastic interaction is not presently available, it was decided to re-test the articulated 6x35 array in the 75'x75'x4.5' deep wave test tank (No.2) in order to assure freedom from tank sidewall influences.

An approach to an analytical description of the deck motion, taking deck elasticity into account, is discussed but an explanation of the tail-wagging does not appear to follow from this analysis.

Plans for a comprehensive test program to determine the effects of variations in parameters such as float spacing and shape, wave frequency and height, deck rigidity and number of floats on the motions of the platform are described.

Mode

Articulated Model

A preliminary design for float-attenuator shape was developed on the basis of a simplified hydrodynamic analysis and a particular limiting vertical motion criterion. The selected float had a relatively shallow draft and large diameter near the lower end. No interaction effect was anticipated in selecting the float shape. A scale ratio of 1/57.6 was selected ; the full-size float has 6-ft diameter at the waterline while the model was fabricated with 1 1/4-in O.D. plastic tubing.

The 210 float elements were made of plexiglas tube and sheet according to the sketch shown in Figure 44. Solvent-bonding was used to assemble the parts in a watertight fashion.

The float elements were connected in sets of 6 to an aluminum channel. The channel was lightened considerably by drilling holes and the tubes were ballasted with brass weights and lead shot so that a row floated at the correct draft and roll angle, with a small positive roll stability. This was checked by floating the sets in a fish tank while lightly restraining them against pitching (the rows are very unstable in pitch).

The rows are connected to each other by linkages consisting of 3-3/4" x 1/2" x 0.050" aluminum strips with 1/8" diameter reamed holes spaced 3-1/4" center-to-center. The linages roll on 0.1245 diameter x 1/8" long shoulder screws which are secured to light posts at the ends of the rows of floats. The vertical spacing of the linkages is 4 inches. The float are arranged in an equilateral triangular fashion, as indicated in the sketch of Figure 45.

Although roll stability of the articulated model is present because each row is suitably ballasted, the pitch behavior is unstable because each row is unstable and the 4-bar-linkage connections provide no restraint unless one row is held so that it can move only vertically. The center row (number 18) was restrained by a vertical tube which slides in a pair of linear-motion ball bearings, as indicated in the sketch of Figure 46.

The linear motion bearing is secured to a light weight (approximately 3 lbs) carriage which rides on low-friction wheels on a monorail about 12 inches avove the water, permitting effective freedom of surge.

The vertical motions of five locations along the lenght of the model, at rows 1, 9, 18, 27 and 35, were measured by systems consisting of a long (approximately 8 ft) vertical string between the measurement point on the model and quadrant connected to the shaft of a rotary variable differential transformer (RVDT). These RVDT's have very low friction ball bearings and the quadrants are very slightly counterbalanced to assure that the string remains in tension.

Motions tests were carried out in November 1971 in Davidson Laboratory Tank No. 3, which is 300-ft long, 12-ft wide and 6-ft deep.

Additional tests were carried out in June 1972 in DL Tank No. 2, which is 75-ft long, 75-ft wide and 4.5-ft deep, to check whether tank

sidewall influences were appreciable. These tests were undertaken after measurements of wave-induced forces were carried out with the same floats, secured to a different mechanism, so the floats and articulating linkages were completely disconnected and reassembled between the two sets of tests in the two tanks.

Wave elevation measurements were made at three locations during these tests : a) at a location about 10-ft forward of the "bow" of the platform model and about 1-ft abeam of the model centerline (the bow of the model was situated 35 feet from the wavemaker; b) at a location about 1-ft abeam of the side of the model at its midlength and, c) at a location about 10-ft aft of the model's stern and about 1-ft abeam of the model's centerline. Wave measurements were made without the model in the test tank for all wavemaker settings used for the test program so that reference measurements without possible reflection effects would be available.

Spring lines were connected to the bow and stern to restrain the model against yawing or excessive drifting. The bow line was connected, through two ordinary rubber bands in series, between the deck of the model and a fixed point at the same elevation about 10-ft forward of the bow. The stern line was connected at the deck and over a pulley about 10-ft aft of the stern, to a 0.10-lb weight. The light tensions in these lines are considered to exert very little influence on the motions of the model.

Wave-Induced Forces

Large Model

In order to study the effect of interaction on wave-induced forces to correlate with motions measurements of the articulated model, the same floats used in the motions tests were adapted for use in a restrained model rig.

The sets of six floats were disconnected from the transverse channels solvent bonded to 1-inch square times 30-inch wide plexiglas bars. The bars were secured to a pair of 2" x 4" x 12' aluminum strongbacks which were, in turn, connected to the bridge spanning the 75-ft length of DL Tank No. 2. The spacing and staggered array of the floats is the could be measured for any desired row of floats.

Wave elevations were measured at three locations : a) 10-ft forward of the row of floats nearest the wavemaker and about 1-ft abeam of the model centerline (the first row was situated 35 feet from the wavemaker for the small model tests also), b) at a location 14-in

from the model centerline directly abeam of the row of floats in which measurements were being made, and d) at a location 4-ft aft of the last row of floats and about 1-ft abeam of the model centerline. Again, wave tests were done at wavemaker settings for which wave measurements with the model present were available.

Results

Motion Tests

Articulated model motions tests were carried out with regular waves in the 75-ft wide Tank No.2 to compare with results previously obtained in the 12-ft wide Tank No.3. Presumably if any effects of tank wall interference were present for the first series of tests, they will not be present in the tests in the wide tank.

Results in the form of heave amplitude divided by wave amplitude, Z/ζ (in/in) for Row 18 are given in Figure 47 as a function of model-scale frequency. The repeat test results of Tank 2 are given with different plotting symbols to distinguish them from the previous Tank 3 results. The differences between the results are not great and similar agreement exists for measurements for Rows 1, 9, 27 and 35. The results have been cross-faired by means of "carpet-plotting" and the smoothed curves are presented in the composite Figure 48 which shows the substantial tail-wagging.

Force Tests

Large Model

Force measurements results, in the form of oscillatory heave force amplitude divided by wave amplitude, Z/ζ (lb/in), for Row 17, are given same as for the articulated motions model.

One row of lfoats is not connected to the strongbacks but is coupled ot a force balance system for measuring vertical and horizontal wave forces. This row may be located in any desired position, while the "fixed" rows are also relocatable so that the forces acting on any one of the 35 rows of floats can be measured.

Wave elevation measurements were made at several locations during these tests : a) at a location 10-ft forward of the row of floats nearest the wavemaker and about 1-ft abeam of the model centerline (this first row was situated 35 feet from the wavemaker) ; b) at a location 27-in from the model centerline directly abeam of the row of floats on which measurements were being made ; and c) at a location 4-ft aft of the last row of floats and about 1-ft abeam of the model

centerline. As for the motions tests, wave measurements were made without the float models present for all wavemaker settings used for the test program.

Small Model

In order to study the effect of model size on hydrodynamic forces, an array of 35 rows of 6 each of smaller scale models was constructed. The scale ratio relative to the larger model was 7/20, corresponding to the ratios of the diameters of the surface piercing tubes, 7/16:5/4. The shape of the floats, similar to that of the large models, was produced by thin-walled wax castings. The damping collars at the top of the conical part of the float are stiff mylar film glued to the tube.

The floats were attached in rows to 30-in wide bars (except for the row used for measuring forces) which were, in turn, attached to a pair of 2" x 4" x 5' aluminum strongbacks which were connected to the bridge in the same way as for the large model tests. The spacing ratio and staggered array are the same as for the large model.

The measurement row of floats was connected to a force balance system for measuring vertical and horizontal wave forces. This row of floats could be moved, as in the tests with the larger model, so that forces in Figure 49 as a function of frequency. Surge force results are given in Figure 50.

Cross-faired results in the form of carpet plots are given in Figures 51 for heave and 52 for surge force.

It is interesting to note that the heave force shown in Figure 51 does not increase dramatically at the stern as does the heave motion, as shown in Figure 48.

Small Models

The force measurements data obtained in the tests in the large tank are presented in the corresponding figures for the large models. Results have been expanded by Froude's Law so that small model data are expressed in large-model-equivalent forces and frequencies. Different plotting symbols are used to distinguish small model results from large model results. A composite carpet plot of the heave force is given in Figure 53 for these small model results which are somewhat different from the large model results.

Discussion of Interaction Test Results

Comparison of Articulated Model Tests

The results, examples of which are given in Figure 47, demonstrate that tests with this model are repeatable. Although the "scatter" of the data points even within a given test program (Tank 3 or Tank 2) is rather large, there is sufficient consistency between the tests to say with confidence that the measured motions - in particular the unexpected "tail wagging" - are characteristic of this articulated model (and its associated apparatus, viz., pitch-restraining heave most at Row 18 and low-tension spring lines at bow and stern). The motions recorded in the tests in Tank 3 were not importantly influenced by tank sidewall effects.

The carpet plot of Figure 48 exhibits the dependency of the deck motions on position along the length of the model and frequency. The tail-wagging phenomena are shown clearly for all gigher frequencies. The frequency range covered here corresponds to full-scale frequencies for which significant wave energy exists for sea states with significant wave height $H_{1/13} < 15$ feet.

Correlation Between Heave Force Measurements and Motions

The heave force results obtained in the large model (an example of which is shown in Figure 49 and a carpet plot in Figure 51) show important interaction effects on the vertical wave-induced force. For instance, for $f = 1.2$ Hz, the force in the middle of the model is 42% greater than that at the bow, while the force at the stern is 36% higher. It may also be shown that, for this frequency, the force at the bow is 30% higher than those reported for the tests with the smaller (five rows of five) array except that the outside rows (front and back) are different from each other and different from isolated float results.

The fore-and-aft asymmetry of the wave-induced heave force suggests that the interaction may be influenced by either free-surface-type frequency dependent effects or, perhaps, some viscous wake effects. If the interaction were purely potential in character and unaffected by wave diffraction effects (as is expected for slender bodies in relatively long waves), a linearized representation of the interaction effect on the vertical force due to waves on the j^{th} float due to the presence of the other floats might be expressed, formalistically at least, as

$$\left(\frac{Z}{\zeta}\right)_{j,K} = \left(\frac{Z}{\zeta}\right)_{j,o} + \sum_{\substack{k=1,K \\ k\neq j}} W_{jk}\left(x_k - x_j,\ y_k - y_j;\ \frac{Z}{\zeta}\right) \qquad (47)$$

where

$(\frac{Z}{\zeta})_{j,o}$ is the vertical force due to waves on the j^{th} float as though it were isolated,

and W_{jk} expresses the interaction effect of the k^{th} float on the vertical force due to waves on the j^{th} float.

The interaction is expressed simply as a function of the distance between the two floats, which would be valid under the assumptions stated of negligible free surface and viscous wake effects. This representation indicates that the interaction effect should be symmetrical, fore-and-aft. It is not possible, at this time, to say whether the asymmetrical characteristic of the force is due to free-surface or viscous wake influence. An investigation of the effect of wave diffraction according to a simplified slender body analysis is presently being planned.

Dynamic Motions Analysis

The response of multi-degree-of-freedom dynamic systems to constant frequency exciting forces can, in general, be expressed as a sum of normal mode components (cf., Biggs 66 or Timoshenko 61), which can be expressed for a beam in the form

$$z(x,t) = \sum^{n} A_{n_{st}} \cdot (DLF)_n \, \varphi_n(x) \qquad (48)$$

where

$\varphi_n(x)$ = is the normalized model shape of the n^{th} mode of oscillation of the structure

$$A_{n_{st}} = \frac{\int p_1(x) \, \varphi_n(x) dx}{\omega_n^2 \int m \, \varphi_n^2(x) dx}$$

$p_1(x)$ = distributed exciting force

m = mass per unit length of beam

ω^2 = $(\text{natural frequency})^2$ of n^{th} normal mode

$$DLF_n = \frac{1}{1-(\omega/\omega_n)^2}$$; for simple harmonic exciting force with frequency ω , neglecting damping

Normal mode shapes, φ_n , may be characterized as symmetrical and asymmetrical about the midlength of the deck (beam).

A set of normal modes and natural frequencies for a particular assumed island structure and float-attenuator size have been calculated by J.Rice of Goodyear Aerospace [67] . The first eight elastic "free-end" modes of oscillation were found to have natural frequencies corresponding within 0.23% of the pure heave natural frequency !

While these results are applicable to the particular large island which Rice considered, it seems probable that the articulated model, with its essentially negligible elastic interconnections, will also have normal modes whose frequencies correspond to the free heaving frequency of the float elements. Thus the dynamic load factors (DLF's) for all modes, symmetric and asymmetric, will be essentially the same. Then, according to the definition of the amplitude function, A_{nst} , the motion should correspond closely to a weighted sum of the distributed load. A detailed evaluation of the response would require significant numerical work but, intuitively, it does not seem reasonable to expect the modest asymmetry of the wave induced heave force (Figure 51) to produce the pronounced asymmetry of the heave motion response (Figure 48).

Surge Force Interaction

Results given in the carpet plot (Figure 52) indicated virtually no influence of position in the array on surge force due to waves at low frequencies, but as much as 43% increase (monotonic with distance from the bow) at f = 1.4 Hz.

Scale Effects

Force measurements shown in Figures 49 and 50 include the small scale model results. They are seen to be somewhat lower, in general, than the larger model results, but the trends of the results are quite similar. Differences may be partly attributable to experimental error. The magnitudes of the oscillatory forces being measured on the small models are of the order of 0.001 lbs : such small measurements are not routinely executed in hydrodynamic laboratories such as Davidson Laboratory. The scale effect exhibited may be due to either viscous effect (Reynolds Number) or surface tension effects (Weber Number).

Wave Measurements

A few wave elevation measurements were made at locations within the array of the rigidly-held large models. The results show that the wave amplitudes are significantly higher (about 10 to 20 per

cent) than in the absence of the model, probably because of the blockage of flow within the nest of obstacles.

Plans for Comprehensive Test Programs

The results of the exploratory tests have not yielded an explanation of the interaction effect, specifically the "tail-wagging" phenomena, associated with the articulated model motions tests. The force measurements reveal that a significant hydrodynamic interaction effect exists which would be expected to importantly influence the heaving response even if the tail wagging behavior were not observed. Consequently, it is necessary for design purposes to systematically investigate the effect of hydrodynamic interaction on the heave motions response of resiliently connected arrays of floats.

An experimental program to study the influence of float center-to-center spacing, expressed in terms of waterline diameter, float slenderness, deck rigidity, size of array, externally provided damping, and yaw-restraining spring-line restraint, has been developed and will be carried out during August 1972.

Three sets of floats, having different spacing ratios (3 to 1, 3.75 to 1 and 4.5 to 1) are being built. Each set will consist of seventeen rows fo ten floats each. The ten floats in each row will, in this case, provide ample roll stability : these rows consist of sufficiently stiff, yet very light weight, T-sections connected to the cylindrical floatation tubes.

The seventeen rows will be connected by two sets of plastic splines, one pair at each gunwale, which provide sufficient pitch restraint for the otherwise unstable rows of floats, and which simulate a specified deck elastic beam-like behavior. The full-size deck stiffness is assumed to be equal to a plate EI of 80×10^6 lb-ft^2 per ft of deck width, a value recommended by GAC engineers. This stiffness scales according to the 4th power of the scale ratio, which is taken to be 1/48, with 1 1/2-in diameter model floats corresponding to 6-ft diameter full-size (waterline diameter). For the middle-spacing set of floats, an additional simulated deck rigidity, twice as large as the nominal value, will be tested by using plastic splines of the same thickness and spacing but each twice as wide.

The float attenuators to be used are thin-walled wax castings with aluminum tubes at their upper ends. The shapes were selected so that their calculated heave responses, assuming no interaction effects, would be the same. The maximum diameters are 1.5 and 1.8 times

the waterline diameter, while the corresponding full-scale drafts are 96 ft and 78ft, respectively.

Since the full-scale floats are expected to require a hinge to alleviate the bending loads due to wave action on the upper part of the float, it has been decided to simulate these hinges for the present comprehensive test program. The hypothesis that the attenuators will oscillate in harmony under the action of waves will consequently be tested at this early stage. The hinges are made of very flexible silicone rubber.

The attenuators are to be ballasted so that when flooded with water, they have effectively neutral buoyancy and the center-of-gravity slightly below the center-of-volume so that a small positive pendular restoring moment exists. The attenuators and hinges can be interchanged from one row of floats to another.

Tests in regular waves to determine the heaving motions will be carried out with all possible combinations of floats and attenuators, plus the increased deck stiffness for the intermediate-spacing floats with one of the sets of attenuators.

An auxiliary investigation will be made of the motions of a smaller array of floats, 10 rows of 10 each, to explore the effect of extent of the array on the interactions.

Other auxiliary investigations will include a brief study of the effect of externally applied (not from appendages immersed in the test tank) viscous damping for a range of frequencies, including as nearly as possible the heaving natural frequency. Some tests will also be carried out without the yaw restraining spring lines in place.

Results will be compared with theoretical calculations and, it is expected, sets of interaction coefficients derived.

DISCUSSION

The chief findings of these investigations may be given as :

1. The vertical wave-induced forces on relatively slender, vertically-oriented, isolated floats can be evaluated with adequate accuracy according to available analytical procedures (Eq.34).

2. The introduction of a hinge to permit lateral pendulum-like motions of the lower (attenuator) portion of the float produces a large reduction of the lateral wave-induced load.

3. This hinge does not have an appreciable effect on the vertical wave-induced forces.

4. Articulated Model Island tests indicate that an important interaction effect on heave motion occurs. This may be due to hydrodynamic effects, or to some kind of elastic or connecting mechanism effects. A simplified elastic normal mode analysis does not appear to indicate "classical" linear elastic effects leading to the interesting "tail wagging" phenomena found in the tests.

5. The vertical wave-induced forces acting on rigidly-fixed floats in an array like that of the articulated model island show an appreciable effect of interaction, principally on floats in the interior of the array. There is, however, a small fore-and-aft asymmetry of this heave producing force, with the stern row of floats experiencing slightly higher forces than the bow but still less than the middle floats. It is felt that this asymmetry of the exciting force is not sufficient to produce the substantial "tail wagging" of the motions tests.

6. The longitudinal wave-induced forces acting on the rigidly-fixed array of floats show only a modest effect of interaction, which is greater for high frequencies than for low.

7. Scale effects on wave-induced forces acting on a large rigidly-fixed array of floats were investigated by testing a model whose size is much smaller than would ordinarily be selected for hydrodynamic testing. The forces measured on the small models were somewhat lower than those obtained with the larger model. The trends of variations of forces with frequency are the same for both sizes of models. It is considered that models sizes ordinarily selected for platform motions tests are generally satisfactory and free of important scale effects except possibly for some viscous effect on damping forces for

well-rounded structural elements. This exception is not expected to be particularly unfavorable unless resonant behavior is of special interest.

ACKNOWLEDGMENTS

The authors must express their gratitude to the members of the staff of Davidson Laboratory who have assisted in the investigations which have been described. Mr. M. Chiocco has been especially helpful in carrying out the experimental work of the large-array float interaction tests. Dr. D. Savitsky and Mr. E. Numata have given helpful advice on all aspects of the work.

REFERENCES

1 HANDLER, E.H., "Tilt and Vertical Float Aircraft for Open Ocean Operations," Journal of Aircraft, Vol.3, No.6, pp.481-489, November-December 1966.

2 DEWEY, D.B., 'Open Ocean Demonstration of Vertical Float Sea Stabilization Concept", General Dynamics/Convair Report 64-197, June 1964.

3 TESSITORE, F.A., "Tests of the Gyrodyne Tilt-Float Helicopter-November 1964", Gyrodyne Co. of America Final Report Y60-313400-1, November 1964.

4 LUEDERS, D.H., "Motions of a 1/4-Scale Model of Gyrodyne Tilt-Float DSN-1 Helicopter in Regular and Irregular Seas", Davidson Laboratory Report R-881, June 1962.

5 MERCIER, J.A., "Motions Response of a Related Series of Vertical Float-Supported Platforms in Irregular Seas", Davidson Laboratory Report SIT-DL-69-1334, November 1969.

6 BARR, R.A., "The Hydrodynamic Design of Float Supported Aircraft II Method for Selection Optimal Vertical Float Support Systems", Hydronautics, Inc., Technical Report 513-6, October 1968.

7 CARRIVE, F. and JULIEN, B., "Designing Highly Stable Floating Platforms", Ocean Industry, Vol.4, No.8, pp.48-52, August 1969.

8 HOOFT, J.P., "Hydrodynamic Aspects of Semi-Submersible Platforms", Doctoral Dissertation, Delft University, 1972.

9 MARSH, K.R., "Feasibility Study, XC-142A Modified for Open Ocean Operation", LTV Vought Aeronautics Division, Report 2-55400/49-963, February 1965.

10 DEWEY, D.B. and FISHER, R.R., "Inflatable Float Design Study", General Dynamics/Convair Final Report 65-193, September 1965.

11 GONSALVES, J., "Design Study for Establishing an Open-Ocean Tilt-Float Configuration Helicopter", Vertol Division, Boeing Report R-452, January 1966.

12 NUMATA, E., "Hydrodynamic Model Tests of Offshore Drilling Structures", Marine Technology, Vol.3, No.3, July 1966.

13 DALZELL, J. and YAMANOUCHI, Y., "Analysis of Model Tests Results in Irregular Head Seas to Determine Motion Amplitudes and Phase Relationships to Waves", Lecture Notes on Ship Behavior at Sea Second summer Seminar at Stevens Institute of Technology, June 16-20, 1958, Experimental Towing Tank Report 708, November 1958.

14 FUCHS, R.A. and MacCAMY, R.A., "A Linear Theory of Ship Motions in Regular Waves", University of California, Institute of Engineering Research, Series 61, No.2, July 1953.

15 CUMMINS, W.E., "The Impulse Response Function and Ship Motions", DTMB Report 1661, 1962.

16 ABKOWITZ, M.A., "The Interim Standard Sea Spectral Formulation of the 11th ITTC - A Review and Evaluation of Its Use", Appendix V of Seakeeping Committee Report, 12th International Towing Tank Conference, Rome, Italy, Sept. 1969 (see also Technical Decisions and Recommendations No. 7-4).

17 PIERSON, W.J., Jr., and MOSKOWITZ, L., "A Proposed Spectral Form for Full Developed Wind Seas Based on the Similarity Theory of S.A. Kitaigorodskii", New York University,

School of Engineering and Sciences, Geophysical Sciences Laboratory Report 63-12, October 1963.

18 BENNET, R., "A Method to Determine the Response of Ships in Irregular Waves", Chalmers University of Technology, Division of Ship Design Report, September 1966.

19 LINDGREN, H. and WILLIAMS, A., "Systematic Tests with Small, Fast Displacement Vessels, Including a Study of the Influence of Spray Strips", Society of Naval Architects and Marine Engineers, 1968, Diamond Jubilee International Meeting.

20 FRIDSMA, G., "A Systematic Study of the Rough-Water Performance of Planing Boats (Irregular Waves-PART II)", Davidson Laboratory Report SIT-DL-71-1495, March 1971.

21 OCHI, M.K. and VUOLO, R.M., "Seakeeping Characteristics of a Multi-Unit Ocean Platform", Society of Naval Architects and Marine Engineers, Spring Meeting, Honolulu, Hawaii 1971.

22 DALZELL, J.F., "A Study of the Distribution of Maxima of Non-Linear Ship Rolling in a Seaway", Davidson Laboratory Report SIT-DL-71-1562, September 1971.

23 OHKUSU, M., "On the Heaving Motion of Two Circular Cylinders on the Surface of a Fluid", Reports of Research Institute of Applied Mechanics, Kyushu University (Japan), Vol.17, No.58 (1969).

24 OHKUSU, M., "On the Motion of Multihull Ships in Waves (I)", Reports of Research Institute of Applied Mechanics, Kyushu University (Japan), Vol.18, No.60 (1970).

25 OHKUSU, M. and TAKAKI, M., "On the Motion of Multihull Ships in Waves (II)", Reports of Research Institute for Applied Mechanics, Kyushu University, Vol.19, No.62, July 1971.

26 WANG, S. and WAHAB, R., "Heaving Oscillations of Twin Cylinders in a Free Surface", Journal of Ship Research, Vol. 15, No. 1, 1971.

27 LEE, C.M., JONES, H. and BEDEL, J.W., "Added Mass and Damping Coefficients of Heaving Twin Cylinders in a Free Surface", Naval Ship Research and Development Center, Report 3695, April 1971.

28 FRANK, W., "Oscillation of Cylinders in or Below the Free Surface of Deep Fluids", NSRDC Report 2375, October 1967.

29 WEHAUSEN, J.V. and LAITONE, E.V., "Surface Waves", Encyclopedia of Physics, Vol. 9, Springer-Verlag, Berlin, 1960.

30 KIM, C.H. and CHOU, F., "Prediction of Drifting Force and Moment on an Ocean Platform Floating in Oblique Waves", Ocean Engineering Report 2, Stevens Institute of Technology, December 1970.

31 HASKIND, M.D., "The Exciting Forces and Wetting of Ships in Waves", DTMB Translation 307 by J.N. Newman, November 1962.

32 NEWMAN, J.N., "The Exciting Forces on Fixed Bodies in Waves", Journal of Ship Research, Vol.6, No.3, Dec. 1962.

33 HASKIND, M.D., "The Pressure of Waves on a Barrier", Imzhen, Sb.4, No.2, 147-160, 1948.

34 MARUO, H., "The Drift of a Body Floating on Waves", Journal of Ship Research, Vol.4, No.3, December 1960.

35 OHKUSU, M., "Wave Action on Groups of Vertical Circular Cylinders", Presented at the Spring Meeting of the Society of Naval Architects in Japan, May 1972.

36 NEWMAN, J.N., "The Motions of a Spar Buoy in Regular Waves", David Taylor Model Basin Report 1499, May 1963.

37 RUDNICK, P., "Motions of a Large Spar Buoy in Sea Waves", Journal of Ship Research, December 1967.

38 ADEE, B. and BAI, K.J., "Experimental Studies of the Behavior of Spar Type Stable Platforms in Waves", Report No. NA-70-4, College of Engineering, University of California, Berkely, July 1970.

39 LAMB, H., Hydrodynamics, Cambridge University Press, 1932, republished by Dover Publications, N.Y., 1945.

40 THOMPSON, F.L. and KIRSCHBAUM, H.W., "The Drag Characteristics of Several Air Ships Determined by Deceleration Tests", NACA Report No.397, 1931.

41 SMITH, S.L., "BSRA Resistance Experiments on the LUCY ASHTON Part IV, Miscellaneous Investigations and General Appraisal Appraisal", Transactions, Institution of Naval Architects, Vol. 97, 1955, See especially Fig. 12, p. 542.

42 BLAGOVESHCHENSKY, S.N., Theory of Ship Motions, Vol. 1, Dover Publications, New York, 1962, pp. 141-143.

43 KEULEGAN, G.H. and CARPENTER, L.H., "Forces on Cylinders and Plates in an Oscillating Fluid", National Bureau of Standards Report 4821, September 1956.

44 McNOWN, J.S., "Drag in Unsteady Flow", Proceedings of IX International Congress of Applied Mechanics, Brussels, 1957.

45 McNOWN, J.S. and KEULEGAN, G.H., "Vortex Formation and Resistance in Periodic Motions", Proceedings of the American Society of Civil Engineers, Engineering Mechanics Division, January 1959.

46 PAAPE, A. and BREUSERS, H.N.C., "The Influence of Pile Dimensions on Forces Exerted by Waves", Proceedings of the Xth Conference on Coastal Engineering, Tokyo, 1966.

47 MARTIN, M., "Roll Damping Due to Bilge Keels", Ph.D. Dissertation, State University of Iowa, June 1959.

48 RIDJANOVIC, M., "Drag Coefficients of Flat Plates Oscillating Normally to Their Planes", Schiffstechnik, Bd 9-Helf 45, 1962.

49 BROWN, P.W., "The Effect of Configuration on the Drag of Oscillating Damping Plates", Davidson Laboratory Report 1021 May 1964.

50 HENRY, C., "Linear Damping Characteristics of Oscillating Rectangular Flat Plates and Their Effect on a Cylindrical Float in Waves", Davidson Laboratory Report 1183, June 1967.

51 WOOLAM, W., "Drag Coefficients for Flat Plates Oscillating Normal to Their Planes-in Air", Southwest Research Institute Final Report 02-1973 (NASA CR-66544), March 1968.

52 TSANT, M. and ALTMANN, R., "The Hydrodynamic Design of Float-Supported Aircraft. I-Float Hydrodynamics", Hydronautics, Inc. Technical Report 513-5, October 1968.

53 NORRIS, K.S. and HANSON, J.A., "Manned Open Sea Experimentation Station (MOSES) A Feasibility Study", Oceanic Institute, Waimanalo, Hawaii, June 1971.

54 FROUDE, W., "On Resistance in Rolling of Ships", Naval Science, 1874.

55 HISHIDA, T., "A Study on the Wavemaking Resistance for the Rolling of Ships, Part VI, Effect of Motion Ahead on Wave Resistance to Rolling", Journal of Zosen Kiokai (Society of Naval Architects of Japan), Vol. 87 (1955).

56 BAKER, G.S., "Rolling of Ships Underway. The Decrement of Roll Due to Hull and Bilge Keels", Transactions North-East Institution of Engineers and Shipbuilders, Vol.56, pp.25-42, 1939-1940.

57 GERRITSMA, J., "The Effect of a Keel on the Rolling Characteristics of a Ship", International Shipbuilding Progress, Vol.6, pp.295-304, 1959.

58 GERSTEN, A., "Effect of Forward Speed on Roll Damping Due to Viscosity and Eddy Generation", Naval Ship Research and Development Center, Report 2725, June 1968.

59 MERCIER, J.A., "Scale Effect on Roll-Damping Forces at Zero Forward Speed", Davidson Laboratory Report 1057, February 1965.

60 GERSTEN, A., "Roll Damping of Circular Cylinders with and without Appendages", Naval Ship Research and Development Center Report 2621, October 1969.

61 TIMOSHENKO, S.P., Vibration Problems in Engineering, 3rd Edition, D. VanNostrand Company, Inc. Princeton, N.J., 1956.

62 MERCIER, J., "A Method for Computing Float-Platform Motions in Waves", Journal of Hydronautics, Vol.4, No.3, July 1970, pp. 98-104.

63 MERCIER, J., "Hydrodynamic Forces on Some Float Forms", Journal of Hydronautics, Vol.5, No.4, October 1971, pp.109-117.

64 MERCIER, J.A., "Hydrodynamic Characteristics of Several Vertical Floats in Waves", Stevens Institute of Technology Report No. 1481, 1970.

65 OCHI, M.K. and VUOLO, R.M., "Seakeeping Characteristics of a Multi-Unit Ocean Platform", Paper No. 2, Spring Meeting, Society of Naval Architects and Marine Engineers, May 25-28, 1971.

66 BIGGS, J.M., Introduction to Structural Dynamics, McGraw Hill Book Company, New York, 1964.

67 GOODYEAR AEROSPACE CORPORATION, "Phase I Technical Report - Expandable Floating Bases", GER-15048, 15 Nov. 1970, pp.206 et seq.

* * *

NOMENCLATURE

FOR MOTIONS RESPONSE OF THREE AND FOUR FLOAT PLATFORMS

A	coefficient in interim standard sea spectral formulation, Eq.(2)
B	coefficient in interim standard sea spectral formulation, Eq.(2)
E_x	variance for x^{th} mode of response of platform to irregular wave excitations, Eq.(6)
$\tilde{E}_x$	dimensionless response variance, (e.g., Eq.7)
$\tilde{E}_{\hat{x}}$	dimensionless response variance, Eq.(10)
GM	metacentric height
g	acceleration of gravity
$H_{1/3}$	significant wave height
k	impulse response function
m_o	variance of wave spectrum
m_1	first moment of wave spectrum about $\omega = 0$ axis
N_o	number of occurrences of irregular response in given duration of time
Prob	probability of computed value of response being exceeded in a given duration of time
S_ζ	wave elevation spectral density
T_1	$2\pi m_o/m_1$, or observed characteristic period of waves
t	time, sec
$\tilde{t}$	dimensionless time, $t\sqrt{g/\nabla^{1/3}}$
$\bar{x}$	average apparent response (crest-to-trough) in x^{th} mode
$(\bar{x})_{1/3}$	average of one-third highest responses, or "significant" response
$(\bar{x})_{1/10}$	average of one-tenth highest responses
$\hat{x}$	calculated extreme value of response in x^{th} mode, Eq.(9)
z	heave motion
α_x	dimensionless response (transfer function) for x^{th} mode, Eq.(8a-f)
∇	craft displaced volume
ζ	wave elevation

θ pitch motion

λ wave length

φ roll motion

ω frequency, rad/sec

$\tilde{\omega}$ dimensionless frequency = $\omega\sqrt{\nabla^{1/3}/g}$

FOR PROBLEMS OF HYDRODYNAMIC INTERACTION IN BEAM SEAS

A_w waterplane area

$A_{\pm}^{(m)}$ complex radiated wave amplitude ratio

$A_{\pm}^{(o+e)}$ diffracted wave amplitude ratio

a incident wave amplitude

B beam

C_{SS}, etc added mass coefficient defined in Table 6

C section contour

F force or moment

$F^{(m)}$, etc wave-exciting force (moment) derived from the radiation of mode m

$f_S^{(\beta)}$, etc non-dimensional exciting force defined in Table 9

G Green's function (source potential)

g gravitational constant

h wave elevation

ℓ hydrodynamic moment arm

K mean wave force or constant defined in Eq.(14)

M integer, moment or inertial mass

m number of mode of motion or sectional mass

m'' two-dimensional added mass

N integer or two- or three-dimensional damping coefficient

0 origin of the coordinate system

p hydrodynamic pressure

Q	source intensity
r	field point
S	amplitude of displacement, surface or spacing
$S_{-\infty}$, etc	surface at $y \to -\infty$, etc.
s	length of contour, segment or spacing
T	draft of hull or period
t	time
x, y, z	Cartesian coordinate system
X, Y, Z	components of force

SUBSCRIPTS

a	indicating body a
b	indicating body b
D	indicating diffraction
f	indicating force
H	indicating heave or heaving force
h	indicating wave
I	indicating incident wave
i	$\sqrt{-1}$, or indicating the imaginary or hydrodynamic damping part
j	indicating j^{th} segment
k	indicating k^{th} segment
o	indicating origin
r	indicating the real or the hydrodynamic inertial part or relative motion
S	indicating swaying
R	indicating rolling
W	indicating waterplane or waterline
$\pm$	indicating $y \to \pm\infty$

SUPERSCRIPTS

e indicating even function

o indicating odd function

m indicating mode of motion

GREEK LETTERS

α slope of a segment

β suffix standing for e, o or (e+o)

γ suffix standing for m for radiation and β for diffraction

δ non-dimensional damping coefficient

ϵ phase angle

φ velocity potential

λ wave length

ν wave number

ρ water density

η the y-coordinate of source distribution, swaying motion or suffix denoting swaying

ζ the z-coordinate of source distribution, heaving motion or suffix denoting heaving

ω circular frequency

FOR SLENDER VERTICAL FLOATS AND LARGE ARRAYS

A frontal area of appendages, Eq.(43)

$A_{n_{st}}$ model static deflection, Eq.(48)

A_w waterplane area

C_{HH} added mass coefficient for heave

C_m damping moment coefficient, Eq.(43)

C_{vp} vertical prismatic coefficient, $\nabla/A_w T$

c' ratio of added mass of damping devices to added mass of attenuation, Eq.(36)

c/c_c	ratio of damping to critical damping coefficient
DLF_n	dynamic load factor
EI	deck rigidity
F	force
f	frequency, cycles per second
g	acceleration of gravity
k	wave number = $\omega^2/g = 2\pi/\lambda$
k_1'	added mass coefficient for float-attenuator in heave, Eq.(35)
L_a	length of attenuator
M	moment
m''	total added mass in vertical direction
m'	element of added mass in vertical direction
m_a'	added mass of attenuator in vertical direction
m_d'	added mass of damping devices in vertical direction
R_a	radius of attenuator
$R_{c.a.}$	radius to center of area of appendage, Eq.(43)
R_o	radius of float waterplane
S	sectional area of float body
T	draft of float
W_jk	interaction effect of k^{th} float on vertical force due to waves on j^{th} float of array, Eq.(47)
x	horizontal coordinate, along deck
Z	vertical force
z	vertical coordinate
z_e	effective depth for evaluating wave acceleration for element of added mass, Eq.(34)
∇	displaced volume
ζ	wave elevation
ζ_o	wave amplitude
ζ_e	wave motion evaluated at depth corresponding to assumed damping source

θ	angular coordinate, Eq.(43)
λ	wave length
λ'	scale ratio, full-size length/model size length
ρ	fluid mass density
ω	frequency, radians per second
ω_n	natural frequency

* * *

Table 1 : Related series of float platforms characteristics of models with four-float (cruciform) configuration

Float Draft / Float Diam	Damping Plate Diam / Float Diam	$GM/\nabla^{1/3}$ Computed	$GM/\nabla^{1/3}$ Measured	Hull Float Spacing $/\nabla^{1/3}$	Wing Float Spacing $/\nabla^{1/3}$	Test Run
GROUP A: Head Seas; Hull Float Diam/Wing Float Diam = 1.5						
			PITCH			
2.0	1.6	0.277	0.201	3.73	5.59	002
2.0	1.4	0.277	0.201	3.73	5.59	012
2.0	1.8	0.277	0.201	3.73	5.59	018
2.0	1.6	0.229	(~.15)*	3.63	5.39	005
2.5	1.6	0.830	0.622	4.17	6.26	006
1.5	1.6	0.277	0.182	4.13	6.20	047
		0.277	0.654	3.28	4.92	032
GROUP B: Head Seas; Hull Float Diam/Wing Float Diam = 1.25						
			PITCH			
2.0	1.6	0.277	0.232	3.91	4.89	060
2.0	1.4	0.277	0.232	3.91	4.89	058
2.0	1.8	0.277	0.232	3.91	4.89	062
2.0	1.4	0.830	(~.78)*	4.37	5.46	066
2.0	1.8	0.830	(~.78)*	4.37	5.46	064
GROUP C: Beam Seas; Hull Float Diam/Wing Float Diam = 1.5						
			ROLL			
2.0	1.6	0.277	0.198	3.73	5.59	003
2.0	1.4	0.277	0.198	3.73	5.59	010
2.0	1.8	0.277	0.198	3.73	5.59	017
2.0	1.6	0.107	(~.05)*	3.63	5.39	004
2.0	1.6	0.830	0.747	4.17	6.26	007
2.5	1.6	0.277	0.182	4.13	6.20	046
1.5	1.6	0.277	0.250	3.28	4.92	031

*Not measured

Table 2 : Related series of float platforms characteristics of models with three-float (triangular) configuration

GROUP D: Head Seas, All Floats Equal

Float Draft / Float Diam	Damping Plate Diam / Float Diam	Pitch $GM/\nabla^{1/3}$ Computed	Pitch $GM/\nabla^{1/3}$ Measured	Radius to Float ℓ / $\nabla^{1/3}$	Test Run
4.0	1.6	0.366	0.271	3.16	074
4.0	1.4	0.366	0.271	3.16	091
4.0	1.8	0.366	0.271	3.16	087
4.0	1.6	1.098	(~1.0)*	3.55	075
5.0	1.6	0.366	0.300	3.50	096
3.0	1.6	0.366	0.716	2.76	083

*not measured

Table 3 : Transfer functions for heave and pitch, Run No.002
Four-Float (cruciform) configuration head seas tests

Hull Float Diam/Wing Float Diam = 1.5
Float Draft/Diameter = 2.0
Damping Plate Diam/Float Diam = 1.6
Metacentric Height/$\nabla^{1/3}$ = 0.201

WAVE-HEAVE RESULTS

$\tilde{\omega} = \omega\sqrt{\nabla^{1/3}/g}$	$\lvert z\rvert/\lvert\zeta\rvert$	Phase*	Coherency
0.0	1.000	0	---
---	---	--	---
0.244	0.867	-2.	0.97317E+00
0.305	0.990	-.	0.98395E+00
0.366	1.011	4.	0.97982E+00
0.427	1.001	7.	0.98670E+00
0.488	1.015	12.	0.98358E+00
0.550	1.037	18.	0.98095E+00
0.611	1.051	26.	0.96360E+00
0.672	1.047	38.	0.93955E+00
0.733	0.992	56.	0.90799E+00
0.794	0.700	83.	0.73138E+00
0.855	0.378	119.	0.71285E+00
0.916	0.223	136.	0.74496E+00
0.977	0.120	156.	0.83387E+00

WAVE-PITCH RESULTS

$\tilde{\omega} = \omega\sqrt{\nabla^{1/3}/g}$	$\lvert\theta\rvert / \frac{\omega^2\lvert\zeta\rvert}{g}$	Phase*	Coherency
0.0	1.000	90.	---
---	---	--	---
0.427	0.289	112.	0.49342E+00
0.488	0.273	117.	0.77833E+00
0.550	0.241	115.	0.89711E+00
0.611	0.206	116.	0.93136E+00
0.672	0.177	120.	0.94658E+00
0.733	0.147	126.	0.95218E+00
0.794	0.103	135.	0.90537E+00
0.855	0.065	146.	0.89384E+00
0.916	0.046	153.	0.88248E+00
0.977	0.029	165.	0.69802E+00
1.038	0.011	251.	0.16130E+00
1.099	0.026	315.	0.65058E+00
1.160	0.027	320.	0.58830E+00

*A positive phase angle indicates that the motion lags the wave trough (max. positive amplitude) passage.

Table 4 : Impulse response functions for heave and pitch, Run N.002
Four-float (cruciform) configuration head sea tests

Hull Float Diam/Wing Float Diam = 1.5
Float Draft/Diameter = 2.0
Damping Plate Diam/Float Diam = 1.6
Metacentric Height/$\nabla^{1/3}$ = 0.201

$\tilde{t} = t\sqrt{g/\nabla^{1/3}}$	$k_z(\tilde{t})$	$k_\theta(\tilde{t})$
-25.72	0.0009	-.0001
-24.01	0.0000	-.0001
-22.29	-.0004	0.0006
-20.58	-.0014	-.0004
-18.86	-.0006	-.0001
-17.15	0.0020	0.0003
-15.43	0.0000	0.0002
-13.72	-.0053	0.0002
-12.00	-.0037	-.0007
-10.29	0.0050	0.0009
- 8.58	0.0081	-.0006
- 6.86	-.0002	0.0004
- 5.14	-.0073	0.0046
- 3.43	0.0183	-.0073
- 1.72	0.1066	-.0130
- .00	0.2208	-.0026
1.71	0.2428	0.0028
3.43	0.1108	0.0132
5.14	-.0583	0.0102
6.86	-.0968	-.0081
8.57	-.0100	-.0028
10.29	0.0533	0.0040
12.00	0.0250	-.0017
13.72	-.0217	0.0003
15.43	-.0203	0.0003
17.15	0.0063	-.0009
18.86	0.0141	0.0005
20.58	0.0023	-.0004
22.29	-.0070	0.0005
24.01	-.0045	-.0001
25.72	0.0020	-.0008

Table 5a : Spectrum responses, Run No.002
Four-float (cruciform) configuration head seas tests

Hull Float Diam/Wing Float Diam = 1.5
Float Draft/Diameter = 2.0
Damping Plate Diam/Float Diam = 1.6
Metacentric Height/$\nabla^{1/3}$ = 0.201

$\frac{H_{1/3}}{\nabla^{1/3}}$	$\frac{E_z}{\nabla^{2/3}}$	$\frac{E_{\dot{z}}}{g\nabla^{1/3}}$	$\frac{z_{1/3}}{\nabla^{1/3}}$	E_θ	$\frac{E_{\dot{\theta}}\nabla^{1/3}}{g}$	$\theta_{1/3}$
0.1??	0.143E-05	0.119E-05	0.478E-02	0.30?E-06	0.433E-06	0.219E-02
0.2??	0.3??E-03	0.218E-03	0.782E-01	0.641E-05	0.455E-05	0.101E-01
0.3??	0.247E-?2	0.118E-02	0.199E+00	0.354E-04	0.182E-04	0.238E-01
0.4??	0.644E-?2	0.271E-02	0.321E+00	0.939E-04	0.403E-04	0.388E-01
0.5??	0.120E-?1	0.449E-02	0.438E+00	0.179E-03	0.670E-04	0.535E-01
0.6??	0.189E-?1	0.647E-02	0.551E+00	0.286E-03	0.961E-04	0.677E-01
0.7??	0.271E-?1	0.836E-02	0.659E+00	0.411E-03	0.126E-03	0.811E-01
0.8??	0.365E-?1	0.103E-01	0.764E+00	0.551E-03	0.156E-03	0.939E-01
0.9??	0.470E-?1	0.123E-01	0.867E+00	0.704E-03	0.185E-03	0.106E+00
1.0??	0.590E-?1	0.143E-01	0.972E+00	0.882E-03	0.214E-03	0.119E+00
1.5??	0.137E+?0	0.243E-01	0.148E+01	0.204E-02	0.363E-03	0.181E+00
2.0??	0.232E+?0	0.336E-01	0.193E+01	0.359E-02	0.503E-03	0.237E+00
2.5??	0.345E+?0	0.420E-01	0.235E+01	0.525E-02	0.633E-03	0.290E+00
3.0??	0.575E+?0	0.508E-01	0.284E+01	0.767E-02	0.765E-03	0.349E+00
3.5??	0.717E+?0	0.604E-01	0.339E+01	0.106E-01	0.905E-03	0.412E+00
4.0??	0.962E+?0	0.704E-01	0.392E+01	0.147E-01	0.105E-02	0.473E+00

Table 5b : Spectrum responses, Run No. 012
Four-float (cruciform) configuration head seas tests

Hull Float Diam/Wing Float Diam = 1.5
Float Draft/Diameter = 2.0
Damping Plate Diam/Float Diam = 1.4
Metacentric Height/$\nabla^{1/3}$ = 0.201

$\frac{H_{1/3}}{\nabla^{1/3}}$	$\frac{E_z}{\nabla^{2/3}}$	$\frac{E_{\dot{z}}}{g\nabla^{1/3}}$	$\frac{z_{1/3}}{\nabla^{1/3}}$	E_θ	$\frac{E_{\dot{\theta}}\nabla^{1/3}}{g}$	$\theta_{1/3}$
0.100	0.536E-05	0.458E-05	0.926E-02	0.277E-06	0.389E-06	0.211E-02
0.200	0.613E-03	0.386E-03	0.998E-01	0.331E-05	0.271E-05	0.728E-02
0.300	0.302E-02	0.158E-02	0.227E+00	0.161E-04	0.885E-05	0.160E-01
0.400	0.719E-02	0.325E-02	0.339E+00	0.419E-04	0.186E-04	0.259E-01
0.500	0.129E-01	0.513E-02	0.454E+00	0.813E-04	0.327E-04	0.361E-01
0.600	0.201E-01	0.711E-02	0.567E+00	0.134E-03	0.447E-04	0.466E-01
0.700	0.286E-01	0.914E-02	0.676E+00	0.205E-03	0.671E-04	0.573E-01
0.800	0.383E-01	0.112E-01	0.783E+00	0.292E-03	0.767E-04	0.683E-01
0.900	0.495E-01	0.132E-01	0.889E+00	0.398E-03	0.947E-04	0.798E-01
1.000	0.622E-01	0.153E-01	0.998E+00	0.528E-03	0.114E-03	0.919E-01
1.500	0.149E+00	0.262E-01	0.154E+01	0.151E-02	0.228E-03	0.155E+00
2.000	0.257E+00	0.366E-01	0.273E+01	0.286E-02	0.350E-03	0.214E+00
2.500	0.387E+00	0.462E-01	0.249E+01	0.453E-02	0.469E-03	0.269E+00
3.000	0.567E+00	0.561E-01	0.321E+01	0.683E-02	0.594E-03	0.330E+00
3.500	0.822E+00	0.669E-01	0.358E+01	0.979E-02	0.730E-03	0.396E+00
4.000	0.117E+01	0.780E-01	0.414E+01	0.131E-01	0.869E-03	0.459E+00

Table 5c : Spectrum responses, Run No.018
Four-float (cruciform) configuration head seas tests

Hull Float Diam/Wing Float Diam = 1.5
Float Draft/Diameter = 2.0
Damping Plate Diam/Float Diam = 1.8
Metacentric Height/$\nabla^{1/3}$ = 0.201

$\frac{H_{1/3}}{\nabla^{1/3}}$	$\frac{E_z}{\nabla^{2/3}}$	$\frac{E_{\dot{z}}}{g\nabla^{1/3}}$	$\frac{z_{1/3}}{\nabla^{1/3}}$	E_θ	$\frac{E_{\dot{\theta}}\nabla^{1/3}}{g}$	$\theta_{1/3}$
2.1[illegible]	0.327E-[illegible]6	[illegible].262E-[illegible]6	0.2295E-02	[illegible].187E-06	0.208E-06	0.173E-02
2.2[illegible]	0.174E-[illegible]3	[illegible].911E-04	0.527E-01	[illegible].998E-05	0.650E-05	0.126E-01
2.3[illegible]	0.159E-[illegible]2	[illegible].691E-[illegible]3	0.160E+00	[illegible].579E-04	0.288E-04	0.304E-01
2.4[illegible]	0.496E-[illegible]2	[illegible].189E-02	0.282E+00	[illegible].157E-03	0.659E-04	0.501E-01
2.5[illegible]	0.1[illegible]0E-[illegible]1	[illegible].344E-02	0.491E+00	[illegible].333E-03	0.112E-03	0.696E-01
2.6[illegible]	0.165E-[illegible]1	[illegible].517E-[illegible]2	0.514E+00	[illegible].488E-03	0.161E-03	0.884E-01
2.7[illegible]	0.241E-[illegible]1	[illegible].696E-02	0.621E+00	[illegible].705E-03	0.213E-03	0.106E+00
2.8[illegible]	0.327E-[illegible]1	[illegible].876E-02	0.724E+00	[illegible].949E-03	0.264E-03	0.123E+00
2.9[illegible]	0.425E-[illegible]1	[illegible].106E-01	0.825E+00	[illegible].122E-02	0.315E-03	0.140E+00
1.[illegible]	0.537E-[illegible]1	[illegible].124E-[illegible]1	0.927E+00	[illegible].152E-02	0.366E-03	0.156E+00
1.5[illegible]	0.130E+[illegible]0	[illegible].219E-01	0.144E+01	[illegible].341E-02	0.614E-03	0.234E+00
2.[illegible]	0.227E+[illegible]0	[illegible].312E-01	0.190E+01	[illegible].565E-02	0.837E-03	0.301E+00
2.5[illegible]	0.345E+[illegible]0	[illegible].398E-01	0.235E+01	[illegible].912E-02	0.103E-02	0.360E+00
3.[illegible]	0.512E+[illegible]0	[illegible].489E-[illegible]1	0.286E+01	[illegible].111E-01	0.121E-02	0.422E+00
3.5[illegible]	0.730E+[illegible]0	[illegible].588E-01	0.342E+01	[illegible].147E-01	0.140E-02	0.485E+00
4.[illegible]	0.980E+[illegible]0	[illegible].691E-01	0.396E+01	[illegible].184E-01	0.157E-02	0.546E+00

Table 5d : Spectrum responses, RunNo.005
Four-float (cruciform) configuration head seas tests

Hull Float Diam/Wing Float Diam = 1.5
Float Draft/Diameter = 2.0
Damping Plate Diam/Float Diam = 1.6
Metacentric Height/$\nabla^{1/3}$ =0.15

$\frac{H_{1/3}}{\nabla^{1/3}}$	$\frac{E_z}{\nabla^{2/3}}$	$\frac{E_{\dot{z}}}{g\nabla^{1/3}}$	$\frac{z_{1/3}}{\nabla^{1/3}}$	E_θ	$\frac{E_\theta \nabla^{1/3}}{g}$	$\theta_{1/3}$
0.100	0.146E-05	0.125E-05	0.484E-02	0.227E-06	0.289E-06	0.187E-02
0.200	0.390E-03	0.217E-03	0.779E-01	0.852E-05	0.560E-05	0.117E-01
0.300	0.245E-02	0.117E-02	0.198E+00	0.488E-04	0.245E-04	0.279E-01
0.400	0.645E-02	0.279E-02	0.321E+00	0.134E-03	0.560E-04	0.464E-01
0.500	0.121E-01	0.452E-02	0.439E+00	0.276E-03	0.979E-04	0.665E-01
0.600	0.191E-01	0.643E-02	0.553E+00	0.483E-03	0.149E-03	0.880E-01
0.700	0.273E-01	0.840E-02	0.661E+00	0.749E-03	0.207E-03	0.109E+00
0.800	0.365E-01	0.104E-01	0.765E+00	0.106E-02	0.269E-03	0.130E+00
0.900	0.469E-01	0.123E-01	0.867E+00	0.143E-02	0.333E-03	0.151E+00
1.000	0.586E-01	0.143E-01	0.969E+00	0.184E-02	0.398E-03	0.171E+00
1.500	0.136E+00	0.241E-01	0.147E+01	0.447E-02	0.734E-03	0.268E+00
2.000	0.233E+00	0.335E-01	0.193E+01	0.756E-02	0.104E-02	0.348E+00
2.500	0.353E+00	0.422E-01	0.238E+01	0.109E-01	0.131E-02	0.418E+00
3.000	0.522E+00	0.514E-01	0.289E+01	0.157E-01	0.156E-02	0.490E+00
3.500	0.744E+00	0.615E-01	0.345E+01	0.209E-01	0.180E-02	0.566E+00
4.000	0.999E+00	0.729E-01	0.420E+01	0.255E-01	0.205E-02	0.639E+00

Table 5e : Spectrum responses, Run No.006
Four-float (cruciform) configuration head seas tests

Hull Float Diam/Wing Float Diam = 1.5
Float Draft/Diameter = 2.0
Damping Plate Diam/Float Diam = 1.6
Metacentric Height/$\nabla^{1/3}$ = 0.622

$\frac{H_{1/3}}{\nabla^{1/3}}$	$\frac{E_z}{\nabla^{2/3}}$	$\frac{E_{\dot{z}}}{g\nabla^{1/3}}$	$\frac{z_{1/3}}{\nabla^{1/3}}$	E_θ	$\frac{E_{\dot{\theta}}\nabla^{1/3}}{g}$	$\theta_{1/3}$
0.100	0.768E-06	0.659E-06	0.355E-02	0.272E-06	0.353E-06	0.209E-02
0.200	0.282E-03	0.155E-03	0.669E-01	0.417E-05	0.319E-05	0.810E-02
0.300	0.228E-02	0.932E-03	0.179E+00	0.199E-04	0.108E-04	0.178E-01
0.400	0.555E-02	0.225E-02	0.298E+00	0.507E-04	0.226E-04	0.285E-01
0.500	0.107E-01	0.387E-02	0.414E+00	0.998E-04	0.374E-04	0.400E-01
0.600	0.174E-01	0.566E-02	0.528E+00	0.172E-03	0.553E-04	0.525E-01
0.700	0.254E-01	0.753E-02	0.638E+00	0.269E-03	0.760E-04	0.656E-01
0.800	0.346E-01	0.943E-02	0.744E+00	0.393E-03	0.991E-04	0.793E-01
0.900	0.451E-01	0.114E-01	0.850E+00	0.551E-03	0.125E-03	0.939E-01
1.000	0.570E-01	0.133E-01	0.955E+00	0.747E-03	0.153E-03	0.109E+00
1.500	0.137E+00	0.233E-01	0.148E+01	0.224E-02	0.325E-03	0.189E+00
2.000	0.237E+00	0.329E-01	0.195E+01	0.421E-02	0.506E-03	0.260E+00
2.500	0.360E+00	0.419E-01	0.240E+01	0.647E-02	0.675E-03	0.322E+00
3.000	0.535E+00	0.514E-01	0.293E+01	0.935E-02	0.841E-03	0.387E+00
3.500	0.765E+00	0.618E-01	0.350E+01	0.129E-01	0.101E-02	0.454E+00
4.000	0.103E+01	0.727E-01	0.406E+01	0.169E-01	0.118E-02	0.519E+00

Table 5f : Spectrum responses, Run No.047
Four-float (cruciform) configuration head seas tests

Hull Float Diam/Wing Float Diam = 1.5
Float Draft/Diameter = 2.5
Damping Plate Diam/Float Diam = 1.6
Metacentric Height/$\nabla^{1/3}$ = 0.182

$\frac{H_{1/3}}{\nabla^{1/3}}$	$\frac{E_z}{\nabla^{2/3}}$	$\frac{E_{\dot{z}}}{g\nabla^{1/3}}$	$\frac{z_{1/3}}{\nabla^{1/3}}$	E_θ	$\frac{E_\theta \nabla^{1/3}}{g}$	$\theta_{1/3}$
2.1[illegible]	0.695E-[illegible]6	[illegible].542E-06	0.333E-02	[illegible].233E-06	0.332E-06	0.193E-02
[illegible].20[illegible]	0.2[illegible]4E-[illegible]3	[illegible].159E-03	0.674E-01	[illegible].255E-05	0.209E-05	0.639E-02
[illegible].32[illegible]	0.191E-[illegible]2	[illegible].926E-03	0.175E+00	[illegible].142E-04	0.745E-05	0.151E-01
[illegible].40[illegible]	0.5[illegible]8E-[illegible]2	[illegible].211E-02	0.285E+00	[illegible].403E-04	0.169E-04	0.254E-01
[illegible].50[illegible]	0.959E-02	[illegible].355E-02	0.392E+00	[illegible].835E-04	0.296E-04	0.366E-01
[illegible].60[illegible]	0.153E-01	[illegible].513E-02	0.495E+00	[illegible].148E-03	0.453E-04	0.486E-01
[illegible].70[illegible]	0.221E-01	[illegible].671E-02	0.595E+00	[illegible].234E-03	0.636E-04	0.612E-01
[illegible].80[illegible]	0.298E-01	[illegible].833E-02	0.691E+00	[illegible].344E-03	0.840E-04	0.742E-01
[illegible].90[illegible]	0.385E-01	[illegible].994E-02	0.784E+00	[illegible].480E-03	0.106E-03	0.877E-01
1.[illegible]00	0.482E-01	[illegible].116E-01	0.878E+00	[illegible].646E-03	0.131E-03	0.102E+00
1.50[illegible]	0.113E+00	[illegible].199E-01	0.134E+01	[illegible].186E-02	0.273E-03	0.172E+00
2.[illegible]00	0.198E+00	[illegible].278E-01	0.178E+01	[illegible].347E-02	0.418E-03	0.233E+00
2.52[illegible]	0.311E+00	[illegible].356E-01	0.223E+01	[illegible].523E-02	0.553E-03	0.289E+00
3.[illegible]00	0.477E+00	[illegible].443E-01	0.276E+01	[illegible].771E-02	0.691E-03	0.351E+00
3.50[illegible]	0.732E+00	[illegible].542E-01	0.335E+01	[illegible].109E-01	0.838E-03	0.418E+00
4.[illegible]00	0.963E+00	[illegible].646E-01	0.392E+01	[illegible].145E-01	0.989E-03	0.482E+00

Table 5g : Spectrum responses, Run No.032
Four-float (cruciform) configuration head seas tests

Hull Float Diam/Wing Float Diam = 1.5
Float Draft/Diameter = 1.5
Damping Plate Diam/Float Diam = 1.6
Metacentric Height/$\nabla^{1/3}$ = 0.654

$\frac{H_{1/3}}{\nabla^{1/3}}$	$\frac{E_z}{\nabla^{2/3}}$	$\frac{E_{\dot{z}}}{g\nabla^{1/3}}$	$\frac{z_{1/3}}{\nabla^{1/3}}$	E_θ	$\frac{E_{\ddot{\theta}}\nabla^{1/3}}{g}$	$\theta_{1/3}$
0.100	0.334E-05	0.286E-05	0.731E-02	0.193E-06	0.200E-06	0.176E-02
0.200	0.492E-03	0.307E-03	0.887E-01	0.974E-05	0.658E-05	0.125E-01
0.300	0.267E-02	0.135E-02	0.287E+00	0.469E-04	0.249E-04	0.274E-01
0.400	0.660E-02	0.297E-02	0.325E+00	0.115E-03	0.517E-04	0.429E-01
0.500	0.120E-01	0.466E-02	0.438E+00	0.209E-03	0.824E-04	0.579E-01
0.600	0.188E-01	0.653E-02	0.548E+00	0.326E-03	0.115E-03	0.722E-01
0.700	0.267E-01	0.844E-02	0.653E+00	0.462E-03	0.148E-03	0.860E-01
0.800	0.355E-01	0.103E-01	0.754E+00	0.618E-03	0.180E-03	0.994E-01
0.900	0.452E-01	0.122E-01	0.851E+00	0.796E-03	0.213E-03	0.113E+00
1.000	0.560E-01	0.140E-01	0.946E+00	0.100E-02	0.247E-03	0.126E+00
1.500	0.124E+00	0.229E-01	0.141E+01	0.238E-02	0.420E-03	0.195E+00
2.000	0.211E+00	0.313E-01	0.184E+01	0.408E-02	0.585E-03	0.256E+00
2.500	0.325E+00	0.393E-01	0.226E+01	0.604E-02	0.734E-03	0.311E+00
3.000	0.492E+00	0.482E-01	0.281E+01	0.857E-02	0.880E-03	0.370E+00
3.500	0.718E+00	0.581E-01	0.339E+01	0.117E-01	0.103E-02	0.434E+00
4.000	0.978E+00	0.686E-01	0.396E+01	0.153E-01	0.118E-02	0.495E+00

Table 5h : Spectrum Responses, Run No.060
Four-float (cruciform) configuration head seas tests

Hull Float Diam/Wing Float Diam = 1.25
Float Draft/Diameter = 2.0
Damping Plate Diam/Float Diam = 1.6
Metacentric Height/$\nabla^{1/3}$ = 0.232

$\frac{H_{1/3}}{\nabla^{1/3}}$	$\frac{E_z}{\nabla^{2/3}}$	$\frac{E_{\ddot{z}}}{g\nabla^{1/3}}$	$\frac{z_{1/3}}{\nabla^{1/3}}$	E_θ	$\frac{E_{\ddot{\theta}}\nabla^{1/3}}{g}$	$\theta_{1/3}$
0.100	0.212E-05	0.177E-05	0.592E-02	0.131E-06	0.157E-06	0.145E-02
0.200	0.426E-03	0.242E-03	0.806E-01	0.687E-05	0.450E-05	0.105E-01
0.300	0.229E-02	0.115E-02	0.191E+00	0.364E-04	0.187E-04	0.241E-01
0.400	0.570E-02	0.248E-02	0.302E+00	0.945E-04	0.428E-04	0.389E-01
0.500	0.105E-01	0.403E-02	0.410E+00	0.181E-03	0.678E-04	0.538E-01
0.600	0.166E-01	0.569E-02	0.515E+00	0.296E-03	0.980E-04	0.688E-01
0.700	0.239E-01	0.741E-02	0.616E+00	0.437E-03	0.130E-03	0.836E-01
0.800	0.322E-01	0.915E-02	0.717E+00	0.601E-03	0.164E-03	0.981E-01
0.900	0.416E-01	0.109E-01	0.816E+00	0.792E-03	0.198E-03	0.113E+00
1.000	0.522E-01	0.127E-01	0.914E+00	0.101E-02	0.233E-03	0.127E+00
1.500	0.123E+00	0.216E-01	0.140E+01	0.249E-02	0.418E-03	0.200E+00
2.000	0.215E+00	0.303E-01	0.186E+01	0.432E-02	0.594E-03	0.263E+00
2.500	0.333E+00	0.387E-01	0.231E+01	0.637E-02	0.752E-03	0.319E+00
3.000	0.503E+00	0.478E-01	0.284E+01	0.897E-02	0.905E-03	0.379E+00
3.500	0.730E+00	0.579E-01	0.342E+01	0.122E-01	0.106E-02	0.442E+00
4.000	0.992E+00	0.685E-01	0.398E+01	0.157E-01	0.122E-02	0.502E+00

Table 5i : Spectrum responses, Run No. 058
Four-float (cruciform) configuration head seas tests

Hull Float Diam/Wing Float Diam = 1.25
Float Draft/Diameter = 2.0
Damping Plate Diam/Float Diam = 1.4
Metacentric Height/$\nabla^{1/3}$ = 0.232

$\frac{H_{1/3}}{\nabla^{1/3}}$	$\frac{E_z}{\nabla^{2/3}}$	$\frac{E_{\dot{z}}}{g\nabla^{1/3}}$	$\frac{z_{1/3}}{\nabla^{1/3}}$	E_θ	$\frac{E_\theta \nabla^{1/3}}{g}$	$\theta_{1/3}$
0.100	0.626E-05	0.561E-05	0.100E-01	0.122E-06	0.164E-06	0.140E-02
0.200	0.592E-03	0.382E-03	0.974E-01	0.250E-05	0.181E-05	0.633E-02
0.300	0.272E-02	0.147E-02	0.289E+00	0.139E-04	0.682E-05	0.144E-01
0.400	0.626E-02	0.291E-02	0.316E+00	0.354E-04	0.150E-04	0.238E-01
0.500	0.111E-01	0.459E-02	0.421E+00	0.767E-04	0.267E-04	0.350E-01
0.600	0.171E-01	0.617E-02	0.523E+00	0.143E-03	0.422E-04	0.479E-01
0.700	0.242E-01	0.788E-02	0.623E+00	0.236E-03	0.611E-04	0.614E-01
0.800	0.323E-01	0.960E-02	0.719E+00	0.354E-03	0.827E-04	0.752E-01
0.900	0.416E-01	0.113E-01	0.816E+00	0.498E-03	0.106E-03	0.893E-01
1.000	0.522E-01	0.131E-01	0.914E+00	0.673E-03	0.132E-03	0.104E+00
1.500	0.124E+00	0.221E-01	0.141E+01	0.194E-02	0.281E-03	0.176E+00
2.000	0.218E+00	0.309E-01	0.197E+01	0.357E-02	0.433E-03	0.239E+00
2.500	0.336E+00	0.394E-01	0.232E+01	0.548E-02	0.575E-03	0.296E+00
3.000	0.506E+00	0.485E-01	0.284E+01	0.791E-02	0.715E-03	0.356E+00
3.500	0.730E+00	0.585E-01	0.342E+01	0.109E-01	0.859E-03	0.418E+00
4.000	0.988E+00	0.697E-01	0.398E+01	0.142E-01	0.100E-02	0.477E+00

Table 5j : Spectrum Responses, Run No.062
Four-float (cruciform) configuration head seas tests

Hull Float Diam/Wing Float Diam = 1.25
raft/Diameter = 2.0
Dampin /Float Diam = 1.8
eight/$\nabla^{1/3}$ = 0.232

$\frac{H_{1/3}}{\nabla^{1/3}}$	$\frac{E_z}{\nabla^{2/3}}$	$\frac{E_{\dot{z}}}{g\nabla^{1/3}}$	$\frac{\ddot{}^{1/3}}{\nabla^{1/3}}$	E_θ	$\frac{E_\theta \nabla^{1/3}}{g}$	$\theta_{1/3}$
0.10?	0.364E-06	?.30?E-06	0.241E-02	?.305E-06	0.347E-06	?.221E-02
0.20?	0.195E-03	?.991E-04	0.544E-01	?.11?E-04	0.762E-05	0.133E-01
0.30?	0.153E-?2	?.684E-03	0.157E+0?	?.549E-04	0.289E-04	0.296E-01
0.40?	0.456E-?2	?.17?E-02	0.270E+00	?.143E-03	0.622E-04	0.479E-01
0.50?	0.913E-?2	?.318E-02	0.382E+00	?.28?E-03	0.104E-03	0.670E-01
0.60?	0.151E-01	?.475E-02	0.491E+0?	0.468E-03	0.152E-03	0.865E-01
0.70?	0.222E-01	?.64?E-02	0.595E+00	?.70?E-03	0.205E-03	0.106E+00
?.80?	0.3?3E-?1	?.?08E-02	0.696E+00	?.973E-03	0.260E-03	0.125E+00
?.90?	0.395E-?1	?.977E-02	0.795E+00	?.129E-02	0.316E-03	0.144E+00
1.00?	0.5?0E-01	?.115E-01	0.894E+00	?.165E-02	0.374E-03	0.162E+00
1.50?	0.121E+0?	?.204E-01	0.139E+01	?.399E-02	0.670E-03	0.253E+00
2.00?	0.212E+00	?.29?E-01	0.184E+01	?.67?E-02	0.945E-03	0.329E+00
2.50?	0.327E+?0	?.373E-01	0.229E+01	?.984E-02	0.119E-?2	0.397E+00
3.00?	0.491E+?0	?.461E-01	0.280E+01	0.136E-01	0.141E-02	0.466E+00
3.50?	0.7?9E+?0	?.55?E-01	0.337E+01	?.181E-01	0.164E-?2	0.538E+00
4.00?	0.959E+?0	?.46?E-01	2.392E+01	?.23?E-01	0.186E-?2	0.606E+00

Table 5k : Spectrum responses, Run No.066
Four-float (cruciform) configuration head seas tests

Hull Float Diam/Wing Float Diam = 1.25
Float Draft/Diameter = 2.0
Damping Plate Diam/Float Diam = 1.4
Metacentric Height/$\nabla^{1/3}$ =0.78

$\frac{H_{1/3}}{\nabla^{1/3}}$	$\frac{E_z}{\nabla^{2/3}}$	$\frac{E_{\dot{z}}}{g\nabla^{1/3}}$	$\frac{z_{1/3}}{\nabla^{1/3}}$	E_θ	$\frac{E_\theta \nabla^{1/3}}{g}$	$\theta_{1/3}$
0.100	0.232E-05	0.198E-05	0.629E-02	0.157E-06	0.204E-06	0.155E-02
0.200	0.335E-03	0.207E-03	0.732E-01	0.155E-05	0.138E-05	0.498E-02
0.300	0.173E-02	0.892E-03	0.167E+00	0.717E-05	0.395E-05	0.107E-01
0.400	0.427E-02	0.189E-02	0.261E+00	0.251E-04	0.968E-05	0.200E-01
0.500	0.792E-02	0.305E-02	0.356E+00	0.667E-04	0.202E-04	0.327E-01
0.600	0.127E-01	0.433E-02	0.451E+00	0.149E-03	0.363E-04	0.474E-01
0.700	0.186E-01	0.569E-02	0.545E+00	0.246E-03	0.571E-04	0.628E-01
0.800	0.254E-01	0.709E-02	0.638E+00	0.384E-03	0.815E-04	0.784E-01
0.900	0.334E-01	0.852E-02	0.731E+00	0.556E-03	0.109E-03	0.943E-01
1.000	0.427E-01	0.100E-01	0.827E+00	0.766E-03	0.139E-03	0.111E+00
1.500	0.107E+00	0.179E-01	0.131E+01	0.231E-02	0.318E-03	0.192E+00
2.000	0.191E+00	0.258E-01	0.175E+01	0.432E-02	0.505E-03	0.263E+00
2.500	0.298E+00	0.334E-01	0.218E+01	0.666E-02	0.678E-03	0.326E+00
3.000	0.452E+00	0.415E-01	0.269E+01	0.963E-02	0.850E-03	0.393E+00
3.500	0.657E+00	0.507E-01	0.324E+01	0.133E-01	0.103E-02	0.461E+00
4.000	0.893E+00	0.603E-01	0.378E+01	0.174E-01	0.120E-02	0.527E+00

Table 5ℓ : Spectrum responses, Run No. 064
Four-float (cruciform) configuration head seas tests

Hull Float Diam/Wing Float Diam = 1.25
Float Draft/Diameter = 2.0
Damping Plate Diam/Float Diam = 1.8
Metacentric Height/$\nabla^{1/3}$ = 0.78

$\frac{H_{1/3}}{\nabla^{1/3}}$	$\frac{E_z}{\nabla^{2/3}}$	$\frac{E_{\dot{z}}}{g\nabla^{1/3}}$	$\frac{z_{1/3}}{\nabla^{1/3}}$	E_θ	$\frac{E_\theta \nabla^{1/3}}{g}$	$\theta_{1/3}$
0.100	0.282E-06	0.219E-06	0.212E-02	0.257E-06	0.339E-06	0.203E-02
0.200	0.154E-03	0.828E-04	0.497E-01	0.768E-05	0.526E-05	0.111E-01
0.300	0.126E-02	0.563E-03	0.142E+00	0.422E-04	0.216E-04	0.260E-01
0.400	0.375E-02	0.146E-02	0.245E+00	0.111E-03	0.477E-04	0.422E-01
0.500	0.761E-02	0.263E-02	0.349E+00	0.211E-03	0.793E-04	0.581E-01
0.600	0.128E-01	0.397E-02	0.452E+00	0.336E-03	0.113E-03	0.734E-01
0.700	0.191E-01	0.541E-02	0.553E+00	0.483E-03	0.148E-03	0.879E-01
0.800	0.264E-01	0.699E-02	0.650E+00	0.649E-03	0.183E-03	0.102E+00
0.900	0.348E-01	0.841E-02	0.746E+00	0.837E-03	0.218E-03	0.116E+00
1.000	0.444E-01	0.996E-02	0.843E+00	0.105E-02	0.254E-03	0.130E+00
1.500	0.110E+00	0.181E-01	0.133E+01	0.250E-02	0.436E-03	0.200E+00
2.000	0.195E+00	0.261E-01	0.177E+01	0.431E-02	0.610E-03	0.263E+00
2.500	0.302E+00	0.338E-01	0.220E+01	0.640E-02	0.769E-03	0.320E+00
3.000	0.456E+00	0.427E-01	0.270E+01	0.906E-02	0.924E-03	0.381E+00
3.500	0.662E+00	0.512E-01	0.325E+01	0.124E-01	0.108E-02	0.445E+00
4.000	0.898E+00	0.608E-01	0.379E+01	0.160E-01	0.124E-02	0.507E+00

Table 5m : Spectrum responses, Run No.003
Four-float (cruciform) configuration beam seas tests

Hull Float Diam/Wing Float Diam = 1.5
Float Draft/Diameter = 2.0
Damping Plate Diam/Float Diam = 1.6
Metacentric Height/$\nabla^{1/3}$ = 0.198

$\frac{H_{1/3}}{\nabla^{1/3}}$	$\frac{E_z}{\nabla^{2/3}}$	$\frac{E_{\dot{z}}}{g\nabla^{1/3}}$	$\frac{z_{1/3}}{\nabla^{1/3}}$	E_φ	$\frac{E_\varphi \nabla^{1/3}}{g}$	$\varphi_{1/3}$
0.100	0.133E-05	0.111E-05	0.462E-02	0.311E-05	0.390E-05	0.705E-02
0.200	0.399E-03	0.221E-03	0.789E-01	0.435E-04	0.375E-04	0.264E-01
0.300	0.254E-02	0.121E-02	0.202E+00	0.131E-03	0.884E-04	0.458E-01
0.400	0.675E-02	0.281E-02	0.329E+00	0.253E-03	0.143E-03	0.636E-01
0.500	0.127E-01	0.472E-02	0.452E+00	0.397E-03	0.196E-03	0.797E-01
0.600	0.204E-01	0.682E-02	0.572E+00	0.555E-03	0.245E-03	0.943E-01
0.700	0.295E-01	0.894E-02	0.687E+00	0.725E-03	0.291E-03	0.108E+00
0.800	0.399E-01	0.111E-01	0.799E+00	0.906E-03	0.334E-03	0.120E+00
0.900	0.518E-01	0.133E-01	0.910E+00	0.111E-02	0.374E-03	0.133E+00
1.000	0.653E-01	0.155E-01	0.102E+01	0.133E-02	0.414E-03	0.146E+00
1.500	0.156E+00	0.279E-01	0.158E+01	0.282E-02	0.608E-03	0.213E+00
2.000	0.269E+00	0.379E-01	0.208E+01	0.472E-02	0.791E-03	0.275E+00
2.500	0.421E+00	0.478E-01	0.253E+01	0.693E-02	0.958E-03	0.333E+00
3.000	0.572E+00	0.576E-01	0.302E+01	0.981E-02	0.112E-02	0.396E+00
3.500	0.786E+00	0.679E-01	0.355E+01	0.134E-01	0.130E-02	0.463E+00
4.000	0.103E+01	0.781E-01	0.405E+01	0.174E-01	0.147E-02	0.528E+00

Table 5n : Spectrum responses, Run No.010
Four-float (cruciform) configuration beam seas tests

Hull Float Diam/Wing Float Diam = 1.5
Float Draft/Diameter = 2.0
Damping Plate Diam/Float Diam = 1.4
Metacentric Height/$\nabla^{1/3}$ = 0.198

$\frac{H_{1/3}}{\nabla^{1/3}}$	$\frac{E_z}{\nabla^{2/3}}$	$\frac{E_{\dot{z}}}{g\nabla^{1/3}}$	$\frac{z_{1/3}}{\nabla^{1/3}}$	E_φ	$\frac{E_\varphi \nabla^{1/3}}{g}$	$\varphi_{1/3}$
0.100	0.358E-05	0.301E-05	0.757E-02	0.331E-05	0.419E-05	0.728E-02
0.200	0.486E-03	0.301E-03	0.882E-01	0.385E-04	0.352E-04	0.248E-01
0.300	0.252E-02	0.130E-02	0.221E+00	0.977E-04	0.729E-04	0.395E-01
0.400	0.616E-02	0.273E-02	0.314E+00	0.172E-03	0.108E-03	0.521E-01
0.500	0.112E-01	0.438E-02	0.423E+00	0.257E-03	0.140E-03	0.641E-01
0.600	0.175E-01	0.612E-02	0.530E+00	0.365E-03	0.172E-03	0.764E-01
0.700	0.250E-01	0.798E-02	0.632E+00	0.496E-03	0.204E-03	0.891E-01
0.800	0.334E-01	0.968E-02	0.731E+00	0.652E-03	0.236E-03	0.102E+00
0.900	0.429E-01	0.115E-01	0.828E+00	0.836E-03	0.270E-03	0.116E+00
1.000	0.536E-01	0.132E-01	0.926E+00	0.105E-02	0.304E-03	0.130E+00
1.500	0.125E+00	0.223E-01	0.141E+01	0.258E-02	0.491E-03	0.203E+00
2.000	0.216E+00	0.310E-01	0.196E+01	0.454E-02	0.676E-03	0.269E+00
2.500	0.331E+00	0.393E-01	0.230E+01	0.687E-02	0.846E-03	0.330E+00
3.000	0.494E+00	0.487E-01	0.281E+01	0.971E-02	0.101E-02	0.394E+00
3.500	0.709E+00	0.577E-01	0.337E+01	0.133E-01	0.119E-02	0.462E+00
4.000	0.957E+00	0.679E-01	0.391E+01	0.174E-01	0.136E-02	0.527E+00

Table 5o : Spectrum responses, Run No.017
Four-float (cruciform) configuration beam seas tests

Hull Float Diam/Wing Float Diam = 1.5
Float Draft/Diameter = 2.0
Damping Plate Diam/Float Diam = 1.8
Metacentric Height/$\nabla^{1/3}$ = 0.198

$\frac{H_{1/3}}{\nabla^{1/3}}$	$\frac{E_z}{\nabla^{2/3}}$	$\frac{E_{\dot{z}}}{g\nabla^{1/3}}$	$\frac{z_{1/3}}{\nabla^{1/3}}$	E_φ	$\frac{E_\varphi \nabla^{1/3}}{g}$	$\varphi_{1/3}$
0.100	0.621E-06	0.594E-06	0.315E-02	0.228E-05	0.266E-05	0.593E-02
0.200	0.163E-03	0.879E-04	0.511E-01	0.358E-04	0.298E-04	0.239E-01
0.300	0.140E-02	0.617E-03	0.149E+00	0.116E-03	0.748E-04	0.430E-01
0.400	0.429E-02	0.165E-02	0.262E+00	0.238E-03	0.127E-03	0.617E-01
0.500	0.899E-02	0.303E-02	0.379E+00	0.401E-03	0.182E-03	0.801E-01
0.600	0.156E-01	0.470E-02	0.500E+00	0.608E-03	0.240E-03	0.986E-01
0.700	0.241E-01	0.656E-02	0.621E+00	0.853E-03	0.299E-03	0.117E+00
0.800	0.341E-01	0.854E-02	0.739E+00	0.113E-02	0.358E-03	0.135E+00
0.900	0.459E-01	0.106E-01	0.857E+00	0.145E-02	0.417E-03	0.152E+00
1.000	0.594E-01	0.127E-01	0.975E+00	0.181E-02	0.477E-03	0.170E+00
1.500	0.151E+00	0.241E-01	0.156E+01	0.419E-02	0.780E-03	0.259E+00
2.000	0.268E+00	0.351E-01	0.227E+01	0.716E-02	0.107E-02	0.338E+00
2.500	0.409E+00	0.455E-01	0.256E+01	0.105E-01	0.132E-02	0.410E+00
3.000	0.606E+00	0.563E-01	0.311E+01	0.146E-01	0.157E-02	0.483E+00
3.500	0.862E+00	0.680E-01	0.371E+01	0.194E-01	0.181E-02	0.558E+00
4.000	0.115E+01	0.801E-01	0.430E+01	0.247E-01	0.205E-02	0.629E+00

Table 5p : Spectrum Responses, Run No.004
Four-float (cruciform) configuration beam seas tests

Hull Float Diam/Wing Float Diam = 1.5
Float Draft/Diameter = 2.0
Damping Plate Diam/Float Diam = 1.6
Metacentric Height/$\nabla^{1/3}$ =~0.05

$\frac{H_{1/3}}{\nabla^{1/3}}$	$\frac{E_z}{\nabla^{2/3}}$	$\frac{E_{\dot{z}}}{g\nabla^{1/3}}$	$\frac{z_{1/3}}{\nabla^{1/3}}$	E_φ	$\frac{E_\varphi \nabla^{1/3}}{g}$	$\varphi_{1/3}$
0.10?	0.146E-?5	?.139E-05	0.483E-?2	?.263E-05	0.328E-05	0.649E-02
?.20?	0.355E-?3	?.201E-03	0.754E-?1	?.381E-04	0.322E-?4	0.247E-01
?.30?	0.239E-?2	?.113E-02	0.196E+?0	?.124E-03	0.804E-?4	0.445E-01
?.40?	0.649E-?2	?.267E-02	0.322E+?0	?.256E-03	0.137E-?3	0.640E-01
?.50?	0.124E-?1	?.454E-02	0.445E+?0	?.431E-03	0.196E-?3	0.830E-01
?.60?	0.199E-?1	?.657E-02	0.565E+?0	?.645E-03	0.257E-?3	0.102E+?0
?.70?	0.289E-?1	?.869E-02	0.680E+?0	?.895E-03	0.318E-?3	0.120E+?0
?.80?	0.392E-?1	?.108E-01	0.792E+?0	?.118E-02	0.379E-?3	0.137E+?0
?.90?	0.509E-?1	?.132E-01	0.902E+?0	?.149E-02	0.439E-?3	0.154E+?0
1.00?	0.643E-?1	?.152E-01	0.101E+01	?.184E-02	0.498E-?3	0.172E+?0
1.50?	0.154E+?0	?.265E-01	0.157E+01	?.408E-02	0.790E-?3	0.255E+?0
2.00?	0.267E+?0	?.373E-01	0.207E+01	?.674E-02	0.105E-?2	0.328E+?0
2.50?	0.403E+?0	?.474E-01	0.254E+01	?.965E-02	0.129E-?2	0.393E+?0
3.00?	0.588E+?0	?.577E-01	0.307E+01	?.132E-01	0.150E-?2	0.460E+?0
3.50?	0.829E+?0	?.687E-01	0.364E+01	?.175E-01	0.172E-?2	0.529E+?0
4.00?	0.110E+?1	?.801E-01	0.420E+01	?.222E-01	0.193E-02	0.596E+?0

Table 5q : Spectrum responses, Run No.007
Four-float (cruciform) configuration beam seas tests

Hull Float Diam/Wing Float Diam = 1.5
Float Draft/Diameter = 2.0
Damping Plate Diam/Float Diam = 1.6
Metacentric Height/$\nabla^{1/3}$ = 0.747

$\frac{H_{1/3}}{\nabla^{1/3}}$	$\frac{E_z}{\nabla^{2/3}}$	$\frac{E_{\dot{z}}}{g\nabla^{1/3}}$	$\frac{z_{1/3}}{\nabla^{1/3}}$	E_φ	$\frac{E_{\dot{\varphi}}\nabla^{1/3}}{g}$	$\varphi_{1/3}$
0.100	0.102E-05	0.934E-06	0.405E-02	0.337E-05	0.425E-05	0.734E-02
0.200	0.283E-03	0.159E-03	0.673E-01	0.395E-04	0.359E-04	0.251E-01
0.300	0.196E-02	0.920E-03	0.177E+00	0.101E-03	0.752E-04	0.403E-01
0.400	0.538E-02	0.229E-02	0.293E+00	0.176E-03	0.111E-03	0.530E-01
0.500	0.104E-01	0.377E-02	0.408E+00	0.265E-03	0.145E-03	0.652E-01
0.600	0.169E-01	0.551E-02	0.520E+00	0.378E-03	0.178E-03	0.778E-01
0.700	0.248E-01	0.734E-02	0.630E+00	0.515E-03	0.211E-03	0.908E-01
0.800	0.339E-01	0.921E-02	0.737E+00	0.679E-03	0.245E-03	0.104E+00
0.900	0.444E-01	0.111E-01	0.843E+00	0.871E-03	0.280E-03	0.118E+00
1.000	0.565E-01	0.131E-01	0.951E+00	0.111E-02	0.316E-03	0.133E+00
1.500	0.139E+00	0.233E-01	0.149E+01	0.272E-02	0.511E-03	0.208E+00
2.000	0.244E+00	0.333E-01	0.198E+01	0.477E-02	0.706E-03	0.276E+00
2.500	0.375E+00	0.427E-01	0.245E+01	0.719E-02	0.887E-03	0.339E+00
3.000	0.558E+00	0.527E-01	0.299E+01	0.103E-01	0.107E-02	0.406E+00
3.500	0.800E+00	0.636E-01	0.358E+01	0.142E-01	0.125E-02	0.476E+00
4.000	0.108E+01	0.758E-01	0.415E+01	0.185E-01	0.144E-02	0.544E+00

Table 5r : Spectrum responses, Run No.046
Four-float (cruciform) configuration beam seas tests

Hull Float Diam/Wing Float Diam = 1.5
Float Draft/Diameter = 2.5
Damping Plate Diam/Float Diam = 1.6
Metacentric Height/$\nabla^{1/3}$ = 0.182

$\frac{H_{1/3}}{\nabla^{1/3}}$	$\frac{E_z}{\nabla^{2/3}}$	$\frac{E_{\dot{z}}}{g\nabla^{1/3}}$	$\frac{z_{1/3}}{\nabla^{1/3}}$	E_φ	$\frac{E_\varphi \nabla^{1/3}}{g}$	$\varphi_{1/3}$
0.100	0.505E-06	0.395E-06	0.294E-02	0.496E-06	0.640E-06	0.282E-02
0.200	0.216E-03	0.128E-03	0.586E-01	0.606E-05	0.536E-05	0.985E-02
0.300	0.145E-02	0.689E-03	0.153E+00	0.179E-04	0.123E-04	0.169E-01
0.400	0.387E-02	0.161E-02	0.249E+00	0.348E-04	0.198E-04	0.236E-01
0.500	0.734E-02	0.271E-02	0.343E+00	0.561E-04	0.273E-04	0.300E-01
0.600	0.118E-01	0.391E-02	0.435E+00	0.827E-04	0.348E-04	0.362E-01
0.700	0.172E-01	0.517E-02	0.524E+00	0.112E-03	0.423E-04	0.424E-01
0.800	0.234E-01	0.645E-02	0.611E+00	0.147E-03	0.497E-04	0.485E-01
0.900	0.304E-01	0.774E-02	0.698E+00	0.187E-03	0.572E-04	0.547E-01
1.000	0.386E-01	0.906E-02	0.786E+00	0.233E-03	0.648E-04	0.611E-01
1.500	0.943E-01	0.162E-01	0.123E+01	0.558E-03	0.105E-03	0.945E-01
2.000	0.168E+00	0.229E-01	0.164E+01	0.979E-03	0.145E-03	0.125E+00
2.500	0.263E+00	0.295E-01	0.205E+01	0.149E-02	0.182E-03	0.154E+00
3.000	0.422E+00	0.369E-01	0.254E+01	0.217E-02	0.220E-03	0.186E+00
3.500	0.588E+00	0.451E-01	0.307E+01	0.303E-02	0.260E-03	0.220E+00
4.000	0.873E+00	0.538E-01	0.359E+01	0.401E-02	0.301E-03	0.253E+00

Table 5s : Spectrum responses, Run No.031
Four-float (cruciform) configuration beam seas tests

Hull Float Diam/Wing Float Diam = 1.5
Float Draft/Diameter = 1.5
Damping Plate Diam/Float Diam = 1.6
Metacentric Height/$\nabla^{1/3}$ = 0.250

$\frac{H_{1/3}}{\nabla^{1/3}}$	$\frac{E_z}{\nabla^{2/3}}$	$\frac{E_{\dot{z}}}{g\nabla^{1/3}}$	$\frac{z_{1/3}}{\nabla^{1/3}}$	E_φ	$\frac{E_\varphi \nabla^{1/3}}{g}$	$\varphi_{1/3}$
0.100	0.365E-05	0.349E-05	0.764E-02	0.394E-05	0.478E-05	0.794E-02
0.200	0.477E-03	0.289E-03	0.873E-01	0.558E-04	0.485E-04	0.299E-01
0.300	0.261E-02	0.132E-02	0.285E+00	0.154E-03	0.109E-03	0.497E-01
0.400	0.645E-02	0.283E-02	0.321E+00	0.287E-03	0.168E-03	0.669E-01
0.500	0.117E-01	0.456E-02	0.434E+00	0.438E-03	0.223E-03	0.830E-01
0.600	0.184E-01	0.639E-02	0.542E+00	0.609E-03	0.277E-03	0.987E-01
0.700	0.262E-01	0.826E-02	0.647E+00	0.816E-03	0.329E-03	0.114E+00
0.800	0.350E-01	0.101E-01	0.748E+00	0.105E-02	0.380E-03	0.130E+00
0.900	0.449E-01	0.120E-01	0.848E+00	0.131E-02	0.431E-03	0.145E+00
1.000	0.562E-01	0.139E-01	0.948E+00	0.161E-02	0.481E-03	0.160E+00
1.500	0.130E+00	0.233E-01	0.144E+01	0.355E-02	0.732E-03	0.238E+00
2.000	0.225E+00	0.324E-01	0.190E+01	0.591E-02	0.963E-03	0.308E+00
2.500	0.345E+00	0.410E-01	0.235E+01	0.859E-02	0.117E-02	0.371E+00
3.000	0.516E+00	0.502E-01	0.297E+01	0.120E-01	0.137E-02	0.438E+00
3.500	0.745E+00	0.604E-01	0.345E+01	0.161E-01	0.157E-02	0.508E+00
4.000	0.101E+01	0.711E-01	0.401E+01	0.207E-01	0.177E-02	0.576E+00

Table 5t : Spectrum responses, Run No.074
Three-float (triangular) configuration head seas tests

Float Draft/Diameter = 4.0
Damping Plate Diam/Float Diam = 1.6
Metacentric Height/$\nabla^{1/3}$ = 0.271

$\frac{H_{1/3}}{\nabla^{1/3}}$	$\frac{E_z}{\nabla^{2/3}}$	$\frac{E_{\dot{z}}}{g\nabla^{1/3}}$	$\frac{z_{1/3}}{\nabla^{1/3}}$	E_θ	$\frac{E_{\dot{\theta}}\nabla^{1/3}}{g}$	$\theta_{1/3}$
0.100	0.534E-06	0.642E-06	0.292E-02	0.895E-06	0.114E-05	0.378E-02
0.200	0.717E-04	0.375E-04	0.339E-01	0.119E-04	0.102E-04	0.138E-01
0.300	0.781E-03	0.325E-03	0.112E+00	0.433E-04	0.267E-04	0.263E-01
0.400	0.272E-02	0.987E-03	0.208E+00	0.104E-03	0.500E-04	0.407E-01
0.500	0.678E-02	0.194E-02	0.312E+00	0.205E-03	0.800E-04	0.572E-01
0.600	0.110E-01	0.313E-02	0.419E+00	0.361E-03	0.118E-03	0.761E-01
0.700	0.172E-01	0.449E-02	0.525E+00	0.579E-03	0.163E-03	0.963E-01
0.800	0.247E-01	0.594E-02	0.629E+00	0.863E-03	0.215E-03	0.118E+00
0.900	0.336E-01	0.748E-02	0.733E+00	0.122E-02	0.272E-03	0.140E+00
1.000	0.439E-01	0.908E-02	0.838E+00	0.167E-02	0.337E-03	0.164E+00
1.500	0.116E+00	0.178E-01	0.136E+01	0.507E-02	0.727E-03	0.285E+00
2.000	0.211E+00	0.267E-01	0.184E+01	0.946E-02	0.114E-02	0.389E+00
2.500	0.331E+00	0.352E-01	0.230E+01	0.144E-01	0.151E-02	0.479E+00
3.000	0.532E+00	0.443E-01	0.283E+01	0.203E-01	0.186E-02	0.570E+00
3.500	0.729E+00	0.545E-01	0.342E+01	0.274E-01	0.222E-02	0.663E+00
4.000	0.990E+00	0.651E-01	0.398E+01	0.352E-01	0.256E-02	0.751E+00

Table 5u : Spectrum responses, Run No. 091
Three-float (triangular) configuration head seas tests

Float Draft/Diameter = 4.0
Damping Plate Diam/Float Diam = 1.4
Metacentric Height/$\nabla^{1/3}$ = 0.271

$\frac{H_{1/3}}{\nabla^{1/3}}$	$\frac{E_z}{\nabla^{2/3}}$	$\frac{E_{\dot{z}}}{g\nabla^{1/3}}$	$\frac{z_{1/3}}{\nabla^{1/3}}$	E_θ	$\frac{E_\theta \nabla^{1/3}}{g}$	$\theta_{1/3}$
0.100	0.583E-06	0.555E-06	0.305E-02	0.174E-05	0.212E-05	0.527E-02
0.200	0.162E-03	0.882E-04	0.589E-01	0.232E-04	0.282E-04	0.193E-01
0.300	0.127E-02	0.576E-03	0.143E+00	0.727E-04	0.481E-04	0.341E-01
0.400	0.370E-02	0.146E-02	0.243E+00	0.154E-03	0.819E-04	0.496E-01
0.500	0.743E-02	0.260E-02	0.345E+00	0.265E-03	0.119E-03	0.651E-01
0.600	0.125E-01	0.399E-02	0.447E+00	0.404E-03	0.158E-03	0.804E-01
0.700	0.197E-01	0.531E-02	0.547E+00	0.567E-03	0.197E-03	0.952E-01
0.800	0.260E-01	0.678E-02	0.646E+00	0.754E-03	0.237E-03	0.110E+00
0.900	0.346E-01	0.831E-02	0.744E+00	0.970E-03	0.276E-03	0.125E+00
1.000	0.446E-01	0.988E-02	0.845E+00	0.122E-02	0.317E-03	0.140E+00
1.500	0.115E+00	0.184E-01	0.136E+01	0.289E-02	0.527E-03	0.215E+00
2.000	0.238E+00	0.271E-01	0.182E+01	0.495E-02	0.727E-03	0.281E+00
2.500	0.326E+00	0.354E-01	0.228E+01	0.725E-02	0.905E-03	0.340E+00
3.000	0.497E+00	0.445E-01	0.282E+01	0.101E-01	0.107E-02	0.402E+00
3.500	0.723E+00	0.546E-01	0.340E+01	0.135E-01	0.125E-02	0.465E+00
4.000	0.993E+00	0.652E-01	0.397E+01	0.173E-01	0.141E-02	0.527E+00

Table 5v : Spectrum responses, Run No.087
Three-float (triangular) configuration head seas tests

Float Draft/Diameter = 4.0
Damping Plate Diam/Float Diam = 1.8
Metacentric Height/$\nabla^{1/3}$ = 0.271

$\frac{H_{1/3}}{\nabla^{1/3}}$	$\frac{E_z}{\nabla^{2/3}}$	$\frac{E_{\dot{z}}}{g\nabla^{1/3}}$	$\frac{z_{1/3}}{\nabla^{1/3}}$	E_θ	$\frac{E_\theta \nabla^{1/3}}{g}$	$\theta_{1/3}$
0.100	0.496E-07	0.453E-07	0.890E-03	0.104E-05	0.130E-05	0.408E-02
0.200	0.410E-04	0.201E-04	0.256E-01	0.169E-04	0.132E-04	0.160E-01
0.300	0.522E-03	0.209E-03	0.914E-01	0.628E-04	0.368E-04	0.315E-01
0.400	0.270E-02	0.691E-03	0.179E+00	0.155E-03	0.720E-04	0.498E-01
0.500	0.481E-02	0.146E-02	0.278E+00	0.319E-03	0.118E-03	0.704E-01
0.600	0.909E-02	0.247E-02	0.381E+00	0.539E-03	0.174E-03	0.928E-01
0.700	0.147E-01	0.366E-02	0.485E+00	0.842E-03	0.239E-03	0.116E+00
0.800	0.216E-01	0.496E-02	0.587E+00	0.122E-02	0.311E-03	0.140E+00
0.900	0.297E-01	0.634E-02	0.689E+00	0.167E-02	0.387E-03	0.164E+00
1.000	0.392E-01	0.781E-02	0.792E+00	0.221E-02	0.469E-03	0.188E+00
1.500	0.107E+00	0.159E-01	0.131E+01	0.591E-02	0.919E-03	0.308E+00
2.000	0.197E+00	0.242E-01	0.177E+01	0.104E-01	0.135E-02	0.407E+00
2.500	0.313E+00	0.323E-01	0.224E+01	0.151E-01	0.173E-02	0.492E+00
3.000	0.482E+00	0.413E-01	0.278E+01	0.208E-01	0.206E-02	0.577E+00
3.500	0.778E+00	0.512E-01	0.336E+01	0.276E-01	0.242E-02	0.664E+00
4.000	0.967E+00	0.617E-01	0.393E+01	0.357E-01	0.275E-02	0.748E+00

Table 5w : Spectrum responses, Run No.075
Three-float (triangular) configuration head seas tests

Float Draft/Diameter = 4.0
Damping Plate Diam/Float Diam = 1.6
Metacentric Height/$\nabla^{1/3}$ = ~1.0

$\frac{H_{1/3}}{\nabla^{1/3}}$	$\frac{E_z}{\nabla^{2/3}}$	$\frac{E_{\dot{z}}}{g\nabla^{1/3}}$	$\frac{z_{1/3}}{\nabla^{1/3}}$	E_θ	$\frac{E_{\dot{\theta}}\nabla^{1/3}}{g}$	$\theta_{1/3}$
0.100	0.510E-06	0.574E-06	0.286E-02	0.767E-06	0.878E-06	0.349E-02
0.200	0.543E-04	0.296E-04	0.295E-01	0.149E-04	0.117E-04	0.155E-01
0.300	0.592E-03	0.245E-03	0.973E-01	0.656E-04	0.366E-04	0.324E-01
0.400	0.215E-02	0.763E-03	0.186E+00	0.184E-03	0.787E-04	0.543E-01
0.500	0.495E-02	0.155E-02	0.281E+00	0.422E-03	0.143E-03	0.821E-01
0.600	0.903E-02	0.254E-02	0.380E+00	0.822E-03	0.234E-03	0.115E+00
0.700	0.143E-01	0.368E-02	0.478E+00	0.137E-02	0.345E-03	0.148E+00
0.800	0.277E-01	0.490E-02	0.575E+00	0.205E-02	0.471E-03	0.181E+00
0.900	0.293E-01	0.620E-02	0.673E+00	0.284E-02	0.606E-03	0.213E+00
1.000	0.372E-01	0.758E-02	0.772E+00	0.373E-02	0.745E-03	0.244E+00
1.500	0.171E+00	0.152E-01	0.127E+01	0.935E-02	0.146E-02	0.387E+00
2.000	0.185E+00	0.230E-01	0.172E+01	0.156E-01	0.210E-02	0.500E+00
2.500	0.293E+00	0.306E-01	0.217E+01	0.227E-01	0.263E-02	0.593E+00
3.000	0.450E+00	0.389E-01	0.268E+01	0.292E-01	0.309E-02	0.683E+00
3.500	0.659E+00	0.482E-01	0.325E+01	0.374E-01	0.353E-02	0.773E+00
4.000	0.970E+00	0.579E-01	0.380E+01	0.461E-01	0.395E-02	0.859E+00

Table 5x : Spectrum responses, Run No.096
Three-float (triangular) configuration head seas tests

Float Draft/Diameter = 5.0
Damping Plate Diam/Float Diam = 1.6
Metacentric Height/$\nabla^{1/3}$ = 0.300

$\frac{H_{1/3}}{\nabla^{1/3}}$	$\frac{E_z}{\nabla^{2/3}}$	$\frac{E_{\dot{z}}}{g\nabla^{1/3}}$	$\frac{z_{1/3}}{\nabla^{1/3}}$	E_θ	$\frac{E_{\dot{\theta}}\nabla^{1/3}}{g}$	$\theta_{1/3}$
0.100	0.284E-06	0.315E-06	0.213E-02	0.927E-06	0.109E-05	0.384E-02
0.200	0.324E-04	0.161E-04	0.221E-01	0.145E-04	0.122E-04	0.152E-01
0.300	0.463E-03	0.177E-03	0.861E-01	0.509E-04	0.316E-04	0.285E-01
0.400	0.283E-02	0.667E-03	0.180E+00	0.121E-03	0.587E-04	0.440E-01
0.500	0.510E-02	0.149E-02	0.286E+00	0.242E-03	0.942E-04	0.623E-01
0.600	0.971E-02	0.258E-02	0.394E+00	0.431E-03	0.139E-03	0.831E-01
0.700	0.157E-01	0.386E-02	0.501E+00	0.695E-03	0.194E-03	0.105E+00
0.800	0.230E-01	0.524E-02	0.606E+00	0.103E-02	0.256E-03	0.129E+00
0.900	0.316E-01	0.671E-02	0.711E+00	0.146E-02	0.325E-03	0.153E+00
1.000	0.417E-01	0.827E-02	0.816E+00	0.198E-02	0.401E-03	0.178E+00
1.500	0.113E+00	0.168E-01	0.134E+01	0.576E-02	0.843E-03	0.304E+00
2.000	0.227E+00	0.255E-01	0.182E+01	0.104E-01	0.129E-02	0.411E+00
2.500	0.326E+00	0.339E-01	0.228E+01	0.159E-01	0.170E-02	0.504E+00
3.000	0.496E+00	0.439E-01	0.282E+01	0.223E-01	0.209E-02	0.597E+00
3.500	0.723E+00	0.532E-01	0.340E+01	0.299E-01	0.247E-02	0.691E+00
4.000	0.984E+00	0.637E-01	0.397E+01	0.381E-01	0.284E-02	0.781E+00

Table 5y : Spectrum responses, Run No. 083
Three-float (triangular) configuration head seas tests

Float Draft/Diameter = 3.0
Damping Plate Diam/Float Diam = 1.6
Metacentric Height/$\nabla^{1/3}$ = 0.716

$\frac{H_{1/3}}{\nabla^{1/3}}$	$\frac{E_z}{\nabla^{2/3}}$	$\frac{E_{\dot{z}}}{g\nabla^{1/3}}$	$\frac{z_{1/3}}{\nabla^{1/3}}$	E_θ	$\frac{E_\theta \nabla^{1/3}}{g}$	$\theta_{1/3}$
0.100	0.634E-06	0.543E-06	0.318E-02	0.196E-05	0.260E-05	0.561E-02
0.200	0.260E-03	0.143E-03	0.645E-01	0.227E-04	0.198E-04	0.191E-01
0.300	0.193E-02	0.857E-03	0.171E+00	0.874E-04	0.531E-04	0.375E-01
0.400	0.499E-02	0.205E-02	0.283E+00	0.227E-03	0.103E-03	0.593E-01
0.500	0.958E-02	0.349E-02	0.391E+00	0.452E-03	0.170E-03	0.851E-01
0.600	0.155E-01	0.508E-02	0.498E+00	0.823E-03	0.257E-03	0.115E+00
0.700	0.226E-01	0.673E-02	0.601E+00	0.133E-02	0.363E-03	0.146E+00
0.800	0.308E-01	0.842E-02	0.702E+00	0.195E-02	0.480E-03	0.177E+00
0.900	0.401E-01	0.101E-01	0.801E+00	0.269E-02	0.605E-03	0.207E+00
1.000	0.508E-01	0.119E-01	0.902E+00	0.353E-02	0.736E-03	0.238E+00
1.500	0.124E+00	0.217E-01	0.141E+01	0.909E-02	0.142E-02	0.379E+00
2.000	0.218E+00	0.299E-01	0.187E+01	0.153E-01	0.205E-02	0.494E+00
2.500	0.336E+00	0.384E-01	0.232E+01	0.219E-01	0.258E-02	0.590E+00
3.000	0.505E+00	0.474E-01	0.284E+01	0.291E-01	0.305E-02	0.683E+00
3.500	0.728E+00	0.574E-01	0.341E+01	0.376E-01	0.350E-02	0.775E+00
4.000	0.984E+00	0.679E-01	0.397E+01	0.466E-01	0.392E-02	0.863E+00

TABLE 6 : ADDED MASSES AND DAMPING COEFFICIENTS

Mode	ADDED MASS COEFFICIENTS		DAMPING COEFFICIENTS	
2	$m''_{SS} = \frac{F^{(2)}_{S_r}}{\omega^2 \cdot}$	$C_{SS} = \frac{m''_{SS}}{\frac{1}{2}\rho\pi r^3}$	$N_{SS} = \frac{F^{(2)}_{S_i}}{\omega^{\cdot}}$	$\delta_{SS} = \frac{N_{SS}}{\frac{1}{2}\omega\rho\pi r^3}$
	$m''_{SH} = \frac{F^{(2)}_{H_r}}{\omega^2 \cdot}$	$C_{SH} = \frac{m''_{SH}}{\frac{1}{2}\rho\pi r^3}$	$N_{SH} = \frac{F^{(2)}_{H_i}}{\omega^{\cdot}}$	$\delta_{SH} = \frac{N_{SH}}{\frac{1}{2}\omega\rho\pi r^3}$
	$m''_{SR} = \frac{F^{(2)}_{R_r}}{\omega^2 \cdot}$	$C_{SR} = \frac{m''_{SR}}{\frac{1}{2}\rho\pi r^3}$	$N_{SR} = \frac{F^{(2)}_{R_i}}{\omega^{\cdot}}$	$\delta_{SR} = \frac{N_{SR}}{\frac{1}{2}\omega\rho\pi r^3}$
3	$m''_{HS} = \frac{F^{(3)}_{S_r}}{\omega^2 \cdot}$	$C_{HS} = \frac{m''_{HS}}{\frac{1}{2}\rho\pi r^3}$	$N_{HS} = \frac{F^{(3)}_{S_i}}{\omega^{\cdot}}$	$\delta_{HS} = \frac{N_{HS}}{\frac{1}{2}\omega\rho\pi r^3}$
	$m''_{HH} = \frac{F^{(3)}_{H_r}}{\omega^2 \cdot}$	$C_{HH} = \frac{m''_{HH}}{\frac{1}{2}\rho\pi r^3}$	$N_{HH} = \frac{F^{(3)}_{H_i}}{\omega^{\cdot}}$	$\delta_{HH} = \frac{N_{HH}}{\frac{1}{2}\omega\rho\pi r^3}$
	$m''_{HR} = \frac{F^{(3)}_{R_r}}{\omega^2 \cdot}$	$C_{HR} = \frac{m''_{HR}}{\frac{1}{2}\rho\pi r^3}$	$N_{HR} = \frac{F^{(3)}_{R_i}}{\omega^{\cdot}}$	$\delta_{HR} = \frac{N_{HR}}{\frac{1}{2}\omega\rho\pi r^3}$
4	$m''_{RS} = \frac{F^{(4)}_{S_r}}{\omega^2 \cdot}$	$C_{RS} = \frac{m''_{RS}}{\frac{1}{2}\rho\pi r^3}$	$N_{RS} = \frac{F^{(4)}_{S_i}}{\omega^{\cdot}}$	$\delta_{RS} = \frac{N_{RS}}{\frac{1}{2}\omega\rho\pi r^3}$
	$m''_{RH} = \frac{F^{(4)}_{H_r}}{\omega^2 \cdot}$	$C_{RH} = \frac{m''_{RH}}{\frac{1}{2}\rho\pi r^3}$	$N_{RH} = \frac{F^{(4)}_{H_i}}{\omega^{\cdot}}$	$\delta_{RH} = \frac{N_{RH}}{\frac{1}{2}\omega\rho\pi r^3}$
	$m''_{RR} = \frac{F^{(4)}_{R_r}}{\omega^2 \cdot}$	$C_{RR} = \frac{m''_{RR}}{\frac{1}{2}\rho\pi r^4}$	$N_{RR} = \frac{F^{(4)}_{R_i}}{\omega^{\cdot}}$	$\delta_{RR} = \frac{N_{RR}}{\frac{1}{2}\omega\rho\pi r^4}$

TABLE 7 : THE HYDRODYNAMIC MOMENT ARMS

MODE	INERTIAL PART	DAMPING PART
2	$\ell_{SS_r} = \ell_{S_r}^{(2)}$ $\ell_{SH_r} = \ell_{H_r}^{(2)}$	$\ell_{SS_i} = \ell_{S_i}^{(2)}$ $\ell_{SH_i} = \ell_{H_i}^{(2)}$
3	$\ell_{HS_r} = \ell_{S_r}^{(3)}$ $\ell_{HH_r} = \ell_{H_r}^{(3)}$	$\ell_{HS_i} = \ell_{S_i}^{(3)}$ $\ell_{HH_i} = \ell_{H_i}^{(3)}$
4	$\ell_{RS_r} = \ell_{S_r}^{(4)}$ $\ell_{RH_r} = \ell_{H_r}^{(4)}$	$\ell_{RS_i} = \ell_{S_i}^{(4)}$ $\ell_{RH_i} = \ell_{H_i}^{(4)}$

TABLE 8 : MOMENT COEFFICIENT RELATIONSHIPS

$$C_{SR} = C_{SS}\,\ell_{SS_r} + C_{SH}\,\ell_{SH_r}$$

$$\delta_{SR} = \delta_{SS}\,\ell_{SS_i} + \delta_{SH}\,\ell_{SH_i}$$

$$C_{HR} = C_{HS}\,\ell_{HS_r} + C_{HH}\,\ell_{HH_r}$$

$$\delta_{HR} = \delta_{HS}\,\ell_{HS_i} + \delta_{HH}\,\ell_{HH_i}$$

$$C_{RR} = C_{RS}\,\ell_{RS_r} + C_{RH}\,\ell_{RH_r}$$

$$\delta_{RR} = \delta_{RS}\,\ell_{RS_i} + \delta_{RH}\,\ell_{RH_i}$$

TABLE 9 : THE NON-DIMENSIONAL EXPRESSION OF THE WAVE-EXCITING FORCES AND MOMENTS

$f_S^{(\beta)} = \dfrac{F_S^{(\beta)}}{\rho g a B}$	sway-exciting force
$f_H^{(\beta)} = \dfrac{F_H^{(\beta)}}{\rho g a B}$	heave-exciting force
$f_R^{(\beta)} = \dfrac{F_R^{(\beta)}}{\rho g a B T}$	roll-exciting moment

where

B = beam of the body (a or b)

β = o or e corresponding to the odd or even potential

$$\varphi_I^{(o)} + \varphi_D^{(o)} \text{ , or } \varphi_I^{(e)} + \varphi_D^{(e)}$$

TABLE 10 : THE RELATIONS BETWEEN THE FORCE COEFFICIENTS DUE TO MOTIONS FOR TWIN BODIES a AND b

$$[C_{SH}]_a = -[C_{SH}]_b \text{ , } [\delta_{SH}]_a = -[\delta_{SH}]_b$$
$$[C_{SS}]_a = [C_{SS}]_b \text{ , } [\delta_{SS}]_a = [\delta_{SS}]_b$$
$$[C_{SR}]_a = [C_{SR}]_b \text{ , } [\delta_{SR}]_a = [\delta_{SR}]_b$$
$$[C_{HS}]_a = -[C_{HS}]_b \text{ , } [\delta_{HS}]_a = -[\delta_{HS}]_b$$
$$[C_{HH}]_a = [C_{HH}]_b \text{ , } [\delta_{HH}]_a = [\delta_{HH}]_b$$
$$[C_{HR}]_a = -[C_{HR}]_b \text{ , } [\delta_{HR}]_a = -[\delta_{HR}]_b$$
$$[C_{RH}]_a = -[C_{RH}]_b \text{ , } [\delta_{RH}]_a = -[\delta_{RH}]_b$$
$$[C_{RS}]_a = [C_{RS}]_b \text{ , } [\delta_{RS}]_a = [\delta_{RS}]_b$$
$$[C_{RR}]_a = [C_{RR}]_b \text{ , } [\delta_{RR}]_a = [\delta_{RR}]_b$$

$$[\ell_{SH_r}]_a = -[\ell_{SH_r}]_b \text{ , } [\ell_{SH_i}]_a = -[\ell_{SH_i}]_b$$
$$[\ell_{SS_r}]_a = [\ell_{SS_r}]_b \text{ , } [\ell_{SS_i}]_a = [\ell_{SS_i}]_b$$
$$[\ell_{HS_r}]_a = [\ell_{HS_r}]_b \text{ , } [\ell_{HS_i}]_a = [\ell_{HS_i}]_b$$
$$[\ell_{HH_r}]_a = -[\ell_{HH_r}]_b \text{ , } [\ell_{HH_i}]_a = -[\ell_{HH_i}]_b$$
$$[\ell_{RH_r}]_a = -[\ell_{RH_r}]_b \text{ , } [\ell_{RH_i}]_a = -[\ell_{RH_i}]_b$$
$$[\ell_{RS_r}]_a = [\ell_{RS_r}]_b \text{ , } [\ell_{RS_i}]_a = [\ell_{RS_i}]_b$$
$$[\ell_H^{(o)}]_a = -[\ell_H^{(o)}]_b \text{ , } [\ell_H^{(e)}]_a = -[\ell_H^{(e)}]_b$$

TABLE 11 : THE RESULTANT HYDRODYNAMIC FORCES AND MOMENTS DUE TO MOTIONS FOR TWIN CYLINDERS

$C_{SS} = 2[C_{SS}]_a$	$\delta_{SS} = 2[\delta_{SS}]_a$
$C_{SH} = 0$	$\delta_{SH} = 0$
$C_{SR} = 2[C_{SR}]_a$	$\delta_{SR} = 2[\delta_{SR}]_a$
$C_{HS} = 0$	$\delta_{HS} = 0$
$C_{HH} = 2[C_{HH}]_a$	$\delta_{HH} = 2[\delta_{HH}]_a$
$C_{HR} = 0$	$\delta_{HR} = 0$
$C_{RS} = C_{SR}$	$\delta_{RS} =$ SR
$C_{RH} = 0$	$\delta_{RH} = 0$
$C_{RR} = 2[C_{RR}]_a$	$\delta_{RR} = 2[\delta_{RR}]_a$

TABLE 12 : THE RELATIONS BETWEEN THE WAVE-EXCITING FORCES AND MOMENTS FOR TWIN BODIES a AND b

$[f_S^{(o)}]_a = [f_S^{(o)}]_b$	$[f_S^{(e)}]_a = -[f_S^{(e)}]_b$
$[f_H^{(o)}]_a = -[f_H^{(o)}]_b$	$[f_H^{(e)}]_a = [f_H^{(e)}]_b$
$[f_R^{(o)}]_a = [f_R^{(o)}]_b$	$[f_R^{(e)}]_a = -[f_R^{(e)}]_b$
$[\ell_S^{(o)}]_a = [\ell_S^{(o)}]_b$	$[\ell_S^{(e)}]_a = [\ell_S^{(e)}]_b$
$[\ell_H^{(o)}]_a = -[\ell_H^{(o)}]_b$	$[\ell_H^{(e)}]_a = -[\ell_H^{(e)}]_b$

TABLE 13 : THE RESULTANT WAVE-EXCITING FORCES AND MOMENTS FOR TWIN CYLINDERS

$$f_S = 2\left[f_S^{(o)}\right]_a$$

$$f_H = 2\left[f_H^{(e)}\right]_a$$

$$f_R = 2\left[f_R^{(o)}\right] = 2\left[\ell_S^{(o)}\, f_S^{(o)} + \ell_H^{(o)}\, f_H^{(o)}\right]_a$$

TABLE 14 : VERTICAL ADDED MASS COEFFICIENT

$L_a/2R_a$	k_1'
1.0	0.5
1.5	0.458
2.0	0.418
2.51	0.392
2.99	0.365
3.99	0.327
4.99	0.294

TABLE 15 : EFFECT OF MODEL SIZE ON ROLL DAMPING MOMENTS FOR CYLINDERS WITH APPENDAGES. (C_m values Eq.(43))

Cyl. Diameter	Bilge Keels	Sharp-Edged Fins	Streamlined Fins
6 in	17	16	4.2
12 in	16	17	3.1
24 in	15	Not Tested	2.9

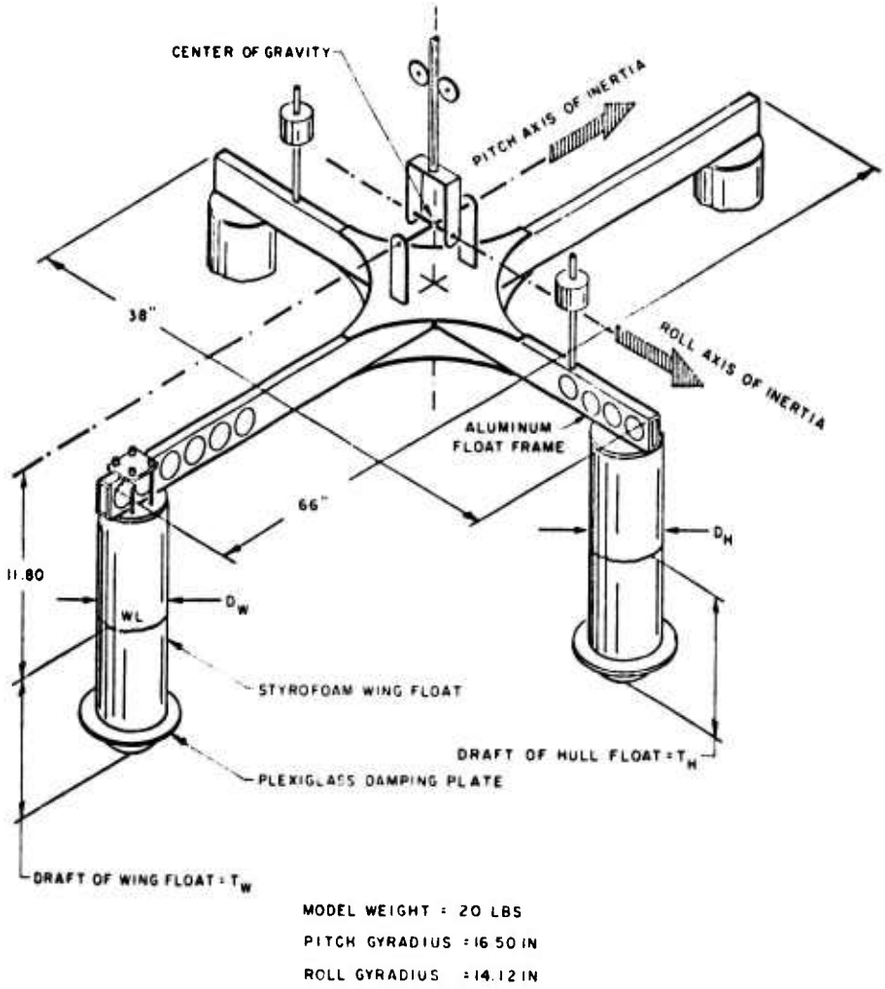
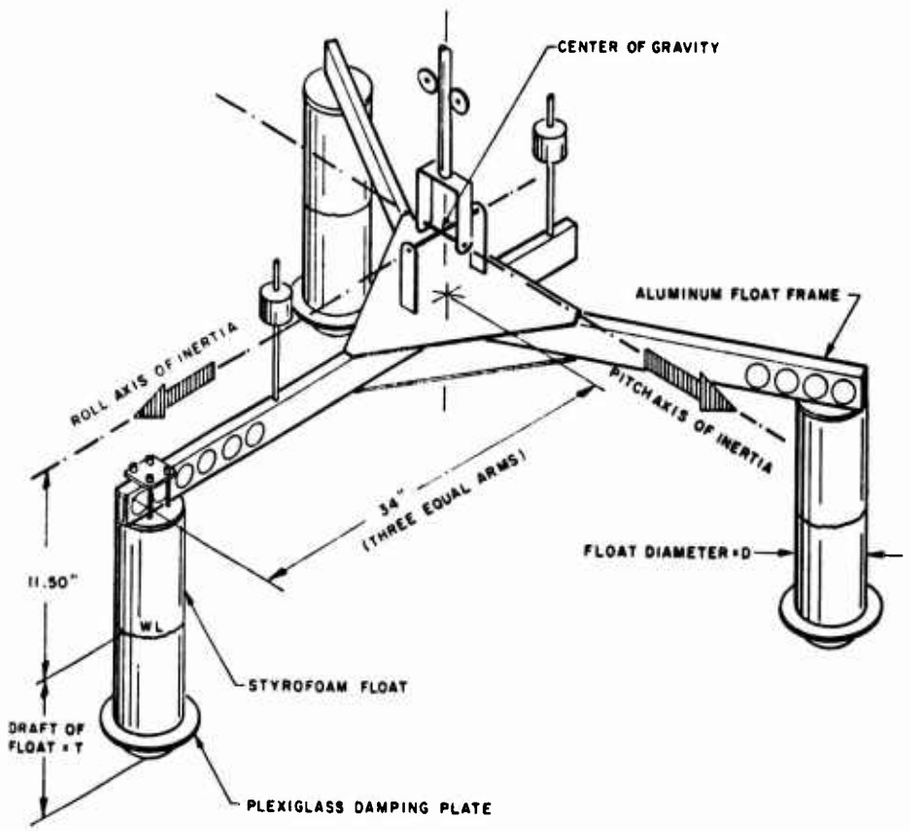


Figure 1 : Sketch of crudiform float platform model



MODEL WEIGHT = 20 LBS
PITCH GYRADIUS = 16.68 IN
ROLL GYRADIUS 9 0 IN

Figure 2 : Sketch of triangular array float platform model

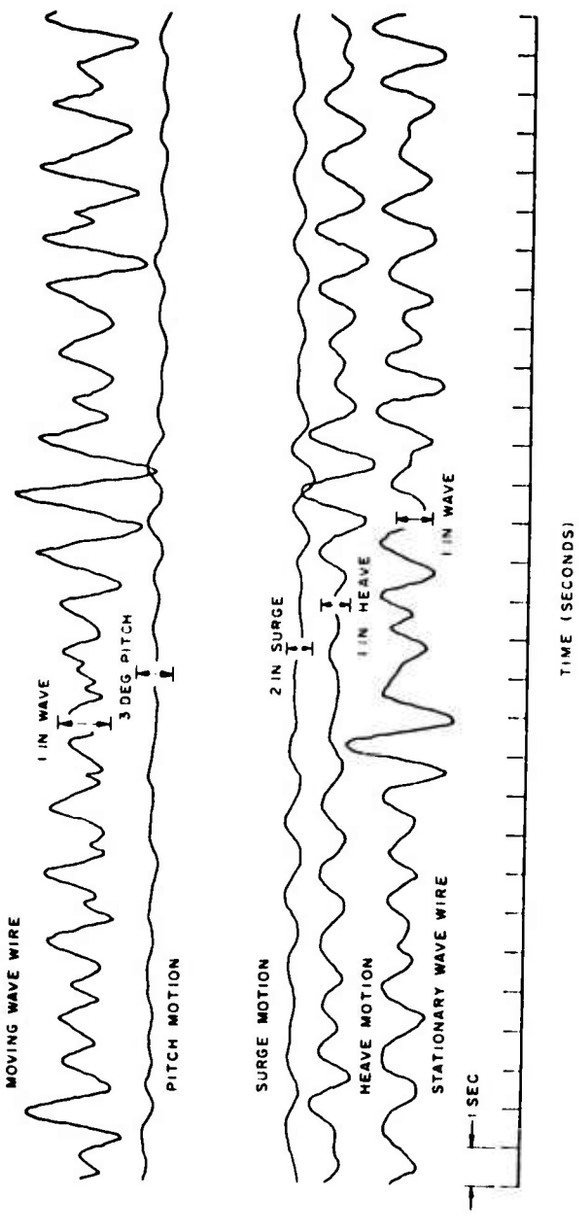


Figure 3 : Example of oscillogram record of float platform motions in irregular seas. Cruciform model in head seas, Run 002.

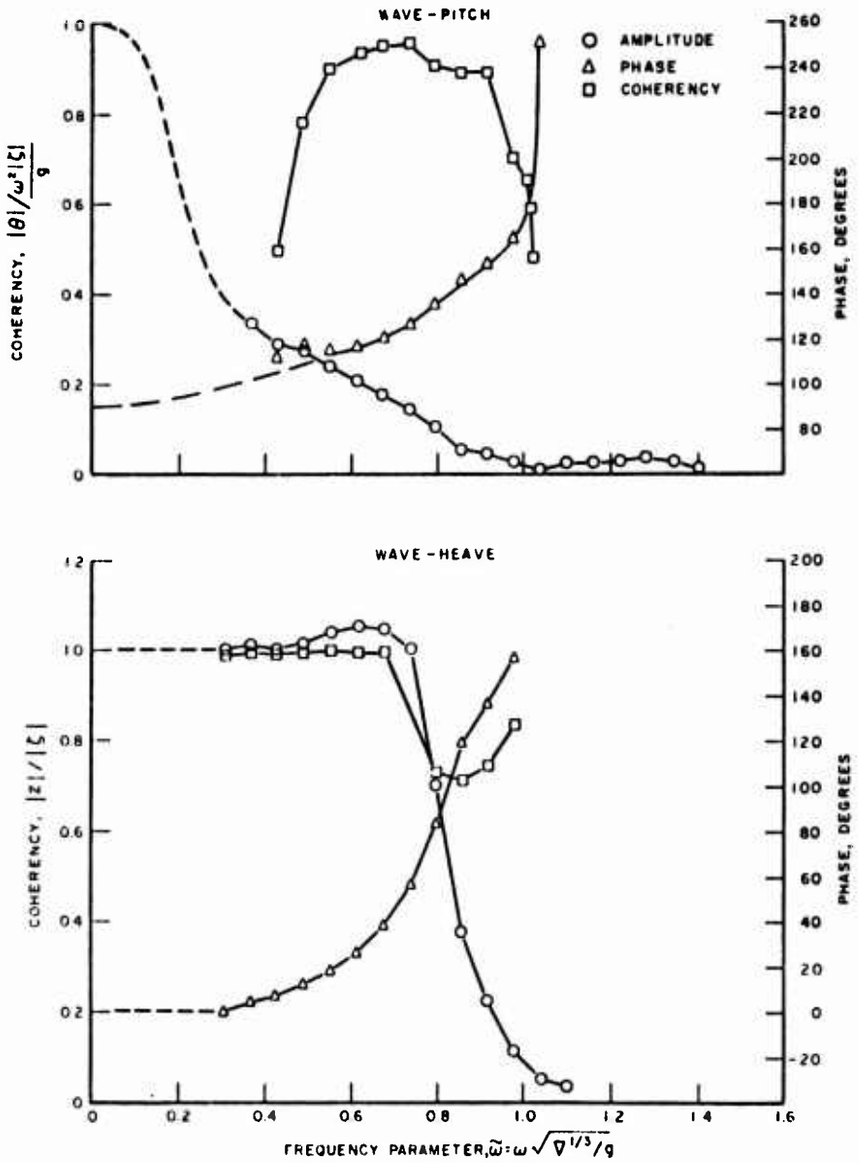


Figure 4 : Examples of transfer functions : amplitude, phase and coherency. Cruciform model in head seas, Run 002.

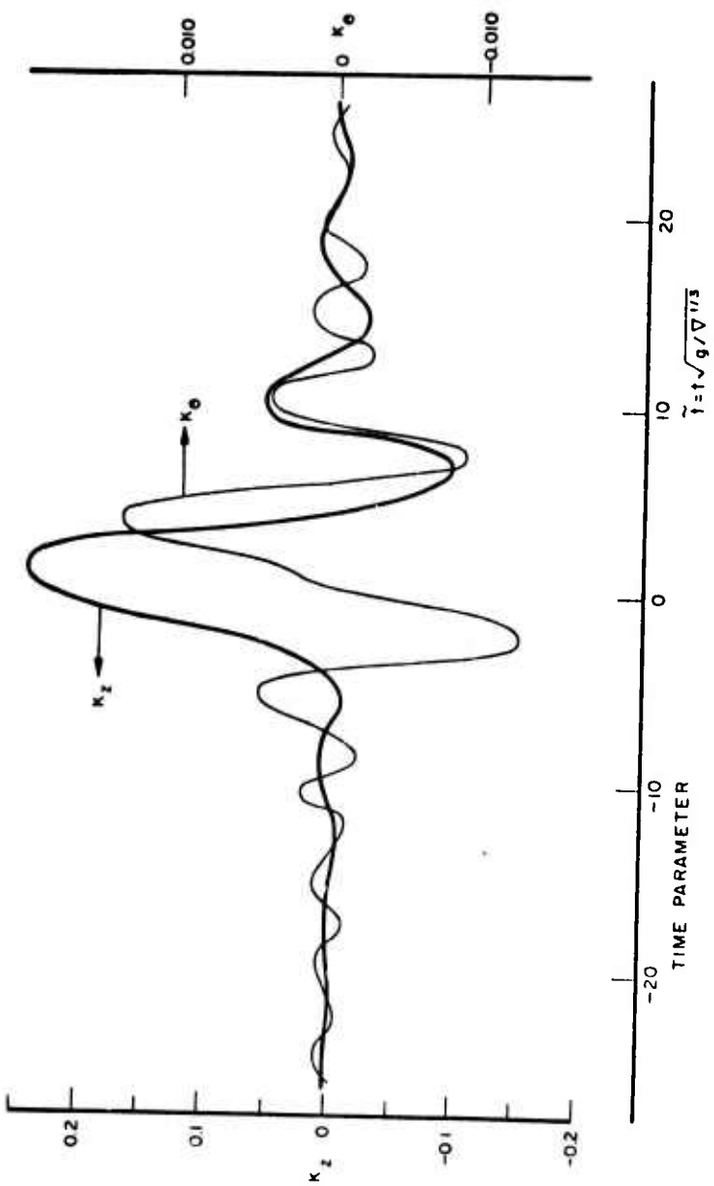


Figure 5 : Examples of impulse response functions : K_Z for heave and K_θ for pitch. Cruciform model in head seas, Run 002

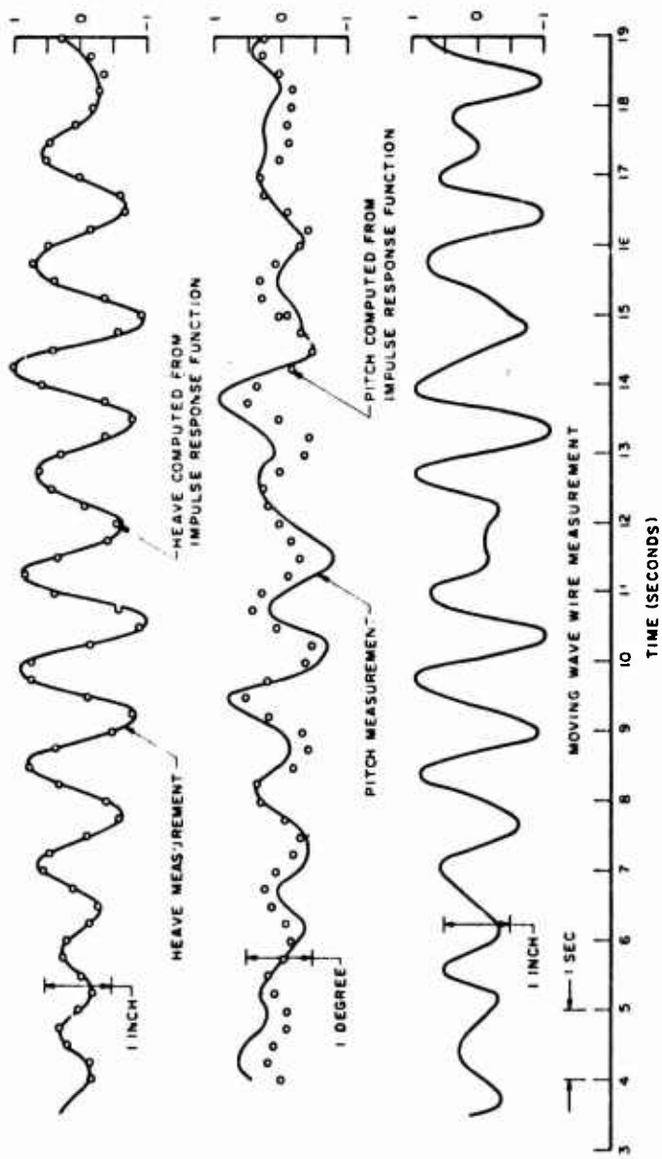


Figure 6 : Heave and pitch motions for cruciform model in head seas predicted by impulse response technique, Run 002

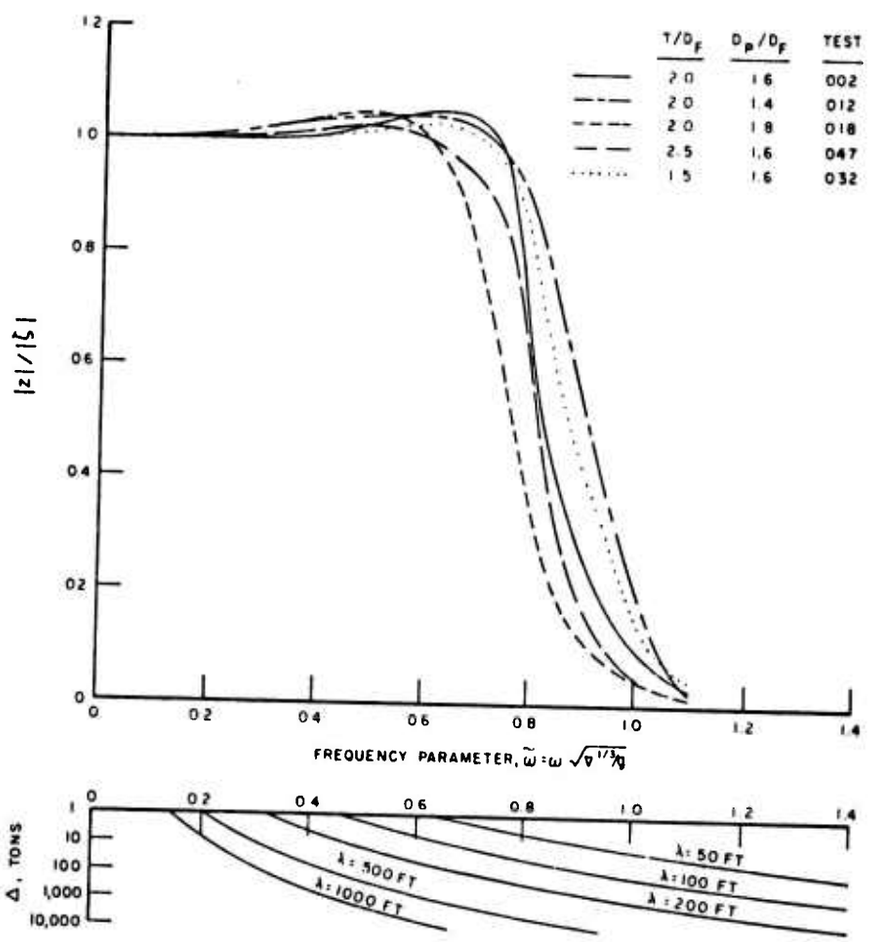


Figure 7 : Transfer functions (amplitude only) for heave of some cruciform float arrays in head seas Group A, hull float diameter/wing float diameter = 1,5

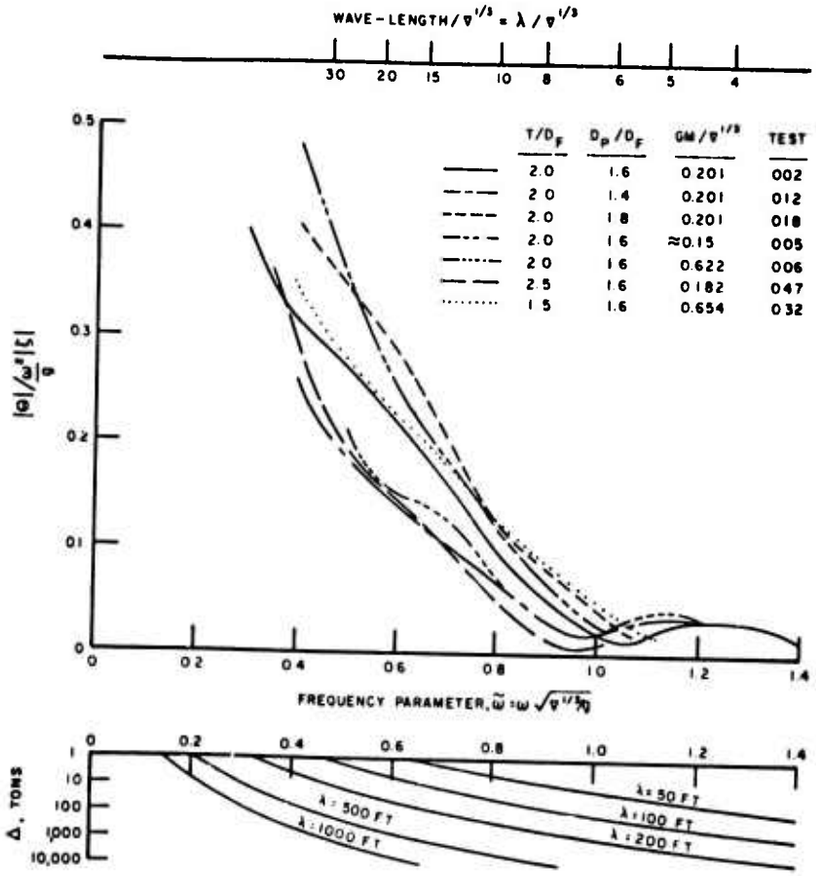


Figure 8 : Transfer functions (amplitude only) for pitch of some cruciform float arrays in head seas group A, hull float diameter/wing float diameter = 1.5

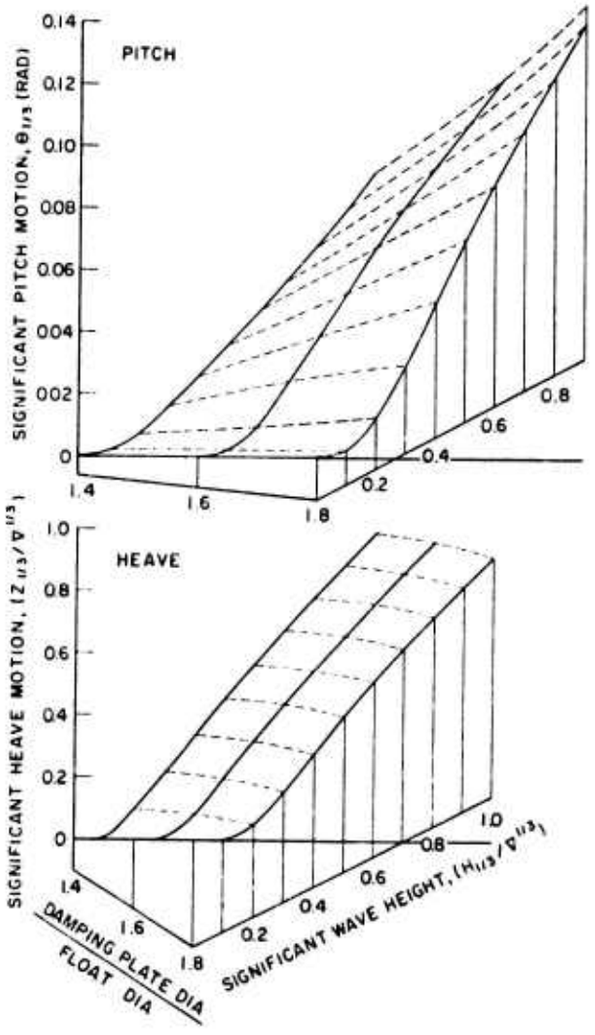


Figure 9 : Effect of damping plate size on spectral response of cruciform array of floats
Hull float diam/wing float diam = 1.5 (head seas)

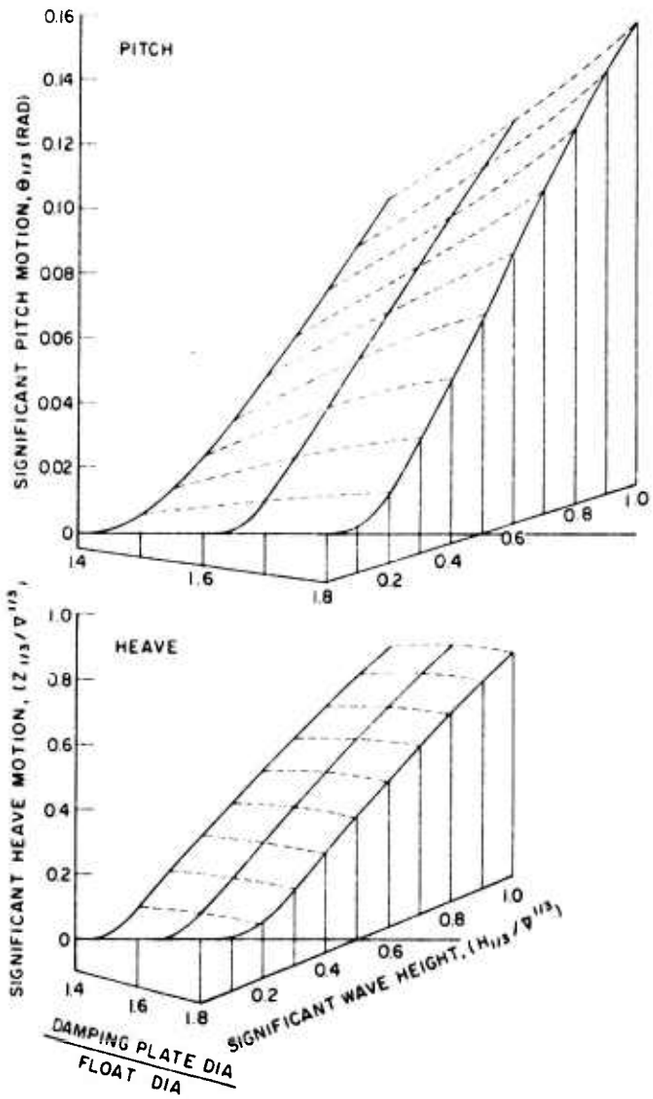


Figure 10 : Effect of damping plate size on spectral response of cruciform array of floats
Hull float diam/wing float diam = 1.25 (head seas)

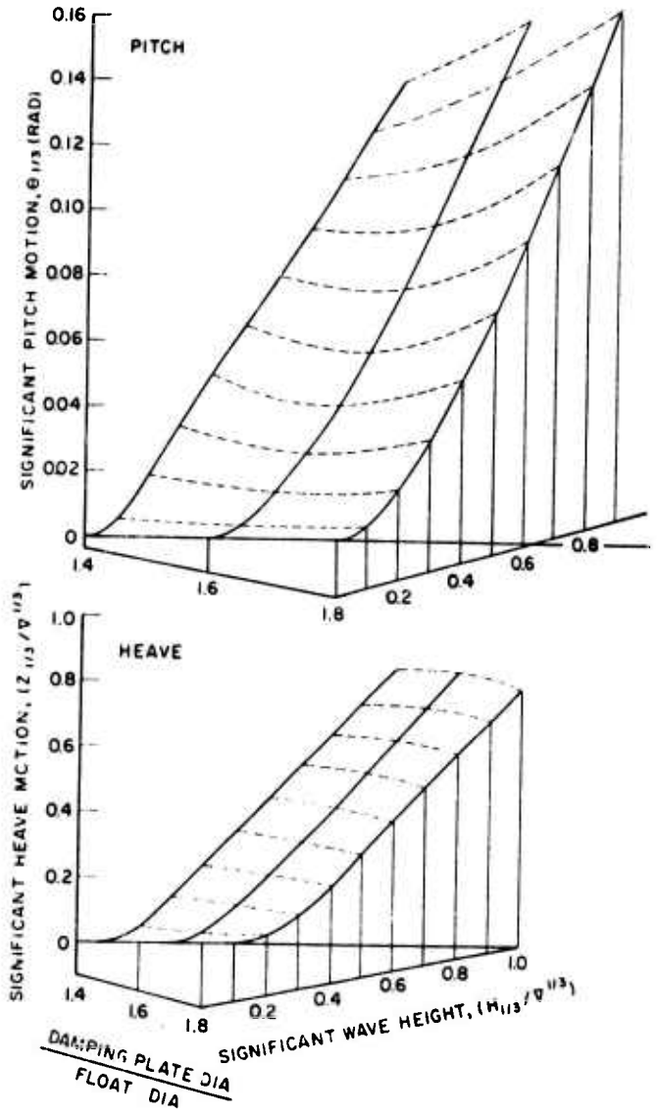


Figure 11 : Effect of damping plate size on spectral response of triangular array of floats (head seas)

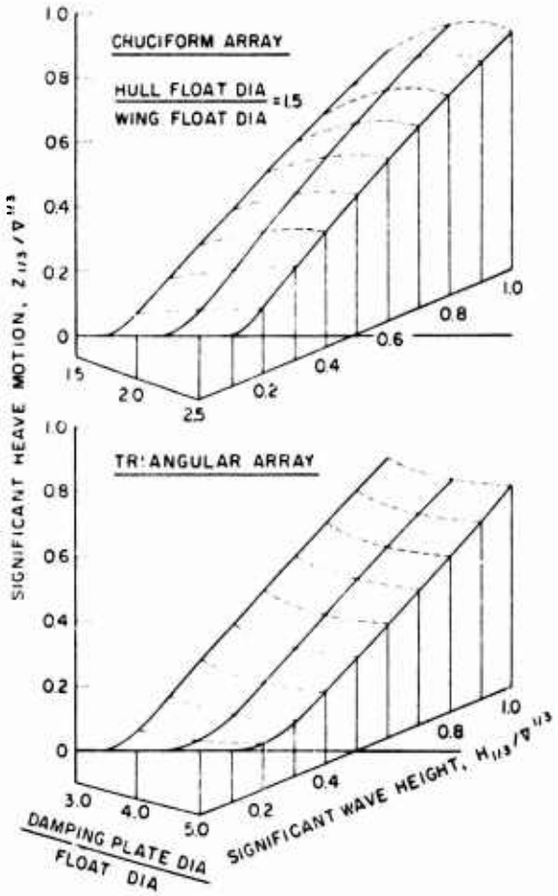


Figure 12 : Effect of slenderness on heave spectral response of crudiform and triangular float arrays (head seas)

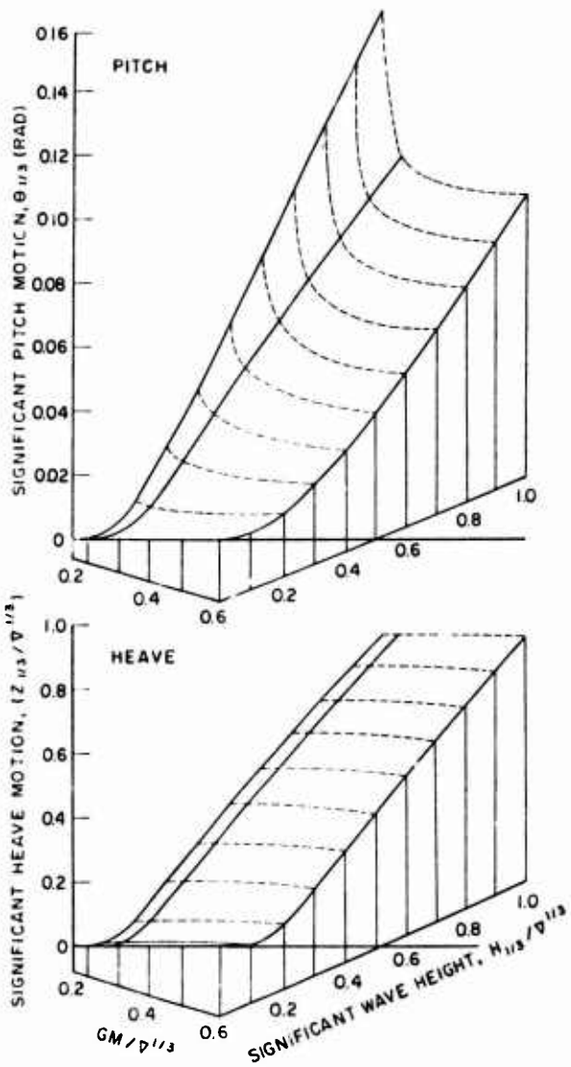


Figure 13 : Effect of metacentric height on spectral response of cruciform array of floats
Hull float diam/wing float diam = 1.5 (head seas)

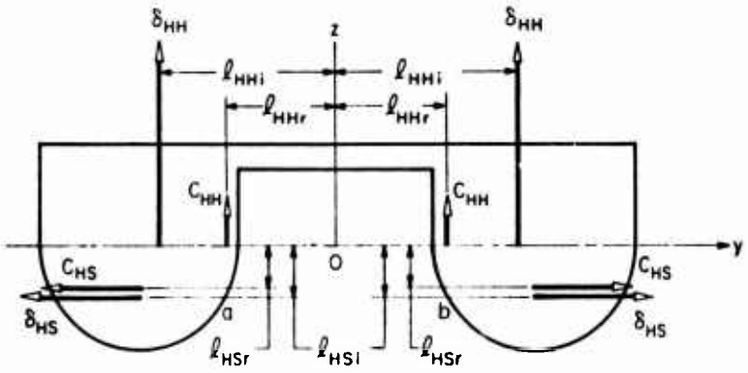


Figure 14a : A typical system of forces induced by heaving motion

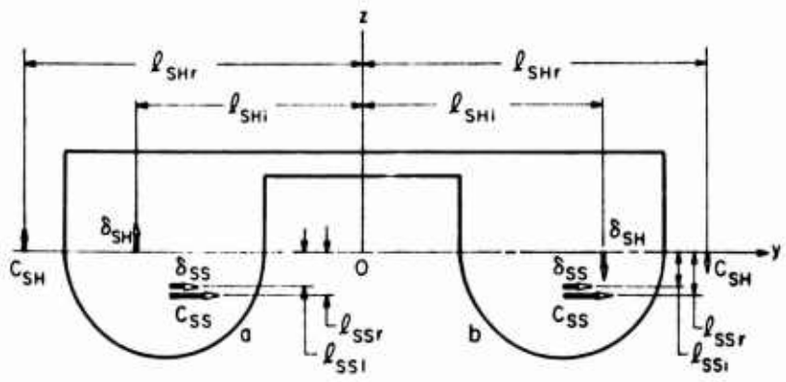


Figure 14b : A typical system of forces induced by swaying motion

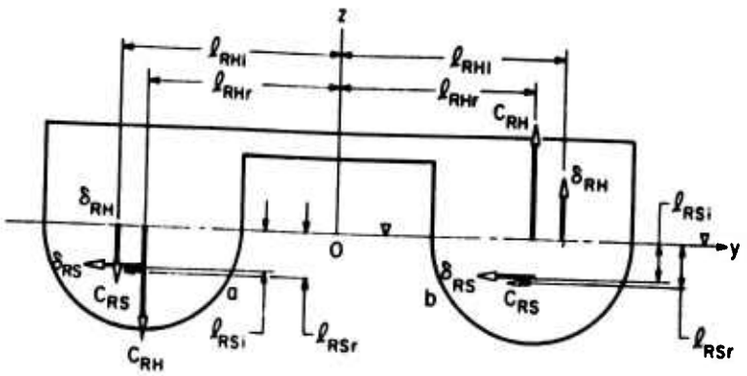


Figure 14c : A typical system of forces induced by rolling motion

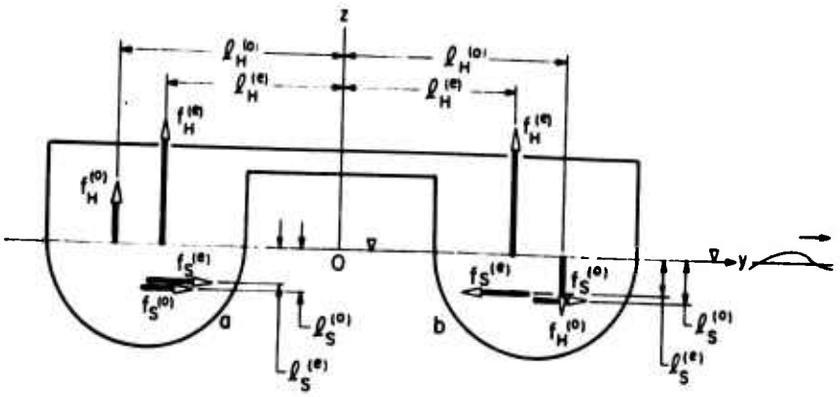


Figure 14d : A typical system of forces induced by waves

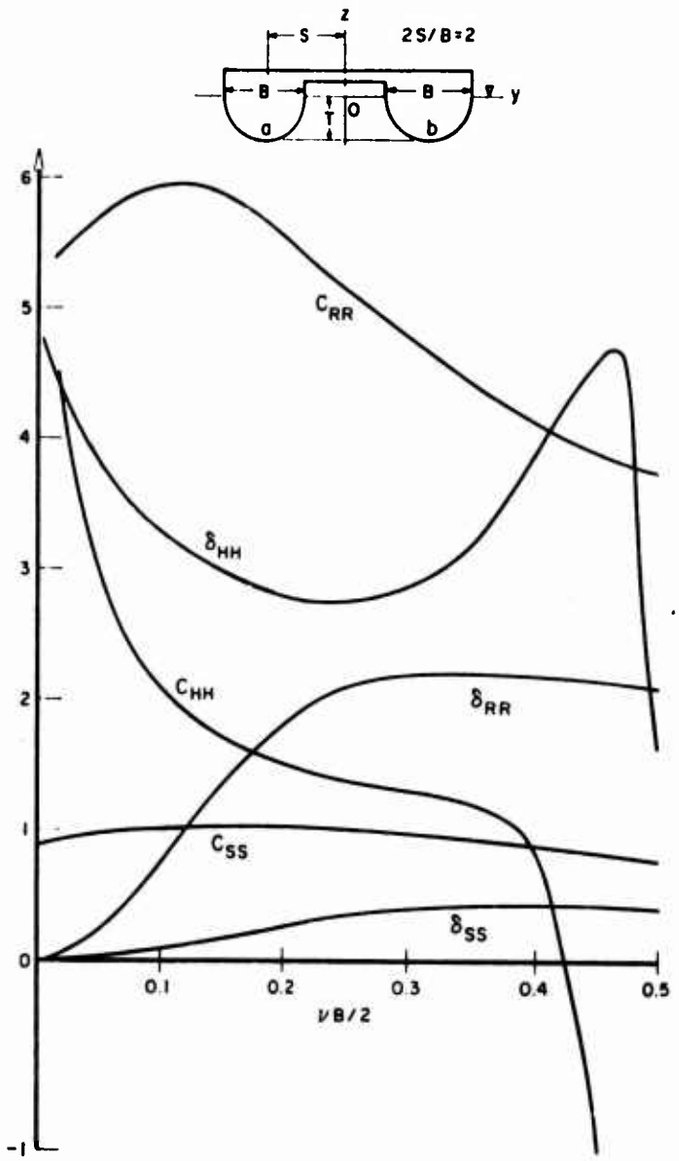


Figure 15 : Heaving, swaying and rolling added mass and damping coefficients for cylinder a

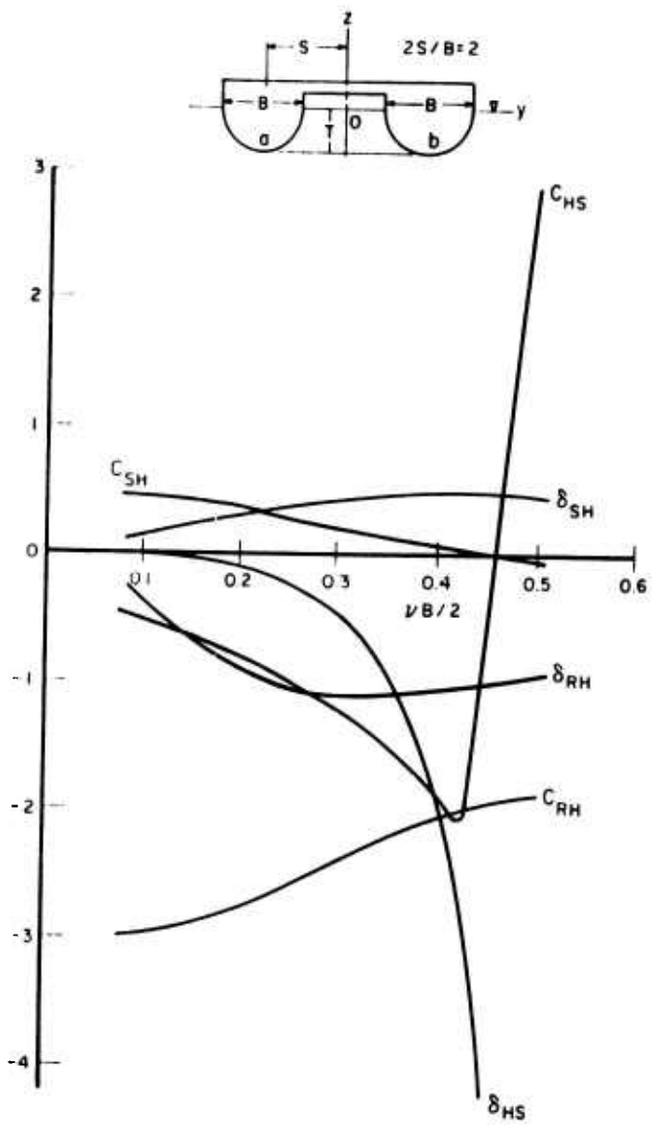


Figure 16 : Heave-induced swaying, sway-induced heaving, and roll-induced heaving and swaying forces on cylinder a

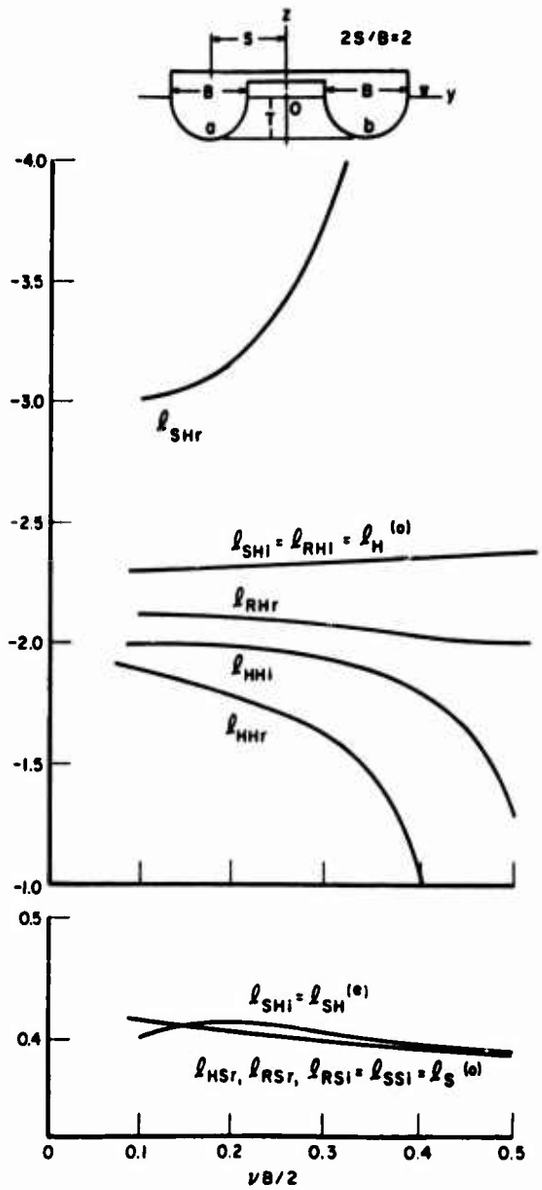


Figure 17 : Hydrodynamic moment arms on cylinder a

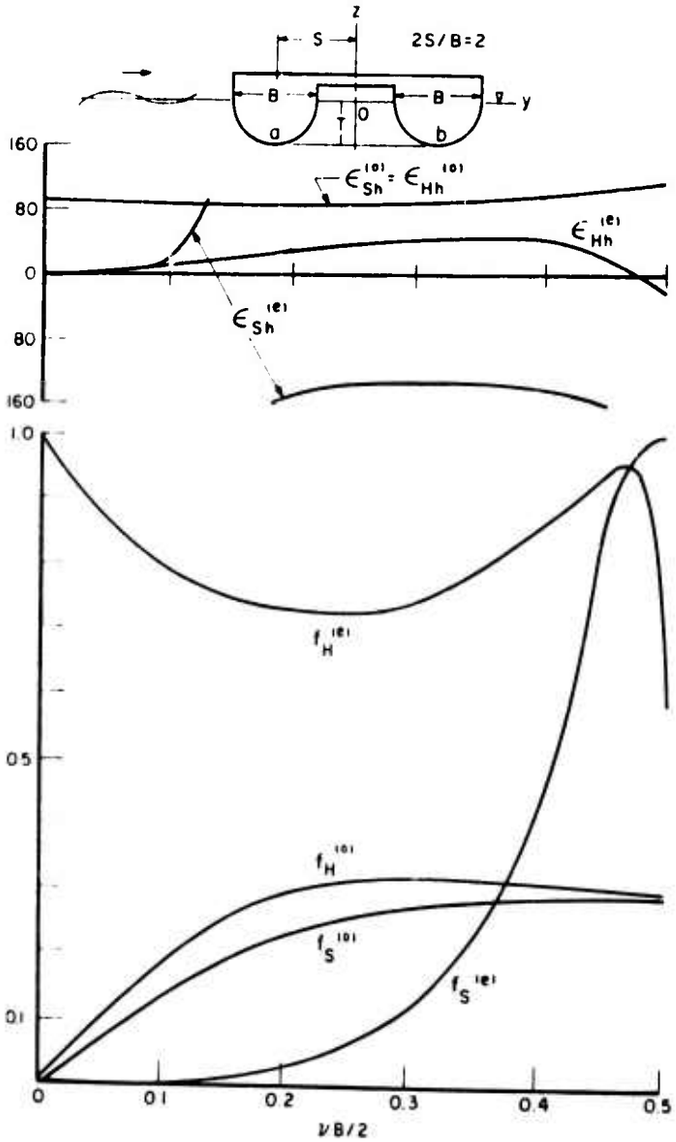


Figure 18 : The sway-and heave-exciting forces on cylinder a induced by even and odd waves

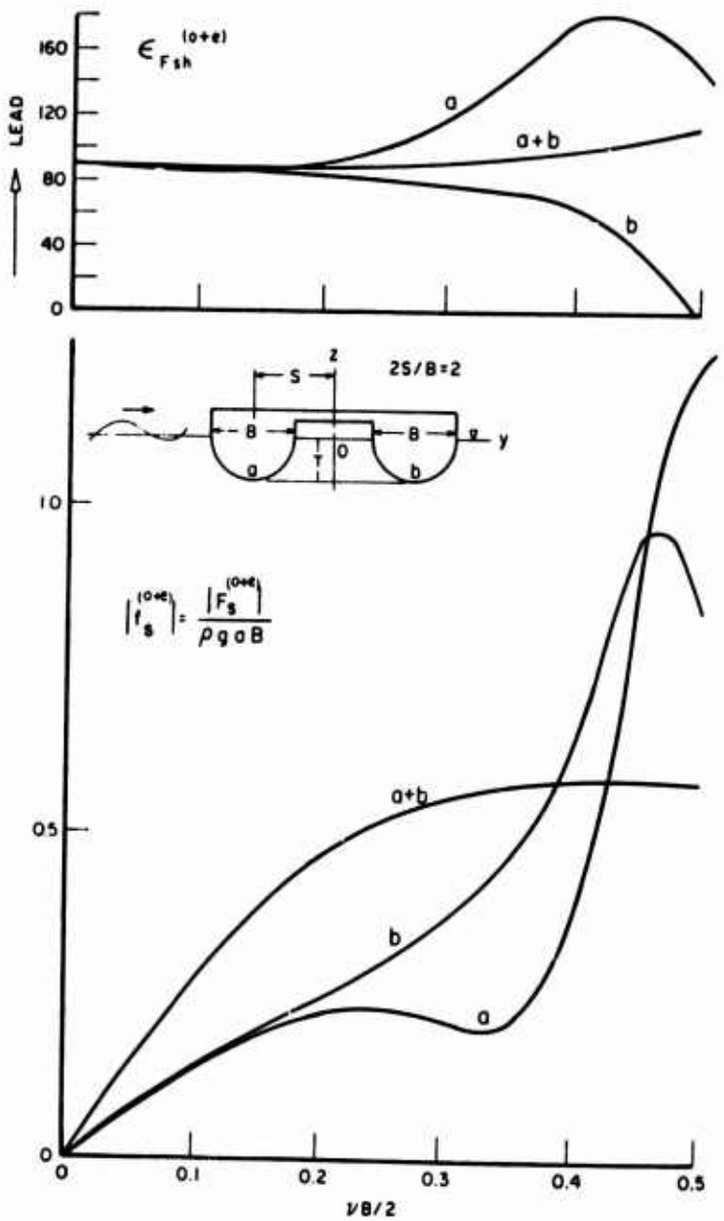


Figure 19 : The sway-exciting forces on cylinders a,b and a+b

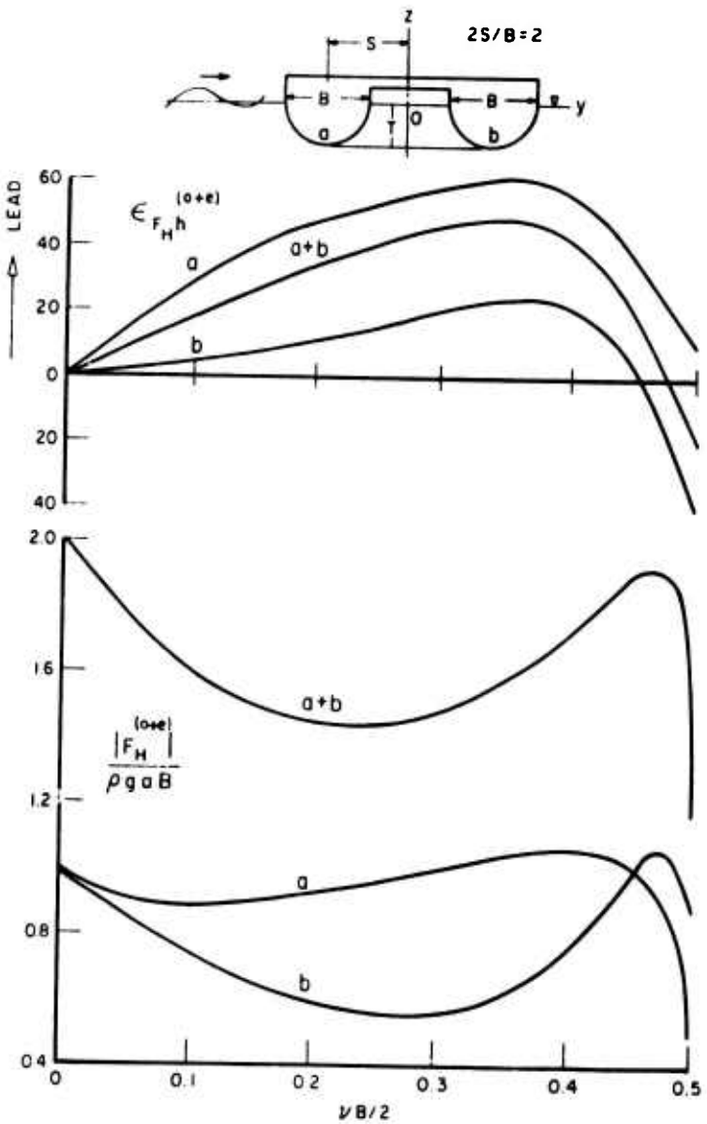


Figure 20 : The heave-exciting forces on cylinders a,b and a+b

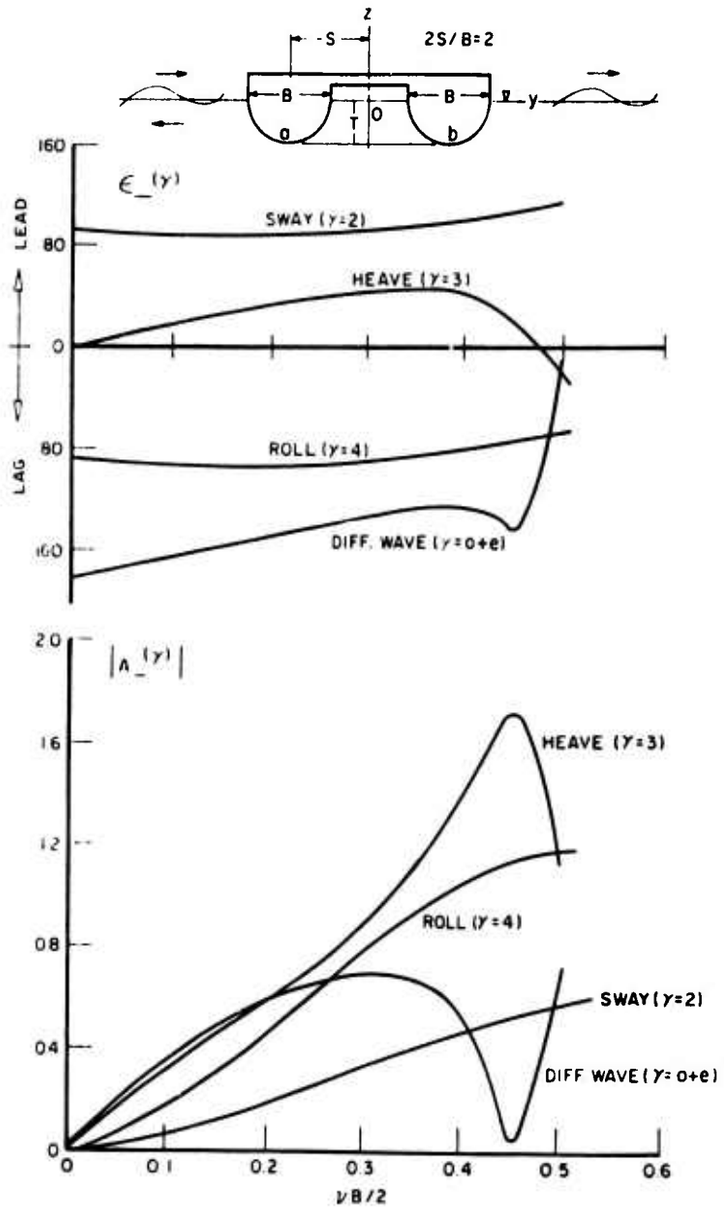


Figure 21 : The radiated and diffracted waves generated from the twin cylinders

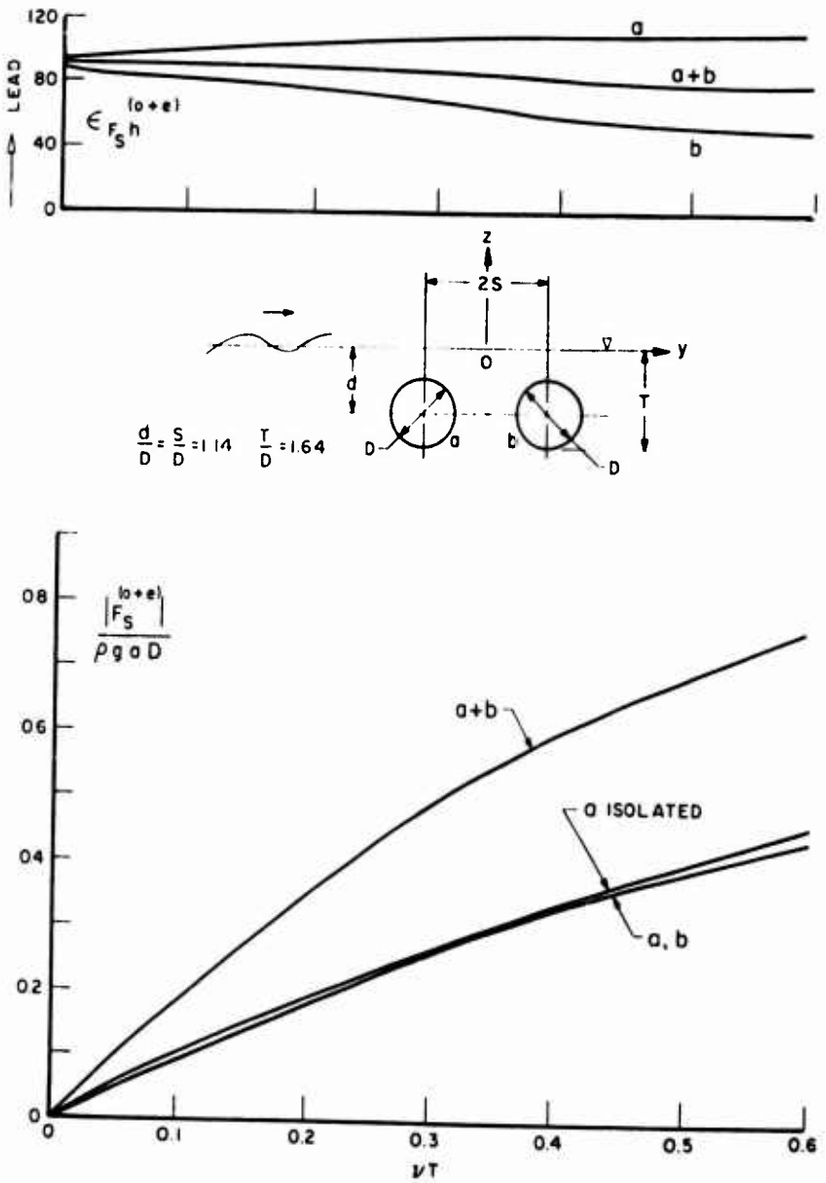


Figure 22a : Sway-exciting forces on the submerged twin circular cylinders

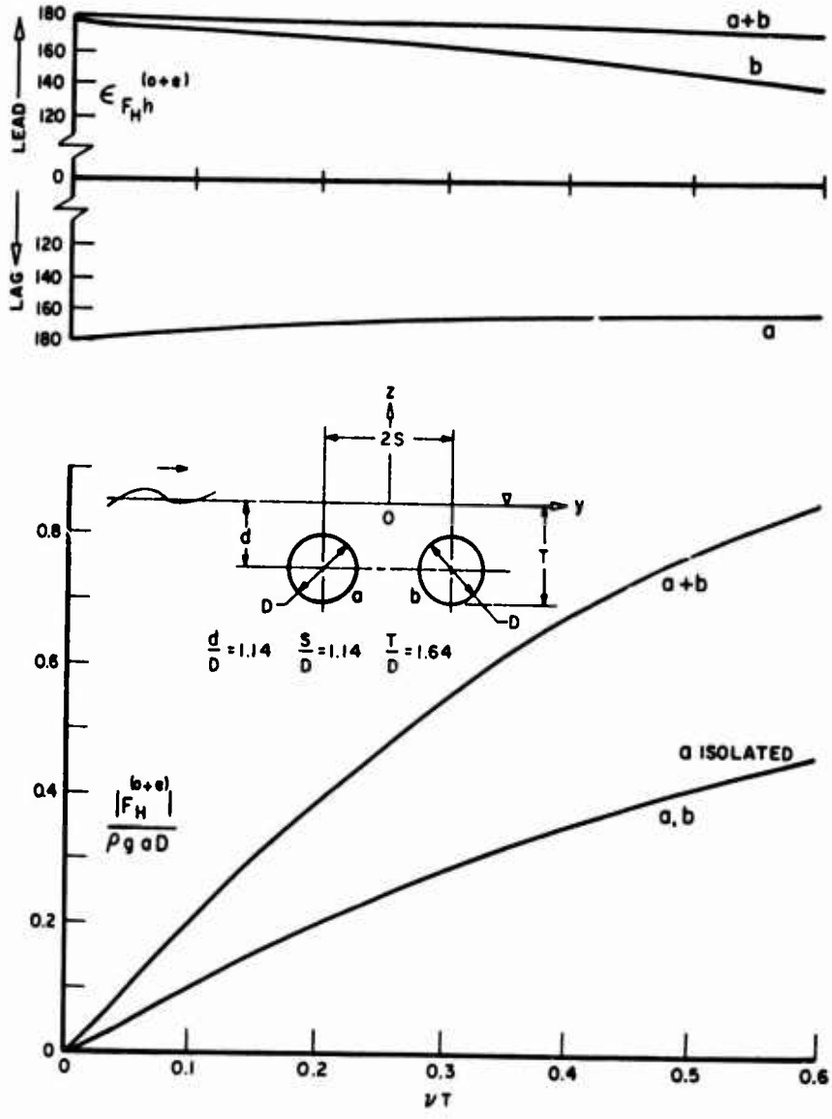


Figure 22b : Heave-exciting forces on the submerged twin circular cylinders

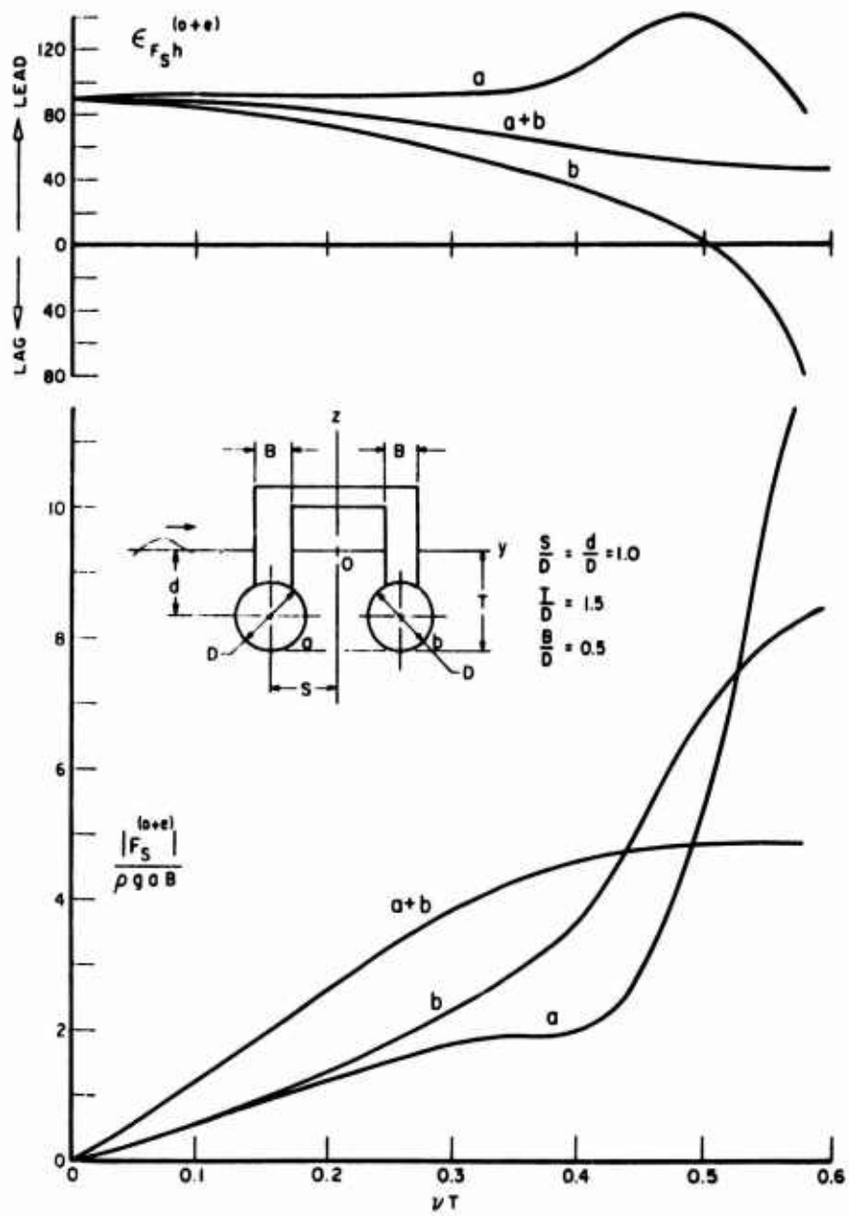


Figure 23a : The sway-exciting force on cylinders a, b and a+b

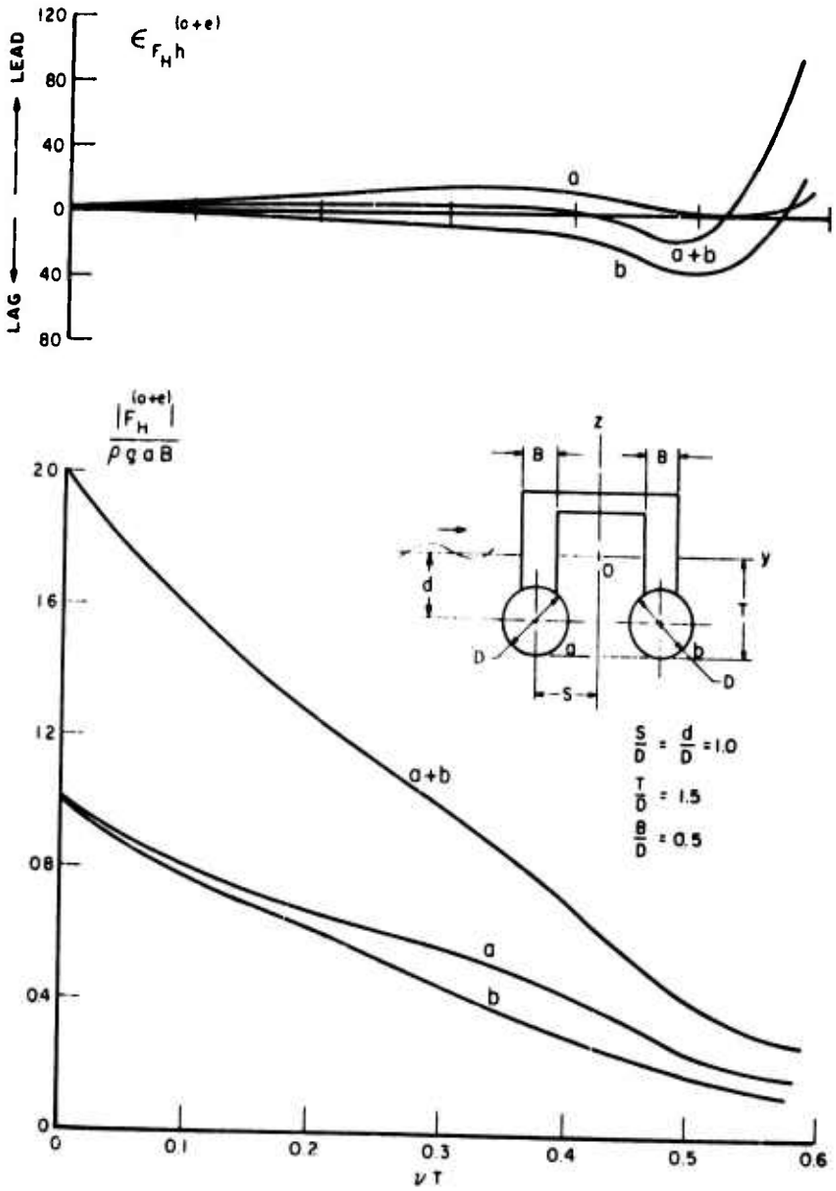


Figure 23b : Heave-exciting forces on cylinders a,b and a+b

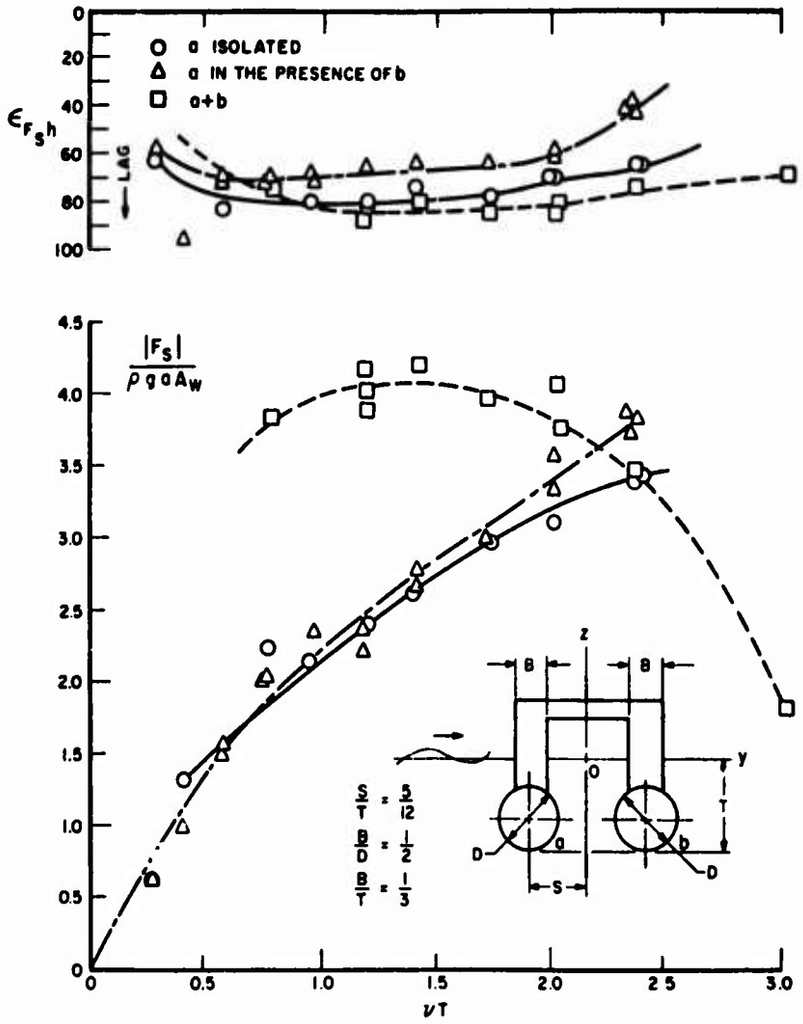


Figure 24a : Sway-exciting force on motora type twin floats

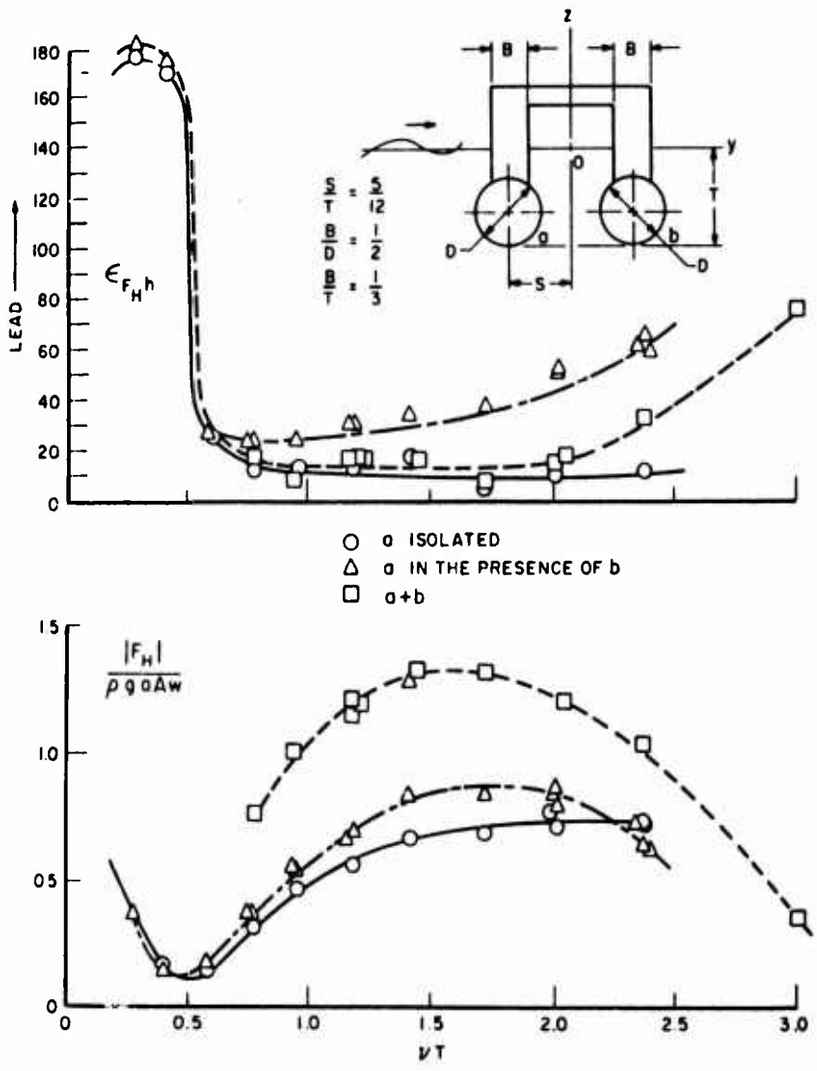


Figure 24b : Heave-exciting forces on motora type twin floats

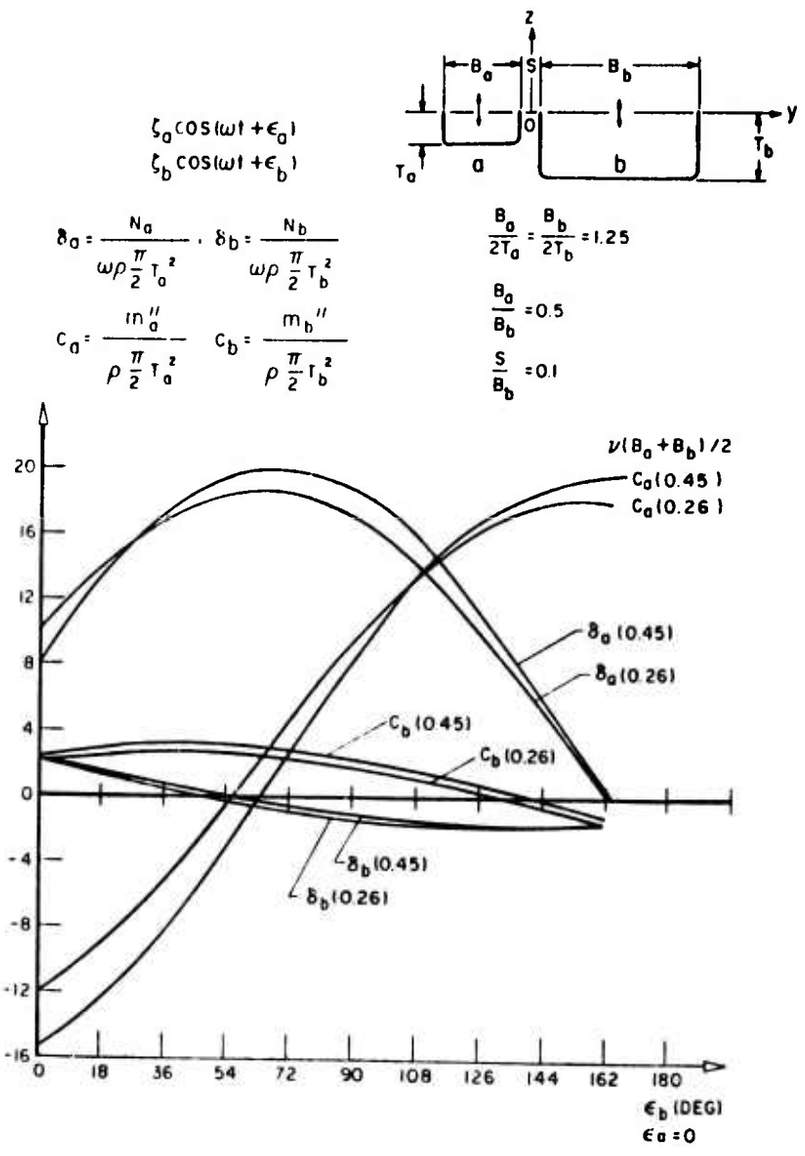


Figure 25a : Hydrodynamic characteristics of two heaving cylinders as function of phase difference

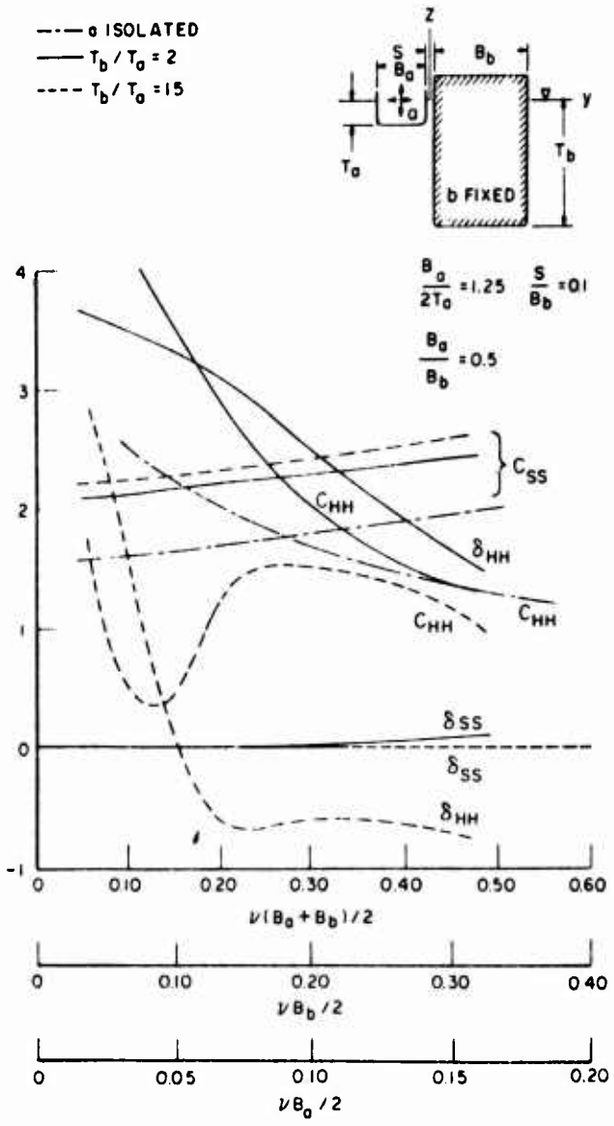


Figure 25b : Swaying and heaving hydrodynamic forces on cylinder a influenced by fixed cylinder b

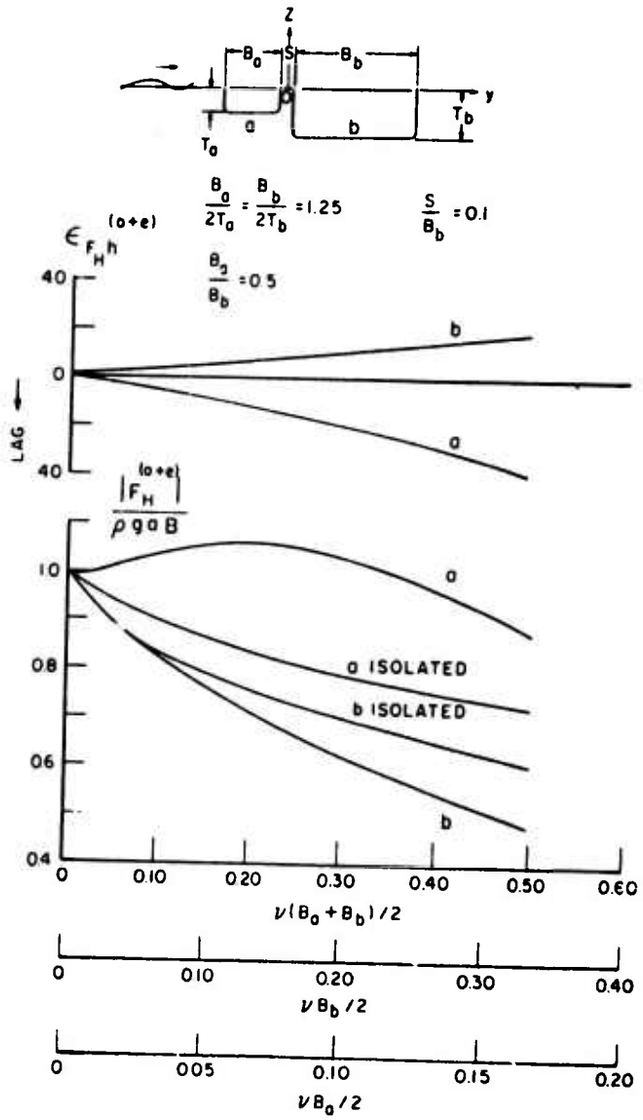


Figure 25c : Heave-exciting forces on cylinders a and b

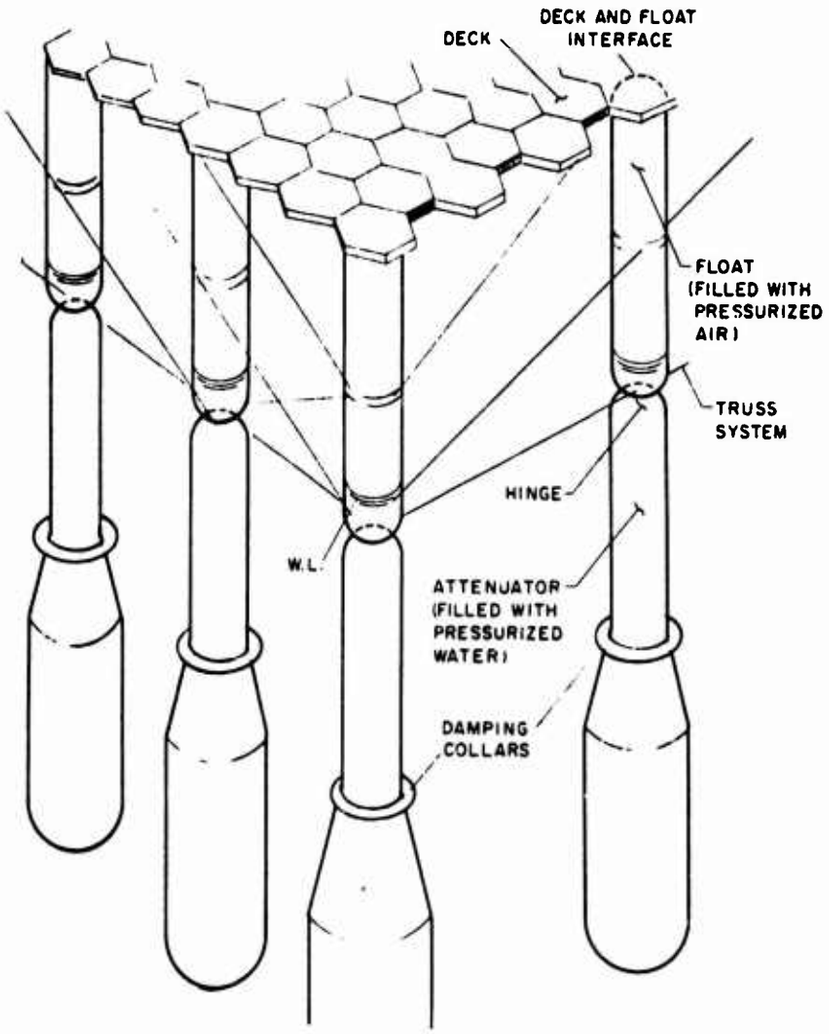


Figure 26 : Illustration of float configuration

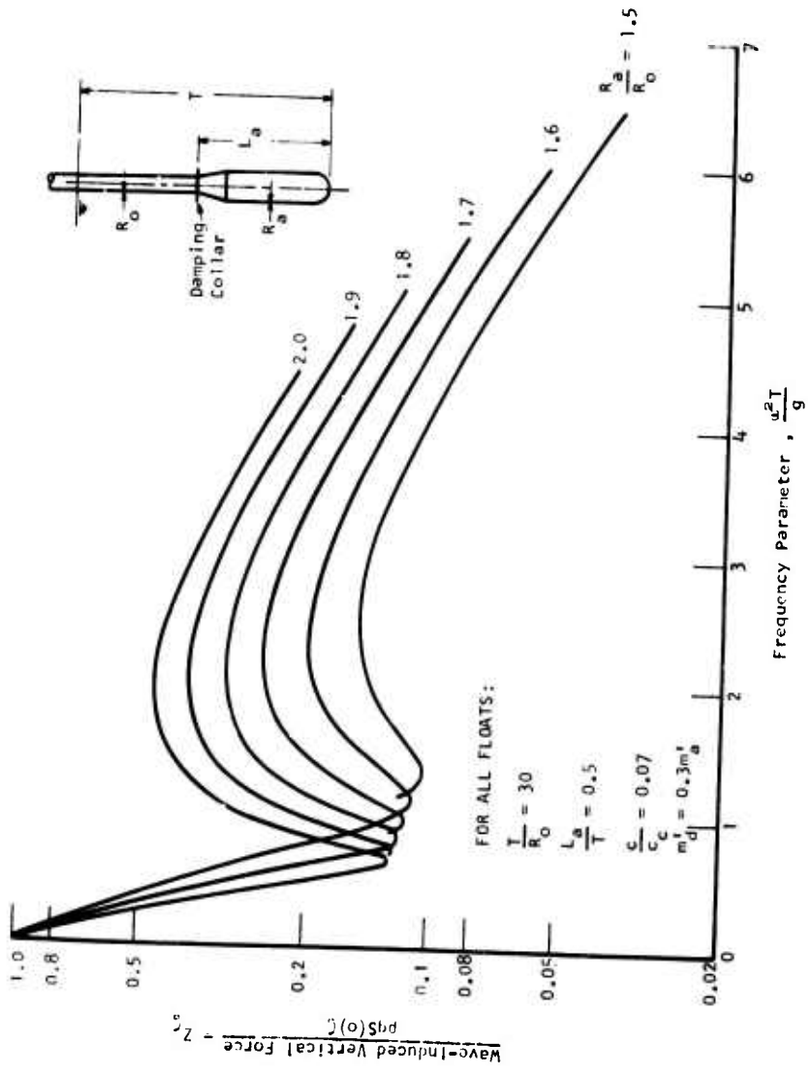


Figure 27 : The influence of $\frac{R_a}{R_o}$ on wave-induced vertical force

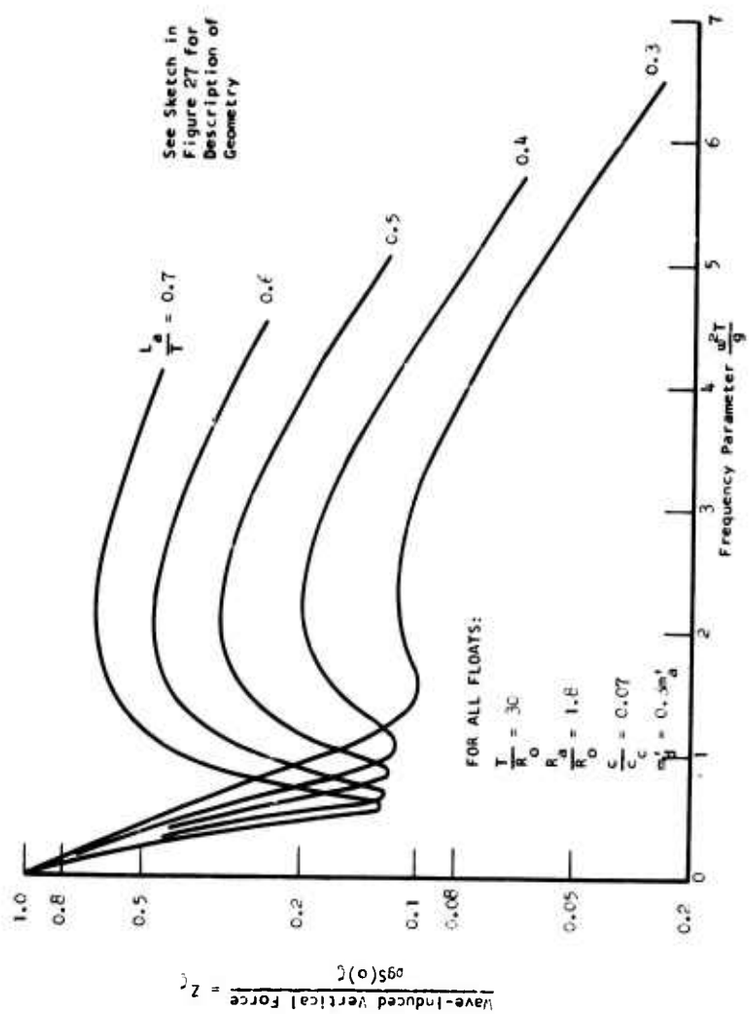


Figure 28 : The influence of $\frac{L_a}{T}$ on wave-induced vertical force

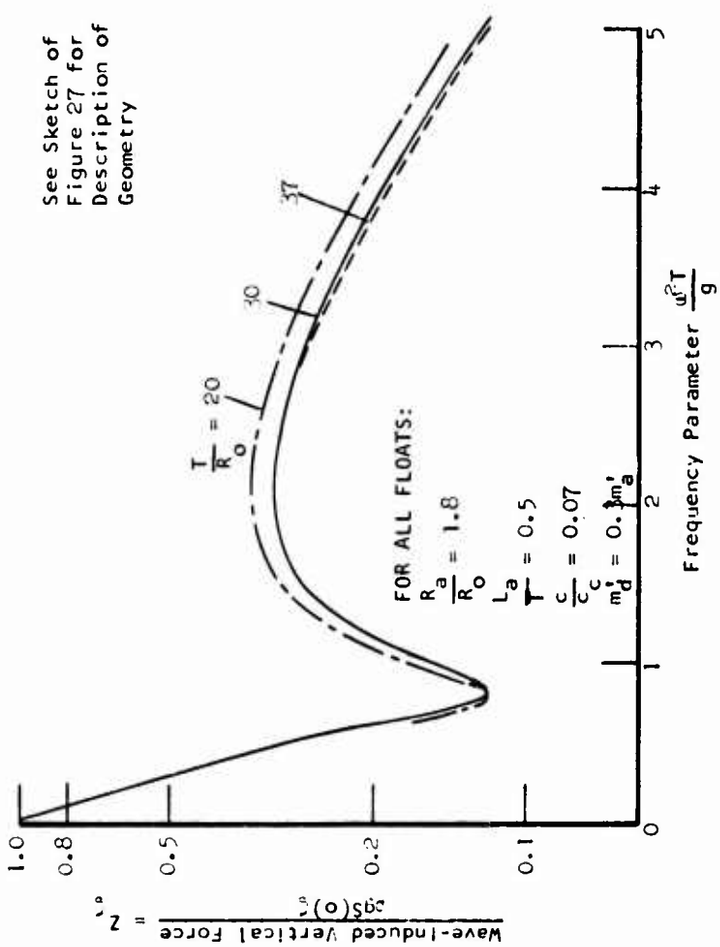


Figure 29 : The influence of $\frac{T}{R_o}$ on wave-induced vertical force

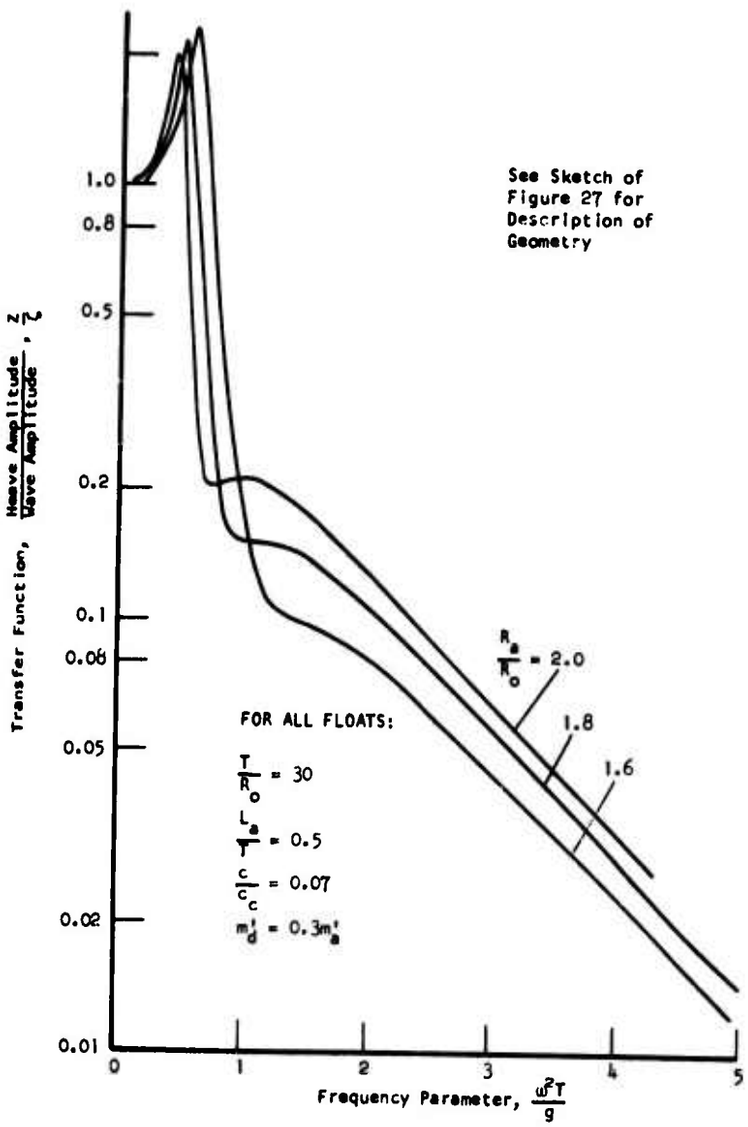


Figure 30 : The influence of $\frac{R_a}{R_o}$ on the heave transfer function

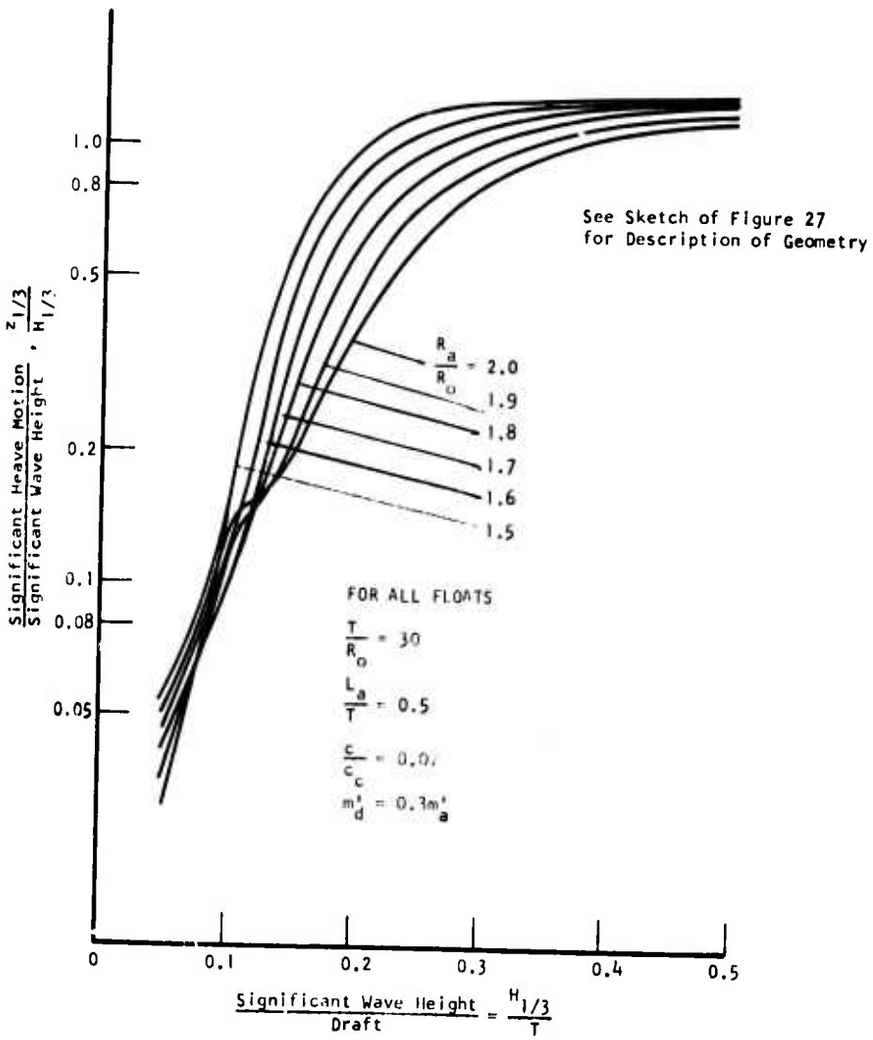


Figure 31 : The influence of $\frac{R_a}{R_o}$ on heave spectral response

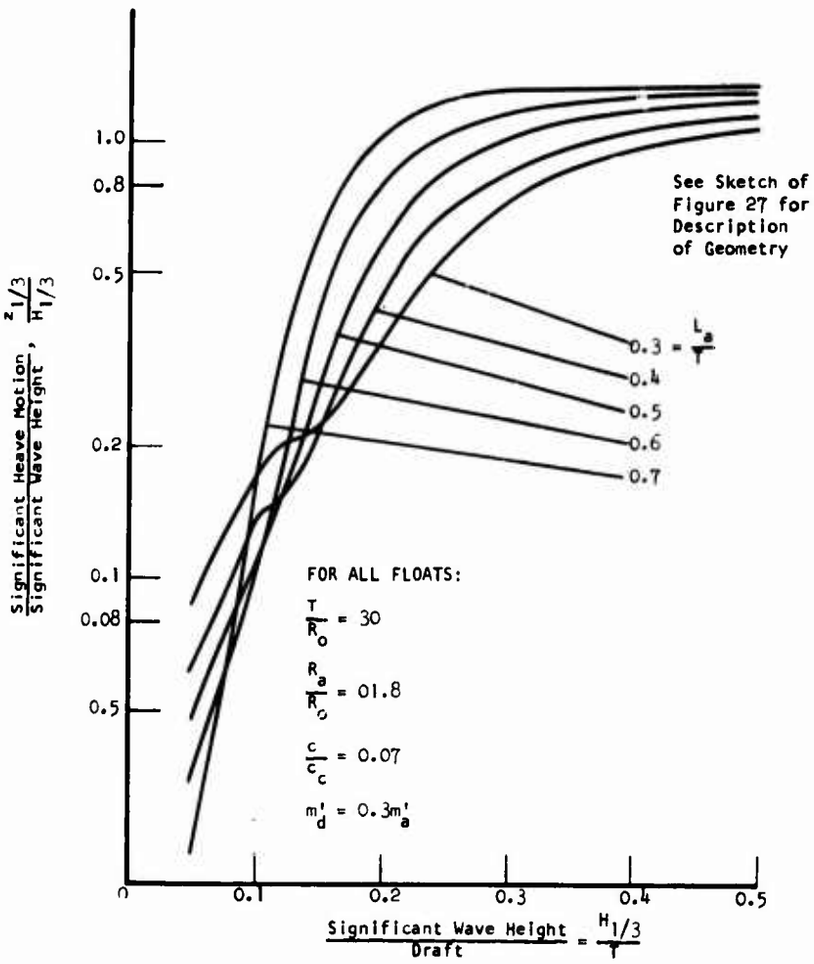


Figure 32 : The influences of $\frac{L_a}{T}$ on heave spectral response

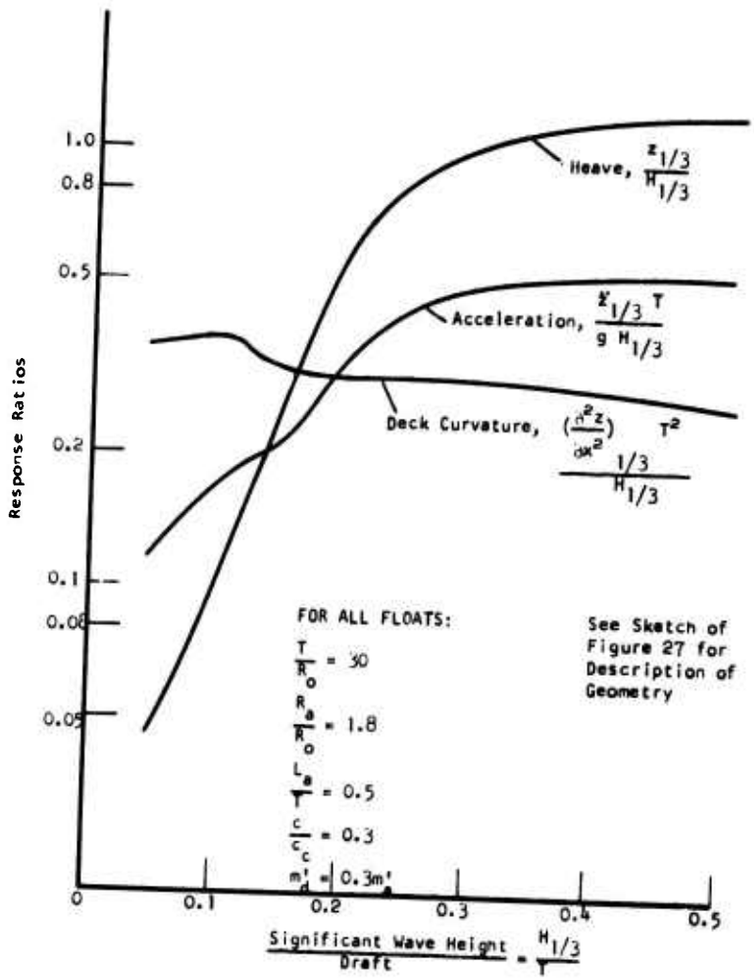


Figure 33 : The effect of sea state (significant wave height) on thre heave-related spectral responses

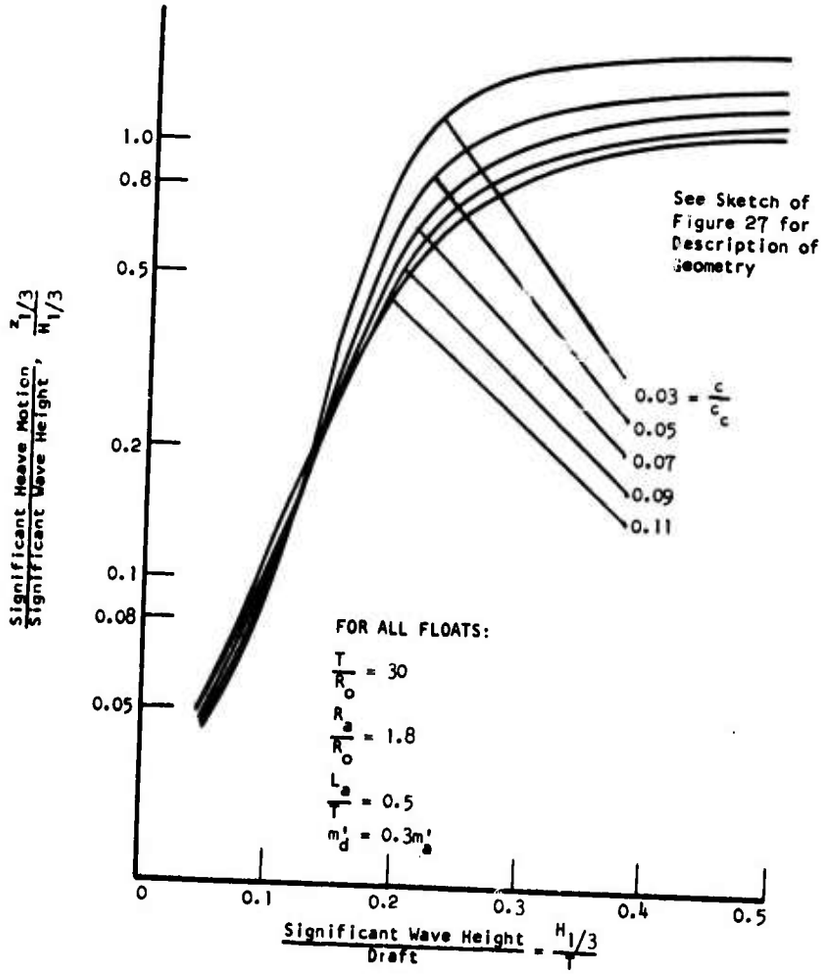


Figure 34 : The influence of damping coefficient $(\frac{c}{c_c})$ on heave spectral response

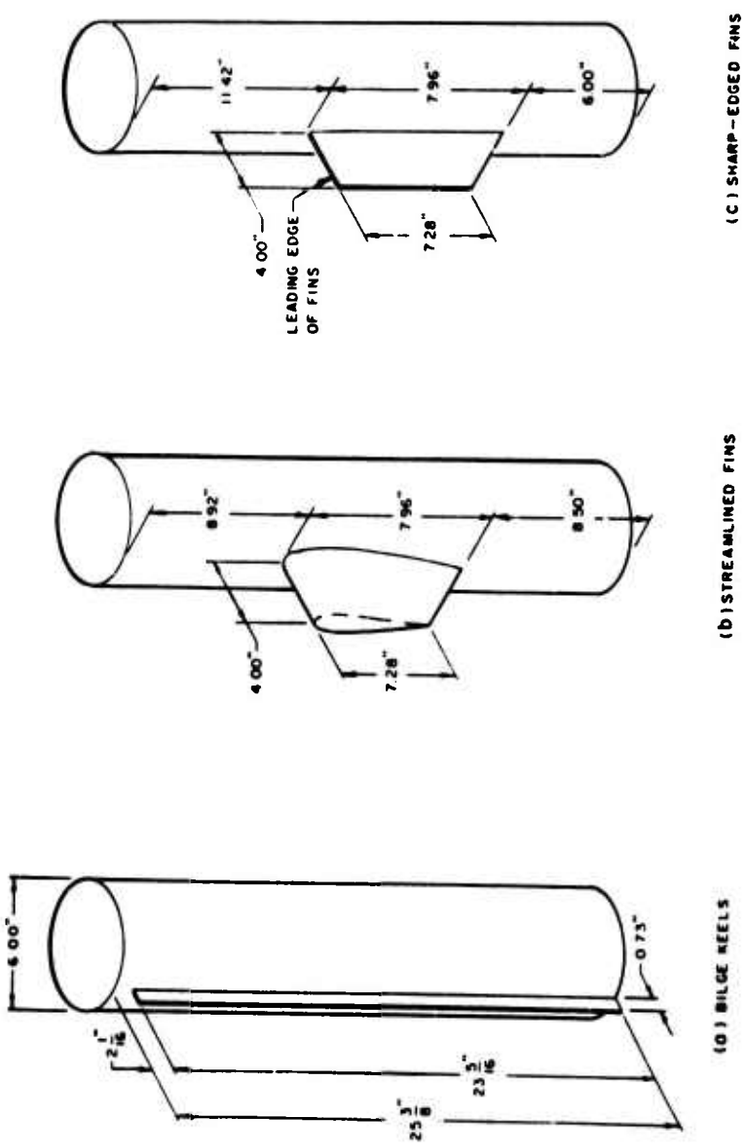


Figure 35 : Sketch of 6" diameter cylinder with various appendages

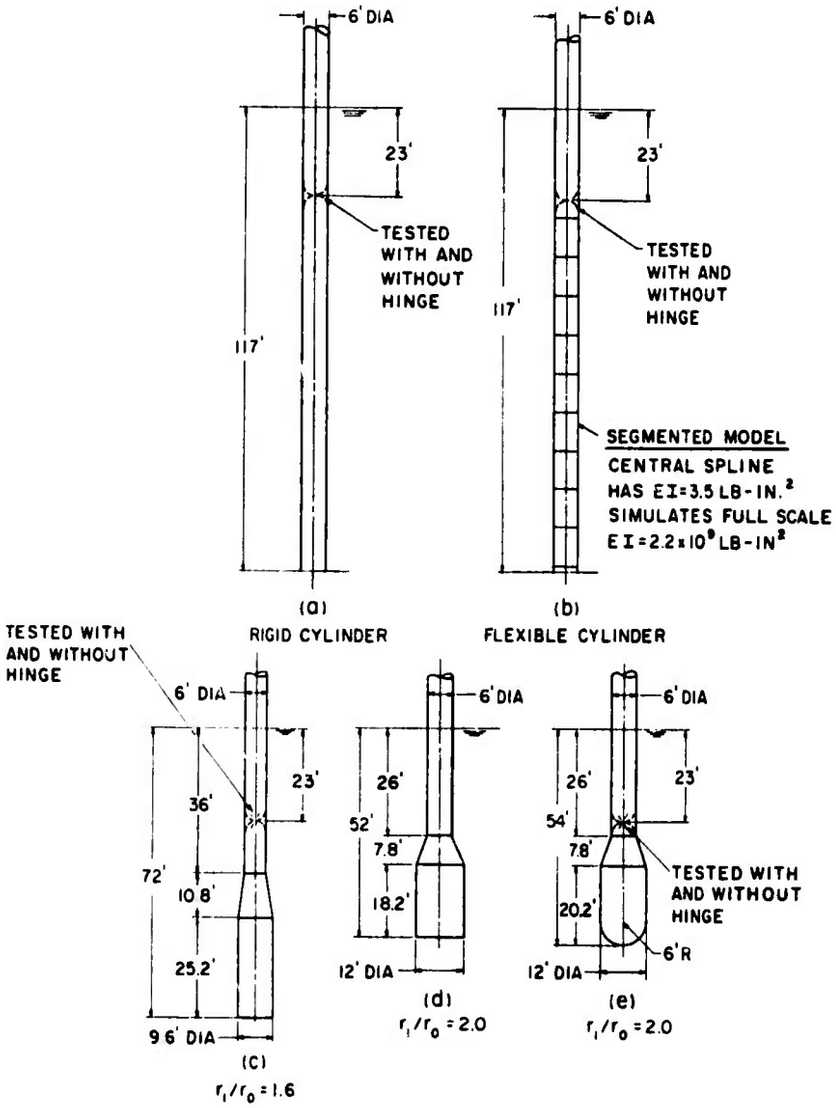


Figure 36 : Models used in test program, scale ratio : 1/57.6

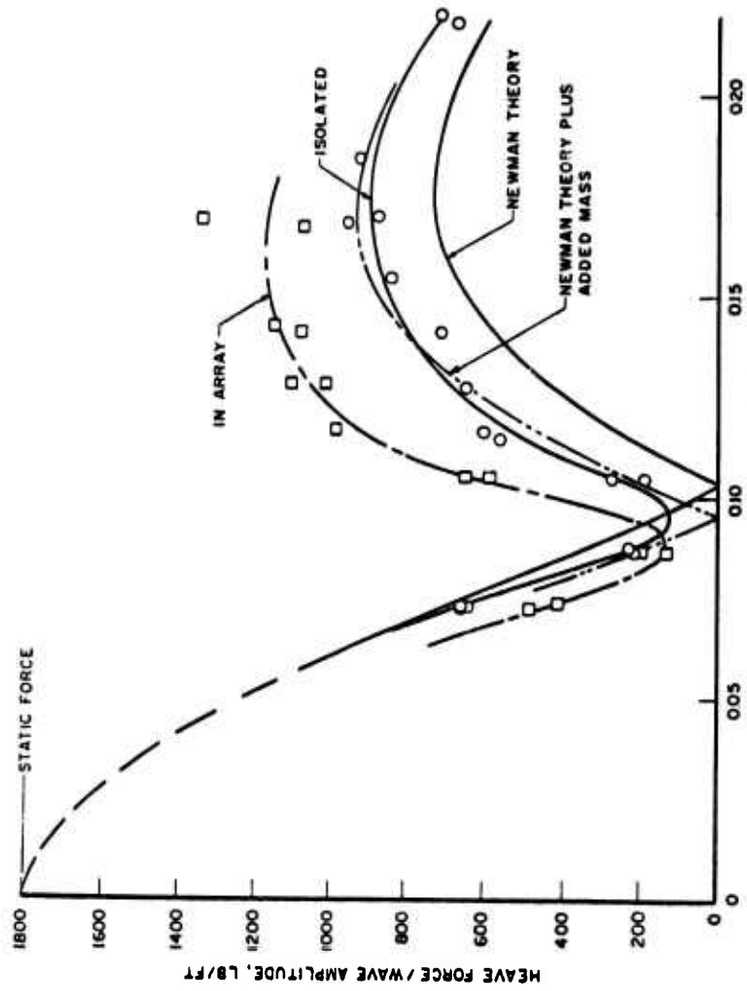


Figure 37 : Wave-induced vertical force on full float (figures 36-d,e)

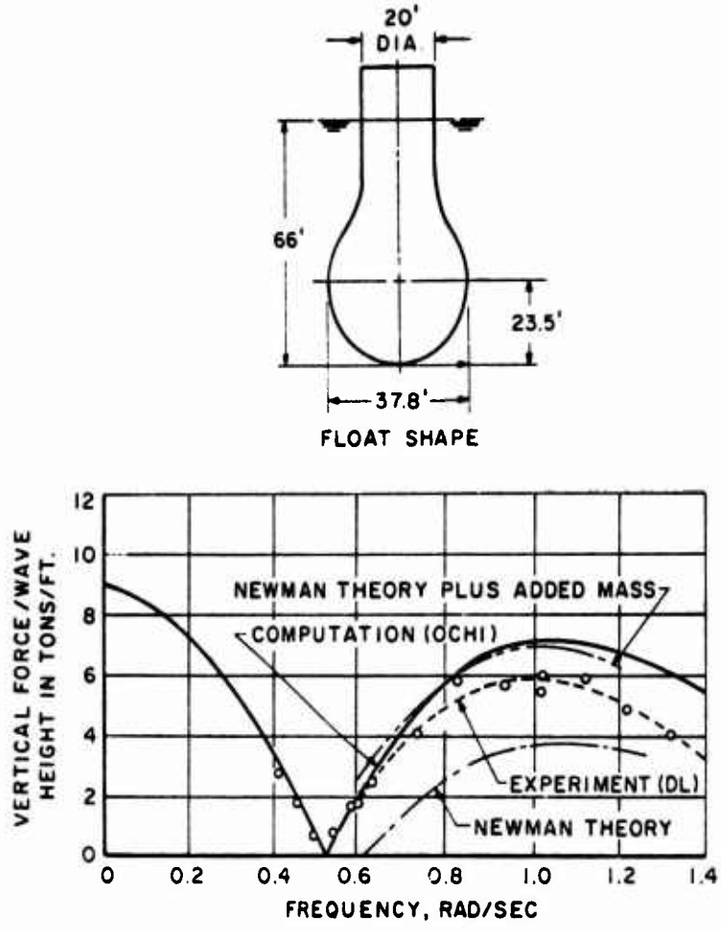


Figure 38 : Wave-induced vertical force on a very full float (references 63, 64)

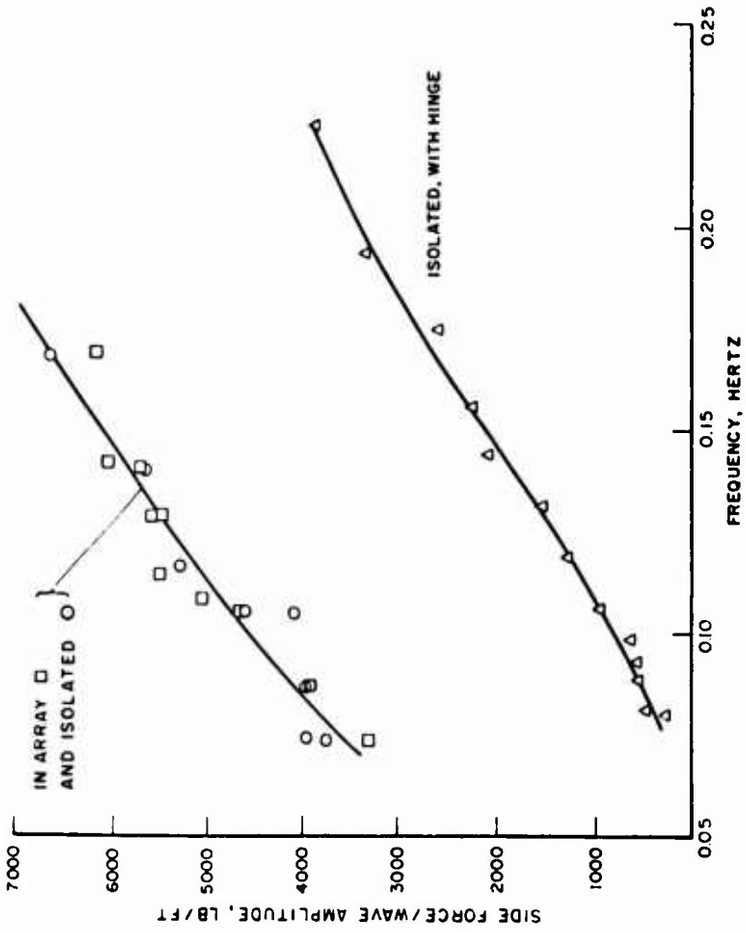


Figure 39 : Wave-induced side force on full float (figures 36-d,e)

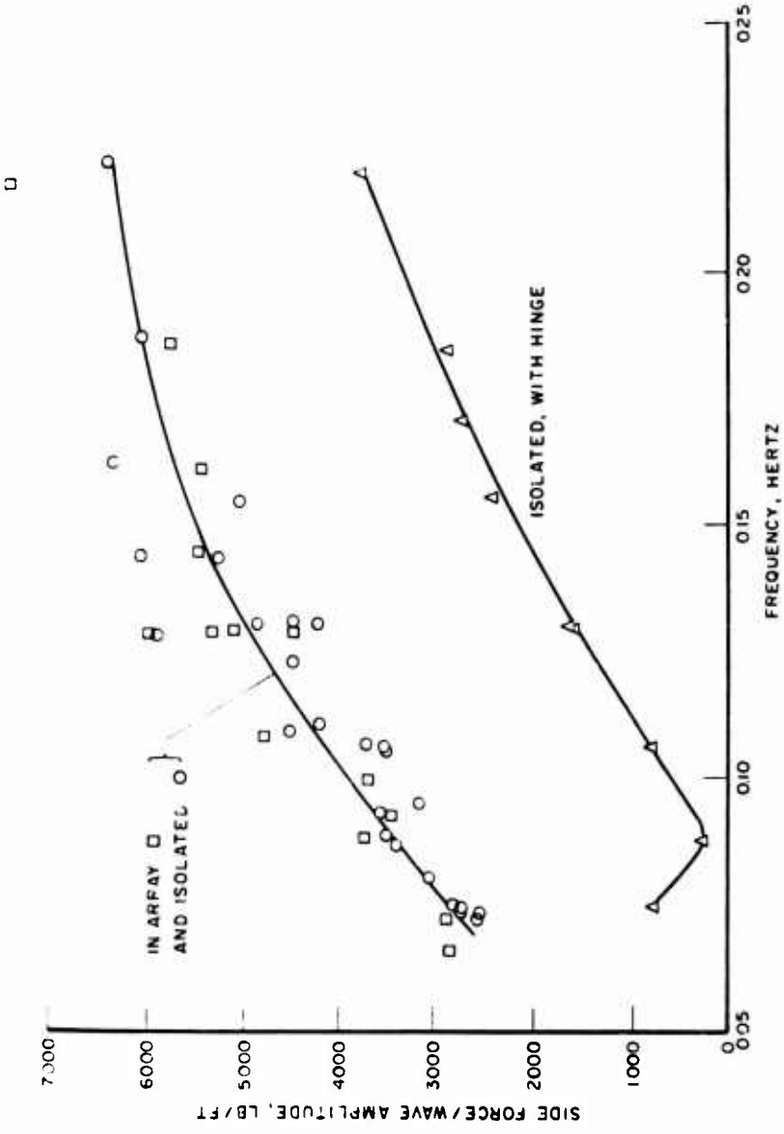


Figure 40 : Wave-induced side force on full float (figures 36-c)

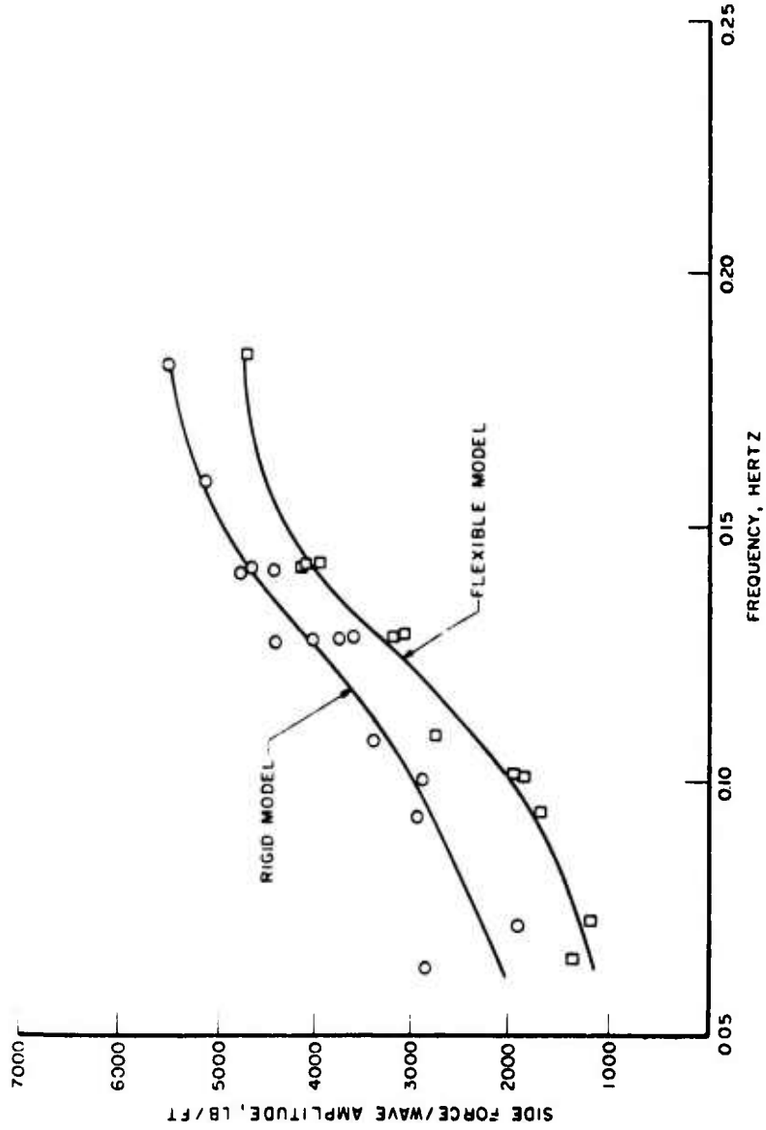


Figure 41 : Wave-induced side force on rigid and elastically-scalled cylindrical models (figures 36-a, b)

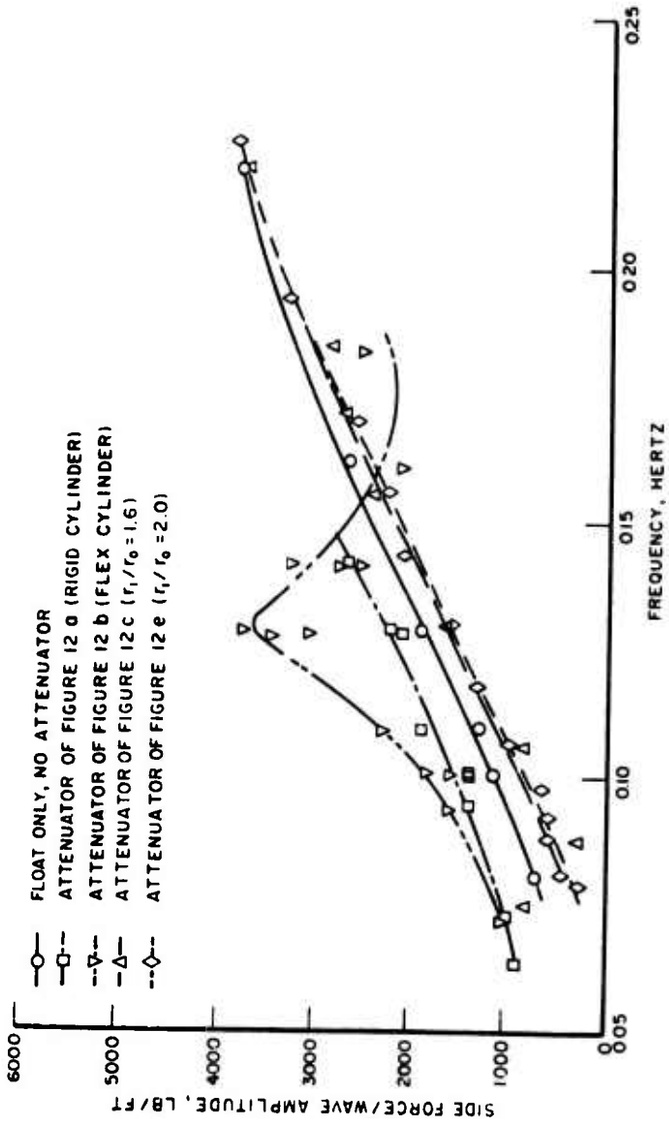


Figure 42 : Wave-induced side force with pitch hinge : all models (figures 36-a,b,c,d,e)

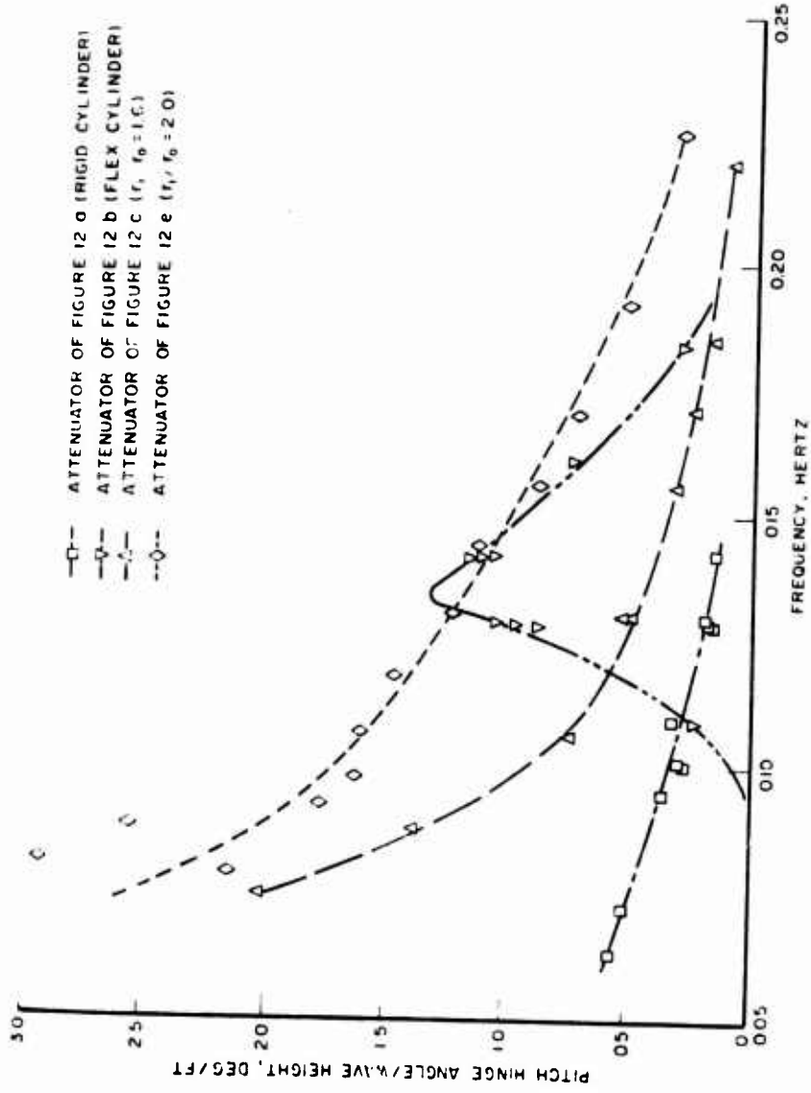


Figure 43 : Wave-induced pitch motions for hinged models (Figures 36-a,b,c,d,e)

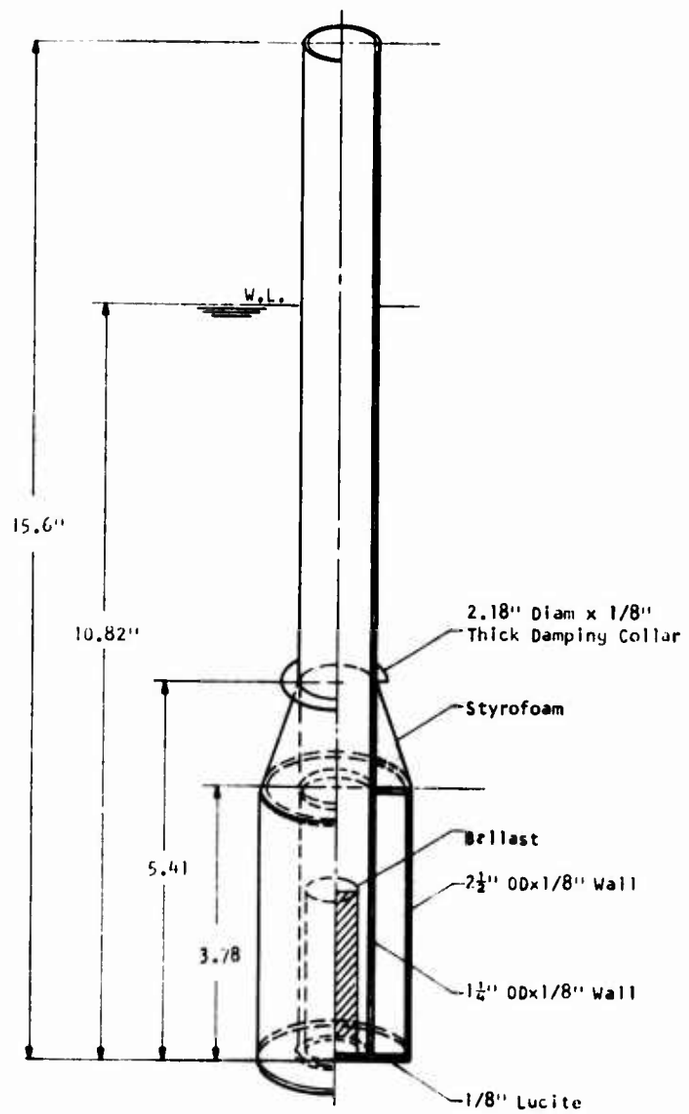


Figure 44 : Sketch of float fabrication method

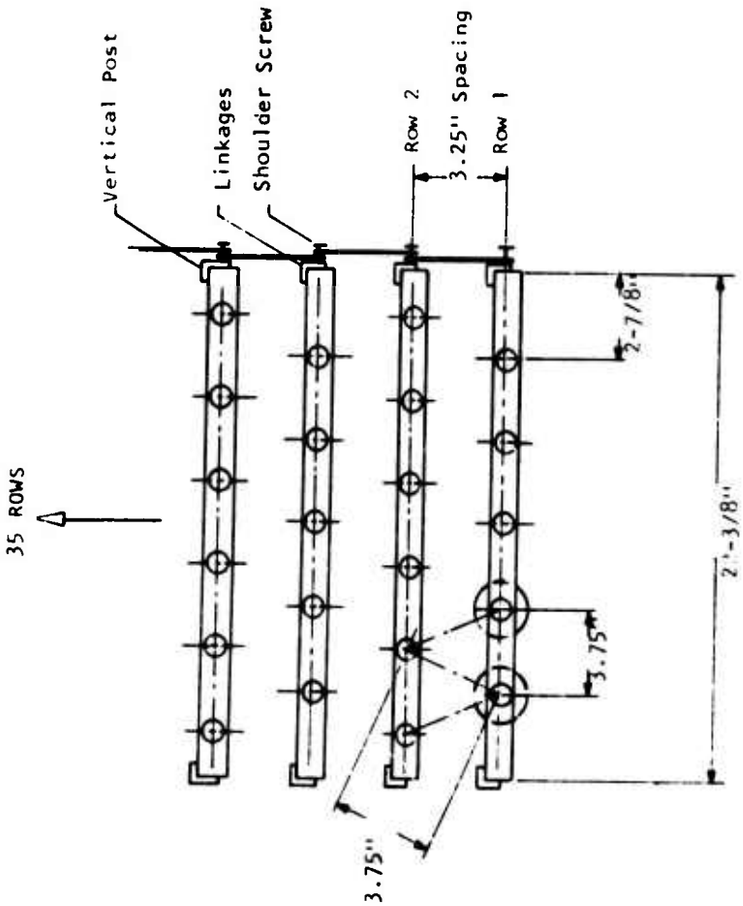


Figure 45 : arrangement and specing of floats

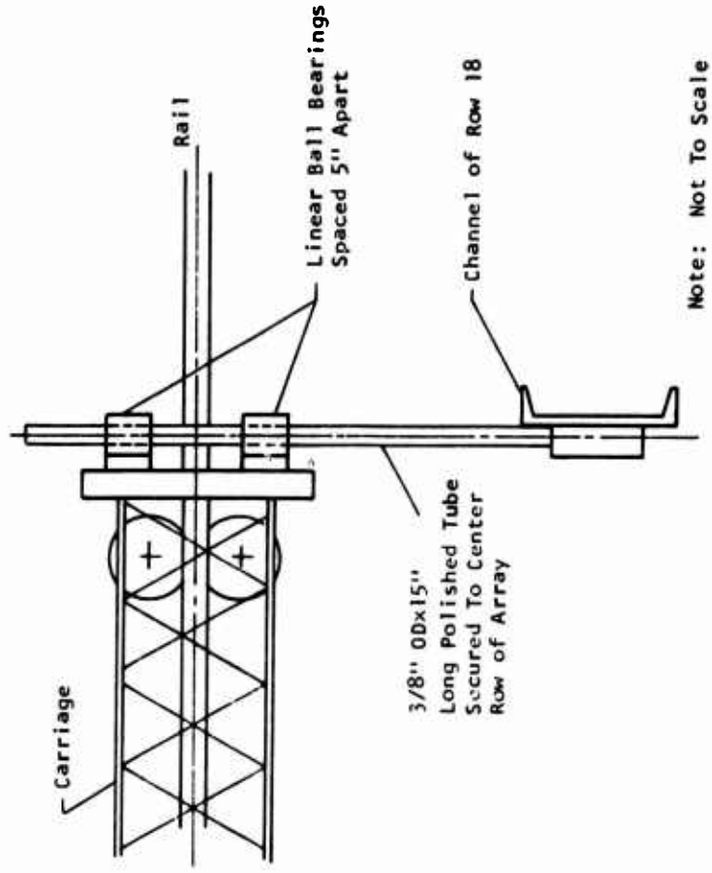


Figure 46 : Sketch of heave mast-pitch restraining device

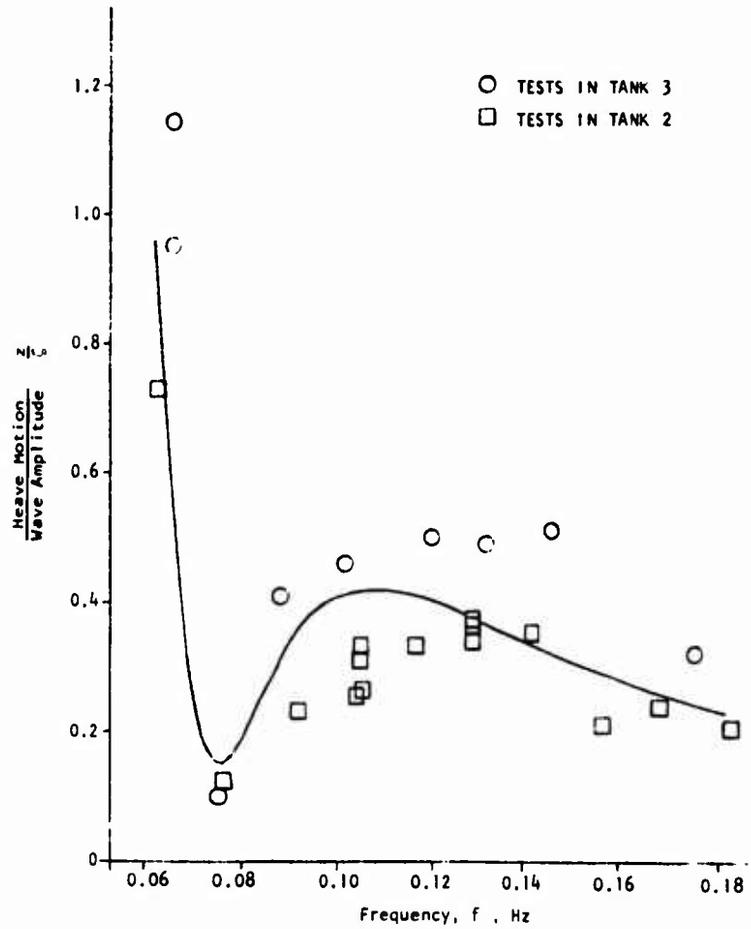


Figure 47 : Heave motions due to waves on row 18 of model island

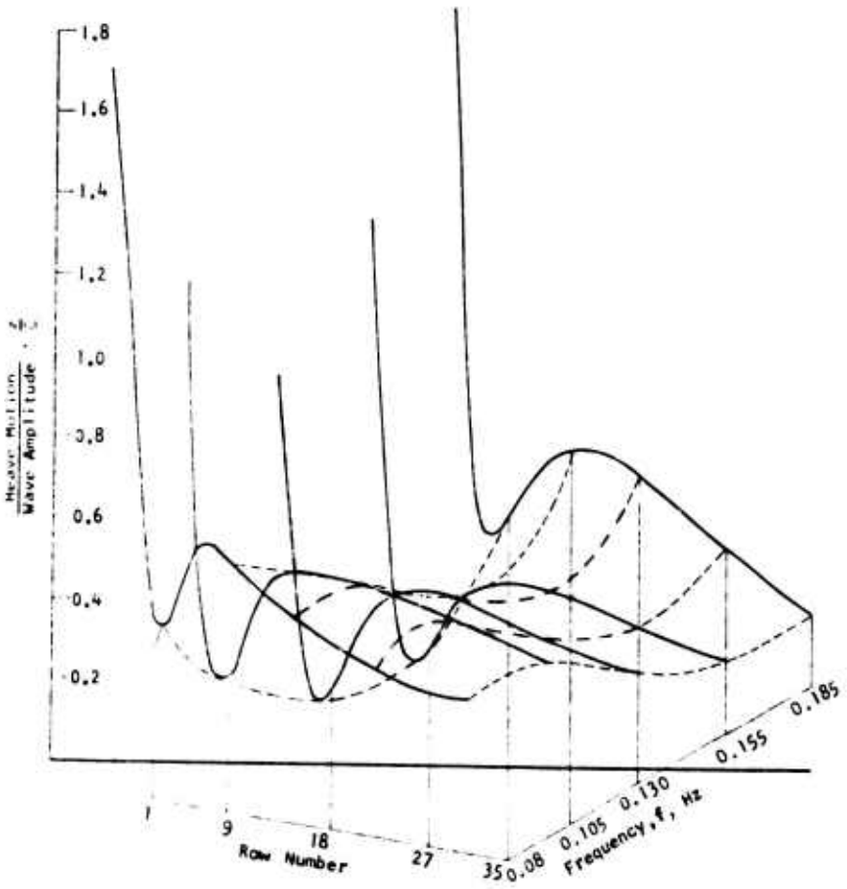


Figure 48 : Carpet plot of heave motion due to waves for articulated model

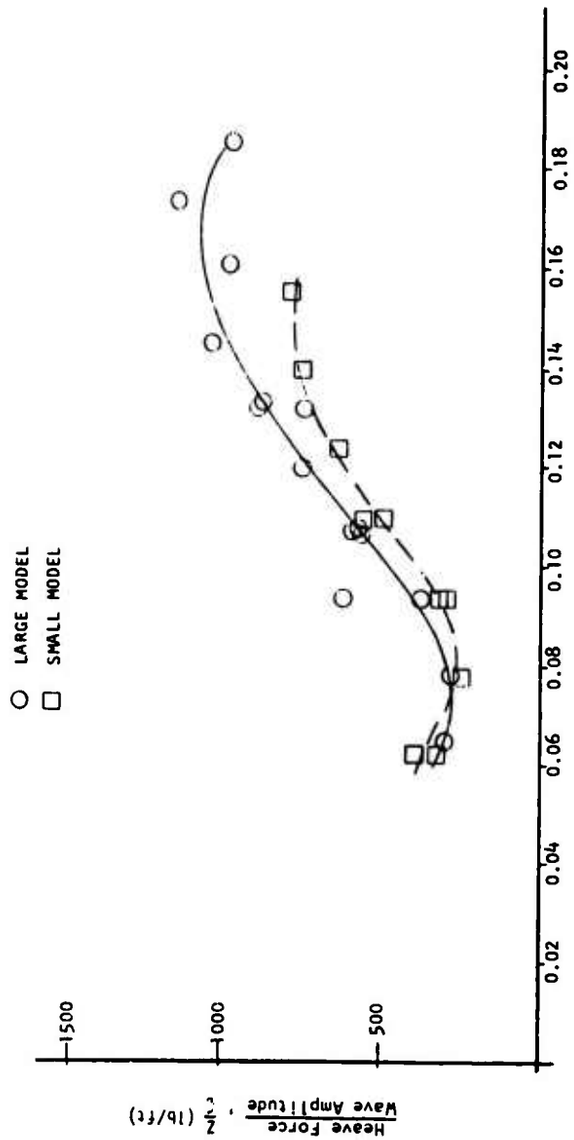


Figure 49 : Heave force due to waves on row 17 of model island

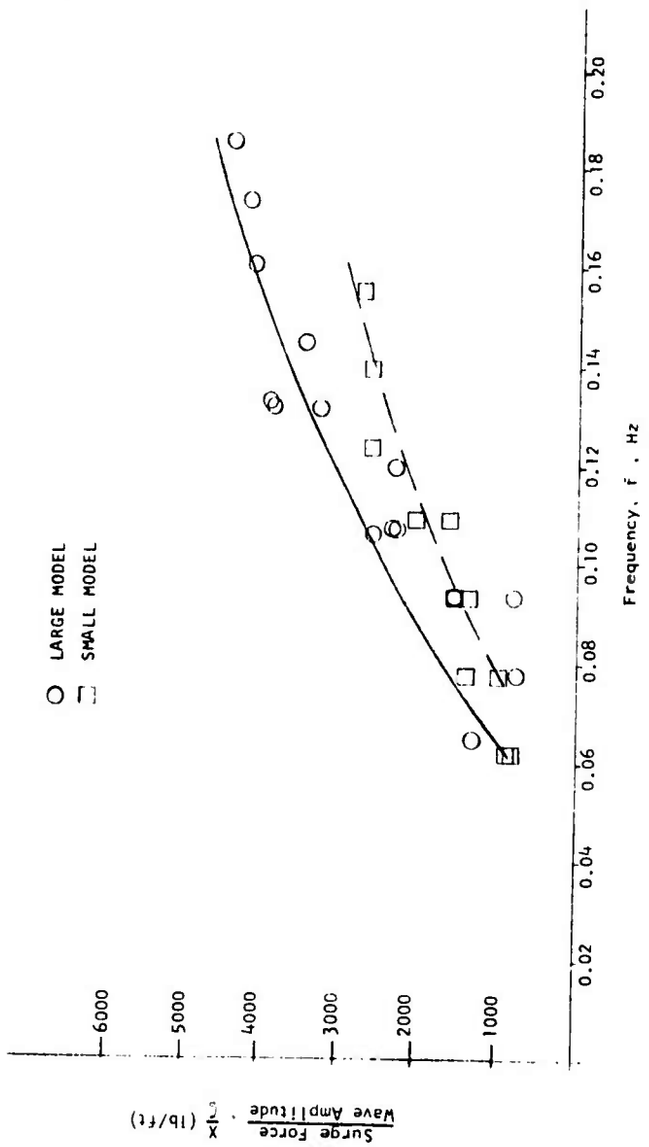


Figure 50 : Surge force due to waves on row 17 from model island

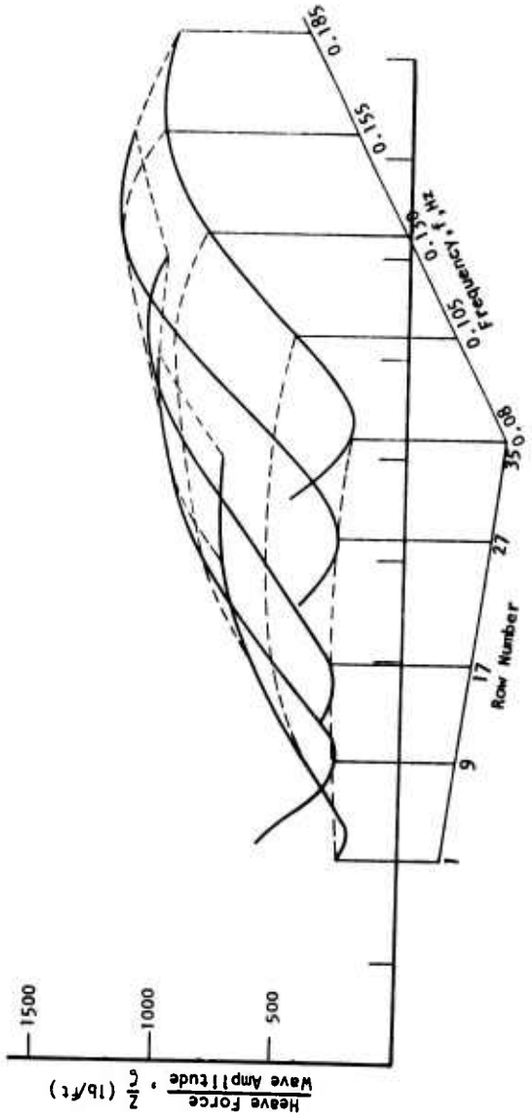


Figure 51 : Carpet plot of wave-induced vertical force on restrained 6 x 35 array of floats

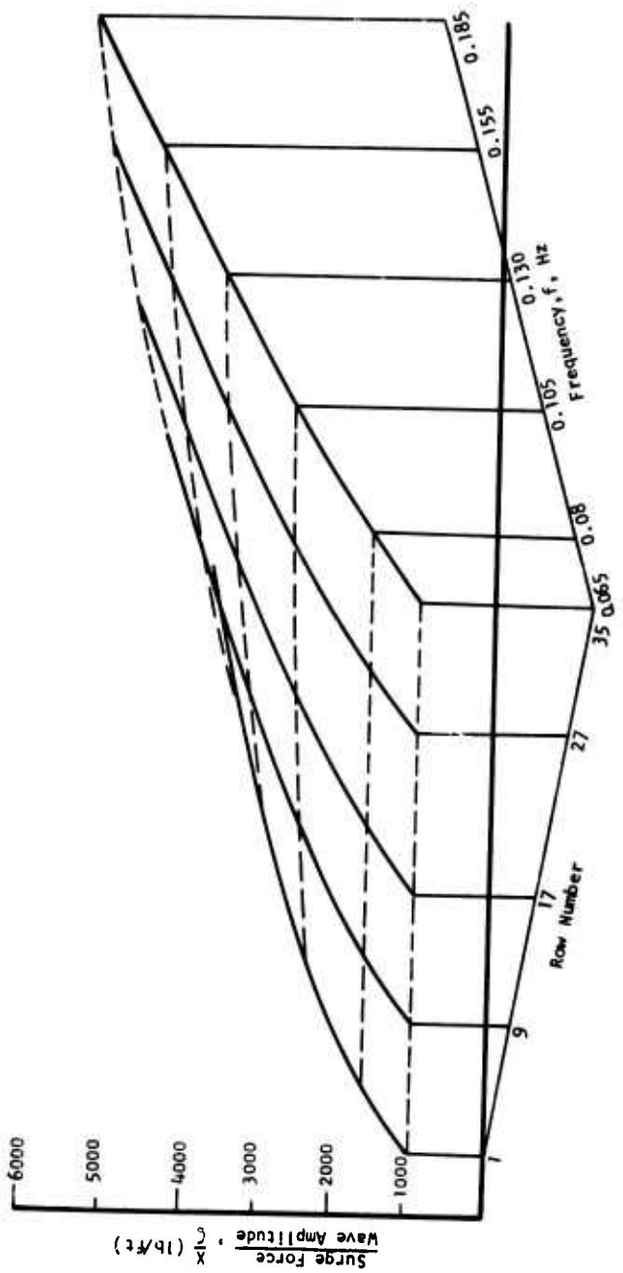


Figure 52 : Carpet plot of surge force due to waves

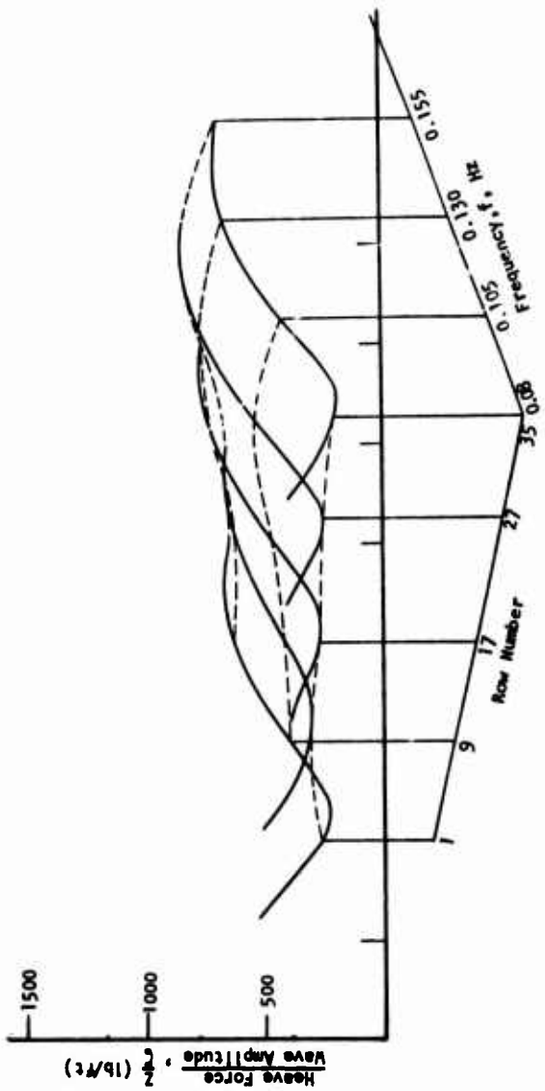


Figure 53 : Carpet plot of heave force due to waves for small model

DISCUSSION

Michel K. Ochi
Naval Ship Research and Development Center
Bethesda, Maryland, U.S.A.

My discussion is directed toward the evaluation of underwater float configuration which is one of the most difficult decisions to make for the design of a float-supported ocean platform.

The authors have derived a significant conclusion that a slender float with displacement relatively uniformly distributed along its length appears to be superior in mild seas, while a float with displacement concentrated near the bottom is preferable in relatively severe seas. This writer concurs with this conclusion. It may be well, however, to call the authors' attention that this conclusion is true from the view point of platform motions, but the validity of the conclusion should also be confirmed from the view point of wave-induced forces and moments of the platform.

To clarify the point of discussion, let us consider the following example : suppose a platform of proper size is floating without any restrictions, the minimumization of motions is of utmost importance. Suppose the platform is moored, on the other hand, a float configuration which yields the minimum wave-induced forces and moments of platform is highly desirable. The same way be true for a platform of relatively large size consisting of several element platforms which have been connected into a single unit. This is because the minimumization of the hydrodynamic forces and moments is necessary for safe connection of each element platform.

Selection of the best float configuration from the view point of motions may be rather difficult ; however, the best configuration from the view point of wave-induced forces can be achieved by adjusting the waterplane area of floats, since the wave-induced force on a floating body can be reduced to almost zero at a certain frequency if the underwater configuration is properly selected. This property was discussed by Motora and Koyama at the 6th Symposium in 1966 and is also demonstrated in the authors'study.

In short, this writer would like to suggest that the evaluation of float configuration should be made from two different view points ; i.e. motions and wave-induced forces and moments of the platform.

REPLY TO DISCUSSION

John A. Mercier
Stevens Institute of Technology
Hoboken, New Jersey, U.S.A.

Doctor Ochi is, of course, right. The proper design characteristics must depend on the design problem and in the case of studying structural characteristics and the behaviour of rigidly connected floats one must be able to calculate the forces and minimize them, rather than the motions responsible, which I studied at that time.

I found that our situation in regard to calculating the vertical forces on such floats was pretty satisfactory so long as the interaction effects could be safely ignored, that is, so long as the floats were sufficiently spaced - and I hope to be able to say what I mean by "sufficiently" at some time in the near future. I know that if they are too closely spaced we cannot calculate them satisfactorily.

The horizontal force, on the other hand, is more complicated, as Weigel has just reported, and we must await further results for this case. In fact, the calculations may be influenced by the presence of ambient currents and other complicating factors.

* * *

SOME ASPECTS OF VERY LARGE OFFSHORE STRUCTURES

G. van Oortmerssen
Netherlands Ship Model Basin
Wageningen, Netherlands

ABSTRACT

Due to the fast development of the offshore industry, there is a rapidly increasing demand for very large unconventional offshore structures, both floating and fixed to the bottom, to be applied for storage and production purposes. The general hydrodynamic aspects of these big objects will be summarized in this paper. In the case of floating structures, the drift force is relatively important and consequently resonance phenomena can occur in the anchor lines. Therefore, in rather shallow water a structure fixed to the bottom will be preferred in many cases.

From calculations and model experiments it appeared that the wave loading on a large object and the wave pattern around it can be calculated with great accuracy with a diffraction theory.

As an example a cylindrical storage tank - 96 m in diameter, fixed to the bottom in 50 m deep water and extending above the water surface - will be discussed.

This example is hardly hypothetical, since structures with comparable dimensions are in the design stage or under construction at present. The wave pressure on the tank and the wave diffraction as calculated with the potential theory are compared with measurements. The agreement is very good.

From the wave pattern around the tank it was found, that it can be advantageous to moor a tanker immediately to the tank. Model tests were con-

ducted with a tanker moored behind the tank in irregular seas, while the tanker motions and the force in the bowhawser were measured.
The results of these tests will be compared with the results of tests conducted with existing mooring systems.

I. INTRODUCTION

The increasing importance of remote offshore oil fields has created a need for very large unconventional structures for production and storage of oil or liquid natural gas. Some very large structures are now in use, as for instance the floating oil storage 'Pazargad' and the submerged tank in Dubai, while others are under construction, as for example the large concrete tank for the Ekofisk field in the North Sea. Besides structures for exploitation and storage of minerals, the use of very large offshore structures is considered for a variety of future purposes. Plans exist to build polluting or dangerous plants on artificial islands, far from the living areas, to prevent a deterioration of the environmental conditions in densely populated industrial countries. Fear for calamities and a need of plenty of cooling water was the reason to study the possibility to build offshore nuclear power plants, and there is even talk of constructing a floating intercontinental air port.

With regard to the design and construction of a large unconventional offshore structure, a lot of problems arise. The structure has to be strong enough to survive the severest weather conditions. In the case of floating structures, it is a problem to design a proper anchor system. When the structure is fixed, the entire construction has to be stable. In most cases, such artificial islands require transshipment of goods from ships to island or vice versa. Consequently, attention has to be paid to the mooring of ships to the island. If a construction on the sea bottom is considered, its behaviour during immersion has to be studied carefully.

In order to be able to cope with future developments, a research program has been performed at the Netherlands Ship Model Basin. A computer program has been developed for the calculation of wave loads on objects of arbitrary shape, using a three-dimensional source technique, while the effects of the free surface and of finite water depth were taken into account. With this program it is also possible to calculate the wave pattern around the structure. Subsequently model experiments were carried out to check the theoretical results.

Also the mooring of a tanker to a large circular storage tank was investigated by means of model tests.

In this paper the following topics will be discussed successively :
- the calculation of wave loads and wave diffraction, with a comparison of theoretical and experimental results;
- anchoring of floating structures;
- mooring of a ship to an artificial island.

The object is not to give practical solutions, but to scan the problems and possibilities which occur in the field of hydrodynamics.

II. WAVE-STRUCTURE INTERACTION

We shall consider the following aspects of the interaction between waves and a structure :
- the pressure distribution on the surface of the body, which has to be known for the structural design;
- the total wave excited forces and moments, which are important for the design of an anchor system in the case of a floating structure, or, if the body is fixed, for the stability of the structure : the amplitude of the vertical force, for instance, must be smaller than the apparent weight of the structure in the case of a submerged structure fixed to the bottom;
- the wave diffraction : if ships are to moor to the structure, it is important to know in which way the incident waves are deformed by the presence of the structure.

The interaction between waves and a structure is governed by inertial, gravitational and viscous effects. The relative importance of each of these effects depends on the ratios of the wave height and the wave length to the body dimensions. In figure 1 the regions of influence of the different effects are indicated for the case of a vertical circular cylinder (See ref.[1]). From this figure it appears, that gravitational effects must be taken into account if ka is larger than 0.6, or in general, if the wave length is smaller than approximately five times the body dimensions. This means that, for the structures with which we are dealing here, both the inertial and gravitational effects must be considered. These phenomena can be described adequately by means of the potential theory; this theory, however, presupposes an inviscid fluid. Fortunately, it can be stated that for large structures the potential forces are predominant to such a degree, that the viscous effects can be neglected.

II. 1 Potential theory approach

Consider a fluid, bounded by a partially or totally submerged rigid body, a fixed bottom and a free surface. The undisturbed free surface will be taken as XOY-plane of the co-ordinate system, with the z-axis pointing vertically upwards. The fluid is assumed to be inviscid, incompressible and irrotational. All motions will be infinitely small. At infinity the fluid motion behaves as a single harmonic wave, travelling in the positive direction of the x-axis. If the undisturbed wave has a frequency ω, the velocity potential may be written as

$$\Phi = \mathrm{Re}\left[\varphi e^{-i\omega t}\right] \tag{1}$$

The function φ has to satisfy the Laplace equation :

$$\nabla^2 \varphi = 0 \tag{2}$$

and the boundary conditions :

- at the bottom $\frac{\partial \varphi}{\partial z} = 0$ for $z = -d$ (3)
- in the free surface $\frac{\partial \varphi}{\partial z} = \nu \varphi$ for $z = 0$ (4)
- at the body contour $\frac{\partial \varphi}{\partial n} = 0$ for $\underline{x} = \underline{s}$ (5)

in which

d	= water depth
ν	$= \omega^2/g$
g	= the acceleration of gravity
$\underline{s}$	= vector which describes the body contour
$\underline{n}$	= vector normal to the contour

The function φ can be split into two components :

$$\varphi = \varphi_i + \varphi_s \tag{6}$$

in which

φ_i	= the wave function of the undisturbed incident waves
φ_s	= the wave function of the scattering waves

Both components have to satisfy the Laplace equation. The function for the incident wave, including the boundary conditions in the free surface and at the bottom, is given by

$$\varphi_i = \frac{\zeta_a g}{\omega} \frac{\cosh k(d+z)}{\cosh kd} e^{ikx} \tag{7}$$

in which :

ζ_a = incident wave amplitude
k = wave number = $2\pi/\lambda$
λ = wave length

The relation between wave frequency and wave length is given by the dispersion equation :

$$\omega^2 = kg \tanh kd \tag{8}$$

The wave function φ_s , corresponding to the motion of the scattered waves must, besides the boundary condition in the free surface and at the bottom, also satisfy the radiation condition. This condition requires that, at infinity, φ_s behaves as a radially outgoing progressive wave and imposes a uniqueness which would otherwise not be present.

In a system of local axes with cylindrical co-ordinates r, θ and z, the radiation condition can be formulated as :

$$\lim_{r \to \infty} r^{1/2} \left(\frac{\partial \varphi_s}{\partial r} - ik\varphi_s \right) = 0 \tag{9}$$

in which :

$r = (x^2 + y^2)^{1/2}$

$\theta = \arctan (y/x)$

II. 2 Analytical solutions

An analytical solution of the potential function can only be given for certain bodies of which the geometry can be described by means of a simple mathematical formula, such as the cylinder, the sphere and the ellipsoid. Havelock [2] for instance, has given the solution for an infinitely long vertical cylinder of circular section. This solution has been adapted for a cylinder fixed to the bottom in shallow water by Mac Camy and Fuchs [3] and Flokstra [4] . According to Flokstra, the analytical solution of the potential in cylindrical co-ordinates is - for this particular case - given by :

$$\Phi (r, \theta, z, t) = \frac{\zeta_a g}{\omega \cosh kd} \cosh k (z+d) \, e^{-i\omega t} \cdot \sum_{n=0}^{\infty} \epsilon_n C_n (i)^{+n} \cos n\theta \tag{10}$$

in which :

$$C_n = i \frac{J_n(kr)\, Y_{n,r}(ka) - J_{n,r}(ka)\, Y_n(kr)}{J_{n,r}(ka) + i\, Y_{n,r}(ka)}$$

ϵ_n = 1 for n = 0

ϵ_n = 2 for n ≠ 0

For the case that the cylinder does not extend to the bottom, Garret [5] has derived an analytical solution, using variational principles.

II. 3 Numerical solutions

For the body of arbitrary shape, the velocity potential can be found from numerical methods. At the Netherlands Ship Model Basin a computer program has been developed for the numerical calculation of the velocity potential, using a source distribution over a surface inside the body. According to Lamb [6] the potential function can be found from :

$$\varphi_s(x) = \iint_A q(\underline{a})\, \gamma(\underline{x}, \underline{a})\, dA \qquad (11)$$

in which :

$\gamma(\underline{x}, \underline{a})$ = the Green's function for a source, singular in $\underline{a}$

$\underline{a}$ = vector which describes the surface A, on which the sources are located.

$q(\underline{a})$ = the unknown source strength.

The Green's function represents the contribution to the velocity potential in $\underline{x}$ due to a unit wave source located in a. A Green's function which satisfies the boundary conditions in the free surface, at the bottom and the radiation condition, has been given by John [7] :

$$\gamma(\underline{x}, \underline{a}) = 2\pi \frac{k^2 - \nu^2}{k^2 d - \nu^2 d + \nu} \cosh k(c+d) \cosh k(z+d) \left[Y_o(kr_j) - iJ_o(kr_j) \right] \qquad (12)$$

$$\ldots + \sum_{n=1}^{\infty} \frac{4(k_n^2 + \nu^2)}{dk_n^2 + d\nu^2 - \nu} \cdot \cos k_n(z+d) \cos k_n(c+d)\, K_o(k_n r_j)$$

in which :

$$r_j = \sqrt{(x-a)^2 + (y-b)^2}$$

$$k_n \tan (k_n . d) + \nu = 0$$

The source strength $q(\underline{a})$ can be obtained after substitution of (11) in the boundary condition at the body surface :

$$\frac{\partial \varphi}{\partial n} = \frac{\partial \varphi_i}{\partial n} + \frac{\partial \varphi_s}{\partial n} = 0 \text{ for } \underline{x} = \underline{s} \qquad (13)$$

or :

$$\frac{\partial}{\partial n} \left\{ \iint_A q(\underline{a}) . \gamma (\underline{x}, \underline{a}) \, dA \right\} = - \frac{\partial \varphi_i(\underline{x})}{\partial n} \text{ for } \underline{x} = \underline{s} \qquad (14)$$

For a restricted number of discrete sources, this integral equation changes into a set of linear equations in the unknown source strengths. For an infinitely great number of sources, the numerical solution approaches the exact solution. It will be clear that the accuracy obtained in the calculations depends on the number of sources applied and on the location of the sources.

II. 4 Pressure, forces and wave diffraction

Once the velocity potential is known, the different aspects of the interaction between structure and waves can be calculated without much difficulty. According to Bernoulli's theorem, the pressure is given by :

$$p = F(t) - \rho g z + \rho \frac{\partial \Phi}{\partial t} + \frac{1}{2} \rho \left\{ \left(\frac{\partial \Phi}{\partial x} \right)^2 + \left(\frac{\partial \Phi}{\partial y} \right)^2 + \left(\frac{\partial \Phi}{\partial z} \right)^2 \right\} \qquad (15)$$

The dynamic wave load on the structure is given by the linearized pressure :

$$p = \rho \frac{\partial \Phi}{\partial t} \qquad (16)$$

The total wave excited forces (and moments) can be found by integration of the pressure over the surface of the body. The total force is composed of a periodic and a constant part. The oscillating part of the wave force is found from the linearized pressure :

$$\underline{F} = \iint_A p(\underline{x}) . \underline{n} . dA \qquad (17)$$

Similarly we find for the moment :

$$\underline{M} = \iint_A p\,(\underline{x}) \cdot \left\{ \underline{x} \times \underline{n} \right\} dA \qquad (18)$$

The constant part of the wave force or drift force can be found from :

$$\underline{F}_c = \frac{1}{2}\rho \iint_A \left\{ \left(\frac{\partial \Phi}{\partial x}\right)^2 + \left(\frac{\partial \Phi}{\partial y}\right)^2 + \left(\frac{\partial \Phi}{\partial z}\right)^2 \right\} \cdot \underline{n} \cdot dA \qquad (19)$$

Evaluation of this integral results in a constant term plus higher harmonic components, which can be neglected. Although the constant force is a second order effect, Havelock [2] has shown that this force may be determined, using a first order approximation for the velocity potential. In general, the constant force is small in comparison with the oscillating wave force; for large structures, however, it may become of interest.

The wave pattern due to the diffraction of waves by the object can also be found from Bernoulli's theorem. In the free surface, the linearized pressure has to be zero, hence :

$$p = -\rho\, gz + \rho \frac{\partial \Phi}{\partial t} = 0 \qquad (20)$$

Consequently we find for the surface elevation :

$$\zeta = -\frac{1}{g} \left\{ \frac{\partial \Phi}{\partial t} \right\}_{z=0} \qquad (21)$$

II. 5 Comparison of theoretical and experimental results.

Model tests were performed at the Netherlands Ship Model Basin in order to check the theoretical calculation of wave forces, pressure and wave diffraction.

In figures 2 and 3 the oscillating horizontal and vertical wave forces on a circular cylinder, as calculated with the computer program of the Netherlands Ship Model Basin, using the three-dimensional source technique, are compared with experimental results. The experimental values, which are given in these figures, were obtained from cross-fairing of the results of a great number of measurements, which were performed with systematically varied cylinders. Also given in these figures are the values according to the analytical solution of Garret. The results of the numerical calculations, which were obtained using only 42 sources to represent the cylinder, closely approximate the analytical results of Garret, while there is also a good agreement between the theoretical and experimental results.

From the measurements of the total horizontal wave force on the cylinders, the mean value which represents the constant resistance or drift force, was also determined. In figure 4 the results are given for a particular case, together with the calculated values.

In order to check a more extreme case, calculations and measurements were performed for a pyramid-like structure, of which the shape is given in figure 5. Due to the sharp edges, it is difficult to represent this object by means of a source distribution. The number of sources, applied in the computer calculations, amounts to 92.

The results of the calculations and the measurements of the horizontal wave force on the structure are given in figure 6. Even in this case the agreement is reasonable.

Some aspects of the interaction between structure and waves were studied in greater detail for a circular model, which - at a scale ratio of 1 : 100 - can be regarded as the representation of a cylindrical island, for instance a storage tank, 96 m in diameter, fixed to the bottom in 50 m deep water and extending to above the water surface. The pressure distribution on this model was determined in regular waves with varying periods. To this end the model was provided with four very sensitive pressure gauges. These gauges were placed on a vertical line at regular distances, to obtain the distribution of the pressure over the water depth. The measurement of the variation of the pressure along the circumference of the cylinder was established by rotating the model. In figures 7 and 8 the results are given for ka = 2 and ka = 3, which for a scale ratio of 1 : 100, correspond to wave periods of 8 and 10 seconds. In general, the measured pressures closely approximate the calculated values. The diffraction of the waves by the cylinder was calculated with the potential theory and also measured in the basin in a large number of points around the model. Figure 9 shows the calculated wave pattern for ka = 1.4. The lines in this figure connect the points with equal values of the ratio of resulting wave height to incident wave height. In figures 10 and 11 the results are given of the calculated and measured wave height behind and in front of the cylinder for ka = 4. Again, the experiments confirm the theoretical calculations.

II. 6 Wave loads in high, irregular and breaking waves.

Up till now only sinusoidal waves of low amplitude were taken into consideration. However, for the design of offshore struc-

tures, the maximum wave condition is important; such a condition usually is an irregular sea-state, consisting of high waves, among which sometimes even breaking waves will occur.

High regular waves are not sinusoidal any longer, the distance of the crest to the still water level becomes greater than the distance of the trough to the still water level. However, a steep regular wave can always be split up into a number of harmonic components. From various experiments the experience was gained, that the forces and pressures in high waves can be found by summation of the forces and pressures, as calculated for the different components according to the potential theory for sinusoidal waves of low amplitude.

In non-periodic waves, as far as the linear phenomena are concerned, force and pressure spectra can be calculated, departing from the wave energy spectrum and the force and pressure response functions. In such a statistic approach, no data can be obtained with regard to drift forces. Since the magnitude of the drift force is proportional to the square of the wave height and also dependent on the wave frequency, this force is no longer constant in irregular seas and is thus known as the slowly oscillating drift force which has a period of oscillation in the order of magnitude of ten times the mean wave period. For an estimation of the drift force a deterministic approach can be applied (see Hsu and Blenkarn [8] and also Remery and Hermans [9]). In this approach the point of departure is not the energy spectrum of the waves, but a record of the wave height to a base of time, which can be obtained either by field measurements, or by calculations, in which case one of the possible realizations of a spectrum is generated by a computer.

The wave record can be regarded as a sequence of separate wave crests and troughs, each with its own period and amplitude. For every part of the wave record the drift force can be calculated, resulting in a record of the drift force to a base of time. The drawback of this method is, that no indication is obtained about the chance of exceeding a certain force. The maximum force, encountered in a certain wave train, will differ from the maximum force in an other wave train with the same energy distribution.

No theoretical approach is available for the determination of peak loads, which can occur in breaking waves. In [10] Wiegel gives a review of experimental work performed on this topic. Most of the investigations were related to the phenomena which occur when a wave breaks against a vertical barrier; a smaller part was concerned with cylinders in breaking waves. From the laboratory tests with vertical barriers it appeared, that when a breaking wave hits the

wall, the chance that a peak load occurs is about two per cent. Wave induced impact forces only occur, when the wave breaks just at the wall, while trapping a thin lense of air. Apparently, the energy of the impact is stored in the compression of the air cushion. Therefore, it is very unlikely that peak forces will occur if the surface of the object is curved. In the case of large structures with flat or practically flat walls, the possibility that peak loads occur due to breaking waves, must be taken into account. The magnitude of the peak loads can only be found by means of experiments.

III. THE ANCHORING OF FLOATING STRUCTURES

The anchoring of very large floating structures involves tremendous problems, since the anchor system must be able to survive the severest weather conditions. In high waves the drift force becomes very important and causes a high mean load in the anchor lines. Due to the non-linear characteristic of the anchor system - which is schematically shown in figure 12 - the spring constant increases considerably by this mean load and consequently the oscillating motion of the structure induces high oscillating forces in the anchor lines.

Let us consider, as an example, a circular storage tank - 120 m in diameter, with a draft of 25 m and a displacement weight of approximately 290, 000 ton - which is anchored in a water depth of 40 m. It was calculated that, in a design wave with a height of 20 m and a period of 19 seconds, this structure is subjected to a drift force of 4, 730 ton and an oscillating force with an amplitude of 58, 900 ton. If it is assumed that the motion of the structure is a pure surge motion and that the damping can be neglected, the motion can be described by :

$$m_v \ddot{x} + cx = F_{xa} \cdot e^{-i\omega t} \qquad (22)$$

in which :

- m_v = the virtual mass
- c = the spring constant in x-direction of the anchor system
- F_{xa} = the amplitude of the oscillating wave excited force in x-direction

Since the relation between the force and excursion of the anchor system is non-linear, this equation has no simple analytical solution.

Due to the drift force, the motion of the structure will be

an oscillating motion around a point which is situated in the steep part of the load-excursion curve, as indicated in figure 12. The relevant part of the curve may be regarded as linear with an inclination c. Consequently, the resulting surge motion is given by the linear approximation of equation (22) :

$$x = x_a \cdot e^{-i\omega t} \tag{23}$$

in which :

x_a = the amplitude of the motion

After substitution of (23) in (22), we find that the amplitude of the surge motion will be :

$$x_a = \frac{F_{xa}}{\left| c - m_v \omega^2 \right|} \tag{24}$$

The resulting maximum reaction force in the anchor system becomes :

$$F_{Rx\ max.} = 4,730 + x_a \cdot c \tag{25}$$

In figure 13 the maximum reaction force in x-direction is given to a base of the spring constant. From this figure it becomes obvious that it will be very hard in this case to design a proper anchor system. Resonance will occur if :

$$c = m_v \omega^2 \tag{26}$$

and, since most of the wave energy is related to wave frequencies between $\omega = 0.2$ and $\omega = 1.0$, values of c between 2,400 and 60,000 ton/m should be avoided.

A value of c higher than 60,000 ton/m means an almost rigid connection to the sea bottom, which must be able to absorb a horizontal force of over 60,000 ton; this does not seem to be a practical solution. On the other hand, if c is chosen to amount to less than 2,400 ton/m, the risk exists that in irregular seas the slowly varying drift force induces resonance phenomena.

In reality the problem is much more complicated than was assumed in this simple calculation : besides the surge motion, also heave and pitch may be of importance, and due to the high waves, the

drift force and the characteristics of the anchor system, the motions will be non-linear. Therefore, model tests are indispensible to investigate the anchoring of large structures.

The above example has shown, however, that enormous problems are involved with the anchoring of very large structures with a small length to breadth ratio. Therefore, in rather shallow water, a structure fixed to the bottom, will be preferred in many cases. If a floating structure is required - for instance because there exists a risk of earthquakes - or if the structure has to be more or less mobile, it is desirable to choose a shape with a minimum drift force, as for example a ship-shaped structure moored to a single point mooring system or a semi-submersible structure.

IV. MOORING OF A SHIP TO A LARGE STRUCTURE

For the oil storage tanks which are now in use or under construction, a concept was selected by which the loading tanker is not moored immediately to the storage tank, but to a separate single buoy mooring system.

If we consider the wave pattern around the circular tank, as given in figure 9, regions where the waves are higher, as well as regions where the waves are lower than the incident waves, can be observed. For other wave lengths, the wave pattern changes, but there is always an area behind the structure where the waves are lower than the incident waves. It can therefore be expected, that the diffraction of waves by a large fixed structure will be advantageous when a ship is moored immediately behind it.

In order to investigate the behaviour of a tanker, moored to a storage tank by means of a bowhawser, a model test program was performed at the Netherlands Ship Model Basin with the cylindrical model - discussed already in a previous section - and a model of a tanker with a displacement of approximately 100,000 ton. The main particulars of the tanker are given in Table I, while figure 14 shows a small scale body plan. The weight distribution and stability characteristics of the tanker were reproduced to scale. The tanker was moored to the storage tank by means of a single bowhawser, representing a nylon mooring line with a breaking strength of 150 ton and a length of 50 m. The load-elongation characteristic of this bowhawser is given in figure 15.

The following tests were preformed :

a- Measurement of the wave height in regular and irregular seas

behind the structure, at the position of the midship section of the tanker;
b- Measurement of the mooring line force and of the surge and heave motions of the bow of the tanker with the tanker moored to the cylindrical tank in irregular seas;
c- Measurement of the mooring line force and of the motions of the bow of the tanker with the tanker moored to a fixed pile of small diameter, in the same sea-states as tests b. These tests were performed in order to determine the influence of the wave diffraction on the behaviour of the moored ship.

The different test arrangements are shown in figure 16.

For the measurement of the wave height a wave transducer of the resistance type was used. The force in the bowhawser was measured by means of a strain gauge transducer and the surge and heave motions of the tanker by means of a pantograph.

The measurements in irregular seas lasted 210 seconds or 35 minutes for the full scale, which is regarded to be long enough to obtain reliable statistic data.

Besides the measurements, the wave diffraction at the position of the midship section of the tanker was also calculated with the potential theory. In figure 17 the calculated ratio of wave amplitude behind the cylinder to incident wave amplitude ζ_a^* / ζ_a is given to a base of the wave frequency ω, together with some experimental values. With the aid of this curve of ζ_a^* / ζ_a, the energy spectrum behind the cylinder can be calculated for any incident wave spectrum.

The spectral density S_ζ of the incident waves is defined by :

$$S_\zeta(\omega_n)\, d\omega = \frac{1}{2} \zeta_{an}^2 \qquad (27)$$

in which :

ζ_{an} = the amplitude of the n th component of $\zeta(t)$ with circular frequency ω_n.

Consequently, the spectral density of the waves at the position of the midship section of the tanker can be found from :

$$S_\zeta^*(\omega_n)\, d\omega = \frac{1}{2} \zeta_{an}^2 \left[\frac{\zeta_{an}^*}{\zeta_{an}} (\omega_n) \right]^2 \qquad (28)$$

or

$$S^{*}_{F}(\omega_n) = S_{F}(\omega_n) \left[\frac{F_{an}}{F_{an}}(\omega_n)\right]^2 \qquad (29)$$

In figures 18, 19 and 20 the spectral densities of the sea-states applied during the tests, are given together with the predicted and measured spectral densities behind the cylinder. There is a good agreement.

The tests with the moored tanker were performed in the spectra 2 and 3, with significant wave heights of 3.36 m and 5.05 m. The most important test results are stated in Table II.

The most remarkable outcome of the experiments is the considerable reduction in the mooring line force, due to the presence of the cylindrical structure. The reduction in the force is relatively much higher than the reduction in the wave height. This can possibly be explained by the fact, that the drift force plays an important role in the behaviour of a moored ship, this drift force being proportional to the square of the wave height.

If, for instance, we have a wave with frequency $\omega = 0.8$, it follows from figure 17, that the wave height is decreased by 20 per cent. at the position of the moored tanker, and consequently the drift force is decreased by 36 per cent. compared with the drift force in the undisturbed waves.

In figure 21 the results of the present tests are compared with results obtained from the statistics of tests performed at the Netherlands Ship Model Basin with different single point mooring systems. For this comparison the following dimensionless coefficients were applied :

- for the mooring line force $\dfrac{\bar{F}_{1/3}}{\rho g \nabla^{2/3} \bar{\zeta}_{w\,1/3}}$

and

- for the wave frequency $\bar{\omega}\sqrt{L_{pp}/g}$

in which :

∇ = the displacement volume
L_{pp} = the length between perpendiculars.

Due to the non-linear characteristic of the bowhawser, the significant force is not proportional to $\nabla^{2/3}$ and $\zeta_w^{1/3}$, and therefore only results of tests with tankers of comparable size in comparable sea-states were selected.

From Figure 21 it appears, that the results obtained with the tanker moored to a fixed point represent approximately the lower limit of the results of conventional single point mooring systems. The forces occurring in the mooring line when the tanker is moored behind the cylindrical storage tank, are much lower than those for all other considered systems.

These model tests have shown that it is advantageous to moor a ship immediately behind a large fixed structure, though it should be admitted that a rather simple case was considered, since the additional effect of current or wind from a direction different from the wave direction was not investigated.

V. CONCLUSIONS

1 - The wave loads on large structures due to non-breaking waves can be predicted fairly accurately by means of a three-dimensional source theory.

2 - For the study of the anchoring of large structures or the mooring of ships to large structures, an entirely theoretical approach is not feasible and consequently model experiments are required.

3 - Very large floating structures anchored in exposed areas should preferably be either slender or semi-submersible; large structures with a small length to breadth ratio will require extremely heavy anchoring equipment.

4 - Mooring a ship on the lee-side of a fixed structure can be of advantage. If the ship is moored to the structure by a single bowhawser, the force in the latter will be smaller than the force which would occur in a conventional single point mooring system.

NOMENCLATURE :

a	= cylinder radius
c	= spring constant of the anchor system
d	= water depth
$\underline{F}$	= oscillating wave excited force
F_{cx}	= drift force
F_R	= reaction force of the anchor system
F_{xa}	= amplitude of the horizontal wave excited force
F_{za}	= amplitude of the vertical wave excited force
g	= acceleration due to gravity
h	= draught
J_n	= Bessel function of the first kind of order n
$J_{n,r}$	= derivative of J_n with respect to r
k	= wave number
K_n	= modified Bessel function of the second kind of order n
L_{pp}	= lenght between perpendiculars
$\underline{M}$	= oscillating wave excited moment
p	= pressure
q	= source strength
S_ζ	= spectral density of the waves
Y_n	= Weber's Bessel function of the second kind of order n
$Y_{n,r}$	= derivative of Y_n with respect to r
λ	= wave length
ω	= circular frequency
$\bar{\omega}$	= mean circular frequency in irregular waves
ρ	= fluid dens ty
γ	= Green's function
Φ	= velocity potential
φ	= wave function

φ_i = wave function of the incident waves

φ_s = wave function of the scattering waves

ν $= \omega^2 / g$

ζ = wave elevation

ζ_a = incident wave amplitude

ζ_{a^*} = local wave amplitude

ζ_w = wave height (crest to trough)

ζ_∇ = volume of displacement

REFERENCES

[1] OORTMERSSEN G. van
"The interaction between a vertical cylinder and regular waves"
Symposium on "Offshore Hydrodynamics", Wageningen (August 1971)

[2] HAVELOCK T. H
"The pressure of water waves upon a fixed obstacle"
Proc. of the Royal Society of London, Series A - N° 963 Vol. 175 (1940)

[3] Mac CAMY R. C. and FUCHS R. A.
"Wave forces on piles : a diffraction theory"
Technical Memorandum N° 69, Beach Erosion Board (1954)

[4] FLOKSTRA C.
"Wave forces on a vertical cylinder in finite water depth"
N. S. M. B. Report N° 69-107-WO, Wageningen (September 1969)

[5] GARRET C. J. R.
"Wave forces on a circular dock"
Journal of Fluid Mechanics - Vol. 46 (1971)

[6] LAMB H.
"Hydrodynamics"
Sixth Edition (1932)

[7] JOHN F.
"On the motion of floating bodies"
Comm. on Pure and Applied Mathematics, 3 (1950)

[8] HSU F. H. and BLENKARN K. A.
"Analysis of peak mooring forces caused by slow vessel drift oscillation in random seas"
Offshore Technology Conference, Houston (1970)

[9] REMERY G. F. M. and HERMANS A. J.
"The slow drift oscillations of a moored object in random seas"
Offshore Technology Conference, Houston (1971)

[10] WIEGEL R. L.
"Oceanographical Engineering"
Prentice-Hall, Englewood Cliffs (1965)

* * *

Table I
Main particulars of the tanker

Designation	Symbol	Unit	
Length between perpendiculars	L_{pp}	m	249.38
Breadth	B	m	37.41
Draft (even keel)	T	m	13.85
Volume of displacement	∇	m^3	106,792
Displacement weight in sea water	Δ	tons	109,462
Block coefficient	C_B	-	0.826
Midship section coefficient	C_M	-	0.985
Longitudinal radius of gyration	$k_{\theta\theta}$	m	58.61
Transverse radius of gyration	$k_{\phi\phi}$	m	8.98
Centre of buoyancy before midship section	f	m	3.78
Centre of gravity above keel	$\overline{GK}$	m	10.09
Metacentric height	$\overline{GM}$	m	5.55

Table II
Results of the mooring tests

Test arrangement B = Tanker moored to the cylindrical tank
Test arrangement C = Tanker moored to a fixed point

Test arrangement	Wave spectrum		Significant force in bowhawser	Surge			Heave
	$\tilde{\zeta}_{a\,1/3}$ in m	T in sec.		$\tilde{x}_{a\,1/3}{}^{+}$	$\tilde{x}_{a\,1/3}{}^{-}$	$\bar{x}$	$2\tilde{\zeta}_{a\,1/3}$
B	5.05	9.98	28.0	-2.37	-10.63	- 6.39	3.40
B	3.36	7.96	7.0	-1.06	- 3.14	- 1.99	1.06
C	5.05	9.98	51.6	-7.23	-13.19	-10.04	3.85
C	3.36	7.96	8.3	-0.92	- 3.21	- 2.23	0.89

The bowhawser force is given in metric tons
The motions are given in metres

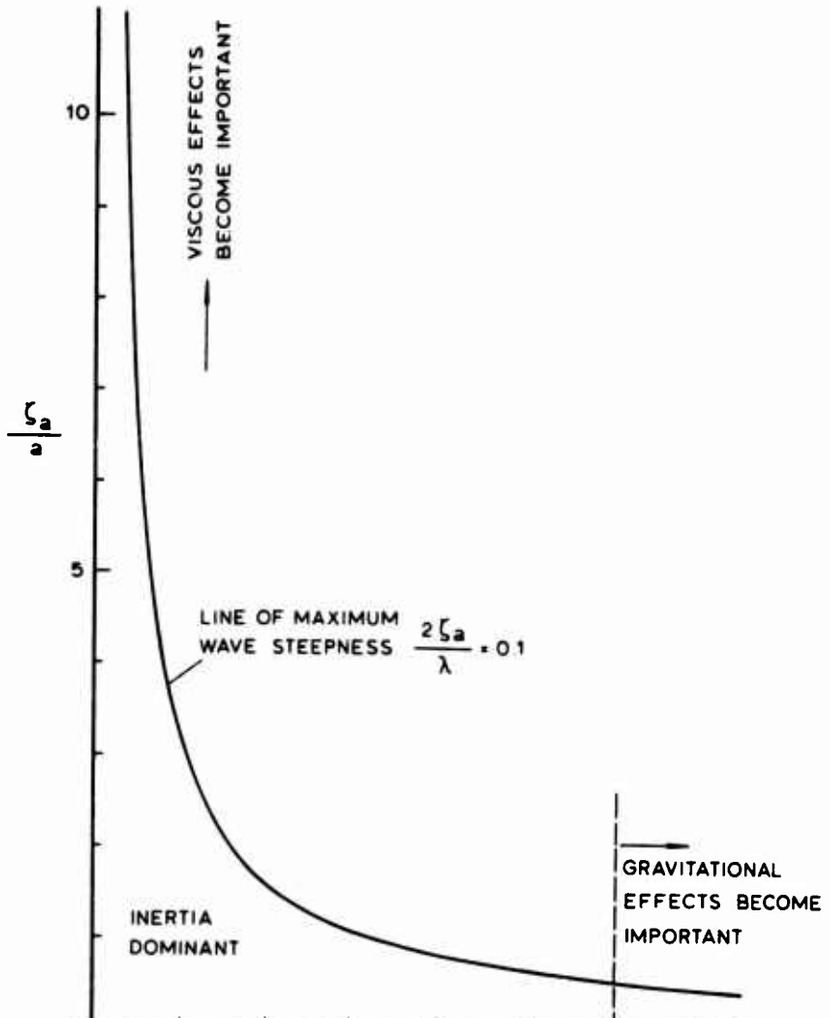


Figure 1 Regions of influence of inertia, gravity and viscosity for a vertical circular cylinder with radius a.

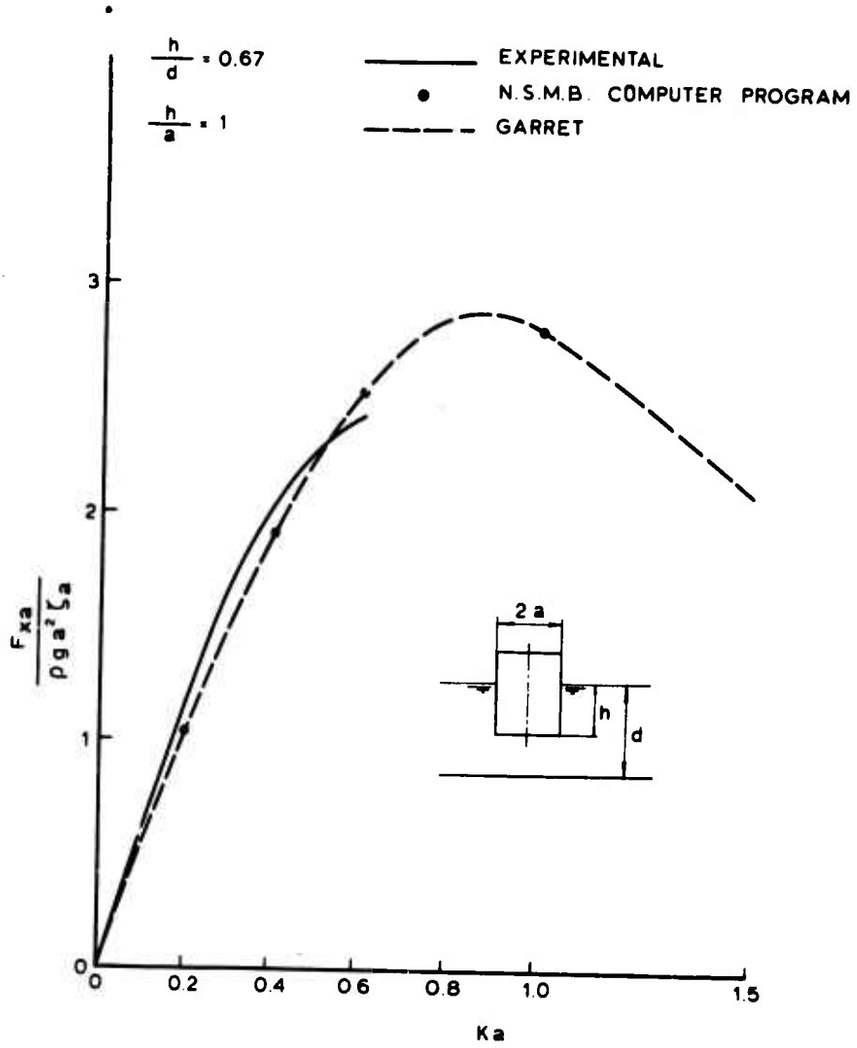


Figure 2 Oscillating horizontal wave force on a circular cylinder

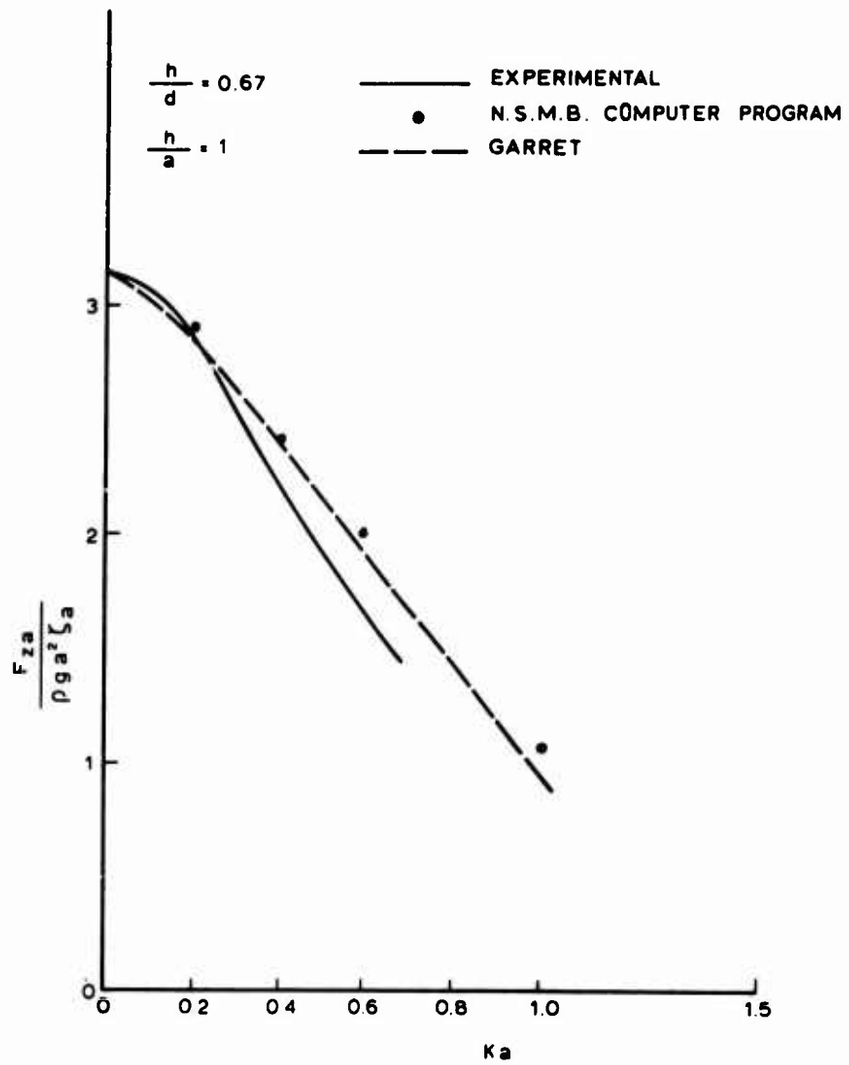


Figure 3 Oscillating vertical wave force on a circular cylinder

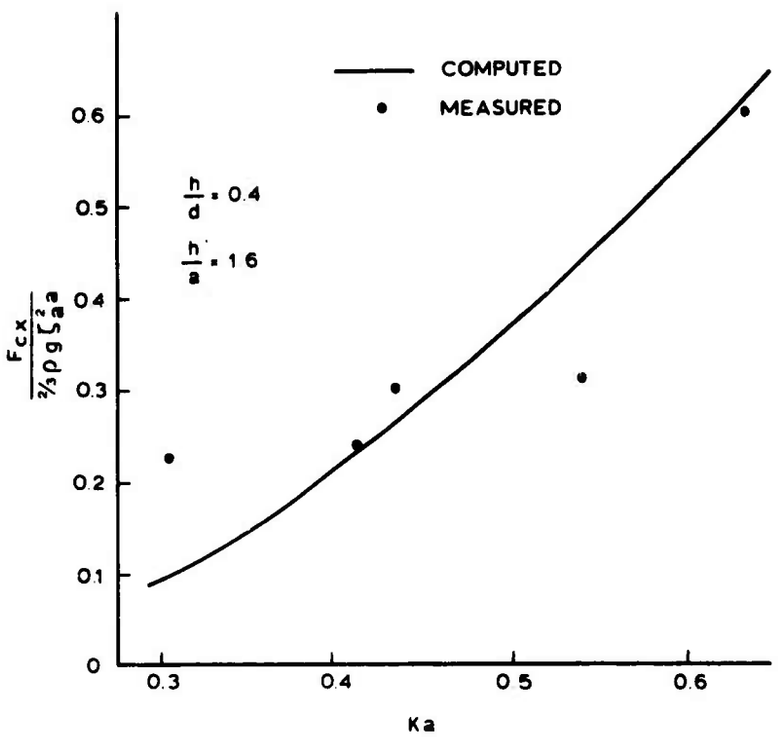


Figure 4 Drift force on a circular cylinder

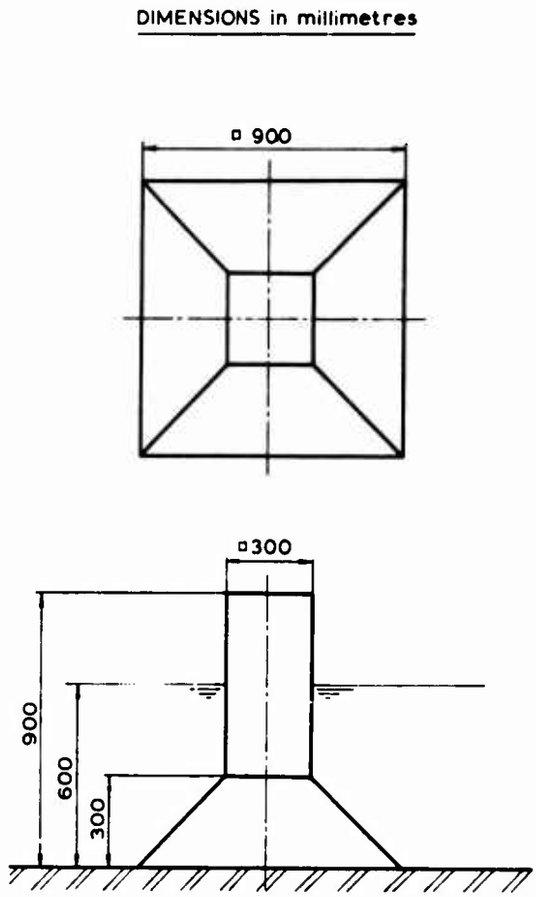


Figure 5 Outline of the pyramid-shaped model

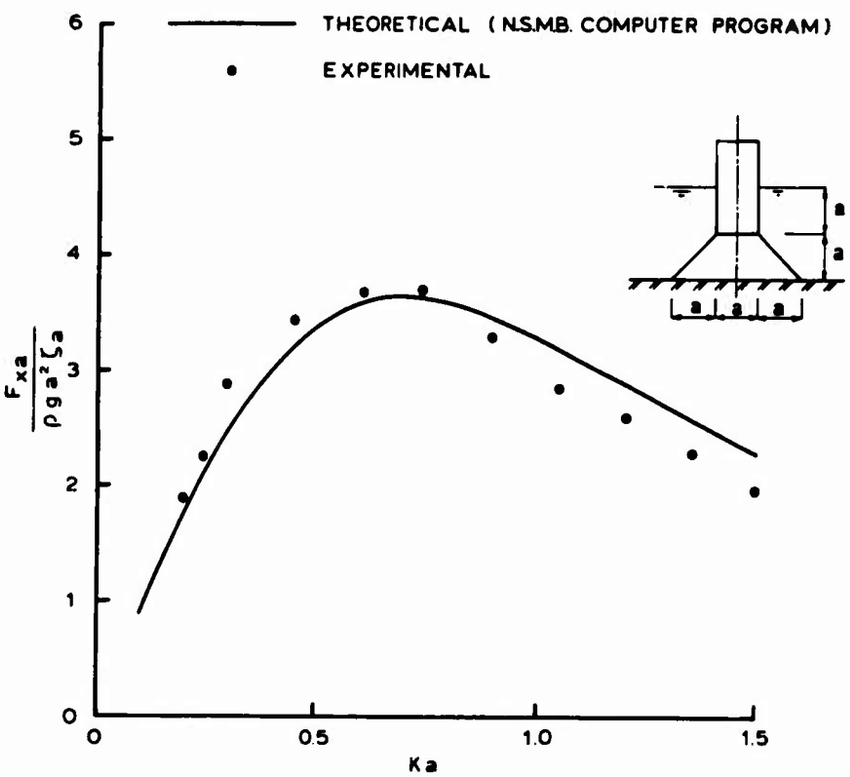


Figure 6 The oscillating horizontal wave force on a pyramid.

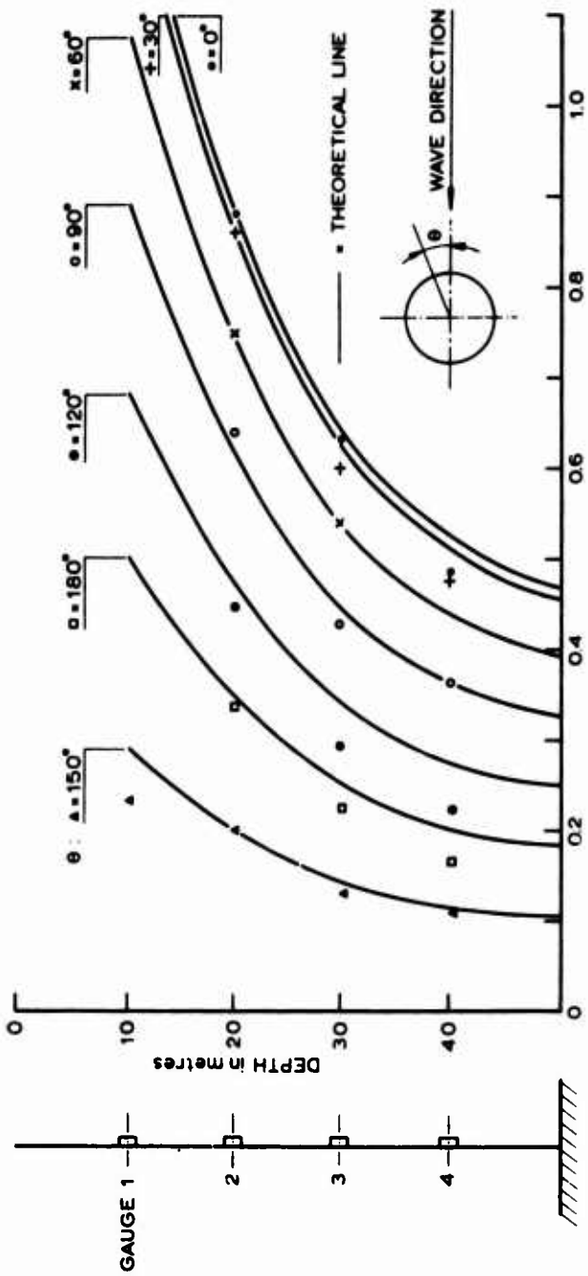


Figure 7 Pressure on a circular cylinder in waves, ka = 2

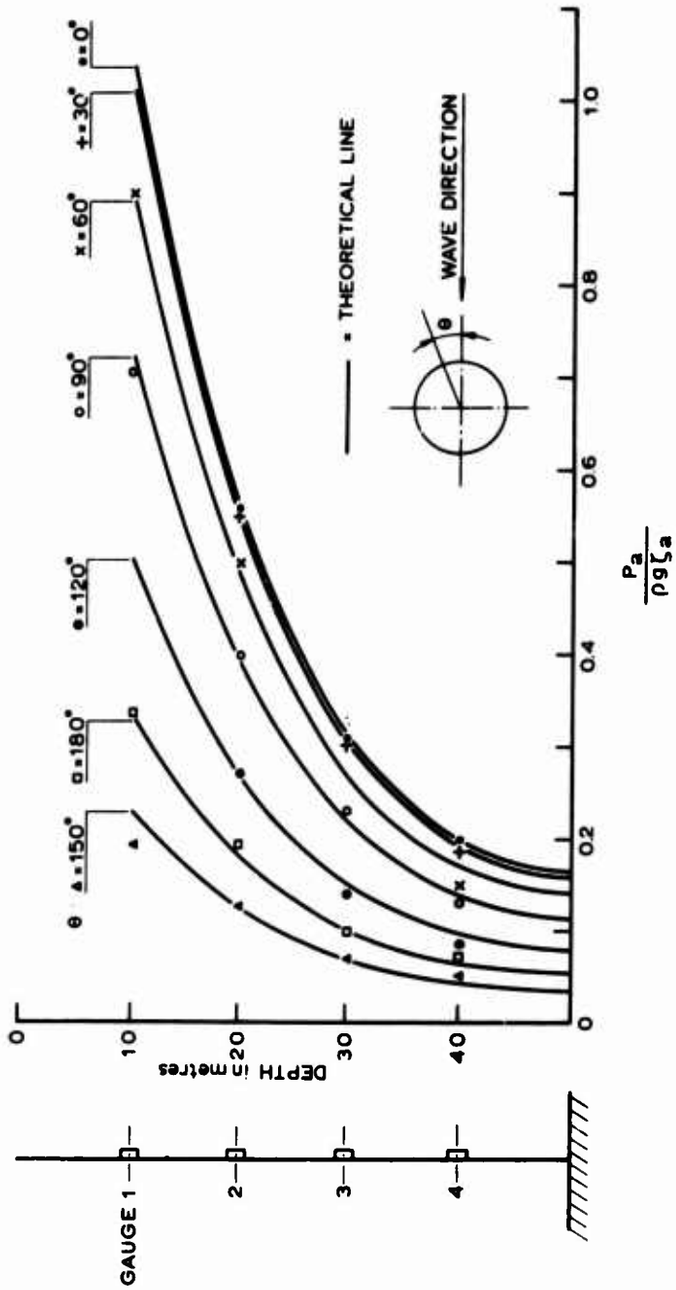


Figure 8 Pressure on a circular cylinder in waves, ka = 3

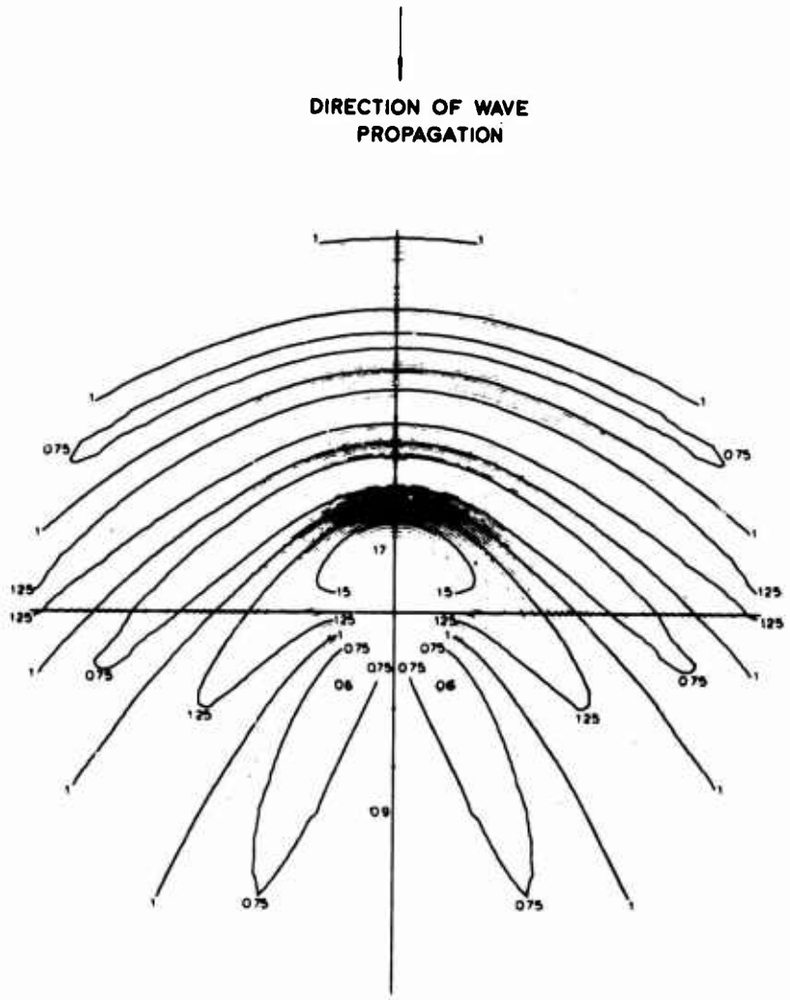


Figure 9 Wave pattern around a circular cylinder, ka = 1.4

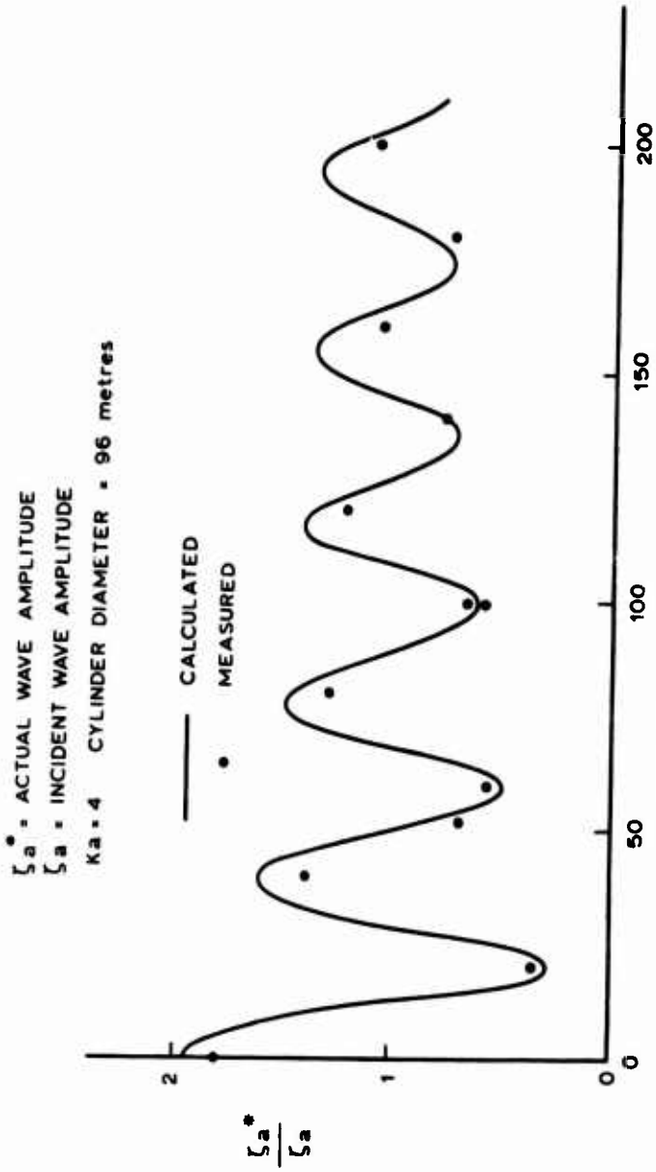


Figure 10 The wave height in front of a circular cylinder

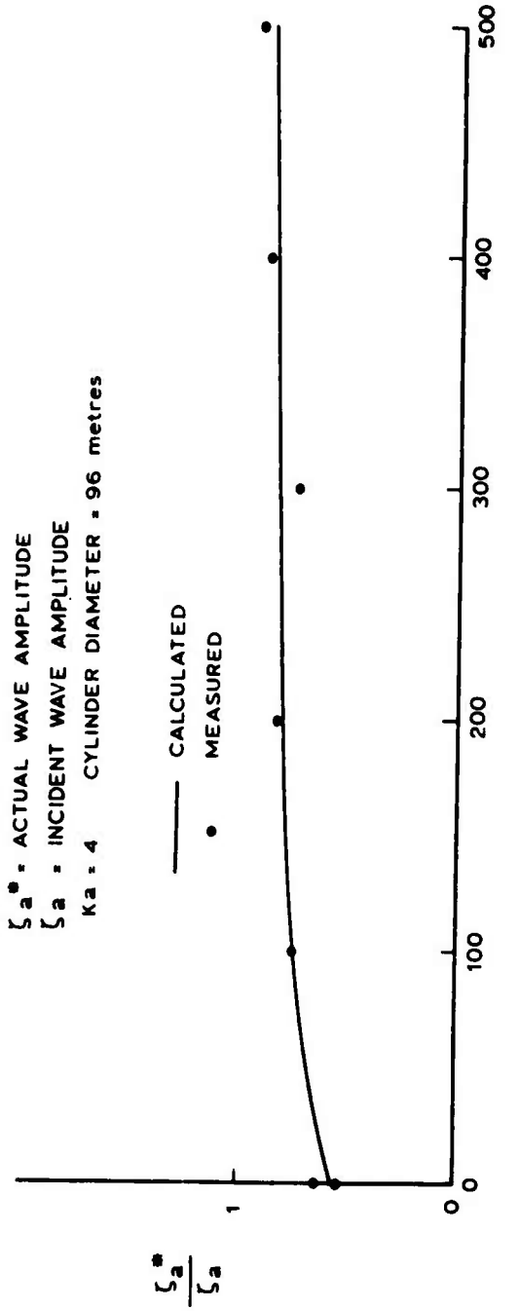


Figure 11 The wave height behind a circular cylinder

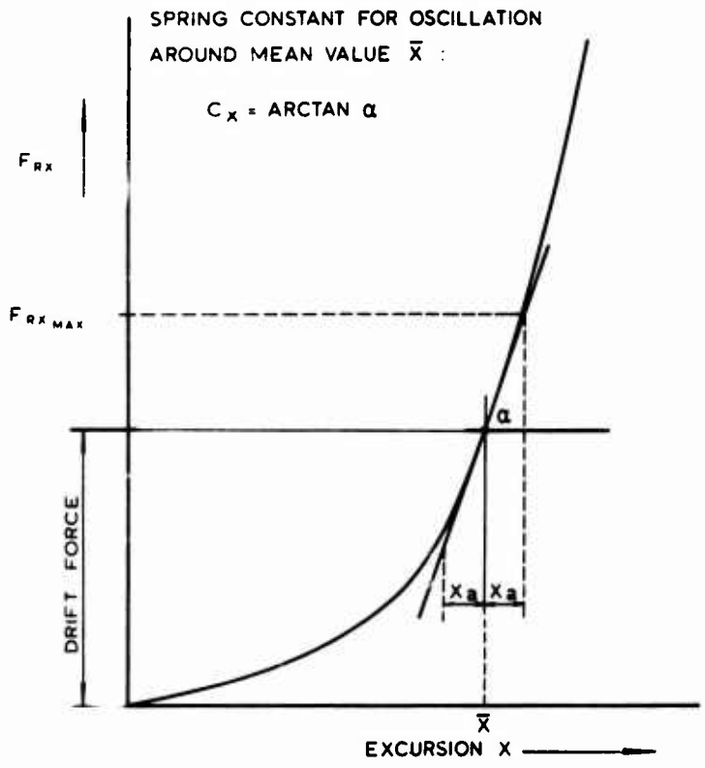


Figure 12 Load-excursion characteristic of the anchor system

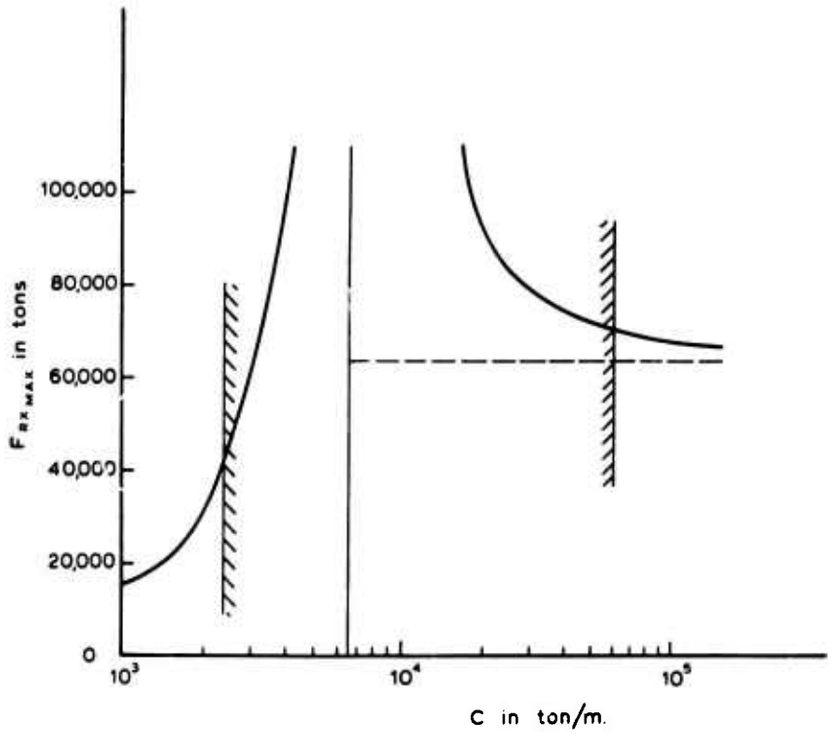
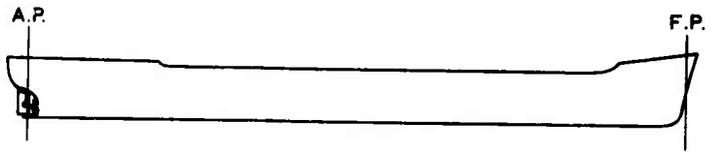
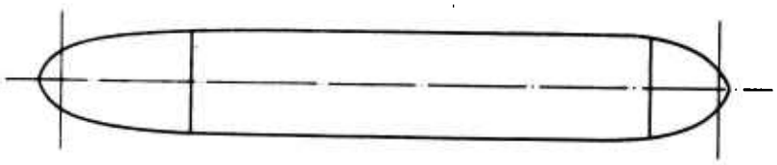


Figure 13 Maximum horizontal reaction of the anchor system on a base of the spring constant for a design wave with wave height 20 meters, period 19 seconds.

LENGTH BETWEEN PERPENDICULARS	249.38 m.
BREADTH	37.41 m.
DRAUGHT	13.85 m.
DISPLACEMENT	106,792 m.^{3}





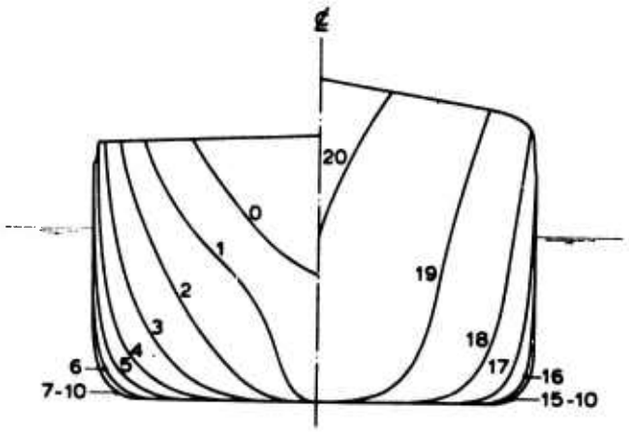


Figure 14 Body plan of the tanker

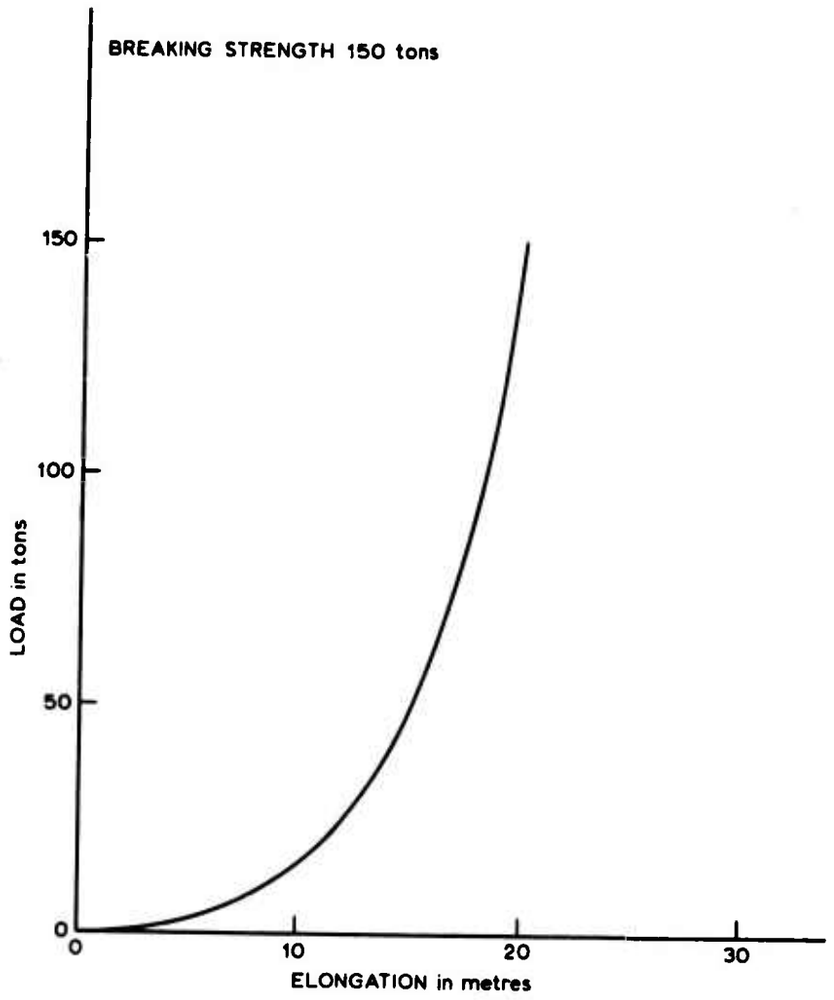


Figure 15 The load-elongation characteristic of the bowhawser.

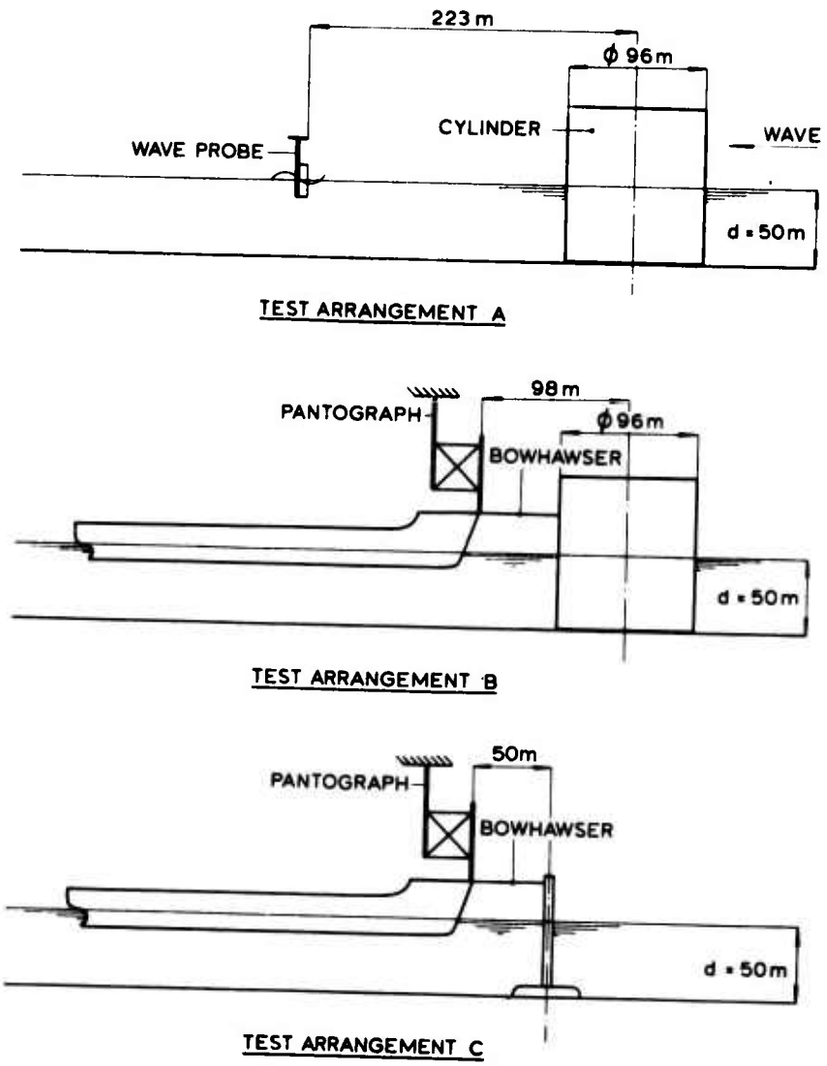


Figure 16 The experimental set-up.

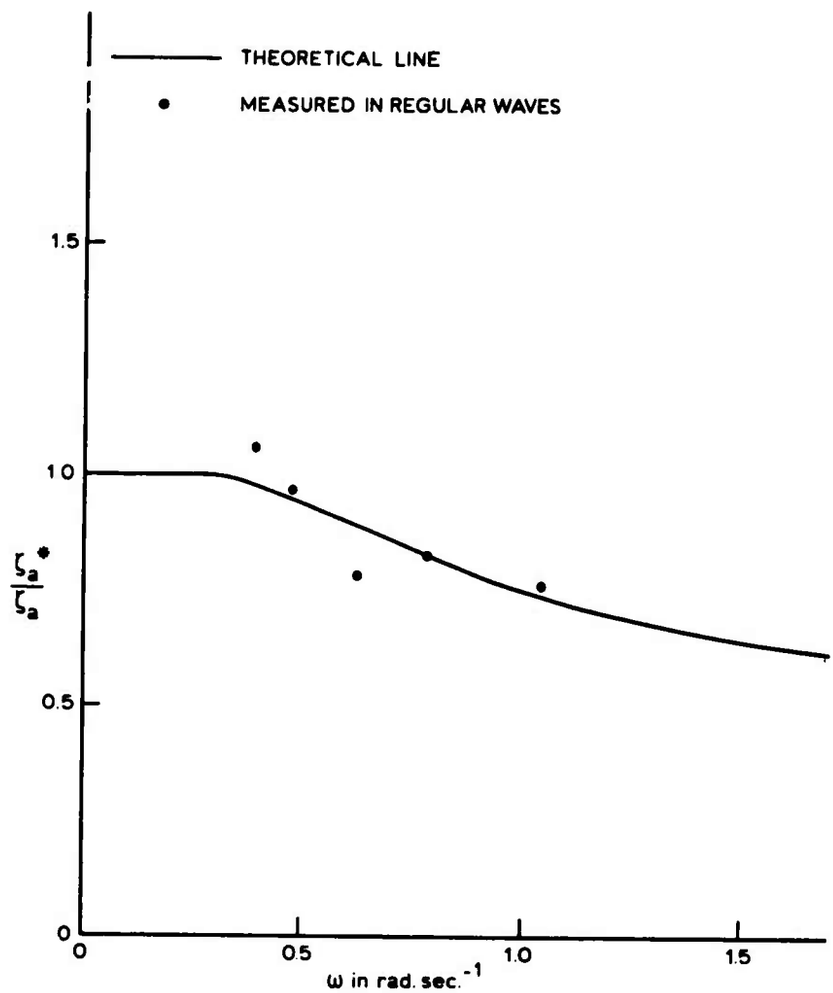


Figure 17 Wave diffraction at the position of the tanker .

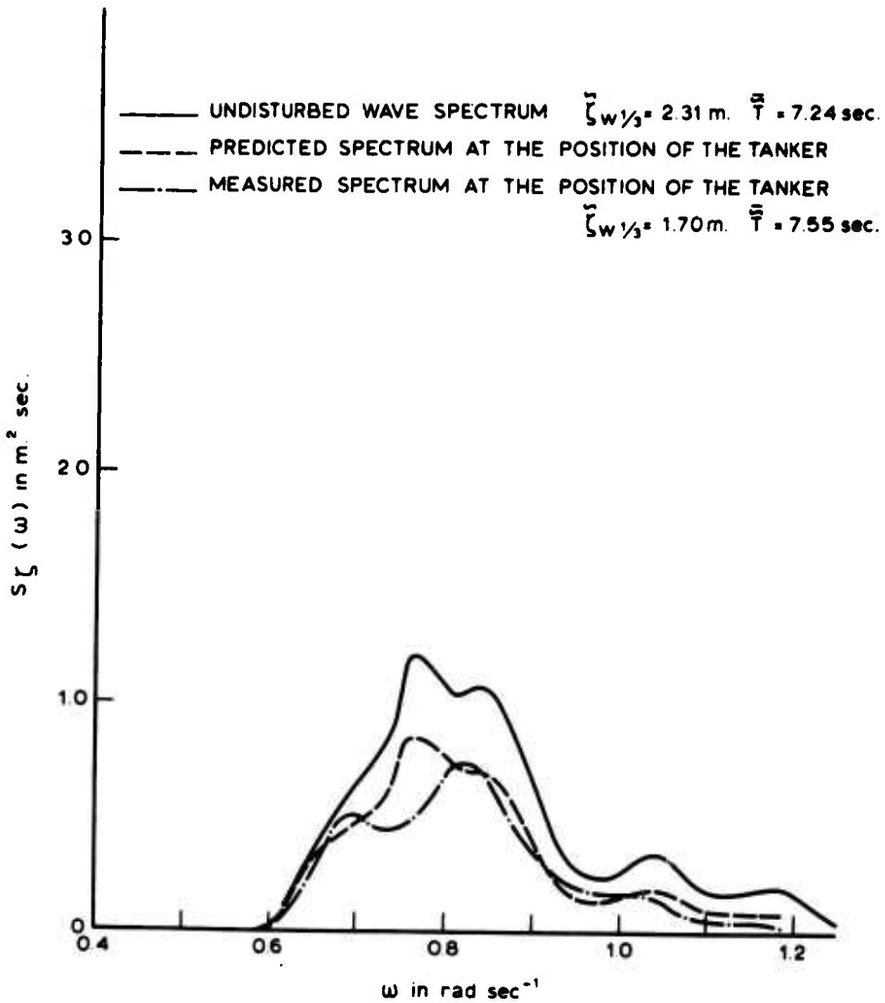


Figure 18 Wave spectrum 1.

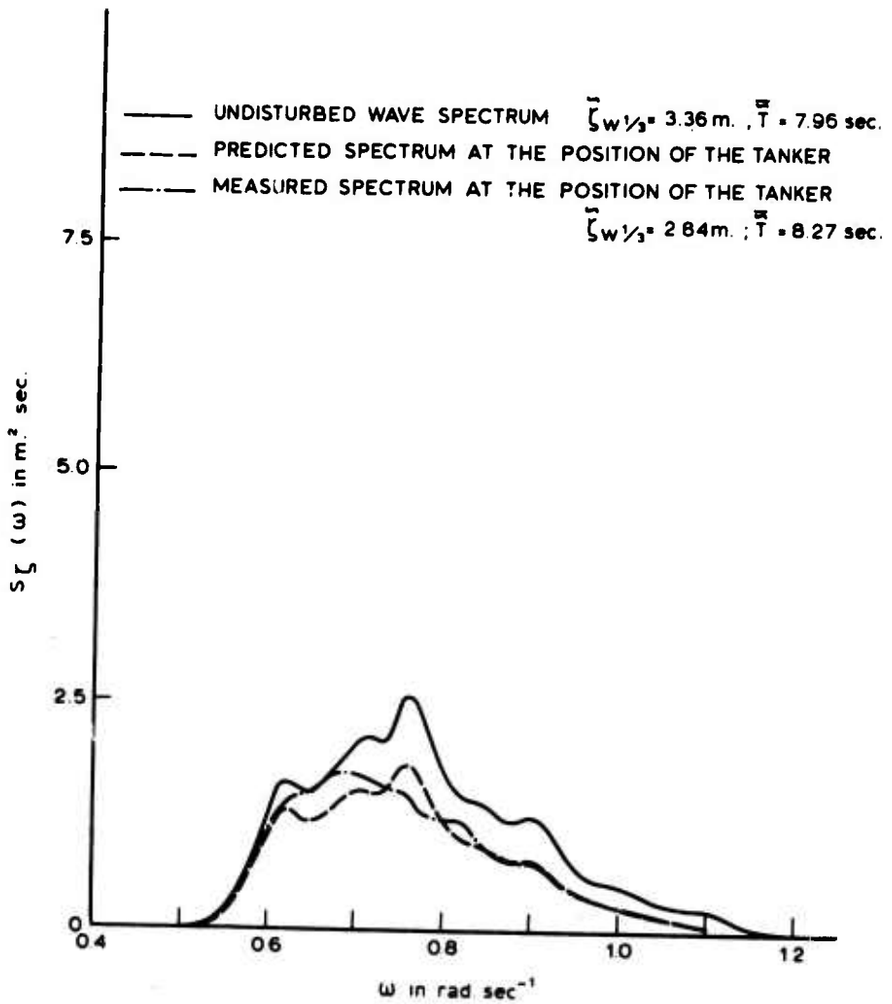


Figure 19 Wave spectrum 2 .

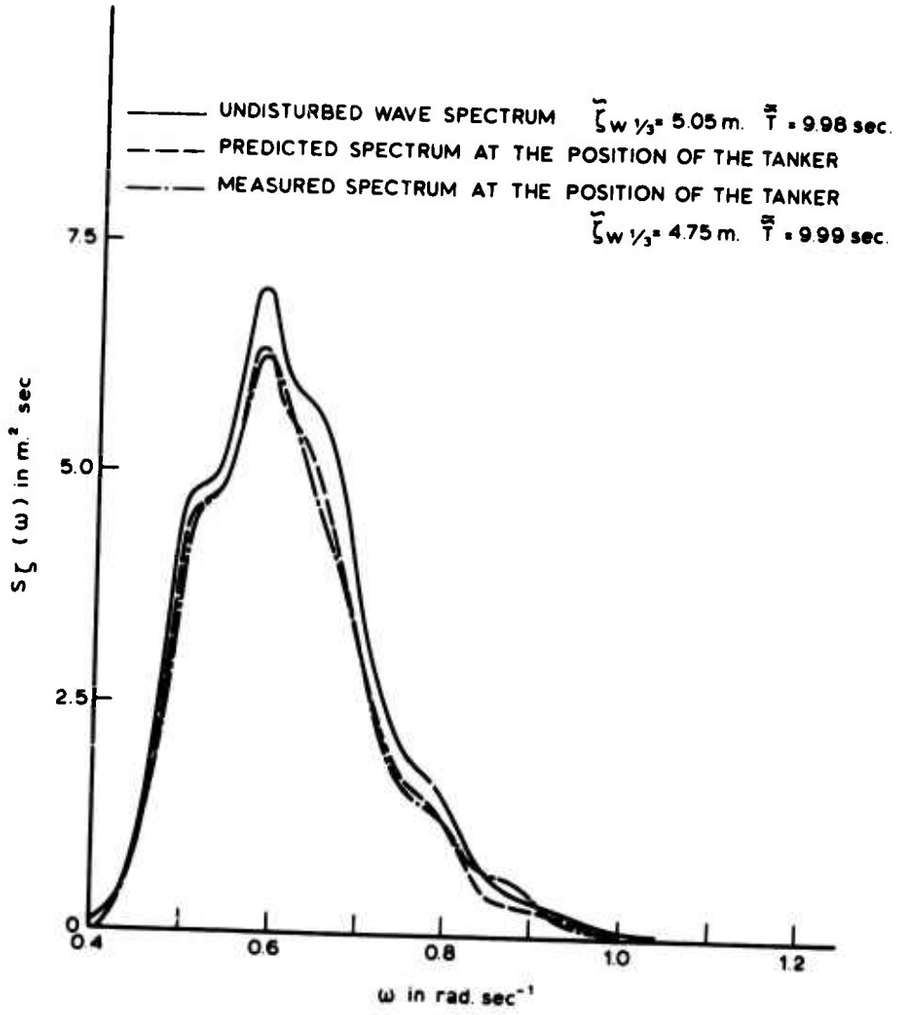


Figure 20 Wave spectrum 3 .

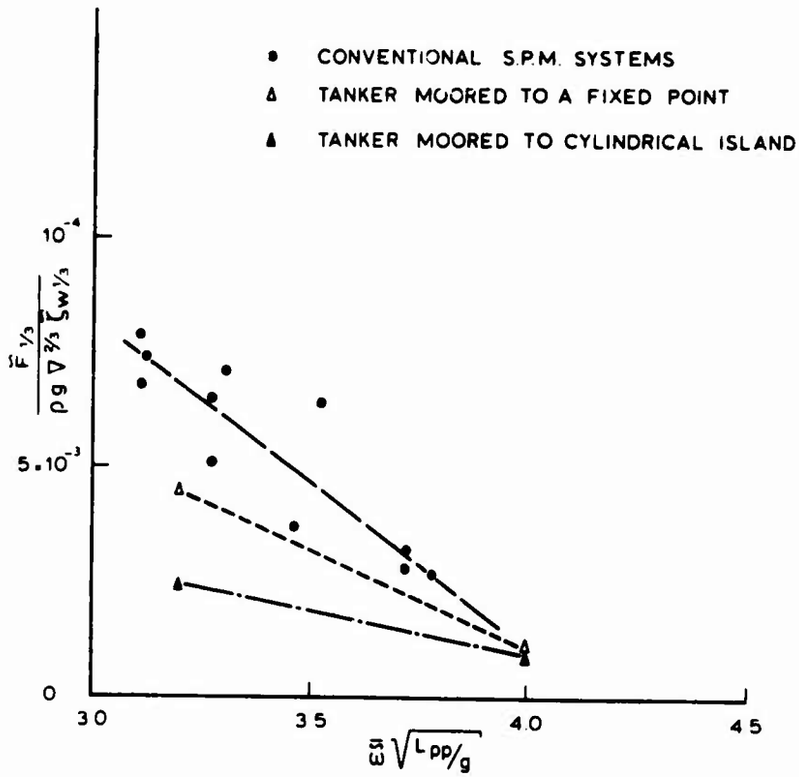


Figure 21 The significant mooring line force for different S. P. M. systems.

DISCUSSION

C. M. Lee
Naval Ship Research and Development Center
Bethesda, Maryland, U.S.A.

I would like to refer to the results given in Figures 2 and 4. Figure 2 presents the amplitude of the oscillatory force in the horizontal direction for the circular cylinder and Figure 4 presents the drift force in the horizontal direction. At Ka equals. 6, which corresponds to the wavelength being approximately 10 times greater than the radius of the circular cylinder, the ratio of the drift force to the oscillatory force is about. 3, if we assume that the wave amplitude is of equal magnitude to the cylinder radius. That means that drift force would comprise about 30 per cent of the oscillatory force. Thus, as the author has already indicated, the drift force cannot be ignored in the calculation of wave forces on a vertical circular cylinder. I would like to point out that when there are multiple wave frequencies as in the case of irregular seas there could exist very slowly-varying forces which in practical cases could be regarded almost like a steady force. The existence of such a force can easily be recognized if we assume two regular waves of slightly different frequencies pinging upon the body. The hydrodynamic pressure on the body contributed by the velocity-square term in the Bernoulli equation would contain a term associated with the difference-frequency of the two frequencies.

REPLY TO DISCUSSION

G. van Oortmerssen
Netherlands Ship Model Basin
Wageningen, Netherlands

I agree with Mr. Lee that the drift force is very important, and especially for moored objects, in irregular seas. The drift has an important influence on the resulting behaviour of the structure. The results presented in this paper dealt only with the drift force in regul-

ar seas and we did not consider the drift force in irregulars seas, which is much more difficult, as you know. There are some methods, approximative methods, to calculate the drift force in irregular seas, but I think there is still a lot of work to be done on this subject.

DISCUSSION

E. J. Plate
University of Karlsruhe
Karlsruhe, Germany

I should like to congratulate the author on an excellent paper. May I ask the author to tell us what computer was used for the work, and how much time it takes to get one of these calculations performed ?

REPLY TO DISCUSSION

G. van Oortmerssen
Netherlands Ship Model Basin
Wageningen, Netherlands

I should like to thank you, Professor Plate, for your kind words. Our calculations were performed on a CDC computer of the 3,000 series, and that is a medium sized computer. For the calculation of the square structure of which I showed some results we used about 100 sources, which is quite a lot, and the computations required about 45 minutes per wave condition for that structure.

DISCUSSION

J. P. Breslin
Stevens Institute of Technology
Hoboken, New Jersey, U.S.A.

It is very comforting to find that measurements and calculations for the forces and pressure distribution on the cylinder having a diameter equal to the wavelength are so well correlated, but I suppose this is not surprising for short waves. I wonder if the author would comment on the comparison of the measurements and calculations for longer wave lengths where viscous effects may be expected to be important.

A second question : there was some information provided on the interference between two cylinders. Would the author let us know how this could be compared with theory as the cylinder spacing is increased ?

REPLY TO DISCUSSION

G. van Oortmerssen
Netherlands Ship Model Basin
Wageningen, Netherlands

On the first question, we have indeed results for longer waves and in that case the agreement is even better, but for the longer waves especially when the wavelength is longer than about five times the body dimensions, we can use approximative methods which give the same results and are much simpler to handle. So I think our computer programme is only of interest for the relatively shorter waves.

On the second question, about the interference of two cylinders, we have indeed performed measurements. We measured the wave force on cylinders for different spacings of the neighbour cylinders, for different wavelengths and for different wave directions, and

we compared those experiments with results obtained with the computer programme. We plan to present those results and the comparison between theoretical and experimental results in the near future, but in that case also the agreement is good.

* * *

UNSTABLE MOTION OF FREE SPAR BUOYS IN WAVES

J-C. Dern
Bassin d'Essais des Carènes
Paris, France

ABSTRACT

The stability of the motions in waves of a particular type of free spar buoys is studied both theoretically and experimentally. In a first step the motions are determined from linearized equations. The coefficients appearing in these equations are obtained from model tests. The obtained results are compared with J. N. Newman's theory.

(i) Tests show that the buoy may perform different stable motions depending on its mass, the position of its center of gravity and its inertia.

In particular, when the buoy has a large static stability in pitching, these motions consist of heaving and pitching, their combination being stable and uniquely determined.

On the contrary for low value of the static stability in pitching, there exist two stable combinations of heaving and pitching motions, they differ from each other by the amplitude of the heave/wave ratio which is moderate in the case of one combination and much higher in the case of the second one.

All the above motions are periodic and their period is that of the waves. The existence of two stable combinations indicates that there also exists a third but unstable combination.

Preceding page blank

(ii) Furthermore, if the period of the wave is in the range between the period of the natural rolling motion and half that of the natural pitching motion and if the static stability in pitching is small, then the motion of the buoy consists of three parts : heaving, rolling and pitching ; two combinations exist, one with a moderate heave value, the other with a larger heave value ; in each case the amplitude of the pitching motion varies irregularly from one oscillation to the next one and gives the impression of being a random function of time.

The above phenomena cannot be predicted from a linearized theory. The phenomenon described in (i) can be explained by the non linearity of the restoring force in pure heave motion ; that described in (ii) by the existence of a term in θZ (θ = pitch angle, Z = heave) in the equations of rolling and pitching.

In the case of irregular waves it is proposed for the rolling and pitching motions a stability criterion similar to that of J. B. Keller and G. F. Carrier for tsunamis.

INTRODUCTION

For some years now, theoretical studies have been devoted to the motion of spar buoys in regular waves. In these works the equations of the heaving motion Z, surging motion X and pitching motion θ are generally linear ([1], [2], [3]). In reference [4] experiments performed on circular cylindrical buoys, of slenderness (draft / radius) larger than 5, in regular and irregular waves are reported. It appears from the results presented in [4] that J. N. Newman's theory is well verified under the condition that an experimentally determined added mass be included in the heaving equation.

In the present paper we present the results of experiments on spar buoy models in regular and irregular waves. In contradiction with reference [4] , motions not predicted by Newman's theory were observed. These particular motions cannot be explained but by the presence of non linear terms in the equations, which come from the fact that in the vicinity of its natural heaving frequency a spar buoy is submitted to vertical oscillations of large amplitude, the damping force being very weak. It is not possible, then, to neglect, even as a first approximation, the variation of the instantaneous waterline area

due to the vertical motion of the buoy. Furthermore the large amplitude of the vertical motion explains why the wave height chosen in our experiments is small ($\zeta_w \leq 0.50$ m. in real scale). For larger wave height, the waves would sometimes overrun the buoy models, the motions would then become quite irregular and would not be amenable by a simple theoretical approach.

The present study was divided as follows :

In Section I, we present results of experiments on regular waves of various models. These experiments show the presence of these phenomena of non linear origin : a double regime for the vertical motions, a rolling motion and an unstable pitching motion.

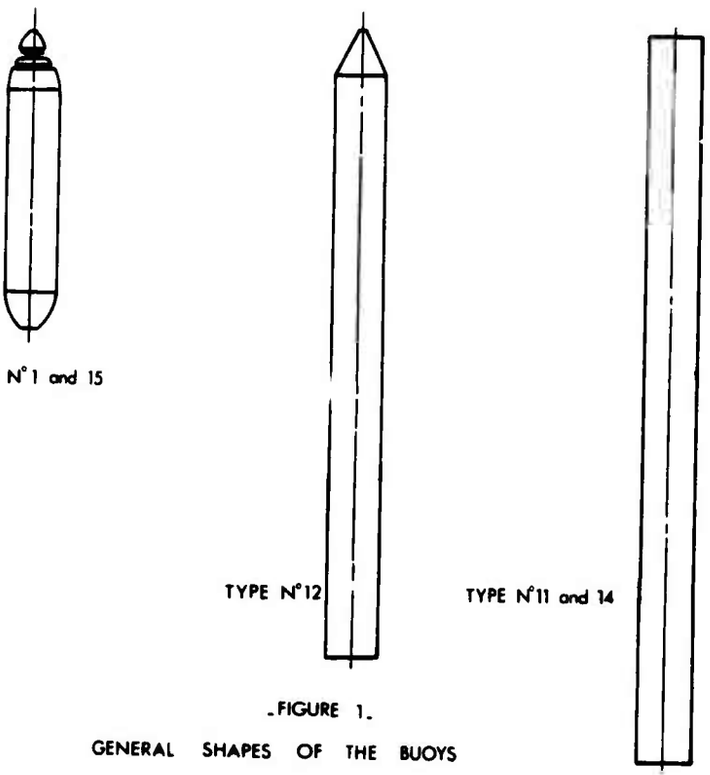
In section II we propose a theory to explain these phenomena. This theory consists essentially in introducing non linear restoring terms in the equations of motion.

Section III deals with the behaviour of the buoy in irregular waves. The unstable rolling motion is studied experimentally and theoretically by using a stability criteria similar to that of J. B. Keller and G. F. Carrier.

TYPE OF BUOYS STUDIED

The buoys studied here are made of a circular cylindrical central part, while the upper and lower parts, though always axisymmetric, may have, in some cases, rather complicated shapes which can sensibly differ from a circular cylinder. The upper part which is out of water is usually of small height. Sketches of the various types of the buoys studied in this paper are given in Figure 1. Their characteristics are given in Table 1 .

Dern



-FIGURE 1-

GENERAL SHAPES OF THE BUOYS

TABLE 1

FULL-SCALE CHARACTERISTICS OF THE STUDIED BUOYS

Type	Buoy radius	Overall length	Mass	Draft	Slender-ness	Position of G/base-line	Position of C/base-line	$\overline{CG}$	Inertia
	R	L_{HT}	m	H	H/R	z'_G	z'_C	$a=z'_C-z'_G$	Kyy/L_{HT}
	meter	meter	kgm.	meter		meter	meter	meter	
1	0.2667	2.800	486	2.297	8.61	1.052	1.225	0.173	0.278
11 and 12	0.2667	5.600	1182	5.155	19.34	1.735	2.578	0.843	0.304
14	0.2667	5.600	1215	5.300	19.9	2.300	2.650	0.350	0.249
15	0.2667	2.800	500	2.181	9.2	0.960	1.090	0.130	0.316

SECTION I

RESULTS OF EXPERIMENTS IN REGULAR WAVES

I - NOMENCLATURE -

1,1 - Characteristics of buoys -
The notations concerning the buoys characteristics are given in Figures 2 and 3 . Furthermore we have :

m	Mass of buoy
Iyy	Moment of inertia around a transversal axis passing through the center of gravity G of the buoy
$Kyy = \sqrt{\frac{Iyy}{m}}$	Transversal radius of inertia

The moment of inertia is preferably defined as the non - dimensional ratio

$$\frac{Kyy}{L_{HT}}$$

1,2 - Regular waves (Figure 4) -

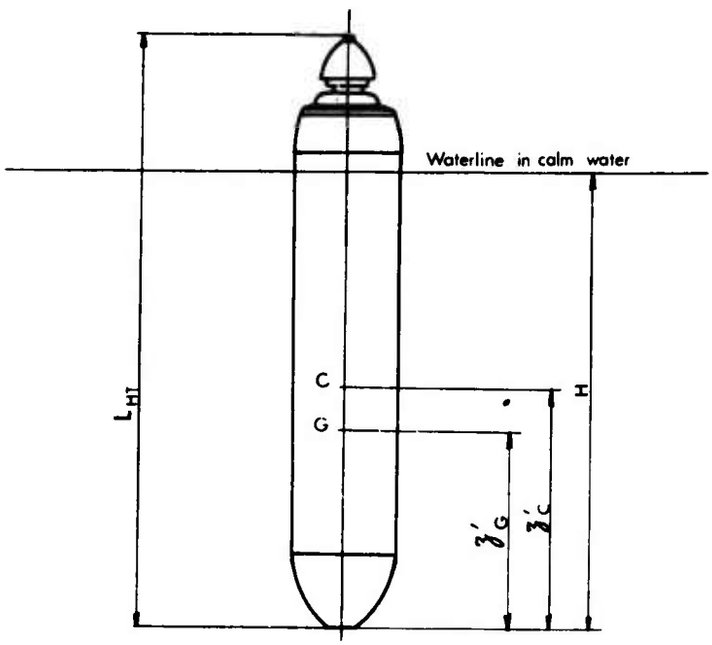
The waves are supposed to be regular and with one only direction of propagation

$O_o x_o y_o z_o$	Fixed systems of axis
$O_o x_o y_o$	Free surface at rest
$O_o x_o$	Axis in the direction of propagation of the waves
$O_o z_o$	Vertical downward axis .

The wave elevation at point O_o is then defined by :

$$\zeta (t) = \zeta_A \cos 2 \pi ft = \rho_A \cos \sigma t$$

f	Wave frequency in Hz
ζ_A	Half wave amplitude
ζ_W	Wave height
σ	Circular frequency



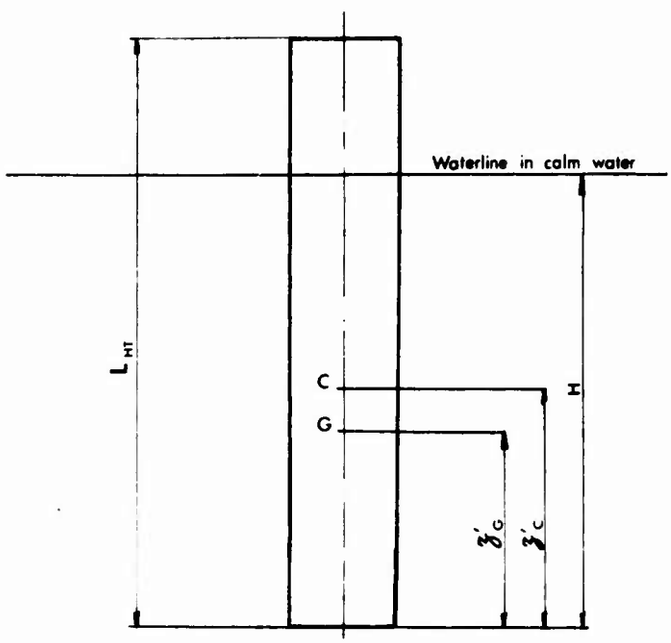
C: CENTER OF BUOYANCY

G: CENTER OF GRAVITY

FIGURE 2

NOMENCLATURE

(TYPE N°1 and 15)



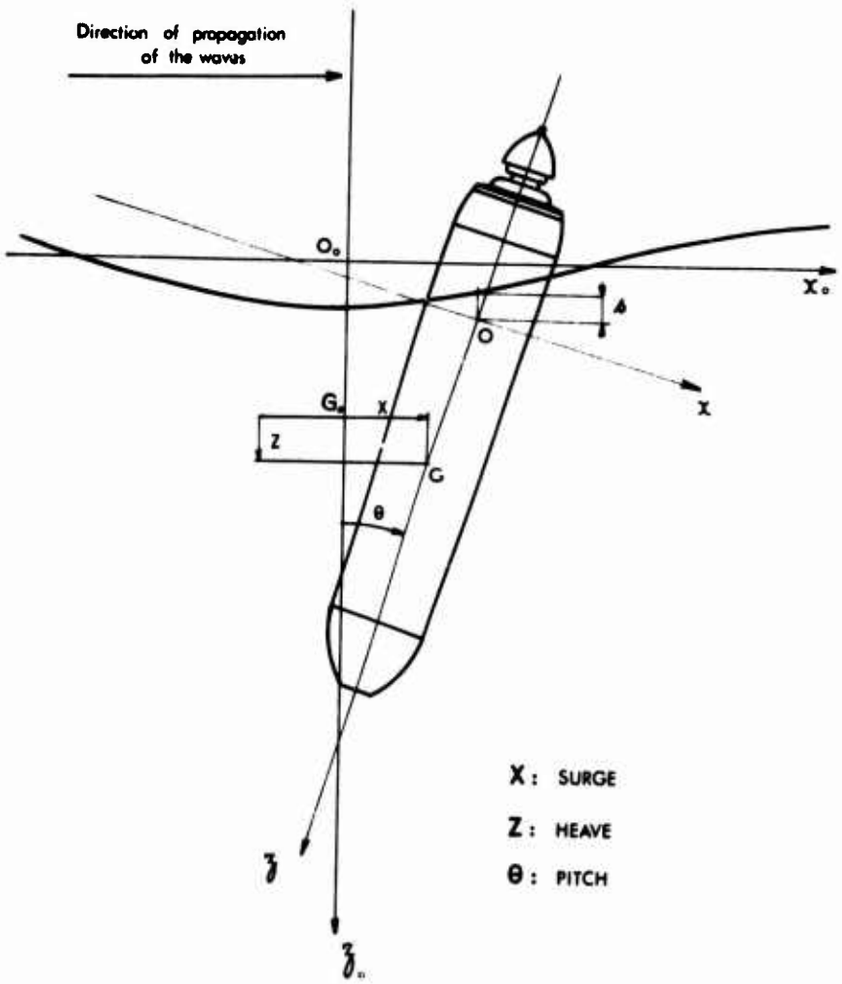
C: CENTER OF BUOYANCY

G: CENTER OF GRAVITY

_ FIGURE 3 _

NOMENCLATURE

(TYPE N° 11 and 14)



-FIGURE 4-

NOMENCLATURE

1, 3 - Buoy motion on waves -

For waves defined as above (1 , 2) , let us put :

φ (t) Roll angle

θ (t) Pitch angle

ψ (t) Yaw angle

The pitching motion (respectively rolling motion) is defined as the motion about an axis parallel to $O_o y_o$ (resp. $O_o x_o$). Thus pitching occurs in a vertical plane parallel to the direction of wave propagation , rolling occurs in a vertical plane parallel to the wave - crest lines .

X (t) Surge of buoy . The surge is a motion parallel to $O_o x_{o,}$, direction of wave propagation

Y (t) Sway of buoy

Z (t) Heave of buoy

s (t) Vertical distance between point O (i. e . the point being in O_o in calm water) and the instantaneous water surface. s (t) defines the relative motion of the buoy with respect to the water .

The index A represents the half - amplitude : e. g. Z_A is the half-amplitude of heaving ($Z(t) = Z_A \cos \sigma t$) .

II - PRINCIPLE OF THE EXPERIMENTAL METHOD -

2, 1 - Models -

Scale : 1 / 4. 2672

The models were adjusted in weight , position of center of gravity and in transversal moment of inertia . In order to adjust the values of these 3 parameters , three weights could be moved along a threaded rod inside the models .

2, 2 - Measurements performed -

In general four quantities were measured . However in some experiments only two or three of these quantities were actually measured .

2, 21 - The wave height ζ (t) was measured with a capa - citance probe , made of a coated wire , and the capacitance between the water and the wire , proportional to the length of wetted wire ,

was measured .

2,22 - The heave Z (t) of the buoy was determined by measuring with an accelerometer set within the model the acceleration - parallel to the axis of revolution of the buoy . Rather than to integrate twice the acceleration a (t) it was assumed that the motion was sinusoidal . The heave is then related to the acceleration by the relationship :

$$Z(t) = -\frac{a(t)}{\sigma^2}$$

This relationship is valid only if a (t) is sinusoidal and if pitching has a small influence on the acceleration . In order to satisfy as well as possible these two conditions , it was decided to simulate only waves with wavelength not too large as compared to tank depth (see shallow water waves theory) and with small steepness ($\gamma = \delta w / \lambda \leq 2 / 100$) . The two purposes of this latter condition are first to reduce the number of harmonics present in the waves , second and more important to avoid large motions of the buoy in pitching (influence on the acceleration a (t) as well as in heaving : experience shows that when the wave steepness is large the buoy performs very irregular vertical motions , which are difficult to interpret (see figure 5) .

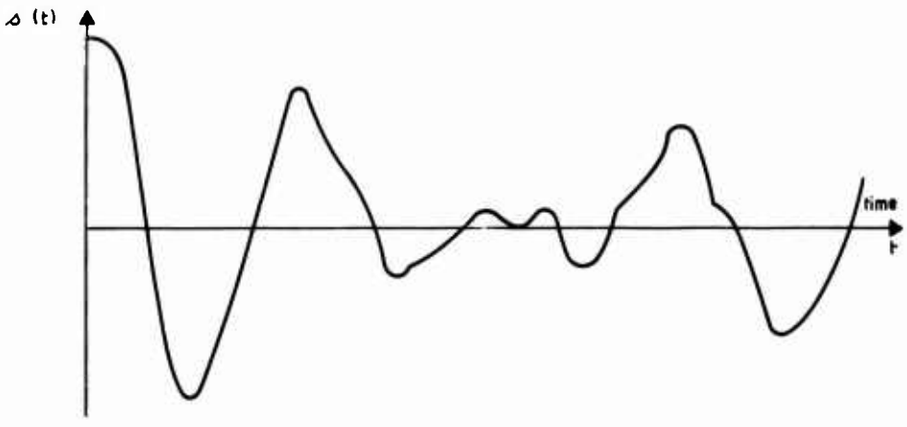


Figure 5

In spite of the care taken , it happens that , under cer - tain conditions one observes vertical motions which differ much from sinusoidal motions . It is then necessary in order to study these vertical motions to use the method described in the following paragraph .

2, 23 - The quantity s (t) is measured by means of three capacitance probes similar to that used to measure the wave height . Figure 6 presents a sketch of the corresponding set-up . Each probe gives a signal proportional to the submerged length of wire , thus the sum of the three signals gives a value proportional to s (t) provided that the pitch angle be small , which was the case in the experi - ments performed (see above paragraph) . The value of s (t) is then related to that of the heave Z (t) by :

$$s(t) = Z(t) - \zeta(t)$$

2, 24 - The pitch and roll angles were measured separa - tely with a Polaroid camera : a picture taken during a time intervall equal to one period of the motion gave the extrem angular positions of a little rod set on top of the model .

2, 25 - The interest of these methods is that they leave the model completely free except for a few very thin electrical wires going from the accelerometer and wave probes .

III - EXPERIMENTS PERFORMED IN REGULAR WAVES -

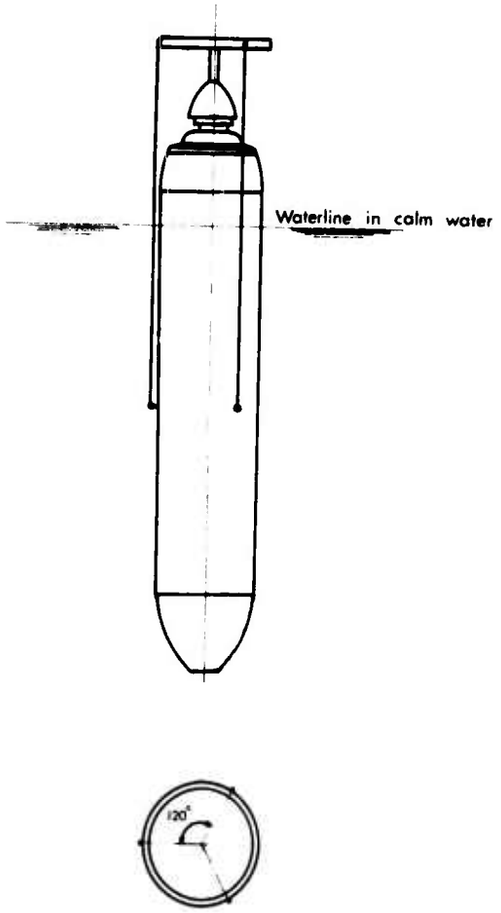
The experiments were conducted partly in the wave tank of the Bassin d'Essais des Carènes (dimensions : 30 m x 7 m x 2.40 m) and partly at the towing tank n° 2 (dimensions : 150 m x 8 m x 2 m). In both tanks the possible waves are $\zeta_w \leq 0.30$ m. , $0.20\ \text{Hz} \leqslant f \leqslant 1\text{Hz}$.

Two types of experiments were performed

- The model was completely free to move in all directions to study the rolling .
- The model was forced to stay in a vertical plane parallel to the direction of wave propagation in order to study its vertical motions and its pitching motion .

IV - EXPERIMENTS IN REGULAR WAVES WITH A COMPLETELY FREE MODEL : STUDY OF ROLLING -

The experiments in one-directional regular waves with



- FIGURE 6 -

PRINCIPLE OF THE MEASUREMENT OF δ (t)

a completely free model showed that for certain types of buoy , the motions of the model are three-dimensional : the model oscillates not only around the y-axis (pitching) but also around the x-axis (rolling) . The top of the model describes then a 8-shaped curve , and the rolling motion has a period equal to twice that of the waves :

$$Tr = 2\ Tw$$

This rolling has the following properties

- it is stable in amplitude ,
- this amplitude is considerable (larger than the corresponding pitching amplitudes)
- rolling occurs but for certain wave frequencies $f = 1 / Tw$
- the wave amplitude has an important effect on the occurence and amplitude of rolling .

Figure 7 presents the rolling and pitching behavior of type 1 buoy .

The following remarks can be made :

- for a given wave amplitude the rolling occurs only if the wave frequency lies between two values , one close to fz , the other close to $2\ f_\theta$

- for a given wave frequency , rolling takes place only if the wave amplitude is sufficiently small . Furthermore for certain amplitudes either rolling occurs or it does not .

- for a given wave amplitude the ratio θ_A / ζ_A varies irregularly with the wave frequency when the model is rolling . One of the reasons of this phenomenon is the following : when there is rolling the top of the model describes a 8-shaped curved but this trajectory is not stable with time , the eight rotates slightly on itself while undergoing deformation . The figure below clearly shows that this modification has little effect on the measurement of rolling but has much effect on that of pitching .

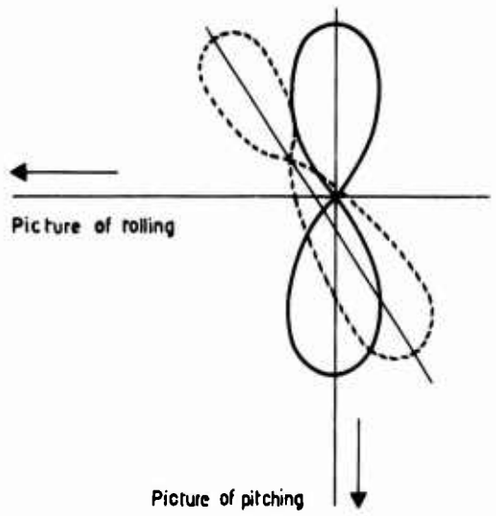
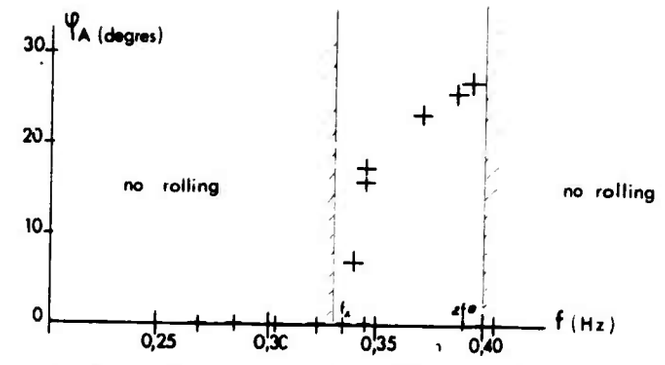


Figure 8 shows the behavior in rolling of the type 14 buoy . Once more one remarks that rolling occurs only if the wave frequency lies between two values one close to fz , the other close to 2 f_θ. For a frequency of 0.240 Hz rolling occurs only if the wave height is larger than some critical value (ζ_w = 0.20 m), but in contrary to the type 1 buoy , the half-amplitude of rolling increases monotically with the wave height up to ζ_w = 1 m . The experiment could not be conducted beyond this value, for the heaving motion became too large and the model was periodically submerged by the waves .

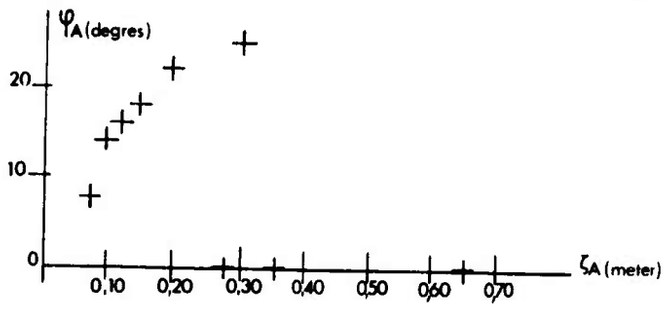
V - EXPERIMENTS IN REGULAR WAVES : STUDY OF THE VERTICAL MOTIONS AND OF PITCHING -

5,1 - Experimental conditions -

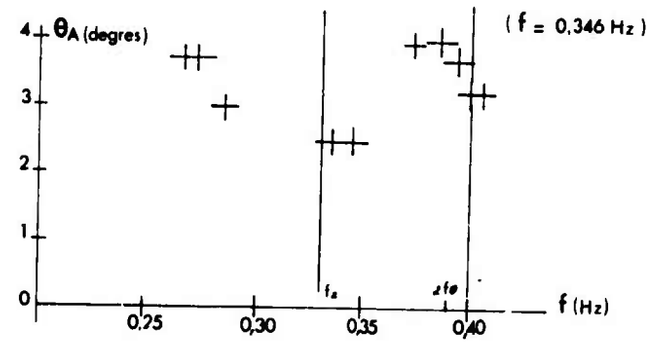
The just mentioned phenomenon of rolling prevented any valid measurement of the pitch angle by photographic method . The experimental set up was then modified to eliminate the rolling motion . The rod on top of the model was set between two guides made of two horizontal steel wires parallel to the direction of wave propagation and located one under the other . It has been verified on a short number of points that this set-up did not perturb the value of the half-amplitude of pitching and heaving .



HALF AMPLITUDE OF ROLLING VS FREQUENCY (ζ_w = 0,255 m)



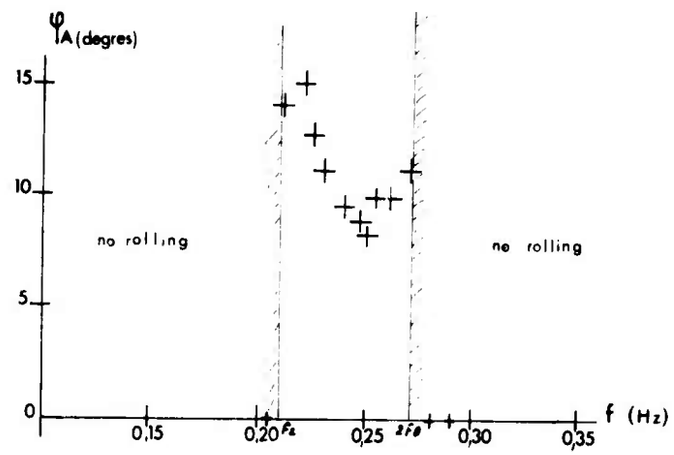
HALF AMPLITUDE OF ROLLING VS HALF AMPLITUDE OF WAVES



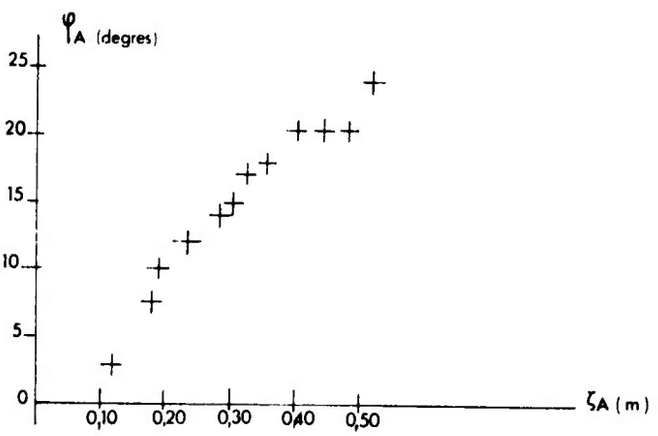
HALF AMPLITUDE OF PITCHING VS FREQUENCY (ζ_w = 0,255 m)

FIGURE 7

ROLLING AND PITCHING OF TYPE 1 BUOY IN REGULAR WAVES



HALF AMPLITUDE OF ROLLING VS FREQUENCY ($\zeta_w = 0{,}340\,m$)



HALF AMPLITUDE OF ROLLING VS HALF AMPLITUDE OF WAVES

($f = 0{,}240$ Hz)

FIGURE 8

ROLLING OF TYPE 14 BUOY IN REGULAR WAVES

The following paragraph is devoted to the study of pitching and vertical motions performed under these particular experimental conditions .

5, 2 - Presentation of results -

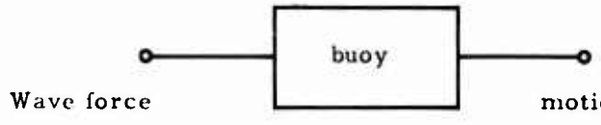
The experimental results are presented under the form of "gain curve" . In other words the following ratios are given :

- pitching θ_A/ζ_A in degree per meter

- relative motion s_A / ζ_A

- heaving Z_A / ζ_A

In principle these ratios should be independant of ζ_A, and each one of them should be equal to the modulus of the transfer function computed from Newman's theory . Together with these experimental gain curves , we also give the modulus of this transfer function (denoted "J. N. Newman" in the figures) and in some cases a curve denoted "second order" on the figures . This last curve was obtained by modeling the dynamic system of the buoy (Input : wave force , output : motion) by a second order differential system .



The wave force acting on the buoy was determined theoretically from the hypothesis of Froude-Krilov (the expression of these forces are given in section II) .

For example , the transfer function of the second order system is for pitching :

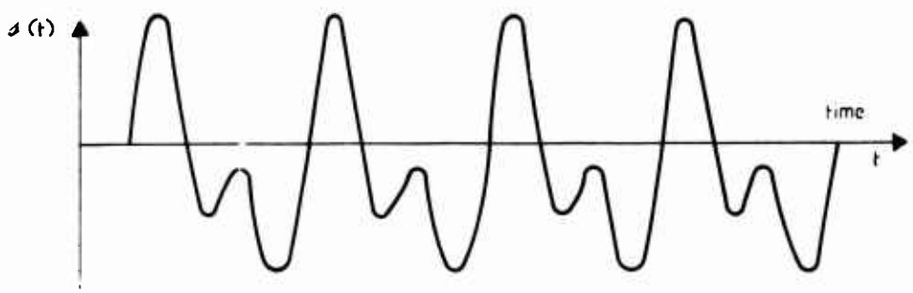
$$H_{\theta\rho}(2\pi i f) = \frac{G_{\theta\rho}(f)}{mg\,(r+a) + (2\pi i f)^2\,(Iyy + Jyy) + 2\pi i f N_{\theta\theta}(\circ)}$$

$G_{\theta\rho}(f)$ is obtained from the expression of the wave force . The constant coefficients in the denominator were experimentally determined (damping test in calm water) .

5,3 - Type 1 Buoy -

Figures 9 and 10 show that Newman's theory is not in agreement with the experiment . At certain frequencies there exist a double regime in the relative motion . For example at f = O. 286 Hz, during the same experiment we obtained the values $\frac{\sigma A}{\zeta A}$ = 1. 1 and $\frac{\sigma A}{\zeta A}$ = 4. 7 simply by giving to the model a vertical impulsion at the right time . The gain curve in s exhibits a slight resonance for $f = f_\theta$ and a zone of unstability for $f = 2\ f_\theta$. For $f < 2\ f_\theta$ but close to $2\ f_\theta$ the signal has the following shape

s (t)



When the frequency is exactly equal to $2\ f_\theta$ the recording of s (t) is untractable , it is very irregular and corresponds to very large va - lues of s (t) .

The gain curve in θ shows the existence of a frequency interval in which the points are very scattered . In this zone pitching varies with time in the same way as s (t) does . The frequency inter - val coincides approximately with $\left[f_z \ , \ 2\ f_\theta \right]$

5. 4 - Type 11 Buoy -

The type 11 buoy was chosen so that all conditions of validity of the slender body theory be satisfied . In particular the slenderness has a large value (H/R = 19. 34) , and the upper part out of water has a cylindrical circular shape as the rest of the buoy . This upper part is quite high (h = 0. 42 m.)

Figures 11, 12 and 13 show that Newman's theory is rather well verified . However two discrepancies can be noted : for $f = 2\ f_\theta$ the experimental points are well above the theoretical curve (see in particular the gain in Z) . Furthermore it is difficult to check experimentally the value of the gain at resonance which is very sharp . At resonance , the gain depends chiefly on the damping coef - ficient . The theoretical heave damping coefficient is 0, 92 , while that determined experimentally in calm water is 85 . It seems there - fore that there is a large inaccuracy for the value of the heave dam -

ping coefficient . The same result exists for the pitch damping coefficient .

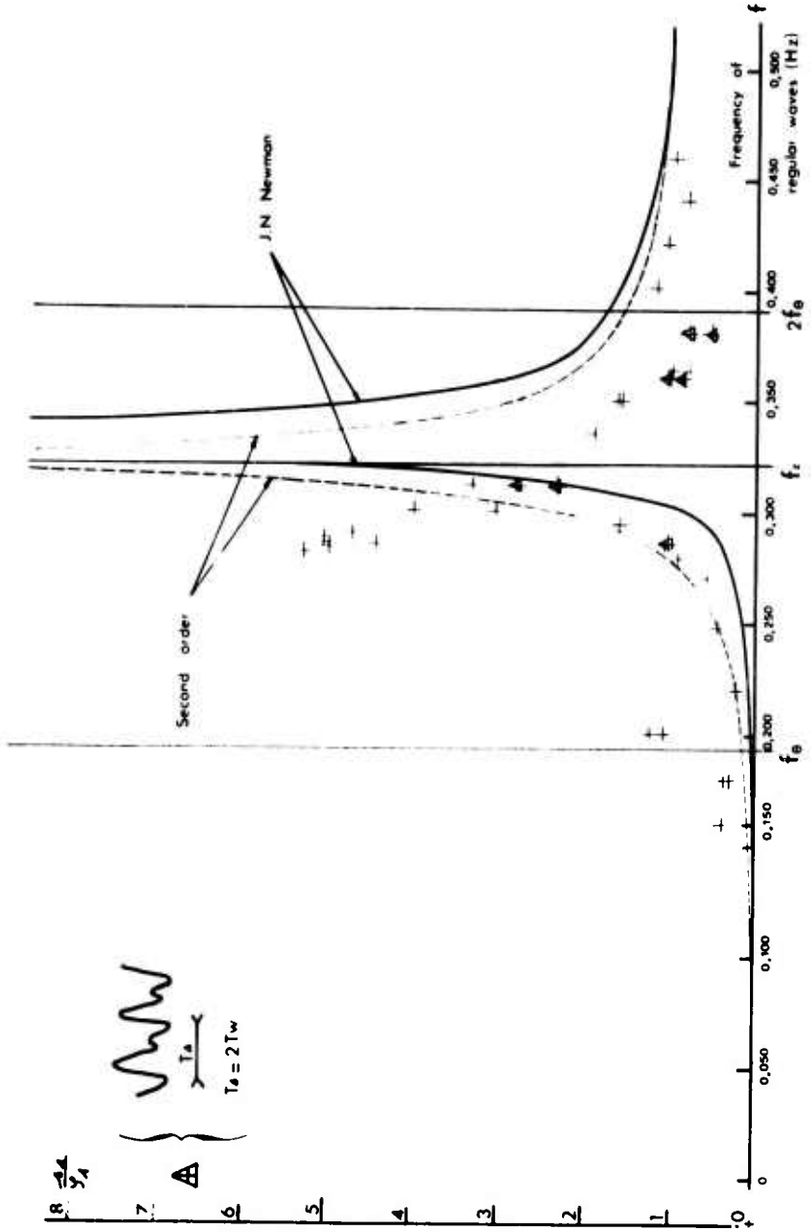
5.5 - Type n° 12 -

In order to confirm the results obtain with the type 1 buoy , we tested a buoy model with the same dynamic characteris - tics as type 11 , but with a conical upper part . This buoy model , denoted type 12 , was tested for various wave amplitudes in order to check the linearity hypothesis . The results of the experiments are given in figures 14 , 15 and 16 , which show that Newman's li - near theory is , here again , not valid . It can be noticed in particu- lar that there is a jump in the gains in s and Z . The results obtai - ned for $f = 2 f_\theta$ show that the three gains are not independent of the wave amplitude . When f is close to but less than $2 f_\theta$, two regimes of motion are possible , in particular for the relative motion s and the heaving Z . These two regimes are characterized first by the value of the gain , second by the frequency of the oscillations . For small gain this frequency is equal to that of the waves , for larger gains it is half the wave frequency . In both regimes the oscillations are approximatively sinusoidal , except for pitching when the regi - me corresponds to the higher gain . Furthermore , for the large gain the model is periodically submerged by the waves .

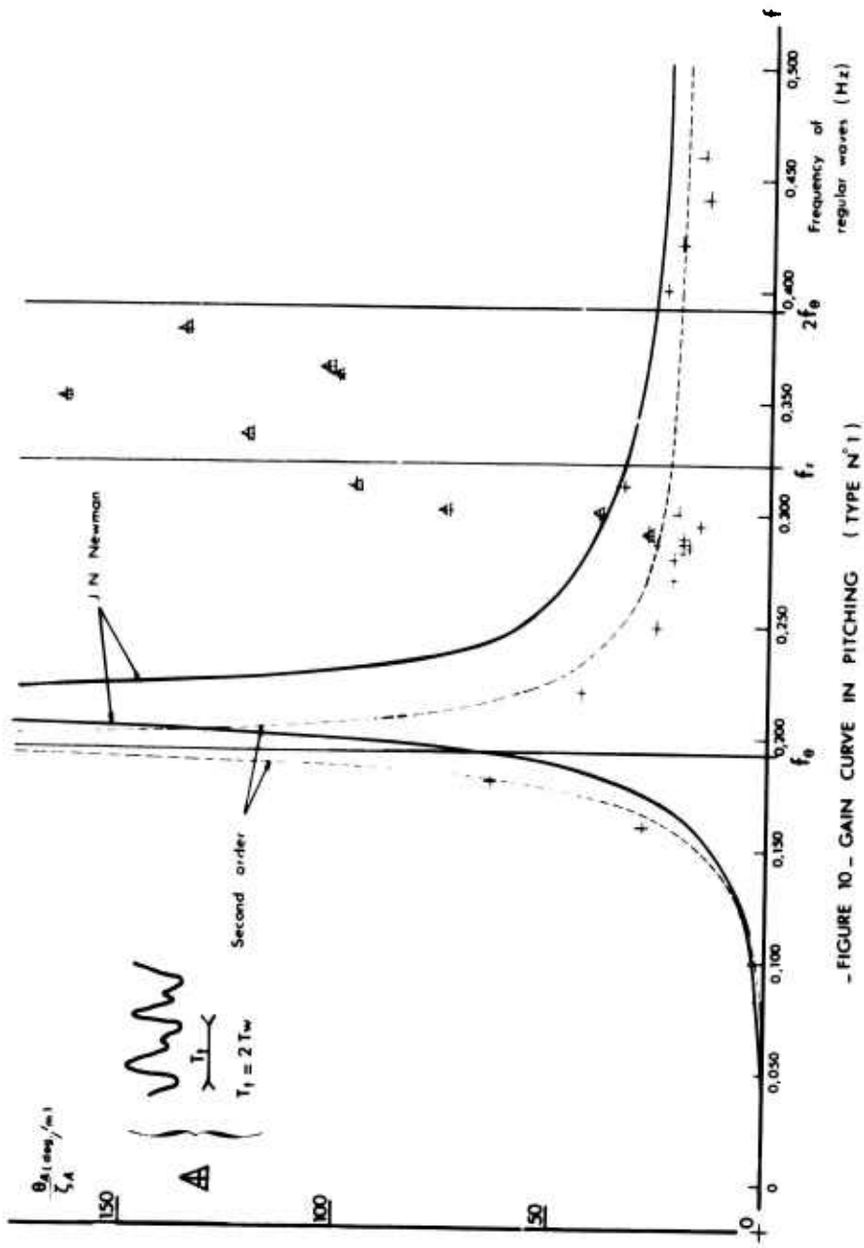
VI - CONCLUSION TO THE EXPERIMENTAL STUDY -

The heave damping of a spar buoy being very weak , when such a buoy is submitted to a wave train of frequency equal to the buoy natural heaving frequency , it then performs motions of large amplitude . Under these conditions if the upper part of the buoy, normally out of the water , does not have a constant sectional area non-linearities appear which modify completely the frequency res - ponse of the buoy . In particular a phenomenon of double regime for the vertical displacements appears . Discrepancies also occur for frequencies close to but less than twice the natural pitching frequency.

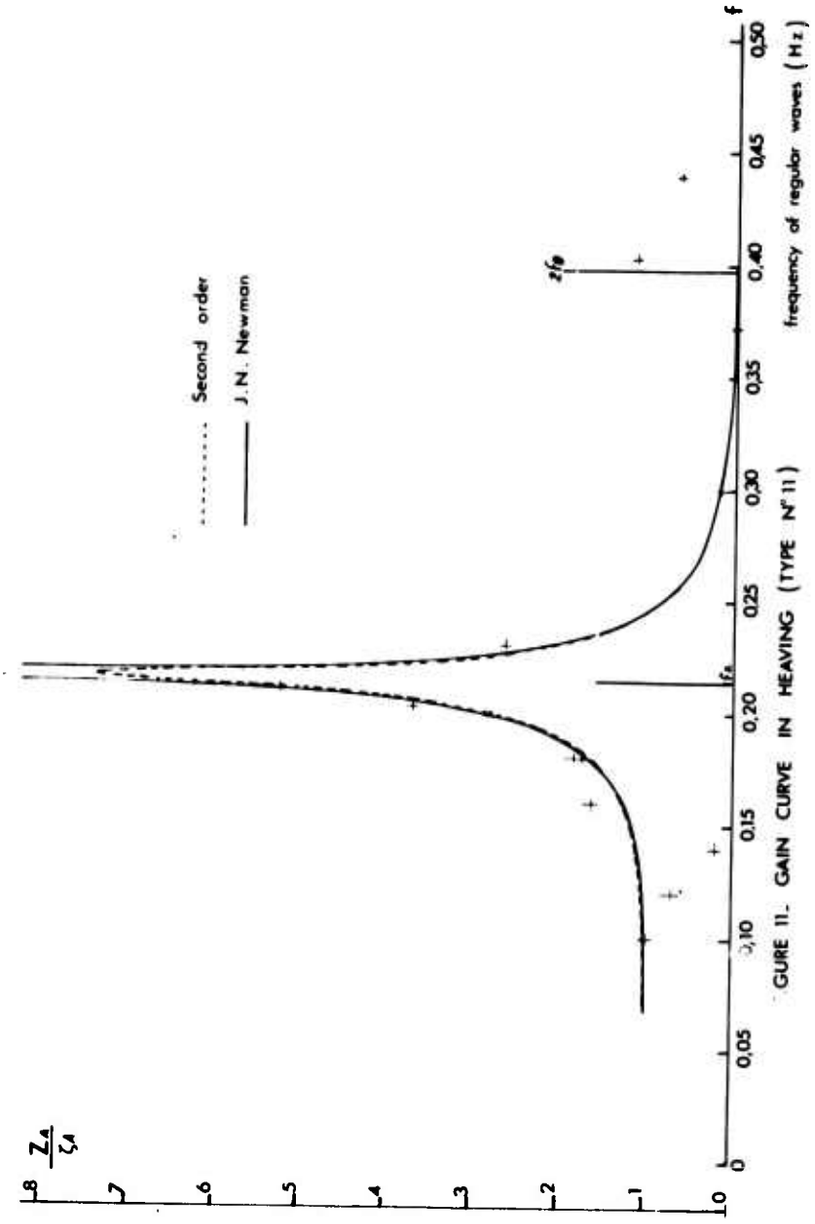
Thus J.N.Newman's linear theory for heaving motion is not valid unless the upper part of these buoys , which is out of the water in calm water , be of constant sectional area on a sufficient length . The conditions of validity of J.N.Newman's theory for pit - ching and rolling motions are more complicated as we shall see in Section II .



- FIGURE 9 - GAIN CURVE OF RELATIVE MOTION (TYPE N° 1)



- FIGURE 10 - GAIN CURVE IN PITCHING (TYPE N°1)



GURE 11- GAIN CURVE IN HEAVING (TYPE N° 11)

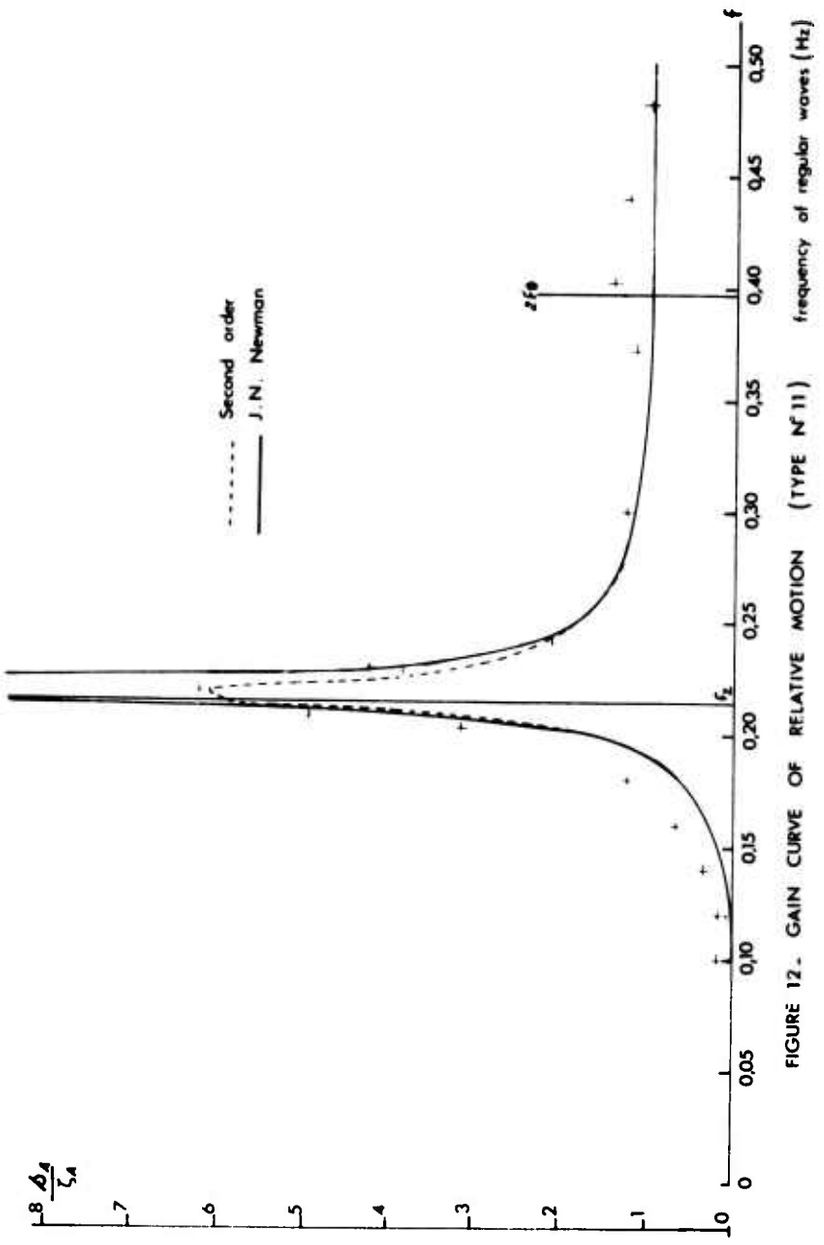


FIGURE 12 - GAIN CURVE OF RELATIVE MOTION (TYPE N° 11) frequency of regular waves (Hz)

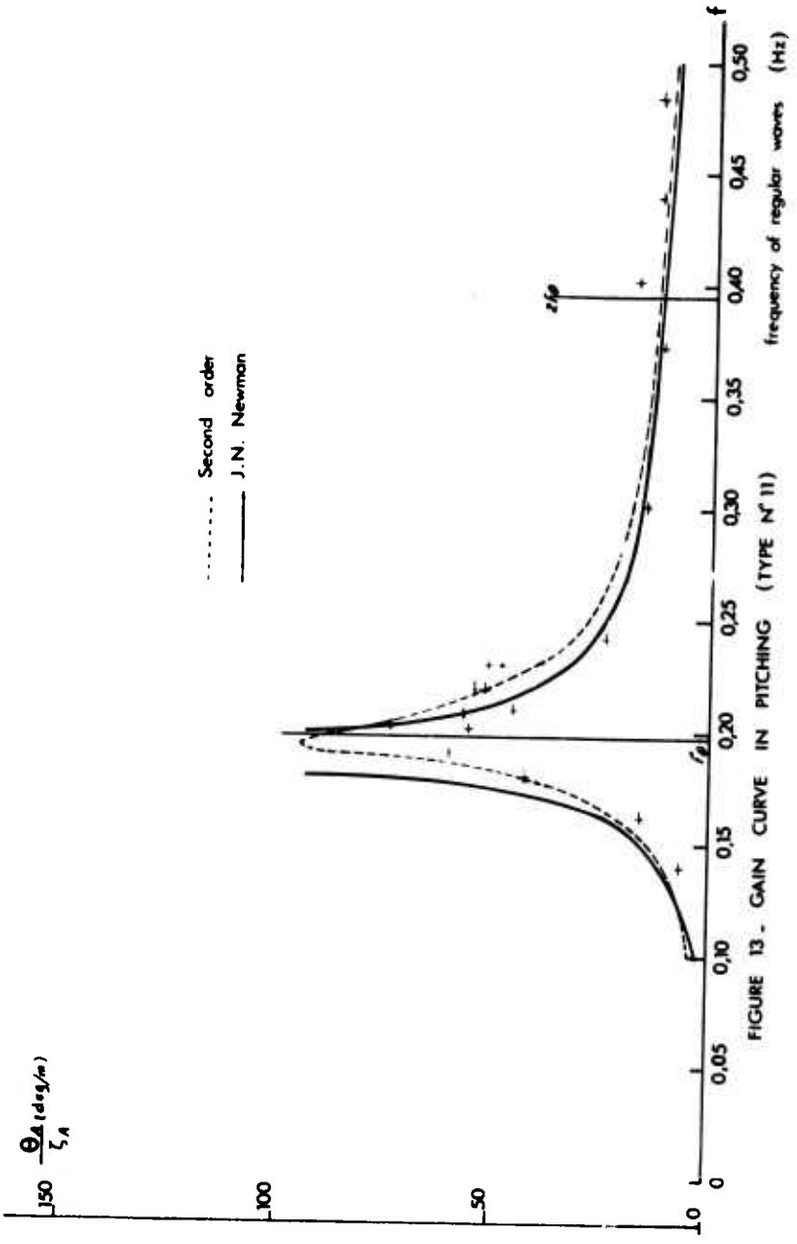


FIGURE 13 - GAIN CURVE IN PITCHING (TYPE N° 11)

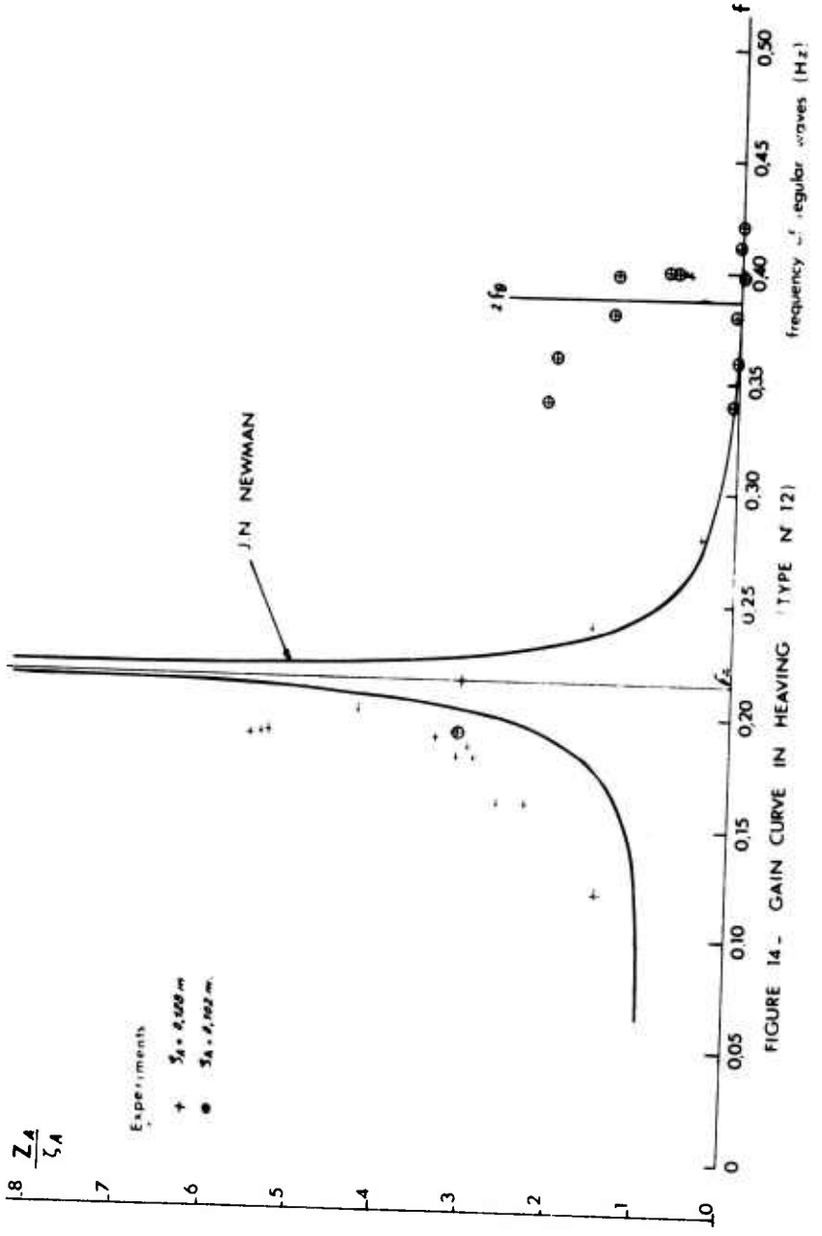


FIGURE 14 - GAIN CURVE IN HEAVING (TYPE N 12)

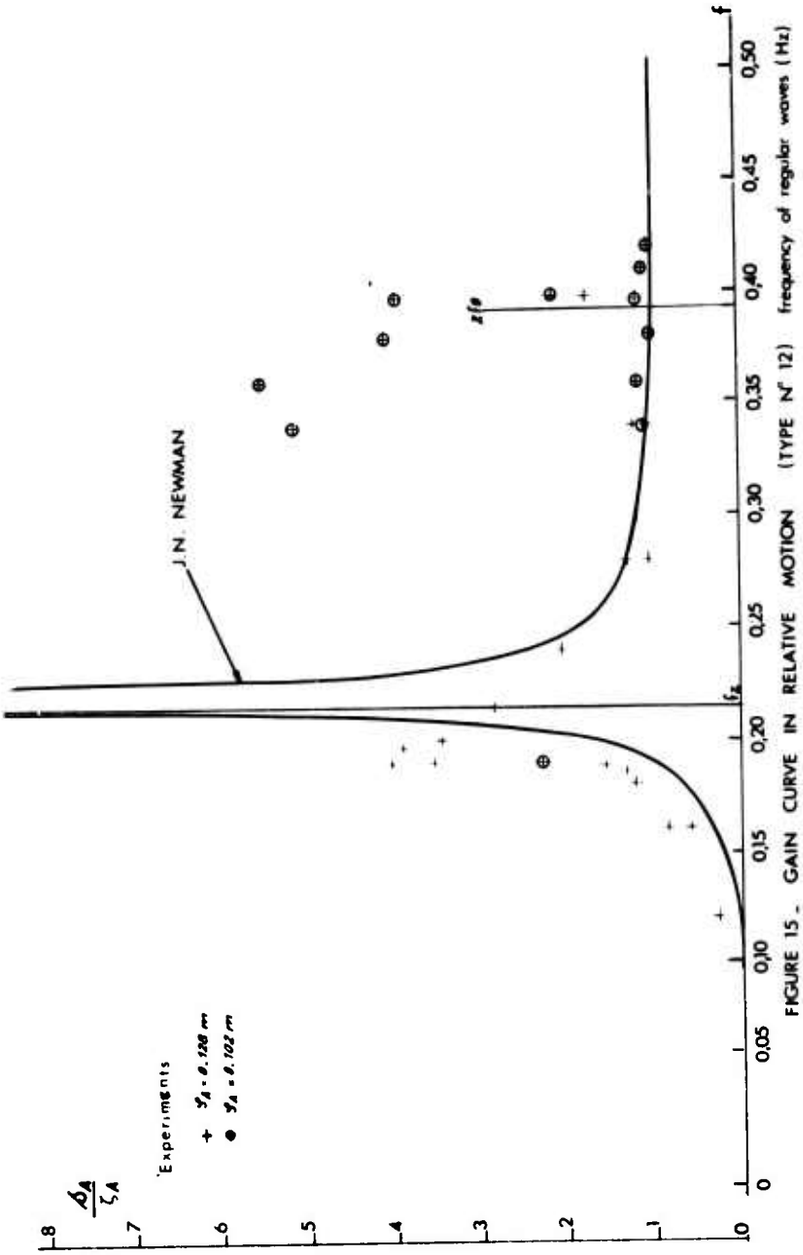


FIGURE 15 - GAIN CURVE IN RELATIVE MOTION (TYPE N° 12) frequency of regular waves (Hz)

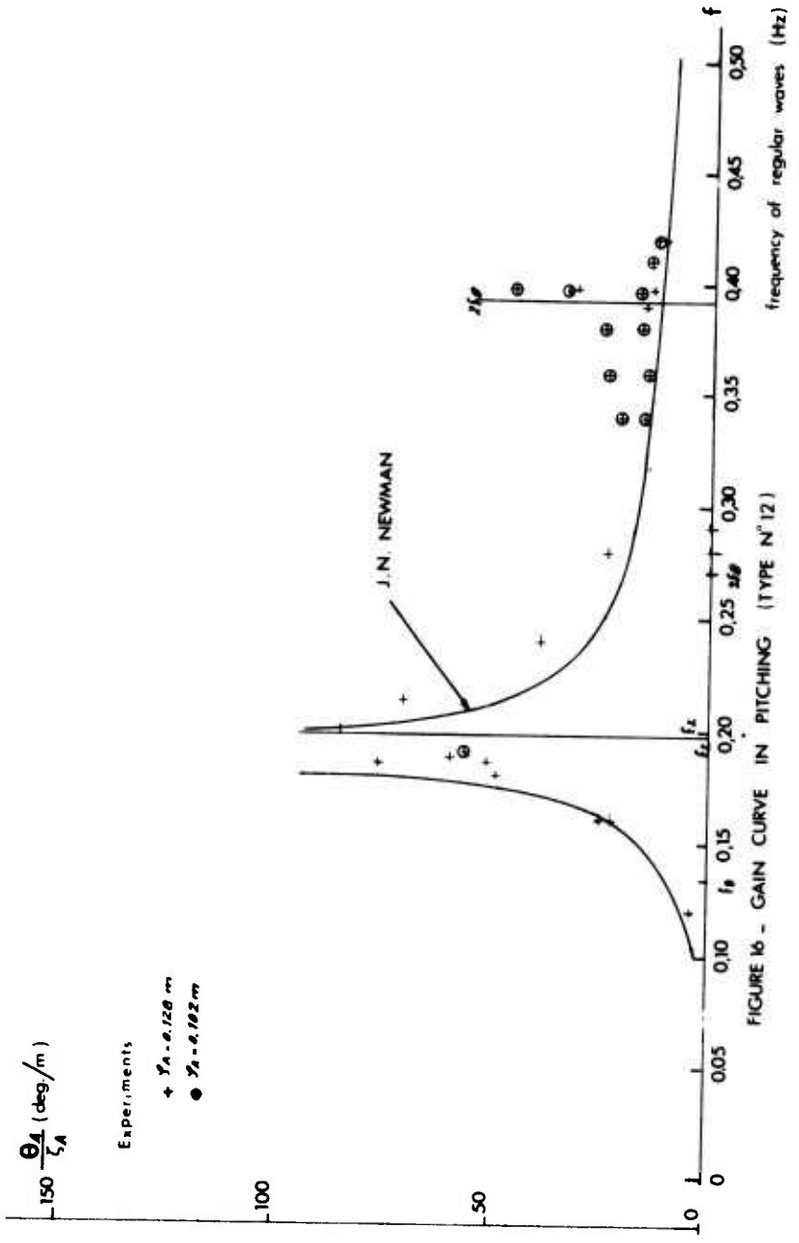


FIGURE 16 - GAIN CURVE IN PITCHING (TYPE N° 12)

SECTION II

THEORETICAL INTERPRETATION OF THE RESULTS OF EXPERIMENTS IN REGULAR WAVES

The experiments , the results of which we have presented in Section I , show that the spar buoy is far from behaving as a linear dynamic system . It is possible to interpret these results qualitatively and sometimes quantitatively using a non linear theory . This theory is simply set by slightly modifying J.N.Newman's equations . In these equations some volume integrals were calculated supposing that the buoy heave was infinitely small . We take back these integral calcu - lations making allowance for the finiteness of the heave amplitude .

I - GENERAL EQUATIONS OF MOTION -

The following classical assumptions are made :

- The buoy is a slender body ($H/R \gg 1$)
- Oncoming wave is Airy wave
- The exciting forces are computed using Froude Krilov hypothesis

With these assumptions , the equations of motion with six degrees of freedom are obtained reasoning as in [2]

$$(\overline{\overline{M}} + \overline{\overline{Q}}) \frac{d}{dt}[V] + [\overline{\overline{N}}][V] + [\Gamma] = [F] + [P]$$

with $$[\Gamma] \triangleq \begin{bmatrix} \int_v \rho \, \vec{g} \, d\mathcal{V} \\ \int_v \rho \, (\vec{GP} \wedge \vec{g}) \, d\mathcal{V} \end{bmatrix}$$

../..

(II-1. 1)

$$\left[F \right] = \overline{\overline{\Delta}} \begin{bmatrix} \int_{\nu} \rho \ (\vec{a_o} + \vec{a_{ox}}) \ d \ \mathcal{V} \\ 2 \int_{\nu} \rho \ (\vec{GP} \wedge \vec{a_{ox}}) \ d \ \mathcal{V} \end{bmatrix}$$

$$\left[P \right] = \overline{\overline{\Delta}} \begin{bmatrix} m \ \vec{g} \\ O \end{bmatrix}$$

ρ	specific mass of water
g	acceleration of gravity
m	mass of the buoy
$\left[V\right] \overline{\overline{\Delta}}$ col	$\left[\frac{dX}{dt} , \frac{dY}{dt} , \frac{d\varphi}{dt} , \frac{d\theta}{dt} , \frac{d\Psi}{dt}\right]$
$\overline{\overline{M}}$, $\overline{\overline{O}}$, $\overline{\overline{N}}$	Tensors of inertia , added inertia and damping
ν	Immersed volume at time t
$\vec{a_c}$	Acceleration of fluid particles due to orbital motion of the waves imperturbated by the buoy
$\vec{a_{ox}} = (\vec{a_o} . \vec{x}) . \vec{x}$	where $\vec{x}$ is unity vector of Ox axis
P	Current point on the buoy axis of revolution

The tensors $\overline{\overline{M}}$, $\overline{\overline{O}}$, and $\overline{\overline{N}}$ are considerably simplified due to the fact that the buoy is a slender boy of revolution .

$$\overline{\overline{M}} = \text{diag} \left[m, \ m, \ m, \ Ixx, \ Iyy, \ 0 \right] + \overline{\overline{0}} (R^2)$$

$$\overline{\overline{Q}} = \begin{bmatrix} m_{xx} & O & O & O & m_{x\theta} & O \\ O & m_{yy} & O & m_{y\varphi} & O & O \\ O & O & m_{zz} & O & O & O \\ O & m_{\rho\varphi} & O & J_{xx} & O & O \\ m_{\theta x} & O & O & O & J_{yy} & O \\ O & O & O & O & O & O \end{bmatrix}$$

$$\bar{\bar{N}} = \begin{bmatrix} N_{xx} & 0 & 0 & 0 & N_{x\theta} & 0 \\ 0 & N_{yy} & 0 & N_{y\varphi} & 0 & 0 \\ 0 & 0 & N_{zz} & 0 & 0 & 0 \\ 0 & N_{\varphi y} & 0 & N_{\varphi\varphi} & 0 & 0 \\ N_{\theta x} & 0 & 0 & 0 & N_{\theta\theta} & 0 \\ 0 & 0 & 0 & 0 & 0 & 0 \end{bmatrix}$$

II - EQUATION OF HEAVE MOTION -

The equation (II-1. 1) gives for heave

$$(II\text{-}2.1)\quad (m + m_{zz})\frac{d^2Z}{dt^2} + N_{zz}\frac{dZ}{dt} + \rho g \int_{\nu} dv = \rho \int_{\nu} a_{ozo}\, dv + mg$$

if the potential of on-coming waves is

$$\phi(x_o, z_o, t) = \frac{g}{\sigma}\zeta_A e^{-k z_o} \sin(\sigma t - k x_o)$$

then $$a_{ozo} = - kg\, \zeta_A\, e^{-k z_o} \cos \sigma t$$

Let S(z) be the area of transverse section at station z

$$\rho g \int_{V} dV = \rho g \int_{-z+\int}^{H} S(z)\, dz = \rho g \int_{-z+\int}^{o} S(z)\, dz + mg$$

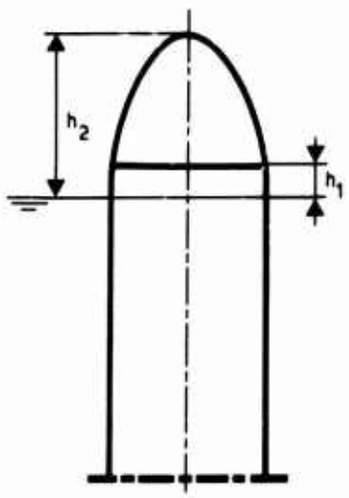
In type 1 buoy , S (z) is roughly :

$$S(z) = S(o)\left[1 + \frac{z + h_1}{h_2 - h_1}\, 1(-z - h_1)\right] 1(+z + h_2)$$

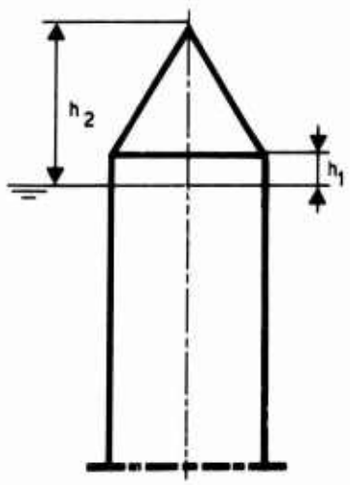
with $$1(z) = \begin{cases} 0 & \text{if } z < 0 \\ 1 & \text{if } z > 0 \end{cases}$$

h_1 and h_2 define the form of upper part of the buoy as indicated on the following figure

.. / ..



Type 1 and 15 buoy
(approximate shape)



Type 12 buoy
(exact shape)

For the type 12 buoy the exact expression of S (z) is

$$S(z) = S(o) \left[1 + \frac{z+h_1}{h_2-h}\, 1(-z-h_1)\right]^2 .\ 1\ (z+h_2)$$

For type 11 or 14

$$S(z) = S(o)\ 1\ (z+h_2)$$

where h_2 is very large .

As an example , for type 1

$$h_1 \simeq 0$$

$$h_2 = 0,42\ m$$

$$\rho g \int_{\mathcal{V}} d\mathcal{V} = m\,g + \rho\,g\,S(o).\begin{cases} s & \text{if } s \leq o \\ s - \dfrac{s^2}{2h_2} & \text{if } o \leq s \leq h_2 \\ \dfrac{h_2}{2} & \text{if } h_2 \leq s \end{cases}$$

$$\rho g \int_{\mathcal{V}} d\mathcal{V} = m\,g + \rho\,g\,S(o).\left[(Z - \zeta) + f(s)\right]$$

with

$$f(s) \begin{cases} 0 \text{ if } s \leq 0 \\ -\dfrac{s^2}{2h_2} \quad \text{if } 0 \leq s \leq h_2 \\ \dfrac{h_2}{2} - s \text{ if } s \geq h_2 \end{cases} \tag{II-2.2}$$

The calculation of the integral in the right hand side of the equation (II-2.1) is much simplified by the hypothesis of slender body theory and if we suppose that

$$h_2 = O(R)$$
$$\text{and } k R_o = o(R)$$
$$\text{then } ks = o(R)$$

$$\rho \int_{\mathcal{V}} a_{ozo}\, d\mathcal{V} = -\rho\,g\,S(o)\,C_p\,kH\,Q_o(k)\zeta + o(R).\zeta$$

with the notations displayed in the nomenclature .

Finally , the heave equation is

$$(II\text{-}2.3)\quad (m + m_{zz})\frac{d^2Z}{dt^2} + N_{zz}\frac{dZ}{dt} + \rho\, g\, S(0)\left[Z + f(s)\right] = \rho g\, S(0)\left[1 - C_p\, kH\, Q_o(k)\right] f(t)$$

where f (s) is given by (II-2.2) for type 1 and where

$$s(t) = Z(t) - f(t)$$

This equation completely determine the buoy heaving behaviour if the values of m_{zz} and N_{zz} are known

$$m_{zz} = \frac{4}{3}\rho R_o^3 \quad \text{from ([5] p. 200)}$$

$$N_{zz} = \pi \frac{\rho}{C_p} \cdot \frac{[S(o)]^2}{H} \cdot f \cdot \left[1 - C_p\, k\, H\, Qo(k)\right]^2 \quad \text{from [1]}$$

Thus , in this theory , the added mass is independent of the frequency but the damping is frequency dependent .

The heave equation in J.N.Newman's theory is obtained by setting $f(s) \equiv 0$ and $m_{zz} = 0$. In fact , in this paper , we mean by J.N.Newman's theory , the theory where $f(s) \equiv 0$ but where m_{zz} is given by the expression above .

III- EQUATION OF SURGE AND PITCH MOTIONS -

Equation (II-1.1) becomes for coupled surge and pitch motions :

$$(m+m_{xx})\frac{d^2X}{dt^2} + m_{x\theta}\frac{d^2\theta}{dt^2} + N_{xx}\frac{dX}{dt} + N_{x\theta}\frac{d\theta}{dt} = 2\rho\int_{\nu} aox\, d\nu$$

$$(I_{yy}+J_{yy})\frac{d^2\theta}{dt^2} + m_{x\theta}\frac{d^2X}{dt^2} + N_{\theta\theta}\frac{d\theta}{dt} + N_{x\theta}\frac{dX}{dt} + \rho\int_{\nu}(\vec{GP}\wedge\vec{g})_x\, d\mathcal{V} = 2\rho\int_{\nu}(\vec{GP}\wedge\vec{aox})_x\, d\mathcal{V}$$

where $(\quad)_x$ designates the projection on the Ox-axis .

The pitch equation obtained by elimination of X in the above two equations is of order 3 . In order to simplify subsequent calculation we shall make use of the fact that the coefficients N_{xx} and $N_{x\theta}$ are small . Neglecting them we obtain a second order equation in θ .

$$\left(I_{yy}+J_{yy}-\frac{m_{x\theta}^2}{m+m_{xx}}\right)\frac{d^2\theta}{dt^2}+N_{\theta\theta}\frac{d\theta}{dt}+\rho\int_{\mathcal{V}}(\vec{GP}\wedge\vec{g})_x\,d\mathcal{V}=2\rho\int_{\mathcal{V}}\left[(\vec{GP}\wedge\vec{a_{ox}})_x-\frac{m_{x\theta}}{m+m_{xx}}a_{ox}\right]d\mathcal{V}$$

The calculation of both integrals is performed in the same way as for the heave equation . Neglecting second order terms in s one gets :

$$(II-3.1)\left(I_{yy}+J_{yy}-\frac{m_{x\theta}^2}{m+m_{xx}}\right)\frac{d^2\theta}{dt^2}+N_{\theta\theta}\frac{d\theta}{dt}+mg\left[\iota+a+\frac{zG}{H}g(s)\right]$$

$$=2\,m\sigma\left[Q_1(k)+\frac{m_{x\theta}}{m+m_{xx}}Qo(k)+\frac{1}{2C_p}\cdot\frac{zG+zC}{H}s\right]\frac{d\zeta}{dt}$$

where the symbols introduced are defined in the nomenclature . The function g (s) is for all types :

$$(II-3.2)\qquad g(s)=\begin{cases}s & \text{if} \quad s\leqslant h_2\\ h_2 & \text{if} \quad s\geqslant h_2\end{cases}$$

with $h_2=\infty$ for the type 11 and 14 .

The coefficients of equation (II-3.1) are the same as n [1]

$$J_{yy}=m\,P_2$$
$$a=P_1$$
$$m_{x\theta}=-a.m$$
$$m_{xx}=m$$
$$r=\frac{\pi R^4}{4W}=o(R)$$
$$N_{\theta\theta}=\frac{1}{2}\rho^2 C_p^2 H^2\left[s(0)\right]^2 k^3 \sigma r\left[Q_1(k)\right]^2$$

IV - EQUATION OF ROLL MOTION -

The roll equation is obtained from the pitch equation by removing the forcing term located in the right hand side of the equation :

$$(II - 4.1)\quad \left(Ixx+Jxx - \frac{m_{y\varphi}^2}{m+m_{yy}}\right)\frac{d^2\varphi}{dt^2} + N_{\varphi\varphi}\frac{d\varphi}{dt} + mg\left[r+a+\frac{zG}{H}g(s)\right]\varphi = 0$$

$$\text{with} \quad J_{xx} = J_{yy} \quad \text{and} \quad N_{\varphi\varphi} = N_{\theta\theta}$$
$$m_{yy} = m_{x\theta} \quad \text{and} \quad m_{yy} = m_{xx}$$

Experiments have shown (cf. Section I) that the roll amplitude may be much higher than the pitch amplitude . This fact suggest the introduction in the equation (II-4. 1) of a new viscous damping term . This term is obtained using the Morison O'Brien equation which gives the force d F (z) acting on a strip of length dz for an infinite length cylinder in an unstationary flow [27]

$$d\,F(z) = \frac{\rho}{2} C_D . D \left|U(t)\right| . U(t) + C_M \rho \frac{\pi D^2}{4} \frac{d\,U(t)}{d\,t}$$

where D is the cylinder diameter , U (t) the velocity of the fluid relative to the cylinder , C_D and C_M are constants

The second term of this equation was already taken into account : the first one corresponds to a non-linear damping . Equation (II-4. 1) becomes

(II-4. 2)

$$\left(Ixx+Jxx - \frac{m_{y\varphi}^2}{m+m_{yy}}\right)\frac{d^2\varphi}{dt^2} + N_{\varphi\varphi}^{(1)}\frac{d\varphi}{dt} + N_{\varphi\varphi}^{(2)}\left|\frac{d\varphi}{dt}\right|\frac{d\varphi}{dt} + mg\left[r+a+\frac{zG}{H}g(s)\right]\varphi = 0$$

with $$N_{\varphi\varphi}^{(1)} = N_{\varphi\varphi}$$

$$N_{\varphi\varphi}^{(2)} = \frac{\rho}{2} C_D . D\left[\frac{z^4 G}{4} + \frac{(H - zG)^4}{4}\right]$$

with D = 2 R .

Equation (II-4.2) is only approximate for roll-sway coupling terms have not been taken into account (cf. previous paragraph for linear terms and Morison - O'Brien formula for non linear ones). Moreover Morison - O'Brien formula is only approximate . The coefficient C_D is actually time-dependent and the value to be attributed to this coefficient varies in a large range [6] . Lastly , the finiteness of the buoy slenderness (H/D) is not taken into account (end effects) .

One should note than equation (II-4.2) does not include the non linearity due to the static restoring moment $\Gamma(\varphi)$. In fact , the exact expression of $\Gamma(\varphi)$ is :

$$\Gamma(\varphi) = -mg\left[r + a + \frac{\pi R^4}{4(W-v)}\left(\frac{v}{W} + tg^2\varphi\right)\right]\sin\varphi$$

with

$$v = \frac{2}{3}R^3 \, tg\,\varphi$$

$$W = \frac{m}{\rho}$$

There is very little difference between this expression and

$$-mg\,(r + a)\sin\varphi$$

even for angles approaching $\varphi = 60°$ (relative variation is about 3 / 100) .

V - APPROXIMATE EQUATIONS FOR HEAVE-PITCH-ROLL MOTIONS -

Figures n° 11 , 12 , 13 relative to the frequency response of version n° 11 show that, in the linear case,the dynamic system associated to the buoy (in the sense of paragraph 1-6, 2) may be approximated by a second order differential system . This result suggests that we may substitute to equations (II-2. 3) , (II-3.1) and (II-4.2) the equations

(II-5.1)

$$(m+mzz)\frac{d^2Z}{dt^2} + N_{zz}^{(o)}\frac{dZ}{dt} + pg\,S(o)\left[Z + f(s)\right] = \rho g\,S(o)\left[1 - C_p kHQo(k)\right]\int(t)$$

(II-5.2)
$$\left(Iyy+Jyy-\frac{m^2 xe}{m+mxx}\right)\frac{d^2\theta}{dt^2} + N_{\theta\theta}^{(o)}\frac{d\theta}{dt} + mg\left[r+a+\frac{zG}{H}g(s)\right]\theta$$

$$= 2\,m\sigma\left[Q_1(k) + \frac{mxe}{m+mxx}Qo\,(k) + \frac{1}{2C_p}\frac{zG+z_c}{H}\right]\frac{df}{dt}$$

(II-5.3)
$$\left(Ixx+Jxx-\frac{m_y^2\varphi}{m+myy}\right)\frac{d^2\varphi}{dt^2} + N_{\varphi\varphi}^{(o)}\frac{d\varphi}{dt} + N_{\varphi\varphi}^{(2)}\left|\frac{d\varphi}{dt}\right|\frac{d\varphi}{dt} + mg\left[r+a+\frac{zG}{H}g(s)\right]\varphi = 0$$

where the coefficients in the left hand sides of the equations are constants and where f (s) and g (s) are given by (II-2.2) and (II-3.2).

In the sequel this particular form of the equations will be used .

VI - EXPLANATION OF THE DOUBLE REGIME IN THE HEAVING MOTION -

The presence of double regimes in a rolling motion has already been investigated by various authors . The experimental finding of this phenomenon was made by E.G.Barillon who explained it by considering a non linear damping proportional to φ_A^r $(r \geq 2)$, a forcing moment proportional to φ_A^m $(m < 1)$ and a restoring moment in the form $\Gamma(\varphi) = -A\varphi - B\varphi^3$ (A and B are constant) [7] . The rigorous mathematical explanation of the phenomenon was given by R. Brard , starting from equation of the form :

(II-6.1)
$$\frac{d^2\varphi}{dt^2} + \beta\, g\left(\frac{d\varphi}{dt}\right) + h\,(\varphi) = F\cos\sigma t$$

where β is a constant , and g (.) and h (.) are analytical functions [8] , but numerous approximative methods exist [9] , [10] .

The double regime in the heaving motion of the buoy is an analogous phenomenon , which can be explained at least qualitatively by equation (II-5.3) . Taking s (t) as the unknown in this equation , it becomes :

$$(m+mzz)\frac{d^2s}{dt^2} + Nzz^{(o)}\frac{ds}{dt} + \rho g\, S\,(o)\, F\,(s)$$

$$= \left[(m+mzz)\sigma^2 - \rho g\, S(o)\, C_p\, k\, H\, Qo\,(k)\right]f_A\cos\sigma t + \sigma Nzz\, f_A \sin\sigma t$$

$$\text{where } F(s) = \triangleq \begin{cases} s & \text{if } s \leq 0 \\ s - \dfrac{s^2}{2h_2} & \text{if } 0 \leq s \leq h_2 \\ \dfrac{h_2}{2} & \text{if } s \geq h_2 \end{cases}$$

Let us assume that the wave amplitude be sufficiently small so that $s \leq h_2$ always . It is then possible to determine the expression relating half the amplitude s_A of s (t) to half the amplitude $\mathcal{S}_A$ of the wave by means of the optimum linear operators theory [11] . For the type 1 buoy , one obtains :

$$\text{(II-6.3)} \quad \frac{s_A}{\mathcal{S}_A} = \frac{\sqrt{\left[(m+m_{zz})\,\sigma^2 - \rho g\, S(o)\, C_p\, k\, H\, Qo\,(k)\right]^2 + \sigma^2 N_{zz}^{(o)2}}}{\sqrt{\left[\rho g\, S(o) - \sigma^2 (m+mzz) - \frac{2}{3\pi h_2} \rho g\, S(o)\, s_A\right]^2 + \sigma^2 N_{zz}^{(o)2}}}$$

For the type 12 buoy one has

$$F(s) = \triangleq \begin{cases} s & \text{if } s \leq h \\ s - \dfrac{(s-h_1)^2}{(h_2-h_1)} + \dfrac{(s-h_1)^3}{3(h_2-h_1)^2} & \text{if } h_1 \leq s \leq h_2 \\ \dfrac{h_2 + 2h_1}{3} & \text{if } s \geq h_2 \end{cases}$$

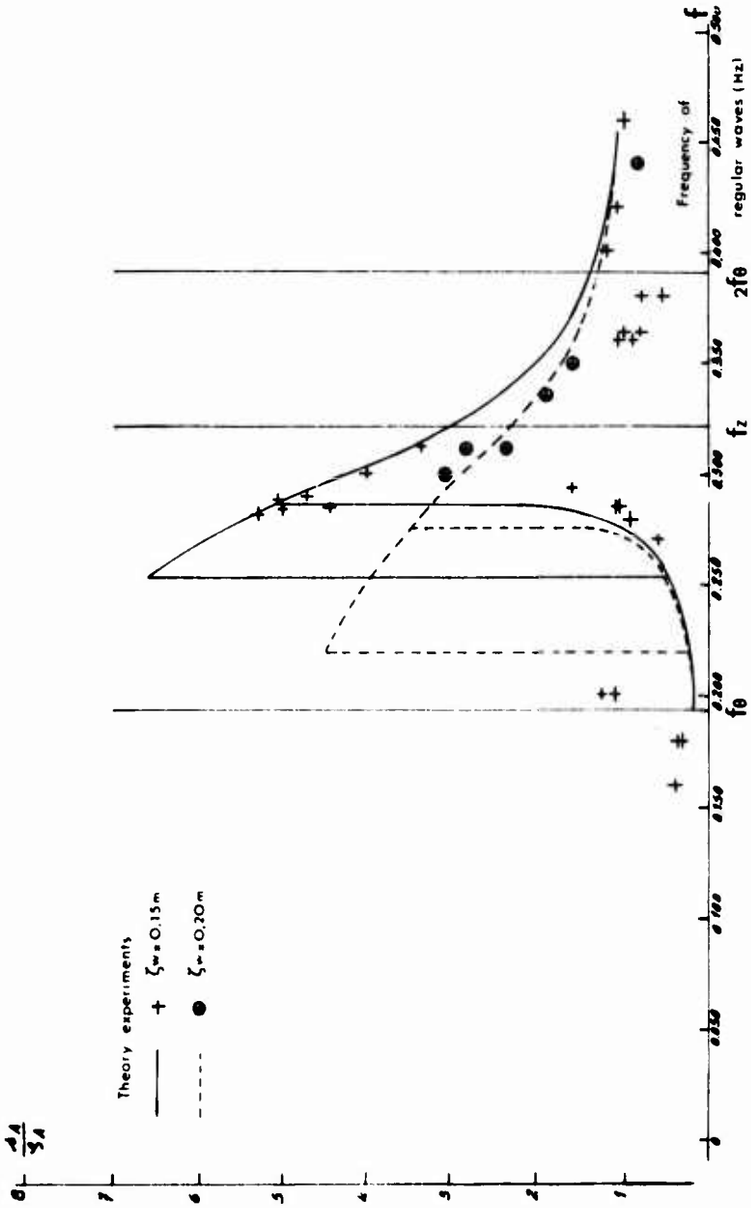


FIGURE 17 - RELATIVE MOTION RESPONSE : COMPARISON THEORY - EXPERIMENTS FOR TYPE 1 BUOY

and if it is assumed that $h_1 \simeq 0$, then

(II-6.4)

$$\frac{\mathcal{A}_A}{f_A} = \frac{\sqrt{\left[(m+mzz)\sigma^2 - \rho g\, S(o)\, C_p\, k\, HQo\,(k) \right]^2 + \sigma^2\, N_{zz}^{(o)2}}}{\sqrt{\left[\rho g\, S(o) - \sigma^2 (m+mzz) + \rho g\, S(o) \left[\frac{1}{8 h_2^2} s_A^2 - \frac{4}{3\pi h_2} s_A \right] \right]^2 + \sigma^2\, 2N_{zz}^{(o)2}}}$$

TYPE 1 BUOY -

From equation (II-6.3) it is easy to see that for a given frequency and a given wave amplitude , there exist one or three positive roots s_A . By a method identical to that used in the following paragraph , it can be verified that when there are 3 roots , one of them is unstable . This explains the jump and hysteresis phenomena observed when solving equation (II-6.2) on an analog computer . Figure 17 presents the gain curve obtained ($\frac{\mathcal{A}_A}{f_A}$ versus f) , and shows a good agreement with experiment .

TYPE 12 BUOY -

Equation (II-6.4) is of degree 6 in s_A . It has therefore six roots but it is difficult to see whether they are real positive . Rather than solving directly this equation on an analog computer , we solved it graphically , which permits to understand better the jump in the gain curve of the relative motion (Figure 15) .

The notations and terminology of [11] are used here, and it is assumed that the wave amplitude is small enough for s (t) to be always less than h_2 . In order to simplify the computations it is also assumed that $h_1 = 0$. In fact $h_1 = 0.08$ m and $h_2 = 0.42$ m . Setting h_1 to zero will thus slightly modify the results . However the general shape of the phenomena will be kept . The describing func - tion of equation (II-6.2) is

$$H(i\sigma, a) = \rho g\, S(o) \left[1 - \frac{4a}{3\pi h_2} + \frac{a^2}{8 h_2^2} \right] - \sigma^2 (m+mzz) - i\, \sigma\, N_{zz}^{(o)}$$

where it has been set $a \triangleq s_A$ for a while .

The characteristic equation of (II-5.2) reads

$$A\ (a\ ,\ \sigma\ )\ \lambda^{2}\ +\ B\ (a\ ,\ \sigma\ )\ \lambda\ +\ C\ (a,\sigma\ )\ =\ 0$$

where

$$A\ (\ a,\ \sigma\ )\ \triangleq\ 4\ a\ \sigma^{2}\ (m+mzz\ )^{2}\ +\ a\ N^{(o)2}_{zz}$$

$$B\ (a\ ,\ \sigma\ )\triangleq N^{(o)}_{zz}\ \left[\ \rho g\ S(o)\ (2a-\frac{4\ a^{2}}{\pi h_{2}}+\frac{a^{3}}{2h_{2}^{2}})\ +2a\sigma^{2}\ (m+m_{zz})\right]$$

$$C\ (a,\ \sigma)\triangleq a\sigma^{2}N^{(o)2}_{zz}+\ \left[\rho g\ S(o)(a-\frac{4\ a^{2}}{3\pi h_{2}}+\frac{a^{3}}{8h_{2}^{2}})\ -a\sigma^{2}(m+m_{zz}\ )\right]\cdot$$

$$\cdot\left[\ \rho g\ S(o)\left(\ 1-\frac{8a}{3\pi h_{2}}\ +\frac{3a^{2}}{8\ h_{2}^{2}}\right)-\sigma^{2}(m+m_{zz})\right]$$

For a given frequency and a given value of a , the quantity a H (i σ , a) defines a point in the Nyquist plane . When a varies , this point describes a curve called an equifrequency curve . The solutions of equation (II-6.2) are obtained as the intersections of this equifrequency curve and a circle centered at the origin and of radius equal to the numerator of expression (II-6.4) times $\int_{A}$ (This construction is but the geometric interpretation of equation II-6.4) . These solutions are stable if the real parts of the roots of the characteristic equation are negative , they are unstable otherwise.

When the wave frequency is small , equation (II-6.2) has only one solution (Figure 18) . For a slightly larger frequency , equation (II-6.2) has two stable solutions and one unstable solution (figure 19) . Only the smallest solution has been obtained experimentally , because during the experiments we did not attempt to see if a second stable motion was possible . When the frequency is 0.182 Hz there are only two solutions both stable (Figure 20) . Figure 21 clearly shows the jump phenomenon . Beyond f = 0.182 , there is only one stable solution (Figure 22) .

From the quantitative point of view , Figures 18 to 22 lead to solutions slightly different from the experimental results . In particular ; the jump phenomenon occurs for f = 0.182 Hz instead of f = 0.190 Hz . It is believed that this discrepancy is due to the

difference between the real value of h_1 ($h_1 = 0.08$ m) and the value actually used in the computations ($h_1 = 0$).

From figures 18 to 22 , it is easy to determine the influence of wave on the value of $a = s_A$. The equifrequency curves are indeed independent from the waves amplitude , and the circle radius is proportional to it . One can see , for example , that for $f = 0.182$ Hz the curve gain VS half-wave-amplitude must exhibit a jump at $\mathcal{S}_A = 0.128$ m .

In conclusion to this investigation of the double regimes , figures 23 and 24 show the effect of h_2 and $\mathcal{S}_A$ on the shape of gain curves computed for the type 1 buoy .

If we turn back to figure 15 we see that the above theory does not explain the double regime in relative motion in the vicinity of $f = 2 f_\theta$. One reason for this discrepancy is that we have assumed that $\mathcal{S}(t) \leq h_2$ (see beginning of this paragraph) . No attempt has been made at explaining the double regime in the vicinity of $f = 2 f_\theta$ by discarding this hypothesis .

VII - EXPLANATION OF ROLLING IN REGULAR WAVES -

It has been known for many years that a ship moving in longitudinal regular waves can perform rolling motions of large amplitude [12] . In 1955 , Kerwin [13] explained the motion by the periodic variation of the restoring moment in rolling due to the on-coming waves . The roll appears as an unstable solution of a Mathieu equation . In 1959 , Paulling and Rosenberg [14] have shown that instabilities in the ship motion could be explained by the effect of second order coupling terms in the equations of motion (see also [15] and [16]). This latter work was pursued by M.R. Haddara for the case of a ship in oblique regular waves [17]

In the case of a spar buoy , Kervin's approach does not apply , since the wave length is considered as large as compared to the buoy diameter . However , the rolli ₒ motion can be explained by the presence of a non linear coupling term between heaving and rol - ling (equation II- 3. 3) .

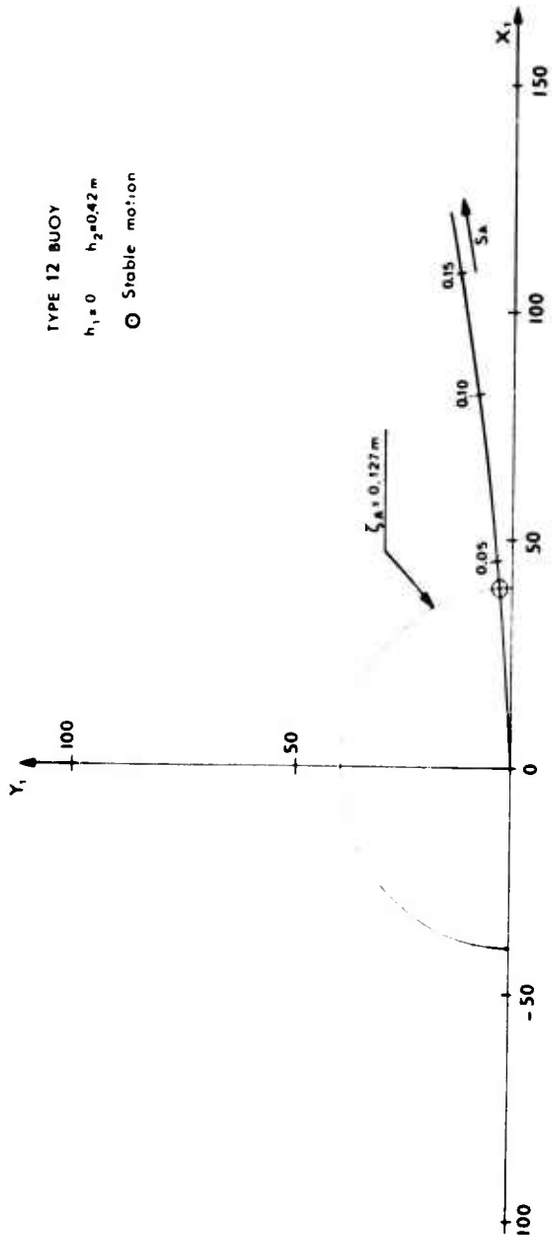


FIGURE 18 - EQUIFREQUENCY CURVE ($f = 0.160$ Hz)

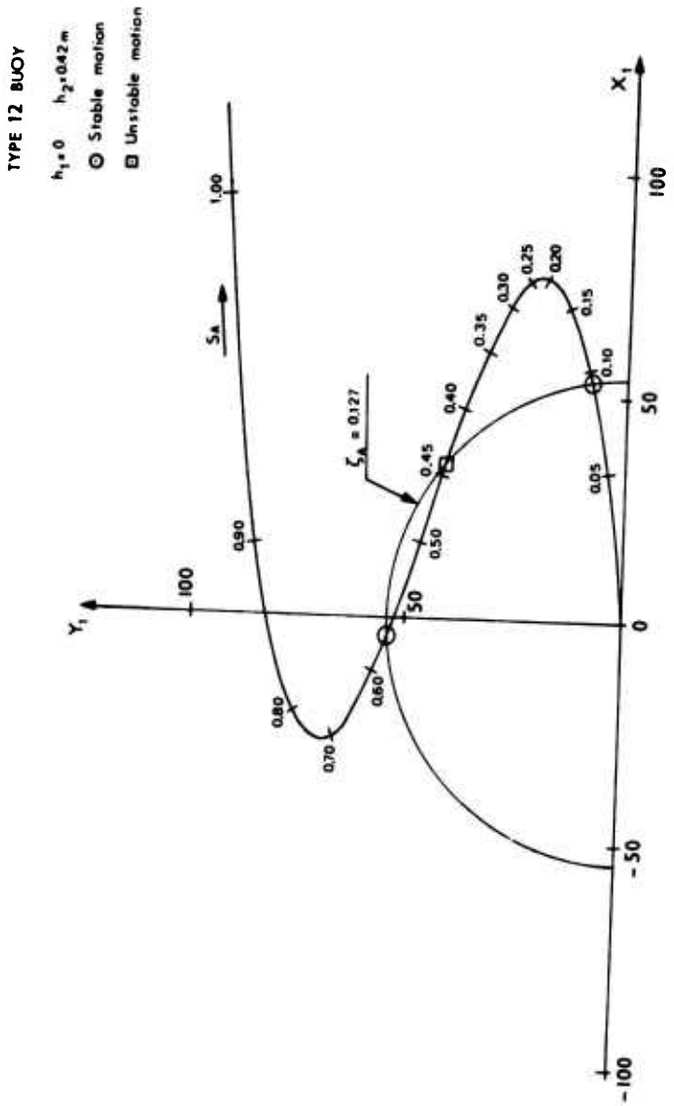


FIGURE 19- EQUIFREQUENCY CURVE (f= 0.176 Hz)

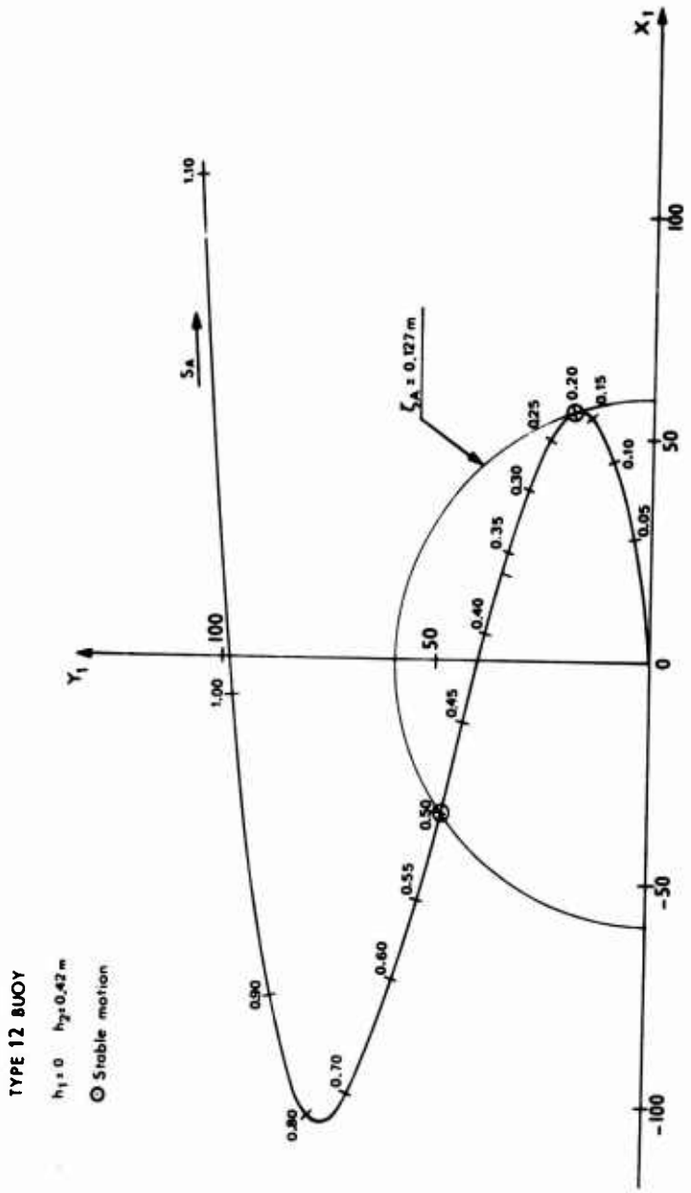


FIGURE 20 – EQUIFREQUENCY CURVE ($f = 0.182$ Hz)

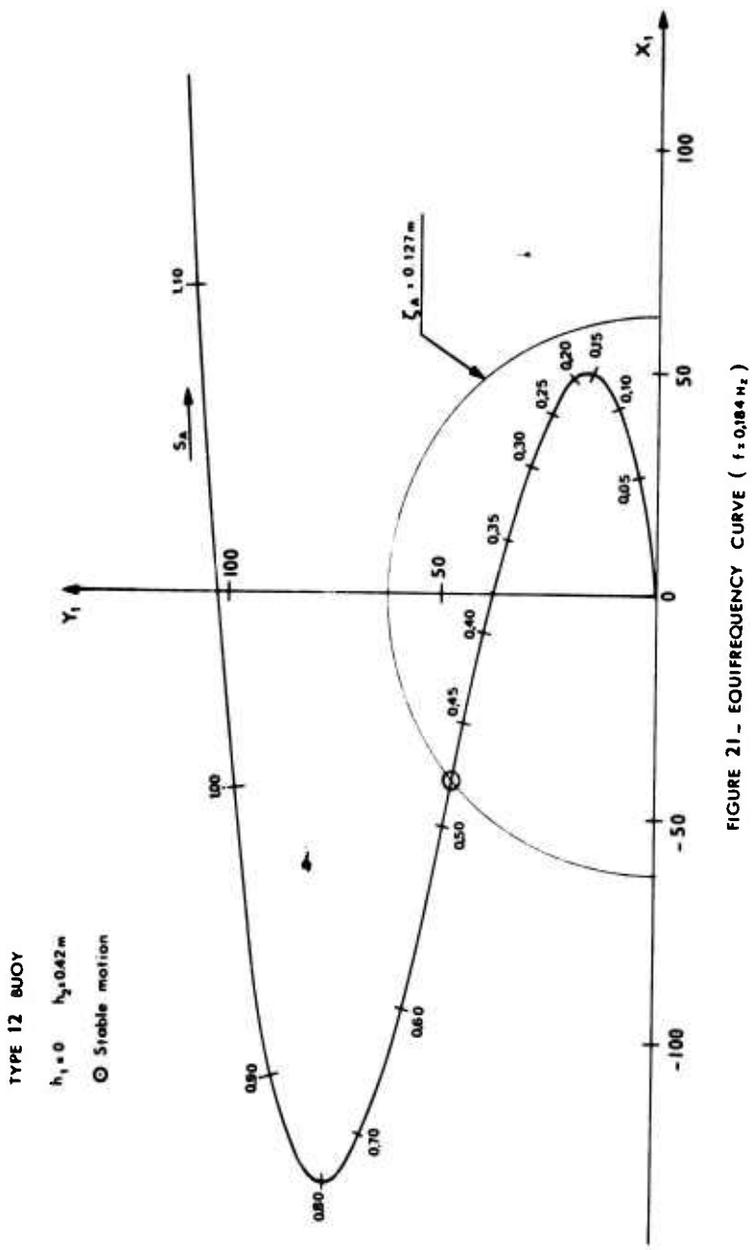


FIGURE 21 - EQUIFREQUENCY CURVE (f = 0.184 Hz)

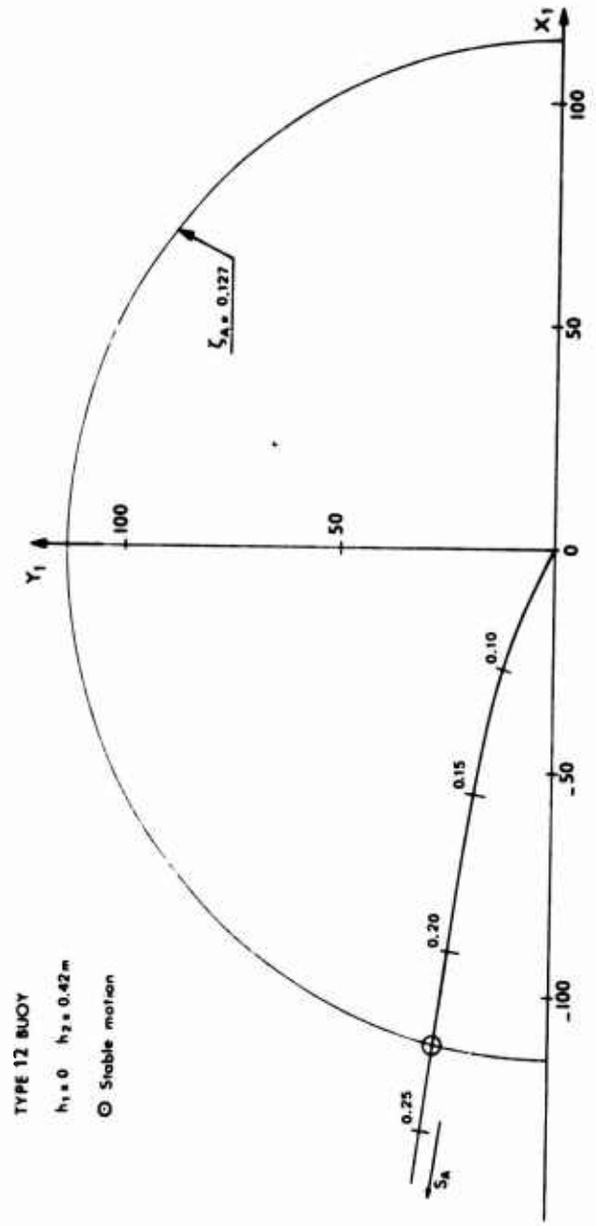


FIGURE 22 - EQUIFREQUENCY CURVE ($f = 0.220$ H_z)

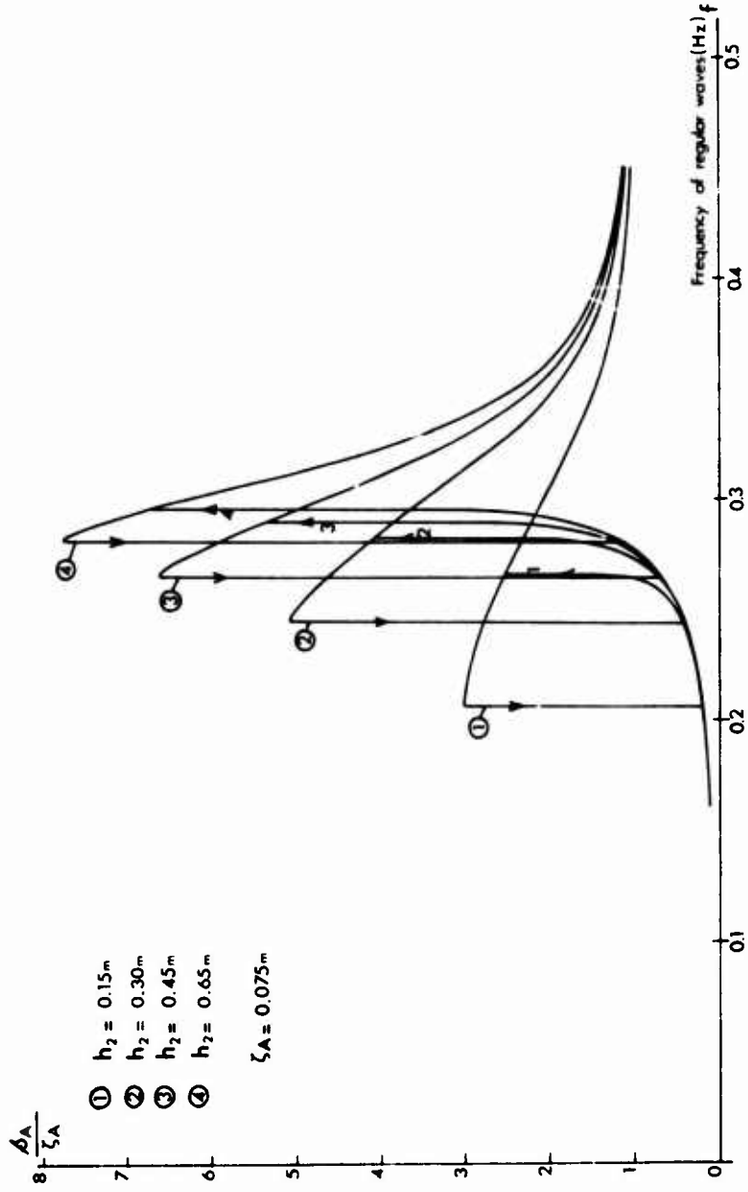


Figure 23 – Effect of the value of h_2 on the shape of the calculated gain curves (β_A/ζ_A)

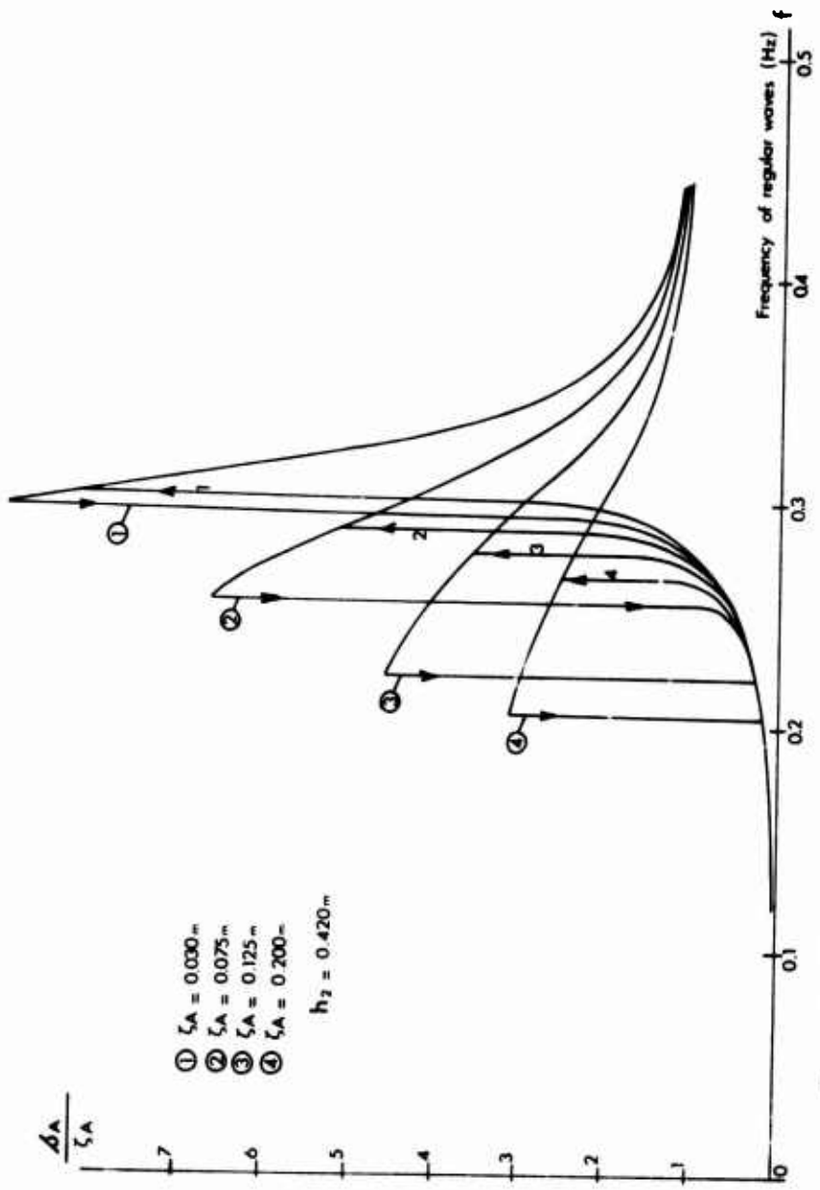


Figure 24 – Effect of the value of ζ_A on the shape of the calculated gain curves (β_A/ζ_A)

If it is assumed that $N^{(2)}_{\varphi\varphi} = 0$, equation (II-5.3) becomes

$$\frac{d^2\varphi}{dt^2} + \beta \frac{d\varphi}{dt} + \left[\gamma - 2\,\delta g \left[s(t) \right] \right] \varphi = 0$$

(II-7.1)

$$\beta \triangleq \frac{N^{(0)}_{\varphi\varphi}}{Ixx + Jxx - \frac{m^2 y\varphi}{m + myy}}$$

$$\gamma \triangleq \frac{mg\,(r + a)}{Ixx + Jxx - \frac{m^2 y\varphi}{m+myy}} \simeq 4\pi^2 f_\theta^2$$

$$\delta \triangleq -\frac{1}{2}\,\frac{z\,G}{H}\,\frac{mg}{Ixx + Jxx - \frac{m^2 y\varphi}{m+myy}}$$

s (t) is given by equation (II-5.1) with s (t) = Z (t) - ζ (t)

Let us assume now that s (t) is a sinusoidal function . This assumption is rigorously verified for the type 11 and 14 buoys., since equation (II-5.1) is then linear . It is only an approximation for the type 1 and 15 buoys , since equation (II-5.1) is then non linear Furthermore , let us assume that s (t) does not take too large a value , so that

$$s\,(t) = s_A \cos \sigma t \leqslant h_2$$

Equation (II-7.1) can then be written as :

$$\frac{d^2y}{dx^2} + (p - 2q \cos 2x)\, y = 0$$

$$y \triangleq e^{\frac{\beta}{2}t}\, \varphi(t)$$

$$x \triangleq \frac{1}{2}\,\sigma\, t$$

$$p \triangleq \frac{4}{\sigma^2}\left(\gamma - \frac{\beta^2}{4}\right) \simeq \frac{4\gamma}{\sigma^2} = 4\,\frac{f_\theta^2}{f^2}$$

$$q \triangleq \frac{\delta s_A}{\pi^2 f^2}$$

Equation (II-7.2) is a Mathieu equation [18] . Its stability chart is recalled in Figure 25 . The values of β , δ and $\flat$ for the buoys type 1 , 11 , 14 and 15 are given in the following table .

Type n°	β	δ	$\flat$	$f_p = f_\theta$
1	0.0667	1.792	-2.867	0.216
11	0.139	1.518	-0.595	0.190
14	0.0800	0.797	-0.639	0.142
15	0.136	1.145	-2.312	0.170

Except for type 11 and 15 , the values of β are quite small , and the stability map of equation (II- 7.2) is thus as a first approximation the stability map of equation (II- 7.1) .

The experimental points obtained for buoys type 1 and 14 are shown on figure 25 , where it can be seen that they agree rather well with the theory .

When the wave height stays constant and that the frequency varies , the point of coordinates (p , q) moves in the stability plane (p - q plane) : when f increases , δ decreases and the point moves to the left . To have an idea of the phenomenon let us replace the curves (a_1) and (b_1) by their tangent at the origin . Instability occur when :

$$q^2 - (p-1)^2 \geq 0$$

i.e. when

$$\sqrt{4 f_\theta^2 + \frac{\delta s_A}{\pi^2}} \leq f \leq \sqrt{4 f_\theta^2 - \frac{\delta s_A}{\pi^2}}$$

In particular for the types 1 and 14 , the experimental values of the relative motion s_A are small in the vicinity of $2 f_\theta$. Therefore there will not be any roll if the frequency is larger than $2 f_\theta$.

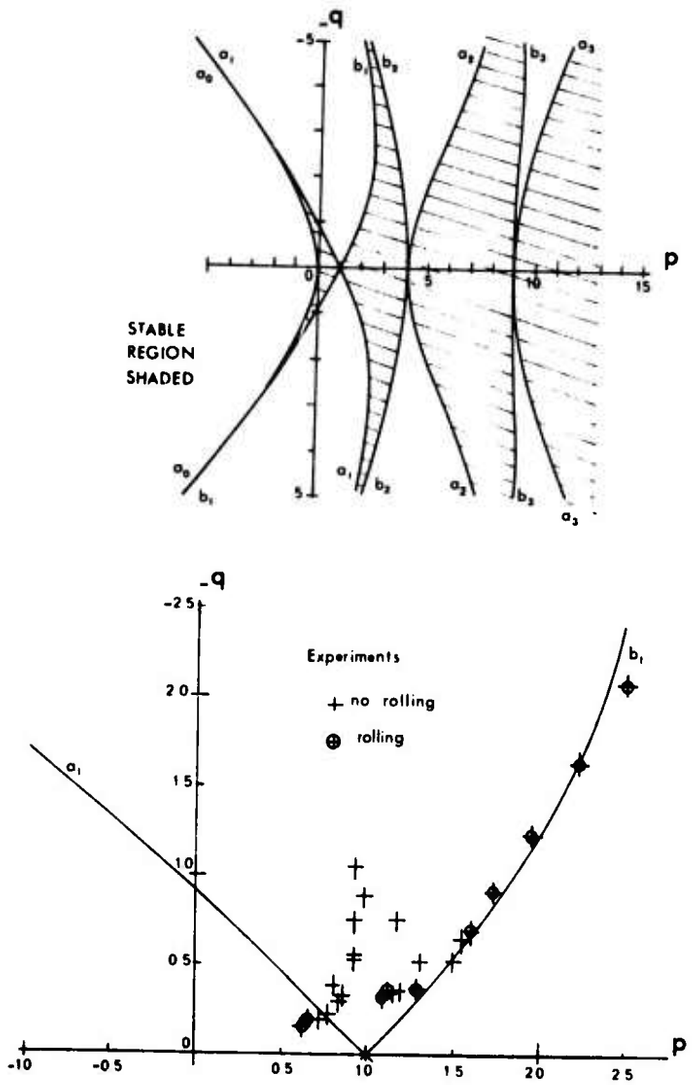


FIGURE 25 - STABILITY PLANE

When the wave height varies while the frequency remains constant the point (p, q) moves along a line parallel to Oq . Thus , when $p \neq 1$, there will be no roll if the wave height is sufficiently small .

The exact solution of equation (II-5. 3) , taking into account equation (II-5. 1) , has been performed on an analog compu - ter . The results are given in Figures 26 and 27 for the type 1 buoy , and in figures 28 and 29 for type 14 . In figures 27 and 29 , the non linear damping term has been taken into account . The coefficient $N^{(2)}_{\varphi\varphi}$ was obtained by trial and error , and such that the theoretical curve be as close as possible to the experimental points . Unfortunately, the value of $N^{(2)}_{pp}$ so obtained corresponds to a value of the coefficient C_D too large for the type 1 buoy and too small for type 14 . The coefficient $N^{(2)}_{pp}$ was set equal to zero in figures 26 and 28 for it was not possible to fall back on the experimental points (figures 7 and 8). In particular in the case of buoy type 14 , the curve is a parabola but with a downward concavity as in Kerwin's work .

It seems therefore that our theory is unsufficient for the prediction of the roll angle . This disagreement may be partly due to the damping coefficient $N^{(1)}_{pp}$ actually varying with frequency , while it was assumed (equation II-5. 3) to be constant ($N^{(1)}_{pp} \equiv N^{(0)}_{pp}$). For example for the type 14 buoy , $N^{(1)}_{pp}$ varies from 1 for $f = f_\varphi$ to 127 for $f = 2 f_\varphi$.

Conditions for cancelling roll in regular waves -

We have shown that rolling occurs when

$$\text{(II-7. 3)} \qquad \sqrt{4 f_\theta^2 + \frac{\delta s_A}{\pi^2}} \leq f \leq \sqrt{4 f_\theta^2 - \frac{\delta s_A}{\pi^2}}$$

Therefore , there is no rolling if and only if

$$\frac{\delta s_A}{\pi^2} \equiv 0$$

which is impossible except for vanishing values of ρ_A . In fact it is necessary to take into account the damping term in pitching . We establish now an approximate condition for no rolling . First we recall that instability occurs in the vicinity of $f = 2 f_\theta$ when ρ_A is small (see II-7. 3) . Then $p \simeq 1$ and $q \simeq \frac{\delta \sigma_A}{4\pi^2 f_\theta^2} = \frac{\delta \sigma_A}{\gamma}$. Unstable solutions of (II-7. 2) grow exponentially as $e^{\frac{\sigma}{2} t}$. Hence, there is

no rolling if and only if $q < \beta$ or

$$s_A < \frac{\beta \gamma}{6}$$

We assume now that the natural frequency for heaving f_θ^z is not too large as compared to the natural frequency for pitching f_θ so that

$$2 f_\theta \gg f_z$$

Then $s_A \simeq \int_A$ for $f = 2 f_\theta$ and the condition for no rolling reads :

(II-7.4) $$\int_A < \frac{\beta \gamma}{6}$$

or

(II-7.5) $$\int_A < 2 H \beta \left(1 - \frac{zc}{zg}\right)$$

Unfortunately β is not theoretically known since $N^{(\omega)}_{\varphi\varphi}$ is determined experimentally . Nevertheless for a given value of $\int_A$, (II-7.5) shows that there is no rolling if the center of gravity is located well below the center of buoyancy .

VIII - EXPLANATION OF THE UNSTABLE PITCHING PHENOMENON -

The unstable pitching observed with the type 1 buoy can be explained qualitatively in the same manner as for rolling , by reducing the problem to an equation where the left member is a Mathieu equation . However there now exists a right member which is a sinusoidal function of same frequency as the perturbation term in the left member . It is known [19] that the regions of stability and unstability are the same as for the equation without a right member . The qualitative results established in paragraph VII are thus valid . Figure 28 shows that the theoretical domain of instability does coincide with the domain of instability determined experimentally .

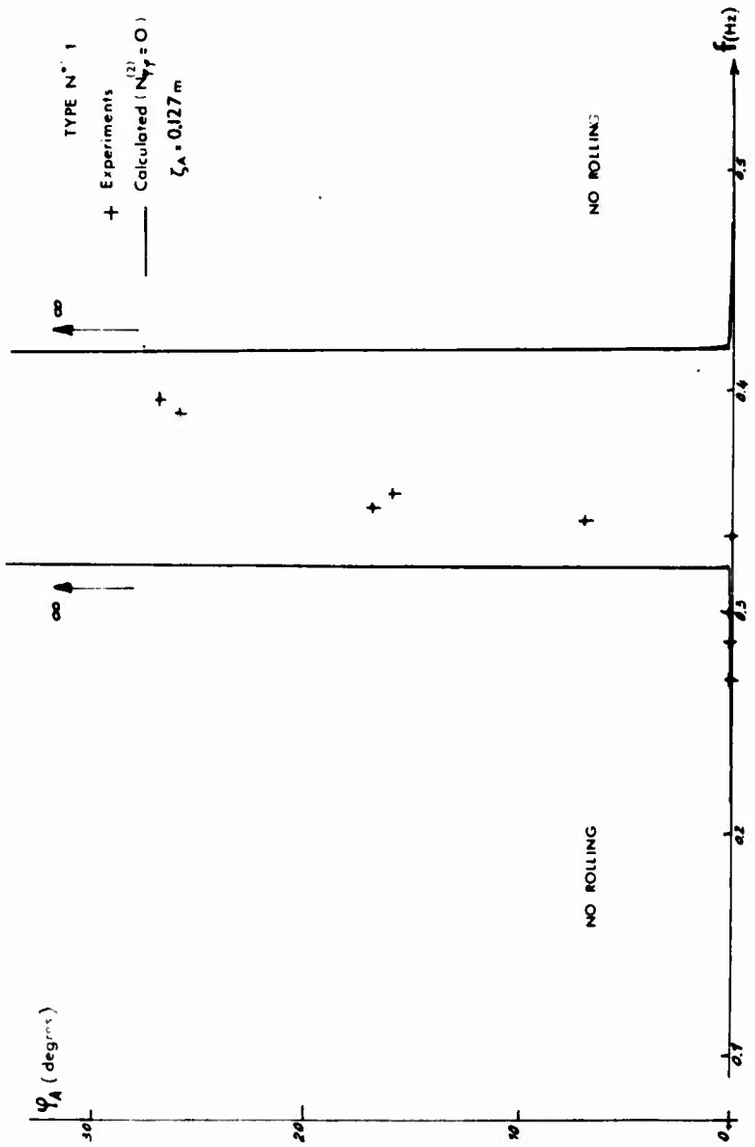


FIGURE 26_ HALF AMPLITUDE OF ROLLING VS FREQUENCY OF REGULAR WAVES

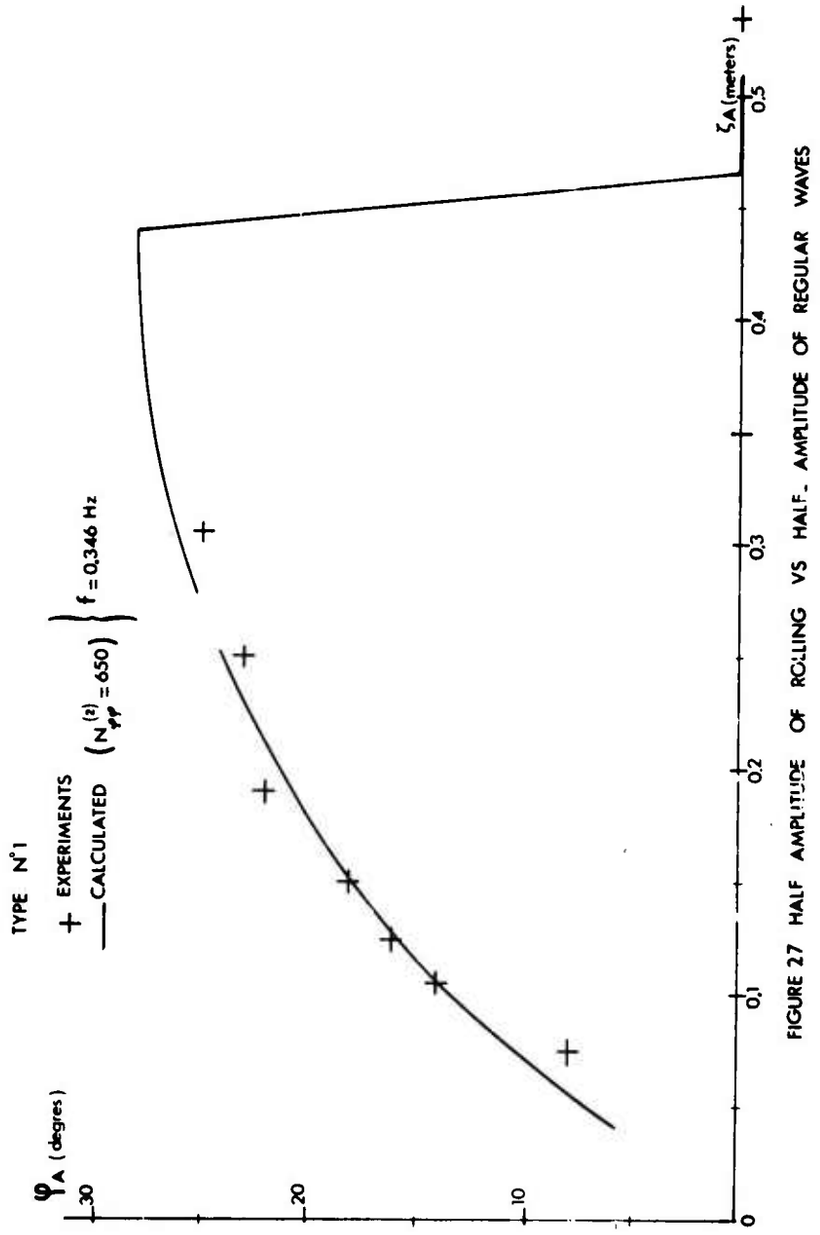


FIGURE 27 HALF AMPLITUDE OF ROLLING VS HALF- AMPLITUDE OF REGULAR WAVES

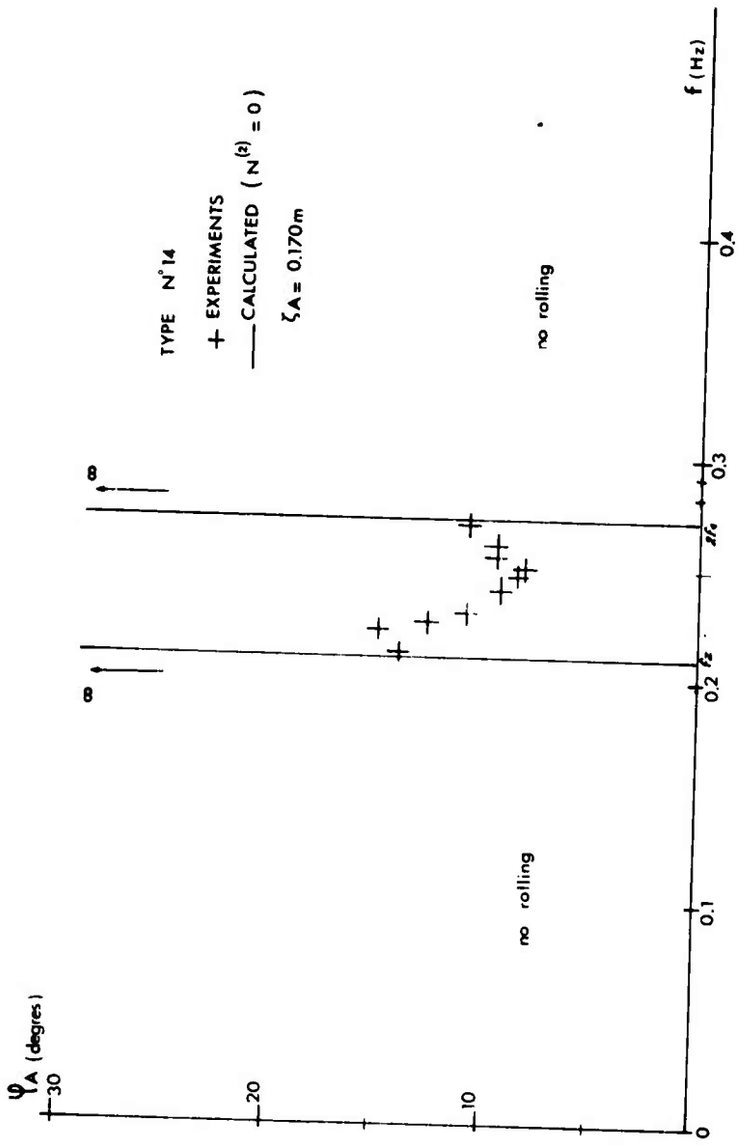


FIGURE 28 HALF AMPLITUDE OF ROLLING VS FREQUENCY OF REGULAR WAVES

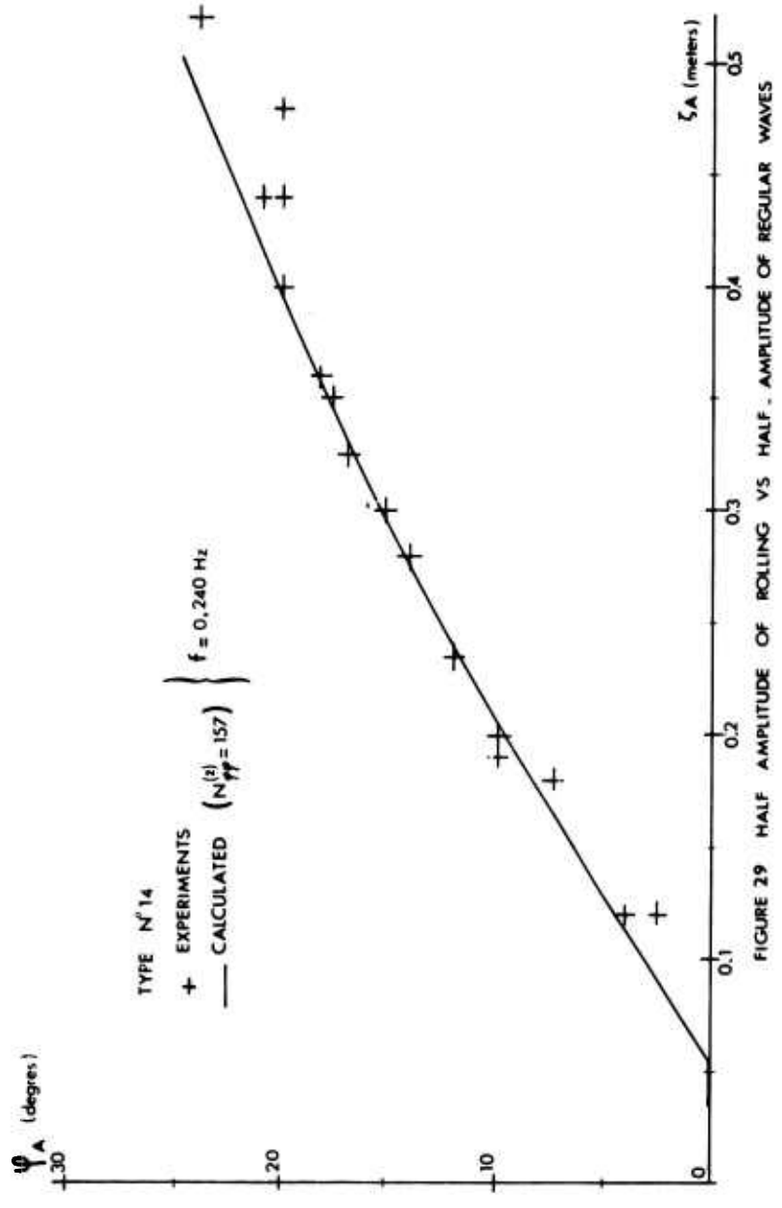


FIGURE 29 HALF AMPLITUDE OF ROLLING VS HALF - AMPLITUDE OF REGULAR WAVES

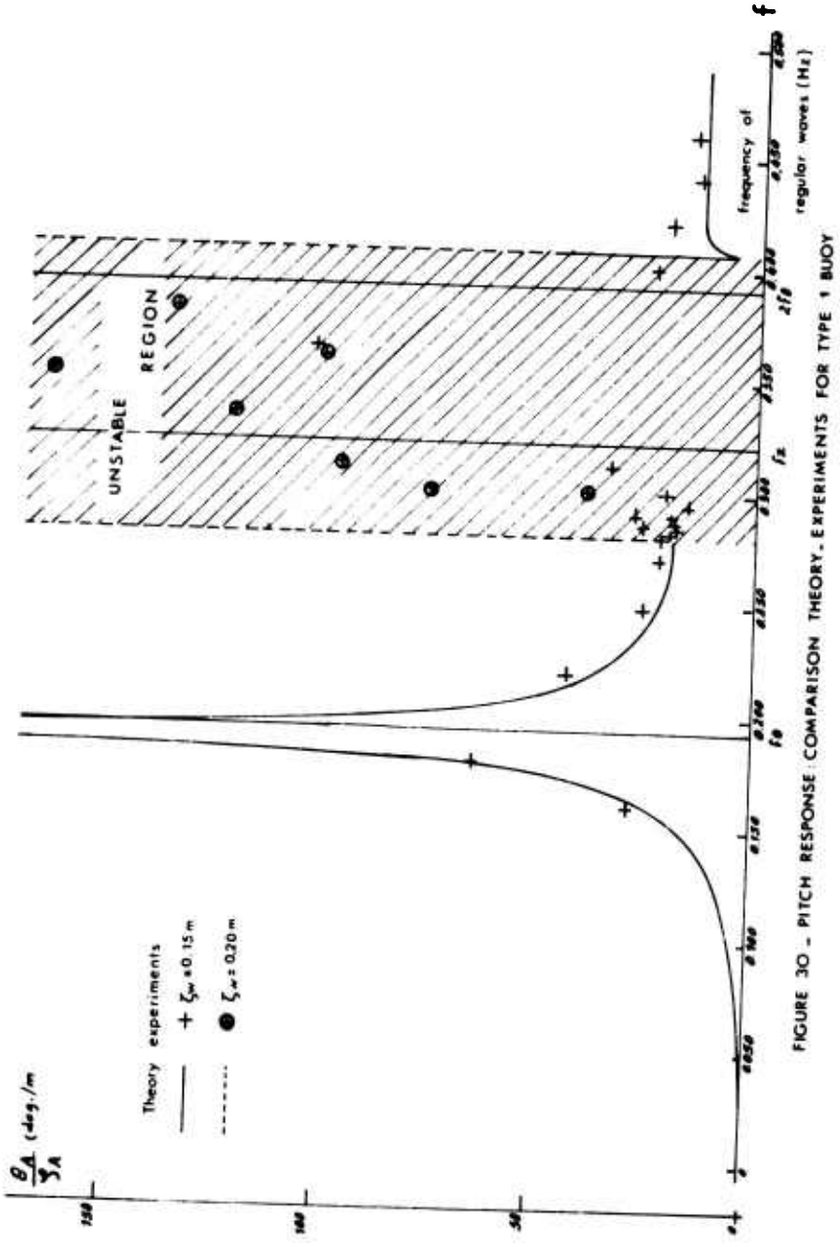


FIGURE 30 - PITCH RESPONSE: COMPARISON THEORY - EXPERIMENTS FOR TYPE 1 BUOY

SECTION III

ROLL BEHAVIOUR OF A SPAR BUOY IN MONODIRECTIONAL IRREGULAR WAVES

I - INTRODUCTION

It seems that no paper has been published to-date on the rolling motion of bodies in monodirectional irregular waves . At least the author has been unable to locate any . One may quote Kastner's study [20] about the righting arm of a ship in a longitudinal irregular sea . In a sense , his study is a continuation of Kerwin's theory but it does not deal with the effect of the irregular variations of the righting arm on the rolling motion of the ship .

From a mathematical point of view , the problem of the rolling motion of a spar buoy is similar to various other problems of mechanics (for example : simply supported beam subjected to stochastic axial load ; vibrating string when the distance between its ends varies stochastically) . All these problems are related to the study of non-autonomous stochastic dynamical systems . Many results exist for these systems but the most interesting one seems to be that of G. F. Carrier [21] . In the present Section , the rolling motion of the spar buoy is studied by using Carrier's theorem whose statement will be given in the next paragraph . The validity of rol - ling criterion is verified experimentally .

II - HYPOTHESES FOR CALCULUS -

In this Section we use equations (II -5.1) and (II -5.3) with the following simplifications :

$$N^{(2)}_{\varphi\varphi} = 0$$

$$h_2 = \infty$$

The approximation $h_2 = \infty$ is valid only for type 11 and 14 buoys . For type 1 and 15 buoys , this assumption is very coarse but it avoids intricate computations . We must recall that $N^{(0)}_{\varphi\varphi}$ is experimentally determined (damping tests) .

We assume that the wave elevation ζ (t) is a normal , strictly stationary random function . We also assume that the sea is monodirectional and that its spectral density is given by the modified Pierson-Moskowitz formula [22], namely .

$$S_{\zeta\zeta}(f) = 0,11 \cdot H_v^2 \; T_v \; (T_v f)^{-5} \exp\left[-0,44\,(Tvf)^{-4}\right]$$

It follows that signal s (t) is also gaussian and strictly stationary .

III - ROLLING CRITERION -

With the above hypothesis the rolling motion equation takes the form (see paragraph 7 of section II)

$$(III\text{-}3.1) \quad \frac{d^2\varphi}{dt^2} + \beta \frac{d\varphi}{dt} + \left[\gamma - 2\delta s(t)\right]\varphi = 0$$

Now the coefficient of φ is no longer harmonic but varies stochastically . For any given initial conditions which are deterministic for example $\varphi_1 = \varphi_0$ and $\left(\frac{d\varphi}{dt}\right)_1 = 0$) we make now the assumption that the buoy is rolling if and only if equation (III-3.1) is unstable in the mean square . By definition , equation (III-3.1) is stable in the mean square if , for any φ_0 :

$$\langle \varphi^2 \; (t) \rangle \to 0 \text{ when } t \to +\infty$$

where $\langle \cdot \rangle$ denotes ensemble average .

Now equation (III-3.1) may be written as

$$(III\text{-}3.2) \quad \frac{d^2\varphi_1}{dt_1^2} + \left[1 + s_1(t_1)\right]\varphi_1(t_1) = 0$$

where $\varphi_1(t) \triangleq e^{\frac{\beta}{2}t}\,\varphi(t)$

../..

(III-3.3) -

$$t_1 \triangleq \sqrt{\gamma - \frac{\beta^2}{4}} \cdot t$$

$$s_1(t) \triangleq -\frac{2\delta}{\sqrt{\gamma - \frac{\beta^2}{4}}} s(t)$$

Equation (III-3.2) has been studied by G. F. Carrier [21] who has given an expression for $\langle \varphi_1^2 (t_1) \rangle$ which is valid under certain conditions (see also Keller [23]). Carrier's expression and relations (III-3.3) permit us to give the expression of $\langle \varphi^2 (t) \rangle$ by the following assertion :

Assertion - If , in equation (III-3.1) , the coefficients β , γ , δ are constants and if s (t) is a gaussian white noise , then , the asymptotic expression for $\langle \varphi^2 (t) \rangle$ is

$$\langle \varphi^2 (t) \rangle \sim \exp \left\{ -\frac{t}{2} \left[2\beta - \frac{\delta^2}{\gamma - \frac{\beta^2}{4}} S_{ss} (2 f_\varphi) \right] \right\}$$

where $S_{ss}(f)$ is the spectral density of s (t) and $f_\varphi \triangleq \frac{1}{2\pi} \sqrt{\gamma - \frac{\beta^2}{4}}$

We note that Carrier's theorem is obtained by setting $\beta = 0$.

When s (t) is not a gaussian white noise this asymptotic expression does not hold any longer . Nevertheless , Carrier has shown that this formula is a good approximation in the following cases :

a/ $s(t) = s_A \cos (4\pi f_\varphi t + \varepsilon)$ where ε is a random variable distributed uniformly over the interval $(0, 2\pi)$

b/ s (t) is a gaussian process with an auto-correlation function given by

$$R(\tau) = 2 k e^{-k|\tau|} \quad (k > 0)$$

For lack of results concerning the case when s(t) is a gaussian process with any autocorrelation function we use the asymptotic expression given by the assertion . This expression permit us to give the stability criterion of equation (III-3.1)

(III-3.1)
$$S_{ss}(2f\varphi) < \frac{2\beta\left(\gamma - \frac{\beta^2}{4}\right)}{\delta^2}$$

For all types $\frac{\beta^2}{4} << \gamma$, hence

(III-3.4)
$$S_{ss}(2f\varphi) < \frac{2\beta\gamma}{\delta^2}$$

This stability criterion may be written in another form by the following transformations :

$$S'_{ff}(f) \triangleq \frac{S_{ff}(f)}{H_v^2} = \text{indep . of } H_v$$

$H_{sf}(2\pi if)$ = transfer function of relative motion

$$S_{ss}(f) = \left|H_{sf}(2\pi if)\right|^2 S_{ff}(f)$$

$$S'_{ss}(f) \triangleq \frac{S_{ss}(f)}{H_v^2} = \text{indep.}$$

(III-3.4) becomes

(III-3.5)
$$H_v < K_z(Tv, f\varphi) \cdot \frac{1}{\left(\frac{zG}{H}\right)} \cdot \sqrt{\frac{2(r+a)\,N\varphi\varphi(o)}{mg}}$$

$$K_z(Tv, f\varphi) \quad \frac{2}{\sqrt{S'ss(2f\varphi)}}$$

$K_s(T_v, f\varphi)$ depends on T_v , $f\varphi$ and on the heave characteristics of the buoy .

In the plane (H_v , T_v) the instability region is located above the curve defined by (III-3.5) . As an example , figure n° 31 gives the range of H_v and T_v in the North Atlantic . Figure n° 32 gives the region of rolling for type 11 buoy .

In practice , relation (III-3.5) does not allow us to study by means of calculus only the effect of the buoy characteristics on the presence of a rolling motion because $N_{p\varphi}^{(0)}$ is not known theoretically but only experimentally .

IV - EXPERIMENTAL STUDY -

4.1 - Experimental apparatus and procedure -

In order to verify the validity of the rolling criterion (III-3.5) we have performed experiments in irregular waves with a spectral density given by the modified Pierson-Moskowitz formula . Only type 1 , 11 , 14 and 15 buoys have been tested in tank n° 2 of Bassin d'Essais des Carènes . This tank is equipped for generating irregular waves [24]: any spectral density may be simulated by using a driving voltage . This driving voltage is obtained by running a pseudo - random white noise through a linear filter so designed that the square of its frequency response has the desired shape . Figures 33 and 34 show an example of a measured spectral density of waves and of relative motion .

The experiments were carried out in the manner discussed below . A driving voltage was selected , corresponding to a given value of T_v . Then the value of H_v was set by adjusting the gain of an amplifier located at the input of the generator of the Ward Leonard group . Unfortunately , during these experiments , the gain could be adjusted only by step . Consequently , the critical value of H_v (i.e. the value above which the model rolls) was not precisely determined .

4.2 - Results -

Figures 32 and 35 to 37 show the results for type 11 , 1 , 14 and 15 buoys . In these figures we can see the "theoretical curves" which give the critical value of H_v versus T_v as given by equation (III-3.5) . As was said before , the number of experimental points are too small for the critical values of H_v to be well-defined . Yet it seems that there is no fundamental discordance between the theoretical curves and the experimental results .

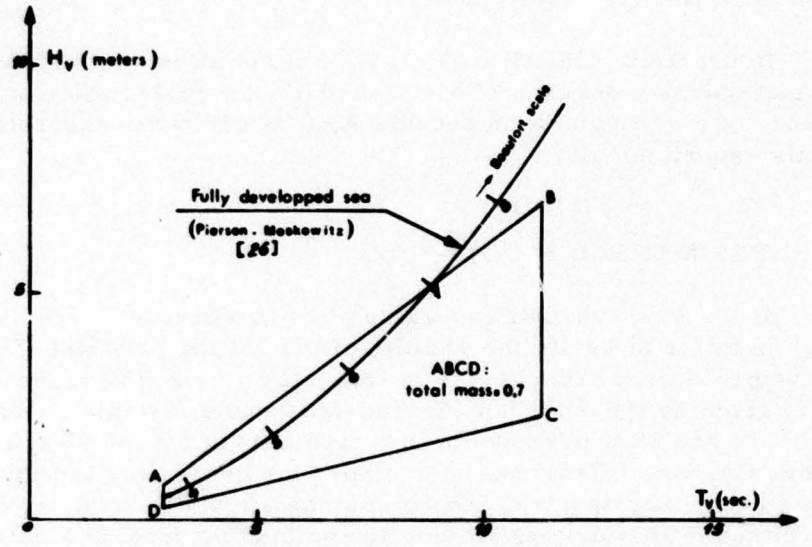


FIGURE 31_ MOST PROBABLE VALUES OF (H_v , T_v) IN NORTH ATLANTIC (Station Atl. of rot [25])

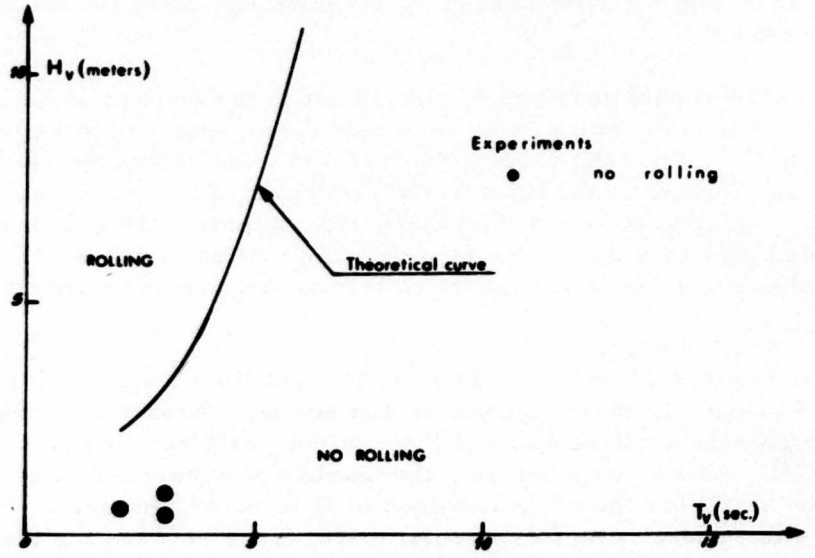


FIGURE 32 _ REGION OF ROLLING OF TYPE 11 BUOY

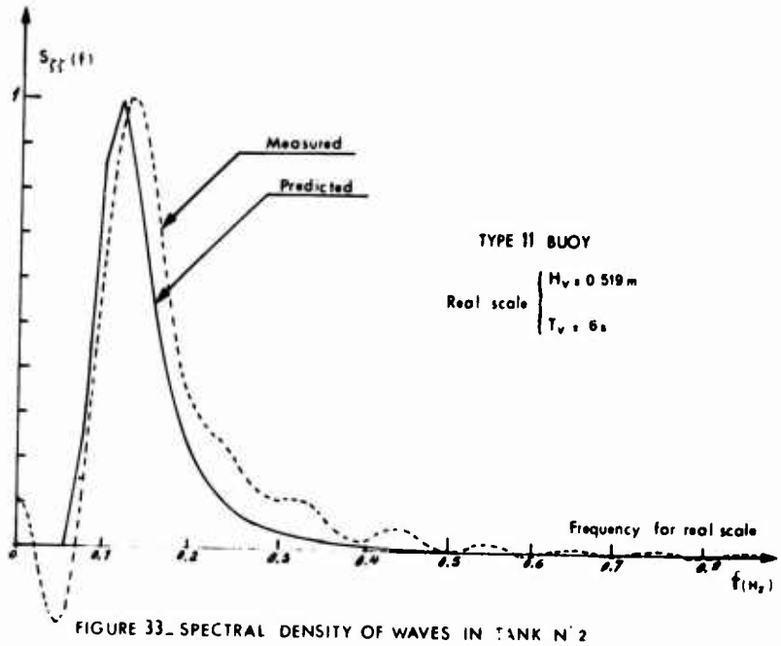


FIGURE 33_ SPECTRAL DENSITY OF WAVES IN TANK N°2

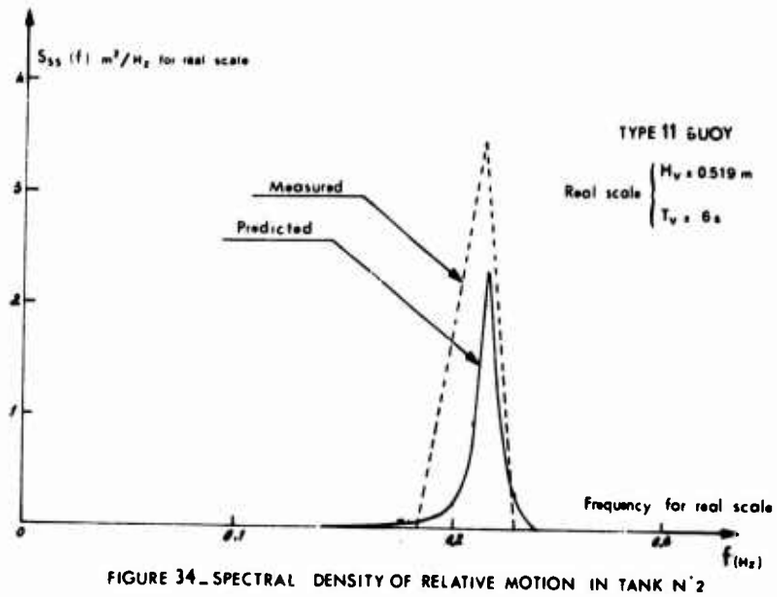


FIGURE 34_ SPECTRAL DENSITY OF RELATIVE MOTION IN TANK N°2

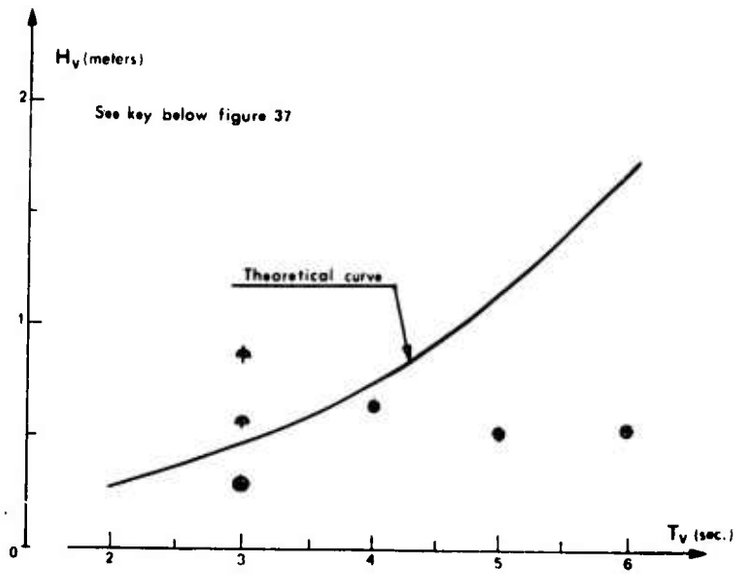


FIGURE 35 - REGION OF ROLLING OF TYPE 1 BUOY

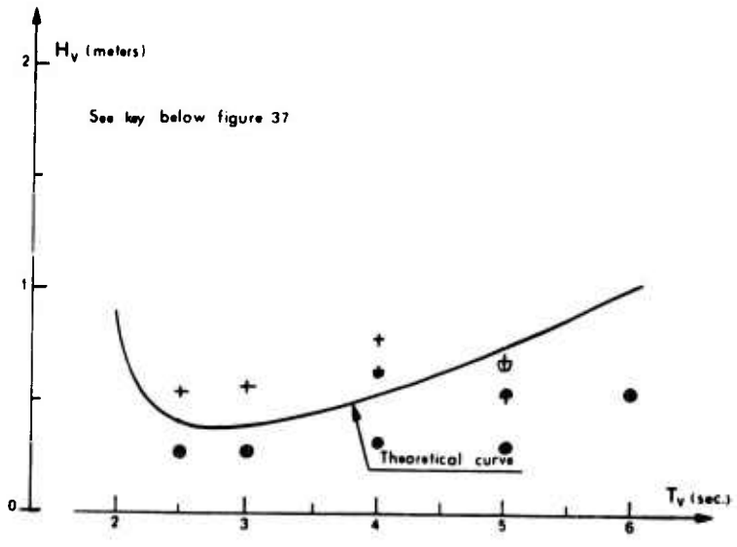


FIGURE 36 - REGION OF ROLLING OF TYPE 14 BUOY

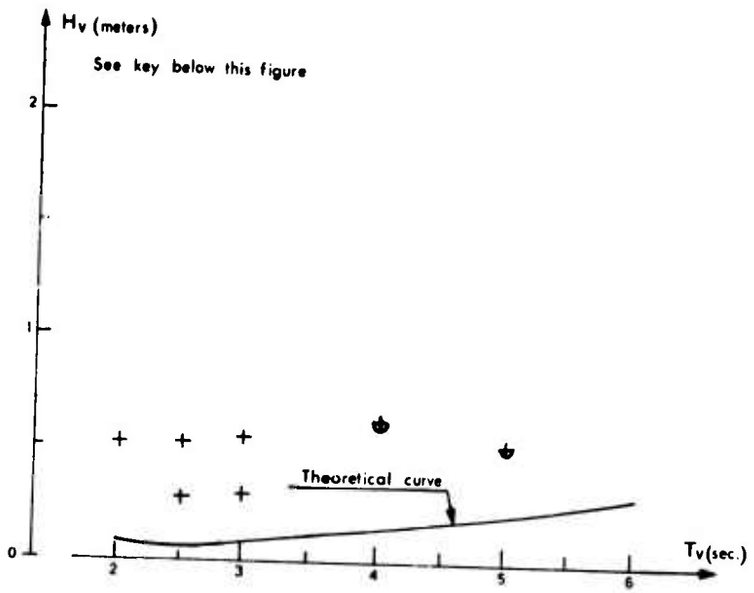


FIGURE 37- REGION OF ROLLING OF TYPE 15 BUOY

KEY FOR FIGURES 35 TO 37

Experiments

+ frequent and important rolling ($\varphi_{max} > 10°$)

frequent but not important rolling ($\varphi_{max} < 10°$)

no frequent but important rolling ($\varphi_{max} > 10°$)

no rolling

IV - CONCLUSION OF SECTION III -

Not enough experimental data has been collected for the validity of rolling criterion to be verified without doubt . Nevertheless this criterion seems reasonable . We must note that it was necessary to introduce in the rolling equation a damping term experimentally determined for J.N.Newman's theory gives too small a value for this term , and , hence , for the critical values of H_v .

GENERAL CONCLUSIONS -

We have shown in sections I and II that J.N.Newman's theory is not valid except if the following conditions are fulfilled :

a/ - the upper part of the buoy which is normally out of water must be of constant sectional area and must be high enough so as to avoid a double regime in the heaving motion .

b/ - It is more difficult to state the conditions for avoiding rolling motions and unstable pitching motions but lowering the center of gravity is an effective method .

When these conditions are fulfilled , J.N.Newman's theory is well verified except for the values of the maxima of the frequency response functions in heaving and pitching . Therefore it seems necessary to determine experimentally the damping terms in heaving and pitching .

In section III we have proposed a criterion for roll in irregular waves . It seems that the criterion is not in disagreement with the few experimental results which are available , provided that one uses an experimentally determined damping term in the rolling equation .

REFERENCES

[1] J.N.NEWMAN - " The motions of a spar buoy in regular waves " - Report 1499 , David Taylor Model Basin, 1963 .

[2] Philip RUDNICK - "Motion of a large spar buoy in sea waves "- Journal of Ship Research , vol. 11, n° 4 , 1967 .

[3] C.BRATU - " Comportement dynamique des bouées océanographiques " - A . T . M . A . 1970 .

[4] Bruce H. ADEE , KWANG JUNE BAI - " Experimental studies of the behaviour of spar type stable platforms in waves " - Report n° NA-70-4 , Collège of Engineering University of California .

[5] H.LAMB - "Hydrodynamics" - Cambridge University Press , 6th edition , 1932 .

[6] A.PAAPE , H.N.C.BREUSERS , J.D.van den BUNT - " L'estimation des forces hydrodynamiques sur les pieux" - Colloques sur la connaissance de la houle , du vent , du courant pour le calcul des ouvrages pétroliers - -Editions Technip , 1970-

[7] E.G.BARILLON - " On the theory of double systems of rolling of ships among waves " - Institution of Naval Architects , 1934 .

[8] R.BRARD - " Contribution à l'étude du roulis . Régimes multiples d'oscillations forcées d'un oscillateur non linéaire " - Bassin d'essais des Carènes , 1944 .

[9] BAUMANN - " Rollzustande grosser amplitude in seitli - cherdünung " - Schiffstechnik , 2 , 1955 .

[10] BLAGOVESHCHENSKY - " Theory of ship motions " - Dover Publications , 1962 .

[11] Austin BLAQUIERE - " Nonlinear system analysis " - - Academic Press - 1966 .

[12] Otto GRIM - " Rollschwingungen , Stabilität und Sicher - heit im Seegang " - Forschungshefte für Schiffstechnik - - Heft 1 , 1952 . -

[13] J.E.KERWIN - " Notes on rolling in longitudinal waves " - International Shipbuilding Progress , vol. 2 , n° 16 , 1955 .

[14] J.R.PAULLING , R.M.ROSENBERG - " On unstable ship motions resulting from nonlinear coupling " - -Journal of Ship Research , vol . n° 3 , n° 1 , June 1959 .

[15] W.D.KINNEY - " On the unstable rolling motions of ships resulting from nonlinear coupling with pitch including the effect of damping in roll " . - Institute of Engineering Research , University of California , Berkeley , October 1961 .

[16] W.D.KINNEY - " On the normal modes of nonlinear coupled ship motions and their stability " - Institute of Engineering Research , University of California , Berkeley , August 1962 .

[17] M.R.HADDARA - " On the stability of ship motions in regular oblique waves " - International Shipbuilding Progress , vol. 18 , November 1971 , n° 207 .

[18] Robert CAMPBELL - " Théorie générale de l'équation de Mathieu " - Masson & Cie , Paris , 1955 .

[19] MINORSKY - " On the stability of nonlinear non autono - mous system " - Proceedings of the US National Congress of Applied Mathematics "- 1954 -

[20] S. KASTNER - " Hebelkurven in unregelmabigem seegang" - Schiffstechnik , vol . 88 , n° 17 , 1970 .

[21] G. F. CARRIER - " Stochastically driven dynamical systems " - Journal of Fluid Mechanics , vol. 44 , part 2 , 11 Novembre 1970 .

[22] Proceedings of the 2nd International Ship Structures Congress 1964 - Delft - Netherlands - 20-24 July 1964 .

[23] J. B. KELLER - " Wave propagation in random media " - Proceedings of Symposia in Applied Mathematics , XIII , 227 - 1960 .

[24] J. L. GIOVACHINI , P. WANTZ - " Generation of Irregular waves of Bassin d'Essais des Carènes , Paris " - 10th ITTC - Teddington - September 1963 .

[25] H. U. ROLL - " Height , Length and Steepness of Seawaves in the North Atlantic " - " Dimensions of Seawaves as functions of Wind Force " SNAME T. R. - Bulletin n° 1 - 19 - 1958 .

[26] W. J. PIERSON and L. MOSKOWITZ - " A proposed spectral form of fully developped wind seas based on the similarity theory of S. A. Kitaigorodski " - Journal of Geophysical Research , vol . 69 , November 1964 .

[27] J. R. MORISON , M. P. O'BRIEN , J. W. JOHNSON and S. A. SCHAAF - " The force exerted by surface waves on piles " - Petroleum Technology , vol. 2 , n° 5 - May 1950 .

NOMENCLATURE

C_D	Coefficient of drag appearing in Morison's formula
C_M	Coefficient of added mass appearing in Morison's formula
C_P	Vertical prismatic coefficient $\frac{m}{\rho H \; S(0)}$
H	Buoy draft
$H(i\sigma, a)$	Describing function
$H_{\Delta f}(2\pi i f)$	Transfer function of relative motion
H_v	Significant wave height
$H_{\theta f}(2\pi i f)$	Transfer function of pitching motion
I_{xx}	Moment of inertia of buoy in roll about the center of gravity
I_{yy}	Moment of inertia of buoy in pitch about the center of gravity
J_{xx}	Added moment of inertia of buoy in roll about the center of gravity
J_{yy}	Added moment of inertia of buoy in pitch about the center of gravity
K_{yy}	Radius of gyration in pitch
L_{HT}	Overall length
N_{zz}	Damping coefficient in heave
$N_{\theta\theta}$	Damping coefficient in pitch
$N_{\varphi\varphi}$	Damping coefficient in roll
$O_o x_o y_o z_o$	Fixed coordinate system
O x y z	Body coordinate system
$P_n = \frac{\rho}{m}\int_o^H (zG - z)^n S(z)\, dz$	
$Q_n(k) = \frac{\rho}{m}\int_o^H e^{-kz} (zG - z)^n S(z)\, dz$	
R	Buoy radius

$S(z)$	Section area of buoy
$S_{ss}(f)$	Spectral density of relative motion
$S_{\zeta\zeta}(f)$	Spectral density of waves
T_p	Period of pitching motion
T_r	Period of rolling motion
T_s	Period of relative motion
T_v	Period of irregular waves
T_w	Period of regular waves
∇	Instantaneous immersed volume of buoy
W	Displaced volume of buoy in calm water
X	Surge displacement of buoy
Y	Sway displacement of buoy
Z	Heave displacement of buoy

$a = z'_C - z'_G$

$\vec{a}_o$ Acceleration of fluid particles due to orbital motion of the on-coming waves

$\vec{a}_{ox} = (\vec{a}_o \cdot \vec{x})\vec{x}$

$\vec{a}_{ozo} = (\vec{a}_o \cdot \vec{z}_o)\vec{z}_o$

f	Frequency
f_z	Natural frequency of heaving motion
f_θ	Natural frequency of pitching motion
g	Acceleration of gravity
h_1, h_2	Characteristics of the upper part of buoy

$i = \sqrt{-1}$

k	Wave number, $\frac{2\pi}{\lambda}$
m	Buoy mass
m_{xx}	Added mass of buoy in the x direction
m_{yy}	Added mass of buoy in the y direction
m_{zz}	Added mass of buoy in the z direction

$m_{x\theta}$	Coupling coefficient between surge and pitch equations
$m_{y\varphi}$	Coupling coefficient between sway and roll equations
r	Metacentric radius
s (t)	Relative motion
t	Time
x , y , z	Cartesian coordinate system
x_o , y_o , z_o	Fixed cartesian coordinate system
$\vec{x}$, $\vec{y}$, $\vec{z}$	Unit vectors of O x y z
$\vec{x}_o$, $\vec{y}_o$, $\vec{z}_o$	Unit vectors of O_o x_o y_o z_o
z_C	Position of center of buoyancy / O x y z
z_G	Position of center of gravity / O x y z
z'_C	Position of center of buoyancy / baseline
z'_G	Position of center of gravity / baseline
ζ (t)	Wave elevation
ζ_A	Half-wave amplitude (preferably to "wave amplitude")
ζ_w	Wave height
θ	Pitch angle of buoy
λ	Length of regular wave
ρ	Density of fluid
σ	Circular frequency of oscillations
φ	Roll angle of buoy
$\Gamma(\varphi)$	Righting moment in roll

AUTO-OSCILLATIONS OF ANCHORED VESSELS UNDER THE ACTION OF WIND AND CURRENT

A. V. Gerassimov, R. Y. Pershitz, N. N. Rakhmanin
Kryloff Ship Research Institute
Leningrad, U.S.S.R.

ABSTRACT

Horizontal plane auto-oscillations of a vessel laid at one anchor are investigated and conditions under which auto-oscillations can be eliminated are established. Ship structure characteristics providing auto-oscillation elimination are considered.

INTRODUCTION

It is known from practice that in the presence of wind an anchored vessel swings from side to side with respect to wind direction line. It performs angular (yaw) and translational (drift) oscillations in the horizontal plane. As is shown by full-scale observations, the intensity of oscillations depends on the wind force, and their amplitude values may reach 90° to 100° for the yaw while for the drift they may be equal to the depth at anchorage or even more than that. The dependence of the oscillatory period on the wind force is weak. When lying at anchor is a working condition for a vessel, such oscillations may prove to be extremely undesirable.

Yawing and drifting of anchored vessels are auto-oscillatory in nature as they may be caused even by the wind of constant direction and force. Such character of motion is due to nonlinear relationships inherent in an oscillatory system formed by the anchored vessel. The most significant of these manifest themselves in the nonlinear relationship between the horizontal component of the anchor chain tension and the shifting of the hawse-hole with respect to the sea bed, as well as

in the nonlinear relationships between the aerodynamic and hydrodynamic forces and the kinematics of the ship's motion.

For the purpose of making a detailed analysis of yawing and drifting of anchored vessels this paper deals with the discussion of forces acting on the vessel in the circumstances, and the derivation of relevant differential equations of motion. In the derivation of these equations great attention was given to determining the tension of the anchor chain as dependent on the shifting of hawse-hole.

The aerodynamic and hydrodynamic forces are defined in accordance with the known results [1], [2], [3]. The general equations of motion obtained for an anchored ship are used for finding her equilibrium positions and analyzing stability of the same. It is shown that the main reason inducing the ship to yaw is instability of her equilibrium position due to wind. Consideration is given to conditions in which stability of equilibrium is ensured for anchored vessels while periodic yawing and drifting is ruled out.

1. Coordinate systems and Nomenclature

To solve the problem under review, four coordinate systems are used. Two of them are applied for the description of ship's motion in the horizontal plane, viz., the fixed coordinate system XOY with OX-axis directed oppositely to the wind and the origin O which coincides with the center of gravity (CG) of a non-diverted vessel, and the body axis system $\xi 0_1 \eta$ with $0_1 \xi$ -axis directed forward and the origin in CG. The $0_1 \eta$ -axis is directed to port side.

Figure 1 shows the directions of coordinate axes and positive directions of angle reading for the two systems. The notation B denotes a point of the anchor chain breaking away from the ground, H_o = initial position of the hawse-hole, H_1 = current position of the same.

Two more coordinate systems (Figure 2) are required for the description of the anchor chain positioning in space. One of these, the $z' Ax'$ system is situated in the plane of the anchor chain sagging. The origin A is made coincident with the anchor lying on the ground. The Az'-axis is directed vertically, while the horizontal axis is coincident with the ground plane and directed to the hawse-hole H_o. The other system of coordinates $h_o \delta$ is characterized by the fact that the vertical axis oh always passes through the point B where the anchor chain breaks away from the ground, and that the origin O is at a distance of

$$a = \frac{T}{W} \qquad (1)$$

below the ground level. Here T denotes the horizontal component of the anchor chain tension and W is the weight per unit length of the chain submerged in water.

Besides, the following designations are also used in this paper :

ρ and ρ_o	=	mass density of water and air,
g	=	acceleration due to gravity,
L	=	length between perpendiculars,
A	=	lateral area of the underwater body,
Q	=	sail area,
m	=	own mass of ship,
λ_{11} and λ_{22}	=	longitudinal and transverse added mass,
J	=	ship's mass moment of inertia for central vertical axis,
λ_{66}	=	added mass moment of inertia for the same axis,
V	=	wind velocity,
V_o	=	flow velocity,
α_o	=	angle between wind and flow directions,
CA	=	center of sail area,
ξ_s	=	abscissa of CA,
ξ_{hh} and η_{hh}	=	hawse-hole coordinates in the body coordinate system $\xi O_1 \eta$,

$\overline{P}_a$, $\overline{P}_{a\xi}$, $\overline{P}_{a\eta}$ = aerodynamic force and its projections on the body axis,

$\overline{P}_h$, $\overline{P}_{h\xi}$, $\overline{P}_{h\eta}$ = hydrodynamic force and its projections on the body axis,

$\overline{P}_{t\xi}$, $\overline{P}_{t\eta}$ = projections of horizontal component of the anchor chain tension on the body axis,

$\overline{M}_a$ = aerodynamic moment about the central vertical axis,

$\overline{M}_h$ = moment of resistance to ship's rotating about the central vertical axis,

$\overline{M}_t$ = moment of anchor chain tension about the central vertical axis,

β, β_m = angle between wind direction and ship's longitudinal axis; the amplitude value of the same angle,

β_o = same angle at static equilibrium,

$\dot{\xi}$ and $\dot{\eta}$ = projections of CG velocity on the body axis,

Y_o = lateral (normal to the wind) displacement of CG,

X_o = displacement of CG towards the wind,

X_{hh} = displacement of hawse-hole towards the wind,

Y_{hh} = lateral displacement of hawse-hole,

$\Delta X'$ = projection of absolute displacement of hawse-hole onto the anchor chain sagging plane,

φ = angle between wind direction and the anchor chain sagging plane,

H = depth of sea at anchorage,

H_h = hawse-hole elevation over the sea bed.

2. Basic assumptions

The discussion of yaw and drift problem for the anchored ships is based on the following assumptions :

1. It is assumed that the coupled pitching and heaving motions do not affect the ship's movement in the horizontal plane.

2. The magnitude of hydrodynamic forces is taken as independent of athwartship inclinations.

3. In the estimation of inertial forces the vessel is considered to be symmetric not only about the centerplane but also about the athwartship plane, and the center of gravity to be located in the athwartship plane.

4. In predicting the noninertial forces and moments acting on the vessel use is made of steadiness hypothesis. It is also assumed that the ship's movement is so slow that the anchor chain inertia forces can be neglected when determining the tension of the chain.

3. Differential equations of motion

According to [1] the differential equations of the ship's horizontal motion in the body coordinate system $\xi 0_1 \eta$ can be written as follows :

$$
\begin{aligned}
&(m + \lambda_{11})\, \dot{\xi} - (m + \lambda_{22})\, V_\eta \dot{\beta} = \overline{F}_\xi , \\
&(m + \lambda_{22})\, \dot{\eta} + (m + \lambda_{11})\, V_\xi \dot{\beta} = \overline{F}_\eta , \\
&(Y + \lambda_{66})\, \dot{\beta} - (\lambda_{11} - \lambda_{22})\, V_\eta \cdot V_\xi = \overline{M}.
\end{aligned} \tag{2}
$$

The right-hand side of equations (2) could most conveniently be written as the sums

$$
\begin{aligned}
\overline{F}_\xi &= -\overline{P}_{a\xi} - \overline{P}_{h\xi} + \overline{P}_{\tau\xi} , \\
\overline{F}_\eta &= -\overline{P}_{a\eta} - \overline{P}_{h\xi} - \overline{P}_{\tau\eta} , \\
\overline{M} &= \overline{M}_a - \overline{M}_h - \overline{M}_\tau .
\end{aligned} \tag{3}
$$

The terms included in the expressions (3) are determined by the aerodynamic forces acting upon the above-water body in the presence of wind, the anchor chain tension, and the noninertial hydrodynamic forces generated on the underwater body during its motion. The inertial forces considered in this problem are taken into account in the left-hand side of equations (2). When defining the signs of formulae (3) it was thought that the forces and moments were calculated for the positive shifts.

In equations (2) provision is made for taking account of the constant current in the vicinity of anchorage. For this purpose you need only to represent the CG velocity projections with respect to water in the form of the following obvious expressions (Figure 1.):

$$V_\xi = \dot{\xi} + V_o \operatorname{Cos}(\alpha_o + \beta),$$
$$V_\eta = \dot{\eta} - V_o \operatorname{Sin}(\alpha_o + \beta). \qquad (4)$$

In the absence of current V_o and α_o are equal to zero. Thus three unknown values can be derived directly from equations (2): yaw angle β and projections $\dot{\xi}$ and $\dot{\eta}$ of the CG velocity. In the fixed coordinate systems these projections will have the form

$$\dot{X}_o = \dot{\xi} \operatorname{Cos}\beta - \dot{\eta} \operatorname{Sin}\beta, \quad \dot{Y}_o = \dot{\xi} \operatorname{Sin}\beta + \dot{\eta} \operatorname{Cos}\beta \qquad (5)$$

By integrating expressions (5) time functions $X_o(t)$ and $Y_o(t)$ can be found which determine the position of CG in space. The position of the hawse-hole can be found from the following obvious relationships :

$$X_{hh} = X_o - \xi_{hh}(1 - \operatorname{Cos}\beta), \quad Y_{hh} = Y_o + \xi_{hh} \operatorname{Sin}\beta \qquad (6)$$

Along with the relationship for β (t) the functions of $X_o(t)$, $Y_o(t)$, $X_{hh}(t)$ and $Y_{hh}(t)$ give rather a full idea of the yawing and drifting of an anchored vessel under the action of wind and current.

4. Estimation of aerodynamic forces

Projections of aerodynamic forces on the axis of the body system of coordinates $\xi\, O_1\, \eta$ are defined by expressions

$$\overline{P}_{a\xi} = C^{o}_{a\xi} \frac{\rho_o V^2}{2} \quad Q \cos \beta ,$$

$$\overline{P}_{a\eta} = C^{o}_{a\eta} \frac{\rho_o V^2}{2} \quad Q \sin \beta , \qquad (7)$$

and the moment about the central vertical axis by

$$\overline{M}_a = C_{ma} \frac{\rho_o V^2}{2} \quad Q \angle \qquad (8)$$

In the latter expression

$$C_{ma} = C_o \left(\sigma_o + \sigma_s - \frac{|\beta|}{2\pi} \right) \sin \beta , \qquad (9)$$

where non-dimensional parameters σ_o and C_o are dependent on the relative position of CA

$$\sigma_s = \frac{\xi s}{\angle} \qquad (10)$$

and defined by the generalized curve (Figure 3) plotted against the data obtained from [2] and [3] . Irrespective of the CA position coefficients $C^{o}_{a\xi}$ and $C^{o}_{a\eta}$ may be considered as constant, viz., $C^{o}_{a\xi} = 0.14$ and $C^{o}_{a\eta} = 0.95\text{-}1.05$.

5. Estimation of hydrodynamic forces

The hydrodynamic force components, the longitudinal one $\overline{P}_{h\xi}$ and the normal $\overline{P}_{h\eta}$, as well as the moment $\overline{M}_h$ originating during rotation of the vessel may be estimated approximately from the formulae

$$\overline{P}_{h\xi} = C^{o}_{h\xi} \left(\dot{\xi} \left| \dot{\xi} \right| + \dot{\tilde{V}}_\xi \left| \tilde{V}_\xi \right| \right) \frac{\rho A}{2} ,$$

$$\overline{P}_{h\eta} = C^{o}_{h\eta} \left(\dot{\eta} \left| \dot{\eta} \right| + \dot{\tilde{V}}_\eta \left| \tilde{V}_\eta \right| \right) \frac{\rho A}{2} , \qquad (11)$$

$$\overline{M}_h = C_{hm} \dot{\beta} \left| \dot{\beta} \right| .$$

Here coefficients $C^{o}_{h\xi}$ and $C^{o}_{h\eta}$ are chosen in conformity with recommendations of Ref. [2], and C_{hm} is determined by the expression

$$C_{hm} = \frac{1}{64} C^{o}_{h\eta} \rho A \angle^{3}, \tag{12}$$

established under the assumption that the centre of ship's rotation in the horizontal plane coincides with the athwartship plane. The second terms of formulae (11) allow for the presence of current

$$\tilde{V}_{\xi} = V_{o} \cos(\alpha_{o} + \beta), \quad \tilde{V}_{\eta} = V_{o} \sin(\alpha_{o} + \beta). \tag{13}$$

6. Estimation of tension of the anchor chain

At an arbitrary moment of time the longitudinal axis $o_1\xi$ forms an angle $(\beta + \varphi)$ with the anchor chain sagging plane (Fig. 1) Projections of tension T for the latter on the body axis will be expressed by the relationships

$$\overline{P}_{T\xi} = T \cos(\beta + \varphi),$$
$$\overline{P}_{T\eta} = T \sin(\beta + \varphi). \tag{14}$$

The moment of force T about the central vertical axis appears to be equal to

$$\overline{M}_{T} = T \cdot \xi_{hh} \sin(\beta + \varphi) - T \cdot \eta_{hh} \cdot \cos(\beta + \varphi). \tag{15}$$

The horizontal component of the anchor chain tension is represented by the sum

$$T = T_{o} + \Delta T \tag{16}$$

Here T_o is taken as

$$T_{o} = C^{o}_{a\xi} \frac{\rho_{o} Q}{2} V^{2}, \tag{17}$$

which corresponds to the longitudinal component $\overline{P}_{a\xi}$ of the aerodynamic force for $\beta = \varphi = 0$. The tension increment ΔT is estimated by the hawse-hole shifts $\Delta X'$ in the course of drifting or yawing of the vessel. The curve of T against $\Delta X'$ plotted with allowance for the chain line characteristics is presented in the dimensionless form in Figure 4 for the case when $K_o = \frac{T_o}{WH_h} = 0$. In all other cases the relationship of $\Delta K = f(\overline{\Delta X'})$ is easily determined, using the same figure, by shifting the origin along the curve to the point where the latter is intersected by the straight line $K = K_o$.

7. The final form of differential equations of motion

Taking into account the results given above and converting the equations (2) to the form where the coefficients for the second derivatives of variables ξ, η, and β are equal to unit, the set of differential equations of motion for an anchored vessel in the presence of wind and current can be presented in the following final form which will be convenient for further analysis :

$$
\left.
\begin{aligned}
&\ddot{\xi} - P_{\xi 1} V_\eta \dot{\beta} + P_{\xi 2} \dot{\xi} \left|\dot{\xi}\right| + P_{\xi 2} V_o^2 \cos(\alpha_o + \beta) \left|\cos(\alpha_o + \beta)\right| - \\
&- P_{\xi 3} \Delta k \cos(\beta + \varphi) = P_{\xi 4} V^2 \cos(\beta + \varphi) - P_{\xi 4} V^2 \cos\beta , \\
&\ddot{\eta} + P_{\eta 1} V_\xi \dot{\beta} + P_{\eta 3} \dot{\eta} \left|\dot{\eta}\right| - P_{\eta 3} V_o^2 \sin(\alpha_o + \beta) \left|\sin(\alpha_o + \beta)\right| + \\
&+ P_{\eta 4} \Delta k \sin(\beta + \varphi) = - P_{\eta 5} V^2 \sin(\beta + \varphi) + P_{\eta 6} V^2 \sin\beta , \\
&\ddot{\beta} + P_{\beta 1} V_\xi V_\eta + P_{\beta 2} \dot{\beta} \left|\dot{\beta}\right| + P_{\beta 3} \Delta k \sin(\beta + \varphi) = \\
&= P_{\beta 4} V^2 \sin\beta - P_{\beta 5} V^2 \left|\beta\right| \sin\beta - P_{\beta 6} V^2 \sin(\beta + \varphi) + \\
&+ P_{\beta 7} V^2 \cos(\beta + \varphi) + P_{\beta 8} \Delta k \cos(\beta + \varphi)
\end{aligned}
\right\} \quad (18)
$$

In equations (18) the values of CG velocity projections V_ξ and V_η are determined from formulae (4) and the following designations are used :

$$P_{\xi 1} = \frac{m + \lambda_{22}}{m + \lambda_{11}} \quad ; \qquad P_{\xi 2} = \frac{C^o_{h\xi}\, \rho\, A}{2\,(m + \lambda_{11})} \quad ,$$

$$P_{\xi 3} = \frac{W\, H_h}{m + \lambda_{11}} \quad ; \qquad P_{\xi 4} = \frac{C^o_{a\xi}\, \rho_o\, Q}{2\,(m + \lambda_{11})} \quad , \qquad (19)$$

$$P_{\eta 1} = \frac{m + \lambda_{11}}{m + \lambda_{22}} \quad ; \qquad P_{\eta 3} = \frac{C^o_{h\eta}\, \rho\, A}{2\,(m + \lambda_{22})} \quad ,$$

$$P_{\eta 4} = \frac{W\, H_h}{m + \lambda_{22}} \quad ; \quad P_{\eta 5} = \frac{C^o_{a\xi}\, \rho_o\, Q}{2\,(m + \lambda_{22})} \quad , \quad P_{\eta 6} = \frac{C^o_{a\eta}\, \rho_o\, Q}{2\,(m + \lambda_{22})} \quad , \qquad (20)$$

$$P_{\beta 1} = \frac{\lambda 22 - \lambda 11}{J + \lambda_{66}} \quad ; \qquad P_{\beta 2} = \frac{1}{32}\, \frac{C^o_{h\eta}\, \rho\, A\, L^3}{2\,(J + \lambda_{66})} \quad ,$$

$$P_{\beta 3} = \frac{W\, H_h\, \xi_{hh}}{J + \lambda_{66}} \quad ; \qquad P_{\beta 4} = \frac{C_o\,(\sigma_o + \sigma_s)\, \rho_o\, Q\, L}{2\,(J + \lambda_{66})} \quad ,$$

$$P_{\beta 5} = \frac{C_o}{2\pi} \cdot \frac{\rho_o\, Q\, L}{2\,(J + \lambda_{66})} \quad ; \qquad P_{\beta 6} = \frac{C^o_{a\xi}\, \rho_o\, Q\, \xi_{hh}}{2\,(J + \lambda_{66})} \quad , \qquad (21)$$

$$P_{\beta 7} = \frac{C^o_{a\xi}\, \rho_o\, Q\, \eta_{hh}}{2\,(J + \lambda_{66})} \quad ; \qquad P_{\beta 8} = \frac{W\, H_h\, \eta_{hh}}{J + \lambda_{66}}$$

8. Equations of equilibrium

Equations of equilibrium for anchored vessels subjected to wind and current action can be derived from differential equations (18) providing $\dot{\xi} = \dot{\eta} = 0$; $\ddot{\xi} = \ddot{\eta} = 0$; $\ddot{\beta} = 0$ and $\ddot{\beta} = 0$.

The set of equations thus obtained makes it possible not only to define the equilibrium position of an anchored ship, with the wind and current prescribed, but also to follow the dependence of this position on the ship's particulars and the coordinates of the hawse-hole.

In the absence of current ($V_o = 0$) this set of equations is reduced to a single equation which determines the angle of equilibrium β_o :

$$\left[(\sigma_o + \sigma_s) - \frac{|\beta|}{2\pi} - \frac{C^o_{a\eta}}{C_o} \cdot \frac{\xi_{hh}}{L}\right] \operatorname{Sin}\beta + \\ + \frac{C^o_{a\xi}}{C_o} \frac{\eta_{hh}}{L} \cdot \operatorname{Cos}\beta = 0 \quad . \tag{22}$$

It follows from equation (22) that the angle β_o is dependent on the coordinates of the hawse-hole ξ_{hh} and η_{hh} and the lengthwise position of the centre of sail area σ_S . The ordinate η_{hh} has no appreciable effect on the equilibrium position of the vessel. Setting $\eta_{hh} = 0$ we shall find that angle β_o is equal to zero if the hawse-hole abscissa satisfies the condition

$$\xi_{ho} \geqslant \frac{C_o}{C^o_{a\eta}} (\sigma_o + \sigma_s) L . \tag{23}$$

Otherwise angle β_o is defined from the formula

$$|\beta_o| = 2\pi \left(\sigma_o + \sigma_s - \frac{C^o_{a\eta}}{C_o} \frac{\xi_{hh}}{L}\right) . \tag{24}$$

9. Stability of equilibrium positions

A vessel may stay in the positions of equilibrium as defined above only on condition that these positions are stable. Considering the stability of the vessel with respect to yawing in conformity with A. M. Liapunov's general theory [4] , the following criterion of stability can be obtained :

$$\frac{\xi_{hh}}{L}\left[\frac{C^o_{a\xi}}{C_o} + \frac{C^o_{a\xi}\,\mathrm{Cos}\,\beta_o + C^o_{a\eta}\,\mathrm{Sin}\,\beta_o}{\overline{\Delta X}_o \cdot C_o} \cdot \frac{L\,\mathrm{Sin}\,\beta_o\,\mathrm{tg}\,\beta_o}{H_h} \cdot \frac{\xi_{hh}}{L}\right] + \tag{25}$$

$$+ \frac{\beta o}{2\pi} + \frac{\mathrm{tg}\,\beta_o}{2\pi} > \sigma_o + \sigma_s ,$$

where $\overline{\Delta X_o}$ is the non-dimensional shifting of the hawse-hole in relation to the anchorage depth H_h as the ship passes from the state of rest in the absence of wind to an equilibrium position with the wind having the velocity of V.

It can practically be assumed that $\frac{\xi_{hh}}{L} = 0.5$. In this case angle β_o is equal to zero, which can easily be verified by using formula (23), and the criterion (25) is simplified taking the form

$$\frac{\xi_{hh}}{L} > (\sigma_o + \sigma_s)\frac{C_o}{C^o_{a\xi}}. \tag{26}$$

Taking into account the curves of Figure 3 it can easily be shown that for the conventional arrangement of the forward hawse-hole condition (26) is not met, i.e. in the absence of current the anchored vessel subjected to wind will not be stable to angular deflections from the course.

Instability of equilibrium of a vessel held in place by the anchor is the main cause of drifting and yawing, which in the absence of current and with constant wind have the nature of auto-oscillations which are symmetrical with respect to the wind directions. Fig. 5 shows the curves obtained by computer simulation of the set of equations (18), which characterize the auto-oscillations of the anchored vessel ($\frac{L}{B} = 5$; $\frac{\xi_{hh}}{L} = 0.5$; $\sigma_s = 0.07$) subjected to constant wind ($V = 12$ m/sec) in the absence of current ($V_o = 0$).

Under the simultaneous action of the wind and current the yawing becomes asymmetric with respect to the wind provided that the direction of the wind differs from that of the current. The average angle β_o and average shifting of the hawse-hole Y_{ho} increase

with the increase in the flow velocity V_o and angle α_o. The amplitude of steady cyclic yaw is but slightly dependent on the flow parameters. On the contrary, the amplitude of lateral displacement of the hawse-hole is substantially decreased with the increase of the flow velocity.

The increase in the flow velocity leads, all other things being equal, to increasing angle β_o. In consequence, as is seen from expression (25), the position of the vessel's equilibrium may change from being instable in respect of yawing to a stable one, which will involve complete ceasing of its oscillations due to yawing and drifting. In the example given the oscillations of the electronic model of an anchored vessel ceased at a flow velocity exceeding 0.8 m/sec.

It is obvious from equations (18) that period τ of the oscillations under consideration is mainly dependent on the depth H at anchorage (Figure 6). At the same time there is a clearly defined dependence of this period on wind velocity. The latter result, however, needs to be explained additionally.

In consequence of the ship's motions and wave action the resistance to drift $P_{\eta 3}$ and yaw $P_{\beta 2}$ must increase much like the resistance of a ship moving in a seaway, which is not taken into account by the set of equations (18). Additional resistance to drift and yaw in a seaway brings about an appreciable reduction in drifting velocity and, consequently, an increase in the period of auto-oscillations of an anchored vessel, all other things being equal. Hence, seaways may be considered as the cause of significant weakening of the relationship between the period of yawing oscillations and the velocity of wind. According to full-scale data, the period of oscillations due to strong wind slightly differs from that when the wind force is 3-4 (on Beaufort scale).

10. Ways to eliminate the auto-oscillations of anchored vessels

Solution of equations (18) indicates that the intensity of auto-oscillations for the given depth at anchorage and wind velocity may be in direct relation to the extent of instability of the ship's equilibrium position. This latter is defined by the difference between the right-hand sides of inequalities (25) and (26). In similar anchorage conditions the left-hand side of these inequalities is substantially dependent upon the position of the hawse-hole along the ship's length. The right-hand side of the inequalities is eventually characterized by the initial (for $\beta_o = 0$) value of the positional

aerodynamic derivative coefficient (9) :

$$C^{\beta}_{ma} = C_o (\sigma_o + \sigma_s), \qquad (27)$$

i. e. by the lengthwise position of the centre of sail area. Figure 7 gives an indication of the relationship between the intensity of yawing and the extent of instability of the ship's equilibrium position. The intensity of yawing is characterized in this figure by the relative amplitude $\bar{\beta} = \frac{\beta_m}{\beta_{mo}}$ versus the derivative C^{β}_{ma}. Here β_m = dimensional amplitude of yaw, β_{mo} = dimensional amplitude of yaw for the vessel with $\frac{L}{B} = 5.0$, $\sigma_s = 0.068$. The curve of β_{mo} against the anchorage depth is presented in Figure 8.

Thus the elimination of the wind-induced auto-oscillations of an anchored vessel may be brought about if stability of its equilibrium position is ensured. This latter can be ensured, as evidenced by the analysis of condition (25), by shifting aft both the centre of sail area and the hawse-hole. This same condition, along with (26), gives the quantitative value of the required shifting of the above points.

When the hawse-hole is located near the forward perpendicular, the auto-oscillations of the anchored vessel subjected to wind may be eliminated at the cost of shifting the centre of sail area well aft. As angle $\beta_o = 0$ corresponds in this case to the ship's equilibrium position, and the $\frac{C_o}{C^o{}_{a\xi}}$ ratio is rather large, so the stability of equilibrium position, as follows from inequality (26), can practically be ensured if the right-hand side of this inequality is close to zero or negative. This will be the case if

$$\sigma_s \leqslant - 0,25 \qquad (28)$$

So considerable a shifting of the centre of sail area, however, adversely affects the controllability of the vessel in wind.

The shifting of the hawse-hole aft of the forward perpendicular must be greater than that where the ship's equilibrium is possible with the value of β_o different from zero. As the angle β_o increases, the instability of equilibrium position decreases, and at a certain value of $(\frac{\xi_h}{L})_{Cr}$ the position becomes stable, viz. inequality (25) is satisfied. Thus, with

$$\frac{\xi_{hh}}{L} < \left(\frac{\xi_{hh}}{L}\right)_{Cr} \tag{29}$$

the auto-oscillations of the anchored vessel are eliminated. Even so, this conclusion based on the analysis of small perturbation stability quite satisfactorily characterizes motion in general.

The test results shown in Figure 9 (a) and (b), for an electronic model of an anchored vessel ($\sigma_s = 0.068$, $\frac{L}{B} = 5.0$) give an idea of the effect the longitudinal arrangement of the hawse-hole has on the intensity of yaw and drift. The dashed lines in the region of unstable equilibrium represent the curves of yaw amplitudes against abscissa ξ_{hh}. During the tests no auto-oscillations were observed at $\left(\frac{2\xi_{hh}}{L}\right)_{cr}$ values beyond the left ends of these curves. The solid lines indicate the β_o and Y_{ho} parameters for the ship's equilibrium position. These relationships were calculated from static equilibrium equations (see section 8); the results obtained from equations (18) are illustrated by points on the solid lines.

It is obvious that the results presented are in good agreement with the boundary of auto-oscillations region determined by calculation from formula (29). Setting $\eta_{hh} = 0$ for the critical abscissa of the hawse-hole the following formula can be obtained

$$\left(\frac{\xi_{hh}}{L}\right)_{cr} \simeq \frac{3}{4}\,\frac{C_o}{C^o_{a\eta}}\,(\sigma_o + \sigma_s). \tag{30}$$

In contrast, for eliminating the auto-oscillations of the anchored vessel by shifting the hawse-hole aft it is desirable that the centre of aerodynamic pressure (CP) should be shifted forward.

Really, in the position of ship's equilibrium the line of aerodynamic action coincides with the anchor chain horizontal projection and passes through the hawse-hole. Hence, no auto-oscillations are present if the following inequalities are met simultaneously:

$$\xi_{hh} < \xi_{cr}, \quad \xi_p < \xi_{cr} \tag{31}$$

where ξ_p = abcissa of CP. But

$$\frac{\xi_p}{L} = \frac{Cma}{L C^o_{a\eta} \sin \beta_o} = \frac{C_o}{C^o_{a\eta}} \left(\sigma_o + \sigma_s - \frac{|\beta_o|}{2\pi} \right) \qquad (32)$$

from which we obtain

$$\frac{\xi_p}{L} = \frac{4}{3} \left(\frac{\xi_{hh}}{L} \right)_{cr} - \frac{C_o |\beta_o|}{2\pi C^o_{a\eta}}$$

It is evident from relationships (24), (30) and (32) that if CP is shifted forward, given the position of the hawse-hole along the ship's length, this will involve an increase of β_o and a reduction of $\frac{\xi_{hh}}{L}$, which will allow satisfaction of the second inequality (31). So, the farther forward CP is displaced, the less is the necessity of shifting the hawse-hole aft of the stem so as to eliminate the wind-induced auto-oscillations of the anchored vessel.

The shifting of the anchor hole aft of the stem is equivalent to springing the vessel as is accepted in maritime practice.

Let us consider the scheme (Figure 10) showing the springing technique. The lengths of the forward $H_f H_s$ and after $H_a H_s$ portions of the spring must be chosen so that in the ship's equilibrium position they will be tensioned. As long as the spring remains tensioned during oscillations, its presence will be equivalent to the hawse-hole shifting to point H_{s1}, and the tension line of the anchor chain will intersect the centre line plane at point K which is coincident with CP. It is evident that the position of equilibrium will not be disturbed if a single anchor rope is secured to the vessel at the point H_{s1}.

As far as research and fishing vessels are concerned for which lying at anchor at various places of the water area is the basic condition of operation, it may prove to be convenient that a special anchor gear be designed so that the point where the anchor chain is secured to the vessel is shifted aft of the stem when at station. This point must satisfy the conditions (31). In the case of a fishing vessel it was found that you need only to locate such a hawse-hole in the

shaded region (Figure 10) covering the centre of sail area in order to eliminate yawing of the anchored ship. This region is likely to be equal for ships which do not differ much in respect of the deck-house architecture. It is expected that such an anchor gear, if properly designed, will create favourable conditions for the operation of the above-mentioned ships.

REFERENCES

1 BASSIN, A. M., "Khodkost' i upravliayemost' sudov" (Performance and controllability of ships), Izd. Transport Leningrad, 1968 (in Russian).

2 VOITKUNSKY, Y.I., PERSHITZ, R.Y., TITOV, I.A., "Spravochnik po teorii korablia" (Reference book on ship theory), Sudpromgiz, Leningrad, 1960 (in Russian).

3 GOFMAN, A.D., ZAIKOV, V.I., SEMIONOVA-TIAN-SHANSKAYA, A.V., "K raschetu upravliayemosti sudna pri vetre" (Analysis of controllability of vessels subjected to wind), Trudy LIIVT, vyp. 81, Rechizdat, Leningrad, 1965 (in Russian).

4 LIAPUNOV, A.M., "Obshchaya zadacha ob ustoichivosti dvizheniya" (General problem of stability of motion), ONTI, Moskva, 1933(in Russian).

5 SAVELOV, A.A., "Ploskiye kriviye" (Plane curves), GIFML, Moskva, 1960.

* * *

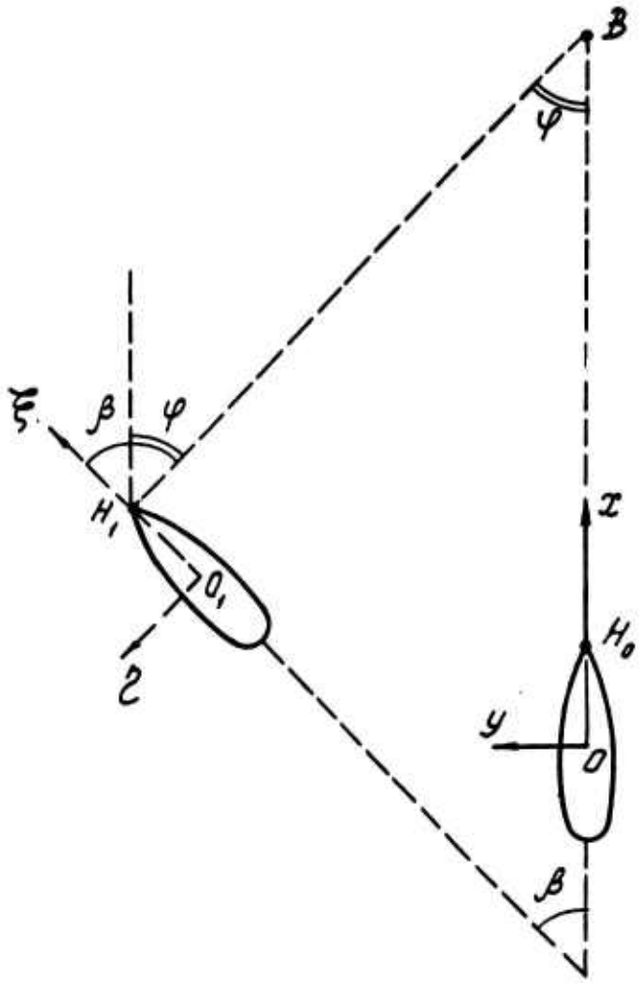


Figure 1 System of coordinates for the description of the anchored ship's motion.

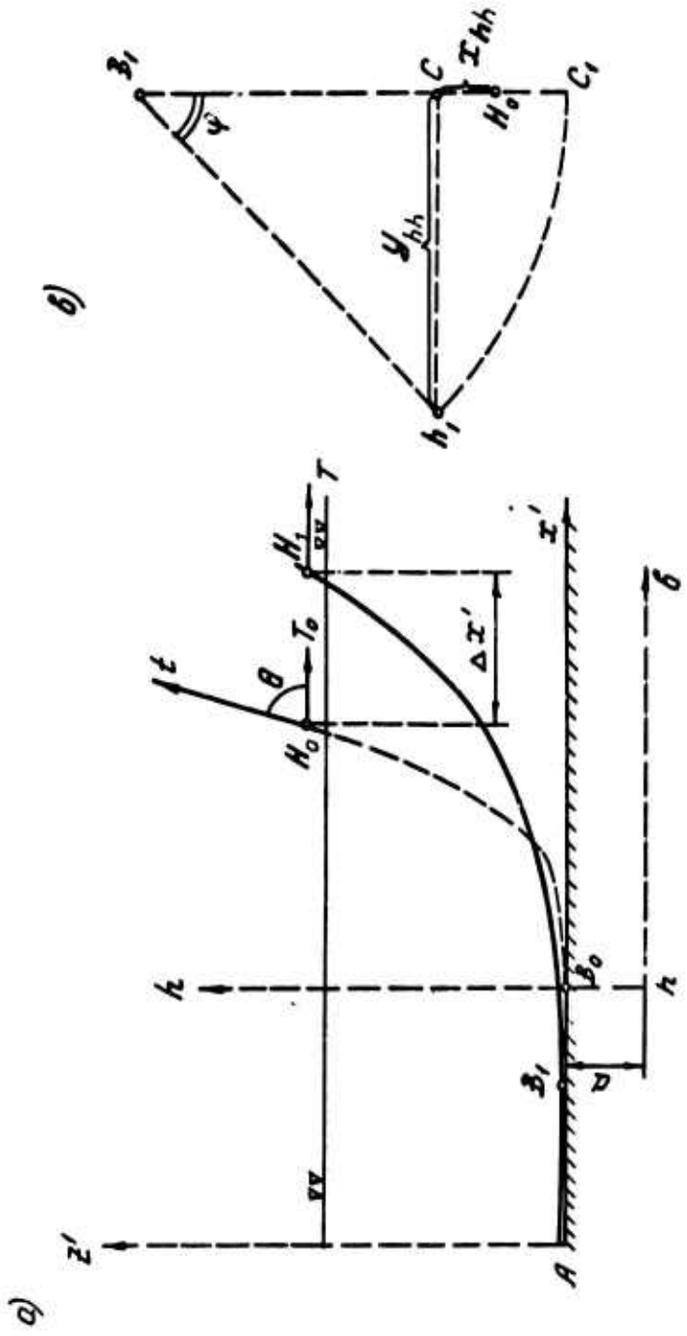


Figure 2 System of coordinates for the description of the anchor chain positioning in space.

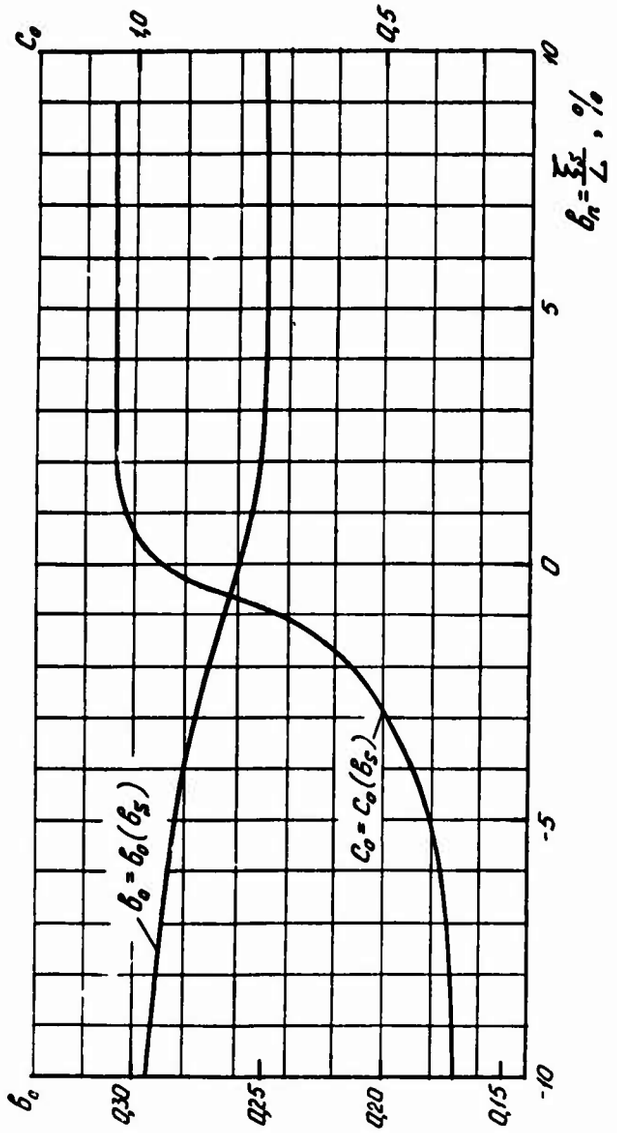


Figure 3 Coefficients C_o and $\bar{b}_o$ versus the lengthwise position of the centre of sail area.

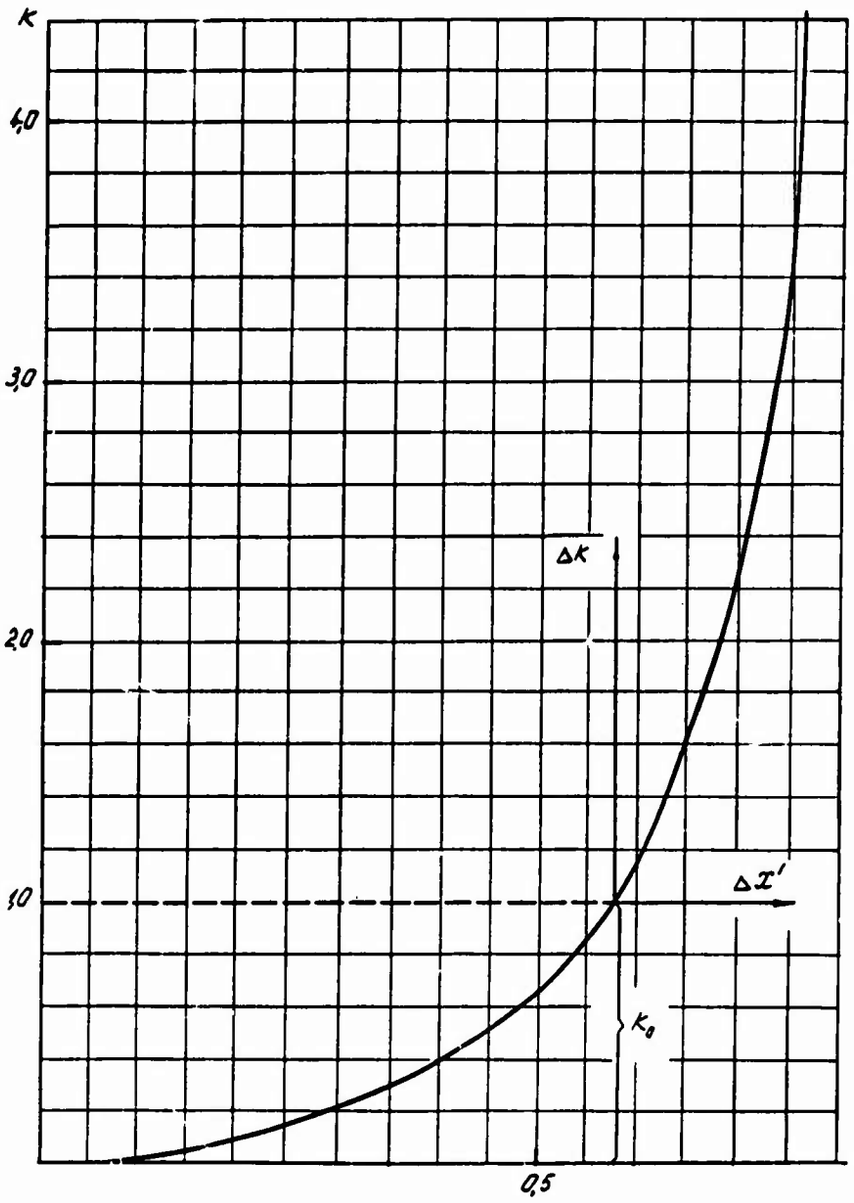


Figure 4 Dimensionless tension of the anchor chain against displacement of the hawse-hole.

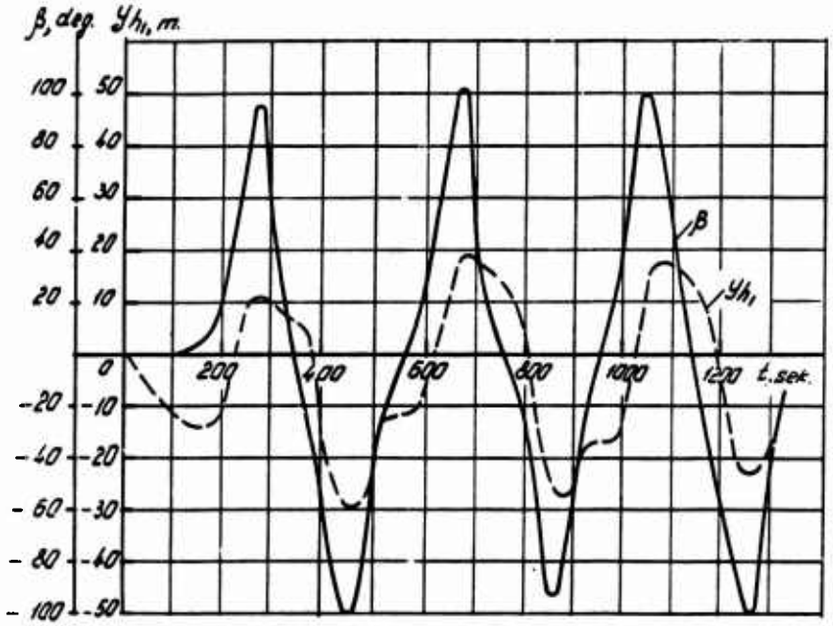


Figure 5 Development of auto-oscillations of the anchored vessel (sea depth H = 100 m, wind velocity v = 12 m/sec.)

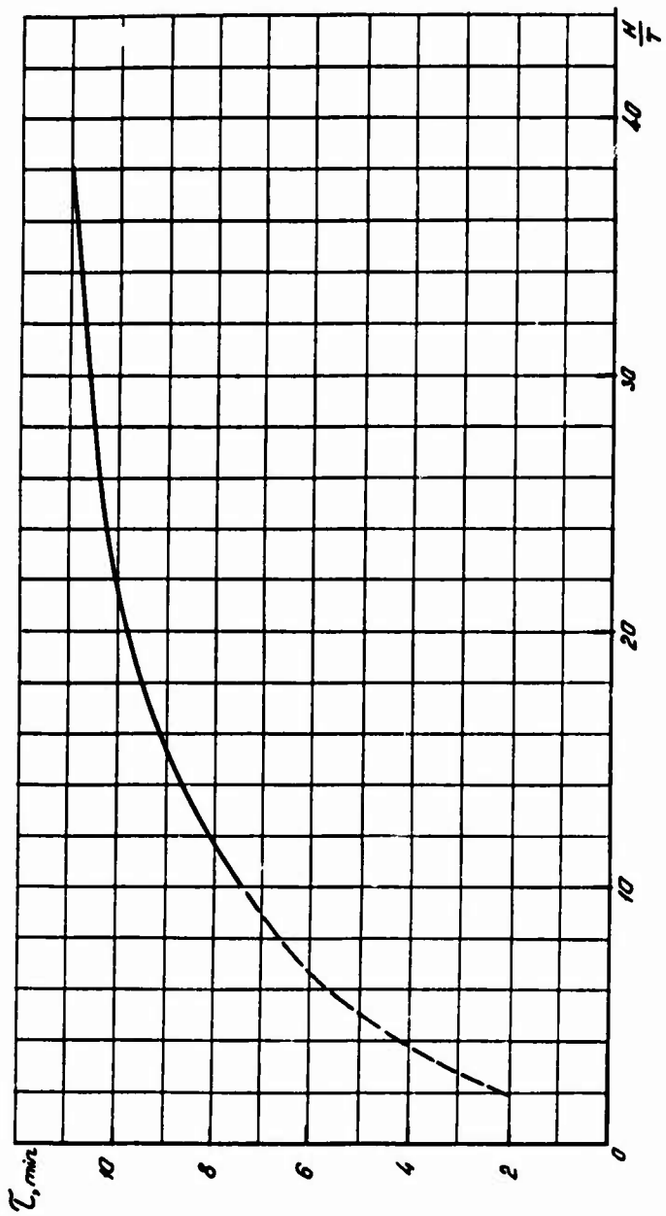


Figure 6 Sea depth effect on the period of oscillations (wind velocity v = 7 m/sec).

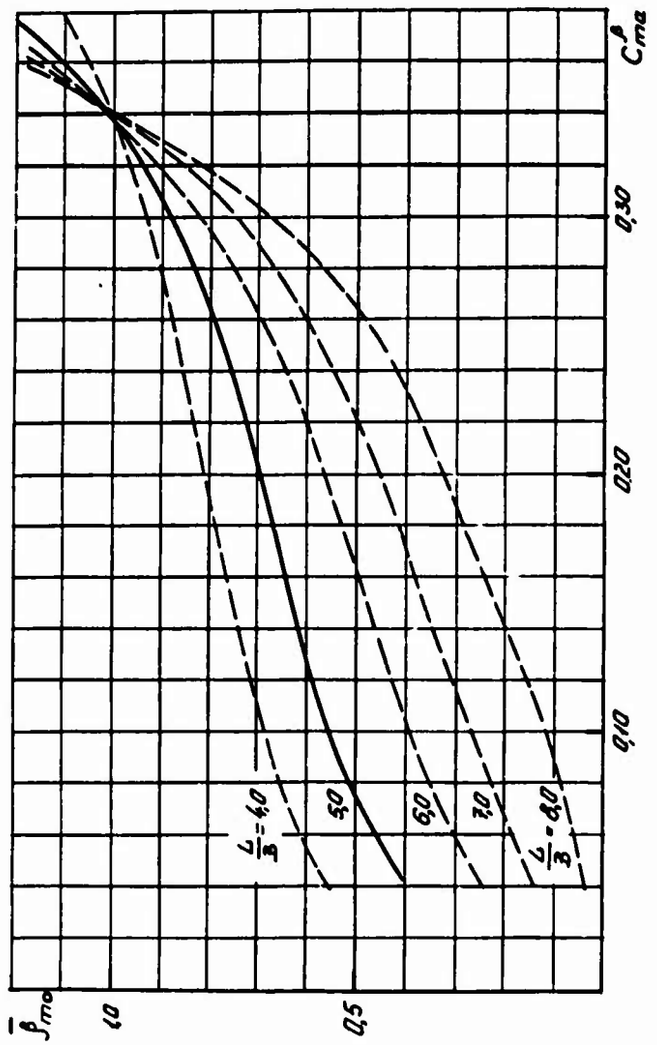


Figure 7 The intensity of yawing versus the derivative of aerodynamic moment.

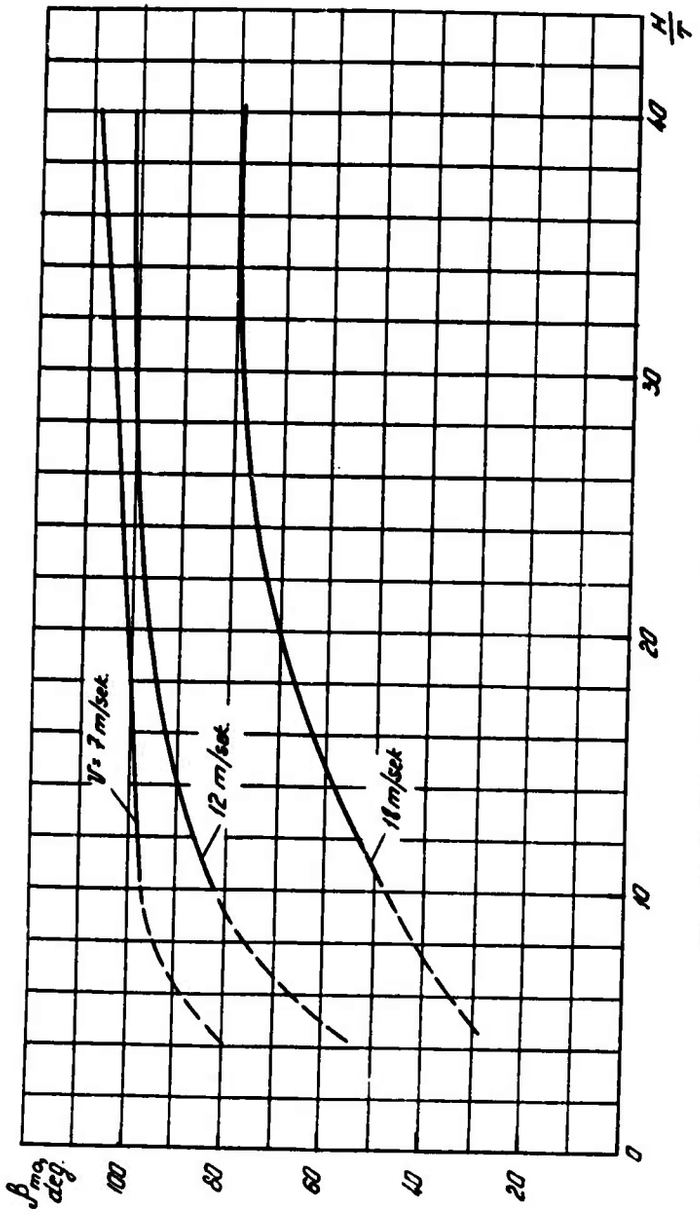


Figure 8 Sea depth effect on the amplitude of yaw.

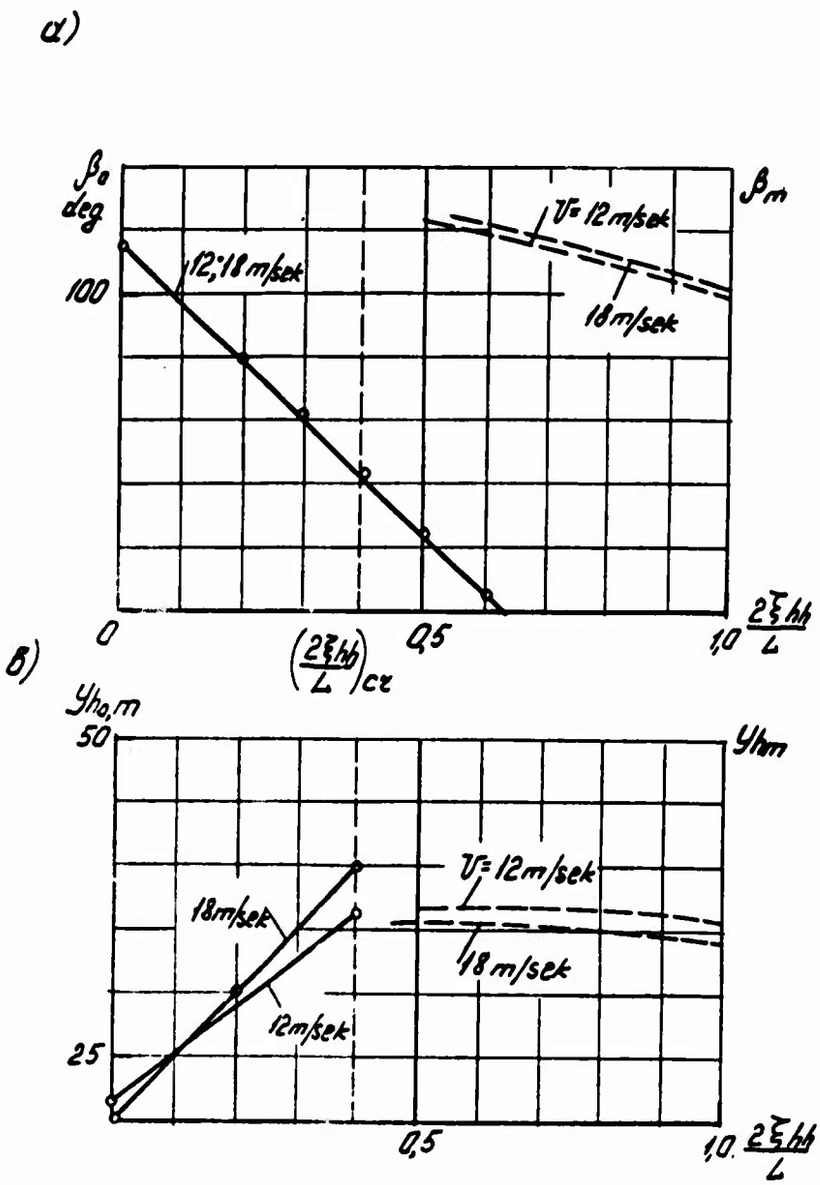


Figure 9 The effect of longitudinal shifting of the hawse-hole on the intensity of yaw (a) and drift (b).

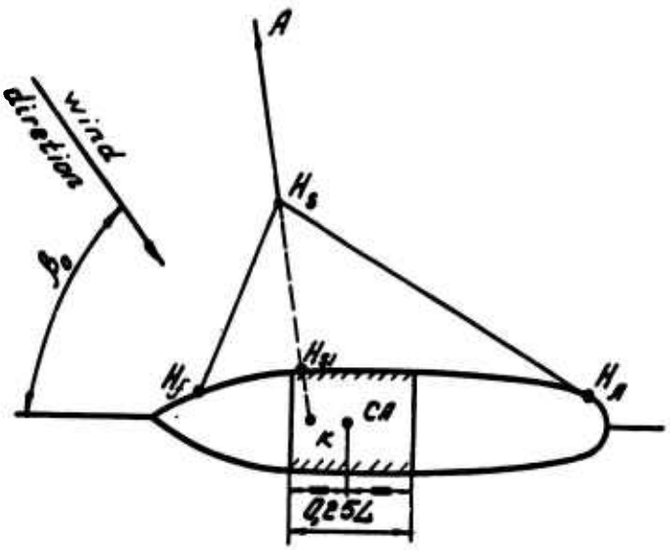


Figure 10 Scheme showing the springing system.

DISCUSSION

J. C. Dern
Bassin d'Essais des Carènes
Paris, France

I have been very interested by the paper we just listened to, for it explains phenomena that I have personnaly encountered during model tests. I would like to make a few remarks.

In the introduction of the paper, it is said that the mean reason for the oscillations in the position of an anchored ship is the instability of her equilibrium position due to the wind. However, it seems to me that under certain conditions, current and waves may also create instabilities. For example the instability due to current is related to the course instability of a towed ship. This instability appears not only with ships but also with buoys. Tests on a 2-ton coastal buoy have shown the presence of transverse oscillations when the current velocity is less than 4 knots. Beyond 4 knots, however, these oscillations disappear.

These results are in agreement with the conclusions of paragraph 9.

The authors assume that the coupled motions of pitching and heaving have no influence on the motions in the horizontal plane. However, in paragraph 9, it is stated that the increase in the period of the sway of an anchored ship is probably due to waves. It seems to me that waves may have a great influence on the behaviour of an anchored ship. For example, for very long waves, the ship may, under certain conditions, go up the waves and her hawser or chain may slacken partially or even completely. In this case, the wave length is the main parameter though it is not taken into account in the equations of the paper.

In any case, waves change the conditions of applications of Liapounov's stability theory since when waves are present, the solution of the motion equations is an oscillatory solution whose stability may notably differ from that of the steady solution of the no-wave case. In some cases, waves may have a stabilizing effect such that the instability oscillations disappear completely. In the case of the

coastal buoy, which I mentionned earlier, the sway oscillations totally disappear in I meter waves.

The authors discussed fully the influence of the position of the centre of pressure of the superstructures on the stability of the equilibrium position. I would like to know the effect of prestretching the chain on the ship oscillations.

REPLY TO DISCUSSION

N. N. Rakhmanin
Kryloff Ship Research Institute
Leningrad, U.S.S.R.

First of all I must thank Dr. Dern for his comments. I should like to make two remarks about them and to answer them.

When we compare the behaviour of a vessel with a buoy we must remember that the buoy has a small LB ratio, which is about I. As to the conventional fishing vessel, her length breadth ratio is about 5 or more. In the Paper there is an indication that this LB ratio has an influence on the oscillation. To my mind these auto-oscillations of a conventional vessel and a buoy have a different character. The auto-oscillations of a vessel, I described in detail in the paper, are connected with the quality of a vessel to turn across the flow, when being the free floating body. Such body has a steady equilibrium position when it is located across the flow.

As to the oscillations which one can observe at a buoy in the current, to my mind the cause of these oscillations is connected with another phenomenon. This phenomenon is the vortex separation behind the cylindric body of a buoy. The eddies separate in turn from the left-hand and the right-hand side of a buoy. As it appears to me that such character of the vortex separation causes the transverse periodic forces to excite the buoy oscillations.

Another point concerns the comparison of the results of the theoretical calculations and that of the experimental data. I must say that this investigation has been started not from a theoretical consideration but from the full-scale observation of the fishing vessel

behaviour in the sea. The fishermen reported that when they observed the behaviour of a vessel in windy weather (the yawing angle and the drifting of the vessel), they were very surprised that the vessel turned not only beam to the wind direction but even more ; the stern of the vessel had turned almost towards to the wind.

We checked this behaviour in details and then set the problem theoretically, I must say that the agreement is good between the theoretical results and the full-scale data. The main purpose of this paper was the representation of the theoretical considerations of the phenomenon.

I certainly agree with Dr. Dern that the presentation of the results of the comparison between the theoretical and the experimental data would have been of interest.

I regret that the authors were not able to check the theory against model tests in order to determine how well their theory is capable of predicting quantitatively the amplitude of the ship oscillations.

* * *

☆ U S GOVERNMENT PRINTING OFFICE 1975 O 565 528